Catalytic and topological aspects of Schiff base supported 3d-4f polynuclear coordination complexes

Kieran Griffiths

Degree of Doctor of Philosophy

University of Sussex

June 2017

DECLARATION

The thesis conforms to an 'article format' in which the middle chapters consist of discrete articles written in a style that is appropriate for publication in peer-reviewed journals in the field. The first (chapter one) and final chapters present synthetic overviews (chapters ten – chapter twelve) and discussions of the field and the research undertaken.

Chapter two is published in *Crystal Growth and Design* as:

"*Four New Families of Polynuclear Zn-Ln Coordination Clusters. Synthetic, Topological, Magnetic and Luminescent Aspects*"

Griffiths, K.; Mayans, J.; Shipman, M. A.; Tizzard, G. J.; Coles, S. J.; Blight, B. A.; Escuer, A.; Kostakis, G. E. *Cryst. Growth Des*. **2017**, *17* (4), 1524-2538.

The author contributions are as follows: Griffiths, K. was responsible for the synthesis and characterisation of the reported PCCs, as well as the topological analysis and UV-Visible studies. Mayans, J., Shipman, M. A. and Blight, B. A. were responsible for fluorescence measurements. Tizzard, G. J. and Coles, S. J. were responsible for some of the single-crystal XRD data collection. Escuer, A. was responsible for the collection of magnetic data. Griffiths, K. and Kostakis, G. E. were collectively responsible for the initial conception of the research and the writing of the paper.

Chapter three is published in the *European Journal of Inorganic Chemistry* as:

"*Synthesis, characterisation, Magnetic Properties, and Topological Aspects of Isoskeletal Heterometallic Hexanuclear* $Co^{II}_4Ln^{III}_2$ *Coordination Clusters Possessing* ***2,3,4M6-1*** *Topology*.

Griffiths, K.; Novitchi, G.; Kostakis, G. E. *Eur. J. Inorg. Chem.* **2016**, *2016* (17), 2750-2756.

The author contributions are as follows: Griffiths, K. was responsible for the synthesis and characterisation of the reported PCCs, as well as the topological analysis. Novitchi, G. was responsible for collection and interpretation of magnetic data. Griffiths, K. and Kostakis, G. E. were collectively responsible for the initial conception of the research and the writing of the paper.

Chapter four has been published in the *European Journal of Inorganic Chemistry* as:

"*Heptanuclear disk-like* $M^{II}_3Ln^{III}_4$ *(M=Ni, Co) coordination clusters: synthesis, structures and magnetocaloric properties*"

Griffiths, K.; Harding, C.; Dokorou, V.N.; Loukopoulos, E.; Sampani, S.I.; Abdul-Sada, A.; Tizzard, G. J.; Coles. S. J.; Lorusso, G.; Evangelisti, M.; Escuer, A.; Kostakis, G. E. *Inorg. Chem.* **2017,** *2017* (33), 3938-3945.

The author contributions are as follows: Griffiths, K. was responsible for the synthesis and characterisation; topological analysis and of the reported ligands and PCCs. Dokorou, V. N. was responsible for the synthesis of two PCCs. Abdul-Sada, A. was responsible for the collection of ESI-MS data. Escuer, A. was responsible for the collection of magnetic data. Tizzard, G. J. and Coles, S. J. were responsible for some of the single-crystal XRD data collection. Lorusso, G. and Evangelisti, M. were responsible for MCE data collection and interpretation. Griffiths, K. and Kostakis, G. E. were collectively responsible for the initial conception of the research and the writing of the paper.

Chapter five is published in *CrystEngComm* as:

"*Isoskeletal Schiff base polynuclear coordination clusters: synthetic and theoretical aspects*"

Griffiths, K.; Dokorou, V. N.; Spencer, J; Abdul-Sada, A.; Vargas, A.; Kostakis, G. E.

CrystEngComm **2016**, *18* (5), 704-713.

The author contributions are as follows: Griffiths, K. was responsible for the synthesis and characterisation of the reported ligands and compounds. Dokorou, V. N. was responsible for the synthesis of two of the reported compounds. Abdul-Sada, A. was responsible for the collection of ESI-MS data. Spencer, J. was responsible for providing feedback on the synthesis of ligands and the manuscript. Vargas, A. was responsible for computational studies. Griffiths, K. and Kostakis, G. E. were collectively responsible for the initial conception of the research and the writing of the paper.

Chapter six has been submitted to *Inorganic Chemistry* as:

"*New twists on the devilishly difficult and ambiguous spin structure of the Ln9-diabolo motif performed by two new* $\{Zn_2Ln_2\}Ln_9\{Zn_2\}$ *coordination clusters*"

Griffiths, K.; Kuhne, I. A.; Tizzard, G.J.; Coles, S.J.; Kostakis, G.E.; Powell, A.K.

The author contributions are as follows: Griffiths, K. was responsible for the synthesis and characterisation of the reported compounds. Kuhne, I. and Powell, A. K. were responsible for the collection and interpretation of magnetic data. All authors were responsible for the writing of the publication.

Chapter seven is a collection of papers published in *Chemistry a European Journal* and *Inorganic Chemistry* as:

"*Heteronuclear 3d/*Dy^{III} *Coordination Clusters as Catalysts in a Domino Reaction*"

Griffiths, K.; Gallop, C. W. D.; Abdul-Sada, A.; Vargas, A.; Navarro, O.; Kostakis, G.E. *Chem. Eur. J.* **2015**, *21* (17), 6358-6361.

"*Efficient $Ni^{II}_2Ln^{III}_2$ Electrocyclization Catalysts for the Synthesis of trans-4,5-Diaminocyclopent-2-enones from 2-Furaldehyde and Primary or Secondary Amines*"

Griffiths, K.; Kumar, P.; Mattock, J. D.; Abdul-Sada, A.; Pitak, M. B.; Coles, S. J.; Navarro, O.; Vargas, A.; Kostakis, G.E. *Inorg. Chem.* **2016**, *55*, 6988-6994.

The author contributions are as follows: Griffiths, K. was responsible for the synthesis and characterisation of the reported compounds, as well development of the catalytic protocols and isolation of catalytic products. Abdul-Sada, A. was responsible for the collection of ESI-MS data of selected compounds. Pitak, M. B. and Coles, S. J. were responsible for the collection of some of the single-crystal XRD data. Vargas, A. and Mattock, J. D. were responsible for computational studies. Navarro, O. and Gallop, C. W. D. were responsible for providing feedback on the catalytic study and the manuscript. Kumar, P. was responsible for the synthesis of the two ligands reported in the second paper and providing feedback on the manuscript. Griffiths, K. and Kostakis, G. E. were collectively responsible for the initial conception of the research and the writing of the paper.

Chapter eight is a collection of papers published in *Chemical Communications*, *Catalysts* and *RSC Advances* as:

"*Tetranuclear Zn/4f coordination clusters as highly efficient catalysts for Friedel–Crafts alkylation*"

Griffiths, K.; Kumar, P.; Akien, G.R.; Chilton, N. F.; Abdul-Sada, A.; Tizzard, G.J.; Coles, S.J.; Kostakis, G.E. *Chem. Commun.* **2016**, *52* (50), 7866-7869.

"*Highly Efficient Tetranuclear $Zn^{II}_2Ln^{III}_2$ Catalysts for the Friedel–Crafts Alkylation of Indoles and Nitrostyrenes*"

Kumar, P.; Lymperopoulou, S.; Griffiths, K.; Sampani, S.; Kostakis, G. *Catalysts* **2016**, *6* (9), 140

"*Tetranuclear Zn_2Ln_2 Coordination Clusters as Catalysts in the Petasis borono-Mannich multicomponent reaction*"

Kumar, P.; Griffiths, K.; Lymperopoulou, S.; Kostakis, G.E.; Kostakis, G. E. *RSC Adv.* **2016**, *6* (82), 79180-79184.

Chemical communications – Griffiths, K. was responsible for the synthesis and characterisation of the reported compounds; UV-Vis binding studies; the development of the catalytic protocols and isolation of the catalytic products. Kumar. P. was responsible for providing feedback on the study and the manuscript. Aiken, G. R. was responsible for collecting and interpreting ^{89}Y NMR and ^{1}H NMR of the Y analogue. Chilton, N. was responsible for collecting and interpreting EPR data. Tizzard, G. J. and Coles, S. J. were responsible for collecting some of the XRD data. Abdul-Sada, A. measured ESI-MS data for compounds and catalytic products. Griffiths, K. and Kostakis, G. E. were collectively responsible for the initial conception of the research and the writing of the paper.

Catalysts - Griffiths, K. was responsible for the synthesis of the reported compounds and UV-Vis binding studies. Kumar, P. was responsible for most of the development of the catalytic protocols and isolation of the catalytic products. Griffiths, K., Lymperopoulou, S. and Sampani, S. were jointly responsible for the remainder of this work. Griffiths, K., Kumar, P. and Kostakis, G. E. were collectively responsible for the initial conception of the research and the writing of the paper.
RSC Advances - Griffiths, K. was responsible for the synthesis of the reported compounds and UV-Vis binding studies. Kumar, P. and Griffiths, K. were responsible for most of the development of the catalytic protocols and isolation of the catalytic products. Lymperopoulou, S. was responsible for the remainder of this work. Griffiths, K., Kumar, P. and Kostakis, G. E. were collectively responsible for the initial conception of the research and the writing of the paper.

Chapter nine has been published in *Inorganic Chemistry* as:
"3d/4f Coordination clusters as cooperative catalysts for highly diastereoselective Michael addition reactions."
Griffiths, K.; Tsipis, A.C.; Kumar, P.; Townrow, P.E.; Abdul-Sada, A.; Akien, G.R.; Baldansuren, A.; Spivey, A.C.; Kostakis, G.E. *Inorg. Chem.* **2017**, 56 (16), 9563-9573.
Griffiths, K. was responsible for the synthesis and characterisation of the reported compounds; UV-Vis binding studies; the development of the catalytic protocols and isolation of the catalytic products and the preparation of samples for EPR and ESI-MS studies. Aiken, G. R. was responsible for collecting and interpreting ^{89}Y NMR and ^{1}H NMR spectra. Abdul-Sada, A. measured ESI-MS data for compounds and catalytic products. Baldansuren, A. was responsible for measuring and interpreting EPR data. Tsipis, A. was responsible for performing DFT studies to support the reaction mechanism. Spivey, A. provided useful insights for the study and writing of the manuscript. Griffiths, K., Kumar, P. and Kostakis, G. E. were collectively responsible for the initial conception of the research and the writing of the paper.

I hereby declare that this thesis has not been and will not be, submitted in whole or in part to another University for the award of any other degree.
Signature……

Summary

The work presented in this thesis deals with the employment of Schiff base ligands used to synthesise novel 3d-4f polynuclear coordination clusters (PCCs) and the investigation into their potential magnetic, luminescent and catalytic properties.

Chapter one provides a general introduction to the chemistry described in the thesis. It includes a general overview of 3d-4f PCC chemistry and the applications of these materials and previous synthetic strategies for the preparation of Schiff base PCCs. A rationale is presented for the ligands employed in the thesis and a synthetic strategy is devised for the synthesis of specific materials.

The initial chapters are focused on the synthesis of 3d-4f PCCs with novel core topologies and the study of their magnetic properties. Several novel series of 3d-4f PCCs are presented with unique core topologies which are previously unobserved in 3d-4f PCC chemistry. In addition, some of the presented PCCs display single-molecule magnet (SMM) properties or a significant magnetocaloric effect (MCE).

Chapter five bridges synthetic aspects discussed in the previous chapters, with a synthetic study targeting 3d-4f PCCs with a defect dicubane core (**2,3M4-1)** and introduces the term "isoskeletal" to describe PCCs which possess the same topology or related organic structures with the same host framework but different guests.

Chapters seven to nine are focused on the development of a well characterised isoskeletal family of 3d-4f PCCs with a defect dicubane core and the investigation of their potential catalytic properties in a range of organic reactions including Michael Addition, Friedel-Crafts alkylations and multicomponent reactions. Characterisation of the 3d-4f PCCs is emphasised and verifies the stability of the **2,3M4-1** core in solution. An attempt at understanding the catalytic system and mechanistic aspects is undertaken, which is not explored in previously reported 3d-4f PCC co-operative catalysis.

Chapter ten provides an overall conclusion to the work presented in the thesis, whilst highlighting the contributions of this work to the reported literature.

Acknowledgements

Above all, I would like to thank my supervisor Dr George E. Kostakis for his excellent guidance, continuous support, patience; freedom to explore different routes in my PhD and a supervisory approach which has helped round me personally and as a professional.

In addition to this, I would again like to thank Dr George E. Kostakis and Dr Mark Roe for teaching me how to operate the single-crystal X-ray diffractometer and the multiple software packages related to crystallographic data interpretation. Furthermore, their help in solving and refining crystal structures has been instrumental in reaching this stage. For the more bewildering crystallographic problems, I would like to thank Dr Graham Tizzard and Dr Simon J Coles from the University of Southampton who were instrumental in deciphering these conundrums.

I would especially like to thank Dr Alaa Abdul-Sada for performing ESI-MS measurements and enhancing my understanding of the technique, but also for providing an inspiration and providing many useful suggestions. I would like to thank Dr Albert Esquer, Dr Irina Kuhne and Dr Ghenadie Novitchi for performing SQUID measurements for all the compounds that are reported in this thesis and for their magnetic studies. A special thanks to Dr Amgalanbaatar Baldansuren for teaching me how to operate the EMX spectrometer at the University of Manchester and for making me comfortable during the trip. I would also like to thank Dr Alfredo Vargas, Mr James Mattock and Dr Athanassios C. Tsipis for providing DFT calculations which support my experimental work, without these the journey in exploring 3d-4f PCC catalysis would have been much more arduous.

I would also like to thank Dr Oscar Navarro, Dr John Spencer and Dr Mark Bagley for providing insightful advice in areas of organic and catalytic chemistry which I was weaker in. Thanks to Dr Prashant Kumar who helped me refine the techniques used for investigating catalytic reactions and all the other knowledge which he passed to me during his time in the lab. I also thank Mr Alex Burns and Mr Paul Andrews and all the other technical staff for their help in the chemical stores and maintenance of the lab. Also, a big thanks to Ben, Eddie, Prashant, Magda, Nikos, Shane, Stravoula, Irina, James, Keith, Tom and Vaso for their help in various projects and for their patience.

Glossary

ac	Altenating Current
β	The Bohr Magneton
BIM	Bis(indolyl)methane
BINOL	1,1'-bi-2-napthol
BVS	Bond Valence Sum
cat	Catalyst
C	Heat Capacity
CC	Coordination Cluster
$CHCl_3$	Chloroform
CH_2Cl_2	Dichloromethane
CN	Coordination Number
CSD	Cambridge Structural Database
CSI-MS	Coldspray Ionisation Mass Spectroscopy
CV	Cyclic Voltammerty
D	Anisotropy
dc	Direct Current
DCM	Dichloromethane
DFT	Density Functional Theory
DME	1,2-Dimethoxyethane
DMF	N, N-Dimethylformaide
DMSO	Dimethylsulphoxide
EA	Elemental Analysis
ESI-MS	Electrospray Ionisation Mass Spectrometry
Et	Ethyl
Et_3N	Triethylamine
EtOH	Ethanol
EPR	Electron Paramagnetic Resonance
FC	Friedel-Crafts
FT-IR	Fourier Transform Infrared Spectroscopy
g	Landé Factor
gp	Gas-Phase

FMO	Frontier Molecular Orbital
H	Magnetic Field
HOMO	Highest Occupied Molecular Orbital
k_B	Boltzmann Constant
Ln	Lanthanide
LUMO	Lowest Unoccupied Molecular Orbital
M	Magnetisation
M	3d Transition Metal
MA	Michael Addition
MCE	Magnetocaloric Effect
MCR	Multicomponent Reaction
Me	Methyl
MeCN	Acetonitrile
MeOH	Methanol
MEP	Molecular Electrostatic Potential
mg	Milligram(s)
min	Minute(s)
mL	Millilitre(s)
mmol	Millimole(s)
MOF	Metal-Organic Framework
N_A	Avogadro Constant
NAC	Natural Atomic Charge
NBO	Natural Bond Orbital
NIR	Near Infrared Spectroscopy
NMR	Nuclear Magnetic Resonance
OAc	Acetate
Oe	Oersted
OEC	Oxygen Evolving Complex
OLED	Organic Light-Emitting Diode
PBR	Petasis Borono Mannich Reaction
PCC	Polynuclear Coordination Cluster
PCM	Polarizable Continuum Media

PES	Potential Energy Surface
Ph	Phenyl
PCM	Polarizable Continuum Media
Py	Pyridine
QTM	Quantum Tunnelling of Magnetisation
R	Gas Constant
RDG	Reduced Density Gradient
r.t	Room Temperature
S	Entropy
S	Energy of the spin state
SE	Slow Evaporation
SIM	Single Ion Magnet
SMM	Single Molecular Magnet
sp	Single Point
SQUID	Superconducting Quantum Interference Device
TGA	Thermogravimetric Analysis
THF	Tetrahydrofuran
UV	Ultra Violet
UV-Vis	Ultra Violet- Visible Spectroscopy
XRD	X-Ray Diffraction
χ	Molar Magnetic Susceptibility
χ'	In-Phase Magnetic Susceptibility
χ''	Out-of-Phase Magnetic Susceptibility
μ_B	Bohr Magnetons
U_{eff}	Effective Energy Barrier
VD	Vapour Diffusion
WOC	Water Oxidation Catalyst
ZFS	Zero Field Splitting

Contents

Synopsis

The initial chapters of this thesis present the synthesis and characterisation of novel 3d-4f Polynuclear Coordination Clusters (PCCs), which exhibit a range of core topologies, some of which demonstrate fascinating magnetic properties and luminescent behaviour. In addition, the latter half of this work introduces the concept of "isoskeletal" PCCs and offers a different perspective, with the first tetranuclear 3d-4f PCCs with the potential to act as catalysts for organic transformations described. This series of 3d-4f PCC catalysts are well characterised in solid and solution state and mechanistic aspects are probed and analysed using a wide range of techniques.

Chapter 1 provides a general introduction to the chemistry described in this thesis. It includes a general overview of 3d-4f PCC chemistry and the previous applications of these materials. Synthetic strategies for the preparation of Schiff base PCCs are also discussed. In addition, a rationale is presented for the ligands employed in this thesis along with a synthetic strategy for the design of specific materials.

In ***chapter 2***, twelve heterometallic Zn^{II}-Ln^{III} PCCs (**1 - 12**) have been synthesised using H_2**L1**-H_3**L3** through serendipitous assembly and a systematic variation of reaction conditions. The first examples, $[Zn^{II}_2Ln^{III}_2(\mathbf{L1})_4(EtOH)_6](ClO_4)_2$ (**1-3**) possess a defect dicubane topology and are the second examples of the **2,3M4-1** topology with a $Zn^{II}_2Ln^{III}_2$ core supported by H_2**L1**. With the omission of perchlorate counter-ions PCCs with the general formula $[Zn^{II}_5Ln^{III}(OH)(\mathbf{L1})_6(H_2O)]$ (**4 - 6**) are formed with a **2,3,4M6-1** core. The incorporation of acetate counter-ions with H_2**L2** resulted in the same **2,3,4M6-1** topology, but with a PCCs formulated $[Zn^{II}_4Ln^{III}_2(OH)_2(\mathbf{L2})_4(OAc)_2(NO_3)_2(DMF)_3]\cdot DMF$ (**7-9**). Compounds **4 - 9** are the first reported examples of the **2,3,4M6-1** topology in Zn^{II}-Ln^{III} chemistry. Finally, a tetranuclear series with the general formula $[Zn^{II}_2Ln^{III}_2(\mathbf{L3})_2(NO_3)_2(CO_3)_2(CH_3OH)_2]$ (**10-12**) are formed from $[Zn^{II}Ln^{III}(H\mathbf{L3})(NO_3)(MeOH)]$ moieties bridges by carbonate ions. A Single Molecule Magnet (SMM) response was not detected for **1** and **10**, however, *ac* measurements indicate that **7** is a Single Ion Magnet (SIM), with an energy barrier (U_{eff}) of 10.2 K and $\tau_0 = 7.1\cdot10^{-6}$ s. The crystal structures of two novel species are also presented including $Zn^{II}_4Dy^{III}_7$ (**13**) (**2,4,4,4M11-1**) and $Zn^{II}_6Dy^{III}_4$ (**14**) (**2,2,3M10-1**).

In ***chapter 3*** a series of hexanuclear isoskeletal $[Co^{II}_4Ln^{III}_2(\mu_3\text{-}OH)_2(\mathbf{L1})_4Cl_2(NO_3)_2(MeOH)_4]\cdot3(Et_2O)$ PCCs (**15-19**) with the **2,3,4M6-1** topology were synthesised from H_2**L1** and H_2**L5**. These are the first examples of $Co^{II}_4Ln^{III}_2$ PCCs displaying the **2,3,4M6-1** topology and the second example of the topology in Co^{II}-Ln^{III} chemistry. Magnetic studies show that Dy^{III} (**17**) and Tb^{III} (**18**) analogues display ferromagnetic interactions. Compound **17** (Dy^{III}) exhibits an out-of-phase signal χ'' in *ac* susceptibility measurements with an energy barrier of (U_{eff}) = 13.4 K and $\tau_0 = 8.5\times10^{-7}$ s.

In ***chapter 4***, five heptametallic $M^{II}_3Ln^{III}_4$ disk-like PCCs are described supported by the monoanionic H**L4** ligand, with the formulas $[Co^{II}_3Ln^{III}_4(\mu_3\text{-}OH)_6(\mathbf{L4})_6(CF_3SO_3)](CF_3SO_3)_5$ (Ln = Gd (**20**), Y (**21**)) and $[Ni^{II}_3Ln^{III}_4(\mu_3\text{-}OH)_6(\mathbf{L4})_6(CF_3SO_3)](CF_3SO_3)_5$ (Ln = Dy (**22**), Gd (**23**), Y(**24**) which are isoskeletal analogues of the previously reported $Co^{II}_3Ln^{III}_4$ cluster.[1] Synthetic issues are identified and the methodology is adapted for more reliable crystallisation which results in higher yields of targeted species. The $M^{II}_3Ln^{III}_4$ core is enumerated **3,6M7-1** and the Ni^{II}-Ln^{III} series are the first examples of Ni^{II}-Ln^{III} disks and the third examples of Co^{II}-Ln^{III} PCC disks. Electrospray Ionisation Mass Spectrometry (ESI-MS) studies of compounds **20 - 23** display a well-defined fragment pattern, all of which are indicative of the $[M^{II}_3Ln^{III}_4(\mathbf{L4})_6(OH)_6]^{x+}$ core. $Ni^{II}_3Gd^{III}_4$ (**23**) displayed a modest MCE effect of 15.4 J kg^{-1} K^{-1} at 5.0 K, the third highest observed for a 3d-4f Schiff base supported PCC.

In ***chapter 5***, the term "isoskeletal" is introduced to describe PCCs that possess cores of the same topology and to describe PCCs constructed from organic ligands that provide a similar coordination environment. This concept is demonstrated by systematically synthesising isoskeletal Ni^{II}/Co^{II}-Dy^{III} PCCs with defect dicubane cores (**2,3M4-1**) from modified derivatives of H_2**L1** (H_2**LX**). The reaction of H_2**L1** and its derivatives resulted in the synthesis of eighteen PCCs (**25 - 42**) which were characterised by single-crystal XRD studies. Compounds **25 - 42** were synthesised by systematically altering conditions, to target isoskeletal $[M^{II}_2Ln^{III}_2(\mathbf{LX})_4(solv)_6](ClO_4)_2$ (**2,3M4-1**) PCCs, including oxidation (**25** and **26**), solvent (**27 - 31**), solvent concentration (**32 - 34**), ratio of reactants (**35** and **36**), crystallisation method (**37**) and co-ligand introduction (**38 - 42**). The resultant PCCs demonstrate that a slight variation in synthetic conditions can drastically alter the formula and topology of the desired $[M^{II}_2Ln^{III}_2(\mathbf{LX})_4(solv)_6](ClO_4)_2$ PCCs. The desired PCCs were further studied by ESI-MS and the **2,3M4-1** core was found to be retained in solution. Further computational studies demonstrate how the activity of the PCCs can be tuned and suggests ways of achieving this.

In ***chapter 6***, two high nuclearity pentadecanuclear PCCs with the general formula $[Zn^{II}_4Ln^{III}_{11}(\mu_4\text{-}OH)_2(\mu_3\text{-}OH)_8(\mu_2\text{-}OH_2)_2(\mu_3\text{-}NO_3)_2(NO_3)_6Cl_4(H\mathbf{L23})_2(\mathbf{L23'})_4(\mu_2\text{-}MeO)_7(\mu_3\text{-}MeO)_2(MeOH)_2(H_2O)_2]$, where Ln = Dy (**43**), Gd (**44**), were synthesised *in situ* and characterised in the solid state. Single-crystal XRD studies elucidate a unique core structure resembling a "purse" with subunits forming a $[Zn^{II}Ln^{III}_2Zn^{II}(H\mathbf{L23})_2(\mu_2\text{-}MeO)_3Cl_2(MeOH)_2]$ "strap" and a $[Zn^{II}Ln^{III}_9(\mu_4\text{-}O)_2(\mu_3\text{-}OH)_8(\mu_2\text{-}OH_2)_2(\mu_3\text{-}NO_3)_6(NO_3)_2Cl_{22}(\mathbf{L23'})_4(\mu_2\text{-}MeO)_4(\mu_2\text{-}MeOH)_2(H_2O)_2]$ "body". This topology is enumerated **1,2,3,4,5,5,5,8M15-1** and has not been previously reported in PCC chemistry. It is also the third highest reported nuclearity for a Zn^{II}-Ln^{III} PCC. Magnetic studies confirm the SMM behaviour of the Dy^{III} analogue (**43**) (U_{eff} = 4.7 K and τ_0 = 4.4x10^{-5} s). With the addition of the "hands and feet" or the "strap" providing a tethering unit which can direct the spin of the central ion of the diabolo unit it was possible, finally, to disentangle the "devil in

the details" directing the spin structure of such diabolo units, which had not previously been described.

In ***chapter 7***, two isoskeletal $Ni^{II}_2Dy^{III}_2$ (**1NiDy-ClO$_4$**) and $Co^{II}_2Dy^{III}_2$ PCCs (**1CoDy-ClO$_4$**) were synthesised possessing the defect dicubane core topology (**2,3M4-1**), with the general formula $[M^{II}_2Ln^{III}_2(\mathbf{L1})_4(EtOH)_6](ClO_4)_2$. ESI-MS studies indicate the stability of the $[M^{II}_2Dy^{III}_2(\mathbf{L1})_4]^{2/1+}$ core in solution. The PCCs were then applied to the catalytic formation of *trans*-4,5-diaminocyclopent-2-enones from 2-furaldehyde and secondary amines. At room temperature, the PCC catalysts perform poorly (41 - 55% conversion, 10 mol% loading) however, under reflux the conversion significantly improves (90 - 95% conversion, 2.5 mol% loading). Refluxing **1NiDy-ClO$_4$** in MeCN leads to the formation of the isoskeletal $[Ni^{II}_2Dy^{III}_2(\mathbf{L1})_4Cl_2(MeCN)_2]$ (**1NiDy-Cl)** and ESI-MS studies confirmed the stability of the $[Ni^{II}_2Ln^{III}_2(\mathbf{L1})_4]^{2+}$ core in solution. When **1NiDy-Cl** was applied to the transformation, conversion drastically improved (quantitative, 1 mol% loading). Ln^{III} analogues of **1NiDy-Cl** were synthesised, **1NiLn-Cl** (Ln = Sm, Eu, Gd, Tb and Y), to determine how the substitution of the Ln^{III} site affected the catalytic efficacy of the PCC. **1NiY-Cl** substantially out-performed the other analogues (98% conversion, 1 mol% loading). Through the systematic testing of Ni^{II}, Ln^{III} salts and H_2**L1** as catalysts in the catalytic reaction, it was determined that only the Ln^{III} ion of the **1NiLn-Cl** was catalytically active and the bimetallic system was not co-operative. Three isoskeletal analogues of **1NiY-Cl** PCCs were synthesised (**2NiY-Cl**, **6NiY-Cl** and **14NiY-Cl**) with modified organic ligands (H_2**L2**, H_2**L6** and H_2**L14**) to optimise the catalytic behaviour of the catalyst. In a comparative study, **1NiDy-Cl** and the **LNiY-Cl** series were all used to test the scope of reaction with a variety of primary and secondary amines to determine the structure-activity relationship. Overall, **1NiY-Cl** was found to be the best catalyst for this reaction. In addition, Density Functional Theory (DFT) studies are presented as well as numerous by-products from various synthetic methods.

In ***chapter 8***, a family of eight novel isoskeletal PCCs with the general formula $[Zn^{II}_2Ln^{III}_2(\mathbf{L1})_4(NO_3)_2(DMF)_2]$ (**1ZnLn-NO$_3$**), where Ln = Sm, Eu, Gd, Tb, Dy, Yb and Y, were synthesised. **1ZnLn-NO$_3$** possess the defect dicubane topology (**2,3M4-1**) and are isoskeletal to those reported in chapters five and seven. Various solution-based studies of **1ZnLn-NO$_3$** (ESI-MS, Electron Paramagnetic Resonance (EPR) spectroscopy, ^{1}H NMR spectroscopy) indicate that the defect dicubane topology is retained in solution. The family of **1ZnLn-NO$_3$** compounds were applied to numerous organic transformations which were previously promoted by either Zn^{II} or Ln^{III} salts or Schiff base complexes. The initial experiments probed the Friedel-Crafts (FC) alkylation of indoles and aldehydes to BIMs. All PCCs display some catalytic efficacy, with the Y^{III} (**1ZnY-NO$_3$**) analogue (1 mol% loading, 96% conversion) surpassing the performance of the corresponding triflate salt (2.5 mol% loading, 55% conversion) substantially. The scope of the reaction was then explored with **1ZnY-NO$_3$** to gain information of the plausible mechanism.

Secondly, the Petasis borono-Mannich multicomponent reaction is explored, some conversion is observed in an uncatalyzed reaction and with Zn^{II} and Ln^{II} triflates (1% loading, 40 - 56%), **1ZnLn-NO$_3$** PCCs surpass this conversion rate, with the Dy^{III} (**1ZnDy-NO$_3$**) analogue reaching 96% conversion at 1 mol% loading. The reaction is optimised for **1ZnDy-NO$_3$** PCCs and the scope of reaction explored. Finally, these compounds are applied to the FC alkylation of indole with nitroalkenes, where **1ZnDy-NO$_3$** substantially out competes uncatalyzed, metal salt or isostructural analogues in the conversion at low yields. For the FC catalytic transformations, plausible mechanisms are proposed and several products are characterised by single-crystal XRD studies. These results confirm the usefulness of altering the 3d or 4f ions in isoskeletal 3d-4f PCCs for catalysis and represent one of the first fully characterised series of 3d-4f PCCs used for promoting catalysis in a range of organic transformations.

In ***chapter 9***, the isoskeletal series of **1ZnLn-NO$_3$** PCCs are applied to the Michael addition reaction between 1,3-dimethyl barbituric acid and *trans*-β-nitrostyrene to confirm co-operative action between Zn^{II} and Ln^{III} metal centres. After initial optimisation, **1ZnY-NO$_3$** (1 mol%, 91% yield, 15 min) was found to have the greatest efficacy (quantitative, 2.5 mol%) and **1ZnY-NO$_3$** was chosen to investigate the ligand structure-activity relationship. A library of twenty isoskeletal PCCs with the general formula $[Zn^{II}_2Y^{III}_2(\mathbf{LX})_4(NO_3)_2(DMF)_2]$ (**LZnY-NO$_3$**) were synthesised and characterised. The **LZnY-NO$_3$** series was applied to the MA reaction and the modified ligands had a noticeable effect on the efficacy of the catalytic reaction. **28ZnY-NO$_3$** was found to be the most catalytically effective (1 mol%, quantitative, 15 min) and the scope of the reaction was expanded to a variety of substituted nitrostyrenes and Michael acceptors in good to excellent yields. Unexpectedly, diastereoselectivity for the R*, R* product was observed for catalytic reactions employing *trans*-β-methyl-β-nitrostyrene. Further investigation revealed stereoselective behaviour on the substitution of the Ln^{III} ion. In addition, a range of evidence for the co-operative action between 3d and 4f metal centres is presented including EPR binding studies, ^{1}H NMR substrate titration, UV-Vis binding studies, the poor performance of simple metal salts and previously reported isoskeletal $Ni^{II}_2Dy^{III}_2$, $Co^{II}_2Dy^{III}_2$ and novel $Cu^{II}_2Dy^{II}_2$ analogues (29%, 34%, 84%).[2] The co-operative action and substrate binding interactions were supported by DFT studies, which also support the observed stereoselectivity of the **LZnLn-NO$_3$** series.

Chapter 10 summarises the work presented in this thesis and relates this work to the previously reported literature to highlight the relevance and importance of the work presented herein.

Chapter 1: General introduction

1.1 Polynuclear coordination clusters

Polynuclear Coordination Clusters (PCCs) incorporate multiple metal ions which are linked by bridging ligands (in particular elements such as N, O and S), which bridge two to six metal centres into a discrete molecular entity.[3] These entities are distinctly different from metal-metal bonded complexes referred to as "clusters" by Cotton et al.[4] PCCs are sub-divided into two categories 1) those formed from inorganic ligands "polyoxometalates" and 2) those supported by organic ligands. The metal core of PCCs can be either comprised of a single metal (homometallic) or combine two or more different metals (heterometallic). Over the last 30 years, the interest and rate of discovery of these molecules has increased exponentially due to advances in single-crystal X-ray crystallography, which has allowed the elucidation of molecules which are of an exceptional size and complexity.

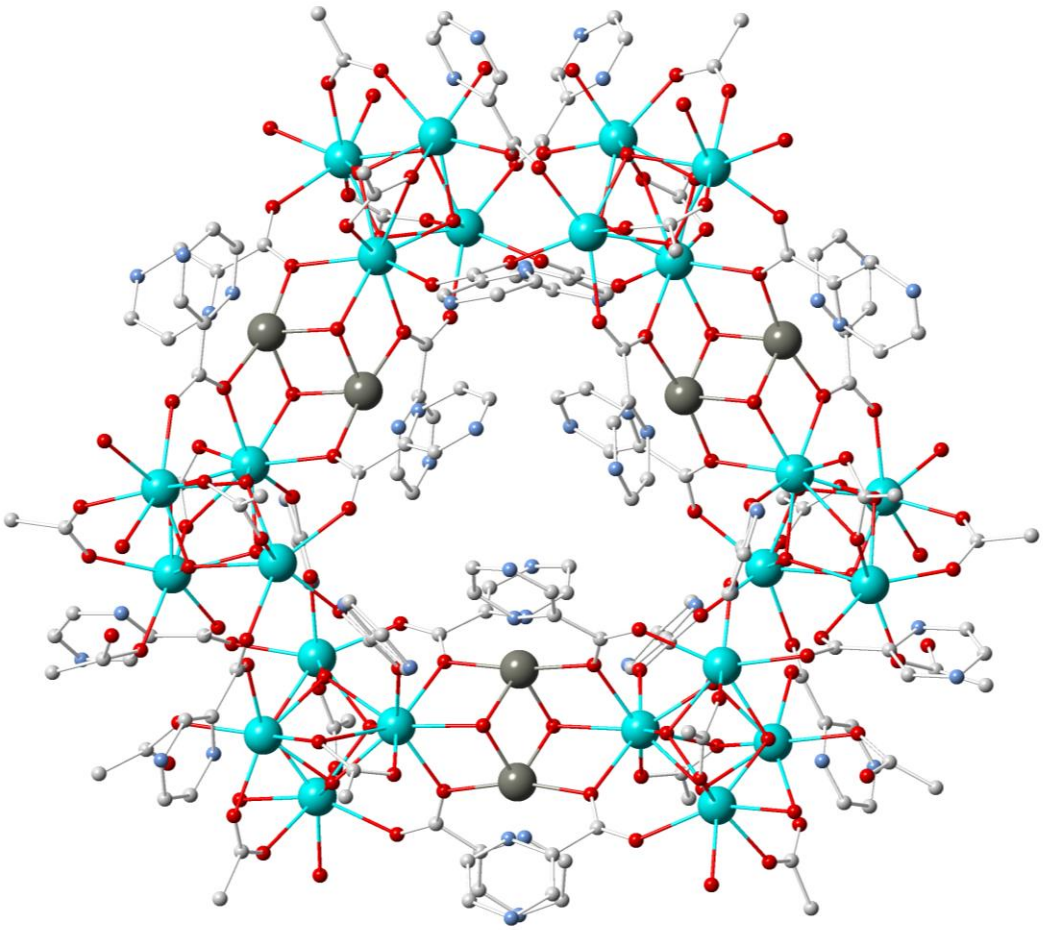

Figure 1.1. The molecular structure of $Zn^{II}_{6}Ln^{III}_{24}$.[5] Colour code: Dy^{III}, light blue; Zn^{II}, grey; O, red; N, pale blue; C, white; S, yellow.[5]

PCCs core nuclearities can range from simple bimetallic species to very high nuclearity species such as Fe_{42},[6] Dy^{III}_{72},[7] Nd^{III}_{104},[8] Mn_{70},[9] $Mn^{III}_{18}Na_6$,[10] $Zn^{II}_6Ln^{III}_{24}$ [5] (Figure 1.1) and Fe^{III}_{168}.[11] The structure of these PCCs is determined both by the geometrical preferences of the metal ions and the steric effects of bridging and terminal ligands that combine to form the PCC. In this way, the metal ions and ligands can be considered ‘‘building blocks’’ which generate an overall structure whose topology is a consequence of the symmetries and connectivity of the constituent parts, however, the targeting of high nuclearity PCCs is much more complicated since various metal ions have many possible coordination geometries. This complexity is further increased with the wide variety of coordination modes that even simple bridging ligands can adopt, including terminal to μ_2, μ_3, and μ_4 bridging modes. PCCs may also be supported by polynucleating ligands which have structural attributes that combine separate coordination pockets.

The ligand–metal combination is one of the most important factors in the overall architecture of the PCC formed. However, the structure of the PCC does not only depend upon the metal ions and oxidation states present but the number of possible binding modes for the ligands, the steric properties of the ligands, the presence of templating units and coordinating solvent, factors such as pH, concentrations and redox potentials of the species present and the type of counter-ions. Consequently, a combination of ligand and metal is often capable of generating a wide range of structures, the favoured structure being the result of a subtle balance of many competing variables.

Due to the variety of PCC structures which have been reported to date, a topological approach has been developed that helps to facilitate the understanding of the growth of the core topology, which in the long term may lead to the targeted synthesis of PCCs.

1.1.1 Topology and notations

The description of the core structure and nuclearity of PCCs has traditionally relied upon representation as a classic Platonic polyhedron. When robust polytopic ligands were employed into a directed assembly process and the resultant PCCs isolated, these were described as (n x n) square grids.[12] High nuclearity PCCs have revealed the limitations of this type of platonic description, due to the difficulty of describing these cores based on Platonic polyhedra.

Topological analysis through the TOPOS program package has successfully described a wide variety of high nuclearity PCCs.[13–16] With this approach, each metal centre of the PCC is designated as a “node” and the bridging monoatomic heteroatoms that bridge these metal ions are then termed as “linkers”. The resulting graph (PCC skeleton) consists of only metal atoms and its topology is described by a characteristic ***ND*k-m** symbol notation. These terms are defined where ***N*** is the number of connections from a single node to topologically non-equivalent nodes through heteroatom linkers, ***D*** is the dimensionality, ***D*** = **M** for finite (molecular) clusters, **k** is the overall

number of nodes within the cluster and **m** enumerates topologically different examples with the same ***ND*k-m** symbol.

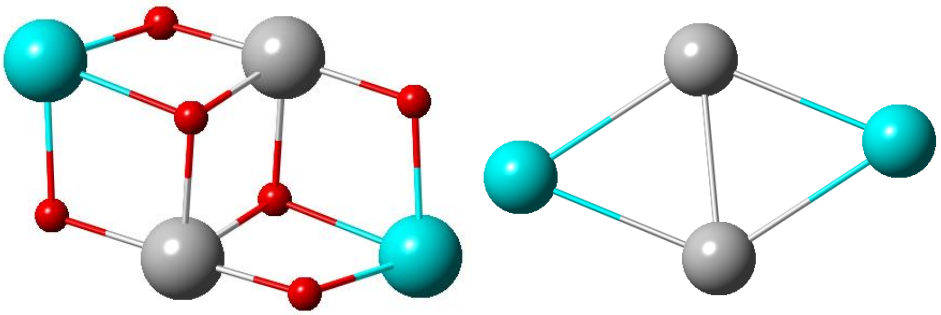

Figure 1.2. A simplified defect dicubane core of a $M^{II}_2Ln^{III}_2$ PCC with heteroatom linkers shown (left) Graph of the defect dicubane (**2,3M4-1**) topology with heteroatoms represented as "linkers" (right). Colour code: M^{II} nodes, grey; Ln^{III} node, light blue and O linkers, red.

The ***ND*K-m** notation will be frequently employed to describe the core topology of PCCs in this work. These notations were first used to describe a database of 439 homometallic $Mn^{II/III/IV}$ PCCs and separate them into 159 separate topologies.[13] This technique has been subsequently employed to categorise homometallic Ni^{II} and $Co^{II/III}$ PCCs,[14,15] high nuclearity 3d-4f PCCs[16] and also adopted for describing newly reported 3d[17,18] and 4f PCCs.[19–21]

With this approach, it is possible to identify structural similarities between seemingly unrelated core topologies whilst providing a universal notation for ligands with different bridging heteroatoms. Similar structural configurations can be identified formed from ligands with specific cavities and bridging modes, which may allow for topologies which exhibit preferential properties to be targeted.

1.2 3d-4f PCCs

The first example of a PCC containing both 3d and 4f elements was reported in 1977 by Lindoy, Drew and co-workers and was first observed by ^{1}H NMR spectroscopy from the changes of the spectrum of tris-(pentane-2,4-dionato_cobalt(III), ($Co(acac)_3$), in $CDCl_3$ upon the addition of tris (1,1,1,2,2,3,3, -heptafluoro-7,7-[$^2H_6$] dimethyl[$^2H_3$] octane-4,6-dionato) europium, (Eu([$^2H_9$] fod)$_3$. This species was subsequently characterised by single-crystal X-Ray Diffraction (XRD) studies and was formulated [$Co(acac)_3${Eu([$^2H_9$]fod)$_3$}].[22]

However, it was not until Gatteschi and co-workers, who eight years later, reported two trinuclear $Cu^{II}_2Gd^{III}$ species, where the observed Gd–Cu coupling was strongly ferromagnetic,[23,24] that opened new perspectives and interest for 3d-4f PCCs in molecular magnetism. The first high nuclearity 3d-4f PCC was reported in 1989, from the reaction of $Cu(OH)_2$, $Ln(NO_3)_3$ and 2-(1H)-

pyridone which afforded a species with an unusual hexanuclear octahedral $Cu^{II}_4Ln^{III}_2$ core, where Ln is Gd or Dy (Figure 1.3).[25]

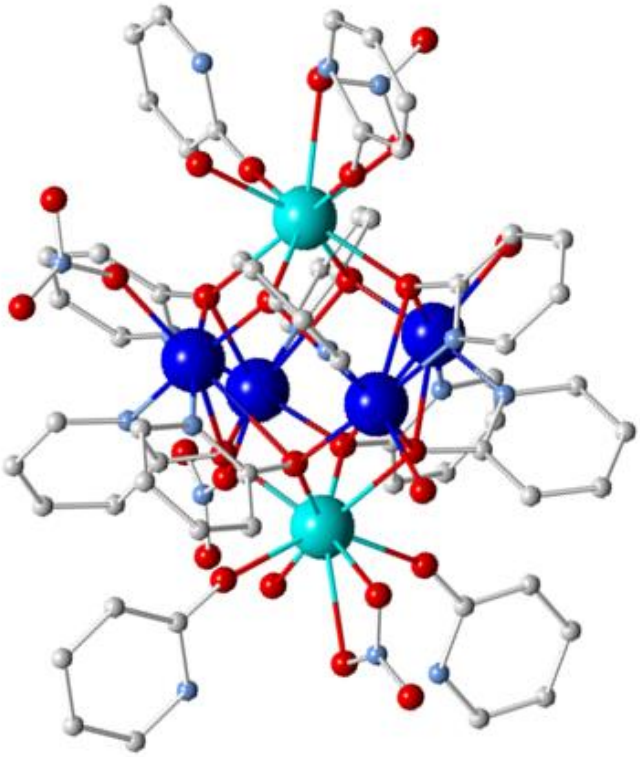

Figure 1.3. The molecular structure of $Cu^{II}_4Ln^{III}_2$. Colour code: Dy^{III}, light blue; Cu^{II}, blue; O, red; N, pale blue; C, white.[25]

1.2.1 Synthetic approach for 3d-4f PCCs

Rationally designing and synthesising 3d-4f PCCs has been difficult due to the complexity of the reaction system. Specifically, according to the "Hard and Soft Acids and Bases" (HSAB) theory,[26] 3d and 4f metal ions have priority to coordinate with different donor atoms (e.g. nitrogen and oxygen). Therefore, simply mixing 3d ions, 4f ions and organic ligands preferentially form pure 3d or 4f PCCs over 3d-4f PCCs.

Traditionally, the synthesis of 3d-4f PCCs has usually relied upon "serendipitous assembly" which allows for the preparation of PCCs which could not have been rationally predicted. Within this approach, poly-functional ligands are used and reliance is often placed on creating a systematic mismatch between the number or type of coordination sites available on a single metal centre and the donor set supplied by the ligand. This method can be employed systematically, to determine how reaction conditions such as solvent effects, reactant ratio, temperature, time of reaction and crystallisation method affect the nature of the product. While the outcome of the reaction cannot be predicted, this method has resulted in many high nuclearity[27–30] and otherwise interesting complexes.[29,31–33]

While serendipitous assembly has resulted in a significant number of 3d-4f PCCs, by applying "rational design", a ligand with specific coordination sites is used in such a way that the resulting product or outcome is predictable. While this approach was initially restricted to mono and dinuclear complexes,[34–37] through the *in situ* studies of PCC formation with various analytical techniques (Electrospray Ionisation Mass Spectrometry (ESI-MS), Cold Spray Ionisation Mass Spectrometry (CSI-MS)), it has been possible to identify common structural units and design high nuclearity PCCs based on these,[38,39] as well as following stepwise syntheses to increase the nuclearity PCCs.[40] These techniques have also been used to control the nuclearity and topology of PCCs with the variation of reaction conditions.[41–45]

3d or 4f metal ions, within 3d-4f PCCs, can be targeted selectively and substituted by either 3d or 4f ions with similar coordination properties without altering the topology of the core. This has been reported in numerous 4f-4f ion and 3d-3d ion substitutions,[43,46–51] as well as 3d-4f ion substitutions which have resulted in enhanced magnetic properties.[52,53] With these synthetic advantages and knowledge of previous heterometallic core topologies, synthesis of novel 3d-4f PCCs can be targeted for specific applications.[54]

With both methods, a wide variety of ligands have been employed for the synthesis of 3d-4f PCCs (Figure 1.4), including, Schiff base ligands,[1,55–77] oximate-based ligands,[78–81] ethanolamines,[82–86] phosphonic acids,[87,88] carboxylates[89–93] and many other varying groups.[94–99]

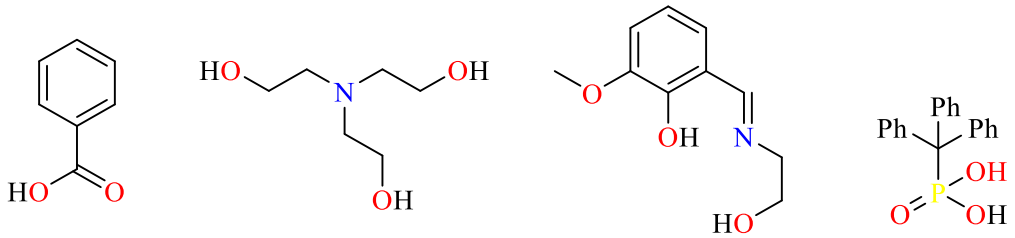

Figure 1.4. Representative examples of ligand types used for 3d-4f PCC synthesis.

1.2.2 Schiff base ligands in 3d-4f chemistry

Schiff base ligands have afforded a variety of 3d-4f PCCs and the reasons for their wide employment are manifold. However, their importance is underlined by the chemistry of Schiff bases being very generous in providing ligands (Figure 1.5). Given the variety and number of keto and amino precursors available for condensation, the number of possible azomethine compounds is extremely vast (Figure 1.5, 1 and 2). Importantly, with the considered selection of these two precursors a great deal of control over, the denticity of the resulting ligand, nature of donor atoms, the coordination "pockets" and chelating moieties of the resultant ligand is granted.[100–103] In addition, precursors may be modified with bulky groups or various functional groups which may affect the nature and properties of the resulting PCC.

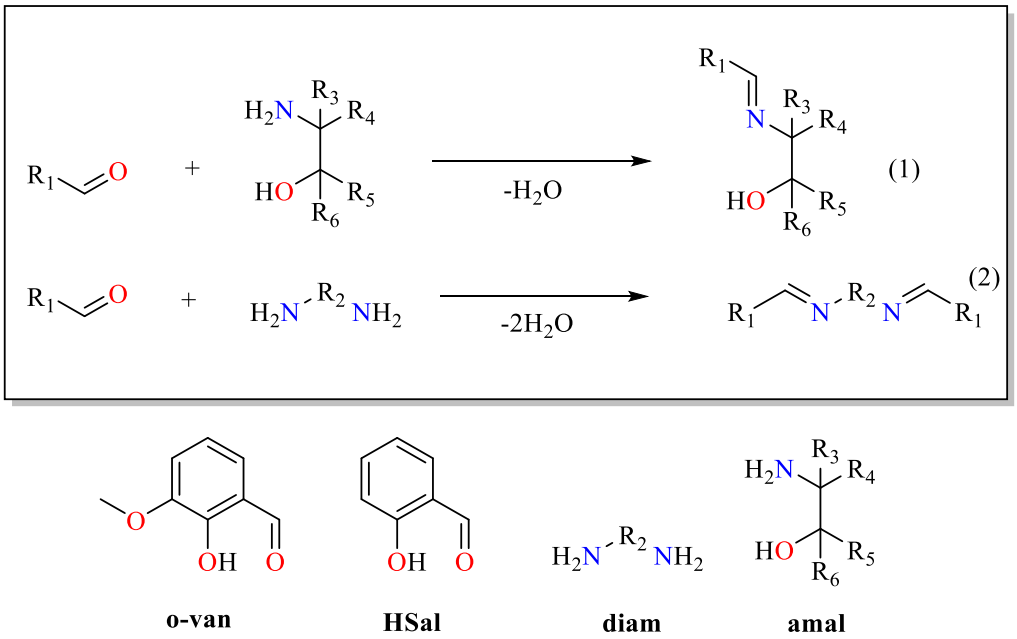

Figure 1.5. The two main classes of reactions to form Schiff base ligands (upper). The structures of commonly used aldehydes and amines (lower).

The most commonly reported keto precursors used to synthesise Schiff base ligands which support high nuclearity 3d-4f PCCs are either o-vanillin (**o-van**) or salicylaldehyde (**HSal**) (Figure 1.5). Whereas the choice of amine precursor is varied, with two main broad categories (Figure 1.5) which are designed either to bridge between metal ions (amino alcohol, **1-amal**) or to form a selective pocket (diamine, **2-diam**) for 3d or 4f ions.

Schiff base ligands have been designed to target specific low nuclearity PCCs (2, 3 or 4), with a fixed number of metal ions in a specific arrangement (Figure 1.6). When 3d-4f PCCs are desired, the ligands compartments must be dissimilar and have a different set of donor ions, specifically Ln^{III} metal ions which are hard Lewis acids with a high oxophilicity and 3d metal ions are less oxophilic and have a greater preference for N donors, therefore pockets can be designed accordingly (Figure 1.6).

A notable example of a bi-compartmental/ dinucleating ligand used to obtain a specific nuclearity is reported by Costes[104,105] who synthesised a series of $Cu^{II}Ln^{III}$ PCCs to study the magnetic interaction between Cu^{II} and Gd^{III} ions. In this example, the inner compartment (N_2O_2) hosts the Cu^{II} ion, while the outer compartment (O_2O_2) hosts the Ln^{III} ion. Many bimetallic complexes with bi-compartmental Schiff base ligands have been reported including M^{II}-Ln^{III} (M = Ni,[106–108] Co,[109] Cu,[37] and Zn[110–112]). PCCs derived from these bi-compartmental ligands have been instrumental in understanding magnetostructural correlations and can be used as building blocks to construct higher nuclearity PCCs.[43,113,114]

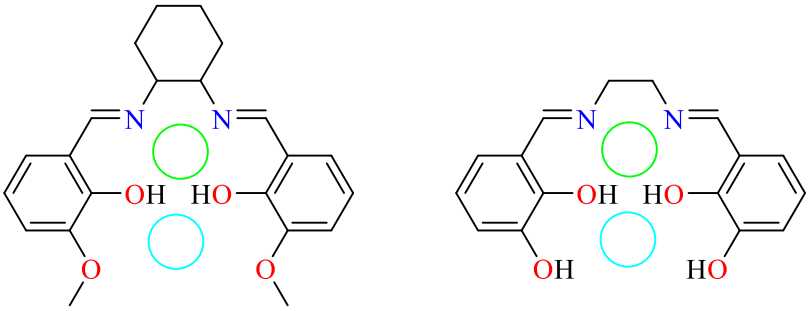

Figure 1.6. Diamine based dinucleating ligands for the synthesis of dinuclear, trinuclear and tetranuclear 3d-4f PCCs. Colour code: O_2N_2 compartment, green; O_2O_2 compartment, light blue.

Another approach has applied amino alcohol (**amal**) (Figure 1.5) based Schiff base ligands which have been successful in synthesising high nuclearity 3d-4f PCCs. While these ligands have quite predictable coordination behaviour, with compartments for specific metal ion coordination (Figure 1.7), the resultant structures cannot be predicted due to extensive bridging modes. The alkoxide oxygen atoms, which result from the deprotonation of the alcohol group, act as a terminal ligand or bridge between several metal centres and the resultant coordination modes cannot be controlled. Due to this the synthesis of 3d-4f PCCs from these ligands usually relies upon serendipitous assembly.

Consequently, this type of Schiff base ligand has generated an array of 3d-4f PCCs which are primarily interesting for their Single-Molecule Magnet (SMM) properties, these include $Co^{II}_2Ln^{III}_4$,[115] $Co^{II}_2Ln^{III}_2$,[2] $Mn^{III}_2Gd^{III}_2$,[116] $Ni^{II}_2Ln^{III}_2$,[117,118] and Cu^{II}_9 Ln^{II}_2[119] PCCs.

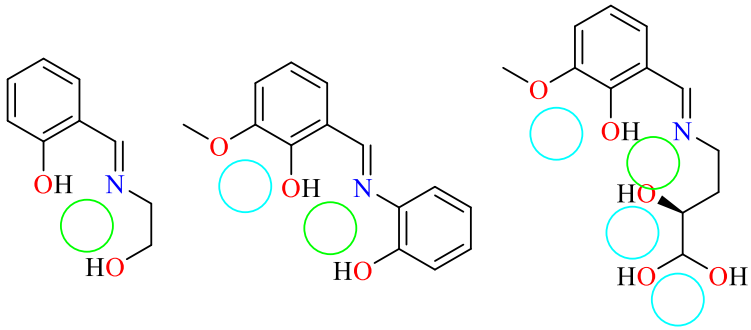

Figure 1.7. Amino-alcohol based Schiff base ligands with specific compartments for binding metal ions. Colour code: NO_2 compartment, green; O_2 compartment, light blue.

1.3 Overview of properties displayed by 3d-4f PCCs

Since the discovery of SMM behaviour in a mixed-valent $[Mn^{IV}_4Mn^{III}_8O_{12}(OAc)_{16}(H_2O)_4]$ (**Mn_{12}-OAc**) PCC (Figure 1.11) and subsequently the observation of the first 3d-4f SMM, $Cu^{II}_2Tb^{III}_2$ (Figure 1.8),[120] there has been a surge in the development of 3d-4f PCCs. 3d-4f PCCs display many interesting magnetic properties which have several applications including ultrahigh-density magnetic data storage devices,[121,122] magnetic refrigeration[123–125] and quantum computation.[126,127]

SMMs can also be used to understand and model several complex quantum phenomena such as quantum tunnelling,[128–130] spin parity[130] and quantum superposition.[131,132]

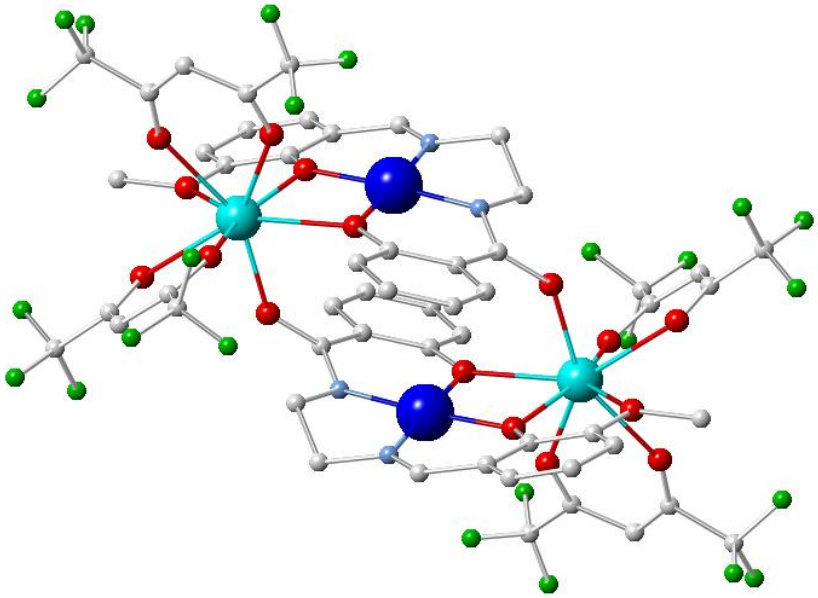

Figure 1.8. The molecular structure of $Cu^{II}_2Tb^{II}_2$ reported by Osa.[120,133] Colour code: Dy^{III}, light blue; Cu^{II}, blue; O, red; N, pale blue; C, white; F, green.

Though many magnetic applications have been studied, 3d-4f PCCs have been successfully applied in various applications. These include fluoro-immunoassays,[134–136] Organic Light-Emitting Diodes (OLED),[137–139] Water Oxidation Catalysts (WOCs)[140–142] and catalysts for organic asymmetric transformations.[143–147]

1.3.1 Overview of magnetic properties

Before discussing the SMM and the Magnetocaloric Effect (MCE) properties of PCCs, it is essential to discuss the fundamental theory behind magnetic interactions. At the atomic level, the angular momentum of unpaired electrons, which is comprised of the spin and orbital angular momenta, creates a magnetic moment.

For both 3d and 4f atoms, the Coulomb interaction between electrons is stronger than the spin-orbit interaction between their individual angular momenta. The electron-electron interaction is typically of the order of 1 eV, whereas spin-orbit interaction is of the order 0.1 eV for 4f lanthanides and 10 – 10^2 meV for 3d transition metal atoms.[148,149] In these cases, the interaction between spin and orbital angular momenta can be described by *LS* or Russell-Saunders coupling.[150]

In this coupling scheme, the Coulomb interaction couples individual orbital momenta into the total orbital momentum **L** and exchange interaction couples the individual spin and orbital angular

momenta into the total spin momentum **S**. Finally, the spin-orbit interaction couples the resulting **L** and **S** into the total angular momentum of an atom, **J**.

The quantum numbers of total angular momentum **J** assume the following values: $|L - S| \leq J \leq L + S$. Further, each J consists of $(2J + 1)$ J_z energy levels which are degenerate in the case of free atoms, and their degeneracy can be lifted by imposing an anisotropy to an atom. The ground state J multiplet can be determined by the three Hund's rules.[151,152]

These rules determine the filling of the electronic orbitals that minimizes the Coulomb interaction between the electrons. The filling of the orbitals is further restricted by Pauli exclusion principle, from which follows that two electrons in the same orbital must have their spins anti-aligned.

According to the first two Hund's rules, the ground state configuration is the one with the maximum S and L values. The third Hund's rule determines the J value for which the energy due to the spin-orbit interaction,

$$H_{SOC} = \zeta \mathbf{L} \cdot \mathbf{S}$$

is the lowest; ζ is the constant of the spin-orbit coupling. In the case of more than half-filled orbitals, the spin and orbital angular momentum are parallel to each other and the ground state is $J = L + S$. Less than half-filled orbitals have their angular momenta anti-parallel and their ground state is given by $J = |L - S|$. Finally, half-filled shells have $L = 0$ and $J = S$. The total magnetic moment of an atom is given in Equation 1.1.

$$\boldsymbol{m} = -\mu_B(g_L \boldsymbol{L} + g_S \boldsymbol{S}) = -\mu_B g_J \boldsymbol{J}$$

Equation 1.1. where μ_B is the Bohr magneton, g_L, g_S and g_J are g -factors of electron orbital, spin, and total angular momentum, respectively. The g_J or Landé factor of the total angular momentum is given by Equation 1.2.

$$g_J = \frac{3}{2} + \frac{S(S+1) - L(L+1)}{2J(J+1)}$$

Equation 1.2. where the two g factors are $g_L = 1$ and $g_S \approx 2$.

In a free atom, the magnetic moment does not have a preferential axis and its orientation fluctuates in space. This results in zero net magnetization of a free atom. Placing an atom in a crystal field or applying a magnetic field creates an anisotropy that stabilizes the magnetic moment in a preferential orientation. Spin-orbit coupling in both 3d and 4f ions leads to a splitting of the spin state levels, known as Zero-Field Splitting (ZFS), which causes magnetic anisotropy and has a profound effect on the magnetic properties.

ZFS in transition metals contains an axial (D) and rhombic (E) component. For odd electron ions, the spin microstates are split by the D component to form Kramer's doublets, the E component is manifested by shifting the energies of the various Kramer's doublets without further splitting. In even-electron systems, the D component also removes the microstate degeneracy by forming non-Kramer's doublets without further splitting. In even-electron systems, the D component also removes the microstate degeneracy by forming non-Kramer's doublets, however, in this case, the E component further splits the $+m_s$ and $-m_s$ components of the doublet.

In transition metals, the spin-orbit coupling may be first or second order depending on the symmetry of the ground state. For 3d ions with orbital T states, a stronger first-order spin order coupling is operative, whereas those with E ground states are split by second-order spin-orbit coupling.[153] Isotropic ions with A ground states have negligible spin-orbit coupling and ZFS. The effect of the D parameter on ZFS is shown in Figure 1.9. When $D = 0$, the m_s sublevels of the ground spin state are degenerate in energy. When $D < 0$, the largest m_s state is lowest and energy; the opposite is true when $D > 0$.

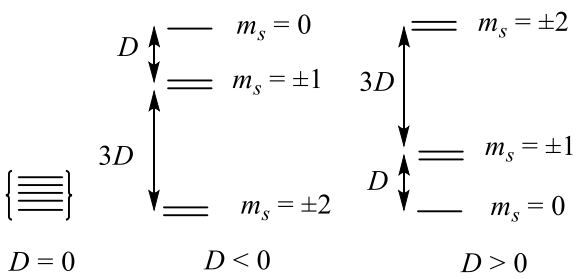

Figure 1.9. The depiction of the m_s sublevels of the ground spin state of an $S = 2$ with $D = 0$.

The magnetism of 4f lanthanide atoms originates from electrons in their well shielded 4f orbitals. In this case, the spin-orbit interaction between electrons is much larger than their interaction with the crystal field, with the latter being of the order of 10 meV. Hence, the crystal field interaction can be viewed as a perturbation to the overall energy of an atom and J remains a good quantum number for describing the system. The cumulative effect of spin-orbit coupling and crystal-field splitting for a Dy^{III} is shown in Figure 1.10.

1.3.1.1 Magnetic coupling

In PCCs, there is a magnetic interaction between neighbouring metal ions known as magnetic coupling, which is described as the parameter, J. The magnitude of J is usually in the order of 0-100 cm^{-1}. The coupling between two metal ions may be ferromagnetic ($J > 0$), where the electron spins are aligned, or antiferromagnetic ($J < 0$), where the spins are orientated antiparallel. The sign and strength of the J coupling parameter is governed by Goodenough-Kanamori rule of superexchange,[154,155] which is dependent on the overlap of the magnetic orbitals.[156] However, in

the case of lanthanides, which have contracted 4f orbitals,[157] magnetic coupling is very weak (<1 cm^{-1}), these weak interactions are important for the properties displayed in SMM and MCE materials.

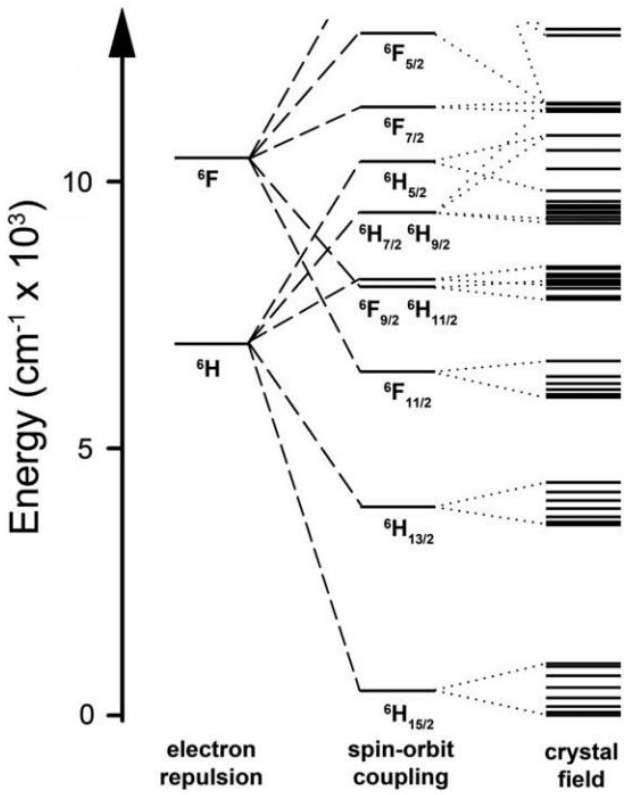

Figure 1.10. Low energy electronic structure of the Dy^{III} ion with sequential perturbations of electron-electron repulsions, spin-orbit coupling and the crystal field.[158]

1.3.1.2 The Zeeman effect

The Zeeman effect describes the removal of the degeneracy of the energies of electrons in an applied field.[159] For an S = ½ metal ion in an applied magnetic field, the energy of the m_s = -1/2 state is stabilised and the energy of the m_s = +1/2 is destabilised. The energy difference between the two states is shown in Equation 1.3.[160]

$$\Delta E = g\beta SH$$

Equation 1.3. where g is the Lande factor, β is the Bohr magneton, S is the spin state and H is the magnetic field.

In magnetic susceptibility measurements, the applied field, H is small and thus Zeeman splitting will be weak (< 1cm^{-1}). Whereas, in magnetisation experiments, H is large and Zeeman splitting will have a pronounced effect on the magnetic properties.

1.3.1.3 Magnetic measurements and data analysis

The Superconducting Quantum Interference Device (SQUID) is the current state-of-the-art in magnetometry. With this instrument, the magnetic moment of a powdered sample can be measured down to 2 K. Magnetisation experiments are the isothermal application of an external field. The molar magnetisation is the Boltzmann average of the magnetic moments (Equation 1.4).[160]

$$M = N_A \frac{\sum_n (-\frac{\partial E_n}{\partial H}) e^{-E_n/k_B T}}{\sum_n e^{-E_n/k_B T}}$$

Equation 1.4. where M is the magnetization, N_A is Avogadro's number, k_B is the Boltzmann constant, E_n is the energy of the quantum state $|n>$, H is the magnetic field.

Equation 1.4 is considered the fundamental equation of molecular magnetism, as it does not rely on any approximations.[161] The use of this expression only requires knowledge of how E_n varies with an applied magnetic field, H for all thermally populated states. To simplify the use of this equation, many of the equations described below are derived from Equation 1.2 based on various assumptions and approximations.[161]

For single spin, paramagnetic compounds with no ZFS, Equation 1.5 can be approximated as the Brillouin function.[161]

$$M = N_A g \beta S B_{s(x)}$$

$$B_s(x) = \frac{2S+1}{2S} coth\left(\frac{2S+1}{2S} x\right) - \frac{1}{2S} coth(\frac{x}{2})$$

Equation 1.5. where g is the Landé factor, β is the Bohr magneton, S is the spin state and $B_s(x)$ is the Brillouin function where $x = \frac{g\beta SH}{k_B T}$.

Simple paramagnetic compounds can be fit with Equation 1.5 to determine the ground S state. However, for molecules with complex and non-negligible coupling, these expressions can't be used. Though at high magnetic fields and low temperatures, the magnetisation can be expressed in Equation 1.6

$$M = N_A \beta S$$

Equation 1.6.

This equation corresponds to the magnetic saturation. This equation can be used for magnetisation experiments at low temperature and high fields and can be used to determine the ground S state for molecular complexes.

In direct current (*dc*) susceptibility measurements, a small magnetic field is applied (usually 1000 or 200 Oe) and the temperature varied. At low magnetic field and high temperatures, the magnetic properties can be described by the simplified van Vleck equation (Equation 1.7).[162]

$$\chi_m = \frac{N_A\, g^2\beta^2}{3k_BT}\, S(S+1)$$

Equation 1.7.

Equation 1.7 can be used to describe the *dc* susceptibility data for well isolated single-spin paramagnets of for PCCs at high temperature. Through perturbation theory, van Vleck was able to derive a more precise approximation for the molar magnetic susceptibility (Equation 1.8).[162]

$$\chi_m = \frac{N_A\, g^2\beta^2}{3k_BT}\, \frac{\sum_S S(S+1)(2S+1)e^{-E_S/k_BT}}{\sum S^{(2S+1)e^{-E_S/k_BT}}}$$

Equation 1.8. where E_S is the energy of spin state, *S*.

It is important to note that the susceptibility is usually plotted as $\chi_m T$ vs *T*, as it can visually give more information about magnetic interactions.[160]

1.3.2 Overview of single-molecule magnetism

3d-4f PCCs have the potential to display SMM behaviour and this is one of the main motivations behind their development. SMMs have many advantages over traditional magnets, these include solubility in organic solvents, uniform size and structure and air stability.

The characteristic property of an SMM is the retention of magnetization (spin orientation) after the removal of the external magnetic field. SMMs display a slow relaxation of the magnetization which is of a molecular origin. Magnetic analysis has previously revealed that there are two important criteria necessary for a molecule to display SMM behaviour, a large ground state spin (*S*) and a negative uni-axial magnetic anisotropy (*D*).[163]

$$U_{eff} = S^2|D| \text{ (integer spin)}$$

$$U_{eff} = (S^2 - 1/4)|D| \text{ (half-integer spin)}$$

Equation 1.9.

The magnetic anisotropy is influenced by the ZFS of the ground state configuration. In a polynuclear molecular system, the ZFS depends on three major factors, the spin-orbit coupling, structural distortions and spin-spin interactions. The combined effect of *S* and *D* create an energy barrier, U_{eff} which needs to be overcome to achieve relaxation of magnetization (Equation 1.9). For SMM behaviour, *D* must be negative in order for the largest M_s sublevel to be the lowest

energy. It is clear from Equation 1.9 that *S* and *D* must be large in order to achieve a large barrier height.

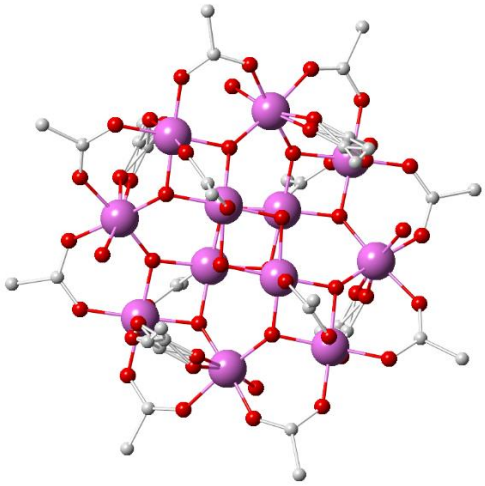

Figure 1.11. The molecular structure of **Mn_{12}-OAc** (left). Colour code**:** $Mn^{III/IV}$, purple; O, red; C, white; hydrogen ions omitted for clarity.

The dodecanuclear mixed valence **Mn_{12}-OAc** PCC was synthesised in an attempt to oxidise Mn^{II} ions by using permanganate in acetic acid solution.[164] **Mn_{12}-OAc** has eight outer Mn^{III} ions and four central Mn^{IV} ions. Dynamic magnetic susceptibility measurements on this complex resulted in the discovery of the slow relaxation of its magnetisation[165] and a hysteresis[166] pattern also revealed steps at below 2 K.

Polynuclear SMMs generally consist of paramagnetic 3d, 4d, 3d-4f or 4f metal ions and a variety of homonuclear 3d and 4f PCCs have been reported with improved SMM properties since.[167–173] An unprecedented example is the recently reported dysprosium metallocene $[(\mathbf{Cp})_2Dy^{III}][(B(C_6F_5)_4]$ (**Cp** = 1,2,4-tri(*tert*-butyl)cyclopentadienide), with a record anisotropy barrier of 1837 K at zero field and a record magnetic blocking temperature of 60 K, which both far exceed any previously reported SMMs.[174] However, as this thesis is concentrated with 3d-4f PCCs only these will be discussed further.

1.3.2.1 SMM characterisation techniques

There are two commonly used techniques for the characterisation of the SMM properties of a molecule:

1) Alternating current (*ac*) magnetic susceptibility measurements.

2) Magnetisation vs field hysteresis measurements.

The first of these techniques is used extensively for the characterisation of materials in this thesis, whereas hysteresis loops were not employed. Only *ac* susceptibility experiments will be described herein.

To identify SMM properties, the PCC is subjected to an *ac* field and susceptibility is measured over a range of temperatures at different frequencies. In this experiment, a small (~3 Oe) oscillating magnetic field is applied to the sample. The susceptibility, χ, is related to the in-phase *ac* susceptibility, χ' and the out-of-phase ac susceptibility χ'' by Equation 1.10.[175]

$$\chi = \chi' + i\chi''$$

Equation 1.10.

For paramagnetic materials, the magnetic moment of the sample will follow the oscillating magnetic field. However, in superparamagnetic materials which include SMMs, at low enough temperatures and high enough frequencies, the magnetic moment of the sample will lag behind the *ac* field, which is measured as the phase shift, φ. The in-phase and out-of-phase susceptibilities are related to the phase shift by Equation 1.11.[175]

$$\chi' = \chi cos\varphi$$

$$\chi'' = \chi sin\varphi$$

Equation 1.11.

The presence of an out-of-phase, χ'' signal is a strong indicator of superparamagnetic behaviour. At a given oscillation frequency, ν, the χ'' peak maximum, T_{max}, is the temperature at which the thermal magnetisation relaxation is given by $1/\tau = 2\pi\upsilon$. The energy barrier, U_{eff}, of an SMM follows an Arrhenius relationship (Equation 1.12).

$$\tau = \tau_0 e^{(\frac{U_{eff}}{k_B T})}$$

Equation 1.12. where τ is the relaxation time and τ_0 is a pre-exponential factor.

Therefore, a plot of ln vs $1/T$ should be linear and fitting the slope and intercept would give values of U_{eff} and τ_0, (Figure 1.12), where the relaxation process follows the thermal activation pathway (Orbach process).[176]

The experimentally determined energy barriers may not reach their theoretical limit due to Quantum Tunnelling of Magnetisation (QTM). This phenomenon is a common occurrence in SMMs and is due to the superposition of the two M_s states that are of degenerate energy.[128,177] QTM is prevalent at low temperatures, therefore the barrier is often extracted from the high-temperature regime. QTM may also be reduced upon application of a magnetic field, which

removes the degeneracy of spin sublevels. Other common strategies to reduce QTM include limiting rhombic anisotropy and increasing the strength of magnetic coupling.[178–180]

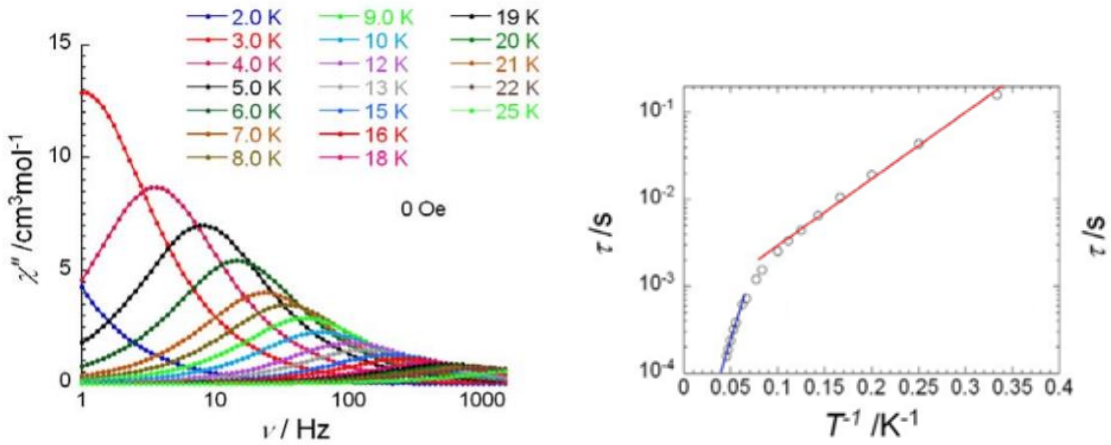

Figure 1.12. Graph of temperature dependent out-of-phase *ac* susceptibility at different frequencies (left) and an Arrhenius plot for $Co^{II}_2Dy^{III}_2$ (right).[2]

Cole and Cole described a relaxation model for dielectrics.[181] This was followed by Mydosh and co-workers who applied this theory to the relaxation of magnetic complexes.[182] The in-phase and out-of-phase *ac* susceptibility can be fit simultaneously with a generalised Debye model in Equation 1.13.

$$\chi'(\upsilon_{ac}) = \chi_s + \frac{(\chi_{T-}\ \chi_S)[1 + (2\pi\upsilon_{ac}\tau)^{1-\alpha}\sin(\frac{\alpha\pi}{2})}{1 + 2(2\pi\upsilon_{ac}\tau)^{1-\alpha}\sin(\frac{\alpha\pi}{2}) + (2\pi\upsilon_{ac}\tau)^{2(1-\alpha)}}$$

$$\chi''(\upsilon_{ac}) = \frac{(\chi_{T-}\ \chi_S)[1 + (2\pi\upsilon_{ac}\tau)^{1-\alpha}\cos(\frac{\alpha\pi}{2})}{1 + 2(2\pi\upsilon_{ac}\tau)^{1-\alpha}\sin(\frac{\alpha\pi}{2}) + (2\pi\upsilon_{ac}\tau)^{2(1-\alpha)}}$$

Equation 1.13. where χ_s is the adiabatic susceptibility, χ_T is the isothermal susceptibility, υ_{ac} is the *ac* frequency, τ is the magnetisation relaxation time and α is a value between 1 and 0 which is a measure of the distribution of relaxation processes.

When α is zero, then there is a single relaxation process (Debye process).[183] when α is larger there are multiple relaxation processes. A plot of χ'' vs χ' is known as a Cole-Cole plot and forms a semi-circular shape. When there is a distribution of single-relaxation processes (α > 0), the semicircle becomes flattened. With complex systems, with more than one relaxation process and largely different relaxation times (τ), multiple semi-circles may be present in the Cole-Cole plot.

1.3.2.2 3d-4f PCC SMMs

3d-4f PCCs merge 3d and 4f ions into a single material which can result in the following advantageous SMM properties including:

1) A large magnetic moment which can be achieved by the intrinsic characteristic of 4f ions.

2) The uniaxial anisotropy can be satisfied more easily from the single ion anisotropy of 4f ions, rather than molecular anisotropy in homometallic 3d complexes.

3) The intermediate magnetic exchange between 3d-4f ions may suppress zero-field QTM and improve the energy barrier for spin reversal.

With the aim of synthesising M^{II}-Ln^{III} PCC SMMs with high core nuclearities, a brief description of previously reported 3d-4f SMMs will be described corresponding to the incorporated 3d ion (Cu^{II}, Zn^{II}, Co^{II}, Ni^{II}).

Cu^{II} ions serve as a paramagnetic centre with a strong Jahn-Teller effect, which makes it magnetically anisotropic. The first 3d-4f magnetic system (Cu^{II}-Ln^{III}) was magnetically characterised in 1985, with isotropic Cu^{II} and Gd^{III} ions.[23] The Gd^{III} ions were exchanged with Ln^{III} ions (Ln = Dy^{III}, Tb^{III}) and resulted in a Cu^{II}-Ln^{III} series which displayed SMM behaviour. The first heterometallic 3d-4f SMM was a $Cu^{II}_2Tb^{III}_2$ complex reported by Osa and co-workers in 2004.[120] Notably, larger Cu^{II}-Ln^{III} PCCs display characteristic SMM behaviour including $Cu^{II}_9Dy^{III}_2$,[119,184] $Cu^{II}_4Dy^{III}_4$,[103] $Cu^{II}_4Dy^{III}$,[19] $Cu^{II}_6Dy^{III}_3$,[19] and $Cu^{II}_{36}Dy^{III}_{24}$.[185]A recently reported $Cu^{II}_6Dy^{III}_{12}$[186] "windmill" displays one of the highest energy barriers of U_{eff} = 17 K for Cu^{II}-Ln^{III} PCCs, with the highest belonging to a $Cu^{II}_4Dy^{III}_4$ PCC with a U_{eff} = 32.2 K.[187]

Ni^{II} ions have a $3d^8$ electron configuration and display paramagnetism in an octahedral field (high-spin) and diamagnetism in a planar square field (low spin). Ni^{II}-Ln^{III} PCCs of various nuclearities have been reported so far, the first of which was a trinuclear $Ni^{II}Dy^{III}_2$ complex reported by Sessoli and co-workers in 2007.[188] Higher nuclearity Ni^{II}-Ln^{III} PCCs (Ln = Dy, Tb) have exhibited a slow relaxation characteristic of SMM behaviour including $Ni^{II}_2Ln^{III}_2$,[50] $Ni^{II}_6Dy^{III}_3$,[189] $Ni^{II}_6Dy^{III}_4$,[190] $Ni^{II}_2Ln^{III}$,[191] and $Ni^{II}_8Ln^{III}_8$,[48]. Many notable examples of Ni^{II}-Ln^{III} PCCs have been reported by Chandrasekhar including $Ni^{II}_3Ln^{III}_3$,[49] $Ni^{II}_4Ln^{III}_4$,[192] and the pentanuclear $Ni^{II}_2Ln^{III}_3$ which displays the highest reported effective energy barrier for Ni^{II}-Ln^{III} PCCs with a U_{eff} of 88 K and a blocking temperature of 3 K.

The orbital angular momentum of $3d^7$ high spin Co^{II} ions is not quenched in octahedral fields, which makes it a good spin carrier for magnetic materials. Chandrasekhar et al. reported the first Co^{II}-Ln^{III} SMM, a trinuclear Co^{II}_2Gd complex,[193] which shows slow magnetic relaxation below 8 K in *ac* susceptibility measurements and reveals an energy barrier of U_{eff} = 27 K and $\tau_0 = 1.7\times10^{-7}$ s. A number of other trinuclear $Co^{II}_2Ln^{III}$ PCCs displaying SMM behaviour have been reported with a variety of ligands.[194–197] Since then the synthesis and magnetic properties of Co^{II}-Ln^{III} PCCs has recently received tremendous attention and a plethora of Co^{II}-Ln^{III} PCCs with a variety of nuclearities including $Co^{II}_2Ln^{III}_2$,[2,67,68,198–203] $Co^{II}Dy^{III}_3$,[68] $Co^{II}_2Dy^{III}_4$,[204] $Co^{II}_3Dy^{III}_4$,[1] $Co^{II}_2Dy^{III}_5$,[68]

$Co^{II}_4Ln^{III}_4$,[68,123] $Co^{II}_6Ln^{III}$,[205] $Co^{II}_2Co^{III}_4Ln^{III}_4$,[206] $Co^{II}_8Ln^{III}_2$,[207] $Co^{II}_2Dy^{III}_{10}$,[64] $Co^{II}_6Ln^{III}_8$,[207] $Co^{II}_8Ln^{III}_8$,[207,208] $Co^{II}_{11}Dy^{III}_6$,[123] $Co^{II}_9Co^{III}Ln^{III}_{42}$,[209] and $Co^{II}_{16}Ln^{III}_{24}$ [75] have all been reported.

Zn^{II} has a stable diamagnetic d^{10} electron configuration. Zn^{II}-Ln^{III} PCCs are usually isolated as analogues to help the study of M^{II}-Ln^{III} PCCs as the diamagnetic centres provide an effective approach to control magnetic interactions between the transition metal and lanthanide ions and study the magnetic contribution of the spin carriers.[188,210,211]A number of dinuclear Zn^{II}-Ln^{III} complexes with compartmental ligands that display SMM behaviour have been reported.[212–214] Interestingly, Zn^{II} ions have also been shown to enhance the U_{eff} of $Zn^{II}Dy^{III}$ and $Zn^{II}_2Dy^{III}_2$ SMMs.[215,216] Further work supports the enhancement of the U_{eff} by investigating the effect of ligand substitution around the Dy^{III} centre.[213] Several larger Zn^{II}-Ln^{III} PCCs display characteristic SMM behaviour including $Zn^{II}_{12}Dy^{III}_{18}$,[28] $Zn^{II}_6Ln^{III}_6$[217] and a giant $Zn^{II}_6Dy^{III}_{24}$[5] metallic-ring (Figure 1.1).

As one of the objectives of this thesis concentrates on the synthesis of high nuclearity 3d-4f PCCs which display SMM behaviour, previously reported examples of M^{II}-Ln^{III} PCCs (Ni^{II}, Co^{II}, Cu^{II}, Zn^{II}) supported by Schiff base ligands (Appendix A, Figure S1.1) are presented in Appendix A (Table S1.1), along with the topology of the core and other characteristics.

1.3.3 Overview of MCE

Sub-Kelvin refrigeration is critical in many technologically advanced applications such as the condensing of hydrogen, methane and propane and the obtaining of sub-Kelvin ultra-low temperatures. Currently, ^3He - ^4He dilution refrigeration is the most popular method of continuous refrigeration below 0.3K,[218] however, the cost of isotopic helium is a drawback of this technique. Other refrigeration methods include adiabatic nuclear diamagnetization[218] and adiabatic demagnetisation of a paramagnetic salt.[218] The latter is based on the MCE.

The MCE phenomenon relies on the field-temperature and entropy change of a paramagnetic material. According to Equation 1.14, in a magnetorefrigerant, the total entropy of the system is the sum of the field and temperature-dependent magnetic entropy, S_M, and the temperature-dependent lattice entropy, S_{latt}:

$$S_{Total}(T,H) = S_M(T,H) + S_{Latt}(T,H)$$

Equation 1.14.

In the magnetic refrigeration process, the MCE material is brought to the starting temperature, T, through a precooling bath. A magnetic field, H, is applied to isothermally magnetize the material; the heat of magnetisation ($Q = T\Delta S$) is absorbed by the precooling bath. With this first step, the magnetic entropy during isothermal magnetisation is lowered due to the ordering of the electronic

spin. Since in an isothermal process $\Delta S_{latt} = 0$, then according to Equation 1.14, $\Delta S_M = \Delta S_{Total} < 0$. Conversely, during isothermal demagnetisation $\Delta S_M > 0$.

In the second step of the cycle, the material is isolated from the precooling bath and adiabatically demagnetized ($\Delta S_{total} = 0$). Here, the spins become disordered and $\Delta S_M > 0$. To compensate, there must be a decrease in lattice entropy ($\Delta S_{Latt} < 0$) which comes with a commensurate decrease in the temperature of the material ($\Delta T_{ad} < 0$). Finally, the refrigerant will warm up along the entropy curve of the final magnetic field, absorbing heat until it reaches the initial T and S_{Total}, hence, the cooling power of the material is related to the entropy change during isothermal magnetization, ΔS_M.

Experimentally, the two most important parameters for MCE materials are the temperature during *adiabatic magnetization*, ΔT_{ad}, and magnetic entropy change during *isothermal magnetization*, ΔS_M. ΔT_{ad}, which is related to the total entropy, S_{Total} (Equation 1.14), must be measured by direct methods[219] or more commonly, indirectly through heat capacity measurements through the thermodynamic expression in Equation 1.15.

$$\Delta T_{ad}(T, \Delta H) = - \int_{Hi}^{Hf} \left(\frac{T}{C\,(T,H)}\right)_H \left(\frac{\partial M(T,H)}{\partial T}\right)_H dH$$

Equation 1.15. H = magnetic field (f = final, I = initial) and C = heat capacity.

The magnetic entropy change, ΔS_M, can also be determined through heat capacity measurements through the application of Equation 1.16.

$$\Delta S_M(T,H) = \int_0^T \frac{C_M(T, H) - C_M(T,0)}{T} dT$$

Equation 1.16. $C_M(T,H)$ and $C_M(T,0)$ are heat capacities in a field H and in zero field, respectively.

Furthermore, ΔS_M may be evaluated through magnetization experiments using the Maxell equation for magnetic entropy:

$$\Delta S_M(T,\Delta H) = \int_{Hi}^{Hf} \left(\frac{\partial M(T, H)}{\partial T}\right)_H dH$$

Equation 1.17. M = Magnetisation.

The total available magnetic entropy in a material is associated with the total magnetic degrees of freedom at $T = \infty$ and is equal to Equation 1.18.

$$S_M = R\ln(2S+1)$$

Equation 1.18. R = the gas constant (8.3144621 J K^{-1} mol^{-1}) and S = spin.

1.3.3.1 3d-4f magnetic coolers

Unlike SMMs, PCCs which display a significant MCE require isotropic metal ions with minimal ZFS, as the presence of magnetic anisotropy reduces the total available magnetic entropy regardless of the sign of D. Therefore, isotropic metal ions such as Fe^{III}, Mn^{III} and Gd^{III} are best suited to synthesise 3d-4f PCCs which display a significant MCE effect.

Consequently, for a PCC to be useful for practical magnetic cooling applications, it must display a large magnetic entropy change per unit weight (J kg^{-1} K^{-1}) at low magnetic fields.[220] Therefore it is important to maximise the ligand weight ratio. In addition to these factors, magnetic coupling may lower the total available magnetic entropy, this makes 3d-4f PCCs ideal for promoting MCE behaviour as the insertion of 3d ions between 4f ions usually results in weak magnetic interactions.[163]

The first reported 3d-4f PCC used for magnetic cooling was a $Mn^{III}_4Gd^{III}_4$ PCC which displayed a larger MCE than any of the previous homometallic PCC.[221] So far, 3d-4f PCCs have been most widely studied molecular coolers.[222] As previously stated only M^{II}-Ln^{III} PCCs (Cu^{II}, Zn^{II}, Co^{II}, and Ni^{II}) are being targeted, therefore only a brief description of the reported examples with a significant MCE in relation to the 3d ion will be described.

The magnetic coupling between Cu^{II} and Ln^{III} ions is usually weak. Several high nuclearity Cu^{II}-Ln^{III} PCCs which display a significant MCE effect have been reported including $Cu^{II}_6Gd^{III}_{12}$ (33.7 J kg^{-1} K^{-1}),[186] $Cu^{II}_6Gd^{III}_2$ (11.9 J kg^{-1} K^{-1}),[223] $Cu^{II}_5Gd^{III}_4$ (31 J kg^{-1} K^{-1}),[124] $Cu^{II}_6Gd^{III}_6$[224] and $Cu^{II}_2Gd^{III}_7$ (34.6 J kg^{-1} K^{-1}).[223]

Ni^{II} ions were shown to enhance the MCE in a series of $M^{II}_8Gd^{III}_4$ complexes by switching the Cu^{II}-Gd^{III} antiferromagnetic interactions (14.6 J kg^{-1} K^{-1}) to Ni^{II}-Gd^{III} ferromagnetic interactions (22 J kg^{-1} K^{-1}).[225,226] The Ni^{II}-Ln^{III} PCC displaying the highest MCE effect is a $Ni^{II}_{12}Gd^{III}_{36}$ cage, where due to the low molecular weight of the ligands a large MCE effect of 36.3 J kg^{-1} K^{-1} is observed.[227]

In contrast to Ni^{II} ions, the use of magnetically highly anisotropic Co^{II} ions is a counter-intuitive route to synthesising 3d-4f molecular coolers, however a variety of these have been reported including a large family of Co-Ln PCCs reported by Zheng et.al,[208] which can be divided into "grids"; $Co^{II}_8Ln^{III}_4$, $Co^{II}_4Ln^{III}_6$, $Co^{II}_4Ln^{III}_2$, $Co^{II}_8Ln^{III}_8$ and "cages"; $Co^{II}_6Ln^{III}_8$, $Co^{II}_8Ln^{III}_2$. The highest entropy changes were observed in the Gd^{III} cages (23.6 J kg^{-1} K^{-1} – 28.6 J kg^{-1} K^{-1}). The

highest value entropy change (41.3 J kg^{-1} K^{-1}) among 3d-4f coolers is exhibited by a $Co^{II}_{10}Gd^{III}_{42}$ "bowl" like PCC.[209]

Very high nuclearity 3d-4f PCCs have proven to display a significant and enhanced MCE, which include the previously mentioned $Co^{II}_{10}Gd^{III}_{42}$ and $Ni^{II}_{12}Gd^{III}_{36}$ PCCs as well as $Ni^{II}_{10}Ln^{III}_{42}$,[209] $Co^{II}_{16}Gd^{III}_{24}$ (26 J $kg^{-1}K^{-1}$),[75] $Cu^{II}_{36}Gd^{III}_{42}$ (21 J kg^{-1} K^{-1})[228] and $Zn^{II}_{6}Gd^{III}_{24}$ (30.0 J kg^{-1} K^{-1}) species.[5]

1.3.4 Luminescence

Near Infrared (NIR) luminescent Ln^{III} (Nd, Yb or Er) complexes[229–233] with long-lived and characteristic line-like emission bands have potential applications in fluoro-immunoassays[134–136] and OLEDs,[137–139,234] though due to forbidden f-f transitions, the absorption coefficient of the Ln^{III} ions is usually very low. The introduction of ligands with chromophoric moieties, with fully allowed π- π^* transitions sensitise the NIR luminescence, in an antenna-like effect.[234] Introducing other metal ions such as Cr^{III}, Ru^{II}, Ir^{III}, Zn^{II} and Cd^{II} as sensitizers into lanthanide complexes is also a common strategy to enhance lanthanide luminescence and has led to an increased interest in the development of bimetallic PCCs.[235–237] Due to the low cost and high abundance of Zn, many Zn^{II}-Ln^{III} PCCs which enhance lanthanide luminescence have been reported.

A distinct type of Zn^{II}-Ln^{III} PCCs, which are supported by compartmental Schiff base ligands (Figure 1.13), have been reported to enhance the luminescent properties of Ln^{III} ions. These PCCs are usually low in nuclearity and include $Zn^{II}_2Ln^{III}$,[238,239] $Zn^{II}Ln^{III}_2$,[240] $Zn^{II}Ln^{III}$,[237,239,241–246] $Zn^{II}_2Ln^{III}_3$[247] and $Zn^{II}_2Ln^{III}_2$,[243,248,249] PCCs (Ln = Nd, Er, Yb, Eu, Tb).

Compartmental Schiff base ligands are chosen due to the chromophores and tuneable coordination geometry which they can provide. Most of the reported 3d-4f PCCs supported by Salen-type Schiff base ligands have an inner N_2O_2 pocket for binding 3d (Zn^{II}) ions and an outer O_2O_2 pocket which can bind both Ln^{III} and 3d ions (Figure 1.13). With the coordination of both 3d and 4f ions to the ligand, luminescent quenching, which would arise from OH-, CH- or NH- oscillators of a solvate, is prevented.

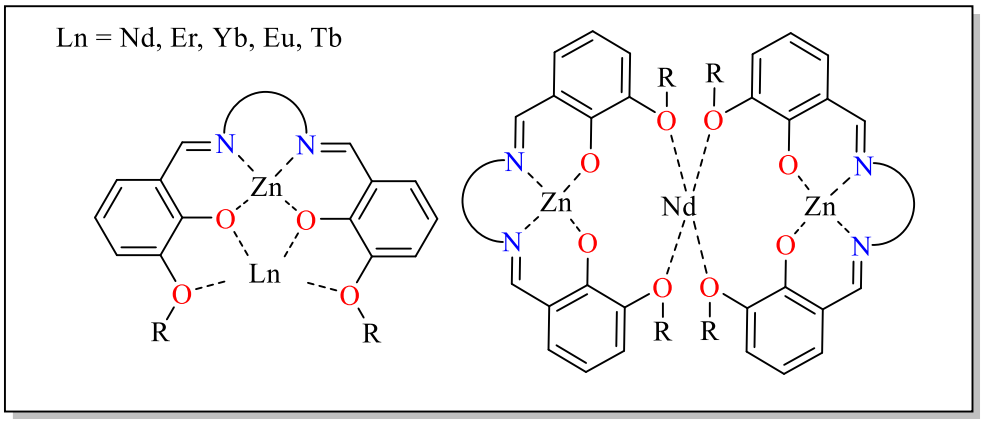

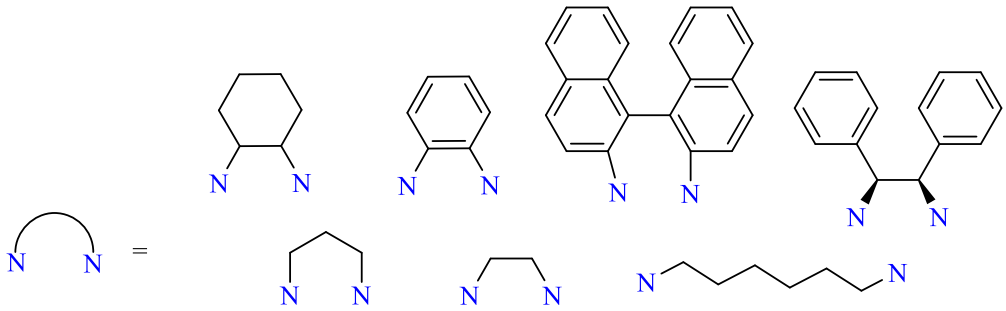

Figure 1.13. The general structure of dinuclear and trinuclear luminescent 3d-4f PCCs (upper). Representative examples of dinucleating ligands for the construction of luminescent 3d-4f PCCs (lower).

Extension of the flexible carbon backbone (Figure 1.13 lower), which is indicative of the Salen-type ligands, has led to the formation of larger $Zn^{II}_{8}Ln^{III}_{4}$ "drum" complexes[114] (Ln = Nd, Yb), which both demonstrate some of the best quantum yields for 3d-4f NIR luminescence.

Particularly striking examples of 3d-4f NIR luminescent complexes are $Zn^{II}_{16}Ln^{III}$ PCCs (Figure 1.14) which have long luminescent lifetimes and the highest reported overall quantum yields for Nd^{III} and Er^{III} (Φ = 1.13% and 3.6 x 10^{-2} % respectively) NIR-emitting lanthanide complexes with C-H bonds.[250] The well-known metallo-crown motif organises several organic sensitizers at a well-controlled distance from the Ln^{III} ion which substantially limits C-H quenching.

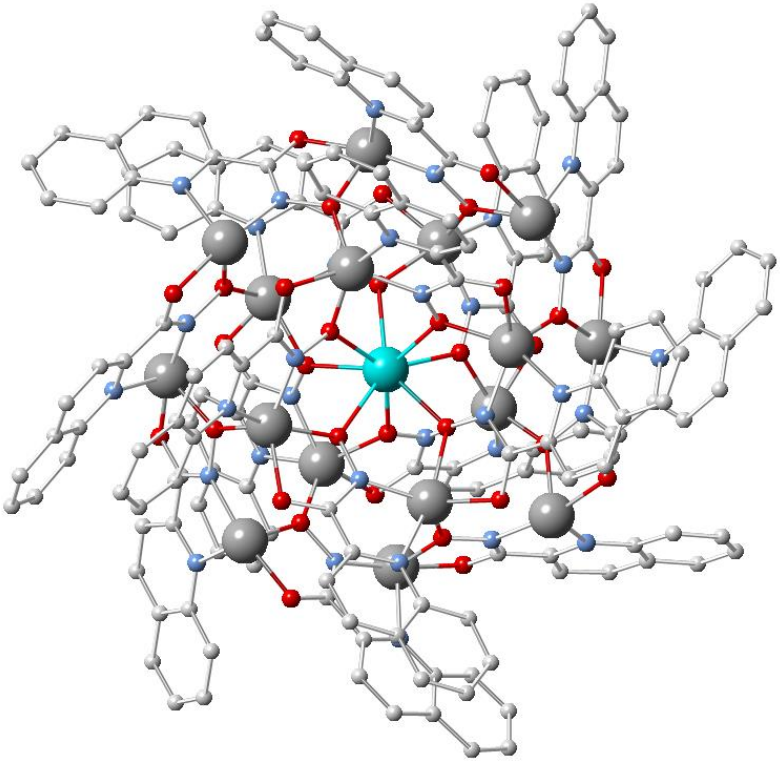

Figure 1.14. The molecular structure of $Zn^{II}_{16}Ln^{III}$. Colour code: Ln^{III}, light blue; Zn^{II}, grey; O, red; C, white. Hydrogen ions omitted for clarity.[250]

1.3.5 Co-operative catalysis

Synergistic, co-operative activation through multiple metal centres can often be found in enzyme biocatalysts such as tyrosinase,[251] superoxide dismutase,[252] urease[253] and phosphohydrolase.[254] With the unrivalled efficacy of these enzymes in their respective transformations, there has been significant interest in developing PCCs which mimic or surpass the behaviour of their natural counterparts.

Two important areas are WOCs based on the Mn_4Ca core of Oxygen-Evolving Complex (OEC) in photosynthesis,[140,255–261] the dinuclear cores of urease (Ni^{II}_2) and class II aldolase in enantioselective C-C bond formation (Zn^{II}_2) for asymmetric transformations.

1.3.5.1 PCC co-operative catalysis

Bimetallic PCCs, with multiple metal centres and different coordination environments, have been employed as catalysts in a variety of asymmetric organic transformations. This arrangement can promote co-operative catalysis between the two metal centres. Bimetallic co-operative catalysis usually functions as Lewis acid-Brønsted base catalysis (Figure 1.15), where one metal centre (Brønsted base) generates a nucleophile and an electrophile is activated by a second metal (Lewis acid). The substrates are brought into proximity (3.5 - 6 Å) and a favourable orientation through this interaction and promote efficient catalysis.

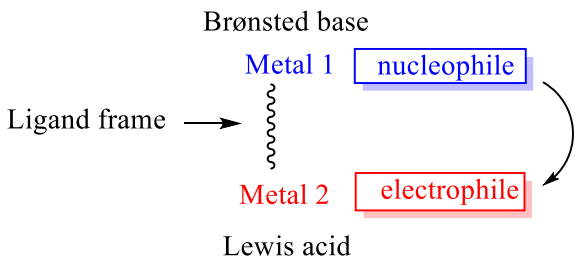

Figure 1.15. Bimetallic catalysis mechanism.

This behaviour is observed in naturally occurring dinuclear metalloenzymes such as urease for urea hydrolysis (Ni^{II}_2, Equation 1.19) and class II aldolase in enantioselective C-C bond formation (Zn^{II}_2).

With the first respective example, two Ni^{II} cations are held in proximity linked by a ligand frame within the active site. One Ni^{II} ion is coordinated to urea (Lewis acid) and the other acts as a Brønsted base with the aid of a histidine chain, which produces the Ni hydroxide. Through synergistic action between the centres, the hydrolysis is significantly accelerated.

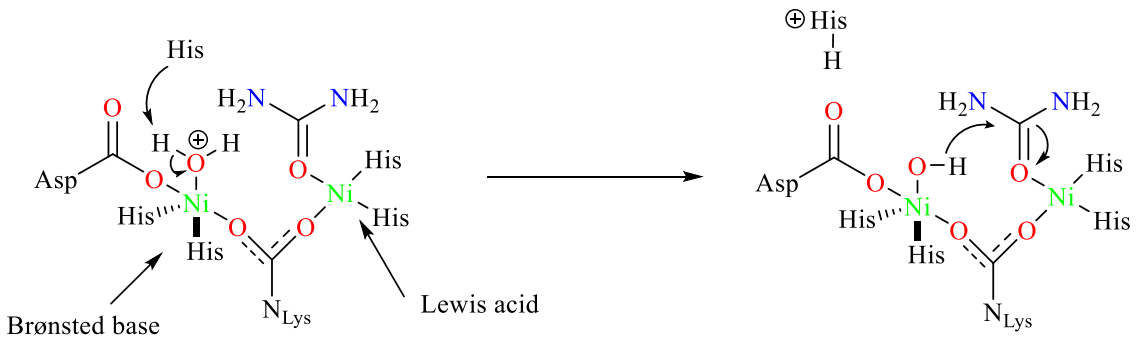

Equation 1.19. Mechanism of hydrolysis of urea by urease.

Bimetallic PCCs modelled after these systems have employed an array of metals such as lanthanides, transitions metals and alkali metals. Structurally, co-operative bimetallic catalysts can be classified into several types, however, this thesis will only concentrate on those that metal ions are held within a single ligand frame.

The careful design of the ligand frame for co-operative asymmetric catalysis is important so that the chiral environment for the targeted reactions is efficient for the dual activation of nucleophiles and electrophiles through co-operation of the metal centres.

Many of the previously reported organic transformations postulate the active species is expected to form *in situ*, which requires specific cavities for the coordination of metal ions. So far there have been three distinct types of single ligand frames reported for the development of PCCs which promote bimetallic catalysis, these include 1,1 binapthol (BINOL) based ligands, amino acids and Schiff base ligands. A brief overview will be given for BINOL and amino acid-based systems and a more detailed account of the co-operative catalysis displayed by Schiff base derived systems.

1.3.5.2 BINOL and amino acid derived co-operative PCC catalysts

The first group of reported PCC catalysts were heterobimetallic with $M^{III}M^{II}_3$ (**1, 3M4-1**) cores, supported by BINOL and various derivatives as chiral bidentate ligands (Figure 1.16). This series promoted a wide range of asymmetric transformations including nitroaldol reactions,[262] aza-henry reactions,[263] conjugate addition of malonates,[264] conjugate addition of malonates to cyclic-enones,[265] epoxide ring opening with thiols,[266] 1,4-addition of Horner-Wadsworth-Emmons reagents[267] and direct asymmetric aldol reactions.[268] When two BINOL units are fused and treated with Et_2Zn a trinuclear Zn^{II} complex forms *in situ* (Figure 1.17), which preferentially affords the syn adducts up to 96% *ee* in the formation of α,β-dihydroxyketones from 2-hydroxyacetophenone and aldehydes.[269–271]

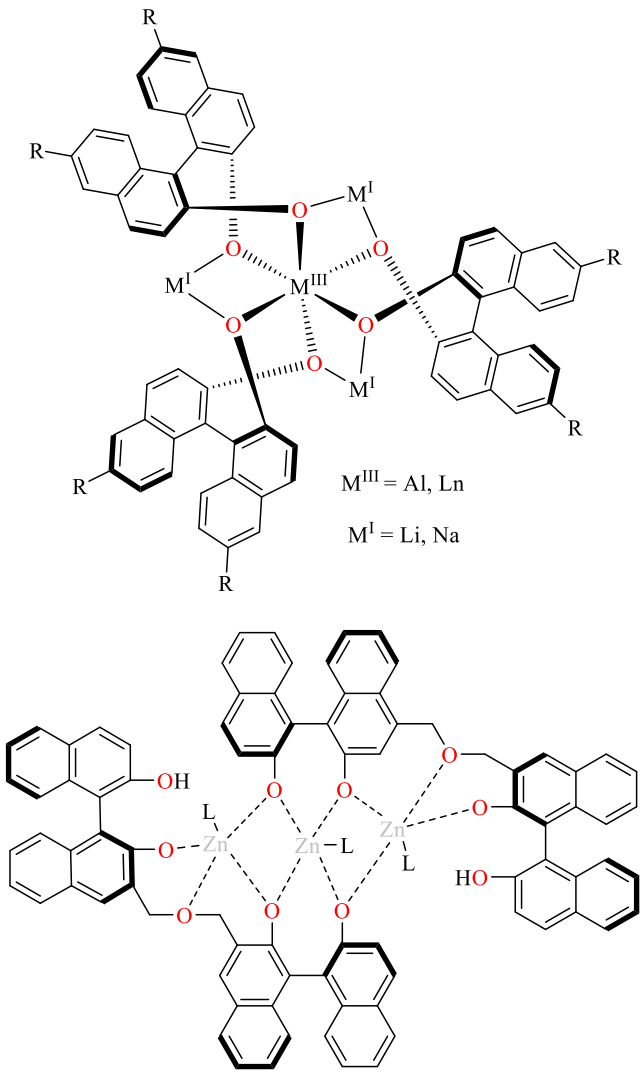

Figure 1.16. The general structure of BINOL supported $M^{I}_{3}M^{III}$ PCC catalysts.

An alternate ligand scaffold, based on abundant homochiral amino-acids has also been employed for the construction of bimetallic co-operative catalysts. Trost et al. reported a dinuclear Zn^{II}_{2} PCC (Figure 1.17, **ZnProPhenol**) which is supported by a prophenol based ligand derived from proline,[272] wherein one zinc metal acts as a Lewis acid and the other delivers the nucleophile.

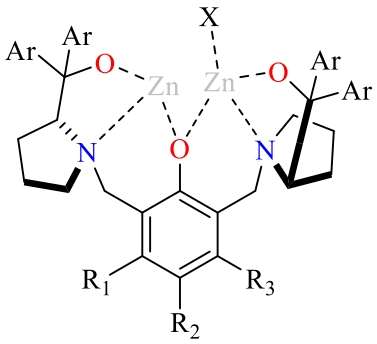

Figure 1.17. The general structure of **ZnProPhenol**.

ZnProPhenol was successfully applied to a variety of direct asymmetric aldol reactions using various aldol donors including methyl ketones,[272] acetone,[273] a-hydroxyl,[274] acetylenic ketones[275] and vinyl ketones.[276] It was subsequently reported that **ZnProPhenol** efficiently catalysed both Mannich[277] and conjugate additions.[278,279]

1.3.5.3 Schiff base derived co-operative PCC catalysts

Shibasaki and Matsunaga et al. reported a series of homo and heterobimetallic dinuclear PCCs which are postulated to form *in situ* and promote a variety of asymmetric transformations reactions. These dinuclear PCCs are based on a chiral dinucleating ligand reported by Kozlowski et al., in which Ni^{II} and Ti^{IV}-Ga^{III} mononuclear complexes promote the asymmetric conjugate addition of dibenzyl malonate to cyclic enones[280–282] and asymmetric ring opening of meso epoxides with thiols and selenols, respectively.[283,284]

These Schiff base ligands share a common ligand structure (Scheme 1.1) and contain two specific cavities for coordination of metal ions. The first is the N_2O_2 cavity which preferentially coordinates transition metal ions. The second is the O_2O_2 cavity which can selectively coordinate oxophilic lanthanide ions. This specificity is important as in all the reported protocols the formation of the active species is during the reaction and the PCC catalyst is not characterised independently. The geometry of the common ligand frame brings the two metal ions into proximity (3.5 – 6 Å) which is essential for the promotion of co-operative catalysis.[143,285]

Various transition metal homometallic dinuclear PCCs supported by these ligands have been reported to form *in situ* and they promote a variety of asymmetric catalytic transformations (Scheme 1.1). A bimetallic Ni^{II}_2 catalyst, bearing a 1,1 binaphthyl diamine as a chiral diamine (H_2**LB**), was particularly versatile and promoted Mannich reactions,[147,286,287] conjugate additions,[286,288,289] amination,[290] desymmetization[291] and aldol-type reactions.[292,293] By substituting Ni^{II} ions and the chiral diamine linker, it was possible to tune the catalytic efficacy of this system to specific reactions with Co^{II} and Mn^{III} analogues which promote 1,4 addition reactions.[146,294,295]

The first example of a heterometallic PCC catalyst of this type was a $Cu^{II}Sm^{II}$ PCC which promoted a *syn*-selective asymmetric nitroaldol reaction,[296] substituting the metal ions with Pd^{II} and La^{III} permitted the use of aldehydes as electrophiles and catalysed an anti-*syn* selective nitroaldol reaction.[297] Further examples of heterometallic 3d-4f PCC catalysed reactions will be discussed in the next section.

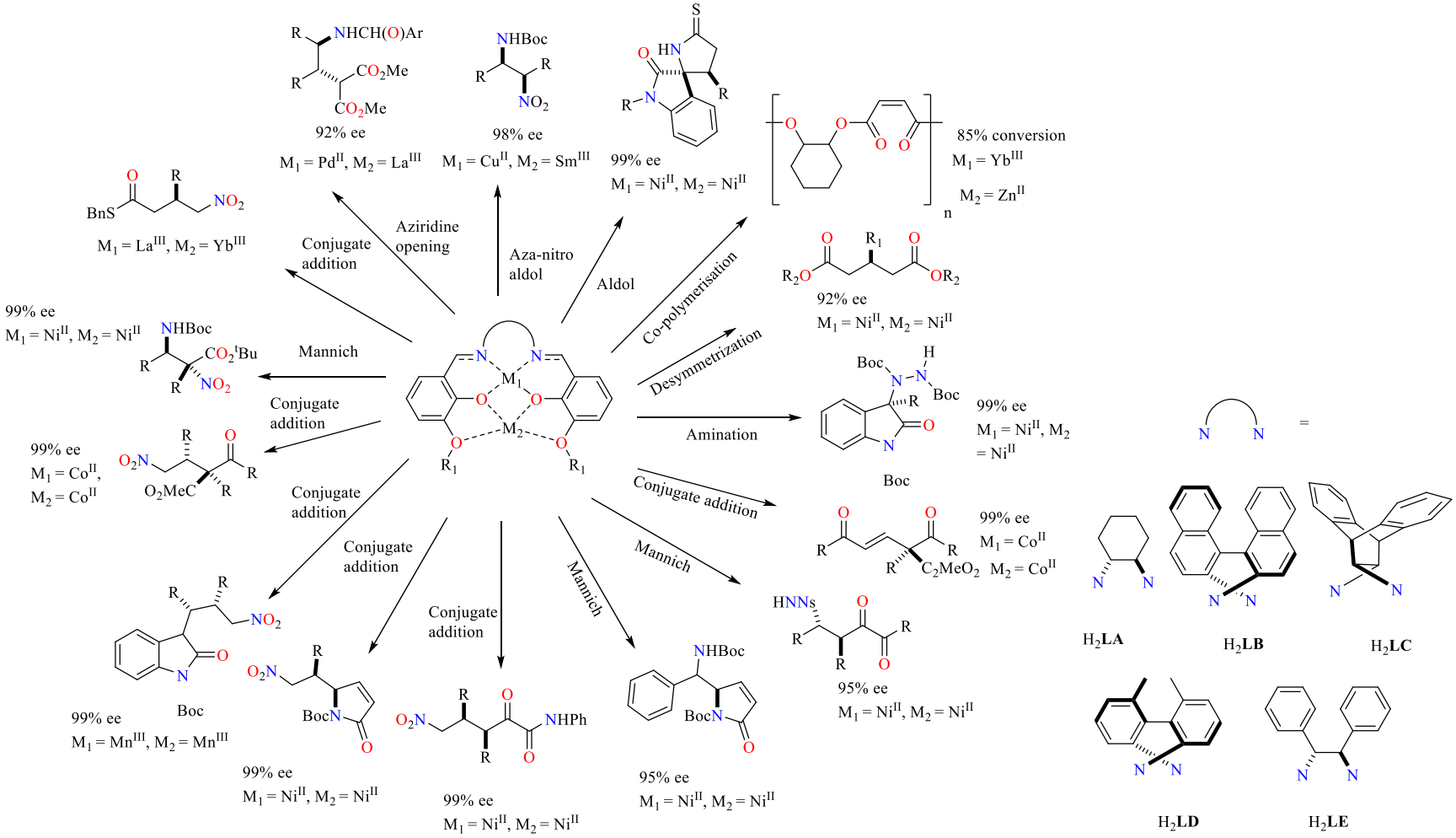

Scheme 1.1. Ligands reported in *in situ* asymmetric transformations with 3d and 4f salts.

1.3.5.4 3d-4f PCCs as co-operative catalysts

Though there are few reported 3d-4f PCCs used for catalysis, the most common are dinuclear PCCs (**1M2-1**), which have been employed for asymmetric transformations. The ligands which have been reported in these systems are shown in Figure 1.18.

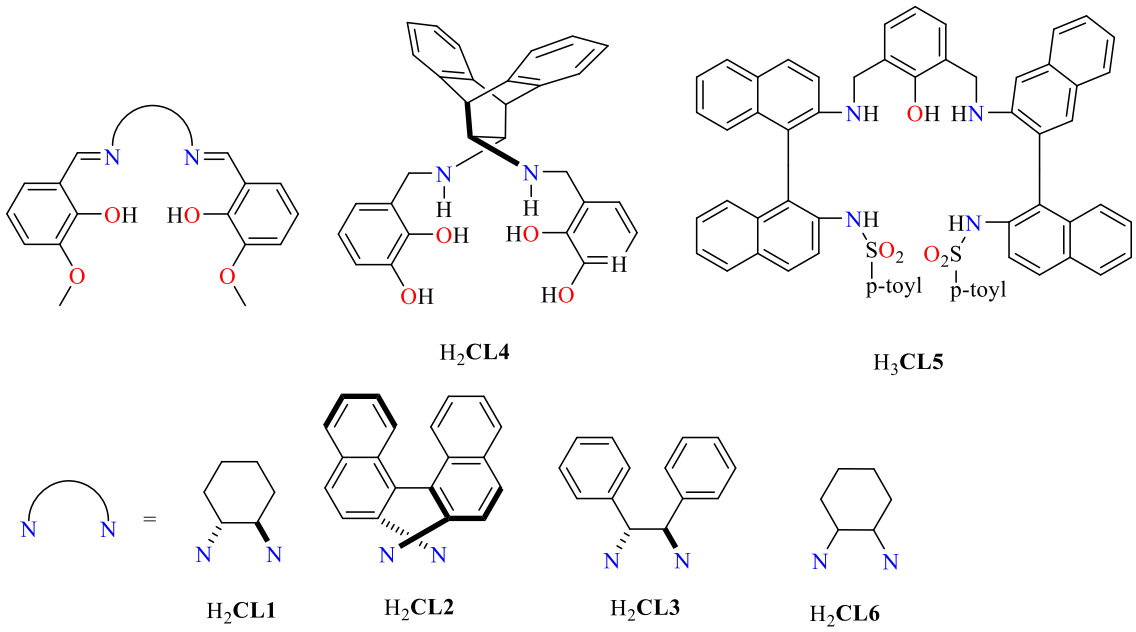

Figure 1.18. Schiff base and Schiff base-derived ligands used to form catalytically active 3d-4f dinuclear PCCs.

The first example of a 3d-4f PCC acting as a co-operative catalyst was reported by Shibasaki for an asymmetric transformation. A bimetallic Lewis acid/Brønsted base Cu^{II}-Sm^{III} (**1M2-1**) PCC which was postulated to form *in situ*, with an achiral phenol additive, catalysed nitro-Mannich reactions with a high *syn* diastereoselectivity (>20:1 - 13:1) and enantioselectivity (66 - 99% *ee*) (Equation 1.20).[297+296] It is suggested that the dinucleating Schiff base ligand, H_2**CL1**, supports the PCC with a Cu^{II} ion coordinated to the N_2O_2 cavity and a Sm^{III} ion in the O_2O_2 pocket to give a dinuclear Cu^{II}-Sm^{III} species.

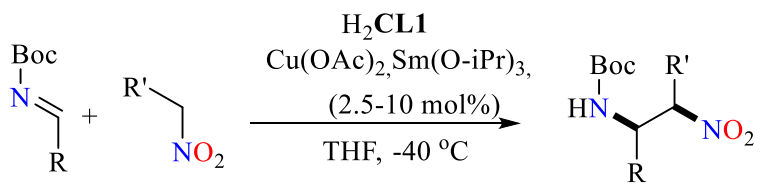

Equation 1.20. A Cu^{II}/Sm^{III} catalysed nitro-Mannich reaction.[297+296]

Interestingly, the substitution of H_2**CL1** with H_2**CL2** or H_2**CL3**, under identical conditions, showed no conversion to product. In addition, with the replacement of the $Cu^{II}(OAc)_2$ with $Zn^{II}(OAc)_2$ or $Ni^{II}(OAc)_2$ no conversion to product was observed, whereas the replacement of the

Sm^{III} salt by other Ln^{III} salts (La^{III}, Pr^{III}, Nd^{III}, Eu^{III}, Gd^{III}, Dy^{III}, Er^{III}, Yb^{III}) resulted in lower yields (63 - 96%) with reduced stereoselectivity (3:1 > 20:1) and enantioselectivity (5 – 80 *ee*).

The co-operative activation of the Sm-OAr moiety as a Brønsted base and the Cu^{II} ion as a Lewis acid is thought to be the key to the efficacy of these transformations. Though ESI-MS and optical purity studies indicated a trimer of Cu^{II}-Sm^{III} dinuclear PCCs with an achiral phenol additive was the active species in the promotion of this selectivity, many other oligomers including Cu_3Sm_3, Cu_6Sm_6, Cu_7Sm_7, Cu_8Sm_8 and Cu_9Sm_9 were detected by ESI-MS. The proposed monomeric and trimeric Cu^{II}-Sm^{III} species was never isolated or characterised.

Subsequently, Zhou et al. reported a dinuclear Cu^{II}-Sm^{III} PCC supported by H_3**CL5** which catalysed an *in situ* anti-selective asymmetric Henry reaction (Equation 1.21).[298] Anti-β-nitro-alcohols are obtained in up to 99% conversion, > 30:1 *dr* and 98% *ee*. The use of other M^{II} and Ln^{III} ions was not investigated. Furthermore, the reaction with only H_3**CL5** and $Sm(OiPr)_3$ lead to a reduction in yield to 90% with an *ee* of 91%. ESI-MS studies indicated the presence of a $[Cu^{II}Sm^{III}$**CL5**$]^+$ dimer, which was postulated to be the active species, however, a $[Cu^{II}_2$**CL5**$]^+$ species is also observed with no further explanation. Although the *in situ* catalysis with H_3**CL5** and $Sm(OiPr)_3$ gave a higher yield than H_3**CL5** and $Cu(OAc)_2$, the species in the more active reaction is not studied via ESI-MS.

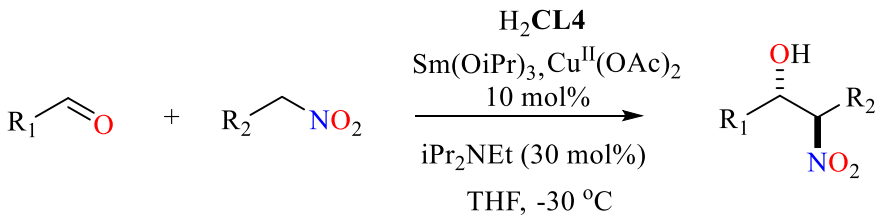

Equation 1.21. A Cu^{II}/Sm^{III} catalysed *anti*-selective asymmetric Henry reaction.[298]

These studies were followed by a proposed Ni^{II}-La^{III} PCC, supported by H_2**CL4**, which catalysed the enantioselective decarboxylation -1,4-addition of malonic acid half thioester to nitroalkenes (Equation 1.22).[299] The Ni^{II}-La^{III} PCC gave products in a 40 - 99% yield with 66 - 94% *ee*. No further identification or characterisation of the active species was presented.

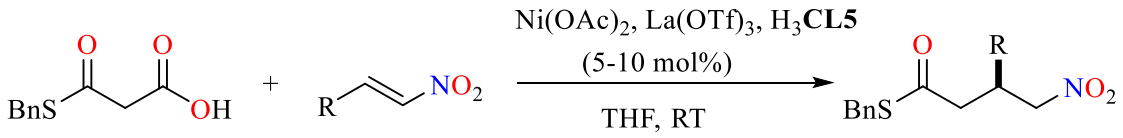

Equation 1.22. A Ni^{II}-La^{III} asymmetric decarboxylative 1,4-addition of Malonic acid half thioester.[299]

More recently, a dinuclear PCC with the general formula $[Zn^{II}Yb^{III}$(**CL6**)$(\mu_1\text{-OAc})_2(\mu_2\text{-OAc})(H_2O)]$ (Figure 1.19) has been reported for the solvent-free copolymerization of cyclohexane

oxide and maleic anhydride (Scheme 1.2).[300] The presence of TPP or DMAP as a co-catalyst leads to the formation of polyester and poly (ester-coether) respectively. The Zn^{II}-Yb^{III} PCC can effectively catalyse the co-polymerisation alone, unlike similar salen-based M^{III} complexes, which may indicate that $[OAc]^-$ initiators are working co-operatively with the active Zn^{II} and Yb^{III} centres.[301] The Zn^{II}-Yb^{III} structure was elucidated by single-crystal XRD studies and has a similar structure to the 3d-4f PCC catalysts which were proposed in Shikasaki's work. ESI-MS confirms the $[Zn^{II}Yb^{III}(\mathbf{CL6})]^+$ core configuration and Thermogravimetric Analysis (TGA) shows an indicative weight loss with the hetero-bimetallic framework stable up to 200 °C.

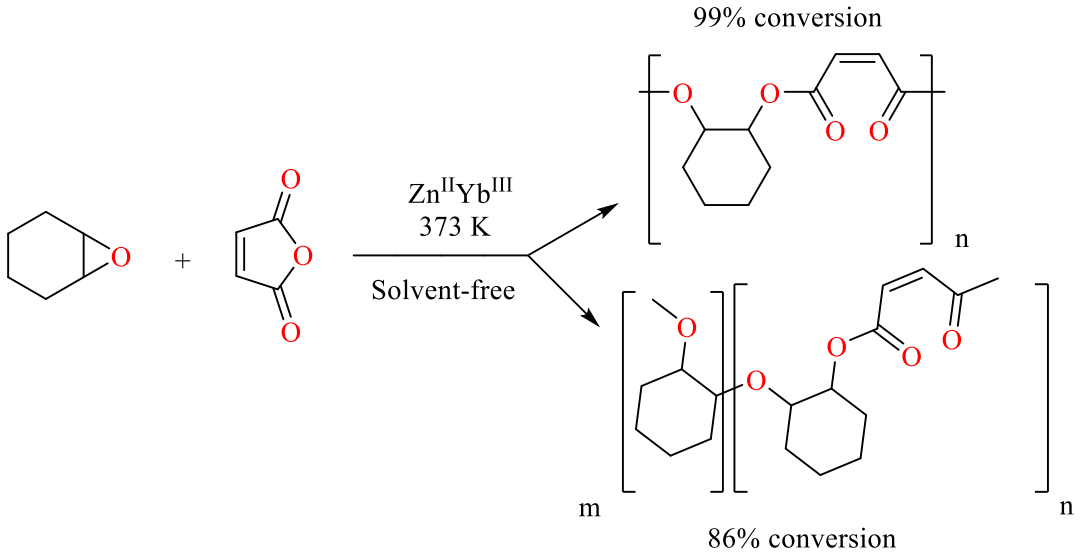

Scheme 1.2. Solvent-free co-polymerisation of cyclohexane oxide and maleic anhydride by Zn^{II}-Yb^{II}.[300]

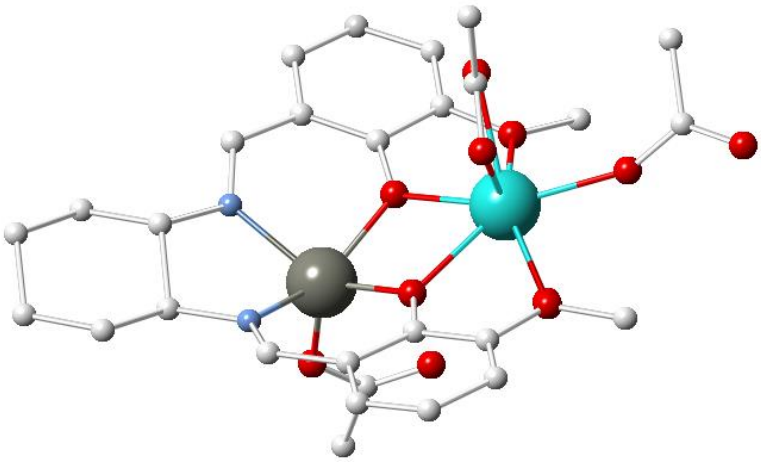

Figure 1.19. The molecular structure of Zn^{II}-Yb^{III}. Colour code: Yb^{III}, light blue; Zn^{II}, grey; O, red; C, white; N, blue. Hydrogen ions and counter-ions are omitted for clarity.[300]

Though all *in situ* 3d-4f catalytic systems promote enantioselective and diastereoselective transformations, the characterisation of the proposed dinuclear 3d-4f PCCs, which are postulated

to promote the transformations, have been overlooked with only ESI-MS studies and the nature of the dinucleating ligands used as evidence to propose their formation. The characterisation of the active species and understanding of the catalytic mechanism are considered vital aspects for the development of 3d-4f PCC catalysis and will be addressed rigorously throughout the rest of this work.

Higher nuclearity 3d-4f PCCs have been reported as catalysts, however, these are limited to oxidation catalysts and WOCs. Further, these examples report the prior synthesis and characterisation of the PCC and attempt to understand the catalytic mechanism.

A heptanuclear $Mn^{IV}_6Ce^{IV}$ (**3M7-1**) PCC with TEMPO, was reported to catalyse the oxidation of benzyl alcohol to benzaldehyde with quantitative yields (Equation 1.23).[302] The $Mn^{IV}_6Ce^{IV}$ PCC was well characterised in the solid state, which includes single-crystal XRD studies (Figure 1.20). The conversion to the product does not decrease with time and Fourier Transform Infrared Spectroscopy (FT-IR) data of the recovered product is consistent with the starting material, suggesting the PCC remains stable during the reaction. It was highlighted that the high efficiency of transformation could only be achieved when both high oxidation Ce^{IV} and Mn^{IV} ions were present in the same cluster. In contrast to previous dinuclear examples, the $Mn^{IV}_6Ce^{IV}$ cluster was well characterised and it was suggested that the catalyst remains stable under the reaction conditions.

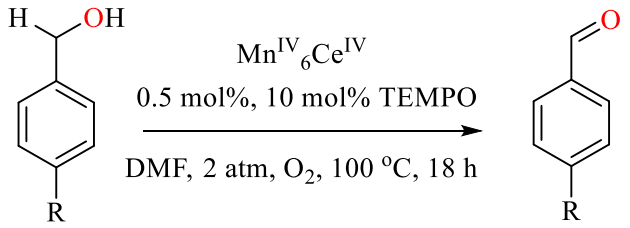

Equation 1.23. The $Mn^{IV}_6Ce^{IV}$ catalysed oxidation of benzyl alcohol to benzaldehyde.[302]

More recently, a family of $Co^{II}_3Ln^{III}$ cubanes (Figure 1.20) (**3M4-1**) with the general formula $[Co^{II}_3Ln^{III}(hmp)_4(OAc)]\cdot 5H_2O$ (Ln = Ho, Er, Tm, Yb, hmp = 2-(hydroxymethyl)pyridine) were reported as the first 3d-4f WOCs.[141,303] Initially synthesised by Wang et al.,[303] the series of $Co^{II}_3Ln^{III}$ WOC activity is highest in a pH 8 borate/HCl buffer solution with yields of O_2 between 90 - 97% and TON vales of 42 - 99. The embedment of the Ln^{III} centres into the cubane was shown to be essential for tunability and performance enhancement, with Er^{III} and Ho^{III} analogues among leading Co^{II} containing molecular WOCs to date.[255,304–306]

The stability of the $Co^{II}_3Ln^{III}$ cores during the reaction was established with three distinct stages including spectroscopic solution tests and exclusion of nanoparticles, trace metal tests with Co^{II} chelators or ICP-MS analysis and post-catalytic structural integrity checks which encompassed

HPLC analyses as well as XANES/EXAFS spectroscopy. In addition, Density Functional Theory (DFT) studies provides proof that Ln^{III} centres are active catalytic promoters with flexible ligand binding modes. Overall, this contribution has opened up 3d-4f PCCs for photocatalytic applications.

In the wake of the $Co^{II}_3Ln^{III}$ cubanes WOC activity, a dinuclear Fe^{III}-Ce^{IV} PCC (Figure 1.20) with the general formula $[Fe^{III}Ce^{IV}(N_4Py)(OH_2)(NO_3)_4]^+$ was reported as a catalyst for water oxidation, which was demonstrated to be a facile and reversible process.[307] The position of this equilibrium depends on the number of nitrate ligands on the Ce centre as controlled by the $MeCN/H_2O$ ratio in the solvent, which tunes the $Ce^{IV/III}$ potential. A variety of characterisation techniques (single-crystal XRD studies, ESI-MS, XAS and TGA) were used to confirm the identity of the $Fe^{III}Ce^{IV}$ PCC. Cyclic Voltammetry (CV) confirms the reversible nature of the process and it represents the first example of a reversible inner-sphere electron transfer between Ce^{III} and Fe^{IV}= O PCCs.

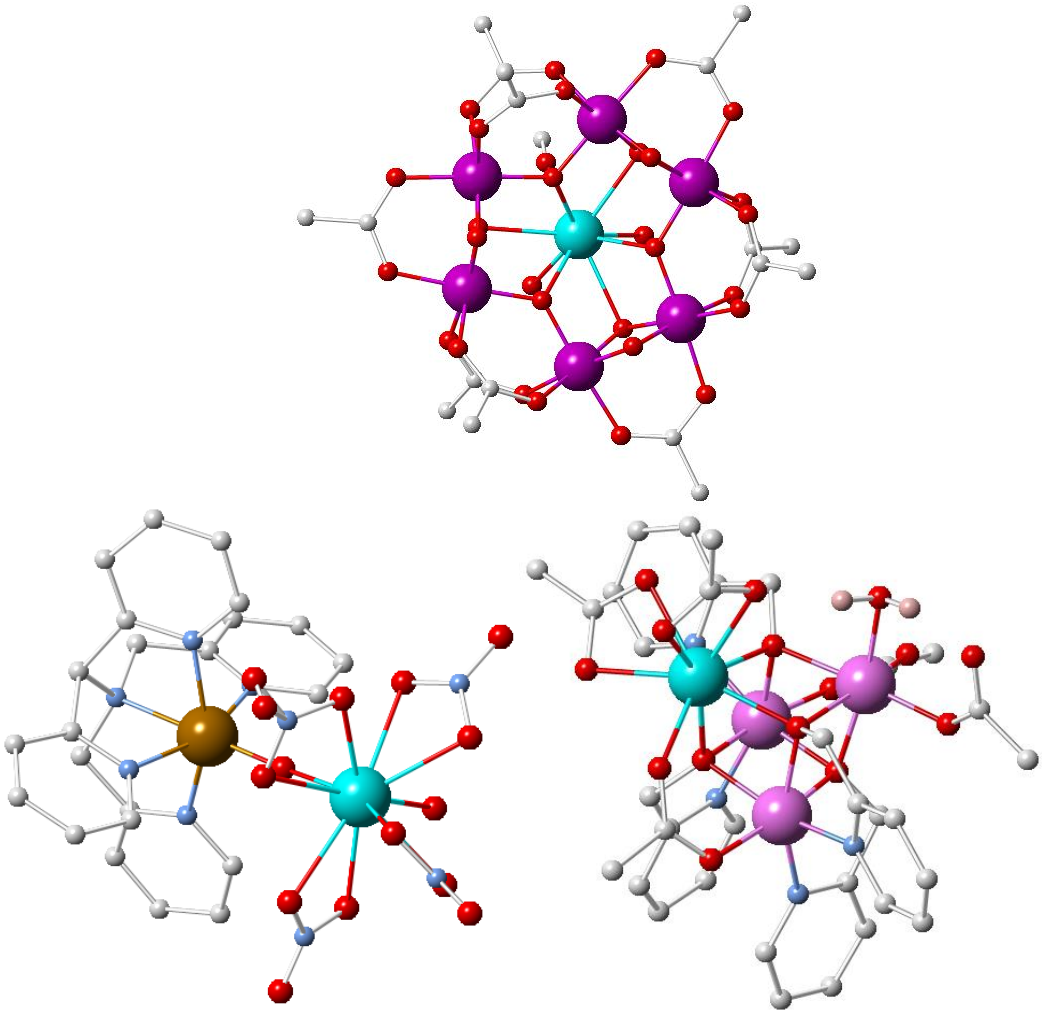

Figure 1.20. The molecular structure of $Mn^{IV}_6Ce^{IV}$ (upper). The molecular structure of Fe^{III}-Ce^{IV} (lower left). The molecular structure of $Co^{II}_3Ln^{III}$ (lower right). Colour code: $Ln^{III/IV}$, light blue; Mn^{IV}, purple; Fe^{III}, brown; Co^{II}, pink; O, red; C, white. Hydrogen ions and lattice molecules omitted for clarity.

1.4 Ligand selection and synthetic strategy for novel topologies and magnetic properties

An objective of this research is to synthesise heterometallic 3d-4f PCCs with novel topologies and to study their enhanced magnetic and/or optical properties. The Schiff-base ligands selected to fulfil this objective were all synthesised from the keto precursor o-vanillin and **amal** (Figure 1.5), which form ligands with a wide range of coordination modes. In this work several diprotic, tripotic and monoprotic Schiff base ligands; (E)-2-(2-hydroxy-3- methoxybenzylideneamino)-phenol (H_2**L1**), (E)-2-(2-hydroxy-3- methoxybenzylideneamino)-naphthol (H_2**L2**), 6,6'-((1E,1'E)-((2-hydroxypropane-1,3-diyl)bis(azanylylidene))bis(methanylylidene))bis(2-methoxyphenol) (H_3**L3**) and (*E*)-4-(2-hydroxy-3-methoxybenzylideneamino)-2,3-dimethyl-1-phenyl-1,2-dihydropyrazol-5-one (H**L4**) have been selected (Figure 1.21).

H_2**L1** has been previously reported for the synthesis of a small number of 3d-4f PCCs. These include isostructural $M^{II/III}_2Ln^{III}_2$ (M = Mn,[116] Ni,[50] Zn,[46] Co,[2,46]) PCCs with a **2,3M4-1** core which all display SMM behaviour, with the Co^{II} analogues displaying some of the highest reported blocking temperatures for 3d-4f PCC SMMs. A dodecanuclear $Ni^{II}_8Ln^{III}_4$ PCC is also reported. H_2**L2** has not been previously reported for the synthesis of 3d-4f PCCs, however, it has identical co-ordination modes to H_2**L1**.

The coordination properties of H_3**L3** have been investigated extensively.[308] This work was extended to synthesise dinuclear PCCs, including $Co^{II}Dy^{III}$,[309] $Cu^{II}Dy^{III}$ [309] and $Cu^{II}Sm^{III}$ [308] all of which display a typical SMM response. The highest nuclearity 3d-4f PCCs synthesised with H_3**L3** were a family of isostructural heptanuclear $Cu^{II}_5Ln^{III}_2$ PCCs reported by Chandrasekhar et al. in 2013,[113] where Dy^{III} and Ho^{III} analogues display SMM behaviour with energy barriers below 5 K.

H**L4** has only been employed for the synthesis of Co^{II}-Dy^{III} PCCs. The first 3d-4f PCC supported by H**L4** was a heptanuclear $Co^{II}_3Dy^{III}_4$ disk.[1] In addition, a family of nine Co^{II}-Dy^{III} PCCs including $Co^{II}_2Dy^{III}_2$, $Co^{II}Dy^{III}_3$, $Co^{II}_4Dy^{III}_4$ and $Co^{II}_2Dy^{III}_5$ were reported, many possessing previously unobserved topologies in 3d-4f chemistry.[68]

The synthesis of novel 3d-4f PCCs with these ligands will rely on serendipitous assembly through a systematic variation of the reaction conditions (metal salts, temperature, reaction time, reactant ratio, solvent, and crystallisation method). In this pursuit, 3d-4f PCCs of new topologies and with magnetically interesting species should be isolated.

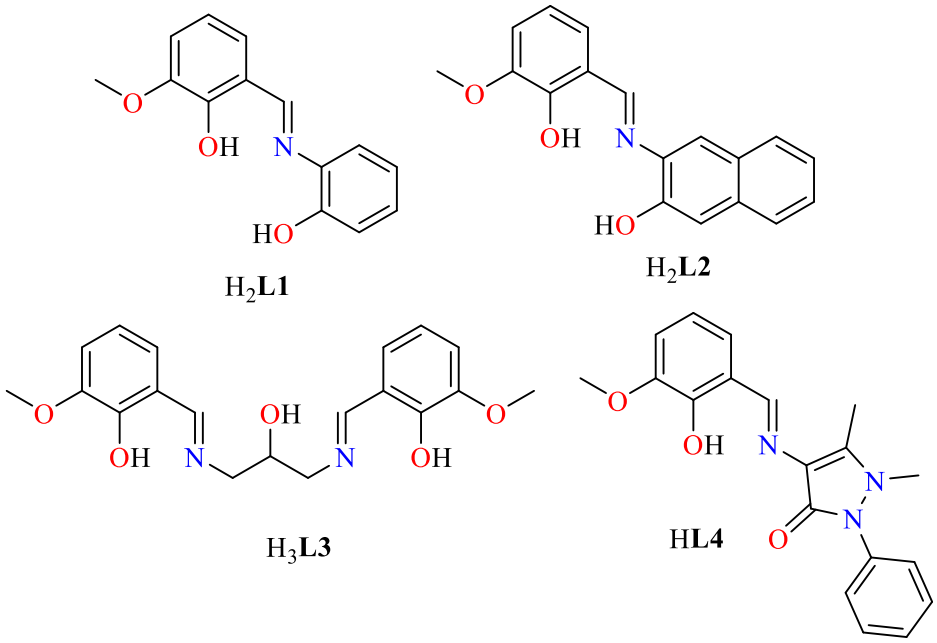

Figure 1.21. Schiff base ligands for targeting novel topologies and enhanced magnetic properties in 3d-4f PCCs.

1.5 Ligand selection and synthetic strategy for catalytic properties

Another main objective of this research is to construct well characterised 3d-4f PCCs which retain a stable core topology in solution and can be applied as catalysts in a variety of organic transformations.

One of the most studied core topologies in 3d-4f PCC chemistry is the defect dicubane structure (**2,3M4-1**) and it is an ideal topology to study for catalytic activity. In this topology, the four metal ions are linked together by two μ_3-O and further bridged by four μ_2-O, forming an $M^{II}_2Ln^{III}_2O_6$ core. The two 3d ions and two 4f ions can be co-planar, and the six oxygen atoms are located above and below the plane with a centrosymmetric feature.

In 3d-4f chemistry, this topology has been formed from a variety of ligands (Figure 1.22) and they display some of the most outstanding SMM properties hitherto reported.[50,215] Notable examples include a $Mn^{III}_2Ln^{III}_2$ PCC formed from 1,1,1-trihydroxymethyl propane,[310] a $Fe^{III}_2Dy^{III}_2$ PCC supported by triethanolamine and carboxylic acids and two $Co^{III}_2Ln^{III}_2$ PCCs were obtained with an analogous structure to the previous $Fe^{III}_2Dy^{III}_2$ PCC.[311,312]

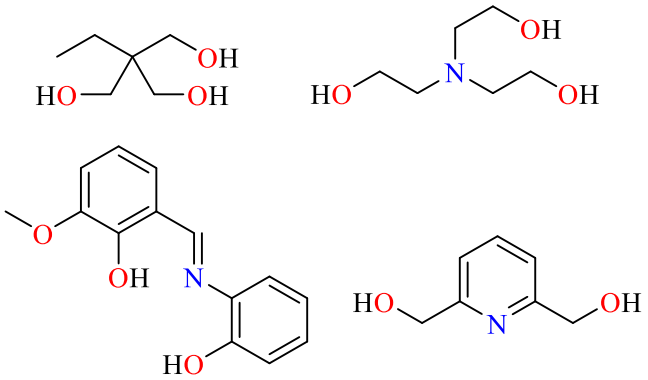

Figure 1.22. Representative examples of ligands used for the synthesis of 3d-4f defect dicubane PCCs.

Additionally, two isostructural $Ni^{II}_2Ln^{III}_2$ and $Co^{II}_2Dy^{III}_2$ (Figure 1.23) defect dicubane PCCs, supported by **L1**, were reported by Powell.[2,50] These PCCs presented an ideal starting point for targeting of catalytically active 3d-4f PCCs. The two crystallographically equivalent M^{II} and two Dy^{III} ions are linked via two u_3-O phenol bridges from two separate **L1** ligands to construct the $M_2Ln_2O_2$ core. The two ligands provide μ_2-O-phenol along the four outer edges of the $M^{II}_2Dy^{III}_2$ rhombus with chelating $[NO_3]^-$ and oxygen from a solvent molecule to complete the respective Ln^{III} and M^{II} coordination spheres. As the core is formed without the support of additional bridging ligands or co-ligands, the $[M^{II}_2Ln^{III}_2(\mathbf{L1})_4]^{2+}$ core may be stable in solution or in a potential catalytic reaction.

The 3d ions coordination sphere also contains solvent molecules (THF/ DMF), which may allow interaction with possible substrate molecules, however, the Ln^{III} node is capped by a nitrate counter-ion (Figure 1.24, **1CoDy-NO$_3$**).

As the $[M^{II}_2Ln^{III}_2(\mathbf{L1})_4]^{2+}$ core is only supported by **L1**, it may be possible to synthesise isostructural analogues without coordinated counter-ions ($[NO_3]^-$, $[Cl]^-$), instead replacing these with lattice counter-ions ($[ClO_4]^-$, $[OTf_3]^-$, $[BF_4]^-$), so that potential substrates are free to interact with the metal centres (Figure 1.24, **1CoDy-Solvent**). The previously reported examples by Powell have already demonstrated that metal centres can be exchanged, 3d ions (Ni^{II} and Co^{II}) and 4f ions (Dy^{III}, Tb^{III}), without affecting the defect dicubane core topology which grants scope for Zn^{II} and Cu^{II} analogues to be synthesised.

The advantages of using H_2**L1** to synthesise defect dicubane isostructural analogues of $M^{II}_2Ln^{III}_2$[2,50] over the previously described examples (Figure 1.22), is the simplicity of H_2**L1** synthesis and the myriad of o-vanillin and modified aminophenol derivatives available. With the possible combinations of substrates to form modified H_2**L1** ligands (Table 1.1, H_2**LX**), it would allow the synthesis of a library of 3d-4f PCCs with the same defect dicubane framework, with

modified ligands (Table 1.1, H_2**LX**), similar coordination environments (Figure 1.24 right) and different guest ions with similar coordination properties.

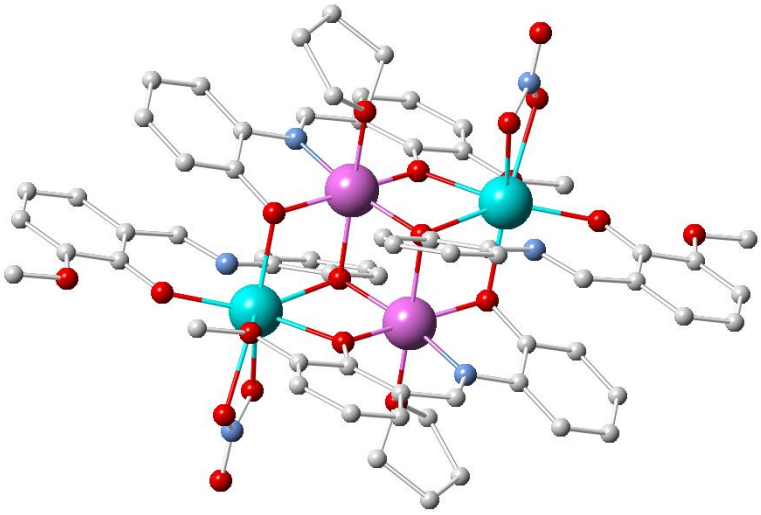

Figure 1.23. The molecular structure of $Co^{II}_2Ln^{II}_2$ (**1CoDy-NO$_3$**). $Ni^{II}_2Ln^{II}_2$ (**1NiDy-NO$_3$**) is isostructural with Co^{II} ions substituted with Ni^{II} ions. Colour code: Ln^{III}, light blue; Co^{II}, pink; O, red; C, white; N, blue; Hydrogen ions omitted for clarity.[2,50]

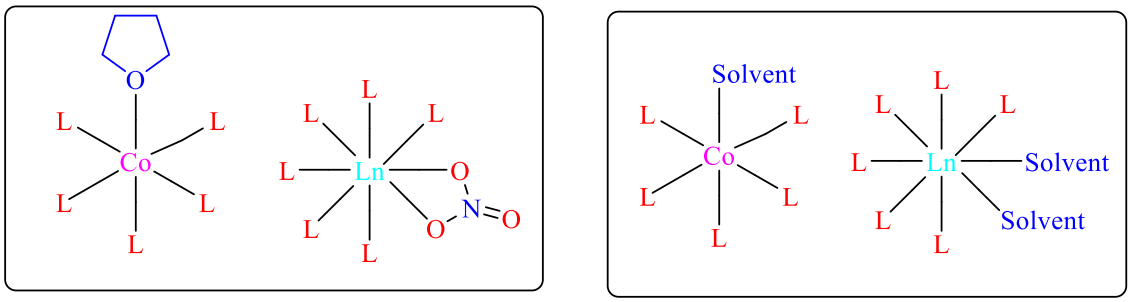

1CoDy-NO$_3$ **1CoDy-Solvent**

Figure 1.24. Coordination spheres of Co^{II} and Ln^{III} observed in **1CoDy-NO$_3$** (left). Hypothesised coordination spheres of Co^{II} and Ln^{III} in an isoskeletal analogue with uncoordinated lattice counter-ions (**1CoDy-Solvent**) (right). Ligand coordination, red; solvent, blue.

With this library**,** the "isoskeletal" PCCs could be applied to a catalytic organic transformation to determine how the second sphere effects of the PCC such as the ligand modification, coordinated counter-ions and coordinated solvent may affect the catalytic efficacy of the PCC. These modifications may also impart other properties such as immobilisation for heterogeneous catalysis, Ultra Violet (UV) activated catalysis or act to promote asymmetric transformations with the correct selection of organic ligand.

The term "isoskeletal" is based on the isoreticular concept introduced by O'Keeffe and Yaghi and it will be used to describe a PCC which possesses the same topology but with a modified organic periphery. This term will be further discussed, with an investigation into targeting the **2,3M4-1**

topology, by varying the reaction conditions (solvent, environment, reactant ratio, temperature, crystallisation method, concentration and reaction time) with each H_2**LX** ligand and determining how this affects the nature of the final product.

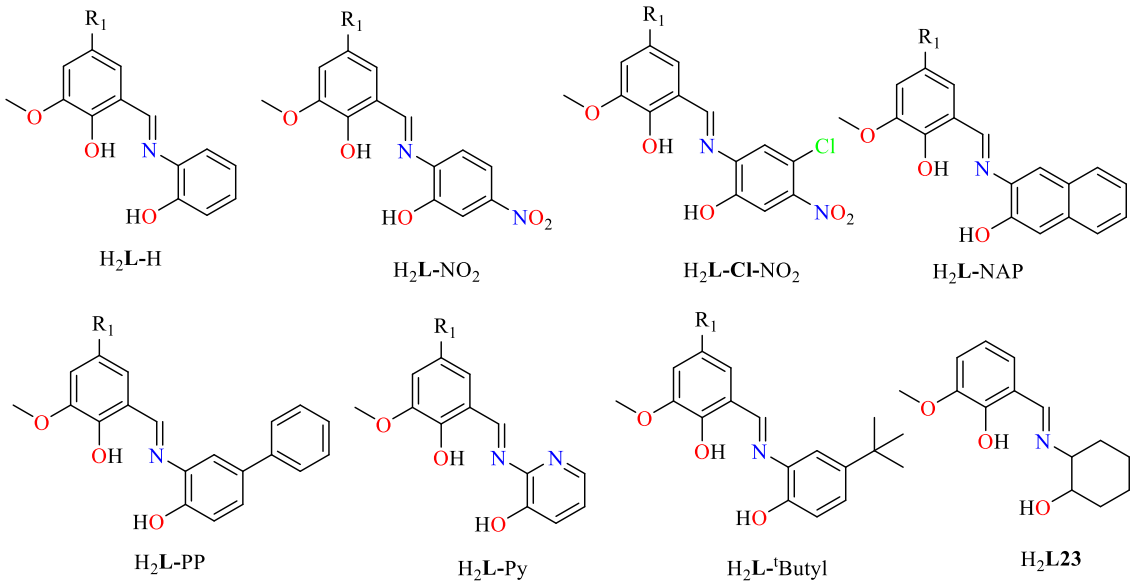

Figure 1.25. Schiff base ligands for targeting catalytically active 3d-4f PCCs.

Table 1.1. Key for modified ligands (H_2**LX**) of H_2**L1**.

		H_2**L**-H	H_2**L**-NO_2	H_2**L**-Cl-NO_2	H_2**L**-NAP	H_2**L**-PP	H_2**L**-Py	H_2**L**-^{t}Butyl
R1 =	H	H_2**L1**	H_2**L8**	H_2L**12**	H_2**L2**	H_2**L19**	H_2**L24**	H_2**L27**
		H_2**L6**	H_2**L9**	H_2L**13**	H_2**L16**	H_2**L20**	H_2**L25**	H_2**L28**
	NO_2	H_2**L7**	H_2L**10**	H_2L**14**	H_2**L17**	H_2**L21**	N/S	N/S
	Br	H_2**L5**	H_2L**11**	H_2L**15**	H_2**L18**	H_2**L22**	H_2**L26**	H_2**L29**

N/S – Not synthesised. Synthetic protocol (chapter eleven) and characterisation (^{1}H NMR and ^{13}C NMR, Appendix B, S1.1-S1.26).

Chapter 2: Four new families of Zn^{II}-Ln^{III} PCCs. Synthetic, topological, magnetic and luminescent aspects.

Abstract: The employment of three structurally related Schiff bases H_2**L1,** H_2**L2,** and H_3**L3** with zinc (II) and lanthanide (III) salts under various reaction conditions, gave four families of compounds formulated as $[Zn^{II}_2Ln^{III}_2(\mathbf{L1})_4(EtOH)_6](ClO_4)_2$ (**1-3**), $[Zn^{II}_5Ln^{III}(OH)(\mathbf{L1})_6(H_2O)]$ (**4-6**), $[Zn^{II}_4Ln^{III}_2(OH)_2(\mathbf{L2})_4(OAc)_2(NO_3)_2(DMF)_3]\cdot DMF$(**7-9**) and $[Zn^{II}_2Ln^{III}_2(\mathbf{L3})_2(NO_3)_2(CO_3)_2(CH_3OH)_2]$ (**10-12**). A comprehensive topological analysis of all reported Zn^{II}-Ln^{III} polynuclear coordination clusters with a core nuclearity of four and above is presented and identifies that families (**4 - 9**) are the first examples of the **2,3,4M6-1** motif in Zn^{II}-Ln^{III} chemistry. Magnetic studies are presented for the Dy^{III} analogues (**1**, **7** and **10**), compound **7** demonstrates a field-induced slow relaxation of the magnetization. Fluorescence studies are also discussed.

2.1 Introduction

This chapter presents the synthesis, topological analysis and magnetic properties of Zn^{II}-Ln^{III} Schiff base PCCs. Previously, Zn^{II}-Ln^{III} PCCs have displayed a number of interesting properties and topologies, with the first example of a heteronuclear Zn^{II} – Eu^{III}/Sm^{III} PCCs reported in 1995 by Brennan et al.[313,314] Many dinuclear Zn^{II}-Ln^{III} examples followed.[315–317] However, the most pivotal example of a Zn^{II}-Ln^{III} PCC was a pentanuclear $Zn^{II}_2Dy^{III}_3$ PCC which exhibited SMM and fluorescent properties and was reported by Murugesu et al.[318] Since then, the synthesis of Zn^{II}-Ln^{III} PCCs has gained a remarkable amount of attention due to their unique characteristics including:

a) A magnetic behaviour which can be explained due to the diamagnetic character of the Zn^{II} ion and which has been shown to enhance the energy barrier in Zn^{II}-Dy^{III} SMMs.[216]

b) Eu^{III} and Tb^{III} ions are attractive luminescent centres, due to their long-lived $^5D_0$ and $^5D_4$ excited states and the accompanying large Stokes' Shifts. In addition, the combination with Zn^{II} ions may produce species with enhanced luminescent properties via 3d-4f energy transfer.[319]

A plethora of such mixed metal species have been reported and the magnetic and luminescent properties of such compounds have been very well investigated.[72,114,210,212,225,237,239,320–335] H_2**L1** and its structurally related pro-ligands, H_2**L2** and H_3**L3** (Figure 2.1), have not been reported for the synthesis of Zn^{II}-Ln^{III} PCCs. Due to these multifunctional properties and the wide range of previously synthesised core topologies in Zn^{II}-Ln^{III} PCC chemistry, it was thought that this combination would provide an ideal starting point for the discovery of novel 3d-4f Schiff base supported PCCs.

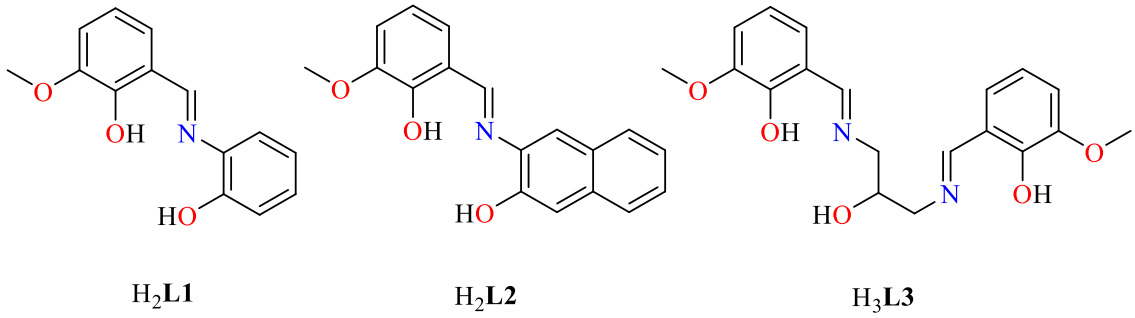

Figure 2.1. Schiff base ligands used in this chapter.

A systematic synthetic study using H_2**L1**, H_2**L2** and H_3**L3,** a variety of solvents, metal salts and crystallisation techniques is presented in an effort to discover novel Zn^{II}-Ln^{III} PCCs. Herein, twelve new PCCs formulated as $[Zn^{II}_2Ln^{III}_2(\mathbf{L1})_4(EtOH)_6](ClO_4)_2$ where Ln is Dy^{III} (**1**), Tb^{III} (**2**) or Eu^{III} (**3**), $[Zn^{II}_5Ln(OH)(\mathbf{L1})_6(H_2O)]$, where Ln is Dy^{III} (**4**), Tb^{III} (**5**) or Eu^{III} (**6**), $[Zn^{II}_4Ln^{III}_2(OH)_2(\mathbf{L2})_4(OAc)_2(NO_3)_2(DMF)_3]\cdot DMF$, where Ln is Dy^{III} (**7**), Tb^{III} (**8**) or Eu^{III} (**9**), $[Zn^{II}_2Ln^{III}_2(\mathbf{L3})_2(CO_3)_2(NO_3)_2(CH_3OH)_2]$ where Ln is Dy^{III} (**10**), Tb^{III} (**11**) and Eu^{III} (**12**) are described. Magnetic studies of the Dy^{III} analogues are presented, as well as luminescent properties in solution.

2.2 Results and discussion

2.2.1 Synthetic strategy

It is well-known that the stoichiometric ratio, metal salt, temperature, atmosphere, solvent and time of reaction, can all affect the nature of the final product. The semi-rigid H_2**L1** ligand has two pockets-I (ONO) and –II (ONO) (Figure 2.3) which are suitable for binding both 3d and 4f metal ions.

The reaction between, $Dy(OTf)_3$, $Zn(ClO_4)_2\cdot 6H_2O$ and H_2**L1** in the presence of Et_3N, in EtOH, in the molar ratio 1:2:2:4.5, afforded yellow needle like crystals of **1** in a moderate yield (57%) after 1 week (Table 2.1, entry 1). The reaction with similar ratios but different counter anions and solvent yielded the recently reported isoskeletal PCCs formulated as $[Zn_2Ln_2(\mathbf{L1})_4(NO_3)_2(DMF)_2]$ (Table 2.1, entry 2).[336]

With the aim of synthesising the isoskeletal Zn^{II} analogue of $[Ni_2Ln_2(\mathbf{L1})_4Cl_2(CH_3CN)_2]$,[337] a reaction with similar ratios of MeCN, $DyCl_3$ and $ZnCl_2$, was performed, which yielded crystals of **4** after 2 weeks (Table 2.1, entry 3). The resultant PCCs displayed a topology previously unobserved in the literature for Zn^{II}-Ln^{III} PCCs.

A modified form of this ligand, H_2**L2** (Figure 2.1 middle), that offers identical pockets to H_2**L1** has been employed to act as a sensitizer to enhance luminescence of the resulting complexes. A reaction was performed with same molar reactant ratios in DMF, with $Dy(NO_3)_3\cdot 5H_2O$ and

$Zn(OAc)_2{\cdot}4H_2O$ and after 1 week of Vapour Diffusion (VD) with Et_2O, large yellow plate-like crystals of **7** formed in 70% yield (Table 2.1, entry 4).

With the retention of the o-vanillin unit and replacement of the aminophenol by 1,3-diamino-2-propanol the ligand, H_3**L3** (Figure 2.1, right), which offers similar pockets to that in H_2**L1** and H_2**L2** and one extra pocket was obtained. The use of H_3**L3** for the first time in Zn^{II}-Ln^{III} chemistry, gave the tetranuclear compounds **10** – **12** (Table 2.1, entry 5). A summary of these synthetic procedures is shown in Table 2.1 and Scheme 2.1.

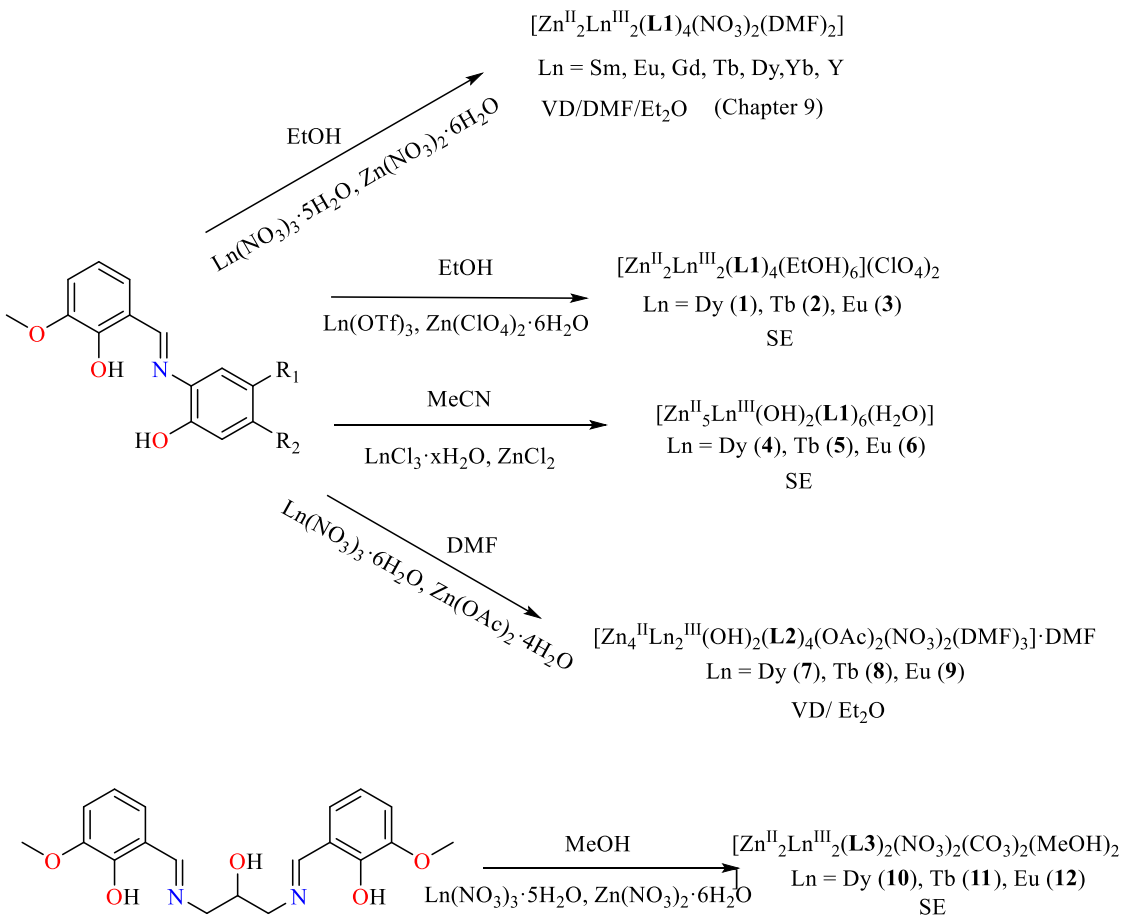

Scheme 2.1. Synthetic scheme for the preparation of (**1-12**).

Table 2.1. Synthetic strategies for the preparation of Zn^{II}-Ln^{III} PCCs.

Entry	Ligand	Ln^{III} salt	Zn^{II} salt	Crystallisation method/ time (days)	Solvent	Compound
1	H_2**L1**	$Ln(OTf)_3$	$Zn(ClO_4)_2 \cdot 6H_2O$	SE / 7	EtOH	$Zn^{II}_2Ln^{III}_2$ (**1**, **2**, **3**)
2	H_2**L1**	$Ln(NO_3)_3 \cdot 5H_2O$	$Zn(NO_3)_2 \cdot 6H_2O$	VD Et_2O / 9	DMF	$Zn^{II}_2Ln^{III}_2$[336] (chapter nine)
3	H_2**L1**	$LnCl_3 \cdot xH_2O$	$ZnCl_2$	SE / 3	MeCN	$Zn^{II}_5Ln^{III}$ (**4**, **5**, **6**)
4	H_2**L2**	$Ln(NO_3)_3 \cdot 5H_2O$	$Zn(CH_3CO_2)_2 \cdot 4H_2O$	VD Et_2O / 7	DMF	$Zn^{II}_4Ln^{III}_2$ (**7**, **8**, **9**)
5	H_3**L3**	$Ln(NO_3)_3 \cdot xH_2O$	$Zn(NO_3)_2 \cdot 6H_2O$	SE / 5	MeOH	$Zn^{II}_2Ln^{III}_2$ (**10**, **11**, **12**)

[a] Ratio of all reactants 1:2:2:4.5 = A: B: C: D. A = Dy^{III} salt, B = Zn^{II} salt, C = H_x**LX**, D = Et_3N. Slow Evaporation (SE). Vapour Diffusion (VD).

2.2.2 Molecular structure and crystal structure descriptions of 1 - 12

In addition to single-crystal XRD studies, compounds **1 - 12** were characterised by FT-IR spectroscopy (Appendix B, S2.1-S2.12), TGA (Appendix B, S2.13-S2.20), ESI-MS (Appendix B, S2.24-S2.26) and Elemental Analysis (EA) (chapter eleven), which all support the following descriptions.

2.2.2.1 Molecular structure of 1 - 3

Compounds **1** – **3** crystallize in the monoclinic *P*21/*n* space group and are isostructural, thus only **1** will be described (Figure 2.2). The asymmetric unit of **1** contains one Zn^{II} ion, one Dy^{III} ion, two doubly deprotonated organic ligands (**L1**), three coordinated ethanol molecules (one to the Zn^{II} and the other two to the Dy^{III} ion), one perchlorate and one ethanol molecule. The main core of **1** can be described as a defect dicubane[338] and is isoskeletal to the previously reported $Ni^{II}_2Ln^{III}_2$[50,337] and $Co^{II}_2Ln^{III}_2$[2,337] cores.

The organic ligands exhibit two different coordination modes (Figure 2.3). In the first mode (Figure 2.3, mode I), the two phenoxide oxygen atoms and the imine nitrogen atom are chelated to the Zn^{II} centre and the two phenoxide atoms are further bonded to two Dy^{III} ions (Dy (1) and its symmetry-related counterpart) and the methoxide oxygen atoms are bound to Dy (1). In the second mode (Figure 2.3, mode II), the two phenoxide oxygen atoms and the imine nitrogen atom are chelated to the Dy^{III} centre, while the phenoxide oxygen atom (from the 2-aminophenol unit), is further bound to two Zn^{II} centres. One ethanol molecule is bound one to the Zn^{II} ion and two others are bound to the Dy^{III} ion.

Each Zn^{II} centre coordinates to six atoms (O_5N) and displays an octahedral coordination, while each Dy^{III} centre coordinates to eight atoms (O_7N). Using SHAPE software,[339] the geometry of Dy(1) can be best described as biaugmented trigonal prismatic, with an S(P) value 1.415. There are two $Zn^{II}\cdots Dy^{III}$ distances at 3.5513(5) Å and 3.5329(5) Å and one $Zn^{II}\cdots Zn^{II}$ distance at 3.172(5) Å. Two coordinating ethanol molecules, one to Zn^{II} and one to Dy^{III} ion, form an H-bond (O8 – H8⋯O9) while the third coordinating ethanol molecule forms an H-bond with the lattice EtOH (O7 – H7⋯O10), which in turn is H-bonded to the uncoordinated methoxide oxygen atom (O10 – H10A⋯ O1).

No other intramolecular interactions (e.g. H-bonds or stacking) can be found between neighbouring entities. According to the ***ND*k-m** topological representation,[13,340] the main core of compound **1** can be enumerated as **2,3M4-1**.[13] According to a literature survey[341] this topology can be found in $Zn^{II}_2Eu^{III}_2$[313] and $Zn^{II}_2Yb^{III}_2$[249] PCCs and other recently reported examples.[336]

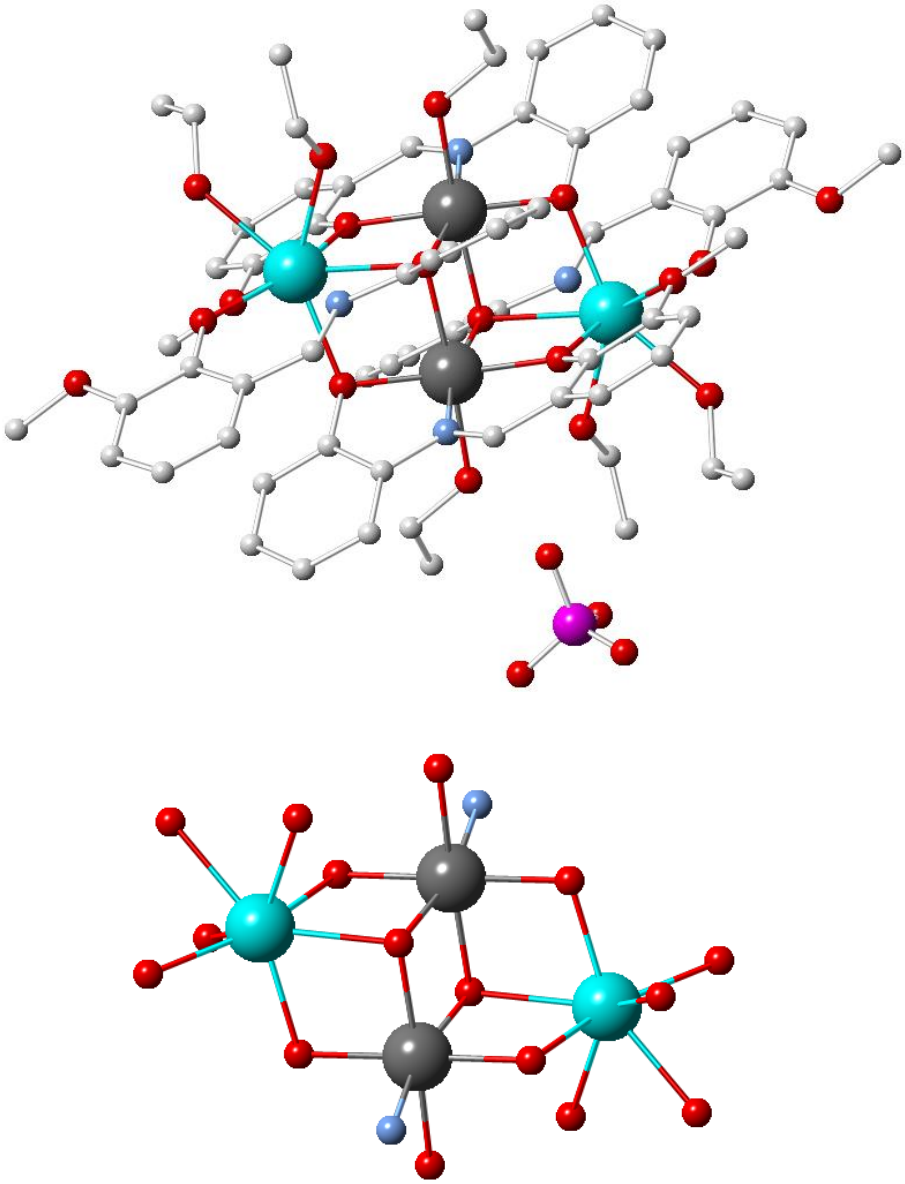

Figure 2.2. The molecular structure of compound **1** (upper) and its core (lower). C, H atoms and lattice molecules are omitted for clarity. Colour code: Zn^{II}, grey; Dy^{III}, light blue; O, red; N, blue; Cl, purple.

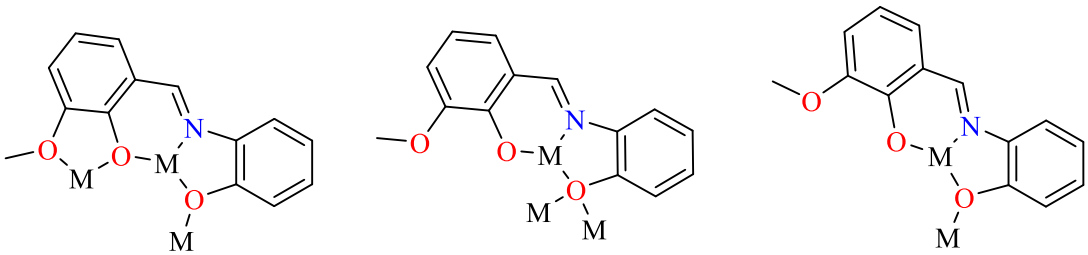

mode I mode II mode III

Figure 2.3. The coordination modes found in **1** and **3**.

2.2.2.2 Molecular structure of 4 - 6

Compounds **4** – **6** crystallize in the triclinic *P*-1 space group and are isostructural, thus only **4** will be further described (Figure 2.4). The asymmetric unit of **4** contains five Zn^{II} ions, one Dy^{III} ion, six doubly deprotonated organic ligands (**L1**), one triply bridging hydroxyl group, one coordinated water molecule and two lattice molecules (one water and one acetonitrile). The main core of **4** can be considered as four fused triangles forming a distorted ‘‘chair’’ shaped core.

The five Zn^{II} ions are situated in a plane, while the Dy^{III} is situated 1.998 Å above this plane. Each of the six organic ligands is chelated to one metal centre and further bridges other metal centres with the phenoxide and methoxide oxygen atoms. Three different coordination modes can be found for the six organic ligands (Figure 2.3, modes I, II and III).

The hydroxyl group bridges Zn2, Zn3 and Dy1 and is situated (0.311 Å) above their plane. The coordination sphere of Zn3 is completed by one water molecule. Zn1 and Zn5 are five coordinated (O_4N) with trigonality index τ = 0.79 and 0.88, respectively, indicating that they adopt distorted trigonal bipyramidal coordination. Zn2 and Zn3 are five coordinated (O_4N) with trigonality index τ = 0.46 and 0.43, respectively, indicating that the coordination is between square pyramidal and trigonal bipyramidal.[342] Zn4 is six-coordinated (O_5N). From SHAPE software,[339] the geometry of Zn4 can be best described as trigonal prismatic, with S(P) value 5.126.

The Dy^{III} centre coordinates to nine atoms (O_8N). From SHAPE software,[339] the coordination of Dy(1) can be best described as between a spherical tricapped trigonal prism and a spherical capped square antiprism [S(P) 1.606 and 1.656, respectively].

There are two $Zn^{II}\cdots Dy^{III}$ distances of 3.4317(3) Å and 3.4452(3) Å and four $Zn^{II}\cdots Zn^{II}$ distances at 3.0942(3) Å, 3.1296(3) Å, 3.527(3) Å and 3.626(3) Å. The coordinating water molecule forms two strong H-bonds, one with the methoxido oxygen atom (O7⋯O1AA) and the other with lattice water (O7⋯O3A). No other supramolecular interactions (H-bonds or stacking) can be found between neighbouring entities.

According to the ***ND*k-m** topological representation,[13,340] the main core of compound **4** can be enumerated as **2,3,4M6-1**[13] and represents the first example of this configuration in Zn^{II}-Dy^{III} chemistry.

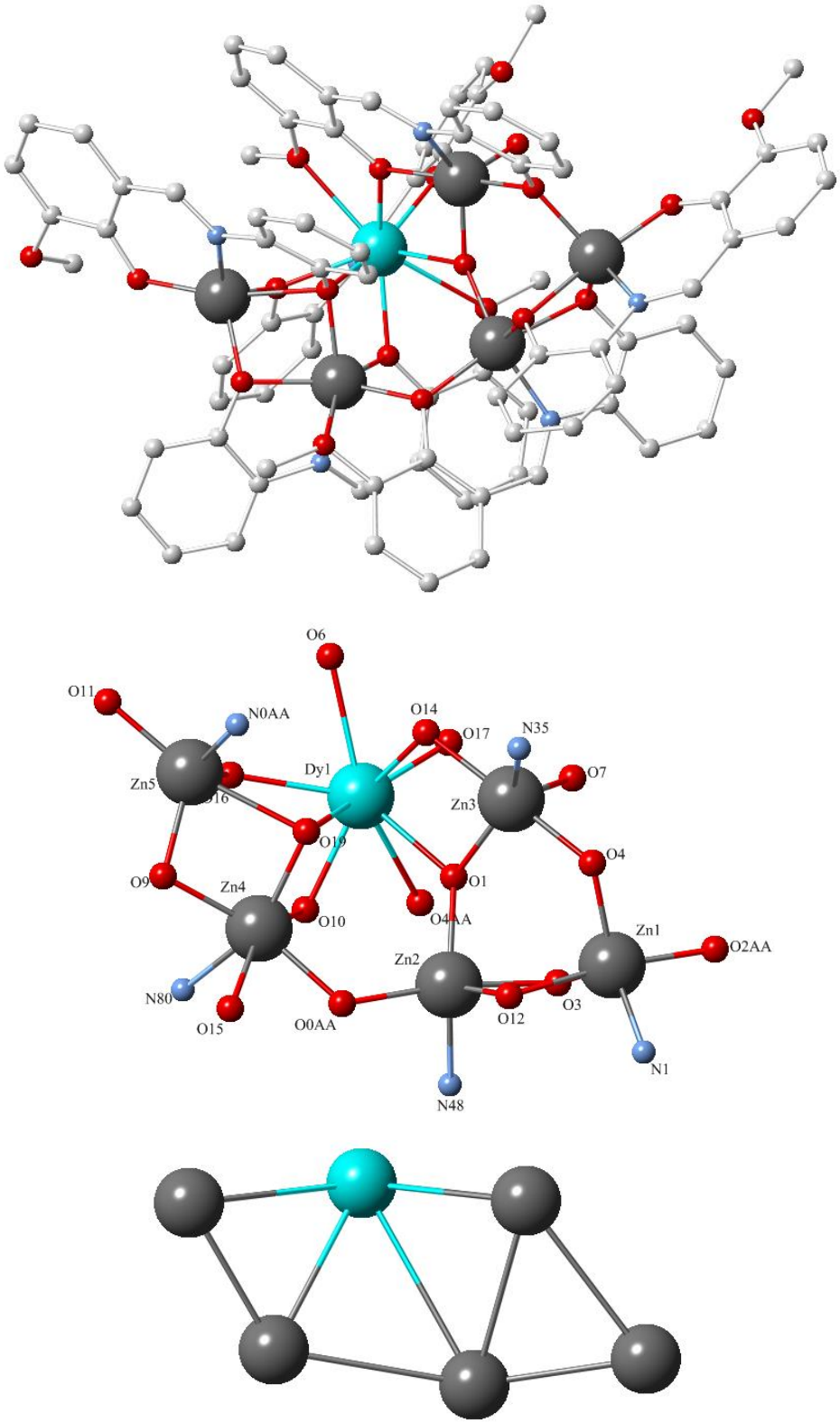

Figure 2.4. The molecular structure of compound **4** (upper) and its core (middle). C, H atoms and lattice molecules are omitted for clarity. The decorated **2,3,4M6-1** motif (lower). Colour code: Zn^{II}, grey; Dy^{III}, light blue; O, red; N, blue.

2.2.2.3 Molecular structure of 7 - 9

Compounds **7** – **9** crystallize in the monoclinic $P2_1/c$ space group and are isostructural, thus only **7** will be further described (Figure 2.5). The asymmetric unit of **7** contains four Zn^{II} ions, two Dy^{III} ions, four doubly deprotonated organic ligands (**L2**), two triply bridging hydroxyl groups, two acetates, three coordinating and one lattice DMF molecule(s). One of the coordination sites of Dy^{III} is disordered with water and a nitrate is present.

The core of **7** can be considered as four fused triangles. Dy2, Zn1, Zn2 and Zn3 are strictly coplanar, while Dy1, Zn4, Zn3 and Zn2 are nearly so. The distorted angle between the two mean planes is 62.39 °. Each organic ligand is chelated to one Zn^{II} ion, forming four neutral metalloligands (Zn**L2**) which are further bridged to neighbouring Zn^{II} and two Dy^{III} ions.

In total each **L2** coordinates to three metal centres; two Zn^{II} and one Dy^{III}, exhibiting a coordination mode analogous to mode I (Figure 2.3). Each hydroxyl group bridges three metal centres, O1 bridges Dy1, Zn2 and Zn4, and O2 bridges Dy2, Zn1 and Zn3, and O1 and O2 are 0.895 and 0.911 Å, respectively above the plane. Each acetate group bridges two metal centres, Dy1 – Zn4 and Dy2, Zn1. Two DMF molecules coordinate to Dy1 and one DMF and one nitrate complete the coordination geometry of Dy2.

Each Zn^{II} ion has a coordination number of six (O_5N) albeit with a distorted octahedral coordination geometry. Each Dy^{III} ion coordinates to eight oxygen atoms. From SHAPE software,[339] the geometry of Dy(1) and Dy(2) can be best described as between biaugmented trigonal prismatic and triangular dodecahedral [S(P) values 1.763 and 1.868, respectively] and biaugmented trigonal prism [S(P) value 1.626], respectively. There are four $Zn^{II}\cdots Dy^{III}$ distances between 3.3598(10) Å - 3.5333(10) Å and four $Zn^{II}\cdots Zn^{II}$ distances 3.1216(12) Å - 3.354(12) Å. The lattice DMF molecule forms strong H-bonds with the two hydroxyl groups.

No other supramolecular interactions (H-bonds or stacking) can be found between neighbouring entities. According to the ***ND*k-m** topological representation,[13,340] the core of compound **7** can be enumerated as **2,3,4M6-1**.[13] A literature survey reveals that the same motif with the same M^{II}/Ln^{III} ratio can be seen in Ni^{II}-Ln^{III} [343] and Co^{II}-Ln^{III} [344] chemistry.

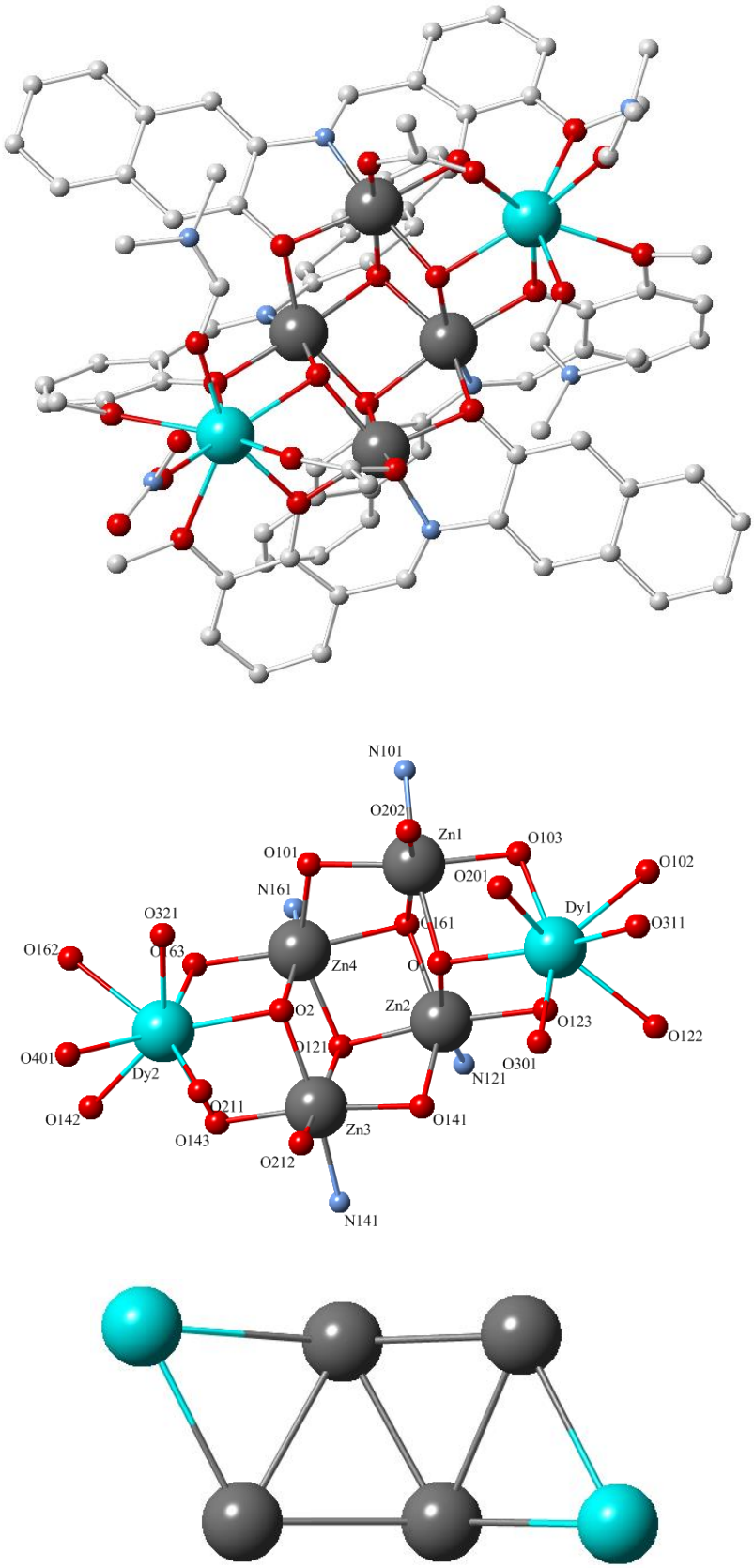

Figure 2.5. The molecular structure of compound **7** (upper) and its core (middle). C, H atoms and lattice molecules are omitted for clarity. The decorated **2,3,4M6-1** motif (lower). Colour code: Zn^{II}, grey; Dy^{III}, light blue; O, red; N, blue.

2.2.2.4 Molecular structure of 10 - 12

Compounds **10** – **12** crystallize in the monoclinic $P2_1/n$ space group and are isostructural, thus only **10** is further described (Figure 2.6). The asymmetric unit contains one Zn^{II} ion, one Dy^{III} ion, one doubly deprotonated organic ligand (H**L3**), one carbonate, one nitrate and one methanol molecule.

The main core of **10** can be considered as two Zn-Dy pairs bridged by two carbonate groups. The four metal centres are situated in a plane (torsion angle Zn1 – Dy1 – Dy1 – Zn1 is 0 ˚). Each organic ligand is chelated to the Zn^{II} ion via the two imino N atoms and the two phenoxide O atoms and to the Dy^{III} ion via the two methoxido and two phenoxide O atoms (Figure 2.3). The carbonate group bridges the two Dy^{III} ions via oxygen O3 and coordinates to Zn1 and the nitrate group is chelated to the Dy^{III} ion.

The distorted octahedral geometry (O_4N_2) of the Zn^{II} ion is completed by the oxygen atom of a methanol molecule. The coordination number of the Dy^{III} ion is completed by one chelated nitrate. From SHAPE software,[339] the geometry of Dy(1) can be best described as spherical capped square antiprism [S(P) 2.489]. There is one $Zn^{II}\cdots Dy^{III}$ distance at 3.446(2) Å and one $Dy^{III}\cdots Dy^{III}$ distance at 4.007(2) Å. The central OH group of the organic ligand remains protonated and forms a strong H-bond with an oxygen atom of a carbonate group of a neighbouring $Zn^{II}_2Dy^{III}_2$ entity forming a two-dimensional (2D) H-bonded framework, which extends perpendicular to the *xy* plane.

According to the ***ND*k-m** topological representation,[13,340] the main core of compound **10** can be enumerated as **1,2M4-1**[13] and it is the fifth example of the motif in Zn^{II}-Dy^{III} chemistry.[72,325,330,332] A comparison between the H_3**L3** ligand, which was used for the synthesis of **10** and the Schiff base ligands used for the synthesis of the previously reported compounds, the same **1,2M4-1** motif indicates that despite the existence of the central OH group, this type of ligand favours the formation of Zn-Ln dimers which combine via the carbonate unit to the tetranuclear motif.[237]

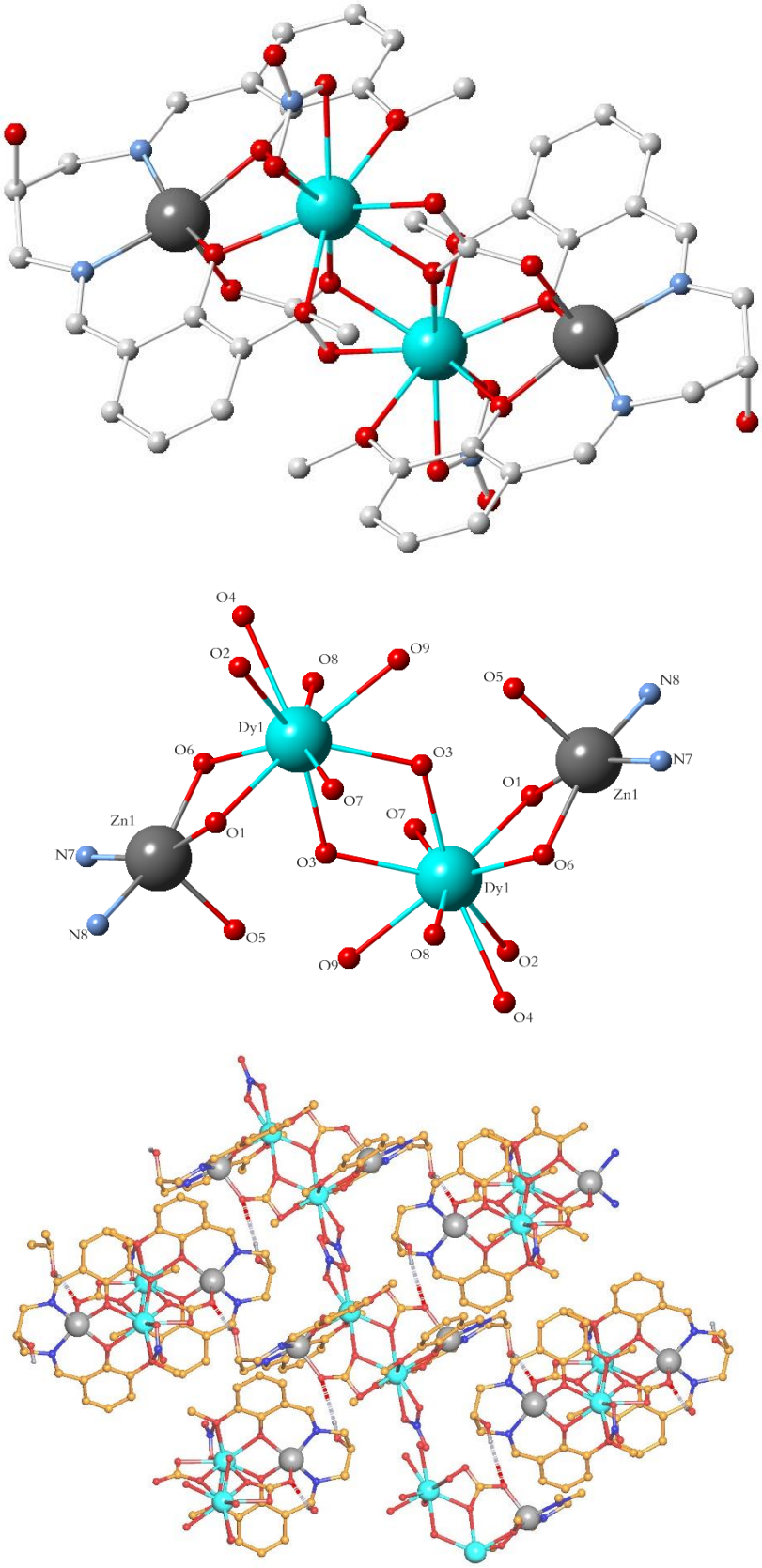

Figure 2.6. The molecular structure of compound **10** (upper) and its core (middle). C, H atoms and lattice molecules are omitted for clarity. The 2D H-bonded framework seen in the crystal structure of **10** (lower). Colour code: Zn^{II}, grey; Dy^{III}, light blue; O, red; N, blue.

2.2.3 Magnetic properties.

Magnetic measurements were made on selected powdered samples of compounds **1**, **7** and **10** to detect any SMM response. In preliminary *ac* measurements at zero field and two frequencies (10 and 1000 Hz) the three compounds showed a similar response, which was only observable by the tail of their *ac* signals (Appendix A, Figure S2.1). A series of new measurements under fields up to 3000 G showed a shift of the signals to a higher temperature but *ac* peaks were not observable for **1** and **10**. In contrast, with the magnetic field $H_{dc} = 0$, *ac* measurement clearly shows the presence of an out-of-phase signal, well-defined peaks were obtained for **7** for frequencies larger than 80 Hz and under a field of 3000 G (Appendix A, Figure S2.2). These measurements are evidence of strong QTM.

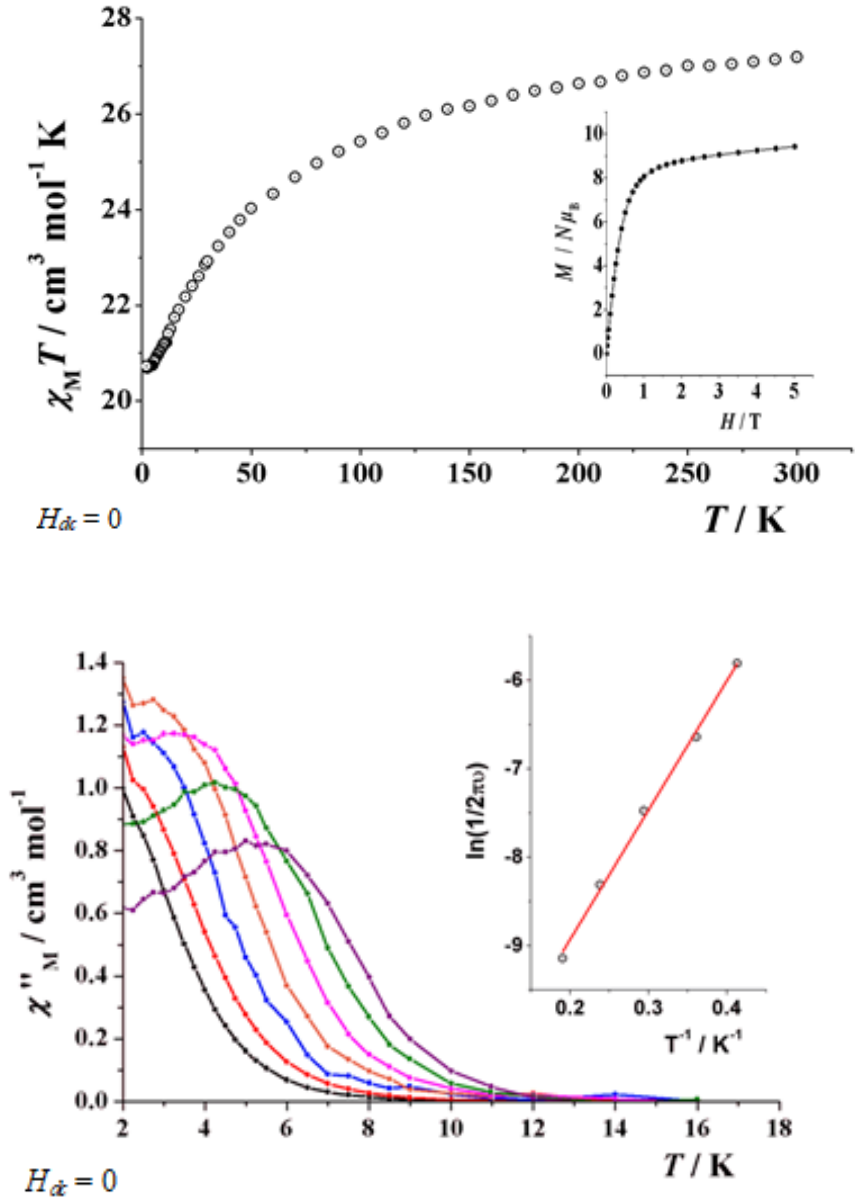

Figure 2.7. $\chi_M T$ product vs. temperature for complex **7** (upper). *ac* susceptibility measurements for **7** at frequencies comprised between 23 and 1500 Hz (lower).

Complementary susceptibility measurements were made for **7**. The $\chi_M T$ product at room temperature is 27.2 $cm^3\,mol^{-1}\,K$, slightly lower than the expected value of 28.3 $cm^3\,mol^{-1}\,K$ for two Dy^{III} cations, (Figure 2.7, upper). On cooling the $\chi_M T$ value decreases monotonically down to a final value of 20.7 $cm^3\,mol^{-1}\,K$ at 2 K. Magnetization experiments show a fast increase of the magnetization and a roughly linear dependence with the applied field in the 2 - 5 T field range. The final value of 9.4 $N\mu_\beta$ (for the two Dy^{III} cations) under the maximum explored field of 5 T is lower than the expected suggesting a moderately high anisotropy, as magnetisation does not saturate.

The *ac* susceptibility measurement in the 80-1500 Hz frequency range show well defined frequency-dependent peaks. An Arrhenius fit of the maxima of the peaks for compound **7** gives an energy barrier of 10.2 cm^{-1} and $\tau_o = 7.1 \cdot 10^{-6}$ s, (Figure 2.7, lower). In the light of the structural data it shows that the two Dy^{III} cations do not interact and are well isolated by the Zn_4 butterfly, compound **7** should be assumed as a Single-Ion Magnet (SIM) with a low barrier for the reversal of magnetization.

The magnitude of the barrier for systems of this kind is sensitive to multiple factors, but the importance of the ligand field and the position of the charged or neutral donors around the lanthanide cation determines whether the spatial arrangement of electronic density fits the ideal oblate-prolate model for the lanthanide cation.[158,345,346]

For the case of Dy^{III}, its oblate electron density will generate larger barriers when negatively charged donors are above and below the radial plane of the cation. For **7** it is far from this situation because the O-phenoxo and O-carboxylate donors (with the shorter Dy⋯O distances) are placed on the same side of the coordination sphere, whereas the other side is occupied by solvent molecules with two Dy⋯O distances larger than 2.5 Å.

Calculation of the direction of the easy axis for the Dy^{III} cations, in low symmetry environments, such as that of **7** (Dy^{III}), which is assumed to be in the $m_j = \pm 15/2$ ground state, can be performed with the MAGELLAN program.[347] The directions are similar, as can be expected from the similar (but not identical) coordination spheres around Dy1 and Dy2. The axes are directed towards the O-phenoxo donors and are inclined at 54.1 º which are not parallel. Both factors in non-ideal arrangements of the charged O-donors around the Dy^{III} cations and the angle between the easy axes contribute to the low energy barrier of the system.

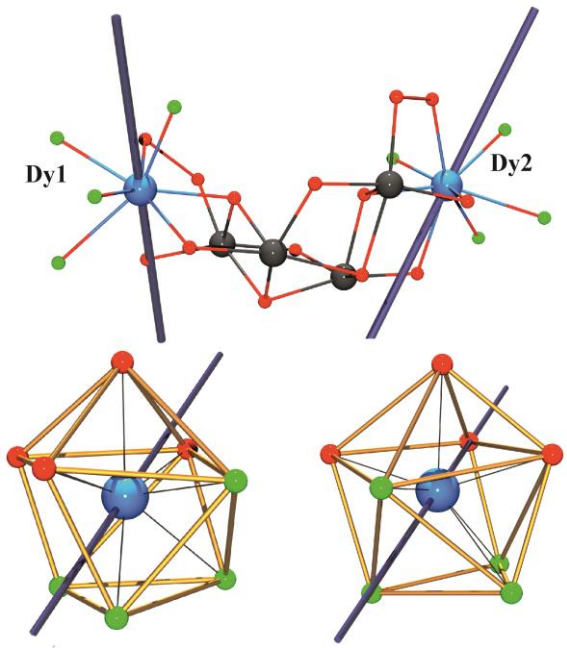

Figure 2.8. The relative position of the easy axis of the two Dy^{III} cations on the core of **7** (upper) and in their DyO_8 coordination spheres (lower). Colour code: red O-atoms corresponds to the O-phenoxo and O-carboxylate donors.

2.2.4 Photoluminescence.

Solution luminescence measurements were made for nine of the Zn^{II}-Ln^{III} PCCs (**4 - 12**) in DMF and each of the three ligands. The spectra of the Dy^{III} containing species (Figure 2.9) show broad ligand-based emissions with some metal contribution (resulting in red-shift of the profile) which dominates for each of the three compounds. Though each of these species has distinctly different absorption spectra, all three emit near 560 nm (**4**: λ_{em} = 560 nm, **7**: λ_{em} = 567 nm, and **10**: λ_{em} = 555 nm) correlating with the $^4F_{9/2}$ - $^6H_{13/2}$ transition that accompanies Dy^{III} emission. The broad nature of these signals indicates a significant ligand contribution to these emitters.

Compounds **4 - 9** which contain **L1** and **L2** exhibited similar behaviour (Appendix B, S2.21). However, Tb^{III} and Eu^{III}-containing complexes supported by **L3** (Appendix B, S2.21-S2.23) displayed more typical emission spectra for lanthanide species with multiple narrow emission bands correlating to specific transitions within a broad ligand emission peak. In particular, **11** exhibits an emission spectrum centred at 550 nm, comparable to that described by Murugesu et al. in 2009 with discrete $^5D_4$ – $^7F_6$, $^5D_4$ - $^7F_5$, $^5D_4$ – $^7F_4$, $^5D_4$ – $^7F_3$ transitions.[318] Emission in the NIR region was not observed below 1100 nm for any of the nine compounds tested.

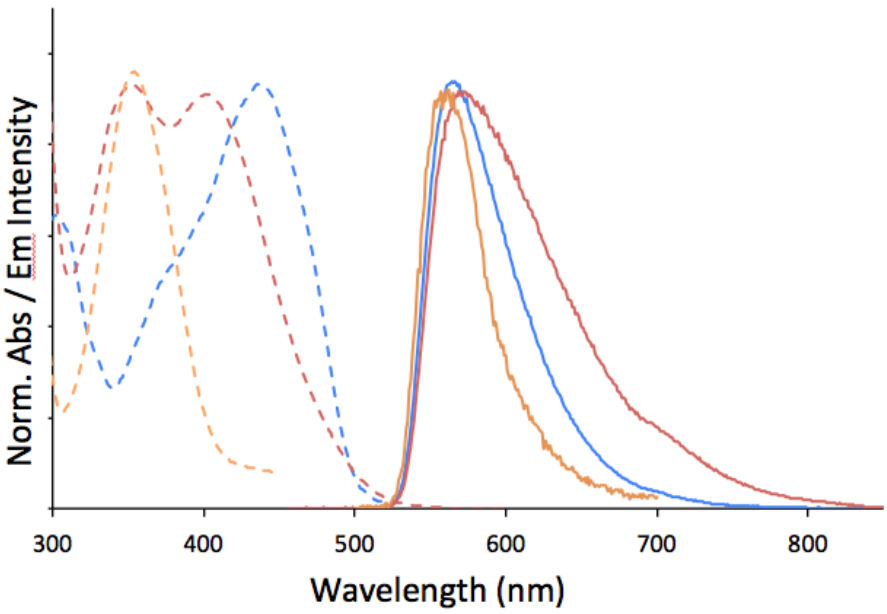

Figure 2.9. Normalised absorption (dashed line) and emission spectra (solid line) of compounds **4** (blue; λ_{ex} = 440), **7** (red; λ_{ex} = 400), and **10** (yellow; λ_{ex} = 355) recorded in DMF (1 x 10^{-5} mol dm^{-3}, 298 K).

2.2.5 Topological aspects.

Many Zn^{II}-Ln^{III} PCCs have been reported in the literature, but a significant number of these are di or tri-nuclear species. There are fewer reported examples with a core nuclearity above four, these higher nuclearity examples are shown in Appendix A (Table S2.1) with their core topology (Figure 2.11) and ligand (Figure 2.10). Recently, two Zn^{II}-Ln^{III} PCC with a core nuclearity of 30 were reported, showcasing the current interest in Zn^{II}-Ln^{III} chemistry.[5,28] The most common core nuclearity reported for Zn^{II}-Ln^{III} PCCs is four, with several topological motifs which are dependent on the structure of the ligand used for their synthesis.

The **1,2M4-1** topology is the most common for Zn^{II}-Ln^{III} PCCs and the supporting ligands share a common structure (Figure 2.10). **1,2M4-1** PCCs are formed in alcoholic solvents (MeOH, EtOH) (Table 2.2, entries 1, 4, 9 and 31), the Zn^{II} ions are co-ordinated between the imine/secondary amine and deprotonated hydroxyl groups, while Ln^{III} ions are bound to the deprotonated hydroxyl and methoxy groups, which form a $[Zn^{II}Ln^{III}(\mathbf{LX})]^{3+}$ unit. In these examples, counter-ions such as $[Cl]^-$ or $[CO_3]_2^-$ (from atmospheric CO_2) bridge between two $[Zn^{II}Ln^{III}(\mathbf{LX})]^{3+}$ units to form the **1,2M4-1** core as a dimer. The coordination sphere is completed by counter-ions such as $[NO_3]^-$ or $[OAc]^-$ for charge balance and solvent molecules.

Of the Schiff base ligands employed in Zn^{II}-Ln^{III} PCC synthesis, few display a core nuclearity above five and tetranuclear Schiff base PCCs are the most frequently reported. This may be due to the many co-ordinating groups usually present and the rigid structural fragments. The **2,3M4-**

1 motif is a very common motif in Zn^{II}-4f chemistry and in this thesis two variations of this topology are reported.

The second most widespread motif in hexanuclear 3d-4f chemistry is **2,3,4M6-1**. According to a survey in Cambridge Structural Database (CSD),[341] 33 crystal structures[55,82,100,115,116,343,348–352] possess this motif. The first reported 3d-4f PCCs with this topology can be found in a family of $Mn_4^{III}Ln_2^{III}$ compounds, where Ln is Gd, Tb, Y, reported in 2008 by Oshi et al.[348] Other examples were reported in Mn-4f, [116,349,350] Ni-4f,[55,343] Co-4f,[115,344,351,352] and Fe-4f [82] chemistry. Although this topology is very common in 3d-4f PCC chemistry, compounds **4 - 9** are the first examples of the **2,3,4M6-1** motif in Zn^{II}-Ln^{III} PCC chemistry.

In the present study, despite using organic ligands that offer similar pockets, a range of topologies were obtained and the unexpected involvement of the fixed carbonate group does not allow for a complete systematic study.

2.3 Conclusion

Reactions of zinc (II) and lanthanide (III) salts with various Schiff bases (H_2**L1** - H_3**L3**) and a variety of reaction conditions yield four families of Zn^{II}-Ln^{III} PCCs with robust and previously unobserved topologies. The most notable of the PCCs reported are the first examples of Zn^{II}-Ln^{III} PCCs with the **2,3,4M6-1** core topology (**4 - 9**). Magnetic studies reveal the SIM behaviour of compound **7** and luminescence studies indicate a significant ligand contribution to the emitters.

Despite incorporating organic ligands that offer similar coordination pockets in similar synthetic ratios, products with a range of nuclearities and motifs are obtained, suggesting that more systematic studies are required to fully understand the growth of such crystalline species and to target specific products. When the reaction that yielded compound **4** was repeated under reflux, instead of room temperature, two different type of crystals were obtained with the general formulas $[Zn^{II}_4Dy^{III}_7(OH)_4(O_2)_2(\mathbf{L1})_8Cl_4(H_2O)_4]Cl_5$ (**13**) and $[Zn^{II}_6Dy^{III}_4(OH)_2(\mathbf{L1})_{10}(MeOH)_2(H_2O)_4]Cl_2$ (**14**) which core topologies are enumerated **2,2,3,3M10-1** and **2,4,4,4M11-1** respectively (Appendix A, Figures S2.3 and S2.4). However, these PCCs could not be isolated independently which highlights the limitations of the applied synthetic strategy.

Future studies should be focused in the following directions:

a) To extend the synthetic study to different 3d metals, ligands, co-ligands and ratios to obtain higher nuclearity 3d-Ln^{III} PCCs.

b) To test the ligand pockets and coordination environment selection in the topological approach to synthetic strategy.[13,353]

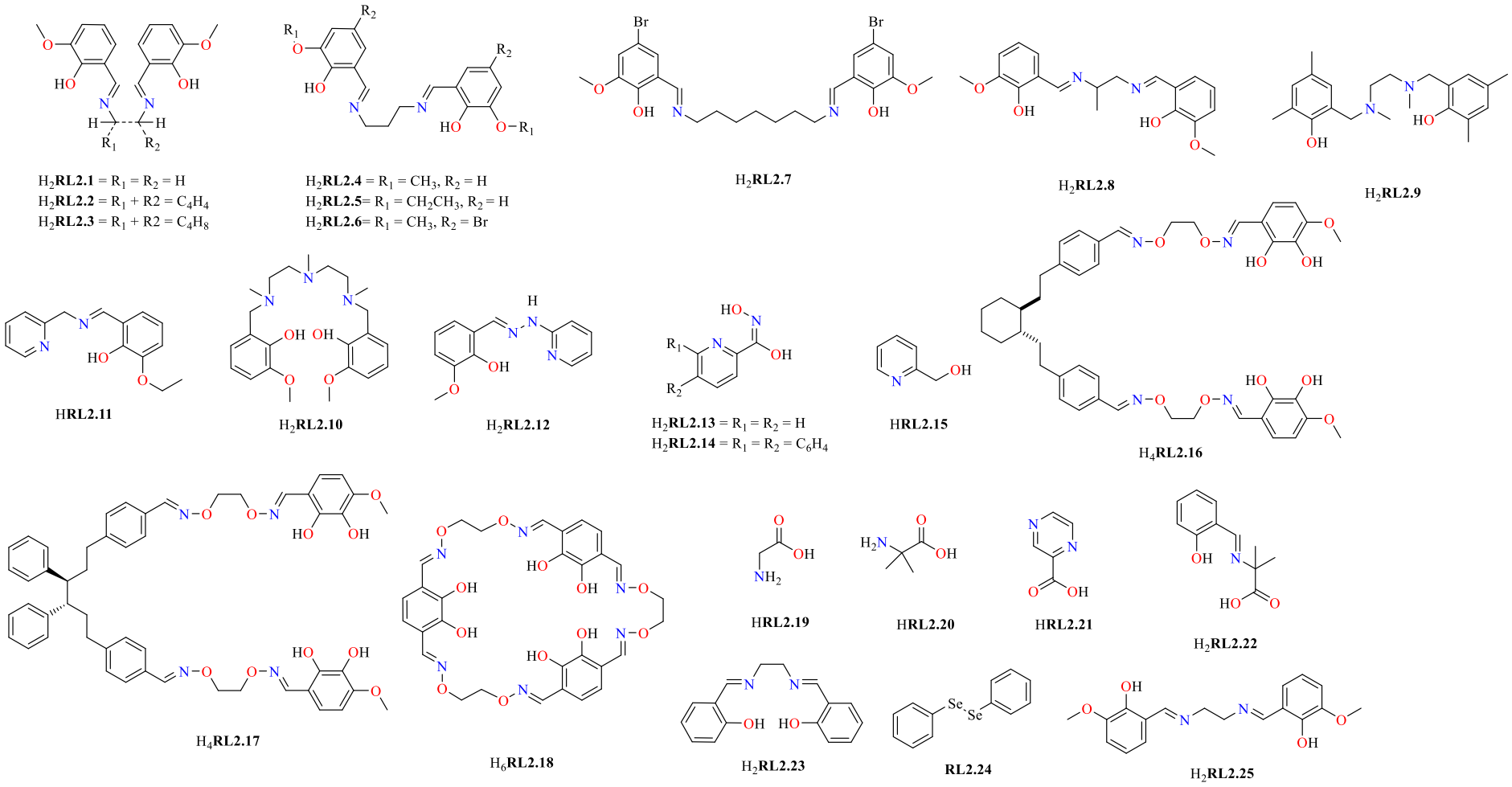

Figure 2.10. The organic ligands used for the synthesis of previously reported Zn^{II}-Ln^{III} PCCs.

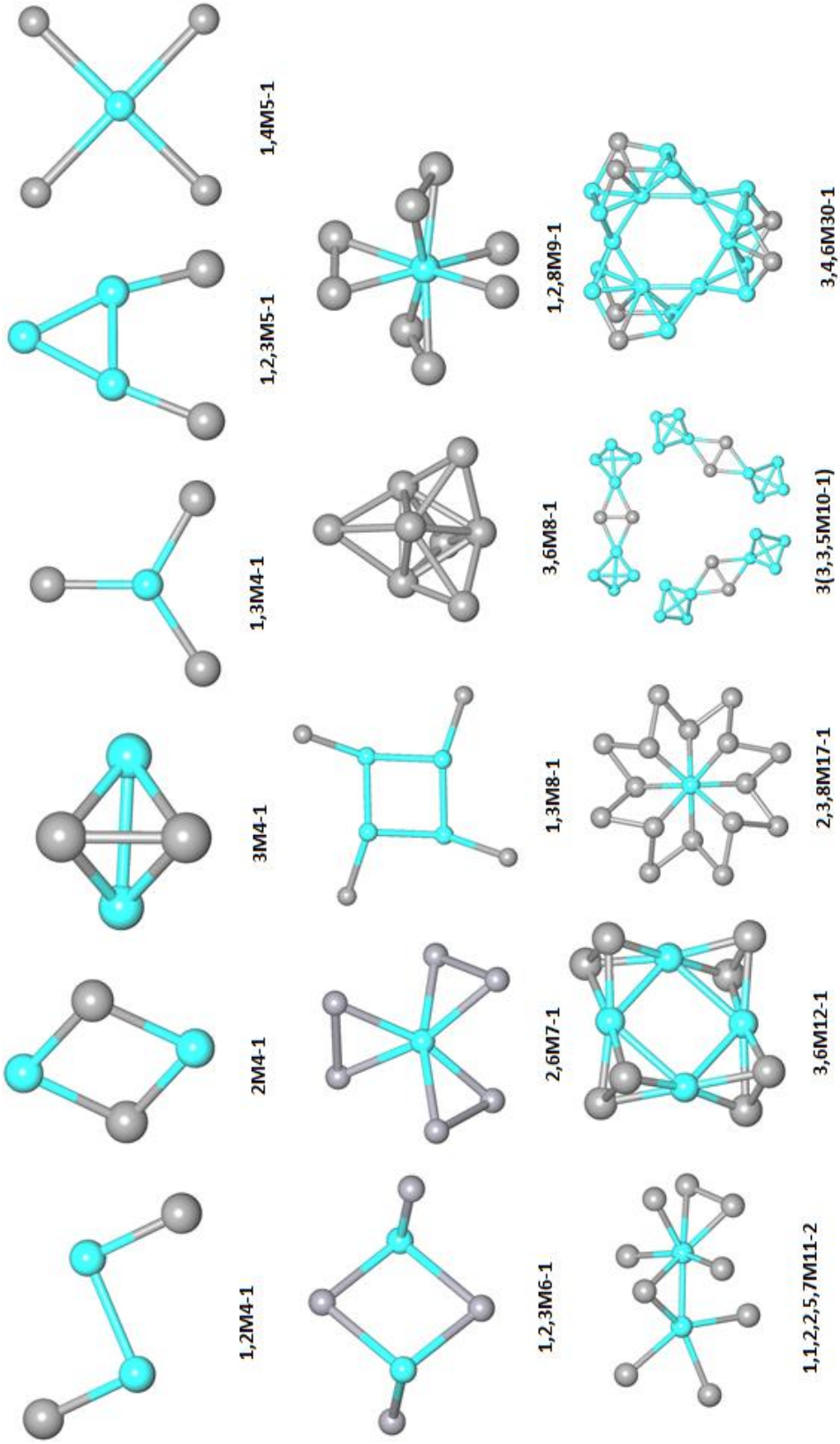

Figure 2.11. The topological representations of all known Zn^{II}-Ln^{III} PCCs with nuclearities of four or higher.

Chapter 3: Synthesis, characterization, magnetic properties and topological aspects of isoskeletal hexanuclear $Co^{II}_4Ln^{III}_2$ PCCs possessing a 2,3,4M6-1 topology

Abstract: The employment of H_2**L1** with $Co(NO_3)_2{\cdot}6H_2O$ and $LnCl_3{\cdot}x(H_2O)$ afforded a family of hexanuclear heterometallic polynuclear coordination clusters formulated $[Co^{II}_4Ln^{III}_2(\mu_3\text{-}OH)_2(\mathbf{L1})_4Cl_2(NO_3)_2(MeOH)_4]{\cdot}3(Et_2O)$ where Ln is Y (**15**), Gd (**16**), Dy (**17**) and Tb (**18**). All the compounds are stable in solution as confirmed by electrospray ionization mass spectrometry studies. The topology of these compounds can be enumerated **2,3,4M6-1**. The use of H_2**L5** with $Co(NO_3)_2{\cdot}6H_2O$ and $DyCl_3{\cdot}x(H_2O)$ afforded a $Co^{II}_4Ln^{III}_2$ PCC which is isoskeletal to compounds **15** – **18** and is formulated $[Co^{II}_4Dy^{III}_2(\mu_3\text{-}OH)_2(\mathbf{L5})_4Cl_2(NO_3)_2(MeOH)_4]$ (**19**). Magnetic studies performed in the temperature range 1.8 – 300 K show that compound **17** shows a slow magnetic relaxation.

3.1 Introduction

Lanthanides, especially dysprosium (III),[354,355] and cobalt (II)[15,356] based PCCs have been widely used to gain access to PCCs behaving as SMMs. The first example of a Co^{II}-Ln^{III} SMM supported by a Schiff base ligand was a trinuclear $Co^{II}_2Gd^{III}$ complex, with a U_{eff} of 27 K and τ_0 of $1.7\text{x}10^{-7}$ s, which was reported by Chandrasekhar.[193] The combination of Co^{II} and Ln^{III} ions with Schiff base ligands has resulted in a variety of low nuclearity species (including $Co^{II}Ln^{III}$,[357] $Co^{II}_2Ln^{III}$,[195,358] and $Co^{II}_2Ln^{III}_2$[2,77,359]) which display SMM behaviour.

There has been few Schiff base supported Co^{II}-Ln^{III} PCCs, with a nuclearity above five, that show SMM behaviour and all of the reported examples of SMM behaviour have been exclusive to the Dy^{III} analogues. The synthesis of these PCCs has traditionally relied upon serendipitous assembly, with Schiff base ligand mixed with Co^{II} and Ln^{III} salts in alcohol or acetonitrile solution and subsequently crystallised.

These examples include a "chair-like" $Co^{II}_2Dy^{III}_4$ PCC (**2,3,4M6-1**) which displays a U_{eff} of 41.9 K and a τ_0 of $1.21 \text{ x } 10^{-7}$ s. Another "chair-like" $Co^{II}_2Dy^{III}_4$ (**2,3,4M6-1**) PCC synthesised from a structurally similar ligand (H_2**CL2.1** and H_2**CL2.2** respectively) and pivalic acid, displays a slightly lower U_{eff} value of 32.4 K and a τ_0 of $4.2 \text{ x } 10^{-7}$ s.

The remaining examples of Co^{II}-Dy^{III} Schiff base PCCs, which display SMM behaviour, are formed from ligands that do not share similar compartments and whose core topologies are unrelated. A dodecanuclear $Co^{II}_2Dy^{III}_{10}$ ring (**2M12-1**) PCC supported by H_2**CL2.3** displays two relaxation pathways, one with a longer relaxation time of $\tau_0 = 1.13 \text{ x}10^{-4}$ s and a lower energy barrier $U_{eff} = 4.3$ K and the other a higher energy barrier of $U_{eff} = 25$ K and a shorter relaxation

time of τ_0 of 1.13 x10^{-4} s. The final example, a $Co^{II}_3Dy^{III}_4$ PCC disk (**3,6M7-1**) formed from H**L4**, displays out-of-phase signals below 4 K.

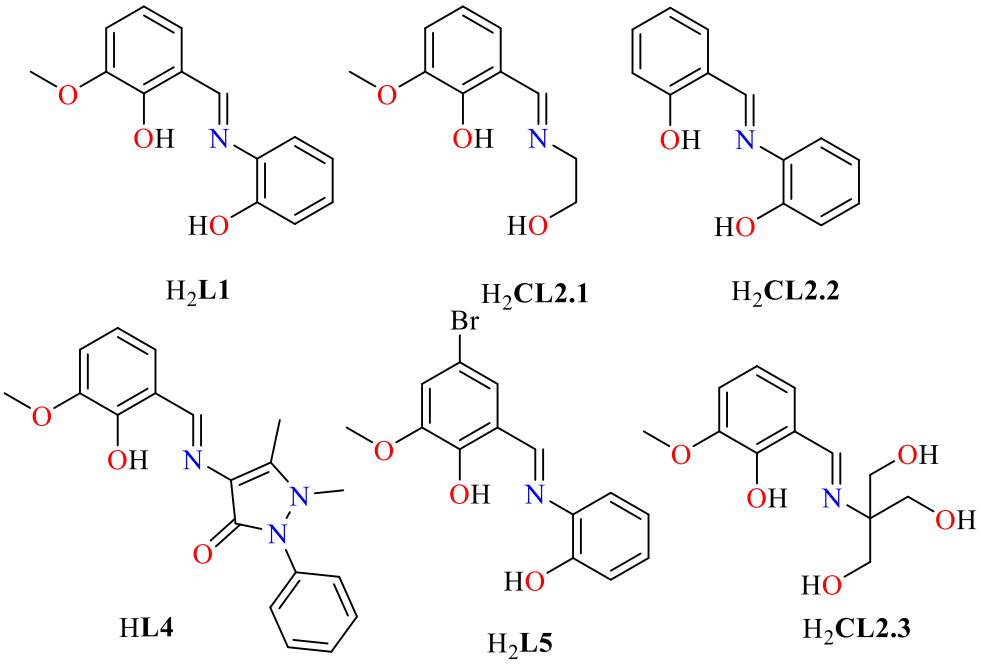

Figure 3.1. Schiff base ligands used for the synthesis of high nuclearity Co^{II}-Dy^{III} PCCs.

Though H_2**L1** has been used for the synthesis of a variety of 3d,[360,361] 4f [362] and 3d-4f PCCs,[2,50,116,343,363–365] the only previous example of H_2**L1** being combined with Co^{II} and Dy^{III} ions resulted in the formation of a defect-dicubane $Co^{II}_2Dy^{III}_2$ which displays SMM behaviour with a blocking temperature of 22 K.[2] With the intention of synthesising high nuclearity Co^{II}-Ln^{III} PCCs which display SMM behaviour, H_2**L1** was employed with $Co(NO_3)_2{\cdot}6H_2O$ and $LnCl_3{\cdot}x(H_2O)$. This combination resulted in a family of hexanuclear heterometallic PCCs formulated as $[Co^{II}_4Ln^{III}_2(\mu_3\text{-}OH)_2(\mathbf{L1})_4Cl_2(NO_3)_2(MeOH)_4]{\cdot}3(Et_2O)$, where Ln is Y (**15**), Gd (**16**), Dy (**17**) and Tb (**18**), in very good yields. For structural purposes, the employment of H_2**L5** (Figure 3.1),[366] under similar reaction conditions afforded an isoskeletal compound formulated as $[Co^{II}_4Dy^{III}_2(\mu_3\text{-}OH)_2(\mathbf{L5})_4Cl_2(NO_3)_2(MeOH)_4]$ (**19**). Topological aspects and magnetic properties of these compounds are discussed.

3.2 Results and discussion

3.2.1 Molecular structures of 15 - 18

Single-crystal XRD studies show three Et_2O molecules[367,368] could be successfully refined in the lattice of **16** and **17**. However, these samples are air sensitive and over time lose their crystallinity. Compounds **15-18** were further characterised by EA (chapter eleven), TGA (Appendix B, S3.5) and ESI-MS (Appendix B, S3.1-3.4).

Compounds **15 - 18** crystallize in the monoclinic space group $P2_1/c$ and are isostructural, thus only compound **16** is discussed further. Four Co^{II} and two Gd^{III} cations form a twisted "boat-like" core with Co^{II} ions occupying the four central body positions and the two Gd^{III} ions occupying positions in the "bow" and "aft" (Figure 3.2), this configuration will be assigned the notation (1Ln: 4Co: 1Ln).

The hexanuclear core is supported by two μ_3-OH groups between the Gd^{III} ion and the two nearest Co^{II} ions. Each of the four organic ligands adopts the same coordination mode (Figure 3.3) and each is bonded to one Gd^{III} and two Co^{II} ions. Each ligand is chelated to a Co^{II} centre through one imino and two phenoxido oxygen atoms, forming a "metalloligand" which is further chelated to a Gd^{III} through a phenoxido and methoxido oxygen atom and another Co^{II} via the phenoxido oxygen atom of the aminophenol moiety. Each hydroxyl group bridges two Co^{II} and one Gd^{III} centres and the angles are within the range 102.16(12) ° - 106.05(13) °.

The coordination environment of Co2 and Co4 is fulfilled by a $[Cl]^-$ ion. All Co centres adopt an essentially distorted octahedral geometry, where the Bond Valence Sum (BVS) analysis is indicative of oxidation state II (2.082, 1.900, 2.040 and 1.913 for Co1, Co2, Co3 and Co4, respectively).

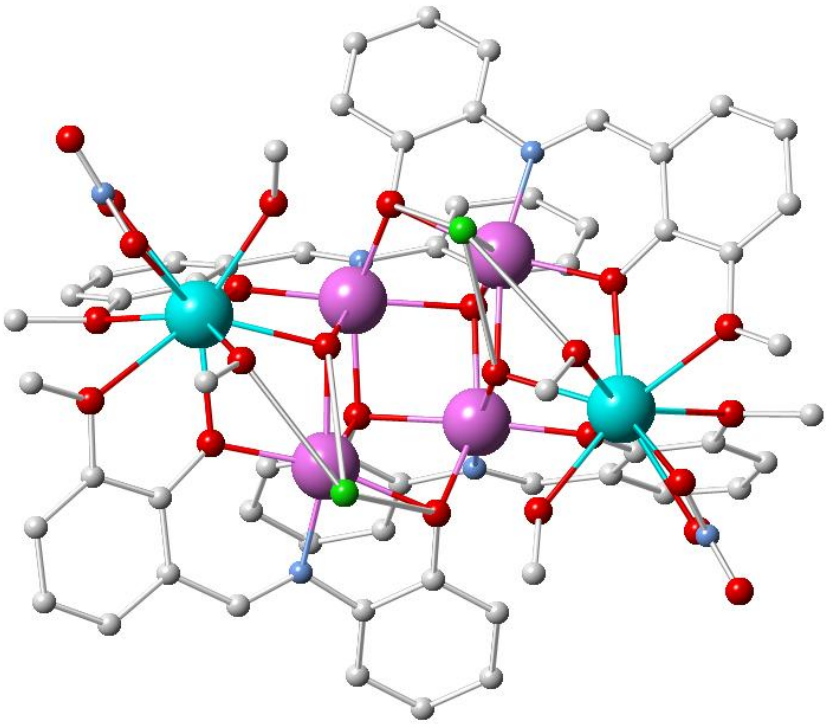

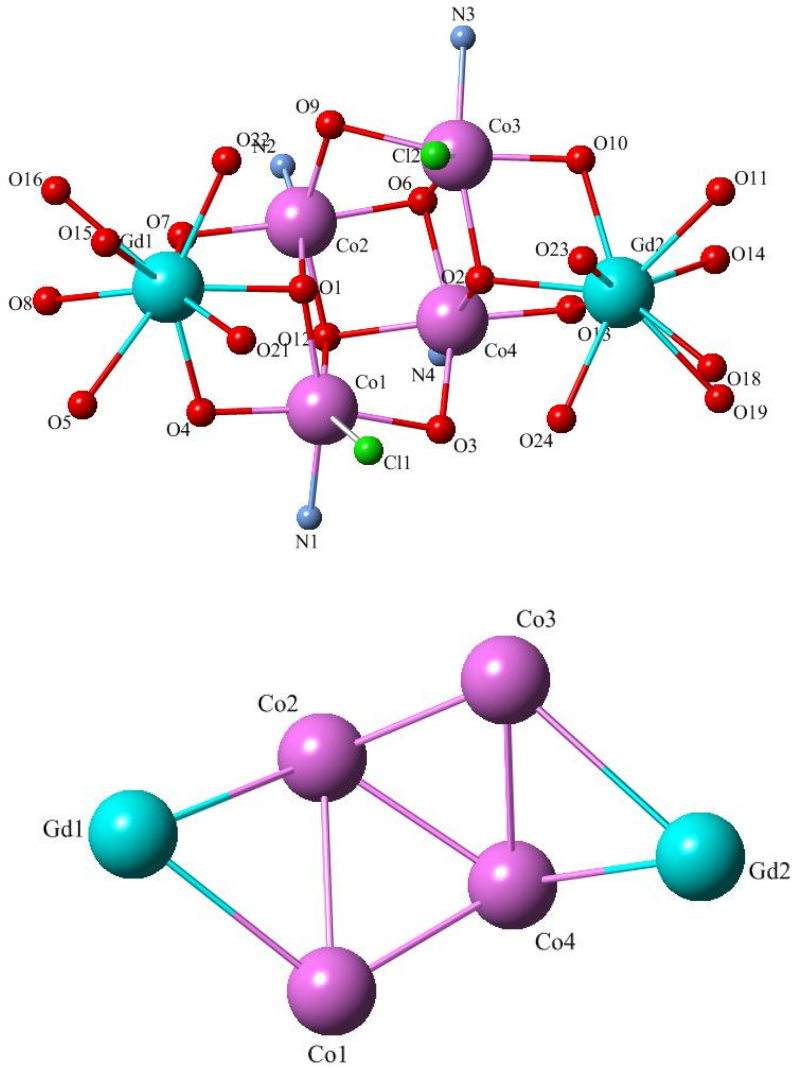

Figure 3.2. The molecular structure of compound **16** (upper). The core of compound **16** (middle) Co1 - Co4 shown in the body positions. Gd1 shown occupying the "bow" and Gd2 the "aft". Representation of **2,3,4M6-1** core of compound **16** (lower). Colour code: Gd^{III}, light blue; Co^{II}, pink; C, yellow; N, pale blue; O, red; Cl, green Hydrogens omitted for clarity

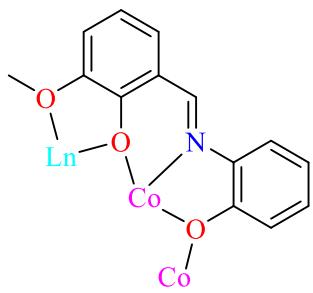

Figure 3.3. The coordination mode of H_2**L1** found in **15 - 18**.

The coordination number of each Gd^{III} ion is nine. Using SHAPE software[339] the geometry of both Gd^{III} ions can be described as capped square antiprism with an S(P) agreement factor of

1.349. There are four $Gd^{III}\cdots Co^{II}$ distances within the range 3.4745(7) - 3.5837(7) Å and four $Co^{II}\cdots Co^{II}$ distances in the range 3.148 (7) -3.366(7) Å. The distance from the "bow" and "aft" between Gd^{III} ions is 7.680 Å. There is no hydrogen bonding between adjacent entities, with the spacing being well defined.

3.2.2 Topological aspects

According to this **NDK-m** nomenclature, the core of **15** - **19** can be enumerated as **2,3,4M6-1** (Figure 3.3). A literature survey indicates that the first example of this topology was found in a heterometallic Co_2Na_4 compound.[369] The first 3d-4f PCCs of this topology were a family of $Mn^{III}_4Ln^{III}_2$ PCCs (2Mn : 2Ln :2Mn) supported by H_3**RL3.1,** which were reported in 2008 by Oshi et al.[348] Since then, few organic ligands (Figure 3.4) have been used for the synthesis of a several of 3d-Ln^{III} PCCs with this topology.

Ligands H_3**RL3.2**, H_3**RL3.3** and H_3**RL3.4** gave access to $Mn^{II}_2Ln^{III}_4$ (1Mn: 4Ln: 1Mn)[116] and $Mn^{III}_2Mn^{II}_2Ln^{III}_2$ (1Ln: $1Mn^{III}$: $2Mn^{II}$: $1Mn^{III}$: 1Ln).[350] In 2009, N-butyl-diethanolamine (H_2**RL3.5**) was used to isolate a $Mn^{IV}_2Ce^{IV}_4$ (1Mn: 4Ce: 1Mn)[349] PCC, while recently its use has resulted in the formation of a $Fe^{III}_4Dy^{III}_2$ (2Fe : 2Dy : 2Fe) PCC.[82] Ligands H_3**RL3.8** and H_2**L1** afforded $Ni^{II}_4Ln^{III}_2$ (1Ln : 4Ni : 1Ln)[343] and (2Ni : 2Dy : 2Ni)[55] PCCs respectively.

More recently, four series of $Co^{II/III}$-Ln^{III} PCCs that possess the **2,3,4M6-1** topology have been described. The first example is a $Co^{III}_2Dy^{III}_4$ PCC based on the (E)-2-((3-hydroxypropylimino)methyl)phenol ligand (H_2**RL3.7**, Figure 3.4) which displays a slow magnetization relaxation.[351]

The second example is a family of eight $Co^{III}_2Ln_4^{III}$ PCCs constructed from H**RL3.8** (Figure 3.4). The Dy^{III} analogue exhibits slow relaxation of magnetization with a U_{eff} = 3.8 K and τ_0 = 4.8 x 10^{-6} s.[352] The third example is a series of four $Co^{II}_2Ln^{III}_4$ PCCs constructed from ligands H_2**RL3.9** and H**RL3.10** (Figure 3.4) reported by Du et al. in 2014,[115] this example demonstrates the importance of Ln – O – Ln bond angles on the magnetic coupling between the centres. The fourth example is a family of $Co^{II}_2Ln^{III}_4$ PCCs derived from 6,6′-{(2-(dimethylamino)ethyl azanediyl)bis(methylene)}bis(2-methoxy-4-methylphenol) (H_2**RL3.11**, Figure 3.4), which exhibits a slow magnetic relaxation behaviour for the Dy^{III} analogue.[204]

In all four reported families the Co^{II}-Ln^{III} ratio is 2/4 and all four Ln^{III} are close together, unlike the compounds reported in this work (**15** – **19**), (1Ln: 4Co: 1Ln)), where the "bow" and "aft" positions are filled by Co^{II} cations (1Co: 4Ln: 1Co). Compounds **15** – **19** are therefore the first examples of the $Co^{II}_4Ln^{III}_2$ core configuration.

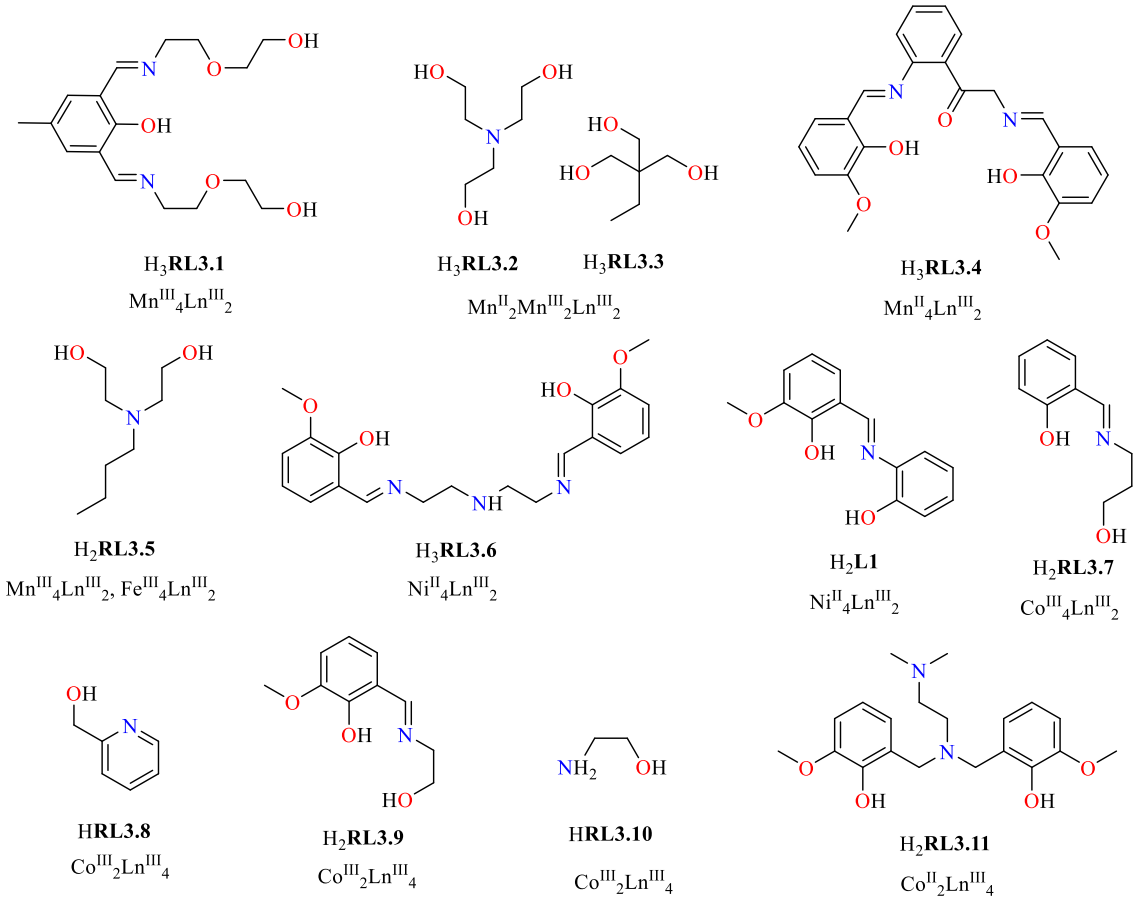

Figure 3.4. The protonated form of the organic ligands used to for the synthesis of 3d-4f PCCs possessing **2,3,4M6-1** topology.

It is worth noting that despite H_2**L1** offering a similar coordination environment to H_2**R3.9**, its employment in Co^{II}-Ln^{III} chemistry resulted in a hexanuclear PCC with 2/4 Co/Ln ratio. This difference may be attributed to the *in situ* synthesis of ligand H_2**RL3.9**.[115]

To further confirm the structural stability of the $Co^{II}_4Ln^{III}_2$ PCCs reported herein, the organic ligand H_2**L5** [366] was applied under similar reaction conditions towards the synthesis of a Co^{II}-Dy^{III} PCC. Ligand H_2**L5** offers similar coordination environment to H_2**L1**. The reaction resulted in compound **19** (Figure 3.5) which is isoskeletal to **15** – **18**.

3.2.3 ESI-MS studies

To confirm the identity of the reported compounds in solution, they were identified by ESI-MS. For **16**, four peaks in the MS (positive-ion mode) were observed at m/z 553.6409, 810.9421, 819.4479 and at m/z 828.8667 which correspond to the fragments, $[Co^{II}_4Ln^{III}_2(\mu_3\text{-}OH)_2(\mathbf{L1})_4(NO_3)_2(MeOH)_2]^{3+}$, $[Co^{II}_2Gd^{III}_2(\mu_3\text{-}OH)_2(\mathbf{L1})_4Cl_2+2H]^{2+}$, $[Co^{II}_2Gd^{III}_2(\mu_3\text{-}OH)_2(\mathbf{L1})_4Cl_2+2H+H_2O]^{2+}$ and $[Co^{II}_2Gd^{III}_2(\mu_3\text{-}OH)_2(\mathbf{L1})_4Cl_2+2H+2H_2O]^{2+}$, respectively (Appendix B, S3.1-S3.4).

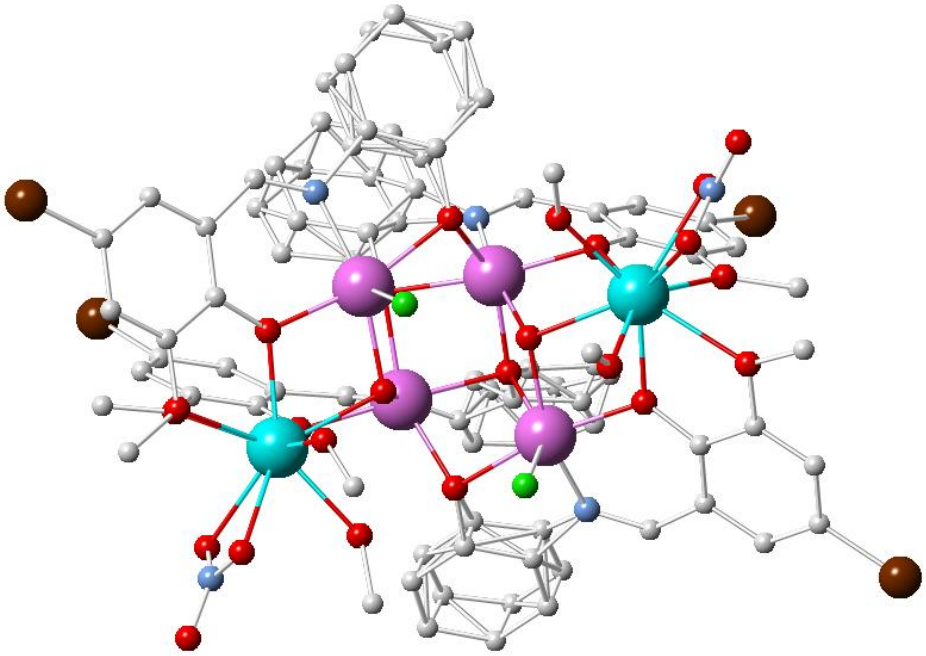

Figure 3.5. The molecular structure of compound **19**. Colour code: Gd^{III}, light blue; Co^{II}, pink; C, white; N, pale blue; O, red; Cl, green; Br, brown. Hydrogen atoms omitted for clarity.

3.2.4 TGA

TGAs of compounds **16** and **18** (Appendix B, S3.5) confirm their solvent sensitivity (Et_2O and MeOH) and degradation of the core begins at 300 ºC and 260 ºC, respectively. The final residue at 1000 ºC perfectly corresponds to a mixture of metal CoO/Gd_2O_3 (34.10% expected - 34.22% found) and CoO/Tb_4O_7 (33.31% expected - 33.22% found) oxides.

3.2.5 Magnetic studies

Variable-temperature *dc* magnetic susceptibility data was collected for compounds **15** - **18** in the temperature range 1.8 – 300 K in an applied field of 0.1 T. The data is shown as $\chi_M T$ vs. T plots in Figure 3.6. The $\chi_M T$ product of compound $Co^{II}{}_4Y^{III}{}_2$ (**15**) has a room temperature value of 11.13 $cm^3\ mol^{-1}$ K which is typical for four uncoupled high spin Co^{II} ions, but larger than that for four free S = 3/2 spins (χT = 7.50cm^3 K mol^{-1} and g = 2.0) as a result of the presence of a significant spin-orbital contribution in the susceptibility of octahedral high-spin Co^{II}.[15,356,370–373] Upon lowering the temperature the value of $\chi_M T$ gradually decreases and reaches a value of 2.17 cm^3 K mol^{-1} at 1.8 K (Figure 3.6).

In the case of PCCs containing octahedral Co^{II} ions, the decrease of the $\chi_M T$ at low temperature can be attributed to the important spin-orbital contribution and dominant antiferromagnetic interaction between the four paramagnetic centres. The value of $\chi_M T$ at low temperature is low for four non-coupling Co^{II} paramagnetic centres and suggests the presence of antiferromagnetic

interaction between the four paramagnetic centres. The antiferromagnetic interaction is further confirmed by magnetization measurements at 2 - 5 K where the magnetization does not saturate at the high-field limit (5 T) and the experimental value of the magnetization at 2.0 K and 5 T, is 6.12 Nβ, which is low for four non coupled Co^{II} ions (Appendix A, S3.1 and S3.2).[372]

The room temperature $\chi_M T$ value for **16** is 27.94 cm^3 K mol^{-1} which is slightly higher than the expected value for two non-interacting Gd^{III} (free ion; S = 7/2; g = 2)[373] and four Co^{II} centres as in compound **16**. The difference between the $\chi_M T$ value of **16** and **15** at 300 K is 17.51 cm^3 K mol^{-1} which is higher of the theoretical expected for two Gd^{III} ions (15.75 cm^3 K mol^{-1}). This can be justified by the presence of ferromagnetic interaction (in conjunction with antiferromagnetic coupling in Co^{II}_4 core) as well as the small variation of g factor for octahedral Co^{II}. By decreasing the temperature, the $\chi_M T$ product decreases steadily up to a value of 27.15 cm^3 mol^{-1} K at 30 K. Upon lowering to 30 K, a rapid increase of the $\chi_M T$ value is observed indicating the presence of ferromagnetic interaction in **16**.

The temperature dependence difference between the $\chi_M T$ value of **16** and $\chi_M T$ value of **15** (see black stars in Figure 3.6) suggest that the ferromagnetic interaction is operated between the Gd ions and Co_4 core. The field dependence of magnetization of compound **16** confirms the presence of important (non-zero) spin state with a significant component of anisotropy.

The room temperature $\chi_M T$ values for **17** (Co_4Dy_2) and **18** (Co_4Tb_2) (39.62 and 36.46 cm^3 K mol^{-1}, respectively) are slightly higher than the expected values for two non-interacting Dy^{III} ($^6H_{15/2}$ free ion; S = 5/2; L = 5; J = 15/2; g_J = 4/3), Tb ($^7F_6$ free ion; S = 3; L = 3; J = 6; g_J = 3/2) and four Co^{II} centres.[149,163] Similar to the Gd analogue, the temperature dependence of $\chi_M T$ values have a minimum at 25 K and 7 K for **17** and **18**, respectively. Upon a further decrease in temperature, the $\chi_M T$ products increase to reach the values of 44.07 and 33.61 cm^3 K mol^{-1} for **17** and **18**, respectively. This behaviour suggests the presence of some ferromagnetic interaction between Co^{II}_4 core and lanthanides ions in **17** and **18**.

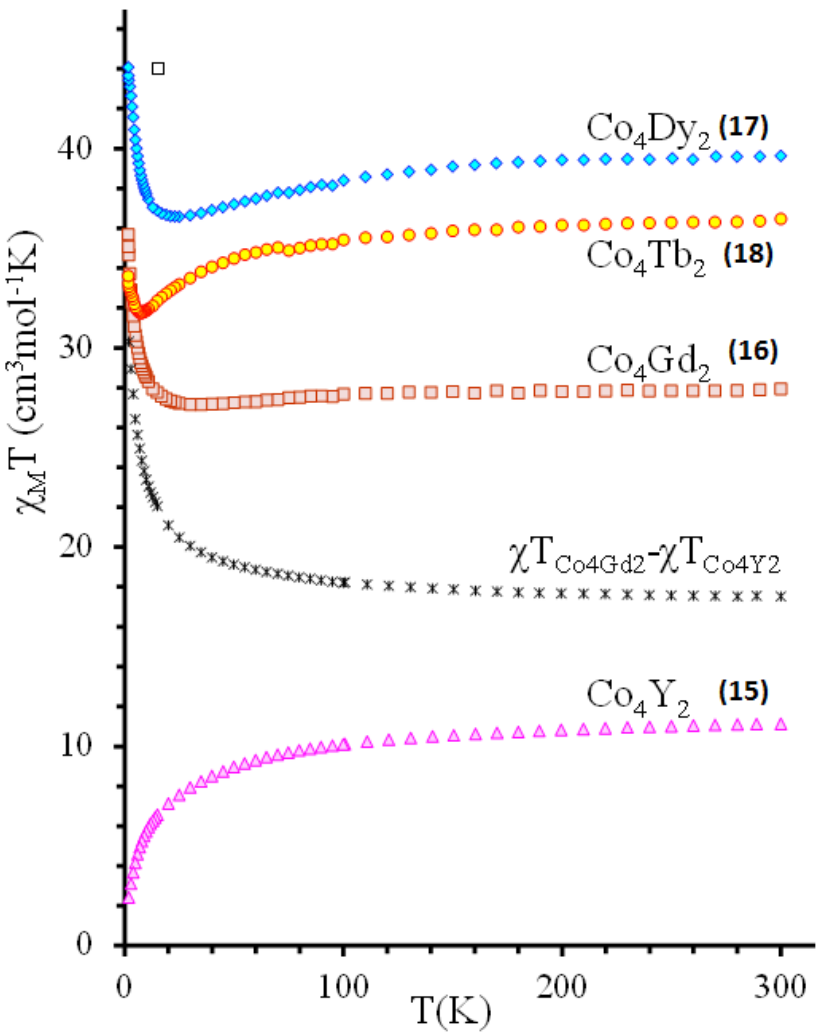

Figure 3.6. Temperature dependence of the $\chi_M T$ product at H_{dc} = 0.1 T for compounds **15** – **18**.

The dynamic properties of **15** - **18** have been investigated using *ac* susceptibility measurements as a function of temperature at varying frequencies and at different temperatures as a function of frequency at 4.0 Oe oscillating field between 1 and 1500 Hz.

Compounds **15**, **16** and **18** do not show an out-of-phase signal at zero *dc* magnetic field. No modifications in out-of-phase susceptibility after applying the *dc* magnetic field (0 - 3.0 T) are detected for **15**, **16** and **18**. In the case of compound **17**, at H_{dc} = 0, the magnetic field *ac* measurement clearly shows the presence of an out-of-phase signal χ'' in *ac* susceptibility with strong temperature and frequency dependence (Figure 3.7).

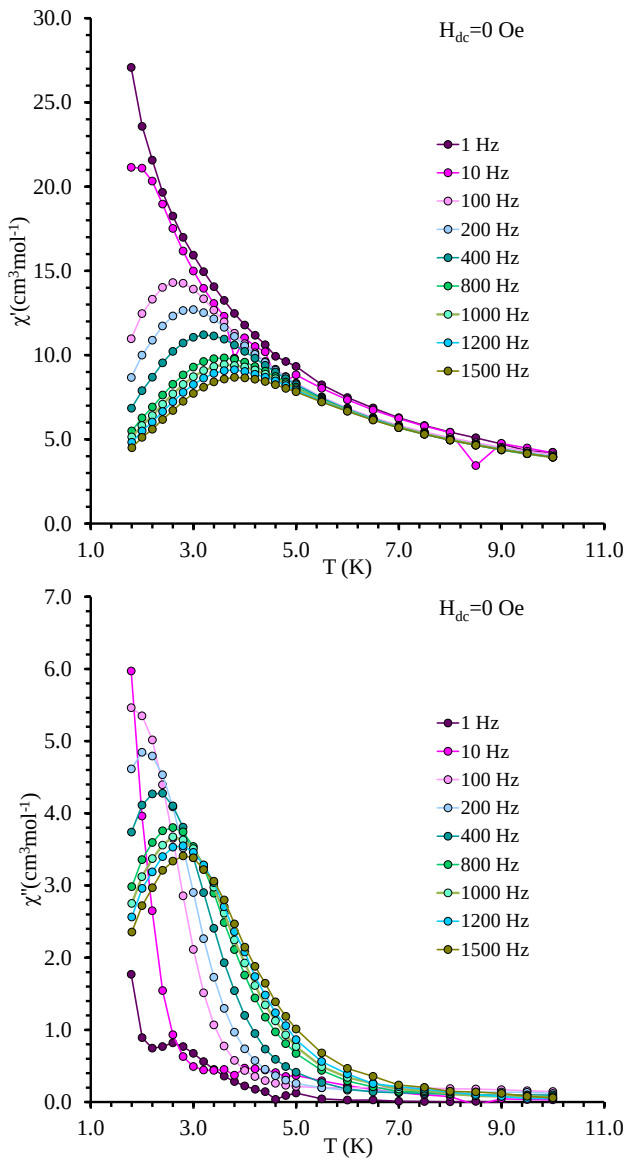

Figure 3.7. Temperature dependence of the in-phase (χ') (upper) and out-of-phase (χ'') (lower) *ac* susceptibility for **17** at indicated frequencies at zero applied *dc* field.

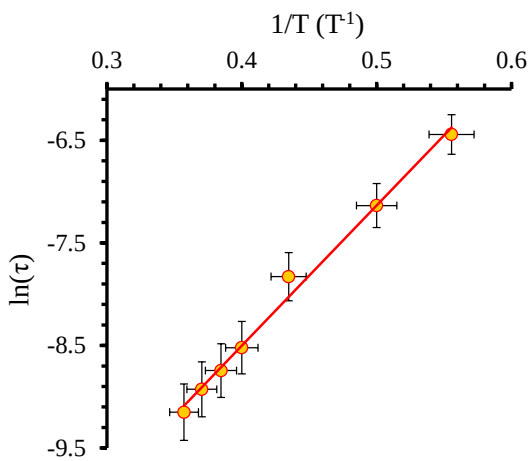

Figure 3.8. Arrhenius plot U_{eff} (**17**) = 13.4 K (τ_0 = 8.5×10^{-7} s) at zero applied *dc* field.

The effective barrier of slow magnetic relaxation, U_{eff} ,is obtained according to the Arrhenius law from temperature (Figure 3.8) measurements (U_{eff} (**17**) = 13.4 K τ_0 = 8.5×10^{-7} s).The *ac* susceptibility follows the generalized Debye model.[153,181] Simultaneous fitting of $\chi'(\nu)$, $\chi''(\nu)$ and Cole-Cole plot are shown in the Appendix A (Figure S3.3). The relatively large value of α (0.015 - 0.388) indicates that more than one relaxation process generated by QTM might be operational at this condition.

3.3 Conclusion

The synthetic strategy of using the dianionic ligand H_2**L1** in Co^{II}-Ln^{III} chemistry resulted in a family of hexametallic $Co^{II}_4Ln^{II}_2$ (**15** – **18**) PCCs possessing a **2,3,4M6-1** topology. After an extensive review, compounds **15** – **18** were determined to be the first $Co^{II}_4Ln^{III}_2$ examples of this topology. Magnetic studies of **15** – **18** reveal the presence of ferromagnetic and antiferromagnetic interactions and interestingly, compound **17** shows SMM behaviour.

The use of H_2**L5**, which provides the same coordination pockets as H_2**L1**, with a similar synthetic strategy that afforded **15** – **18**, results in the formation of compound **19** which is isoskeletal to $Co^{II}_4Ln^{III}_2$ series. In contrast when H_2**RL3.9**, which provides similar coordination modes similar to those of H_2**L1**, was employed in Co^{II}-Ln^{III} chemistry a PCC with the **2,3,4M6-1** topology but with a different core configuration is observed.

Future studies will be focused in two directions:

a) To perform further systematic synthetic studies which employ organic ligands with similar coordination pockets to H_2**L1**, H_2**L5** and H_2**RL3.4** in Co^{II}-Ln^{III} chemistry, to afford hexanuclear PCCs bearing **2,3,4M6-1** topology and determine how ligand structure determines the core configuration.

b) To further develop the topological approach[353] by including valuable information for the synthesis of a specific topology.

Chapter 4: Heptanuclear disk-like $M^{II}_3Ln^{III}_4$ PCCs: synthesis, structures and MCE properties

Abstract: The synthesis, characterization, crystal structures and magnetic properties of isoskeletal heptanuclear disk-like $M^{II}_3Ln^{III}_4$ polynuclear coordination clusters with the general formula $[Co^{II}_3Ln^{III}_4(\mu_3\text{-OH})_6(\mathbf{L4})_6(CF_3SO_3)](CF_3SO_3)_5$, where Ln = Gd (**20**), Y (**21**) and $[Ni^{II}_3Ln^{III}_4(\mu_3\text{-OH})_6(\mathbf{L4})_6(CF_3SO_3)](CF_3SO_3)_5$, where Ln = Dy (**22**), Gd (**23**), Y (**24**), are presented. All the compounds are stable in solution which is confirmed by electrospray ionization mass spectrometry studies. Magnetic studies indicate ferromagnetic coupling for all compounds. The magnetocaloric effect properties of **23** are characterized by $\Delta S_m = -15.4$ J kg^{-1} K^{-1} at $T = 5.0$ K and $\Delta T_{ad} = 5.9$ K at $T = 2.3$ K, for $\mu_0\Delta H = 7$ T.

4.1 Introduction

Chapter three and previously reported examples[2] demonstrate that the combination of H_2**L1** with Co^{II} and Dy^{III} is a plausible route to SMM behaviour and novel topological motifs. With the idea of exploring other potential magnetic applications of 3d-4f Schiff base supported PCCs, it was noted that H_2**L1** is structurally related to the monoanionic H**L4** ligand and has similar coordination pockets (Figure 4.1).

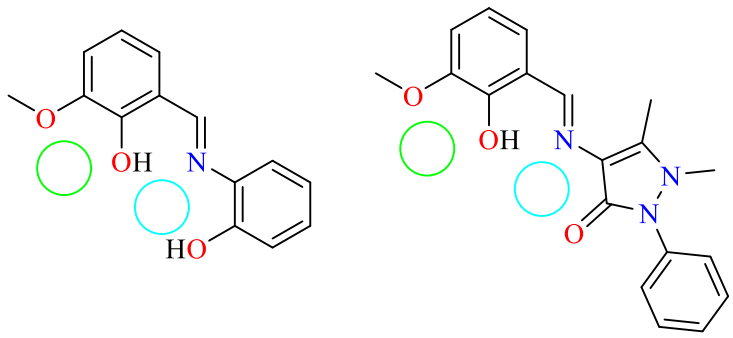

Figure 4.1. Structures of H_2**L1** (left) and H**L4** (right). Colour code: OO coordination pocket, green; ONO coordination pocket, light blue.

Recently, H**L4** was reported for the synthesis of a $Co^{II}_3Dy^{III}_4$ disk PCC which displayed behaviour indicative of an SMM below 4K.[1] The $Co^{II}_3Dy^{III}_4$ disk displays a **3,6M7-1** core topology, where the heptanuclear pentacationic core has alternating Co^{II} and Dy^{III} ions around a central Dy^{III} ion which are bridged by six μ_3-OH groups. The alternating fashion of Co^{II}-Dy^{III} ions is similar to many previously reported 3d-4f PCC magnetic coolers, where coupling of 3d metal ions with Gd^{III} ions leads to weak magnetic interactions[23] which are ideal for achieving the maximum entropy per mole and an enhanced MCE effect.

Notable examples of 3d-4f PCC coolers include $Mn^{III}_4Gd^{III}_4$,[221] $Cu^{II}_5Gd^{III}_4$ [124] and $Zn^{II}_8Gd^{III}_4$.[225] Of particular interest, alternating Co^{II}-Ln^{III} PCCs were reported by Winpenny,[208] which were divided into grids ($Co^{II}_8Gd^{III}_4$, $Co^{II}_4Gd^{III}_6$, $Co^{II}_8Gd^{III}_8$) and cages ($Co^{II}_6Gd^{III}_8$, $Co^{II}_8Gd^{III}_2$) and displayed prominent MCE effects (11.8 – 28.6 J kg^{-1} K^{-1}). Due to the counter-intuitive route of using anisotropic Co^{II} ions for synthesising magnetic coolers, an attempt was made to substitute them with Ni^{II} ions, which resulted in two Ni^{II}-Gd^{III} PCCs with enhanced entropy changes. These examples include a 48-member metallocycle $Ni^{II}_{12}Gd^{III}_{36}$ (36.3 J kg^{-1} K^{-1})[227] and a $Ni^{II}_6Gd^{III}_6$ cage (37.4 J kg^{-1} K^{-1}).[374]

Though 3d-4f PCCs are the most common examples of molecular magnetic coolers studied,[222] there are few reported examples of 3d-4f Schiff base PCCs which display a significant MCE effect. The best performing examples of Schiff base supported magnetic cooler include $Co^{II}_2Gd^{III}_4$ (24 J kg^{-1} K^{-1})[115] and $Cu^{II}_6Gd^{II}_6$ (23.5 J kg^{-1} K^{-1}) PCCs.[224] Other higher nuclearity examples include $Ni^{II}_2Gd^{III}$,[375] $Ni^{II}_4Gd^{III}_4$,[376] $Ni^{II}_2Gd^{III}_4$,[377] and $Cu^{II}_6Gd^{III}_6$ [223] all of which display an MCE above 11.9 J kg^{-1} K^{-1}.

Upon exchanging the Co^{II} ions of the $Co^{II}_3Dy^{III}_4$ disk with Ni^{II} ions to maximise the MCE effect and retain SMM behaviour, this resulted in a series of five isostructural $M^{II}_3Ln^{III}_4$ disks (where M = Ni, Co and Ln = Dy, Gd, Y). The reported examples are isoskeletal to the previously reported $Co^{II}_3Dy^{III}_4$ disk and are formulated $[Co^{II}_3Gd^{III}_4(\mu_3\text{-}OH)_6(\mathbf{L4})_6(CF_3SO_3)](CF_3SO_3)_5$ (**20**), $[Co^{II}_3Y^{III}_4(\mu_3\text{-}OH)_6(\mathbf{L4})_6(CF_3SO_3)](CF_3SO_3)_5$ (**21**), $[Ni^{II}_3Dy^{III}_4(\mu_3\text{-}OH)_6(\mathbf{L4})_6(CF_3SO_3)](CF_3SO_3)_5$ (**22**), $[Ni^{II}_3Gd^{III}_4(\mu_3\text{-}OH)_6(\mathbf{L4})_6(CF_3SO_3)](CF_3SO_3)_5$ (**23**) and $[Ni^{II}_3Y^{III}_4(\mu_3\text{-}OH)_6(\mathbf{L4})_6(CF_3SO_3)](CF_3SO_3)_5$ (**24**). Synthetic insights, topological analysis and magnetic properties of compounds **20 - 24** are discussed.

4.2 Results and discussion

4.2.1 Synthetic issues

The previously reported $Co^{II}_3Dy^{III}_4$ PCC (**CoDy-MeCN**) was prepared from the room temperature reaction of $Dy(OTf)_3$ and $Co(ClO_4)_2{\cdot}6H_2O$ with H**L4** in a molar ratio of 2:1:2.5:2.5 (Dy: Co: H**L4**: Et_3N) using MeOH as solvent and resulted in crystals forming, after 3 weeks, in a moderate yield (30 - 35%).[1] When a similar reaction was performed in EtOH, under reflux, an isoskeletal compound formulated $[Co^{II}_3Dy^{III}_4(\mu_3\text{-}OH)_6(\mathbf{L4})_6(CF_3SO_3)](ClO_4)_3(CF_3SO_3)_2$ (**CoDy-EtOH**) was isolated in only 3 days with moderate yield (Table 4.1).[1] The latter indicates that the temperature and the solvent of the reaction had a profound effect on the crystallization time and yield of the product.

When these two methods were applied to synthesise the $Co^{II}_3Ln^{III}_4$ (Ln = Gd, Y) analogues the yield greatly decreased and when applied to the synthesis of $Ni^{II}_3Ln^{III}_4$ analogues the expected

products were formed in very low yields (Table 4.1, entry 6) or hexagonal shaped crystals were obtained after almost 6 weeks (Table 4.1, entry 7).

However, an adaption of the synthetic procedure leads to the formation of the expected disk-like PCCs with all $M^{II}{}_3Ln^{III}{}_4$ combinations in very good yields (63 - 85%) and shorter crystallization times (Table 4.1, entries 3, 4, 5, 8 and 9).

Compounds **20 - 24** were prepared from the refluxed reaction of $Dy(OTf)_3$ and $M(NO_3)_2{\cdot}6H_2O$ with H**L4** in a molar ratio of 2:1:2.5:12 (Dy: M: H**L4**: Et_3N) with EtOH as a solvent and crystallisation times ranged between 2 - 7 days. The change in synthetic protocol resulted in the replacement of the $[ClO_4]^-$ counter-ions molecules with $[CF_3SO_3]^-$ and did not alter the central $[M^{II}{}_3Ln^{III}{}_4(\mu_3\text{-OH})_6(\mathbf{L4})_6(CF_3SO_3)]^{5+}$ cation.

4.2.2 Molecular structure and crystal structure descriptions

Unit cell determinations (chapter twelve), FT-IR spectra (Appendix B, S4.1-S4.6), EA (chapter eleven), ESI-MS (Appendix B, S4.7-S4.10) and TGA (Appendix B, S4.11-S4.15) show that compounds **20 - 24** are isoskeletal. Therefore, only a detailed crystallographic description of **22** will be described herein and the molecular structure is shown in Figure 4.2.

Crystallographic studies show that **20 - 24** crystallize in the orthorhombic space group *Pbca*. Three Ni^{II} and three Dy^{III} cations form a heterometallic wheel, in an alternating fashion and lay within the same plane, whereas the central Dy^{III} lies 0.671 Å out of the plane. The heptanuclear pentacationic core is supported by six μ_3-OH groups, alternating above and below the $Ni^{II}{}_3Dy^{III}{}_4$ plane, while a triflate group caps the central Dy centre ion.

The coordination number of the three peripheral and one central Dy^{III} ions is eight and seven, respectively. The geometry of the central Dy^{III} cation can be described as a capped octahedron whereas the Dy^{III} ions lying within the wheel is that of a bicapped trigonal prism. The Ni^{II} centres adopt what can be best described as a distorted octahedral geometry.

The H**L4** ligands display the same coordination mode (Figure 4.3) and are each bonded to two Dy^{III} and one Ni^{II} ion. Each ligand is chelated to a Ni^{II} ion, through the phenoxido oxygen and the imino nitrogen atoms; to a Dy^{III} ion, through the phenoxido and methoxido oxygen atoms and bonded to another Dy^{III} ion through a carbonyl oxygen atom. The angles of the μ_3-OH bridges are within the range 97.2(3) – 106.7(3) °.

There are three Dy⋯Dy distances, 3.6470(9) Å, 3.6561(9) Å and 3.6619(12) Å; and nine Ni⋯Dy distances within the range 3.3715(19) - 3.4806(16) Å. The diameter of the disk is 18.799 Å.

Table 4.1. Synthetic conditions for the reported disk-like PCCs.

Entry	PCC	Synthetic ratio[a]	Formula	Solvent	Yield/ %[a]	Crystallisation time/ days
1	**CoDy-EtOH**	2:1:2.5:2.5	$[Co^{II}_3Dy^{III}_4(\mu_3\text{-}OH)_6(\mathbf{L4})_6(CF_3SO_3)](ClO_4)_5$	EtOH	45	3
2	**CoDy-MeCN**	2:1:2.5:2.5	$[Co^{II}_3Dy^{III}_4(\mu_3\text{-}OH)_6(\mathbf{L4})_6(CF_3SO_3)](ClO_4)_5$	MeCN	22	21
3	**20**	2:1:2.5:12	$[Co^{II}_3Gd^{III}_4(\mu_3\text{-}OH)_6(\mathbf{L4})_6(CF_3SO_3)](CF_3SO_3)_5$	EtOH	81	2
4	**21**	2:1:2.5:12	$[Co^{II}_3Y^{III}_4(\mu_3\text{-}OH)_6(\mathbf{L4})_6(CF_3SO_3)](CF_3SO_3)_5$	EtOH	77	5
5	**22**	2:1:2.5:12	$[Ni^{II}_3Dy^{III}_4(\mu_3\text{-}OH)_6(\mathbf{L4})_6(CF_3SO_3)](CF_3SO_3)_5$	EtOH	69	3
6	**22'**	2:1:2.5:2.5	$[Ni^{II}_3Dy^{III}_4(\mu_3\text{-}OH)_6(\mathbf{L4})_6(H_2O)](ClO_4)_6$	EtOH	5	25
7	**22''**	2:1:2.5:2.5	$[Ni^{II}_3Dy^{III}_4(\mu_3\text{-}OH)_6(\mathbf{L4})_6(H_2O)](ClO_4)_6$	MeOH	12	38
8	**23**	2:1:2.5:12	$[Ni^{II}_3Gd^{III}_4(\mu_3\text{-}OH)_6(\mathbf{L4})_6(CF_3SO_3)](CF_3SO_3)_5$	EtOH	71	2
9	**24**	2:1:2.5:12	$[Ni^{II}_3Y^{III}_4(\mu_3\text{-}OH)_6(\mathbf{L4})_6(CF_3SO_3)](CF_3SO_3)_5$	EtOH	68	7

[a] (Ln: M: H**L4**: Et_3N). [b] Yield % based on Ln^{III}.

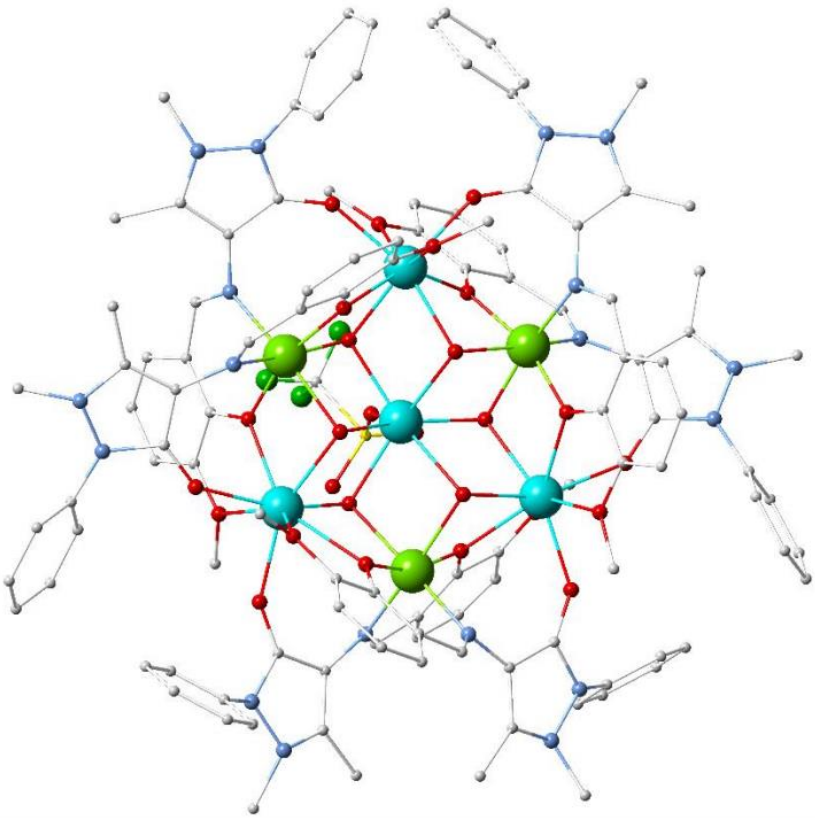

Figure 4.2. The molecular structure of **22**. Colour code: Ni^{II}, green; Dy^{III}, light blue; C, white; N, blue; O, red; S, yellow; F, light green.

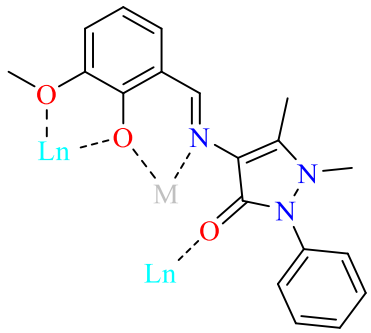

Figure 4.3. Observed co-ordination mode of H**L4** in compounds **20 - 24**.

4.2.3 ESI-MS Studies

To further confirm the identity of the reported compounds a broad ESI-MS for **20 - 23** was performed (Appendix B, S4.7-S4.10). Three main regions were identified for the analogues showing three distinct fragments in each region. These perfectly correspond to the tetracationic, tricationic and dianionic fragments respectively: $[M_3Ln_4(OH)_6(C_{19}H_{18}N_3O_3)_6(CF_3SO_3)]^{4+}$, $[M_3Ln_4(OH)_6(C_{19}H_{18}N_3O_3)_6(CF_3SO_3)_3]^{3+}$ and $[M_3Ln_4(OH)_6(C_{19}H_{18}N_3O_3)_6(CF_3SO_3)_4]^{2+}$. Only the **24** analogue displays the $[Ni_3Y_4(OH)_6(C_{19}H_{18}N_3O_3)_6(CF_3SO_3)_4]^{2+}$ fragment (Appendix B, S4.10). Values assigned to these fragments and the corresponding PCC are shown in Table 4.2. Each of

these fragments corresponds to the $[M_3Ln_4(OH)_6(\mathbf{L4}_6)]$ core with additional trifluorosulphonate counter-ions.

Table 4.2. m/z fragment vales for reported $M^{II}_3Ln^{III}_4$ PCC.

PCC	$[M_3Ln_4(OH)_6(C_{19}H_{18}N_3O_3)_6(CF_3SO_3)_4]^{2+}$ /m/z	$[M_3Ln_4(OH)_6(C_{19}H_{18}N_3O_3)_6(CF_3SO_3)_3]^{3+}$ /m/z	$[M_3Ln_4(OH)_6(C_{19}H_{18}N_3O_3)_6(CF_3SO_3)]^{4+}$ /m/z
20	1762.06	1125.39	807.06
21	1624.03	1038.02	761.19
22	1771.14	1132.07	774.82
23	1760.61	1124.41	768.09
24	1624.09	N/A	N/A

4.2.4 TGA.

TGA measurements were performed to examine the thermal stability of selected compounds. In the cases of **20** and **24** (Appendix B, S4.11 – S4.15), the first mass loss corresponds to the loss of the counter-anions. The stability of the remaining core is then retained up to the region of ~300 °C, where gradual decomposition takes place. The final residue fits well to the analogous oxide $Co_3Gd_4O_9$ for **20** calculated (24.86%) found (24.14%) and $Ni_3Y_4O_9$ for **24** calculated (19.05%) found (19.43%).

4.2.5 Topological aspects

There are a limited number of examples of 3d-4f disk-like PCCs, the first reported examples demonstrating the **3,6M7-1** topology were the $Mn^{IV}_6Ce^{IV}$ disks reported by Christou et al.[378,379] These were followed by $Cu^{II}_6Pr^{III}$,[380] $Mn^{II}_3Ln^{III}_4$,[381] $Cu^{II}_5Ln^{III}_2$,[113] $Co^{II}_3Dy^{III}_4$[1] and $Co^{II}_2Dy^{III}_5$[68] examples.

The seven previously reported examples of 3d-4f PCCs which are enumerated **3,6M7-1** are shown in Table 4.3. Compounds **22 - 24** are the first reported Ni^{II}-Ln^{III} PCCs of this topology. Whereas **20** and **21** are the first examples of Co^{II}-Y^{III} and Co^{II}-Gd^{III} disks respectively, whilst both are also the fourth and fifth examples of Co^{II}-Ln^{III} disks.

There are three configurations for the 3d and 4f nodes within the disk, which are dependent on the 3d and 4f ratio. The first (Figure 4.5, 3/4 (A)) incorporates an Ln node in the centre of the disk, with Ln and M nodes alternating around the central node. This configuration is found in all $M^{II}_3Ln^{III}_4$ PCCs (Table 4.3, entries 1, 6, 7 and 8) and all form $[Mn^{II}_3Ln^{III}_4(\mu_3\text{-}O)_6]$ cores. The next (Figure 4.5, 5/2 or 2/5 (B)) configuration is observed in $Cu^{II}_5Ln^{II}_2$ and $Co^{II}_2Dy^{III}_5$ (Table 4.3,

entries 2 and 7). The Ln or the M nodes can be found in the periphery sandwiched between two 3d nodes each side, with a central M or Dy node, respectively. The last (Figure 4.6, 6/1 (C)) configuration is seen in $Mn^{IV}{}_6Ce^{IV}$ and $Cu^{II}{}_6Pr$ PCCs; the 3d ions form the periphery and the 4f ion only occupies the central node.

The Schiff base ligands (H**L4** and H_3**RL4.2**) have now been the most successful in synthesizing 3d-4f PCCs which display the **3,6M7-1** core topology, however, these are limited to the M^{II}-Ln^{III} valences. Ligands containing carboxylic acid groups have been used to form unique Mn^{IV}-Ln^{IV} disk PCCs as well as the M^{II}-Ln^{III} PCCs. Though it is evident there are distinct types of **3,6M7-1** PCCs, it is difficult to relate the configuration of the core to the types of ligand with the limited number of examples.

None of the previously reported examples have been investigated for the magnitude of their MCE, whereas $Co^{II}{}_3Dy^{III}{}_4$, $Cu^{II}{}_5Dy^{III}{}_2$ and $Cu^{II}{}_5Ho^{III}{}_2$ PCCs were found to display SMM properties with low energy barriers.

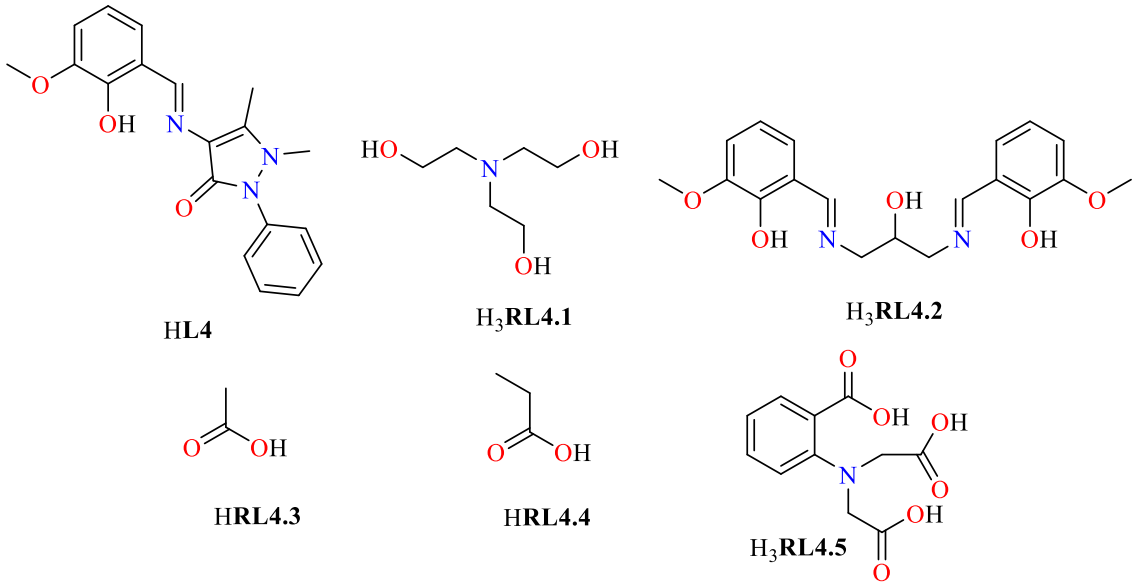

Figure 4.4. Ligands used for the synthesis of 3d-4f PCCs with a **3,6M7-1** core topology.

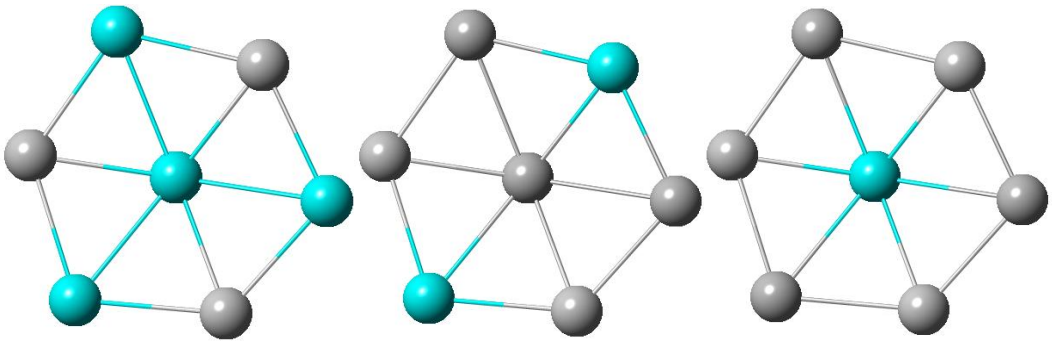

Figure 4.5. Configurations of 3d and 4f nodes in the **3,6M7-1** topology. A (left), B (middle) and C (right). Colour code: Ln node, light blue; M node, grey.

Table 4.3. Reported 3d-4f PCCs with a **3, 6M7-1** topology.

Entry	Formula	Core nuclearity	Ligand	Reference
1	$[Mn^{II}_3Ln^{III}_4(Piv)_{12}(\mathbf{RL4.1})_2(H_2O)_3]\cdot H_2O$	$Mn^{II}_3Ln^{III}_4$	H_3**RL4.1**	381
	Ln = La, Pr, Nd, Gd			
2	$[Cu^{II}_5Ln^{III}_2(\mathbf{RL4.2})_2(\mu_3\text{-}OH)_4(\mu\text{-}OH_2)_2(\mu\text{-}OAc)_2(OAc)_2(OH_2)_2](NO_3)_2\cdot 2H_2O$	$Cu^{II}_5Ln^{III}_2$	H_3**RL4.2**	113
	Ln = Y, Lu, Dy, Ho, Er, Yb			
3	$[Mn^{IV}_6Ce^{IV}O_9(\mathbf{RL4.3})_9(H_2O)_2(MeOH)](ClO_4)$	$Mn^{IV}_6Ce^{IV}$	H_3**RL4.3**	378
4	$[Mn^{IV}_6Ce^{IV}O_9(\mathbf{RL4.3/RL4.4})_9(X)(H_2O)_2]$	$Mn^{IV}_6Ce^{IV}$	H_3**RL4.3**, H_3**RL4.4**	379
5	$[Cu^{II}_6Pr^{III}(\mathbf{RL4.5})][Pr^{III}(H_2O)_{10}]\cdot 14H_2O$	$Cu^{II}_6Pr^{III}$	H_3**RL4.5**	380
6	$[Co^{II}_3Dy^{III}_4(\mu_3\text{-}OH)_6(\mathbf{L4})_6(CF_3SO_3)](ClO_4)_5$	$Co^{II}_3Dy^{III}_4$	H**L4**	1
7	$[Co^{II}_2Dy^{III}_5(\mu_3\text{-}OH)_6(\mathbf{L4})_2(Piv)_8(NO_3)_4]\cdot 4CH_3CN$	$Co^{II}_2Dy^{III}_5$	H**L4**	68
8	$[Co^{II}_3Ln^{III}_4(\mu_3\text{-}OH)_6(\mathbf{L4})_6(CF_3SO_3)](CF_3SO_3)_5$	$Co^{II}_3Ln^{III}_4$	H**L4**	This work
	Ln = Gd, Y			
9	$[Ni^{II}_3Ln^{III}_4(\mu_3\text{-}OH)_6(\mathbf{L4})_6(CF_3SO_3)](CF_3SO_3)_5$	$Ni^{II}_3Ln^{III}_4$	H**L4**	This work
	Ln = Dy, Gd, Y			

4.2.6 Magnetic properties

Susceptibility measurements were performed for **20**, **22** and **23** and for the Ni^{II}-Y^{III} complex **24** to check the degree of interaction between the d cations (Figure 4.6).

The $\chi_M T$ value for **20** at room temperature is 42.87 cm^3 mol^{-1} K, larger than the corresponding spin-only value for three Co^{II} and four Gd^{III} non-interacting cations of 37.125 cm^3 mol^{-1} K. On cooling the $\chi_M T$ value decreases very slightly in the 300 - 40 K region and below this temperature $\chi_M T$ increases continuously up to 60.23 cm^3 mol^{-1} K at 2 K.

22 shows a room temperature $\chi_M T$ value of 61.43 cm^3 mol^{-1} K that decreases to a minimum value of 57.21 cm^3 mol^{-1} K at 15 K, increasing at lower temperatures up to 98.5 cm^3 mol^{-1} K at 2 K. The initial decrease should be attributed to the depopulation of the Stark levels of the Dy^{III} cation.

23 shows a $\chi_M T$ value of 36.09 cm^3 mol^{-1} K at 300 K, somewhat larger than the 34.50 cm^3 mol^{-1} K value expected for three Ni^{II} and four Gd^{III} non-interacting cations per molecule, suggesting that correlations are sizeable at room temperature. On cooling, the $\chi_M T$ product increases slightly in the 300-50 K range and fast below 50 K, reaching the maximum value of 76.2 cm^3 mol^{-1} K at 2.6 K, below which it decays to 75.0 cm^3 mol^{-1} K at 2 K, likely because of weak antiferromagnetic interactions or crystal-field effects. The shape and low-temperature $\chi_M T$ values clearly indicate that the dominant interactions are ferromagnetic for the three complexes.

Magnetization experiments (Figure 4.6) show a fast increase at low fields and a further slow increase of the magnetization, reaching quasi-saturated values of 28.1 $N_{\mu B}$ for **22**, 35.7 $N_{\mu B}$ for **20** and 34.9 $N_{\mu B}$ for **23**, coherent with the maximum ferromagnetic *S* ground states for **20** and **23** (*S* = 18.5 and 17 respectively). The fit of the experimental data was not possible for the anisotropic $Co^{II}_3Gd^{III}_4$ and $Ni^{II}_3Dy^{III}_4$ complexes **20** and **22**, but a spin-only attempt was performed for the $Ni^{II}_3Gd^{III}_4$ (**23**). The response of the Ni_3Y_4 (**24**) was also measured and shows a constant $\chi_M T$ value of 3.5 cm^3 mol^{-1} K between 300 - 6 K and a decay below this temperature down to a final value of 2.80 $cm^3 \cdot mol^{-1}$ K at 2 K. This measure indicates that there is no interaction between the Ni^{II} cations and that **24** magnetically behaves as three isolated Ni^{II} cations with a *g* value of 2.16.

Next, simultaneous fits of $\chi_M T$ and *M (H, T)* data (Figure 4.7) were carried out for **23** by using the PHI program, if only the Ni-Gd and the Gd-Gd pathways are operative and that *g*(Ni) = 2.16. The best fit, solid lines in Figures 4.6 and 4.7, gives: J_1(Gd-Gd) = -0.17 cm^{-1} and J_2(Ni-Gd) = 0.62 cm^{-1}. It is worth noting that similar fitting curves of $\chi_M T$ and *M (H, T)* can also be obtained by constraining J_1(Gd-Gd) and J_2(NiGd) to be both ferromagnetic and by adding a weak antiferromagnetic effective J_z interaction to consider intermolecular couplings. However, this second set of parameters can be safely disregarded because contrary to the first one, it cannot be used to reproduce satisfactorily the heat capacity results that are reported herein.

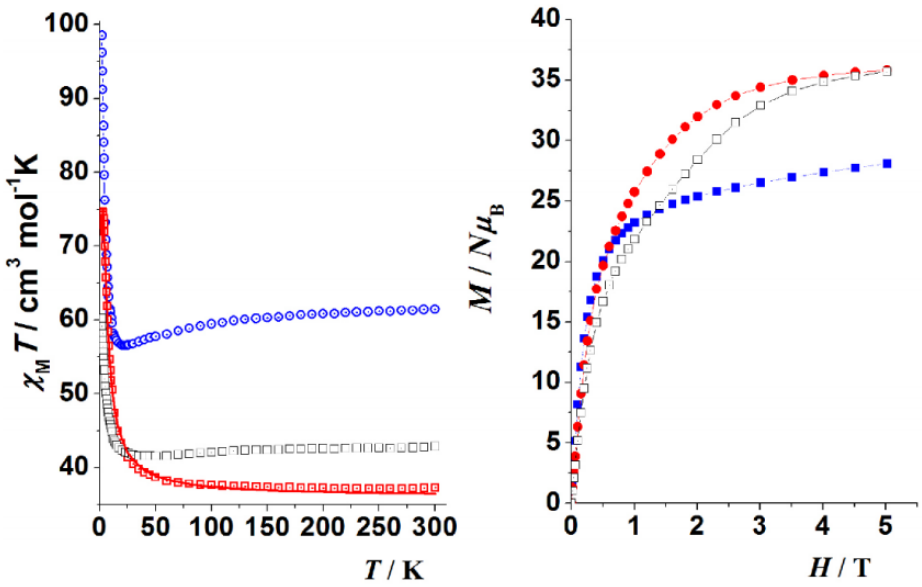

Figure 4.6. $\chi_M T$ product for complexes **20** (black), **22** (blue) and **23** (red), for applied field 0.1 T (left). The solid line shows the fit of the experimental data for **23**. Magnetization plots for **20** (black), **22** (blue) and **23** (red) (right). Solid lines are eye-guide.

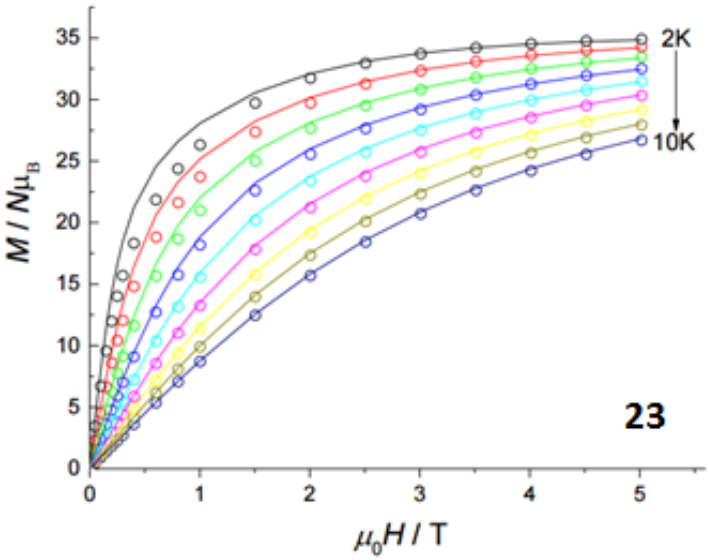

Figure 4.7. Isothermal magnetization curves for T = 2 − 10 K, step 1 K. Solid lines are the best-fit curves obtained by using spin-only model and by fixing g_{Ni} = 2.16; the coupling constant found from the fitting are J_1(Gd-Gd) = –0.17 cm^{-1} and J_2(Ni-Gd) = 0.62 cm^{-1}.

Figure 4.8 shows the experimental molar heat capacity C for **23**, collected for the temperature range 0.35 – 30 K and for several applied magnetic fields. The heat capacity is best understood by comparing the experimental data with the calculated curves (solid lines) on the basis of the spin-only model and parameters J_1(Gd-Gd) = –0.17 cm^{-1} and J_2(Ni-Gd) = 0.62 cm^{-1} obtained from fitting the susceptibility and magnetization data. Overall, the agreement is good, with the main

discrepancy gradually taking place on increasing T above 10 - 15 K. This discrepancy is due to a non-magnetic contribution that is ascribed to lattice vibrations and can be described by the Debye model (dotted line), which simplifies to a $C/R = \alpha T^3$ dependence at the lowest temperatures, where $\alpha = 2.3 \times 10^{-2}$ K^{-3}. The magnetic contribution to the heat capacity is strongly dependent on the applied field, especially for fields larger than 1 T. At the lowest temperatures, the calculated curves deviate from the experimental ones for zero field and less so for $\mu_0 H = 1$ T. This is very likely due to weak, though sizeable, magnetic interactions acting between the molecules, probably of dipolar origin, which are not included in the calculations.

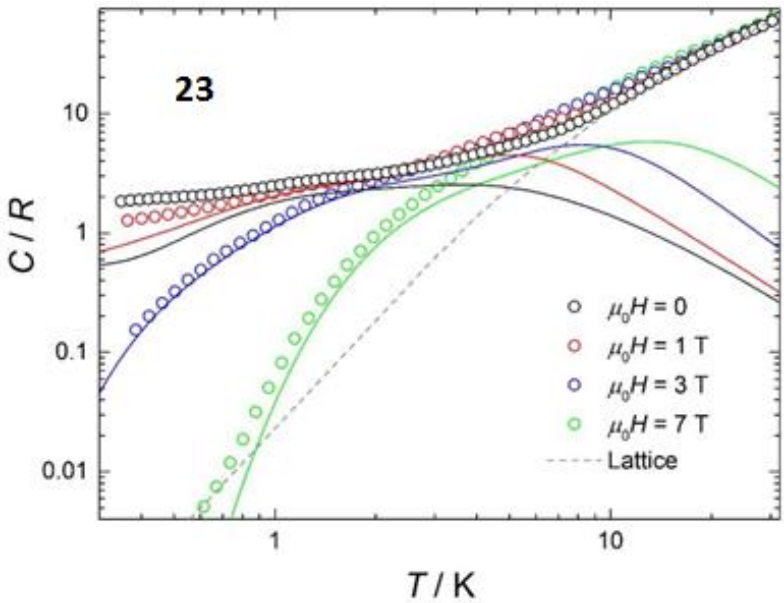

Figure 4.8. Temperature-dependence of the molar heat capacity, normalized to the gas constant R, for **23**, collected for the labelled applied fields. Solid lines are the calculated magnetic contributions for J_1(Gd-Gd) = –0.17 cm^{-1} and J_2(Ni-Gd) = 0.62 cm^{-1}, while dashed line is the non-magnetic lattice contribution.

Finally, the MCE for Ni_3Gd_4 (**23**) was evaluated, namely the magnetic entropy change was determined, ΔS_m, and adiabatic temperature change ΔT_{ad} for selected values of the applied field change $\Delta H = H - 0$. The results are shown in Figure 4.9, where one can notice that the two sets of data for ΔS_m that were obtained from $C(T, H)$ and $M(T, H)$ are consistent to each other, thus confirming that the procedures used are correct. For $\mu_0 \Delta H = 7$ T, $-\Delta S_m$ reaches 7.3 R = 15.4 J kg^{-1} K^{-1} at T = 5.0 K, while $\Delta T_{ad} = 5.9$ K at T = 2.3 K. Magnetic correlations inhibit the system to reach the whole available magnetic entropy that for four Gd^{III} and three Ni^{II} ions per molecule amounts to $4R\ln(2S_{Gd} + 1) + 3R\ln(2S_{Ni} + 1) = 11.62\ R$, where $S_{Gd} = 7/2$ and $S_{Ni} = 1$. The values of ΔS_m for **23**, when expressed per molar R, are like the corresponding ones reported for other Ni^{II}-Gd^{III} compounds,[376,382] whereas they compare less favourably when expressed per unit mass because the metal/non-metal ratio is relatively modest in **23**.

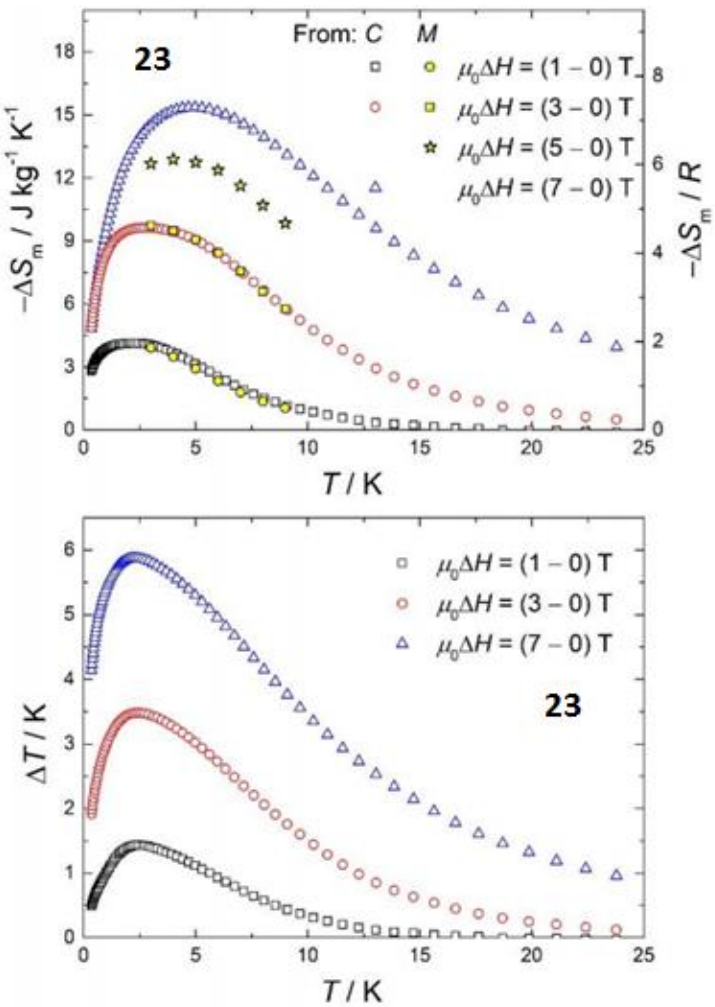

Figure 4.9. Magnetic entropy change vs *T*, for several values of the applied field change Δ*H*, as labelled (upper). Vertical axis reports units in J kg^{-1} K^{-1} (left) and molar *R* (right). Adiabatic temperature change vs *T* for the labelled applied field change, as obtained from heat capacity data (lower).

4.3 Conclusion

By altering the synthetic procedure of the previously reported heptanuclear disk-like PCC (**CoDy-EtOH**), a family of isoskeletal compounds formulated $[M^{II}_3Ln^{III}_4(\mu_3\text{-}OH)_6(\mathbf{L4})_6(CF_3SO_3)](CF_3SO_3)_5$ is obtained in higher yields and shorter crystallization times. Compounds **22** – **24** represent the first examples of Ni^{II}-Ln^{III} PCCs derived from the H**L4** ligand and the first to bear the disk-like topology (**3,6M7-1**). Moreover, **20** and **21** are respectively, the first disk-like examples in Co^{II}/ Gd^{III} and Co^{II}/Y^{III} cluster chemistry. All reported compounds are solution stable and demonstrate three characteristic regions of peaks when analysed with ESI-MS. The study of their magnetic properties revealed a dominant ferromagnetic coupling, while compound **23** displays MCE properties at liquid-helium temperatures. The present work illustrates the effectiveness of the proposed synthetic strategy to synthesize PCCs with fascinating magnetic properties.

Chapter 5: Isoskeletal Schiff base PCCs: synthetic and theoretical aspects

Abstract: This work addresses and explores the synthetic aspects derived from the effort to systematically construct isoskeletal polynuclear coordination clusters with the general formula $[M^{II}_2Ln^{III}_2(\mathbf{LX})_4(solv)_6](ClO_4)_2$ which possess the specific defect dicubane core topology. A variety of substituted Schiff base organic ligands ($H_2\mathbf{LX}$) and Ni^{II}-Co^{II} and $Dy(OTf)_3$ salts are employed. Nineteen novel Schiff base ligands are synthesised ($H_2\mathbf{L2}$, $H_2\mathbf{L6}$-$H_2\mathbf{L22}$), as well as a series of isoskeletal $Ni^{II}_2Dy^{II}_2$ (**27** – **34**, **36** – **43**) PCCs and by-products are also discussed. The $[Ni^{II}_2Ln^{II}_2(\mathbf{LX})_4]^{2+}$ core is found to be stable in solution. This work is further supported by density functional theory studies.

5.1 Introduction

3d-4f PCC catalysed organic transformations have only been studied *in situ* and the active species in these transformations are either unidentified or a mixture of different species.[296–299] To develop tetranuclear PCCs with the general formula $[M^{II}_2Ln^{III}_2(\mathbf{LX})_4(solv)_6](ClO_4)_2$ and study their behaviour in catalytic reactions, knowledge of the exact structure and purity of these species is of the utmost importance to differentiate this work from previous studies.

Previously, the blending of $H_2\mathbf{L1}$ with M^{II} (M = Ni, Co) salts and Ln^{III} nitrate salts, resulted in tetranuclear PCCs[2,50] with the general formula $[M^{II}_2Ln^{III}_2\mathbf{(L1)}_4(NO_3)_2(solv)_2]$, (solv = THF, MeOH) which possess a defect dicubane, "butterfly"[338] (Figure 5.1, middle) or **2,3M4-1** (Figure 5.1 , right) core topology.[13,340,362] The main goal of this study is to alter the "second sphere" of these PCCs and to replace the coordinated $[NO_3]^-$ ions with solvent molecules and uncoordinated $[ClO_4]^{2-}$ ions, which are more suitable for catalytic transformations. These second sphere effects include ligand modification, coordinating solvent and the types of counter-ion. Additionally, the influence of a variety of reaction conditions on the final structure of the product is evaluated.

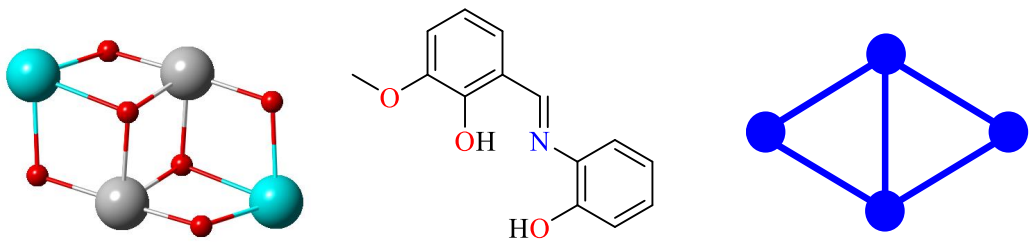

Figure 5.1. The defect dicubane motif (left). The $H_2\mathbf{L1}$ ligand (middle) and the **2,3M4-1** topology (right).

Ligand modification has successfully enhanced the properties of PCCs, such as when Murugesu et al.[65] reported a seven-fold enhancement of the energy barrier, U_{eff}, of a Dy^{III}_2 complex that

behaves as an SMM, by introducing electron-withdrawing terminal ligands. Additionally, in previously reported catalytic transformations, modification of the ligand frame of the active complex was shown to improve efficacy.[383–386] In this chapter, a variety of modified Schiff base ligands, with the same coordination modes as H_2**L1**, were synthesised to study the influence of the modified groups for the formation of the defect dicubane core topology (termed H_2**LX**).

Adopting the isoreticular concept, which was defined by O'Keeffe and Yaghi in Metal-Organic Framework (MOF) chemistry,[387] the term "isoskeletal" is introduced. This term is used to describe PCCs that possess the same topology[388,389] or related organic structures with the same host framework but different guests.[390,391] This term will be used to describe the targeted PCCs constructed from the modified organic ligands with a similar coordination environment and the same underlying **2,3M4-1** topology. Herein, the synthesis of nineteen Schiff base ligands are described and they are used to systematically construct isoskeletal PCCs with the general formula $[M^{II}_2Ln^{III}_2(\mathbf{LX})_4(solv)_6](ClO_4)_2$. A variety of reaction conditions are explored and a series of isoskeletal defect dicubane $M^{II}_2Ln^{III}_2$ PCCs are isolated (**27** – **34, 36** – **43**). ESI-MS studies are presented to confirm the solution stability of the defect dicubane motif.

5.2 Results and discussion

5.2.1 Synthesis of modified H_2L1 analogues (H_2L2 - H_2L22)

A typical synthesis of a Schiff base ligand takes place in an alcoholic solution sometimes in the presence of acidic or basic catalysts, although other synthetic methods such as microwave-mediated[392] or solvent-free mechanochemical synthesis[393,394] can be employed.

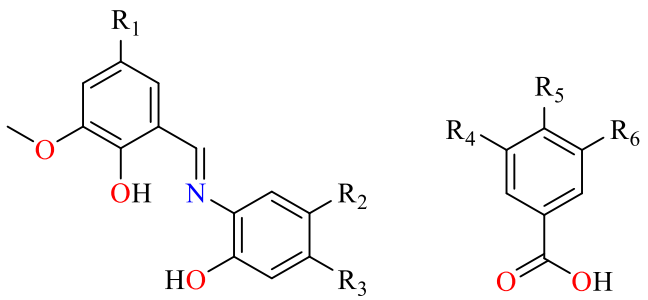

Figure 5.2. The modified organic ligands used in this work (left). R_1 = H, allyl, NO_2; R_2 = H, Cl, C_6H_5; R_3 = H, NO_2; R_2-R_3 = C_4H_4. The substituted monocarboxylates used in this work; **M1** (R_4 = R_5 = NO_2, R_5 = H); **M2** (R_4 = NO_2, R_5 = R_6 = H).

The attempts to synthesize Schiff base ligands which bear electron withdrawing groups (Figure 5.2, left) (Table 5.1, entries 2 - 20) via a typical synthesis, *viz*. reflux in an alcoholic solution of equivalent amounts of the corresponding aldehyde and amine, resulted in the desired products, but in very low yields. Microwave-assisted organic synthesis enables the rapid synthesis of organic molecules, often with excellent yields and selectivity. Interestingly, by applying

microwave-assisted synthesis[395,396] for the synthesis of the corresponding Schiff base ligands, the yield increases drastically.

In total, nineteen new Schiff Base ligands (Table 5.1, entries 2 - 19) were synthesised and two examples, H_2**L12** and H_2**L22**, were characterized via single-crystal XRD studies (Figure 5.3). Single-crystal XRD studies at 173 K reveal that both H_2**L12** and H_2**L22** are a mixture of keto-enol tautomer. In H_2**L12**, where two molecules can be found in the asymmetric unit, the enol form of the ligand is indicative of the existence of protons H3 and H8A that could be freely refined with chemical occupancy 22 and 23%, respectively.

However, to obtain a suitable structure solution, both protons were restrained to have 25% occupancy and their O – H bond distance to be at 0.88 Å. The C – O bond distances are 1.282(3) and 1.282(3) Å which are slightly higher than a typical C = O double bond. Similarly, for ligand H_2**L22**, protons H1 and H2 (Figure 5.3) could be free refined and have 79% and 21% occupancies, indicating a 79/21 existence of ketonic/enolic form, while the C – O bond distance is 1.285(2) Å. These findings are consistent with previously reported compounds.[393] Solution studies (^{1}H and ^{13}C NMR spectroscopy) of the synthesized compounds, revealed the existence of both keto and enol forms.

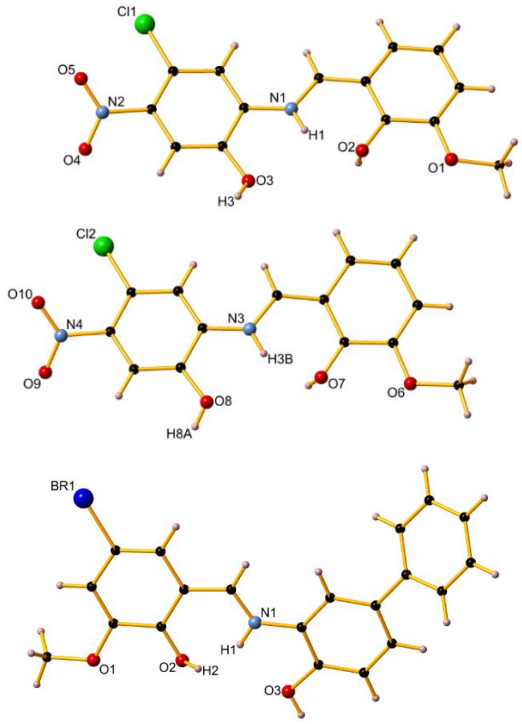

Figure. 5.3. A schematic representation of H_2**L12** (upper) and H_2L**22** (lower) ligands. Colour code; O, red; N, pale blue; C, black; Cl, green; Br, blue.

Table 5.1. A list of all substituted Schiff bases synthesized for this study. R_1, R_2 and R_3 correspond to the substituted groups seen in Figure 5.2.

Entry	Ligand (H_2**LX**)	R_1	R_2	R_3	Yield/ %
1	H_2**L1**	H	H	H	95
2	H_2**L2**	H	C_4H_4		88
3	H_2**L6**	allyl	H	H	70 [98][a]
4	H_2**L7**	NO_2	H	H	93
5	H_2**L8**	H	H	NO_2	66 [96][a]
6	H_2**L9**	allyl	H	NO_2	72
7	H_2**L10**	NO_2	H	NO_2	94
8	H_2**L11**	Br	H	NO_2	79
9	H_2**L12**	H	Cl	NO_2	76 [95][a]
10	H_2**L13**	allyl	Cl	NO_2	70
11	H_2**L14**	NO_2	Cl	NO_2	80
12	H_2**L15**	Br	Cl	NO_2	35 [85][a]
13	H_2**L16**	allyl	C_4H_4		61 [95][a]
14	H_2**L17**	NO_2	C_4H_4		74
15	H_2**L18**	Br	C_4H_4		79
16	H_2**L19**	H	C_6H_5	H	91
17	H_2**L20**	allyl	C_6H_5	H	69
18	H_2**L21**	NO_2	C_6H_5	H	92
19	H_2**L22**	Br	C_6H_5	H	83

[a] MW technique

5.2.2 Synthetic protocols for targeting $[M^{II}_2Ln^{III}_2(LX)_4(solv)_6](ClO_4)_2$ PCCs

Based on the previously reported synthetic protocols that resulted in the isolation of tetranuclear PCCs, with the general formula $[M^{II}_2Ln^{III}_2(\mathbf{LX})_4(solv)_6](ClO_4)_2$,[337] and considering that a subtle change in the synthetic procedure may affect the shape, dimensionality and nuclearity of the final product, several molecular ratios to isolate the corresponding-targeted isoskeletal PCCs were screened. It is worth mentioning that to avoid complicating the synthetic procedures only $Dy(OTf)_3$ as the lanthanide source was employed. During this screening procedure, several interesting and unexpected results were obtained, which are grouped and presented below.

5.2.2.1 Oxidation

Reaction of H_2**L8** with $Co(ClO_4)_2{\cdot}6H_2O$, $Dy(OTf)_3$ and Et_3N in the molar ratio 2:1:1:5 in MeOH resulted after 3 days, in approximately 82% yield, in dark-red crystals formulated as

$(Et_3NH)[Co^{III}(\mathbf{L8})_2]\cdot 3MeOH$ (**25**·3MeOH) (Figure 5.4 left). Similarly, the reaction of H_2**L18** with $Co(ClO_4)\cdot 6H_2O$, $Dy(OTf)_3$ and Et_3N in the molar ratio 1:1:1:3 in MeOH resulted after 6 days, in approximately 82% yield, dark red crystals formulated as $(Et_3NH)[Co^{III}(\mathbf{L18})_2]\cdot 2MeOH$ (**26**·2MeOH). (Figure 5.4, right).

In the cases of **25** and **26**, during crystallization at room temperature, Co^{II} is oxidized to Co^{III}. To target for the isoskeletal **2,3M4-1** $Co^{II}_2Dy^{III}_2$ analogues, it is important to perform the synthesis and crystallization under an inert atmosphere to prevent oxidation of Co^{II} to Co^{III}.

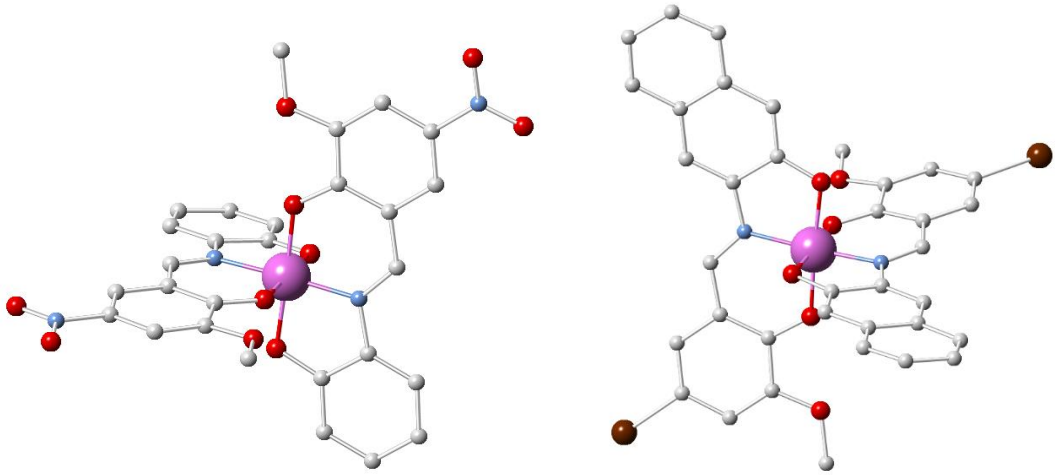

Figure 5.4. The crystal structure of compound **25** (left). The crystal structure of compound **26** (right). Colour code: Co^{III}, pink; N, light blue; O, red; C, white; Br, blue. Hydrogen atoms and solvent molecules are omitted for clarity.

5.2.2.2 Solvent influence

As anticipated, modification of the organic periphery of the parent organic ligand (H_2**L1**) drastically affects its solubility. However, when targeting for the corresponding isoskeletal tetranuclear species, the use of a mixture of solvents enhanced solubility, resulting in the formation of undesired compounds.

For example, the reaction of ligand H_2**L14** with $Ni(ClO_4)_2.6H_2O$, $Dy(OTf)_3$ and Et_3N in the molar ratio 2:1:1:5 in a mixture of $EtOH/CH_2Cl_2$ results in the formation of a tetranuclear compound, formulated as $[Ni^{II}_2Dy^{III}_2(\mathbf{L20})_4(\text{allyl-o-vanillin})_2(EtOH)_2]\cdot 3CH_2Cl_2$ (**27**·$3CH_2Cl_2$) (Figure 5.5). The two allyl-o-vanillin moieties derive from the disassembling of H_2**L20** during the reaction. Interestingly, performing a similar reaction, in solely DMF results in the formation of the desired $[Ni^{II}_2Dy^{III}_2(\mathbf{L20})_4(DMF)_6](ClO_4)_2\cdot 4DMF$ (**28**·4DMF) (Figure 5.5).

This observation was additionally proven by performing a reaction of ligand H_2**L22** with $Ni(ClO_4)_2\cdot 6H_2O$, $Dy(OTf)_3$ and Et_3N in the molar ratio 2:1:1:5 in a mixture of $EtOH/CH_2Cl_2$

which resulted in the isolation of compound $[Ni^{II}_2Dy^{III}_2(\mathbf{L22})_4(\text{bromo-o-vanillin})_2(EtOH)_2]\cdot 6EtOH$ (**29**·6EtOH) (Figure 5.5). Moreover, using a blend of EtOH/THF in the following reaction with $Ni(ClO_4)_2\cdot 6H_2O$, $Dy(OTf)_3$ and Et_3N in the molar ratio 2:1:1:5 results in $[Ni^{II}_2Dy^{III}_2(\mathbf{L16})_4(\text{allyl-o-vanillin})_2(EtOH)_2]\cdot 2THF\cdot 2EtOH$ (**30**·2THF·2EtOH) (Figure 5.5). However, performing a similar reaction in DMF results in the formation of the desired compound formulated $[Ni^{II}_2Dy^{III}_2(\mathbf{L16})_4(DMF)_2](ClO_4)_2$ (**31**) (Figure 5.5).

These examples indicate that the use of a second solvent increases the chance of by-product formation and thus the mixture of solvents may not be an ideal synthetic protocol when targeting high purity compounds.

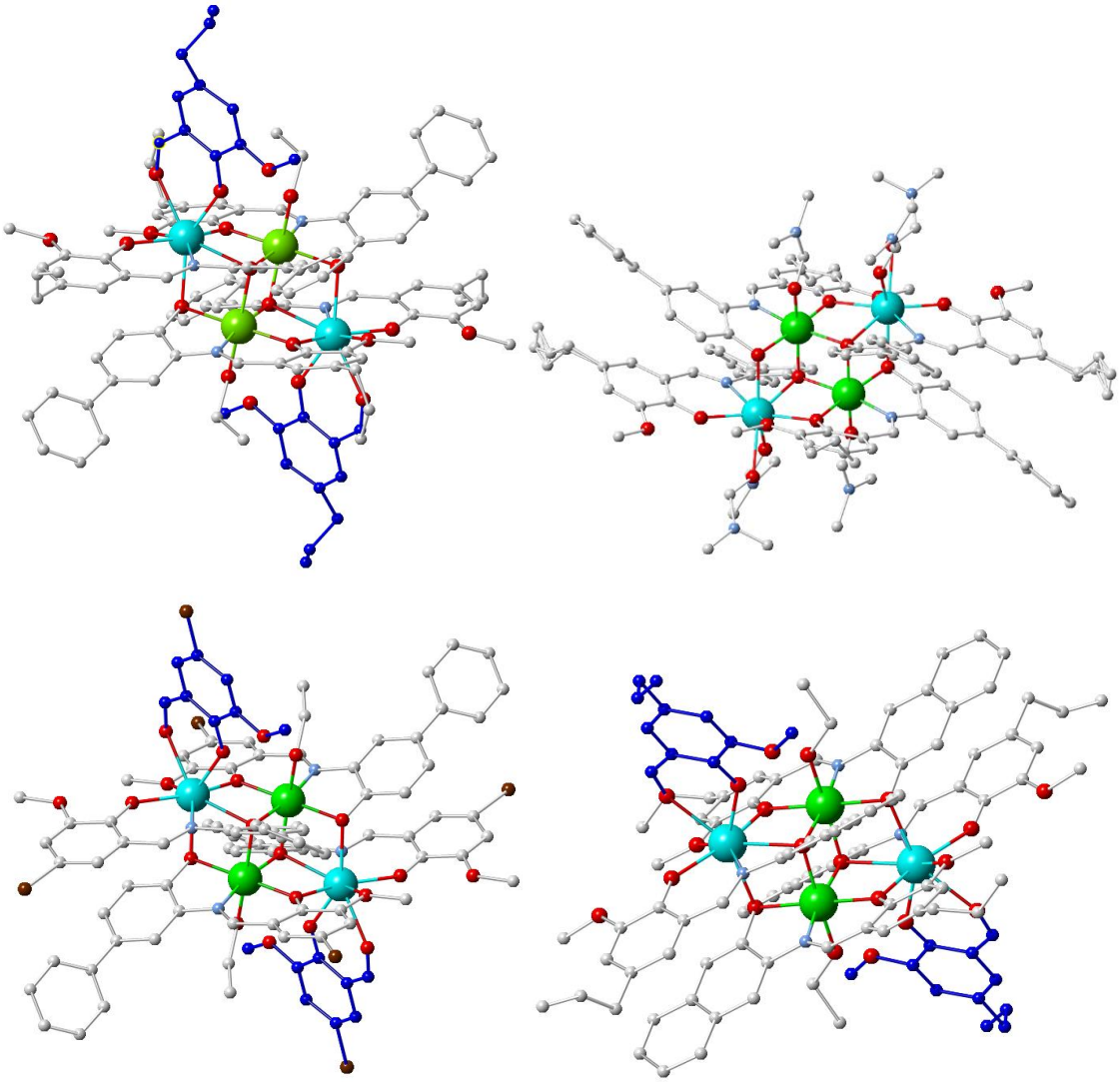

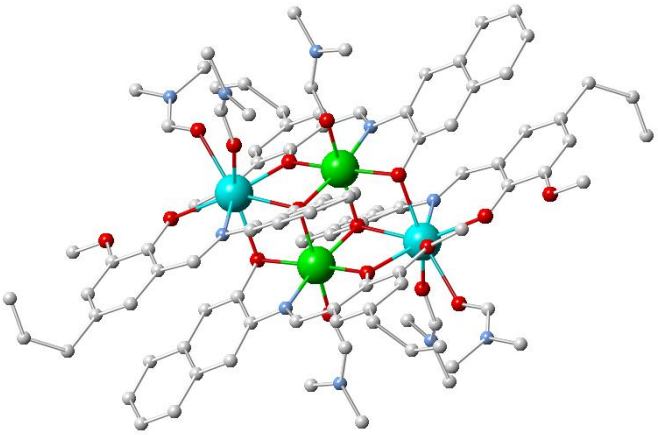

Figure 5.5. The crystal structures of compounds **27 - 31**. The substituted o-vanillin moiety is indicated with blue colouring. Colour code: Ni^{II}, green; Dy^{III}, light blue; N, blue; O, red; C, white; Br, brown. Hydrogen atoms and solvent molecules omitted for clarity.

5.2.2.3 Solvent concentration influence

When reactions were performed with less solvent (10 mL instead of 20 mL) or the reactant ratio was tripled, a different product was obtained, formulated as $[Ni^{II}_2Dy^{III}_2(\mathbf{L1})_4(EtOH)_4(H_2O)_2](ClO_4)_2$ (**32**) (Figure 5.6). Two water molecules coordinate to Ni^{II} centres in **32**. Moreover, performing a similarly scaled-up reaction in a different solvent such as DMF another compound is formed formulated as $[Ni^{II}_2Dy^{III}_2(\mathbf{L1})_4(DMF)_6](OTf)_2\cdot 2DMF$ (**33**·2DMF) (Figure 5.6), instead of the expected perchlorate derivative. In addition, performing a concentrated reaction of $Ni(ClO_4)\cdot 6H_2O$, $Dy(OTf)_3$, Et_3N and $\mathbf{H_2L18}$ in the molar ratio 1:1:2:8 resulted in a PCC with the formula $[Ni^{II}_2Dy^{III}_2(\mathbf{L18})_4(DMF)_6]$ $[Ni^{II}_2Dy^{III}_2(\mathbf{L18})_4(DMF)_4(H_2O)_2](ClO_4)_4\cdot 5DMF$ (**34**·5DMF). (Figure 5.6).

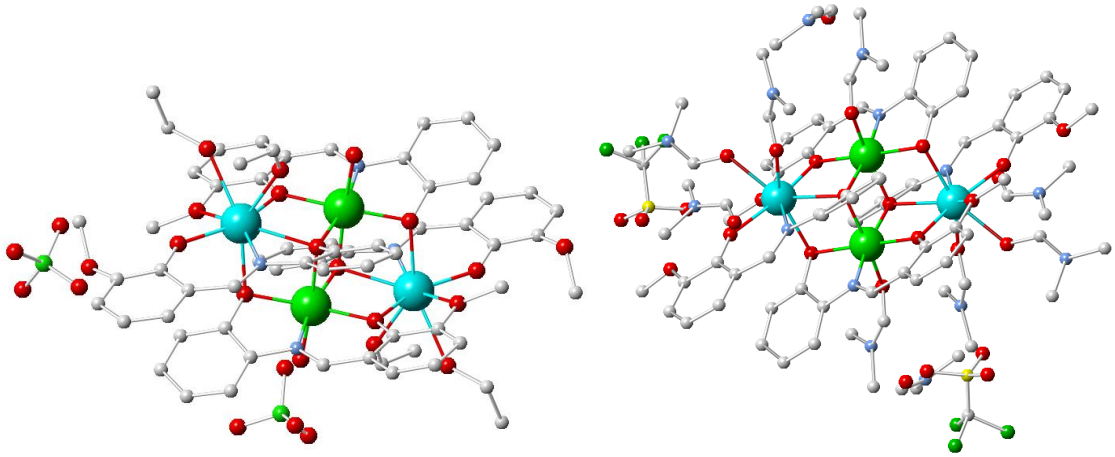

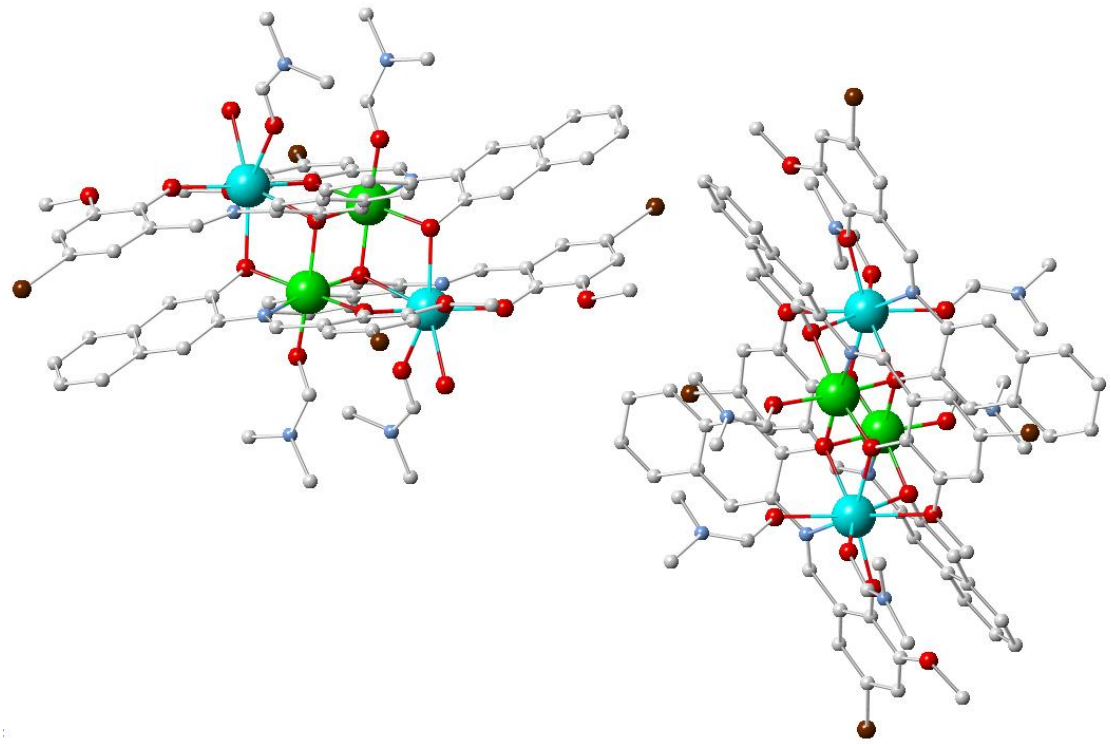

Figure 5.6. The crystal structures of **32 - 34**. Colour code: Ni^{II}, green; Dy^{III}, light blue; N blue; O, red; C, white; Br, blue; F, green; S, yellow. Hydrogen atoms omitted for clarity.

5.2.2.4 Molar ratio

The reaction of $Ni(ClO_4)_2 \cdot 6(H_2O)$, $Dy(OTf)_3$ and H_2**L2** with Et_3N in MeOH, in the molar ratio 1:1:2:5, resulted in the isolation of a tetranuclear cubane formulated as $[Ni^{II}_4(\mathbf{L2})_4(MeOH)_4] \cdot 6MeOH$ (**35**·6MeOH) which is isoskeletal to a cubic Ni_4 PCC reported recently.[361] However, performing the same reaction in EtOH, results in the isolation of the targeted isoskeletal tetranuclear $[Ni^{II}_2Dy^{III}_2(\mathbf{L2})_4(EtOH)_6](ClO_4)_2 \cdot 4EtOH$ (**36**·4EtOH) (Figure 5.7).

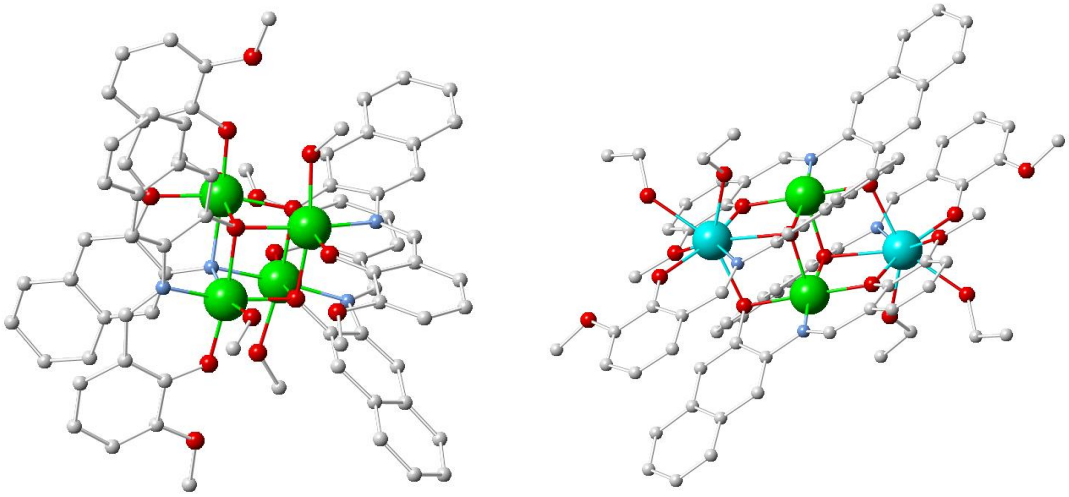

Figure. 5.7. The crystal structures of compounds **35** (left) and **36** (right). Colour code: Ni^{II}, green; Dy^{III}, light blue; N, blue; O, red; C, white. Hydrogen atoms omitted for clarity.

5.2.2.5 Solvent diffusion crystallization

In the effort to obtain the targeted tetranuclear $Ni^{II}_2Dy^{III}_2$ analogues with H_2**L19** as a ligand via the diffusion crystallization technique, a compound formulated as $[Ni^{II}_2Dy^{III}_2(\mathbf{L19})_4(DMF)_6](ClO_4)_2\cdot 2Et_2O$ (**37**·$2Et_2O$) (Figure 5.8, left) which contains two ether molecules as lattice solvent, was isolated.[367,368,397,398] Upon standing at room temperature, compound **37** immediately loses its crystallinity.

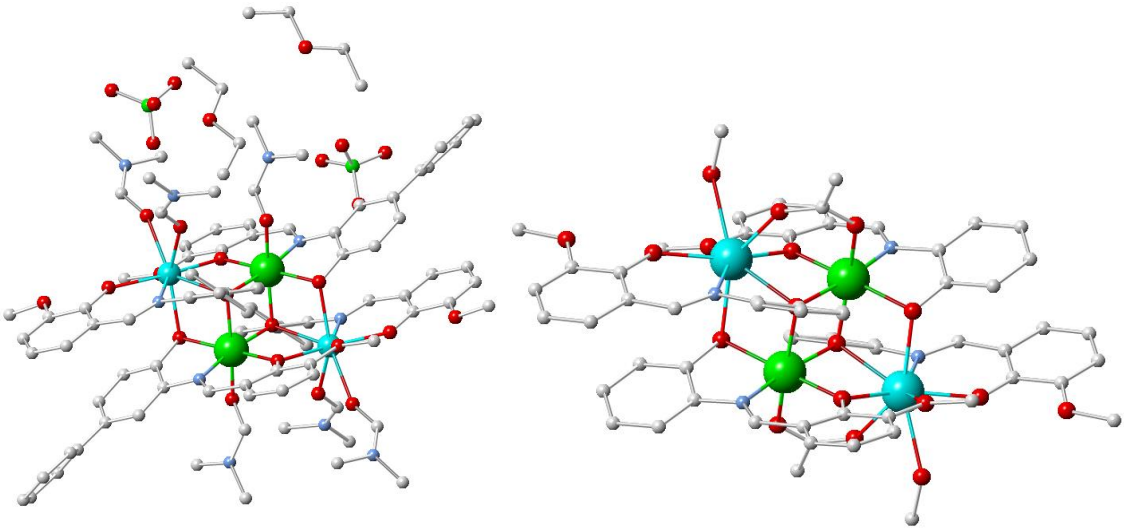

Figure. 5.8. The crystal structures of compound **37** (left) and **38** (right). Colour code: Ni^{II}, green; Dy^{III}, light blue; N, blue; O, red; C, white; Cl, light green. Hydrogen atoms omitted for clarity.

5.2.2.6 Co-ligand introduction

To identify the possibility of whether a monocarboxylate co-ligand could bridge between Ni^{II} and Dy^{III} centres, a pilot reaction with H_2**L1**, $Ni(OAc)_2\cdot 4(H_2O)$, $Dy(OTf)_3$ and Et_3N in the molar ratio 2:1:1:2 in MeOH was performed and resulted in the isolation of a compound formulated as $[Ni^{II}_2Dy^{III}_2(\mathbf{L1})_4(OAc)_2(MeOH)_2]\cdot 2MeOH$ (**38**·2MeOH) (Figure 5.8, right). Each acetate group bridges the Ni^{II} and Dy^{III} centres, which contrasts with the NO_3 analogues that prefer to chelate to the Ln^{III} centres.[2,50]

Employment of the bulky co-ligands **M1** and **M2** along with ligand H_2**L9**, $Co(ClO_4)_2\cdot 6H_2O$ and $Dy(OTf)_3$ in the molar ratio of 2:1:1:5 and in DMF as solvent results in the isolation of two compounds formulated as $[Co^{II}_2Dy^{III}_2(\mathbf{L9})_4(\mathbf{M1})_2(DMF)_2]$ (**39**) and $[Co^{II}_2Dy^{III}_2(\mathbf{L9})_4(\mathbf{M2})_2(DMF)_2]\cdot 2DMF$ (**40**·2DMF), respectively (Figure 5.9).

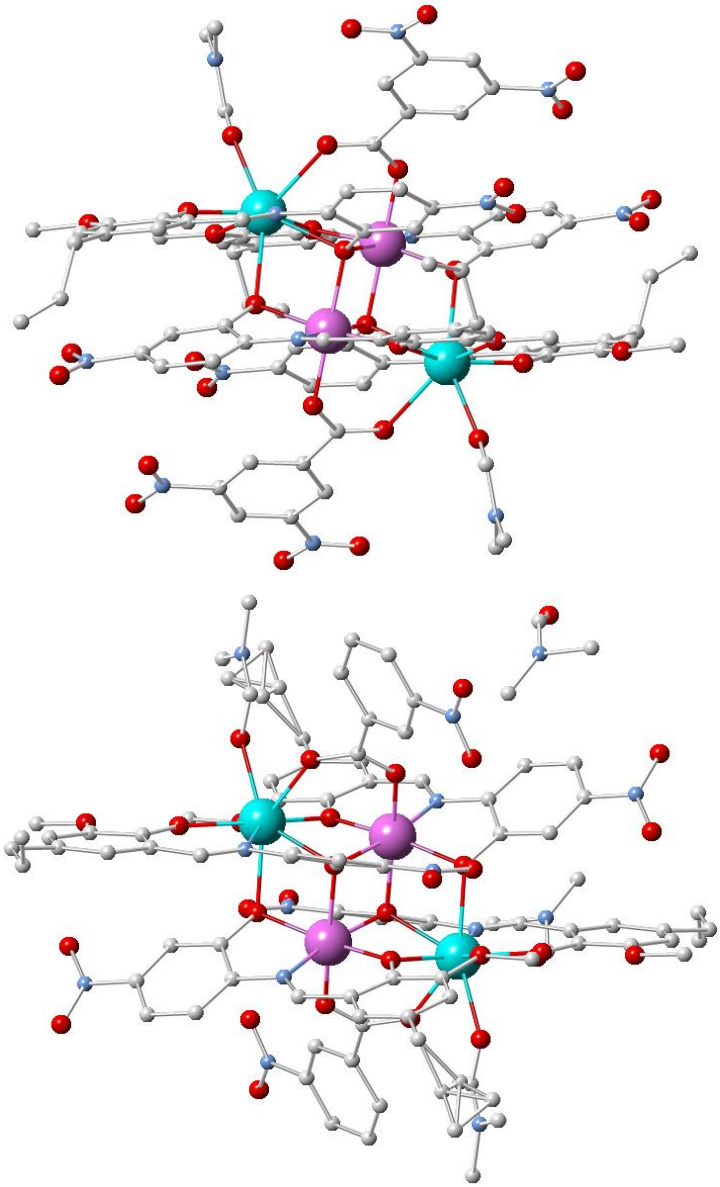

Figure. 5.9. The crystal structures of compounds **39** (upper) and **40** (lower). Colour code: Co^{II}, pink; Dy^{III}, light blue; N, blue; O, red; C, white. Hydrogen atoms omitted for clarity.

The effort to obtain the isoskeletal **M1** $Co^{II}_2Dy^{III}_2$ compound with **H_2L8** instead of **H_2L9**, by performing a similar reaction, resulted in red plate crystals formulated as $[Dy^{III}(\mathbf{M1})_3(DMF)_2]$ (**41**) (Figure 5.10). Compound **41** is a one dimensional (1D) coordination polymer and can be considered as a polymorph to a recently reported compound.[399]

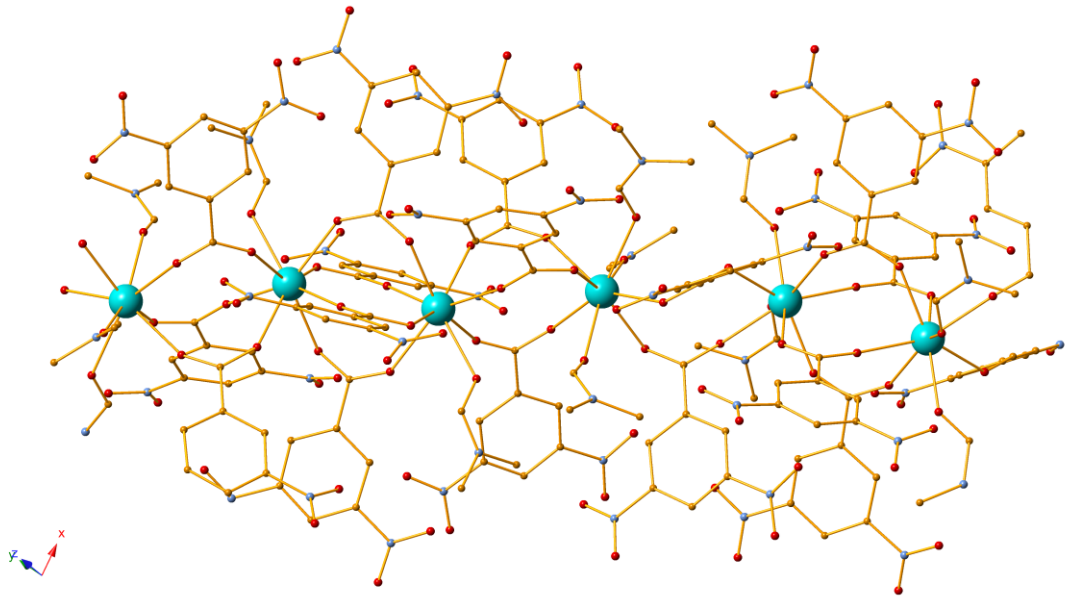

Figure. 5.10. The crystal structure of compound **41**. Colour code: Dy^{III}, light blue; N, blue; O, red; C, orange. Hydrogen atoms omitted for clarity.

Finally, the diffusion of Et_2O to a concentrated reaction of ligand H_2**L5** along with $Ni(ClO_4)\cdot 6H_2O$, $Dy(OTf)_3$, **M1** and Et_3N in DMF resulted in the formation of a compound formulated as $[Ni^{II}_2Dy^{III}_2(OH)(\mathbf{L2})_3(\mathbf{M1})_3(DMF)_2]\cdot 1.5DMF\cdot Et_2O$ (**42**$\cdot$1.5DMF$\cdot Et_2O$) which possesses the **2,3M4-1** topology. Surprisingly, only three organic ligands are involved in the aggregation in contrast to four ligands used in other **2,3M4-1** PCCs supported by H_2**LX**. The skeleton of **42** is further supported by the presence of a hydroxyl μ_3-OH group and one Et_2O molecule is trapped in the lattice.

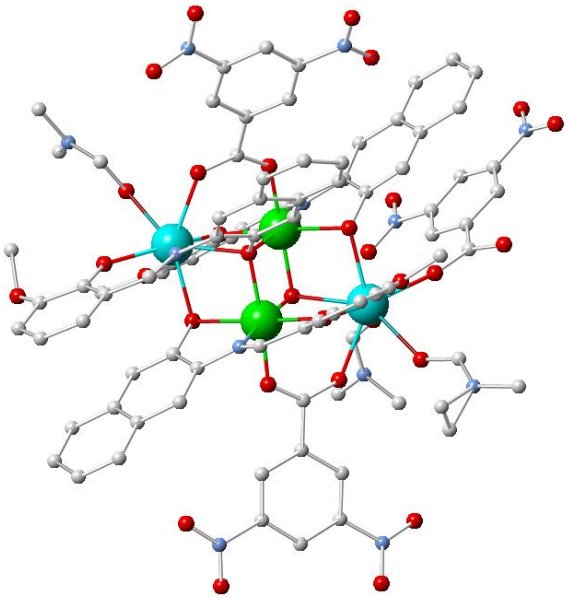

Figure. 5.11. The crystal structure of compound **42**. Colour code: Ni, green; Dy, light blue; N, blue; O, red; C, white. Hydrogen atoms omitted for clarity.

5.2.2.7 ESI-MS studies

To confirm the identity of compounds **28**, **31** and **37** in solution, ESI-MS studies were performed. (Table 5.2). For compound **28**, three peaks in the MS (positive-ion mode) which correspond perfectly to three dicationic fragments were observed (Appendix B, S5.18). For compounds **31** and **37,** four peaks in the MS (positive-ion mode) which correspond to a cationic fragment and three dicationic fragments were observed (Appendix B, S5.19 and S5.20)

Table 5.2. Observed peaks for **28**, **31** and **37** in ESI-MS with corresponding peak assignments.

	Observed fragments and corresponding peaks / m/z	
	$[Ni^{II}_2Dy^{III}_2(\mathbf{LX})_4(MeOH)]^+$	$[Ni^{II}_2Dy^{III}_2(\mathbf{LX})_4]^{2+}$
28	n/a	936.1485
X = 20		+(DMF) 972.1730
		+2(DMF) 1009.2113
31	1742.2549	803.067
X = 16		+(DMF) 840.0702
		+2(DMF) 876.6074
37	1847.228	855.5781
X = 19		+(DMF) 892.1121
		+2(DMF) 929.1356

All the efforts to obtain similar ESI-MS spectra for compounds **39** and **40,** which contain a co-ligand, were unsuccessful.

5.2.2.8 Theoretical studies

To gain further insight into the tuning and modulation of, *inter alia*, the catalytic activities of the tetranuclear **2,3M4-1** PCCs, computational studies were performed. Specifically, the influence of the Schiff base ligands on the electronic properties of the metals was studied, in effect, the 'activity' of the ligands themselves can be, in turn, modified by employing diverse functional groups at specific sites/positions.

Quantitative and qualitative metrics of the functional group effects were established and in parallel, several congeners of the ligands were examined (Tables 5.3 and 5.4). Several model systems of the PCCs were used. Figure 5.12 shows the visualization of the mapped Molecular Electrostatic Potential (MEP) in ligands L1m to L12m, as with the usual MEP rendering, with blue zones depicting 'positively' charged zones while red zones the 'negatively charged zones'.

One way to assess the effect of the electron withdrawing groups on the Schiff base is to qualitatively render the MEP mapped onto the van der Waals surface. The nature of the R groups has a profound effect on the surface charge of the base on its 'inner cove' – that is, the O-O-N-O core pattern directly interacting with the metals. Figure 5.12 and Table 5.6 qualitatively illustrate

this idea. Unsurprisingly, results show charge distribution along the cove can be modulated upon modification of the groups.

Table 5.3. Recapitulative table of the model ligands used.

LX	R_1	R_2	R_3
L1m	H	H	H
L2m	OMe	H	H
L3m	$N(CH_2CH_3)_2$	H	H
L4m	F	H	H
L5m	H	H	NO_2
L6m	$CH_2CH{=}CH_2$	H	NO_2
L7m	NO_2	H	H
L8m	NO_2	H	H
L9m	H	Cl	NO_2
L10m	Br	H	NO_2
L11m	NO_2	H	NO_2
L12m	NO_2	Cl	NO_2

L7m: An additional NO_2 is substituted at the ortho position adjacent to R_2.

Table 5.4. Recapitulative table of the co-ligands used.

coL	R_4	R_5	R_6
coL1m	H	H	H
coL2m	H	F	H
coL3m	NO_2	H	NO_2

In the gas phase, in their most stable geometrical configuration, the ‘simplest’ functionalization, i.e. having $R_1 = R_2 = R_3 = H$ turns out to confer the most of negative charge accumulation on the ligand 'anchor' points, the least being with $R_1 = NO_2$, $R_2 = Cl$, $R_3 = NO_2$. Interestingly, for a given R_1, changing R_3 has a profound effect on the charge distribution which is illustrated by considering L1m and L5m. On the other hand, for a given R_3, changing R_1 does not have a noticeable altering effect, as shown for example by L5m versus L10m and L1m versus L2m. More crucially, the conformation of the ligand ultimately determines the extent, nature and motifs of interaction between the metal-interacting side of the ligands and the metals (Figure 5.13).

Single point (sp) calculations on L6m in its ligand-bound geometry exhibits a different charge distribution signature with respect to that of its gas-phase optimized structure (gp). The geometries differ by having the nitrogen-bound aryl group (ring 2) rotated clockwise (gp) or

counter-clockwise (sp) around the N-C(aryl) bond. This observation can be rationalized when one considers the Frontier Molecular Orbitals (FMO)s.

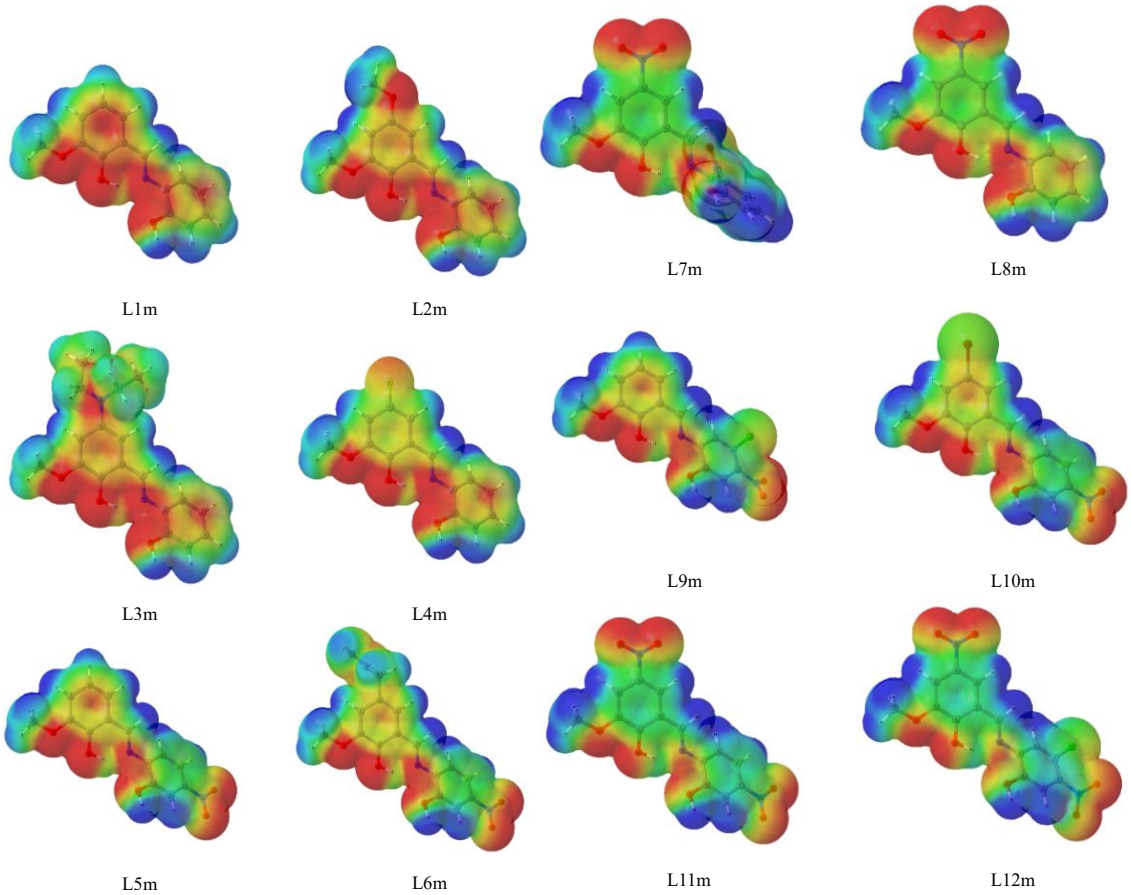

Figure. 5.12. The rendition of the MEP of the model ligands.

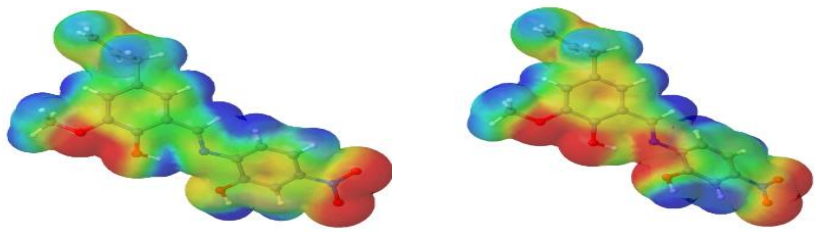

Figure. 5.13. The rendition of the MEP of L6m in its ligand-bound (left) and in its free conformation (right).

Inspection of the LUMO – HOMO-2 of the L6m (sp), indicates that the Molecular Orbitals (MO) consist mainly of a π network running throughout the whole of the molecule. Even more remarkable is the low mixing of atomic p orbitals perpendicular to the molecular plane, defined by ring 1 (the aryl-containing R1) and the N-centred p orbital that is parallel to this plane (Figure 5.14). This very orientation of the p orbital should also be responsible for the dependence of the cove charge distribution on the orientation of the hydrogens over the OH functions on both rings (data not shown).

In terms of partial atomic charge within the Mulliken partitioning scheme, it can be noted that there are variations in values on the metals on the two oxygen and the nitrogen atoms (see Table 5.6) depending on the makeup of the ligand. Close examination suggests that, in terms of partial charges, both M2 and O1 (OH on ring 1) are spectator elements, i.e. the value of their partial charge does not depend on that of the other atoms whereas there is a correlation between the partial charge on N, O2 (OH on ring 2) and M1, there exist an interdependence of the values of partial charge on these centres. The largest of such variations occur for metal M1 and is observed between model m2 11a and model m3 12. These results perfectly correspond with that of the charge distribution being dependent on the orientation of ring 2.

Table 5.5. Recapitulative table of the models used.

Model	**M1**	**M2**	**LX**	coL	S
m1 11	Zn	Y	L1m	coL2m	$(CH_3)_2NCOH$
m2 11a	Ni	Y	L1m	coL2m	$(CH_3)_2NCOH$
m3 12	Zn	Y	L5m	MeOH	NO_3
m4 12a	Ni	Y	L5m	MeOH	NO_3
m5 13	Zn	Y	L1m	EtOH	-
m6 14	Zn	Y	L6m	coL3m	S1m
m7 14b	Zn	Y	L1m	coL3m	S1m

Table 5.6. Mulliken charges.

model	q(M1)	q(M2)	q(O1)	q(N)	q(O2)
m1 11	0.79	1.49	-0.64	-0.20	-0.61
m2 11a	0.53	1.49	-0.61	-0.16	-0.59
m3 12	0.93	1.34	-0.55	-0.26	-0.73
m4 12a	0.69	1.36	-0.62	-0.17	-0.58
m5 13	0.86	1.32	-0.56	-0.30	-0.73
m6 14	0.85	1.56	-0.55	-0.27	-0.70
m7 14b	0.85	1.55	-0.56	-0.27	-0.71

The above results clearly show the richness of the chemistry of the presented PCCs. The nature of metal ions and the identity of the R groups in the ligands play preponderant roles in both the tuning and control of the behaviour of the clusters. With the trends and rationale hereby demonstrated, it should be possible in future work to better modulate the activity of the clusters through tuning of the electronic structure and control of structural constraints.

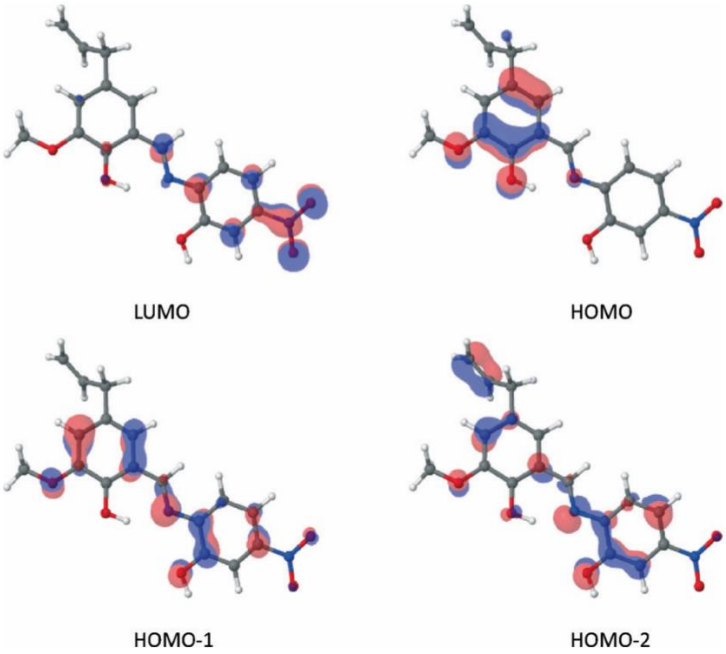

Figure 5.14. FMOs of L6m (sp).

5.3 Conclusion

In this work, the synthesis of nineteen new modified Schiff base organic ligands (H_2**L2** - H_2**L22**) and eighteen new PCCs is presented. The term "isoskeletal" is introduced, which ideally describes structural and topological similarities found in compounds **30** – **37**, **39** – **43** and **45**.

Microwave synthesis has proven to be very effective for the synthesis of the substituted Schiff base ligands.[400] To target defect dicubane isoskeletal species, it is shown that several parameters must be taken into account. It is shown here that a slight change in the synthetic procedure drastically affects the formula of the desired PCC. However, the usage of different lanthanide sources and the lanthanide contraction are two parameters that have not been considered in this study and are anticipated to have a major impact in the shape, nuclearity and formula of the final product.

The possibility of producing isoskeletal species and exchanging the 3d and/or the 4f element with diamagnetic elements such as Zn^{II} or Y^{III}, presents the opportunity to further study the targeted molecules in the solid and/or solution state, with additional spectroscopic techniques such as NMR (^{1}H, ^{13}C, ^{89}Y) or Electron Paramagnetic Resonance (EPR) studies for the Gd^{III} analogue.
ESI-MS studies of compounds **31**, **34** and **40** are indicative that the targeted species retain intact in solution. However, upon introduction of co-ligands, the targeted PCCs do not remain intact in solution. Computational studies demonstrate how the likely activity of the PCCs can be tuned and modulated and suggesting ways of achieving this, hence demonstrating the richness of the chemistry of the hereby reported constructs.

Chapter 6: Two unprecedented purse-shaped pentadecanuclear $Zn^{II}_4Ln^{III}_{11}$ (Ln = Gd, Dy) PCCs

Abstract: The *in situ* reaction of o-vanillin and *trans*-2-amino-cyclohexanol with $Zn(NO_3)_2{\cdot}6H_2O$, $LnCl_3{\cdot}5H_2O$ afforded a family of pentadecanuclear heterometallic polynuclear coordination clusters formulated $[Zn^{II}_4Ln^{III}_{11}(\mu_4\text{-}OH)_2(\mu_3\text{-}OH)_8(\mu_2\text{-}OH_2)_2(\mu_3\text{-}NO_3)_2(NO_3)_6Cl_4(H\mathbf{L23})_2(\mathbf{L23'})_4(\mu_2\text{-}MeO)_7(\mu_3\text{-}MeO)_2(MeOH)_2(H_2O)_2]$ where Ln = Dy (**43**), Gd = (**44**). These compounds display a unique topology and are enumerated as **1,2,3,4,5,5,5,8M15-1**. The core displays many unique features including a Ln^{III} diabolo motif (**4,8M9-1**) and a previously unseen ligand transformation. Magnetic studies demonstrate the importance of the central spin orientation in the spin structure of the ambiguous Ln_9-diabolo motif. The single-molecule magnet properties of the Dy^{III} analogue (**43**) are elucidated through disentangling the magnetic properties of the isostructural Gd^{III} analogue (**44**).

6.1 Introduction

A few 3d-4f, crystallographically characterised[141,302] or formed *in situ*,[296–298] bimetallic catalysts have been reported. Previously the catalytic efficiency of a series of tetranuclear $Zn^{II}_2Ln^{III}_2$ PCCs, built from H_2**L1** (Figure 6.1, left) towards Friedel-Crafts (FC) alkylation[344] and Petasis-Mannich[401] reactions were reported. Aiming to develop a class of bimetallic co-operative catalysts for enantioselective purposes, it was envisioned that ligand H_2**L23** (Figure 6.1), that offers similar coordination pockets to H_2**L1**, was an excellent candidate to harvest the corresponding isoskeletal defect dicubane tetranuclear PCCs.[366] The coordination chemistry of H_2**L23** has received less attention and has never been used in 3d, 4f or 3d-4f chemistry.[402]

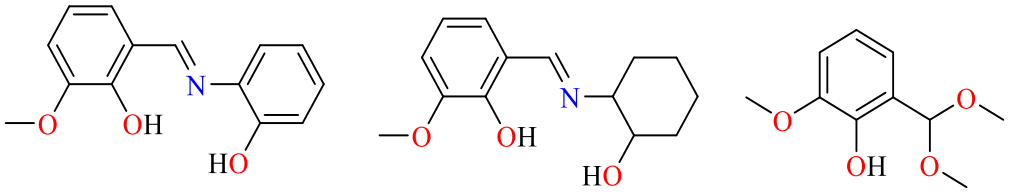

H_2**L1** H_2**L23** H_2**L23'**

Figure 6.1. The protonated form of H_2**L1** (left). The protonated form of H_2**L23** (middle). The protonated form of the transformed ligand (H_2**L23'**) (right).

In a reaction aimed at yielding such a chiral $Zn^{II}_2Ln^{III}_2$ defect cicubanes, the *in situ* reaction of o-vanillin and *trans*-2-amino-cyclohexanol in methanolic solvent with $LnCl_3{\cdot}xH_2O$, $Zn(NO_3)_2{\cdot}6H_2O$ and Et_3N was performed which resulted instead in an unprecedented transformation of some of the H_2**L23** ligand to the achiral H_2**L23'** ligand (Figure 6.1, right) accompanied by the stabilization of one of the largest Zn^{II}-4f PCCs so far reported with the general

formula $[Zn^{II}_4Ln^{III}_{11}(\mu_4\text{-}OH)_2(\mu_3\text{-}OH)_8(\mu_2\text{-}OH_2)_2(\mu_3\text{-}NO_3)_2(NO_3)_6Cl_4(H\mathbf{L23})_2(\mathbf{L23'})_4(\mu_2\text{-}MeO)_7(\mu_3\text{-}MeO)_2(MeOH)_2(H_2O)_2]$ where Ln = Dy (**43**), Gd = (**44**). The resulting structure forms around the well known Ln^{III}_9 "diabolo" motif encapsulated within units of $Zn^{II}_2Ln^{II}_2$ and Zn^{II}_2, which provide a C_2 symmetry and thereby confer the system with a chirality which aids in understanding the spin structure of the central Ln_9 diabolo unit. The molecular structure, topological representations and magnetic studies are discussed.

6.2 Results and discussion

6.2.1 Molecular structure of compounds 43 and 44

Single-crystal XRD studies reveal the formation of a pentadecanuclear PCC with the general formula $[Zn^{II}_4Ln^{III}_{11}(\mu_4\text{-}OH)_2(\mu_3\text{-}OH)_8(\mu_2\text{-}OH_2)_2(\mu_3\text{-}NO_3)_2(NO_3)_6Cl_4(H\mathbf{L23})_2(\mathbf{L23'})_4(\mu_2\text{-}MeO)_7(\mu_3\text{-}MeO)_2(MeOH)_2(H_2O)_2]$ where Ln is Gd (**43**) and Dy (**44**) (Figure 6.3). Compounds **43** and **44** are isostructural and isomorphous, as identified by single-crystal XRD studies (chapter twelve), EA (chapter eleven), FT-IR (Appendix B) and TGA (Appendix B, S6.1).

Compounds **43** and **44** crystallize in the monoclinic space group C2/c with *Z* = 4. The pentadecanuclear core consists of two units, a trianionic undecanuclear $[Zn^{II}_2Ln^{III}_9(\mu_4\text{-}O)_2(\mu_3\text{-}OH)_8(\mu_2\text{-}OH)_2(NO_3)_8Cl_2(\mathbf{L23'})_4(\mu_2\text{-}MeO)_4(\mu_3\text{-}MeO)_2(H_2O)_2]^{3-}$ "body" unit (Figure 6.2) and a tetranuclear $[Zn^{II}Ln^{III}_2Zn^{II}(H\mathbf{L23})_2(\mu_2MeO)_3Cl_2(MeOH)_2]^{3+}$ "handlebar" unit (Figure 6.2).

Within the $Zn^{II}_2Ln^{III}_9$ part, the nonanuclear lanthanide unit is held together by two μ_4- O (O29), eight μ_3-OH (O25, O26, O27, O28 and their symmetry-related counterparts), two μ_2-OH molecules (O30) and four *in situ* formed *o*-vanillin derivatives (**L23'**) (Figure 6.1). This nonanuclear motif is often referred to as "diabolo" shaped and has been identified in several compounds.[403–405]

The diabolo description derives from the similarity to the topology of a double spinning top which a player performs tricks with using a two-handled rope. In the compound that is described here, the hands and rope are provided by the "handlebar unit", corresponding to Zn2 and Ln6 and their symmetry equivalents, respectively, the diabolo is provided by the Ln_9 core, where Ln2, Ln3, Ln4 and Ln5 (and their symmetry-related counterparts) form two square planes arranged as a square antiprism with Ln1 in the middle. The "feet" of the player corresponding to the lower two Zn2 and Zn2' ions (Figure 6.2).

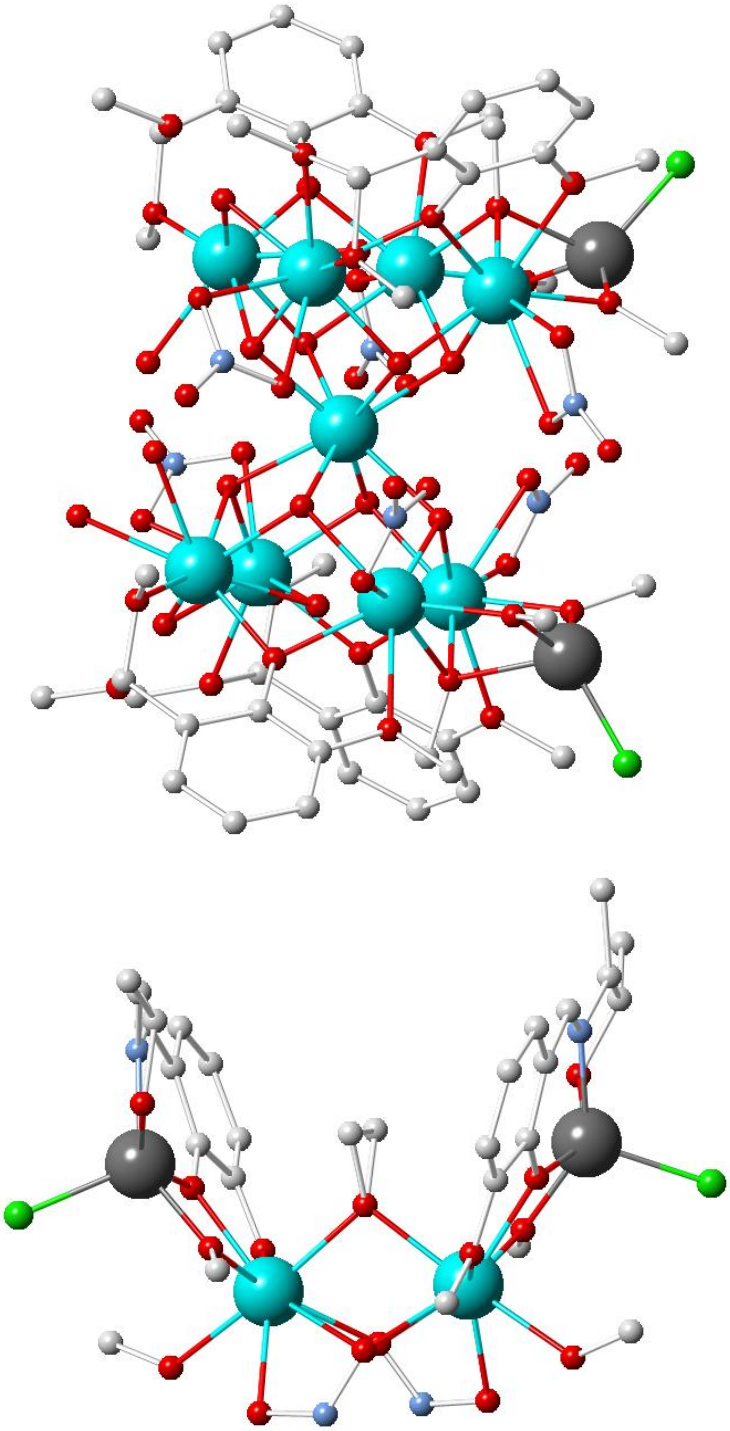

Figure. 6.2. The undecanuclear $[Zn^{II}_2Ln^{III}_9(\mu_4\text{-}O)_2(\mu_3\text{-}OH)_8(\mu_2\text{-}OH)_2(NO_3)_8Cl_2(\mathbf{L23'})_4(\mu_2MeO)_4(\mu_3\text{-}MeO)_2(H_2O)_2]^{3-}$ "body" unit (upper) and tetranuclear $[Zn^{II}Ln^{III}_2Zn^{II}(H\mathbf{L23})_2(\mu_2MeO)_3Cl_2(MeOH)2]^{3+}$ "handlebar" unit (lower). Colour code: Ln^{III}, light blue; Zn^{II}, grey; C, black; N, blue; O, red; C, green; H atoms omitted for clarity.

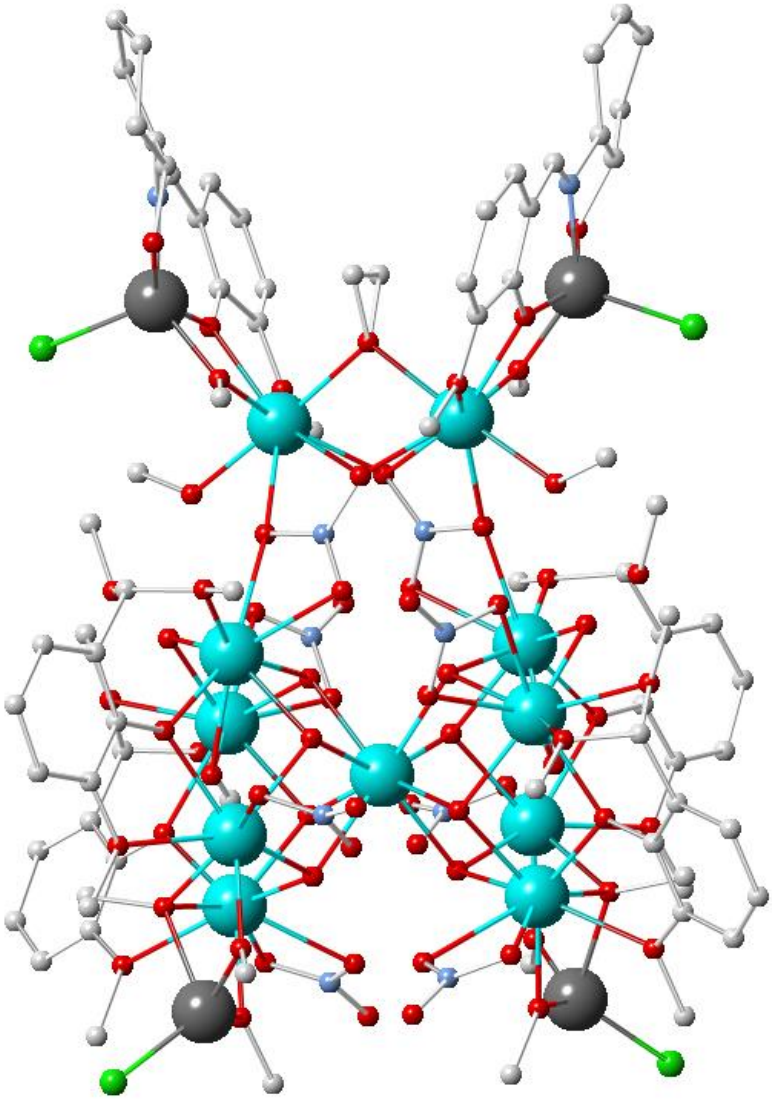

Figure 6.3. The molecular structure of **44**. Colour code: Gd^{III}, light blue; Zn^{II}, grey; C, black; N, blue; O, red; C, green; H atoms omitted for clarity.

The nonanuclear Ln_9 core is connected by two triply bridging methoxido units (O3) bridging Gd3, Gd4 to Zn1 and the symmetry equivalents, thereby forming the undecanuclear core. The attachment of Zn1 to the Gd_9 unit is further supported by two doubly bridging methoxido moieties (O2 and O4). Gd2, Gd3 and Gd4 are chelated by a nitrate moiety, whereas Gd5, Gd 6 and Gd6' are linked by another tridentate nitrate group thereby providing attachment to the main core and the tetranuclear unit. Gd6 and Gd6' are bridged by a methoxido moiety (O32), whereas Gd6 is linked to Zn2 by doubly bridging methoxido (O33) and phenoxido (O35) units. Both Zn metal centres are five coordinate. Zn1 has a coordination geometry between square based pyramidal and trigonal bipyramidal with a trigonality index (τ) = 0.46, whereas Zn2 possesses an almost idea square pyramidal geometry (trigonality index (τ) = 0.06).

Gd1 and Gd6 are eight-coordinate and Gd2, Gd3, Gd4 and Gd5 are nine-coordinate. An analysis (S) using the SHAPE program (Appendix B, S6.3 and S6.4) shows that that the central Ln1 ion has an almost perfectly square antiprismatic geometry (0.33% deviation from SAPR-8) whilst the nine-coordinate Ln^{III} ions are close to a spherical capped square antiprismatic (CSAPR-9). These were determined as follows, Ln3 to Ln5 have a nitrate anion to fulfil their coordination sphere, where the Ln-N bond is within the range of 2.90 - 2.96 Å and are therefore not considered. In the case of Ln2 and Ln6 which are linked together via two nitrate groups, the Ln-N bond is shortened to 2.84 Å, but with the electron density coming most from the oxygens, these Ln-N are not considered either. Ln2 to Ln5 and Ln2' to Ln5' which are generated by symmetry operation respectively, are surrounded by nine oxygens, while Ln1, which is the metal ion located in the centre of the "sandglass", and the two Ln6 metal ions, which are part of the tetranuclear handle bar, are only eight-coordinated.

It appears here that, from the SHAPE analysis, Gd3/Dy4 and Gd4/Dy3 resemble each other. A similar behaviour occurs for Gd2/ Dy5, and Dy2/ Gd5 respectively. This is a consequence of having refined **44** anticlockwise in comparison to **43**. The nine-coordinate Ln^{III} ions are close to a spherical capped square antiprism (CSAPR-9, Appendix B, Table S6.3), with a deviation between 1.41-1.87% from the perfect geometry, although in case of Gd3, the surrounding atoms are closer to a "muffin" topology with a deviation of 1.34%. Gd6 is more distorted in the coordination environment and the smallest deviation was found to be biaugmented trigonal prismatic (BTPR-8, Appendix B, Table S6.4) with a deviation of 3.86%.

The *o*-vanillin derivative (H_2**L23**, Figure 6.1) and the *in situ* formed Schiff base ligand (H**L23'**, Figure 6.1) both bridge two metal centres respectively (Figure 6.4). Notably, the transformation of the o-vanillin moiety has never been observed before and moreover, the chiral framework of the ligand retains its stereochemistry.

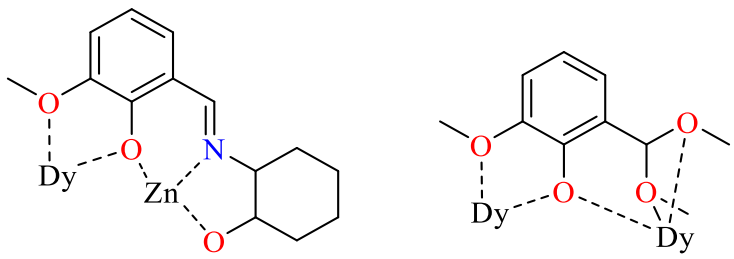

Figure 6.4. Observed coordination modes for H_2**L23** and H**L23'**.

TGA of compounds **43** and **44** (Appendix B, S6.2) show that they are stable up to 250 ºC, with only a 4.82% loss in mass before this temperature, which corresponds to a loss of methanolic solvent. Decomposition starts at 300 ºC and has a significant mass loss between 300 ºC - 320 ºC

(~40 - 42%). The mass slowly decreases until 500 ºC, where the final residue corresponds to the $Zn_4Ln_{11}O_{20.5}$ oxide 51.62% for Gd (**44**) and 52.36% for Dy (**43**).

6.2.2 Topological descriptions

The $Zn^{II}_4Ln^{III}_{11}$ core of compounds **43** and **44** can be enumerated as **1,2,3,4,5,5,5,8M15-1** (Figure 6.5) and has never been observed in PCC chemistry before. The pentadecanuclear compound is the third highest nuclearity example in Zn^{II}-Ln^{III} chemistry.[5,28,250]

From the automatic graph-based search of TOPOS, a comparison of the topology of the present compounds with previously reported compounds containing the diabolo motif (**4,8M9-1** graph, Figure 6.6) provides very interesting structural data which has not been identified previously in any structural description (Table 6.1).

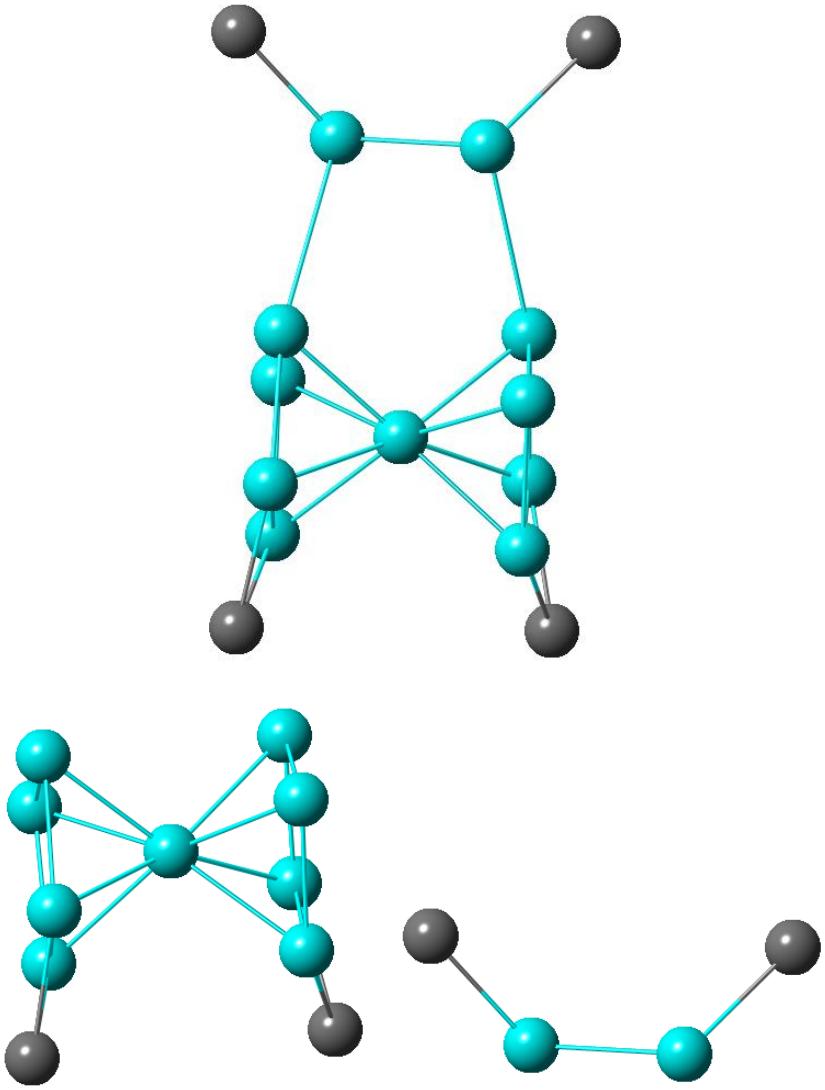

Figure 6.5. The **1,2,3,4,5,5,5,8M15-1** purse topology (upper), the **2,4,5,8M11-1** "body" topology (lower left) and the **1,2M4-1** "strap" topology (lower right). Colour code: Ln^{III} node, light blue; Zn^{II} node, grey.

In both **44** and **43**, the two Ln_4 planes of the diabolo are not parallel to each other. For **44** they are tilted at an angle of 0.888 ° and for **43** at 1.157 ° These values lie between those reported for previous examples, which range from 0.290 ° – 0.535 ° for the nearly co-parallel examples to the significantly tilted Dy_9 example reported by Tang et al. where the angle is 1.809 °. The two μ_4-O_2- bridge are placed 0.382 Å (in **44**) and 0.393 Å (in **43**) above the Ln_4 plane; these values are significantly higher than those previously reported ranging from 0.147 Å to 0.325 Å. The nonanuclear core in **44** and **43** is tetra-anionic, while all previously reported compounds are singly positively or negatively charged. The observed structural features for the compounds reported here are probably directed by the attachment of the $Zn^{II}Ln^{III}_2Zn^{II}$ handlebar unit to the nonanuclear core providing the twist to the structure.

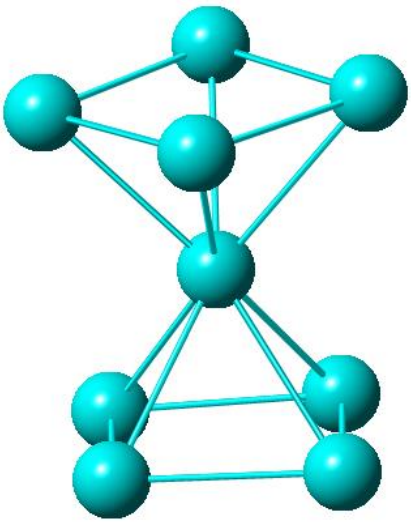

Figure 6.6. Diabolo topology **(4,8M9-1**). Colour code: Ln^{III} node, light blue.

6.2.3 Magnetic properties of compounds 43 and 44

The magnetic properties of both **43** and **44** complexes were recorded. The magnetic susceptibility of both compounds was measured between 1.9 and 300 K under an applied field of 1000 Oe (Figure 6.7).

The $\chi_M T$ value of 60.6 cm^3 K mol^{-1} at 300 K for Zn_4Gd_{11} (**44**) is smaller than the expected value of 86.7 cm^3 K mol^{-1} for eleven non-interacting Gd^{III} ions (S = 7/2, $^8S_{7/2}$, g = 2, C = 7.88 cm^3 K mol^{-1}). On lowering the temperature, the $\chi_M T$ product stays almost constant until 100 K, below which it steadily decreases until it reaches a minimum value of 58.9 cm^3 K mol^{-1} at 13.8 K. Below 4.7 K further cooling results in the $\chi_M T$ value increasing sharply to reach a value of 61.5 cm^3 K mol^{-1} at 1.8 K, indicating an onset of dominant ferromagnetic interactions among the lanthanide centres within the complex.

Table 6.1. Structural characteristic of reported compounds containing the diabolo **(4,8M9-1**) motif.

Compound core	Reference	Ln^{III} ion	Ln_9 Charge	Ln_4 plane CN	Ln central CN	Ln_4 planes angle	Ln_4 planes distance / Å	Nuclearity	O distance from Ln_4 plane/ Å	Space Group
Gd_{17}	[406]	Gd	neutral	9	8	0	5.499	17	0.319	*P*4212
Dy_{17}	[406]	Dy	neutral	9	8	0	5.482	17	0.325	*P*4212
Dy_9	[403]	Dy	1^+	8	8	1.809	5.772	9	0.147	*C*2/*c*
Dy_9	[404]	Dy	1^+	9	8	0.535	5.672	9	0.300	*C*2/*c*
Dy_9	[405]	Dy	1^+	9	8	0	5.759	9	0.248	*P*4/*n*
Gd_9	[405]	Gd	1^+	9	8	0	5.759	9	0.248	*P*4/*n*
Gd_9	[407]	Gd	1^+	8	8	0	5.427	9	0.266	*Pn*-3*n*
Dy_9	[407]	Dy	1^+	8	8	0	5.372	9	0.270	*Pn*-3*n*
Gd_9	[408]	Gd	1^-	8	8	0.541	5.319	9	0.236	*C*2/*c*
Gd_9	[409]	Gd	1^+	8	8	0.326	5.329	9	0.271	*Pbcn*
Dy_9	[408]	Dy	1^+	8	8	0.29	5.328	9	0.236	*C*2/*c*
Zn_4Gd_{11} (**44**)	This work	Gd	4^-	9	8	0.888	5.559	15	0.382	*C*2/*c*
$Zn4Dy_{11}$ (**43**)	This work	Dy	4^-	9	8	1.157	5.599	15	0.393	*C*2/*c*

Coordination Number (CN)

In the case of Zn_4Dy_{11} (**43**) the $\chi_M T$ value at 300 K of 105.9 cm^3 K mol^{-1} is also smaller than the expected value of 155.8 cm^3 K mol^{-1} for eleven non-interacting Dy^{III} ions (S = 5/2, $^6H_{15/2}$, g = 4/3, C = 14.17 cm^3 K mol^{-1}). On lowering the temperature, the $\chi_M T$ value steadily decreases until it reaches a minimum value of 85.6 cm^3 K mol^{-1} at 12.0 K and then steeply increases upon further cooling to reach a value of 116.0 cm^3 K mol^{-1} at 1.9 K, which again suggests the presence of intramolecular ferromagnetic interactions. This contrasts with other "diabolo" or "hourglass" shaped Gd_9 or Dy_9 cores reported in the literature, which are found to be antiferromagnetically coupled. It is believed this is the result of the presence of the tetranuclear $[Zn^{II}Ln^{III}_2Zn^{II}(H\mathbf{L23})_2(\mu_2\text{-MeO})_3Cl_2(MeOH)_2]^{3+}$ "handlebar" unit (Figure 6.1), containing a dimeric triply-oxygen bridged Ln^{III} motif and the chiral H**L23** ligand, with the C_2 axis lying between the two-lanthanide metal centres.

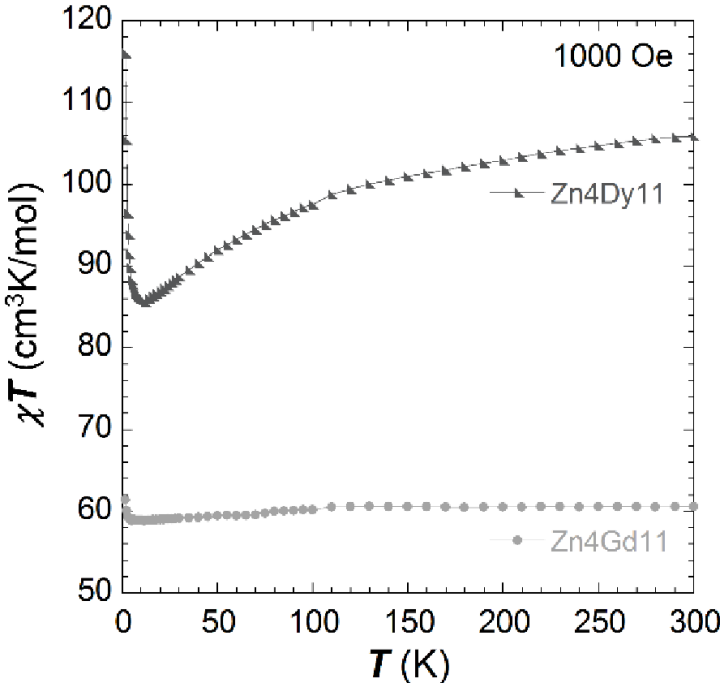

Figure 6.7. Temperature dependence of the $\chi_M T$ product at 1000 Oe for $Zn^{II}_4Gd^{III}_{11}$ (**44**) (light grey points) and $Zn^{II}_4Dy^{III}_{11}$ (**43**) (grey triangles).

The field dependence of the magnetization (Figure 6.8 and Figure 6.9) was measured between 2.0 to 5.0 K. For $Zn^{II}_4Dy^{III}_{11}$ (**43**) the lack of saturation in the magnetization values indicates the presence of magnetic anisotropy and/or low-lying excited states.

The magnetization curve for compound **43** shows no saturation up to 7.0 T and the values of the isotherms rapidly increase at small fields before following a more gradual linear increase above 1.0 T without saturation. The reduced magnetization plot shown as M vs. H/T in Figure 6.9, shows the magnetization isotherms which clearly do not superpose onto a single master curve, which indicates the presence of anisotropy within the system.

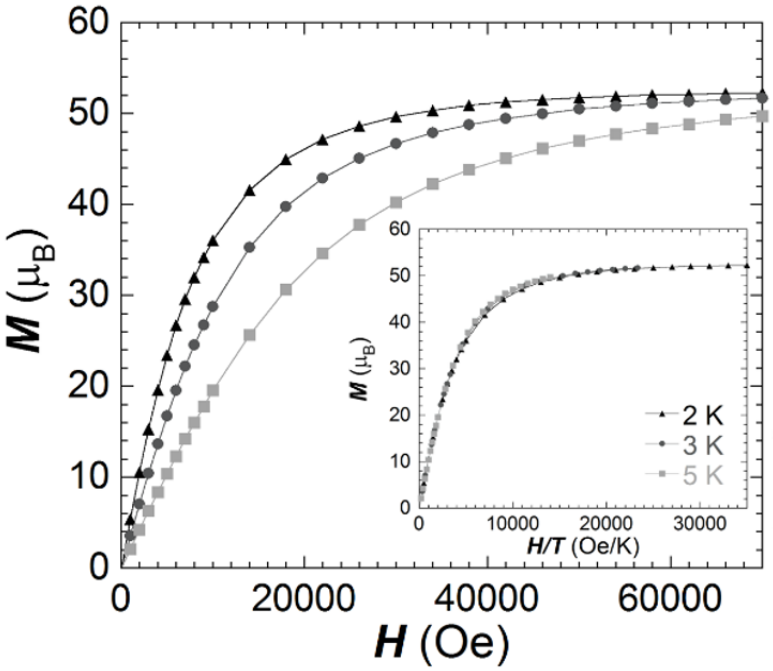

Figure 6.8. Field dependence of the magnetization plot of $Zn^{II}_4Gd^{III}_{11}$ (**44**) measured between 0 and 7 T at different temperatures; inset: the reduced magnetization.

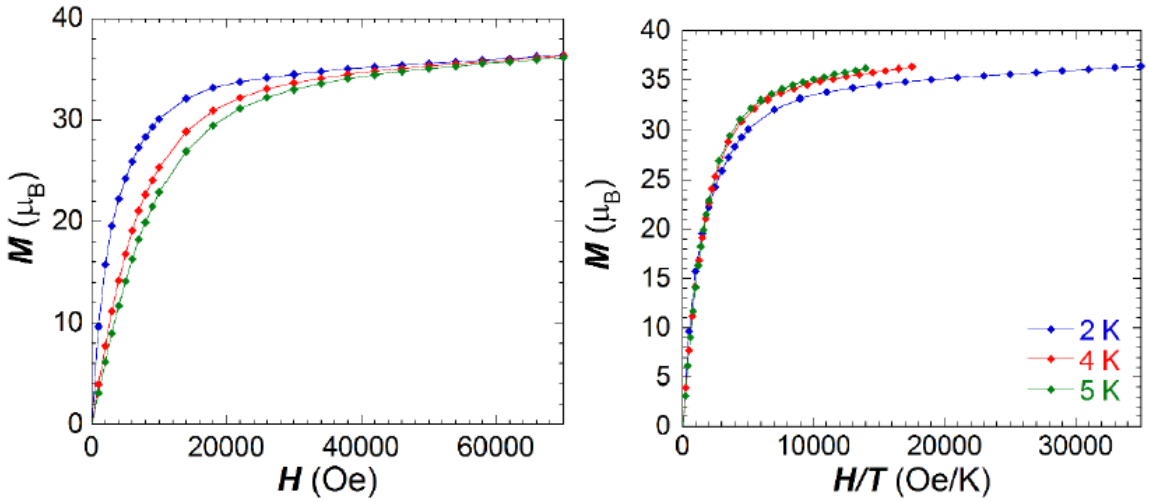

Figure 6.9. Field dependence of the magnetization plot of $Zn^{II}_4Dy^{III}_{11}$ (**43**) (left) measured between 0 and 7 T at different 2 K (blue), 4 K (red) and 5 K (green) reduced magnetization (right).

On the other hand, for $Zn^{II}_4Gd^{III}_{11}$ (**44**), which contains the isotropic Gd^{III} ions, the magnetization shows a rapid increase at small magnetic fields, which also follows a more gradual slope after 1.0 T, and reaches a clear saturation above 4.0 T. The reduced magnetization (Figure 6.8) shows a superposition of the three isotherms onto one master curve, as expected for an isotropic system. The saturation value of 52.2 μ_B at 7.0 T and 2.0 K is lower than the expected value of 77.0 μ_B for eleven Gd^{III} ions, which are uncoupled or completely ferromagnetically coupled, suggesting that not all metal centres have the same spin orientation.

ac magnetic susceptibility measurements were performed on $Zn^{II}_4Dy^{III}_{11}$ (**43**) to explore the presence of any slow relaxation of the magnetization compatible with SMM behaviour. The frequency dependent *ac* susceptibility was measured using various applied fields in attempts to suppress any QTM.

The optimum *dc* field, where the QTM is smallest, was found to be at 1000 Oe (Figure 6.10). The data obtained (Figure 6.11) between 1.8 and 4.0 K show temperature-dependent signals with shifting maxima clearly visible. The relaxation time as a function of the temperature (Figure 6.12) was analysed in terms of an ln(τ) versus 1/T points and fitted to an Arrhenius law to give U_{eff} = 4.7 K and τ_0 = 4.4.10^{-5} s (R = 0.99) (Figure 6.12).

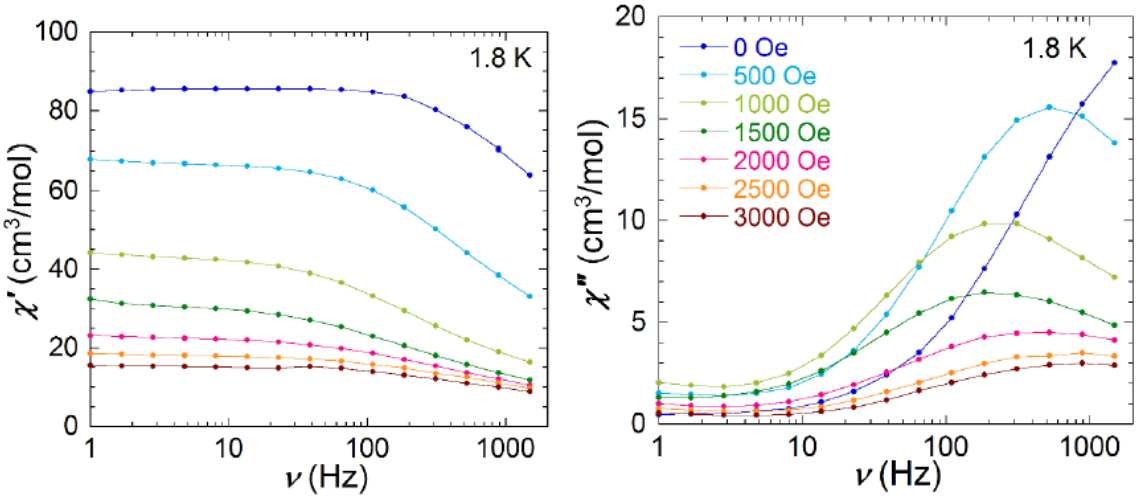

Figure 6.10. In-phase (left) and out-of-phase susceptibility (right) of $Zn^{II}_4Dy^{III}_{11}$ (**43**) at the varying field at 1.8 K.

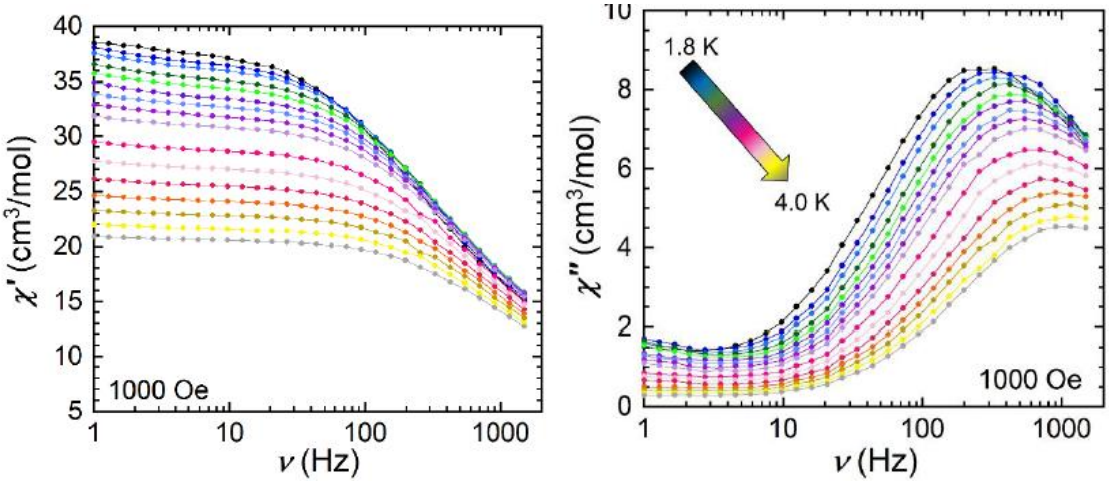

Figure 6.11. Frequency dependence of the in-phase χ_M' (left) and out-of phase χ_M'' (right) susceptibility for $Zn^{II}_4Dy^{III}_{11}$ (**43**) at different temperatures under an applied field of 1000 Oe.

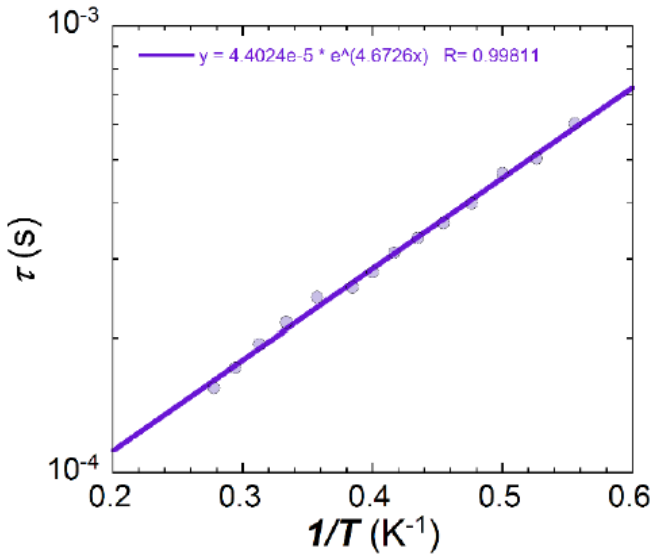

Figure 6.12. Arrhenius fit for $Zn^{II}_4Dy^{III}_{11}$ (**43**), leading to U_{eff} = 4.7 K and τ_0 = 4.4.10^{-5} s (R = 0.99).

On its own, the Ln_9 diabolo spin structure is ambiguous as discussed here for the Gd_9 spin structure. The spins on the squares forming the "sandwich" motifs providing the square antiprismatic coordination environment of the central Ln^{III} ion lead to two limiting cases.

The known Ln_9 diabolo structures tend towards the first case where the overall contribution of the two sandwich slices is effectively a zero-giant spin as a result of antiparallel arrangements of the eight S = 7/2 spins. In this case, the central spin is frustrated and possibly takes an overall average position essentially at right angles to the antiprismatic sandwiching squares. This leads to an observable but small S = 7/2 spin.

In the second limiting case, all the spins would be aligned parallel, which for nine x Gd^{III} would mean an expected spin ground state of S = 63/2. Neither limiting case has ever been identified. The compounds that are described in this chapter may provide the answer.

For case one, it is assumed eight antiparallel aligned spins are supplied by the sandwiching parts and thus a contribution of S = 0. The central spin number nine is essentially frustrated. In case two, where the spins on the "sandwich" part are all parallel, the contribution is S = eight x 7/2 = 56/2 and one might expect the central spin to be parallel, to these (S = 63/2). Case two is tended towards here in the central diabolo.

However, a key feature of the structure is that the introduction of the zinc "feet and hands" along with the tethering rope provided by the connecting Ln ions emphasizes the importance of the C_2 symmetry for the diabolo motif. The tethering rope provides a means for directing the spin on the central Ln of the diabolo unit and neatly explains why the spin structure for such units has always seemed ambiguous. Simply put, the central spin does not know which way to turn and is therefore

frustrated in the absence of any external influence. Here it can be seen that through the twisting action provided by the C_2 axis and emphasized by the handlebar motif, the resolution of the inherent chirality into “left or right” explains the induced spin ambiguity of the central Ln of the diabolo.

The electrostatically based modelling of Magellan fitting procedure was used to estimate the orientations of the magnetic anisotropy of the lanthanide ions. Layfield et al. showed for a dimeric Dy^{III} complex, that using the Magellan approach provided results similar to those obtained from ab initio calculations. This analysis provides insights into the interplay of the additional $Zn^{II}_2Dy^{III}_2$ handle-bar with the Dy_9 diabolo motif. The results of the analysis are shown in Figure 6.13 and indicate that the magnetic moments are oriented toroidally within the squares of the hourglass motif, pointing each towards their coordinating nitrate anion on the outside and the μ_4-O_2^- link in the middle of the metal plane. The axes lie at an angle of 37 ° to the plane defined by the four Dy^{III} ions (Dy_2 to Dy_5 and symmetry equivalents).

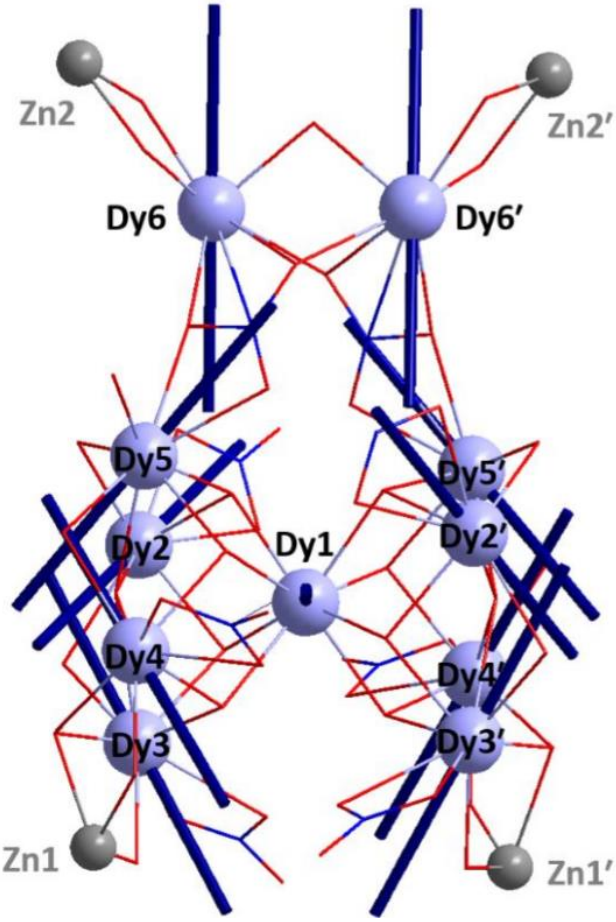

Figure 6.13. The orientation of the magnetic moments of the ground doublet according to an electrostatic model using the Magellan program, shown as dark blue lines for complex **43**. In this orientation, the uppermost pairs of Zn^{II}/Ln^{III} ions can be pictured as the hands (Zn) and handles to the (imaginary) rope which will twist the central Ln_9 diabolo in a left or right-handed sense whilst the bottom pair of Zn ions can be imagined as the feet of the diabolo artist.

If the alternative description is considered of the central hourglass as a diabolo, it is a useful description for the role of the outer Dy and Zn (Dy6 and Zn2 and symmetry equivalent) ions. When playing with a diabolo a two-handled rope, the $ZnLn_2Zn$ unit, provides a spin direction through the centre of the diabolo (here Dy (1)) and the performance of the diabolo depends on the applied spin direction induced on the central ion by either a slightly stronger left-hand or right-hand pull on the rope. This inherent induced chirality is clarified by examining the fine details of the molecular structure. Just as in the case of chiral bisphenoid and analogous structures, the scissor angle is crucial in deciding the degree to which the natural chirality of two homochiral scissor blades allows or blocks a cutting action. In the case here, it is concluded that the distorted orientation of the magnetic anisotropy axes can explain the ambiguity in the orientation of the spin of the central "bottleneck" Dy (1) centre of the hourglass motif.

In this case, the Magellan analysis suggests that the constriction at the centre of the hourglass corresponding to Dy1, has an orientation where its magnetic anisotropy axis points towards the *a* axis of the crystal system and is thus displaced from the central position of the axially elongated square antiprism sandwiching this central Dy1 ion. The magnetic anisotropy axes of the Dy6 and Dy6' ions are perpendicular to this and thus point towards the *b* axis of the crystal system. This distorted orientation of the magnetic anisotropy axes provides an explanation as to why the magnetization values at 7.0 T and 2.0 K are *ca* 1/3 smaller than the value expected for eleven Ln^{III} ions, which are either uncoupled or ferromagnetically coupled.

6.3 Conclusion

In conclusion, the first examples of 3d-4f PCCs containing the nonanuclear "diabolo" motif and the first example of a PCC with the **1,2,3,4,5,5,5,8M15-1** topology are presented. By extending the diabolo unit with "hands and feet" and by providing a tethering unit, which can direct the spin of the central ion of the diabolo unit, it has been possible to disentangle the "devil in the details" directing the spin structure of such diabolo units. In addition, the o-vanillin moiety gives an unseen chemical transformation yielding the organic ligand H**L23'**. Moreover, the isolation and characterization of these species showcase the importance of structural determination of potential catalysts and avoid their *in situ* formation. Future work will focus to develop other congeners of this system as well as new Zn^{II}-Ln^{III} PCCs with unusual topologies and interesting catalytic properties.

Chapter 7: Heteronuclear 3d/Ln^{III} PCCs as catalysts for the efficient synthesis of trans-4,5-diaminocyclopent-2-enones from 2-furaldehyde and primary or secondary amines

Abstract: Two isoskeletal defect dicubane polynuclear coordination clusters (PCCs) formulated $[M^{II}_2Dy^{III}_2(\mathbf{L1})_4(EtOH)_6](ClO_4)_2\cdot 2EtOH$ (M = Ni (**1NiDy-ClO$_4$**), Co (**1CoDy-ClO$_4$**) were synthesized and applied to the domino ring-opening electrocyclization synthesis of *trans*-4,5-diaminocyclopentanones from 2-furaldehyde and primary or secondary amines. Under reflux, an improved catalytic efficacy was observed and two isoskeletal PCCs were isolated, with the general formulas $[M^{II}_2Dy^{III}_2(\mathbf{L1})_4(Cl)_2(MeCN)_2]\cdot 2MeCN$ (M = Ni (**1NiDy-Cl**), Co (**1CoDy-Cl**).

Isoskeletal analogues of **1NiDy-Cl** were synthesized to investigate the influence of the Ln^{III} ion towards catalytic efficacy, with the general formula $[Ni^{II}_2Ln^{III}_2(\mathbf{L1})_4(Cl)_2(MeCN)_2]\cdot 2MeCN$ (**1NiLn-Cl** where Ln = Sm, Eu, Gd, Tb, Y). **1NiY-Cl** demonstrated a significantly improved catalytic efficacy over the other Ln^{III} analogues with half the catalytic loading. Optimized isoskeletal analogues (**LNiY-Cl**) with a modified organic periphery were synthesized, however, **1NiY-Cl** remained the catalyst of choice for the transformation. Density functional theory studies are presented to support catalytic data.

7.1 Introduction

This chapter represents the first attempt at developing well-characterised tetranuclear 3d-4f PCC catalysts, which are subsequently applied to an organic transformation. The isoskeletal $M^{II}_2Ln^{III}_2$ frameworks investigated in chapter five will be the basis for the PCC catalysts developed in this chapter.

Chapter five targeted 3d-Dy^{III} PCCs possessing a defect dicubane topology derived from H_2**L1** with 3d and 4f ions and were synthesised in high yields.[410] This topology bears two divalent 3d ions (centre) and two trivalent 4f ions (wings) (Figure 7.1), in the absence of any additional bridging atom,[2,50] with five out of six and six out of seven or eight coordination sites occupied by H_2**L1** for the 3d and the Dy^{III} centres, respectively (Figure 7.1). The key point in developing these catalytic species, from H_2**L1**, is the absence of any additional bridging atoms as the four metal centres assemble into the desired topology and the PCC can, therefore, remain intact in the solution.[337]

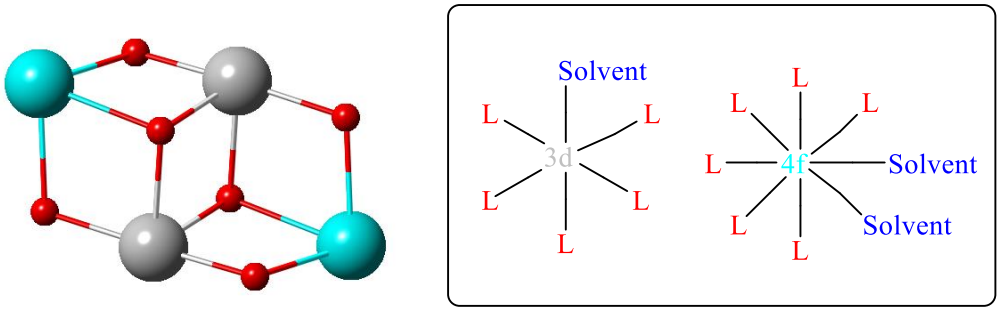

Figure 7.1. The defect dicubane motif (left). A representation of the coordination environment of the 3d and 4f ions in this motif (right).

The choice of the 4f ion, in the $M^{II}_2Ln^{III}_2$ framework, that could demonstrate catalytic efficacy in a corresponding transformation was paramount. Previously, dysprosium salts, due to their mild nature, have proven to be excellent catalysts for reactions where both nitrogen and oxygen functionalities are present.[411] Of particular interest is its ability to retain catalytic activity in the presence of Lewis-basic nitrogen groups, allowing for its use in transformations involving unprotected amines.[412–414]

With these factors in mind a potential reaction in which the efficacy of 3d-Dy^{III} PCCs could be tested was sought. Batey and co-workers reported on the use of $Dy(OTf)_3$ as a Lewis acid catalyst for the domino condensation/ring-opening/electrocyclization of secondary amines and 2-furaldehyde, leading to the synthesis of exclusively *trans*-4,5-diaminocyclopent-2-enones.[412] This is a remarkably atom-efficient reaction with only one equivalent of water generated as a side product. The authors postulated that the reaction proceeds through a deprotonated Stenhouse salt intermediate, although they showed that the lanthanide is not involved in the cyclization step. Primary amines required the use of the more expensive $Sc(OTf)_3$ to produce the corresponding products, albeit with considerably lower yields. The synthesis of $M^{II}_2Ln^{III}_2$ defect dicubane PCCs, as well as, catalytic and theoretical aspects are discussed for the development of this reaction system.

7.2 Results and discussion

7.2.1 Initial efforts

7.2.1.1 Synthetic strategy

With the initial objective of developing 3d-Dy^{III} PCCs which were catalytically active towards the domino condensation/ring-opening/electrocyclization of secondary amines and 2-furaldehyde, the synthetic insights discussed in chapter five were followed. The targeted compounds have no coordinated counter-ions, with vacant positions only coordinated to by solvent molecules (Figure 7.1, middle), for the possible binding or interaction with substrates.

The reaction, under aerobic conditions of $M(ClO_4)_2{\cdot}6H_2O$ (M = Ni, Co), $Dy(OTf)_3$, H_2**L1** and in the presence of Et_3N in a 1:1:2:5 ratio, in EtOH, followed by Slow Evaporation (SE) led to the formation of block shape crystals after 6 - 9 days. These crystals were determined to be the targeted , air stable, tetranuclear defect dicubane PCCs (Figure 7.1) by single-crystal-XRD studies (chapter twelve), with the general formula $[M^{II}_2Dy^{III}_2(\mathbf{L1})_4(EtOH)_6](ClO_4)_2{\cdot}2(EtOH)$ (**1MDy-ClO$_4$**) where M is Co (**1CoDy-ClO$_4$**) and Ni (**1NiDy-ClO$_4$**). The two compounds were further characterized by FT-IR spectra (Appendix B), ESI-MS (Appendix B, S7.1-S7.4) and EA (chapter eleven).

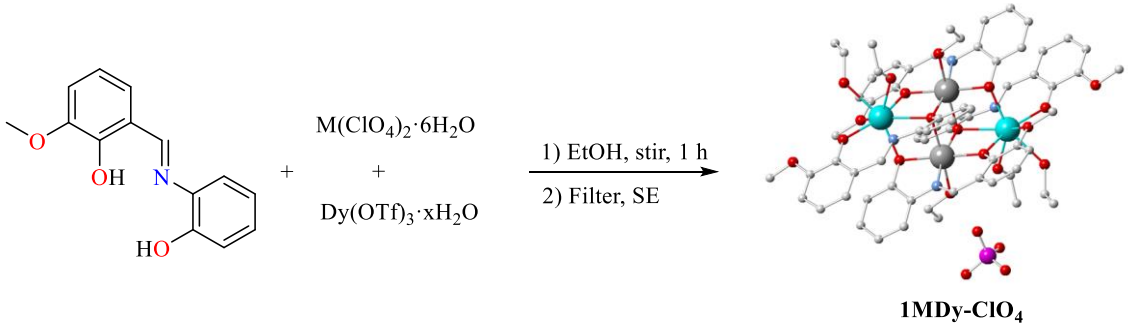

Equation 7.1. Pictorial representation of the synthesis of **1MDy-ClO$_4$**.

7.2.1.2 Molecular structure of 1MDy-ClO$_4$ PCCs

1NiDy-ClO$_4$ and **1CoDy-ClO$_4$** are isoskeletal to the previously described Zn^{II} PCC (**1**) described in chapter two. As **1NiDy-ClO$_4$** and **1CoDyClO$_4$** are analogues, only the full structure of **1NiDy-ClO$_4$** will be described (Figure 7.2).

1NiDy-ClO$_4$ crystallizes in the monoclinic *P*21/*n* space group. The asymmetric unit of **1NiDy-ClO$_4$** contains one Ni^{II} ion, one Dy^{III} ion, two doubly deprotonated organic ligands (**L1**), three coordinated ethanol molecules, one to Ni^{II} and the other two to the Dy^{III} ion and one lattice perchlorate counter-ion.

The main core of **1NiDy-ClO$_4$** can be described as a defect dicubane (**2,3M4-1**). Each 3d metal ion has an octahedral geometry and each Dy^{III} centre has a square-antiprismatic geometry. The H_2**L1** ligand exhibits two different coordination modes (Figure 7.3, modes I and II). In the first mode (Figure 7.3, mode I), the two phenoxide oxygen atoms and the imine nitrogen atom are chelated to the Ni^{II} centre, and the two phenoxide atoms are further bonded to two Dy^{III} ions (Dy (1) and its symmetry-related counterpart) and the methoxide oxygen atoms are bound to Dy (1).

In the second mode (Figure 7.3, mode II), the two phenoxide oxygen atoms and the imine nitrogen atom are chelated to the Dy^{III} centre, while the phenoxide oxygen atom (from the 2-aminophenol unit), is further bound to two Ni^{II} centres, occupying five and six vertices for the 3d and the Dy^{III}

centres, respectively. The remaining vertices are occupied by one (Ni^{II}) and two (Dy^{III}) ethanol molecules.

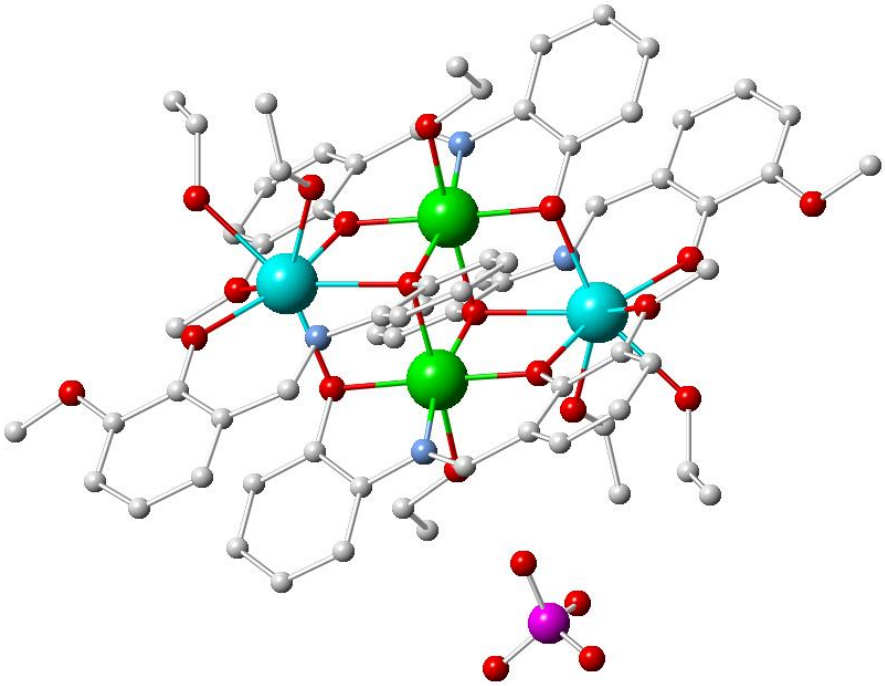

Figure 7.2. The molecular structure of **1NiDy-ClO$_4$**. Colour code: Ni^{II}, green; Dy^{III}, light blue; O, red; N, blue; C, white; Cl, purple. Hydrogen atoms omitted for clarity.

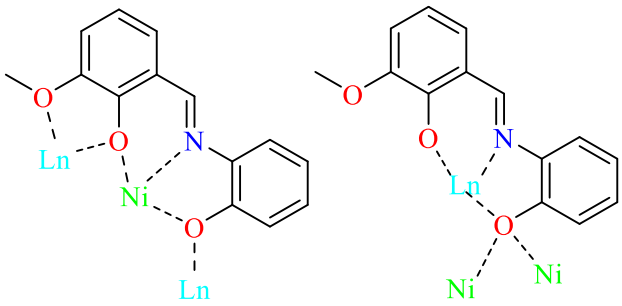

I II

Figure 7.3. Coordination modes of H_2**L1** in **1NiDy -ClO$_4$**.

7.2.1.3 ESI-MS studies of 1MDy -ClO$_4$

A broad ESI-MS study was performed for **1MDy-ClO$_4$** PCCs.

For **1CoDy-ClO$_4$**, two prominent peaks in the MS (positive ion mode) were observed at 1506.9719 m/z and at 736.0393 m/z which perfectly correspond to two fragments, $[Co^{II}_2Dy^{III}_2(\mathbf{L1})_4(ClO_4)\text{-}H]^+$ and $[Co^{II}_2Dy^{III}_2(\mathbf{L1})_4(MeOH)_2\text{-}H]^{2+}$, respectively (Appendix B, S7.1-S7.2).

Similarly, for **1NiDy-ClO$_4$**, peaks at 1520.0169 and 744.55 correspond to $\{[Ni^{II}_2Dy^{III}_2(\mathbf{L1})_4(MeOH)_2(EtOH)]+2H\}^+$ and $\{[Ni^{II}_2Dy^{III}_2(\mathbf{L1})_4(MeOH)(EtOH)]+2H\}^{2+}$ fragments respectively (Appendix B, S7.3-S7.4). This data indicates that the $[M^{II}_2Dy^{III}_2(\mathbf{L1})_4]^{2/1+}$ core remains intact in solution.

7.2.1.4 Benchmarking studies

Initial experiments were performed to determine the catalytic efficacy of the **1MDy-ClO$_4$** PCCs for a domino condensation ring-opening electrocyclization process toward the formation of (4*S*,5*R*)-dimorpholinocyclopent-2-enone (**C7a**) from 2-furaldehyde (**C7S1**) and morpholine (**C7S2**) in acetonitrile solution (Scheme 7.1).[412]

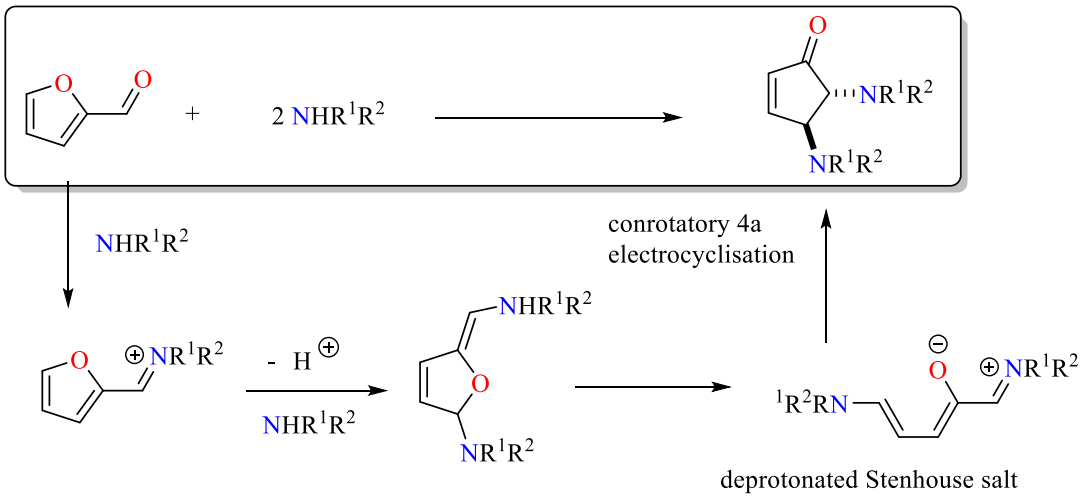

Scheme 7.1. The previously proposed mechanism for the Dy^{III} catalysed synthesis of *trans*-4,5-diaminocyclopent-2-enones.[412]

Previously, the reactions were carried out in acetonitrile solution under a nitrogen atmosphere, at room temperature and using a catalyst ($Dy(OTf)_3$) loading of 10 mol%. Under these conditions, the reaction between 2-furaldehyde (**C7S1**) and morpholine (**C7S2**) led to a quantitative amount of (4*S*,5*R*)-dimorpholinocyclopent-2-enone (**C7a**) (Table 7.1, entry 1) with $Dy(OTf)_3$ as a catalyst.[412]

To make the protocol more user-friendly, the reactions were conducted without an inert atmosphere and all the reactions were set up in the open air. Under these conditions, both complexes (**1NiDy-ClO$_4$** and **1CoDy-ClO$_4$**) only afforded moderate yields of the desired product after 16 h (Table 7.1, entries 2 and 3). Upon increasing the temperature (refluxing), both complexes allowed the reaction to take place with excellent yields and a reduced time (2 h) (Table 7.1, entries 4 and 5). At this temperature and in both cases, the catalyst loading could be decreased to 2.5 mol% with only a slight decrease in the yields (Table 7.1, entries 6 - 11). Interestingly, the

use of $Dy(OTf)_3$ under these conditions led to a considerable decrease in the yield when compared with the reaction at room temperature (Table 7.1, entry 12). As expected, neither $Co(ClO_4)_2{\cdot}6(H_2O)$ nor $Ni(ClO_4)_2{\cdot}6(H_2O)$, showed catalytic behaviour (Table 7.1, entries 13 - 14).

Table 7.1. Comparison of catalytic activity for compounds **1NiDy-ClO$_4$**, **1CoDy-ClO$_4$** and **1NiDy-Cl**.

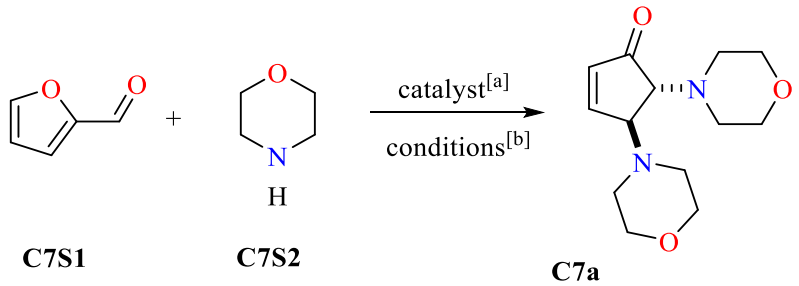

Entry	PCC	*T*	Loading / mol%[a]	Time / h	Yield / %[b]
1	$Dy(OTf)_3$[c]	r.t	10	16	quantitative
2	**1CoDy-ClO$_4$**	r.t	10	16	55
3	**1NiDy-ClO$_4$**	r.t	10	16	41
4	**1CoDy-ClO$_4$**	reflux	10	2	93
5	**1NiDy-ClO$_4$**	reflux	10	2	95
6	**1CoDy-ClO$_4$**	reflux	5	2	92[d]
7	**1CoDy-ClO$_4$**	reflux	2.5	2	90[d]
8	**1CoDy-ClO$_4$**	reflux	1	2	79[d]
9	**1NiDy-ClO$_4$**	reflux	5	2	94[d]
10	**1NiDy-ClO$_4$**	reflux	2.5	2	94[d]
11	**1NiDy-ClO$_4$**	reflux	1	2	80[d]
12	$Dy(OTf)_3$	reflux	10	2	63
13	$Co(ClO_4)_2{\cdot}6H_2O$	reflux	10	2	0
14	$Ni(ClO_4)_2{\cdot}6H_2O$	reflux	10	2	0
15	**1NiDy-Cl**	r.t	1	16	quantitative
16	**1CoDy-Cl**	r.t	1	16	98

[a] Catalyst loading calculated per equivalent of Dy^{III}; [b] Reaction conditions: amine, 1 mmol; 2-furaldehyde, 0.5 mmol; 4 Å MS, 100 mg; catalyst; anhydrous MeCN, 4 mL; room temperature. [c] Batey. [d] Product not isolated, yield determined by ^{1}H NMR spectroscopy.

With promising results at high temperature and at low catalyst loadings, it was considered that **1NiDy-ClO$_4$** and **1CoDy-ClO$_4$** could be under-going structural changes under these reaction conditions. To test this hypothesis, **1NiDy-ClO$_4$**, which had a slightly higher efficacy was

refluxed in acetonitrile for 2 h. This reaction provided the air-stable $[Ni^{II}_2Dy^{III}_2(\mathbf{L1})_4Cl_2(CH_3CN)_2]\cdot 2(CH_3CN)$ (**1NiDy-Cl**) (Scheme 7.2, A)[415] upon SE.

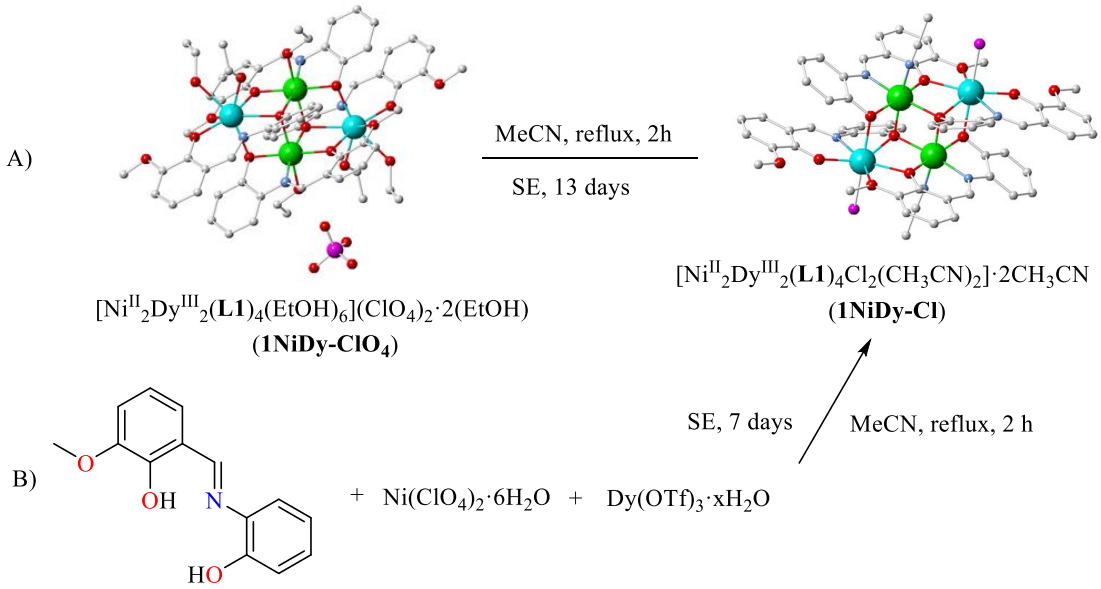

Scheme 7.2. Pictorial representation of the synthesis of **1NiDy-Cl**.

The use of 1 mol% of **1NiDy-Cl** at room temperature in the benchmarking reaction led to the quantitative formation of **C7a** (Table 7.1, entry 13). This is a decrease of catalyst loading of one order of magnitude when compared to the state-of-the-art for this Multicomponent Reaction (MCR), as well as a more user-friendly protocol that does not require the use of an inert atmosphere.

Realising the convenience of circumventing the need to synthesize **1NiDy-ClO$_4$** to obtain **1NiDy-Cl**, the original procedure was modified by substituting ethanol with acetonitrile and refluxing for 1 h (Figure 7.3, B). After SE for 7 days, small green crystals were afforded with the general formula $[Ni^{II}_2Dy^{III}_2(\mathbf{L1})_4Cl_2(CH_3CN)_2]\cdot 2(CH_3CN)$ (**1NiDy-Cl**) in 68% yield. Following this adapted procedure (Scheme 7.2, B) but substituting $Ni(ClO_4)_2\cdot 6H_2O$ for $Co(ClO_4)_2\cdot 6H_2O$, in the same ratio, led to the formation of small needle-like pink crystals with the general formula $[Co^{II}_2Dy^{III}_2(\mathbf{L1})_4Cl_2(CH_3CN)_2]\cdot 2(CH_3CN)$ (**1CoDy-Cl**) in a 61% yield**.**

Though **1CoDy-Cl** demonstrated an improved catalytic efficacy, at room temperature, over **1CoDy-ClO$_4$** (Table 7.1, entries 16 and 2 respectively) the efficacy was slightly lower than the Ni^{II} analogue (Table 7.1, entry 17). These transformed PCCs will be abbreviated, in the collective, as **1MDy-Cl**. Compounds **1MDy-Cl** were characterized in full by single-crystal XRD studies (chapter twelve), FT-IR spectra (Appendix B), ESI-MS (Figure 7.5) and EA (chapter eleven).

7.2.1.5 Molecular structure of 1MDy-Cl

1NiDy-Cl and **1CoDy-Cl** are isostructural and crystallise in the same triclinic *P*1 space group with the same unit cell parameters, therefore only the structure of **1NiDy-Cl** will be described. The molecular structure of **1NiDy-Cl** is shown in Figure 7.4. A similar coordination behaviour to **1NiDy-ClO$_4$** and **1CoDy-ClO$_4$** is observed for the **L1** ligands in **1MDy-Cl**, but a perchlorate to chlorine transformation is observed.[416]

The asymmetric unit of **1NiDy-Cl** contains one Ni^{II} ion, one Dy^{III} ion, two doubly deprotonated organic ligands (**L1**), one coordinated chloride ion, one coordinated MeCN molecule and two lattice MeCN molecules.

The main core of **1NiDy-Cl** is a defect dicubane (**2,3M4-1**). The H_2**L1** ligands exhibit the two-previously described coordinated modes (Figure 7.3). One MeCN molecule is bound to the Ni^{II} ion and a chloride anion is coordinated to the Dy^{III} ion. The Ni^{II} atom coordinates to six atoms (O_5N) and displays an octahedral geometry with one vertex occupied by a CH_3CN molecule, while Dy^{III} is coordinated to seven atoms (O_5NCl) and has an almost ideal pentagonal bipyramidal geometry with one phenolic oxygen and the chlorine atoms occupying the axial positions. There are two $Ni^{II}\cdots Dy^{III}$ distances at 3.464 (5) Å and 3.428 (5) Å and one $Ni^{II}\cdots Ni^{II}$ distance at 3.521(4) Å. No intramolecular interactions (e.g. H-bonds or stacking) can be found between neighbouring entities.

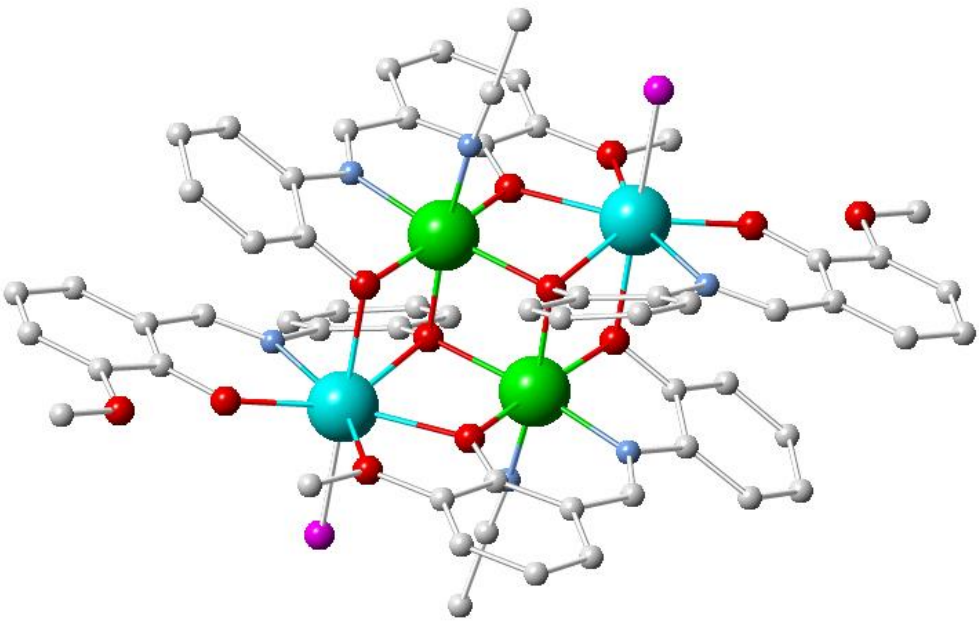

Figure 7.4. The molecular structure of **1NiDy-Cl**. Colour code: Ni^{II}, green; Dy^{III}, light blue; O, red; N, blue; C, white; Cl, purple. Hydrogen atoms are omitted for clarity.

7.2.1.6 ESI-MS studies of 1NiDy-Cl

ESI-MS studies for **1NiDy-Cl** show that it retains its topology in solution. Two main peaks were observed at 1556.1150 m/z and 703.5109 m/z corresponding to $\{[Ni^{II}_2Dy^{III}_2(\mathbf{L1})_4Cl_2(CH_3CN)(CH_3OH)]+4H\}^+$ and $\{[Ni^{II}_2Dy^{III}_2(\mathbf{L1})_4]-H\}^{2+}$ fragments, respectively (Figure 7.5).

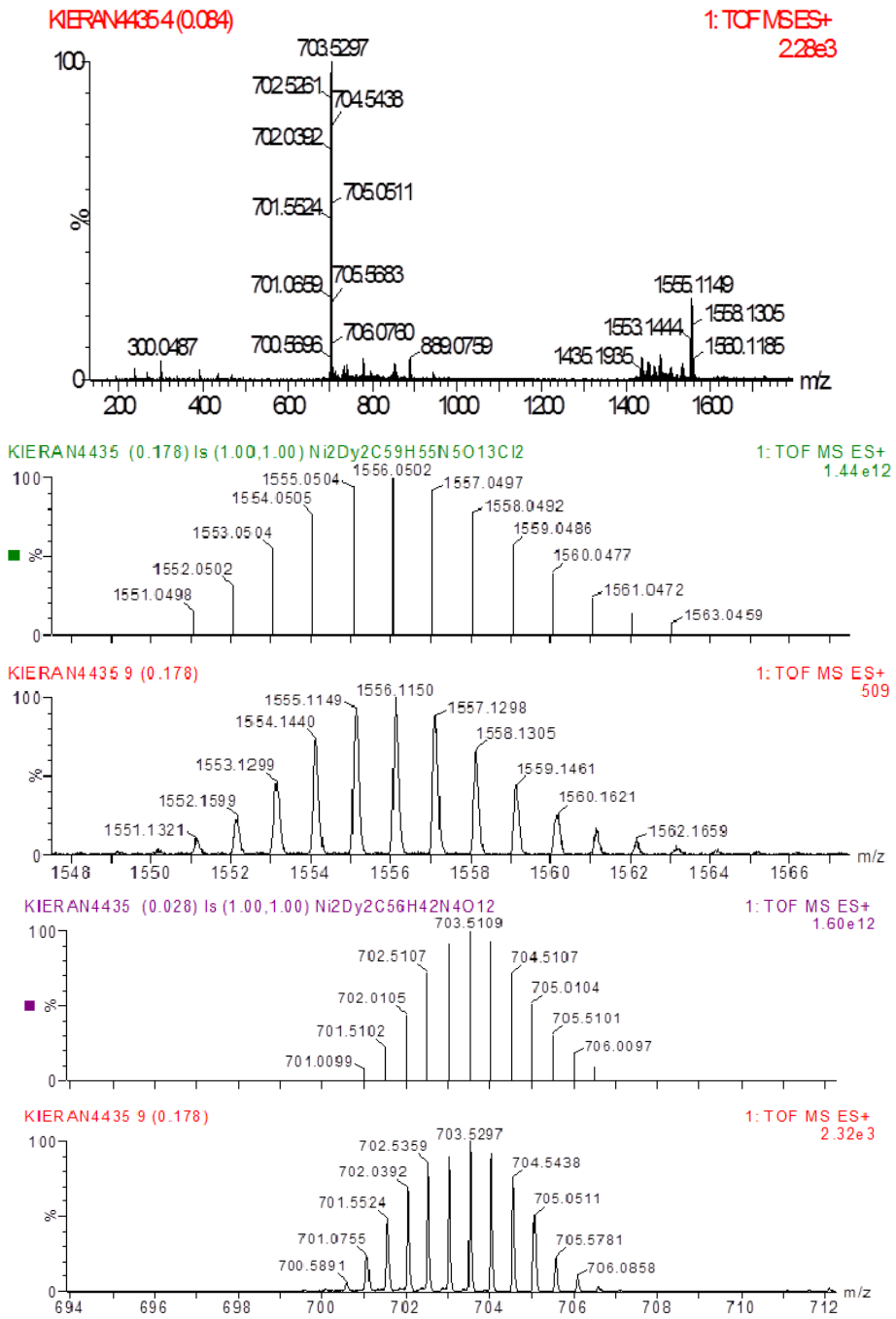

Figure 7.5. Experimental and theoretical ESI-MS patterns of **1NiDy-Cl** corresponding to $\{[Ni^{II}_2Dy^{III}_2(\mathbf{L1})_4Cl_2(CH_3CN)(CH_3OH)]+4H\}^+$ (upper) and $\{[Ni^{II}_2Dy^{III}_2(\mathbf{L1})_4]-H\}^{2+}$ (lower) fragments.

7.2.1.7 Scope of reaction

The scope of the reaction was then investigated with **1NiDy-Cl** due to its slightly higher efficacy and a variety of secondary amines as substrates were employed (Table 7.2). In all cases, the reactions proceeded smoothly, and it was possible to isolate the corresponding products (**C7a - C7e**) in excellent yields. Interestingly, when the same conditions were applied to primary amines, **1NiDy-Cl** catalysed the formation of the corresponding deprotonated Stenhouse salts (**C7f - C7e**). The combination of **C7f** or **C7g** with very dilute HCl or silica gel promoted the ring-closing leading to the corresponding *trans*-4,5-diaminocyclopent-2-enones in very high yields (Scheme 7.3, 95% and 56% overall yield, for **C7j** and **C7k**, respectively). The latter transformations are consistent with Batey's proposition that Dy^{III} is not involved in the cyclization step.[412] Interestingly, the same treatment when applied to **C7h** and **C7i** did not afford the cyclized products to any extent, the substrates remaining unaltered.

Table 7.2. 1NiDy-Cl catalysed condensation/ring-opening/cyclization of secondary amines with 2-furaldehyde and condensation/ring-opening of primary amines with 2-furaldehyde.

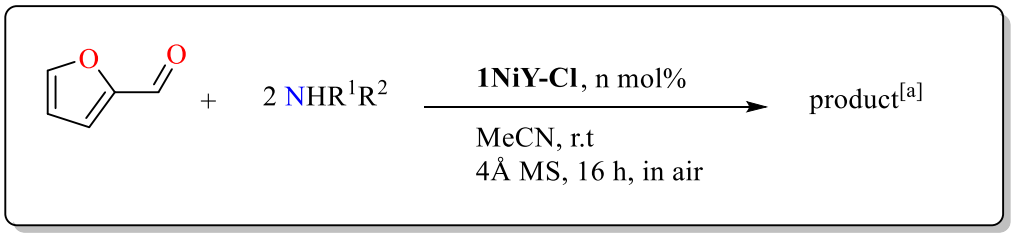

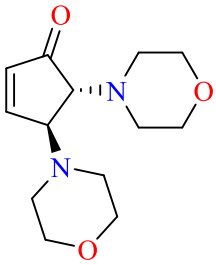

C7a
n = 1, quantitative

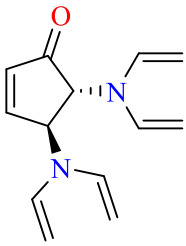

C7b
n = 1, 99%

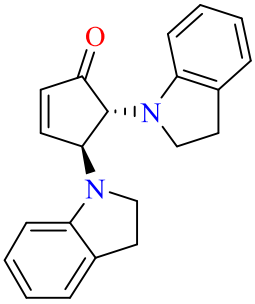

C7c
n = 1, 95%

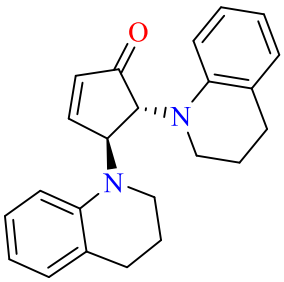

C7d
n = 1, 61%
n = 2.5, 99%

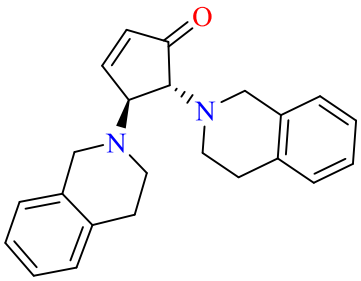

C7e
n = 1, 63%
n = 2.5, 99%

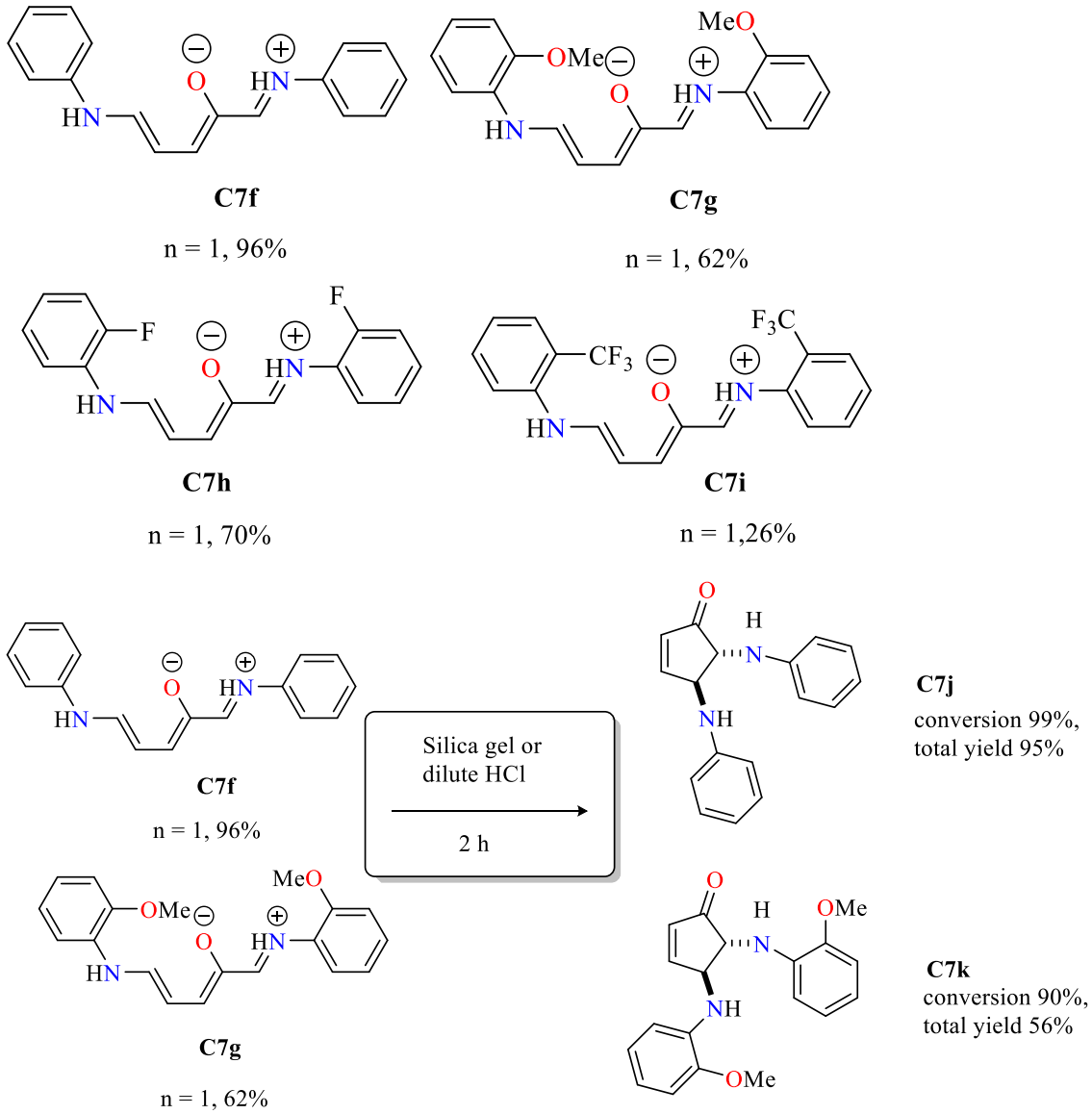

Scheme 7.3. The ring closing of **C7f** or **C7g** is promoted by very dilute HCl or silica gel leading to the corresponding *trans*-4,5-diaminocyclopent-2-enones **C7j** and **C7k**, respectively.

7.2.2 Optimization of the $Ni^{II}_2Ln^{III}_2$ catalysts

Considering the effectiveness of **1NiDy-Cl** at catalysing the condensation/ring-opening/cyclization of secondary amines with 2-furaldehyde (**C7S1**) and condensation/ring-opening of primary amines with 2-furaldehyde, it was reasoned that substitution of the Dy^{III} ion with lanthanides of lower cost would allow the evaluation of the relationship between cost and effectiveness. Therefore, an attempt was made to isolate and characterize isoskeletal analogues of compound **1NiDy-Cl** with Y^{III}, Sm^{III}, Eu^{III}, Gd^{III}, and Tb^{III}.

7.2.2.1 Synthetic insights and characterization of 1NiLn-Cl

Reproducing both reaction procedures that had produced **1NiDy-Cl** (Scheme 7.3, A and B), attempts to synthesize and isolate Ln^{III} analogues of **1NiDy-Cl** were not successful.

In an adapted procedure, where the mixture of $LnCl_3{\cdot}xH_2O$ (Ln = Y, Sm, Eu, Gd and Tb), $NiCl_2{\cdot}6H_2O$ and H_2**L1** in the presence of Et_3N (in a molecular ratio of 1/1/2/5) in CH_3CN was refluxed for 1 h, resulted in all samples producing a large amount of green precipitate. The precipitate was filtered and dried overnight for all reactions (Equation 7.2). A range of techniques including ESI-MS (Table 7.3, Appendix B, S7.6-S7.14), EA (chapter eleven), FT-IR spectroscopy (Appendix B, S7.15-S7.23), and TGA (Appendix B, S7.24-S7.29) confirmed that the filtrates were identical to **1NiDy-Cl** and have the general formula $[Ni^{II}_2Ln^{III}_2(\mathbf{L1})_4(Cl)_2(MeCN)_2]{\cdot}2MeCN$ (**1NiLn-Cl**) (Ln = Sm (**1NiSm-Cl**), Eu (**1NiEu-Cl**), Gd (**1NiGd-Cl**), Tb (**1NiTb-Cl**), Y (**1NiY-Cl**)] (Equation 7.2).

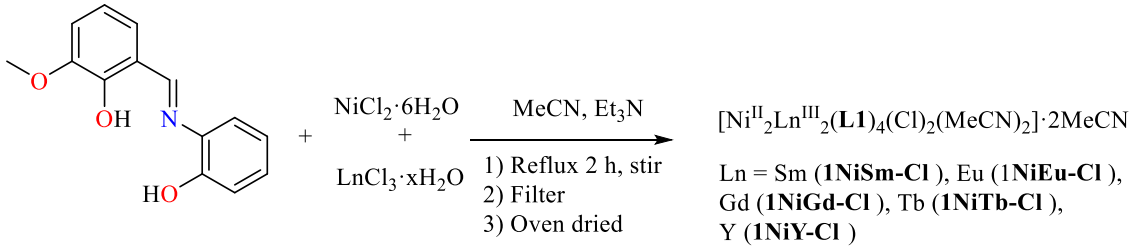

Equation 7.2. Pictorial representation of the synthesis of **1NiLn-Cl**.

The TGA data (Appendix B, S7.24-S7.29) for all solid compounds indicated the loss of four CH_3CN molecules (lattice and coordinated) up to 290 °C and decomposition at higher temperatures.

ESI-MS spectra of all **1NiLn-Cl** species were similar, with two main peaks in the positive ion mode corresponding to the $\{[Ni^{II}_2Ln^{III}_2(\mathbf{L1})_4Cl(CH_3CN)(CH_3OH)]+4H\}^+$ and$\{[Ni^{II}_2Ln^{III}_2(\mathbf{L1})_4]\}^{2+}$ fragments (Appendix B, S7.6-S7.14 with Table 7.3 for peak assignments).

Table 7.3. Observed peaks for **1NiLn-Cl** PCCs in ESI-MS with corresponding peak assignments.

Observed peaks and corresponding fragments in ESI-MS /m/z		
PCC	$[Ni_2Ln_2(\mathbf{L1})_4(CH_3CN)]^{1+}$	$[Ni_2Ln_2(\mathbf{L1})_4]^{2+}$
1NiY-Cl	1302.9743	628.9899
1NiSm-Cl	1428.9876	692.0004
1NiEu-Cl	1430.9948	693.0042
1NiTb-Cl	1443.0186	699.0098
1NiGd-Cl	1441.0109	698.0069
1NiDy-Cl	1556 / + MeOH	703.5109

Finally, EA are consistent with the calculated values without lattice CH_3CN molecules (chapter eleven).

In the attempt to characterize the species via single-crystal XRD studies, several unexpected products were structurally characterized, indicating that the synthesis of these species is not a simple task.

For example, the effort to obtain crystals of **1NiSm-Cl** resulted in the structural characterization of three different compounds, formulated as $[Ni^{II}_5Sm^{III}_2(CO_3)(\mathbf{L1})_7(\mathbf{L1'})(H_2O)_3]$ (**1NiSm-Cl-A**), $[Ni^{II}_2Sm^{III}_2(\mathbf{L1})_4(\mathbf{o\text{-}van})_2(H_2O)_2]\cdot 4CH_3CN$ (**1NiSm-Cl-B**), and $[Sm^{III}_4(OH)_2(\mathbf{L1})_4(H\mathbf{L1})_2]\cdot 2CH_3CN$ (**1NiSm-Cl-C**), where **L1′** is 2-aminophenol and **o-van** is o-vanillin (Appendix B, S7.33-S7.35). In the attempt to obtain crystals of **1NiEu-Cl**, a compound formulated as $[Ni^{II}_8Eu^{III}_4(\mathbf{L1})_8(CO_3)_4Cl_4(H_2O)_{14}]$ (**1NiEu-Cl-A**) was obtained (Appendix B, S7.33-7.35). The latter molecule is isoskeletal to compounds recently reported by Ke et al.[417]

7.2.2.2 Comparison of catalytic activity of 1NiLn-Cl (Ln^{III}) analogues

To ascertain whether the catalytic activity of these species is driven solely by the 4f ions or co-operative action between 4f and 3d ions, various blank tests were performed (Table 7.4).

Firstly, three Ni^{II} salts each with three different loadings (Table 7.4, entries 2 - 10) were used in the prototype reaction. $NiCl_2\cdot 6H_2O$ was found to catalyse the reaction with very high loadings and very low yields after 24 h (Table 7.4, entry 2) reflecting that its contribution is negligible for the shorter time. An *in situ* mixture of Ni^{II} salt and H_2**L1** (Table 7.4, entries 11 - 13) gave none of the anticipated product after 24 h.

In Batey's protocol, since $Dy(OTf)_3$ was found to be an excellent catalyst using a loading of 10 mol%, the catalytic efficacy of other lanthanide salts (Table 7.4, entries 14 - 20) along with yttrium salts were tested. Y^{III} has a size and Lewis acidity like Ho^{III} and its use allows a catalytic reaction to be possibly monitored with NMR spectroscopy (^{1}H, ^{13}C, ^{15}N, or ^{89}Y), because of its diamagnetic character. $Y(OTf)_3$ showed similar excellent catalytic performance (Table 7.4, entry 14) to $Dy(OTf)_3$, and the lanthanide chlorides showed the poorest performance (Table 7.4, entries 15 - 20).

To further understand the nature of the system, a mixture of Ni^{II} and Ln^{III} salts (Table 7.4, entries 21 - 26), reveal that the presence of the Ni^{II} salt had negligible influence on the catalytic performance. Finally, the use of $Ni(ClO_4)_2\cdot 6H_2O$ and $Dy(OTf)_3$ or $Y(OTf)_3$ (Table 7.4, entries 27 and 28) exhibited an insignificant influence of the Ni^{II} source on the catalytic performance. The Y^{III} salt had a higher efficacy the Dy^{III} salt. All these experiments confirmed the superior catalytic behaviour of **1NiDy-Cl** (1 mol%; Table 7.4, entry 1) over the simple metal salts as catalysts and the insignificant role of Ni^{II} in the catalysis.

Table 7.4. Comparison of Ni^{II}, Ln^{III}, a combination of Ni^{II}/Ln^{III} and Ni^{II}/H_2**L1** sources catalytic activity.

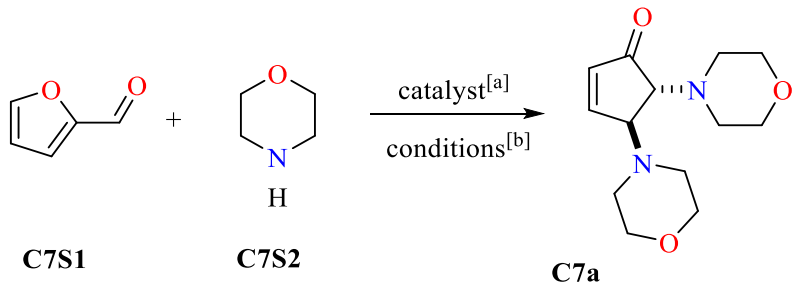

Entry	Catalyst	*T*	Loading / mol%[b]	Time / h	Yield / %[c]
1	None	r.t	N/A	24	0.1
2	$NiCl_2$	r.t	30	24	6.5
3	$NiCl_2$	r.t	20	24	2.0
4	$NiCl_2$	r.t	10	24	0.2
5	$Ni(NO_3)_2{\cdot}6H_2O$	r.t	30	24	2.9
6	$Ni(NO_3)_2.6H_2O$	r.t	20	24	1.0
7	$Ni(NO_3)_2{\cdot}6H_2O$	r.t	10	24	0.0
8	$Ni(ClO_4)_2{\cdot}6H_2O$	r.t	30	24	0.3
9	$Ni(ClO_4)_2{\cdot}6H_2O$	r.t	20	24	0.0
10	$Ni(ClO_4)_2{\cdot}6H_2O$	r.t	10	24	0.0
11	$Ni(NO_3)_2/H_2$**L1**	r.t	10/10	24	0.0
12	$Ni(ClO_4)_2/H_2$**L1**	r.t	10/10	24	0.0
13	$NiCl_2/H_2$**L1**	r.t	10/10	24	0.0
14	$Y(OTf)_3$	r.t	10	24	99
15	$SmCl_3$	r.t	10	24	37
16	$EuCl_3$	r.t	10	24	22
17	$GdCl_3$	r.t	10	24	41
18	$TbCl_3$	r.t	10	24	43
19	$DyCl_3$	r.t	10	24	72
20	YCl_3	r.t	10	24	73
21	$NiCl_2/SmCl_3$	r.t	10/10	24	31
22	$NiCl_2/EuCl_3$	r.t	10/10	24	21
23	$NiCl_2/GdCl_3$	r.t	10/10	24	41
24	$NiCl_2/TbCl_3$	r.t	10/10	24	39
25	$NiCl_2/DyCl_3$	r.t	10/10	24	72
26	$NiCl_2/YCl_3$	r.t	10/10	24	71
27	$Ni(ClO_4)_2/Dy(OTf)_3$	r.t	10/10	24	95
28	$Ni(ClO_4)_2/Y(OTf)_3$	r.t	10/10	24	98

[a]Reaction conditions: amine, 1 mmol; 2-furaldehyde, 0.5 mmol; 4 Å MS, 100 mg; catalyst; anhydrous MeCN, 4 mL; r.t; [b] Catalyst loading calculated per equivalent of M; [c] determined by ^{1}H NMR spectroscopy.

1NiLn-Cl PCCs (Table 7.5, entries 2 - 5) catalyse the formation of **C7a** in moderate to good yields in comparison to **1NiDy-Cl** but display higher yields than simple salts. When **1NiY-Cl** (Table 7.5, entry 6) was employed, a catalytic performance similar to **1NiDy-Cl** was observed. A further decrease of the catalytic amount of **1NiY-Cl** to 0.5 mol% loading results in excellent conversion (Table 7.5, entry 7). The higher efficacy of Y^{III} than Ln^{III} in Lewis acid catalysis has been previously reported,[418,419] but no rationale has been proposed. All attempts to recover the **1NiLn-Cl** catalyst, to reuse it, were unsuccessful.

Table 7.5. Comparison of **1NiLn-Cl** PCC catalytic activity.

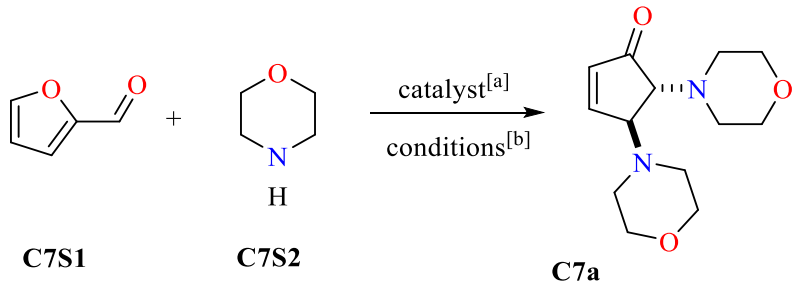

Entry	Catalyst	*T*	Loading /mol%[b]	Time /h	Yield / %[c]
1	**1NiDy-Cl**	r.t	1	2	quantitative
2	**1NiSm-Cl**	r.t	1	2 (24)	55 (75)
3	**1NiEu-Cl**	r.t	1	2 (24)	60 (99)
4	**1NiGd-Cl**	r.t	1	2 (24)	63 (99)
5	**1NiTb-Cl**	r.t	1	2 (24)	63 (86)
6	**1NiY-Cl**	r.t	1	2	quantitative
7	**1NiY-Cl**	r.t	0.5	2 (24)	98 (100)

[a] Reaction conditions: amine, 1 mmol; 2-furaldehyde, 0.5 mmol; 4 Å MS, 100 mg; catalyst; anhydrous MeCN, 4 mL; r.t; [b] Catalyst loading calculated per equivalent of Ln; [c] determined by ^{1}H NMR spectroscopy.

7.2.3 Tuning the organic periphery

7.2.3.1 Synthetic strategy

1NiY-Cl shows similar or better catalytic behaviour than **1NiDy-Cl** (Table 7.5). Given the excellent results that were obtained using even lower catalyst loadings (0.5 mol% for **1NiY-Cl**, instead of 1.0 mol% for **1NiDy-Cl**), along with the less-expensive lanthanide source, it was considered that **1NiY-Cl** could be structurally modified to achieve immobilization or to demonstrate photosensitivity.

From the nineteen Schiff base ligands synthesised in chapter five, the three organic ligands shown in Figure 7.6 were selected for the synthesis of the corresponding tetranuclear defect dicubane PCCs. These were chosen with the following considerations (i) to increase the solubility, as well

to offer the possibility for deposition of these species on surfaces by the introduction of an allyl group (H_2**L6**); (ii) to create "photosensitive" catalysts by inclusion of a naphtho group (H_2**L2**); and (iii) to combine both features (H_2**L16**).

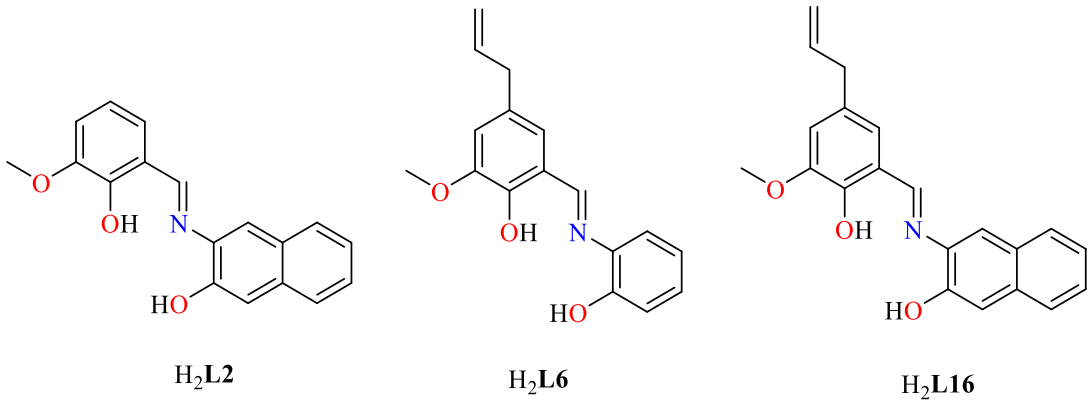

Figure 7.6. The three modified organic ligands used for the synthesis of **LNiY-Cl** PCCs.

From a generalized reaction procedure, using initial steps identical to the previously discussed protocols for **1NiLn-Cl** (Scheme 7.2), H_2**L2**, H_2**L6** and H_2**L16** were blended with $NiCl_2{\cdot}6H_2O$, and $YCl_3{\cdot}xH_2O$, in the presence of Et_3N in a 1:1:2:5 ratio in MeCN and refluxed for 2 h. All three samples resulted in a green precipitate, which was subsequently recrystallized from DMF and Et_2O by VD (Scheme 7.4). Each sample resulted in needle-like green crystals which will be described.

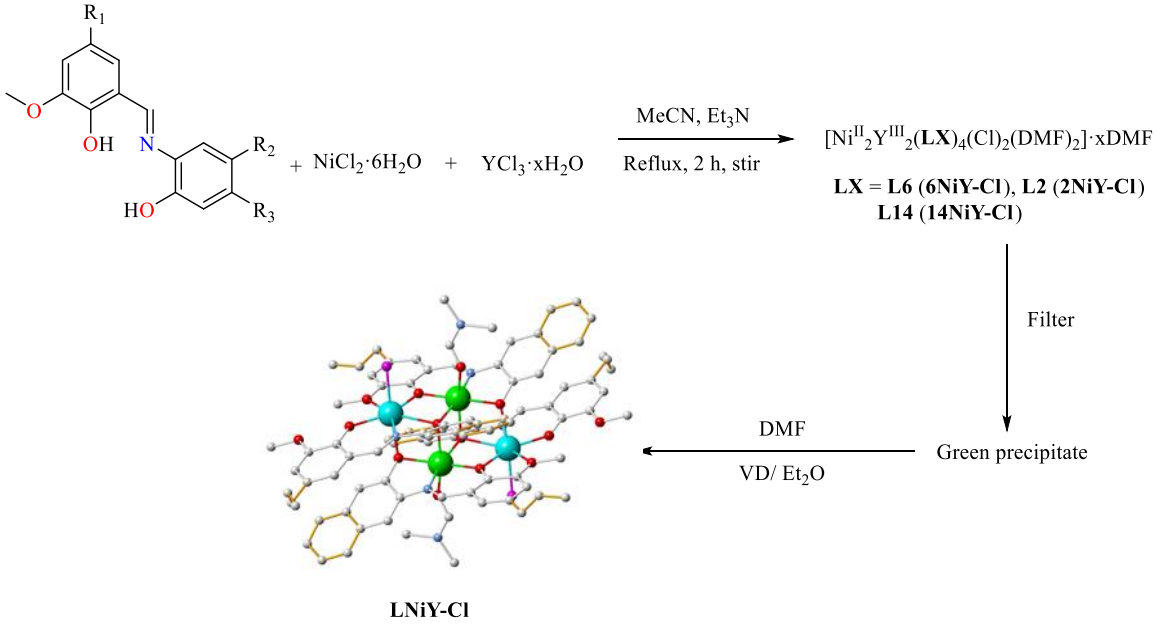

Scheme 7.4. Pictorial representation of the synthesis of **LNiY-Cl**.

From ligand H_2**L6** (Figure 7.6, left), in a slightly different synthetic ratio to **1NiY-Cl**, a compound formulated as $[Ni^{II}_2Y^{III}_2(\mathbf{L6})_4Cl_2(DMF)_2]$ (**6NiY-Cl**) (Figure 7.7, upper) was obtained. Also, the

ligands H_2**L2** and H_2**L16** (Figure 7.6), with slightly different synthetic ratios, gave $[Ni^{II}_2Y^{III}_2(\mathbf{L2})_4Cl_2(DMF)_2]\cdot 2DMF\cdot 2Et_2O$ (**2NiY-Cl**$\cdot$2DMF$\cdot$2Et_2O) (Figure 7.7, middle) and $[Ni^{II}_2Y^{III}_2(\mathbf{L14})_4Cl_2(DMF)_2]$ (**14NiY-Cl**) (Figure 7.7, lower), respectively.

These compounds were characterized by single-crystal XRD studies (Figure 7.7), FT-IR spectra (Appendix B, S7.21-S7.23), ESI-MS (Appendix B, S7.12-7.14), EA (chapter eleven) and TGA (Appendix B, S7.20-S7.22). Single-crystal XRD studies indicate that compounds **2NiY-Cl**, **6NiY-Cl**, and **14NiY-Cl** are isoskeletal to **1NiDy -Cl**. These PCCs will be collectively referred to as **LNiY-Cl**.

7.2.3.2 Molecular structures of LNiY-Cl

LNiY-Cl are isoskeletal to the previously described defect dicubane **1NiLn-Cl** PCCs. The ligands display the same coordination modes as previously described (Figure 7.3). The coordination environments around each metal centre are the same as **1NiDy-Cl**. Each Ni^{II} centre coordinates to six atoms (O_5N environment) possessing an octahedral geometry and each Y^{III} centre coordinates to seven atoms (O_5NCl environment) possessing a pentagonal bipyramidal geometry. No intermolecular interactions are observed and selected bond lengths can be found in Appendix B.

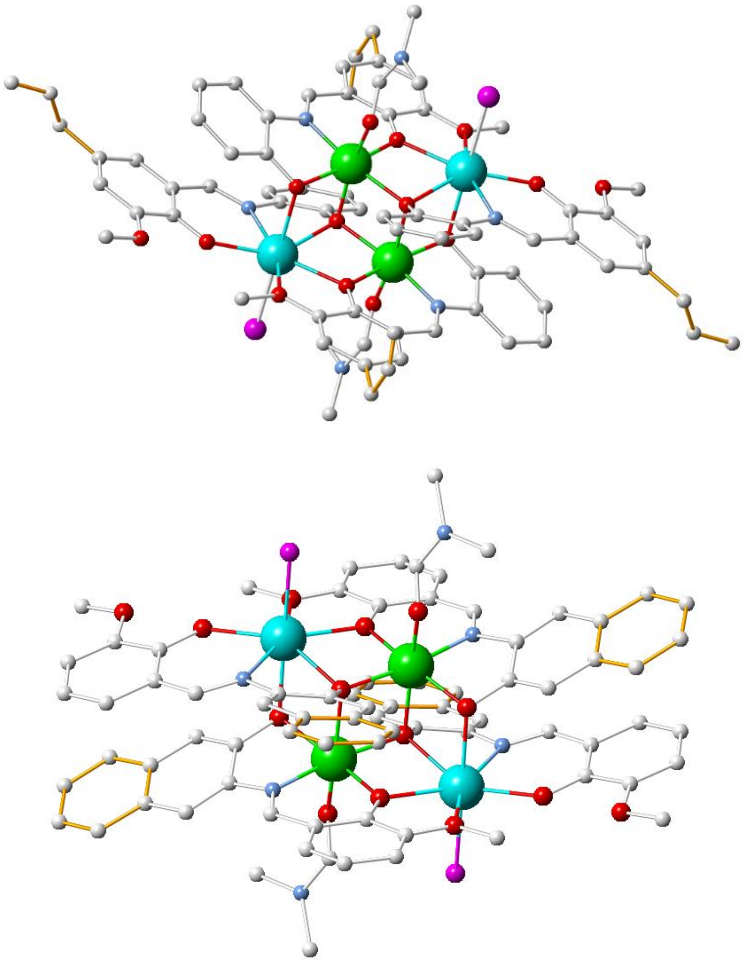

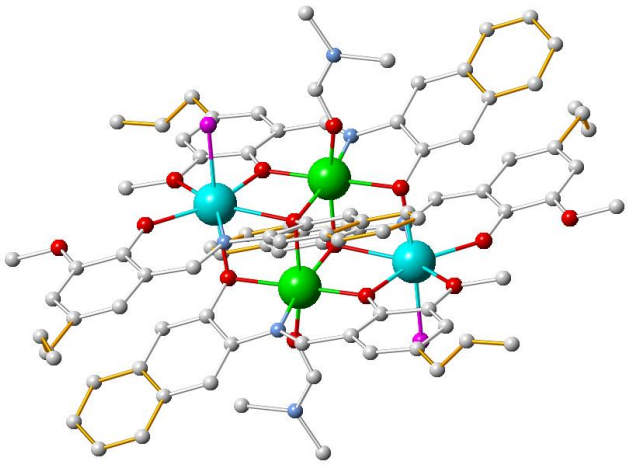

Figure 7.7. Molecular structures of **6NiY-Cl** (upper), **2NiY-Cl** (middle) and **14NiY-Cl** (lower). Colour code: Ni^{II}, green; Dy^{III}, light blue; O, red; N, blue; C, white; Cl, purple. Hydrogen atoms and disordered solvent molecules are omitted for clarity.

7.2.3.3 ESI-MS studies

Broad ESI-MS data from **2NiY-Cl**, **6NiY-Cl** and **14NiY-Cl** indicate that all three compounds retain their core structures in solution, shown by two prominent peaks in the MS (positive ion mode). These two peaks were observed for **6NiY-Cl** and **2NiY-Cl** and perfectly correspond to the $\{[Ni^{II}_2Y^{II}_2(\mathbf{L6})_4Cl_2]\}^+$ and $\{[Ni^{II}_2Y^{III}_2(\mathbf{L6})_4]\}^{2+}$ or $\{[Ni_2Ln_2(\mathbf{L2})_4(CH_3OH)Cl]\}^{2+}$ fragments respectively (Table 7.6). However, for **14NiY-Cl** only a peak corresponding to the $\{[Ni_2Ln_2(\mathbf{L1})_4(CH_3CN)]\}^{1+}$ is observed. This data, as with other isoskeletal $M^{II}_2Ni^{II}_2$ PCCs in this chapter, indicates that the $[M^{II}_2Dy^{III}_2(\mathbf{LX})_4]$ core remains intact in solution.

Table 7.6. Observed Peaks and corresponding fragments of **1NiY-Cl** in ESI-MS.

	Observed Peaks	
	$[Ni_2Ln_2(\mathbf{L6})_4(CH_3CN)]^{1+}$	$[Ln_2Ni_2(\mathbf{L6})_4]^{2+}$
6NiY-Cl	1465.1169	710.488
	$[Ni_2Ln_2(\mathbf{L2})_4(CH_3OH)\ Cl]^{1+}$	$[Ni_2Ln_2(\mathbf{L2})_4(CH_3OH)\ Cl]^{2+}$
2NiY-Cl	1430.9948	762.0541
	$[Ni_2Ln_2(\mathbf{L14})_4(CH_3CN)]^{1+}$	n/a
14NiY-Cl	1663.2231	n/a

7.2.3.4 Scope of reaction for optimized $Ni^{II}_2Ln^{II}_2$ PCCs

The catalytic activity of **6NiY-Cl**, **2NiY-Cl**, and **14NiY-Cl** toward the prototype reaction is shown in Table 7.7. Compounds **14NiY-Cl** and **6NiY-Cl** are not as efficient, relative to **1NiY-Cl** (1.0 mol% loading, instead of 0.5 mol% loading, and slightly lower yields), but these results can be

attributed to the decreased solubility in MeCN. When **2NiY-Cl** was employed as a catalyst (Table 7.7), yields similar to those with **1NiY-Cl** were obtained.

7.2.3.5 Immobilization of $Ni^{II}_2Ln^{II}_2$ PCCs

To explore the potential of these catalysts for immobilization and therefore heterogeneous catalysis, attempts were made to synthesize the organic ligands H_4**L30** and H_4**L31** shown in Figure 7.8.

Ligand H_4**L30** offers a similar coordination environment to H_2**L1** and thus it was anticipated to form coordination polymers upon complexation with the Ni^{II} and Y^{III} salts. However, H_4**L30** is slightly soluble in the polar solvents DMF or DMSO. To overcome the solubility issue, the organic ligand H_4**L31** was synthesized, this provides two *t*-butyl groups, but, similarly to H_4**L30**, it is slightly soluble in polar solvents. All efforts to synthesize the corresponding coordination polymers were unsuccessful.

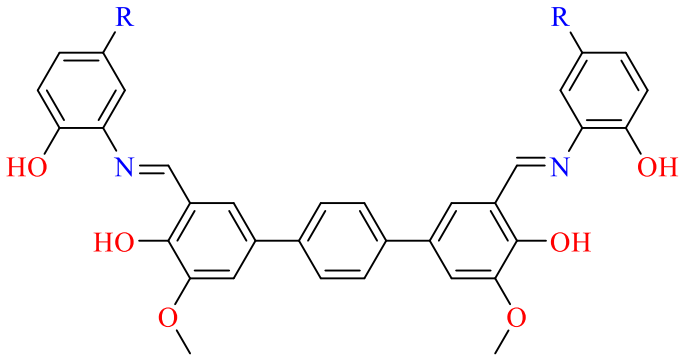

Figure 7.8. The modified organic ligands H_4**L30** (R = H) and H_4**L31** [R = $C(CH_3)_3$].

7.3 Theoretical studies

To further identify the formation of the previously discussed deprotonated Stenhouse salt intermediate a computational study was undertaken. Energy minimization calculations within the Kohn–Sham DFT at the B3LYP/6-311G** level employing the Polarizable Continuum Media (PCM) formalism were carried out on model compounds **C7f**, **C7j**, **C7II** and **C7I** (Figure 7.9).

Table 7.7. Comparison of catalytic activity of **LNiY-Cl** (where **L** = **1**, **2**, **6** and **14**) and **1NiDy-Cl** with secondary and primary substrates.

	Compound	**1NiDy-Cl**	**1NiY-Cl**	**6NiY-Cl**	**2NiY-Cl**	**14NiY-Cl**
	Loading /mol%[b]	1	0.5	1	0.5	1
	Time/ h	16	8	12	8	12
Entry	Product	Yield / %[c]	Yield / %[c]	Yield / %[c]	Yield / %[c]	Yield / %[c]
1	**C7a**	quantitative	quantitative	91	quantitative	85
2	**C7b**	99	96	85	95	80
3	**C7c**	95	99	70	94	64
4	**C7d**	61	53	58	51	52
5	**C7e**	63	71	69	69	62
6	**C7f**	96	99	96	99	94
7	**C7g**	62	91	91	93	91
8	**C7h**	70	95	94	94	92
9	**C7i**	26	90	81	86	81

[a] Reaction conditions: amine, 1 mmol; 2-furaldehyde, 0.5 mmol; 4 Å MS, 100 mg; catalyst; anhydrous MeCN, 4 mL; r.t; [b] Catalyst loading calculated per equivalent of Dy; [c] Determined by ^{1}H NMR spectroscopy.

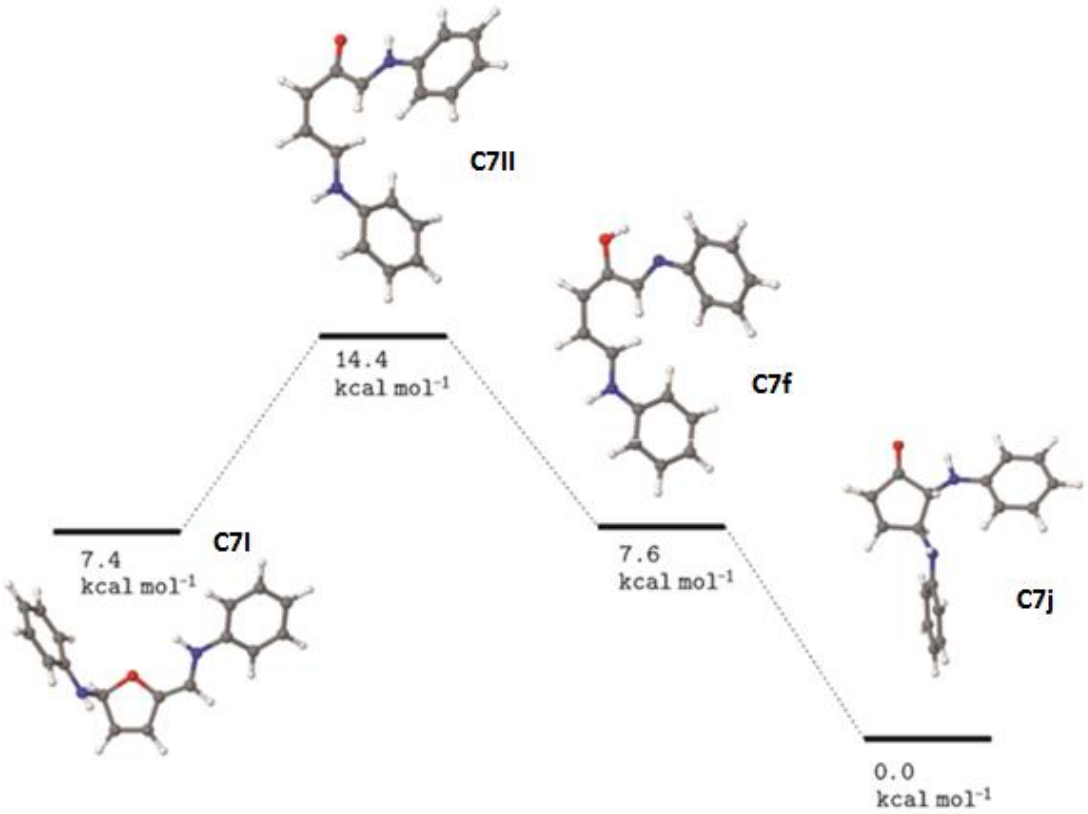

Figure 7.9. Energy profile of the reaction with aniline of the ring-opening (**C7f**) and closure (**C7j**) products.

The overall energy profile together with the calculated NMR data (Appendix B, Table S7.1) suggests:

a) The pathway from intermediate **C7II** – **C7f** towards the final product is highly favourable, which confirms that the catalysis takes place prior to this step.

b) The intermediate **C7II** – **C7f** likely resembles a configuration somewhere between **C7II** (in which the nitrogen bears a hydrogen) and **C7f** (in which the hydrogen migrates to the neighbouring oxygen.

c) That one factor that highly affects the total electronic energy of **C7i** concerns a pyramidal-to-planar evolution of the beta-nitrogen, a key feature that is likely involved in the catalytic process.

Computational studies also show that it was possible to modify ligand sterics without compromising the electrostatic properties that are key to the activities of the complexes.

Renditions of the MEP for H_2**L2**, H_2**L6**, and H_2**L16** are shown in Figure 7.10. The results also suggest that the charge distribution within the O−O−N−O core pattern directly interacting with the metals is a function of the conformation of the ligands.

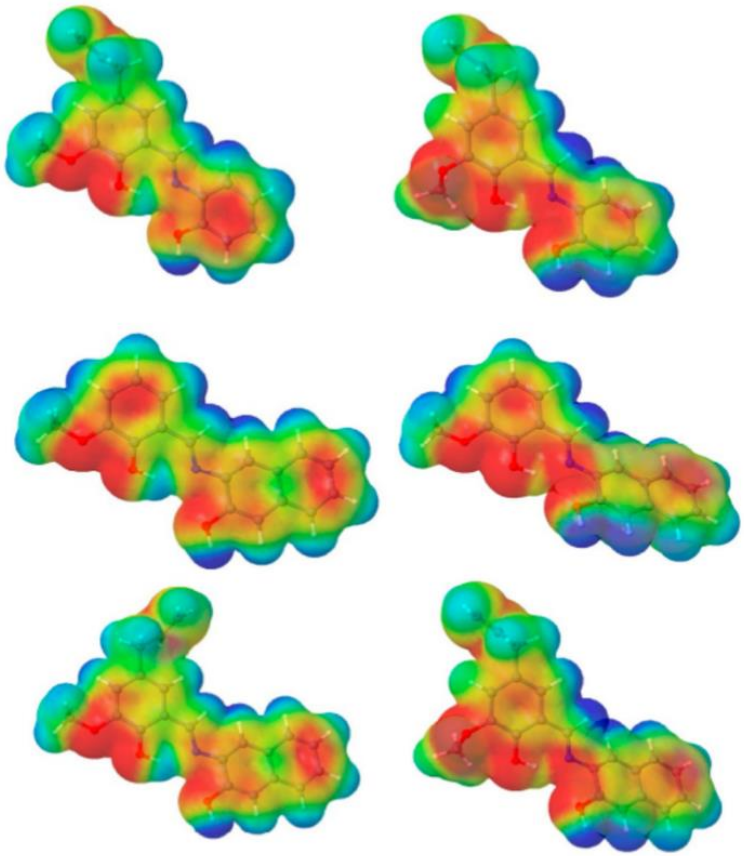

Figure 7.10. The rendition of the MEP of H_2**L6** (upper), H_2**L2** (middle), and H_2**L16** (lower) organic ligands: Bound (left) and free conformation (right).

7.4 Conclusion

This chapter presents and demonstrates a simple and high yielding isoskeletal series of $M^{II}_2Ln^{III}_2$ (M = Ni, Co) PCCs, supported by structurally homologous Schiff base ligands, which show remarkable catalytic activity towards the synthesis of *trans*-4,5-diaminocyclopent-2-enones from 2-furaldehyde and primary or secondary amines.

From two poorly performing 3d-Dy^{III}, defect dicubane PCCs (**1MDy-ClO$_4$**) under mild conditions, it was possible to synthesize an optimized isoskeletal analogue with an altered coordination environment (**1NiDy-Cl**) and generate an analogous family (**1NiLn-Cl**) with the substitution of the 4f ion. It was then possible to determine the relationship between efficacy and 4f ion node.

In addition, considering the catalyst loadings and the reaction times, the Ni^{II} contribution appears negligible and it is, therefore, safe to conclude that the domino reaction is driven solely by the 4f ion. Remarkably, the employment of Y^{III} (**1NiY-Cl**) instead of Dy^{III} (**1NiDy-Cl**) results in a lower loading and reduced cost catalyst.

With further optimization, it was demonstrated that the functionalization of the organic skeleton is feasible (**2NiY-Cl**, **6NiY-Cl** and **14NiY-Cl**), without deterioration of the catalytic activity. Moreover, the modified species **6NiY-Cl** and **14NiY-Cl**, that bear allyl groups, can be immobilized by deposition on surfaces, but this is the goal of a following study. The results presented herein show the richness of this chemistry and pave the way for the future employment of 3d-4f PCCs in catalysis.

Chapter 8: Tetranuclear Zn/4f PCCs as highly efficient catalysts for Friedel-Crafts alkylations and for the Petasis borono-Mannich multicomponent reaction

Abstract: A series of novel, high yielding, isoskeletal tetranuclear polynuclear coordination clusters formulated $[Zn^{II}_2Ln^{III}_2(\mathbf{L1})_4(NO_3)_2(DMF)_2]$ (**1ZnLn-NO$_3$**) which display a defect dicubane (**2,3M4-1**) core topology were synthesised and characterised. Synthetic insights are discussed. The ability to substitute the 4f centres in these catalysts without altering the core topology was studied and allows further confirmation of their solution stability via electrospray ionization mass spectrometry, electron paramagnetic resonance and NMR studies. **1ZnLn-NO$_3$** are shown to be high-efficiency catalysts with low catalytic loadings in two types of Friedel-Crafts (FC) alkylations and in a Petasis Borono-Mannich (PBR) transformation. The **1ZnY-NO$_3$** analogue demonstrates the highest efficacy in the FC alkylation of indoles by aldehydes, whereas **1ZnDy-NO$_3$** surpasses the rest of the series for the FC alkylation of indoles by nitrostyrenes and the PBR reaction. Insights into plausible reaction mechanisms are presented which are supported by ultra violet visible spectroscopy substrate binding studies.

8.1 Introduction

Chapter seven established the catalytic activity of a series of tetranuclear Ni^{II}/Co^{II}-Ln^{III} PCCs (**1MLn-ClO$_4$** and **LMLn-Cl**) for the domino ring-opening electrocyclization reaction between furaldehyde and a wide range of secondary and primary amine substrates. Furthermore, the organic periphery of the catalysts could be modified without a substantial impact on the efficacy of the catalytic transformation. A noticeable limitation of this study was that only the Ln^{III} ion of the Ni^{II}/Co^{II}-Ln^{III} PCCs was catalytically active and there was no evidence of a co-operative action between the 3d and 4f metal centres. Considering that $Ln(OTf)_3$[420] and $Zn(ClO)_4$/Schiff base[421] compounds have been employed as catalysts in the reactions of indole derivatives with aldehydes and ketones, it was envisioned that $Zn^{II}_2Ln^{III}_2$ PCCs isoskeletal to those in chapter seven could be applied to these types of reactions and have a significant co-operative catalytic effect.

Catalysts based on zinc or lanthanide elements have been extensively employed in FC reactions and sizeable development has taken place.[411,422] FC reactions are an important carbon-carbon bond forming reaction in organic and medicinal chemistry.[423] In particular, the indole ring system represents one of the most abundant and important heterocycles in nature exhibiting wide-ranging biological activity.[424]

The nucleophilic addition of aldehydes or ketones to indoles, in the presence of a Lewis acid, is a facile route towards the synthesis of bis indolyl-methane (BIM) derivatives with only one equivalent of water generated as a side product. BIMs have recently been shown to be useful in

the treatment of fibromyalgia,[425] as antibacterial agents[426] and even in the prevention of cancer.[426] Various catalytic systems and metal salts have been reported for the synthesis of BIMS, however, these methods suffer from a number of disadvantages such as expense, the toxicity of reagents, high temperatures, high catalytic loading and photosensitivity.[427–430]

Another important FC reaction is the reaction between indole and β-nitrostyrene which gives access to indole-based alkaloids such as melatonin analogues, 1,2,3,4-tetrahydro-β-carbolines (THBCs) and "triptans". Nitroalkenes have received considerable attention as active Michael acceptors[431] because the nitro derivatives can be transformed into amino compounds with a variety of different functionalities.[432–436] In streamlining the reaction between indole and β-nitrostyrene various catalytic systems have been proposed. These include hydrogen-bond-based compounds[437–442] such as thiourea,[437,440,441,443–446] phosphoric acid,[442] silanediols,[447,448] sulfamic acid,[449] 2,6-bis(amido)benzoic acid,[450] metal based compounds[451–467] such as Al^{III},[451,465] Cu^{II},[452–456,467] Zn^{II},[422,457–461,466] Fe^{III},[462] Pd^{II},[463] Rh^{II} [468,469] and SmI_3[464] and heterogeneous systems including MOFs,[470,471] nano *n*-propylsulfonated γ-Fe_2O_3 (NPS-γ-Fe_2O_3) [472] and zeolite HY.[473] However efficient metal-based catalytic systems for this transformation are very rare. Du developed an efficient catalyst containing bisoxazolines, bisimidazolines and $Zn(OTf)_2$.[452,474–477] Wang reported the involvement of a dimeric Cu^{II} PCC and piperidine as a catalyst for reactions between aromatic nitroalkenes and ortho-substituted indoles.[467] However, some of the reported protocols have drawbacks such as high catalyst loading, long reaction time, multi-step designed ligands, the need for additives and the reaction at low temperature (0 to -20 ^{o}C) which limits their practical applications.

MCRs have dominated synthetic chemistry for the following reasons, they yield products from simple starting materials, in fewer steps and in a shorter time when the reactions are carried out in a combinatorial way.[478–489] Among these transformations, the Mannich-type condensation that involves amines, aldehydes and boronic acids, developed by Petasis,[490] known as Petasis Borono-Mannich Reaction (PBR) has received considerable attention because it produces skeletons that can easily convert to amino acids, heterocycles and alkylaminophenols.[491] More specifically, the reaction between aryl boronic acids, amines and salicylaldehydes yield, in a single step, novel aminophenol derivatives[492] which are suitable for the preparation of dihydro-1,3-oxazines,[493,494] triarylmethanes[495] and polycyclic N, O-acetals.[30] It is worth noting that aldehydes lacking an OH group in position 2 failed to deliver the desired product, highlighting the importance of the hydroxyl group in the aldehyde to activate the boronic acid.[491] The first report for the specific transformation included a reaction at 90 ^{o}C, in dioxane as a solvent, in 16 hours and in absence of catalyst in very good yields.[496] In 2004, Tye et al developed a rapid, microwave-assisted protocol for carrying this reaction that required a 10 min reaction time.[497] In 2009, Gois et al., reported the synthesis of several alkylaminophenols in moderate to good yields, in water, at 80 ^{o}C, in absence

of a catalyst.[498] Recently, an effective and rapid synthesis was carried out using protonated trititanate ($H_2Ti_3O_7$) nanotubes as a heterogeneous solid–acid catalyst.[499] However, these methods all suffer from a number of disadvantages such as high temperatures, high catalyst loadings (10 mol%) and long-time reactions.

Herein a series of isoskeletal defect dicubane PCCs with the general formula $[Zn^{II}_2Ln^{III}_2(\mathbf{L1})_4(NO_3)_2(DMF)_2]$ (**1ZnLn-NO$_3$)** where Ln is Y, Sm, Eu, Gd, Tb and Yb were synthesised and characterised. For the first time, they were applied towards the aforementioned FC reactions. In addition, bearing in mind that the Zn-Y/Ln metals are very close (~ 3.3 Å) in this specific topology and observing a chelation preference of aldehydes to Y-Ln metals,[336] it was anticipated that these catalysts would be an ideal synergistic template for the PBR reaction.

8.2 Results and discussion

8.2.1 Synthetic strategy

To develop $Zn^{II}_2Ln^{II}_2$ defect dicubane PCC catalysts, isoskeletal to those $Ni^{II}_2Ln^{II}_2$ discussed in chapter five, several synthetic procedures were employed. As discussed in chapter two, $Zn^{II}_2Ln^{II}_2$ defect dicubane PCCs (**1-3**) were synthesized, though these display the targeted defect dicubane topology supported by H_2**L1**, the presence of perchlorate counter-ions previously had an adverse effect on the catalytic efficacy with the isoskeletal **1MDy-ClO$_4$** PCCs described in chapter seven. For this reason, (**1-3**) were not considered for promoting FC or MCR reactions.

Attempts were made to synthesize Zn^{II} analogues of the previously described **1MLn-Cl** PCCs, however, these efforts failed. Following an adapted method, a series of isoskeletal defect dicubane $Zn^{II}_2Ln^{II}_2$ PCCs supported by H_2**L1** with nitrate counter-ions were synthesized with the following procedure.

The stirred reaction of $Dy(NO_3)_3{\cdot}6H_2O$, $Zn(NO_3)_2{\cdot}6H_2O$, EtOH and H_2**L1** in the presence of Et_3N in a 1:2:2:4.5 ratio under aerobic conditions afforded a yellow precipitate. The precipitate was subsequently crystallized by VD of Et_2O in DMF solution which afforded block shape crystals of air-stable tetranuclear defect dicubane compound formulated $[Zn^{II}_2Dy^{III}_2(\mathbf{L1})_4(NO_3)_2(DMF)_2]$ (**1ZnDy-NO$_3$**) after 1 week (Scheme 8.1) in very good yields (78%).

When the same reaction was performed with other lanthanide salts, isoskeletal analogues with the general formula $[Zn^{II}_2Ln^{III}_2(\mathbf{L1})_4(NO_3)_2(DMF)_2]$ (**1ZnLn-NO$_3$**) where Ln is Y (**1ZnY-NO$_3$**), Sm (**1ZnSm-NO$_3$**), Eu (**1ZnEu-NO$_3$**) Gd (**1ZnGd-NO$_3$**), Tb (**1ZnTb-NO$_3$**) and Yb (**1ZnYb-NO$_3$**) were isolated. These compounds were characterized in full by single-crystal XRD studies (Figure 8.1), FT-IR spectra (Appendix B, S8.1-S8.7), ESI-MS (Appendix B, S8.8-S8.25), TGA (Appendix B, S8.26-S8.32) and EA (chapter eleven).

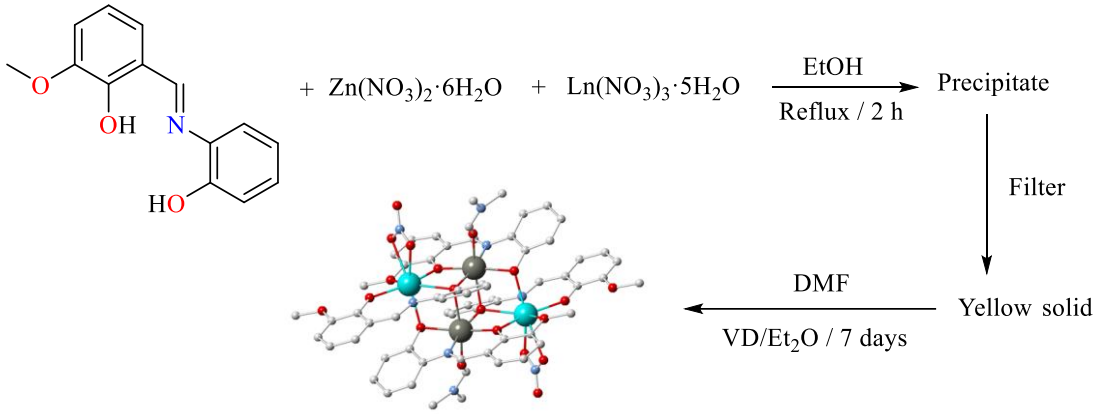

Scheme 8.1. Pictorial representation of the synthesis of **1ZnLn-NO$_3$**.

8.2.2 Crystal structures of 1ZnLn-NO$_3$

As **1ZnLn-NO$_3$** PCCs are isostructural, which is confirmed by single-crystal XRD studies (chapter twelve) and the aforementioned characterisation, only the crystal structure of **1ZnGd-NO$_3$** is described herein.

1ZnGd-NO$_3$ crystallises in the monoclinic space group $P2_1/c$. The asymmetric unit cell contains one Zn^{II} ion, one Gd^{III} ion, two doubly deprotonated (**L1**) ligands, one coordinated nitrate anion and one coordinated DMF molecule (Figure 8.1). The main core of **1ZnGd-NO$_3$** can be described as a defect dicubane (**2,3M4-1**).

L1 exhibits two different coordination modes (Figure 8.2). In the first mode (Figure 8.2, mode I), the two phenoxide oxygen atoms and the imine nitrogen atom are chelated to the Zn^{II} centre and the two phenoxide atoms are further bonded to two Gd^{III} ions Gd (1) (and its symmetry-related counterpart) and the methoxide oxygen atom is bound to Gd (1).

In the second mode (Figure 8.2, mode II), the two phenoxide oxygen atoms and the imine nitrogen atom are chelated to the Gd^{III} centre, while the phenoxide oxygen atom (from the 2-aminophenol unit), is further bound to two Zn^{II} centres. The DMF molecule is bound to the Zn^{II} ion and the $[NO_3]^-$ anion is bound to the Gd^{III}. The Zn^{II} ion adopts a slightly distorted octahedral geometry with an O_5N donor set, while the Ln ion has a very distorted square antiprismatic geometry, due to the chelating nitrate anion with an O_7N donor set. Gd⋯ Zn distances are 3.505 - 3.564 Å and the Zn⋯Zn distance 3.291 Å. No intramolecular interactions (e.g. H-bonds or stacking) can be found between neighbouring entities.

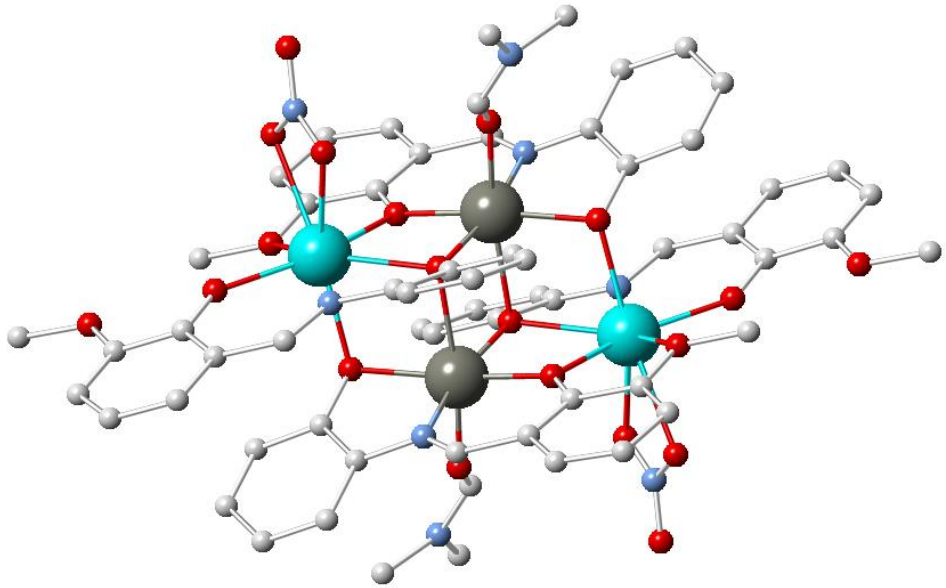

Figure 8.1. Molecular Structure of **1ZnGd-NO$_3$**. Colour code: Zn^{II}, grey; Gd^{III}, light blue; O, red; N, blue; C, white. Hydrogen atoms have been omitted for clarity.

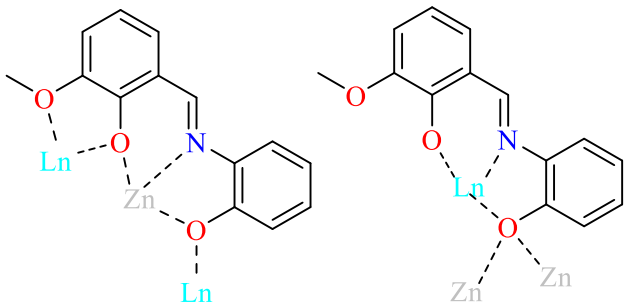

Figure 8.2. Observed coordination modes of **L1** in **1ZnLn -NO$_3$**.

8.2.3 Solution studies of 1ZnLn-NO$_3$

To verify that the $[Zn^{II}_2Ln^{III}_2(\mathbf{L1})_4]^{2+}$ core is stable in solution and that it is the active species towards the catalytic efficacy in the following investigated reactions, several solution-based studies were conducted (ESI-MS, EPR, ^{1}H NMR spectroscopy). These verify core stability and determine that other by-product species are not present.

8.2.3.1 ESI-MS studies of 1ZnLn-NO$_3$

The identity of **1ZnLn-NO$_3$** was confirmed by ESI-MS studies. In all cases, two peaks (positive-ion mode) in the MS were observed at an m/z which correspond respectively to the monocationic $[Zn^{II}_2Ln^{III}_2(\mathbf{L1})_4(NO_3)]^+$ and the dicationic $[Zn^{II}_2Ln^{III}_2(\mathbf{L1})_4(MeOH)]^{2+}$ fragments perfectly (Table 8.1, Appendix B, S8.8-S8.25.). The identification of these fragments indicates that the defect dicubane core is retained in solution.

Table 8.1. ESI-MS peak assignments

	Observed Peaks	
PCC	$[Zn_2Ln_2(\mathbf{L1})_4(NO_3)]^{1+}$	$[Zn_2Ln_2(\mathbf{L1})_4(MeOH)]^{2+}$
1ZnY-NO$_3$	1335.9672	652.9971
1ZnSm-NO$_3$	1457.0803	717.0056
1ZnEu-NO$_3$	1460.0661	718.9654
1ZnTb-NO$_3$	1476.0757	720.1311
1ZnGd-NO$_3$	1471.9936	722.0254
1ZnDy-NO$_3$	1482.0975	726.0345
1ZnYb-NO$_3$	1504.9225	737.9388

8.2.3.2 EPR studies of 1ZnGd-NO$_3$

To further confirm the solution stability of the **1ZnLn-NO$_3$** PCCs, Q-band EPR studies of **1ZnGd-NO$_3$** in both solid and solution (80% DMF, 20% Et_2O) phase were performed, (Figure 8.3). Simulations with PHI[500] confirm that the spectra are owed to S = 7/2 Gd^{III} ions with ZFS (Figure 8.3). The highly sensitive, finger-print-like ZFS of the S = 7/2 state directly indicates that the coordination environment of the Gd^{III} ion is unchanged in solution.

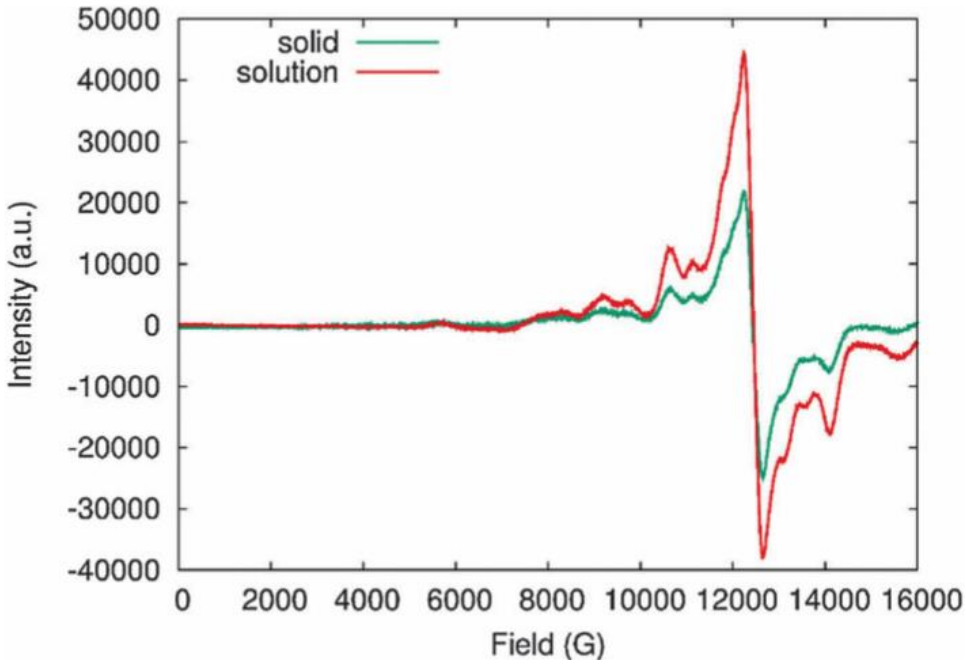

Figure 8.3. Experimental EPR spectra at the Q-band (34.0865 GHz) of **1ZnGd-NO$_3$**, recorded at 7 K in the solid (green line) and solution phase (red line).

8.2.3.3 ^{1}H NMR studies of 1ZnY-NO$_3$

Despite the diamagnetic nature of **1ZnY-NO$_3$**, characterizing it in the solution state by ^{1}H NMR spectroscopy proved difficult due to its asymmetry, dynamic behaviour and its relatively low

solubility. However, the peak areas for the imine, aromatic, and methoxy protons were all consistent with the structure as determined by single-crystal XRD studies (Figure 8.1). Gradually warming to 75 °C in 10 °C steps caused gradual broadening of the peaks, which then recoalesced on cooling back to room temperature, without any apparent decomposition of the complex.

8.2.4 1ZnLn-NO_3 as catalysts for organic transformations

With the series of **1ZnLn-NO_3** PCCs characterised in both solid and solution state, this series of PCCs was applied as potential catalysts to the FC alkylation reaction of indoles with aldehydes, FC alkylation reaction of indoles with nitrostyrenes and the PBR reaction between salicylaldehydes, secondary amines and boronic acids. Initial steps involved identifying the best reaction conditions and PCC for the respective catalytic reaction, followed by an exploration of the scope of reaction. In addition, mechanistic insights are proposed and supported by UV-Vis substrate binding studies.

8.2.4.1 1ZnLn-NO_3 catalysed FC alkylation of indoles and aldehydes

To determine whether **1ZnLn-NO_3** had a catalytic effect for the synthesis of BIMs, indole (**C8S1**) and benzaldehyde (**C8S2**) were selected as reactants for the benchmarking studies for the catalytic synthesis of the BIM adduct, **C8aa**. In initial studies, **1ZnDy-NO_3** was used as the catalyst at 10 mol% loading, based on a previously reported catalytic procedure with $Dy(OTf)_3$.[420]

8.2.4.1.1 Benchmarking and optimisation

To determine the optimised catalytic system, several reaction parameters were investigated, including the solvent medium (Table 8.2 and 8.3), different catalysts (Table 8.4) and catalyst loading (Table 8.4).

The first set of reactions were performed to identify the ideal solvent system. After screening several solvents (Table 8.2), the ethanol/water (2: 1) solvent system (Table 8.2, entry 7) was identified to give the best catalytic yield. The use of DMF, acetonitrile or EtOH as solvent (Table 8.2, entries 4 - 6) resulted in the same product but with lower yields, indicating that the presence of H_2O is crucial to obtain high yields. No conversion to product was observed in low polarity solvents in which **1ZnDy-NO_3** is insoluble (Table 8.2, entries 1 - 3), suggesting that the catalytic action is homogeneous.

Table 8.2. Comparison of catalytic activity of **1ZnDy-NO$_3$** with multiple solvent systems.

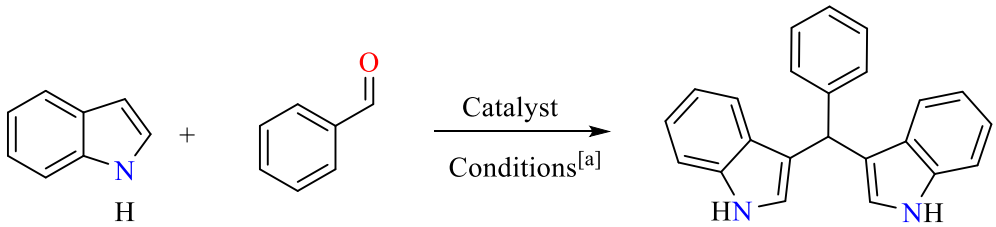

C8S1 **C8S2** **C8aa**

Entry[a]	Solvent	Loading/ mol%[b]	Time/ h	Yield/ %[c]
1	Toluene	10	12	0
2	$CHCl_3$	10	12	0
3	DME	10	12	0
4	DMF	10	12	16
5	MeCN	10	12	30
6	EtOH	10	12	95
7	EtOH/H_2O	10	12	Quantitative
8	MeCN/H_2O	10	12	42
9	MeOH/ H_2O	10	12	92
10	iPrOH/H_2O	10	12	70

[a] Reactions conditions: **C8S1**, 1 mmol; **C8S2**, 0.5 mmol; solvent 10 mL; r.t. [b] Catalyst loading calculated per equivalent of Ln^{III}. [c] Determined by ^{1}H NMR spectroscopy.

Table 8.3. Comparison of catalytic activity of **1ZnDy-NO$_3$** with a range of EtOH and H_2O ratios.

Entry [a]	%EtOH	Loading/ mol% [b]	Time / h	Yield / % [c]
1	100	2.5	12	89
2	90	2.5	12	92
3	80	2.5	12	95
4	70	2.5	12	97
5	60	2.5	12	Quantitative
6	50	2.5	12	Quantitative

[a] Reaction conditions: **C8S1**, 1 mmol; **C8S2**, 0.5 mmol; solvent 10 mL; r.t. [b]Catalyst loading calculated per equivalent of Ln^{III}. [c] Determined by ^{1}H NMR spectroscopy

Subsequently, a series of reactions was performed at 2.5 mol% catalyst loading with a varied H_2O/ EtOH ratio (Table 8.3). Quantitative yields (Table 8.3, entries 5 - 6) were obtained in the 3: 2 and 1: 1 EtOH/H_2O ratio.

After selecting the optimum solvent system, reactions were sought in the absence of any potential catalyst (Table 8.4, entry 1) and no product was obtained. Next, due to the heteronuclear (Zn^{II}/Ln^{III}) character of **1ZnLn-NO$_3$**, lanthanide and zinc triflates were used at 10 mol% loading (Table 8.4, entries 2 - 5) to identify their influence on the conversion to **C8aa**. Yttrium triflate (Table 8.4, entry 3) was found to give quantitative yields whilst dysprosium triflate (Table 8.4, entry 2) produced only slightly lower yields, zinc triflate (Table 8.4, entry 5), however, exhibited poor catalytic performance. Compound **1ZnDy-NO$_3$** afforded almost quantitative yields of the desired product after 2 h at 10 mol% loading. With the use of **1ZnLn-NO$_3$** PCCs, comparable performance to **1ZnDy-NO$_3$** was observed, however, the use of **1ZnY-NO$_3$** at 2.5 mol% loading afforded the desired material in quantitative yield (Table 8.4, entry 10).

Table 8.4 Comparison of catalytic activity for compounds **1ZnLn-NO$_3$**.

Entry	Catalyst	*T*	Loading / mol%[b]	Time / h	Yield / %[c]
1	None	r.t	N/A	12	0
2	$Dy(OTf)_3$	r.t	10	12	95
3	$Y(OTf)_3$	r.t	10	12	quantitative
4	$Y(OTf)_3$	r.t	5	12	55
5	$Zn(OTf)_3$	r.t	10	12	18
6	**1ZnDy-NO$_3$**	r.t	10	12	quantitative
7	**1ZnDy-NO$_3$**	r.t	5	12	96
8	**1ZnDy-NO$_3$**	r.t	2.5	12	92
9	**1ZnDy-NO$_3$**	r.t	1	12	87
10	**1ZnY-NO$_3$**	r.t	2.5	12	quantitative
11	**1ZnY-NO$_3$**	r.t	1	12	96
12	**1ZnSm-NO$_3$**	r.t	2.5	12	87
13	**1ZnEu-NO$_3$**	r.t	2.5	12	53
14	**1ZnTb-NO$_3$**	r.t	2.5	12	80
15	**1ZnGd-NO$_3$**	r.t	2.5	12	75
16	**1ZnYb-NO$_3$**	r.t	2.5	12	94

[a] Reaction conditions: **C8S1**, 1 mmol; **C8S2**, 0.5 mmol; catalyst; 10 mL EtOH/H_2O (2:1); r.t. [b] Catalyst loading calculated per equivalent of Ln^{III}. [c] Determined by ^{1}H NMR spectroscopy.

Promisingly, the catalyst loading for **1ZnY-NO$_3$** could be decreased to 1 mol% with only a slight decrease in the yields (Table 8.4, entry 11), a catalyst loading which is lower than other reported systems. Importantly, reducing the catalyst loading for yttrium triflate to 2.5 mol% (Table 8.4, entry 4) results in a severe decrease in yield, compared to the ability of **1ZnDy-NO$_3$** and **1ZnY-NO$_3$** to maintain high yields at only a few mol%.

8.2.4.1.2 Scope of reaction

The scope of the reaction was then explored by employing a variety of aldehydes and substituted indoles with **1ZnY-NO$_3$** (Table 8.5). The reactions proceed smoothly with very good to excellent yields. Products **C8aa**, **C8am** and **C8au** were characterized via single-crystal XRD studies (Figure 8.4).

The next step was to involve ketones in place of aldehydes. Long reaction times, even with a slight increase of the temperature (50 °C) did not yield any product with either aliphatic (acetone, cyclohexanone) or aromatic ketones (acetophenone) and no unexpected side products were observed. This opposite behaviour recalls the selective reduction of ketones in presence of aldehydes (Luche reaction).[501] In this reaction, aldehydes bond to Ln centres via hemiketal form, whilst ketone remains unprotected and is thus reduced by $NaBH_4$. Efforts to monitor the formation of the hemiketal form by ^{1}H NMR spectroscopy were not successful.

Table 8.5. 1ZnY-NO$_3$ catalysed FC alkylation of indoles and aldehydes.[a]

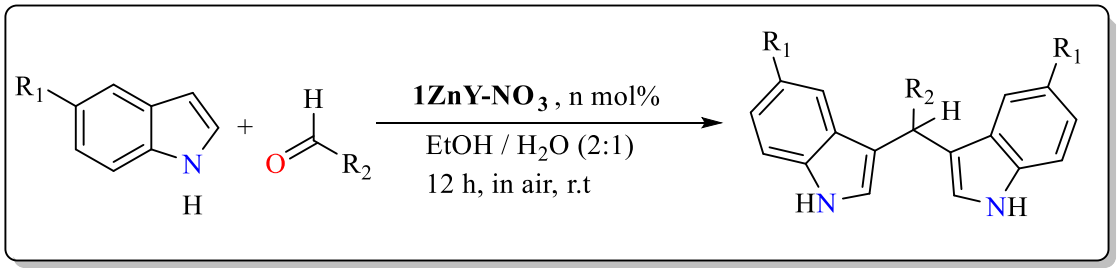

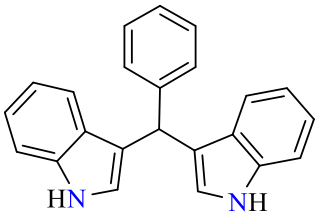

C8aa
n = 2.5 mol%, quantitative

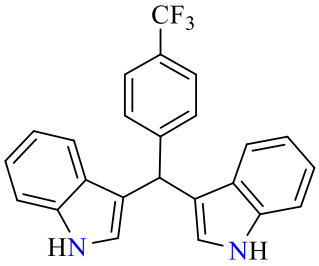

C8ab
n = 2.5 mol%, 95%

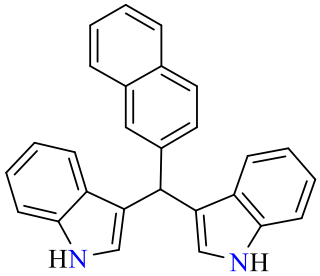

C8ac
n = 1 mol%, 98%

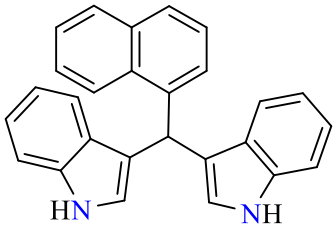

C8ad
n = 1 mol%, 96%

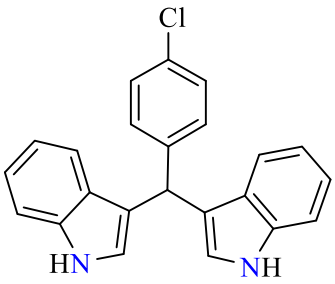

C8ae
n = 2.5 mol%, 89%

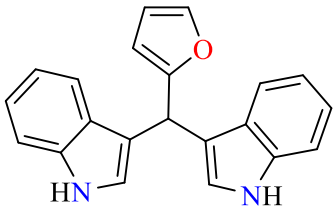

C8af
n = 2.5 mol%, 79%

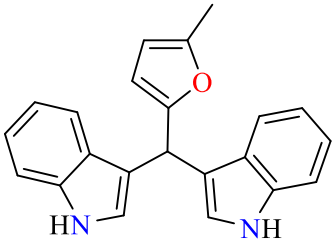

C8ag
n = 2.5 mol%, 77%

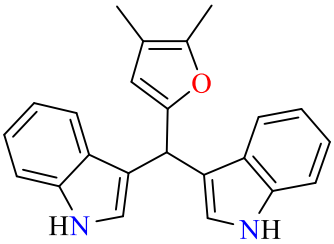

C8ah
n = 2.5 mol%, 72%

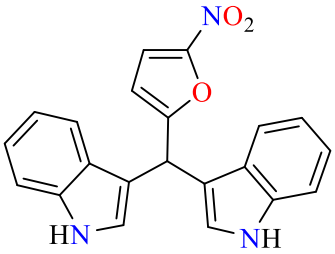

C8ai
n = 2.5 mol%, 65%

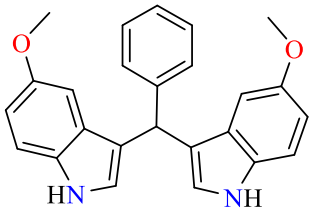

C8aj
n = 2.5 mol%, 99%

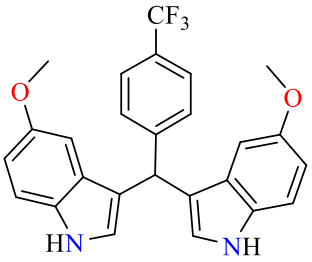

C8ak
n = 2.5 mol%, 88%

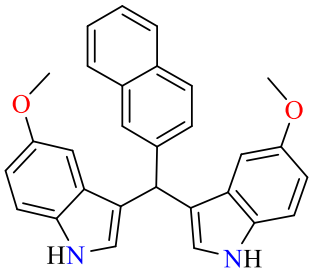

C8al
n = 2.5 mol%, 99%

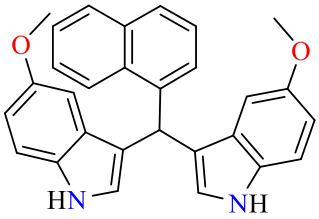

C8am
n = 2.5 mol%, 6 h, 99%

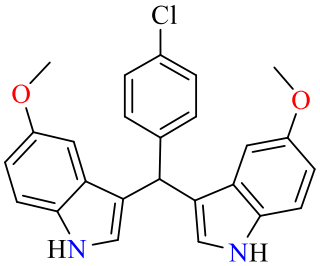

C8an
n = 2.5 mol%, 89%

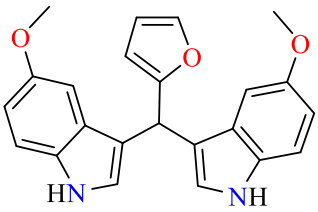

C8ao
n = 2.5 mol%, 82%

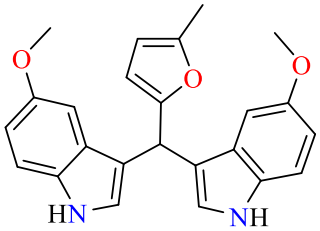

C8ap

n = 2.5 mol%, 82%

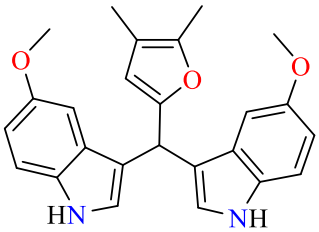

C8aq

n = 2.5 mol%, 75%

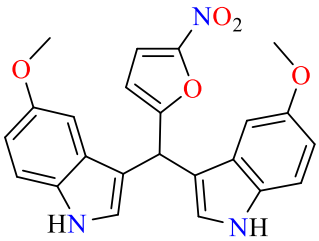

C8ar

n = 2.5 mol%, 62%

[a] Reaction conditions: **C8S1**, 1 mmol; **C8S2**, 0.5 mmol; catalyst; 10 mL EtOH/H_2O (2:1); r.t. [b] Catalyst loading calculated per equivalent of Y^{III}. [c] Determined by ^1H NMR spectroscopy.

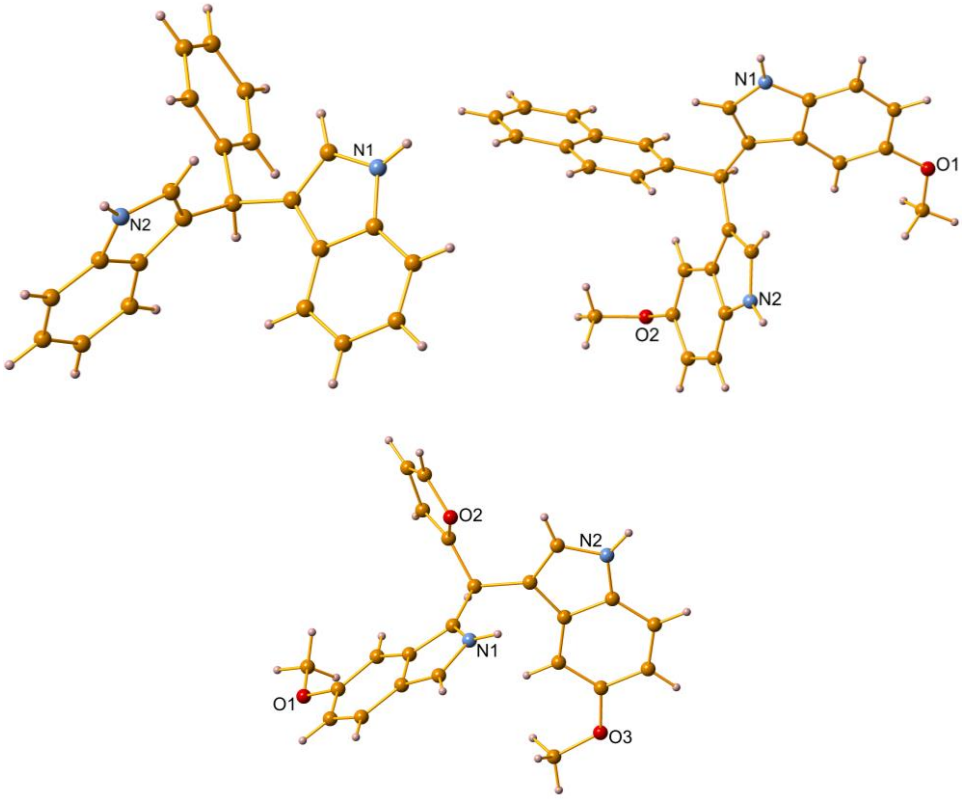

Figure 8.4. Crystal structures of **C8aa** (upper left), **C8al** (upper right) and **C8ao** (lower)**.** Colour code: C, gold; H, pink; N, pale blue; O, red.

8.2.4.1.3 Mechanistic insights

To gain information regarding the reaction mechanism and whether substrates were indeed binding or interacting with the $Zn^{II}_2Ln^{II}_2$ core, UV-Vis binding studies of 2-naphthaldehyde with $Zn(OTf)_2$, $Dy(OTf)_3$ and **1ZnDy-NO$_3$** were performed (Appendix B, S8.34-S8.36).

A 0.1 mM water/ethanol solution of 2-naphthaldehyde exhibited a strong absorption at 290 nm. **1ZnDy-NO$_3$** was added to the solution and the absorption was recorded over 3 h with 5 min intervals between measurements. It was observed that the intensities of the peak at 290 nm gradually decreased with time (Appendix B, S8.36). The quenching of this band may be attributed

to the bonding of 2-naphthaldehyde with **1ZnDy-NO$_3$** through weak Van der Waals interactions. Similar quenching was observed with the indole substrate (Appendix B, S8.41), indicating the binding behaviour of both substrates to **1ZnDy-NO$_3$**. Thus, both substrates can be activated after coordination with the two metal centres in **1ZnDy-NO$_3$** which favours the conjugate addition of the nucleophiles.

Similar studies were conducted with Zn(OTf)$_2$ and Dy(OTf)$_3$ to determine the preference of each substrate for the Ln^{III} or Zn^{II} metal centres (Appendix B, S8.37 - S8.38 and S8.40 - S.41). 2-naphthaldehyde shows almost double the rate quenching with Dy(OTf)$_3$ when compared to Zn(OTf)$_2$. This may suggest that 2-naphthaldehyde preferentially binds to the Dy^{III} centre. The **1ZnDy-NO$_3$** catalyst displays a greater rate of quenching for both substrates, than either Zn(OTf)$_2$ or Dy(OTf)$_3$, perhaps indicating a stronger interaction with the metal centres in tandem.

With the insights gathered from the UV-Vis binding study, the following set of reactions were performed to determine further mechanistic information.

Firstly, aliphatic aldehyde (cyclohexanecarbaldehyde) was employed instead of an aromatic aldehyde in reaction with indole, this gave very low yields of the expected product (**C8as**) (Table 8.6) after 72 hours.

Secondly, substituted indoles such as 2-methyl-indole, 2-(trifluoromethyl)-indole, 3-methyl indole, indole-3-acetic acid and N-methyl indole were examined in a reaction with benzaldehyde. The use of 2-methyl-indole gave the expected product (**C8at**) (Table 8.6) in quantitative yield in only 2 hours, indicating that substitution in position 2 promotes the reaction. Compound **C8at** was characterized via single-crystal XRD studies (Figure 8.5).

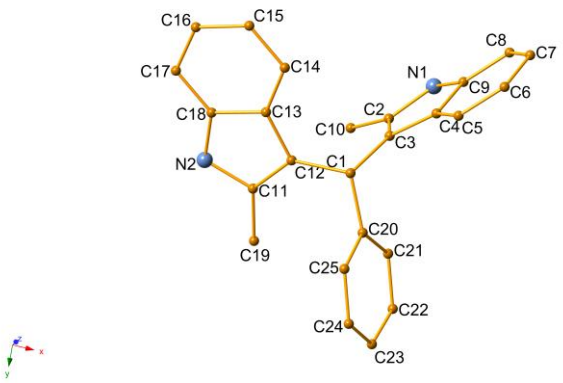

Figure 8.5. The molecular structure of **C8at**. Colour code: C, gold; H, pink; N, pale blue.

However, the use of the electron withdrawing group -CF$_3$ in place of -CH$_3$ [reaction with 2-(trifluoromethyl)-indole] gave a yield of only 16% of product **C8au**, indicating a substantial influence on the catalytic activity. The use of indole-3-acetic acid did not yield any product. A

logical explanation for the deterioration of catalytic activity is that indole-3-acetic acid is in competition with the benzaldehyde to coordinate to the Ln^{III} centre, leading to a poisoning of the catalyst.

In addition, the use of 3-methyl-indole also did not result in the formation of the corresponding BIM. The latter indicates that if the most active site (C-3) of the indole group is blocked the reaction does not proceed. Finally, the reaction of N-methyl-indole with benzaldehyde did not yield any product, revealing that coordination of the nitrogen atom to Zn^{II} is crucial.

Table 8.6. Reactions for mechanistic insights.[a]

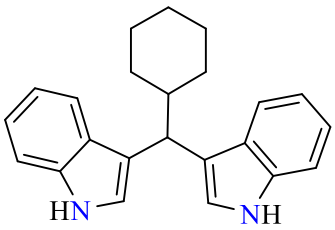	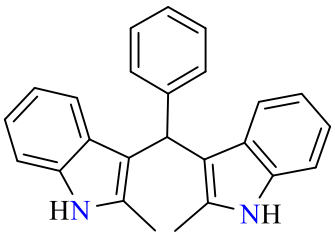	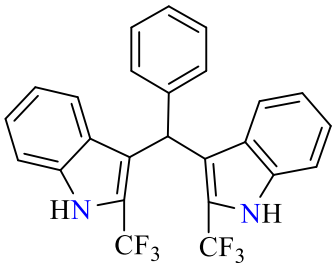
C8as	**C8at**	**C8au**
n = 2.5 mol%, 72 h, 12 %	n = 2.5 mol%, 2 h, 100 %	n = 2.5 mol%, 24 h, 16 %

[a] Reaction conditions: indole, 1 mmol; benzaldehyde (**C8S2**), 0.5 mmol; catalyst; 10 mL EtOH/H_2O (2:1); r.t. Yields determined by ^{1}H NMR spectroscopy.

Given the knowledge of the structure of the catalyst and the insights derived from above, the following mechanism for the FC reaction is proposed (Scheme 8.2). The first step of the reaction involves the coordination of the N_{indole} atom to the Zn^{II} and the $O_{carbonyl}$ atom of the aldehyde to the Ln part of the catalyst (Step 1). Then, deprotonation of the coordinated indole leads to the formation of negative centre at C-3 of the indole moiety (Step 2). The two organic moieties are very close [Y⋯Zn distances are 3.34882(7) and 3.5272(8) Å] which favours the formation of benzaldehyde-indole hemiaminal, as suggested by the ^{1}H NMR studies. This is followed (Steps 3-4) by alkylation of one more indole moiety (Step 5). Finally, the catalytic cycle ends by a proton exchange with an additional indole moiety (Step 6) and release of the bis-adduct product and water to reform the active catalyst species (Step 7).

8.2.4.2 1ZnLn-NO_3 catalysed FC alkylation of indoles and nitrostyrenes

With the promising results of the **1ZnY-NO_3** PCCs towards the catalysing of the FC alkylation of indoles with aldehydes to form BIM adducts, **1ZnLn-NO_3** were applied to the FC alkylation of indoles with nitrostyrenes to further confirm their efficacy as FC alkylation catalysts.

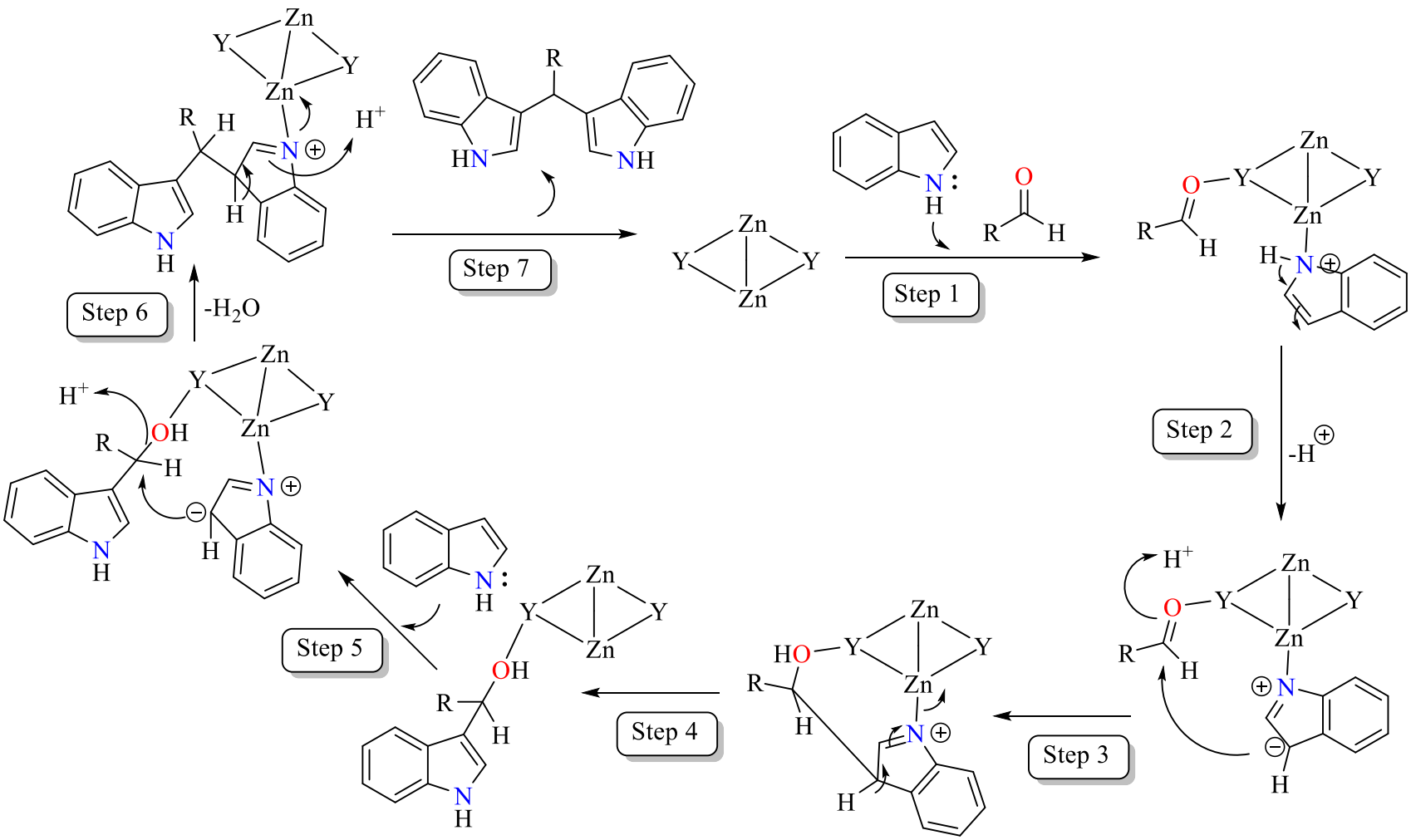

Scheme 8.2. Proposed mechanism for the catalytic reaction of indoles and aldehydes by **1ZnY-NO$_3$**.

The reaction between indole (**C8S1**) and *trans*-β-nitrostyrene (**C8S3**), in EtOH, at room temperature and a catalyst loading of 1.0 mol% (Table 8.7, entries 1 - 9) was chosen to optimise the reaction conditions.

8.2.4.2.1 Benchmarking and optimisation

To determine an optimised catalytic system several reaction parameters were investigated, including the solvent (Table 8.7, entries 10 - 13), catalysts (Table 8.7, entries 2 - 9) catalyst loading (Table 8.7, entries 18 - 20) and temperature of reaction (Table 8.7, entries 15 - 17).

Firstly, to determine the efficacy of the reaction without a catalyst, a blank experiment was performed and showed no conversion (Table 8.7, entry 1). In addition, very low conversions to product (**C8ba**) were obtained in the presence of Dy^{III} or Zn^{II} salts (Table 8.7, entries 2 - 3). In contrast, the first reactions with **1ZnDy-NO$_3$** and **1ZnY-NO$_3$** after 24 h show very high yields, 99% and 94%, respectively (Table 8.7, entries 4 - 5). Other catalysts such as **1ZnLn-NO$_3$**, where Ln = Eu, Gd, Sm and Tb, displayed lower yields (Table 8.7, entries 1 - 6). **1ZnDy-NO$_3$** was determined to be the best choice for this FC reaction.

The influence of the solvent on the catalytic performance was then investigated. **1ZnDy-NO$_3$** showed a high activity in ethanol with 99% yield for the desired product **C8ba** (Table 8.7, entry 4). Solvents such as THF, water, acetonitrile and DMF had a negative influence on the catalytic activity, therefore ethanol was deemed the best choice for further studies. At room temperature, the yield of **C8ba** was 99%, but only 5% at 0 °C. Lower yields were obtained at 60 °C (Table 8.7, entry 18), so the following reactions were made at room temperature.

As shown in Table 8.7, it was sufficient to use a catalyst loading of 1.0 mol% to obtain a yield up to 99% (Table 8.7, entry 4). An increase of the catalyst loading from 1.0 mol% to 5 mol% led to a remarkable decrease in the product yield (Table 8.7, entries 19 - 20). This finding can be explained due to the low solubility of the catalyst.

Further, a decrease in the catalyst loading to 0.5 mol% also displayed a lower yield of **C8ba** (Table 8.7, entry 18). Therefore, 1.0 mol% **1ZnDy-NO$_3$** in ethanol at room temperature for further experiments was subsequently used.

Table 8.7. Optimization of the FC alkylation of **C8S1** with **C8S3** catalysed by **1ZnLn-NO$_3$.**[a]

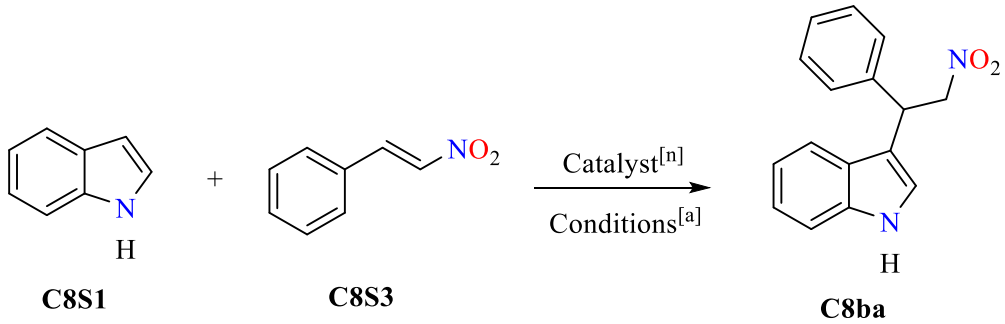

Entry	Catalyst[n]	Yield/ %[b]
1	none	0
2	Dy(OTf)$_3$	8
3	Zn(OTf)$_2$	20
4	**1ZnDy-NO$_3$**	99
5	**1ZnY-NO$_3$**	94
6	**1ZnEu-NO$_3$**	55
7	**1ZnGd-NO$_3$**	30
8	**1ZnSm-NO$_3$**	12
9	**1ZnTb-NO$_3$**	24
10	**1ZnDy-NO$_3$** (Toluene)	30
11	**1ZnDy-NO$_3$** (Water)	0
12	**1ZnDy-NO$_3$** (THF)	0
13	**1ZnDy-NO$_3$** (Acetonitrile)	0
14	**1ZnDy-NO$_3$** (DMF)	5
15	**1ZnDy-NO$_3$** (-30 ºC)	0
16	**1ZnDy-NO$_3$** (0 ºC)	5
17	**1ZnDy-NO$_3$** (60 ºC)	30
18	**1ZnDy-NO$_3$** (0.5 mol%)	26
19	**1ZnDy-NO$_3$** (2.5 mol%)	62
20	**1ZnDy-NO$_3$** (5.0 mol%)	17

[a] Reaction conditions: **C8S1** (0.50 mmol), **C8S3** (0.50 mmol) in 3 mL of EtOH under 1.0 mol% **1ZnLn-NO$_3$** complexes, 24 h, in air, stirred. [b] Isolated yield by column chromatography.

8.2.4.2.2 Scope of reaction

To explore the scope of the reaction, various nitroalkenes were treated with indole (Table 8.8). In the first of these experiments R_2 was aromatic (Table 8.8, **C8ba - C8bh**). Several catalytic systems gave slightly lower yields due to the electronic effect of para substitution of the phenyl group of

aromatic nitroalkenes. In all these cases, very good yields were obtained, ranging from the 4-fluoro substrate (**C8bd**) to 98% for the tolyl substituted compound (**C8bb**). A slight improvement of the yield up to 99% was observed with the use of a heteroaromatic nitroalkene bearing a furan substituent (**C8bf**). The effect of substitution of the indole is also shown in Table 8.8 (**C8bg - C8bo**). The substituent at position at 5 of the indole had little effect on the yield except for the electron-drawing group (**C8bj**) (Table 8.8).

Table 8.8. The scope of the FC alkylation of indoles with various nitrostyrenes catalysed by **1ZnDy-NO$_3$.**[a]

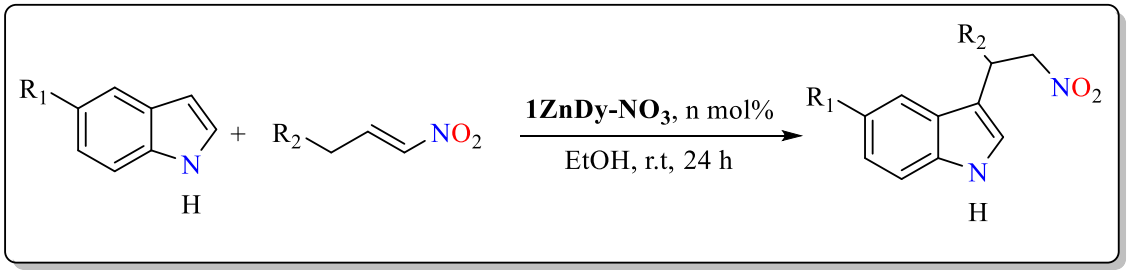

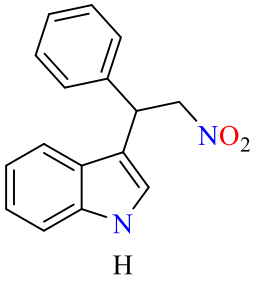

C8ba
n = 1 mol%, 99%

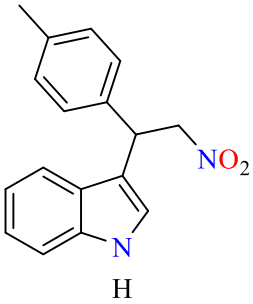

C8bb
n = 1 mol%, 98%

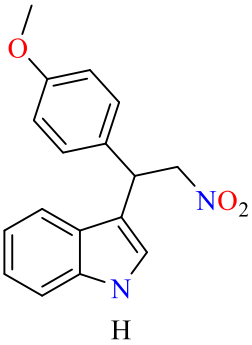

C8bc
n = 1 mol%, 96%

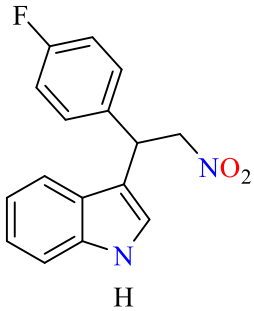

C8bd
n = 1 mol%, 92%

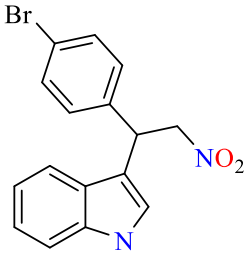

C8be
n = 1 mol%, 94%

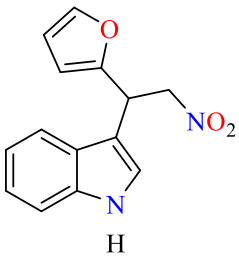

C8bf
n = 1 mol%, 99%

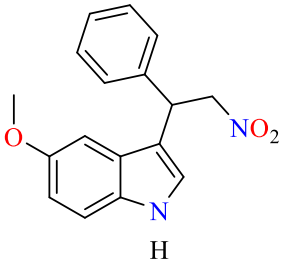

C8bg
n = 1 mol%, 97%

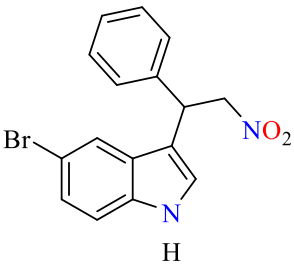

C8bh
n = 1 mol%, 95%

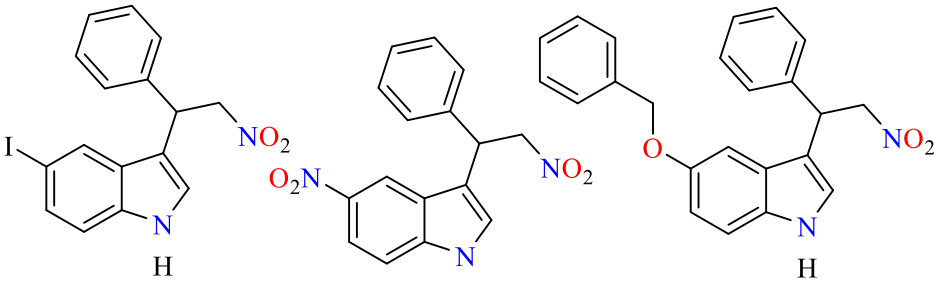

C8bi
n = 1 mol%, 94%

C8bj
n = 1 mol%, 76%

C8bk
n = 1 mol%, 96%

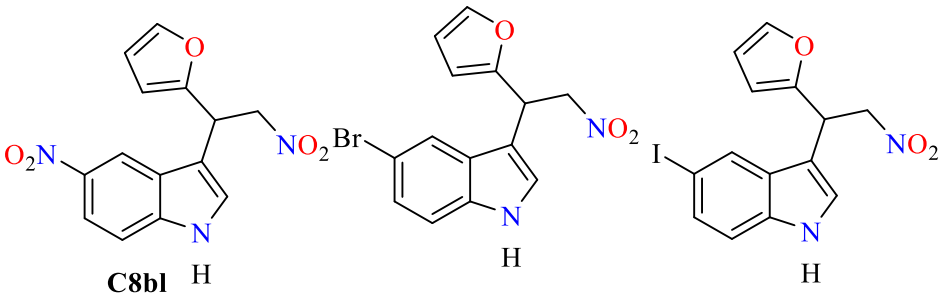

C8bl
n = 1%, 98%

C8bm
n = 1%, 95%

C8bo
n = 1%, 95%

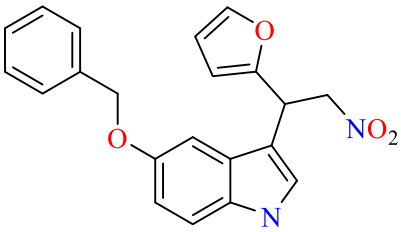

C8bn
n = 1%, 96%

[a] Reaction conditions: indoles (0.5 mmol) with nitroalkene (0.5 mmol) in 3 mL of EtOH, 1.0 mol% of **1ZnDy-NO$_3$**. [b] isolated yield by column chromatography.

The scope of the reaction was further investigated with N-alkylated and 2-methyl indole with various nitrostyrenes. The products were isolated in good to excellent yields (Table 8.9). A change of the substituent at the nitrogen atom in position 5, and at the 2-position of indole did not show any profound effect on the yield of the desired product (99%, Table 8.9). **C8bw** was characterized via single-crystal XRD studies (Figure 8.6).

Table 8.9. FC alkylation of N-alkylated and 2-methyl indoles and various nitrostyrenes.[a]

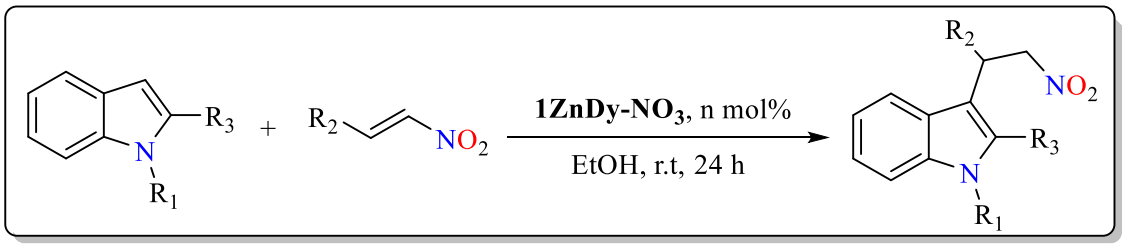

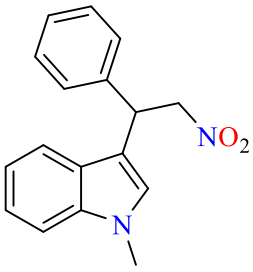

C8bp
n = 1 mol%, 99 %

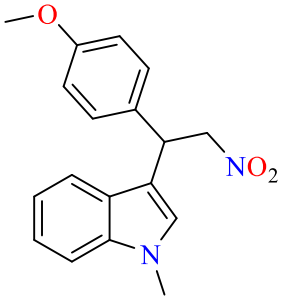

C8bq
n = 1 mol%, 99 %

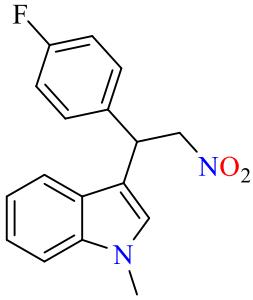

C8br
n = 1 mol%, 93 %

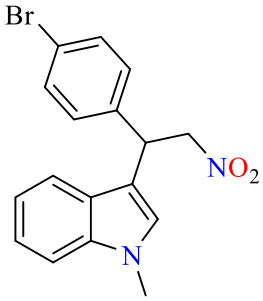

C8bs
n = 1 mol%, 95 %

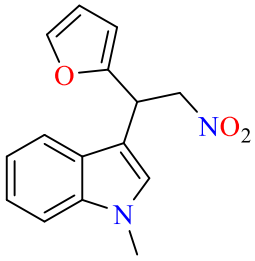

C8bt
n = 1 mol%, 99 %

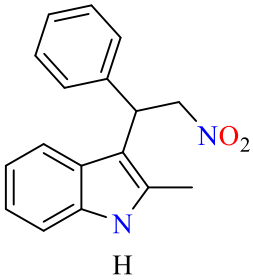

C8bu
n = 1 mol%, 99 %

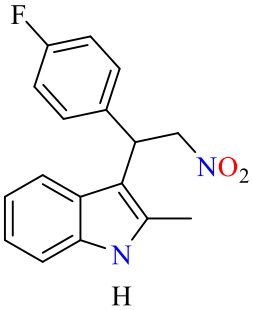

C8bv
n = 1 mol%, 94 %

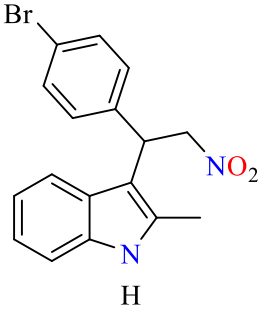

C8bw
n = 1 mol%, 96 %

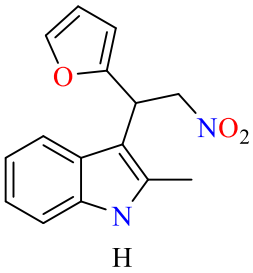

C8bx
n = 1 mol%, 99 %

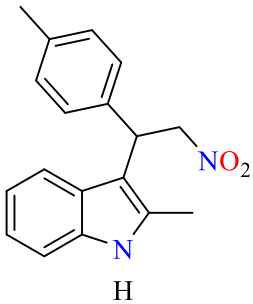

C8by
n = 1 mol%, 98 %

[a] Reaction conditions: indoles (0.3 mmol), nitrostyrenes (0.3 mmol), 3 mL of EtOH, 1.0 mol% **1ZnDy -NO$_3$** complex. [b] Isolated yield by column chromatography.

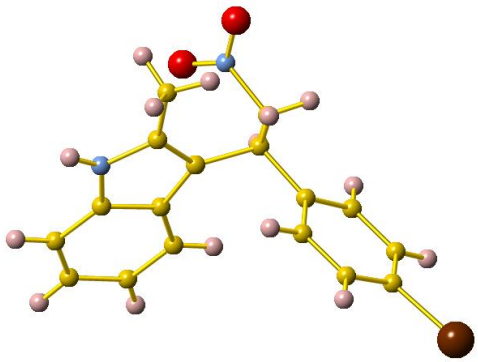

Figure 8.6. Crystal structure of **C8bw**. Colour code: C, gold; H, pink; N, pale blue; O, red; Br, brown.

8.2.4.2.3 Mechanistic insights and UV studies

UV-Vis binding studies were performed to determine whether there was any interaction between **C8S3** and **1ZnDy-NO$_3$**.

A 0.1 mM water/ethanol solution of **C8S3** exhibited a strong absorption at 320 nm. **1ZnDy-NO$_3$** was added to the solution and the absorption was recorded over 3 h with 5 min intervals between measurements. It was observed (Appendix B, Figure S8.38) that the intensities of the peak at 320 nm gradually decreased. The quenching of the band may be attributed to Van der Waals interactions between nitrostyrene and **1ZnDy-NO$_3$**. Similar quenching was observed with the **C8S1** substrate as discussed previously, indicating the binding behaviour of both substrates to **1ZnDy-NO$_3$**. Thus, both substrates can be activated after coordination with the two metal centres in **1ZnDy-NO$_3$** which favours the conjugate addition of the nucleophiles.

Repeat studies were conducted with Zn(OTf)$_2$ and Dy(OTf)$_3$ to determine the preference of each substrate for the Ln^{III} or Zn^{II} metal centres. **C8S3** shows a greater rate of quenching with Dy(OTf)$_3$ than Zn(OTf)$_2$, whereas with **1ZnDy-NO$_3$** the rates are similar. This may suggest that **C8S3** preferentially binds to the Dy^{III} centre. The **1ZnDy-NO$_3$** catalyst for both substrates demonstrates a greater rate of quenching than either Zn(OTf)$_2$ or Dy(OTf)$_3$, perhaps indicating a stronger interaction with the metal centres in tandem.

Based on the previously discussed results and the crystal structure of **1ZnDy-NO$_3$**,[336] in which a nitrate group chelates to Dy^{III} (**C8S3** can be considered as an alternative of nitrate), then a plausible mechanism and transition state can be proposed, as shown in Scheme 8.3. It is envisioned that the nitroalkenes are activated by chelation to Dy^{III} and π-π stacking between the phenyl group of the coordinating ligand **L1** and the phenyl group of nitroalkenes.[469] In addition,

the indole substrate will bond to the Zn^{II} ion through the nitrogen atom and bring the two organic moieties efficiently close to favour the formation of the alkylated product.

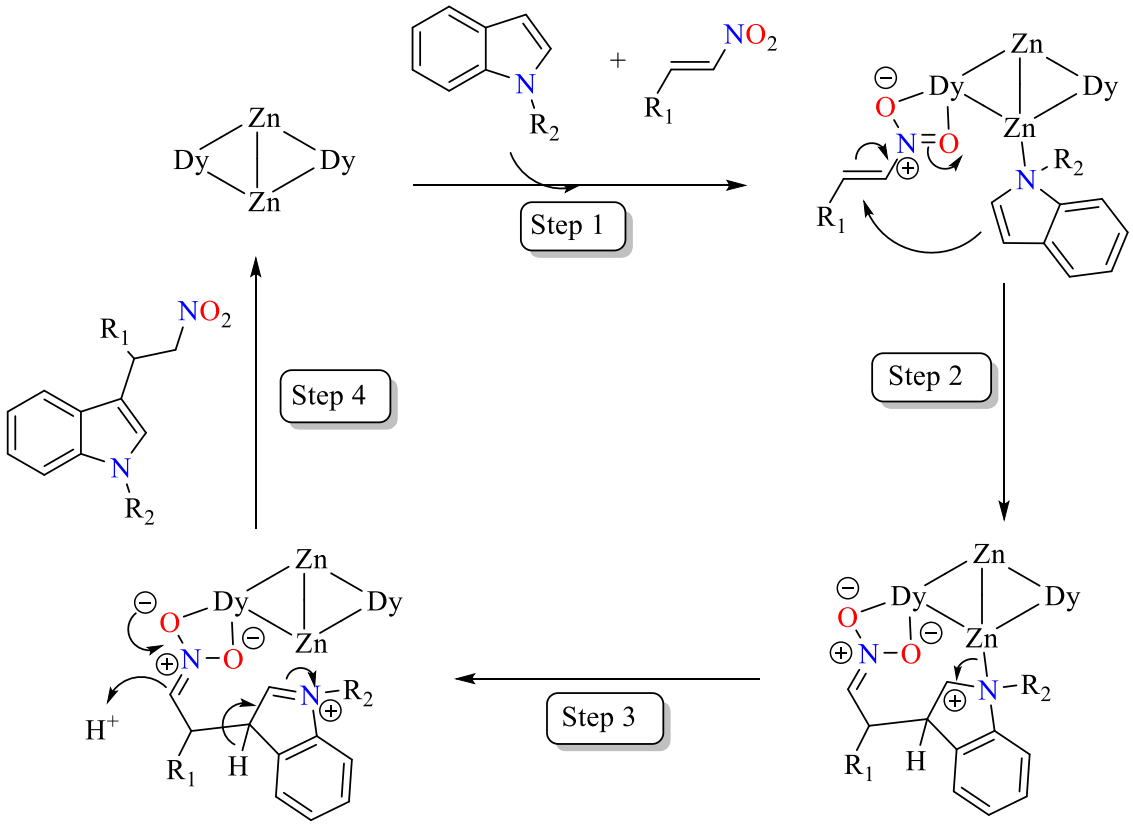

Scheme 8.3. A plausible mechanism for the FC alkylation.

8.2.4.3 A 1ZnLn-NO_3 catalysed PBR reaction

With the success of the **1ZnLn-NO_3** PCC series in the previous two FC alkylation reactions, they were applied to a PBR. The reaction between salicylaldehyde (**C8S4)**, indoline (**C8S5**) and boronic acid (**C8S6**) at room temperature and a catalyst loading of 1.0 mol% was chosen to optimise the reaction conditions.

8.2.4.3.1 Benchmarking and optimisation

Several reaction parameters, such as the use of solvents (Table 8.10), different catalysts (Table 8.11), temperature (Table 8.12) and catalyst loading (Table 8.13) were studied. **1ZnY-NO_3** and **1ZnDy-NO_3** showed a similar catalytic efficacy at room temperature, therefore solvent screening reactions were performed with **1ZnDy-NO_3**.

DME appears to be the most suitable solvent where almost full conversion is achieved (Table 8.10, entry 5). The use of THF, toluene or ethanol, provided the anticipated product in substantially lower yields (Table 8.10, entries 1 - 4), demonstrating an inhibitory influence on the

reaction. Interestingly, the use of DMSO or DMF yielded very low conversions (Table 8.10, entries 6 - 7).

Table 8.10. Influence of the solvent.[a]

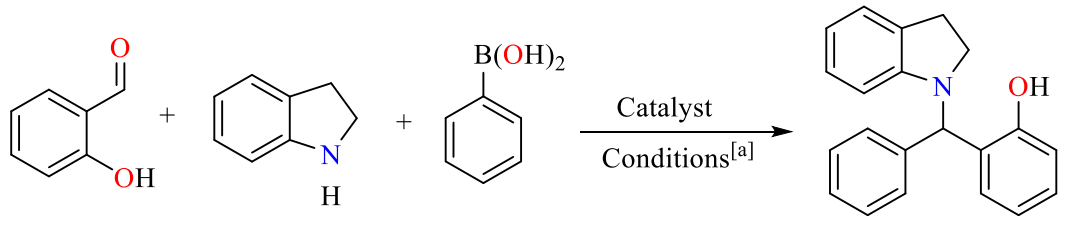

C8S4 **C8S5** **C8S6** **C8ca**

Entry	Solvent	Yield / %[b]
1	Toluene	34
2	Water	28
3	THF	40
4	Ethanol	80
5	DME	96
6	DMSO	12
7	DMF	14

[a] Reaction conditions: **C8S4** (0.50 mmol), **C8S5** (0.50 mmol), **C8S6** (0.50 mmol), 5 mL solvent, 1.0 mol% **1ZnDy-NO$_3$** catalyst, r.t. [b] Isolated yield by column chromatography.

With the optimised solvent established, the remainder of the $Zn^{II}_2Ln^{III}_2$ series (**1ZnLn-NO$_3$**) were tested for their catalytic efficacy. The results are summarized in Table 8.11. **C8ca** was obtained in moderate to excellent yields. A control experiment in the absence of the 3d-4f PCCs catalyst showed 40% conversion (Table 8.11, entry 1). Moderate conversions were obtained in the presence of Dy^{III} or Zn^{II} salts (Table 8.11, entries 2 - 3).

Both **1ZnDy-NO$_3$** and **1ZnY-NO$_3$** show higher activity than **1ZnLn-NO$_3$**, where Ln = Gd, Eu, Yb and Tb (Table 8.11, entries 4 - 9). Therefore, **1ZnDy-NO$_3$** was selected for subsequent experiments. Efforts to recover the catalyst after the MCR completion were not successful.

The influence of the temperature on the catalytic performance was then studied. The reactions were carried out at various temperatures ranging from room temperature to 120 °C (Table 8.12, entries 1 - 6). At room temperature (Table 8.12) the yield of **C8ca** was 96%, however, no conversion was observed at 0 °C. Lower yields were obtained at 60 °C, 80 °C, 100 °C and 120 °C (Table 8.12, entries 3 - 6), therefore subsequent reactions were performed at room temperature.

Table 8.11. MCR of **C8S4**, **C8S5** and **C8S6** catalyzed by **1ZnLn-NO$_3$** complexes.[a]

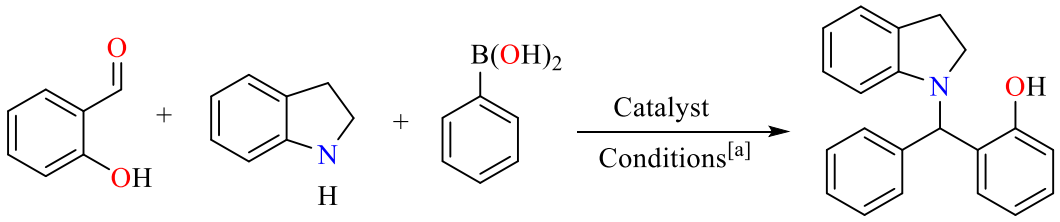

C8S4 **C8S5** **C8S6** **C8ca**

Entry	Catalyst	Yield / %
1	none	40
2	$Zn(OTf)_2$	56
3	$Dy(OTf)_3$	36
4	**1ZnY-NO$_3$**	74
5	**1ZnEu-NO$_3$**	55
6	**1ZnGd-NO$_3$**	54
7	**1ZnDy-NO$_3$**	96
8	**1ZnTb-NO$_3$**	66
9	**1ZnYb-NO$_3$**	57

[a] Reaction conditions: **C8S4** (0.50 mmol), **C8S5** (0.50 mmol), **C8S6** (0.50 mmol), 5 mL solvent, 1.0 mol% **1ZnDy-NO$_3$** catalyst, r.t. [b] Isolated yield by column chromatography.

Table 8.12. Influence of the temperature.[a]

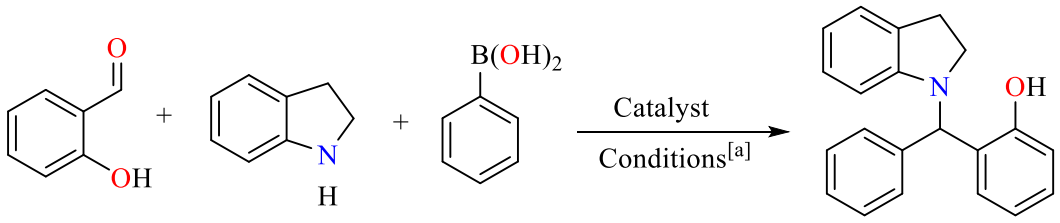

C8S4 **C8S5** **C8S6** **C8ca**

Entry	Temperature/ ºC	Yield/ %
1	0	0
2	r.t	96
3	60	76
4	80	72
5	100	65
6	120	62

[a] Reaction conditions: **C8S4** (0.50 mmol), **C8S5** (0.50 mmol), **C8S6** (0.50 mmol), 5 mL solvent, 1.0 mol% **1ZnDy-NO$_3$** catalyst, r.t. [b] Isolated yield by column chromatography.

After optimisation of the reaction conditions, the loadings of catalyst **1ZnDy-NO$_3$** were varied (Table 8.13). It was sufficient to use a catalyst loading of 1.0 mol% to obtain a yield up to 96% (Table 8.13, entry 3). An increase of the catalyst loading from 1.0 mol% to 5 mol% led to a remarkable decrease in the yield of **C8ca** (Table 8.13, entries 3 - 6). Further, a decrease in the catalyst loading to 0.5 mol% lowered the yield of **C8ca** (Table 8.13, entry 2). In absence of catalyst, a 40% conversion is observed (Table 8.13, entry 1). Finally, it was determined that the use of 1.0 mol% **1ZnDy-NO$_3$**, in DME and at room temperature, were the optimal conditions to further explore the scope of the MCR.

Table 8.13. Influence of catalyst (**1ZnDy-NO$_3$**) loading.[a]

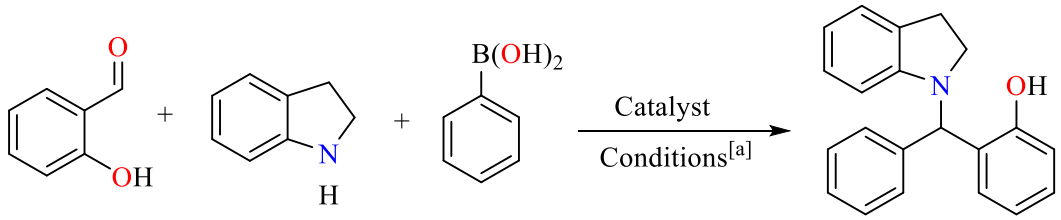

C8S4 **C8S5** **C8S6** **C8ca**

Entry	Catalyst loading / mol%	Yield / %
1	-	40
2	0.5	57
3	1.0	96
4	1.5	70
5	2.0	40
6	5.0	24

[a] Reaction conditions: **C8S4** (0.50 mmol), **C8S5** (0.50 mmol), **C8S6** (0.50 mmol), 5 mL solvent, 1.0 mol% **1ZnDy-NO$_3$** catalyst, r.t. [b] Isolated yield by column chromatography.

8.2.4.3.2 Scope of reaction and mechanistic insights

To demonstrate the applicability of the optimised reaction conditions, different secondary amines, aldehydes and boronic acids were employed in this MCR, using **1ZnDy-NO$_3$** as catalyst (Table 8.14). The reaction proceeds in very good to excellent yields (84 - 98%, **C8ca** - **C8cq**) at room temperature with a catalyst loading of 1.0 mol%. Compound **C8cb** was characterized via single-crystal XRD studies (Figure 8.7).

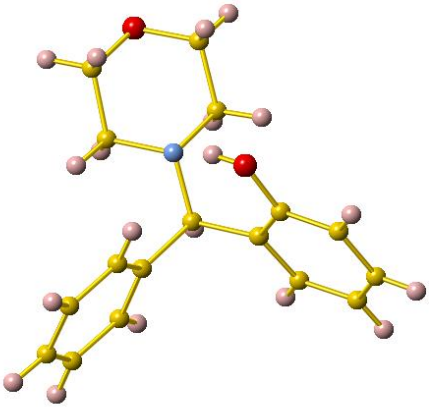

Figure 8.7. Crystal structure of **C8cb**. Colour code: C, gold; O, red; N, blue; H, pink.

Very good yields were obtained for the reaction involving indoline as a secondary amine (Table 8.14), but the reaction with N-methylaniline and N-benzylmethylamine, also gave very good yields, 94 and 93%, respectively (Table 8.14). The presence of an electron donating group in the para position of boronic acid gives the multicomponent product in very good yields, whereas the nature of secondary amine influences the total yield (Table 8.14). Compounds **C8cj**, **C8ck**, **C8cl** and **C8cm** (allyl functional group) were isolated only in moderate yields. Moreover, the MCRs between a salicylic aldehyde or o-vanillin, secondary amines and benzene 1, 4-diboronic acid afforded products **C8cn**, **C8co**, **C8cp** and **C8cq** in very good yields (Table 8.14).

After an extensive literature review, it is believed that this is the first time that benzene 1, 4-diboronic acid has successfully been involved in the titled reaction. It is worth mentioning that the reaction does not progress with the use of primary amines or benzaldehyde indicating the importance of the hydroxyl group in the aldehyde to activate the boronic acid.[31]

Table 8.14. 1ZnDy-NO$_3$ catalysed MCR of aldehydes, amines and boronic acids. [a+b]

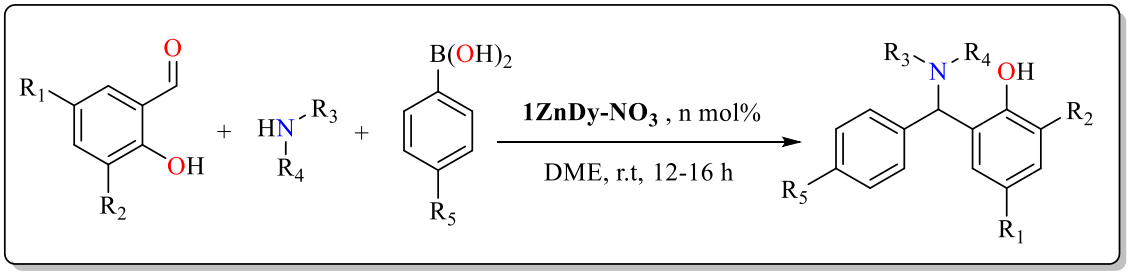

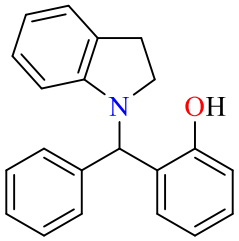

C8ca
n = 1 mol%, 96%

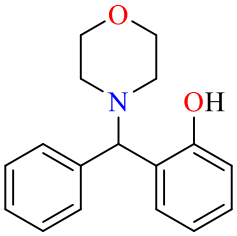

C8cb
n = 1 mol%, 95%

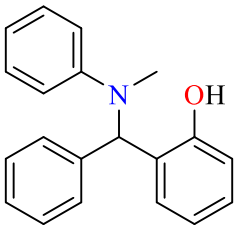

C8cc
n = 1 mol%, 94%

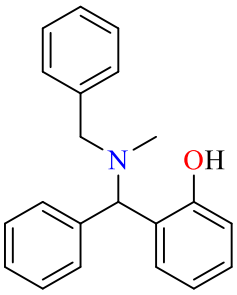

C8cd
n = 1 mol%, 93%

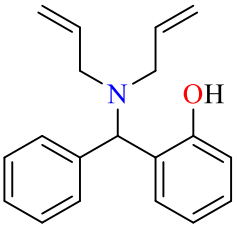

C8ce
n = 1 mol%, 90%

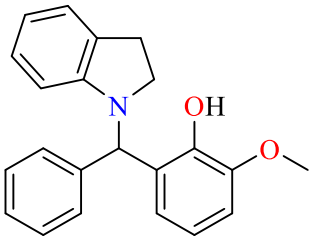

C8cf
n = 1 mol%, 95%

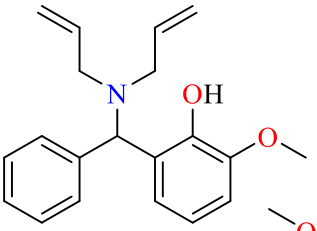

C8cg
n = 1 mol%, 93%

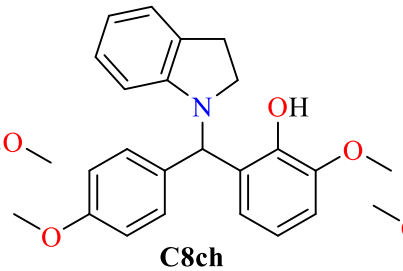

C8ch
n = 1 mol%, 98%

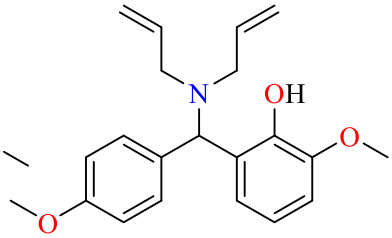

C8ci
n = 1 mol%, 93%

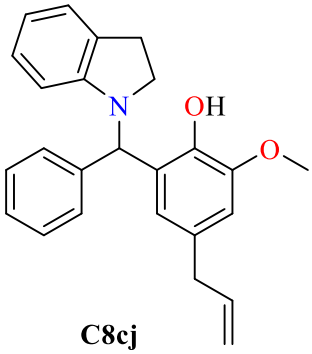

C8cj
n = 1 mol%, 87%

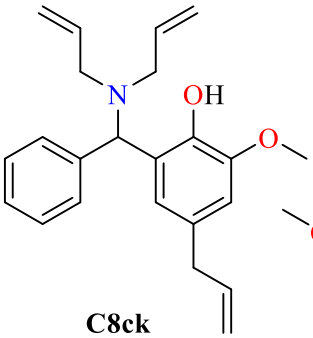

C8ck
n = 1 mol%, 84%

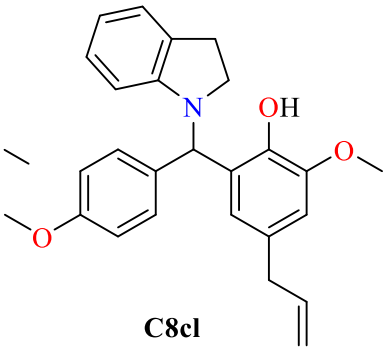

C8cl
n = 1 mol%, 89%

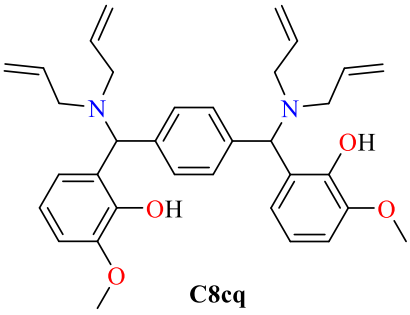

C8cq
n = 1 mol%, 88%

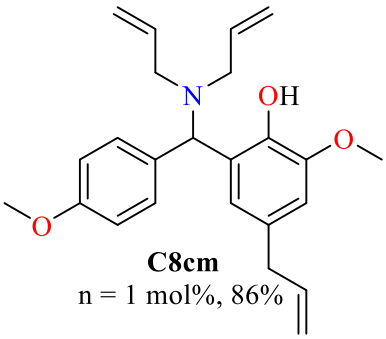

C8cm
n = 1 mol%, 86%

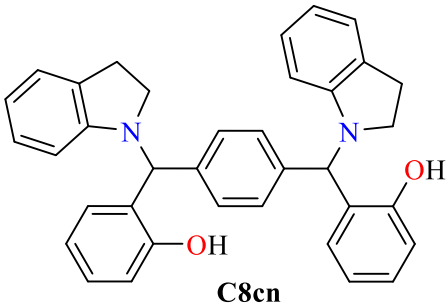

C8cn
n = 1 mol%, 92%

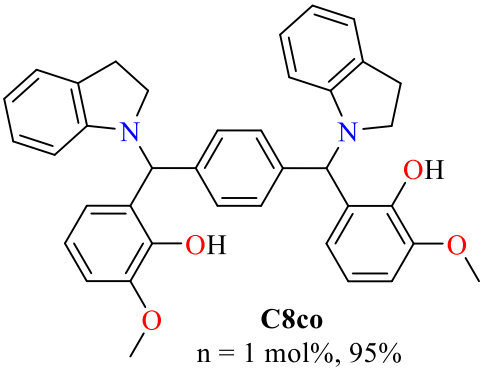

C8co
n = 1 mol%, 95%

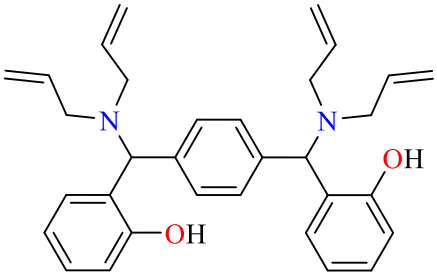

C8cp
n = 1 mol%, 86%

[a] Reaction conditions: **aldehyde** (0.50 mmol), **secondary amine** (0.50 mmol), **boronic acid** (0.50 mmol), 5 mL solvent, 1.0 mol% **1ZnDy-NO$_3$** catalyst, r.t. [b] Isolated yield by column chromatography.

8.3 Conclusion

The results presented in this chapter confirm for the first time that Zn^{II}-Ln^{II} PCCs may be useful as catalysts for FC alkylation and MCR reactions with low catalyst loadings and mild reaction conditions. $Zn^{II}_2Ln^{III}_2$ defect dicubane PCCs (**1ZnLn-NO$_3$**) were synthesised and characterised. By substituting the 4f elements in the isoskeletal frame and substituting the 3d ion to the diamagnetic Zn^{II}, it was possible to confirm the solution stability of these 3d-4f bimetallic species via EPR, NMR and ESI-MS studies. This also allowed mechanistic insights into possible reaction mechanisms of both MCR and FC reactions. UV-Vis binding studies further support the proposed mechanisms and give insights into possible substrate-core interactions. In addition, it was possible to tune the 4f ion to optimise efficient conversion to a broad variety of products, with both **1ZnDy-NO$_3$** and **1ZnY-NO$_3$** found to be the optimal PCC for either MCR or FC reactions. The fine-tuning of the organic periphery and further extending mechanistic studies of these catalysts will be the focus of chapter nine.

Chapter 9: Co-operative $Zn^{II}_2Ln^{III}_2$ PCC catalysts for a diastereoselective Michael addition reaction

Abstract: Michael Additions (MA) are one of the most well-studied chemical transformations in synthetic chemistry. Herein, the synthesis and crystal structures of a library of 3d-4f polynuclear coordination clusters (PCCs) formulated $[M^{II}_2Ln^{III}_2(\mathbf{L1})_4(solv)_X(Z)_Y]$ (**LMLn-NO_3**) and a study of their catalytic properties towards a MA reaction are reported. All these PCCs combine a hard and a borderline hard/soft Lewis acid within a defect dicubane framework that brings the two metals within 3.3 Å. Valuable mechanistic information for the co-operative catalytic character can be extracted via ^{1}H NMR, electrospray ionisation mass spectrometry, electron paramagnetic resonance, UV-Vis studies and theoretical studies. This chapter demonstrates for the first time the successful use of 3d-4f PCCs as efficient and highly diastereoselective catalysts in a MA reaction. Density functional theory calculations shed light on the possible catalytic mechanism.

9.1 Introduction

Chapters seven and eight reported the ease of ambient and high yielding synthesis of a library of heterometallic 3d-4f PCCs possessing a rigid defect dicubane topology (Figure 9.1) with the general formula $[M^{II}_2Ln^{III}_2(\mathbf{L1})_4(solv)_X(Z)_Y]$ (**1MLn**), where M is Co/Ni/Zn, Ln is Y/Sm/Eu/Gd/Dy/Tb/Yb, solv is EtOH/CH_3CN/DMF, Z = Cl/NO_3/ClO_4, when Z = Cl, (X = 2, Y = 2), Z = NO_3 (X = 2, Y = 2) and Z = ClO_4 (X = 6, Y = 2). In addition, the solution stability of these 3d-4f PCCs and their effectiveness to construct organic building blocks, at room temperature and low catalyst 1% loading, in domino (chapter seven) as well FC alkylation, and PBR (chapter eight) reactions were presented. Chapter eight also suggested a co-operative effect between 3d and 4f metal centres, an observation which is absent in chapter seven.

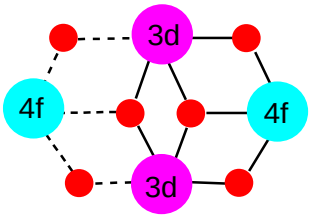

Figure 9.1. A pictorial representation of the present catalytic system (**LMLn**). Colour code: O, red.

This well-defined and crystallographically characterised bimetallic catalytic system, in addition to having characterisation handles, brings the two metals in a proximity of 3.3 Å, lower than recommended,[285] and offers the unique possibility to combine a hard and a borderline hard/soft Lewis acid. Therefore, by retaining the hard 4f centre and upon tuning the 3d centre (Co^{II}, Ni^{II}, Cu^{II}, or Zn^{II}, Figure 9.1), valuable mechanistic information can be extracted by correlating product

distributions/selectivities *vs*. metal properties, *e.g*. Co^{II} and Ni^{II} that have a lower preference to O-atoms in comparison to Zn^{II} and Cu^{II} (Pearson table).[502] Such information cannot be obtained by the use of homometallic polynuclear 3d-3d or 4f-4f catalysts.

The employment of the previously described **1MLn** PCCs in a Michael Addition (MA) reaction was considered, as these are one of the most well-studied chemical transformations in synthetic chemistry and various catalytic protocols including organocatalysts,[503,504] simple salts, and complexes[505,506] have been developed. Inspired by Shibasaki's pioneering study of a dinuclear Cu^{II}-Sm^{III} PCC in nitro Mannich reactions,[296,297] in which binding of both substrates on both metal centres is recommended, and having all the above in mind, it was envisaged that the present library of catalysts will co-operatively catalyse a MA reaction.

The catalytic MA reaction of *trans*-β-nitrostyrene and 1,3-dimethyl barbituric was identified as an ideal system to be studied. Previously this reaction has been tested to elucidate the catalytic mechanism of a "molecular prism" and investigate the binding properties to these substrates.[507] The reaction proceeds smoothly and is not very well explored.[507–509] There is also no previous report into the use of bimetallic 3d-4f PCCs as catalysts in MA reactions.

Modification of the ligand and metal centres as well as *in situ* studies of the catalytic reaction with UV-Vis, NMR and EPR spectroscopic techniques to gain mechanistic aspects and theoretical support are provided.

9.2 Results and discussion

9.2.1 Synthetic aspects

One of the objectives of this chapter is to further optimise the catalytic efficacy of the previously described **1MLn** catalysts**,** more specifically the **1ZnLn-NO$_3$** analogues towards the previously discussed MA reaction. It was envisioned that by modifying the organic periphery of H_2**L1**, this may result in $Zn^{II}_2Ln^{III}_2$ PCCs with increased solubility and steric effects, which could lead to improved catalytic efficacy.

With sixteen of the Schiff base ligands described in chapter five and an additional six synthesised in this chapter (H_2**L24** - H_2**L29**), twenty-one novel $Zn^{II}_2Ln^{III}_2$ PCCs (**LZnY-NO$_3$**) with a defect dicubane core topology (**2,3M4-1**) were synthesised according to the following synthetic procedure.

LZnY-NO$_3$ PCCs were synthesized from the one-step reaction of H_2**LX** (Figure 9.2) (0.2 mmol), Et_3N (0.5 mmol), $Zn(NO_3)_2{\cdot}6H_2O$ (0.1 mmol) and $Ln(NO_3)_3{\cdot}x(H_2O)$ (0.1 mmol), in EtOH, under reflux for 2 h with very high yields of solid (over 90%). Crystals suitable for single-crystal XRD studies were obtained by dissolving solid in DMF followed by VD with Et_2O.

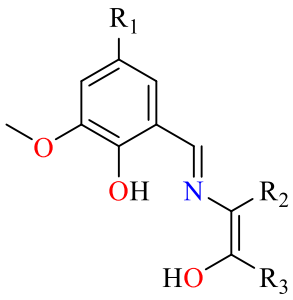

R_1	R_2 R_3						
	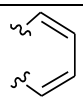	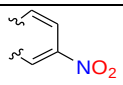	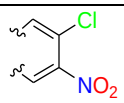	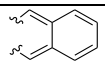	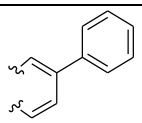	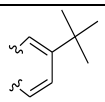	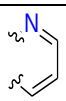
H	H_2**L1**	H_2**L8**	H_2**L12**	H_2**L2**	H_2**L19**	H_2**L27**	H_2**L24**
CH_2-CH=CH_2	H_2**L6**	H_2**L9**	H_2**L13**	H_2**L16**	H_2**L20**	H_2**L28**	H_2**L25**
Br	H_2**L5**	H_2**L11**	H_2**L15**	H_2**L18**	H_2**L22**	H_2**L29**	H_2**L26**

Figure 9.2. The organic ligands (H_2**LX**) used in this chapter.

9.2.2 Molecular structures

In chapter five the term "isoskeletal" was introduced to describe PCCs that possess the same topology. All PCCs synthesised in this study were isoskeletal and possess a defect dicubane topology. The 3d metal is in the centre and the 4f in the wings. The 3d and 4f ions are within a proximity of 3.3 Å. Five out of six and six out of eight positions of the 3d and 4f centres are occupied by the ligand, respectively. The ligands used in this study display a similar coordination environment, aiming always to yield the same **2,3M4-1** motif as to identify the influence of the second coordination sphere on the catalysis.

In total, twenty-one ligands (Figure 9.2) were used, to synthesise the PCCs formulated as $[M^{II}_2Ln^{III}_2(\mathbf{LX})_4(NO_3)_2(DMF)_2]$, which were isoskeletal analogues to **1ZnLn-NO$_3$** described in chapter eight. All these PCCs were characterised by FT-IR spectra (Appendix B, Figures S9.1-S9.20), TGA (Appendix B, Figures S9.21-S9.40), EA (chapter 11), ESI-MS (Appendix B, Figure S9.41-9.51) and several were characterised via single-crystal XRD studies including **LZnY-NO$_3$**, where **L** = 2, 6, 8, 9, 12, 13, 22, 24 and 27. Crystallographic representations are given in Figure 9.3. The crystallographic characterization of **1ZnLn-NO$_3$**, where Ln = Y, Sm, Eu, Gd, Dy, Tb and Yb, have been reported been previously discussed in chapter eight.

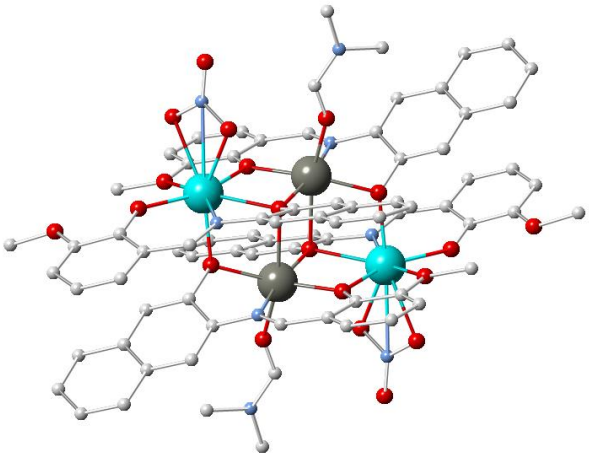

2ZnY-NO$_3$

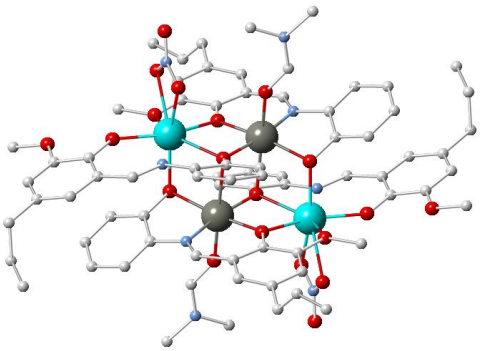

6ZnY-NO$_3$

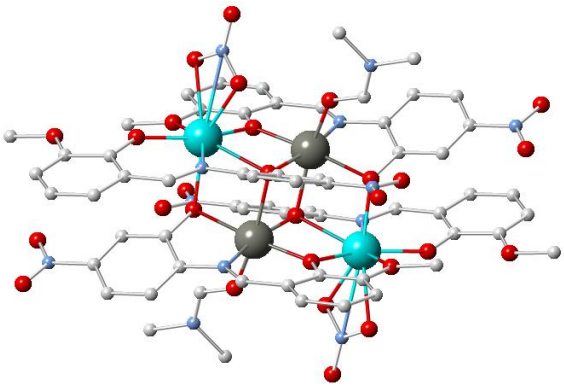

8ZnY-NO$_3$

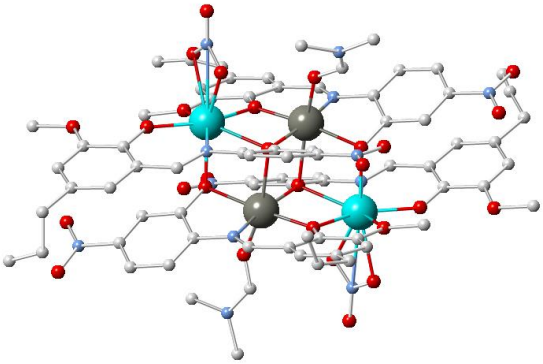

9ZnY-NO$_3$

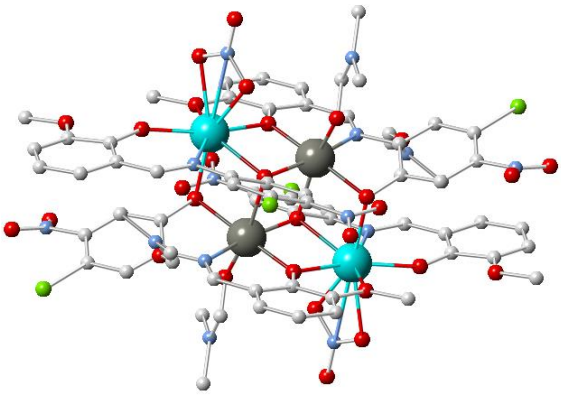

12ZnY-NO$_3$

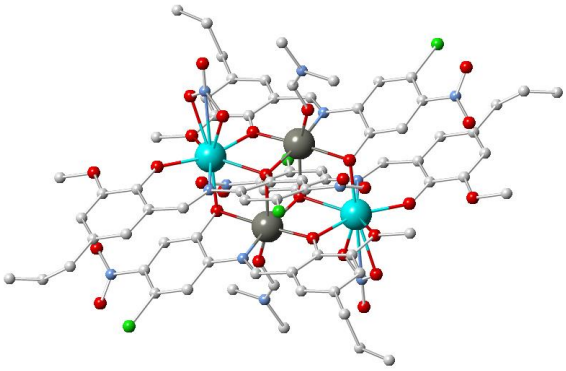

13ZnY-NO$_3$

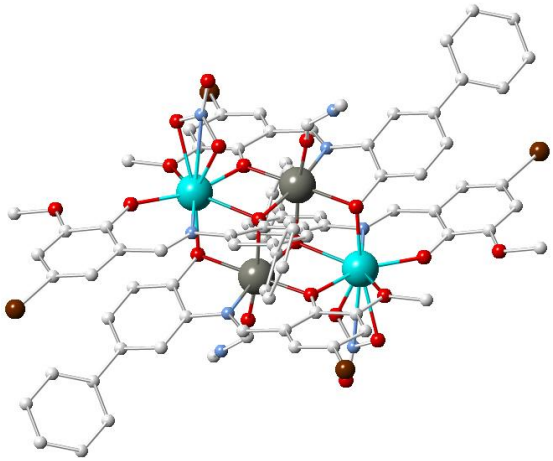

22ZnY-NO$_3$

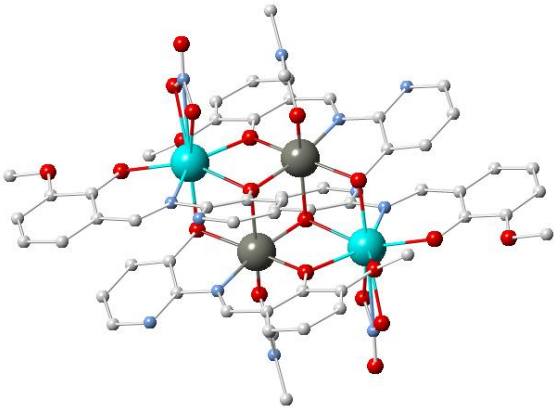

24ZnY-NO$_3$

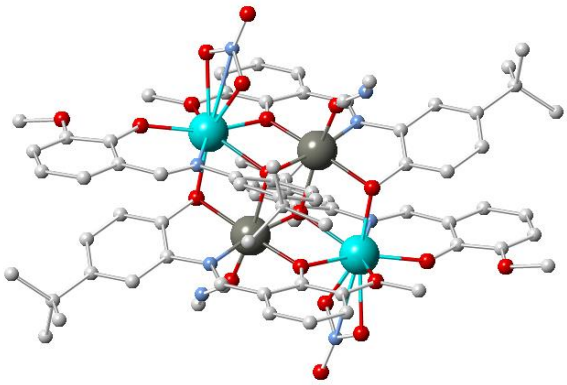

27ZnY-NO$_3$

Figure 9.3. The crystal structures of **LZnY-NO$_3$**, where **L** = 2, 6, 8, 9, 12, 13, 22, 24 and 27. Colour code: Zn^{II}, grey; Y^{III}, light blue; O, red; N, blue; C, white.

TGAs for compounds **2ZnY** - **21ZnY** (Appendix B, Figure S9.21-S9.40) display similar behaviour. Initially, the PCCs mass decreases slowly up to 280 - 320 ^{o}C, this decrease is between 6 - 13% depending on overall molecule weight. Which corresponds to a loss of the two solvent DMF molecules co-ordinated to Y^{III} and Zn^{II} metal centres. Once this temperature is exceeded the molecular weight rapidly decreases up to 400 ^{o}C, which is indicative of the organic ligands decomposing and the overall structure breaking down. This decrease becomes less significant and plateaus after 600 ^{o}C and with all examples, the remaining mass is unchanging by 800 ^{o}C. The remaining % mass is between 19 - 25% depending on initial molecular mass and corresponds to the remaining metal oxides (ZnO and Y_2O_3).

9.2.3 Catalytic testing

9.2.3.1 Initial studies and benchmarking

For benchmarking studies, *trans*-β-nitrostyrene (**C9S1**) and 1,3-dimethyl barbituric acid (**C9S2**) were selected as reactants to form the MA product **C9a**, using **1ZnLn-NO$_3$** as the catalyst with a 2.5 mol% loading in EtOH.

The reaction parameters were subsequently optimized with numerous reaction parameters including metal salt catalyst (Table 9.1), **1ZnLn-NO$_3$** catalyst (Table 9.2), solvent (Table 9.3), temperature (Table 9.4) and modification of the catalysts organic periphery (Table 9.6 and 9.7).

Firstly, metal salts of Zn^{II} and Ln^{III} were tested with the above reaction procedure, albeit with a 10 mol% loading. A blank experiment was performed where a low yield was obtained (Table 9.1, entry 1), increased reaction time to 24 h did show any additional conversion to **C9a**. Zn^{II} salts do not promote the transformation (Table 9.1, entries 2 - 5), whereas the reactions with Ln^{III} salts gave low yields (Table 9.1, entries 7 - 11) in comparison to the blank (Table 9.1). Noticeably, nitrate analogues significantly lower the conversion to **C9a** in comparison to the blank (Table 9.1, entries 4 and 8). This indicates a single Zn^{II} or Ln^{III} metal ion may not be sufficient for high conversion to the product in this MA reaction.

Table 9.1. Comparison of efficacy for Y^{III} and Zn^{II} metal salts.

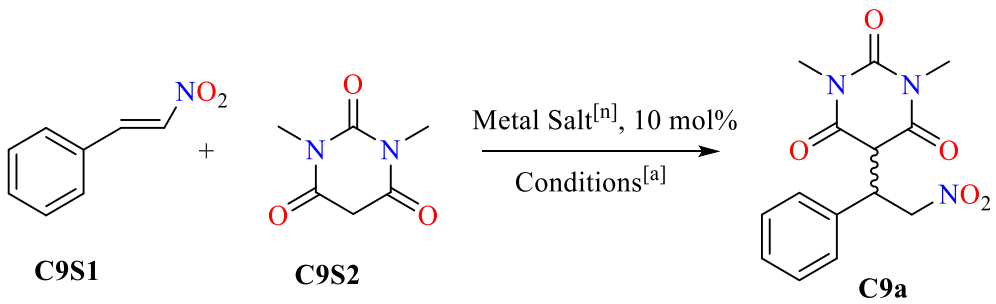

Entry	Loading / mol%	Metal salt[n]	Yield/ %[b]	Time/ h
1	n/a	None	40	2
2	10	$Zn(OTf)_2$	41	2
3	10	$ZnCl_2$	44	2
4	10	$Zn(NO_3)_2$	Trace	2
5	10	$ZnBr_2$	43	2
6	10	$Dy(OTf)_3$	49	2
7	10	$DyCl_3$	48	2
8	10	$Dy(NO_3)_3$	3	2
9	10	$DyBr_3$	39	2
10	10	YCl_3	39	2
11	10	$Y(OTf)_3$	48	2
12	10	$Y(OTf)_3$	51	24

[a] **C9S1** (0.5 mmol), **C9S2**(0.5 mmol); solvent (EtOH 10 mL); stirred at r.t.[b] Yields calculated via ^{1}H NMR spectroscopy.

The previously described isoskeletal lanthanide analogues (**1ZnLn-NO$_3$**) were tested to determine which had the highest efficacy of conversion from reactants to **C9a**. **1ZnLn-NO$_3$**,

(where Ln is Sm, Eu, Tb and Gd) analogues displayed a comparable performance to **1ZnDy-NO$_3$**, however, the use of **1ZnY-NO$_3$** and **1ZnYb-NO$_3$** at 2.5 mol% loading afforded the desired material in quantitative yield (Table 9.2**,** entries 8 and 7 respectively). All PCCs significantly outcompete the single Ln^{III} or M^{II} salts tested in Table 9.1. Due to the diamagnetic nature of the PCC and lower cost of lanthanide salt, **1ZnY-NO$_3$** was chosen for the following optimization tests.

Table 9.2. Optimisation of Ln^{III} ion of **1ZnLn-NO$_3$** catalysts.

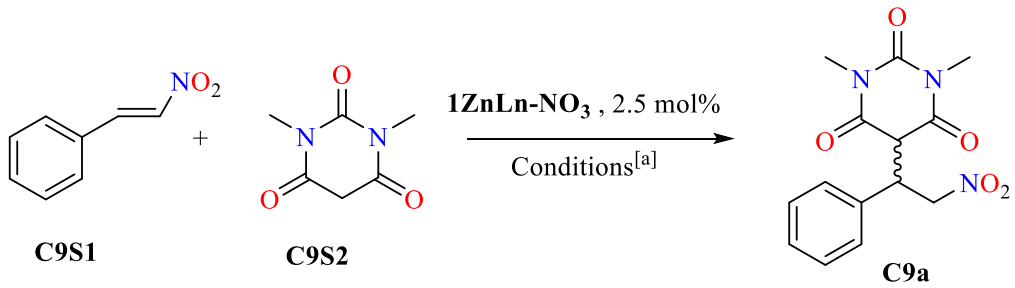

Entry	Loading / mol%	Catalyst	Yield/ %[b]	Time/min
1	0	None	35	60
2	2.5	**1ZnSm-NO$_3$**	75	15
3	2.5	**1ZnEu-NO$_3$**	81	15
4	2.5	**1ZnGd-NO$_3$**	89	15
5	2.5	**1ZnTb-NO$_3$**	88	15
6	2.5	**1ZnDy-NO$_3$**	94	15
7	2.5	**1ZnYb-NO$_3$**	quantitative	15
8	2.5	**1ZnY-NO$_3$**	quantitative	15

[a] **C9S1** (0.5 mmol), **C9S2**(0.5 mmol); solvent (EtOH 10 mL); stirred at r.t [b] Yields calculated via ^{1}H NMR spectroscopy.

Next, after screening several solvents (Table 9.3), an ethanol/water (6/4) (Table 9.3, entry 9) solvent system was identified to provide the best catalytic yield, however other protic solvents also demonstrated a high efficacy. Solvents, where **1ZnY-NO$_3$** had a low solubility, had an equally low yield (Table 9.3, entries 2, 3 and 7), suggesting the catalysis may be homogenous. Additionally, The use of a mixed EtOH/H_2O solution had some advantages from the environmental point of view.[510] Finally, it was identified that the reactions at room temperature yield excellent results (Table 9.4) in comparison with (-5 ^{o}C or reflux).

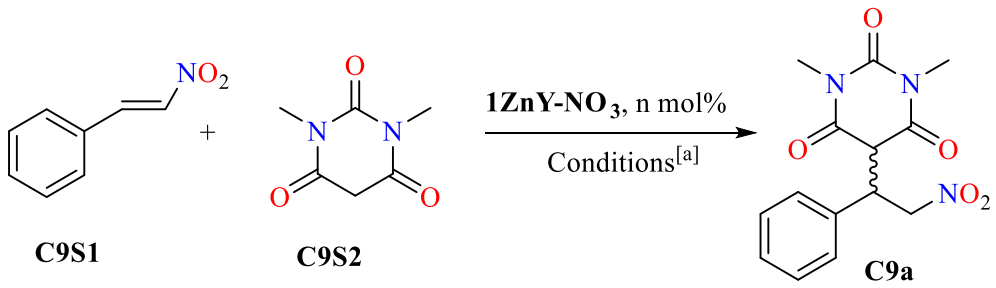

Equation 9.1. General catalytic scheme for catalyst optimisation.

Table 9.3 Optimisation of solvent.

Entry	Catalyst	Solvent [b]	Yield / % [c]	Loading/ mol%[n]
1	**1ZnY-NO$_3$**	MeOH	95	2.5
2	**1ZnY-NO$_3$**	Water	27	2.5
3	**1ZnY-NO$_3$**	DCM	trace	2.5
4	**1ZnY-NO$_3$**	DMF	98	2.5
5	**1ZnY-NO$_3$**	DMSO	trace	2.5
6	**1ZnY-NO$_3$**	iPrOH	71	2.5
7	**1ZnY-NO$_3$**	$CHCl_3$	trace	2.5
8	**1ZnY-NO$_3$**	EtOH	99	2.5
9	**1ZnY-NO$_3$**	EtOH/H_2O	quantitative	2.5

[a] **C9S1** (0.5 mmol), **C9S2**(0.5 mmol); [b] solvent 10 mL); stirred at r.t for 15 min.). [c] Yields calculated via ^{1}H NMR spectroscopy.

Table 9. 4. Optimisation of temperature.

Entry	*T*	Catalyst	Loading /mol%[n]	Yield/ %[b]
1	-5	**1ZnY-NO$_3$**	2.5	23
2	0	**1ZnY-NO$_3$**	2.5	41
3	15	**1ZnY-NO$_3$**	2.5	89
4	r.t	**1ZnY-NO$_3$**	2.5	quantitative
5	40	**1ZnY-NO$_3$**	2.5	97
6	Reflux	**1ZnY-NO$_3$**	2.5	95

[a] **C9S1** (0.5 mmol), **C9S2**(0.5 mmol); EtOH 10 mL); stirred at r.t for 15 min.). [b] Yields calculated via ^{1}H NMR spectroscopy.

The scope of the reaction was then extended and explored (Table 9.5) with **1ZnY-NO$_3$**, with barbituric acids (Table 9.5, entries 1 - 7), 6-amino-1,3-dimethyluracil (Table 9.5, entries 8 - 14), 1,3-diethyl-2-thiobarbituric acid (Table 9.5, entries 15 - 21) and a range of nitrostyrenes, functionalised with groups at the R_3 and R_4 positions.

1ZnY-NO$_3$ affords **C9S2** and 6-amino-1,3-dimethyluracil products in very good to quantitative yields (Table 9.5, entries 1 - 14), with 1,3-diethyl-2-thiobarbituric acid products slightly lower (79 - 81%). This may be due to the lower acidity of the α-C. The structure of compounds **C9f**, **C9h** and **C9l** were confirmed by single-crystal XRD studies (Figure 9.4).

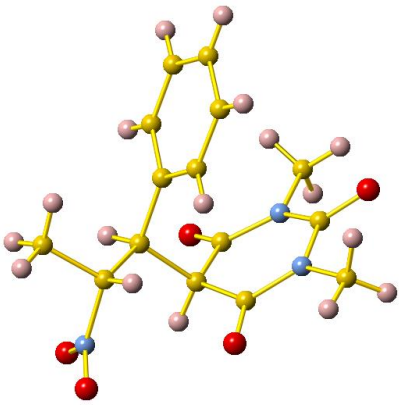

C9f

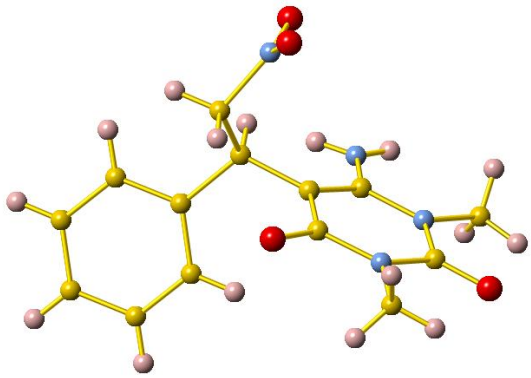

C9h

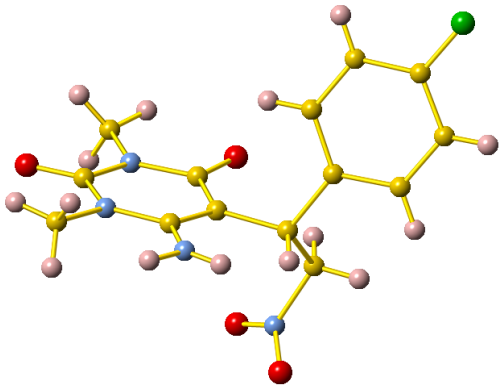

C9i

Figure 9.4. Molecular structures of **C9f** (upper left), **C9h** (upper right) and **C9i** (lower). Colour code: C, gold; H, pink; O, red; N, pale blue; Cl, green.

After determining the scope of reaction, the next step was to substitute **1ZnY-NO$_3$** with the isoskeletal analogues (**2ZnY-NO$_3$ - 29ZnY-NO$_3$**) to identify how the altered organic periphery of the ligand determines the efficacy of the $Zn^{II}_2Y^{II}_2$ core in promoting the MA reaction (Table 9.6 and 9.7).

Table 9.5. The scope of the reaction (**1ZnY-NO$_3$**, 2.5 mol% loading).

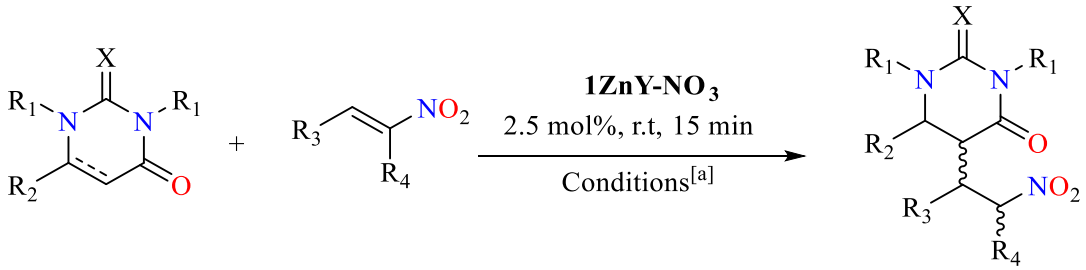

Entry	Compound	R_1	R_2	R_3	R_4	X	Yield / %[b]	Time /min
1	**C9a**	CH_3	O	C_6H_5	H	O	quantitative	15
2	**C9b**	CH_3	O	p-CH_3O-C_6H_4	H	O	75	15
3	**C9c**	CH_3	O	p-CH_3-C_6H_4	H	O	99	15
4	**C9d**	CH_3	O	p-Br-C_6H_4	H	O	99	15
5	**C9e**	CH_3	O	p-F-C_6H_4	H	O	99	15
6	**C9f**	CH_3	O	C_6H_5	CH_3	O	94	15
7	**C9g**	CH_3	O	C_4H_4O	H	O	quantitative	15
8	**C9h**	CH_3	NH_2	C_6H_5	H	O	quantitative	15
9	**C9i**	CH_3	NH_2	p-CH_3O-C_6H_4	H	O	95	20

10	**C9j**	CH_3	NH_2	p-CH_3-C_6H_4	H	O	80	20
11	**C9k**	CH_3	NH_2	p-Br-C_6H_4	H	O	quantitative	20
12	**C9l**	CH_3	NH_2	p-F-C_6H_4	H	O	96	20
13	**C9m**	CH_3	NH_2	C_6H_5	CH_3	O	81	15
14	**C9n**	CH_3	NH_2	C_4H_4O	H	O	96	15
15	**C9o**	CH_2CH_3	O	C_6H_5	H	S	81	60
16	**C9p**	CH_2CH_3	O	p-CH_3O-C_6H_4	H	S	80	60
17	**C9q**	CH_2CH_3	O	p-CH_3-C_6H_4	H	S	76	60
18	**C9r**	CH_2CH_3	O	p-Br-C_6H_4	H	S	79	60
19	**C9s**	CH_2CH_3	O	p-F-C_6H_4	H	S	80	60
20	**C9t**	CH_2CH_3	O	C_6H_5	CH_3	S	78	60
21	**C9u**	CH_2CH_3	O	C_4H_4O	H	S	79	60

[a] barbituric acid (0.5 mmol), nitrostyrene (0.5 mmol), EtOH/H_2O 6/4 mL); stirred at r.t. [b] Yields calculated via ^{1}H NMR spectroscopy.

Table 9.6. Comparison of efficacy of **1ZnY-NO$_3$-21YZn-NO$_3$** catalysts.

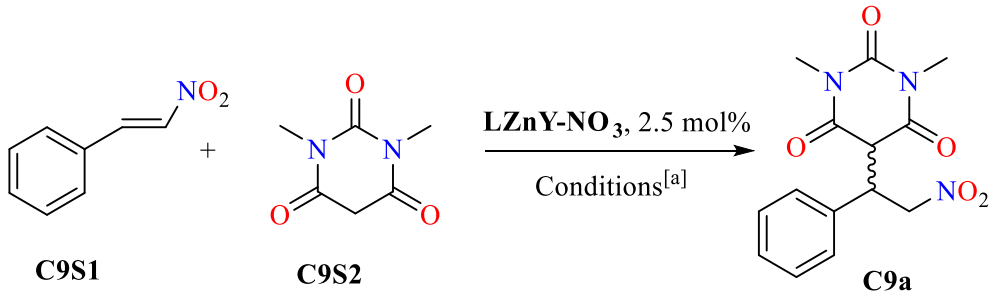

Entry	Catalyst	Yield /% [b]	Entry	Catalyst	Yield /% [b]
1	**1ZnY-NO$_3$**	100	13	**19ZnY-NO$_3$**	90
2	**6ZnY-NO$_3$**	100	14	**20ZnY-NO$_3$**	86
3	**4ZnY-NO$_3$**	76	15	**22ZnY -NO$_3$**	42
4	**8ZnY-NO$_3$**	43	16	**27ZnY- NO$_3$**	100
5	**9ZnY-NO$_3$**	56	17	**28ZnY- NO$_3$**	100
6	**11ZnY-NO$_3$**	56	18	**29ZnY- NO$_3$**	95
7	**12ZnY-NO$_3$**	55	19	**24ZnY- NO$_3$**	98
8	**13ZnY-NO$_3$**	73	20	**25ZnY- NO$_3$**	100
9	**15ZnY-NO$_3$**	59	21	**26ZnY -NO$_3$**	89
10	**2ZnY-NO$_3$**	86			
11	**16ZnY-NO$_3$**	100			
12	**18ZnY-NO$_3$**	54			

[a] **C9S1** (0.25 mmol), **C9S2** (0.25mmol); solvent (EtOH 6 mL: H_2O 4 mL); stirred at r.t for 15 min. [b] Yields calculated by ^{1}H NMR spectroscopy.

The results indicated that **28ZnY-NO$_3$** (R1 = allyl, R_2/R_3 = *t*-butyl) affords the highest conversion to the product (**C9a**) **(**Table 9.6, entry 17**)**. The presence of the allyl groups and *t*-butyl groups in the R_1 and R_2/R_3 (Figure 9.2), generally improved the catalytic efficacy in comparison to Br and H analogues, this may be due to an increase in solubility of the PCC leading to more of the active species for homogeneous catalysis. Whereas PCCs with Br and NO_2 groups significantly decreased the yields obtained (Table 9.7, **2ZnY-NO$_3$ - 29ZnY-NO$_3$**). The catalyst loading was further lowered (Table 9.7), and **28ZnY -NO$_3$** gave excellent yields with a 0.5 mol% loading, a five-fold reduction in efficacy.

Table 9.7. Comparison of efficacy for compounds **LZnY-NO$_3$** (where **L** = 1, 6, 27 and 28) at lower loading.

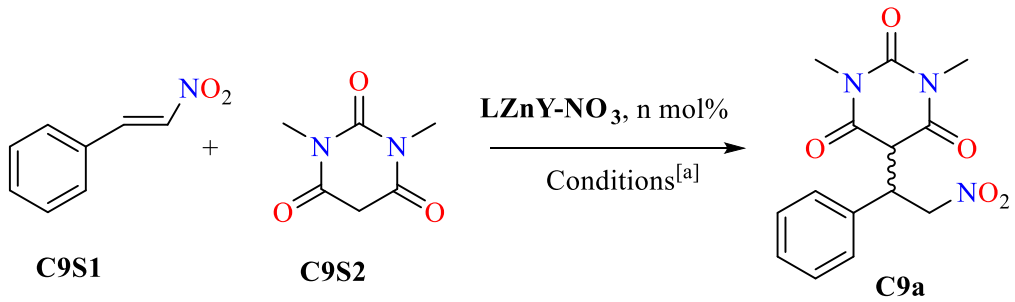

Entry	Catalyst	Loading / mol%[n]	Yield of Product/ %[b]
1	**1ZnY-NO$_3$**	1	91
2	**6ZnY- NO$_3$**	1	98
3	**27ZnY- NO$_3$**	1	100
4	**28ZnY- NO$_3$**	1	100
5	**25ZnY- NO$_3$**	1	95
6	**27ZnY- NO$_3$**	0.5	95
7	**28ZnY- NO$_3$**	0.5	99

[a] **C9S1** (0.5 mmol), **C9S2** (0.5 mmol); solvent (EtOH 6 mL: H_2O 4 mL);**;** stirred at r.t for 15 min. [b] Yields calculated via ^{1}H NMR spectroscopy.

The scope of reaction, with the optimised catalyst (**28ZnY-NO$_3$**), was further investigated at 0.5 mol% loading (Figure 9.5). Conversion to the respective products was good, with all conversions above 60%. In comparison with the previous results with **1ZnY-NO$_3$** at 2.5 mol% loading, the conversion to product was generally similar, with a notable exception where **28ZnY-NO$_3$** significantly outperformed **1ZnY-NO$_3$** (**C9b** and **C9j**).

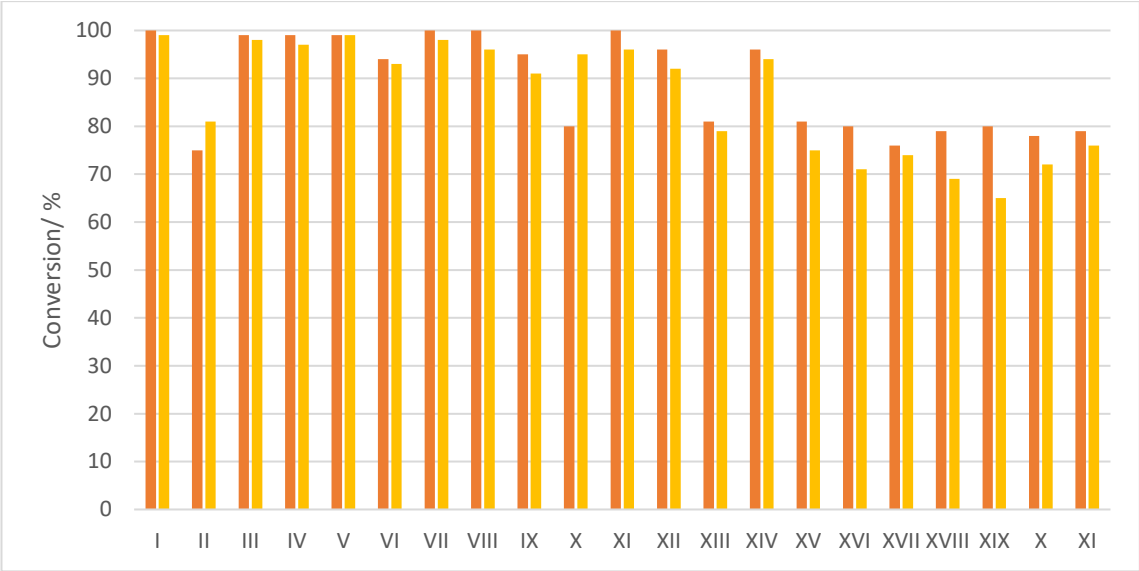

Figure 9.5. A comparative study of the performance of **1ZnY-NO$_3$** and **28ZnY-NO$_3$** for the conversion of substrates to products (**C9a-C9u**). **1ZnY-NO$_3$** (orange), **28ZnY-NO$_3$** (yellow). **C9S2** (0.25 mmol), **C9S1** (0.25 mmol); solvent (EtOH 6 mL: H_2O 4 mL); 2.5 mol% loading of **1ZnY-NO$_3$** and 0.5 mol% loading of **28ZnY-NO$_3$**; stirred at r.t for 15 min.) Yields calculated via ^{1}H NMR spectroscopy.

9.2.3.2 Mechanistic investigation of LMLn-NO$_3$ catalysts towards the MA reaction.

To gain further information on the plausible mechanism and to identify the limitations of the present 3d-4f PCC catalysts, the following sets of reactions and experimental techniques were explored.

These include the influence of base on reaction, substitution of the 3d ion of $M^{II}_2Ln^{III}_2$ (**LMLn**) PCCs, ^{1}H NMR titration of $Zn^{II}_2Ln^{III}_2$ PCCs with substrates, EPR *in situ* binding studies, ESI-MS studies of **1ZnLn-NO$_3$** and *in situ* ESI-MS **1ZnLn-NO$_3$** with substrate studies. DFT studies further support the presented mechanism.

9.2.3.2.1 Base influence.

Two sets of reactions were performed in presence of base (Table 9.8, entries 2 - 6 (NaOH) and entries 7 - 11 (Et_3N)), however with both sets of reactions, with an increasing amount of base the catalytic conversion to **C9a** significantly lowered. NaOH had a more detrimental effect per equivalent of base to the catalyst. This influence could be attributed to the instability of the catalyst when exposed to basic conditions.

Table 9.8. Influence of base on the efficacy of **1ZnY-NO$_3$**.

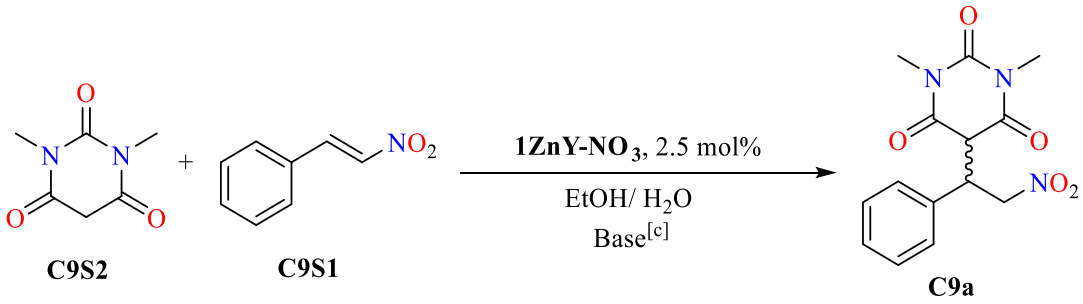

Entry	(Substrate: base)[c]	Time/ min	Yield / %[b]
1	No base	15	quantitative
2	NaOH	15	
3	(1:0.025)	15	83
4	(1:1)	15	79
5	(1:2)	15	52
6	(1:5)	15	33
7	Et_3N	15	
8	(1:0.025)	15	91
9	(1:1)	15	85
10	(1:2)	15	76
11	(1:5)	15	61

[a] **C9S1** (0.5 mmol), **C9S2** (0.5 mmol); solvent (EtOH 6 mL: H_2O 4 mL). [b] Yields calculated via ^{1}H NMR spectroscopy.

9.2.3.2.2 Tuning the 3d ion.

To further determine and understand the role of the bimetallic catalyst the isoskeletal compounds **1NiDy-NO$_3$**, **1CoDy-NO$_3$**[2,50] and **1CuDy-NO$_3$** were tested (Table 9.9).

$[Cu^{II}_2Dy^{III}_2(\mathbf{L1})_4(NO_3)_2]\cdot 2MeCN$ (**1CuDy-NO$_3$**, Figure 9.6) was synthesised following a modified synthetic procedure which is fully described in chapter eleven. Single-crystal XRD studies (chapter twelve) show the molecular structure is isoskeletal to the previously described **1MLn** PCCs described in chapters seven, eight and this chapter.

Interestingly, unlike the previously reported PCCs, solvent (MeCN) molecules do not coordinate to the 3d (Cu^{II}) ion, instead, the Cu^{II} ion adopts a square planar geometry. The PCC was characterised by EA (chapter eleven), TGA (Appendix B) and FT-IR spectra (Appendix B).

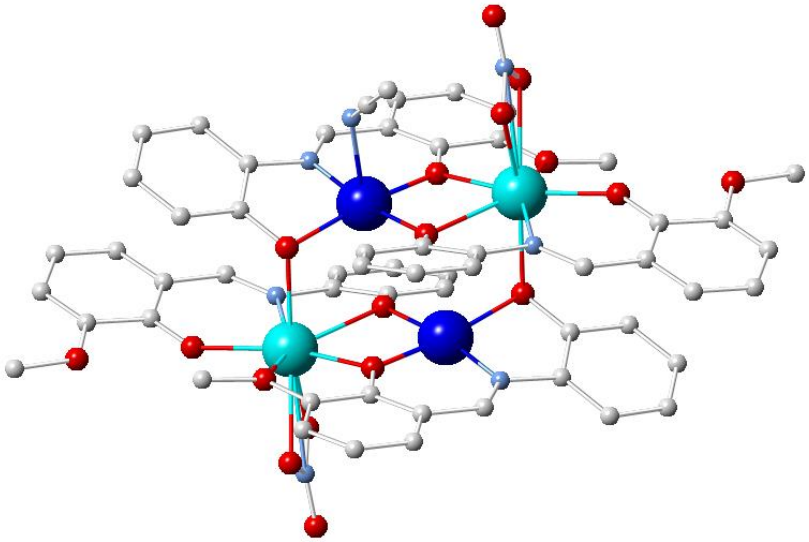

Figure 9.6. The molecular structure of **1CuDy-NO$_3$**. Colour code: Cu^{II}, dark blue; Dy^{III}, light blue; C, black; N, pale blue; O, red. Hydrogen atoms omitted for clarity.

According to the Pearson table, Cu^{II} and Zn^{II} have a higher preference to O atoms, whereas Ni^{II} and Co^{II} have a higher preference for N atoms. The reactions of **1CuDy-NO$_3$** and **1ZnDy-NO$_3$** yielded the desired product in very good yields (90%) (Table 9.9, entry 2 and 4 respectively) whereas **1NiDy-NO$_3$** and **1CoDy-NO$_3$** displayed a poor efficacy. This may be an indication that activation (binding) of both substrates at the same time is required. These results suggest that the catalytic action between metals is co-operative and that not only one metal centre is active in the transformation of reactants to **C9a**.

Table 9.9. Comparison of efficacy for compounds **1MLn-NO$_3$**.

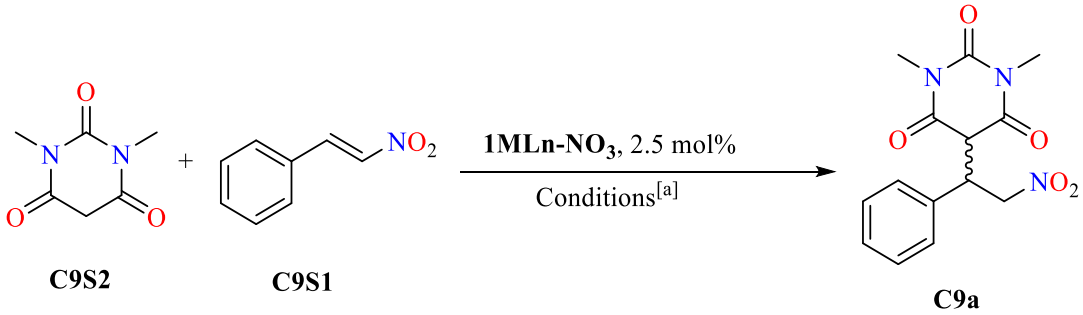

Entry	Catalyst	Yield/ %[b]	Time/min
1	**1ZnY-NO$_3$**	quantitative	15
2	**1ZnDy-NO$_3$**	94	15
3	**1NiDy-NO$_3$**	29	15
4	**1CoDy-NO$_3$**	34	15
5	**1CuDy-NO$_3$**	85	15

[a] **C9S1** (0.5 mmol), **C9S2** (0.5 mmol); solvent (EtOH 6 mL: H_2O 4 mL**;** stirred at r.t for 15 min.)

[b] Yields calculated via ^{1}H NMR spectroscopy.

9.2.3.2.3 Simple salts.

Reactions with Zn^{II} salts do not promote the MA reaction however the use of Ln^{III} salts form the desired product in good yields (Table 9.1). This may indicate that the Ln^{III} ion in **1MLn-NO$_3$** is essential for catalytic action towards the MA reaction and that the 3d ion is only synergistic (Table 9.1).

9.2.3.2.4 Diastereoselectivity tests.

trans-β-methyl-nitrostyrene (**C9S3**) instead **C9S1** was employed in the reaction with **C9S2**, which gave excellent yields of the expected product (**C9f**). ^{1}H NMR spectra showed the presence of one diastereoisomer (> 20:1 *dr*).

Crystallographic determination of the crystalline material **C9f**, derived after the filtration of the reaction in the presence of the catalyst, revealed the formation of the R* R* derivative. The influence of the lanthanide radii on the diastereoselectivity of the PCC was then explored, thus **1ZnLn-NO$_3$**, (where Ln is Sm, Eu, Tb, Gd, Dy and Yb) were tested (Table 9.10, entries 1 - 7). Slightly different diastereoselectivity behaviour was observed (20:1 for **1ZnY-NO$_3$** to >20:1 for **1ZnSm-NO$_3$**) which can be attributed to the different ionic the radii of the Ln^{III}.

Subsequently, **1CoDy-NO$_3$** and **1NiDy-NO$_3$** were studied and a similar diastereoselectivity behaviour (20:1) was observed, but with significantly lower yields (Table 9.10, entries 8 and 9). The use of **1CuDy-NO$_3$** (Table 9.10, entry 10) gave a similar diastereoselectivity and yield to that of **1ZnY-NO$_3$**.

To further obtain mechanistic information, the reaction of *cis*-β-methyl-4-methoxy-nitrostyrene (**C9S4**) with **C9S2** and **1ZnY-NO$_3$** as a catalyst was investigated, this yielded product **C9v** (Figure 9.7). The ^{1}H NMR data displays the presence of only one diastereoisomer, while the single-crystal XRD characterisation revealed the formation of the S*, S* derivative (Figure 9.8). Incorporation of **1ZnLn-NO$_3$**, (where Ln is Sm, Eu, Tb, Gd, Dy and Yb), **1CoDy-NO$_3$**, **1NiDy-NO$_3$** and **1CuDy-NO$_3$** as catalysts showed similar *dr* and conversion behaviour in comparison to the *trans* (Table 9.10, entries 1 and 8 - 10). This data indicates a *syn* addition.

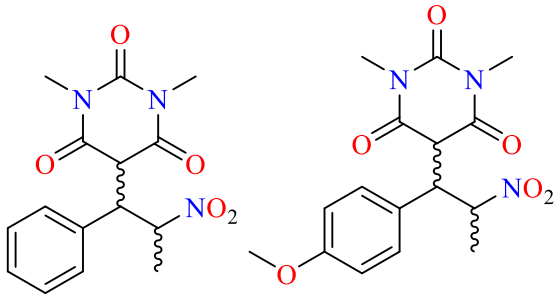

Figure 9.7. Structure of **C9f** (left) and **C9v** (right).

Table 9.10. Comparison of efficacy for compounds **1ZnLn-NO$_3$**, **1NiDy-NO$_3$**, **1CoDy-NO$_3$** and **1CuDy-NO$_3$**.

Entry	Catalyst	Yield of **C9f** / %[b]	*dr* [b] (R*, R*/R*, S*)	Yield of **C9v** / %[b]	*dr* [b] (R*, R*/R*, S*)
1	**1ZnY-NO$_3$**	quantitative	20:1	96	20:1
2	**1ZnSm-NO$_3$**	75	>20:1	69	>20:1
3	**1ZnEu-NO$_3$**	81	>20:1	74	>20:1
4	**1ZnGd-NO$_3$**	89	>20:1	77	>20:1
5	**1ZnDy-NO$_3$**	94	>20:1	89	>20:1
6	**1ZnTb-NO$_3$**	88	>20:1	85	>20:1
7	**1ZnYb-NO$_3$**	quantitative	20:1	93	20:1
8	**1CoDy-NO$_3$**	24	20:1	41	20:1
9	**1NiDy-NO$_3$**	19	20:1	30	20:1
10	**1CuDy-NO$_3$**	71	20:1	94	20:1

[a] **C9S3** (0.5 mmol), **C9S2** (0. 5mmol); solvent (EtOH 6 mL: H_2O 4 mL); 1 mol% loading of **1MLn-NO$_3$;** stirred at r.t for 15 min.) [b] Yields calculated via ^{1}H NMR spectroscopy.

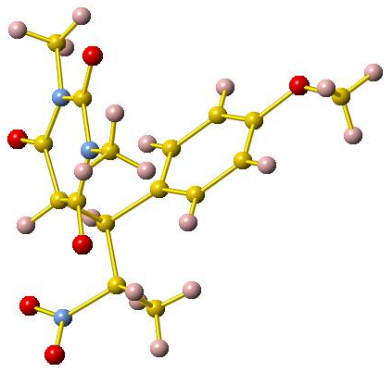

Figure 9.8. Molecular Structure of **C9v**. Colour code: C, gold; H, pink; O, red; N, pale blue.

9.2.3.2.5 ^{1}H NMR *in situ* studies

To gain insights to how **1MLn-NO$_3$** PCCs interact with substrates, DMF solutions of **1ZnY-NO$_3$** were titrated with 0.25-10 eq. of Michael acceptor (**C9S1** and **C9S3**) or donors (1,3-cyclohexanedione or 6-amino-1,3-dimethyluracil) which lead to no significant observable changes in the ^{1}H NMR spectra. Dimedone gave no apparent changes for **1ZnY-NO$_3$** but the dimedone peaks that were initially twice as broad then narrowed with more equivalents (i.e. intermediate-fast exchange).

C9S2 showed significant differences for both the **C9S2** and **1ZnY-NO$_3$** peaks. Evidently binding of the individual substrates to the **1ZnY-NO$_3$** is not strong but is no impediment to the catalytic activity of the complex. Owing to the difficulty in characterising **1ZnY-NO$_3$** alone in the solution state, a more detailed mechanistic was not possible in this investigation.

9.2.3.2.6 *In situ* EPR studies.

As previously demonstrated in chapter eight, the $[Zn^{II}_2Gd^{III}_2(\mathbf{L1})_4(NO_3)_2]$ core of **1ZnGd-NO$_3$** was found to give the same EPR signal in solution to the solid state, suggesting the coordination environment around the Gd^{III} ion remains unchanged and the core topology is retained.

To gain further insights into **LMLn-NO$_3$** interaction with substrates, the following Q-band EPR studies at 15 K of **1ZnGd-NO$_3$** in solution were performed. **C9S1** or **C9S2**, dissolved in EtOH, were added to solutions of **1ZnGd-NO$_3$** in ratios (1:1, 20:1 and 40:1). Finally, a mixture of **C9S1** and **C9S2**, dissolved in EtOH, in a 1:1 ratio, and then added to ethanolic solutions of **1ZnGd-NO$_3$** in ratios (1:1, 20:1 and 40:1) (Figure 9.9). The experiments in ratios 20:1 and 40:1 were performed to mimic the catalytic conversion (100:5 and 100:2.5) conditions and identify the stability of the bimetallic system.

From these studies, it can be concluded that the coordination environment of Gd in **1ZnGd-NO$_3$** alters (shifted signals) but its coordination number (eight) remains intact in the ratios of 1:1 and 20:1, with **C9S1**, **C9S2** and **C9S1**/ **C9S2** and in 40:1 for **C9S2** and **C9S1**/ **C9S2**.

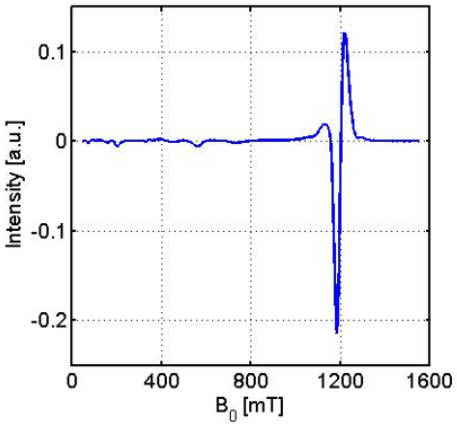

1ZnGd-NO$_3$ with **C9S2** (1:1)

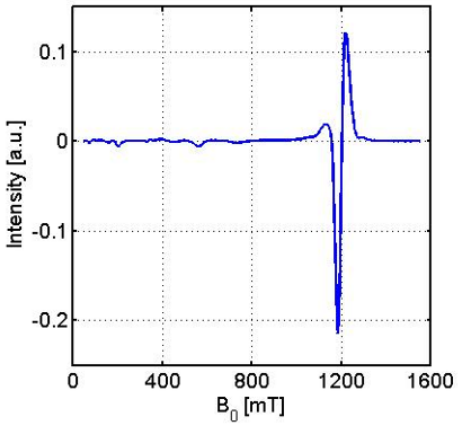

1ZnGd-NO$_3$ with **C9S1** (1:1)

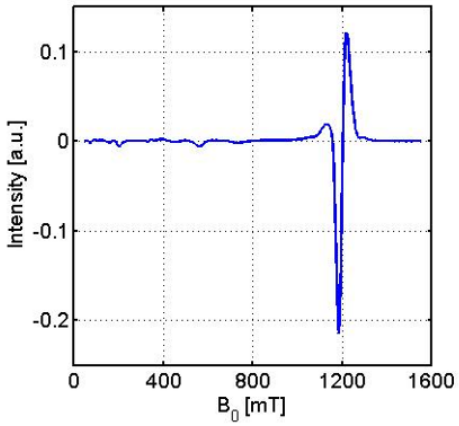

1ZnGd-NO$_3$ with **C9S1** and **C9S2** (1:1)

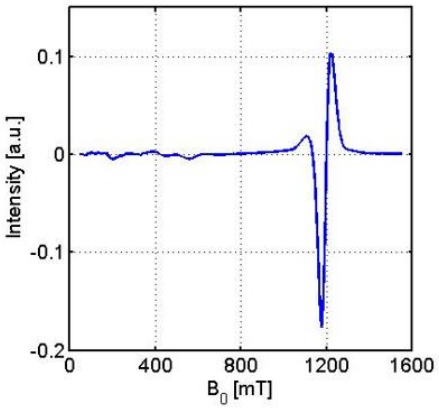

1ZnGd-NO$_3$ with **C9S2** (1:20)

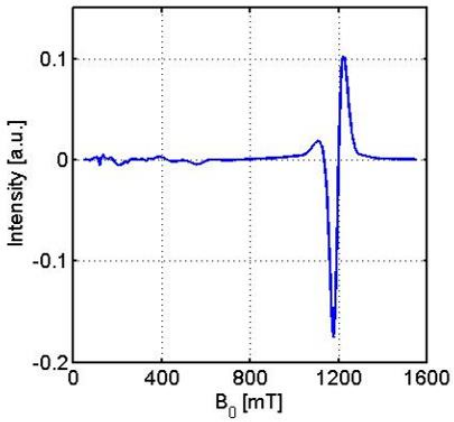

1ZnGd-NO$_3$ with **C9S1** (1:20)

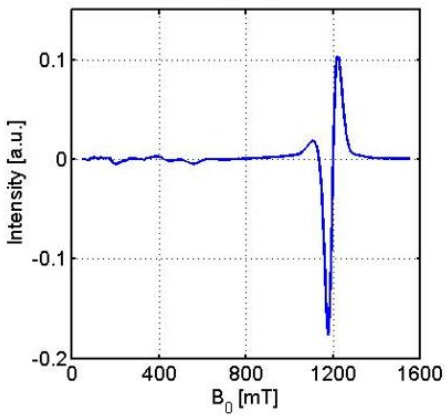

1ZnGd-NO$_3$with **C9S1** and **C9S2** (1:20)

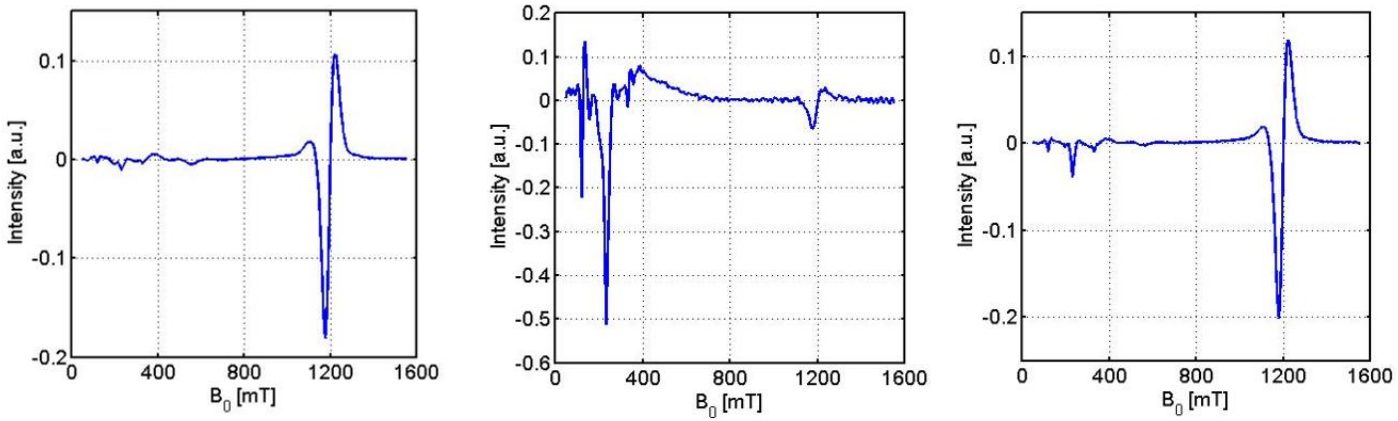

1ZnGd-NO$_3$ with **C9S2** (1:40) **1ZnGd-NO$_3$** with **C9S1** (1:40) 1**ZnGd-NO$_3$** with **C9S1** and **C9S2**

Figure 9.9. *In situ* EPR studies with **C9S1**, **C9S2** and **1ZnGd-NO$_3$**.

9.2.3.2.7 UV-Vis studies

To further understand how the substrates interact with **1MLn-NO$_3$**, the reaction between **C9S1** and **C9S2** was followed with UV-Vis spectroscopy. Solutions of 1 x 10^{-5} mmol of **C9S1** and **C9a** were (in 9:1 H_2O/EtOH solution) recorded initially to determine their maximum absorbance peak positions, these were found to be at 320 nm and 347 nm respectively. The absorbance of the product (**C9a**) peak was found to be much weaker than **C9S1**. **C9S2** did not show any absorbance in the 250 - 450 nm range.

A solution of **C9S1** (1 x 10^{-5} mmol in 9:1 H_2O/EtOH) was prepared and an equimolar amount of **C9S2** was added, the uncatalyzed solution was followed for 2 h with measurements at 5 min intervals (Appendix B, S9.2). The 320 nm **C9S1** peak decreased marginally over the 2 h period (0.66 - 0.61), which could be attributed to the conversion of substrate to product, albeit the **C9a** peak was not observable due to the strength of the **C9S1** absorbance.

A similar solution of **C9S1** (1 x 10^{-5} mmol) and **1ZnY-NO$_3$** (1.25 x 10^{-6} mmol) in 9:1 H_2O/EtOH was prepared and an equimolar amount of **C9S2** was added, the catalysed solution was followed for 2 h with measurements at 5 min intervals (Appendix B, S9.3). The 320 nm peak decreased far more drastically over the 2 h period than the uncatalyzed solution (0.71 - 0.18). In addition, during reaction the 320 nm peak shifts to the 347 nm peak position of the product **C9S1**, which is indicative of product formation. Due to the imposition of both **C9S1** and **C9a** peaks, it was not possible to determine the rate of reaction under these conditions.

9.2.3.2.8 ESI-MS studies of LZnY-NO$_3$

The identity of the **LZnY-NO$_3$** analogues was confirmed by ESI-MS studies. In most cases, two peaks (positive-ion mode) were observed in the MS at an m/z which correspond to monocationic $[Zn^{II}_2Ln^{III}_2(\mathbf{L1})_4(NO_3)]^+$ and the dicationic $[Zn^{II}_2Ln^{III}_2(\mathbf{L1})_4(NO_3)]^{2+}$ fragments**.**

The fragments corresponding peak value for each PCC is shown in Table 9.11 and Figures are included in Appendix B S9.41 - 9.51. Some of the PCCs had many other peaks, however, these correspond to the $[Zn^{II}_2Y^{III}_2(\mathbf{LX})_4]^{2/1+}$ core with various solvent molecules (MeOH/ H_2O) associated with the molecule. PCCs whose ligands were modified with Br in the R_1 position were not soluble enough in MeOH to obtain an ESI-MS spectrum. In all successfully measured **1ZnY-NO$_3$** PCCs the defect dicubane core is retained when dissolved in solution.

Table 9.11. ESI-MS data for **LZnY-NO$_3$ PCCs**

	Observed peaks and corresponding fragments	
	$[Zn^{II}_2Y^{III}_2(\mathbf{LX})_4(NO_3)]^{2+}$	$[Zn^{II}_2Y^{III}_2(\mathbf{LX})_4(NO_3)]^{1+}$
6Zn-NO$_3$	n/a	+$(CH_3OH)_2$ 1561.1385
8Zn-NO$_3$	789.0073	n/a
9Zn-NO$_3$	n/a	Multiple species with $[Zn^{II}_2Ln^{III}_2(\mathbf{LX})_4]^{+}$ core
2Zn-NO$_3$	769.0489	1534.0425
16Zn-NO$_3$	849.1129	1696.2066
19Zn-NO$_3$	821.0808	1640.0883
20Zn-NO$_3$	901.1491	1800.2494
27Zn-NO$_3$	781.1411	1560.2788
28Zn-NO$_3$	861.2108	1720.4364
24Zn-NO$_3$	+(H_2O) 710.0302	1336.9400
25Zn-NO$_3$	749.0456	1500.0715

9.2.3.2.9 Theoretical studies.

To complement the practical studies discussed in this chapter and gain further insights into the plausible mechanism of the MA reaction of **C9S2** acid with *trans*-nitrostyrenes catalysed by 3d-4f co-operative catalysts, a series of calculations was performed on possible reaction pathways employing DFT methods and monitoring the Natural Atomic Charge (NAC) distribution and the nature of the FMOs on both the catalyst and the substrates.

Barbiturate substrates were selected the **C9S2** and 6-amino-1,3-dimethyl barbituric acid and for the *trans*-nitrostyrenes the **C9S1**, (*Z*)-(2-nitroprop-1-enyl)benzene and (*Z*)-1-methoxy-4-(2-nitroprop-1-enyl)benzene. The thermodynamics of the uncatalyzed MA reactions in aqueous solution employing the PBE0/6-311++G(d,p) computational protocol were calculated. The NACs calculated by the Natural Bond Orbital (NBO) population analysis scheme and the relevant FMOs are shown in Figure 9.10.

It is well established that the α-carbon of barbituric acid has a reactive hydrogen atom and is quite acidic (pK_a = 4.01) because of the additional aromatic stabilization of the carbanion. DFT

calculations at the PBE0/6-311++G(d,p) level of theory revealed that the keto form of 1,3-dimethyl barbituric acid in aqueous solution can co-exist in equilibrium with the diketo-enol form, which is found at 8.7 kcal mol^{-1} higher in energy than the triketo form (Figure 9.10). Notice that *ab initio* and DFT calculations on the tautomers of barbituric acid showed that the triketo form is found to be the most stable form in the gas phase and in solution, which is in agreement with the experimental result.[511–515] On the other hand, the aminodiketo form of 6-amino-1,3-dimethyl barbituric acid is the most stable form relative to the aminoketo-enol and diketo-ammonium forms, which are found 47.0 and 63.6 kcal mol^{-1} higher in energy.

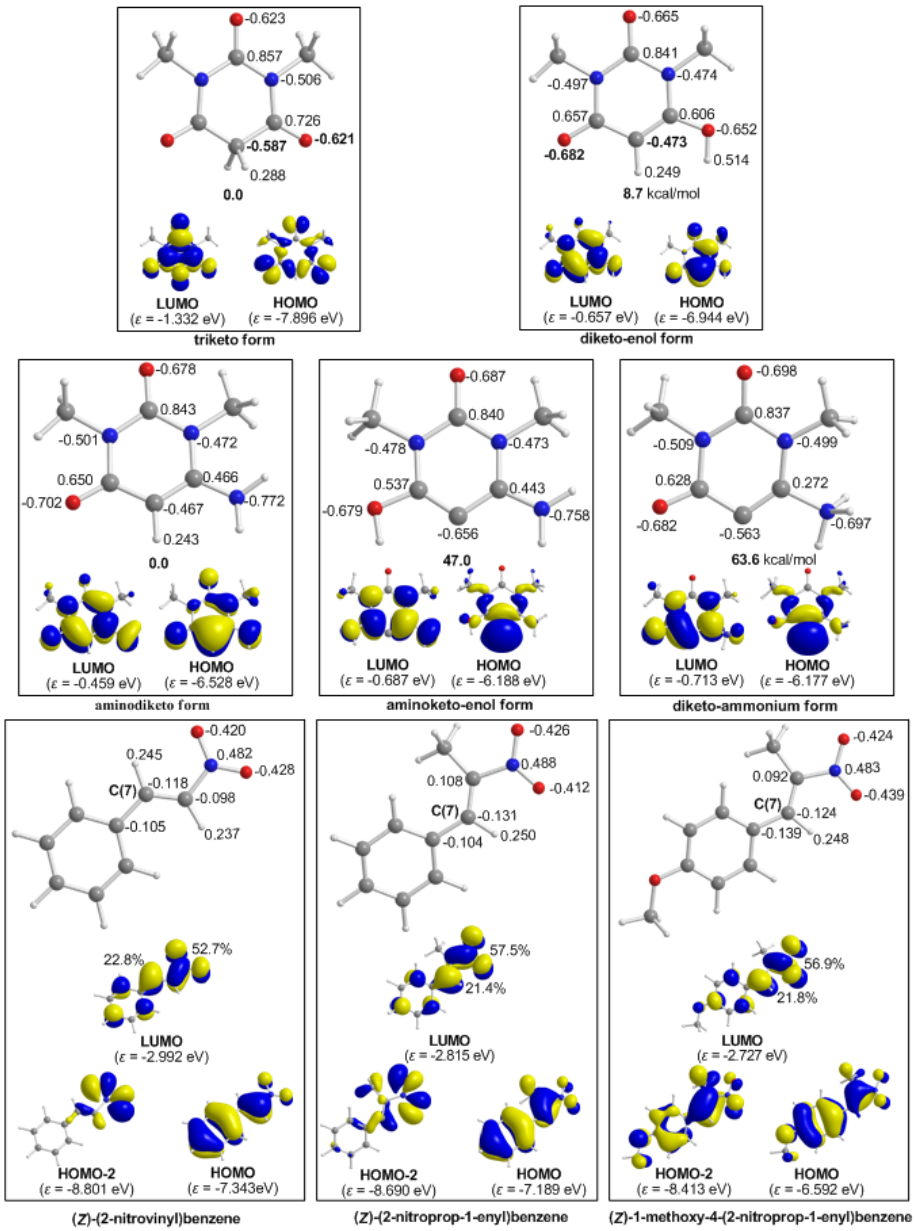

Figure 9.10. NACs and the relevant FMOs of the triketo and diketo-enol forms of **C9S2**, the aminodiketo, aminoketo-enol and diketo-ammonium forms of 6-amino 1,3-dimethyl barbituric acid and the **C9S1**, (*Z*)-(2-nitroprop-1-enyl)benzene and (*Z*)-1-methoxy-4-(2-nitroprop-1-enyl)benzene calculated at the PBE0/6-311++G(d,p) level of theory in aqueous solutions.

According to NBO population analysis, the keto and enolic oxygen atoms of the diketo-enolic tautomer acquire higher negative NACs by 0.03 up to 0.06 |e| relative to the corresponding oxygen atoms of the triketo tautomer. On the other hand, the α-carbon atom in the enolic tautomer acquires less negative NAC by 0.114 |e| relative to the α-carbon atom of the triketo tautomer. In the 6-amino 1,3-dimethyl barbiturate substrate the keto oxygen atoms of the acquire higher negative NACs by 0.055 up to 0.080 |e| relative to the corresponding oxygen atoms of the triketo tautomer of the 1,3-dimethyl barbiturate substrate. Alternatively, the α-carbon atom in the enolic tautomer acquires less negative NAC by 0.114 |e| relative to the α-carbon atom of the triketo tautomer. In the 6-amino 1,3-dimethyl barbiturate substrate the α-carbon atom acquires less negative NAC by 0.12 |e| relative to the α-carbon atom of the triketo tautomer of the 1,3-dimethyl barbiturate substrate.

The Highest Occupied Molecular Orbital (HOMO) in the triketo tautomer is mainly localized on the keto oxygen atoms adjacent to the α-carbon atom (64.4% having 2*p* character), while in the diketo-enolic tautomer is mainly localized on the α-carbon atom (44.6% having 2*p* character) and the adjacent keto- oxygen atom (13.5% with 2*p* character). Both the nature of the HOMOs and the negative charge distribution suggest that the triketo form of the 1,3-dimethyl barbiturato ligand could be coordinated to a metal centre through the keto- oxygen donor atoms, while the diketo-enolic form through the α-carbon atom. Similarly, the nature of HOMO of the 6-amino-1,3-dimethyl barbiturate substrate supports coordination through the α-carbon atom.

The uncatalyzed MA reactions of the triketo tautomer of **C9S2** to (*Z*)-(2-nitrovinyl)benzene, (*Z*)-(2-nitroprop-1-enyl)benzene and (Z)-1-methoxy-4-(2-nitroprop-1-enyl)benzene are predicted to be exothermic by 11.9, 9.9 and 10.9 kcal mol^{-1} respectively. The exothermicity of the addition of the diketo-enol tautomer of 1 **C9S2** to (*Z*)-(2-nitrovinyl)benzene, (*Z*)-(2-nitroprop-1-enyl)benzene and (Z)-1-methoxy-4-(2-nitroprop-1-enyl)benzene are 20.7, 18.6 and 19.6 kcal mol^{-1} respectively at the PBE0/6-311++G(d,p) level of theory.

The uncatalyzed MA reactions of the 6-amino-1,3-dimethyl barbiturate substrate to (*Z*)-(2-nitrovinyl)benzene, is predicted to be also exothermic by 13.2 kcal mol^{-1}. Considering the nature of the Lowest Unoccupied Molecular Orbital (LUMO) of the (*Z*)-(2-nitrovinyl)benzene, (*Z*)-(2-nitroprop-1-enyl)benzene and (Z)-1-methoxy-4-(2-nitroprop-1-enyl)benzene being a π^* MO mainly localized on the NO_2 moiety (51.2%, 57.5% and 56.9%) and on the C(7) unsaturated carbon atom (22.8%, 21.4% and 21.8%), the MA reactions under study are FMO controlled supported by HOMO-LUMO interactions.

An alternative plausible reaction pathway involves the nucleophilic attack of the C(2) electrophilic centre of the protonated *trans*-nitrostyrenes, namely **C9S1**, (*Z*)-(2-nitroprop-1-

enyl)benzene and (Z)-1-methoxy-4-(2-nitroprop-1-enyl)benzene and by the nucleophilile 1,3-dimethyl barbiturate carbanion (Figure 9.11).

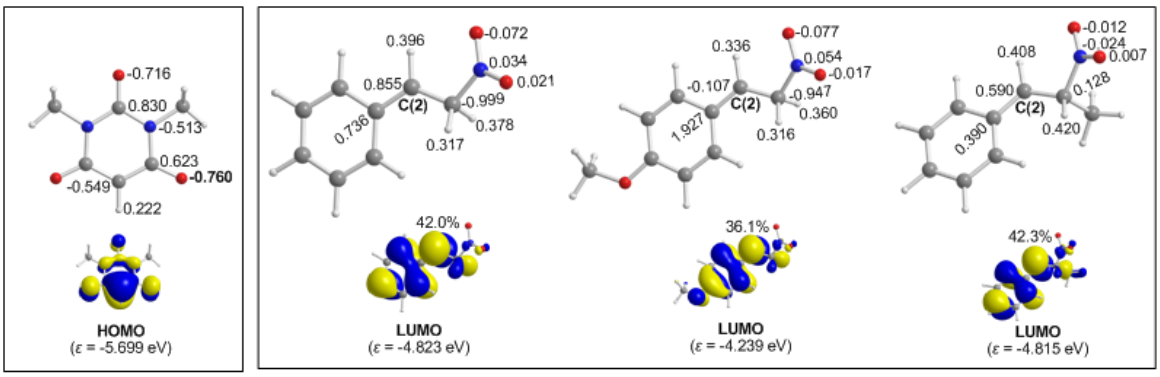

Figure 9.11. NACs and relevant FMOs of the 1,3-dimethyl barbiturate carbanion and the protonated **C9S1**, (Z)-1-methoxy-4-(2-nitrovinyl)benzene and (*Z*)-(2-nitroprop-1-enyl)benzene calculated at the PBE0/6-311++G(d,p) level of theory in aqueous solutions.

The deprotonation of the triketo form of **C9S2** to form the 1,3-dimethyl barbiturate carbanion is predicted to be endothermic by 45.1 kcal mol^{-1}. Notice a remarkable increase of the negative atomic charge of the keto oxygen atoms in the carbanion relative to the corresponding keto oxygen atoms of the triketo tautomer. On the other hand, the negative NAC on the deprotonated α-carbon atom of the carbanion decreases by 0.04|e|. Interestingly, the HOMO of the nucleophile is primarily localized on the deprotonated α-carbon atom (52.3%) and the two adjacent keto oxygen atoms (28.9%) being π*-type MOs, while the LUMOs of the protonated **C9S1**, (*Z*)-(2-nitroprop-1-enyl)benzene and (Z)-1-methoxy-4-(2-nitrovinyl)benzene are mainly localized on the electrophilic C(2) carbon atom (42.0%; 36.1% and 42.3% respectively) (Figure 9.11).

It is obvious that the nucleophilic attack at the electrophilic C(2) carbon atom by the carbanion is a FMO controlled process, supported by the interaction of the HOMO (nucleophile) with the LUMO (electrophile). The nucleophilic attack at the electrophilic C(2) carbon atom of the protonated **C9S1**, (*Z*)-(2-nitroprop-1-enyl)benzene and (Z)-1-methoxy-4-(2-nitrovinyl)benzene by the 1,3-dimethyl barbiturate carbanion are predicted to be strongly exothermic by 61.4, 58.7 and 49.1 kcal mol^{-1} respectively.

To probe the electrophilic/nucleophilic character of the *trans*-nitrostyrene molecules selected electronic descriptors (condensed Fukui function, f^{-}C(7), condensed dual descriptor ΔfC(7), proton affinity, *PA* and chemical potential, μ) were calculated by the PBE0/6-311++G(d,p)/PCM computational protocol in order to find out how the electrophilic/nucleophilic character of the electrophilic/nucleophilic centres of the *trans*-nitrostyrenes affect the efficacy of the MA reaction. The results are summarized in Table 9.12.

Table 9.12. Selected electronic descriptors related to the nucleophilic character of the *trans*-nitrostyrene molecules calculated at the PBE0/6-311++G(d,p) level of theory in aqueous solutions.

trans-nitrostyrene	Yield /%[a]	Yield /%[b]	ΔfC(7)	f^-C(7)	PA	μ
C9S1	100	100	0.213(	-0.017	130.97	-5.168
p-Me-Nitrovinylbenzene	88	80	0.226	-0.029	135.74	-5.015
p-MeO-Nitrovinylbenzene	75	80	0.234	-0.037	140.93	-4.788
p-F-Nitrovinylbenzene	99	96	0.214	-0.018	131.90	-5.134
p-Br-Nitrovinylbenzene	99	100	0.213	-0.023	130.93	-5.132

[a] For the addition of **C9S2**. [b] For the addition of 6-amino-1,3-dimethyl barbituric acid.

Excellent linear relationships (Figure 9.12) are obtained for the yield (%) vs ΔfC(7) and yield (%) vs f^-C(7) correlations. Good linear relationships are also obtained for the yield (%) vs *PA* and yield (%) vs μ correlations ($\mu = (\varepsilon_{HOMO} + \varepsilon_{LUMO})/2$). These correlations show that the nucleophilic character of the C(7) carbon atom of the *trans*-nitrostyrenes affects the efficacy of the MA reaction. Upon protonation the C(2) carbon atom in the protonated *trans*-nitrostyrenes becomes an electrophilic centre. The calculated electronic descriptors related to the electrophilic character of the C(2) carbon atom in the protonated *trans*-nitrostyrene molecules are compiled in Tables 9.13.

Table 9.13. Selected electronic descriptors related to the electrophilic character of the C(2) carbon atom in the protonated *trans*-nitrostyrene molecules calculated at the PBE0/6-311++G(d,p) level of theory in aqueous solutions.

Protonated *trans*-nitrostyrenes	Yield / %[a]	Yield / %[b]	f^+C(2)	f^-C(2)	QC(2)
$[C_6H_5CHCH(Me)NO_2]^+$	100	100	0.306	0.08	0.166
$[p\text{-}Me\text{-}C_6H_4CHCH(Me)NO_2]^+$	99	n/a	0.285	0.081	0.129
$[p\text{-}MeO\text{-}C_6H_4CHCH(Me)NO_2]^+$	75	80	0.424	0.167	0.071
$[p\text{-}F\text{-}C_6H_4CHCH(Me)NO_2]^+$	99	96	0.297	0.083	0.147
$[p\text{-}Br\text{-}C_6H_4CHCH(Me)NO_2]^+$	99	100	0.28	0.123	0.143

[a] For the addition of **C9S2**. [b] For the addition of 6-amino-1,3-dimethyl barbituric acid.

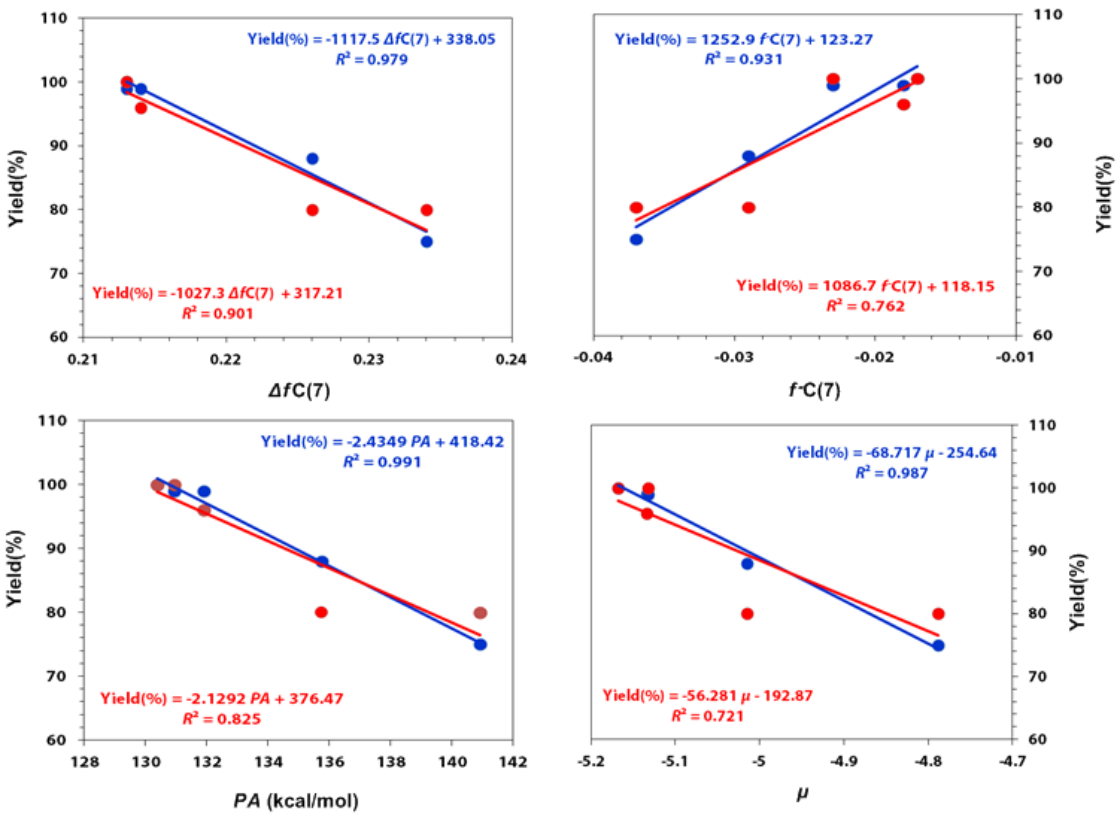

Figure 9.12. Linear relationships between yield (%) vs ΔfC(7), yield (%) vs f^-C(7), yield (%) vs *PA* and yield (%) vs μ correlations calculated at the PBE0/6-311++G(d,p) level of theory in aqueous solutions.

Excellent linear relationships **(**Figure 9.13) are obtained for the yield (%) vs f^-C(2) and yield (%) vs *Q*C(2) correlations (f^+C(2) is the condensed Fukui function for electrophilic attack). However, the poor linear relationship is obtained for the yield (%) vs f^-C(2) correlation, since the C(2) carbon atom in the protonated *trans*-nitrostyrene molecules is not susceptible to electrophilic attack.

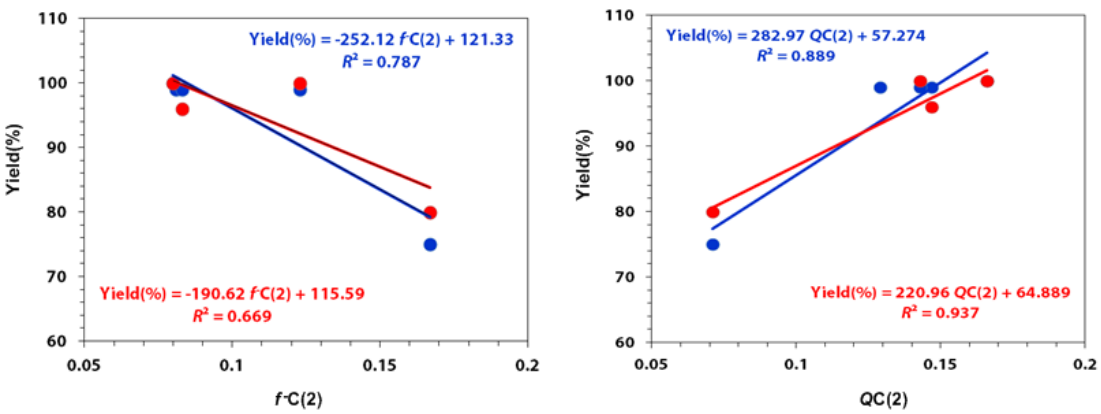

Figure 9.13. Linear relationships between yield (%) vs f^-C(2) and yield (%) vs *Q*C(2) correlations calculated at the PBE0/6-311++G(d,p) level of theory in aqueous solutions.

The above correlations show that the electrophilic character of the C(2) carbon atom would affect the efficacy of the MA reaction since it determines the strength of the nucleophilic attack by the 1,3-dimethyl barbiturate carbanion nucleophile. In summary, the MA reaction should involve first a proton transfer from the 1,3-dimethyl barbituric acid to the $C(NO_2)Me$ carbon atom, which is accompanied by charge density redistribution rendering the C(2) carbon atom electrophilic centre that is attacked by the nucleophile 1,3-dimethyl barbiturate carbocation formed.

To gain insights into the activation of the substrates of the MA reaction catalysed by the bimetallic $Zn^{II}Y^{III}$ catalysts, all possible coordination modes of the substrates to the metal centres of the catalysts were explored by means of DFT calculations at the PBE0/Def2-TZVP(Zn,Y) ∪ 6-31G(d,p)(E) (E = main group element) level of theory in aqueous solution using a representative catalyst, **12ZnY-NO$_3$**.

Firstly, the NACs on the metal centres of the **12ZnY-NO$_3$** bimetallic catalysts were calculated, using their crystal structures in aqueous solution and analysed the MOs for only the representative catalyst **12ZnY-NO$_3$**. The NACs along with the efficacy for these catalysts are compiled in Table 9.14, while the 3D plots of FMOs of the representative catalyst **12ZnY-NO$_3$** are shown in the Appendix B (S9.6).

Table 9.14. NACs on the metal centres of 3*d*-4*f* ZnY bimetallic catalyst calculated at the PBE0/Def2-TZVP(Zn,Y) ∪ 6-31G(d,p)(E) (E = main group element) level of theory in aqueous solutions.

Catalyst	Yield /% [a]	Q_{Zn}	Q_Y
6ZnY-NO$_3$	100	1.308	1.935
8ZnY-NO$_3$	43	1.331	1.926
12ZnY-NO$_3$	55	1.330	1.927
13ZnY-NO$_3$	73	1.322	1.937
2ZnY-NO$_3$	86	1.320	1.945
20ZnY-NO$_3$	86	1.325	1.932
22ZnY-NO$_3$	42	1.307	1.935
27ZnY-NO$_3$	100	1.311	1.929
24ZnY-NO$_3$	98	1.326	1.942

[a] For the addition of **C9S2**.

A perusal of the FMOs of the **12ZnY-NO$_3$** catalyst reveals that the virtual acceptor FMOs (LUMO, LUMO+1, LUMO+2, LUMO+3, etc) are of π*-type located on the ligands. As no acceptor orbital is located on the metal centres of the ZnY bimetallic catalyst, coordination of the MA substrates to the metal centres supported by the interaction of the acceptor orbitals with the donor orbitals (HOMO, HOMO-1, HOMO-2, etc) of the substrates is not feasible. Therefore, the substrates interact with the bimetallic catalyst through non-covalent interactions (electrostatic and dispersion forces).

All attempts to optimize the geometry of the **12ZnY-NO$_3$ -**barbiturate substrate adducts, with the barbiturate substrate approaching the Y^{III} centre failed. In contrast, a local minimum was located on the Potential Energy Surface (PES) of a **12ZnY-NO$_3$** barbiturate adduct involving coordination of barbiturate to Zn metal atom of the catalyst upon dissociation of the coordinated DMF ligand. Notice that the estimated binding energy of DMF to Zn^{II} metal centre is 10.7 kcal mol^{-1} at the PBE0/Def2-TZVP(Zn,Y) $\cup$ 6-31G(d,p)(E) (E = main group element) level of theory in aqueous solutions.

The binding of the barbiturate substrate to Zn^{II} centre is very weak, the estimated binding energy found to be 2.8 kcal mol^{-1}, which is indicative of weak non-covalent interactions. The calculated distance between the Zn^{II} and the keto O atom of the triketo form of **C9S2** was found to be 2.140 Å. On the other hand, *trans*-nitro-styrene substrates showed a preference to be coordinated to Y^{III} centre of the **12ZnY-NO$_3$** catalyst, via a unidentate coordination mode,[469] the estimated binding energy is predicted to be 4.3 kcal mol^{-1} at the PBE0/Def2-TZVP(Zn,Y) $\cup$ 6-31G(d,p)(E) (E = main group element) level of theory in aqueous solutions.

The calculated distance between the Y and the O atom of the unidentate *trans*-nitro-styrene substrate was found to be 2.445 Å. On approaching the *trans*-nitro-styrene substrate to Zn central atom resulted in a local minimum corresponding to a very weak association of the barbiturate substrate with the **12ZnY-NO$_3$** catalyst, but the binding energy is marginal (0.2 kcal mol^{-1}).

The geometry of the adduct formed upon interaction of the *trans*-nitro-styrene substrate was optimised with the Y metal centre of the **12ZnY-NO$_3$** barbiturate adduct. In this adduct the barbiturate and *trans*-nitro-styrene substrates are both coordinated to the Zn and Y metal centres of the **12ZnY-NO$_3$ -**catalyst respectively. The estimated Zn⋯O and Y⋯O bond distances are predicted to be 2.135 and 2.454 Å respectively. For this adduct, the estimated binding energy of the *trans*-nitro-styrene-yttrium interaction is 4.1 kcal mol^{-1}. The equilibrium geometries of the **12ZnY-NO$_3$** barbiturate and **12ZnY-NO$_3$** *trans*-nitro-styrene adducts optimized at the PBE0/Def2-TZVP(Zn,Y) $\cup$ 6-31G(d,p)(E) (E = main group element) level of theory in aqueous solutions are given in Appendix B (S9.7).

It can be concluded that that the barbiturate and *trans*-nitro-styrene substrates of the MA reaction catalysed by the $Zn^{II}Y^{III}$ bimetallic catalyst are co-operatively activated through their interaction with the Zn^{II} and Y^{III} centres of the catalyst following the proposed mechanism is shown in Figure 9.14.

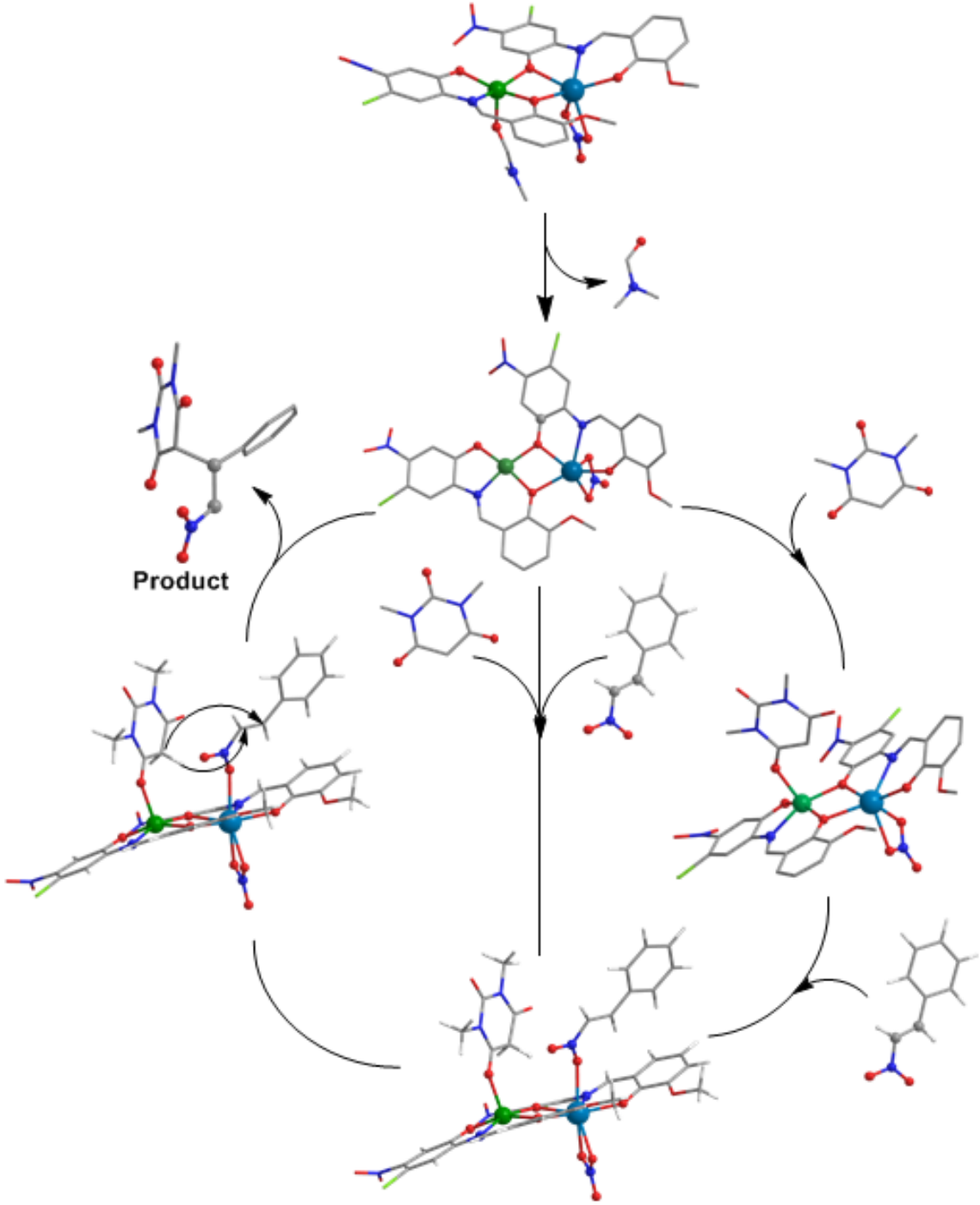

Figure 9.14. A proposed mechanism involving the co-operative activation of both the barbiturate and *trans*-nitro-styrene substrates. Colour code: Zn^{II}, green; Y^{III}, pale blue; C, grey; N, blue; O, red.

In the proposed mechanism, initially, the barbiturate substrate is coordinated to Zn^{II} centre of the **12ZnY-NO$_3$** catalyst after dissociation of the coordinated DMF solvent molecule followed by the coordination of the *trans*-nitro-styrene substrate to the Y^{III} centre of the catalyst. This could be a stepwise process or both substrates are simultaneously coordinated to the metal centres of the catalyst.

The two substrates upon coordination to the metal centres are brought into proximity where a proton can be transferred from the a-carbon atom of the barbiturate substrate to the CH(NO_2) carbon atom of the coordinated *trans*-nitro-styrene substrate, followed by the nucleophilic attack of the electrophilic **C** (7) carbon atom of the *trans*-nitro-styrene substrate by the barbiturate carbanion releasing the product of the MA reaction.

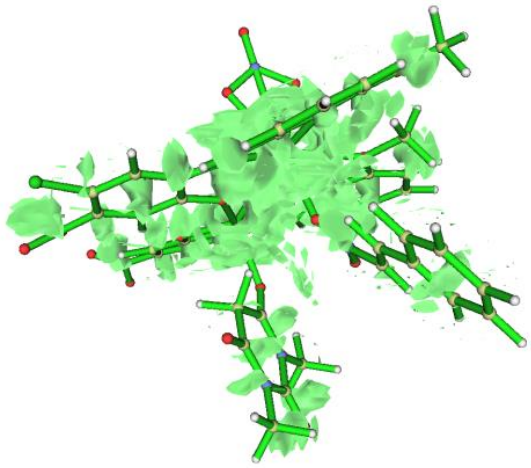

Figure 9.15. The 3D plot of the RDG of the **LZnY-NO$_3$** substrates molecule.

The diastereoselectivity could be explained by considering the very loose association of the two substrates with the catalyst, where their orientation is mainly determined by maximization of the non-covalent interactions between the substrates leading always to the formation of R*/ R* or S*/ S* enantiomers irrespective of what isomer of the nitro-styrene is used. These non-covalent interactions are shown in the 3D plot of the Reduced Density Gradient (RDG) of the catalyst-substrates molecule (Figure 9.15)

9.2.3.2.10 *In situ*-ESI-MS studies

In situ ESI-MS studies were performed to confirm the dissociation of the tetranuclear core to the two dinuclear moieties, on the addition of substrate and to identify any possible adducts.

Firstly, **1ZnGd-NO$_3$** and **C9S2** were dissolved in a 1:1 ratio in MeOH, a peak was observed at 946.0920 m/z which perfectly corresponds to a $[Zn^{II}Gd^{III}(\mathbf{L1})_2(\mathbf{C9S2})(NO_3)(H_2O)]^+$ (Appendix B, S9.10) fragment, which would support the coordination of **C9S2** to a dinuclear species of **1ZnGd-NO$_3$**.

Furthermore, a [$Zn^{II}Gd^{III}$(**L1**)$_2$(**C9S3**)(NO_3)(CH_3OH)$_2$(H_2O)] fragment at 1009.0995 m/z is observed when **C9S2** is substituted **C9S1**, indicating that both substrates have the ability to coordinate to the dinuclear species (Appendix B, S9.9).

On addition of both substrates, a peak at 1345.2556 m/z is observed, which may correspond to [$Zn^{II}Gd^{III}$(**L1**)$_2$(**C9S2**)(**C9S1**)$_2$(NO_3)(CH_3OH)$_3$] fragment (Appendix B, S9.12).

9.3 Conclusion

In summary, this chapter presents a multidisciplinary study that for the first time demonstrates the successful use of 3d-4f PCCs as efficient and highly diastereoselective catalysts in a MA reaction.

The synthesis of a library of twenty-one isoskeletal $Zn^{II}_2Y^{III}_2$ PCCs (**LZnY-NO$_3$**) with a modified organic periphery, demonstrated that the modification of the ligand sterics does not compromise the electrostatic properties of the catalyst. By tuning the metal centres, it was possible to obtain useful mechanistic information and reveal the co-operative character of the proposed catalytic system, through the use of a pallet of spectroscopic techniques.

Finally, by altering the structural character of the **1MLn-NO$_3$** catalysts it was possible to tune the PCCs to maximise efficacy. DFT calculations throw light on the possible mechanism of the MA reaction catalyzed by the **1MLn-NO$_3$** catalysts. Such information cannot be obtained by the use of homometallic polynuclear 3d-3d, 4f-4f catalysts or organocatalysts. The successful employment of this library of co-operative catalysts paves the way to expand this approach to other 3d-4f PCCs and catalytic reactions.

Chapter 10: Summary and conclusions

This chapter summarizes the thesis, discusses its findings and contributions, points out limitations of the current work and also outlines directions for potential future research.

This thesis aimed to investigate two main ideas:

1) to use structurally related Schiff base ligands to synthesise novel high nuclearity 3d-4f PCCs that display interesting magnetic and luminescent behaviour.

2) to develop the first tetranuclear 3d-4f PCCs, supported by Schiff base ligands, used as catalysts in organic transformations and to understand and manipulate their structure to maximise catalytic efficacy.

A summary of the main findings of the thesis are presented below.

10.1 Summary

The attempts to synthesise novel high nuclearity 3d-4f PCCs with structurally similar compartmental Schiff base ligands (H_2**L1**-H_2**L5**), through a systematic variation of the reaction conditions, formed a wealth of 3d-4f PCCs with novel structures and topologies.

Herein, the first examples of the **2,3,4M6-1** core topology in Zn^{II}-Ln^{III} chemistry, the first examples of $Co^{II}_4Ln^{III}_2$ PCCs which display the **2,3,4M6-1** core topology and the first examples of Ni^{II}-Ln^{III} PCCs with a **3,6M7-1** core topology are reported. Perhaps most importantly, the first examples of the **1,2,3,4,5,5,5,8M15-1** topology in PCC chemistry are also described. However, the limitations of the methodology are evident as the synthesis of PCCs with the **2,3,4M6-1** and **1,2,3,4,5,5,5,8M15-1** core topologies could not be predicted and $Zn^{II}_4Dy^{III}_7$ (**13**) and $Zn^{II}_6Dy^{III}_4$ (**14**) PCCs could only be identified by single-crystal XRD studies and were not isolated independently.

Though a myriad of novel structures with new topologies were formed, only a few have been confirmed to display SMM behaviour. Of the reported PCCs in this thesis, only $Zn^{II}_4Dy^{III}_2$ (**7**), $Co^{II}_4Dy^{III}_2$ (**17**) and $Zn^{II}_4Dy^{III}_{11}$ (**43**) were shown to display a slow relaxation of magnetisation. The U_{eff} and τ_0 of these PCCs are 10.2 cm^{-1}, $\tau_0 = 7.1 \cdot 10^{-6}$ s; 13.4 K, $\tau_0 = 8.5 \times 10^{-7}$ s and 4.7 K, $\tau_0 = 4.4.10^{-5}$ s respectively. Previously, higher nuclearity 3d-4f Schiff base supported PCC SMMs, with similar 3d metal ions (Cu^{II}, Ni^{II}, Zn^{II}, Co^{II}) display enhanced SMM properties when compared to the examples described herein., with U_{eff} values ranging from 3 K – 85 K and τ_0 values between 1 x 10^{-9} s to 5.5 x 10^{-3} s.[56,103,318,516]

Furthermore, low nuclearity 3d-4f Schiff base supported PCC SMMs have been reported which display comparable SMM properties to the larger examples.[170,517–520] Therefore, synthesising high

nuclearity 3d-4f PCCs may be a counter-intuitive route to SMM behaviour. Moreover, structurally simple monometallic complexes have been reported with greatly enhanced SMM properties all of which surpass the values observed in 3d-4f PCC chemistry.[174,521–524] The synthetic control over the symmetry of the lanthanide coordination site, and therefore over magnetic axial field, gives rise to these exceptional properties. This degree of synthetic control has not yet been demonstrated with 3d-4f PCCs and the synthetic protocols employed in this study are far from this level.

The development of the first tetranuclear 3d-4f PCC catalysts has been detailed and in comparison to the previously reported 3d-4f PCC catalysts, which were prepared *in situ*,[296–299] these are characterised in both the solid and solution state with a wide range of techniques. This thesis has demonstrated the range of catalytic reactions that they can be successfully employed in which include FC alkylations, a MA reaction, a PBR and a domino ring-opening cyclization. The optimised catalytic protocols provides mild conditions, reduced catalytic loading and high catalytic efficacies which improves on many of the previously reported procedures. [412,422,427–430,451,457–461,465,466,498,499]

The synthesis of the series of isoskeletal defect dicubane $M^{II}_2Ln^{III}_2$ PCC catalysts did not prove straightforward and many variables determined the structure of the targeted PCC (chapter five). Chapter seven demonstrated that the catalytic conditions could alter the structure of the catalyst (transformation from **1NiDy-ClO$_4$** to **1NiDy-Cl**), the targeted substitution of Ln^{III} ions could result in a myriad of by-products (**1NiSm-A, B, C**) and that certain PCCs could not reliably crystallise (**1NiLn-Cl**). Furthermore, the substitution of the Ni^{II}/Co^{II} ion to Zn^{II}, in chapter eight, required a significant adaption of the synthetic procedure. However, with the insights from these chapters, a reliable synthetic protocol was developed to synthesise a library of isoskeletal $Zn^{II}_2Ln^{III}_2$ (**LZnLn-NO$_3$**) PCCs with modified Schiff base ligands (H_2**LX**).

The ratio of reactants (M^{II}: Ln^{III}: H_2**LX**: Et_3N) is the most important variable for reliably synthesising $M^{II}_2Ln^{III}_2$ PCCs, with the $Ni^{II}/Co^{II}_2Ln^{III}_2$ ratio, 1:1:2:5, and the $Cu^{II}/Zn^{II}_2Ln^{III}_2$ ratio, 1:2:2:4.5, the most successful. Other synthetic variables such as solvent or metal salt can be carefully altered depending on the desired structure of the targeted tetranuclear PCC. Whereas long reaction times, mixed or non-polar solvents and high temperatures either led to significant impurities or formation of undesired species. The crystallisation of the $M^{II}_2Ln^{III}_2$ PCCs from DMF/Et_2O via VD was the most successful method of isolating $M^{II}_2Ln^{III}_2$ PCCs, with well-defined crystals forming without impurities co-crystallising.

With the $M^{II}_2Ln^{III}_2$ PCCs the catalytic effects of the substitution of 3d and 4f ions within the framework, the replacement of modified Schiff base ligands and altered coordination environments were studied. With these insights and a range of characterisation techniques (ESI-MS, UV-Vis, EPR, ^{1}H NMR) and DFT studies, the coordination of substrates to either 3d or 4f

metal centres was rationalised and the co-operative nature of the 3d-4f PCC catalysts was confirmed, an effect which had not previously fully studied.

10.2 Discussion

It is felt the most significant contribution of this thesis to the already existing literature is the development and methodology for studying the $M^{II}_2Ln^{III}_2$ Schiff base ligand framework for catalytic reactions. With this framework, it was possible to tune the PCCs to obtain the highest possible catalytic efficacy and manipulate the magnetic character of the PCC so that both the framework and mechanistic aspects could be studied with EPR and NMR spectroscopy. While the magnetic character of a 3d-4f PCC framework has been previously altered to study SMM and magnetic coupling interactions, this has never been studied in 3d/4f/ligand *in situ* organic transformations. This thesis emphasises that 3d-4f PCCs offer a unique opportunity for the study of catalytic reactions, due to their exploitable dual nature and the number of structural aspects which can be tuned. The adaption of this methodology to pre-existing or newly synthesised 3d-4f PCCs provides a new avenue for the continued development of 3d-4f PCCs, in general, and specifically to catalyse organic transformations.

Synthetic methods. Two broad synthetic methodologies have been employed. The first, serendipitous assembly, has led to the discovery of novel 3d-4f PCCs with an array of interesting properties. However, none of these structures could be predicted and required a large number of reactions and subsequent crystallisation procedures to synthesise them. This is a highly time-consuming process which could be partially avoided by employing rational/ targeted design.

Secondly, the targeted synthesis of defect dicubane 3d-4f PCCs, based on the $Co^{II}_2Dy^{III}_2$ PCC reported by Powell,[2] resulted in a series of catalytically active PCCs with tunable properties. This work shows that this approach is far more applicable for the study of catalytic behaviour and correlating magnetic behaviour in PCC cores, whereas serendipitous assembly should only be applied as the initial stage for the discovery of new 3d-4f PCCs.

Even so, it is very difficult to predict the nuclearity or the core topology of a 3d-4f PCC with either method. Nevertheless, with a move away from serendipitous assembly and towards rational/targeted design, a deeper understanding of the relationships between synthesis, structure and physical properties will be developed.

Topological implications. The topological approach employed throughout this thesis has identified similarities between the core structures of 3d-4f PCCs within the thesis and in the literature. Though some relationships between ligand structure and core topology are identified it could not be used to predict the synthesis of compounds with specific properties. Additionally, the ***ND*k-m** notation does not discriminate between O, N, S and P donors which are assigned as

linkers. The type of donor will significantly affect the coupling between 3d/3d, 4f/4f and 3d/4f ions which will influence the magnetic properties.

While this approach has been useful for the identification of related core motifs (such as the diabolo in chapter six), it is not yet developed enough to rationally predict the synthesis of 3d-4f PCCs with specific properties and relating the existing properties of 3d-4f PCCs to their core motif is tenuous at best.

Ligand selection – high nuclearity 3d-4f PCCs. The ligands used for the synthesis of high nuclearity 3d-4f PCCs (H_2**L1**, H_2**L2**, H_3**L3** and H**L4**) did not manage to generate a 3d-4f PCC whose core nuclearity was greater than seven. The common structure of these ligands contains three identical pockets for the selective binding of 3d and 4f ions and are structurally rigid. In addition, co ligands were not introduced into the reactions. These factors may have restricted the growth of larger 3d-4f PCCs due to the limited number of coordination and bridging modes of the ligands.

The use of structurally flexible Schiff bases and co-ligands, which have extensive bridging modes, has resulted in some of the highest nuclearity 3d-4f PCCs such as those reported by Milios,[205] Li[525] and Powell[119] which resulted in $Zn^{II}_{12}Dy^{III}_{18}$, $Co^{II}_{2}Dy^{III}_{10}$ and $Cu^{II}_{9}Dy^{III}_{2}$ PCCs respectively. Considering these examples and the results obtained, more flexible Schiff base ligands which retain the salicylaldehyde or o-vanillin moieties should be used for future studies and combined with co-ligands such as azides, acetates and carboxylic acids.

Ligand selection – catalysis. The use of H_2**L1** and the modified (H_2**LX**) ligands for the synthesis of catalytically active defect dicubane 3d-4f PCCs proved very successful. These ligands could reliably synthesise isoskeletal $M^{II}_{2}Ln^{III}_{2}$ PCCs which host a variety of guest 3d and 4f ions. However, the ligands reported by Shibasaki may have provided a better starting point for this type of research, as the system is already known and partially defined. In addition, the previously reported *in situ* 3d-4f / Schiff base catalytic systems all demonstrate their potential efficacy in catalysing enantioselective transformations.[296–299] Although unexpected diastereoselectivity was observed in the $M^{II}_{2}Ln^{III}_{2}$ series for the MA catalysis (chapter nine), it was not possible to develop an enantioselective 3d-4f tetranuclear PCC catalyst, which is a noticeable omission from this work.

Though these ligands reliably synthesised the targeted $M^{II}_{2}Ln^{III}_{2}$ PCCs, the use of a tetranuclear PCC over the previously reported dinuclear examples presented many challenges. It is recommended that 3d-4f catalysis is further explored with low nuclearity 3d-4f PCCs, with metal ions held within a single Schiff base ligand frame, before extending these studies to more complex examples. Though as an initial foray into the area of 3d-4f PCC catalysis, the development of the

catalytic system was much more successful than initially anticipated and provides a solid foundation for future work.

Ligand Modification- The modified ligands (H_2**LX**) allowed a wide range of $M^{II}_2Ln^{III}_2$ PCCs with modified organic peripheries to be studied. However, ligand modification had little or no impact on the efficacy of the studied catalytic reactions, instead changes in efficacy were due to the solubility of the respective PCC. Though it is disappointing that ligand modification does not change the efficacy, considering some of the limitations 3d-4f PCC catalysts have which include their poor solubility, lack of enantioselectivity and limited recoverability, this opens new perspectives for 3d-4f PCC catalysis. With the astute selection of modified ligand, these limitations could be overcome without altering the underlying effectiveness of the $M^{II}_2Ln^{III}_2$ core. This discovery was unexpected, however, it uncovers a new feature in 3d-4f PCC catalysis one which may lead to applications which have not yet been considered and with this toolkit of modification methods a 3d-4f PCC may be tailored for a variety of catalytic procedures.

Characterisation – solid state. The combination of characterisation methods for materials in the solid state in this thesis is consistent with the characterisation described in 3d-4f PCC literature. Single-crystal XRD studies are unparalleled in determining the molecular structure of crystalline materials and without it, much of the subject matter in this thesis would be indiscernible. The combination of this technique with other characterisation methods which measure the bulk material (CHN, FT-IR and TGA) ensure that the structure of these materials is as reported.

Characterisation – solution state. The measurement of $M^{II}_2Ln^{III}_2$ PCCs in the solution state proved much more difficult. For previously reported *in situ* 3d/4f / Schiff base catalytic reactions ESI-MS was used to confirm the formation of the proposed 3d-4f PCC, however many of these spectra displayed several peaks which corresponded to 3d-4f and homometallic 3d fragments. Using the same technique but with defect dicubane 3d-4f PCCs structure determined in the solid state, only peaks identified as the [$M^{II}_2Ln^{III}_2$(**LX**)$_4$] core were observed. This observation emphasises the importance of ensuring the purity of 3d-4f PCCs and questions the previously reported results.

EPR and ^{1}H NMR studies were employed to confirm the structure of the series in solution, by substitution of the 3d and 4f ion. The characterisation of the 3d-4f PCC structure and substrate interaction in this way is unique and offers a completely new way of analysing 3d-4f PCCs in solution. However, these methods have their limitations and several issues must be overcome for these methods to become commonplace.

Impact. The effort to synthesise novel 3d-4f PCCs from Schiff base ligands has expanded upon the many reported examples where a serendipitous approach has resulted in 3d-4f PCCs with novel topologies and interesting magnetic behaviour. Though the compounds in these chapters do

not display outstanding SMM or luminescent properties, many contain structural motifs and core configurations which have not been observed before in 3d-4f PCC chemistry. Although the selection of organic ligands and co-ligands could have been more astute, it is believed with the synthetic approach employed the outcome of this research has fulfilled the original criteria, helped to further explore topological relationships between 3d-4f PCCs, as well as to further develop the topological approach.

Impact. The demonstration that 3d-4f PCCs can be used as catalysts for organic transformations opens a new pathway in 3d-4f PCC chemistry. Currently, the drive to synthesise new 3d-4f PCCs is dominated by investigating the SMM properties that they display. While the work by Shibasaki and others,[296] did demonstrate that the combination of 3d and 4f ions with Schiff base ligands can successfully catalyse asymmetric organic transformations, there was little evidence that the active species was a 3d-4f PCC. With the methodology employed in this thesis, it is certain that a 3d-4f PCC is successfully catalysing the organic transformations studied. The demonstration of this behaviour may generate a new impetus for the synthesis of catalytically active 3d-4f PCCs following the methodology employed in this thesis. It is hoped that this avenue of research helps to further broaden the field of 3d-4f PCC chemistry and a new generation of 3d-4f PCC catalysts will be developed.

10.3 Future work

Rational design is essential for the targeting of 3d-4f PCCs with specific properties, however there are few reported examples of targeting the same core topology with specific ligand cavities. Previously, H_2**L10.1** (Figure 10.1) has been used to synthesise 3d-4f PCCs with nonanuclear $[M^{II}_6Ln^{III}_3(OH)_6]$ cores,[189,526,527] where Dy^{III} analogues all display SMM behaviour. The H_2**L10.1** ligand has coordination pockets which are similar to the ligands shown in Figure 10.1.

The aim of this study would be to determine whether, with the same reaction conditions, if substituting Schiff base ligands (Figure 10.1) with the same coordination pockets would allow for the targeting of $[Cu^{II}_6Ln^{III}_3(OH)_6]$ cores. Which would demonstrate that ligands with specific pockets can be applied to reliably form a desired core topology.

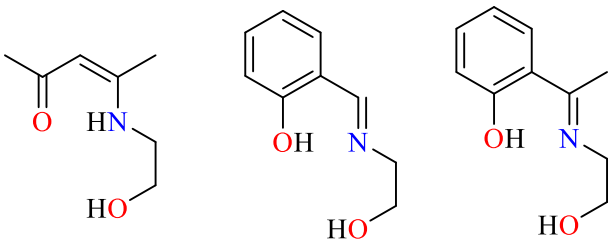

H_2**L10.1** $[M^{II}_6Ln^{III}_3(OH)_6]$ $[Cu^{II}_6Ln^{III}_3(OH)_6]$ $[Cu^{II}_6Ln^{III}_3(OH)_6]$

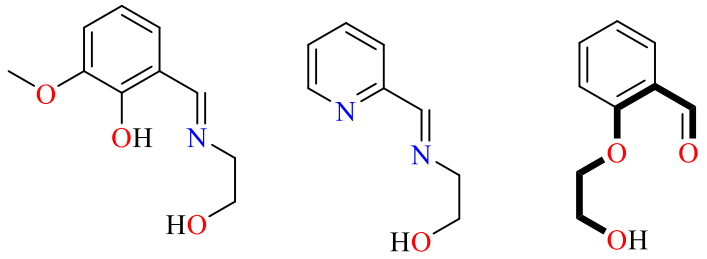

H_2**L1**

$[Cu^{II}_2Ln^{III}_2]$ $[Cu^{II}_6Ln^{III}_3(OH)_6]$ $[Cu^{II}_6Ln^{III}_3(OH)_6]$

Figure 10.1. Schiff base ligands for targeting $[Cu^{II}_6Ln^{III}_3(OH)_6]$ PCCs.

As enantioselectivity was one of the most significant omissions from the studied $M^{II}_2Ln^{III}_2$ PCCs behaviour, further efforts to study this system should concentrate on this. To develop an enantioselective 3d-4f PCC catalyst based on the isoskeletal defect dicubane PCC described herein, it may be possible to employ chiral Schiff base ligands which are structurally similar to H_2**L1**, with the same coordination pockets but with bulkier functional groups added.

However, the ligands used in Shibasaki's work may provide a better starting point. Instead of following an *in situ* protocol, synthetic inspiration taken from this thesis could be applied to fully characterise the dinuclear species, substitute M^{II} and Ln^{III} ions and to use a pallet of spectroscopic techniques to probe the asymmetric organic transformations. Some potential organic transformations that these catalysts could be applied in include the MA addition discussed in chapter nine or the oxa Michael reaction between 2-acyl-imidazole with indoles. This new generation of catalysts may also be applicable in the multicomponent synthetic strategy that is currently gaining a lot of interest from research industrially and in academia.

Chapter 11: Synthetic part

11.1 General methods

Materials. Chemicals (reagent grade) were purchased from Sigma Aldrich and Alfa Aesar. All experiments were performed under aerobic conditions using materials and solvents as received.

Instrumentation. ^{1}H and ^{13}C NMR spectra were recorded on a Varian VNMRS solution-state spectrometer at 500 MHz at 30 °C using a residual isotopic solvent (DMSO, δ_H = 2.50 ppm) as an internal reference. Chemical shifts are quoted in ppm. Coupling constants (J) are recorded in Hz.

FT-IR spectra of the samples were recorded over the range of 4000-650 cm^{-1} on a Perkin Elmer Spectrum One FT-IR spectrometer fitted with a UATR polarization accessory.

ESI-MS data were obtained on a VG Autospec Fissions instrument (EI at 70 eV).

TGAs weres performed on a TA Instruments Q-50 model (TA, Surrey, UK) under nitrogen and at a scan rate of 10 °C/min.

All steady-state UV−Vis absorbance measurements (University of Kent) were made by use of a Shimadzu UV-1800 UV−Vis spectrophotometer in DMF as indicated with quartz cuvettes, while all steady-state solution fluorescence emission measurements were carried out using a Cary Eclipse fluorescence spectrometer in either acetonitrile or DMF as indicated with quartz cuvettes.

Crystallography. Data was obtained either at the University of Sussex by use of an Agilent Xcalibur Eos Gemini Ultra diffractometer with CCD plate detector under a flow of nitrogen gas at 173(2) K using Mo Kα radiation (λ = 0.71073 Å). CRYSALIS CCD or RED software programs were used, respectively, for data collection and processing. Reflection intensities were corrected for absorption by the multiscan method. Other data was collected at the UK National Crystallography Service, University of Southampton, on a Rigaku Saturn 724+ area detector mounted at the window of an FR-E+ rotating anode generator with a Mo anode (λ = 0.71075 Å) under a flow of nitrogen gas at 100(2) K. The X-ray data was collected and processed using Rigaku CrystalClear or where Rigaku Oxford Diffraction CrystallisPro was used for data processing. Crystal structures were solved by dual-space methods with SHELXT or using charge flipping methods with Superflip. All crystal structures were then refined on Fo2 by full-matrix least-squares refinements using SHELXL. All non-H atoms were refined with anisotropic thermal parameters, and H atoms were introduced at calculated positions and allowed to ride on their carrier atoms. Geometric/crystallographic calculations were performed using PLATON, Olex2 and WINGX packages; graphics were prepared with Crystal Maker.

Magnetic Studies. *Chapter 2, 3, 4 and 6*- Variable-temperature magnetic studies were made by use of an MPMS-5 Quantum Design magnetometer operating at 0.03 T in the 300 2.0 K range. Magnetization measurements were made under a magnetic field range of 0 − 5 T. Diamagnetic corrections were applied to the observed paramagnetic susceptibility using Pascal's constants. *Chapter 4* - Heat capacity measurements were carried out by using a Quantum Design PPMS system, equipped with a ^{3}He cryostat. The experiments were performed on a thinly pressed pellet (ca. 1 mg) of a polycrystalline sample, thermalized by ca. 0.2 mg of Apiezon N grease, whose contribution was subtracted by using a phenomenological expression.

Continuous wave EPR measurements. *Chapter 8 and 9*-The continuous wave EPR spectra were recorded on a Bruker EMX spectrometer operating at X-band with a microwave frequency of ~ 9.4 GHz. The microwave frequency and magnetic field were measured using the Bruker internal frequency counter and field controller, respectively. To avoid a saturation of signals, an optimized microwave power of 0.8 and 1 mW (23 and 24 dB) was applied for all measurements. Modulation amplitude of 2 – 4 G was applied to prevent an artificial signal broadening, combined with a fixed modulation frequency of 100 KHz applying a receiver gain of 3.2×10^3 depending upon the signal-to-noise ratio. The Bruker SHQE (ER 4122) resonator was used for measurements at variable temperatures. The applied magnetic field was calibrated using a Bruker standard sample with a well-known *g*-value, and all the measurements were performed at 3400 G.

Computational details. *Chapter 5 and 7*- Energy minimization on strategically designed model compounds were conducted within the Kohn-Sham DFT approach at the B3LYP/SDD and B3LYP/6-311G* levels.[528–538] Calculations were carried using the Gaussian09 software. The Jmol program was used for visualization purposes.

Chapter 9 - All DFT calculations were performed using the Gaussian09, D.01 program suite. The geometry of all organic molecules and of representative ZnY dinuclear complexes were fully optimized, employing the Perdew, Burke and Ernzerhof,[539–545] PBE0 (also called PBE1PBE) hybrid density functional. Calculations on the organic molecules are performed by the PBE0/6-311++G(d,p) computational protocol, while for the ZnY dinuclear complexes the PBE0/Def2-TZVP(Zn,Y)$\cup$6-31G(d,p)(E) (E = main group element) computational protocol was used. Notice the use of the Def2-TZVP basis set[546] for Zn and Y. The stationary points were identified as local minima by the absence of imaginary frequencies ($N_{\mathrm{Imag}} = 0$). Water solvent effects were taken into account employing the polarizable continuum model (PCM) using the integral equation formalism variant (IEFPCM) being the default self-consistent reaction field (SCRF) method.[547] The NBO population analysis was performed using Weinhold's methodology as implemented in the NBO 6.0 software.[548,549]

11.2 Ligand synthesis

Supporting Figures for ^{1}H NMR spectra, ^{13}C NMR spectra and ESI-MS are found in Appendix B.

Preparation of H_2L1

O-vanillin (0.025mol, 3.35g) and 2-amino-phenol (0.025mol, 2.73g) were dissolved in MeOH (5 mL). The suspension was refluxed for 1 h, during which time a bright orange solid precipitated. After cooling to room temperature, the solid was filtered off and washed with cold MeOH and Et_2O. The solid was dried in vacuo. Yield 95%. ^{1}H NMR (500 MHz, DMSO-d_6) δ 9.75 – 9.71 (m, 1H), 8.95 (s, 1H), 7.36 (dd, *J* = 8.0, 1.6 Hz, 1H), 7.21 – 6.99 (m, 3H), 6.96 (dd, *J* = 8.1, 1.4 Hz, 1H), 6.91 – 6.81 (m, 2H), 3.80 (s, 3H). ^{13}C NMR (126 MHz, DMSO) δ 162.01, 152.27, 151.42, 148.63, 134.95, 128.46, 124.26, 120.05, 119.96, 119.70, 118.37, 116.97, 115.71, 56.34, 40.62, 40.53, 40.45, 40.36, 40.28, 40.19, 40.11, 40.03, 39.95, 39.86, 39.69, 39.53.

Preparation of H_2L2

o-vanillin (0.025 mol, 3.35 g) and 3-amino-2-napthol (0.025 mol, 3.98 g) were dissolved in MeOH (5 mL). The suspension was refluxed for 1 h, during which time a bright orange solid precipitated. After cooling to room temperature, the solid was filtered off and washed with cold MeOH and Et_2O. The solid was dried in vacuo. Yield 88 %. ^{1}H NMR (500 MHz, DMSO-d_6) δ 13.78 (s, 0H), 10.12 (s, 0H), 9.07 (s, 1H), 7.85 – 7.77 (m, 2H), 7.69 (d, *J* = 8.2 Hz, 1H), 7.41 – 7.34 (m, 1H), 7.33 – 7.22 (m, 3H), 7.12 (dd, *J* = 8.0, 1.3 Hz, 1H), 6.89 (t, *J* = 7.9 Hz, 1H), 3.83 (s, 3H); ^{13}C NMR (126 MHz, DMSO-d_6) δ 163.49 , 152.35 , 150.36 , 128.07 , 126.38 , 126.17 , 124.37 , 123.85 , 118.60 , 117.52 , 116.06 , 110.42 , 56.38 , 40.56 , 40.31 (d, *J* = 20.9 Hz), 40.06

Preparation of H_3L3

o-vanillin (0.025 mol, 3.35 g) and 1,3-diamino-2-propanol (0.025 mol, 2.73 g) were dissolved in MeOH (50 mL). The suspension was refluxed for 1 h, during which time the solution became a bright yellow. The solution was reduced under pressure to form a yellow oil. The oil was treated with hot toluene (20 mL) and stirred. Upon treatment, a bright yellow precipitate formed and was filtered and washed with cold MeOH (15 mL) and Et_2O (3 x 15 mL). The solid was dried in vacuo. Yield 96 %. ^{1}H NMR (500 MHz, chloroform-*d*) δ 8.37 (d, *J* = 1.5 Hz, 2H), 6.94 – 6.84 (m, 4H), 6.79 (tt, *J* = 7.9, 0.9 Hz, 2H), 4.24 (h, *J* = 4.8, 4.3 Hz, 1H), 3.93 – 3.82 (m, 8H), 3.75 (dd, *J* = 12.5, 6.3 Hz, 2H), 2.78 (s, 1H). ^{13}C NMR (126 MHz, $CDCl_3$) δ 167.40, 152.08, 148.48, 145.81, 123.20, 118.42, 118.00, 117.73, 114.35, 77.28, 77.03, 76.77, 70.29, 62.42, 56.10, -0.04.

Preparation of H_2L16

5-bromo-3-methoxy salilcyldahyde (0.025 mol, 4.666 g) and 2-amino-phenol (0.025mol, 2.73 g) were dissolved in MeOH (5 mL). The suspension was refluxed for 1 h, during which time a red solid precipitated. After cooling to room temperature, the solid was filtered off and washed with

Et_2O and dried in vacuo. Yield 84 %. ^{1}H NMR (500 MHz, DMSO-d_6) δ 9.85 (s, 1H), 8.94 (d, *J* = 1.7 Hz, 1H), 7.42 – 7.34 (m, 2H), 7.18 – 7.10 (m, 2H), 6.96 (dd, *J* = 8.0, 1.5 Hz, 1H), 6.88 (t, *J* = 7.6 Hz, 1H), 3.82 (s, 3H), 2.49 (s, 1H); ^{13}C NMR (126 MHz, DMSO d_6) δ 160.11, 152.85, 151.42, 150.09, 133.98, 128.85, 125.58, 120.42, 120.10, 119.68, 117.71, 117.01, 108.62, 56.64, 40.62, 40.53, 40.45, 40.36, 40.28, 40.20, 40.11, 40.03, 39.95, 39.86, 39.70, 39.53.

Preparation of HL4

o-vanillin (0.025 mol) and 4-aminoantipyrine (0.025 mol) were refluxed in MeOH (20 mL) to form a clear bright yellow solution. The solution was reduced under pressure to form a viscous yellow oil. The oil was recrystallized from toluene to form a bright yellow powder the powder was collected via filtration and washed with MeOH (20 mL x 2) and Et_2O (15 ml) before being dried over night. (Yield 74 %) ^{1}H NMR (500 MHz, chloroform-*d*) δ 9.81 (s, 1H), 7.52 – 7.44 (m, 2H), 7.41 – 7.29 (m, 3H), 6.98 (dd, *J* = 7.9, 1.7 Hz, 1H), 6.91 (dd, *J* = 8.0, 1.7 Hz, 1H), 6.83 (td, *J* = 7.9, 1.3 Hz, 1H), 3.92 (d, *J* = 1.3 Hz, 3H), 3.16 (d, *J* = 1.2 Hz, 3H), 2.40 (d, *J* = 1.3 Hz, 3H). ^{13}C NMR (126 MHz, $CDCl_3$) δ 160.41, 160.19, 150.42, 149.89, 148.08, 134.32, 129.28, 127.31, 124.66, 123.58, 120.15, 118.47, 117.73, 115.97, 113.60, 77.33, 77.07, 76.82, 56.06, 35.57, 28.60, 10.10, -0.02. {338.15 m/z} M+

Preparation of H_2L6

2-hydroxy-3-methoxy-5-allyl-benzaldehyde (0.025 mol, 4.81 g) and 2-aminophenol (0.025 mol, 2.73 g) were dissolved in MeOH (5 mL). The suspension was refluxed for 1 h, during which time a bright red solid precipitated. After cooling to room temperature, the solid was filtered off and washed with cold MeOH and Et_2O. The solid was dried in vacuo. Yield 70 %. ^{1}H NMR (500 MHz, chloroform-*d*) δ 13.80 (s, 1H), 9.71 (s, 1H), 8.90 (s, 1H), 7.38 – 7.32 (m, 1H), 7.14 – 7.07 (m, 1H), 7.01 – 6.83 (m, 4H), 6.04 – 5.92 (m, 1H), 5.14 – 5.03 (m, 2H), 3.79 (d, *J* = 1.2 Hz, 3H), 3.35 – 3.28 (m, 3H). ^{13}C NMR (126 MHz, DMSO d_6) δ 192.25, 149.64, 148.79, 145.41, 142.08, 137.90, 133.24, 131.18, 122.66, 120.71, 119.51, 118.56, 116.44, 113.68, 111.69, 56.56, 40.61, 40.52, 40.44, 40.35, 40.27, 40.19, 40.11, 40.02, 39.94, 39.85, 39.68, 39.52, 39.19.

Preparation of H_2L7

2-hydroxy-3-methoxy-5-nitro benzaldehyde (0.025 mol, 3.853 g) and 2-amino-phenol (0.025 mol, 2.73 g) were dissolved in MeOH (5 mL). The suspension was refluxed for 1 h, during which time a clay brown solid precipitated. After cooling to room temperature, the solid was filtered off and washed with cold MeOH and Et_2O. The solid was dried in vacuo. Yield 93%. ^{1}H NMR (500 MHz, DMSO-d_6) δ 15.63 (d, *J* = 10.3 Hz, 1H), 10.68 (s, 1H), 9.33 (d, *J* = 9.1 Hz, 1H), 8.25 (d, *J* = 2.6 Hz, 1H), 7.70 (d, *J* = 8.1 Hz, 1H), 7.47 (d, *J* = 2.7 Hz, 1H), 7.22 (t, *J* = 7.4 Hz, 1H), 7.11 – 6.86 (m, 2H), 3.83 (s, 3H). ^{13}C NMR (126 MHz, DMSO-d_6) δ 171.05, 158.90, 151.81, 149.73,

134.62, 129.63, 127.09, 125.03, 120.44, 118.44, 116.92, 113.36, 106.48, 56.17, 40.61, 40.52, 40.44, 40.35, 40.28, 40.19, 40.11, 40.02, 39.94, 39.85, 39.69, 39.52.

Preparation of H_2L8

o-vanillin (0.025 mol, 3.35 g) and 2-amino-5-nitrophenol (0.025 mol, 3.30 g) were dissolved in MeOH (5 mL). The suspension was refluxed for 1 h, during which time a dark brown to red solid separated. After cooling to room temperature, the solid was filtered off and washed with cold MeOH and Et_2O. The solid was dried in vacuo. Yield 66%. ^{1}H NMR (500 MHz, DMSO-d_6) δ 13.18 (s, 1H), 10.72 (s, 1H), 9.01 (s, 1H), 7.77 (dd, J = 8.4, 1.7 Hz, 2H), 7.57 – 7.51 (m, 1H), 7.26 (dd, J = 7.9, 1.5 Hz, 1H), 7.15 (dd, J = 8.0, 1.5 Hz, 1H), 6.90 (t, J = 7.9 Hz, 1H), 3.82 (s, 3H).

Preparation of H_2L9

5-allyl-2 hydroxy-3-methoxy benzaldehyde (0.0125 mol, 2.290 g) and 2-amino-5-nitrophenol (0.0125 mol, 1.926 g) were dissolved in MeOH (5 mL). The suspension was refluxed for 1 h, during which time the dark brown solution had formed a dark red precipitate. After cooling to room temperature, the solid was filtered off and washed with cold MeOH and Et_2O. The solid was dried in vacuo. Yield 72%. ^{1}H NMR (500 MHz, DMSO-d_6) δ 12.94 (s, 1H), 10.69 (s, 1H), 8.97 (s, 1H), 7.79 – 7.73 (m, 2H), 7.56 – 7.50 (m, 1H), 7.07 (d, J = 1.9 Hz, 1H), 6.98 (d, J = 2.1 Hz, 1H), 5.98 (ddt, J = 16.7, 9.7, 6.6 Hz, 1H), 5.15 – 5.04 (m, 2H), 3.81 (s, 3H), 3.37 – 3.31 (m, 2H).

Preparation of H_2L10

2-hydroxy-3-methoxy-5-nitro benzaldehyde (0.025 mol, 3.853 g) and 2-amino-5-nitrophenol (0.025 mol, 4.923 g) were dissolved in MeOH (5 mL). The suspension was refluxed for 1 h, during which time the orange solution had formed a deep orange precipitate. After cooling to room temperature, the solid was filtered off and washed with cold MeOH and Et_2O. The solid was dried in vacuo. Yield 95.69%. ^{1}H NMR (500 MHz, DMSO-d_6) δ 13.79 (s, 1H), 9.71 (s, 1H), 8.90 (s, 1H), 7.35 (d, J = 7.8 Hz, 1H), 7.11 (t, J = 7.8 Hz, 1H), 7.01 – 6.83 (m, 4H), 6.04 – 5.92 (m, 1H), 5.14 – 5.03 (m, 2H), 3.79 (d, J = 1.3 Hz, 3H); ^{13}C NMR (126 MHz, DMSO-d_6) δ 189.82, 149.55, 145.99, 142.88, 122.04, 118.73, 116.25, 111.63, 110.78, 109.12, 57.28, 40.61, 40.52, 40.44, 40.35, 40.27, 40.18, 40.10, 40.02, 39.94, 39.85, 39.68, 39.51.

Preparation of H_2L11

5-bromo-3-methoxy salilyldahyde (0.0125 mol, 2.333 g) and 2-amino-5-nitrophenol (0.0125 mol, 1.926 g) were dissolved in MeOH (5 mL). The suspension was refluxed for 1 h, during which time the orange solution had formed a red precipitate. After cooling to room temperature, the solid was filtered off and washed with cold MeOH and Et_2O. The solid was dried in vacuo. Yield 79%. ^{1}H NMR (500 MHz, DMSO-d_6) δ 13.16 (s, 1H), 10.76 (s, 1H), 8.98 (s, 1H), 7.81 – 7.73 (m, 2H),

7.55 – 7.47 (m, 2H), 7.25 (d, *J* = 2.3 Hz, 1H), 3.85 (s, 3H);^{13}C NMR (126 MHz, DMSO-d_6) δ 190.35, 150.67, 150.30, 145.99, 142.89, 121.73, 120.18, 118.73, 111.63, 110.89, 109.12, 57.07, 40.53, 40.45, 40.36, 40.29, 40.19, 40.12, 40.03, 39.95, 39.86, 39.69, 39.53.

Preparation of H_2L12

o-vanillin (0.01 mol, 1.541 g) and 2-amino-4-chloro-5-nitro phenol (0.01 mol, 1.541 g) were suspended in MeOH (5 mL). The suspension was refluxed for 1 h, during which time the dark brown solution had formed a grey precipitate. After cooling to room temperature, the solid was filtered off and washed with cold MeOH and Et_2O. The solid was dried in vacuo. Yield 76%. ^{1}H NMR (500 MHz, DMSO-d_6) δ 12.95 (s, 1H), 10.89 (s, 1H), 9.02 (s, 1H), 7.72 (s, 1H), 7.59 (s, 1H), 7.25 (dd, *J* = 7.9, 1.5 Hz, 1H), 7.16 (dd, *J* = 8.0, 1.5 Hz, 1H), 6.92 (t, *J* = 7.9 Hz, 1H), 3.82 (s, 3H), 2.49 (s, 3H); ^{13}C NMR (126 MHz, DMSO-d_6) δ 192.46, 142.07, 122.97, 120.62, 119.65, 119.11, 118.10, 113.68, 111.69, 109.99, 56.57, 56.42, 40.62, 40.53, 40.45, 40.36, 40.29, 40.20, 40.12, 40.03, 39.96, 39.86, 39.69, 39.53.

Preparation of H_2L13

2-hydroxy-3-methoxy-5-allyl-benzaldehyde (0.025 mol, 4.81 g) and 2-amino-4-chloro-5-nitro phenol (0.025 mol, 4.71 g) were dissolved in MeOH (4 mL). The suspension was refluxed for 1 h, during which time a cream brown solid precipitated. After cooling to room temperature, the solid was filtered off and washed with Et_2O and dried in vacuo. Yield 70%. ^{1}H NMR (500 MHz, DMSO-d_6) δ 12.70 (s, 1H), 10.86 (s, 1H), 8.97 (s, 1H), 7.71 (s, 1H), 7.59 (s, 1H), 7.06 (d, *J* = 2.0 Hz, 1H), 6.99 (d, *J* = 2.0 Hz, 1H), 5.98 (ddt, *J* = 16.7, 9.8, 6.6 Hz, 1H), 5.15 – 5.04 (m, 2H), 3.81 (s, 3H), 3.34 (d, *J* = 6.6 Hz, 2H); ^{13}C NMR (126 MHz, DMSO-d_6) δ 192.25, 149.64, 148.79, 145.41, 142.08, 137.90, 133.24, 131.18, 122.66, 120.71, 119.51, 118.56, 116.44, 113.68, 111.69, 56.56, 40.61, 40.52, 40.44, 40.35, 40.27, 40.19, 40.11, 40.02, 39.94, 39.85, 39.68, 39.52, 39.19.

Preparation of H_2L14

2-hydroxy-3-methoxy-5-nitro benzaldehyde (0.025 mol, 3.853 g) and 2-amino-4-chloro-5-nitro phenol (0.025 mol, 4.71 g) were dissolved in MeOH (4 mL). The suspension was refluxed for 1 h, during which time dark brow solid precipitated. After cooling to room temperature, the solid was filtered off and washed with Et_2O and dried in vacuo. Yield 80%. ^{1}H NMR (500 MHz, DMSO-d_6) δ 12.70 (s, 1H), 10.86 (s, 1H), 8.97 (s, 1H), 7.71 (s, 1H), 7.59 (s, 1H), 7.06 (d, *J* = 2.0 Hz, 1H), 6.99 (d, *J* = 2.0 Hz, 1H), 5.98 (ddt, *J* = 16.7, 9.8, 6.6 Hz, 1H), 5.15 – 5.04 (m, 2H), 3.81 (s, 3H), 3.34 (d, *J* = 6.6 Hz, 2H).

Preparation of H_2L15

5-bromo-3-methoxy saliyladehyde (0.0072 mol, 1.650 g) and 2-amino-4-chloro-5-nitro phenol were dissolved in MeOH (4 mL). The suspension as refluxed for 1 h, during which time orange-

red solid precipitated. After cooling to room temperature, the solid was filtered off and washed with Et_2O and dried in vacuo. Yield 35 %. ^{1}H NMR (500 MHz, DMSO-d_6) δ 12.85 – 12.80 (m, 2H), 10.91 (s, 2H), 8.97 (d, *J* = 1.4 Hz, 2H), 7.69 (d, *J* = 1.6 Hz, 2H), 7.59 (s, 2H), 7.48 (d, *J* = 2.2 Hz, 2H), 7.27 (d, *J* = 2.2 Hz, 2H), 3.85 (s, 6H), 3.29 (s, 2H), 3.19 – 3.14 (m, 1H); ^{13}C NMR (126 MHz, DMSO-d_6) δ 190.35, 164.19, 150.67, 150.30, 145.41, 142.07, 125.41, 124.07, 122.71, 121.73, 120.71, 120.17, 118.70, 113.68, 113.63, 111.69, 110.89, 57.06, 56.80, 40.62, 40.53, 40.45, 40.36, 40.28, 40.19, 40.12, 40.03, 39.94, 39.86, 39.69, 39.52.

Preparation of H_2L16

2-hydroxy-3-methoxy-5-allyl-benzaldehyde (0.025 mol, 4,81 g) and 3-amino-2-napthol (0.025 mol, 3.98 g) were dissolved in MeOH (5 mL). The suspension was refluxed for 1 h, during which time a dark red solid precipitated. After cooling to room temperature, the solid was filtered off and washed with cold MeOH and Et_2O. The solid was dried in vacuo. Yield 61%. ^{1}H NMR (500 MHz, Chloroform-*d*) δ 10.96 (s, 0H), 9.89 (d, *J* = 0.9 Hz, 0H), 8.80 (s, 1H), 7.77 (d, *J* = 8.2 Hz, 1H), 7.72 (d, *J* = 8.3 Hz, 1H), 7.55 (s, 1H), 7.47 – 7.30 (m, 4H), 7.23 (s, 0H), 7.02 – 6.92 (m, 2H), 6.88 (d, *J* = 1.6 Hz, 1H), 6.06 – 5.92 (m, 2H), 5.18 – 5.08 (m, 3H), 3.93 (d, *J* = 7.8 Hz, 4H), 3.39 (dd, *J* = 7.0, 5.0 Hz, 3H).

Preparation of H_2L18

5-bromo-3-methoxy salilcyldahyde (0.025 mol, 4.666 g) and 3-amino-2-napthol (0.025 mol, 3.98 g) were dissolved in MeOH (5 mL). The suspension was refluxed for 1 h, during which time a dark red solid precipitated. After cooling to room temperature, the solid was filtered off and washed with cold MeOH and Et_2O. The solid was dried in vacuo. Yield 79%. ^{1}H NMR (500 MHz, DMSO-d_6) δ 13.90 (s, 1H), 10.14 (s, 1H), 9.06 (s, 1H), 7.86 – 7.77 (m, 2H), 7.70 (d, *J* = 8.2 Hz, 1H), 7.50 – 7.45 (m, 1H), 7.39 (t, *J* = 7.5 Hz, 1H), 7.34 – 7.26 (m, 2H), 7.21 (dd, *J* = 2.2, 1.1 Hz, 1H), 3.85 (s, 3H); ^{13}C NMR (126 MHz, DMSO-d_6) δ 161.63, 128.11, 126.55 , 126.23 , 125.63 , 123.98 , 118.06 , 117.46 , 56.71 , 40.55 , 40.30 (d, *J* = 21.0 Hz).

Preparation of H_2L19

o-vanillin (0.025 mol, 3.35 g) and 2-amino-5-phenylphenol (0.025 mol,4.63 g) were dissolved in MeOH (5 mL). The suspension was refluxed for 1 h, during which time a dark orange solid precipitated. After cooling to room temperature, the solid was filtered off and washed with cold MeOH and Et_2O. The solid was dried in vacuo. Yield 91%. ^{1}H NMR (500 MHz, DMSO-d_6) δ 9.92 (s, 1H), 9.10 (d, *J* = 2.0 Hz, 1H), 7.72 – 7.65 (m, 3H), 7.50 – 7.27 (m, 4H), 7.21 (dt, *J* = 7.8, 1.4 Hz, 1H), 7.12 – 7.02 (m, 2H), 6.87 (tt, *J* = 7.8, 1.3 Hz, 1H), 3.84 – 3.80 (m, 3H), 3.17 (s, 1H), -1.96 (s, 0H); ^{13}C NMR (126 MHz, DMSO-d_6) δ 162.56 , 152.41 , 151.14 , 140.22 , 135.32 , 129.22 , 127.17 , 126.64 (d, *J* = 9.2 Hz), 124.37 , 119.77 , 118.39 , 118.05 , 117.39 , 115.83 , 56.37 , 40.55 , 40.38 , 40.21 , 40.05 .

Preparation of H_2L20

2-hydroxy-3-methoxy-5-allyl-benzaldehyde (0.025 mol, 4.8 1g) and 2-amino-5-phenylphenol (0.025 mol, 4.63 g) were dissolved in MeOH (5 mL). The suspension was refluxed for 1 h, during which time a dark orange solid precipitated. After cooling to room temperature, the solid was filtered off and washed with cold MeOH and Et_2O. The solid was dried in vacuo. Yield 69%. ^{1}H NMR (500 MHz, Chloroform-*d*) δ 10.96 (s, 0H), 8.76 (s, 1H), 7.61 – 7.51 (m, 2H), 7.49 – 7.41 (m, 2H), 7.40 – 7.30 (m, 2H), 7.27 (s, 1H), 7.12 (d, *J* = 8.3 Hz, 1H), 7.02 – 6.94 (m, 1H), 6.89 (dd, *J* = 21.8, 1.9 Hz, 2H), 5.99 (ddt, *J* = 17.4, 9.2, 6.7 Hz, 1H), 5.13 (ddq, *J* = 12.9, 4.1, 1.9 Hz, 2H), 3.93 (d, *J* = 6.5 Hz, 3H), 3.39 (d, *J* = 6.6 Hz, 2H).

Preparation of H_2L22

5-bromo-3-methoxy salilcyldahyde (0.025 mol, 4.666 g) and 2-amino-5-phenylphenol (0.025 mol, 4.63 g) were dissolved in MeOH (5 mL). The suspension was refluxed for 1 h, during which time a dark orange solid precipitated. After cooling to room temperature, the solid was filtered off and washed with cold MeOH and Et_2O. The solid was dried in vacuo. Yield 83%. ^{1}H NMR (500 MHz, DMSO-d_6) δ 10.03 (s, 1H), 9.10 (s, 1H), 7.74 – 7.65 (m, 3H), 7.50 – 7.39 (m, 4H), 7.35 – 7.27 (m, 1H), 7.18 (d, *J* = 2.3 Hz, 1H), 7.06 (d, *J* = 8.4 Hz, 1H), 4.07 (p, *J* = 5.1, 4.3 Hz, 1H), 3.84 (s, 3H), 3.20 – 3.15 (m, 2H); ^{13}C NMR (126 MHz, DMSO-d_6) δ 160.71 , 152.98 , 151.11 , 150.14 , 140.11 , 134.39 , 132.31 , 129.24 , 127.24 , 126.97 , 126.65 , 125.73 , 120.46 , 117.82 , 117.45 , 56.67 , 40.46 (d, *J* = 21.1 Hz), 40.21 .

Preparation of H_2L23 – Only synthesised *in situ*

Preparation of H_2L24

o-vanillin (6.5 mmol, 1 g) and 2-amino-3-hydroxy-pyridine (6.5 mmol,0.72 g) were refluxed in MeOH (25 mL) for 2 h. The cloudy orange solution was filtered and the bright orange precipitate collected. The precipitate was washed with cold MeOH (15 mL x 3) and Et_2O (15 mL x 3). The solid was dried in vacuo. Yield 81%. ^{1}H NMR (500 MHz, Chloroform-*d*) δ 9.45 (s, 1H), 8.09 – 8.04 (m, 1H), 7.39 (s, 1H), 7.22 – 7.13 (m, 2H), 7.03 (d, *J* = 7.9 Hz, 1H), 6.90 (t, *J* = 7.9 Hz, 1H), 3.94 (s, 3H), 1.29 – 1.24 (m, 0H).

Preparation of H_2L25

5-allyl-2-hydroxy-3-methoxy-benzaldehyde (5.2 mmol, 1 g) and 2-amino-3-hydroxy-pyridine (5.2 mmol, 0.57 g) were refluxed in MeOH (25 mL) for 2 h. The cloudy orange solution was filtered and the bright orange precipitate collected. The precipitate was washed with cold MeOH (15 mL x 3) and Et_2O (15 mL x 3). The solid was dried in vacuo. Yield 81%. ^{1}H NMR (500 MHz, Chloroform-*d*) δ 9.25 (s, 1H), 7.95 (s, 1H), 7.37 (s, 1H), 7.27 (d, *J* = 1.1 Hz, 1H), 7.12 (s, 1H),

6.88 – 6.84 (m, 1H), 6.76 (s, 1H), 5.97 (dq, *J* = 16.4, 7.2 Hz, 1H), 5.16 – 5.08 (m, 2H), 3.91 – 3.81 (m, 19H), 3.36 – 3.30 (m, 2H).

Preparation of H_2L26

5-bromo-2-hydroxy-3-methoxy-benzaldehyde (4.3 mmol, 1 g) and 2-amino-3-hydroxy-pyridine (4.3 mmol, 0.47 g) were refluxed in MeOH (25 mL) for 2 h. The cloudy orange solution was filtered and the bright orange precipitate collected. The precipitate was washed with cold MeOH (15 mL x 3) and Et_2O (15 mL x 3). The solid was dried in vacuo. Yield 81%.

Preparation of H_2L27

o-vanillin (6.5 mmol, 1 g) and 4-*tert*-butyl-2-amino-phenol (6.5 mmol, 1.07 g) were refluxed in MeOH (25 mL) for 2 h. The cloudy orange solution was filtered and the bright orange precipitate collected. The precipitate was washed with cold MeOH (15 mL x 3) and Et_2O (15 mL x 3). The solid was dried in vacuo. Yield 71%. ^{1}H NMR (500 MHz, Chloroform-*d*) δ 13.08 (s, 1H), 8.67 (s, 1H), 7.27 – 7.21 (m, 1H), 7.16 (d, *J* = 2.3 Hz, 1H), 7.07 – 6.95 (m, 3H), 6.88 (t, *J* = 7.8 Hz, 1H), 3.89 (s, 3H), 1.35 (s, 9H). ^{13}C NMR (126 MHz, $CDCl_3$) δ 162.47, 151.69, 148.59, 147.64, 143.97, 134.38, 125.70, 123.92, 119.24, 118.69, 115.72, 115.16, 115.10, 77.32, 77.06, 76.81, 56.15, 34.36, 31.52.

Preparation of H_2L28

5-allyl-2-hydroxy-3-methoxy-benzaldehyde (5.2 mmol, 1 g) and 4-*tert*-butyl-2-amino-phenol (5.2 mmol, 0.86 g) were refluxed in MeOH (25 mL) for 2 h. The cloudy orange solution was filtered and the bright orange precipitate collected. The precipitate was washed with cold MeOH (15 mL x 3) and Et_2O (15 mL x 3). The solid was dried in vacuo Yield 81%. ^{1}H NMR (500 MHz, Chloroform-*d*) δ 8.66 (s, 1H), 7.25 (dd, *J* = 8.5, 2.3 Hz, 1H), 7.15 (d, *J* = 2.2 Hz, 1H), 6.97 (d, *J* = 8.5 Hz, 1H), 6.90 (d, *J* = 1.8 Hz, 1H), 6.86 – 6.82 (m, 1H), 5.99 (ddt, *J* = 17.6, 9.6, 6.6 Hz, 1H), 5.17 – 5.09 (m, 2H), 3.91 (s, 3H), 3.38 (d, *J* = 6.5 Hz, 2H), 1.34 (s, 8H), 1.26 (s, 1H). ^{13}C NMR (126 MHz, $CDCl_3$) δ 162.79, 149.52, 148.40, 147.62, 144.01, 137.20, 134.69, 130.60, 125.68, 123.27, 119.00, 116.09, 115.92, 115.54, 115.07, 109.99, 77.28, 77.02, 76.77, 56.21, 39.58, 34.36, 31.52.

Preparation of H_2L29

5-bromo-2-hydroxy-3-methoxy-benzaldehyde (4.3 mmol, 1 g) and 4--*tert*-butyl -2-amino-phenol (4.3 mmol, 0.71 g) were refluxed in MeOH (25 mL) for 2 h. The cloudy orange solution was filtered and the bright orange precipitate collected. The precipitate was washed with cold MeOH (15 mL x 3) and Et_2O (15 mL x 3). The solid was dried in vacuo. Yield 86%. ^{1}H NMR (500 MHz, Chloroform-*d*) δ 12.95 (s, 1H), 8.62 (s, 1H), 7.27 (d, *J* = 4.0 Hz, 1H), 7.22 (s, 1H), 7.17 – 7.13 (m, 1H), 7.07 (s, 1H), 6.97 (s, 1H), 5.90 (s, 1H), 3.93 (s, 3H), 1.63 (s, 2H), 1.34 (s, 9H).

11.3 Synthetic protocols for PCCs

Supporting Figures for TGA, FT-IR and ESI-MS are found in Appendix B.

Preparation of $[Zn^{II}_2Ln^{III}_2(L1)_4(EtOH)_4](ClO_4)_2$ (1-3)

To a solution of H_2**L1** (48.2 mg, 0.2 mmol) in EtOH (20 mL), $Zn(ClO_4)_2{\cdot}6H_2O$ (74 mg, 0.2 mmol) and $Ln(OTf)_3$ (61 mg, 0.1 mmol) were added and the resultant solution was stirred for 5 min, Et_3N (62 µL, 0.45 mmol) was added and the mixture was stirred for a further 1 h. The resulting cloudy yellow solution was filtered and allowed to stand at room temperature. After 4 days, small yellow crystals were obtained with yields in the range of 52% based on Zn. For **1**, CHN $[Zn^{II}_2Dy^{III}_2(\mathbf{L1})_4(EtOH)_6](ClO_4)_2$ observed: C-43.19%, H-4.06%, N-2.79%; expected: C-43.08%, H-4.26%, N-2.96%. For **2** CHN $[Zn^{II}_2Tb^{III}_2(\mathbf{L1})_4(EtOH)_6](ClO_4)_2$ observed: C-43.21%, H-4.44%, N-3.04%; expected: C-43.30%, H-4.28%, N-2.97%. For **3** CHN $[Zn^{II}_2Eu^{III}_2(\mathbf{L1})_4(EtOH)_6](ClO_4)_2$ observed: C-43.53%, H-4.26%, N-2.92%; expected: C-43.59%, H-4.31%, N-2.99%.

Preparation of $[Zn^{II}_5Ln^{III}(L1)_6(OH)(H_2O)]$ (4-6)

To a solution of H_2**L1** (48.2 mg, 0.2 mmol) in MeCN (20 mL), $LnCl_3{\cdot}xH_2O$ (37 mg, 0.1 mmol) and $ZnCl_2$ (27.2 mg, 0.2 mmol) were added and the mixture was stirred for 5 min, Et_3N (62 µL, 0.45 mmol) was added and the mixture stirred for a further 1 h. The resulting cloudy yellow solution was filtered and allow to stand at room temperature. After 3 days, small yellow crystals were collected with yields in the range of 67% based on Zn. CHN for (**4**) $[Zn^{II}_5Dy^{III}(\mathbf{L1})_6(OH)(H_2O)]$ observed: C-51.32%, H-3.41%, N-4.19%; expected C-51.29%, H-3.53%, N-4.27%. For **5** $[Zn^{II}_5Tb^{III}(\mathbf{L1})_6(OH)(H_2O)]$ observed: C-51.41%, H-3.50%, N-4.35%; expected C-51.29%, H-3.53%, N-4.27%. For **6** $[Zn^{II}_5Eu^{III}(\mathbf{L1})_6(OH)(H_2O)]$ observed: C-51.45%, H-3.60%, N-4.14%; expected C-51.58%, H-3.55%, N-4.29%**.**

Preparation of $[Zn^{II}_4Ln^{III}_2(OH)_2(L2)_4(OAc)_2(NO_3)_2(DMF)_3]{\cdot}DMF$ (7-9)

To a solution of H_2**L2** (52 mg, 0.2 mmol) in DMF (10 mL), $Ln(NO_3)_3{\cdot}5H_2O$ (44 mg, 0.1 mmol), $Zn(CH_3CO_2)_2{\cdot}4H_2O$ (45 mg, 0.2 mmol) and Et_3N (62 µL, 0.45 mmol) were added and the solution was stirred for 1h. The clear yellow solution was filtered and underwent VD with Et_2O. After 7 days, yellow needle-like crystals were obtained with yields of 44%. CHN for $[Zn^{II}_4Dy^{III}_2(OH)_2(\mathbf{L2})_4(OAc)_2(NO_3)_2(DMF)_3]{\cdot}DMF$ (**7**) observed: C-45.41%, H-3.86%, N-6.19%; expected C-45.59%, H-3.83%, N-6.05%. For $[Zn^{II}_4Tb^{III}_2(OH)_2(\mathbf{L2})_4(OAc)_2(NO_3)_2(DMF)_3]{\cdot}DMF$ (**8**) observed: C-45.67%, H-3.79%, N-6.11%; expected C-45.79%, H- 3.85%, N-6..07%. For $[Zn^{II}_4Eu^{III}_2(OH)_2(\mathbf{L2})_4(OAc)_2(NO_3)_2(DMF)_3]{\cdot}DMF$ (**9**) observed: C-45.99%, H-3.90%, N-6.15%; expected C-46.03%, H- 3.86%, N-6.10%.

Preparation of $[Zn^{II}_2Ln^{III}_2(L3)_2(CO_3)_2(NO_3)_2(CH_3OH)_2]$ (10-12)

To a solution of H_3**L3** (71.6 mg, 0.1 mmol) in MeOH (20 mL), Et_3N (61.5 µL, 0.45 mmol) was added and the solution was stirred for 10 min. $Ln(NO_3)_3{\cdot}5H_2O$ (44 mg, 0.1 mmol) and

$Zn(NO_3)_2 \cdot 6H_2O$ (58 mg, 0.2 mmol) were added and the resultant solution was stirred for a further 40 min. The clear yellow solution was filtered and left to stand at room temperature. After 5 days, small yellow crystals were obtained with a yield of 80% based on Zn. CHN for (**10**) $[Zn^{II}_2Dy^{III}_2(\mathbf{L3})_2(CO_3)_2(NO_3)_2(CH_3OH)_2]$ observed C-34.89%, H-3.16%; N-5.88%; expected C-34.95%, H-3.21%, N-5.83%. For (**11**) $[Zn^{II}_2Tb^{III}_2(\mathbf{L3})_2(CO_3)_2(NO_3)_2(CH_3OH)_2]$ observed C-35.21%, H-3.34%; N-5.81%; expected C-35.19%, H-3.23%, N-5.86%. For (**12**) $[Zn^{II}_2Eu^{III}_2(\mathbf{L3})_2(CO_3)_2(NO_3)_2(CH_3OH)_2]$ observed C-34.55%, H-3.24%; N-5.89%; expected C-35.49%, H-3.26%, N-5.91%.

Preparation of 13 and 14 (mixed product)

To a solution of H_2**L1** (48 mg, 0.2 mmol) in EtOH/THF (1:1 10 mL), $Dy(Cl)_3 \cdot xH_2O$ (35 mg, 0.1 mmol), $ZnCl_2$ (24 mg, 0.2 mmol) and Et_3N (62 µL, 0.45 mmol) were added and the solution was stirred for 1 h. The clear yellow solution was filtered and left for SE. After 9 days, a mixture of crystals of **13** and **14** were identified.

Preparation of $[Co^{II}_4Ln^{III}_2(\mu_3\text{-}OH)_2(L1)_4Cl_2(NO_3)_2(MeOH)_4]\cdot 3(Et_2O)$ (15-18)

H_2**L1** (48 mg, 0.2 mmol) was suspended in a mixture of CH_2Cl_2 (10 mL) and MeOH (5 mL) and stirred for 5 min before the addition of $Co(NO_3)_2 \cdot 6\ H_2O$ (58 mg, 0.2 mmol), $LnCl_3 \cdot xH_2O$ (37 mg ,0.1 mmol) and Et_3N (0.42 mmol, 59.2 µL). The resultant solution was stirred for 2 h, upon which time it was filtered and the filtrate underwent vapor diffusion with Et_2O. After 9 d small red crystals were collected with a yield of 68% based on Gd. IR: ν ˜ = 3293, 1782, 1609, 1552, 1454, 1388, 1291, 1224, 1182, 1073, 1033, 964, 820, 733, 635 cm^{-1}. CHN for (**15**) $[Co^{II}_4Y^{III}_2(\mu_3\text{-}OH)_2(\mathbf{L1})_4Cl_2(NO_3)_2(MeOH)_4]$ observed C-41.48%, H-3.59%; N-4.83%; expected C-41.53%, H-3.60%, N-4.85%. CHN for (**16**) $[Co^{II}_4Y^{III}_2(\mu_3\text{-}OH)_2(\mathbf{L1})_4Cl_2(NO_3)_2(MeOH)_4]$ observed C-38.41%, H-3.30%; N-4.52%; expected C-38.46%, H-3.34%, N-4.49%. CHN for (**17**) $[Co^{II}_4Dy^{III}_2(\mu_3\text{-}OH)_2(\mathbf{L1})_4Cl_2(NO_3)_2(MeOH)_4]$ observed C-38.25%, H-3.41%; N-4.39%; expected C-38.22%, H-3.32%, N-4.46%. CHN for (**18**) $[Co^{II}_4Tb^{III}_2(\mu_3\text{-}OH)_2(\mathbf{L1})_4Cl_2(NO_3)_2(MeOH)_4]$ observed C-38.41%, H-3.39%; N-4.45%; expected C-38.42%, H-3.33%, N-4.48%.

Preparation of $[Co^{II}_4Dy^{III}_2(\mu_3\text{-}OH)_2(L5)_4Cl_2(NO_3)_2(MeOH)_4]\cdot 3(Et_2O)$ (19)

H_2**L1** (48 mg, 0.2 mmol) was suspended in a mixture of CH_2Cl_2 (10 mL) and MeOH (5 mL) and stirred for 5 min before the addition of $Co(NO_3)_2 \cdot 6H_2O$ (58 mg, 0.2 mmol), $DyCl_3 \cdot xH_2O$ (37 mg,0.1 mmol), and Et_3N (0.42 mmol, 59.2 µL). The resultant solution was stirred for 2 h, upon which time it was filtered and the filtrate underwent vapor diffusion with Et_2O. After 9 days small red crystals were collected with a yield of 68% based on Dy. IR: ν ˜ = ˜ 3290, 1605, 1551, 1452, 1389, 1295, 1228, 1183, 1076, 1035, 965, 819, 735, 638 cm^{-1}. CHN for (**18**) $[Co^{II}_4Dy^{III}_2(\mu_3\text{-}OH)_2(\mathbf{L5})_4Cl_2(NO_3)_2(MeOH)_4]$ observed C-32.59%, H-3.11%; N-3.77%; expected C-32.67%, H-3.02%, N-3.81%.

Preparation of $[Co^{II}_3Ln^{III}_4(\mu_3\text{-}OH)_6(L4)_6(CF_3SO_3)](CF_3SO_3)_5$ (20-21)

$Ln(OTf)_3$ (0.2 mmol), $Co(NO_3)_2{\cdot}6H_2O$ (0.1 mmol, 58 mg), H**L1** (0.2 mmol, 34 mg) and Et_3N (1.2 mmol, 26.8 μL) were refluxed for 2 h in EtOH (20 mL). The reaction mixture was subsequently cooled and filtered. The filtrate was left for SE between 4-8 days before green crystals suitable for single-crystal XRD data were collected. These were dried overnight. CHN for (**20**) $[Co^{II}_3Gd^{III}_4(\mu_3\text{-}OH)_6(\mathbf{L4})_6(CF_3SO_3)](CF_3SO_3)_5$ (expected) C-37.68%, H-3.01%, N-6.60% (observed) C-37.59%, H.3.04%, N-6.71%. CHN for (**21**) $[Co^{II}_3Y^{III}_4(\mu_3\text{-}OH)_6(\mathbf{L4})_6(CF_3SO_3)](CF_3SO_3)_5$ (expected) C-40.62%, H-3.24%, N-7.11% (observed) C-40.71%, H-3.33%, N-7.21%.

Preparation of $[Ni^{II}_3Ln^{III}_4(\mu_3\text{-}OH)_6(L4)_6(CF_3SO_3)](CF_3SO_3)_5$ (22-24)

$Ln(OTf)_3$ (0.2 mmol), $Ni(NO_3)_2.6H_2O$ (0.1 mmol, 58 mg), H**L1** (0.2 mmol, 34 mg) and Et_3N (1.2 mmol, 26.8 μL) were refluxed for 2 h in EtOH (20 mL). The reaction mixture was subsequently cooled and filtered. The filtrate was left for SE between 4-8 days before green crystals suitable for single-crystal XRD data were collected. These were dried overnight. CHN for (**23**) $[Ni^{II}_3Gd^{III}_4(\mu_3\text{-}OH)_6(\mathbf{L4})_6(CF_3SO_3)](CF_3SO_3)_5$ (expected) C-37.71%, H-3.01%, N-6.60% (observed) C-37.82%, H-2.98%, N-6.55%; CHN for (**22**) $[Ni^{II}_3Dy^{III}_4(\mu_3\text{-}OH)_6(\mathbf{L4})_6(CF_3SO_3)](CF_3SO_3)_5$ (expected) C-37.47%, H-2.99%, N-6.56% (observed) C-37.50%, H-3.09%, N-6.46% .CHN for (**24**) $[Ni^{II}_3Y^{III}_4(\mu_3\text{-}OH)_6(\mathbf{L4})_6(CF_3SO_3)](CF_3SO_3)_5$ (expected) C-40.66%, H-3.24%, N-7.12% (observed) C-40.59%, H-3.23%, N-7.15%.

Preparation of $(Et_3NH)[Co^{III}(L8)_2]{\cdot}3MeOH$ (25·3MeOH)

H_2**L8** (0.2 mmol, 56 mg) was suspended in a methanolic solution (20 mL), to which $Co(ClO_4)_2{\cdot}6H_2O$ (0.1 mmol), $Dy(OTf)_3$ (0.1 mmol, 61 mg) and Et_3N (0.5 mmol, 69μL) was added. The resultant solution was stirred for 1 h and on completion filtered. The filtrate was left for SE and after 3 days dark red crystals formed.

Preparation of $(Et_3NH)[Co^{III}(L18)_2]$ [26·2MeOH]

H_2L18 (0.2 mmol, 74 mg) was suspended in a methanolic solution (20 mL), to which $Co(ClO_4)_2{\cdot}6H_2O$ (0.1 mmol), $Dy(OTf)_3$ (0.1 mmol, 61 mg) and Et_3N (0.5 mmol, 69 μL) was added. The resultant solution was stirred for 1 h and on completion filtered. The filtrate was left for SE and after 6 days dark red crystals formed.

Preparation of $[Ni^{II}_2Dy^{III}_2(L20)_4(\text{allyl-o-vanillin})_2(EtOH)_2]{\cdot}3CH_2Cl_2$ [27·3CH_2Cl_2]

H_2**L20** (0.2 mmol, 72 mg) was suspended in EtOH (10 mL) and Et_3N (0.5 mmol, 69 μL) was immediately added. The solution was left to stir and $Ni(ClO_4)_2{\cdot}6H_2O$ (0.1 mmol, 37 mg) and $Dy(Of)_3$ (0.1 mmol, 61 mg) were added after 5 min. The resultant solution was refluxed for 1 h, before CH_2Cl_2 (5 mL) was added and left for SE. After 3 days' brown, block-like crystals had formed.

Preparation of $[Ni^{II}_2Dy^{III}_2(L20)_4(DMF)_6](ClO_4)_2\cdot4DMF$ [28·4DMF]

H_2**L20** (0.2 mmol, 72 mg), $Ni(ClO_4)_2\cdot6H_2O$ (0.1 mmol, 37 mg), $Dy(OTf)_3$ (0. 1mmol, 61 mg) and Et_3N (0.5 mmol, 69 μL) were added to DMF (10 mL) and left to stir for 1 h. The solution was filtered and filtrate underwent VD with Et_2O. After 7 days large brown crystals were formed.

Preparation of $[Ni^{II}_2Dy^{III}_2(L22)_4(bromo\text{-}o\text{-}vanillin)_2(EtOH)_2]\cdot6EtOH$ [29·6EtOH]

H_2**L22** (0.2 mmol, 80 mg) was suspended in EtOH (15 mL) and Et_3N (0.5 mmol, 69 μL) was immediately added. The solution was left to stir and $Ni(ClO_4)_2\cdot6H_2O$ (0.1 mmol, 37 mg) and $Dy(OTf)_3$ (0.1 mmol, 61 mg) were added after 5 min. The resultant solution was stirred for 1 h, before THF (5 mL) was added and left for SE. After 5 days brown, block-like crystals had formed.

Preparation of $[Ni^{II}_2Dy^{III}_2(L16)_4(allyl\text{-}o\text{-}vanillin)_2(EtOH)_2]\cdot2THF\cdot2EtOH$ [30·2THF·2EtOH]

H_2**L16** (0.2 mmol, 66 mg), $Ni(ClO_4)_2\cdot6H_2O$ (0.1 mmol, 37 mg), $Dy(OTf)_3$ (0.1 mmol, 61 mg) and Et_3N **(**0.5 mmol, 69 μL) were added to a mixture a 1:1 of CH_2Cl_2 and THF (20 mL). The reaction mixture was stirred for 1 h and on completion filtered. The filtrate was left for 6 days after which time small red block crystals had formed.

Preparation of $[Ni^{II}_2Dy^{III}_2(L16)_4(DMF)_2](ClO_4)_2$ [31]

H_2**L16** (0.2 mmol, 66 mg), $Ni(ClO_4)_2\cdot6H_2O$ (0.1 mmol, 37 mg), $Dy(OTf)_3$ (0.1 mmol, 61 mg) and Et_3N (0.5 mmol, 69 μL) were added to DMF (10 mL) and left to stir for 1 h. The solution was filtered and filtrate underwent VD with Et_2O. After 9 days, large brown cuboid crystals were formed.

Preparation of $[Ni^{II}_2Dy^{III}_2(L1)_4(EtOH)_4(H_2O)_2](ClO_4)_2$ (32)

H_2**L1** (0.6 mmol, 144 mg), $Ni(ClO_4)_2\cdot6H_2O$ (0.3 mmol, 111 mg), $Dy(OTf)_3$ (0.3 mmol, 183 mg) and Et_3N (1.5 mmol, 205.5 μL) were added to EtOH (20 mL) and left to stir for 1 h. The solution was filtered and left for SE. After 5 days' brown needle-like crystals had formed.

Preparation of $[Ni^{II}_2Dy^{III}_2(L1)_4(DMF)_6]\ (OTf_3)_2\cdot2DMF$ (33·2DMF)

H_2**L1** (0.6 mmol, 144 mg), $Ni(ClO_4)_2\cdot6H_2O$ (0.3 mmol, 111 mg), $Dy(OTf)_3$ (0.3 mmol, 183 mg) and Et_3N (1.5 mmol, 205.5 μL) were added to DMF (10 mL) and left to stir for 1 h. The solution was filtered and underwent VD with Et_2O. After 3 days' brown block-like crystals had formed.

Preparation of $[Ni^{II}_2Dy^{III}_2(L18)_4(DMF)_4(H_2O)_2](ClO_4)_4\cdot5DMF$ (34·5DMF).

H_2**L18** (0.2 mmol, 74 mg), $Ni(ClO_4)_2\cdot6H_2O$ (0.1 mmol, 37 mg), $Dy(OTf)_3$ (0.1 mmol, 61 mg) and an excess of Et_3N were added to DMF(10 mL) and left to sir for 1 h. The solution was filtered and underwent VD with Et_2O. After 2 weeks, light brown crystals were formed.

Preparation of $[Ni^{II}_4(L2)_4(MeOH)_4]\cdot 6MeOH$ (35·6MeOH)

H_2**L2** (0.1 mmol, 58 mg), $Ni(ClO_4)_2\cdot 6H_2O$ (0.1 mmol, 37 mg), $Dy(OTf_3)_3$ (0.1 mmol, 61 mg) and Et_3N (0.5 mmol) were suspended in methanol forming a light-yellow solution. The solution was stirred for 1 h before being filtered and the filtrate left for SE. After 2 days' light green crystals were collected.

Preparation of $[Ni^{II}_2Dy^{III}_2(L2)_4(EtOH)_6](ClO_4)_2\cdot 4EtOH$ (36·4EtOH)

H_2**L2** (0.2 mmol, 58 mg), $Ni(ClO_4)_2\cdot 6H_2O$ (0.1 mmol, 37 mg), $Dy(OTf)_3$ (0.1 mmol, 61 mg) and Et_3N (0.5 mmol, 69 μL) were added to EtOH (20 mL) and left to stir for 1 h. The solution was filtered and left for SE. After 13 days' brown cuboid crystals were formed.

Preparation of $[Ni^{II}_2Dy^{III}_2(L19)_4(DMF)_6](ClO_4)_2\cdot 2Et_2O$ (37·2Et_2O)

H_2**L19** (0.2 mmol, 64 mg), $Ni(ClO_4)_2\cdot 6H_2O$ (0.1 mmol, 37 mg), $Dy(OTf)_3$ (0.1 mmol, 61 mg) and Et_3N (0.5 mmol, 69 μL) were added to DMF (10 mL) and left to stir for 1 h. The solution was filtered and the filtrate underwent VD with Et_2O. After 4 days, brown cuboid crystals were formed.

Preparation of $[Ni^{II}_2Dy^{III}_2(L1)_4(OAc)_2(MeOH)_2]\cdot 2MeOH$ (38·2MeOH)

H_2**L1** (0.1 mmol, 25 mg), $Dy(OTf)_3$ (122 mg, 0.2 mmol) and Et_3N (27.6 μL) were added to MeOH (20 mL) and left to stir for 20 min. $Ni(OAc)_2\cdot 4H_2O$ (0.1 mmol, 25 mg) was added at the end of this time and left to stir for a further 20 min. The solution was filtered and left for SE. Small rectangular black crystals formed after 3 days.

Preparation of $[Co^{II}_2Dy^{III}_2(L9)_4(M1)_2(DMF)_2]$ (39)

H_2**L9** (0.25 mmol, 65 mg) and 3,5-dinirtobenzoic acid (0.5 mmol,) was suspended in DMF (10 mL) to form a cloudy brown solution. Upon addition of $Co(ClO_4)_2.6H_2O$ (0.1 mmol, 37 mg), $Dy(OTf_3)_3$ (0.1 mmol, 61 mg) and Et_3N (0.9 mmol, 121 μL) the solution became a clear porter red. The solution was stirred for 1 h and upon completion filtered. The filtrate underwent VD with Et_2O and after 2 weeks large dark red crystals were collected.

Preparation of $[Co^{II}_2Dy^{III}_2(L9)_4(M2)_2(DMF)_2]\cdot 2DMF$ (40·2DMF),

H_2**L9** (0.25 mmol, 85 mg) and 3-nirtobenzoic acid (0.5 mmol) were suspended in DMF (10 mL) to form a cloudy brown solution. Upon addition of $Co(ClO_4)_2\cdot 6H_2O$ (0.1 mmol, 37 mg), $Dy(OTf_3)_3$ (0.1 mmol, 61 mg) and Et_3N (0.9 mmol, 121 μL) the solution became a clear porter red. The solution was stirred for 1 h and upon completion filtered. The filtrate underwent VD with Et_2O and after 2 weeks large dark red crystals were collected.

Preparation of $[Dy^{III}(M1)_3(DMF)_2]$ (20)

H_2**L9** (0.25 mmol, 85 mg) and 3,5-dinirtobenzoic acid (0.5 mmol) were suspended in DMF (10 mL) to form a cloudy brown solution. Upon addition of $Co(ClO_4)_2\cdot 6H_2O$ (0.1 mmol, 37 mg),

$Dy(OTf_3)_3$ (0. 1mmol, 61 mg) and Et_3N (0.9 mmol, 121 µL) the solution became a clear porter red. The solution was stirred for 1 h and upon completion filtered. The filtrate underwent VD with Et_2O and after 3 days' clear needle-like crystals were collected.

Preparation of $[Ni^{II}_2Dy^{III}_2(OH)(L2)_3(M1)_3(DMF)_2]\cdot1.5DMF\cdot Et_2O$ (42·1.5DMF·Et_2O)

H_2**L2** (0.2 mmol, 58 mg), $Ni(ClO_4)_2\cdot6H_2O$ (0.1 mmol, 37 mg), $Dy(OTf)_3$ (0.1 mmol, 61 mg), 3,5 -dintrobenzoic acid (0.5 mmol, 70 mg) and Et_3N (0.5 mmol, 69 µL) were added to DMF(10 mL) and left to stir for 1 h. The solution was filtered and underwent VD with Et_2O. After 8 days, black small cube crystals were formed.

Preparation of $[Zn^{II}_4Ln^{III}_{11}(\mu_4\text{-}OH)_2(\mu_3\text{-}OH)_8(\mu_2\text{-}OH_2)_2(\mu_3\text{-}NO_3)_2(NO_3)_6Cl_4(HL23)_2(L23')_4(\mu_2\text{-}MeO)_7(\mu_3\text{-}MeO)_2(MeOH)_2(H_2O)_2]$ (43-44)

O-vanillin (0.2 mmol) and *trans*-2-amino-cyclohexanol (0.2 mmol) were stirred in MeOH (20 mL) for 2 h to form a clear light-yellow solution. $LnCl_3\cdot5H_2O$ (0.1 mmol) and $Zn(NO_3)_2\cdot6H_2O$ (0.2 mmol, 56 mg) were subsequently added with Et_3N (0.45 mmol, 61 µL). The solution was stirred for a further 1 h upon which the solution had become colourless. The solution was filtered and the filtrate left for SE. After 13-27 days' colourless needle like crystals were collected. **43** (15%), **44** (21%) based on Ln^{III}. CHN for $C_{80}H_{135}Cl_4Dy_{11}N_{10}O_{70}Zn_4$ (**43**) (expected) C-21.08%, H-2.99, N-3.07% (observed) C-20.95%, H-3.27%, N-3.11%. CHN for $C_{80}H_{135}Cl_4Gd_{11}N_{10}O_{70}Zn_4$ (**44**) (expected) C-21.39%, H-3.03, N-3.12% (observed) C-21.52%, H-2.88%, N-3.00%.

Preparation of $[Ni^{II}_2Dy^{III}_2(L1)_4(EtOH)_6](ClO_4)_2\cdot2EtOH$(1NiDy-$ClO_4$)

$Dy(OTf)_3\cdot xH_2O$ (61 mg, 0.1 mmol), $Ni(ClO_4)_2\cdot6H_2O$ (37 mg, 0.1 mmol), H_2**L1** (48 mg, 0.2 mmol) and Et_3N (69 µl, 0.5 mmol) were added in EtOH (20 mL), and the resulting mixture was stirred for 1 hour. After filtration, yellow-greenish crystals were obtained in 49 % yield and collected by filtration, washed with Et_2O and dried in air.

Preparation of $[Co^{II}_2Dy^{III}_2(L1)_4(EtOH)_6](ClO_4)_2\cdot2EtOH$ (1CoDy-ClO_4)

$Dy(OTf)_3\cdot xH_2O$ (61 mg, 0.1 mmol), $Co(ClO_4)_2\cdot6H_2O$ (37 mg, 0.1 mmol), H_2**L1** (48 mg, 0.2 mmol) and Et_3N (69 µl, 0.5 mmol) were added in EtOH (20 mL), and the resulting mixture was stirred for 1 hour. After filtration, orange crystals were obtained in 57 % yield and collected by filtration, washed with Et_2O and dried in air.

Preparation of $[Ni_2Ln_2(L1)_4Cl_2(CH_3CN)_2]\cdot2CH_3CN$ (1NiLn-Cl)

To a solution of acetonitrile (20 mL), H_2**L1** (0.2 mmol, 48 mg) and Et_3N (0.5 mmol, 69 µL) were added and stirred for 10 min. On completion, $NiCl_2\cdot6H_2O$ (0.1 mmol, 24 mg) and $LnCl_3\cdot xH_2O$ (0.1 mmol) (Ln = Y, Sm, Eu, Gd, Tb, Dy) were added and the resultant solution was heated under reflux for 2 h. In this time the clear yellow solutions precipitated and on completion were left to cool where a green precipitate settled. The solution was filtered and washed with cold MeCN (20

mL) and Et_2O (10 mL). The precipitate (**1NiLn-Cl**) was then collected and dried overnight at 60 °C. Yield = 69 - 95% based on Ln for **1NiLn-Cl**. Elemental analysis for $[Ni_2Dy_2(C_{14}H_{11}NO_3)_4Cl_2(CH_3CN)_2]$ (**1NiDy-Cl**): expected C-46.55%, H-3.23%, N-5.38%; found C-46.84%, H-3.21%, N-5.16%. Elemental analysis for $[Ni_2Y_2(C_{14}H_{11}NO_3)_4Cl_2(CH_3CN)_2]$ (**1NiY-Cl**): C-51.06%, H-3.57%, N-5.95%.; found C-51.32%, H-3.51%, N-6.09%. Elemental analysis for $[Ni_2Gd_2(C_{14}H_{11}NO_3)_4Cl_2(CH_3CN)_2]$ (**1NiGd-Cl**): C-46.15%, H-3.25%, N-5.42%; found C-46.51%, H-3.18%, N-4.82%. Elemental analysis for $[Ni_2Eu_2(C_{14}H_{11}NO_3)_4Cl_2(CH_3CN)_2]$ (**1NiEu-Cl**): C-46.81%, H-3.47%, N-5.46%.; found C-47.08%, H-3.79%, N-5.52%. Elemental analysis for $[Ni_2Tb_2(C_{14}H_{11}NO_3)_4\text{-}Cl_2(CH_3CN)_2]$ (**1NiTb-Cl**): C-46.85%, H-3.25%, N-5.42%.; found C-47.20%, H-3.33%, N-4.98%. Elemental analysis for $[Ni_2Sm_2(C_{14}H_{11}NO_3)_4Cl_2(CH_3CN)_2]$ (**1NiSm-Cl**): C-46.87%, H-3.28%, N-5.16%; found: C-46.81%, H-3.22%, N-4.91%.

Preparation of $[Ni^{II}_5Sm^{III}_2(CO_3)(L1)_7(L1')(H_2O)_3]$ (1NiSm-A), $[Ni^{II}_2Sm^{III}_2(L1)_4(O\text{-}Van)_2(H_2O)_2]\cdot 4CH_3CN$ (1NiSm-B) and $[Sm^{III}_4(OH)_2(L1)_4(HL1)_2]\cdot 2CH_3CN$ (1NiSm-C)

To a solution of acetonitrile (20 mL), H_2**L1** (0.2 mmol, 48 mg) and Et_3N (0.5 mmol, 69 µL) were added and stirred for 10 min. On completion, $NiCl_2\cdot 6H_2O$ (0.1 mmol, 24 mg) and $SmCl_3\cdot xH_2O$ (0.1 mmol) were added and the resultant solution was heated under reflux for 2 h. In this time, the clear yellow solutions precipitated and on completion were left to cool where a green precipitate settled. The filtrate underwent SE and from 3-15 days mixed crystals of **1NiSm-A**, **1NiSm-B** and **1NiSm-C** were collected.

Preparation of 1NiEu-A

To a solution of acetonitrile (20 mL), H_2**L1** (0.2 mmol, 48 mg) and Et_3N (0.5 mmol, 69 µL) were added and stirred for 10 min. On completion, $NiCl_2\cdot 6H_2O$ (0.1 mmol, 24 mg) and $EuCl_3\cdot xH_2O$ (0.1 mmol) were added and the resultant solution was heated under reflux for 2 h. In this time, the clear yellow solutions precipitated and on completion were left to cool where a green precipitate settled. The filtrate underwent SE and from 6 days mixed crystals of **1NiSm-Eu** were collected.

Preparation of $[Co_2Dy_2(C_{14}H_{11}NO_3)_4Cl_2(CH_3CN)_2]$ (1CoLn-Cl)

To a solution of acetonitrile (20 mL), H_2**L1** (0.2 mmol, 48 mg) and Et_3N (0.5 mmol, 69 µL) were added and stirred for 10 min. On completion, $CoCl_2$ (0.1 mmol, 18 mg) and $DyCl_3\cdot xH_2O$ (0.1 mmol, 35 mg) were added and the resultant solution was heated under reflux for 2 h. In this time, the clear yellow solutions precipitated and on completion were left to cool where a pink precipitate settled. The solution was filtered and washed with cold MeCN (20 mL) and Et_2O (10 mL). The precipitate (**1CoLn-Cl**) was then collected and dried overnight at 60 °C.). Crystals were obtained by recrystallization in MeCN (10 mL) Yield = 69-95% based on Ln (for **1CoLn-Cl**). Elemental

analysis for $[Co_2Dy_2(C_{14}H_{11}NO_3)_4Cl_2(CH_3CN)_2]$ (**1CoLn-Cl**): C-46.55%, H-3.23%, N-5.38%; found C-46.84%, H-3.21%, N-5.16%.

Preparation of $[Zn^{II}_2Ln^{III}_2(L1)_4(NO_3)_2(DMF)_2]$ (1ZnLn-NO$_3$)

H_2**L1** (0.2 mmol, 48 mg) and Et_3N (61 µL,0.4 mmol) were added to EtOH (20 mL) and the resultant solution was stirred for 5 min under reflux. Upon completion, $Zn(NO_3)_2{\cdot}6H_2O$ (56, 0.2 mmol) and $Ln(NO_3)_3{\cdot}xH_2O$ were added and the solution was refluxed for a further 2 h. After cooling, the yellow precipitate was filtered, washed with Et_2O and dissolved in DMF (10mL). The resultant solution underwent vapour diffusion and after 1 week long yellow crystals with the formula $[Zn^{II}_2Ln^{III}_2(C_{14}H_{11}NO_3)_4(NO_3)_2(DMF)_2]$ had formed. Yield 45-71%.

Compound **1ZnDy-NO$_3$** - $[Zn^{II}_2Dy^{III}_2(C_{14}H_{11}NO_3)_4(NO_3)_2(DMF)_2]$ CHN (expected) -C-44.02%, H-3.46%, N-6.63. (measured): C-41.90%, H-2.84%, N-5.61% corresponding to $[Zn^{II}_2Dy^{III}_2(C_{14}H_{11}NO_3)_4(NO_3)_2(H_2O)_2]{\cdot}2H_2O$: C-41.58%; H-3.24%; N-5.19%.

Compound **1ZnY-NO$_3$** - $[Zn^{II}_2Y^{III}_2(C_{14}H_{11}NO_3)_4(NO_3)_2(DMF)_2]$ CHN (Expected) – C-48.31%, H-3.80%, N-7.27%. (measured): C-45.34%, H-3.12%, N-5.90% corresponding to a formula $[Zn^{II}_2Y^{III}_2(C_{14}H_{11}NO_3)_4(NO_3)_2(H_2O)_2]{\cdot}2H_2O$: C-45.84%, H-3.57%, N-5.73%.

Compound **1ZnGd-NO$_3$** - $[Zn^{II}_2Gd^{III}_2(C_{14}H_{11}NO_3)_4(NO_3)_2\text{-}(DMF)_2]$ CHN (expected) C-44.33%, H-3.48%, N-6.68%. (measured): C-41.50%, H-2.86%, N-5.20% corresponding to a formula $[Zn^{II}_2Gd^{III}_2(C_{14}H_{11}NO_3)_4(NO_3)_2\text{-}(H_2O)_2]{\cdot}2H_2O$: C-41.89%, H-3.26%, N-5.24%.

Preparation of $[(Zn^{II}_2Y^{III}_2(L6)_4(NO_3)_2(C_3H_7NO)_2]$ (6ZnY-NO$_3$)

H_2**L6** (0.2 mmol) and Et_3N (0.45 mmol, 61 µL) was stirred under reflux for 5 min. $Zn(NO_3)_2{\cdot}6H_2O$ (0.2mmol, 58mg) and $Y(NO_3)_3{\cdot}5H_2O$ (0.1mmol, 39mg) were added and the solution was refluxed for a further 1h. The cloudy yellow solution was left to cool to room temperature and filtered. The yellow precipitate was collected and washed with EtOH (20ml) and Et_2O (15 mL). The precipitate was dissolved in DMF (10 mL) and underwent VD with Et_2O. Square yellow crystals of (**6ZnY**) were collected after 8 days and dried overnight. 60% yield calculated via Y^{III}. CHN (expected) $[(Zn^{II}_2Y^{III}_2(\mathbf{L6})_4(NO_3)_2(C_3H_7NO)_2]$ C-52.23%; H-4.38%, N-6.59%. CHN (observed) $[(Zn^{II}_2Y^{III}_2(\mathbf{L6})_4(NO_3)_2(C_3H_7NO)_2]$ C-51.50%; H-4.12%; N-5.34%.

Preparation of $[(Zn^{II}_2Y^{III}_2(L4)_4(NO_3)_2(C_3H_7NO)_2]$ (4ZnY-NO$_3$)

H_2**L4** (0.2 mmol) and Et_3N (0.45 mmol, 61 µl) was stirred under reflux for 5 min. $Zn(NO_3)_2{\cdot}6H_2O$ (0.2 mmol, 58mg) and $Y(NO_3)_3{\cdot}5H_2O$ (0.1 mmol, 39mg) were added and the solution was refluxed for a further 1 h. The cloudy yellow solution was left to cool to room temperature and filtered. The yellow precipitate was collected and washed with EtOH (20 ml) and Et_2O (15 ml). The precipitate was dissolved in DMF (10 mL) and underwent VD with Et_2O. Square brown crystals were collected after 14 days and dried overnight. 41% yield calculated via Y^{III}. CHN

(expected) [($Zn^{II}_2Y^{III}_2$(**L4**)$_4$(NO_3)$_2$(C_3H_7NO)$_2$] C-40.17%, H-2.93%, N-6.04%. CHN (observed) C-39.99%, H-3.02%, N 5.98.

Preparation of [($Zn^{II}_2Y^{III}_2$(L8)$_4$(NO_3)$_2$(C_3H_7NO)$_2$] (8ZnY-NO_3)

H_2**L8** (0.2 mmol) and Et_3N (0.45 mmol, 61 μL) was stirred under reflux for 5 min. $Zn(NO_3)_2·6H_2O$ (0.2 mmol, 58 mg) and $Y(NO_3)_3·5H_2O$ (0.1 mmol, 39 mg) were added and the solution was refluxed for a further 1 h. The cloudy red solution was left to cool to room temperature and filtered. The dark red precipitate was collected and washed with EtOH (20 mL) and Et_2O (15 mL). The precipitate was dissolved in DMF (10 mL) and underwent VD with Et_2O. Square red crystals of (**8ZnY**) were collected after 8 days and dried overnight. 71% yield calculated via Y^{III}. CHN (expected) [($Zn^{II}_2Y^{III}_2$(**L8**)$_4$(NO_3)$_2$(C_3H_7NO)$_2$] C-43.26. %; H-3.16%, N-9.76%. CHN (observed) [($Zn^{II}_2Y^{III}_2$(**L8**)$_4$(NO_3)$_2$(H_2O)$_2$] C-41.67%; H-2.80%; N-8.75%.

Preparation of [($Zn^{II}_2Y^{III}_2$(L9)$_4$(NO_3)$_2$(C_3H_7NO)$_2$] (9ZnY-NO_3)

H_2**L9** (0.2 mmol) and Et_3N (0.45 mmol, 61 μL) was stirred under reflux for 5 min. $Zn(NO_3)_2·6H_2O$ (0.2 mmol, 58 mg) and $Y(NO_3)_3·5H_2O$ (0.1 mmol, 39 mg) were added and the solution was refluxed for a further 1 h. The cloudy red solution was left to cool to room temperature and filtered. The dark red precipitate was collected and washed with EtOH (20 mL) and Et_2O (15 mL). The precipitate was dissolved in DMF(10ml) and underwent VD with Et_2O. Square red crystals were collected after 8 days and dried overnight. 91% yield calculated via Y^{III}. CHN (expected) [($Zn^{II}_2Y^{III}_2$(**L9**)$_4$(NO_3)$_2$(C_3H_7NO)$_2$] C-47.23%, H-3.75%, N-8.90%. CHN (Observed) C-47.31%. H-3.90%, N-8.95%

Preparation of [($Zn^{II}_2Y^{III}_2$(L11)$_4$(NO_3)$_2$(C_3H_7NO)$_2$] (11ZnY-NO_3)

H_2**L11** (0.2 mmol) and Et_3N (0.45 mmol, 61 μL) was stirred under reflux for 5 min. $Zn(NO_3)_2·6H_2O$ (0.2 mmol, 58 mg) and $Y(NO_3)_3·5H_2O$ (0.1 mmol, 39 mg) were added and the solution was refluxed for a further 1 h. The cloudy red solution was left to cool to room temperature and filtered. The dark red precipitate was collected and washed with EtOH (20 mL) and Et_2O (15 mL). The precipitate was dissolved in DMF (10 mL) and underwent VD with Et_2O. Square light brown crystals were collected after 8 days and dried overnight. 91% yield calculated via Y^{III}. CHN (expected) [($Zn^{II}_2Y^{III}_2$(**L11**)$_4$(NO_3)$_2$(C_3H_7NO)$_2$] C-36.62%, H-2.48%, N-8.27%. CHN(observed) C-36.48%, H-2.31%, N-8.26%.

Preparation of [($Zn^{II}_2Y^{III}_2$(L12)$_4$(NO_3)$_2$(C_3H_7NO)$_2$] (12ZnY-NO_3)

H_2**L12** (0.2 mmol) and Et_3N (0.45 mmol, 61 μL) was stirred under reflux for 5 min. $Zn(NO_3)_2·6H_2O$ (0.2 mmol, 58 mg) and $Y(NO_3)_3·5H_2O$ (0.1 mmol, 39 mg) were added and the solution was refluxed for a further 1 h. The cloudy red solution was left to cool to room temperature and filtered. The dark red precipitate was collected and washed with EtOH (20 mL) and Et_2O (15 mL). The precipitate was dissolved in DMF (10 mL) and underwent VD with Et_2O.

Square red crystals of (**12ZnY**) were collected after 6 days and dried overnight. 65% yield calculated via Y^{III}. CHN (expected) [($Zn^{II}_2Y^{III}_2$(**L12**)$_4$(NO_3)$_2$(C_3H_7NO)$_2$] C-40.08%, H-2.72%, N-9.05%. CHN (observed) [($Zn^{II}_2Y^{III}_2$(**L12**)$_4$(NO_3)$_2$(H_2O)$_2$] C-38.40%; H-2.29%; N-7.98%.

Preparation of [($Zn^{II}_2Y^{III}_2$(L13)$_4$(NO_3)$_2$(C_3H_7NO)$_2$] (13ZnY-NO_3)

H_2**L13** (0.2 mmol) and Et_3N (0.45 mmol, 61 μL) was stirred under reflux for 5 min. $Zn(NO_3)_2·6H_2O$ (0.2 mmol, 58 mg) and $Y(NO_3)_3·5H_2O$ (0.1 mmol, 39 mg) were added and the solution was refluxed for a further 1 h. The cloudy red solution was left to cool to room temperature and filtered. The dark red precipitate was collected and washed with EtOH (20 mL) and Et_2O (15 mL). The precipitate was dissolved in DMF (10 mL) and underwent VD with Et_2O. Square red crystals of (**13ZnY**) were collected after 6 days and dried overnight. 71% yield calculated via Y^{III}. CHN (expected) [($Zn^{II}_2Y^{III}_2$(**L13**)$_4$(NO_3)$_2$(C_3H_7NO)$_2$] C-44.05%, H-3.29%, N-8.34%. CHN (observed) [($Zn^{II}_2Y^{III}_2$(**L13**)$_4$(NO_3)$_2$(C_3H_7NO)$_2$] C-43.98%, H-3.28%, N-8.29%.

Preparation of [($Zn^{II}_2Y^{III}_2$(L15)$_4$(NO_3)$_2$(C_3H_7NO)$_2$] (15ZnY-NO_3)

H_2**L15** (0.2 mmol) and Et_3N (0.45 mmol, 61 μL) was stirred under reflux for 5 min. $Zn(NO_3)_2·6H_2O$ (0.2 mmol, 58 mg) and $Y(NO_3)_3·5H_2O$ (0.1 mmol, 39 mg) were added and the solution was refluxed for a further 1 h. The cloudy red solution was left to cool to room temperature and filtered. The dark red precipitate was collected and washed with EtOH (20 mL) and Et_2O (15 mL). The precipitate was dissolved in DMF (10 mL) and underwent VD with Et_2O. Square red crystals were collected after 6 days and dried overnight. 66% yield calculated via Y^{III}. CHN (expected) [($Zn^{II}_2Y^{III}_2$(**L15**)$_4$(NO_3)$_2$(C_3H_7NO)$_2$] C-34.20%, H-2.50%, N-7.72%. CHN (observed) [($Zn^{II}_2Y^{III}_2$(**L15**)$_4$(NO_3)$_2$(C_3H_7NO)$_2$] C-34.27%, H-2.61%, N.81%.

Preparation of [($Zn^{II}_2Y^{III}_2$(L2)$_4$(NO_3)$_2$(C_3H_7NO)$_2$] (2ZnY-NO_3)

H_2**L2** (0.2 mmol) and Et_3N (0.45 mmol, 61 μL) was stirred under reflux for 5 min. $Zn(NO_3)_2·6H_2O$ (0.2 mmol, 58 mg) and $Y(NO_3)_3·5H_2O$ (0.1 mmol, 39 mg) were added and the solution was refluxed for a further 1 h. The cloudy yellow solution was left to cool to room temperature and filtered. The yellow precipitate was collected and washed with EtOH (20ml) and Et_2O (15 mL). The precipitate was dissolved in DMF (10 mL) and underwent VD with Et_2O. Square yellow crystals of (**2ZnY**) were collected after 8 days and dried overnight. 58% yield calculated via Y^{III}. CHN (expected) [($Zn^{II}_2Y^{III}_2$(**L2**)$_4$(NO_3)$_2$(C_3H_7NO)$_2$] C-53.78%; H-3.82%, N-6.43%. CHN (observed) [($Zn^{II}_2Y^{III}_2$(**L2**)$_4$(NO_3)$_2$(H_2O)$_2$] C-53.01%; H-3.47%; N-5.18%.

Preparation of [($Zn^{II}_2Y^{III}_2$(L16)$_4$(NO_3)$_2$(C_3H_7NO)$_2$] (16ZnY-NO_3)

H_2**L16** (0.2 mmol) and Et_3N (0.45 mmol, 61 μL) was stirred under reflux for 5 min. $Zn(NO_3)_2·6H_2O$ (0.2 mmol, 58 mg) and $Y(NO_3)_3·5H_2O$ (0.1 mmol, 39 mg) were added and the solution was refluxed for a further 1 h. The cloudy yellow solution was left to cool to room temperature and filtered. The yellow precipitate was collected and washed with EtOH (20 mL)

and Et_2O (15 mL). The precipitate was dissolved in DMF (10 mL) and underwent VD with Et_2O. Square yellow crystals were collected after 8 days and dried overnight. 81% yield calculated via Y^{III}. CHN (expected) [$(Zn^{II}_2Y^{III}_2(\mathbf{L16})_4(NO_3)_2(C_3H_7NO)_2]$ C-56.76%; H-4.29%, N-5.76%. CHN (observed) [$(Zn^{II}_2Y^{III}_2(\mathbf{L16})_4(NO_3)_2(H_2O)_2]$ C-56.29%; H-4.74%; N-4.66%.

Preparation of [$(Zn^{II}_2Y^{III}_2(L18)_4(NO_3)_2(C_3H_7NO)_2$] (18ZnY-$NO_3$)

H_2**L18** (0.2 mmol) and Et_3N (0.45 mmol, 61 μL) was stirred under reflux for 5 min. $Zn(NO_3)_2{\cdot}6H_2O$ (0.2 mmol, 58 mg) and $Y(NO_3)_3{\cdot}5H_2O$ (0.1 mmol, 39 mg) were added and the solution was refluxed for a further 1 h. The cloudy yellow solution was left to cool to room temperature and filtered. The yellow precipitate was collected and washed with EtOH (20 mL) and Et_2O (15 mL). The precipitate was dissolved in DMF (10 mL) and underwent VD with Et_2O. Square brown crystals were collected after 8 days and dried overnight. 56% yield calculated via Y^{III}. CHN (expected) [$(Zn^{II}_2Y^{III}_2(\mathbf{L18})_4(NO_3)_2(C_3H_7NO)_2]$ C-45.44%; H-3.24%, N-5.43%. CHN (observed) [$(Zn^{II}_2Y^{III}_2(\mathbf{L18})_4(NO_3)_2(C_3H_7NO)_2]$ C-45.49%; H-3.18%; N-5.29%.

Preparation of [$(Zn^{II}_2Y^{III}_2(L19)_4(NO_3)_2(C_3H_7NO)_2$] (19ZnY-$NO_3$)

H_2**L19** (0.2 mmol) and Et_3N (0.45 mmol, 61μL) was stirred under reflux for 5 min. $Zn(NO_3)_2{\cdot}6H_2O$ (0.2 mmol, 58 mg) and $Y(NO_3)_3{\cdot}5H_2O$ (0.1 mmol, 39 mg) were added and the solution was refluxed for a further 1 h. The cloudy yellow solution was left to cool to room temperature and filtered. The yellow precipitate was collected and washed with EtOH (20 mL) and Et_2O (15 mL). The precipitate was dissolved in DMF (10 mL) and underwent VD with Et_2O. jagged Yellow crystals were collected after 4 days and dried overnight. 89% yield calculated via Y^{III}. CHN (expected) [$(Zn^{II}_2Y^{III}_2(\mathbf{L19})_4(NO_3)_2(C_3H_7NO)_2]$ C-55.96%; H-4.04%, N-6.07%. CHN (observed) [$(Zn^{II}_2Y^{III}_2(\mathbf{L19})_4(NO_3)_2(C_3H_7NO)_2]$ C-55.86%; H-3.92%; N-6.06%.

Preparation of [$(Zn^{II}_2Y^{III}_2(H_2L20)_4(NO_3)_2(C_3H_7NO)_2$] (20ZnY-$NO_3$)

H_2**L20** (0.2 mmol) and Et_3N (0.45 mmol, 61 μL) was stirred under reflux for 5 min. $Zn(NO_3)_2{\cdot}6H_2O$ (0.2 mmol, 58 mg) and $Y(NO_3)_3{\cdot}5H_2O$ (0.1 mmol, 39 mg) were added and the solution was refluxed for a further 1 h. The cloudy yellow solution was left to cool to room temperature and filtered. The yellow precipitate was collected and washed with EtOH (20 mL) and Et_2O (15 mL). The precipitate was dissolved in DMF(10 mL) and underwent VD with Et_2O. Square yellow crystals of (**20ZnY-NO_3**) were collected after 9 days and dried overnight. 81% yield calculated via Y^{III}. CHN (expected) [$(Zn^{II}_2Y^{III}_2(H_2\mathbf{L20})_4(NO_3)_2(C_3H_7NO)_2]$ C-58.67%; H-4.52%, N-5.59%. CHN (observed) [$(Zn^{II}_2Y^{III}_2(H_2\mathbf{L20})_4(NO_3)_2(H_2O)_2]$ C-58.21%; H-4.33%; N-4.52%.

Preparation of [$(Zn^{II}_2Y^{III}_2(H_2L22)_4(NO_3)_2(C_3H_7NO)_2$] (22ZnY-$NO_3$)

H_2**L22** (0.2 mmol) and Et_3N (0.45 mmol, 61 μL) was stirred under reflux for 5 min. $Zn(NO_3)_2{\cdot}6H_2O$ (0.2 mmol, 58 mg) and $Y(NO_3)_3{\cdot}5H_2O$ (0.1 mmol, 39 mg) were added and the

solution was refluxed for a further 1 h. The cloudy yellow solution was left to cool to room temperature and filtered. The yellow precipitate was collected and washed with EtOH (20 mL) and Et_2O (15 mL). The precipitate was dissolved in DMF (10 mL) and underwent VD with Et_2O. Jagged brown crystals of (**22ZnY-NO$_3$**) were collected after 3 days and dried overnight. 44% yield calculated via Y^{III}. CHN (expected) $[(Zn^{II}_2Y^{III}_2(H_2\mathbf{L22})_4(NO_3)_2(C_3H_7NO)_2]$ C-47.87%; H-3.27%, N-5.19%. CHN (observed) $[(Zn^{II}_2Y^{III}_2(H_2\mathbf{L22})_4(NO_3)_2(C_3H_7NO)_2]$ C-47.92%; H-3.39%; N-5.14%.

Preparation of $[(Zn^{II}_2Y^{III}_2(H_2L27)_4(NO_3)_2(C_3H_7NO)_2]$ (27ZnY-NO$_3$)

H_2**L27** (0.2 mmol) and Et_3N (0.45 mmol, 61 μL) was stirred under reflux for 5 min. $Zn(NO_3)_2{\cdot}6H_2O$ (0.2 mmol, 58 mg) and $Y(NO_3)_3{\cdot}5H_2O$ (0.1 mmol, 39 mg) were added and the solution was refluxed for a further 1 h. The cloudy yellow solution was left to cool to room temperature and filtered. The yellow precipitate was collected and washed with EtOH (20 mL) and Et_2O (15 mL). The precipitate was dissolved in DMF (10 mL) and underwent VD with Et_2O. Square yellow crystals of (**27ZnY-NO$_3$**) were collected after 12 days and dried overnight. 71% yield calculated via Y^{III}. CHN (expected) $[(Zn^{II}_2Y^{III}_2(H_2\mathbf{L27})_4(NO_3)_2(C_3H_7NO)_2]$ C-53.05%; H-5.14%, N-6.34%. CHN (observed) $[(Zn^{II}_2Y^{III}_2(H_2\mathbf{L27})_4(NO_3)_2(C_3H_7NO)_2]$ C-52.98%; H-5.12%; N-6.40%.

Preparation of $[(Zn^{II}_2Y^{III}_2(H_2L28)_4(NO_3)_2(C_3H_7NO)_2]$ (28ZnY-NO$_3$)

H_2**L28** (0.2 mmol) and Et_3N (0.45 mmol, 61 μL) was stirred under reflux for 5 min. $Zn(NO_3)_2{\cdot}6H_2O$ (0.2 mmol, 58 mg) and $Y(NO_3)_3{\cdot}5H_2O$ (0.1 mmol, 39 mg) were added and the solution was refluxed for a further 1 h. The cloudy yellow solution was left to cool to room temperature and filtered. The yellow precipitate was collected and washed with EtOH (20 mL) and Et_2O (15 mL). The precipitate was dissolved in DMF (10 mL) and underwent VD with Et_2O. Square yellow crystals were collected after 15 days and dried overnight. 66% yield calculated via Y^{III}. CHN (expected) $[(Zn^{II}_2Y^{III}_2(H_2\mathbf{L28})_4(NO_3)_2(C_3H_7NO)_2]$ C-56.12%; H-5.55%, N-5.82%. CHN (observed) $[(Zn^{II}_2Y^{III}_2(H_2\mathbf{L28})_4(NO_3)_2(C_3H_7NO)_2]$ C-56.10%; H-5.52%; N-5.79%.

Preparation of $[(Zn^{II}_2Y^{III}_2(H_2L29)_4(NO_3)_2(C_3H_7NO)_2]$ (29ZnY-NO$_3$)

H_2**L29** (0.2 mmol) and Et_3N (0.45 mmol, 61 μL) was stirred under reflux for 5 min. $Zn(NO_3)_2{\cdot}6H_2O$ (0.2 mmol, 58 mg) and $Y(NO_3)_3{\cdot}5H_2O$ (0.1 mmol, 39 mg) were added and the solution was refluxed for a further 1 h. The cloudy yellow solution was left to cool to room temperature and filtered. The yellow precipitate was collected and washed with EtOH (20 mL) and Et_2O (15 mL). The precipitate was dissolved in DMF (10 mL) and underwent VD with Et_2O. Cubic orange crystals were collected after 7 days and dried overnight. 51% yield calculated via Y^{II}. CHN (expected) $[(Zn^{II}_2Y^{III}_2(H_2\mathbf{L29})_4(NO_3)_2(C_3H_7NO)_2]$ C-45.09%; H-4.18%, N-5.39%. CHN (observed) $[(Zn^{II}_2Y^{III}_2(H_2\mathbf{L29})_4(NO_3)_2(C_3H_7NO)_2]$ C-44.98%; H-4.09%; N-5.28%.

Preparation of [($Zn^{II}_2Y^{III}_2(H_2L24)_4(NO_3)_2(C_3H_7NO)_2$] (24ZnY-$NO_3$)

H_2**L19** (0.2 mmol) and Et_3N (0.45 mmol, 61 μL) was stirred under reflux for 5 min. $Zn(NO_3)_2·6H_2O$ (0.2 mmol, 58 mg) and $Y(NO_3)_3·5H_2O$ (0.1 mmol, 39 mg) were added and the solution was refluxed for a further 1 h. The cloudy yellow solution was left to cool to room temperature and filtered. The yellow precipitate was collected and washed with EtOH (20 mL) and Et_2O (15 mL). The precipitate was dissolved in DMF (10 mL) and underwent VD with Et_2O. Needle like yellow crystals of (**24ZnY**) were collected after 5 days and dried overnight. 80% yield calculated via Y^{II}. CHN (expected) [($Zn^{II}_2Y^{III}_2(H_2$**L24**$)_4(NO_3)_2(C_3H_7NO)_2$] C-45.08%; H-3.52%, N-10.88%. CHN (observed) [($Zn^{II}_2Y^{III}_2(H_2$**L24**$)_4(NO_3)_2(H_2O)_2$] C-43.58%, H- 3.12%, N-9.96%

Preparation of [($Zn^{II}_2Y^{III}_2(H_2L25)_4(NO_3)_2(C_3H_7NO)_2$] (25ZnY-$NO_3$)

H_2**L25** (0.2 mmol) and Et_3N (0.45 mmol, 61 μL) was stirred under reflux for 5 min. $Zn(NO_3)_2·6H_2O$ (0.2 mmol, 58 mg) and $Y(NO_3)_3·5H_2O$ (0.1 mmol, 39 mg) were added and the solution was refluxed for a further 1 h. The cloudy yellow solution was left to cool to room temperature and filtered. The yellow precipitate was collected and washed with EtOH (20 mL) and Et_2O (15 mL). The precipitate was dissolved in DMF (10 mL) and underwent VD with Et_2O. Needle like yellow crystals were collected after 4 days and dried overnight. 91% yield calculated via Y^{II}. CHN (expected) [($Zn^{II}_2Y^{III}_2(H_2$**L25**$)_4(NO_3)_2(C_3H_7NO)_2$] C-49.29%; H-4.13%, N-9.86%. CHN (observed) [($Zn^{II}_2Y^{III}_2(H_2$**L25**$)_4(NO_3)_2(H_2O)_2$] C-48.25%, H- 3.83%, N-8.73%

Preparation of [($Zn^{II}_2Y^{III}_2(H_2L26)_4(NO_3)_2(C_3H_7NO)_2$] (26ZnY-$NO_3$)

H_2**L26** (0.2 mmol) and Et_3N (0.45 mmol, 61 μL) was stirred under reflux for 5 min. $Zn(NO_3)_2·6H_2O$ (0.2 mmol, 58 mg) and $Y(NO_3)_3·5H_2O$ (0.1 mmol, 39 mg) were added and the solution was refluxed for a further 1 h. The cloudy yellow solution was left to cool to room temperature and filtered. The yellow precipitate was collected and washed with EtOH (20 mL) and Et_2O (15 mL). The precipitate was dissolved in DMF (10 mL) and underwent VD with Et_2O. Needle-like yellow crystals were collected after 4 days and dried overnight. 91% yield calculated via Y^{II}. CHN (expected) [($Zn^{II}_2Y^{III}_2(H_2$**L26**$)_4(NO_3)_2(C_3H_7NO)_2$] C-37.51%; H-2.72%, N-9.06%. CHN (observed) [($Zn^{II}_2Y^{III}_2(H_2$**L26**$)_4(NO_3)_2(H_2O)_2$] C-35.87%, H- 2.37%, N-8.09%.

11.4 Catalytic protocols

Supporting Figures for ^{1}H NMR, ^{13}CNMR and ESI-MS are found in Appendix B.

Synthesis of *trans*-4,5-dimorpholin-4-yl-cyclopent-2-enone (C7a)

In air, powdered 4 Å molecular sieves (100mg) were weighed into a 10 mL capped vial equipped with a magnetic stirbar. MeCN (dry, 4 mL), furfural (0.5 mmol, 41 μL), morpholine (1 mmol) and the appropriate amount of catalyst (10 -1 mol% total of Dy) were added. The resultant mixture was stirred at room temperature for 24 h. The reaction mixture was diluted with DCM (20 mL) and filtered through Celite. The resultant solution was concentrated under reduced pressure and

the residue purified by column chromatography (30 % ethyl acetate in 70 % hexanes). The product was obtained as a yellow oil which solidified on standing. ^{1}H NMR (500 MHz, $CDCl_3$) δ 7.59 (1H, dd, J = 6.0, 2.0 Hz), 6.22 (1H, dd, J = 6.0, 2.0Hz), 3.79 (1H, ddd, J = 3.0, 2.0, 2.0 Hz), 3.71 (4H, t, J = 4.5 Hz), 3.67 (4H, t, J = 4.5 Hz), 3.28(1H, d, J = 3.0 Hz), 2.84-2.79 (2H, m), 2.67-2.55 (6H, m)

Synthesis of *trans*-4,5-bis-diallylaminocyclopent-2-enone (C7b)

In air, powdered 4 Å molecular sieves (100 mg) were weighed into a 10 mL capped vial equipped with a magnetic stirbar. MeCN (dry, 4 mL), furfural (0.5 mmol, 41 μL), diallylamine (1 mmol) and the appropriate amount of catalyst (10 -1 mol% total of Dy) were added. The resultant mixture was stirred at room temperature for 24 h. The reaction mixture was diluted with DCM (20 mL) and filtered through Celite. The resultant solution was concentrated under reduced pressure and the residue purified by column chromatography (5% ethyl acetate in 95% hexanes). The product was obtained as a yellow oil which solidified on standing. ^{1}H NMR (500 MHz, $CDCl_3$) δ 7.46 (1H, dd, J = 6.0, 2.0 Hz), 6.16 (1H, dd, J = 6.0, 2.0 Hz), 5.91-5.77 (4H, m), 5.26-5.10 (8H, m), 4.11 (1H, ddd, J = 3.0, 2.0, 2.0 Hz), 3.59 (1H, d, J = 3.0Hz), 3.38-3.31 (2H, m), 3.23-3.10 (6H, m)

Synthesis of *trans*-4,5-bis-(2,3-dihydroindol-1-yl)-cyclopent-2-enone (C7c)

In air, powdered 4 Å molecular sieves (100 mg) were weighed into a 10 mL capped vial equipped with a magnetic stirbar. MeCN (dry, 4 mL), furfural (0.5 mmol, 41 μL), indoline (1 mmol) and the appropriate amount of catalyst (10 -1 mol% total of Dy) were added. The resultant mixture was stirred at room temperature for 24 h. The reaction mixture was diluted with DCM (20 mL) and filtered through Celite. The resultant solution was concentrated under reduced pressure and the residue purified by column chromatography (20% ethyl acetate in 80% hexanes). The product was obtained a yellow oil which solidified on standing. ^{1}H NMR (500 MHz, $CDCl_3$) δ 7.68 (1H, dd, J = 6.0, 2.0 Hz), 7.08 (1H, d, J = 7.0 Hz), 7.05 (1H, d, J = 7.5 Hz),6.96 (1H, dd, J = 7.5, 7.5 Hz), 6.91 (1H, dd, J = 7.5, 7.5 Hz), 6.67 (1H, dd, J = 7.5, 7.5 Hz), 6.63(1H, dd, J = 7.5, 7.5 Hz), 6.49 (1H, dd, J = 6.0, 2.0 Hz), 6.35 (1H, d, J = 8.0 Hz), 6.07 (1H, d, J =8.0 Hz), 5.01-4.99 (1H, m), 4.40 (1H, d, J = 3.5 Hz), 3.52 (1H, ddd, J = 7.5, 7.5, 7.5 Hz), 3.50(1H, ddd, J = 8.0, 8.0, 8.0 Hz), 3.41 (1H, ddd, J = 8.0, 8.0, 8.0 Hz), 3.34 (1H, ddd, J = 8.0, 8.0,8.0 Hz), 3.06-2.90 (4H, m)

Synthesis of *trans*-4,5-bis-(3,4-dihydro-2H-quinolin-1-yl)-cyclopent-2-enone (C7d)

In air, powdered 4 Å molecular sieves (100 mg) were weighed into a 10 mL capped vial equipped with a magnetic stirbar. MeCN (dry, 4 mL), furfural (0.5 mmol, 41 μL), 1,2,3,4-tetrahydroquinoline (1 mmol) and the appropriate amount of catalyst (10 -1 mol% total of Dy) were added. The resultant mixture was stirred at room temperature for 24 h. The reaction mixture was diluted with DCM (20 mL) and filtered through Celite. The resultant solution was

concentrated under reduced pressure and the residue purified by column chromatography (20% ethyl acetate in 80% hexanes). The product was obtained a yellow oil which solidified on standing. ^{1}H NMR (500 MHz, $CDCl_3$) δ 7.67 (1H, dd, J = 6.0, 2.0 Hz), 6.99-6.87 (4H, m), 6.65-6.50 (4H, m), 6.09 (1H, d, J = 8.0 Hz),5.38 (1H, br s), 4.32 (1H, br s), 3.33-3.15 (4H, m), 2.822.66 (4H, m), 2.00-1.88 (4H, m)

Synthesis of *trans*-4,5-Bis-(3,4-dihydro-1H-isoquinolin-2-yl)-cyclopent-2-enone (C7e)

In air, powdered 4 Å molecular sieves (100 mg) were weighed into a 10 mL capped vial equipped with a magnetic stirbar. MeCN (dry, 4 mL), furfural (0.5 mmol, 41 μL), 1,2,3,4-tetrahydroisoquinoline (1 mmol) and the appropriate amount of catalyst (10 -1 mol% total of Dy) were added. The resultant mixture was stirred at room temperature for 24 h. The reaction mixture was diluted with DCM (20 mL) and filtered through Celite. The resultant solution was concentrated under reduced pressure and the residue purified by column chromatography (30% ethyl acetate in 70% hexanes). The product was obtained a yellow oil which solidified on standing. ^{1}H NMR (500 MHz, $CDCl_3$) δ 7.70 (1H, dd, J = 6.0, 2.0 Hz), 7.16-7.00 (8H, m), 6.32 (1H, dd, J= 6.0, 2.0 Hz), 4.25-4.13 (2H, m), 3.95-3.90 (3H, m), 3.62 (1H, d, J = 3.0 Hz), 3.12-2.86 (8H, m)

Synthesis of (1E,2Z,4E)-5-(phenylamino)-1-(phenyliminio)penta-2,4-dien-2-olate (C7f)

In air, powdered 4 Å molecular sieves (100 mg) were weighed into a 10 mL capped vial equipped with a magnetic stirbar. MeCN (dry, 4 mL), furfural (0.5 mmol, 41 μL), aniline (1 mmol) and the appropriate amount of catalyst (10 -1 mol% total of Dy) were added. The resultant mixture was stirred at room temperature for 24 h. The reaction mixture was diluted with DCM (20 mL) and filtered through Celite. The resultant solution was concentrated under reduced pressure. The residue was purified by column chromatography (10% ethyl acetate in 90% hexanes). The product was obtained as red oil which solidified on standing. ^{1}H NMR (500 MHz, DMSO-d6) δ 7.68 (dd, J = 6.1, 1.9 Hz, 1H), 7.11 – 7.01 (m, 4H), 6.63 – 6.44 (m, 6H), 6.39 (dd, J = 6.1, 1.5 Hz, 1H), 6.20 (d, J = 8.6 Hz, 1H), 6.06 (d, J = 7.5 Hz, 1H), 4.63 – 4.57 (m, 1H), 4.01 (dd, J = 7.6, 3.4 Hz, 1H), 1.22 (s, 1H) ^{13}C NMR (126 MHz, DMSO-d6) δ 205.12, 161.93, 152.43, 151.61, 149.03, 148.77, 146.81, 132.63, 129.66, 129.53, 129.22, 126.47, 121.37, 117.33, 116.75, 116.12, 114.36, 113.17, 112.93, 64.86, 40.56, 40.40, 40.23, 40.06, 39.90, 39.73, 39.56, 28.28

Synthesis of (1E,2Z,4E)-5-((2-methoxyphenyl)amino)-1-((2-methoxyphenyl)iminio)penta-2,4-dien-2olate (C7g)

In air, powdered 4 Å molecular sieves (100 mg) were weighed into a 10 mL capped vial equipped with a magnetic stirbar. MeCN (dry, 4 mL), furfural (0.5 mmol, 41 μL), O-anisidine (1 mmol) and the appropriate amount of catalyst (10 -1 mol% total of Dy) were added. The resultant mixture was stirred at room temperature for 24 h. The reaction mixture was diluted with DCM (20 mL)

and filtered through Celite. The resultant solution was concentrated under reduced pressure. The residue was purified by column chromatography (10% ethyl acetate in 90% hexanes). The product was obtained as red oil. ^{1}H NMR (500 MHz, DMSO-d6) δ 8.35 (s, 1H), 7.61 (dt, J = 6.1, 1.7 Hz, 2H), 7.29 – 7.17 (m, 2H), 7.07 (d, J = 7.8 Hz, 1H), 7.02 – 6.94 (m, 3H), 6.89 – 6.69 (m, 19H), 6.55 (dt, J = 3.5, 1.7 Hz, 1H), 6.41 (dt, J = 6.1, 1.4 Hz, 1H), 3.96 – 3.69 (m, 23H).

Synthesis of (1E,2Z,4E)-5-((2-fluorophenyl)amino)-1-((2-fluorophenyl)iminio)penta-2,4-dien-2-olate (C7h)

In air, powdered 4 Å molecular sieves (100 mg) were weighed into a 10 mL capped vial equipped with a magnetic stirbar. MeCN (dry, 4 mL), furfural (0.5 mmol, 41 μL), 2-fluoroanaline (1 mmol) and the appropriate amount of catalyst (10 -1 mol% total of Dy) were added. The resultant mixture was stirred at room temperature for 24 h. The reaction mixture was diluted with DCM (20 mL) and filtered through Celite. The resultant solution was concentrated under reduced pressure. The residue was purified by column chromatography (5% ethyl acetate in 95% hexanes). The product was obtained as yellow oil. ^{1}H NMR (500 MHz, DMSO-d6) δ 8.35 (s, 1H), 7.61 (dt, J = 6.1, 1.7 Hz, 2H), 7.29 – 7.17 (m, 2H), 7.07 (d, J = 7.8 Hz, 1H), 7.02 – 6.94 (m, 4H), 6.89 – 6.69 (m, 22H), 6.55 (dt, J = 3.5, 1.7 Hz, 1H), 6.41 (dt, J = 6.1, 1.4 Hz, 1H), 3.96 – 3.69 (m, 27H)

Synthesis of (1E,2Z,4E)-5-((2-(trifluoromethyl)phenyl)amino)-1-((2(trifluoromethyl)phenyl)iminio)penta-2,4-dien-2-olate (C7i)

In air, powdered 4 Å molecular sieves (100 mg) were weighed into a 10 mL capped vial equipped with a magnetic stirbar. MeCN (dry, 4 mL), furfural (0.5 mmol, 41 μL), 2(trifluoromethyl)-analine (1 mmol) and the appropriate amount of catalyst (10 -1% total of Dy) were added. The resultant mixture was stirred at room temperature for 24 h. The reaction mixture was diluted with DCM (20 mL) and filtered through Celite. The resultant solution was concentrated under reduced pressure. The residue was purified by column chromatography (20% ethyl acetate in 80% hexanes). The product was obtained as red oil which solidified on standing. ^{1}H NMR (500 MHz, DMSO-d^{6}) δ 9.71 – 9.66 (m, 3H), 8.19 (s, 1H), 8.01 – 7.94 (m, 1H), 7.75 – 7.44 (m, 13H), 7.36 – 7.23 (m, 11H), 7.06 (d, J = 7.5 Hz, 1H), 6.94 – 6.84 (m, 6H), 6.64 – 6.57 (m, 4H), 4.13 (qd, J = 7.2, 1.6 Hz, 5H), 3.94 (d, J = 1.5 Hz, 2H), 2.18 (q, J = 0.8 Hz, 2H).

Synthesis of 3,3'-(phenylmethylene)bis(1H-indole) (**C8aa**)

To a mixed solution of EtOH/H_2O (2:1 in 10 mL), benzaldehyde (0.5 mmol) and indole (1 mmol) were added followed by catalyst (2.5 mol% with respect to benzaldehyde). The resultant solution was stirred for 12 h, upon which time product had precipitated. The cloudy solution was filtered and precipitate washed with hexanes (3 x 10 mL) and water (3 x 10 mL). ^{1}H NMR (500 MHz, $CDCl_3$) δ 7.74 (s, 2H), 7.47 – 7.17 (m, 10H), 7.05 (ddd, J = 8.0, 7.0, 1.0 Hz, 2H), 6.61 (dd, J = 2.5, 1.1 Hz, 2H), 5.92 (s, 1H). ^{13}C NMR (126 MHz, CDCl3) δ 165.91, 144.07, 136.72, 128.75,

128.23, 127.13, 126.15, 123.63, 123.61, 121.93, 119.95, 119.72, 119.26, 117.73, 111.06, 77.30, 77.04, 76.79, 40.26, 40.24, -8.79.

Synthesis of 3,3'-((4-(trifluoromethyl)phenyl)methylene)bis(1H-indole) (C8ab)

To a mixed solution of EtOH/H_2O (2:1 in 10 mL), 4-(trifluroro) benzaldehyde (0.5 mmol) and indole (1 mmol) were added followed by catalyst (2.5 mol% with respect to benzaldehyde). The resultant solution was stirred for 12 h, upon which time product had precipitated. The cloudy solution was filtered and precipitate washed with hexanes (3 x 10 mL) and water (3 x 10 mL). ^{1}H NMR (500 MHz, $CDCl_3$) δ 8.28 (s, 2H), 7.53 (d, J = 8.1 Hz, 2H), 7.45 (d, J = 8.1 Hz, 2H), 7.36 (t, J = 7.8 Hz, 4H), 7.18 (ddd, J = 8.0, 7.0, 1.2 Hz, 2H), 7.02 (ddd, J = 8.0, 7.0, 1.1 Hz, 2H), 6.62 (dd, J = 2.5, 1.1 Hz, 2H), 5.95 (s, 1H). ^{13}C NMR (126 MHz, $CDCl_3$) δ 136.71, 128.99, 126.85, 125.22, 125.19, 125.16, 123.59, 122.17, 119.70, 119.45, 118.83, 111.10, 77.23, 76.97, 76.72, 40.12. ESI-MS expected $C_{24}H_{17}F_3N_2$: 390.1; observed 389.1243.

Synthesis of 3,3'-(naphthalen-1-ylmethylene)bis(1H-indole) (C8ac)

To a mixed solution of EtOH/H_2O (2:1 in 10 mL), 1-naphthaldehyde (0.5 mmol) and indole (1 mmol) were added followed by catalyst (2.5 mol% with respect to aldehyde). The clear solution was concentrated under reduced pressure and extracted in ethyl acetate (30 mL) from water (20 mL). The ethyl acetate layer was dried with $MgSO_4$ and concentrated under reduced pressure. The resulting oil was washed with hexanes (60 mL) resulting in a red solid which was further washed with water (3 x 10 mL).^{1}H NMR (500 MHz, $CDCl_3$) δ 8.21 – 8.15 (m, 1H), 7.89 (d, J = 8.0 Hz, 3H), 7.75 (d, J = 8.1 Hz, 1H), 7.37 (pd, J = 20.9, 20.4, 10.5 Hz, 8H), 7.19 (t, J = 7.7 Hz, 2H), 7.01 (t, J = 7.9 Hz, 2H), 6.68 (s, 1H), 6.59 (s, 2H).

Synthesis of 3,3'-((4-chlorophenyl)methylene)bis(1H-indole) (C8ae)

To a mixed solution of EtOH/H_2O (2:1 in 10 mL), 4-chlorobenzaldehyde (0.5 mmol) and indole (1 mmol) were added followed by catalyst (2.5 mol% with respect to aldehyde). The clear solution was concentrated under reduced pressure and extracted in ethyl acetate (30 mL) from water (20 mL). The ethyl acetate layer was dried with $MgSO_4$ and concentrated under reduced pressure. The resulting oil was washed with hexanes (60 mL) resulting in a red solid which was further washed with water (3 x 10mL). ^{1}H NMR (500 MHz, $CDCl_3$) 7.90 (s, 2H), 7.37 (t, J = 8.5 Hz, 5H), 7.31 – 7.15 (m, 6H), 7.03 (t, J = 7.5 Hz, 2H), 6.63 (d, J = 2.4 Hz, 2H), 5.87 (s, 1H), 1.29. ^{13}C NMR (126 MHz, $CDCl_3$) δ 142.57, 136.72, 131.79, 130.05, 128.33, 126.91, 123.55, 122.06, 119.79, 119.35, 119.23, 111.08, 77.24, 76.99, 76.73, 39.65. ESI-MS expected $C_{23}H_{17}ClN_2$: 356.1; observed 355.0977.

Synthesis of 3,3'-(naphthalen-2-ylmethylene)bis(1H-indole) (C8ad)

To a mixed solution of EtOH/H_2O (2:1 in 10 mL), 2-napthaldehyde (0.5 mmol) and indole (1 mmol) were added followed by catalyst (2.5 mol% with respect to benzaldehyde). The resultant

solution was stirred for 12 h, upon which time product had precipitated. The cloudy solution was filtered and precipitate washed with hexanes (3 x 10 mL) and water (3 x 10 mL). ^{1}H NMR (500 MHz, $CDCl_3$) δ 7.89 (s, 2H), 7.75 (td, J = 29.9, 24.9, 5.8 Hz, 4H), 7.55 – 7.49 (m, 1H), 7.41 (d, J = 7.9 Hz, 4H), 7.35 (d, J = 8.2 Hz, 2H), 7.20 – 7.13 (m, 2H), 6.99 (d, J = 7.9 Hz, 2H), 6.67 (s, 2H), 6.06 (s, 1H). ^{13}C NMR (126 MHz, $CDCl_3$) δ 141.58, 136.73, 133.61, 132.37, 127.88, 127.72, 127.70, 127.53, 127.13, 126.74, 125.63, 125.23, 123.72, 121.96, 119.94, 119.60, 119.29, 110.99, 77.23, 76.98, 76.78, 76.73, 40.34, 1.00.

Synthesis of 3,3'-(furan-2-ylmethylene)bis(1H-indole) (C8af)

To a mixed solution of EtOH/H_2O (2:1 in 10 mL), furaldehyde (0.5 mmol) and indole (1 mmol) were added followed by catalyst (2.5 mol% with respect to aldehyde). The clear solution was concentrated under reduced pressure and extracted in ethyl acetate (30 mL) from water (20 mL). The ethyl acetate layer was dried with $MgSO_4$ and concentrated under reduced pressure. The resulting oil was washed with hexanes (60 mL) resulting in a white solid which was further washed with water (3 x 10 mL). ^{1}H NMR (500 MHz, $CDCl_3$) δ 7.64 – 7.54 (m, 5H), 7.43 (dd, J = 1.8, 0.9 Hz, 1H), 7.18 (ddd, J = 7.9, 6.6, 1.5 Hz, 3H), 6.75 – 6.70 (m, 2H), 6.39 (dd, J = 3.2, 1.8 Hz, 1H), 6.18 – 6.13 (m, 1H), 6.06 – 6.02 (m, 1H). ^{13}C NMR (126 MHz, $CDCl_3$) δ 157.04, 153.87, 141.19, 131.74, 127.23, 123.81, 116.89, 112.06, 111.73, 110.12, 109.99, 106.64, 101.73, 77.24, 76.99, 76.74, 34.21. ESI-MS expected $C_{21}H_{16}N_2O$: 312.1; observed 311.1173.

Synthesis of 3,3'-(phenylmethylene)bis(5-methoxy-1H-indole) (C8aj)

To a mixed solution of EtOH/H_2O (2:1 in 10 mL), benzaldehyde (0.5 mmol) and 5-methoxyindole (1 mmol) were added followed by catalyst (2.5 mol% with respect to benzaldehyde). The resultant solution was stirred for 12 h, upon which time product had precipitated. The cloudy solution was filtered and precipitate washed with hexanes (3 x 10mL) and water (3 x 10 mL). ^{1}H NMR (500 MHz, $CDCl_3$) δ 7.80 (s, 2H), 7.35 (d, J = 7.7 Hz, 2H), 7.25 (dt, J = 21.8, 10.3 Hz, 5H), 6.86 – 6.78 (m, 4H), 6.67 (d, J = 2.3 Hz, 2H), 5.77 (s, 1H), 3.69 (s, 6H). ^{13}C NMR (126 MHz, $CDCl_3$) δ 153.75, 143.91, 131.90, 128.71, 128.17, 127.55, 126.08, 124.37, 119.36, 111.92, 111.59, 102.08, 77.22, 76.97, 76.94, 76.72, 55.85, 40.32. ESI-MS expected $C_{25}H_{22}N_2O_2$: 382.2; observed 381.1582.

Synthesis of 3,3'-((4-(trifluoromethyl)phenyl)methylene)bis(5-methoxy-1H-indole) (C8ak)

To a mixed solution of EtOH/H_2O (2:1 in 10 mL), 4-(trifluoromethyl)benzaldehyde (0.5 mmol) and 5-methoxyindole (1 mmol) were added followed by catalyst (2.5 mol% with respect to benzaldehyde). The resultant solution was stirred for 12 h, upon which time product had precipitated. The cloudy solution was filtered and precipitate washed with hexanes (3 x 10 mL) and water (3 x 10mL).^{1}H NMR (500 MHz, $CDCl_3$) δ 7.83 (s, 2H), 7.52 (d, J = 8.0 Hz, 2H), 7.47 – 7.41 (m, 2H), 7.22 (s, 1H), 6.87 – 6.81 (m, 2H), 6.75 (s, 2H), 6.62 (s, 2H), 5.82 (s, 1H), 3.68 (s,

6H). ^{13}C NMR (126 MHz, $CDCl_3$) δ 162.17, 153.90, 148.12, 131.91, 129.02, 128.60, 128.34, 127.31, 125.46, 125.22, 125.19, 125.15, 125.13, 124.46, 123.30, 118.37, 112.09, 111.89, 111.80, 109.99, 101.92, 77.25, 76.99, 76.74, 55.88, 40.19. ESI-MS expected $C_{26}H_{21}F_3N_2O_2$: 450.2; observed 449.1446.

Synthesis of 3,3'-(naphthalen-1-ylmethylene)bis(5-methoxy-1H-indole) (C8al)

To a mixed solution of EtOH/H_2O (2:1 in 10 mL), 1-napthaldehyde (0.5 mmol) and 5-methoxyindole (1 mmol) were added followed by catalyst (2.5 mol% with respect to aldehyde). The clear solution was concentrated under reduced pressure and extracted in ethyl acetate (30 mL) from water (20 mL). The ethyl acetate layer was dried with $MgSO_4$ and concentrated under reduced pressure. The resulting oil was washed with hexanes (60 mL) resulting in a pink solid which was further washed with water (3 x 10 mL). ^{1}H NMR (500 MHz, $CDCl_3$) δ 8.16 (d, J = 8.5 Hz, 1H), 7.87 (d, J = 8.2 Hz, 1H), 7.80 – 7.71 (m, 3H), 7.47 – 7.22 (m, 4H), 6.87 – 6.78 (m, 4H), 6.58 (s, 2H), 6.52 (s, 1H), 3.66 (s, 6H). ^{13}C NMR (126 MHz, $CDCl_3$) δ 153.83, 131.96, 128.60, 126.94, 126.14, 125.71, 125.44, 125.17, 125.06, 124.34, 119.01, 111.87, 111.63, 109.99, 102.04, 88.22, 77.22, 76.97, 76.72, 55.92, 36.03. ESI-MS expected $C_{29}H_{24}O_2N_2$: 432.2; observed 431.1744.

Synthesis of 3,3'-((4-chlorophenyl)methylene)bis(5-methoxy-1H-indole) (C8an)

To a mixed solution of EtOH/H_2O (2:1 in 10 mL), 4-chlorobenzaldehyde (0.5 mmol) and 5-methoxyindole (1 mmol) were added followed by catalyst (2.5 mol% with respect to benzaldehyde). The resultant solution was stirred for 12 h, upon which time product had precipitated. The cloudy solution was filtered and precipitate washed with hexanes (3 x 10 mL) and water (3 x 10 mL).^{1}H NMR (500 MHz, $CDCl_3$) δ 7.81 (s, 2H), 7.24 (p, J = 9.0 Hz, 5H), 6.87 – 6.81 (m, 2H), 6.78 (s, 2H), 6.60 (s, 2H), 5.74 (s, 1H), 3.70 (s, 6H). ^{13}C NMR (126 MHz, $CDCl_3$) δ 206.29, 153.82, 142.50, 131.92, 131.77, 130.05, 128.32, 127.36, 124.42, 118.76, 111.99, 111.74, 102.04, 89.91, 77.25, 77.00, 76.75, 55.90, 39.71. ESI-MS expected $C_{25}H_{21}ClO_2N_2$: 416.1; observed 415.118.

Synthesis of 3,3'-(naphthalen-2-ylmethylene)bis(5-methoxy-1H-indole) (C8am)

To a mixed solution of EtOH/H_2O (2:1 in 10 mL), 2-napthadehyde (0.5 mmol) and 5-methoxyindole (1 mmol) were added followed by catalyst (2.5 mol% with respect to aldehyde). The clear solution was concentrated under reduced pressure and extracted in ethyl acetate (30 mL) from water (20 mL). The ethyl acetate layer was dried with $MgSO_4$ and concentrated under reduced pressure. The resulting oil was washed with hexanes (60 mL) resulting in a pink solid which was further washed with water (3 x 10 mL). ^{1}H NMR (500 MHz, $CDCl_3$) δ 7.77 (s, 3H), 7.72 (s, 2H), 7.68 (s, 1H), 7.49 (s, 1H), 7.38 (s, 2H), 6.80 (s, 4H), 6.64 (s, 2H), 6.37 (s, 1H), 5.91 (s, 1H), 3.64 – 3.60 (m, 6H). ^{13}C NMR (126 MHz, $CDCl_3$) δ 165.91, 144.07, 136.72, 128.75,

128.23, 127.13, 126.15, 123.63, 123.61, 121.93, 119.95, 119.72, 119.26, 117.73, 111.06, 77.30, 77.04, 76.79, 40.26, 40.24, -8.79. ESI-MS expected $C_{29}H_{24}O_2N_2$: 432.2; observed 431.1734.

Synthesis of 3,3'-(furan-2-ylmethylene)bis(5-methoxy-1H-indole) (C8ao)

To a mixed solution of EtOH/H_2O (2:1 in 10 mL), furfural (0.5 mmol) and 5-methoxyindole (1 mmol) were added followed by catalyst (2.5 mol% with respect to aldehyde). The clear solution was concentrated under reduced pressure and extracted in ethyl acetate (30 mL) from water (20 mL). The ethyl acetate layer was dried with $MgSO_4$ and concentrated under reduced pressure. The resulting oil was washed with hexanes (60 mL) resulting in a pink solid which was further washed with water (3 x 10 mL) ^{1}H NMR (500 MHz, $CDCl_3$) δ 7.85 (s, 2H), 7.38 (s, 1H), 7.24 (d, J = 8.8 Hz, 2H), 6.92 (s, 2H), 6.85 (d, J = 7.8 Hz, 4H), 6.32 (s, 1H), 6.09 (s, 1H), 5.85 (s, 1H), 3.75 (s, 6H). ^{13}C NMR (126 MHz, $CDCl_3$) δ 157.04, 153.87, 141.19, 131.74, 127.23, 123.81, 116.89, 112.06, 111.73, 110.12, 109.99, 106.64, 101.73, 77.24, 76.99, 76.74, 55.87, 34.21.

Synthesis of 3,3'-((5-methylfuran-2-yl)methylene)bis(5-methoxy-1H-indole) (C8ap)

To a mixed solution of EtOH/H_2O (2:1 in 10 mL), 5-methyl-2-furaldehyde (0.5 mmol) and 5-methoxyindole (1 mmol) were added followed by catalyst (2.5 mol% with respect to aldehyde). The clear solution was concentrated under reduced pressure and extracted in ethyl acetate (30 mL) from water (20 mL). The ethyl acetate layer was dried with $MgSO_4$ and concentrated under reduced pressure. ^{1}H NMR (500 MHz, $CDCl_3$) δ 7.82 (s, 2H), 7.25 – 7.19 (m, 2H), 6.95 (s, 2H), 6.84 (d, J = 9.9 Hz, 4H), 5.93 (s, 1H), 5.89 (s, 1H), 5.79 (s, 1H), 3.75 (s, 6H), 2.27 (s, 3H). ^{13}C NMR (126 MHz, $CDCl_3$) δ 153.77, 153.72, 145.68, 131.76, 127.35, 123.76, 117.32, 114.23, 111.94, 111.60, 109.85, 101.93, 77.23, 76.98, 76.72, 55.86, 34.13, 11.42, 9.93.

Synthesis of 3,3'-((5-nitrofuran-2-yl)methylene)bis(5-methoxy-1H-indole) (C8ar)

To a mixed solution of EtOH/H_2O (2:1 in 10 mL), 2-nitro-2-furaldehyde (0.5 mmol) and 5-methoxyindole (1 mmol) were added followed by catalyst (2.5 mol% with respect to aldehyde). The clear solution was concentrated under reduced pressure and extracted in ethyl acetate (30 mL) from water (20 mL). The ethyl acetate layer was dried with $MgSO_4$ and concentrated under reduced pressure. ^{1}H NMR (500 MHz, $CDCl_3$) δ 8.03 (s, 2H), 7.32 – 7.22 (m, 4H), 6.96 (d, J = 2.5 Hz, 2H), 6.93 – 6.85 (m, 4H), 6.35 – 6.30 (m, 1H), 5.91 (d, J = 1.4 Hz, 1H), 3.77 (d, J = 1.9 Hz, 6H).

Synthesis of 3,3'-((5-methylfuran-2-yl)methylene)bis(1H-indole) (C8ag)

To a mixed solution of EtOH/H_2O (2:1 in 10 mL), 5-methyl-furaldehyde (0.5 mmol) and indole (1 mmol) were added followed by catalyst (2.5 mol% with respect to aldehyde). The clear solution was concentrated under reduced pressure and extracted in ethyl acetate (30 mL) from water (20mL). The ethyl acetate layer was dried with $MgSO_4$ and concentrated under reduced pressure. ^{1}H NMR (500 MHz, $CDCl_3$) δ 7.86 (s, 2H), 7.23 (d, J = 8.7 Hz, 2H), 6.95 (d, J = 2.7 Hz, 2H),

6.90 – 6.81 (m, 4H), 5.83 (s, 1H), 5.74 (s, 1H), 3.75 (s, 6H), 2.18 (d, J = 3.9 Hz, 6H). ^{13}C NMR (126 MHz, $CDCl_3$) δ 155.06, 153.79, 150.59, 132.28, 131.76, 127.31, 123.82, 117.17, 111.98, 111.66, 107.33, 105.96, 101.87, 77.25, 77.00, 76.74, 55.87, 34.24, 13.69.

Synthesis of 3,3'-((5-nitrofuran-2-yl)methylene)bis(1H-indole) (C8ai)

To a mixed solution of EtOH/H_2O (2:1 in 10 mL), 2-nitro-2-furaldehyde (0.5 mmol) and indole (1 mmol) were added followed by catalyst (2.5 mol% with respect to aldehyde). The clear solution was concentrated under reduced pressure and extracted in ethyl acetate (30 mL) from water (20 mL). The ethyl acetate layer was dried with $MgSO_4$ and concentrated under reduced pressure. ^{1}H NMR (500 MHz, $CDCl_3$) δ 8.08 (s, 2H), 7.50 – 7.44 (m, 2H), 7.43 – 7.31 (m, 3H), 7.29 – 7.19 (m, 4H), 7.16 – 7.05 (m, 2H), 6.96 (dd, J = 2.5, 1.2 Hz, 2H), 6.34 – 6.29 (m, 1H), 6.01 (s, 1H). ^{13}C NMR (126 MHz, $CDCl_3$) δ 161.40, 136.58, 126.29, 123.35, 122.42, 119.79, 119.20, 114.73, 112.72, 111.35, 110.59, 77.23, 76.98, 76.72, 60.35, 34.77.

Synthesis of 3,3'-((4,5-methylfuran-2-yl)methylene)bis(1H-indole) (C8ah)

To a mixed solution of EtOH/H_2O (2:1 in 10 mL), 2-nitro-2-furaldehyde (0.5 mmol) and indole (1 mmol) were added followed by catalyst (2.5 mol% with respect to aldehyde). The clear solution was concentrated under reduced pressure and extracted in ethyl acetate (30 mL) from water (20mL). The ethyl acetate layer was dried with $MgSO_4$ and concentrated under reduced pressure. ^{1}H NMR (500 MHz, $CDCl_3$) δ 7.90 (s, 2H), 7.58 (d, J = 7.9 Hz, 2H), 7.36 (d, J = 7.9 Hz, 4H), 7.04 (dd, J = 16.9, 8.9 Hz, 3H), 6.95 (s, 2H), 5.87 (d, J = 17.3 Hz, 1H), 4.69 (s, 1H), 1.83 (s, 3H). ESI-MS expected $C_{22}H_{17}N_2O$: 326.1; observed 325.1326

Synthesis of 3,3'-((4,5-dimethylfuran-2-yl)methylene)bis(1H-indole) (C8aq)

To a mixed solution of EtOH/H_2O (2:1 in 10 mL), 2-nitro-2-furaldehyde (0.5 mmol) and indole (1 mmol) were added followed by catalyst (2.5 mol% with respect to aldehyde). The clear solution was concentrated under reduced pressure and extracted in ethyl acetate (30 mL) from water (20 mL). The ethyl acetate layer was dried with $MgSO_4$ and concentrated under reduced pressure. ^{1}H NMR (500 MHz, $CDCl_3$) δ 7.72 (d, 1H), 7.63 – 7.54 (m, 2H), 7.39 (d, 1H), 7.37 – 7.16 (m, 7H), 7.14 – 7.04 (m, 2H), 6.60 (s, 1H), 5.89 (s, 1H), 2.20 (s, 3H), 1.92 (s, 3H). ESI-MS expected $C_{23}H_{19}N_2O$: 340.1; observed 360.1475.

Synthesis of 3,3'-(cyclohexylmethylene)bis(1H-indole) (C8as)

To a mixed solution of EtOH/H_2O (2:1 in 10 mL), cyclohexanecarboxaldehyde (0.5 mmol) and indole (1 mmol) were added followed by catalyst (2.5 mol% with respect to aldehyde). The clear solution was concentrated under reduced pressure and extracted in ethyl acetate (30 mL) from water (20 mL). The ethyl acetate layer was dried with $MgSO_4$ and concentrated under reduced pressure. The compound was isolated via column chromatography (40 ethyl acetate: 60 hexanes) and concentrated under reduced pressure to yield a colourless oil. 12%. ^{1}H NMR (500 MHz,

$CDCl_3$) δ 7.89 (s, 2H), 7.67 (ddd, J = 7.9, 1.6, 0.8 Hz, 2H), 7.41 – 7.25 (m, 2H), 7.21 – 7.02 (m, 6H), 4.29 (d, J = 8.8 Hz, 1H), 2.27 (dtt, J = 11.8, 8.7, 3.3 Hz, 1H), 1.85 (dd, J = 13.9, 4.0 Hz, 2H), 1.67 (ddt, J = 17.4, 12.3, 3.9 Hz, 3H), 1.20 – 1.01 (m, 3H), 0.94 – 0.84 (m, 3H). ESI-MS expected $C_{23}H_{24}N_2$: 328.2; observed 351.1837 ($C_{23}H_{24}N_2Na$).

Synthesis of 3,3'-(phenylmethylene)bis(2-methyl-1H-indole) (C8at)

To a mixed solution of EtOH/H_2O (2:1 in 10 mL),) benzaldehyde (0.5 mmol) and 5-methoxyindole (1 mmol) were added followed by catalyst (2.5 mol% with respect to benzaldehyde). The resultant solution was stirred for 12 h, upon which time product had precipitated. The cloudy solution was filtered and precipitate washed with hexanes (3 x 10mL) and water (3 x 10mL). ^{1}H NMR (500 MHz, $CDCl_3$) δ 7.72 (s, 2H), 7.32 – 7.18 (m, 6H), 7.08 – 6.96 (m, 4H), 6.86 (t, J = 7.9 Hz, 2H), 6.02 (s, 1H), 2.07 (d, J = 2.5 Hz, 6H), 1.27 (s, 1H).

Synthesis of 3-(2-nitro-1-phenylethyl)-1H-indole (**C8ba**)

Indole (58 mg, 0.5 mmol), *trans*-β-nitrostyrene (74 mg, 0.5 mmol), 1.0 mol% pre-catalyst (**1ZnDy-NO$_3$**), 3 mL EtOH, r.t, 24 h. The crude product was purified by column chromatography with silica (20% ethyl acetate in hexanes) to afford the title compound **C8ba**. ^{1}H NMR ($CDCl_3$, 500 MHz): = 8.10 (s, 1H), 7.45 (d, *J*= 8.0 Hz, 1H), 7.35-7.26 (m, 5H), 7.21-7.18(m, 1H), 7.08-7.02 (m ,2H), 5.21 (t, *J*= 8.0 Hz, 1H), 5.08 (dd, *J*= 7.5 Hz, 2.5Hz, 1H), 4.96 (dd, *J*=8.5 Hz, 8.0 Hz, 1H). ^{13}C NMR ($CDCl_3$, 126 MHz): 139.46, 136.41, 128.88, 127.73, 127.52, 125.90, 122.71, 121.56, 119.98, 118.93, 114.66, 111.32, 79.52, 41.56.

Synthesis of 3-(2-nitro-1-(p-tolyl)ethyl)-1H-indole (**C8bb**)

Indole (58 mg, 0.5 mmol), *trans*-4-methyl-β-nitrostyrene (81 mg, 0.5 mmol), 1.0 mol% pre-catalyst (**1ZnDy-NO$_3$**), 3 mL EtOH, r.t, 24 h. The crude product was purified by column chromatography with silica (20% ethyl acetate in hexanes) to afford the title compound **C8bb** (274 mg, 0.98 mmol, 98%). ^{1}H NMR ($CDCl_3$, 500 MHz): = 8.08 (s, 1H), 7.46 (d, *J*= 7.2 Hz, 1H), 7.37 (d, *J* = 8.0, 1H), 7.21-7.16(m, 3H), 7.15-7.10 (m ,2H), 7.09 (d, *J* = 2.5 Hz, 1H) 7.04 (d, *J*= 2.0 Hz, 1H), 5.17 (t, *J*= 7.8 Hz, 1H), 5.06 (dd, *J*= 7.0 Hz, 2.5Hz, 1H), 4.95 (dd, *J*=8.2 Hz, 8.1 Hz, 1H), 2.32 (s, 1H). ^{13}C NMR ($CDCl_3$, 126 MHz): 139.60, 137.17, 134.62, 129.56, 127.59, 126.15, 124.76, 122.66, 121.49, 119.93, 118.96, 114.68, 111.29, 79.63, 41.21, 20.99.

Synthesis of 3-(1-(4-methoxyphenyl)-2-nitroethyl)-1H-indole (**C8bc**)

Indole (58 mg, 0.5 mmol), *trans*-4-methoxy-β-nitrostyrene (89 mg, 0.5 mmol), 1.0 mol% pre-catalyst (**1ZnDy-NO$_3$**), 3 mL EtOH, r.t, 24 h. The crude product was purified by column chromatography with silica (20% ethyl acetate in hexanes) to afford the title compound **C8bc**. ^{1}H NMR ($CDCl_3$, 500 MHz): = 8.09 (s, 1H), 7.45 (d, *J*= 6.9 Hz, 1H), 7.37 (d, *J* = 8.2, 1H), 7.26-7.19(m, 3H), 7.09 (d, *J* = 3.0 Hz, 1H) 7.03 (d, *J* = 2.8 Hz, 1H), 6.86 – 6.78 (m, 2H), 5.15 (t, *J* = 7.2 Hz, 1H), 5.06 (dd, *J*= 7.0 Hz, 2.5Hz, 1H), 4.91 (dd, *J*=7.8 Hz, 7.6 Hz, 1H), 3.79 (s, 3H).^{13}C

NMR ($CDCl_3$, 126 MHz): 158.93, 131.30, 128.78, 122.68, 121.42, 119.93, 118.99, 114.30, 111.31, 109.99, 107.75, 103.39, 79.75, 55.23, 40.87.

Synthesis of 3-(1-(4-fluorophenyl)-2-nitroethyl)-1H-indole (**C8bd**)

Indole (58 mg, 0.5 mmol), *trans*-4-fluoro-β-nitrostyrene (83 mg, 0.5 mmol), 1.0 mol% pre-catalyst (**1ZnDy-NO$_3$**), 3 mL EtOH, r.t, 24 h. The crude product was purified by column chromatography with silica (20% ethyl acetate in hexanes) to afford the title compound **C8bd**. ^{1}H NMR ($CDCl_3$, 500 MHz): = 8.11 (s, 1H), 7.40 – 7.34 (m, 2H), 7.31 – 7.26 (m, 2H), 7.22 (dd, J = 6.8 Hz, , 2.4 Hz, 1H), 7.10 (dd, *J* = 7.1 Hz, 3.0 Hz, 1H) 7.02 – 6.94 (m, 3H), 5.19 (t, *J* = 6.6 Hz, 1H), 5.07 (dd, *J*= 7.2 Hz, 2.4 Hz, 1H), 4.92 (dd, *J*=7.6 Hz, 7.3 Hz, 1H). ^{13}C NMR ($CDCl_3$, 126 MHz): 161.1, 136.5, 131.3, 129.4, 128.3, 125.9, 122.8, 121.4, 120.0, 118.8, 115.8 (2C), 115.7, 114.3, 79.5, 40.8.

Synthesis of 3-(1-(4-bromophenyl)-2-nitroethyl)-1H-indole (**C8be**)

Indole (58 mg, 0.5 mmol), *trans*-4-bromo-β-nitrostyrene (114 mg, 0.5 mmol), 1.0 mol% pre-catalyst (**1ZnDy-NO$_3$**), 3 mL EtOH, r.t, 24 h. The crude product was purified by column chromatography with silica (20% ethyl acetate in hexanes) to afford the title compound **C8be**. ^{1}H NMR ($CDCl_3$, 500 MHz): = 8.15 (s, 1H), 7.46 – 7.38 (m, 2H), 7.37 – 7.30 (m, 2H), 7.22 – 7.14(m, 3H), 7.10 (dd, *J* = 6.8 Hz, *J* = 2.6 Hz, 1H), 7.03 (d, *J* = 3.0 Hz, 1H), 5.16 (t, *J* = 7.4 Hz, 1H), 5.06 (dd, *J*= 6.9 Hz, 2.8 Hz, 1H), 4.92 (dd, *J*=8.0 Hz, 7.7 Hz, 1H).^{13}C NMR ($CDCl_3$, 126 MHz): 138.2, 136.8, 132.0, 131.3, 129.4, 122.8, 121.5 (2C), 120.1, 118.7, 115.1, 111.5, 79.1, 41.0.

Synthesis of 3-(1-(2-furanyl)-2-nitroethyl)-1H-indole (C8bf)

Indole (58 mg, 0.5 mmol), *trans*-2-furanyl-β-nitrostyrene (69 mg, 0.5 mmol), 1.0 mol% pre-catalyst (**1ZnDy-NO$_3$**), 3 mL EtOH, r.t, 24 h. The crude product was purified by column chromatography with silica (20% ethyl acetate in hexanes) to afford the title compound **C8bf**. ^{1}H NMR ($CDCl_3$, 500 MHz): = 8.12 (s, 1H), 7.58 (d, *J*= 5.8 Hz, 1H), 7.39 – 7.33 (m, 2H), 7.25-7.18(m, 1H), 7.16-7.10 (m, 2H), 6.33 (d, *J* = 4.2 Hz, 1H), 6.18 (d, *J*= 4.0 Hz, 1H), 5.27 (t, *J* = 8.2 Hz, 1H), 5.07 (dd, *J*= 6.8 Hz, 2.8Hz, 1H), 4.92 (dd, *J*=7.2 Hz, 7.0 Hz, 1H). ^{13}C NMR ($CDCl_3$, 126 MHz): 152.2, 142.2, 136.3, 125.7, 122.6 (2C), 120.3, 120.1, 118.7, 111.8, 111.4, 110.4, 107.3, 77.8, 35.7.

Synthesis of 5-methoxy-3-(2-nitro-1-phenylethyl)-1H-indole (**C8bg**)

5-methoxyindole (73 mg, 0.5 mmol), *trans*-β-nitrostyrene (74 mg, 0.5 mmol), 1.0 mol% pre-catalyst (**1ZnDy-NO$_3$**), 3 mL EtOH, r.t, 24 h. The crude product was purified by column chromatography with silica (20% ethyl acetate in hexanes) to afford the title compound **C8bg**. ^{1}H NMR ($CDCl_3$, 500 MHz): = 8.00 (s, 1H), 7.34 (d, *J*= 8.0 Hz, 4H), 7.26-7.18 (m, 2H), 7.21-7.18(m, 1H), 7.02 – 6.92 (m ,2H), 5.15 (t, *J*= 7.2 Hz, 1H), 5.06 (dd, *J*= 8.0 Hz, 2.8 Hz, 1H), 4.95 (dd,

J=7.6 Hz, 6.8 Hz, 1H), 3.78 (s, 3H).^{13}C NMR ($CDCl_3$, 126 MHz): 154.39, 139.06, 131.46, 128.75, 127.30, 127.05, 126.22, 123.77, 112.81, 112.19, 111.45, 110. 45, 100.68, 77.83, 55.91, 40.85.

Synthesis of 5-bromo-3-(2-nitro-1-phenylethyl)-1H-indole (**C8bh**)

5-bromoindole (98 mg, 0.5 mmol), *trans*-β-nitrostyrene (74 mg, 0.5 mmol), 1.0 mol% pre-catalyst (**1ZnDy-NO$_3$**), 3 mL EtOH, r.t, 24 h. The crude product was purified by column chromatography with silica (20% ethyl acetate in hexanes) to afford the title compound **C8bh**. ^{1}H NMR ($CDCl_3$, 500 MHz): = 8.22 (s, 1H), 7.6 (d, *J* = 1Hz, 1H), 7.33-7.18 (m ,7H), 7.03 (d, *J* = 2.5 Hz, 1H), 5.12 (t, *J* = 8.0 Hz, 1H), 5.01 (dd, *J* = 8.0 Hz, 8.0 Hz, 1H), 4.91(dd, *J* = 8.0 Hz, 8.0 Hz, 1H). ^{13}C NMR ($CDCl_3$, 126 MHz):138.29, 136.54, 132.05, 129.46, 127.86, 126.95, 125.90, 122.88, 121.51, 120.12, 118.78, 113.96, 111.43, 79.19, 41.04.

Synthesis of 5-iodo-3-(2-nitro-1-phenylethyl)-1H-indole (**C8bi**)

5-iodoindole (121 mg, 0.5 mmol), *trans*-β-nitrostyrene (74 mg, 0.5 mmol), 1.0 mol% pre-catalyst (**1ZnDy-NO$_3$**), 3 mL EtOH, r.t, 24 h. The crude product was purified by column chromatography with silica (20% ethyl acetate in hexanes) to afford the title compound **C8bi**. ^{1}H NMR ($CDCl_3$, 500 MHz): = 8.15 (s, 1H), 7.77 (d, *J* = 2.0 Hz, 1H), 7.45 (d, *J* = 2.8 Hz, 1H), 7.33-7.24 (m ,5H), 7.15 (d, *J* = 2.8 Hz, 1H), 7.04 (d, *J* = 2.0 Hz, 1H), 5.14 (t, *J* = 7.6 Hz, 1H), 5.03 (dd, *J* = 8.2 Hz, 8.0 Hz, 1H), 4.93(dd, *J* = 8.1 Hz, 7.8 Hz, 1H). ^{13}C NMR ($CDCl_3$, 126 MHz): 138.63, 135.5, 131.18, 129.02, 128.6, 127.7 (2C), 127.63, 127.63, 126.13, 122.33, 120.88, 114.47, 113.9, 113.26, 79.39, 41.26.

Synthesis of 5-nitro-3-(2-nitro-1-phenylethyl)-1H-indole (**C8bj**)

5-nitroindole (81 mg, 0.5 mmol), *trans*-β-nitrostyrene (74 mg, 0.5 mmol), 1.0 mol% pre-catalyst (**1ZnDy-NO$_3$**), 3 mL EtOH, r.t, 24 h. The crude product was purified by column chromatography with silica (20% ethyl acetate in hexanes) to afford the title compound **C8bj**. ^{1}H NMR ($CDCl_3$, 500 MHz): = 8.47 (s, 1H), 8.38 (d, *J* = 2.5 Hz, 1H), 8.13 (dd, *J* = 3.5 Hz, 3.0 Hz, 1H), 7.35-7.22 (m ,7H), 5.25 (t, *J* = 7.2 Hz, 1H), 5.08 (dd, *J* = 7.8 Hz, 7.6 Hz, 1H), 4.97 (dd, *J* = 8.0 Hz, 7.8 Hz, 1H) .^{13}C NMR ($CDCl_3$, 126 MHz): 142.6, 139.0, 132.30, 128.7, 126.5, 126.23, 124.10, 122.18, 117.3, 114.2, 113.2, 111.58, 79.78, 40.85.

Synthesis of 5-benzoxy-3-(2-nitro-1-phenylethyl)-1H-indole (**C8bk**)

5-benzoxyindole (111 mg, 0.5 mmol), *trans*-β-nitrostyrene (74 mg, 0.5 mmol), 1.0 mol% pre-catalyst (**1ZnDy-NO$_3$**), 3 mL EtOH, r.t, 24 h. The crude product was purified by column chromatography with silica (20% ethyl acetate in hexanes) to afford the title compound **C8bk** (357 mg, 0.96 mmol, 96%). ^{1}H NMR ($CDCl_3$, 500 MHz): = 7.98 (s, 1H), 7.48 – 7.42 (m, 2H), 7.38 – 7.34 (m, 2H), 7.33 - 7.26 (m ,4H), 7.25 (d, *J* = 2.5 Hz, 1H), 7.02 (d, *J* = 2.0 Hz, 1H), 6.94 (d, *J* = 3.0 Hz, 2H), 5.12 (t, *J* = 6.5 Hz, 1H), 5.02 - 4.98 (m, 3H), 4.93 (dd, *J* = 8.0 Hz, 7.8 Hz,

1H). ^{13}C NMR ($CDCl_3$, 126 MHz): 153.4, 152.1, 142.2, 137.4, 131.6, 128.5, 127.8, 127.5, 126.1, 123.3, 122.18, 113.5, 112.1, 111.5, 110.4, 107.3, 102.4, 77.7, 71.03, 35.7.

Synthesis of 5-methoxy- 3-(1-(2-furanyl)-2-nitroethyl)-1H-indole (**C8bl**)

5-methoxyindole (73 mg, 0.5 mmol), *trans*-2-furanyl-β-nitrostyrene (69 mg, 0.5 mmol), 1.0 mol% pre-catalyst (**1ZnDy-NO$_3$**), 3 mL EtOH, rt, 24 h. The crude product was purified by column chromatography with silica (20% ethyl acetate in hexanes) to afford the title compound **C8bl.** ^{1}H NMR ($CDCl_3$, 500 MHz): = 8.08 (s, 1H), 7.40 (d, *J* = 4.2 Hz, 1H), 7.27- 7.21 (m, 1H), 7.10 (d, *J* = 2.8 Hz, 1H), 6.97 (d, *J* = 2.5 Hz, 1H), 6.89 (d, J = 3.0, 1H), 6.33 (d, *J* = 3.0 Hz, 1H), 6.19 (d, *J*= 3.8 Hz, 1H), 5.22 (t, *J* = 7.6 Hz, 1H), 5.05 (dd, *J* = 7.4 Hz, 7.3 Hz, 1H), 4.91(dd, *J* = 7.6 Hz, 7.4 Hz, 1H), 3.85 (s, 3H).^{13}C NMR ($CDCl_3$, 126 MHz): 154.39, 152.25, 142.20, 131.46, 126.22, 123.27, 112.81, 112.19, 111.45, 110.45, 107.33, 100.68, 77.83, 55.91, 35.69.

Synthesis of 5-bromo- 3-(1-(2-furanyl)-2-nitroethyl)-1H-indole (**C8bm**)

5-bromoindole (98 mg, 0.5 mmol), *trans*-2-furanyl-β-nitrostyrene (69 mg, 0.5 mmol), 1.0 mol% pre-catalyst (**1ZnDy-NO$_3$**), 3 mL EtOH, r.t, 24 h. The crude product was purified by column chromatography with silica (20% ethyl acetate in hexanes) to afford the title compound **C8bm.** ^{1}H NMR ($CDCl_3$, 500 MHz): = 8.20 (s, 1H), 7.56 (d, *J* = 5.8 Hz, 1H), 7.44 (d, *J* = 4.2 Hz, 1H), 7.38 – 7.34 (m, 1H), 7.25-7.18(m, 1H), 7.04 (d, *J* = 2.0 Hz, 1H), 6.28 (d, *J* = 3.8 Hz, 1H), 6.18 (d, *J*= 4.0 Hz, 1H), 5.16 (t, *J* = 7.4 Hz, 1H), 5.06 (dd, *J* = 8.2 Hz, 8.0 Hz, 1H), 4.94(dd, *J* = 8.1 Hz, 8.0 Hz, 1H). ^{13}C NMR ($CDCl_3$, 126 MHz): 155.37, 142.22, 136.34, 129.40, 122.6 (2C), 120.11, 118.71, 115.81, 111.47, 110.44, 107.36, 77.87, 35.72.

Synthesis of 5- benzoxy-3-(1-(2-furanyl)-2-nitroethyl)-1H-indole (**C8bn**)

5-benzoxyindole (111 mg, 0.5 mmol), *trans*-2-furanyl-β-nitrostyrene (69 mg, 0.5 mmol), 1.0 mol% pre-catalyst (**1ZnDy-NO$_3$**), 3 mL EtOH, r.t, 24 h. The crude product was purified by column chromatography with silica (20% ethyl acetate in hexanes) to afford the title compound **C8bn.** ^{1}H NMR ($CDCl_3$, 500 MHz): = 8.04 (s, 1H), 7.48 – 7.41 (m, 2H), 7.39 – 7.34 (m, 3H), 7.33 - 7.28 (m ,1H), 7.27 – 7.22 (m, 1H), 7.10 (t, J = 4.2 Hz, 1H), 7.06 (t, *J* = 3.6 Hz, 1H), 6.97 (d, *J* = 2.8 Hz, 2H), 6.31 (d, *J* = 4.0 Hz, 1H), 6.15 (d, *J*= 3.8 Hz, 1H), 5.20 (t, *J* = 7.0 Hz, 1H), 5.10 – 5.03 (m, 3H), 4.87 (dd, *J* = 7.6 Hz, 7.4 Hz, 1H). ^{13}C NMR ($CDCl_3$, 126 MHz): 153.4, 152.1, 142.2, 137.4, 131.6, 128.5, 127.8, 127.5, 126.1, 123.3, 122.18, 113.5, 112.1, 111.5, 110.4, 107.3, 102.4, 77.7, 71.03, 35.7.

Synthesis of 5- iodo -3-(1-(2-furanyl)-2-nitroethyl)-1H-indole (**C8bo**)

5-iodoindole (137 mg, 0.5 mmol), *trans*-2-furanyl-β-nitrostyrene (69 mg, 0.5 mmol), 1.0 mol% pre-catalyst (**1ZnDy-NO$_3$**), 3 mL EtOH, r.t, 24 h. The crude product was purified by column chromatography with silica (20% ethyl acetate in hexanes) to afford the title compound **C8bo**. ^{1}H NMR ($CDCl_3$, 500 MHz): = 8.22 (s, 1H), 7.89 (d, *J* = 4.0 Hz, 1H), 7.48 (dd, *J* = 6.2 Hz, 4.0 Hz,

1H), 7.40 – 7.35 (m, 1H), 7.15 – 7.08 (m, 2H), 6.33 (d, *J* = 4.0 Hz, 1H), 6.16 – 6.10 (m, 1H), 5.19 (t, *J* = 8.0 Hz, 1H), 5.04 – 4.98 (m, 1H), 4.90 (dd, *J* = 8.2 Hz, 8.0 Hz, 1H). ^{13}C NMR ($CDCl_3$, 126 MHz): 156.58, 142.37, 131.14, 127.61, 126.15, 123.43, 119.91, 113.38, 110.51, 107.51, 88.11, 35.47.

Synthesis of 3-(2-nitro-1-phenylethyl)-1-methyl-indole (**C8bp**)

N-methylindole (39 mg, 0.3 mmol), *trans*-β-nitrostyrene (44 mg, 0.3 mmol), 1.0 mol% pre-catalyst (**1ZnDy-NO$_3$**), 3 mL EtOH, r.t, 24 h. The crude product was purified by column chromatography with silica (20% ethyl acetate in hexanes) to afford the title compound **C8bp**. ^{1}H NMR ($CDCl_3$, 500 MHz): = 7.45 (d, *J*= 7.6 Hz, 1H), 7.33-7.26 (m, 5H), 7.24-7.18(m, 1H), 7.08-7.02 (m , 2H), 6.87 (s, 1H), 5.19 (t, *J*= 7.8 Hz, 1H), 5.06 (dd, *J*= 7.2 Hz, 2.8Hz, 1H), 4.95 (dd, *J* = 8.0 Hz, 7.8 Hz, 1H), 3.76 (s, 3H). ^{13}C NMR ($CDCl_3$, 126 MHz): 139.46, 136.41, 128.88, 127.73, 127.52, 125.90, 122.71, 121.56, 119.98, 118.93, 114.66, 111.32, 79.52, 41.56.

Synthesis of 3-(1-(4-methoxyphenyl)-2-nitroethyl)-1-methyl-indole (**C8bq**)

N-methylindole (39 mg, 0.3 mmol), *trans*-4-methoxy-β-nitrostyrene (54 mg, 0.3 mmol), 1.0 mol% pre-catalyst (**1ZnDy-NO$_3$**), 3 mL EtOH, r.t, 24 h. The crude product was purified by column chromatography with silica (20% ethyl acetate in hexanes) to afford the title compound **C8bq**. ^{1}H NMR ($CDCl_3$, 500 MHz): = 7.48 (d, *J*= 7.0 Hz, 1H), 7.35 – 7.28 (m, 4H), 7.25-7.18 (m, 1H), 6.89 (d, *J* = 3.0 Hz, 3H), 5.18 (t, *J* = 7.0 Hz, 1H), 5.06 (dd, *J*= 7.2 Hz, 2.8Hz, 1H), 4.86 (dd, *J*=8.2 Hz, 7.8 Hz, 1H), 3.67 (s, 3H), 3.62 (s, 3H). ^{13}C NMR ($CDCl_3$, 126 MHz): 158.90, 137.35, 131.41, 128.75, 126.56, 126.23, 124.10, 122.18, 119.40, 119.03, 117.73, 114.28, 113.22, 109.45, 79.78, 55.23, 40.85, 32.76.

Synthesis of 3-(1-(4-fluorophenyl)-2-nitroethyl)-1-methyl-indole (**C8br**)

N-methylindole (39 mg, 0.3 mmol), *trans*-4-fluoro-β-nitrostyrene (50 mg, 0.3 mmol), 1.0 mol% pre-catalyst (**1ZnDy-NO$_3$**), 3 mL EtOH, r.t, 24 h. The crude product was purified by column chromatography with silica (20% ethyl acetate in hexanes) to afford the title compound **C8br.** ^{1}H NMR ($CDCl_3$, 500 MHz): = 7.42 – 7.37 (m, 1H), 7.32 – 7.24 (m, 3H), 7.24 (dd, *J* = 7.0 Hz, , 2.6 Hz, 1H), 7.09 (dd, *J* = 7.4 Hz, 2.8 Hz, 1H) 7.02 – 6.96 (m, 2H), 6.86 (s, 1H) 5.18 (t, *J* = 7.2 Hz, 1H), 5.05 (dd, *J*= 8.0 Hz, 2.5 Hz, 1H), 4.91 (dd, *J*=8.0 Hz, 8.1 Hz, 1H), 3.77 (s, 3H). ^{13}C NMR ($CDCl_3$, 126 MHz): 161.09, 137.37, 135.20, 135.17, 129.35, 129.29, 126.42, 126.19, 122.35, 119.55, 118.90, 115.86, 115.69, 109.56, 79.57, 40.87, 32.80.

Synthesis of 3-(1-(4-bromophenyl)-2-nitroethyl)-1-methyl-indole (**C8bs**)

N-methylindole (39 mg, 0.3 mmol), *trans*-4-bromo-β-nitrostyrene (68 mg, 0.3 mmol), 1.0 mol% pre-catalyst (**1ZnDy-NO$_3$**), 3 mL EtOH, r.t, 24 h. The crude product was purified by column chromatography with silica (20% ethyl acetate in hexanes) to afford the title compound **C8bs**. ^{1}H NMR ($CDCl_3$, 500 MHz): = 7.46 – 7.42 (m, 2H), 7.41 – 7.34 (m, 1H), 7.31 (dd, *J* = 2.8 Hz, 1H),

7.24 – 7.16 (m, 3H), 7.09 (dd, *J* = 7.0 Hz, *J* = 2.8 Hz, 1H), 6.85 (s, 1H), 5.15 (t, *J* = 7.6 Hz, 1H), 5.04 (dd, *J*= 7.2 Hz, 2.5 Hz, 1H), 4.91 (dd, *J*=8.0 Hz, 7.8 Hz, 1H), 3.76 (s, 3H) . ^{13}C NMR ($CDCl_3$, 126 MHz): 139.46, 136.26, 134.43, 132.03, 129.26, 126.26, 125.27, 122.39, 119.60, 118.82, 109.99, 109.57, 79.21, 41.01, 32.82.

Synthesis of 3-(1-(2-furanyl)-2-nitroethyl)-1-methyl-indole (**C8bt**)

N-methylindole (39 mg, 0.3 mmol), *trans*-2-furanyl-β-nitrostyrene (42 mg, 0.3 mmol), 1.0 mol% pre-catalyst (**1ZnDy-NO$_3$**), 3 mL EtOH, r.t, 24 h. The crude product was purified by column chromatography with silica (20% ethyl acetate in hexanes) to afford the title compound **C8bt** (267 mg, 0.99 mmol, 99%). ^{1}H NMR ($CDCl_3$, 500 MHz): = 7.56 – 7.48 (m, 1H), 7.40 (dd, *J* = 4.3 Hz, 1H), 7.32 – 7.29 (m, 1H), 7.27 – 7.21 (m, 1H), 7.14 (dd, *J* = 7.1 Hz, *J* = 2.8 Hz, 1H), 6.99 (s, 1H), 6.33 (d, *J* = 4.0 Hz, 1H), 6.18 (d, *J*= 4.2 Hz, 1H), 5.25 (t, *J* = 8.0 Hz, 1H), 5.05 (dd, *J*= 7.0 Hz, 3.0 Hz, 1H), 4.92 (dd, *J*=7.2 Hz, 7.0 Hz, 1H), 3.77 (s, 3H). ^{13}C NMR ($CDCl_3$, 126 MHz): 152.38, 142.16, 137.16, 127.25, 126.19, 122.17, 119.58, 118.76, 110.42, 110.05, 109.60, 107.23, 77.99, 35.68, 32.80.

Synthesis of 3-(2-nitro-1-phenylethyl)-2-methyl-1H-indole (**C8bu**)

2-methylindole (39 mg, 0.3 mmol), *trans*-β-nitrostyrene (44 mg, 0.3 mmol), 1.0 mol% pre-catalyst (**1ZnDy-NO$_3$**), 3 mL EtOH, r.t, 24 h. The crude product was purified by column chromatography with silica (20% ethyl acetate in hexanes) to afford the title compound **C8bu**. ^{1}H NMR ($CDCl_3$, 500 MHz): = 7.86 (s, 1H), 7.39 (d, *J*= 8.1 Hz, 1H), 7.30-7.21 (m, 6H), 7.13-7.08(m, 1H), 7.05 (dd, *J* = 6.0 Hz, 1H), 5.23 – 5.16 (m, 2H), 5.13 (dd, *J*= 8.0 Hz, 2.6Hz, 1H), 2.40 (s, 3H) .^{13}C NMR ($CDCl_3$, 126 MHz): 139.54, 135.44, 132.77, 128.75, 127.30, 127.73, 127.05, 126.91, 122.71, 121.36, 119.77, 110.67, 109.99, 108.98, 78.63, 41.47, 11.99.

Synthesis of 3-(1-(4-fluorophenyl)-2-nitroethyl)- 2-methyl-1H-indole (**C8bv)**

2-methylindole (39 mg, 0.3 mmol), *trans*-4-fluoro-β-nitrostyrene (50 mg, 0.3 mmol), 1.0 mol% pre-catalyst (**1ZnDy-NO$_3$**), 3 mL EtOH, r.t, 24 h. The crude product was purified by column chromatography with silica (20% ethyl acetate in hexanes) to afford the title compound **C8bv.** ^{1}H NMR ($CDCl_3$, 500 MHz): = 7.89 (s, 1H), 7.35 (d, *J*= 7.8 Hz, 1H), 7.29-7.20 (m, 3H), 7.14-7.08(m, 1H), 7.05 (dd, *J* = 6.2 Hz, 1H), 6.99 – 6.92 (m, 2H), 5.20 – 5.12 (m, 2H), 5.09 (dd, *J*= 8.2 Hz, 3.0 Hz, 1H), 2.42 (s, 3H).^{13}C NMR ($CDCl_3$, 126 MHz): 162.74, 135.42, 132.69, 128.90, 128.84, 126.72, 121.50, 119.89, 118.44, 115.69, 115.52, 115.69, 110.72, 109.99, 108.83, 78.66, 40.87, 39.85, 12.03.

Synthesis of 3-(1-(4-bromophenyl)-2-nitroethyl)- 2-methyl-1H-indole (**C8bw**)

2-methylindole (39 mg, 0.3 mmol), *trans*-4-bromo-β-nitrostyrene (68 mg, 0.3 mmol), 1.0 mol% pre-catalyst (**1ZnDy-NO$_3$**), 3 mL EtOH, r.t, 24 h. The crude product was purified by column chromatography with silica (20% ethyl acetate in hexanes) to afford the title compound **C8bw**.

^{1}H NMR ($CDCl_3$, 500 MHz): = 7.91 (s, 1H), 7.43 – 7.38 (m, 2H), 7.30 - 7.24 (m, 2H), 7.20 - 7.15(m, 2H), 7.14 – 7.09 (m, 1H), 7.05 – 6.99 (m, 1H), 5.21 (d, *J* = 8.0 Hz, 7.8 Hz, 1H), 5.15 – 5.10 (m, 1H), 5.08 (dd, *J*= 7.6 Hz, 3.2 Hz, 1H), 2.42 (s, 3H). ^{13}C NMR ($CDCl_3$, 126 MHz): 138.59, 135.43, 132.79, 131.85, 130.50, 129.02, 126.65, 124.79, 121.04, 119.94, 118.38, 110.75, 108.46, 78.32, 41.01, 39.97, 12.02.

Synthesis of 3-(1-(2-furanyl)-2-nitroethyl)- 2-methyl-1H-indole (**C8bx**)

2-methylindole (39 mg, 0.3 mmol), *trans*-2-furanyl-β-nitrostyrene (42 mg, 0.3 mmol), 1.0 mol% pre-catalyst (**1ZnDy-NO$_3$**), 3 mL EtOH, r.t, 24 h. The crude product was purified by column chromatography with silica (20% ethyl acetate in hexanes) to afford the title compound **C8bx.** ^{1}H NMR ($CDCl_3$, 500 MHz): = 7.90 (s, 1H), 7.39 – 7.32 (m, 2H), 7.28 - 7.22 (m, 1H), 7.14 – 7.08 (m, 1H), 7.06 – 6.99 (m, 1H), 6.31 (d, *J* = 3.8 Hz, 1H), 6.10 (d, *J* = 4.0 Hz, 1H), 5.20 – 5.12 (m, 2H), 4.95 – 4.88 (m, 1H), 2.41 (s, 3H). ^{13}C NMR ($CDCl_3$, 126 MHz): 152.31, 141.94, 135.40, 133.07, 126.63, 121.47, 119.75, 118.53, 110.63, 110.43, 109.99, 107.21, 78.71, 35.68, 35.29, 11.77.

Synthesis of 3-(2-nitro-1-(p-tolyl)ethyl)-2-methyl-1H-indole (**C8by**)

2-methylindole (39 mg, 0.3 mmol), *trans*-4-methyl-β-nitrostyrene (49 mg, 0.3 mmol), 1.0 mol% pre-catalyst (**1ZnDy-NO$_3$**), 3 mL EtOH, r.t, 24 h. The crude product was purified by column chromatography with silica (20% ethyl acetate in hexanes) to afford the title compound **C8by**. ^{1}H NMR ($CDCl_3$, 500 MHz): = 7.85 (s, 1H), 7.38 (d, J = 4.2 Hz, 1H), 7.32 - 7.25 (m, 3H), 7.20 - 7.12(m, 3H), 7.08 – 7.01 (m, 1H), 5.20 – 5.08 (m, 3H), 2.46 (s, H), 2.42 (s, 3H). ^{13}C NMR ($CDCl_3$, 126 MHz): 136.66, 136.45, 135.42, 132.64, 129.41, 127.16, 126.93, 121.31, 119.72, 118.65, 110.60, 109.60, 78.73, 41.01, 40.14, 20.91, 12.02.

Synthesis of compound (**C8ca)**

Salicylaldehyde (61 mg, 0.5 mmol), indoline (59 mg, 0.5 mmol), benzene boronic acid (61 mg, 0.5 mmol), 1.0 mol% **1ZnDy-NO$_3$**, 5 mL DME, r.t, 16 h. The crude product was purified by column chromatography with silica (10% ethyl acetate in hexanes) to afford the title compound **C8ca** (289 mg, 0.96 mmol, 96%). ^{1}H NMR ($CDCl_3$, 500 MHz): δ = 11.03 (s, 1H), 7.54 – 7.48 (m, 1H), 7.46 – 7.39 (m, 2H), 7.32 – 7.26 (m, 3H), 7.19 – 7.15 (m, 1H), 7.14 – 7.11 (m, 1H), 6.99 – 6.92 (m , 3H), 6.90 (dd, J = 5.2 Hz, 3.8 Hz, 1H), 6.83 – 6.78 (m, 2H), 6.49 (d, *J*=6.0 Hz, 1H), 5.34 (s, 1H), 3.21 (m, 1H), 3.01 (m, 1H), 2.93 (m, 1H). ^{13}C NMR ($CDCl_3$, 126 MHz): δ = 156.22, 151.08, 139.54, 132.12, 128.50, 128.02, 127.37, 124.60, 121.08, 119.79, 117.02, 111.76, 69.98, 53.00, 28.51.

Synthesis of compound (**C8cb)**

Salicylaldehyde (61 mg, 0.5 mmol), morpholine (43 mg, 0.5 mmol), benzene boronic acid (61 mg, 0.5 mmol), 1.0 mol% **1ZnDy-NO$_3$**, 5 mL DME, r.t, 16 h. The crude product was purified by

column chromatography with silica (10% ethyl acetate in hexanes) to afford the title compound **C8cb** (255 mg, 0.95 mmol, 95%). ^{1}H NMR ($CDCl_3$, 500 MHz): δ = 10.36 (s, 1H), 7.43 – 7.38 (m, 2H), 7.46 – 7.39 (m, 2H), 7.28 – 7.24 (m, 3H), 7.19 – 7.16 (m, 1H), 7.01 – 6.96 (m, 1H), 6.74 – 6.69 (m ,2H), 4.64 (s, 1H), 3.60 (t, *J* = 5.2, 4H), 2.34 – 2.26 (m, 4H). ^{13}C NMR (DMSO-d_6, 126 MHz): δ = 155.74, 147.70, 128.90, 128.88, 128.82, 128.58, 128.47, 128.14, 127.53, 127.36, 119.65, 116.31, 66.69, 52.50.

Synthesis of compound (C8cc)

Salicylaldehyde (61 mg, 0.5 mmol), N-methylaniline (53 mg, 0.5 mmol), benzene boronic acid (61 mg, 0.5 mmol), 1.0 mol% **1ZnDy-NO$_3$**, 5 mL DME, r.t, 16 h. The crude product was purified by column chromatography with silica (10% ethyl acetate in hexanes) to afford the title compound **C8cc** (271 mg, 0.94 mmol, 94%). ^{1}H NMR ($CDCl_3$, 500 MHz): δ = 9.79 (s, 1H), 7.24 – 7.12 (m, 8H), 7.03 – 6.94 (m, 2H), 6.96 – 6.89 (m, 3H), 6.79 – 6.74 (m, 1H), 5.86 (s, 1H), 2.83 (s, 3H). ^{13}C NMR ($CDCl_3$, 126 MHz): δ = 157.63, 149.45, 142.71, 131.90, 128.14, 26.88, 123.99, 121.72, 119.60, 117.33, 114.66, 68.55, 37.50.

Synthesis of compound (C8cd)

Salicylaldehyde (61 mg, 0.5 mmol), N-benzylmethylamine (60 mg, 0.5 mmol), benzene boronic acid (61 mg, 0.5 mmol), 1.0 mol% **1ZnDy-NO$_3$**, 5 mL DME, r.t, 16 h. The crude product was purified by column chromatography with silica (10% ethyl acetate in hexanes) to afford the title compound **C8cd** (282 mg, 0.93 mmol, 93%). ^{1}H NMR ($CDCl_3$, 500 MHz): δ = 12.31 (s, 1H), 7.50 – 7.54 (m, 2H), 7.33 – 7.23 (m, 8H), 7.16 – 7.10 (m, 1H), 6.93 – 6.84 (m, 2H), 6.73 – 6.68 (m, 1H), 4.72 (s, 1H), 3.58 (s, 2H), 2.19 (s, 3H). ^{13}C NMR ($CDCl_3$, 126 MHz): δ = 156.94, 138.79, 136.90, 129.25, 129.10, 128.94, 128.76, 128.63, 128.55, 128.02, 127.51, 125.24, 122.58, 118.83, 117.21, 75.53, 59.65, 38.92.

Synthesis of compound (C8ce)

Salicylaldehyde (61 mg, 0.5 mmol), diallylamine (48 mg, 0.5 mmol), benzene boronic acid (61 mg, 0.5 mmol), 1.0 mol% **1ZnDy-NO$_3$**, 5 mL DME, r.t, 16 h. The crude product was purified by column chromatography with silica (10% ethyl acetate in hexanes) to afford the title compound **C8ce** (251 mg, 0.90 mmol, 90%). ^{1}H NMR ($CDCl_3$, 500 MHz): δ = 12.08 (s, 1H), 7.43 – 7.37 (m, 2H), 7.37 – 7.32 (m, 2H), 7.31 – 7.27 (m, 1H), 7.13 – 7.09 (m, 1H), 6.86 – 6. 78 (m, 2H), 6.69 (t, *J* = 6.2, 1H), 5.91 – 5.83 (m, 2H), 5.25 – 5.18 (m, 2H), 5.16 – 5.08 (m, 2H), 5.06 (s, 1H), 3.38 – 3.32 (m, 2H), 3.07 – 3.02 (m, 2H). ^{13}C NMR ($CDCl_3$, 126 MHz): δ = 143.32, 133.50, 130.18, 129.53, 128.36, 127.83, 126.76, 121.28, 119.48, 118.41, 116.12, 71.39, 56.22.

Synthesis of compound C8cf

2-methoxybenzaldehyde (68 mg, 0.5 mmol), indoline (59 mg, 0.5 mmol), benzene boronic acid (61 mg, 0.5 mmol), 1.0 mol% **1ZnDy-NO$_3$**, 5 mL DME, r.t, 16 h. The crude product was purified

by column chromatography with silica (10% ethyl acetate in hexanes) to afford the title compound **C8cf** (314 mg, 0.95 mmol, 95%). ^{1}H NMR ($CDCl_3$, 500 MHz): δ = 7.56 (s, 1H), 7.44 – 7.36 (m, 2H), 7.31 – 7.24 (m, 3H), 7.10 (dd, *J* = 4.5, *J* = 3.6, 1H), 6.95 – 6.90 (m, 1H), 6.82 – 6.75 (m, 3H), 6.72 – 6.68 (m, 1H), 6.33 (d, *J* = 4.8 Hz), 5.72 (s, 1H), 3.90 (s, 3H), 3.21- 3.14 (m, 2H), 2.95 (t, *J* = 6.2 Hz, 2H). ^{13}C NMR ($CDCl_3$, 126 MHz): δ = 151.78, 147.15, 144.31, 140.67, 130.87, 128.55, 128.41, 127.32, 127.19, 124.22, 121.14, 120.65, 119.42, 118.70, 109.88, 109.53, 63.54, 55.98, 52.32, 28.43.

Synthesis of compound (C8cg)

2-methoxybenzaldehyde (68 mg, 0.5 mmol), indoline (59 mg, 0.5 mmol), benzene boronic acid (61 mg, 0.5 mmol), 1.0 mol% **1ZnDy-NO$_3$**, 5 mL DME, r.t, 16 h. The crude product was purified by column chromatography with silica (10% ethyl acetate in hexanes) to afford the title compound **C8cg** (287 mg, 0.93 mmol, 93%).^{1}H NMR ($CDCl_3$, 500 MHz): δ = 12.32 (s, 1H), 7.48 – 7.37 (m, 4H), 6.58 – 6.52 (m, 1H), 6. 51 – 6. 44 (m, 3H), 5.86 – 6.77 (m, 2H), 5.24 – 5. 12 (m, 5H), 3.78 (s, 3H), 3.44 – 3. 38 (m, 2H), 3.24 – 2.17 (m, 2H). ^{13}C NMR ($CDCl_3$, 126 MHz): δ = 148.68, 144.39, 142.91, 134.23, 129.35, 128.49, 127.98, 126.99, 123.60, 121.15, 118.47, 110.72, 73.03, 58.13, 52.28.

Synthesis of compound (C8ch)

2-methoxybenzaldehyde (68 mg, 0.5 mmol), indoline (59 mg, 0.5 mmol), 4-Methoxyphenylboronic acid (76 mg, 0.5 mmol), 1.0 mol% **1ZnDy-NO$_3$**, 5 mL DME, r.t, 16 h. The crude product was purified by column chromatography with silica (10% ethyl acetate in hexanes) to afford the title compound **C8ch** (354 mg, 0.98 mmol, 98%). ^{1}H NMR ($CDCl_3$, 500 MHz): δ = 7.36 – 7.28 (m, 2H), 7.13 – 7.08 (m, 1H), 7.05 – 6.99 (m, 1H), 6.96 - 6.88 (m, 3H), 6.87 – 6. 82 (m, 2H), 6.80 – 6. 74 (m, 1H), 6.36 (d, J = 4.8 Hz, 1H), 5.64 (s, 1H), 3.90 (s, 3H), 3.81 (s, 3H), 3.21 – 3.14 (m, 2H), 2.95 (t, *J* = 5.2 Hz, 2H). ^{13}C NMR ($CDCl_3$, 126 MHz): δ = 158.61, 151.92, 147.43, 144.20, 132.39, 130.89, 129.80, 126.81, 124.21, 120.76, 119.26, 118.39, 113.27, 109.69, 109.46, 63.58, 55.96, 55.20.

Synthesis of compound (C8cl)

2-methoxybenzaldehyde (68 mg, 0.5 mmol), diallylamine (48 mg, 0.5 mmol), 4-Methoxyphenylboronic acid (76 mg, 0.5 mmol), 1.0 mol% **1ZnDy-NO$_3$**, 5 mL DME, r.t, 16 h. The crude product was purified by column chromatography with silica (10% ethyl acetate in hexanes) to afford the title compound **C8cl** (315 mg, 0.93 mmol, 93%). ^{1}H NMR ($CDCl_3$, 500 MHz): δ = 12.45 (s, 1H), 7.34 –7. 27 (m, 2H), 6.88 – 6.80 (m, 2H), 6.77 – 6.72 (m, 1H), 6.65 (t, 1H), 6.46 – 6.39 (m, 1H), 5.91 – 5. 84 (m, 2H), 5.22 -5.15 (m, 3H), 5.02 (s, 1H), 3.89 (s, 3H), 3.81 (s, 3H), 3.37 – 3.31 (m, 2H), 3.06 – 2.99 (m, 2H). ^{13}C NMR ($CDCl_3$, 126 MHz): δ = 159.30,

148.30, 146.97, 135.50, 130.61, 130.18, 125.51, 121.20, 119.35, 118.41, 113.93, 113.56, 110.68, 69.24, 55.20, 52.27.

Synthesis of compound (C8cj)

5-allyl-2-hydroxy-3-methoxybenzaldehyde (96 mg, 0.5 mmol), indoline (59 mg, 0.5 mmol), benzene boronic acid (61 mg, 0.5 mmol), 1.0 mol% **1ZnDy-NO$_3$**, 5 mL DME, r.t, 16 h. The crude product was purified by column chromatography with silica (10% ethyl acetate in hexanes) to afford the title compound **C8cj** (322 mg, 0.87 mmol, 87%). ^{1}H NMR (CDCl$_3$, 500 MHz): δ = 7.45 (dd, *J* = 6.4 Hz, 4.5 Hz, 2H), 7.31 – 7.24 (m, 3H), 7.20 – 7.15 (m, 1H), 7.13 – 7.06 (m, 3H), 6.95 – 6.88 (m, 1H), 6.55 – 6.48 (m, 2H), 5.91 – 5. 86 (m, 1H), 5.65 (s, 1H), 5.02 – 4.94 (m, 2H), 3.88 (s, 3H), 3.29 – 3.23 (m, 2H), 3.20 – 3.08 (m, 3H), 2.94 – 2.87 (m, 2H). ^{13}C NMR (CDCl$_3$, 126 MHz): δ = 151.87, 147.13, 142.58, 140.72, 137.81, 131.06, 128.54, 128.40, 128.16, 127.30, 127.19, 124.19, 120.88, 119.56, 118.82, 115.47, 110.34, 109.75, 64.13, 56.04, 52.45, 39.95, 28.45.

Synthesis of compound (C8ck)

5-allyl-2-hydroxy-3-methoxybenzaldehyde (96 mg, 0.5 mmol), diallylamine (48 mg, 0.5 mmol), benzene boronic acid (61 mg, 0.5 mmol), 1.0 mol% **1ZnDy-NO$_3$**, 5 mL DME, r.t, 16 h. The crude product was purified by column chromatography with silica (10% ethyl acetate in hexanes) to afford the title compound **C8ck** (293 mg, 0.84 mmol, 84%). ^{1}H NMR (CDCl$_3$, 500 MHz): δ = 12.08 (s, 1H), 7.44 – 7.38 (m, 2H), 7.32 – 7.24 (m, 3H), 6.59 (d, 1H), 6.31 (d, 1H), 5.89 – 5.81 (m, 3H), 5.22 – 5.17 (m, 2H), 5.13 – 5.09 (m, 2H), 5.00 – 4.94 (m, 3H), 3.88 (s, 3H), 3.44 – 3.39 (m, 2H), 3.19 – 3.14 (m, 2H), 3.10 – 3.05 (m, 2H). ^{13}C NMR (CDCl$_3$, 126 MHz): δ = 148.19, 144.87, 137.80, 133.29, 129.24, 127.91, 123.71, 122.48, 120.92, 119.38, 110.09, 70.39, 55.91, 52.28.

Synthesis of compound (C8cl)

5-allyl-2-hydroxy-3-methoxybenzaldehyde (96 mg, 0.5 mmol), indoline (59 mg, 0.5 mmol), 4-methoxyphenylboronic acid (76 mg, 0.5 mmol),1.0 mol% **1ZnDy-NO$_3$**, 5 mL DME, r.t, 16 h. The crude product was purified by column chromatography with silica (10% ethyl acetate in hexanes) to afford the title compound **C8cl** (357 mg, 0.89 mmol, 89%). ^{1}H NMR (CDCl$_3$, 500 MHz): δ = 7.90 (s, 1H), 7.34 – 7.28 (m, 2H), 7.10 – 7.04 (m, 2H), 6.95 – 6.91 (m, 1H), 6.88 – 6.82 (m, 2H), 6.66 – 6.56 (m, 4H), 6.35 – 6.30 (m, 1H), 5.94 – 5.90 (m, 1H), 5.54 (s, 1H), 5.05 – 4.94 (m, 2H), 3.87 (m, 3H), 3.80 (m, 3H) 3.28 – 3.24 (m, 2H), 3.11 – 3. 05 (m, 3H), 2.98 (t, *J* = 4.6 Hz, 2H). ^{13}C NMR (CDCl$_3$, 126 MHz): δ = 158.86, 151.68, 146.99, 142.72, 137.83, 132.72, 131.14, 129.75, 129.46, 127.20, 124.20, 121.37, 120.63, 119.03, 115.54, 113.94, 113.81, 110.33, 110.03, 64.11, 55.11, 52.70, 40.32, 28.53.

Synthesis of compound (C8cm)

5-allyl-2-hydroxy-3-methoxybenzaldehyde (96 mg, 0.5 mmol), diallylamine (48 mg, 0.5 mmol), 4-methoxyphenylboronic acid (76 mg, 0.5 mmol), 1.0 mol% **1ZnDy-NO$_3$**, 5 mL DME, r.t, 16 h. The crude product was purified by column chromatography with silica (10% ethyl acetate in hexanes) to afford the title compound **C8cm** (326 mg, 0.86 mmol, 86%).^{1}H NMR ($CDCl_3$, 500 MHz): δ = 9.98 (s, 1H), 7.33 (dd, *J* = 6.2 Hz, 4.5Hz, 2H), 6.85 – 6.79 (m, 2H), 6.64 (t, J = 4.8 Hz, 1H), 6.59 – 6.54 (m, 1H), 5.85 – 5. 79 (m, 3H), 5.14 – 5.08 (m, 2H), 5.04 – 4.94 (m, 5H), 3.71 (s, 3H), 3.69 (s, 3H), 3.32 (s, 2H), 3.20 – 3.14 (m, 2H), 3.09 – 3.02 (m, 3H). ^{13}C NMR ($CDCl_3$, 126 MHz): δ = 158.76, 148.08, 143.29, 138.45, 134.66, 133.60, 130.29, 129.64, 127.87, 127.63, 120.13, 118.59, 115.93, 114.40, 111.32, 65.70, 56.01, 55.36, 52.23.

Synthesis of compound (C8cn)

Salicylaldehyde (122 mg, 1.0 mmol), indoline (118 mg, 1.0 mmol), benzene 1, 4-diboronic acid (83 mg, 0.5 mmol), 1.0 mol% **1ZnDy-NO$_3$**, 5 mL DME, r.t, 16 h. The crude product was purified by column chromatography with silica (10% ethyl acetate in hexanes) to afford the title compound **C8cn** (482 mg, 0.92 mmol, 92%).^{1}H NMR ($CDCl_3$, 500 MHz): δ = 9.99 (s, 2H), 7.43 (s, 3H), 7.21 – 7.17 (m, 2H), 7.15 – 7.10 (m, 2H), 6.98 – 6.93 (m , 3H), 6.91 – 6.87 (m, 2H), 6.85 – 6.80 (m, 3H), 6.44 – 6.40 (m, 2H), 5.31 (s, 2H), 3.17 – 3.13 (m, 2H), 3.07 – 3.02 (m, 2H), 2.93 – 2.86 (m, 4H) . ^{13}C NMR ($CDCl_3$, 126 MHz): δ = 156.24, 151.01, 150.99, 139.38, 139.37, 132.10, 129.30, 129.26, 128.92, 128.47, 127.36, 126.19, 126.13, 124.63, 121.30, 120.06, 117.73, 117.10, 112.06, 69.84, 69.81, 53.57, 53.52, 28.51.

Synthesis of compound (C8co)

2-methoxybenzaldehyde (136 mg, 1.0 mmol), indoline (118 mg, 1.0 mmol), benzene 1, 4-diboronic acid (83 mg, 0.5 mmol), 1.0 mol% **1ZnDy-NO$_3$**, 5 mL DME, r.t, 16 h. The crude product was purified by column chromatography with silica (10% ethyl acetate in hexanes) to afford the title compound **C8co** (555 mg, 0.95 mmol, 95%). ^{1}H NMR ($CDCl_3$, 500 MHz): δ = 7.35 (s, 4H), 7.08 (d, 2H), 6.92 (t, 2H), 6.79 – 6. 72 (m, 6H), 6.69 (t, 2H), 6.30 (d, 2H), 5.69 (d, 2H), 3.89 (s, 6H), 3.18 – 3.12 (m, 4H), 2.92 (t, 4H). ^{13}C NMR ($CDCl_3$, 126 MHz): δ = 151.78, 147.15, 144.31, 140.67, 130.87, 128.55, 128.41, 127.32, 127.19, 124.22, 121.14, 120.65, 119.42, 118.70, 109.88, 109.53, 63.54, 55.98, 52.32, 28.43.

Synthesis of compound (C8cp)

Salicylaldehyde (122 mg, 1.0 mmol), diallylamine (96 mg, 1.0 mmol), benzene 1, 4-diboronic acid (83 mg, 0.5 mmol), 1.0 mol% **1ZnDy-NO$_3$**, 5 mL DME, r.t, 16 h. The crude product was purified by column chromatography with silica (10% ethyl acetate in hexanes) to afford the title compound **C8cp** (413 mg, 0.86 mmol, 86%).^{1}H NMR ($CDCl_3$, 500 MHz): δ = 11.97 (s, 2H), 7.40 (s, 4H), 7.14 – 7.10 (m, 2H), 6.84 – 6. 79 (m, 4H), 6.70 – 6.65 (m, 2H), 5.88 – 5. 81 (m, 4H), 5.22

– 5. 16 (m, 4H), 5.13 – 5.08 (m, 4H), 5.00 (m, 2H), 3.34 – 3.29 (m, 4H), 3.07 – 2.97 (m, 4H). ^{13}C NMR ($CDCl_3$, 126 MHz): δ = 157.43, 137.73, 133.28, 129.64, 129.20, 128.64, 124.80, 119.46, 119.04, 116.92, 69.99, 51.91.

Synthesis of compound (C8cq)

2-methoxybenzaldehyde (136 mg, 1.0 mmol), diallylamine (96 mg, 1.0 mmol), benzene 1, 4-diboronic acid (83 mg, 0.5 mmol), 1.0 mol% **1ZnDy-NO$_3$**, 5 mL DME, r.t, 16 h. The crude product was purified by column chromatography with silica (10% ethyl acetate in hexanes) to afford the title compound **C8cq** (475 mg, 0.88 mmol, 88%).^{1}H NMR ($CDCl_3$, 500 MHz): δ = 12.15 (s, 2H), 7.40 (s, 4H), 6.78 – 6.73 (m, 2H), 6.66 – 6.60 (m, 2H), 6.47 – 6.42 (m, 2H), 5.88 – 5.79 (m, 4H), 5.16 – 5. 05 (m, 8H), 4.98 (d, 2H), 3.89 (s, 6H), 3.33 – 3.27 (m, 4H), 3.09 – 3.04 (m, 4H). ^{13}C NMR ($CDCl_3$, 126 MHz): δ = 148.21, 146.94, 141.78, 133.24, 129.74, 123.78, 121.16, 119.43, 110.64, 69.79, 55.92, 52.23.

Synthesis of 1,3-dimethyl-5-(2-nitro-1-phenyl-ethyl)-pyrimidine-2,4,6-trione (C9a)

trans-β-nitrostyrene (44 mg, 0.3 mmol), 1,3-dimethylbarbituric acid (47 mg ,0.3 mmol), 2.5 mol% **1ZnY-NO$_3$** were stirred in a mixture of EtOH/H_2O (2:1) (10 mL) for 15 min. The crude product was purified by column chromatography with silica (20% ethyl acetate in hexanes) to afford the title compound **C9a.** ^{1}H NMR (500 MHz, Chloroform-*d*) δ 7.35 – 7.23 (m, 3H), 7.07 – 6.97 (m, 2H), 5.28 (ddd, *J* = 14.3, 7.9, 1.3 Hz, 1H), 4.99 (ddd, *J* = 14.2, 7.6, 1.4 Hz, 1H), 4.48 (td, *J* = 7.7, 3.5 Hz, 1H), 3.88 – 3.81 (m, 1H), 3.18 – 3.02 (m, 6H). ^{13}C NMR (126 MHz, $CDCl_3$) δ 166.82, 166.79, 150.46, 133.76, 129.73,129.12, 127.61, 51.47, 45.47, 39.36, 28.34, 28.1

Synthesis of 5-[1-(4-methoxy-phenyl)-2-nitro-ethyl]-1,3-dimethyl-pyrimidine-2,4,6-trione (C9b)

trans-4-methoxy-β-nitrostyrene (48 mg, 0.3 mmol), 1,3-dimethylbarbituric acid (47 mg ,0.3 mmol), 2.5 mol% **1ZnY-NO$_3$** were stirred in a mixture of EtOH/H_2O (2:1) (10 mL) for 15 min. The crude product was purified by column chromatography with silica (15% ethyl acetate in hexanes) to afford the title compound **C9c.** ^{1}H NMR (500 MHz, $CDCl_3$) δ 7.12 – 7.03 (m, 2H), 6.93 – 6.84 (m, 2H), 5.30 – 5.20 (m, 1H), 4.95 (ddd, *J* = 14.2, 7.8, 1.7 Hz, 1H), 4.43 (td, *J* = 7.9, 3.3 Hz, 1H), 3.83 (dd, *J* = 3.5, 1.8 Hz, 1H), 3.18 – 3.04 (m, 6H), 2.34 – 2.25 (m, 3H). ^{13}C NMR (126 MHz, $CDCl_3$) δ 167.12, 150.54, 149.29, 139.74, 130.59, 129.76, 127.47 53.57, 45.24, 28.34, 28.15, 21.00.

Synthesis of 5-[1-(4-fluoro-phenyl)-2-nitro-ethyl]-1,3-dimethyl-pyrimidine-2,4,6-trione (C9e)

trans-4-fluoro-β-nitrostyrene (50 mg, 0.3 mmol), 1,3-dimethylbarbituric acid (47 mg ,0.3 mmol), 2.5 mol% **1ZnY-NO$_3$** were stirred in a mixture of EtOH/H_2O (2:1) (10 mL) for 15 min. The crude product was purified by column chromatography with silica (10% ethyl acetate in hexanes) to

afford the title compound **C9e.** ^{1}H NMR (500 MHz, $CDCl_3$) δ 7.09 (ddd, *J* = 8.6, 5.4, 2.8 Hz, 2H), 7.05 – 6.94 (m, 2H), 5.27 (dd, *J* = 14.2, 7.7 Hz, 1H), 5.05 – 4.97 (m, 1H), 4.55 (td, *J* = 7.8, 3.3 Hz, 1H), 3.85 (d, *J* = 3.4 Hz, 1H), 3.18 (s, 3H), 3.13 (s, 3H). ^{13}C NMR (126 MHz, $CDCl_3$) δ 166.63, 166.49, 163.89, 150.36, 129.50, 129.44, 116.36, 116.18, 51.42, 44.32, 28.53, 28.33.

Synthesis of 5-[1-(4-Methyl-phenyl)-2-nitro-ethyl]-1,3-dimethyl-pyrimidine-2,4,6-trione (C9c)

trans-4-methyoxy-β-nitrostyrene (54 mg, 0.3 mmol), 1,3-dimethylbarbituric acid (47 mg ,0.3 mmol), 2.5 mol% **1ZnY-NO$_3$** were stirred in a mixture of EtOH/H_2O (2:1) (10 mL) for 15 min. The crude product was purified by column chromatography with silica (10% ethyl acetate in hexanes) to afford the title compound **C9b.** ^{1}H NMR (500 MHz, $CDCl_3$) δ 6.97 (d, *J* = 8.5 Hz, 2H), 6.83 – 6.77 (m, 2H), 5.25 (dd, *J* = 14.0, 7.9 Hz, 1H), 4.97 (dd, *J* = 14.0, 7.8 Hz, 1H), 4.47 (td, *J* = 7.9, 3.4 Hz, 1H), 3.82 (d, *J* = 3.5 Hz, 1H), 3.77 (d, *J* = 1.0 Hz, 3H), 3.16 (d, *J* = 1.0 Hz, 3H), 3.11 (d, *J* = 1.0 Hz, 3H). ^{13}C NMR (126 MHz, $CDCl_3$) δ 167.12, 166.90, 150.54, 129.76, 127.47, 127.27, 53.57, 51.50, 45.24, 39.35, 28.79, 28.67

Synthesis of 5-[1-(4-Bromo-phenyl)-2-nitro-ethyl]-1,3-dimethyl-pyrimidine-2,4,6-trione (C9d)

trans-4-bromo-β-nitrostyrene (66 mg, 0.3 mmol), 1,3-dimethylbarbituric acid (47 mg ,0.3 mmol), 2.5 mol% **1ZnY-NO$_3$** were stirred in a mixture of EtOH/H_2O (2:1) (10 mL) for 15 min. The crude product was purified by column chromatography with silica (5% ethyl acetate in hexanes) to afford the title compound **C9d.** ^{1}H NMR (500 MHz, $CDCl_3$) δ 7.47 – 7.41 (m, 2H), 7.03 – 6.97 (m, 2H), 5.28 (dd, *J* = 14.2, 7.8 Hz, 1H), 5.01 (dd, *J* = 14.2, 7.8 Hz, 1H), 4.55 (td, *J* = 7.8, 3.4 Hz, 1H), 3.87 (d, *J* = 3.4 Hz, 1H), 3.68 (s, 3H), 3.18 (d, *J* = 19.1 Hz, 6H). ^{13}C NMR (126 MHz, $CDCl_3$) δ 166.71, 166.53, 162.73, 130.22, 129.27, 116.36, 109.98, 101.25, 77. 24, 76.81, 76.94, 51.35, 43.91, 29.01

Synthesis of C9f

trans-β-methyl-β-nitrostyrene (48 mg, 0.3 mmol), 1,3-dimethylbarbituric acid (47 mg ,0.3 mmol), 2.5 mol% **1ZnY-NO$_3$** were stirred in a mixture of EtOH/H_2O (2:1) (10 mL) for 15 min. The crude product was purified by column chromatography with silica (15% ethyl acetate in hexanes) to afford the title compound **C9f.** ^{1}H NMR (500 MHz, $CDCl_3$) δ 7.29 (dd, *J* = 4.9, 2.0 Hz, 3H), 7.05 – 6.99 (m, 2H), 5.61 (dd, *J* = 11.6, 6.6 Hz, 1H), 4.13 (dd, *J* = 11.5, 3.6 Hz, 1H), 3.72 (d, *J* = 3.6 Hz, 1H), 3.14 (s, 3H), 3.01 (s, 3H), 1.39 (d, *J* = 6.8 Hz, 3H). ^{13}C NMR (126 MHz, $CDCl_3$) δ 166.81, 166.75, 150.54, 133.73, 129.24, 129.21, 129.13, 128.17, 88.25, 82.93, 77.31, 77.05, 76.80, 51.86, 50.81, 28.27, 28.15, 19.50

Synthesis of 5-(1-Furan-2-yl-2-nitro-ethyl)-1,3-dimethyl-pyrimidine-2,4,6-trione (C9g)

2-(2-Nitrovinyl) furan (45 mg, 0.3 mmol), 1,3-dimethylbarbituric acid (47 mg ,0.3 mmol), 2.5 mol% **1ZnY-NO$_3$** were stirred in a mixture of EtOH/H_2O (2:1) (10 mL) for 1 h. The crude product was purified by column chromatography with silica (15% ethyl acetate in hexanes) to afford the title compound **C9g.** ^{1}H NMR (500 MHz, $CDCl_3$) δ 7.29 (s, 1H), 6.32 – 6.27 (m, 1H), 6.18 – 6.14 (m, 1H), 5.18 (dd, *J* = 14.3, 7.6 Hz, 1H), 4.97 (dd, *J* = 14.3, 7.5 Hz, 1H), 4.69 (td, *J* = 7.6, 3.2 Hz, 1H), 3.88 – 3.83 (m, 1H), 3.23 (s, 6H). ^{13}C NMR (126 MHz, $CDCl_3$) δ 166.34, 150.81, 147.88, 143.22, 110.86, 108.82, 77.27, 77.02, 76.76, 74.72, 49.79, 46.33, 39.04, 28.69, 28.51, 8.61.

Synthesis of C9h

trans-β-nitrostyrene (44 mg, 0.3 mmol), 6-amino-1,3-dimethyluracil (47 mg ,0.3 mmol), 2.5 mol% **1ZnY-NO$_3$** were stirred in a mixture of EtOH/H_2O (2:1) (10 mL) for 15 min. The crude product was purified by column chromatography with silica (15% ethyl acetate in hexanes) to afford the title compound **C9h.** ^{1}H NMR (500 MHz, $CDCl_3$) δ 7.37 – 7.23 (m, 5H), 5.42 (dd, *J* = 13.2, 8.0 Hz, 1H), 5.10 (dd, *J* = 13.4, 6.7 Hz, 1H), 4.84 (d, *J* = 12.3 Hz, 2H), 4.67 (t, *J* = 7.5 Hz, 1H), 3.39 (d, *J* = 5.1 Hz, 4H), 3.28 (s, 3H). ^{13}C NMR (126 MHz, $CDCl_3$) δ 162.05, 151.69, 151.00, 138.63, 128.98, 127.63, 127.22, 109.99, 77.32, 77.06, 77.00, 76.81, 60.42, 40.21, 29.48, 29.04, 28.06, 21.01, 14.15. ESI-MS [$C_{14}H_{16}N_4Na_1O_4$] – 327.1064

Synthesis of C9i

trans-4-methoxy-β-nitrostyrene (54 mg, 0.3 mmol), 6-amino-1,3-dimethyluracil (47 mg ,0.3 mmol), 2.5 mol% **1ZnY-NO$_3$** were stirred in a mixture of EtOH/H_2O (2:1) (10 mL) for 15 min. The crude product was purified by column chromatography with silica (15% ethyl acetate in hexanes) to afford the title compound **C9i.** ^{1}H NMR (500 MHz, $CDCl_3$) δ 7.00 – 6.90 (m, 2H), 6.90 – 6.83 (m, 2H), 5.41 (dd, *J* = 13.4, 7.7 Hz, 1H), 5.08 (dd, *J* = 13.3, 6.9 Hz, 1H), 4.65 – 4.56 (m, 1H), 4.54 (s, 2H), 3.43 (s, 3H), 3.32 (s, 3H), 1.25 (d, *J* = 0.6 Hz, 3H). ESI-MS [$C_{15}H_{18}N_4Na_1O_4$] – 357.1169

Synthesis of C9j

trans-4-methyl-β-nitrostyrene (48 mg, 0.3 mmol), 6-amino-1,3-dimethyluracil (47 mg ,0.3 mmol), 2.5 mol% **1ZnY-NO$_3$** were stirred in a mixture of EtOH/H_2O (2:1) (10 mL) for 15 min. The crude product was purified by column chromatography with silica (5% ethyl acetate in hexanes) to afford the title compound **C9j.** ^{1}H NMR (500 MHz, $CDCl_3$) δ 7.30 – 7.24 (m, 2H), 7.21 (s, 0H), 7.15 (d, *J* = 7.8 Hz, 2H), 5.45 – 5.37 (m, 1H), 5.13 – 5.05 (m, 1H), 4.63 (t, *J* = 7.4 Hz, 1H), 4.53 (s, 2H), 3.43 (d, *J* = 2.9 Hz, 3H), 3.32 (d, *J* = 2.9 Hz, 3H), 2.33 (d, *J* = 2.9 Hz, 3H), ^{13}C NMR (126 MHz, $CDCl_3$) δ 161.91, 150.98, 137.54, 135.50, 129.79, 127.17, 87.85, 77.23, 77.10, 76.98, 76.72, 40.18, 29.26, 28.10, 20.98. ESI-MS [$C_{15}H_{18}N_4Na_1O_4$] – 341.1222

Synthesis of C9k

trans-4-bromo-β-nitrostyrene (66 mg, 0.3 mmol), 6-amino-1,3-dimethyluracil (47 mg ,0.3 mmol), 2.5 mol% **1ZnY-NO$_3$** were stirred in a mixture of EtOH/H_2O (2:1) (10 mL) for 15 min. The crude product was purified by column chromatography with silica (7% ethyl acetate in hexanes) to afford the title compound **C9k**. ^{1}H NMR (500 MHz, $CDCl_3$) δ 7.48 – 7.41 (m, 2H), 7.29 – 7.21 (m, 2H), 5.43 (ddd, *J* = 13.6, 8.0, 2.7 Hz, 1H), 5.09 (ddd, *J* = 13.5, 6.6, 2.7 Hz, 1H), 4.71 (s, 2H), 4.57 – 4.46 (m, 1H), 3.44 (d, *J* = 2.6 Hz, 3H), 3.29 (d, *J* = 2.7 Hz, 3H. ^{13}C NMR (126 MHz, $CDCl_3$) δ 161.98, 151.64, 134.44, , 128.99, 115.83, 77.31, 77.19, 77.05, 76.80, 60.45, 39.72, 29.54, 29.06, 28.04

Synthesis of C9l

trans-4-fluoro-β-nitrostyrene (50 mg, 0.3 mmol), 6-amino-1,3-dimethyluracil (47 mg ,0.3 mmol), 2.5 mol% **1ZnY-NO$_3$** were stirred in a mixture of EtOH/H_2O (2:1) (10mL) for 15 min. The crude product was purified by column chromatography with silica (10% ethyl acetate in hexanes) to afford the title compound **C9l.** ^{1}H NMR (500 MHz, $CDCl_3$) δ 7.34 (dd, *J* = 8.2, 4.6 Hz, 2H), 7.05 – 6.97 (m, 2H), 5.47 – 5.39 (m, 1H), 5.14 – 5.05 (m, 1H), 4.70 (s, 2H), 4.59 – 4.52 (m, 1H), 3.42 (d, *J* = 2.0 Hz, 3H), 3.30 (d, *J* = 2.3 Hz, 3H). ^{13}C NMR (126 MHz, $CDCl_3$) δ 162.97, 161.98, 161.00, 151.64, 150.96, 134.44, 129.05, 128.99, 127.17, 115.83, 115.66, 86.83, 77.31, 77.19, 77.05, 76.80, 60.45, 29.54, 29.06, 28.04, 21.01. ESI-MS [$C_{14}H_{16}FN_4Na_1O_4$] – 357.1169

Synthesis of C9m

trans- β -methyl-β-nitrostyrene (48 mg, 0.3 mmol), 6-amino-1,3-dimethyluracil (47 mg ,0.3 mmol), 2.5 mol% **1ZnY-NO$_3$** were stirred in a mixture of EtOH/H_2O (2:1) (10 mL) for 1 h. The crude product was purified by column chromatography with silica (10% ethyl acetate in hexanes) to afford the title compound **C9m.**^{1}H NMR (500 MHz, $CDCl_3$) δ 7.34 (dd, *J* = 8.2, 4.6 Hz, 2H), 7.27 (d, *J* = 2.2 Hz, 1H), 7.05 – 6.97 (m, 2H), , 5.47 – 5.39 (m, 1H), 5.14 – 5.05 (m, 1H), 4.70 (s, 2H), 4.59 – 4.52 (m, 1H), 3.50 – 3.40 (m, 5H), 3.30 (d, *J* = 2.3 Hz, 3H). ^{13}C NMR (126 MHz, $CDCl_3$) δ 161.91, 150.98, 137.54, 135.50, 129.79, 127.17, 87.85, 77.23, 77.10, 76.98, 76.72, 40.18, 29.26, 28.10, 20.98. ESI-MS [$C_{15}H_{18}N_4Na_1O_4$] – 341.1553

Synthesis of C9n

2-(2-Nitrovinyl) furan (45 mg, 0.3 mmol), 6-amino-1,3-dimethyluracil (47 mg ,0.3 mmol), 2.5 mol% **1ZnY-NO$_3$** were stirred in a mixture of EtOH/H_2O (2:1) (10 mL) for 1 h. The crude product was purified by column chromatography with silica (15% ethyl acetate in hexanes) to afford the title compound **C9n.** ^{1}H NMR (500 MHz, $CDCl_3$) δ 7.35 (d, *J* = 1.6 Hz, 1H), 7.27 (s, 1H), 6.35 (dd, *J* = 3.2, 1.7 Hz, 1H), 6.31 – 6.26 (m, 1H), 5.18 – 4.99 (m, 3H), 4.80 (s, 2H), 3.56 – 3.42 (m, 8H). ^{13}C NMR (126 MHz, $CDCl_3$) δ 151.28, 141.95, 110.87, 107.18, 88.29, 77.23, 76.98, 76.73, 74.79, 34.47, 29.27, 28.15

Synthesis of C9o

trans-β-nitrostyrene (44 mg, 0.3 mmol), 1,3-diethyl-2-thiobarbituric acid (60 mg ,0.3 mmol), 2.5 mol% **1ZnY-NO$_3$** were stirred in a mixture of EtOH/H_2O (2:1) (10 mL) for 1 h. The crude product was purified by column chromatography with silica (20% ethyl acetate in hexanes) to afford the title compound **C9o.** ^{1}H NMR (500 MHz, $CDCl_3$) δ 7.32 – 7.25 (m, 3H), 7.10 – 7.04 (m, 2H), 5.28 (dd, *J* = 14.2, 7.9 Hz, 1H), 4.99 (dd, *J* = 14.1, 7.6 Hz, 1H), 4.52 (d, *J* = 3.9 Hz, 1H), 4.33 – 4.19 (m, 4H), 3.90 (d, *J* = 3.8 Hz, 1H), 1.17 (t, *J* = 6.9 Hz, 3H), 1.03 (t, *J* = 7.0 Hz, 3H). ^{13}C NMR (126 MHz, $CDCl_3$) δ 165.93, 149.82, 133.56, 127.63, 126.96, 88.34, 75.09, 53.91, 44.86, 38.57, 27.09. CHN $C_{16}H_{19}N_3O_4S$ (observed) C-54.91%, H-5.33%, N-11.99% (expected) C-54.99%, H-5.49%, N-12.03%.

Synthesis of C9p

trans-4-methoxy-β-nitrostyrene (54 mg, 0.3 mmol), 1,3-diethyl-2-thiobarbituric acid (60 mg ,0.3 mmol), 2.5 mol% **1ZnY-NO$_3$** were stirred in a mixture of EtOH/H_2O (2:1) (10 mL) for 1h. The crude product was purified by column chromatography with silica (25% ethyl acetate in hexanes) to afford the title compound **C9p.** ^{1}H NMR (500 MHz, $CDCl_3$) δ 6.97 (dd, *J* = 11.4, 8.1 Hz, 3H), 6.81 – 6.75 (m, 2H), 5.24 (dd, *J* = 14.0, 7.8 Hz, 1H), 4.96 (dd, *J* = 14.1, 7.7 Hz, 1H), 4.47 (td, *J* = 7.9, 3.8 Hz, 1H), 4.27 (ddt, *J* = 34.0, 13.3, 6.6 Hz, 4H), 3.89 – 3.84 (m, 1H), 2.19 – 2.15 (m, 3H), 1.18 (dd, *J* = 7.6, 6.4 Hz, 3H), 1.06 (dd, *J* = 7.5, 6.4 Hz, 3H). ^{13}C NMR (126 MHz, $CDCl_3$) δ 168.43, 149.76, 188.43, 129.70, 126.54, 87.09, 75.01, 52.69, 45.13, 27.84, 19.99

Synthesis of C9s

trans-4-fluoro-β-nitrostyrene (54 mg, 0.3 mmol), 1,3-diethyl-2-thiobarbituric acid (60 mg ,0.3 mmol), 2.5 mol% **1ZnY-NO$_3$** were stirred in a mixture of EtOH/H_2O (2:1) (10 mL) for 1 h. The crude product was purified by column chromatography with silica (20% ethyl acetate in hexanes) to afford the title compound **C9s.**^{1}H NMR (500 MHz, $CDCl_3$) δ 7.14 – 7.07 (m, 2H), 7.02 – 6.94 (m, 2H), 5.26 (dd, *J* = 14.0, 7.6 Hz, 1H), 5.00 (dd, *J* = 14.1, 7.9 Hz, 1H), 4.56 (dt, *J* = 7.9, 4.0 Hz, 1H), 4.36 – 4.22 (m, 4H), 3.91 – 3.86 (m, 1H), 1.22 – 1.15 (m, 3H), 1.11 – 1.04 (m, 3H). ^{13}C NMR (126 MHz, $CDCl_3$) δ 166.76, 151.23, 128.22, 117.53, 88.91, 53.06, 43.09, 27.62

Synthesis of C9t

trans- β -methyl-β-nitrostyrene (48 mg, 0.3 mmol) 1,3-diethyl-2-thiobarbituric acid (60 mg, 0.3 mmol), 2.5 mol% **1ZnY-NO$_3$** were stirred in a mixture of EtOH/H_2O (2:1) (10 mL) for 1 h. The crude product was purified by column chromatography with silica (15% ethyl acetate in hexanes) to afford the title compound **C9t.** ^{1}H NMR (500 MHz, $CDCl_3$) δ 7.32 – 7.25 (m, 3H), 7.04 (dt, *J* = 7.9, 1.6 Hz, 2H), 5, 4.36 – 4.28 (m, 2H), 4.20 – 4.10 (m, 3H), 3.80 (dd, *J* = 3.9, 1.3 Hz, 1H), 2.03 (d, *J* = 1.3 Hz, 1H), 1.43 – 1.38 (m, 3H), 1.20 (td, *J* = 7.1, 1.3 Hz, 3H), 0.95 (td, *J* = 7.1, 1.3 Hz, 3H). ^{13}C NMR (126 MHz, $CDCl_3$) δ 167.79, 150.93, 134.22, 128.55, 128.03, 87.11, 83.45,

52.78, 49.82, 28.45, 19.29. CHN $C_{17}H_{21}N_3O_4S$ (observed) C-56.15%, H-5.81%, N-11.60% (expected) C-56.18%, H-5.83%, N-11.56%.

Synthesis of C9u

2-(2-Nitrovinyl) furan (45 mg, 0.3 mmol), 1,3-diethyl-2-thiobarbituric acid (60 mg ,0.3 mmol), 2.5 mol% **1ZnY-NO$_3$** were stirred in a mixture of EtOH/H_2O (2:1) (10 mL) for 1 h. The crude product was purified by column chromatography with silica (15% ethyl acetate in hexanes) to afford the title compound **C9u.** ^{1}H NMR (500 MHz, $CDCl_3$) 6.28 (s, 1H), 6.18 – 6.13 (m, 1H), 5.15 (dd, *J* = 14.5, 7.6 Hz, 1H), 4.94 (dd, *J* = 14.4, 7.9 Hz, 1H), 4.69 – 4.62 (m, 1H), 4.33 (q, *J* = 6.8, 6.4 Hz, 4H), 1.16 (dt, *J* = 21.0, 7.4 Hz, 6H). ^{13}C NMR (126 MHz, $CDCl_3$) δ 164.44, 147.51, 143.23, 110.82, 109.19, 77.27, 77.01, 76.76, 74.78, 50.20, 43.66, 43.45, 39.58, 11.91.

Synthesis of C9r

trans-4-bromo-β-nitrostyrene (66 mg, 0.3 mmol), 1,3-diethyl-2-thiobarbituric acid (60 mg ,0.3mmol), 2.5 mol% **1ZnY-NO$_3$** were stirred in a mixture of EtOH/H_2O (2:1) (10 mL) for 1 h. The crude product was purified by column chromatography with silica (20% ethyl acetate in hexanes) to afford the title compound **C9r**.^{1}H NMR (500 MHz, $CDCl_3$) δ 7.12 – 7.05 (m, 2H), 7.01 – 6.95 (m, 2H), 5.31 (dd, *J* = 14.0, 7.5 Hz, 1H), 5.00 (dd, *J* = 14.1, 7.9 Hz, 1H), 4.60(dt, *J* = 7.9, 4.0 Hz, 1H), 4.34 – 4.21 (m, 4H), 3.91 – 3.88 (m, 1H), 1.20 – 1.17 (m, 3H), 1.12 – 1.06 (m, 3H). ^{13}C NMR (126 MHz, $CDCl_3$) δ 167.81, 153.01, 130.47, 116.21, 87.88, 54.12, 44.39, 28.61

Synthesis of C9q

trans-4-methyl-β-nitrostyrene (48 mg, 0.3 mmol), 1,3-diethyl-2-thiobarbituric acid (60 mg, 0.3 mmol), 2.5 mol% **1ZnY-NO$_3$** were stirred in a mixture of EtOH/H_2O (2:1) (10 mL) for 1 h. The crude product was purified by column chromatography with silica (25% ethyl acetate in hexanes) to afford the title compound **C9q.** ^{1}H NMR (500 MHz, $CDCl_3$) δ 7.34 – 7.29 (2H), 7.03 – 7.01 (2H), 5.30 – 5.20 (1H), 5.01 (1H), 4.47 (1H), 3.99(1H), 3.19 – 3.10 (6H), 2.41 – 2.39 (3H). ^{13}C NMR (126 MHz, $CDCl_3$) δ 169.32, 154.49, 150.21, 142.67, 132.99, 125.69, 122.81, 51.78, 43.67, 28.76, 28.01, 22.06.

Synthesis of C9v

cis-4-methoxy- β-methyl- β-nitrostyrene (58 mg, 0.3 mmol), 1,3-dimethylbarbituric acid (47 mg ,0.3 mmol), 2.5 mol% **1ZnY-NO$_3$** were stirred in a mixture of EtOH/H_2O (2:1) (10 mL) for 1 h. The crude product was purified by column chromatography with silica (15% ethyl acetate in hexanes) to afford the title compound **C9v.** ^{1}H NMR (500 MHz, Chloroform-*d*) δ 6.97 – 6.91 (m, 2H), 6.83 – 6.77 (m, 2H), 5.64 – 5.54 (m, 1H), 4.13 – 4.06 (m, 1H), 3.76 (t, *J* = 1.1 Hz, 3H), 3.69 (dd, *J* = 3.6, 1.4 Hz, 1H), 3.17 (d, *J* = 1.3 Hz, 3H), 3.05 (d, *J* = 1.3 Hz, 3H), 1.41 – 1.35 (m, 3H). ^{13}C NMR (126 MHz, $CDCl_3$) δ 166.91, 166.85, 159.92, 150.60, 129.33, 125.32, 114.60, 83.18, 77.29, 77.04, 76.78, 55.22, 51.13, 50.81, 28.36, 28.21, 19.

Chapter 12: Crystallographic data

13.1 Crystallographic tables of PCCs

13.1.1 Chapter 2

Table 13.1 Crystallographic table of compounds **1-3**.

Identification code	**1**	**2**	**3**
Empirical formula	$C_{72}H_{92}Cl_2Dy_2N_4O_{28}Zn_2$	$C_{72}H_{92}Cl_2Tb_2N_4O_{28}Zn_2$	$C_{72}H_{92}Cl_2Eu_2N_4O_{28}Zn_2$
Formula weight	1988.14	1976.23	1964.22
Temperature/K	173	173	173
Crystal system	monoclinic	monoclinic	monoclinic
Space group	$P2_1/n$	$P2_1/n$	$P2_1/n$
a/Å	12.8750(3)	12.8759(4)	12.9329(7)
b/Å	20.9336(5)	20.9432(5)	20.8123(4)
c/Å	15.2275(2)	15.2346(4)	15.2261(8)
α/°	90	90	90
β/°	108.549(2)	108.395(6)	108.824(2)
γ/°	90	90	90
Volume/Å^3	3890.93(14)	3898.29(12)	3901.37(19)
Z	2	2	2
ρ_{calc}g/cm^3	1.697		
μ/mm^{-1}	12.141		
F(000)	2004		
Crystal size/mm^3	0.14 × 0.1 × 0.04		
Radiation	Cu Kα (λ = 1.54184)		
2Θ range for data collection/°	7.44 to 141.24		
Index ranges	$-13 \leq h \leq 15$, $-25 \leq k \leq 14$, $-18 \leq l \leq 15$		
Reflections collected	10935		
Independent reflections	7014 [R_{int} = 0.0222, R_{sigma} = 0.0374]		
Data/restraints/parameters	7014/9/512		
Goodness-of-fit on F^2	1.019		
Final R indexes [I>=2σ (I)]	R_1 = 0.0371, wR_2 = 0.0925		
Final R indexes [all data]	R_1 = 0.0414, wR_2 = 0.0965		
Largest diff. peak/hole / e Å^{-3}	1.18/-1.08		

Table 13.2 Crystallographic table of compounds **4-6**.

Identification code	**4**	**5**	**6**
Empirical formula	$C_{86}H_{73}DyN_7O_{21}Zn_5$	$C_{86}H_{74}N_7O_{21}TbZn_5$	$C_{86}H_{73}N_7O_{21}EuZn_5$
Formula weight	2029.86	2027.29	2012.15
Temperature/K	173	173	173
Crystal system	triclinic	triclinic	triclinic
Space group	P-1	P-1	P-1
a/Å	13.1526(9)	13.1739(7)	13.1746(12)
b/Å	16.8229(12)	16.8279(12)	16.8285(10)
c/Å	20.5069(14)	20.5073(13)	20.5092(9)
α/°	72.907(2)	73.274(6)	72.998(5)
β/°	72.829(2)	72.920(5)	72.908(7)
γ/°	68.596(2)	68.553(6)	68.582(3)
Volume/Å^3	3946.8(5)	3960.8(5)	3959.3(6)
Z	2	2	2
ρ_{calc}g/cm^3	1.708	1.7	
μ/mm^{-1}	2.511	2.452	
F(000)	2044	2044	
Crystal size/mm^3	0.21 × 0.15 × 0.12	0.2 × 0.18 × 0.12	
Radiation	MoKα (λ = 0.71075)	MoKα (λ = 0.71073)	
2Θ range for data collection/°	4.252 to 55.092	6.996 to 51.362	
Index ranges	$-17 \leq h \leq 17$, $-21 \leq k \leq 21$, $-25 \leq l \leq 26$	$-16 \leq h \leq 15$, $-20 \leq k \leq 17$, $-24 \leq l \leq 15$	
Reflections collected	72629	14632	
Independent reflections	18032 [R_{int} = 0.0457, R_{sigma} = 0.0315]	10744 [R_{int} = 0.0401, R_{sigma} = 0.0869]	
Data/restraints/parameters	18032/0/1092	10744/0/1092	
Goodness-of-fit on F^2	1.042	1.002	
Final R indexes [I>=2σ (I)]	R_1 = 0.0257, wR_2 = 0.0669	R_1 = 0.0425, wR_2 = 0.0743	
Final R indexes [all data]	R_1 = 0.0283, wR_2 = 0.0682	R_1 = 0.0647, wR_2 = 0.0854	
Largest diff. peak/hole / e Å^{-3}	0.89/-0.99	1.07/-0.82	

Table 13.3 Crystallographic table of compound **7**.

Identification code	**7-Squeezed**	**7-Unsqueezed**
Empirical formula	$C_{88}H_{89}Dy_2N_{8.5}O_{24}Zn_4$	$C_{88}H_{87.99}Dy_2N_{8.51}O_{24.01}Zn_4$
Formula weight	2236.15	2235.4
Temperature/K	100(2)	100(2)
Crystal system	monoclinic	monoclinic
Space group	$P2_1/c$	$P2_1/c$
a/Å	19.17440(10)	19.17440(10)
b/Å	19.54640(10)	19.54640(10)
c/Å	31.9584(2)	31.9584(2)
α/°	90	90
β/°	103.2960(10)	103.2960(10)
γ/°	90	90
Volume/Å^3	11656.64(12)	11656.64(12)
Z	4	4
ρ_{calc}g/cm^3	1.274	1.274
μ/mm^{-1}	2.136	2.136
F(000)	4482	4478
Crystal size/mm^3	0.1 × 0.08 × 0.006	0.1 × 0.08 × 0.006
Radiation	MoKα (λ = 0.71073)	MoKα (λ = 0.71073)
2Θ range for data collection/°	4.312 to 54.97	3.776 to 54.97
Index ranges	$-24 \leq h \leq 24$, $-25 \leq k \leq 25$, $-41 \leq l \leq 41$	$-24 \leq h \leq 24$, $-25 \leq k \leq 25$, $-41 \leq l \leq 41$
Reflections collected	255761	255761
Independent reflections	26535 [R_{int} = 0.0274, R_{sigma} = 0.0120]	26544 [R_{int} = 0.0274, R_{sigma} = 0.0120]
Data/restraints/parameters	26535/43/1171	26544/43/1172
Goodness-of-fit on F^2	0.983	1.936
Final R indexes [I>=2σ (I)]	R_1 = 0.0340, wR_2 = 0.1050	R_1 = 0.1051, wR_2 = 0.3834
Final R indexes [all data]	R_1 = 0.0377, wR_2 = 0.1079	R_1 = 0.1108, wR_2 = 0.3939
Largest diff. peak/hole / e Å^{-3}	1.54/-0.69	20.05/-1.59

Table 13.4 Crystallographic table of compounds **8** and **9**.

Identification code	**8 -Squeezed**	**8 -Unsqueezed**	**9**
Empirical formula	$C_{88}H_{89}N_{8.5}O_{24}Tb_2Zn_4$	$C_{88}H_{89}N_{8.5}O_{24}Tb_2Zn_4$	$C_{88}H_{88}Eu_2N_9O_{25}Zn_4$
Formula weight	2228.99	2228.99	2232.14
Temperature/K	100(2)	100(2)	173
Crystal system	monoclinic	monoclinic	monoclinic
Space group	$P2_1/c$	$P2_1/c$	$P2_1/c$
a/Å	19.2227(6)	19.2227(6)	19.2415(13)
b/Å	19.5355(5)	19.5355(5)	19.4913(5)
c/Å	31.9960(7)	31.9960(7)	32.1383(15)
α/°	90	90	90
β/°	103.254(3)	103.254(3)	104.401(9)
γ/°	90	90	90
Volume/Å^3	11695.3(6)	11695.3(6)	11883.1(10)
Z	4	4	4
ρ_{calc}g/cm^3	1.266	1.266	
μ/mm^{-1}	2.061	2.061	
F(000)	4474	4474	
Crystal size/mm^3	0.1 × 0.09 × 0.04	0.1 × 0.09 × 0.04	
Radiation	MoKα (λ = 0.71075)	MoKα (λ = 0.71075)	
2Θ range for data collection/°	4.534 to 50.054	4.534 to 50.054	
Index ranges	$-22 \leq h \leq 22$, $-16 \leq k \leq 23$, $-30 \leq l \leq 38$	$-22 \leq h \leq 22$, $-16 \leq k \leq 23$, $-30 \leq l \leq 38$	
Reflections collected	64883	64883	
Independent reflections	20622 [R_{int} = 0.0925, R_{sigma} = 0.1067]	20622 [R_{int} = 0.0925, R_{sigma} = 0.1067]	
Data/restraints/parameters	20622/43/1165	20622/43/1165	
Goodness-of-fit on F^2	0.973	0.973	
Final R indexes [I>=2σ (I)]	R_1 = 0.0588, wR_2 = 0.1478	R_1 = 0.0588, wR_2 = 0.1478	
Final R indexes [all data]	R_1 = 0.0962, wR_2 = 0.1620	R_1 = 0.0962, wR_2 = 0.1620	
Largest diff. peak/hole / e Å^{-3}	1.61/-0.85	1.61/-0.85	

Table 13.5 Crystallographic table of compounds **10-12**.

Identification code	**10**	**11**	**12**
Empirical formula	$C_{42}H_{48}Dy_2N_6O_{24}Zn_2$	$C_{42}H_{48}N_6O_{23}Tb_2Zn_2$	$C_{42}H_{46}Eu_2N_6O_{24}Zn_2$
Formula weight	1476.6	1453.44	1453.51
Temperature/K	173	172	173
Crystal system	monoclinic	monoclinic	monoclinic
Space group	$P2_1/n$	$P2_1/n$	$P2_1/n$
a/Å	14.415(2)	14.4046(7)	14.3947(6)
b/Å	11.9895(10)	12.0096(8)	12.0517(8)
c/Å	14.4978(9)	14.5335(6)	14.5717(6)
α/°	90	90	90
β/°	92.014(6)	92.016(5)	91.998(4)
γ/°	90	90	90
Volume/Å^3	2504.0(5)	2512.6(2)	2526.4(2)
Z	2	2	2
ρ_{calc}g/cm^3	1.958	1.921	1.911
μ/mm^{-1}	17.581	15.427	19.373
F(000)	1452	1432	1436
Crystal size/mm^3	0.26 × 0.2 × 0.12	0.21 × 0.18 × 0.12	0.21 × 0.17 × 0.14
Radiation	CuKα (λ = 1.54184)	CuKα (λ = 1.54184)	CuKα (λ = 1.54184)
2Θ range for data collection/°	12.288 to 133.198	9.556 to 143.164	9.574 to 140.114
Index ranges	$-12 \leq h \leq 10$, $-10 \leq k \leq 14$, $-15 \leq l \leq 17$	$-17 \leq h \leq 17$, $-13 \leq k \leq 14$, $-15 \leq l \leq 17$	$-13 \leq h \leq 17$, $-14 \leq k \leq 11$, $-17 \leq l \leq 14$
Reflections collected	5442	9661	6153
Independent reflections	3208 [R_{int} = 0.0345, R_{sigma} = 0.0549]	4788 [R_{int} = 0.0856, R_{sigma} = 0.1009]	3871 [R_{int} = 0.0712, R_{sigma} = 0.1007]
Data/restraints/parameters	3208/505/348	4788/23/349	3871/504/349
Goodness-of-fit on F^2	1.061	1.049	1.046
Final R indexes [I>=2σ (I)]	R_1 = 0.0787, wR_2 = 0.1917	R_1 = 0.1058, wR_2 = 0.2759	R_1 = 0.0855, wR_2 = 0.2241
Final R indexes [all data]	R_1 = 0.0884, wR_2 = 0.2006	R_1 = 0.1246, wR_2 = 0.3029	R_1 = 0.1190, wR_2 = 0.2570
Largest diff. peak/hole / e Å^{-3}	2.49/-1.50	2.74/-2.87	1.34/-1.19

Table 13.6 Crystallographic table of compounds **13** and **14**.

Identification code	**13**	**14**
Empirical formula	$C_{112}H_{100}Cl_4Dy_7N_8O_{36}Zn_4$	$C_{71}H_{64}Dy_2N_5O_{19}Zn_3$
Formula weight	3674.77	1812.38
Temperature/K	100(2)	100(2)
Crystal system	monoclinic	monoclinic
Space group	C2/c	$P2_1/c$
a/Å	35.4471(14)	17.2803(10)
b/Å	16.1080(7)	22.8749(9)
c/Å	28.2724(12)	20.9155(8)
α/°	90	90
β/°	113.449(5)	110.500(5)
γ/°	90	90
Volume/Å^3	14809.8(12)	7744.0(7)
Z	4	4
ρ_{calc}g/cm^3	1.648	1.555
μ/mm^{-1}	4.257	2.89
F(000)	7064	3596
Crystal size/mm^3	0.1 × 0.05 × 0.05	0.04 × 0.04 × 0.01
Radiation	MoKα (λ = 0.71075)	MoKα (λ = 0.71075)
2Θ range for data collection/°	4.276 to 50.056	5.034 to 50.054
Index ranges	$-40 \leq h \leq 42$, $-19 \leq k \leq 19$, $-29 \leq l \leq 33$	$-20 \leq h \leq 20$, $-26 \leq k \leq 27$, $-24 \leq l \leq 24$
Reflections collected	43506	84485
Independent reflections	13082 [R_{int} = 0.0435, R_{sigma} = 0.0480]	13646 [R_{int} = 0.2122, R_{sigma} = 0.1532]
Data/restraints/parameters	13082/1109/777	13646/1039/922
Goodness-of-fit on F^2	1.06	0.945
Final R indexes [I>=2σ (I)]	R_1 = 0.0877, wR_2 = 0.1966	R_1 = 0.0628, wR_2 = 0.1446
Final R indexes [all data]	R_1 = 0.1038, wR_2 = 0.2036	R_1 = 0.1226, wR_2 = 0.1683
Largest diff. peak/hole / e Å^{-3}	2.32/-3.31	1.93/-1.53

13.1.2 Chapter 3

Table 13.7 Crystallographic table of compounds **16** and **17**.

Identification code	**16**	**17**
Empirical formula	$C_{132}H_{154}Cl_4Co_8Gd_4N_{12}O_{51}$	$C_{120}H_{124}Cl_4Co_8Dy_4N_{12}O_{48}$
Formula weight	3966.9	3765.54
Temperature/K	173(2)	173
Crystal system	monoclinic	monoclinic
Space group	$P2_1/c$	$P2_1/c$
a/Å	15.7924(10)	15.8067(10)
b/Å	21.4805(10)	21.4624(15)
c/Å	25.0254(15)	25.0731(16)
α/°	90	90
β/°	98.932(5)	99.651(5)
γ/°	90	90
Volume/Å^3	8386.4(8)	8385.7(10)
Z	2	2
ρ_{calc}g/cm^3	1.571	1.491
μ/mm^{-1}	2.468	2.663
F(000)	3956	3720
Crystal size/mm^3	0.300 × 0.240 × 0.140	0.14 × 0.12 × 0.08
Radiation	MoKα (λ = 0.71073)	MoKα (λ = 0.71073)
2Θ range for data collection/°	5.024 to 50.216	4.744 to 50.248
Index ranges	? ≤ h ≤ ?, ? ≤ k ≤ ?, ? ≤ l ≤ ?	-16 ≤ h ≤ 18, -23 ≤ k ≤ 25, -29 ≤ l ≤ 29
Reflections collected	?	37054
Independent reflections	14651 [R_{int} = ?, R_{sigma} = 0.0568]	14593 [R_{int} = 0.1405, R_{sigma} = 0.2390]
Data/restraints/parameters	14651/180/1044	14593/2484/788
Goodness-of-fit on F^2	0.916	0.767
Final R indexes [I>=2σ (I)]	R_1 = 0.0372, wR_2 = 0.0827	R_1 = 0.0857, wR_2 = 0.1791
Final R indexes [all data]	R_1 = 0.0565, wR_2 = 0.0868	R_1 = 0.1960, wR_2 = 0.2112
Largest diff. peak/hole / e Å^{-3}	1.20/-1.46	1.47/-1.02

Table 13.8 Crystallographic table of compounds **18** and **19**.

Identification code	**18**	**19**
Empirical formula	$C_{132}H_{152}Cl_4Co_8N_{12}O_{51}Tb_4$	$C_{62}H_{59.33}Br_4Cl_{3.33}Co_4Dy_2N_6O_{25.33}$
Formula weight	3971.57	2292.34
Temperature/K	173	173
Crystal system	monoclinic	trigonal
Space group	$P2_1/c$	$P3_121$
a/Å	15.7073(6)	16.2445(5)
b/Å	21.4916(12)	16.2445(5)
c/Å	24.8869(10)	29.8880(11)
α/°	90	90
β/°	98.906(3)	90
γ/°	90	120
Volume/Å^3	8299.9(7)	6830.3(5)
Z	2	3
ρ_{calc}g/cm^3	1.589	1.672
μ/mm^{-1}	2.6	4.251
F(000)	3960	3338
Crystal size/mm^3	0.25 × 0.2 × 0.18	0.12 × 0.1 × 0.08
Radiation	MoKα (λ = 0.71073)	MoKα (λ = 0.71073)
2Θ range for data collection/°	3.446 to 51.424	5.198 to 49.528
Index ranges	$-19 \leq h \leq 17$, $-26 \leq k \leq 26$, $-30 \leq l \leq 30$	$-17 \leq h \leq 19$, $-17 \leq k \leq 5$, $-31 \leq l \leq 35$
Reflections collected	51035	16320
Independent reflections	15507 [R_{int} = 0.0809, R_{sigma} = 0.0660]	6621 [R_{int} = 0.0844, R_{sigma} = 0.1090]
Data/restraints/parameters	15507/354/1020	6621/46/394
Goodness-of-fit on F^2	0.901	0.915
Final R indexes [I>=2σ (I)]	R_1 = 0.0389, wR_2 = 0.0900	R_1 = 0.0563, wR_2 = 0.1187
Final R indexes [all data]	R_1 = 0.0612, wR_2 = 0.0960	R_1 = 0.1317, wR_2 = 0.1451
Largest diff. peak/hole / e Å^{-3}	1.08/-0.94	0.54/-0.54

13.1.3 Chapter 4

Table 13.9 Crystallographic table of compounds **20, 22** and **22'**.

Identification code	**20**	**22**	**22'**
Empirical formula	$C_{120}H_{114}Co_3F_{18}N_{18}O_{42}S_6Y_4$	$C_{120}H_{116}Dy_4F_{18}N_{18}Ni_3O_{43}S_6$	$C_{114}H_{114}Cl_3Dy_4N_{18}Ni_3O_{37}$
Formula weight	3547.08	3858.79	3260.71
Temperature/K	100(2)	100(2)	100(2)
Crystal system	orthorhombic	orthorhombic	trigonal
Space group	Pbca	Pbca	R3c
a/Å	36.2555(6)	22.6480(2)	20.9581(2)
b/Å	22.6457(4)	35.8769(6)	20.9581(2)
c/Å	36.5878(8)	36.2728(3)	58.0341(8)
α/°	90	90	90
β/°	90	90	90
γ/°	90	90	120
Volume/Å^3	30039.7(10)	29473.1(6)	22075.9(5)
Z	8	8	6
ρ_{calc}g/cm^3	1.569	1.739	1.472
μ/mm^{-1}	2.038	2.569	2.508
F(000)	14328	15296	9714
Crystal size/mm^3	0.25 × 0.13 × 0.01	0.1 × 0.08 × 0.06	0.14 × 0.13 × 0.11
Radiation	MoKα (λ = 0.71075)	MoKα (λ = 0.71075)	MoKα (λ = 0.71075)
2Θ range for data collection/°	4.23 to 50.058	3.936 to 50.056	4.42 to 55.118
Index ranges	$-43 \leq h \leq 40$, $-25 \leq k \leq 26$, $-43 \leq l \leq 42$	$-26 \leq h \leq 26$, $-33 \leq k \leq 42$, $-41 \leq l \leq 43$	$-27 \leq h \leq 27$, $-27 \leq k \leq 27$, $-75 \leq l \leq 75$
Reflections collected	162614	147024	164374
Independent reflections	26516 [R_{int} = 0.1027, R_{sigma} = 0.0755]	26026 [R_{int} = 0.0767, R_{sigma} = 0.0459]	11346 [R_{int} = 0.0372, R_{sigma} = 0.0114]
Data/restraints/parameters	26516/2783/1855	26026/2734/1849	11346/535/521
Goodness-of-fit on F^2	1.031	1.111	1.058
Final R indexes [I>=2σ (I)]	R_1 = 0.0982, wR_2 = 0.2643	R_1 = 0.0881, wR_2 = 0.2198	R_1 = 0.0374, wR_2 = 0.1038
Final R indexes [all data]	R_1 = 0.1745, wR_2 = 0.3165	R_1 = 0.1121, wR_2 = 0.2322	R_1 = 0.0382, wR_2 = 0.1048
Largest diff. peak/hole / e Å^{-3}	1.18/-0.70	2.11/-2.00	1.46/-0.53

Table 13.10 Crystallographic table of compounds **25-27**.

Identification code	**25**	**26**	**27**
Empirical formula	$C_{36}H_{44}CoN_5O_{12}$	$C_{45}H_{52}Br_2CoN_3O_9$	$C_{120.5}H_{115}Cl_5Dy_2N_4Ni_2O_{20}$
Formula weight	797.69	997.64	2558.83
Temperature/K	100	173	173
Crystal system	monoclinic	monoclinic	monoclinic
Space group	$P2_1/c$	$P2_1/n$	C2/c
a/Å	18.8624(5)	13.0590(8)	22.1776(15)
b/Å	17.0300(4)	22.7258(11)	18.8940(11)
c/Å	25.6461(18)	15.4472(13)	27.8333(11)
α/°	90	90	90
β/°	108.353(8)	109.616(8)	100.127(4)
γ/°	90	90	90
Volume/$Å^3$	7819.2(7)	4318.3(5)	11481.1(11)
Z	8	4	4
ρ_{calc}g/cm^3	1.355	1.535	1.48
μ/mm^{-1}	0.505	2.307	1.795
F(000)	3344	2048	5196
Crystal size/mm^3	0.24 × 0.13 × 0.02	0.12 × 0.1 × 0.06	0.1 × 0.05 × 0.02
Radiation	MoKα (λ = 0.71075)	MoKα (λ = 0.71073)	MoKα (λ = 0.71073)
2Θ range for data collection/°	6.104 to 54.962	4.88 to 52.742	5.564 to 58.632
Index ranges	$-24 \leq h \leq 24$, $-19 \leq k \leq 22$, $-26 \leq l \leq 33$	$-14 \leq h \leq 16$, $-27 \leq k \leq 26$, $-14 \leq l \leq 19$	$? \leq h \leq ?$, $? \leq k \leq ?$, $? \leq l \leq ?$
Reflections collected	61781	13404	?
Independent reflections	17458 [R_{int} = 0.0518, R_{sigma} = 0.0621]	8410 [R_{int} = 0.0365, R_{sigma} = 0.0800]	12896 [R_{int} = ?, R_{sigma} = 0.1362]
Data/restraints/parameters	17458/93/955	8410/0/543	12896/264/535
Goodness-of-fit on F^2	1.054	1.041	1.041
Final R indexes [I>=2σ (I)]	R_1 = 0.0855, wR_2 = 0.2181	R_1 = 0.0590, wR_2 = 0.1182	R_1 = 0.1138, wR_2 = 0.2803
Final R indexes [all data]	R_1 = 0.1216, wR_2 = 0.2379	R_1 = 0.1023, wR_2 = 0.1402	R_1 = 0.1828, wR_2 = 0.3192
Largest diff. peak/hole / e $Å^{-3}$	1.40/-1.25	0.77/-0.81	2.48/-2.56

Table 13.11 Crystallographic table of compounds **28-30**.

Identification code	**28**	**29**	**30**
Empirical formula	$C_{122}H_{146}Cl_2Dy_2N_{14}Ni_2O_{30}$	$C_{112}H_{114}Br_6Dy_2N_4Ni_2O_{26}$	$C_{122}H_{130}Dy_2N_4Ni_2O_{24}$
Formula weight	2801.84	2848.01	2478.64
Temperature/K	173	173	100
Crystal system	triclinic	monoclinic	trigonal
Space group	P-1	C2/c	R-3
a/Å	12.5403(7)	20.4620(7)	38.159(3)
b/Å	14.7915(10)	20.8069(7)	38.159(3)
c/Å	18.880(2)	27.3553(7)	18.7654(13)
α/°	100.291(8)	90	90
β/°	106.198(7)	98.444(3)	90
γ/°	105.143(5)	90	120
Volume/Å^3	3124.5(5)	11520.3(7)	23664(4)
Z	1	4	9
ρ_{calc}g/cm^3	1.489	1.592	1.507
μ/mm^{-1}	1.602	3.754	1.832
F(000)	1438	5472	10962
Crystal size/mm^3	0.38 × 0.32 × 0.24	0.12 × 0.08 × 0.03	0.15 × 0.12 × 0.06
Radiation	MoKα (λ = 0.71073)	MoKα (λ = 0.71073)	MoKα (λ = 0.71075)
2Θ range for data collection/°	4.956 to 58.074	5.06 to 58.266	4.992 to 54.966
Index ranges	$-15 \leq h \leq 10$, $-9 \leq k \leq 18$, $-24 \leq l \leq 6$	$-27 \leq h \leq 14$, $-14 \leq k \leq 26$, $-29 \leq l \leq 37$	$-38 \leq h \leq 49$, $-49 \leq k \leq 39$, $-24 \leq l \leq 22$
Reflections collected	9418	22076	56666
Independent reflections	7781 [R_{int} = 0.0478, R_{sigma} = 0.0683]	12759 [R_{int} = 0.0281, R_{sigma} = 0.0604]	11972 [R_{int} = 0.0483, R_{sigma} = 0.0370]
Data/restraints/parameters	7781/23/779	12759/7/652	11972/73/638
Goodness-of-fit on F^2	1.083	1.018	0.992
Final R indexes [I>=2σ (I)]	R_1 = 0.0437, wR_2 = 0.1070	R_1 = 0.0501, wR_2 = 0.1310	R_1 = 0.0408, wR_2 = 0.1095
Final R indexes [all data]	R_1 = 0.0524, wR_2 = 0.1165	R_1 = 0.0746, wR_2 = 0.1431	R_1 = 0.0553, wR_2 = 0.1157
Largest diff. peak/hole / e Å^{-3}	1.03/-0.62	2.77/-3.54	1.46/-0.90

Table 13.12 Crystallographic table of compounds **31-32**.

Identification code	**31**	**32**	**33**
Empirical formula	$C_{102}H_{110}Cl_2Dy_2N_{10}Ni_2O_{26}$	$C_{64}H_{72}Cl_2Dy_2N_4Ni_2O_{26}$	$C_{82}H_{100}Dy_2F_6N_{12}Ni_2O_{26}S_2$
Formula weight	2405.31	1826.57	2290.27
Temperature/K	173	173	173
Crystal system	monoclinic	monoclinic	monoclinic
Space group	$P2_1/n$	$P2_1/n$	$P2_1/c$
a/Å	15.8855(6)	12.1724(12)	16.6632(4)
b/Å	17.2105(11)	14.1352(15)	18.8674(3)
c/Å	20.5903(11)	19.123(2)	15.7017(3)
α/°	90	90	90
β/°	96.747(4)	99.425(11)	109.993(3)
γ/°	90	90	90
Volume/Å^3	5590.3(5)	3245.9(6)	4638.96(19)
Z	2	2	2
ρ_{calc}g/cm^3	1.429	1.869	1.64
μ/mm^{-1}	1.774	3.019	2.13
F(000)	2444	1828	2316
Crystal size/mm^3	0.36 × 0.28 × 0.2	0.12 × 0.1 × 0.04	0.26 × 0.2 × 0.06
Radiation	MoKα (λ = 0.71073)	MoKα (λ = 0.71073)	MoKα (λ = 0.71073)
2Θ range for data collection/°	5.072 to 58.376	5.184 to 58.058	6.762 to 52.744
Index ranges	$-21 \leq h \leq 19$, $0 \leq k \leq 23$, $0 \leq l \leq 26$	$-15 \leq h \leq 13$, $-10 \leq k \leq 18$, $-13 \leq l \leq 25$	$-20 \leq h \leq 20$, $-23 \leq k \leq 23$, $-18 \leq l \leq 19$
Reflections collected	13138	12310	17646
Independent reflections	13129 [R_{int} = 0.0000, R_{sigma} = 0.0495]	7192 [R_{int} = 0.1031, R_{sigma} = 0.2047]	9384 [R_{int} = 0.0267, R_{sigma} = 0.0449]
Data/restraints/parameters	13129/446/664	7192/5/462	9384/0/599
Goodness-of-fit on F^2	1.075	0.872	1.039
Final R indexes [I>=2σ (I)]	R_1 = 0.0464, wR_2 = 0.1115	R_1 = 0.0650, wR_2 = 0.0947	R_1 = 0.0382, wR_2 = 0.0885
Final R indexes [all data]	R_1 = 0.0708, wR_2 = 0.1220	R_1 = 0.1319, wR_2 = 0.1300	R_1 = 0.0501, wR_2 = 0.0976
Largest diff. peak/hole / e Å^{-3}	1.24/-1.24	1.35/-1.82	1.03/-1.20

Table 13.13 Crystallographic table of compounds **34-33**.

Identification code	**34**	**35**	**36**
Empirical formula	$C_{174}H_{170}Br_8Cl_4Dy_4N_{18}Ni_4O_{52}$	$C_{164}H_{184}N_8Ni_8O_{44}$	$C_{92}H_{112}Cl_2Dy_2N_4Ni_2O_{30}$
Formula weight	5011.19	3432.72	2267.18
Temperature/K	100	100	173
Crystal system	triclinic	triclinic	monoclinic
Space group	P-1	P-1	$P2_1/n$
a/Å	13.4199(5)	18.0377(13)	12.19560(19)
b/Å	19.4201(7)	18.3422(13)	19.3817(6)
c/Å	20.7033(15)	29.900(2)	20.2019(7)
α/°	88.220(6)	71.347(2)	90
β/°	85.020(6)	71.670(2)	98.464(2)
γ/°	84.859(6)	67.774(2)	90
Volume/Å^3	5352.1(5)	8462.6(11)	4723.1(2)
Z	1	2	2
ρ_{calc}g/cm^3	1.555	1.262	1.594
μ/mm^{-1}	3.34	0.941	2.095
F(000)	2480	3348	2308
Crystal size/mm^3	0.12 × 0.08 × 0.04	0.22 × 0.08 × 0.03	0.28 × 0.14 × 0.1
Radiation	MoKα (λ = 0.71075)	MoKα (λ = 0.71075)	Mo Kα (λ = 0.71073)
2Θ range for data collection/°	6.118 to 54.97	4.49 to 55.226	5.32 to 58.32
Index ranges	$-17 \leq h \leq 16$, $-25 \leq k \leq 25$, $-26 \leq l \leq 26$	$-23 \leq h \leq 23$, $-23 \leq k \leq 23$, $-38 \leq l \leq 38$	$-14 \leq h \leq 16$, $-26 \leq k \leq 22$, $-26 \leq l \leq 25$
Reflections collected	72585	106354	29019
Independent reflections	24304 [R_{int} = 0.0441, R_{sigma} = 0.0524]	38045 [R_{int} = 0.0854, R_{sigma} = 0.0739]	11050 [R_{int} = 0.0320, R_{sigma} = 0.0412]
Data/restraints/parameters	24304/1/1203	38045/206/1922	11050/9/613
Goodness-of-fit on F^2	1.112	1.049	1.053
Final R indexes [I>=2σ (I)]	R_1 = 0.0480, wR_2 = 0.1253	R_1 = 0.0643, wR_2 = 0.1750	R_1 = 0.0322, wR_2 = 0.0687
Final R indexes [all data]	R_1 = 0.0603, wR_2 = 0.1312	R_1 = 0.0845, wR_2 = 0.1896	R_1 = 0.0451, wR_2 = 0.0755
Largest diff. peak/hole / e Å^{-3}	2.65/-3.19	0.91/-1.15	1.18/-0.54

Table 13.14 Crystallographic table of compounds **37-39**.

Identification code	**37**	**38**	**39**
Empirical formula	$C_{106}H_{122}Cl_2Dy_2N_{10}Ni_2O_{28}$	$C_{62}H_{58}Dy_2N_4Ni_2O_{18}$	$C_{88}H_{76}Co_2Dy_2N_{14}O_{34}$
Formula weight	2497.46	1589.54	2316.48
Temperature/K	173	173	100
Crystal system	monoclinic	monoclinic	triclinic
Space group	$P2_1/c$	$P2_1/c$	P-1
a/Å	15.0768(5)	10.4776(4)	13.1490(9)
b/Å	20.6499(5)	21.3408(8)	13.6200(10)
c/Å	17.8256(8)	14.3681(5)	15.4701(11)
α/°	90	90	68.869(5)
β/°	103.010(4)	106.977(4)	65.650(4)
γ/°	90	90	63.614(4)
Volume/Å^3	5407.3(3)	3072.7(2)	2207.1(3)
Z	2	2	1
ρ_{calc}g/cm^3	1.534	1.718	1.743
μ/mm^{-1}	1.838	14.105	2.141
F(000)	2548	1580	1160
Crystal size/mm^3	0.28 × 0.24 × 0.12	0.08 × 0.06 × 0.03	0.03 × 0.03 × 0.01
Radiation	Mo Kα (λ = 0.71073)	CuKα (λ = 1.54184)	MoKα (λ = 0.71075)
2Θ range for data collection/°	5.08 to 58.5	9.75 to 140.882	4.986 to 55.256
Index ranges	-19 ≤ h ≤ 19, -26 ≤ k ≤ 27, -23 ≤ l ≤ 16	? ≤ h ≤ ?, ? ≤ k ≤ ?, ? ≤ l ≤ ?	-17 ≤ h ≤ 17, -17 ≤ k ≤ 17 , -20 ≤ l ≤ 20
Reflections collected	27684	?	49522
Independent reflections	12547 [R_{int} = 0.0313, R_{sigma} = 0.0458]	5641 [R_{int} = ?, R_{sigma} = 0.0927]	10202 [R_{int} = 0.1033, R_{sigma} = 0.0580]
Data/restraints/parameters	12547/0/686	5641/3/386	10202/15/621
Goodness-of-fit on F^2	1.065	0.99	1.078
Final R indexes [I>=2σ (I)]	R_1 = 0.0362, wR_2 = 0.0816	R_1 = 0.0666, wR_2 = 0.1672	R_1 = 0.0745, wR_2 = 0.1889
Final R indexes [all data]	R_1 = 0.0491, wR_2 = 0.0908	R_1 = 0.0899, wR_2 = 0.1837	R_1 = 0.0859, wR_2 = 0.1971
Largest diff. peak/hole / e Å^{-3}	1.05/-0.94	3.24/-1.36	4.51/-2.63

13.1.4 Chapter 5

Table 13.15. Crystallographic table of compounds **40-42**.

Identification code	**40**	**41**	**42**
Empirical formula	$C_{94}H_{90}Co_2Dy_2N_{14}O_{32}$	$C_{81}H_{69}Dy_3N_{24}O_{60}$	$C_{181}H_{171}Dy_4N_{27}Ni_4O_{66}$
Formula weight	2370.65	2826.1	4665.28
Temperature/K	100	100	173
Crystal system	triclinic	triclinic	triclinic
Space group	P-1	P-1	P-1
a/Å	12.7821(9)	16.5657(12)	14.1586(6)
b/Å	13.5743(10)	17.6842(12)	17.2590(7)
c/Å	14.1583(10)	18.4698(13)	22.3936(8)
α/°	106.940(3)	81.572(2)	98.527(3)
β/°	91.065(2)	80.148(2)	98.268(3)
γ/°	97.754(2)	83.020(2)	111.403(4)
Volume/Å^3	2324.2(3)	5247.5(6)	4920.7(4)
Z	1	2	1
ρ_{calc}g/cm^3	1.694	1.789	1.574
μ/mm^{-1}	2.034	2.233	1.966
F(000)	1194	2802	2350
Crystal size/mm^3	0.14 × 0.12 × 0.04	0.13 × 0.1 × 0.05	0.2 × 0.18 × 0.14
Radiation	MoKα (λ = 0.71075)	MoKα (λ = 0.71075)	MoKα (λ = 0.71073)
2Θ range for data collection/°	4.98 to 55.026	4.68 to 55.01	6.714 to 58.828
Index ranges	$-16 \leq h \leq 16$, $-17 \leq k \leq 16$, $-18 \leq l \leq 16$	$-21 \leq h \leq 21$, $-22 \leq k \leq 22$, $-22 \leq l \leq 23$	$-18 \leq h \leq 19$, $-23 \leq k \leq 21$, $-30 \leq l \leq 25$
Reflections collected	37052	76415	33792
Independent reflections	10595 [R_{int} = 0.0498, R_{sigma} = 0.0413]	23648 [R_{int} = 0.0367, R_{sigma} = 0.0304]	21989 [R_{int} = 0.0315, R_{sigma} = 0.0630]
Data/restraints/parameters	10595/112/653	23648/0/1489	21989/19/1284
Goodness-of-fit on F^2	1.047	1.05	1.053
Final R indexes [I>=2σ (I)]	R_1 = 0.0427, wR_2 = 0.1152	R_1 = 0.0314, wR_2 = 0.0764	R_1 = 0.0425, wR_2 = 0.0968
Final R indexes [all data]	R_1 = 0.0469, wR_2 = 0.1197	R_1 = 0.0360, wR_2 = 0.0797	R_1 = 0.0618, wR_2 = 0.1096
Largest diff. peak/hole / e Å^{-3}	2.80/-1.53	2.10/-1.47	1.32/-0.93

13.1.5 Chapter 6

Table 13.16 Crystallographic table of compounds **43** and **44**.

Identification code	**43**	**44**
Empirical formula	$C_{79}H_{137}Cl_4Dy_{11}N_{10}O_{71}Zn_4$	$C_{79}H_{135}Cl_4Gd_{11}N_{10}O_{71}Zn_4$
Formula weight	4553.76	4493.99
Temperature/K	100(2)	100(2)
Crystal system	monoclinic	monoclinic
Space group	C2/c	C2/c
a/Å	21.5114(3)	21.5153(3)
b/Å	35.0488(4)	35.0390(3)
c/Å	22.5248(3)	22.6388(2)
α/°	90	90
β/°	101.3200(10)	101.2930(10)
γ/°	90	90
Volume/Å^3	16652.2(4)	16736.4(3)
Z	4	4
ρ_{calc}g/cm^3	1.816	1.784
μ/mm^{-1}	5.574	4.994
F(000)	8652	8556
Crystal size/mm^3	0.18 × 0.08 × 0.03	0.25 × 0.14 × 0.03
Radiation	MoKα (λ = 0.71075)	Mo Kα (λ = 0.71075)
2Θ range for data collection/°	4.36 to 54.97	4.544 to 54.972
Index ranges	$-27 \leq h \leq 27$, $-45 \leq k \leq 45$, $-29 \leq l \leq 25$	$-27 \leq h \leq 27$, $-45 \leq k \leq 45$, $-29 \leq l \leq 29$
Reflections collected	107258	109848
Independent reflections	19099 [R_{int} = 0.0369, R_{sigma} = 0.0244]	19130 [R_{int} = 0.0342, R_{sigma} = 0.0215]
Data/restraints/parameters	19099/1659/879	19130/40/881
Goodness-of-fit on F^2	1.01	1.082
Final R indexes [I>=2σ (I)]	R_1 = 0.0328, wR_2 = 0.0833	R_1 = 0.0333, wR_2 = 0.0804
Final R indexes [all data]	R_1 = 0.0392, wR_2 = 0.0859	R_1 = 0.0387, wR_2 = 0.0823
Largest diff. peak/hole / e Å^{-3}	2.98/-1.14	1.92/-1.37

13.1.6 Chapter 7

Table 13.17 Crystallographic table of compounds **1MDy-ClO$_4$**.

Identification code	**1CoDy-ClO$_4$**	**1NiDy-ClO$_4$**
Empirical formula	$C_{72}H_{88}Cl_2Co_2Dy_2N_4O_{28}$	$C_{72}H_{90}Cl_2Dy_2N_4Ni_2O_{28}$
Formula weight	1971.28	1972.79
Temperature/K	173	173
Crystal system	monoclinic	monoclinic
Space group	$P2_1/n$	$P2_1/n$
a/Å	12.8227(4)	12.7440(4)
b/Å	20.9384(5)	20.9329(5)
c/Å	15.3817(5)	15.3458(5)
α/°	90	90
β/°	108.995(4)	108.920(4)
γ/°	90	90
Volume/Å^3	3904.9(2)	3872.6(2)
Z	2	2
ρ_{calc}g/cm^3	1.6764	1.692
μ/mm^{-1}	14.67	2.539
F(000)	1943	1992
Crystal size/mm^3	0.24 × 0.2 × 0.18	0.5604 × 0.5354 × 0.2879
Radiation	Cu Kα (λ = 1.54184)	MoKα (λ = 0.71073)
2Θ range for data collection/°	7.4 to 142.92	4.798 to 58.67
Index ranges	$-14 \leq h \leq 15$, $-25 \leq k \leq 25$, $-18 \leq l \leq 17$	$-16 \leq h \leq 13$, $-25 \leq k \leq 28$, $-18 \leq l \leq 21$
Reflections collected	26009	19340
Independent reflections	7576 [R_{int} = 0.0490, R_{sigma} = 0.0482]	8980 [R_{int} = 0.0330, R_{sigma} = 0.0510]
Data/restraints/parameters	7576/9/511	8980/9/512
Goodness-of-fit on F^2	1.033	1.055
Final R indexes [I>=2σ (I)]	R_1 = 0.0388, wR_2 = N/A	R_1 = 0.0375, wR_2 = 0.0814
Final R indexes [all data]	R_1 = 0.0469, wR_2 = 0.1028	R_1 = 0.0508, wR_2 = 0.0887
Largest diff. peak/hole / e Å^{-3}	1.94/-1.00	1.69/-0.87

Table 13.17 Crystallographic table of compounds **1MDy-Cl**.

Identification code	**1NiDy-Cl**	**1CoDy-Cl**
Empirical formula	$C_{66}H_{59}Cl_2Dy_2N_9Ni_2O_{12}$	$C_{68}H_{56}Cl_2Co_2Dy_2N_{10}O_{12}$
Formula weight	1683.54	1719.03
Temperature/K	273(2)	N/A
Crystal system	triclinic	triclinic
Space group	P-1	P-1
a/Å	11.696(3)	11.6965(3)
b/Å	11.973(4)	12.0424(3)
c/Å	13.084(4)	13.1724(3)
α/°	88.597(16)	89.1070(19)
β/°	64.494(10)	64.281(3)
γ/°	81.504(15)	81.938(2)
Volume/Å^3	1633.9(9)	1652.92(8)
Z	1	1
ρ_{calc}g/cm^3	1.711	1.7268
μ/mm^{-1}	2.978	2.879
F(000)	836	851.1
Crystal size/mm^3	0.01 × 0.01 × 0.01	N/A × N/A × N/A
Radiation	MoKα (λ = 0.71075)	Mo Kα (λ = 0.71075)
2Θ range for data collection/°	4.768 to 50.166	3.42 to 55.12
Index ranges	$-13 \leq h \leq 13$, $-14 \leq k \leq 14$, $-15 \leq l \leq 15$	$-15 \leq h \leq 14$, $-14 \leq k \leq 15$, $-17 \leq l \leq 16$
Reflections collected	17528	20820
Independent reflections	5748 [R_{int} = 0.1337, R_{sigma} = 0.1331]	7623 [R_{int} = 0.0193, R_{sigma} = 0.0173]
Data/restraints/parameters	5748/1/423	7623/0/429
Goodness-of-fit on F^2	1.111	1.248
Final R indexes [I>=2σ (I)]	R_1 = 0.0671, wR_2 = 0.1265	R_1 = 0.0211, wR_2 = 0.0684
Final R indexes [all data]	R_1 = 0.1124, wR_2 = 0.1492	R_1 = 0.0250, wR_2 = 0.0876
Largest diff. peak/hole / e Å^{-3}	1.70/-1.01	1.84/-1.24

Table 13.18 Crystallographic table of compounds **LNiY-Cl**.

Identification code	**2NiY-Cl**	**6NiY-Cl**	**16NiY-Cl**
Empirical formula	$C_{328}H_{302}Cl_8N_{28}Ni_8O_{61}Y_8$	$C_{74}H_{74}Cl_2N_6Ni_2O_{14}Y_2$	$C_{90}H_{82}Cl_2N_6Ni_2O_{14}Y_2$
Formula weight	7076.52	1637.53	1837.75
Temperature/K	173	173	173
Crystal system	monoclinic	triclinic	triclinic
Space group	C2/c	P-1	P-1
a/Å	28.0407(5)	11.9923(4)	12.4631(7)
b/Å	13.00973(16)	12.8768(4)	12.9437(6)
c/Å	24.9789(6)	16.6543(6)	15.0457(10)
α/°	90	107.146(3)	100.653(4)
β/°	111.550(3)	107.314(3)	101.291(5)
γ/°	90	95.136(3)	103.269(4)
Volume/Å^3	8475.4(3)	2301.43(14)	2248.5(2)
Z	1	1	1
ρ_{calc}g/cm^3	1.386	1.182	1.357
μ/mm^{-1}	3.392	3.067	3.204
F(000)	3626	840	944
Crystal size/mm^3	0.12 × 0.1 × 0.06	0.12 × 0.08 × 0.06	0.12 × 0.08 × 0.06
Radiation	CuKα (λ = 1.54184)	CuKα (λ = 1.54184)	CuKα (λ = 1.54184)
2Θ range for data collection/°	11.61 to 133.2	11.62 to 133.202	10.584 to 102.16
Index ranges	$-34 \leq h \leq 34$, $-9 \leq k \leq 15$, $-30 \leq l \leq 29$	$-9 \leq h \leq 14$, $-15 \leq k \leq 15$, $-20 \leq l \leq 19$	$-10 \leq h \leq 12$, $-13 \leq k \leq 9$, $-14 \leq l \leq 15$
Reflections collected	29597	15855	8229
Independent reflections	7467 [R_{int} = 0.0331, R_{sigma} = 0.0293]	8024 [R_{int} = 0.0587, R_{sigma} = 0.0785]	4659 [R_{int} = 0.0348, R_{sigma} = 0.0479]
Data/restraints/parameters	7467/54/475	8024/48/455	4659/58/527
Goodness-of-fit on F^2	1.077	1.04	1.015
Final R indexes [I>=2σ (I)]	R_1 = 0.0721, wR_2 = 0.2106	R_1 = 0.0870, wR_2 = 0.2350	R_1 = 0.0476, wR_2 = 0.1253
Final R indexes [all data]	R_1 = 0.0791, wR_2 = 0.2205	R_1 = 0.1003, wR_2 = 0.2471	R_1 = 0.0542, wR_2 = 0.1292
Largest diff. peak/hole / e Å^{-3}	2.55/-1.51	2.09/-2.04	1.14/-0.83

13.1.7 Chapter 8

Table 13.19 Crystallographic tables of compounds **1ZnDy-NO$_3$**.and **1ZnY-NO$_3$**.

Identification code	**1ZnDy-NO$_3$**	**1ZnY-NO$_3$**
Empirical formula	$C_{62}H_{58}Dy_2N_8O_{20}Zn_2$	$C_{62}H_{58}N_8O_{20}Y_2Zn_2$
Formula weight	1690.9	1543.72
Temperature/K	173	173
Crystal system	monoclinic	monoclinic
Space group	$P2_1/c$	$P2_1/c$
a/Å	13.75033(18)	13.7448(6)
b/Å	14.3147(2)	14.3133(7)
c/Å	16.9418(2)	16.9268(7)
α/°	90	90
β/°	95.2801(12)	95.068(5)
γ/°	90	90
Volume/Å^3	3320.55(8)	3317.0(3)
Z	2	2
ρ_{calc}g/cm^3	1.691	1.546
μ/mm^1	3.016	2.525
F(000)	1676	1568
Crystal size/mm^3	0.32 × 0.20 × 0.18	0.28 × 0.22 × 0.16
Radiation	MoKα (λ = 0.71073)	MoKα (λ = 0.71073)
2Θ range for data collection/°	6.766 to 54.964	6.77 to 58.646
Index ranges	$-17 \leq h \leq 18$, $-18 \leq k \leq 12$, $-23 \leq l \leq 13$	$-18 \leq h \leq 15$, $-18 \leq k \leq 14$, $-22 \leq l \leq 20$
Reflections collected	14238	10546
Independent reflections	7145 [R_{int} = 0.0295, R_{sigma} = 0.0479]	6364 [R_{int} = 0.0364, R_{sigma} = 0.0586]
Data/restraints/parameters	7145/0/428	6364/0/428
Goodness-of-fit on F^2	1.064	1.162
Final R indexes [I>=2σ (I)]	R_1 = 0.0367, wR_2 = 0.0946	R_1 = 0.0558, wR_2 = 0.1467
Final R indexes [all data]	R_1 = 0.0462, wR_2 = 0.0992	R_1 = 0.0791, wR_2 = 0.1627
Largest diff. peak/hole / e Å^{-3}	2.51/-0.60	2.25/-0.71

Table 13.20 Crystallographic tables of compounds **1ZnGd-NO$_3$**.and **1ZnEu-NO$_3$**.

Identification code	**1ZnGd-NO$_3$**	**1ZnEu-NO$_3$**
Empirical formula	$C_{62}H_{58}Gd_2N_8O_{20}Zn_2$	$C_{62}H_{58}Eu_2N_8O_{20}Zn_2$
Formula weight	1678.1	1669.91
Temperature/K	173	173
Crystal system	monoclinic	monoclinic
Space group	$P2_1/c$	$P2_1/c$
a/Å	13.8175(6)	13.8125(4)
b/Å	14.3074(6)	14.3087(5)
c/Å	16.9999(8)	16.9783(5)
α/°	90	90
β/°	95.503(4)	95.498(3)
γ/°	90	90
Volume/Å^3	3345.3(3)	3340.12(18)
Z	2	2
ρ_{calc}g/cm^3	1.668	1.6603
μ/mm^1	14.089	14.709
F(000)	1668	1627.8
Crystal size/mm^3	0.30 × 0.24 × 0.20	0.34 × 0.22 × 0.20
Radiation	CuKα (λ = 1.54184)	Cu Kα (λ = 1.54184)
2Θ range for data collection/°	8.092 to 122.2	8.1 to 122.28
Index ranges	$-15 \leq h \leq 14$, $-16 \leq k \leq 15$, $-19 \leq l \leq 17$	$-12 \leq h \leq 15$, $-15 \leq k \leq 16$, $-19 \leq l \leq 19$
Reflections collected	17350	16615
Independent reflections	5096 [R_{int} = 0.0723, R_{sigma} = 0.0602]	5100 [R_{int} = 0.0717 , R_{sigma} = 0.0651]
Data/restraints/parameters	5096/0/428	5100/0/427
Goodness-of-fit on F^2	1.053	1.072
Final R indexes [I>=2σ (I)]	R_1 = 0.0644, wR_2 = 0.1795	R_1 = 0.0572, wR_2 = 0.1605
Final R indexes [all data]	R_1 = 0.0701, wR_2 = 0.1883	R_1 = 0.0619, wR_2 = 0.1685
Largest diff. peak/hole / e Å^{-3}	3.02/-1.79	3.06/-1.19

Table 13.21 Unit Cell parameters for **1ZnLn-NO$_3$**

Identification code	**1ZnSm-NO$_3$**	**1ZnYb-NO$_3$**	**1ZnTb-NO$_3$**
Temperature/K	173	173	173
Crystal system	monoclinic	monoclinic	monoclinic
Space group	$P2_1/c$	$P2_1/c$	$P2_1/c$
a/Å	13.803(5)	13.53(2)	13.758(13)
b/Å	14.26(4)	14.06(4)	14.344(12)
c/Å	16.98(2)	17.98(6)	16.952(8)
α/°	90.00	90.00	90.00
β/°	95.56(6)	95.21(13)	95.56(6)
γ/°	89.94(8)	90.12(4)	90.21(8)
Volume/Å^3	3326(10)	3329(11)	3333(3)

13.1.8 Chapter 9

Table 13.22 Crystallographic table of compounds **2ZnLn-NO$_3$** and **6ZnLn-NO$_3$**.

Identification code	**2ZnY-NO$_3$**	**6ZnY-NO$_3$**
Empirical formula	$C_{84}H_{80}N_{10}O_{22}Y_2Zn_2$	$C_{74}H_{74}N_8O_{20}Y_2Zn_2$
Formula weight	1890.14	1703.97
Temperature/K	100(2)	173
Crystal system	monoclinic	triclinic
Space group	I2/c	P-1
a/Å	30.1992(13)	12.2132(7)
b/Å	13.1382(3)	12.5056(8)
c/Å	24.8811(12)	13.6386(8)
α/°	90	107.799(6)
β/°	120.298(6)	94.432(5)
γ/°	90	113.574(6)
Volume/Å^3	8523.5(7)	1769.7(2)
Z	4	1
ρ_{calc}g/cm^3	1.473	1.599
μ/mm^{-1}	1.983	3.579
F(000)	3872	872
Crystal size/mm^3	0.13 × 0.05 × 0.04	0.18 × 0.16 × 0.12
Radiation	MoKα (λ = 0.71073)	CuKα (λ = 1.54184)
2Θ range for data collection/°	5.38 to 54.968	9.426 to 143.07
Index ranges	$-39 \leq h \leq 38$, $-17 \leq k \leq 17$, $-28 \leq l \leq 32$	$-14 \leq h \leq 14$, $-14 \leq k \leq 15$, $-16 \leq l \leq 16$
Reflections collected	37307	10989
Independent reflections	9751 [R_{int} = 0.0482, R_{sigma} = 0.0452]	6649 [R_{int} = 0.0676, R_{sigma} = 0.0954]
Data/restraints/parameters	9751/66/547	6649/0/482
Goodness-of-fit on F^2	1.033	1.047
Final R indexes [I>=2σ (I)]	R_1 = 0.0548, wR_2 = 0.1535	R_1 = 0.0563, wR_2 = 0.1315
Final R indexes [all data]	R_1 = 0.0739, wR_2 = 0.1642	R_1 = 0.0740, wR_2 = 0.1509
Largest diff. peak/hole / e Å^{-3}	1.91/-0.74	1.24/-0.79

Table 13.22 Crystallographic table of compounds **8ZnLn-NO$_3$** and **9ZnLn-NO$_3$**.

Identification code	**8ZnY-NO$_3$**	**9ZnY-NO$_3$**
Empirical formula	$C_{62}H_{54}N_{12}O_{28}Y_2Zn_2$	$C_{80}H_{84}N_{14}O_{30}Y_2Zn_2$
Formula weight	1723.73	2030.17
Temperature/K	100	173
Crystal system	monoclinic	monoclinic
Space group	$P2_1/c$	$P2_1/c$
a/Å	15.5167(6)	20.4636(14)
b/Å	14.3778(5)	15.5850(6)
c/Å	15.9946(5)	27.6252(15)
α/°	90	90
β/°	93.649(3)	102.669(6)
γ/°	90	90
Volume/Å^3	3561.1(2)	8595.8(8)
Z	2	4
ρ_{calc}g/cm^3	1.608	1.569
μ/mm^{-1}	2.371	3.163
F(000)	1744	4160
Crystal size/mm^3	0.1 × 0.09 × 0.05	0.18 × 0.1 × 0.08
Radiation	MoKα (λ = 0.71073)	CuKα (λ = 1.54184)
2Θ range for data collection/°	5.104 to 52.744	8.858 to 142.702
Index ranges	$-20 \leq h \leq 20$, $-18 \leq k \leq 16$, $-20 \leq l \leq 20$	$-24 \leq h \leq 25$, $-18 \leq k \leq 10$, $-33 \leq l \leq 32$
Reflections collected	23681	31658
Independent reflections	7255 [R_{int} = 0.0408, R_{sigma} = 0.0576]	16320 [R_{int} = 0.0947, R_{sigma} = 0.1491]
Data/restraints/parameters	7255/0/482	16320/126/1156
Goodness-of-fit on F^2	1.052	1.005
Final R indexes [I>=2σ (I)]	R_1 = 0.0442, wR_2 = 0.1075	R_1 = 0.0793, wR_2 = 0.1733
Final R indexes [all data]	R_1 = 0.0680, wR_2 = 0.1150	R_1 = 0.1505, wR_2 = 0.2190
Largest diff. peak/hole / e Å^{-3}	0.76/-0.44	0.81/-0.68

Table 13.23 Crystallographic table of compounds **12ZnLn-NO$_3$** and **13ZnLn-NO$_3$**.

Identification code	**12ZnY-NO$_3$**	**13ZnY-NO$_3$**
Empirical formula	$C_{68}H_{64}Cl_4N_{14}O_{30}Y_2Zn_2$	$C_{80}H_{80}Cl_4N_{14}O_{30}Y_2Zn_2$
Formula weight	2007.69	2167.94
Temperature/K	100(2)	100(2)
Crystal system	triclinic	monoclinic
Space group	P-1	$P2_1/c$
a/Å	11.4670(6)	14.6309(5)
b/Å	14.2497(5)	21.5296(4)
c/Å	14.3350(7)	14.1004(3)
α/°	114.638(4)	90
β/°	112.569(5)	96.537(3)
γ/°	94.342(3)	90
Volume/Å^3	1886.96(16)	4412.7(2)
Z	1	2
ρ_{calc}g/cm^3	1.767	1.632
μ/mm^{-1}	2.39	2.051
F(000)	1016	2208
Crystal size/mm^3	0.07 × 0.04 × 0.03	0.08 × 0.04 × 0.02
Radiation	MoKα (λ = 0.71075)	MoKα (λ = 0.71075)
2Θ range for data collection/°	4.408 to 54.968	4.246 to 52.744
Index ranges	$-14 \leq h \leq 14$, $-18 \leq k \leq 18$, $-18 \leq l \leq 18$	$-18 \leq h \leq 17$, $-26 \leq k \leq 26$, $-17 \leq l \leq 15$
Reflections collected	22827	27584
Independent reflections	8613 [R_{int} = 0.0668, R_{sigma} = 0.0740]	9009 [R_{int} = 0.0516, R_{sigma} = 0.0694]
Data/restraints/parameters	8613/0/547	9009/0/601
Goodness-of-fit on F^2	0.983	1.023
Final R indexes [I>=2σ (I)]	R_1 = 0.0513, wR_2 = 0.1234	R_1 = 0.0459, wR_2 = 0.0829
Final R indexes [all data]	R_1 = 0.0773 , wR_2 = 0.1344	R_1 = 0.0781, wR_2 = 0.0923
Largest diff. peak/hole / e Å^{-3}	1.98/-0.67	1.07/-0.57

Table 13.23 Crystallographic table of compounds **20ZnLn-NO$_3$** and **22ZnLn-NO$_3$**.

Identification code	**20ZnY-NO$_3$**	**22ZnY-NO$_3$**
Empirical formula	$C_{98}H_{90}Dy_2N_8Ni_2O_{20}$	$C_{86}H_{70}Br_4N_8O_{20}Y_2Zn_2$
Formula weight	2142.19	2163.7
Temperature/K	100(2)	100
Crystal system	triclinic	monoclinic
Space group	P-1	C2/c
a/Å	11.64167(16)	26.7727(5)
b/Å	14.56081(18)	16.6603(2)
c/Å	14.80148(19)	20.4411(3)
α/°	70.2523(12)	90
β/°	77.1776(11)	92.4692(16)
γ/°	68.9971(12)	90
Volume/Å^3	2190.02(5)	9109.1(3)
Z	1	4
ρ_{calc}g/cm^3	1.624	1.578
μ/mm^{-1}	2.189	3.608
F(000)	1082	4320
Crystal size/mm^3	0.05 × 0.05 × 0.02	0.24 × 0.16 × 0.02
Radiation	MoKα (λ = 0.71075)	MoKα (λ = 0.71073)
2Θ range for data collection/°	4.864 to 54.97	5.282 to 52.742
Index ranges	$-15 \leq h \leq 15$, $-18 \leq k \leq 18$, $-19 \leq l \leq 19$	$-34 \leq h \leq 34$, $-21 \leq k \leq 21$, $-26 \leq l \leq 26$
Reflections collected	66515	78750
Independent reflections	10027 [R_{int} = 0.0357, R_{sigma} = 0.0181]	9234 [R_{int} = 0.0380, R_{sigma} = 0.0195]
Data/restraints/parameters	10027/0/590	9234/219/526
Goodness-of-fit on F^2	1.054	1.089
Final R indexes [I>=2σ (I)]	R_1 = 0.0207, wR_2 = 0.0519	R_1 = 0.0592, wR_2 = 0.1817
Final R indexes [all data]	R_1 = 0.0231, wR_2 = 0.0528	R_1 = 0.0680, wR_2 = 0.1901
Largest diff. peak/hole / e Å^{-3}	0.83/-0.37	2.00/-1.06

Table 13.24 Crystallographic table of compounds **24 ZnLn-NO$_3$**,**27ZnLn-NO$_3$** and **1CuDy-NO$_3$**

Identification code	**24ZnY-NO$_3$**	**27ZnY-NO$_3$**	**1CuDy-NO$_3$**
Empirical formula	$C_{64}H_{68}N_{14}O_{22}Y_2Zn_2$	$C_{78}H_{90}N_8O_{20}Y_2Zn_2$	$C_{64}H_{56}Cu_2Dy_2N_{10}O_{18}$
Formula weight	1693.88	1768.13	1705.26
Temperature/K	173	100(2)	173
Crystal system	monoclinic	monoclinic	orthorhombic
Space group	$P2_1/c$	$P2_1/c$	Pbca
a/Å	11.012(2)	14.15839(16)	14.0995(4)
b/Å	21.610(3)	13.05838(14)	16.9713(6)
c/Å	14.825(2)	25.7485(3)	25.9304(8)
α/°	90	90	90
β/°	100.762(19)	90.8307(10)	90
γ/°	90	90	90
Volume/Å^3	3466.0(10)	4760.02(9)	6204.8(3)
Z	2	2	4
ρ_{calc}g/cm^3	1.623	1.234	1.825
μ/mm^{-1}	3.698	1.768	14.139
F(000)	1728	1824	3376
Crystal size/mm^3	0.11 × 0.08 × 0.06	0.24 × 0.1 × 0.08	0.24 × 0.16 × 0.1
Radiation	CuKα (λ = 1.54184)	MoKα (λ = 0.71073)	CuKα (λ = 1.54184)
2Θ range for data collection/°	9.142 to 123.278	4.244 to 54.968	6.818 to 134.34
Index ranges	$-12 \leq h \leq 7$, $-24 \leq k \leq 24$, $-14 \leq l \leq 16$	$-18 \leq h \leq 18$, $-16 \leq k \leq 16$, $-33 \leq l \leq 33$	$-16 \leq h \leq 15$, $-19 \leq k \leq 16$, $-16 \leq l \leq 29$
Reflections collected	10484	128151	18682
Independent reflections	5214 [R_{int} = 0.1091, R_{sigma} = 0.1149]	10892 [R_{int} = 0.0484, R_{sigma} = 0.0219]	4863 [R_{int} = 0.0927, R_{sigma} = 0.0754]
Data/restraints/parameters	5214/0/475	10892/36/497	4863/0/437
Goodness-of-fit on F^2	1.199	1.117	1.049
Final R indexes [I>=2σ (I)]	R_1 = 0.1062, wR_2 = 0.2791	R_1 = 0.0441, wR_2 = 0.1301	R_1 = 0.0513, wR_2 = 0.1138
Final R indexes [all data]	R_1 = 0.1326, wR_2 = 0.3351	R_1 = 0.0513, wR_2 = 0.1351	R_1 = 0.0757, wR_2 = 0.1289
Largest diff. peak/hole / e Å^{-3}	2.50/-1.42	1.95/-0.87	0.80/-1.04

13.2 Crystallographic tables of ligands

Table 13.25 Crystallographic table of ligands H_2**L12** and H_2**L22**.

Identification code	**H_2L12**	**H_2L22**
Empirical formula	$C_{14}H_{11}ClN_2O_5$	$C_{21}H_{20}BrNO_4$
Formula weight	322.7	430.29
Temperature/K	173	173
Crystal system	triclinic	triclinic
Space group	P-1	P-1
a/Å	6.9697(4)	7.5662(4)
b/Å	12.6645(7)	8.5456(4)
c/Å	15.0866(8)	14.8304(8)
α/°	76.153(5)	84.747(4)
β/°	89.966(5)	84.775(4)
γ/°	88.423(5)	82.090(4)
Volume/Å^3	1292.45(13)	942.80(8)
Z	4	2
ρ_{calc}g/cm^3	1.658	1.516
μ/mm^{-1}	2.9	2.207
F(000)	664	440
Crystal size/mm^3	0.12 × 0.08 × 0.01	0.28 × 0.14 × 0.04
Radiation	CuKα (λ = 1.54184)	Mo Kα (λ = 0.71073)
2Θ range for data collection/°	10.444 to 142.68	5.36 to 58.26
Index ranges	$-5 \leq h \leq 8$, $-15 \leq k \leq 15$, $-18 \leq l \leq 18$	$-10 \leq h \leq 10$, $-11 \leq k \leq 11$, $-19 \leq l \leq 19$
Reflections collected	7064	21895
Independent reflections	4806 [R_{int} = 0.0243, R_{sigma} = 0.0398]	4630 [R_{int} = 0.0562, R_{sigma} = 0.0474]
Data/restraints/parameters	4806/2/417	4630/2/253
Goodness-of-fit on F^2	1.054	1.049
Final R indexes [I>=2σ (I)]	R_1 = 0.0493, wR_2 = 0.1324	R_1 = 0.0373, wR_2 = 0.0719
Final R indexes [all data]	R_1 = 0.0593, wR_2 = 0.1451	R_1 = 0.0506, wR_2 = 0.0768
Largest diff. peak/hole / e Å^{-3}	0.66/-0.33	0.40/-0.50

13.3 Crystallographic tables of organic products

13.3.1 Chapter 8

Table 13.26 Crystallographic table of organic products **C8aa** and **C8al**.

Identification code	**C8aa**	**C8al**
Empirical formula	$C_{23}H_{18}N_2$	$C_{29}H_{24}N_2O_2$
Formula weight	322.39	432.5
Temperature/K	100(2)	100
Crystal system	monoclinic	triclinic
Space group	$P2_1/c$	P-1
a/Å	10.0681(7)	9.9468(4)
b/Å	9.7551(7)	10.2850(5)
c/Å	17.5082(11)	11.5735(5)
α/°	90	75.327(4)
β/°	94.291(6)	82.383(4)
γ/°	90	81.347(4)
Volume/Å^3	1714.7(2)	1126.82(9)
Z	4	2
ρ_{calc}g/cm^3	1.249	1.275
μ/mm^{-1}	0.069	0.08
F(000)	680	456
Crystal size/mm^3	0.05 × 0.05 × 0.02	0.12 × 0.04 × 0.02
Radiation	? (λ = 0.6889)	MoKα (λ = 0.71073)
2Θ range for data collection/°	4.636 to 53.132	4.816 to 52.736
Index ranges	$-13 \leq h \leq 13$, $-12 \leq k \leq 12$, $-22 \leq l \leq 22$	$-11 \leq h \leq 12$, $-12 \leq k \leq 12$, $-14 \leq l \leq 14$
Reflections collected	11331	27043
Independent reflections	3894 [R_{int} = 0.0786, R_{sigma} = 0.0803]	4603 [R_{int} = 0.0597, R_{sigma} = 0.0393]
Data/restraints/parameters	3894/0/226	4603/1/304
Goodness-of-fit on F^2	1.033	1.045
Final R indexes [I>=2σ (I)]	R_1 = 0.0626, wR_2 = 0.1375	R_1 = 0.0558, wR_2 = 0.1337
Final R indexes [all data]	R_1 = 0.1319, wR_2 = 0.1681	R_1 = 0.0788, wR_2 = 0.1463
Largest diff. peak/hole / e Å^{-3}	0.26/-0.21	0.39/-0.24

Table 13.27 Crystallographic table of organic products **C8ao** and **C8as**

Identification code	**C8ao**	**C8as**
Empirical formula	$C_{23}H_{20}N_2O_3$	$C_{25}H_{22}N_2$
Formula weight	372.41	350.44
Temperature/K	173	100(2)
Crystal system	monoclinic	monoclinic
Space group	$P2_1/n$	I2/a
a/Å	8.8491(5)	18.3322(16)
b/Å	10.6531(7)	10.0821(6)
c/Å	20.9154(13)	20.0451(10)
α/°	90	90
β/°	96.794(6)	90.573(6)
γ/°	90	90
Volume/Å^3	1957.8(2)	3704.7(4)
Z	4	8
ρ_{calc}g/cm^3	1.263	1.257
μ/mm^{-1}	0.085	0.074
F(000)	784	1488
Crystal size/mm^3	0.28 × 0.18 × 0.15	0.08 × 0.05 × 0.01
Radiation	MoKα (λ = 0.71073)	MoKα (λ = 0.71075)
2Θ range for data collection/°	6.872 to 52.74	4.522 to 50.056
Index ranges	$-11 \leq h \leq 9$, $-7 \leq k \leq 13$, $-26 \leq l \leq 19$	$-17 \leq h \leq 21$, $-11 \leq k \leq 12$, $-23 \leq l \leq 23$
Reflections collected	6886	19320
Independent reflections	3957 [R_{int} = 0.0376, R_{sigma} = 0.0635]	3261 [R_{int} = 0.1120, R_{sigma} = 0.0883]
Data/restraints/parameters	3957/2/262	3261/0/246
Goodness-of-fit on F^2	1.023	1.032
Final R indexes [I>=2σ (I)]	R_1 = 0.0696, wR_2 = 0.1801	R_1 = 0.0575, wR_2 = 0.1015
Final R indexes [all data]	R_1 = 0.1108, wR_2 = 0.2212	R_1 = 0.1149, wR_2 = 0.1202
Largest diff. peak/hole / e Å^{-3}	0.46/-0.41	0.21/-0.23

Table 13.28 Crystallographic table of organic products **C8bw** and **C8cb**.

Identification code	**C8bw**	**C8cb**
Empirical formula	$C_{17}H_{15}BrN_2O_2$	$C_{17}H_{19}NO_2$
Formula weight	359.22	269.33
Temperature/K	173	173
Crystal system	monoclinic	monoclinic
Space group	$P2_1/c$	Ia
a/Å	13.8437(7)	13.4472(5)
b/Å	12.9564(6)	9.3180(4)
c/Å	8.5035(4)	11.5805(4)
α/°	90	90
β/°	96.989(5)	90.109(4)
γ/°	90	90
Volume/Å^3	1513.89(12)	1451.06(10)
Z	4	4
ρ_{calc}g/cm^3	1.576	1.233
μ/mm^{-1}	3.776	0.64
F(000)	728	576
Crystal size/mm^3	0.2 × 0.08 × 0.06	0.18 × 0.14 × 0.08
Radiation	CuKα (λ = 1.54184)	CuKα (λ = 1.54184)
2Θ range for data collection/°	9.382 to 142.13	11.554 to 142.016
Index ranges	$-14 \leq h \leq 16$, $-15 \leq k \leq 11$, $-10 \leq l \leq 8$	$-16 \leq h \leq 15$, $-11 \leq k \leq 11$, $-14 \leq l \leq 10$
Reflections collected	4684	4020
Independent reflections	2826 [R_{int} = 0.0454, R_{sigma} = 0.0492]	1939 [R_{int} = 0.0281, R_{sigma} = 0.0334]
Data/restraints/parameters	2826/0/200	1939/2/182
Goodness-of-fit on F^2	1.05	1.037
Final R indexes [I>=2σ (I)]	R_1 = 0.0595, wR_2 = 0.1530	R_1 = 0.0413, wR_2 = 0.1052
Final R indexes [all data]	R_1 = 0.0650, wR_2 = 0.1627	R_1 = 0.0424, wR_2 = 0.1061
Largest diff. peak/hole / e Å^{-3}	1.09/-0.82	0.16/-0.26

13.3.2 Chapter 9

Table 13.29 Crystallographic table of organic products **C9f** and**C9h**.

Identification code	**C9f**	**C9h**
Empirical formula	$C_{15}H_{17}N_3O_5$	$C_{14}H_{16}N_4O_4$
Formula weight	319.32	304.31
Temperature/K	373(2)	100(2)
Crystal system	monoclinic	orthorhombic
Space group	$P2_1/c$	$Pna2_1$
a/Å	21.4080(6)	13.8265(3)
b/Å	8.64361(19)	10.2290(3)
c/Å	25.2347(5)	10.7482(3)
α/°	90	90
β/°	93.733(2)	90
γ/°	90	90
Volume/Å^3	4659.59(19)	1520.13(7)
Z	12	4
ρ_{calc}g/cm^3	1.366	1.33
μ/mm^{-1}	0.875	0.1
F(000)	2016	640
Crystal size/mm^3	? × ? × ?	0.2 × 0.1 × 0.06
Radiation	CuKα (λ = 1.54184)	MoKα (λ = 0.71073)
2Θ range for data collection/°	10.506 to 133.198	5.894 to 52.736
Index ranges	? ≤ h ≤ ?, ? ≤ k ≤ ?, ? ≤ l ≤ ?	-15 ≤ h ≤ 17, -12 ≤ k ≤ 12, -13 ≤ l ≤ 13
Reflections collected	?	15711
Independent reflections	8177 [R_{int} = ?, R_{sigma} = 0.0615]	3005 [R_{int} = 0.0392, R_{sigma} = 0.0220]
Data/restraints/parameters	8177/381/646	3005/3/209
Goodness-of-fit on F^2	1.479	1.032
Final R indexes [I>=2σ (I)]	R_1 = 0.1003, wR_2 = 0.3050	R_1 = 0.0624, wR_2 = 0.1695
Final R indexes [all data]	R_1 = 0.1126, wR_2 = 0.3310	R_1 = 0.0675, wR_2 = 0.1758
Largest diff. peak/hole / e Å^{-3}	1.78/-0.74	0.95/-0.30

Table 13.30 Crystallographic table of organic products for **C9l** and **C9v**.

Identification code	**C9l**	**C9v**
Empirical formula	$C_{14}H_{15}FN_4O_4$	$C_{16}H_{19}N_3O_6$
Formula weight	322.3	349.34
Temperature/K	100(2)	173
Crystal system	orthorhombic	triclinic
Space group	$Pna2_1$	P-1
a/Å	13.8506(4)	8.0625(8)
b/Å	10.5093(3)	8.9689(9)
c/Å	10.5961(2)	11.7791(9)
α/°	90	80.019(8)
β/°	90	85.910(7)
γ/°	90	83.179(8)
Volume/$Å^3$	1542.38(7)	831.82(14)
Z	4	2
ρ_{calc}g/cm^3	1.388	1.395
μ/mm^{-1}	0.112	0.912
F(000)	672	368
Crystal size/mm^3	0.12 × 0.1 × 0.07	0.14 × 0.1 × 0.08
Radiation	MoKα (λ = 0.71073)	CuKα (λ = 1.54184)
2Θ range for data collection/°	5.882 to 52.74	10.074 to 142.272
Index ranges	$-11 \leq h \leq 17$, $-12 \leq k \leq 13$, $-13 \leq l \leq 13$	$-8 \leq h \leq 9$, $-10 \leq k \leq 7$, $-12 \leq l \leq 14$
Reflections collected	10359	4562
Independent reflections	3077 [R_{int} = 0.0175, R_{sigma} = 0.0182]	2946 [R_{int} = 0.0310, R_{sigma} = 0.0376]
Data/restraints/parameters	3077/1/216	2946/0/230
Goodness-of-fit on F^2	1.065	1.063
Final R indexes [I>=2σ (I)]	R_1 = 0.0626, wR_2 = 0.1832	R_1 = 0.0574, wR_2 = 0.1570
Final R indexes [all data]	R_1 = 0.0638, wR_2 = 0.1849	R_1 = 0.0679, wR_2 = 0.1672
Largest diff. peak/hole / e $Å^{-3}$	2.27/-0.27	0.51/-0.25

Chapter 13: Bibliography

1 E. Loukopoulos, B. Berkoff, A. Abdul-Sada, G. J. Tizzard, S. J. Coles, A. Escuer and G. E. Kostakis, *Eur. J. Inorg. Chem.*, 2015, **2015**, 2646–2649.

2 K. C. Mondal, A. Sundt, Y. Lan, G. E. Kostakis, O. Waldmann, L. Ungur, L. F. Chibotaru, C. E. Anson and A. K. Powell, *Angew. Chem. Int. Ed. Engl.*, 2012, **51**, 7550–4.

3 J. Fielden and L. Cronin, in *Encyclopedia of Supramolecular Chemistry*, CRC Press, 2004, vol. null, pp. 1–10.

4 F. A. Cotton, *Inorg. Chem.*, 1964, **3**, 1217–1220.

5 L. Zhang, L. Zhao, P. Zhang, C. Wang, S. W. Yuan and J. Tang, *Inorg. Chem.*, 2015, **54**, 11535–11541.

6 S. Kang, H. Zheng, T. Liu, K. Hamachi, S. Kanegawa, K. Sugimoto, Y. Shiota, S. Hayami, M. Mito, T. Nakamura, M. Nakano, M. L. Baker, H. Nojiri, K. Yoshizawa, C. Duan and O. Sato, *Nat. Commun.*, 2015, **6**, 5955.

7 L. Qin, Y. Z. Yu, P. Q. Liao, W. Xue, Z. Zheng, X. M. Chen and Y. Z. Zheng, *Adv. Mater.*, 2016, **28**, 10772–10779.

8 J. B. Peng, X. J. Kong, Q. C. Zhang, M. Orendáč, J. Prokleška, Y. P. Ren, L. S. Long, Z. Zheng and L. S. Zheng, *J. Am. Chem. Soc.*, 2014, **136**, 17938–17941.

9 A. Vinslava, A. J. Tasiopoulos, W. Wernsdorfer, K. A. Abboud and G. Christou, *Inorg. Chem.*, 2016, **55**, 3419–3430.

10 M. Manoli, R. Inglis, S. Piligkos, L. Yanhua, W. Wernsdorfer, E. K. Brechin and A. J. Tasiopoulos, *Chem. Commun.*, 2016, **52**, 12829–12832.

11 Z.-M. Zhang, S. Yao, Y.-G. Li, R. Clérac, Y. Lu, Z.-M. Su and E.-B. Wang, *J. Am. Chem. Soc.*, 2009, **131**, 14600–14601.

12 L. N. Dawe, K. V Shuvaev and L. K. Thompson, *Chem. Soc. Rev.*, 2009, **38**, 2334.

13 G. E. Kostakis, V. A. Blatov and D. M. Proserpio, *Dalt. Trans.*, 2012, **41**, 4634.

14 P. Wix, G. E. Kostakis, V. A. Blatov, D. M. Proserpio, S. P. Perlepes and A. K. Powell, *Eur. J. Inorg. Chem.*, 2013, **2013**, 520–526.

15 G. E. Kostakis, S. P. Perlepes, V. A. Blatov, D. M. Proserpio and A. K. Powell, *Coord. Chem. Rev.*, 2012, 256, 1246–1278.

16 G. E. Kostakis, in *Elsevier Reference Module in Chemistry, Molecular Sciences and Chemical Engineering*, ed. J. Reedijk, Elsevier, Waltham, MA, 2016, pp. 1–53.

17 A. N. Bilyachenko, M. S. Dronova, A. I. Yalymov, F. Lamaty, X. Bantreil, J. Martinez, C. Bizet, L. S. Shul'Pina, A. A. Korlyukov, D. E. Arkhipov, M. M. Levitsky, E. S. Shubina, A. M. Kirillov and G. B. Shul'Pin, *Chem. - A Eur. J.*, 2015, **21**, 8758–8770.

18 A. N. Bilyachenko, A. N. Kulakova, M. M. Levitsky, A. A. Petrov, A. A. Korlyukov, L. S. Shul'pina, V. N. Khrustalev, P. V Dorovatovskii, A. V Vologzhanina, U. S. Tsareva, I. E. Golub, E. S. Gulyaeva, E. S. Shubina and G. B. Shul'pin, *Inorg. Chem.*, 2017, **56**, 4093–4103.

19 R. Modak, Y. Sikdar, G. Cosquer, S. Chatterjee, M. Yamashita and S. Goswami, *Inorg. Chem.*, 2016, **55**, 691–699.

20 R. Modak, Y. Sikdar, A. Bieńko, M. Witwicki, M. Jerzykiewicz and S. Goswami, *Polyhedron*, 2016, **119**, 202–215.

21 S. Biswas, P. Bag, S. Das, S. Kundu, J. van Leusen, P. Kögerler and V. Chandrasekhar, *Eur. J. Inorg. Chem.*, 2017, **2017**, 1129–1142.

22 L. F. Lindoy, H. C. Lip, H. W. Louie, M. G. B. Drew and M. J. Hudson, *J. Chem. Soc. Chem. Commun.*, 1977, 778.

23 A. Bencini, C. Benelli, A. Caneschi, R. L. Carlin, A. Dei and D. Gatteschi, *J. Am. Chem. Soc.*, 1985, **107**, 8128–8136.

24 A. Bencini, C. Benelli, A. Caneschi, A. Dei and D. Gatteschi, *Inorg. Chem.*, 1986, **25**, 572–575.

25 D. M. L. Goodgame, D. J. Williams and R. E. P. Winpenny, *Polyhedron*, 1989, **8**, 1531–1536.

26 R. G. Pearson, *J. Chem. Educ.*, 1968, **45**, 581.

27 X. Yang, S. Wang, D. Schipper, L. Zhang, Z. Li, S. Huang, D. Yuan, Z. Chen, A. J. Gnanam, J. W. Hall, T. L. King, E. Que, Y. Dieye, J. Vadivelu, K. A. Brown and R. A. Jones, *Nanoscale*, 2016, **8**, 11123–11129.

28 N. Stavgianoudaki, M. Siczek, T. Lis, R. Inglis and C. J. Milios, *Chem. Commun.*, 2016, **52**, 343–345.

29 C. G. Efthymiou, I. Mylonas-Margaritis, C. P. Raptopoulou, V. Psycharis, A. Escuer, C. Papatriantafyllopoulou and S. P. Perlepes, *Magnetochemistry*, 2016, **2**, 30.

30 Z.-M. Zhang, L.-Y. Pan, W.-Q. Lin, J.-D. Leng, F.-S. Guo, Y.-C. Chen, J.-L. Liu and M.-L. Tong, *Chem. Commun.*, 2013, **49**, 8081.

31 X. Lü, W. Bi, W. Chai, J. Song, J. Meng, W. Y. Wong, W. K. Wong, X. Yang and R. A. Jones, *Polyhedron*, 2009, **28**, 27–32.

32 S. Schmidt, D. Prodius, V. Mereacre, G. E. Kostakis and A. K. Powell, *Chem. Commun.*, 2013, **49**, 1696–1698.

33 R. E. P. Winpenny, *J. Chem. Soc. Dalt. Trans.*, 2001, **6**, 1–10.

34 Q. Meng, J. K. Clegg, A. J. Brock, K. A. Jolliffe, L. F. Lindoy and G. Wei, *Polyhedron*, 2014, **74**, 113–121.

35 D. Cangussu, E. Pardo, M.-C. Dul, R. Lescouëzec, P. Herson, Y. Journaux, E. F. Pedroso, C. L. M. Pereira, H. O. Stumpf, M. C. Muñoz, R. Ruiz-garcía, J. Cano, M. Julve and F. Lloret, *Inorganica Chim. Acta*, 2008, **361**, 3394–3402.

36 T. Glaser, G. F. von Mollard and D. Anselmetti, *Inorganica Chim. Acta*, 2016, **452**, 62–72.

37 F. Z. Chiboub Fellah, S. Boulefred, A. Chiboub Fellah, B. El Rez, C. Duhayon and J.-P. Sutter, *Inorganica Chim. Acta*, 2016, **439**, 24–29.

38 C. H. Zhan, R. S. Winter, Q. Zheng, J. Yan, J. M. Cameron, D. L. Long and L. Cronin, *Angew. Chemie - Int. Ed.*, 2015, **54**, 14308–14312.

39 H. N. Miras, E. F. Wilson and L. Cronin, *Chem. Commun.*, 2009, 1297.

40 H. X. Na, P. Y. Yang, Z. Yin, Y. H. Wang, L. X. Chang, R. Si, M. Kurmoo and M. H. Zeng, *Chem. - A Eur. J.*, 2016, **22**, 18404–18411.

41 G. J. T. Cooper, G. N. Newton, D. L. Long, P. Kögerler, M. H. Rosnes, M. Keller and L. Cronin, *Inorg. Chem.*, 2009, **48**, 1097–1104.

42 G. N. Newton, G. J. T. Cooper, P. Kögerler, D. L. Long and L. Cronin, *J. Am. Chem. Soc.*,

2008, **130**, 790–791.

43 L. Jiang, B. Liu, H.-W. Zhao, J.-L. Tian, X. Liu and S.-P. Yan, *CrystEngComm*, 2017, **19**, 1816–1830.

44 F. Li, J. K. Clegg, P. Jensen, K. Fisher, L. F. Lindoy, G. V Meehan, B. Moubaraki and K. S. Murray, *Angew. Chem. Int. Ed. Engl.*, 2009, **48**, 7059–63.

45 J. Bunzen, J. Iwasa, P. Bonakdarzadeh, E. Numata, K. Rissanen, S. Sato and M. Fujita, *Angew. Chemie Int. Ed.*, 2012, **51**, 3161–3163.

46 Y. Peng, V. Mereacre, C. E. Anson and A. K. Powell, *Dalt. Trans.*, 2017, **46**, 5337–5343.

47 S. Chen, V. Mereacre, G. E. Kostakis, C. E. Anson and A. K. Powell, *Inorg. Chem. Front.*, 2017, **4**, 927–934.

48 E. Guarda, K. Bader, J. van Slageren and P. Alborés, *Dalt. Trans.*, 2016, **45**, 8566–8572.

49 J. Goura, R. Guillaume, E. Rivière and V. Chandrasekhar, *Inorg. Chem.*, 2014, **53**, 7815–7823.

50 K. C. Mondal, G. E. Kostakis, Y. Lan, W. Wernsdorfer, C. E. Anson and A. K. Powell, *Inorg. Chem.*, 2011, **50**, 11604–11611.

51 A. Zabala-Lekuona, J. Cepeda, I. Oyarzabal, A. Rodríguez-Diéguez, J. A. García, J. M. Seco and E. Colacio, *CrystEngComm*, 2017, **19**, 256–264.

52 A. M. Ako, V. Mereacre, R. Clérac, W. Wernsdorfer, I. J. Hewitt, C. E. Anson and A. K. Powell, *Chem. Commun.*, 2009, **5**, 544–546.

53 M. Ledezma-Gairaud, L. Grangel, G. Aromí, T. Fujisawa, A. Yamaguchi, A. Sumiyama and E. C. Sañudo, *Inorg. Chem.*, 2014, **53**, 5878–5880.

54 Y. Q. Hu, M. H. Zeng, K. Zhang, S. Hu, F. F. Zhou and M. Kurmoo, *J. Am. Chem. Soc.*, 2013, **135**, 7901–7908.

55 L. Zhao, J. Wu, H. Ke and J. Tang, *Inorg. Chem.*, 2014, **53**, 3519–3525.

56 V. Chandrasekhar, P. Bag, W. Kroener, K. Gieb and P. Müller, *Inorg. Chem.*, 2013, **52**, 13078–13086.

57 S. Hossain, S. Das, A. Chakraborty, F. Lloret, J. Cano, E. Pardo and V. Chandrasekhar, *Dalt. Trans.*, 2014, **43**, 10164.

58 V. Chandrasekhar, S. Das, A. Dey, S. Hossain, F. Lloret and E. Pardo, *Eur. J. Inorg. Chem.*, 2013, **2013**, 4506–4514.

59 M. Nematirad, W. J. Gee, S. K. Langley, N. F. Chilton, B. Moubaraki, K. S. Murray and S. R. Batten, *Dalt. Trans.*, 2012, **41**, 13711.

60 M. Towatari, K. Nishi, T. Fujinami, N. Matsumoto, Y. Sunatsuki, M. Kojima, N. Mochida, T. Ishida, N. Re and J. Mrozinski, *Inorg. Chem.*, 2013, **52**, 6160–6178.

61 M. Sarwar, A. M. Madalan, C. Tiseanu, G. Novitchi, C. Maxim, G. Marinescu, D. Luneau and M. Andruh, *New J. Chem.*, 2013, **37**, 2280.

62 L.-L. Fan, F.-S. Guo, L. Yun, Z.-J. Lin, R. Herchel, J.-D. Leng, Y.-C. Ou and M.-L. Tong, *Dalt. Trans.*, 2010, **39**, 1771–1780.

63 L. Zhao, S. Xue and J. Tang, *Inorg. Chem.*, 2012, **51**, 5994–5996.

64 L.-F. Zou, L. Zhao, Y.-N. Guo, G.-M. Yu, Y. Guo, J. Tang and Y.-H. Li, *Chem. Commun.*, 2011, **47**, 8659.

65 F. Habib, G. Brunet, V. Vieru, I. Korobkov, L. F. Chibotaru and M. Murugesu, *J. Am. Chem. Soc.*, 2013, **135**, 13242–13245.

66 J. P. Costes and C. Duhayon, *Eur. J. Inorg. Chem.*, 2014, **2014**, 4745–4749.

67 V. Gómez, L. Vendier, M. Corbella and J.-P. Costes, *Inorg. Chem.*, 2012, **51**, 6396–6404.

68 B. Berkoff, K. Griffiths, A. Abdul-Sada, G. J. Tizzard, S. J. Coles, A. Escuer and G. E. Kostakis, *Dalt. Trans.*, 2015, **44**, 12788–12795.

69 M. Andruh, *Dalt. Trans.*, 2015, **44**, 16633–16653.

70 J. Wu, L. Zhao, P. Zhang, L. Zhang, M. Guo and J. Tang, *Dalt. Trans.*, 2015, **44**, 11935–11942.

71 H. Wang, H. Ke, S.-Y. Lin, Y. Guo, L. Zhao, J. Tang and Y.-H. Li, *Dalt. Trans.*, 2013, **42**, 5298.

72 P. Zhang, L. Zhang, S. Y. Lin and J. Tang, *Inorg. Chem.*, 2013, **52**, 6595–6602.

73 H. Ke, L. Zhao, Y. Guo and J. Tang, *Dalton Trans.*, 2012, **41**, 2314–9.

74 H. Ke, L. Zhao, Y. Guo and J. Tang, *Dalt. Trans.*, 2012, **41**, 9760.

75 Z.-M. Zhang, L.-Y. Pan, W.-Q. Lin, J.-D. Leng, F.-S. Guo, Y.-C. Chen, J.-L. Liu and M.-L. Tong, *Chem. Commun. (Camb).*, 2013, **49**, 8081–80813.

76 A. A. Athanasopoulou, M. Pilkington, C. P. Raptopoulou, A. Escuer and T. C. Stamatatos, *Chem. Commun.*, 2014, **50**, 14942–14945.

77 L. Zhao, J. Wu, S. Xue and J. Tang, *Chem. Asian J.*, 2012, **7**, 2419–2423.

78 O. Iasco, G. Novitchi, E. Jeanneau and D. Luneau, *Inorg. Chem.*, 2013, **52**, 8723–8731.

79 C. Papatriantafyllopoulou, T. C. Stamatatos, C. G. Efthymiou, L. Cunha-Silva, F. A. A. Paz, S. P. Perlepes and G. Christou, *Inorg. Chem.*, 2010, **49**, 9743–9745.

80 X.-T. Wang, H.-M. Dong, X.-G. Wang, E.-C. Yang and X.-J. Zhao, *Zeitschrift fur Anorg. und Allg. Chemie*, 2016, **2016**, 1166–1172.

81 L. Wang, J. C. Ma, W. K. Dong, L. C. Zhu and Y. Zhang, *Zeitschrift fur Anorg. und Allg. Chemie*, 2016, **642**, 834–839.

82 S. Chen, V. Mereacre, D. Prodius, G. E. Kostakis and A. K. Powell, *Inorg. Chem.*, 2015, **54**, 3218–3227.

83 H. Chen, C.-B. Ma, M.-Q. Hu, H.-M. Wen, H.-H. Cui, J.-Y. Liu, X.-W. Song and C.-N. Chen, *Dalt. Trans.*, 2013, **42**, 4908.

84 A. Baniodeh, C. E. Anson and A. K. Powell, *Chem. Sci.*, 2013, **4**, 4354.

85 V. Mereacre, F. Klöwer, Y. Lan, R. Clérac, J. A. Wolny, V. Schünemann, C. E. Anson and A. K. Powell, *Beilstein J. Nanotechnol.*, 2013, **4**, 807–814.

86 M. Li, A. M. Ako, Y. Lan, W. Wernsdorfer, G. Buth, C. E. Anson, A. K. Powell, Z. Wang and S. Gao, *Dalton Trans.*, 2010, **39**, 3375–3377.

87 X. Tang, W. Ye, J. Hua, M. Chen, H. Cheng, Y. Ma and R. Yuan, *Inorganica Chim. Acta*, 2016, **453**, 142–148.

88 J. Goura and V. Chandrasekhar, *Chem. Rev.*, 2015, 115, 6854–6965.

89 X. Tan, X. Ji and J.-M. Zheng, *Inorg. Chem. Commun.*, 2015, **60**, 27–32.

90 X. Tan, Y.-X. Che and J.-M. Zheng, *Inorg. Chem. Commun.*, 2013, **37**, 17–20.

91 O. Botezat, J. Van Leusen, V. C. Kravtsov, P. Kögerler and S. G. Baca, *Inorg. Chem.*, 2017, **56**, 1814–1822.

92 T. N. Hooper, R. Inglis, G. Lorusso, J. Ujma, P. E. Barran, D. Uhrin, J. Schnack, S. Piligkos, M. Evangelisti and E. K. Brechin, *Inorg. Chem.*, 2016, **55**, 10535–10546.

93 I. Radu, V. C. Kravtsov, S. M. Ostrovsky, O. S. Reu, K. Krämer, S. Decurtins, S. X. Liu, S. I. Klokishner and S. G. Baca, *Inorg. Chem.*, 2017, **56**, 2662–2676.

94 S. Mameri and V. Mereacre, *Inorganica Chim. Acta*, 2016, 451, 52–58.

95 X. Zhu and W. Liao, *Polyhedron*, 2016, **111**, 185–189.

96 S. Wu, B. Deng, X. Jiang, R. Li, J. Guo, F. Lai, X. Huang and C. Huang, *J. Solid State Chem.*, 2012, **196**, 451–457.

97 Y.-Q. Sun, Y.-Y. Xu, D.-Z. Gao, G.-Y. Zhang, Y.-X. Liu, J. Wang and D.-Z. Liao, *Dalt. Trans.*, 2012, **41**, 5704.

98 D. Visinescu, L. M. Toma, O. Fabelo, C. Ruiz-Pérez, F. Lloret and M. Julve, *Polyhedron*, 2009, **28**, 851–859.

99 A. J. Tasiopoulos and S. P. Perlepes, *Dalt. Trans.*, 2008, **0**, 5537.

100 A. Chakraborty, P. Bag, J. Goura, A. K. Bar, J.-P. P. Sutter and V. Chandrasekhar, *Cryst. Growth Des.*, 2015, **15**, 848–857.

101 J. Goura, V. Mereacre, G. Novitchi, A. K. Powell and V. Chandrasekhar, *Eur. J. Inorg. Chem.*, 2015, **2015**, 156–165.

102 T. G. Tziotzi, D. A. Kalofolias, D. I. Tzimopoulos, M. Siczek, T. Lis, R. Inglis and C. J. Milios, *Dalt. Trans.*, 2015, **44**, 6082–6088.

103 I. A. Kühne, N. Magnani, V. Mereacre, W. Wernsdorfer, C. E. Anson and A. K. Powell, *Chem. Commun. (Camb).*, 2014, **50**, 1882–1885.

104 J.-P. Costes and L. Vendier, *Comptes Rendus Chim.*, 2010, **13**, 661–667.

105 C. Benelli, A. J. Blake, P. E. Y. Milne, J. M. Rawson and R. E. P. Winpenny, *Chem. Eur. J.*, 1995, **1**, 614–618.

106 H. J. Im and S. W. Lee, *Polyhedron*, 2015, **101**, 48–55.

107 Y. Sui, R.-H. Hu, D.-S. Liu and Q. Wu, *Inorg. Chem. Commun.*, 2011, **14**, 396–398.

108 N. P. Kuzmina, I. P. Malkerova, A. S. Alikhanyan and A. N. Gleizes, in *Journal of Alloys and Compounds*, 2004, vol. 374, pp. 315–319.

109 W. K. Dong, J. C. Ma, Y. J. Dong, L. C. Zhu and Y. Zhang, *Polyhedron*, 2016, **115**, 228–235.

110 W.-K. Lo, W.-K. Wong, J. Guo, W.-Y. Wong, K.-F. Li and K.-W. Cheah, *Inorganica Chim. Acta*, 2004, **357**, 4510–4521.

111 W. K. Lo, W. K. Wong, W. Y. Wong, J. Guo, K. T. Yeung, Y. K. Cheng, X. Yang and R. A. Jones, *Inorg. Chem.*, 2006, **45**, 9315–9325.

112 X. Yang, R. A. Jones, Q. Wu, M. M. Oye, W.-K. Lo, W.-K. Wong and A. L. Holmes, *Polyhedron*, 2006, **25**, 271–278.

113 V. Chandrasekhar, A. Dey, S. Das, M. Rouzières and R. Clérac, *Inorg. Chem.*, 2013, **52**,

2588–2598.

114 X. Yang, Z. Li, S. Wang, S. Huang, D. Schipper and R. A. Jones, *Chem. Commun.*, 2014, **50**, 15569–15572.

115 C.-B. Tian, D.-Q. Yuan, Y.-H. Han, Z.-H. Li, P. Lin and S.-W. Du, *Inorg. Chem. Front.*, 2014, **1**, 695–704.

116 H. Ke, W. Zhu, S. Zhang, G. Xie and S. Chen, *Polyhedron*, 2015, **87**, 109–116.

117 N. Ahmed, C. Das, S. Vaidya, A. K. Srivastava, S. K. Langley, K. S. Murray and M. Shanmugam, *Dalt. Trans.*, 2014, **43**, 17375–17384.

118 N. Ahmed, C. Das, S. Vaidya, S. K. Langley, K. S. Murray and M. Shanmugam, *Chem. - A Eur. J.*, 2014, **20**, 14235–14239.

119 I. A. Kühne, G. E. Kostakis, C. E. Anson and A. K. Powell, *Inorg. Chem.*, 2016, **55**, 4072–4074.

120 S. Osa, T. Kido, N. Matsumoto, N. Re, A. Pochaba and J. Mrozinski, *J. Am. Chem. Soc.*, 2004, **126**, 420–421.

121 R. Sessoli, *Angew. Chemie - Int. Ed.*, 2012, **51**, 43–45.

122 E. M. Chudnovsky, *Science* , 1996, 274, 938–939.

123 S. K. Langley, N. F. Chilton, B. Moubaraki and K. S. Murray, *Polyhedron*, 2013, **66**, 48–55.

124 S. K. Langley, N. F. Chilton, B. Moubaraki, T. Hooper, E. K. Brechin, M. Evangelisti and K. S. Murray, *Chem. Sci.*, 2011, **2**, 1166.

125 S. K. Langley, N. F. Chilton, M. Massi, B. Moubaraki, K. J. Berry and K. S. Murray, *Dalt. Trans.*, 2010, **39**, 7236.

126 B. Lapo and W. Wolfgang, *Nat. Mater.*, 2008, **7**, 179.

127 S. Kahle, Z. Deng, N. Malinowski, C. Tonnoir, A. Forment-Aliaga, N. Thontasen, G. Rinke, D. Le, V. Turkowski, T. S. Rahman, S. Rauschenbach, M. Ternes and K. Kern, *Nano Lett.*, 2012, **12**, 518–521.

128 W. Wernsdorfer and R. Sessoli, *Science* , 1999, **284**, 133–135.

129 L. Lecren, W. Wernsdorfer, Y. G. Li, A. Vindigni, H. Miyasaka and R. Clérac, *J. Am. Chem. Soc.*, 2007, **129**, 5045–5051.

130 G. A. Timco, T. B. Faust, F. Tuna and R. E. P. Winpenny, *Chem. Soc. Rev.*, 2011, **40**, 3067.

131 Z. Shu-Qun and C. Zhi-De, *Chinese Phys. B*, 2008, **1436**, 1436.

132 L. Lecren, O. Roubeau, C. Coulon, Y. G. Li, X. F. Le Goff, W. Wernsdorfer, H. Miyasaka and R. Clérac, *J. Am. Chem. Soc.*, 2005, **127**, 17353–17363.

133 T. Kido, Y. Ikuta, Y. Sunatsuki, Y. Ogawa, N. Matsumoto and N. Re, *Inorg. Chem.*, 2003, **42**, 398–408.

134 M. F. Rega, J. C. Reed and M. Pellecchia, *Bioorg. Chem.*, 2007, **35**, 113–120.

135 A. Indapurkar, B. Henriksen, J. Tolman and J. Fletcher, *J. Pharm. Sci.*, 2013, **102**, 2589–2598.

136 E. F. Gudgin Dickson, A. Pollak and E. P. Diamandis, *J. Photochem. Photobiol. B Biol.*,

1995, **27**, 3–19.

137 J. P. Martins, P. Martín-Ramos, C. Coya, A. L. Álvarez, L. C. Pereira, R. Díaz, J. Martín-Gil and M. Ramos Silva, *Mater. Chem. Phys.*, 2014, **147**, 1157–1164.

138 I. V Taydakov, A. A. Akkuzina, R. I. Avetisov, A. V Khomyakov, R. R. Saifutyarov and I. C. Avetissov, *J. Lumin.*, 2016, **177**, 31–39.

139 V. V Utochnikova, N. N. Solodukhin, A. N. Aslandukov, L. Marciniak, I. S. Bushmarinov, A. A. Vashchenko and N. P. Kuzmina, *Org. Electron.*, 2017, **44**, 85–93.

140 A. R. Parent, T. Nakazono, S. Lin, S. Utsunomiya and K. Sakai, *Dalt. Trans.*, 2014, **43**, 12501–12513.

141 F. Evangelisti, R. Moré, F. Hodel, S. Luber and G. R. Patzke, *J. Am. Chem. Soc.*, 2015, **137**, 11076–11084.

142 C. Zhang, C. Chen, H. Dong, J. R. Shen, H. Dau and J. Zhao, *Science* , 2015, **348**, 690–693.

143 S. Matsunaga and M. Shibasaki, *Chem. Commun.*, 2014, **50**, 1044–1057.

144 H. Mihara, Y. Xu, N. E. Shepherd, S. Matsunaga and M. Shibasaki, *J. Am. Chem. Soc.*, 2009, **131**, 8384–8385.

145 K. Endo, M. Ogawa and T. Shibata, *Angew. Chemie Int. Ed.*, 2010, **49**, 2410–2413.

146 Z. Chen, M. Furutachi, Y. Kato, S. Matsunaga and M. Shibasaki, *Angew. Chemie Int. Ed.*, 2009, **48**, 2218–2220.

147 Z. Chen, H. Morimoto, S. Matsunaga and M. Shibasaki, *J. Am. Chem. Soc.*, 2008, **130**, 2170–2171.

148 H. C. Stöhr, Joachim, Siegmann, *Magnetism*, Springer Berlin Heidelberg, Berlin, Heidelberg, 2006.

149 R. Layfield and M. Murugesu, *Lanthanides and Actinides in Molecular Magnetism*, Wiley-VCH Verlag GmbH & Co. KGaA, Weinheim, Germany, 2015.

150 H. N. Russell and F. A. Saunders, *Astrophys. J.*, 1925, **61**, 38.

151 F. Hund, *Zeitschrift für Phys.*, 1927, **40**, 742–764.

152 F. Hund, *Zeitschrift für Phys.*, 1927, **42**, 93–120.

153 D. Gatteschi, R. Sessoli, J. Villain and W. Wernsdorfer, in *Advanced Magnetic Nanostructures*, eds. D. Sellmyer and R. Skomski, Springer US, Boston, MA, 2006, pp. 147–181.

154 J. Kanamori, *J. Phys. Chem. Solids*, 1959, **10**, 87–98.

155 J. B. Goodenough, *J. Phys. Chem. Solids*, 1958, **6**, 287–297.

156 J. McMaster, *Annu. Reports Sect. 'A' (Inorganic Chem.*, 2001, **97**, 567–586.

157 S. Cotton, *Lanthanide and Actinide Chemistry*, John Wiley & Sons, Ltd, Chichester, UK, 2006.

158 J. D. Rinehart and J. R. Long, *Chem. Sci.*, 2011, **2**, 2078.

159 A. Rieger, D. Collinson, B. C. Gilbert, D. M. Murphy, P. H. R. Trust, R. G. Lawler and P. Rieger, *Electron Spin Resonance: Analysis and Interpretation*, Royal Society of Chemistry, 2007.

160 G. Aromí, P. Gamez and O. Roubeau, in *Spin States in Biochemistry and Inorganic Chemistry*, John Wiley & Sons, Ltd, Oxford, UK, 2015, pp. 263–296.

161 O. Kahn, *J. Chem. Educ.*, 1995, **72**, A19.

162 S. Best, *Appl. Organomet. Chem.*, 2009, **23**, 482–483.

163 C. Benelli and D. Gatteschi, *Chem. Rev.*, 2002, **102**, 2369–2387.

164 T. Lis, *Acta Crystallogr. Sect. B Struct. Crystallogr. Cryst. Chem.*, 1980, **36**, 2042–2046.

165 R. Sessoli, D. Gatteschi, A. Caneschi and M. A. Novak, *Nature*, 1993, **365**, 141–143.

166 L. Thomas, F. Lionti, R. Ballou, D. Gatteschi, R. Sessoli and B. Barbara, *Nature*, 1996, **383**, 145–147.

167 Y.-Z. Zheng, E. M. Pineda, M. Helliwell and R. E. P. Winpenny, *Chemistry*, 2012, **18**, 4161–4165.

168 D. I. Alexandropoulos, T. N. Nguyen, L. Cunha-Silva, T. F. Zafiropoulos, A. Escuer, G. Christou and T. C. Stamatatos, *Inorg. Chem.*, 2013, **52**, 1179–1181.

169 K. S. Pedersen, J. Bendix and R. Clérac, *Chem. Commun.*, 2014, **50**, 4396–4415.

170 K. Liu, W. Shi and P. Cheng, *Coord. Chem. Rev.*, 2015, 289–290, 74–122.

171 L. Rosado Piquer and E. C. Sañudo, *Dalt. Trans.*, 2015, **44**, 8771–8780.

172 H. L. C. Feltham and S. Brooker, *Coord. Chem. Rev.*, 2014, 276, 1–33.

173 J.-L. Liu, Y.-C. Chen, F.-S. Guo and M.-L. Tong, *Coord. Chem. Rev.*, 2014, **281**, 26–49.

174 F. S. Guo, B. M. Day, Y. C. Chen, M. L. Tong, A. Mansikkamäki and R. A. Layfield, *Angew. Chemie - Int. Ed.*, 2017, **56**, 11445–11449.

175 R. M. White, *Quantum Theory of Magnetism*, Springer Berlin Heidelberg, Berlin, Heidelberg, 2007, vol. 32.

176 R. Orbach, *Proc. R. Soc. A Math. Phys. Eng. Sci.*, 1961, **264**, 458–484.

177 D. Gatteschi and R. Sessoli, *Angew. Chemie Int. Ed.*, 2003, **42**, 268–297.

178 J. D. Rinehart, M. Fang, W. J. Evans and J. R. Long, *J. Am. Chem. Soc.*, 2011, **133**, 14236–14239.

179 J. D. Rinehart, M. Fang, W. J. Evans and J. R. Long, *Nat. Chem.*, 2011, **3**, 538–542.

180 W. Wernsdorfer, N. Aliaga-Alcalde, D. N. Hendrickson and G. Christou, *Nature*, 2002, **416**, 406–409.

181 K. S. Cole and R. H. Cole, *J. Chem. Phys.*, 1941, **9**, 341–351.

182 C. Dekker, A. F. M. Arts, H. W. de Wijn, A. J. van Duyneveldt and J. A. Mydosh, *Phys. Rev. B*, 1989, **40**, 11243–11251.

183 Y.-N. Guo, G.-F. Xu, Y. Guo and J. Tang, *Dalt. Trans.*, 2011, **40**, 9953–9963.

184 W.-W. Kuang, L.-L. Zhu, L.-C. Li and P.-P. Yang, *Eur. J. Inorg. Chem.*, 2015, **2015**, 2245–2253.

185 J.-D. Leng, J.-L. Liu and M.-L. Tong, *Chem. Commun.*, 2012, **48**, 5286.

186 D. I. Alexandropoulos, K. M. Poole, L. Cunha-Silva, J. Ahmad Sheikh, W. Wernsdorfer, G. Christou and T. C. Stamatatos, *Chem. Commun.*, 2017, **53**, 4266–4269.

187 J. Wu, L. Zhao, M. Guo and J. Tang, *Chem. Commun.*, 2015, **51**, 17317–17320.

188 F. Pointillart, K. Bernot, R. Sessoli and D. Gatteschi, *Chem. - A Eur. J.*, 2007, **13**, 1602–1609.

189 A. B. Canaj, D. I. Tzimopoulos, M. Siczek, T. Lis, R. Inglis and C. J. Milios, *Inorg. Chem.*, 2015, **54**, 7089–7095.

190 H.-M. Dong, Y. Li, Z.-Y. Liu, E.-C. Yang and X.-J. Zhao, *Dalt. Trans.*, 2016, **45**, 11876–11882.

191 H. L. C. Feltham, S. Dhers, M. Rouzieres, R. Clerac, A. K. Powell and S. Brooker, *Inorg. Chem. Front.*, 2015, **2**, 982–990.

192 S. Biswas, J. Goura, S. Das, C. V. Topping, J. Brambleby, P. A. Goddard and V. Chandrasekhar, *Inorg. Chem.*, 2016, **55**, 8422–8436.

193 V. Chandrasekhar, B. M. Pandian, R. Azhakar, J. J. Vittal and R. Clérac, *Inorg. Chem.*, 2007, **46**, 5140–5142.

194 R. Modak, Y. Sikdar, A. E. Thuijs, G. Christou and S. Goswami, *Inorg. Chem.*, 2016, **55**, 10192–10202.

195 T. Yamaguchi, J.-P. Costes, Y. Kishima, M. Kojima, Y. Sunatsuki, N. Bréfuel, J.-P. Tuchagues, L. Vendier and W. Wernsdorfer, *Inorg. Chem.*, 2010, **49**, 9125–9135.

196 V. Chandrasekhar, B. M. Pandian, J. J. Vittal and R. Clérac, *Inorg. Chem.*, 2009, **48**, 1148–1157.

197 V. Chandrasekhar, S. Das, A. Dey, S. Hossain, S. Kundu and E. Colacio, *Eur. J. Inorg. Chem.*, 2014, **2014**, 397–406.

198 J. Li, R.-M. Wei, T.-C. Pu, F. Cao, L. Yang, Y. Han, Y. Zhang, J.-L. Zuo and Y. Song, *Inorg. Chem. Front.*, 2017, **2**, 114–122.

199 A. V. Funes, L. Carrella, Y. Rechkemmer, J. van Slageren, E. Rentschler and P. Alborés, *Dalt. Trans.*, 2017, **46**, 3400–3409.

200 S. She, Y. Li and W. Li, *Dalt. Trans.*, 2016, **45**, 10830–10835.

201 S. K. Langley, C. Le, L. Ungur, B. Moubaraki, B. F. Abrahams, L. F. Chibotaru and K. S. Murray, *Inorg. Chem.*, 2015, **54**, 3631–3642.

202 Z. Y. Li, Y. Dai, H. Zhang, J. Zhu, J. J. Zhang, S. Q. Liu and C. Y. Duan, *Eur. J. Inorg. Chem.*, 2014, **2014**, 384–391.

203 X.-Q. Zhao, Y. Lan, B. Zhao, P. Cheng, C. E. Anson and A. K. Powell, *Dalton Trans.*, 2010, **39**, 4911–7.

204 J. Goura, A. Chakraborty, J. P. S. Walsh, F. Tuna and V. Chandrasekhar, *Cryst. Growth Des.*, 2015, **15**, 3157–3165.

205 G. J. Sopasis, M. Orfanoudaki, P. Zarmpas, A. Philippidis, M. Siczek, T. Lis, J. R. O'Brien and C. J. Milios, *Inorg. Chem.*, 2012, **51**, 1170–1179.

206 S. Hill, S. Datta, J. Liu, R. Inglis, C. J. Milios, P. L. Feng, J. J. Henderson, E. del Barco, E. K. Brechin and D. N. Hendrickson, *Dalt. Trans.*, 2010, **39**, 4693.

207 Y. Z. Zheng, M. Evangelisti, F. Tuna and R. E. P. Winpenny, *J. Am. Chem. Soc.*, 2012, **134**, 1057–1065.

208 Y.-Z. Zheng, M. Evangelisti and R. E. P. Winpenny, *Chem. Sci.*, 2011, **2**, 99–102.

209 J. B. Peng, Q. C. Zhang, X. J. Kong, Y. Z. Zheng, Y. P. Ren, L. S. Long, R. Bin Huang, L. S. Zheng and Z. Zheng, *J. Am. Chem. Soc.*, 2012, **134**, 3314–3317.

210 Z.-S. Meng, F.-S. Guo, J.-L. Liu, J.-D. Leng and M.-L. Tong, *Dalton Trans.*, 2012, **41**, 2320–2329.

211 G. F. Xu, P. Gamez, J. Tang, R. Clérac, Y. N. Guo and Y. Guo, *Inorg. Chem.*, 2012, **51**, 5693–5698.

212 M. A. Palacios, S. Titos-Padilla, J. Ruiz, J. M. Herrera, S. J. A. Pope, E. K. Brechin and E. Colacio, *Inorg. Chem.*, 2014, **53**, 1465–1474.

213 J. P. Costes, S. Titos-Padilla, I. Oyarzabal, T. Gupta, C. Duhayon, G. Rajaraman and E. Colacio, *Inorg. Chem.*, 2016, **55**, 4428–4440.

214 N. C. Anastasiadis, C. D. Polyzou, G. E. Kostakis, V. Bekiari, Y. Lan, S. P. Perlepes, K. F. Konidaris and A. K. Powell, *Dalt. Trans.*, 2015, **44**, 19791–19795.

215 S. M. T. Abtab, M. C. Majee, M. Maity, J. Titiš, R. Boča and M. Chaudhury, *Inorg. Chem.*, 2014, **53**, 1295–1306.

216 A. Upadhyay, S. K. Singh, C. Das, R. Mondol, S. K. Langley, K. S. Murray, G. Rajaraman and M. Shanmugam, *Chem. Commun.*, 2014, **50**, 8838–8841.

217 X.-Q. Song, P.-P. Liu, Y.-A. Liu, J.-J. Zhou and X.-L. Wang, *Dalt. Trans.*, 2016, **45**, 8154–8163.

218 Olivier Kahn, O. Kahn and F. Pobell, *J. Chem. Educ.*, 1995, **72**, A19.

219 E. Brück, ed. K. H. J. Buschow, Elsevier, 2007, vol. 17, pp. 235–291.

220 A. M. T. and Y. I. Spichkin, *Mater. Today*, 2003, **6**, 51.

221 G. Karotsis, M. Evangelisti, S. J. Dalgarno and E. K. Brechin, *Angew. Chemie - Int. Ed.*, 2009, **48**, 9928–9931.

222 Y.-Z. Zheng, G.-J. Zhou, Z. Zheng and R. E. P. Winpenny, *Chem. Soc. Rev.*, 2014, **43**, 1462–75.

223 S. Xue, Y. N. Guo, L. Zhao, H. Zhang and J. Tang, *Inorg. Chem.*, 2014, **53**, 8165–8171.

224 A. S. Dinca, A. Ghirri, A. M. Madalan, M. Affronte and M. Andruh, *Inorg. Chem.*, 2012, **51**, 3935–3937.

225 T. N. Hooper, J. Schnack, S. Piligkos, M. Evangelisti and E. K. Brechin, *Angew. Chem. Int. Ed. Engl.*, 2012, **51**, 4633–4636.

226 Y. Z. Zheng, M. Evangelisti and R. E. P. Winpenny, *Angew. Chemie - Int. Ed.*, 2011, **50**, 3692–3695.

227 J. B. Peng, Q. C. Zhang, X. J. Kong, Y. P. Ren, L. S. Long, R. Bin Huang, L. S. Zheng and Z. Zheng, *Angew. Chemie - Int. Ed.*, 2011, **50**, 10649–10652.

228 J.-D. Leng, J.-L. Liu and M.-L. Tong, *Chem. Commun. (Camb).*, 2012, **48**, 5286–5288.

229 G. A. Kumar, R. E. Riman and J. G. Brennan, *Coord. Chem. Rev.*, 2014, **273**–**274**, 111–124.

230 R. X. Chen, T. Gao, W. Bin Sun, H. F. Li, Y. H. Wu, M. M. Xu, X. Y. Zou and P. F. Yan, *Inorg. Chem. Commun.*, 2015, **56**, 79–82.

231 L. Maria, V. R. Sousa, I. C. Santos, E. Mora and J. Marçalo, *Polyhedron*, 2016, **119**, 277–285.

232 L. Aboshyan-Sorgho, M. Cantuel, S. Petoud, A. Hauser and C. Piguet, *Coord. Chem. Rev.*, 2012, 256, 1644–1663.

233 R. Łyszczek and L. Mazur, *Polyhedron*, 2012, **41**, 7–19.

234 X. Yang, R. a. Jones and S. Huang, *Coord. Chem. Rev.*, 2014, 273–274, 63–75.

235 J. Song, C.-R. Li, Q. Xu, X.-T. Xu, L.-X. Sun and Y.-H. Xing, *Spectrochim. Acta Part A Mol. Biomol. Spectrosc.*, 2015, **150**, 308–315.

236 X. Q. Lü, W. X. Feng, Y. N. Hui, T. Wei, J. R. Song, S. S. Zhao, W. Y. Wong, W. K. Wong and R. A. Jones, *Eur. J. Inorg. Chem.*, 2010, **2010**, 2714–2722.

237 T. D. Pasatoiu, C. Tiseanu, A. M. Madalan, B. Jurca, C. Duhayon, J. P. Sutter and M. Andruh, *Inorg. Chem.*, 2011, **50**, 5879–5889.

238 T. Wei, S. Zhao, W. Bi, X. Lü, Y. Hui, J. Song, W.-K. Wong and R. A. Jones, *Inorg. Chem. Commun.*, 2009, **12**, 1216–1219.

239 Z.-P. Zheng, Y.-J. Ou, X.-J. Hong, L.-M. Wei, L.-T. Wan, W.-H. Zhou, Q.-G. Zhan and Y.-P. Cai, *Inorg. Chem.*, 2014, **53**, 9625–9632.

240 Z. Wang, W. Feng, P. Su, H. Liu, Z. Zhang, Y. Zhang, T. Miao, X. Lü, D. Fang, W.-K. Wong and R. A. Jones, *Inorg. Chem. Commun.*, 2013, **36**, 11–13.

241 W.-K. Wong, H. Liang, W.-Y. Wong, Z. Cai, K.-F. Li and K.-W. Cheah, *New J. Chem.*, 2002, **26**, 275–278.

242 Q.-W. Li, J.-L. Liu, J.-H. Jia, Y.-C. Chen, J. Liu, L.-F. Wang and M.-L. Tong, *Chem. Commun.*, 2015, **51**, 10291–10294.

243 C. Yu, Z. Zhang, L. Liu, H. Li, Y. He, X. Lu, W.-K. Wong and R. A. Jones, *New J. Chem.*, 2015, **39**, 3698–3707.

244 G. Fu, P. Su, X. Lü and W.-K. Wong, *Inorg. Chem. Commun.*, 2017, **76**, 12–14.

245 W. Feng, Y. Hui, T. Wei, X. Lü, J. Song, Z. Chen, S. Zhao, W. K. Wong and R. A. Jones, *Inorg. Chem. Commun.*, 2011, **14**, 75–78.

246 W. Y. Bi, X. Q. Lü, W. L. Chai, W. J. Jin, J. R. Song and W. K. Wong, *Inorg. Chem. Commun.*, 2008, **11**, 1316–1319.

247 H. Feng, Z. Zhang, W. Feng, P. Su, X. Lü, D. Fan, W. K. Wong, R. A. Jones and C. Su, *Inorg. Chem. Commun.*, 2014, **43**, 151–154.

248 K. Ehama, Y. Ohmichi, S. Sakamoto, T. Fujinami, N. Matsumoto, N. Mochida, T. Ishida, Y. Sunatsuki, M. Tsuchimoto and N. Re, *Inorg. Chem.*, 2013, **52**, 12828–12841.

249 P. Chen, H. Chen, P. Yan, Y. Wang and G. Li, *CrystEngComm*, 2011, **13**, 6237.

250 E. R. Trivedi, S. V. Eliseeva, J. Jankolovits, M. M. Olmstead, S. Petoud and V. L. Pecoraro, *J. Am. Chem. Soc.*, 2014, **136**, 1526–1534.

251 Y. Matoba, T. Kumagai, A. Yamamoto, H. Yoshitsu and M. Sugiyama, *J. Biol. Chem.*, 2006, **281**, 8981–8990.

252 J. J. P. Perry, D. S. Shin, E. D. Getzoff and J. A. Tainer, *Biochim. Biophys. Acta - Proteins Proteomics*, 2010, **1804**, 245–262.

253 S. Benini, W. R. Rypniewski, K. S. Wilson, S. Miletti, S. Ciurli and S. Mangani, *Structure*, 1999, **7**, 205–216.

254 O. Kristensen, M. Laurberg, A. Liljas, J. S. Kastrup and M. Gajhede, *Biochemistry*, 2004,

43, 8894–8900.

255 N. S. McCool, D. M. Robinson, J. E. Sheats and G. C. Dismukes, *J. Am. Chem. Soc.*, 2011, **133**, 11446–11449.

256 P. Kurz, G. Berggren, M. F. Anderlund and S. Styring, *Dalt. Trans.*, 2007, **38**, 4258.

257 J. Limburg, J. S. Vrettos, L. M. Liable-Sands, A. L. Rheingold, R. H. Crabtree and G. W. Brudvig, *Science* , 1999, **283**, 1524–1527.

258 A. K. Poulsen, A. Rompel and C. J. McKenzie, *Angew. Chemie - Int. Ed.*, 2005, **44**, 6916–6920.

259 Y. Liu, R. Xiang, X. Du, Y. Ding and B. Ma, *Chem. Commun.*, 2014, **50**, 12779–12782.

260 M. Okamura, M. Kondo, R. Kuga, Y. Kurashige, T. Yanai, S. Hayami, V. K. K. Praneeth, M. Yoshida, K. Yoneda, S. Kawata and S. Masaoka, *Nature*, 2016, **530**, 465–468.

261 B.-L. Lee, M. D. Kärkäs, E. V. Johnston, A. K. Inge, L.-H. Tran, Y. Xu, Ö. Hansson, X. Zou and B. Åkermark, *Eur. J. Inorg. Chem.*, 2010, **2010**, 5462–5470.

262 H. Sasai, T. Suzuki, S. Arai, T. Arai and M. Shibasaki, *J. Am. Chem. Soc.*, 1992, **114**, 4418–4420.

263 H. Sasai, T. Arai, Y. Satow, M. Shibasaki and K. N. Houk, *J. Am. Chem. Soc.*, 1995, **117**, 6194–6198.

264 Y. M. A. Yamada, N. Yoshikawa, H. Sasai and M. Shibasaki, *Angew. Chemie Int. Ed. English*, 1997, **36**, 1871–1873.

265 T. Arai, H. Sasai, K. I. Aoe, K. Okamura, T. Date and M. Shibasaki, *Angew. Chemie (International Ed. English)*, 1996, **35**, 104–106.

266 T. Iida, N. Yamamoto, H. Sasai and M. Shibasaki, *J. Am. Chem. Soc.*, 1997, **119**, 4783–4784.

267 T. Arai, H. Sasai, K. Yamaguchi and M. Shibasaki, *J. Am. Chem. Soc.*, 1998, **120**, 441–442.

268 N. Yamagiwa, H. Qin, S. Matsunaga and M. Shibasaki, *J. Am. Chem. Soc.*, 2005, **127**, 13419–13427.

269 N. Yoshikawa, N. Kumagai, S. Matsunaga, G. Moll, T. Ohshima, T. Suzuki and M. Shibasaki, *J. Am. Chem. Soc.*, 2001, **123**, 2466–2467.

270 N. Kumagai, S. Matsunaga, T. Kinoshita, S. Harada, S. Okada, S. Sakamoto, K. Yamaguchi and M. Shibasaki, *J. Am. Chem. Soc.*, 2003, **125**, 2169–2178.

271 N. Kumagai, S. Matsunaga, N. Yoshikawa, T. Ohshima and M. Shibasaki, *Org. Lett.*, 2001, **3**, 1539–1542.

272 B. M. Trost and H. Ito, *J. Am. Chem. Soc.*, 2000, 122, 12003–12004.

273 B. M. Trost, E. R. Silcoff, H. Ito and S. U. V, *Org. Lett.*, 2001, **3**, 2497–2500.

274 V. César, N. Lugan and G. Lavigne, *Eur. J. Inorg. Chem.*, 2010, **123**, 361–365.

275 B. M. Trost, A. Fettes and B. T. Shireman, *J. Am. Chem. Soc.*, 2004, **126**, 2660–2661.

276 B. M. Trost, S. Shin, J. A. Sclafani and S. U. V, *J. Am. Chem. Soc.*, 2005, **127**, 2497–2500.

277 B. Trost, *J. Am. Chem. Soc.*, 2006, **128**, 2778.

278 B. M. Trost and K. Hirano, *Org. Lett.*, 2012, **14**, 2446–2449.

279 B. M. Trost and K. Hirano, *Angew. Chemie Int. Ed.*, 2012, **51**, 6480–6483.

280 E. F. DiMauro and M. C. Kozlowski, *Org. Lett.*, 2001, **3**, 1641–1644.

281 V. Annamalai, E. F. DiMauro, P. J. Carroll and M. C. Kozlowski, *J. Org. Chem.*, 2003, **68**, 1973–1981.

282 E. P. DiMauro and M. C. Kozlowski, *Organometallics*, 2002, **21**, 1454–1461.

283 M. Yang, C. Zhu, F. Yuan, Y. Huang and Y. Pan, *Org. Lett.*, 2005, **7**, 1927–1930.

284 J. Sun, F. Yuan, M. Yang, Y. Pan and C. Zhu, *Tetrahedron Lett.*, 2009, **50**, 548–551.

285 J. Park and S. Hong, *Chem. Soc. Rev.*, 2012, **41**, 6931.

286 N. E. Shepherd, H. Tanabe, Y. Xu, S. Matsunaga and M. Shibasaki, *J. Am. Chem. Soc.*, 2010, **132**, 3666–3667.

287 Z. Chen, K. Yakura, S. Matsunaga and M. Shibasaki, *Org. Lett.*, 2008, **10**, 3239–3242.

288 Y. Kato, Z. Chen, S. Matsunaga and M. Shibasaki, *Synlett*, 2009, **2009**, 1635–1638.

289 Y. Xu, S. Matsunaga and M. Shibasaki, *Org. Lett.*, 2010, **12**, 10–13.

290 S. Mouri, Z. Chen, H. Mitsunuma, M. Furutachi, S. Matsunaga and M. Shibasaki, *J. Am. Chem. Soc.*, 2010, **132**, 1255–1257.

291 P. Gopinath, T. Watanabe and M. Shibasaki, *Org. Lett.*, 2012, **14**, 1358–1361.

292 S. Mouri, Z. Chen, S. Matsunaga and M. Shibasaki, *Chem. Commun.*, 2009, 5138.

293 S. Kato, M. Kanai and S. Matsunaga, in *Chemistry - An Asian Journal*, WILEY-VCH Verlag, 2013, vol. 8, pp. 1768–1771.

294 M. Furutachi, Z. Chen, S. Matsunaga and M. Shibasaki, *Molecules*, 2010, **15**, 532–544.

295 Y. Kato, M. Furutachi, Z. Chen, H. Mitsunuma, S. Matsunaga and M. Shibasaki, *J. Am. Chem. Soc.*, 2009, **131**, 9168–9169.

296 S. Handa, V. Gnanadesikan, S. Matsunaga and M. Shibasaki, *J. Am. Chem. Soc.*, 2007, **129**, 4900–4901.

297 S. Handa, V. Gnanadesikan, S. Matsunaga and M. Shibasaki, *J. Am. Chem. Soc.*, 2010, **132**, 4925–4934.

298 Y. Li, P. Deng, Y. Zeng, Y. Xiong and H. Zhou, *Org. Lett.*, 2016, **18**, 1578–1581.

299 M. Furutachi, S. Mouri, S. Matsunaga and M. Shibasaki, *Chem. - An Asian J.*, 2010, **5**, 2351–2354.

300 Q. Shi, X. Yang, X. Zhang, X. Li, J. Yang and X. Lü, *Inorg. Chem. Commun.*, 2016, **73**, 4–6.

301 D. J. Darensbourg, R. R. Poland and C. Escobedo, *Macromolecules*, 2012, **45**, 2242–2248.

302 G. Maayan and G. Christou, *Inorg. Chem.*, 2011, **50**, 7015–7021.

303 P. Wang, S. Shannigrahi, N. L. Yakovlev and T. S. A. Hor, *Inorg. Chem.*, 2012, **51**, 12059–12061.

304 S. Berardi, G. La Ganga, M. Natali, I. Bazzan, F. Puntoriero, A. Sartorel, F. Scandola, S. Campagna and M. Bonchio, *J. Am. Chem. Soc.*, 2012, **134**, 11104–11107.

305 F. Evangelisti, R. Güttinger, R. Moré, S. Luber and G. R. Patzke, *J. Am. Chem. Soc.*, 2013,

135, 18734–18737.

306 E. Pizzolato, M. Natali, B. Posocco, A. Montellano López, I. Bazzan, M. Di Valentin, P. Galloni, V. Conte, M. Bonchio, F. Scandola and A. Sartorel, *Chem. Commun.*, 2013, **49**, 9941.

307 A. Draksharapu, W. Rasheed, J. E. M. N. Klein and L. Que, *Angew. Chemie - Int. Ed.*, 2017, **56**, 9091–9095.

308 M. Dolai, T. Mistri, A. Panja and M. Ali, *Inorganica Chim. Acta*, 2013, **399**, 95–104.

309 M. Dolai, M. Ali, J. Titiš and R. Boča, *Dalt. Trans.*, 2015, **44**, 13242–13249.

310 A. Mishra, W. Wernsdorfer, S. Parsons, G. Christou and E. K. Brechin, *Chem. Commun. (Camb).*, 2005, **0**, 2086–8.

311 M. Murugesu, A. Mishra, W. Wernsdorfer, K. A. Abboud and G. Christou, *Polyhedron*, 2006, **25**, 613–625.

312 S. K. Langley, N. F. Chilton, L. Ungur, B. Moubaraki, L. F. Chibotaru and K. S. Murray, *Inorg. Chem.*, 2012, **51**, 11873–11881.

313 M. Brewer, J. Lee and J. G. Brennan, *Inorg. Chem.*, 1995, **34**, 5919–5924.

314 M. Berardini, T. J. Emge and J. G. Brennan, *Inorg. Chem.*, 1995, **34**, 5327–5334.

315 S. Daniele, L. G. Hubert-Pfalzgraf and J. Vaissermann, *Polyhedron*, 1998, **17**, 4249–4256.

316 Y. Cui, Y. T. Qian and J. S. Huang, *Polyhedron*, 2001, **20**, 1795–1802.

317 R. Rodríguez-Cortiñas, F. Avecilia, C. Platas-Iglesias, D. Imbert, J. C. G. Bünzli, A. De Blas and T. Rodríguez-Blas, *Inorg. Chem.*, 2002, **41**, 5336–5349.

318 C. E. Burrow, T. J. Burchell, P.-H. Lin, F. Habib, W. Wernsdorfer, R. Clérac and M. Murugesu, *Inorg. Chem.*, 2009, **48**, 8051–8053.

319 M. Sakamoto, K. Manseki and H. Kawa, *Coord. Chem. Rev.*, 2001, 219–221, 379–414.

320 S. M. T. Abtab, M. C. Majee, M. Maity, J. Titiš, R. Boča and M. Chaudhury, *Inorg. Chem.*, 2014, **53**, 1295–306.

321 J. Long, J. Rouquette, J. M. Thibaud, R. A. S. Ferreira, L. D. Carlos, B. Donnadieu, V. Vieru, L. F. Chibotaru, L. Konczewicz, J. Haines, Y. Guari and J. Larionova, *Angew. Chemie - Int. Ed.*, 2015, **54**, 2236–2240.

322 W. Sethi, S. Sanz, K. S. Pedersen, M. A. Sørensen, G. S. Nichol, G. Lorusso, M. Evangelisti, E. K. Brechin and S. Piligkos, *Dalt. Trans.*, 2015, **44**, 10315–10320.

323 J. Jankolovits, J. W. Kampf and V. L. Pecoraro, *Inorg. Chem.*, 2014, **53**, 7534–7546.

324 S. K. Samanta, S. M. T. Abtab, P. S. Sardar, S. Sanyal, M. Chaudhury and S. Ghosh, *Eur. J. Inorg. Chem.*, 2014, **2014**, 3101–3113.

325 J. Ruiz, G. Lorusso, M. Evangelisti, E. K. Brechin, S. J. A. Pope and E. Colacio, *Inorg. Chem.*, 2014, **53**, 3586–3594.

326 B. Zhang, X. Zheng, H. Su, Y. Zhu, C. Du and M. Song, *Dalt. Trans.*, 2013, **42**, 8571.

327 W.-R. Yu, G.-H. Lee and E.-C. Yang, *Dalt. Trans.*, 2013, **42**, 3941.

328 A. S. Dinca, J. Vallejo, S. Shova, F. Lloret, M. Julve and M. Andruh, *Polyhedron*, 2013, **65**, 238–243.

329 J. Jankolovits, J. W. Kampf and V. L. Pecoraro, *Polyhedron*, 2013, **52**, 491–499.

330 K. Ehama, Y. Ohmichi, S. Sakamoto, T. Fujinami, N. Matsumoto, N. Mochida, T. Ishida, Y. Sunatsuki, M. Tsuchimoto and N. Re, *Inorg. Chem.*, 2013, **52**, 12828–12841.

331 S. M. T. Abtab, M. Maity, K. Bhattacharya, E. C. Sañudo and M. Chaudhury, *Inorg. Chem.*, 2012, **51**, 10211–10221.

332 S. Titos-Padilla, J. Ruiz, J. M. Herrera, E. K. Brechin, W. Wersndorfer, F. Lloret and E. Colacio, *Inorg. Chem.*, 2013, **52**, 9620–9626.

333 J. Long, R. Vallat, R. A. S. Ferreira, L. D. Carlos, F. A. Almeida Paz, Y. Guari and J. Larionova, *Chem. Commun.*, 2012, **48**, 9974.

334 H. L. C. Feltham, Y. Lan, F. Klöwer, L. Ungur, L. F. Chibotaru, A. K. Powell and S. Brooker, *Chem. - A Eur. J.*, 2011, **17**, 4362–4365.

335 I. Oyarzabal, J. Ruiz, E. Ruiz, D. Aravena, J. M. Seco and E. Colacio, *Chem. Commun.*, 2015, **51**, 12353–12356.

336 K. Griffiths, P. Kumar, G. R. Akien, N. F. Chilton, A. Abdul-Sada, G. J. Tizzard, S. J. Coles and G. E. Kostakis, *Chem. Commun.*, 2016, **52**, 7866–7869.

337 K. Griffiths, C. W. D. Gallop, A. Abdul-Sada, A. Vargas, O. Navarro and G. E. Kostakis, *Chem. - A Eur. J.*, 2015, **21**, 6358–6361.

338 P. King, R. Clerac, W. Wernsdorfer, C. E. Anson and A. K. Powell, *Dalton Trans.*, 2004, **977**, 2670–2676.

339 S. A. M. Llunell, D. Casanova, J. Cirera, P. Alemany, *SHAPE version 2.0.*, 2010, **Barcelona**.

340 G. E. Kostakis and A. K. Powell, *Coord. Chem. Rev.*, 2009, 253, 2686–2697.

341 F. H. Allen, *Acta Crystallogr. Sect. B Struct. Sci.*, 2002, **58**, 380–388.

342 A. W. Addison, T. N. Rao, J. Reedijk, J. van Rijn and G. C. Verschoor, *J. Chem. Soc., Dalt. Trans.*, 1984, **0**, 1349–1356.

343 H. Ke, L. Zhao, Y. Guo and J. Tang, *Inorg. Chem.*, 2012, **51**, 2699–2705.

344 K. Griffiths, G. Novitchi and G. E. Kostakis, *Eur. J. Inorg. Chem.*, 2016, **2016**, 2750–2756.

345 N. F. Chilton, S. K. Langley, B. Moubaraki, A. Soncini, S. R. Batten and K. S. Murray, *Chem. Sci.*, 2013, **4**, 1719.

346 J. Sievers, *Zeitschrift für Phys. B Condens. Matter*, 1982, **45**, 289–296.

347 N. F. Chilton, D. Collison, E. J. L. McInnes, R. E. P. Winpenny and A. Soncini, *Nat. Commun.*, 2013, **4**, 1–7.

348 T. Shiga, N. Hoshino, M. Nakano, H. Nojiri and H. Oshio, *Inorganica Chim. Acta*, 2008, **361**, 4113–4117.

349 V. Mereacre, A. M. Ako, M. N. Akhtar, A. Lindemann, C. E. Anson and A. K. Powell, *Helv. Chim. Acta*, 2009, **92**, 2507–2524.

350 J. Liu, C. Ma, H. Chen, M. Hu, H. Wen, H. Cui, X. Song and C. Chen, *Dalt. Trans.*, 2013, **42**, 2423–2430.

351 S.-Y. Jhan, S.-H. Huang, C.-I. Yang and H.-L. Tsai, *Polyhedron*, 2013, **66**, 222–227.

352 J. Feuersenger, D. Prodius, V. Mereacre, R. Clérac, C. E. Anson and A. K. Powell, *Polyhedron*, 2013, **66**, 257–263.

353 V. A. Blatov, A. P. Shevchenko and D. M. Proserpio, *Cryst. Growth Des.*, 2014, **14**, 3576–3586.

354 P. Zhang, Y. N. Guo and J. Tang, *Coord. Chem. Rev.*, 2013, 257, 1728–1763.

355 D. N. Woodruff, R. E. P. Winpenny and R. A. Layfield, *Chem. Rev.*, 2013, 113, 5110–5148.

356 M. Murrie, *Chem. Soc. Rev.*, 2010, **39**, 1986–95.

357 M. Towatari, K. Nishi, T. Fujinami, N. Matsumoto, Y. Sunatsuki, M. Kojima, N. Mochida, T. Ishida, N. Re and J. Mrozinski, *Inorg. Chem.*, 2013, **52**, 6160–6178.

358 L. Ungur, M. Thewissen, J.-P. Costes, W. Wernsdorfer and L. F. Chibotaru, *Inorg. Chem.*, 2013, **52**, 6328–6337.

359 J.-P. Costes, L. Vendier and W. Wernsdorfer, *Dalt. Trans.*, 2011, **40**, 1700–1706.

360 D. Dey, G. Kaur, A. Ranjani, L. Gayathri, P. Chakraborty, J. Adhikary, J. Pasan, D. Dhanasekaran, A. R. Choudhury, M. A. Akbarsha, N. Kole and B. Biswas, *Eur. J. Inorg. Chem.*, 2014, **2014**, 3350–3358.

361 S. Saha, S. Pal, C. J. Gómez-García, J. M. Clemente-Juan, K. Harms and H. P. Nayek, *Polyhedron*, 2014, **74**, 1–5.

362 K. C. Mondal, G. E. Kostakis, Y. Lan and A. K. Powell, *Polyhedron*, 2013, **66**, 268–273.

363 I. Nemec, M. Machata, R. Herchel, R. Boča and Z. Trávníček, *Dalt. Trans.*, 2012, **41**, 14603.

364 W.-W. Kuang, C.-Y. Shao and P.-P. Yang, *J. Coord. Chem.*, 2015, **68**, 1412–1422.

365 H. Ke, S. Zhang, W. Zhu, G. Xie and S. Chen, *J. Coord. Chem.*, 2015, **8972**, 1–28.

366 K. Griffiths, V. N. Dokorou, J. Spencer, A. Abdul-Sada, A. Vargas and G. E. Kostakis, *CrystEngComm*, 2016, **18**, 704–713.

367 G. C. Vlahopoulou, T. C. Stamatatos, V. Psycharis, S. P. Perlepes and G. Christou, *Dalt. Trans.*, 2009, **0**, 3646.

368 G. S. Papaefstathiou, C. P. Raptopoulou, A. Tsohos, A. Terzis, E. G. Bakalbassis and S. P. Perlepes, *Inorg. Chem.*, 2000, **39**, 4658–4662.

369 H. Muller, A. Holzmann, W. Hinrichs and G. Klar, *Zeitschrift für Naturforsch. B*, 1982, **37**, 341–347.

370 E.-C. C. Yang, D. N. Hendrickson, W. Wernsdorfer, M. Nakano, L. N. Zakharov, R. D. Sommer, A. L. Rheingold, M. Ledezma-Gairaud and G. Christou, *J. Appl. Phys.*, 2002, **91**, 7382–7384.

371 K. W. Galloway, A. M. Whyte, W. Wernsdorfer, J. Sanchez-Benitez, K. V Kamenev, A. Parkin, R. D. Peacock and M. Murrie, *Inorg. Chem.*, 2008, **47**, 7438–7442.

372 F. Lloret, M. Julve, J. Cano, R. Ruiz-García and E. Pardo, *Inorganica Chim. Acta*, 2008, **361**, 3432–3445.

373 Olivier Kahn, *J. Chem. Educ.*, 1995, **72**, A19.

374 Y.-Z. Zheng, M. Evangelisti and R. E. P. Winpenny, *Angew. Chemie Int. Ed.*, 2011, **50**, 3692–3695.

375 A. Upadhyay, N. Komatireddy, A. Ghirri, F. Tuna, S. K. Langley, A. K. Srivastava, E. C. Sañudo, B. Moubaraki, K. S. Murray, E. J. L. McInnes, M. Affronte and M. Shanmugam,

Dalt. Trans., 2014, **43**, 259–266.

376 T. D. Pasatoiu, A. Ghirri, A. M. Madalan, M. Affronte and M. Andruh, *Dalt. Trans.*, 2014, **43**, 9136–9142.

377 C. Meseguer, S. Titos-Padilla, M. M. Hänninen, R. Navarrete, A. J. Mota, M. Evangelisti, J. Ruiz and E. Colacio, *Inorg. Chem.*, 2014, **53**, 12092–12099.

378 A. J. Tasiopoulos, T. A. O'Brien, K. A. Abboud and G. Christou, *Angew. Chemie - Int. Ed.*, 2004, **43**, 345–349.

379 A. J. Tasiopoulos, P. L. Milligan, K. A. Abboud, T. A. O'Brien and G. Christou, *Inorg. Chem.*, 2007, **46**, 9678–9691.

380 Y.-J. Zhang, B.-Q. Ma, S. Gao, J.-R. Li, Q.-D. Liu, G.-H. Wen and X.-X. Zhang, *J. Chem. Soc. Dalt. Trans.*, 2000, **0**, 2249–2250.

381 J. Liu, C. Ma, H. Chen, M. Hu, H. Wen, H. Cui and C. Chen, *Dalt. Trans.*, 2013, **42**, 3787.

382 D. Aguilà, L. A. Barrios, F. Luis, A. Repollés, O. Roubeau, S. J. Teat and G. Aromí, *Inorg. Chem.*, 2010, **49**, 6784–6786.

383 S. K. U. Riederer, P. Gigler, M. P. Högerl, E. Herdtweck, B. Bechlars, W. A. Herrmann and F. E. Kühn, *Organometallics*, 2010, **29**, 5681–5692.

384 L.-Z. Tang, C.-N. Lin and S.-Z. Zhan, *Polyhedron*, 2016, **110**, 247–253.

385 E. W. Dahl, T. Louis-Goff and N. K. Szymczak, *Chem. Commun.*, 2017, **53**, 2287–2289.

386 W. Wang, G. B. Hammond and B. Xu, *J. Am. Chem. Soc.*, 2012, **134**, 5697–5705.

387 O. M. Yaghi, M. O'Keeffe, N. W. Ockwig, H. K. Chae, M. Eddaoudi and J. Kim, *Nature*, 2003, 423, 705–714.

388 R. Della Pergola, F. Demartin, L. Garlaschelli, M. Manassero, S. Martinengo, N. Masciocchi and D. Strumolo, *Inorg. Chem.*, 1991, **30**, 846–849.

389 D. Collini, F. F. De Biani, S. Fedi, C. Femoni, F. Kaswalder, M. C. Iapalucci, G. Longoni, C. Tiozzo, S. Zacchini and P. Zanello, *Inorg. Chem.*, 2007, **46**, 7971–7981.

390 J. W. Steed and J. L. Atwood, *Supramolecular Chemistry*, 2009.

391 S. Bhattacharya and B. K. Saha, *CrystEngComm*, 2011, **13**, 6941–6944.

392 A. J. Close, P. Kemmitt, M. K. Emmerson and J. Spencer, *Tetrahedron*, 2014, **70**, 9125–9131.

393 B. Kaitner and M. Zbačnik, *Acta Chim. Slov.*, 2012, **59**, 670–679.

394 G. T. Tigineh, Y. S. Wen and L. K. Liu, *Tetrahedron*, 2015, **71**, 170–175.

395 J. Spencer, N. Anjum, H. Patel, R. P. Rathnam and J. Verma, *Synlett*, 2007, **2007**, 2557–2558.

396 J. Spencer, C. B. Baltus, H. Patel, N. J. Press, S. K. Callear, L. Male and S. J. Coles, *ACS Comb. Sci.*, 2011, **13**, 24–31.

397 C. C. Stoumpos, T. C. Stamatatos, H. Sartzi, O. Roubeau, A. J. Tasiopoulos, V. Nastopoulos, S. J. Teat, G. Christou and S. P. Perlepes, *Dalt. Trans.*, 2009, **0**, 1004.

398 T. C. Stamatatos, K. a Abboud, S. P. Perlepes and G. Christou, *Dalton Trans.*, 2007, **0**, 3861–3863.

399 W.-H. Zhu, Y. Zhang, Z. Guo, S. Wang, J. Wang, Y.-L. Huang, L. Liu, Y.-Q. Fan, F. Cao

and S.-W. Xiang, *RSC Adv.*, 2014, **4**, 49934–49941.

400 J. Tönnemann, J. Risse, Z. Grote, R. Scopelliti and K. Severin, *Eur. J. Inorg. Chem.*, 2013, **2013**, 4558–4562.

401 P. Kumar, K. Griffiths, S. Lymperopoulou and G. E. Kostakis, *RSC Adv.*, 2016, **6**, 79180–79184.

402 D. J. Darensbourg, O. Karroonnirun and S. J. Wilson, *Inorg. Chem.*, 2011, **50**, 6775–6787.

403 X. Xu, L. Zhao, G.-F. Xu, Y.-N. Guo, J. Tang and Z. Liu, *Dalt. Trans.*, 2011, **40**, 6440.

404 H. H. Zou, L. B. Sheng, Z. L. Chen and F. P. Liang, *Polyhedron*, 2015, **88**, 110–115.

405 D. I. Alexandropoulos, S. Mukherjee, C. Papatriantafyllopoulou, C. P. Raptopoulou, V. Psycharis, V. Bekiari, G. Christou and T. C. Stamatatos, *Inorg. Chem.*, 2011, **50**, 11276–11278.

406 Y. Y. Zhou, B. Geng, Z. W. Zhang, Q. Guan, J. L. Lu and Q. B. Bo, *Inorg. Chem.*, 2016, **55**, 2037–2047.

407 G. Xu, Z. Wang, Z. He, Z. Lü, C. Liao and C. Yan, *Inorg. Chem.*, 2002, **41**, 6802–6807.

408 M. A. Singh-Wilmot, R. A. Sinclair, M. Andrews, C. Rowland, C. L. Cahill and M. Murugesu, *Polyhedron*, 2013, **53**, 187–192.

409 S. Omagari, T. Nakanishi, Y. Kitagawa, T. Seki, K. Fushimi, H. Ito, A. Meijerink and Y. Hasegawa, *Sci. Rep.*, 2016, **6**, 37008.

410 R. Kannappan, D. M. Tooke, A. L. Spek and J. Reedijk, *Inorganica Chim. Acta*, 2006, **359**, 334–338.

411 G. K. Veits and J. Read De Alaniz, *Tetrahedron*, 2012, 68, 2015–2026.

412 S.-W. Li and R. A. Batey, *Chem. Commun.*, 2007, **0**, 3759.

413 D. R. Wenz and J. R. De Alaniz, *Org. Lett.*, 2013, **15**, 3250–3253.

414 L. I. Palmer and J. R. De Alaniz, *Org. Lett.*, 2013, **15**, 476–479.

415 S. J. Coles and P. A. Gale, *Chem. Sci.*, 2012, **3**, 683–689.

416 B. Bhattacharya, R. Dey, D. K. Maity and D. Ghoshal, *CrystEngComm*, 2013, **15**, 9457.

417 H. Ke, S. Zhang, W. Zhu, G. Xie and S. Chen, *J. Coord. Chem.*, 2015, **68**, 808–822.

418 G. Zhang, Y. Wei, L. Guo, X. Zhu, S. Wang, S. Zhou and X. Mu, *Chem. - A Eur. J.*, 2015, **21**, 2519–2526.

419 M. Jha, O. Enaohwo and S. Guy, *Tetrahedron Lett.*, 2011, **52**, 684–687.

420 D. Chen, L. Yu and P. G. Wang, *Tetrahedron Lett.*, 1996, **37**, 4467–4470.

421 Y. H. Hui, Y. C. Chen, H. W. Gong and Z. F. Xie, *Chinese Chem. Lett.*, 2014, **25**, 163–165.

422 Y. Hui, L. Lin, X. Liu and X. Feng, *Zinc Catalysis*, Wiley-VCH Verlag GmbH & Co. KGaA, Weinheim, Germany, 2015.

423 A. des sciences (France) and C. national de la recherche scientifique (France), *Comptes rendus hebdomadaires des séances de l'Académie des sciences.*, 1920, vol. v.171 (192.

424 M. Inman and C. J. Moody, *Chem. Sci.*, 2013, **4**, 29–41.

425 S. Sarva, J. S. Harinath, S. P. Sthanikam, S. Ethiraj, M. Vaithiyalingam and S. R. Cirandur, *Chinese Chem. Lett.*, 2016, **27**, 16–20.

426 V. Jamsheena, G. Shilpa, J. Saranya, N. A. Harry, R. S. Lankalapalli and S. Priya, *Chem. Biol. Interact.*, 2016, **247**, 11–21.

427 C. Karami, H. Ahmadian, M. Nouri, F. Jamshidi, H. Mohammadi, K. Ghodrati, A. Farrokhi and Z. Hamidi, *Catal. Commun.*, 2012, **27**, 92–96.

428 S. Khaksar, M. Tajbakhsh and M. Gholami, *Comptes Rendus Chim.*, 2014, **17**, 30–34.

429 M. A. Zolfigol, P. Salehi, M. Shiri and Z. Tanbakouchian, *Catal. Commun.*, 2007, **8**, 173–178.

430 J. Beltrá, M. C. Gimeno and R. P. Herrera, *Beilstein J. Org. Chem.*, 2014, **10**, 2206–2214.

431 O. M. Berner, L. Tedeschi and D. Enders, *European J. Org. Chem.*, 2002, **2002**, 1877–1894.

432 T. N. Drug, in *The Nitro Group in Organic Synthesis*, John Wiley & Sons, Inc., New York, USA, 2010, vol. 3, pp. 325–363.

433 I. T. Papadas, S. Fountoulaki, I. N. Lykakis and G. S. Armatas, *Chem. - A Eur. J.*, 2016, **22**, 4600–4607.

434 S. Fountoulaki, V. Daikopoulou, P. L. Gkizis, I. Tamiolakis, G. S. Armatas and I. N. Lykakis, *ACS Catal.*, 2014, **4**, 3504–3511.

435 M. Stratakis and H. Garcia, *Chem. Rev.*, 2012, 112, 4469–4506.

436 H.-U. Blaser, H. Steiner and M. Studer, *ChemCatChem*, 2009, **1**, 210–221.

437 R. P. Herrera, V. Sgarzani, L. Bernardi and A. Ricci, *Angew. Chemie - Int. Ed.*, 2005, **44**, 6576–6579.

438 W. Zhuang, R. G. Hazell and K. A. Jørgensen, *Org. Biomol. Chem.*, 2005, **3**, 2566–2571.

439 E. M. Fleming, T. McCabe and S. J. Connon, *Tetrahedron Lett.*, 2006, **47**, 7037–7042.

440 M. Ganesh and D. Seidel, *J. Am. Chem. Soc.*, 2008, **130**, 16464–16465.

441 E. Marqués-Lõpez, A. Alcaine, T. Tejero and R. P. Herrera, *European J. Org. Chem.*, 2011, **2011**, 3700–3705.

442 J. Itoh, K. Fuchibe and T. Akiyama, *Angew. Chemie - Int. Ed.*, 2008, **47**, 4016–4018.

443 D. M. Nickerson, V. V. Angeles, T. J. Auvil, S. S. So and A. E. Mattson, *Chem. Commun.*, 2013, **49**, 4289–4291.

444 D. Roca-López, E. Marqués-López, A. Alcaine, P. Merino and R. P. Herrera, *Org. Biomol. Chem.*, 2014, **12**, 4503–4510.

445 M. Turks, E. Rolava, D. Stepanovs, A. Mishnev and D. Markovi, *Tetrahedron Asymmetry*, 2015, **26**, 952–960.

446 C. M. McGuirk, J. Mendez-Arroyo, A. M. Lifschitz and C. A. Mirkin, *J. Am. Chem. Soc.*, 2014, **136**, 16594–16601.

447 A. G. Schafer, J. M. Wieting and A. E. Mattson, *Org. Lett.*, 2011, **13**, 5228–31.

448 N. T. Tran, S. O. Wilson and A. K. Franz, *Org. Lett.*, 2012, **14**, 186–189.

449 L. T. An, J. P. Zou, L. L. Zhang and Y. Zhang, *Tetrahedron Lett.*, 2007, **48**, 4297–4300.

450 K. Moriyama, T. Sugiue, Y. Saito, S. Katsuta and H. Togo, *Adv. Synth. Catal.*, 2015, **357**, 2143–2149.

451 M. Bandini, A. Garelli, M. Rovinetti, S. Tommasi and A. Umani-Ronchi, *Chirality*, 2005, **17**, 522–529.

452 P. K. Singh, A. Bisai and V. K. Singh, *Tetrahedron Lett.*, 2007, **48**, 1127–1129.

453 H. Y. Kim, S. Kim and K. Oh, *Angew. Chemie Int. Ed.*, 2010, **49**, 4476–4478.

454 T. Arai and N. Yokoyama, *Angew. Chemie - Int. Ed.*, 2008, **47**, 4989–4992.

455 T. Arai, N. Yokoyama and A. Yanagisawa, *Chem. - A Eur. J.*, 2008, **14**, 2052–2059.

456 N. Yokoyama and T. Arai, *Chem. Commun. (Camb).*, 2009, **0**, 3285–7.

457 Y. Jia, S. Zhu, Y. Yang, Q. Zhou and R. V August, *J. Org. Chem.*, 2006, **71**, 75–80.

458 F. Guo, G. Lai, S. Xiong, S. Wang and Z. Wang, *Chem. - A Eur. J.*, 2010, **16**, 6438–6441.

459 Z. L. Yuan, Z. Y. Lei and M. Shi, *Tetrahedron Asymmetry*, 2008, **19**, 1339–1346.

460 S. Lin and T. You, *Tetrahedron*, 2009, **65**, 1010–1016.

461 S. C. McKeon, H. Müller-Bunz and P. J. Guiry, *European J. Org. Chem.*, 2009, **2009**, 4833–4841.

462 S. Jalal, S. Sarkar, K. Bera, S. Maiti and U. Jana, *European J. Org. Chem.*, 2013, **2013**, 4823–4828.

463 T. Kitanosono, M. Miyo and S. Kobayashi, *Tetrahedron*, 2015, **71**, 7739–7744.

464 Z. P. Zhan, R. F. Yang and K. Lang, *Tetrahedron Lett.*, 2005, **46**, 3859–3862.

465 H. Firouzabadi, N. Iranpoor and F. Nowrouzi, *Chem. Commun.*, 2005, **0**, 789–791.

466 G. V. More and B. M. Bhanage, *Catal. Sci. Technol.*, 2015, **5**, 1514–1520.

467 F. Guo, D. Chang, G. Lai, T. Zhu, S. Xiong, S. Wang and Z. Wang, *Chem. - A Eur. J.*, 2011, **17**, 11127–11130.

468 D. Carmona, M. P. Lamata, A. Sánchez, F. Viguri and L. A. Oro, *Tetrahedron Asymmetry*, 2011, **22**, 893–906.

469 I. Méndez, R. Rodríguez, V. Polo, V. Passarelli, F. J. Lahoz, P. García-Orduña and D. Carmona, *Chem. - A Eur. J.*, 2016, **22**, 11064–11083.

470 X.-W. Dong, T. Liu, Y.-Z. Hu, X.-Y. Liu and C.-M. Che, *Chem. Commun.*, 2013, **49**, 7681.

471 C. M. McGuirk, M. J. Katz, C. L. Stern, A. A. Sarjeant, J. T. Hupp, O. K. Farha and C. A. Mirkin, *J. Am. Chem. Soc.*, 2015, **137**, 919–925.

472 S. Sobhani and R. Jahanshahi, *New J. Chem.*, 2013, **37**, 1009–1015.

473 M. Jeganathan, K. Kanagaraj, A. Dhakshinamoorthy and K. Pitchumani, *Tetrahedron Lett.*, 2014, **55**, 2061–2064.

474 H. Liu and D. M. Du, *Adv. Synth. Catal.*, 2010, **352**, 1113–1118.

475 H. Liu, J. Xu and D. M. Du, *Org. Lett.*, 2007, **9**, 4725–4728.

476 H. Liu, S. F. Lu, J. Xu and D. M. Du, *Chem. - An Asian J.*, 2008, **3**, 1111–1121.

477 H. Liu and D.-M. M. Du, *European J. Org. Chem.*, 2010, **2010**, 2121–2131.

478 B. H. Rotstein, S. Zaretsky, V. Rai and A. K. Yudin, *Chem. Rev.*, 2014, 114, 8323–8359.

479 R. Kakuchi, *Angew. Chemie - Int. Ed.*, 2014, 53, 46–48.

480 M. Shiri, *Chem. Rev.*, 2012, 112, 3508–3549.

481 A. Dömling, W. Wang and K. Wang, *Chem. Rev.*, 2012, 112, 3083–3135.

482 E. Ruijter, R. Scheffelaar and R. V. A. Orru, *Angew. Chemie - Int. Ed.*, 2011, 50, 6234–6246.

483 N. Isambert, M. del M. S. Duque, J.-C. Plaquevent, Y. Génisson, J. Rodriguez and T. Constantieux, *Chem. Soc. Rev.*, 2011, **40**, 1347–1357.

484 C. Kalinski, M. Umkehrer, L. Weber, J. Kolb, C. Burdack and G. Ross, *Mol. Divers.*, 2010, **14**, 513–522.

485 R. Zhou, Q. Wu, M. Guo, W. Huang, X. He, L. Yang, F. Peng, G. He and B. Han, *Chem. Commun.*, 2015, **51**, 13113–13116.

486 M. Varyani, P. K. Khatri and S. L. Jain, *CATCOM*, 2016, **77**, 113–117.

487 T. Flagstad, M. T. Petersen and T. E. Nielsen, *Angew. Chemie - Int. Ed.*, 2015, **54**, 8395–8397.

488 S. Roy and O. Reiser, *Angew. Chemie - Int. Ed.*, 2012, **51**, 4722–4725.

489 I. Ibrahem, P. Breistein and A. Córdova, *Chem. - A Eur. J.*, 2012, **18**, 5175–5179.

490 N. A. Petasis and I. Akritopoulou, *Tetrahedron Lett.*, 1993, **34**, 583–586.

491 N. R. Candeias, F. Montalbano, P. M. S. D. Cal and P. M. P. Gois, *Chem. Rev.*, 2010, **110**, 6169–6193.

492 N. A. Petasis and S. Boral, *Tetrahedron Lett.*, 2001, **42**, 539–542.

493 M. L. Deb, S. S. Dey, I. Bento, M. T. Barros and C. D. Maycock, *Angew. Chemie - Int. Ed.*, 2013, **52**, 9791–9795.

494 M. T. Richers, M. Breugst, A. Y. Platonova, A. Ullrich, A. Dieckmann, K. N. Houk and D. Seidel, *J. Am. Chem. Soc.*, 2014, **136**, 6123–6135.

495 Y. Huang and T. Hayashi, *J. Am. Chem. Soc.*, 2015, **137**, 7556–7559.

496 Q. Wang and M. Finn, *Org. Lett.*, 2000, **2**, 4063–4065.

497 N. J. McLean, H. Tye and M. Whittaker, *Tetrahedron Lett.*, 2004, **45**, 993–995.

498 N. R. Candeias, L. F. Veiros, C. A. M. Afonso and P. M. P. Gois, *European J. Org. Chem.*, 2009, 1859–1863.

499 B. R. Prasad Reddy, P. V. Govardhana Reddy, D. P. Kumar, B. N. Reddy and M. V Shankar, *RSC Adv.*, 2016, **6**, 14682–14691.

500 N. F. Chilton, R. P. Anderson, L. D. Turner, A. Soncini and K. S. Murray, *J. Comput. Chem.*, 2013, **34**, 1164–1175.

501 A. L. Gemal and J. L. Luche, *J. Am. Chem. Soc.*, 1981, **103**, 5454–5459.

502 R. G. Parr and R. G. Pearson, *J. Am. Chem. Soc.*, 1983, **105**, 7512–7516.

503 J. Wang, H. Li, W. Duan, L. Zu and W. Wang, *Org. Lett.*, 2005, **7**, 4713–4716.

504 M. Terada, H. Ube and Y. Yaguchi, *J. Am. Chem. Soc.*, 2006, **128**, 1454–1455.

505 M. A. Kacprzynski, S. A. Kazane, T. L. May and A. H. Hoveyda, *Org. Lett.*, 2007, **9**, 3187–90.

506 X. Yang and F. D. Toste, *Chem. Sci.*, 2016, **7**, 2653–2656.

507 P. Howlader, P. Das, E. Zangrando and P. S. Mukherjee, *J. Am. Chem. Soc.*, 2016, **138**, 1668–1676.

508 H. J. Al-Najjar, A. Barakat, A. M. Al-Majid, Y. N. Mabkhot, M. Weber, H. A. Ghabbour and H. K. Fun, *Molecules*, 2014, **19**, 1150–1162.

509 F. Seeliger, S. T. A. Berger, G. Y. Remennikov, K. Polborn and H. Mayr, *J. Org. Chem.*, 2007, **72**, 9170–9180.

510 D. Prat, J. Hayler and A. Wells, *Green Chem.*, 2014, **16**, 4546–4551.

511 X.-L. Wang, L.-L. Hou, J.-W. Zhang, J.-X. Zhang, G.-C. Liu and S. Yang, *CrystEngComm*, 2012, **14**, 3936.

512 D. A. Buckingham, C. R. Clark, R. H. Mckeown and O. Wong, *J. Am. Chem. Soc.*, 1987, **109**, 466–476.

513 V. B. Delchev, *J. Struct. Chem.*, 2004, **45**, 570–578.

514 K. Senthilkumar and P. Kolandaivel, *J. Comput. Aided. Mol. Des.*, 2002, **16**, 263–272.

515 M. U. Schmidt, J. Brüning, J. Glinnemann, M. W. Hützler, P. Mörschel, S. N. Ivashevskaya, J. Van De Streek, D. Braga, L. Maini, M. R. Chierotti and R. Gobetto, *Angew. Chemie - Int. Ed.*, 2011, **50**, 7924–7926.

516 H. Zhang, R. Liu, J. Zhang, Y. Li and W. Liu, *CrystEngComm*, 2016, **18**, 8246–8252.

517 S. Das, K. S. Bejoymohandas, A. Dey, S. Biswas, M. L. P. Reddy, R. Morales, E. Ruiz, S. Titos-Padilla, E. Colacio and V. Chandrasekhar, *Chem. – A Eur. J.*, 2015, **21**, 6449–6464.

518 I. Oyarzabal, J. Ruiz, J. M. Seco, M. Evangelisti, A. Camón, E. Ruiz, D. Aravena and E. Colacio, *Chem. – A Eur. J.*, 2014, **20**, 14262–14269.

519 E. Colacio, J. Ruiz-Sanchez, F. J. White and E. K. Brechin, *Inorg. Chem.*, 2011, **50**, 7268–7273.

520 C. D. Polyzou, E. S. Koumousi, Z. G. Lada, C. P. Raptopoulou, V. Psycharis, M. Rouzières, A. C. Tsipis, C. Mathonière, R. Clérac and S. P. Perlepes, *Dalt. Trans.*, 2017, **46**, 14812–14825.

521 S. Biswas, K. S. Bejoymohandas, S. Das, P. Kalita, M. L. P. Reddy, I. Oyarzabal, E. Colacio and V. Chandrasekhar, *Inorg. Chem.*, 2017, **56**, 7985–7997.

522 F. Gao, L. Cui, Y. Song, Y. Z. Li and J. L. Zuo, *Inorg. Chem.*, 2014, **53**, 562–567.

523 A. J. Brown, D. Pinkowicz, M. R. Saber and K. R. Dunbar, *Angew. Chemie*, 2015, **127**, 5962–5966.

524 D.-P. Lyu, J.-Y. Zheng, Q.-W. Li, J.-L. Liu, Y.-C. Chen, J.-H. Jia and M.-L. Tong, *Inorg. Chem. Front.*, 2017, **4**, 1776–1782.

525 L.-F. Zou, L. Zhao, Y.-N. Guo, G.-M. Yu, Y. Guo, J. Tang and Y.-H. Li, *Chem. Commun.*, 2011, **47**, 8659.

526 C. Aronica, G. Pilet, G. Chastanet, W. Wernsdorfer, J. F. Jacquot and D. Luneau, *Angew. Chemie - Int. Ed.*, 2006, **45**, 4659–4662.

527 C. Aronica, G. Chastanet, G. Pilet, B. Le Guennic, V. Robert, W. Wernsdorfer and D.

Luneau, *Inorg. Chem.*, 2007, **46**, 6108–6119.

528 A. D. Becke, *J. Chem. Phys.*, 1993, **98**, 1372–1377.

529 A. D. McLean and G. S. Chandler, *J. Chem. Phys.*, 1980, **72**, 5639–5648.

530 R. Krishnan, J. S. Binkley, R. Seeger and J. A. Pople, *J. Chem. Phys.*, 1980, **72**, 650–654.

531 S. Jose, *Chem. Phys.*, 1968, **1033**, 3–6.

532 P. J. Hay, *J. Chem. Phys.*, 1977, **66**, 4377–4384.

533 K. Raghavachari and G. W. Trucks, *J. Chem. Phys.*, 1989, **91**, 1062–1065.

534 T. Clark, J. Chandrasekhar, G. W. Spitznagel and P. V. R. Schleyer, *J. Comput. Chem.*, 1983, **4**, 294–301.

535 M. J. Frisch, J. A. Pople and J. S. Binkley, *J. Chem. Phys.*, 1984, **80**, 3265–3269.

536 P. Fuentealba, H. Preuss, H. Stoll and L. Von Szentpály, *Chem. Phys. Lett.*, 1982, **89**, 418–422.

537 M. Pélissier, J. P. Daudey, J. P. Malrieu and G. H. Jeung, *Quantum Chemistry: The Challenge of Transition Metals and Coordination Chemistry*, Springer Netherlands, Dordrecht, 1986.

538 M. F. Summers, *Coord. Chem. Rev.*, 1988, **86**, 43–134.

539 J. P. Perdew, K. Burke and M. Ernzerhof, *Phys. Rev. Lett.*, 1996, **77**, 3865–3868.

540 M. Ernzerhof and G. E. Scuseria, *J. Chem. Phys.*, 1999, **110**, 5029–5036.

541 C. Adamo and V. Barone, *Chem. Phys. Lett.*, 1997, **274**, 242–250.

542 C. Adamo and V. Barone, *J. Chem. Phys.*, 1999, **110**, 6158–6170.

543 C. Adamo, G. E. Scuseria and V. Barone, *J. Chem. Phys.*, 1999, **111**, 2889–2899.

544 C. Adamo and V. Barone, *Theor. Chem. Accounts Theory, Comput. Model. (Theoretica Chim. Acta)*, 2000, **105**, 169–172.

545 V. Vetere, C. Adamo and P. Maldivi, *Chem. Phys. Lett.*, 2000, **325**, 99–105.

546 F. Weigend and R. Ahlrichs, *Phys. Chem. Chem. Phys.*, 2005, **7**, 3297.

547 J. Tomasi, B. Mennucci and R. Cammi, *Chem. Rev.*, 2005, 105, 2999–3093.

548 A. E. Reed, L. A. Curtiss and F. Weinhold, *Chem. Rev.*, 1988, **88**, 899–926.

549 J. G. AD MacKerell Jr. Protein force fields. In: PvR Schleyer, NL Allinger, T Clark and E. PA Kollman, HF Schaefer III, PR Schreiner, *Encycl. Comput. Chem. UK, Wiley 1998*, 1998, **3**, 2191–2200.

550 C. E. Burrow, T. J. Burchell, P.-H. Lin, F. Habib, W. Wernsdorfer, R. Clérac and M. Murugesu, *Inorg. Chem.*, 2009, **48**, 8051–8053.

551 S. Biswas, P. Bag, S. Das, S. Kundu, J. van Leusen, P. Kögerler and V. Chandrasekhar, *Eur. J. Inorg. Chem.*, 2017, **2017**, 1129–1142.

552 J. Goura, R. Guillaume, E. Rivière and V. Chandrasekhar, *Inorg. Chem.*, 2014, **53**, 7815–7823.

553 C.-B. Tian, D.-Q. Yuan, Y.-H. Han, Z.-H. Li, P. Lin and S.-W. Du, *Inorg. Chem. Front.*, 2014, **1**, 695–704.

554 E. Loukopoulos, B. Berkoff, A. Abdul-Sada, G. J. Tizzard, S. J. Coles, A. Escuer and G. E. Kostakis, *Eur. J. Inorg. Chem.*, 2015, **2015**, 2646–2649.

555 S. Biswas, J. Goura, S. Das, C. V. Topping, J. Brambleby, P. A. Goddard and V. Chandrasekhar, *Inorg. Chem.*, 2016, **55**, 8422–8436.

556 I. A. Kühne, G. E. Kostakis, C. E. Anson and A. K. Powell, *Inorg. Chem.*, 2016, **55**, 4072–4074.

557 X.-Q. Song, P.-P. Liu, Y.-A. Liu, J.-J. Zhou and X.-L. Wang, *Dalt. Trans.*, 2016, **45**, 8154–8163.

558 C. Papatriantafyllopoulou, T. C. Stamatatos, C. G. Efthymiou, L. Cunha-Silva, F. A. A. Paz, S. P. Perlepes and G. Christou, *Inorg. Chem.*, 2010, **49**, 9743–9745.

559 X. P. Yang, R. A. Jones, V. Lynch, M. Oye and A. L. Holmes, *Dalt. Trans.*, 2005, **0**, 849–851.

560 S. K. Samanta, S. M. T. Abtab, P. S. Sardar, S. Sanyal, M. Chaudhury and S. Ghosh, *Eur. J. Inorg. Chem.*, 2014, **2014**, 3101–3113.

561 S. M. T. Abtab, A. Audhya, N. Kundu, S. K. Samanta, P. S. Sardar, R. J. Butcher, S. Ghosh and M. Chaudhury, *Dalt. Trans.*, 2013, **42**, 1848–1861.

562 Z.-S. Meng, F.-S. Guo, J.-L. Liu, J.-D. Leng and M.-L. Tong, *Dalt. Trans.*, 2012, **41**, 2320–2329.

563 S. Akine, S. Hotate, T. Matsumoto and T. Nabeshima, *Chem. Commun.*, 2011, **47**, 2925.

564 S. Akine, T. Matsumoto and T. Nabeshima, *Chem. Commun. (Camb).*, 2008, **0**, 4604–4606.

565 G. Xiong, X.-Y. Qin, P.-F. Shi, Y.-L. Hou, J.-Z. Cui and B. Zhao, *Chem. Commun.*, 2014, **50**, 4255–4257.

566 A. Kornienko, L. Huebner, D. Freedman, T. J. Emge and J. G. Brennan, *Inorg. Chem.*, 2003, **42**, 8476–8480.

Chapter 14: Appendix

Appendix A

Chapter 1

Table S1.1 Representative examples of 3d-4f PCCs (3d = Ni^{II}, Co^{II}, Cu^{II}, Zn^{II}) supported by Schiff base ligands with a nuclearity above five that display SMM properties.

Entry	Ligand	Core	Topology	SMM properties	Reference
1	**H_4RL1.1**	$Ni^{II}_2Dy^{III}_3$	**1,2,2M5-1**	U_{eff} = 85 K τ_0 = 5.9 x 10^{-7} s T_B = 3 K	56
2	**H_2 RL1.2**	$Zn^{II}_2Dy^{III}_3$	**1,2,3M5-1**	U_{eff} = 85 K τ_0 = 3.3 x 10^{-7} s	550
3	**H_4RL1.3**	$Co^{III}_3Co^{II}Dy$	**1,1,2,3M5-1**	U_{eff} = 13 K τ_0 = 2.3 x 10^{-7} s	74
4	H_2**RL1.4**	$Cu^{II}_4Dy^{III}$	**2,4M5-1**	U_{eff} = 12.876 K τ_0 = 2.268 x 10^{-7} s	19
5	H_4**RL1.5**	$Cu^{II}_2Dy^{III}_3$	**1,2,2M5-1**	U_{eff} = 5.4 K τ_0 = 2.6 x 10^{-5} s	551
6	**H_2RL1.6**	$Ni^{II}_3Dy^{III}_3$	**2,4M6-1**	U_{eff} = 10 K τ_0 = 1 x 10^{-6} s	552
7	H_2**RL1.7**	$Co^{II}_2Dy^{III}_4$	**2,3,4M6-1**	U_{eff} = 32.4 K τ_0 = 4.2 x 10^{-7} s	553
8	H_2**RL1.8**	$Ni^{II}_4Ln^{III}_2$	**2,3,4M6-1**	(**Tb^{III}**) T_B= 2.9 K, τ_0 = 2.09 x 10^{-9} s U_{eff} = 30 K (**Dy^{III}**) = T_B-.2 K τ_0 = 1.41 x 10^{-8} s U_{eff} = 32 K	55
9	H_2**RL1.9**	$Co^{II}_2Dy^{III}_4$	**2,3,4M6-1**	U_{eff} = 41.9 K τ_0 = 1.21 x 10^{-7} s	516

10	H_4**RL1.5**	$Cu^{II}_4Dy^{III}_2$	**1,2,2M6-1**	U_{eff} = 6.5 K τ_0 = 2.9x10^{-7} s	551
11	H_3**RL1.10**	$Cu^{II}_5Dy^{III}_2$	**3,6M7-1**	U_{eff} = 4 K τ_0 = 3x10^{-6} s	113
12	H**RL1.11**	$Co^{II}_3Dy^{III}_4$	**3,6M7-1**	Out-of-phase signal below 4 K	554
13	H_2**RL1.12**	$Cu^{II}_4Dy^{III}_4$	**2M8-1**	U_{eff} = 41.6 K τ_0 = 2.1x10^{-5} s	103
14	H_2**RL1.13**	$Ni^{II}_5Dy^{III}_3$	**2,3,5,6M8-4**	Out-of-phase sign below 4 K	71
15	H_4**RL1.14**	$Ni^{II}_4Dy^{III}_4$	**2M8-1**	Out-of-phase sign below 4K	555
16	H**RL1.15**	$Cu^{II}_6Dy^{III}_3$	**3,6M9-1**	U_{eff} = 25 K τ_0 = 1.5x10^{-7} s	526
17	H_2**RL1.7**	$Cu^{II}_6Dy^{III}_3$	**3,6M9-1**	U_{eff} = 25.293 K τ_0 = 3.939 ×10^{-9} s,	19
18	H_3**RL1.16**	$Dy^{III}_3Cu^{II}_8$	**2,3,4M11-1**	Out-of-phase signal below 4 K	78
19	**H_2RL1.17**	$Dy^{II}_2Cu^{II}_9$	**1,2,3,4,6M11-1**	U_{eff} = 16.1 K τ_0 = 3.6 × 10^{-7} s	556
20	H_2**RL1.18**	$Ni^{II}_8Dy^{II}_4$	**2M12-1**	Frequency-dependent maxima below 3.5 K	365
21	H_2**RL1.19**	$Co^{II}_2Dy^{III}_{10}$	**(2,3,3M12-1)+2(0)**	Dual relaxation pathways U_{eff} = 4.3 K, τ_0 = 1.13 ×10^{-4} s; U_{eff} = 25 K τ_0 = 3.14 ×10^{-6} s	525
22	H_3**RL1.20**	$Zn^{II}_6Dy^{III}_6$	**2M12-1**	Frequency dependent maxima 2-10 K	557
24	H_2**RL1.21**	$Cu^{II}_{16}Dy^{III}_2$	**3,4,6,8M16-1**	U_{eff} = 5.2 K τ_0 = 6.5 × 10^{-6} s	223
23	H**RL**1.**22**	$Ni^{II}_8Dy^{III}_8$	**(2,5M8-1)+8(0)**	May be an SMM	558
24	H**RL1.23**	$Zn^{II}_{12}Dy^{III}_{18}$		Frequency-dependent signal-below 4.5K	28

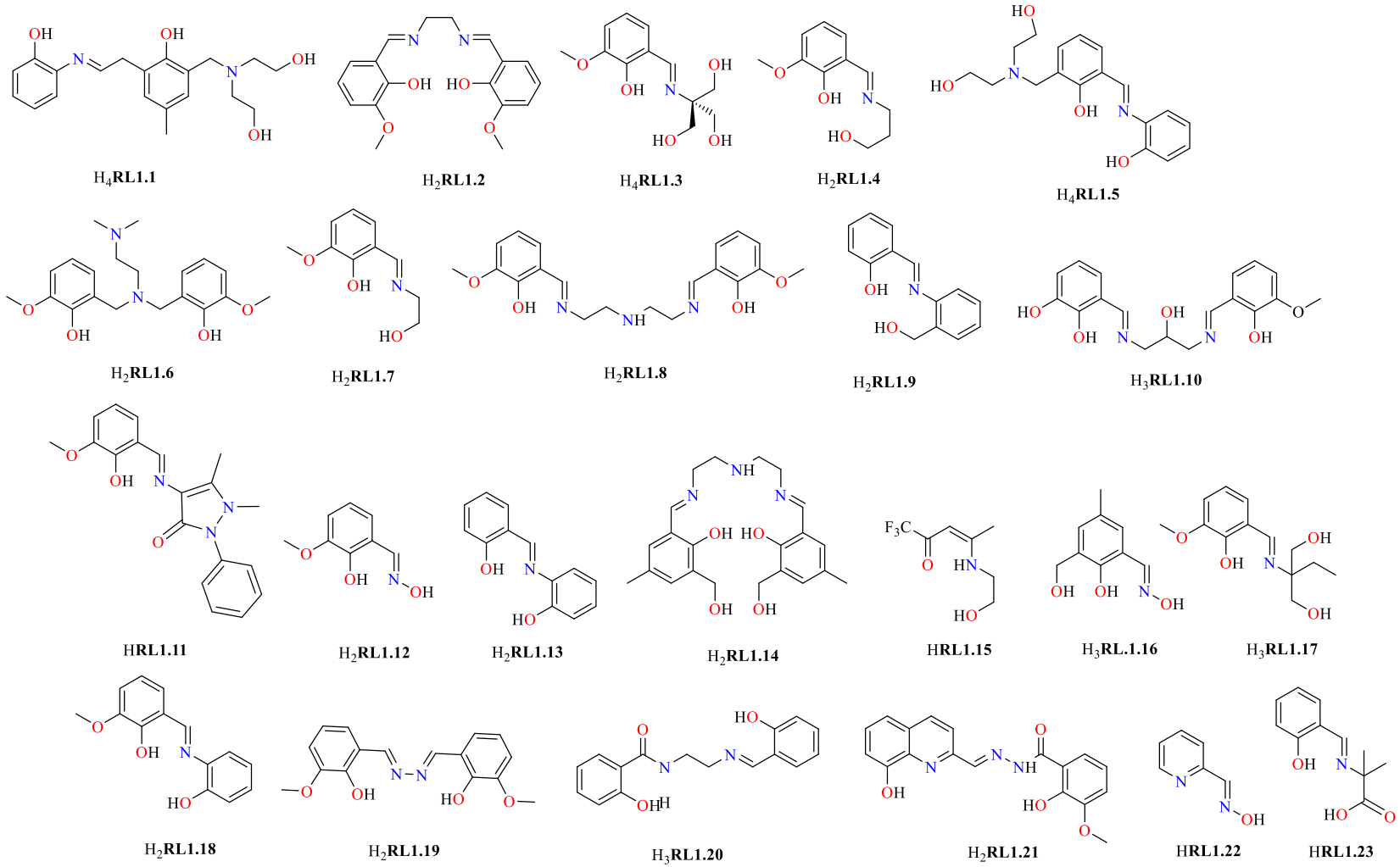

Figure S1.11. Schiff base ligands used to support 3d-4f PCCs with SMM properties.

Chapter 2

Table S2.1. Reported polynuclear Zn^{II}-Ln^{III} PCCs with a nuclearity of 4 and above.

Entry	Compound formula	Ligand	Nuclearity	Topological nomenclature	Reference
1	$[Zn^{II}_2Nd^{III}_2(\mathbf{RL2.2})_2Cl_6(MeOH)_2]\cdot MeOH$	H_2**RL2.2**	$Zn^{II}_2Ln^{III}_2$	**1,2M4-1**	[72,111]
	$[Zn^{II}_2Dy^{III}_2(\mathbf{RL2.3})_2(OAc)_2(CO_3)_2]\cdot 10CH_3OH$	H_2**RL2.3**			
2	$[Zn^{II}_2Ln^{III}_3(\mathbf{RL2.1})_3(N_3)_5(OH)_2]$	H_2**RL2.1**	$Zn^{II}_2Ln^{III}_3$	**1,2,3M5-1**	[318]
	Ln = (Tb, Eu, Ho, Dy)				
3	$[Zn^{II}_2\ Ln^{III}_3(\mathbf{RL2.3})_3Cl_2(OH)_3(N_3)_2]$	H_2**RL2.3**	$Zn^{II}_2Ln^{III}_3$	**1,2,3M5-1**	[247]
	Ln = (La, Nd, Yb, Er)				
4	$[Zn^{II}_2Ln^{III}_2(\mathbf{RL2.4})_2(CO_3)_2(NO_3)_2]\cdot$solv	H_2**RL2.4**	$Zn^{II}_2Ln^{III}_2$	**1,2M4-1**	[330]
	Ln = Dy, Tb, Gd				
5	$[Zn^{II}_2Ln^{III}_2(\mathbf{RL2.5})_2(CO_3)_2(NO_3)_2]\cdot$solv	H_2**RL2.5**	$Zn^{II}_2Ln^{III}_2$	**1,2M4-1**	[330]
	Ln = Dy, Tb, Gd				
6	$[Zn^{II}_2Yb^{III}_2(\mathbf{RL2.6})_2(OH)_2Cl_4]\cdot 2MeCN$	H_2**RL2.6**	$Zn^{II}_2Ln^{III}_2$	**1,2M4-1**	[559]

7	$[Zn^{II}_8Ln^{III}_4(R\mathbf{L2.7})_2(OAc)_{20}(OH)_4]$	H_2**RL2.7**	$Zn^{II}_8Ln^{III}_4$	**2(1,2,3M6-1)**	[234]
	Ln = Nd, Yb				
8	$[Zn^{II}_4Eu^{III}_4(\mathbf{R2.L8})_4(CO_3)_6]\cdot EtOH$	H_2**RL2.8**	$Zn^{II}_4Ln^{III}_4$	**1,3M8-1**	[326]
9	$[Zn^{II}_2Eu^{III}_2(PhCOO)_2\ (\mathbf{RL2.9})_4]$	H_2**RL2.9**	$Zn^{II}_2Ln^{III}_2$	**2M4-1**	[560,320,561]
	$[Zn^{II}_2Dy^{III}_2(PhCOO)_2(\mathbf{RL2.9})_4]$				
	$[Zn^{II}_2Tb^{III}_2(PhCOO)_2\ (\mathbf{RL2.9})_4]$				
10	$[Zn^{II}_2Dy^{III}_2(\mathbf{RL2.9})_2(\mu_3\text{-}OH)_2(\mu_4\text{-}OH)(dbm)_2(MeOH)_2]X$ X = NO_3, ClO_4	H_2**RL2.9**	$Zn^{II}_2Ln^{III}_2$	**3M4-1**	[331]
11	$[Zn^{II}_2Ln^{III}_2(\mathbf{RL2.10})_2(CO_3)_2(NO_3)_2]\cdot 4CH_3OH$	H_2**RL2.10**	$Zn^{II}_2Ln^{III}_2$	**1,2M4-1**	[325]
	Ln = Gd, Yb				
12	$[(Yb^{III}\mathbf{RL2.11})_2(H_2O)Cl(OAc)]_2\cdot[Zn^{II}Cl_4]_2$	H**RL2.11**	$Zn^{II}_2Ln^{III}_2$	**3M4-1**	[562]

13	$[Zn^{II}_2Ln^{III}_2(OH)_2(\mathbf{RL2.12})_2(OAc)_5(EtOH)(H_2O)](ClO_4)\cdot 2EtOH\cdot 1.5H_2O$ Ln = Gd, Dy	H_2**RL2.12**	$Zn^{II}_2Ln^{III}_2$	**3M4-1**	239
14	$[Zn^{II}_3La^{III}$**(RL2.16)** $(OAc)_3]$	H_4**RL2.16**	$Zn^{II}_3Ln^{III}$	**1,3M4-1**	563
15	$[Zn^{II}_3La^{III}$**(RL2.17)** $(OAc)_3]$	H_4**RL2.17**	$Zn^{II}_3Ln^{III}$	**1,3M4-1**	564
17	$[Zn^{II}_4Dy^{III}(\mathbf{RL2.14})_4(DMF)_4(NO_3)_3]$ Ln = Dy, Tb, Y, Er	H_2**RL2.14**	$Zn^{II}_4Ln^{III}$	**1,4M5-1**	329
18	$[Zn^{II}_{16}Ln^{III}(\mathbf{RL2.14})_{16}(Py)_8(CF_3SO_4)]$ Ln = Tb, Dy, Yb, Er, Nd	H_2**RL2.14**	$Zn^{II}_{16}Ln^{III}$	**2,3,8M17-1**	250
19	$[Zn^{II}_9Ln^{III}_2(\mathbf{RL2.14})_{10}(OH)(NO_3)_{2.25}Cl_{0.75}]$ Ln = Dy, Tb, Eu	H2**RL2.14**	$Zn^{II}_9Ln^{III}_2$	**1,1,2,2,5,7M11-2**	323
20	$[Zn^{II}_8Ln^{III}(\mathbf{RL2.13})_8(OH)_3]$ Ln = Dy, Nd	H_2**RL2.13**	$Zn^{II}_8Ln^{III}$	**1,2,8M9-1**	323

21	$[Zn^{II}_8Gd^{III}_4(OH)_8(\mathbf{RL2.15})_8(O_2CHMe_2)_8]\ (ClO_4)_4$	H**RL2.15**	$Zn^{II}_8Ln^{III}_4$	**3,6M12-1**	225
22	$[Zn^{II}_2Ln^{III}_2(\mathbf{RL2.15})_4(PhCO_2)_5(ROH)_2](ClO_4)\cdot 2MeOH$ Ln = Dy, Gd	H**RL2.15**	$Zn^{II}_2Ln^{III}_2$	**3M4-1**	327
23	$[Zn^{II}_6Ln^{III}(OH)(\mathbf{RL2.19})_6(NO_3)_3](OH)(NO_3)_2\cdot 8H_2O$ Ln = Er, Dy	H**RL2.19**	$Zn^{II}_6Ln^{III}$	**2,6M7-1**	565
24	$[Zn^{II}_6Dy^{III}(\mathbf{RL2.20})_6(OH)_3(OAc)_3(NO_3)_3]$	H**RL2.20**	$Zn^{II}_6Ln^{III}$	**2,6M7-1**	205
25	$[Zn^{II}_6Ln^{III}_{24}(\mathbf{RL2.21})_{24}(OAc)_{22}(\mu_3OH)_{30}(H_2O)_{14}](ClO_4)_7(OAc)\cdot 2CH_3OH\cdot 26H_2O$ Ln = Gd, Tb, Dy	H**RL2.21**	$Zn^{II}_6Ln^{III}_{24}$	**3(3,3,5M10-1)**	5
26	$[Zn^{II}_{12}Dy^{III}_{18}(OH)_{30}(\mathbf{RL2.22})_{12}(sal)_6(OAc)_6(NO_3)_3(H_2O)_6](NO_3)_3\cdot 12MeOH\cdot 5H_2O$	H_2**RL2.22**	$Zn^{II}_{12}Ln^{III}_{18}$	**3,4,6,8M30-1**	28
27	$[Zn^{II}_3Ln^{III}_2(\mathbf{RL2.23})_2(Py)_2(NO_3)_2]$ $[ZnLn(\mathbf{RL2.23})(Py)(NO_3)_3(H_2O)](NO_3)\cdot solv$ Ln = Er, Gd	H_2**RL2.23**	$Zn^{II}_3Ln^{III}_2$	**(1,2M3-1) +(1M2-1)**	238
28	$[(THF)_8Ln^{III}_4Se(\mathbf{RL2.24})_8]\ [Zn^{II}_8Se(\mathbf{L2.27})_{16}]\ THF$	**RL2.24**	$Zn^{II}_8Ln^{III}_4$	**(3,6M8-1) +(3M4-1)**	566

29	$[Zn^{II}_4Nd^{III}_2(\mathbf{RL2.25})_4(1,4\text{-BDC})_2]$ $[ZnNd(\mathbf{RL2.25})(NO_3)_3(OAc)]_2$	$H_2\mathbf{RL2.25}$	$Zn^{II}_6Ln^{III}_4$	**2(1,2M3-1) +2(1M2-1)**	[31]
30	$[Zn^{II}_2Ln^{III}_2(\mathbf{L1})_4(EtOH)_6](ClO_4)_2$	$H_2\mathbf{L1}$	$Zn^{II}_2Ln^{III}_2$	**2,3M4-1**	This work
31	$[Zn^{II}_5Ln^{III}(OH)(\mathbf{L1})_6(H_2O)]$	$H_2\mathbf{L1}$	$Zn^{II}_5Ln^{III}$	**2,3,4M6-1**	This work
32	$[Zn^{II}_4Dy^{III}_2(OH)_2(\mathbf{L2})_4(OAc)_2(NO_3)_2(DMF)_3]\cdot DMF$	$H_2\mathbf{L2}$	$Zn^{II}_4Dy^{III}_2$	**2,3,4M6-1**	This work
33	$[Zn^{II}_2Ln^{III}_2(\mathbf{L3})_2(CO_3)_2(NO_3)_2(CH_3OH)_2]$	$H_3\mathbf{L3}$	$Zn^{II}_2Ln^{III}_2$	**1,2M4-1**	This work
34	$[Zn^{II}_2Ln^{III}_2(\mathbf{L1})_4(NO_3)_2(DMF)_2]$	$H_2\mathbf{L1}$	$Zn^{II}_2Ln^{III}_2$	**2,3M4-1**	[336]

Magnetic measurements

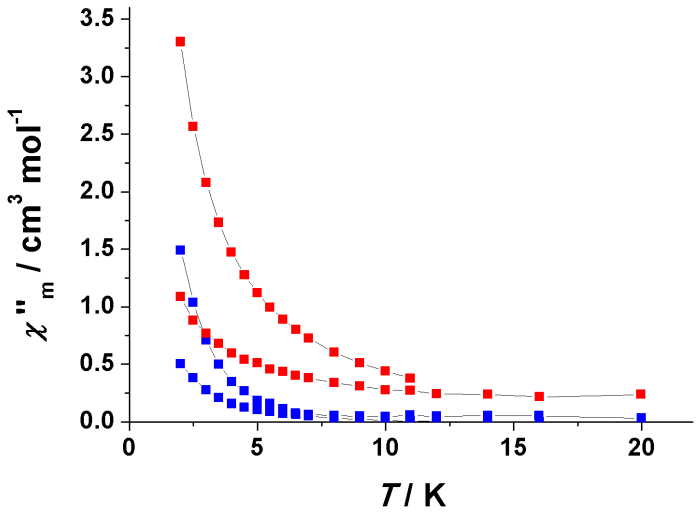

Figure S2.1. *ac* susceptibility measures for **1** (red squares) and **10** (blue squares) for the frequencies 10 and 1000 Hz and under a field of 0.1 T. Both systems show a very weak response, showing the tails of the out-of-phase signals.

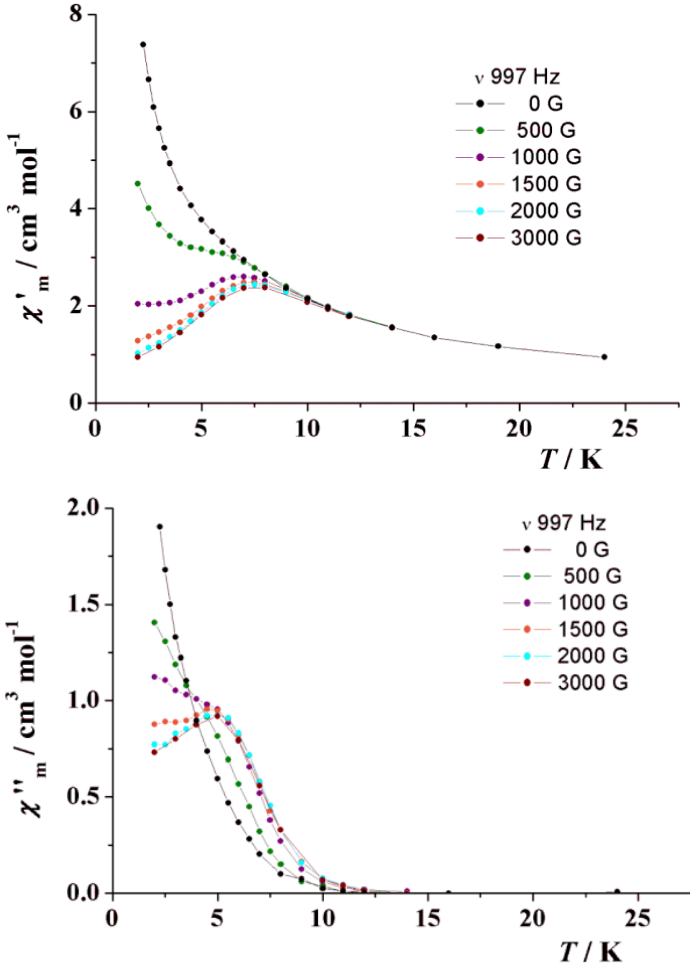

Figure S2.2. *ac* susceptibility measurements for **7** under variable transverse field and a fixed frequency of 997 Hz, showing the displacement of the *ac* peaks as consequence of the breaking of the tunnelling relaxation.

Molecular Structures of 13 and 14

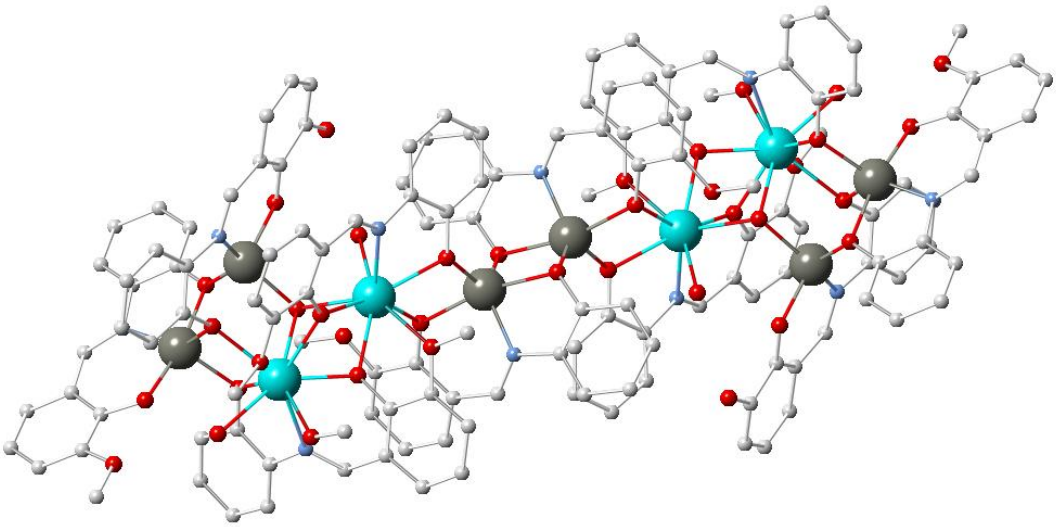

Figure S2.3 Molecular Structure of **13**. Colour code: Zn^{II}, grey; Dy^{III}, light blue; O, red; N, blue and C, white. Crystallographic data (chapter 11).

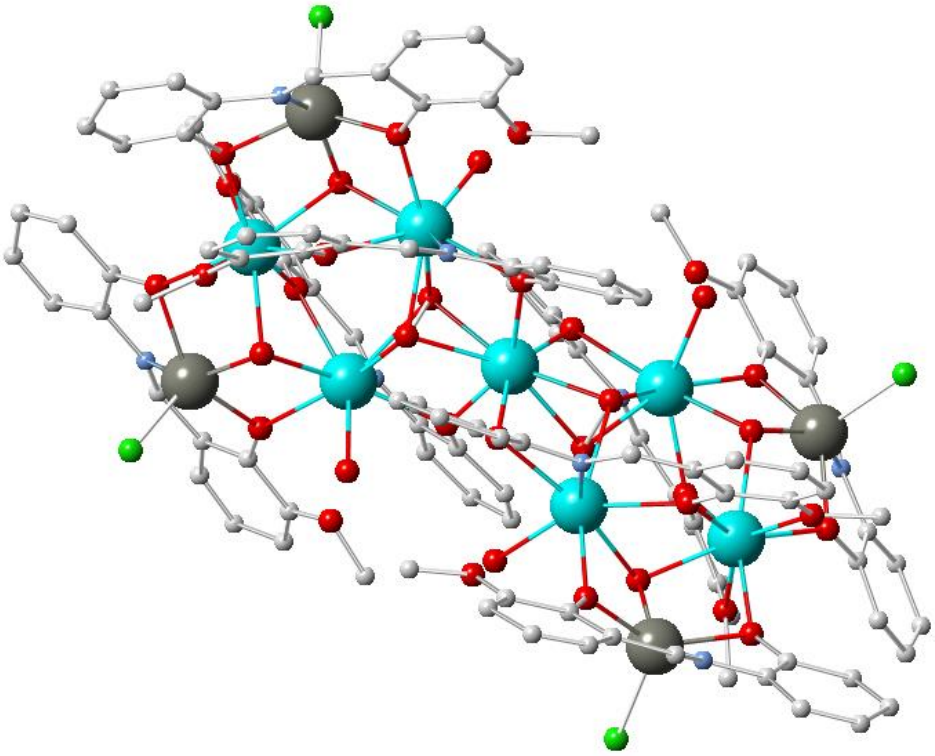

Figure S2.4 Molecular Structure of **14.** Colour code: Zn^{II}, grey; Dy^{III}, light blue; O, red; N, blue; Cl, green and C, white. Crystallographic data (chapter 11).

Chapter 3

Magnetics measurements

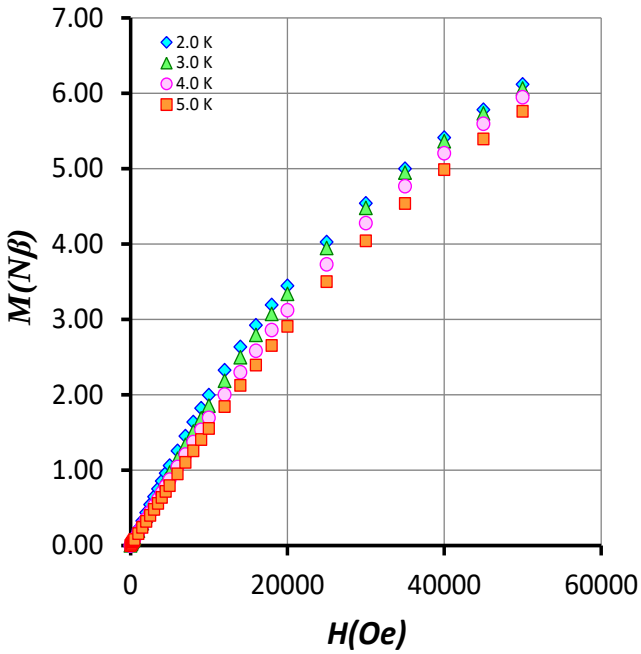

Figure S3.1 Field dependence of the magnetization of **18** at the indicated temperatures.

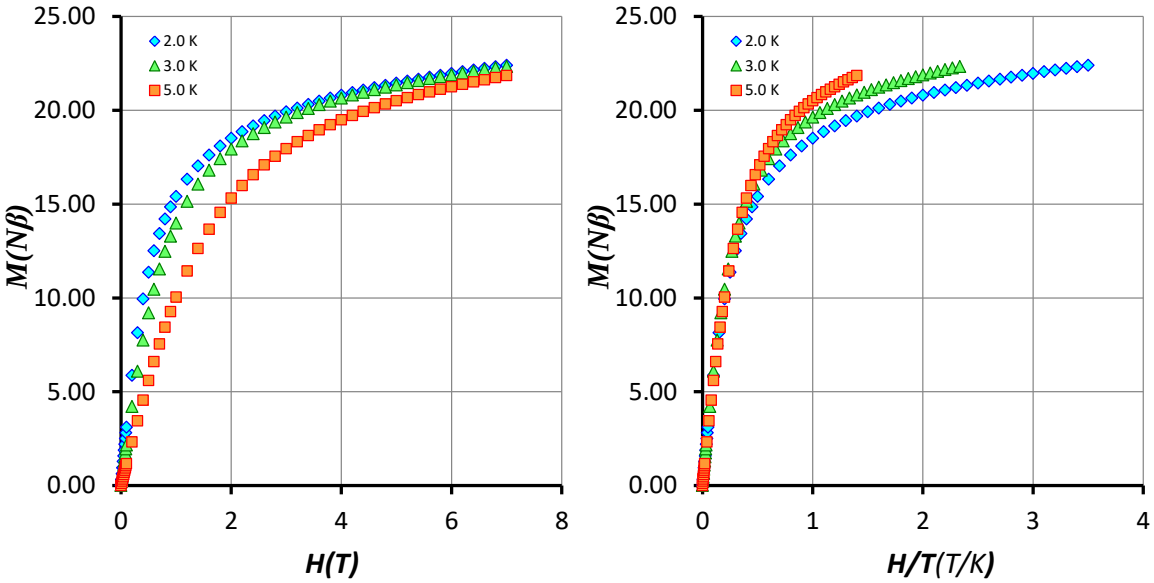

Figure S3.2 Field dependence of the magnetization and reduced magnetization for **16** at the indicated temperatures.

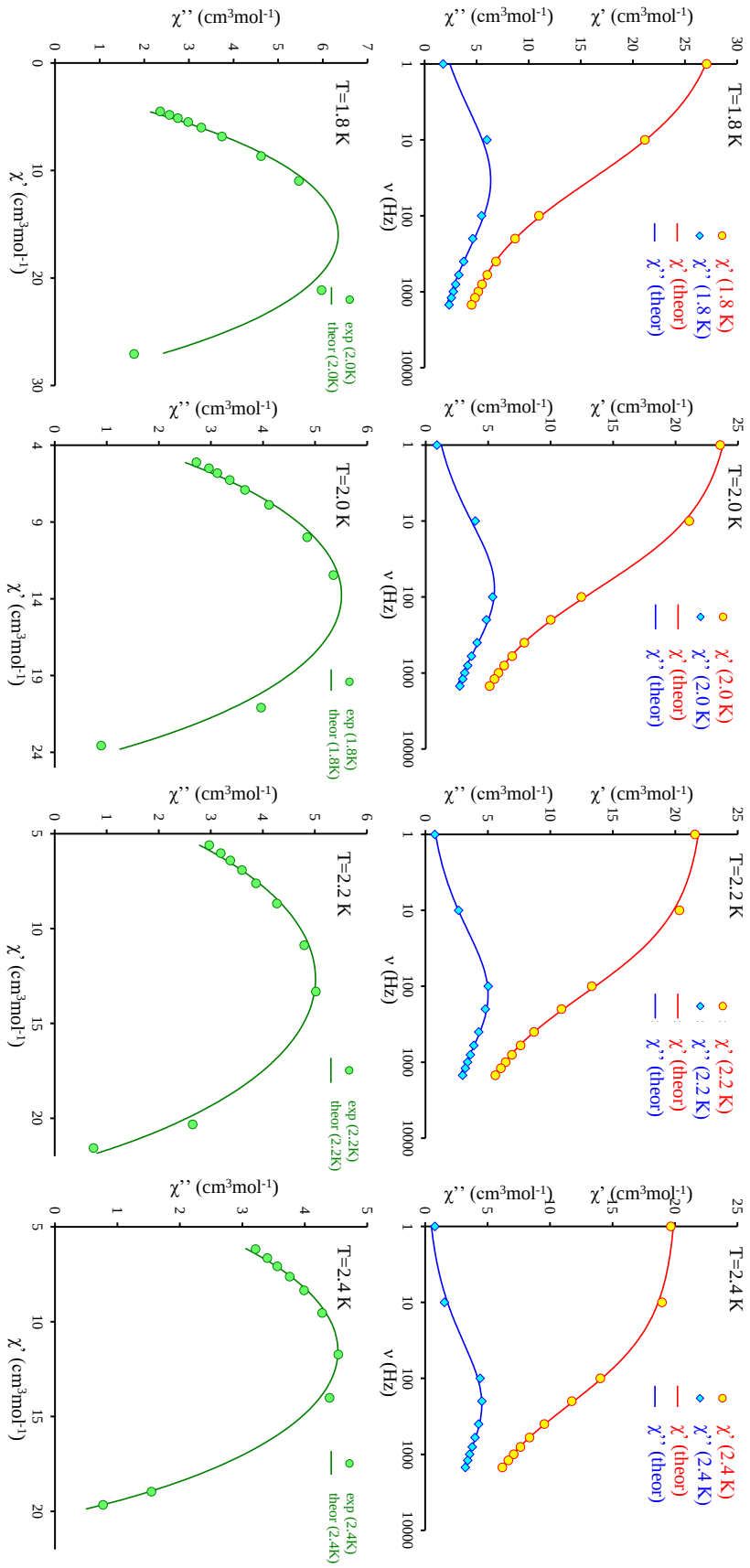

Figure S3.3. In-phase (χ' red) and out-of-phase (χ'' blue) *ac* susceptibility *versus* frequency and Cole-Cole plot (green) for **17** (Co_4Dy_2) at indicated temperatures. The solid line is a least-squares fitting of the data to a generalized Debye model.

Appendix B - Supporting data and supplemental material.

For supporting data, supplemental Figures, tables and schemes (SX), see attached CD.

Catalytic and topological aspects of Schiff Base supported 3d-4f polynuclear coordination complexes

Kieran Griffiths

Degree of Doctor of Philosophy

University of Sussex

June 2017

Appendix B

Table of Contents

Chapter 1

1.1 ^{1}H NMR and ^{13}C NMR of ligands (H_2L1-H_2L29)

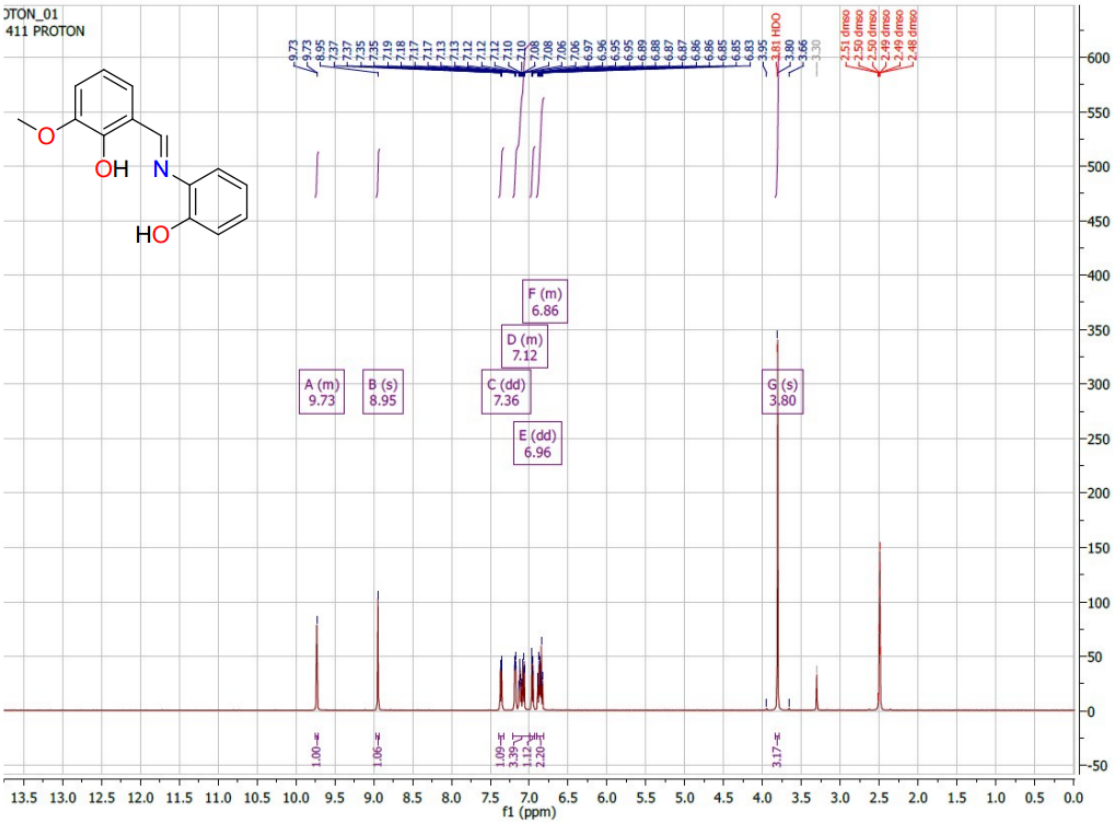

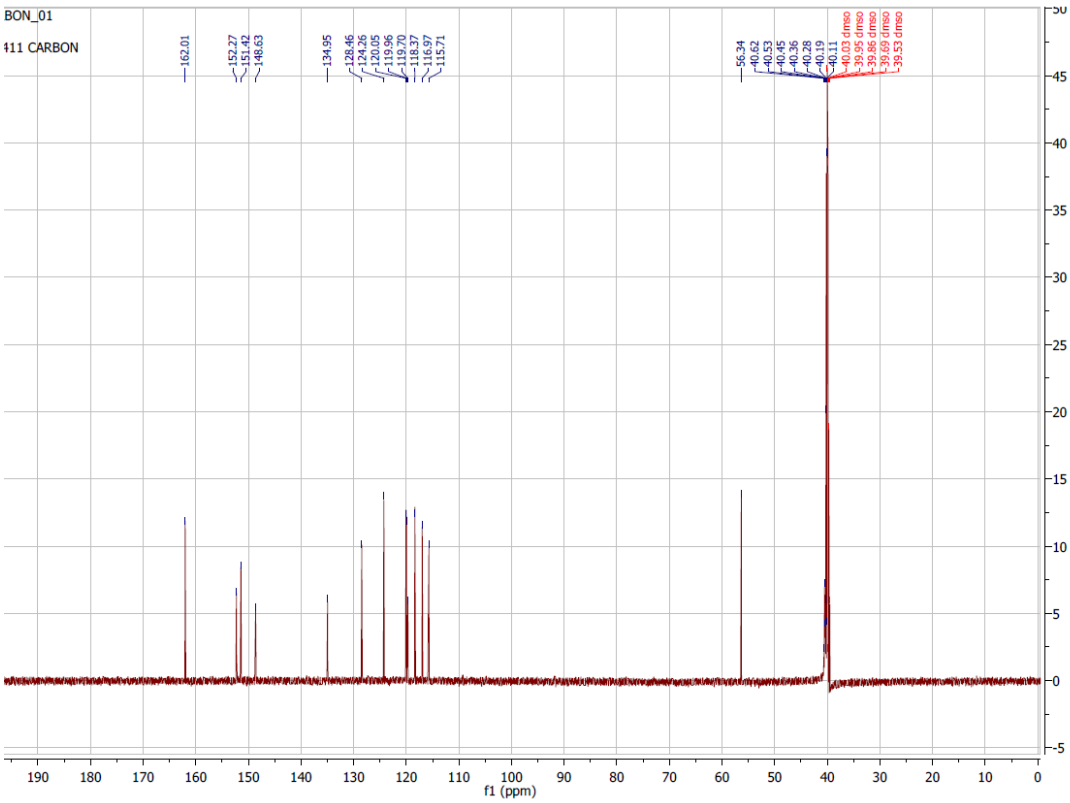

S1.1 (Top) ^{1}H NMR of H_2**L1. (**Bottom**)** ^{13}C NMR of H_2**L1**.

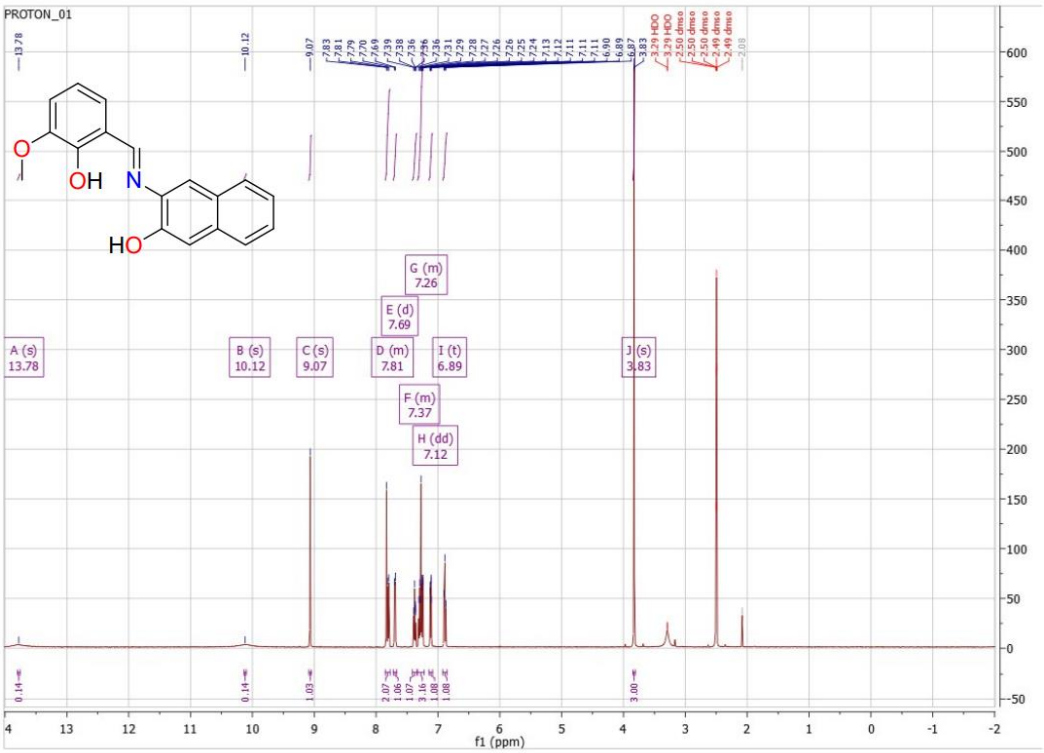

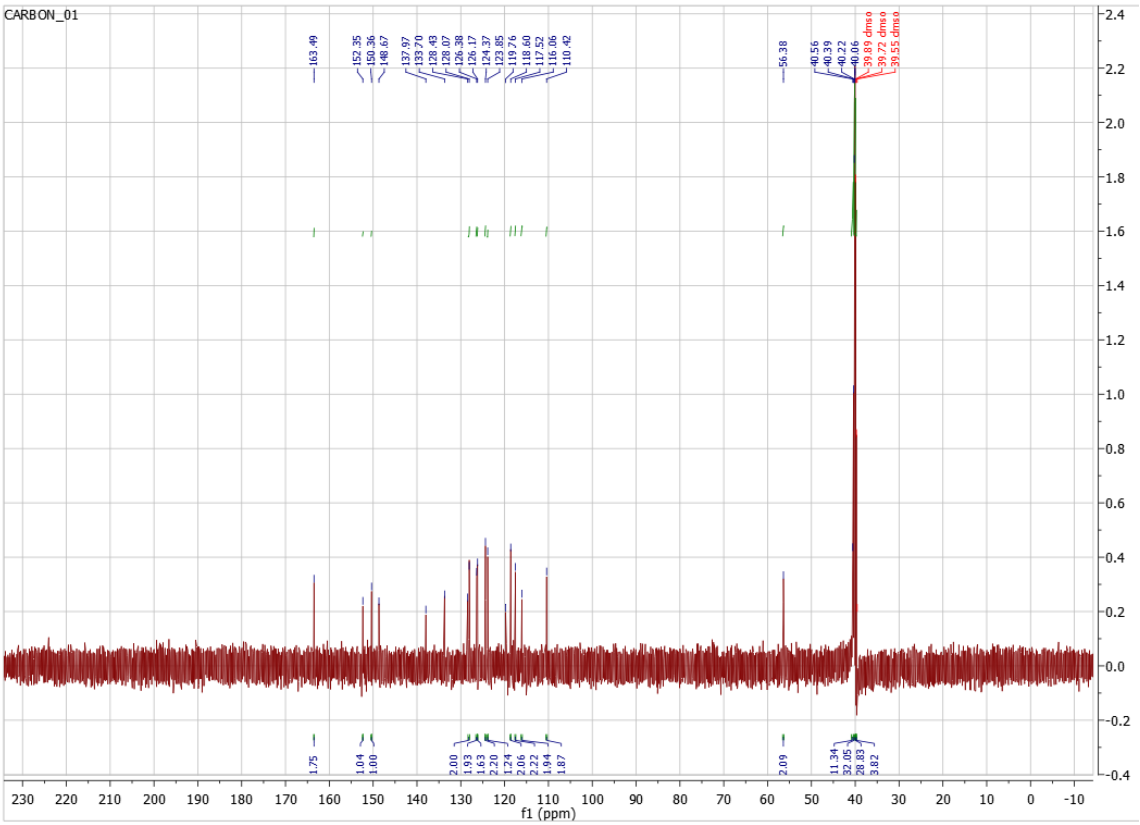

S1.2 (Top) ^{1}H NMR of H_2**L2** **(**Bottom**)** ^{13}C NMR of H_2**L2**

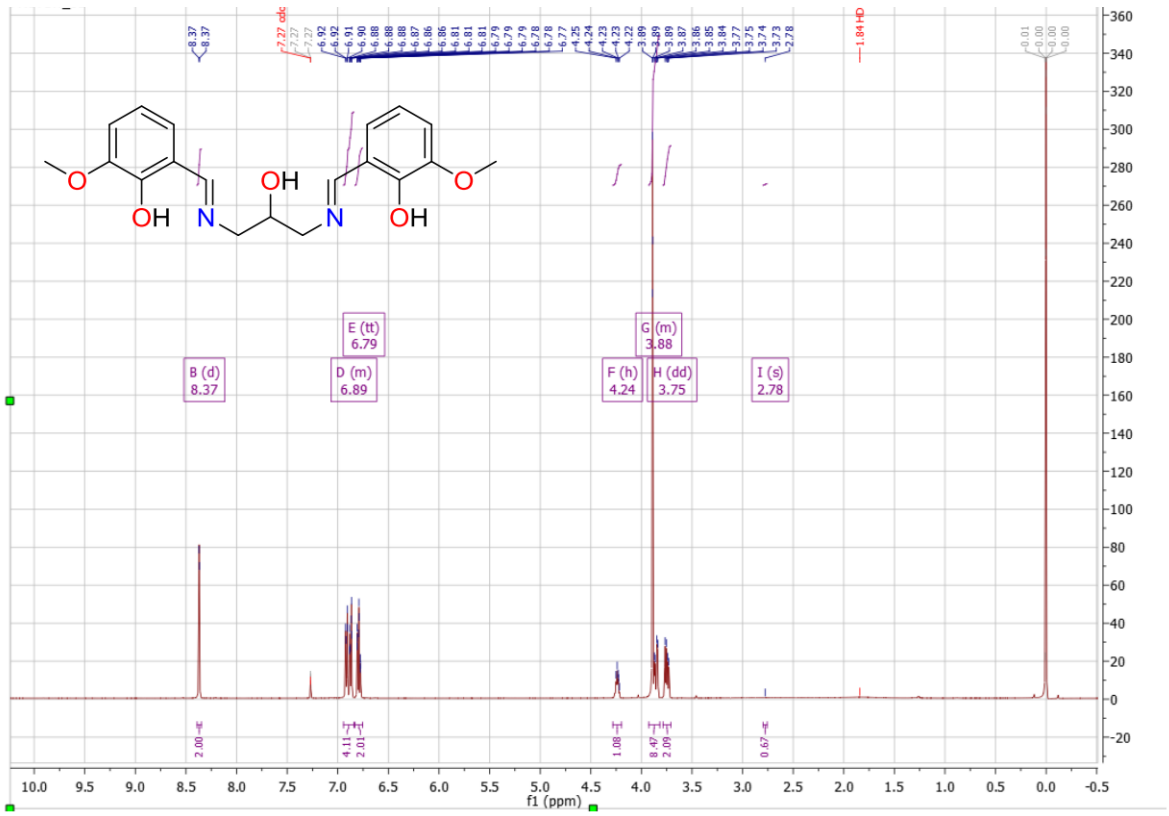

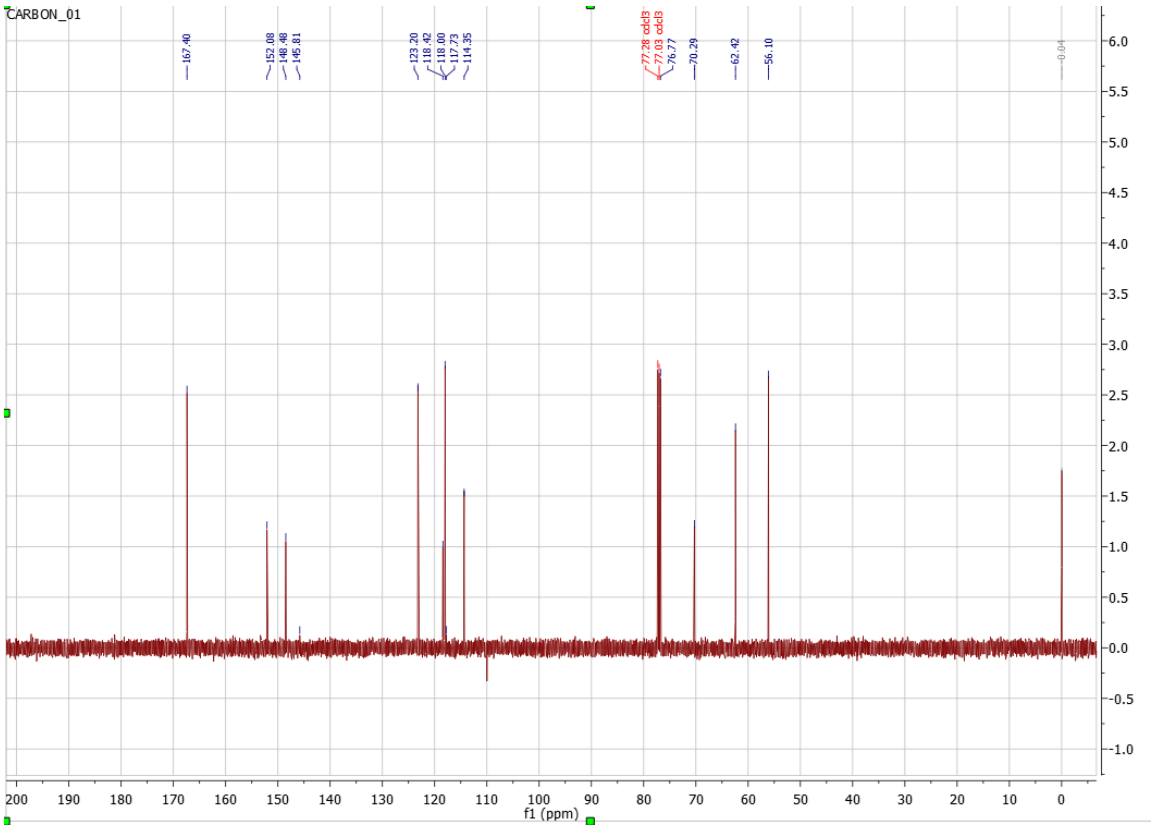

S1.3 (Top) ^{1}H NMR of H_3**L3 (**Bottom**)** ^{13}C NMR of H_3**L3**

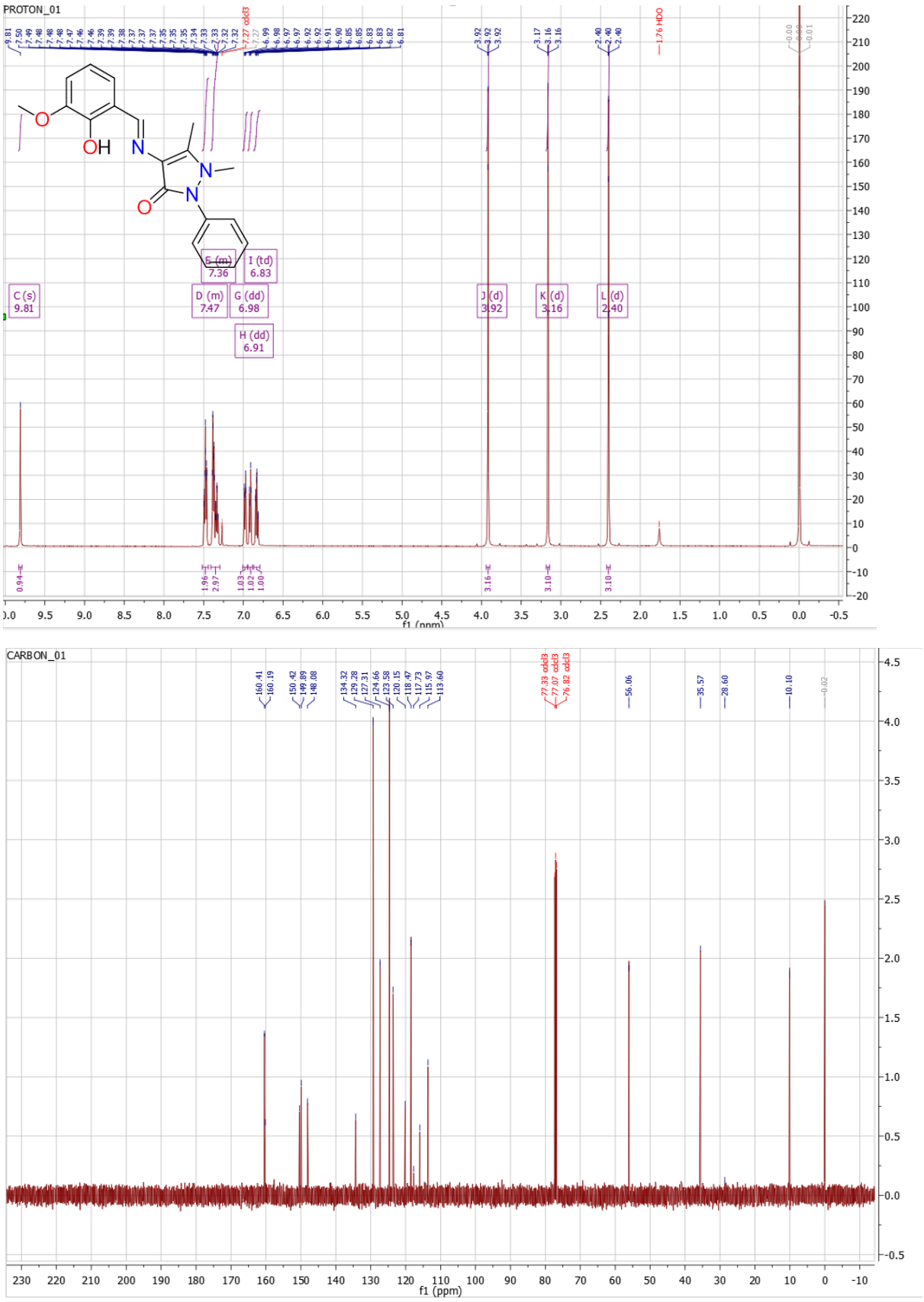

S1.4 (Top) ^{1}H NMR of H**L4** (Bottom) ^{13}C NMR of H**L4**

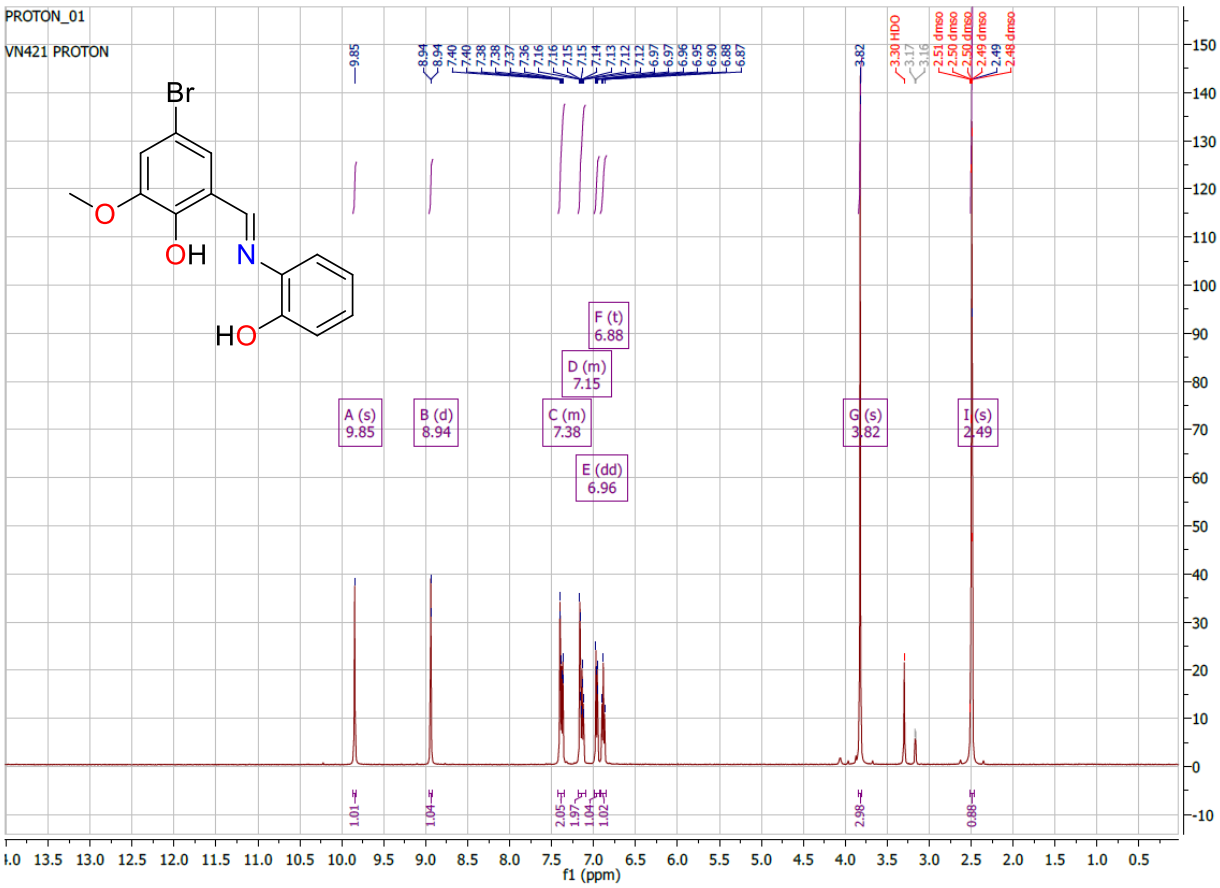

S1.5. ^{1}H NMR of H_2**L5**

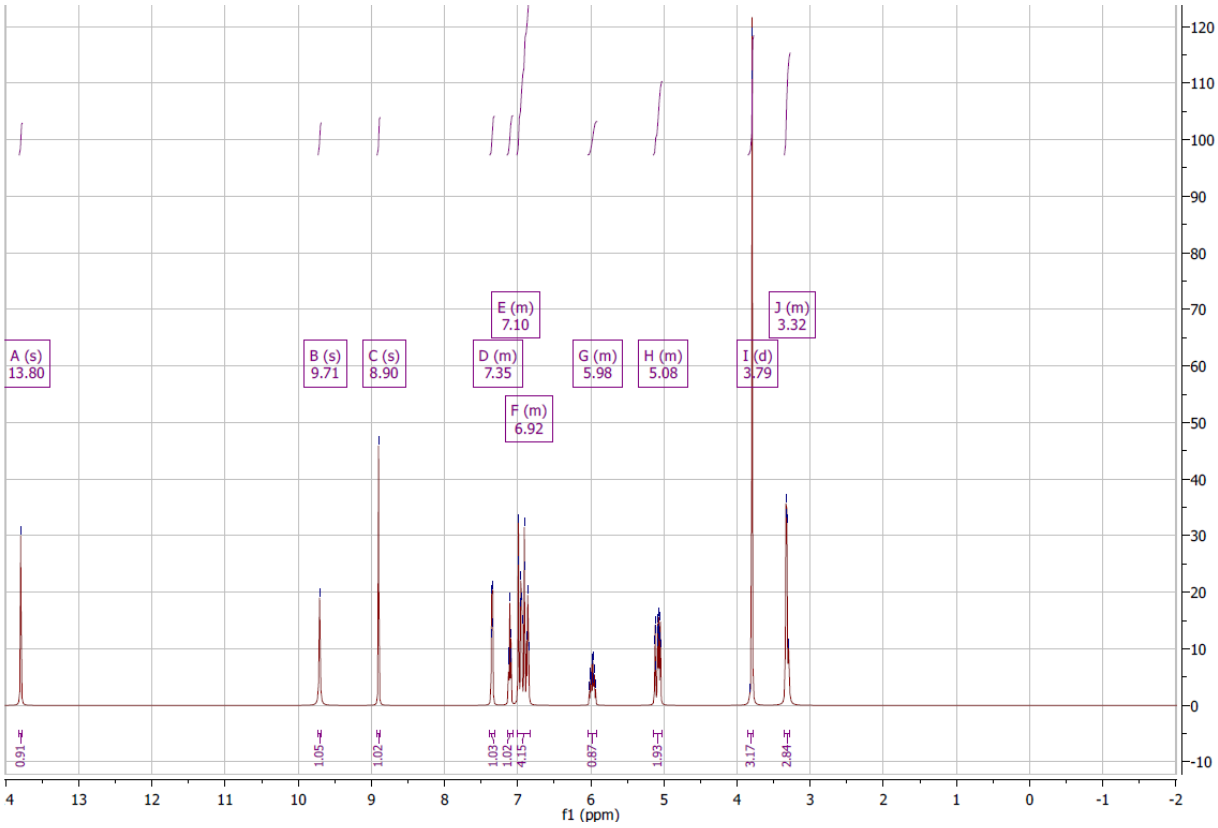

S1.6. ^{1}H NMR of H_2**L6**

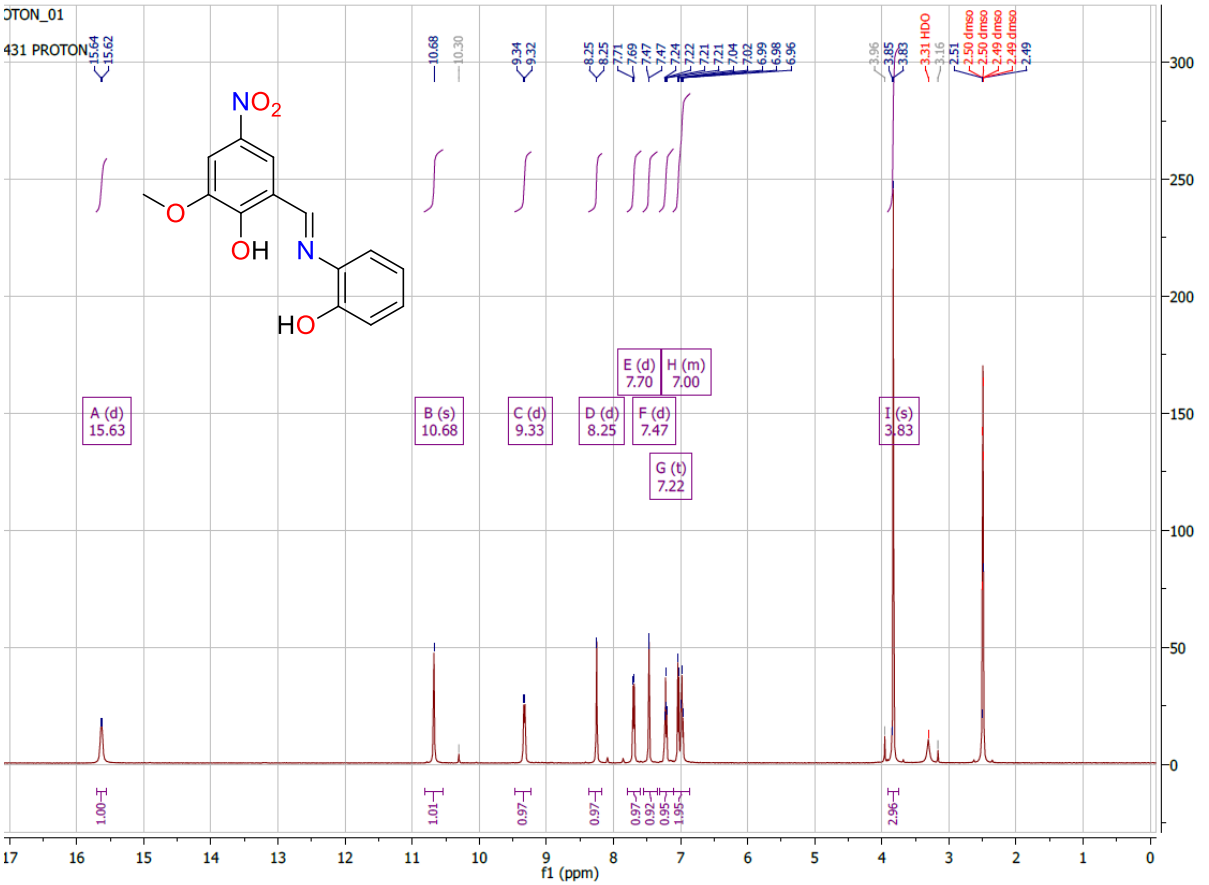

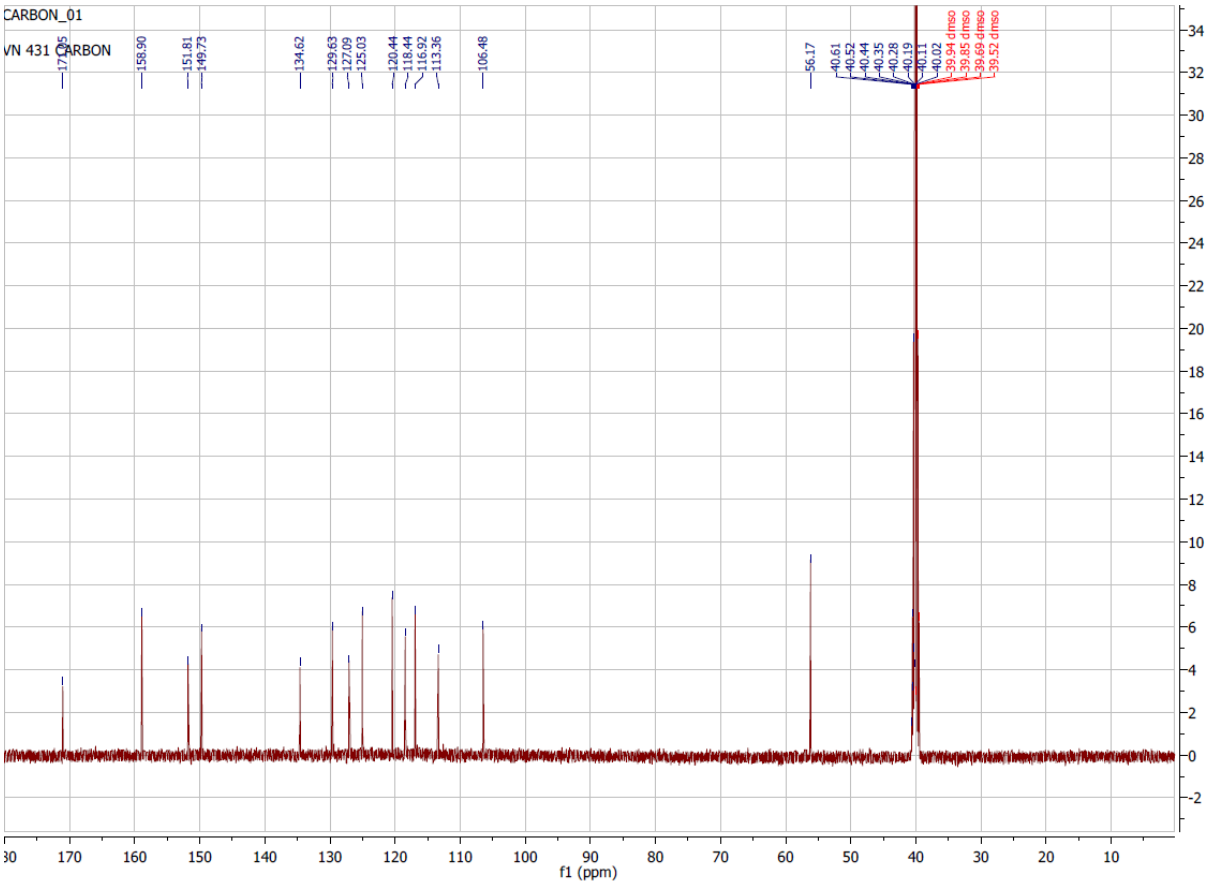

S1.7. (Top) ^{1}H NMR of H_2**L2** (Bottom) ^{13}C NMR of H_2**L7**

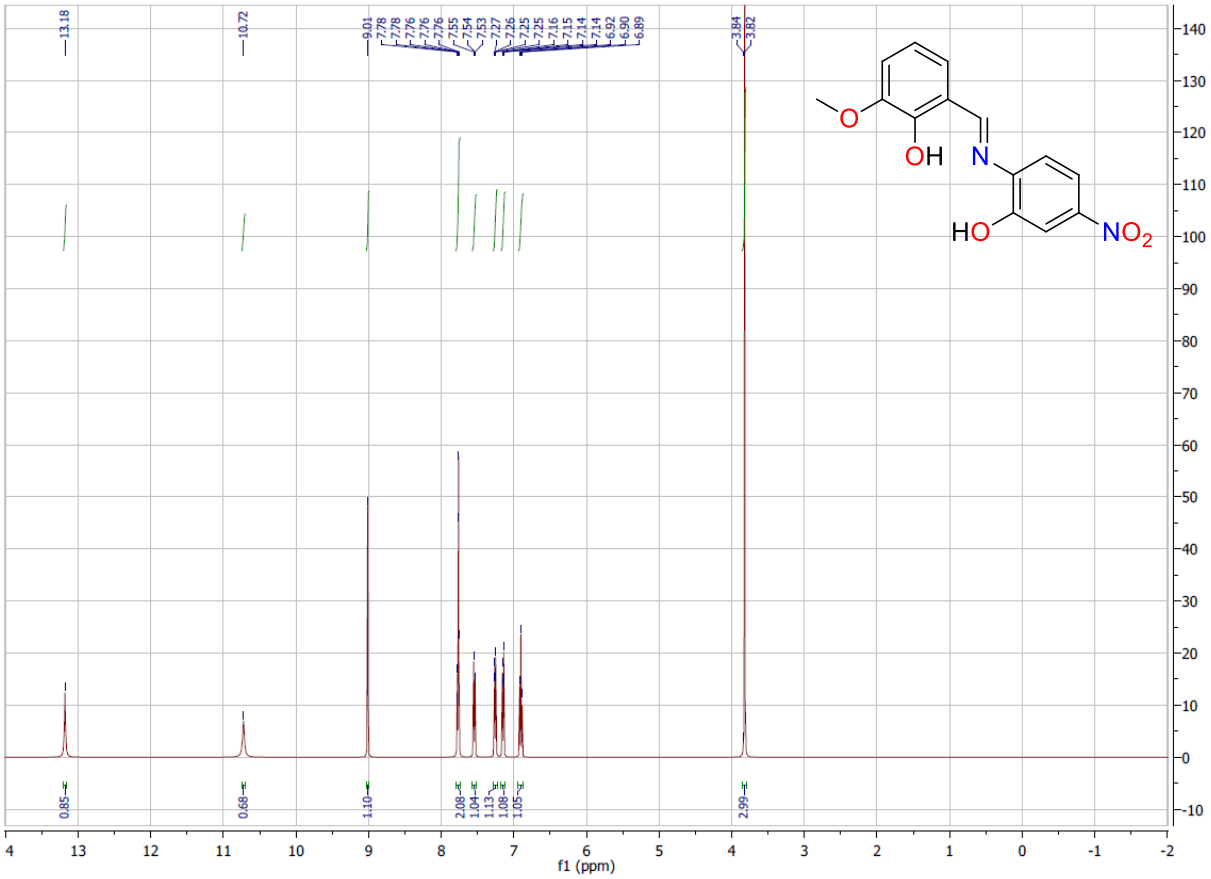

S1.8. ^{1}H NMR of H_2**L8**.

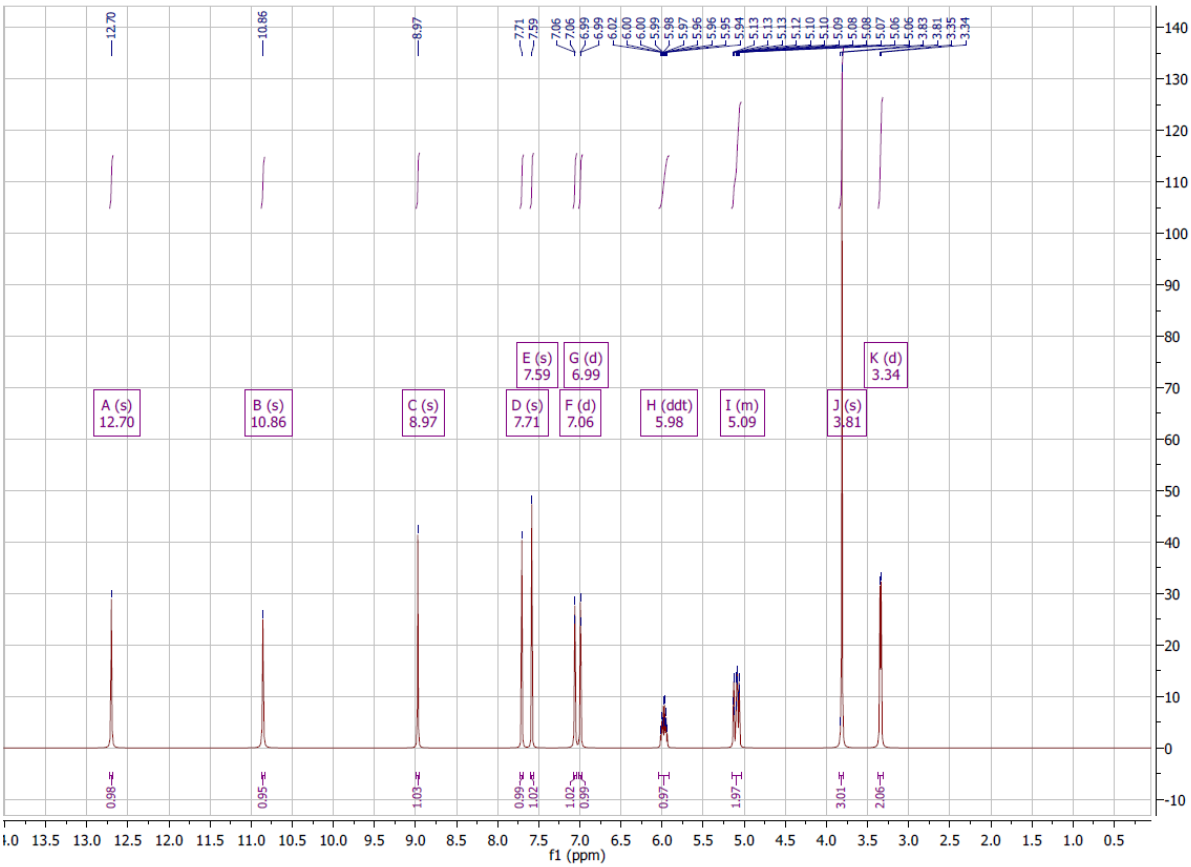

S1.9. ^{1}H NMR of H_2**L9**

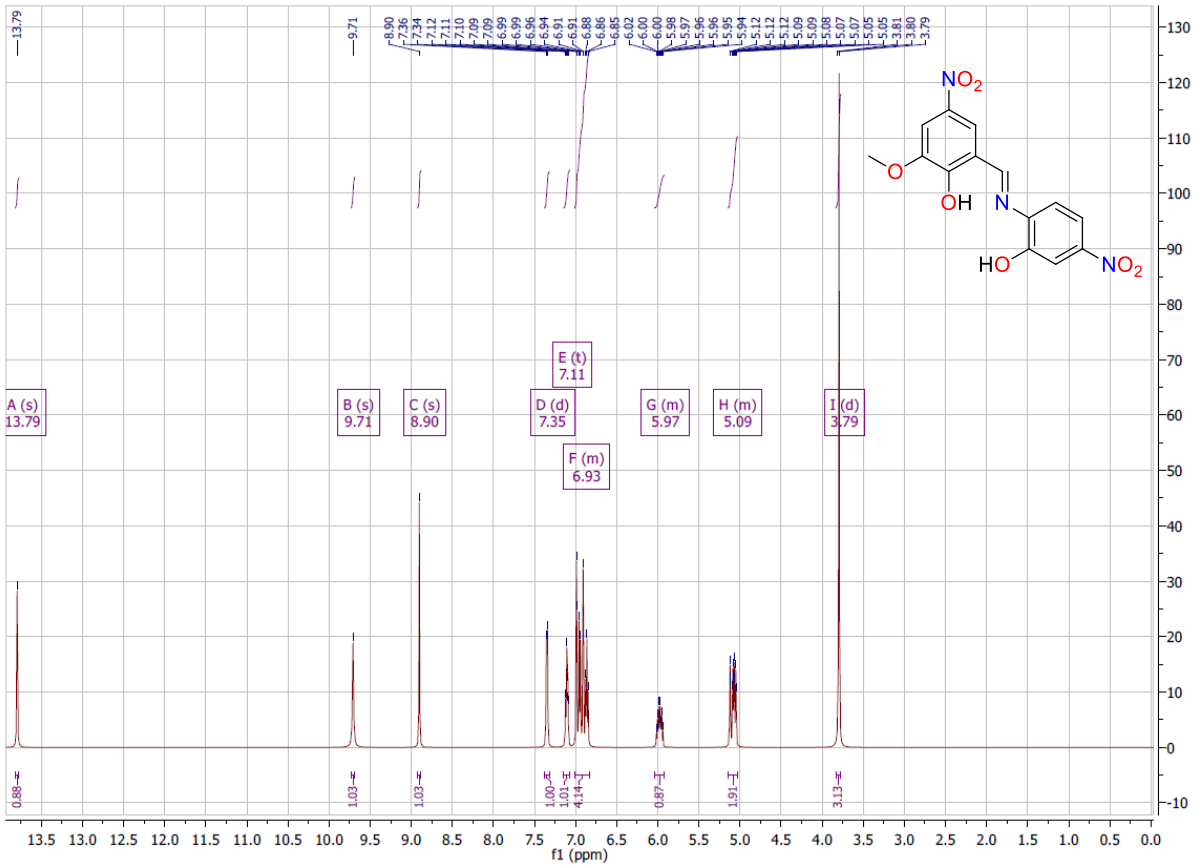

S1.10. ^{1}H NMR of H_2**L10**

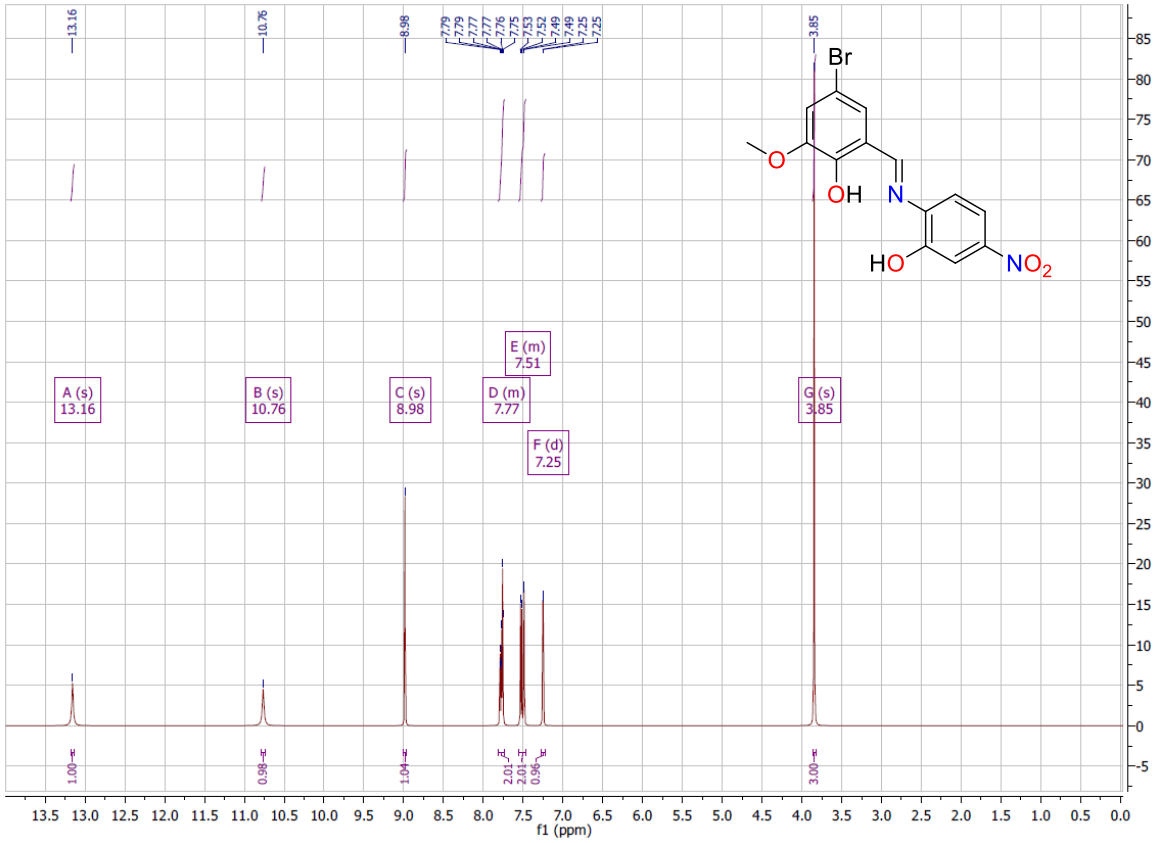

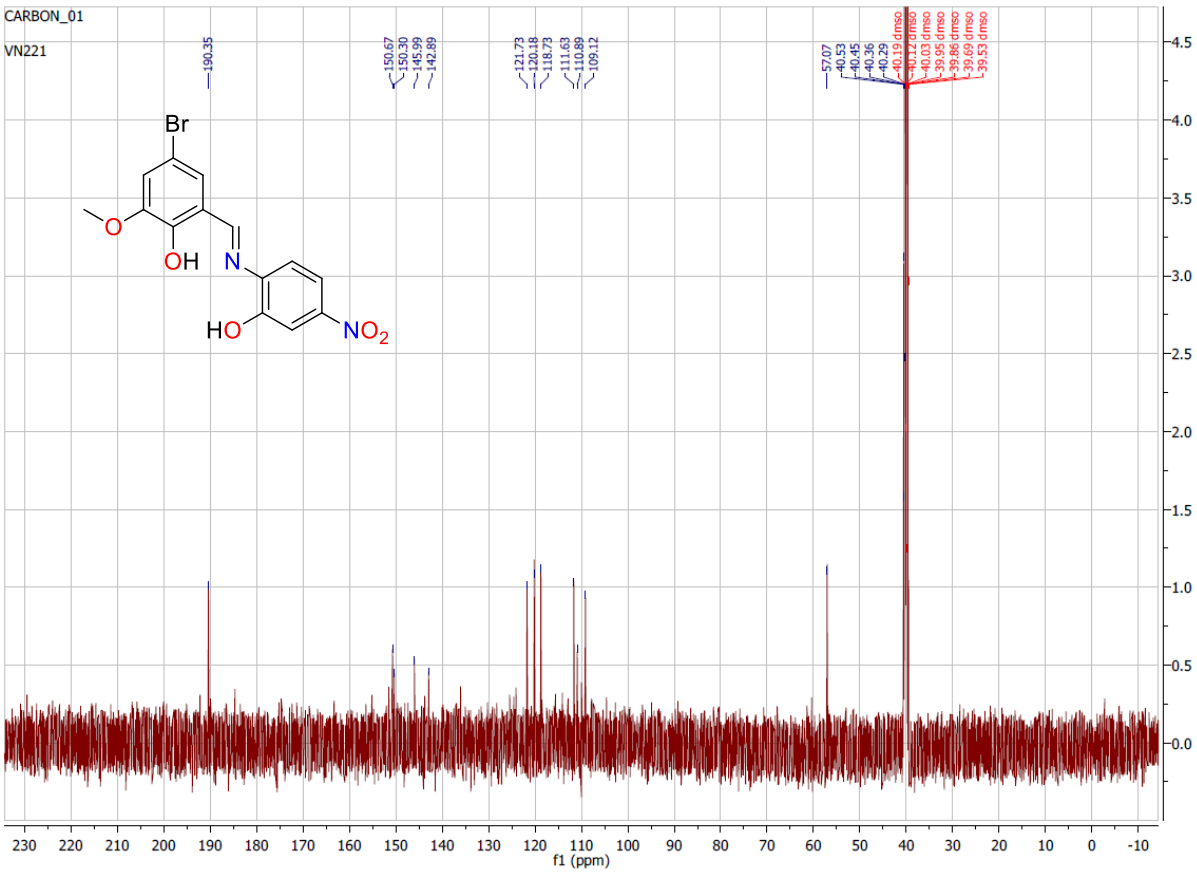

S1.11. (Top) ^{1}H NMR of H_2**L11** **(**Bottom**)** ^{13}C NMR of H_2**L11**

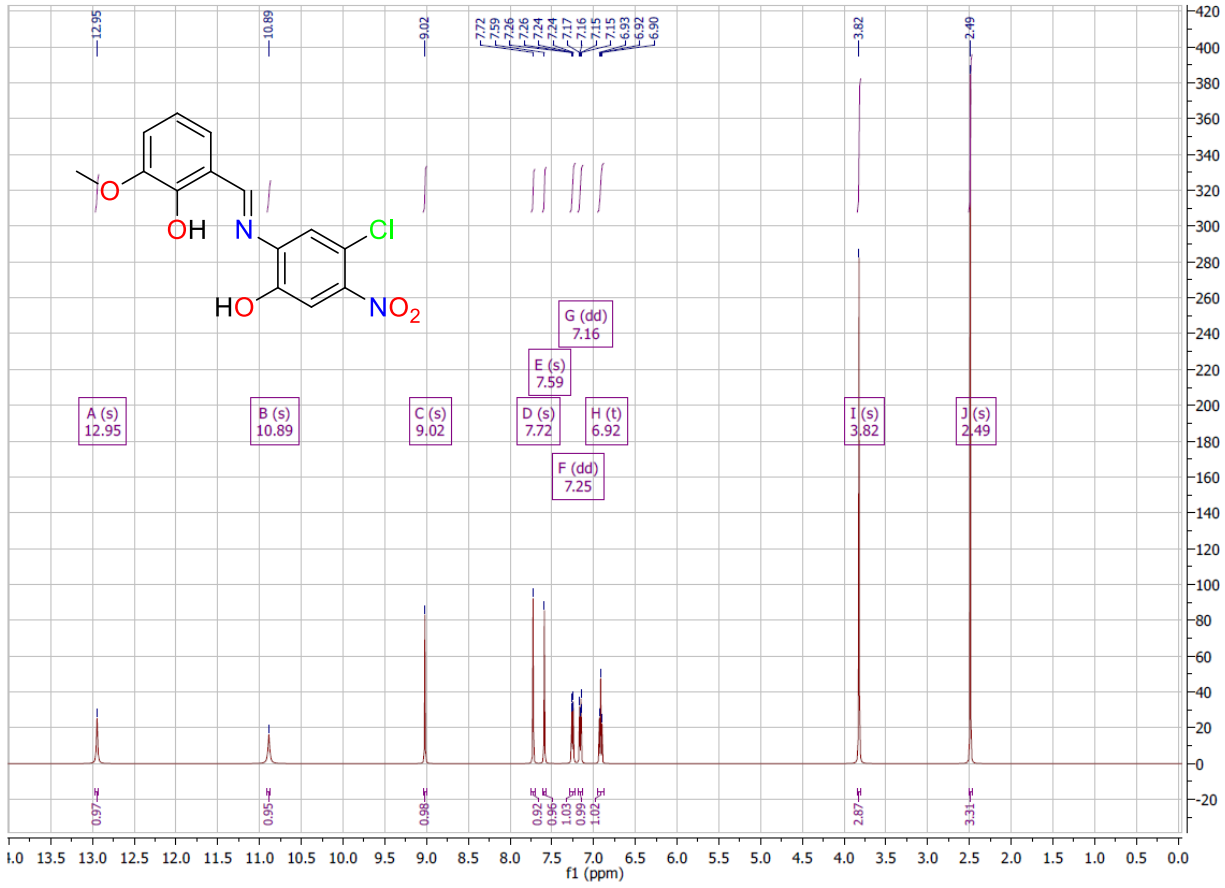

#

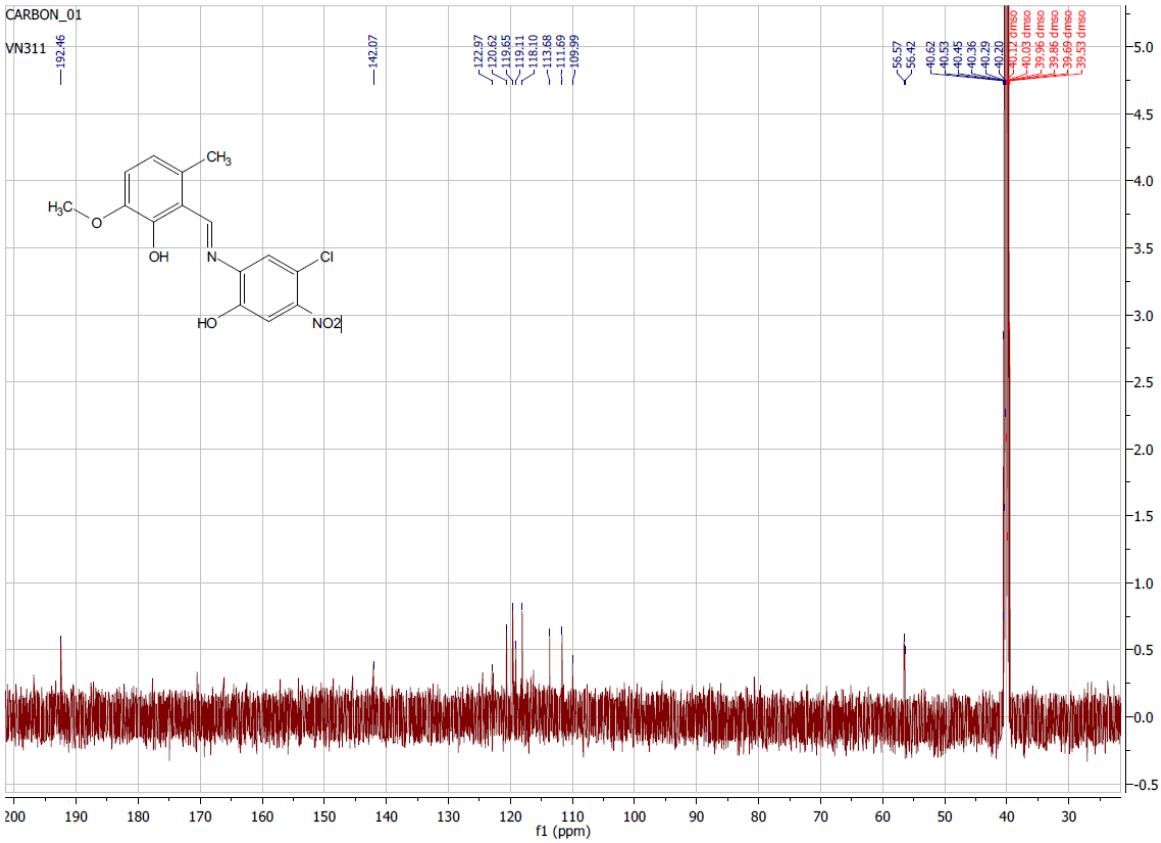

S1.12. (Top) ^{1}H NMR of H_2**L12** (Bottom) ^{13}C NMR of H_2**L12**

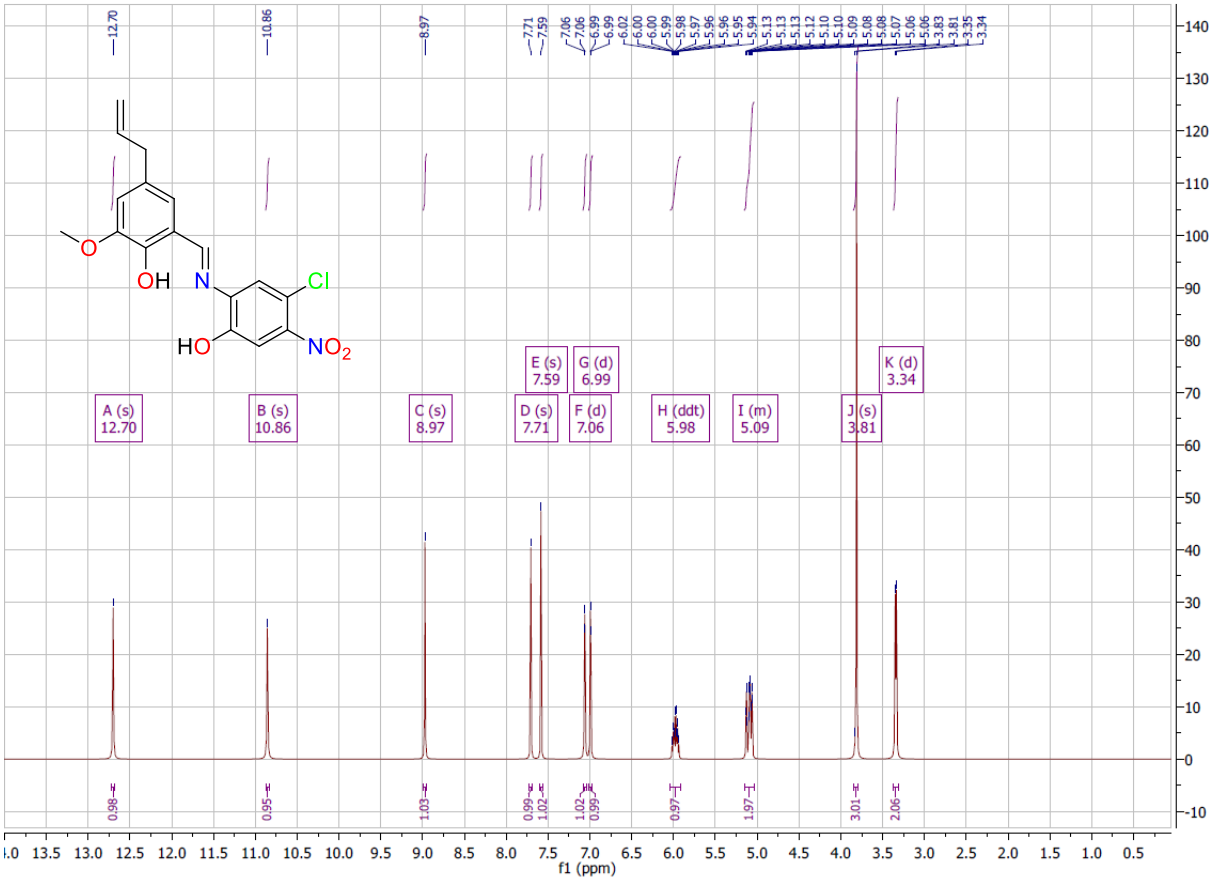

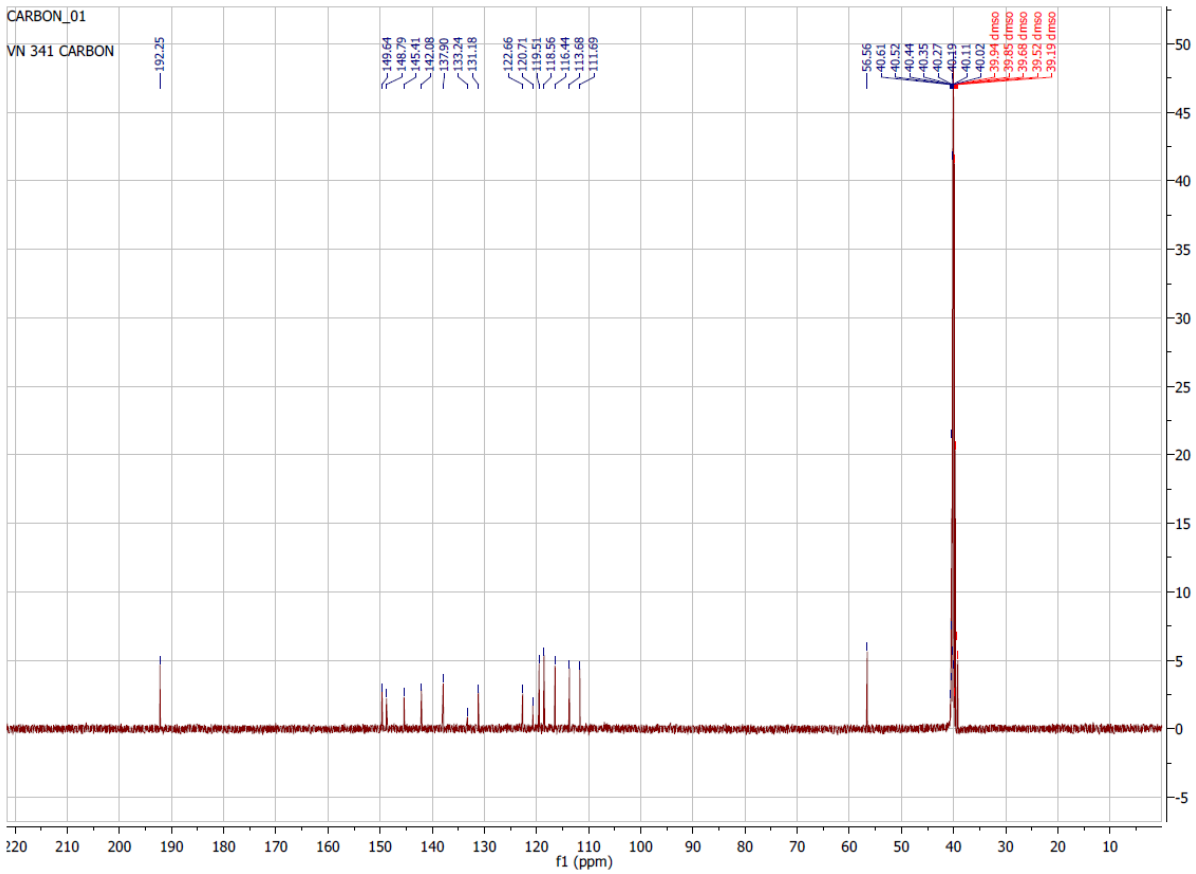

S1.13. (Top) ^{1}H NMR of H_2**L13** (Bottom) ^{13}C NMR of H_2**L13**

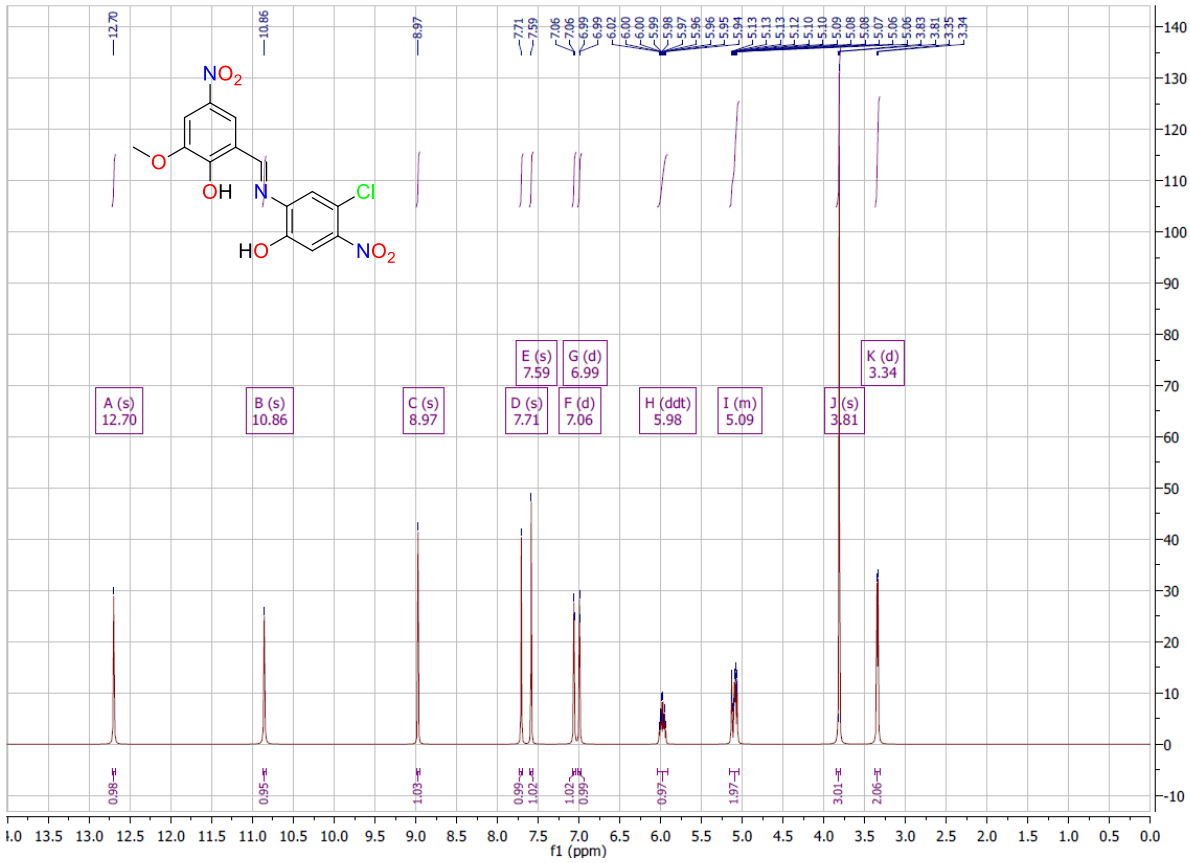

S1.14. ^{1}H NMR of H_2**L14**

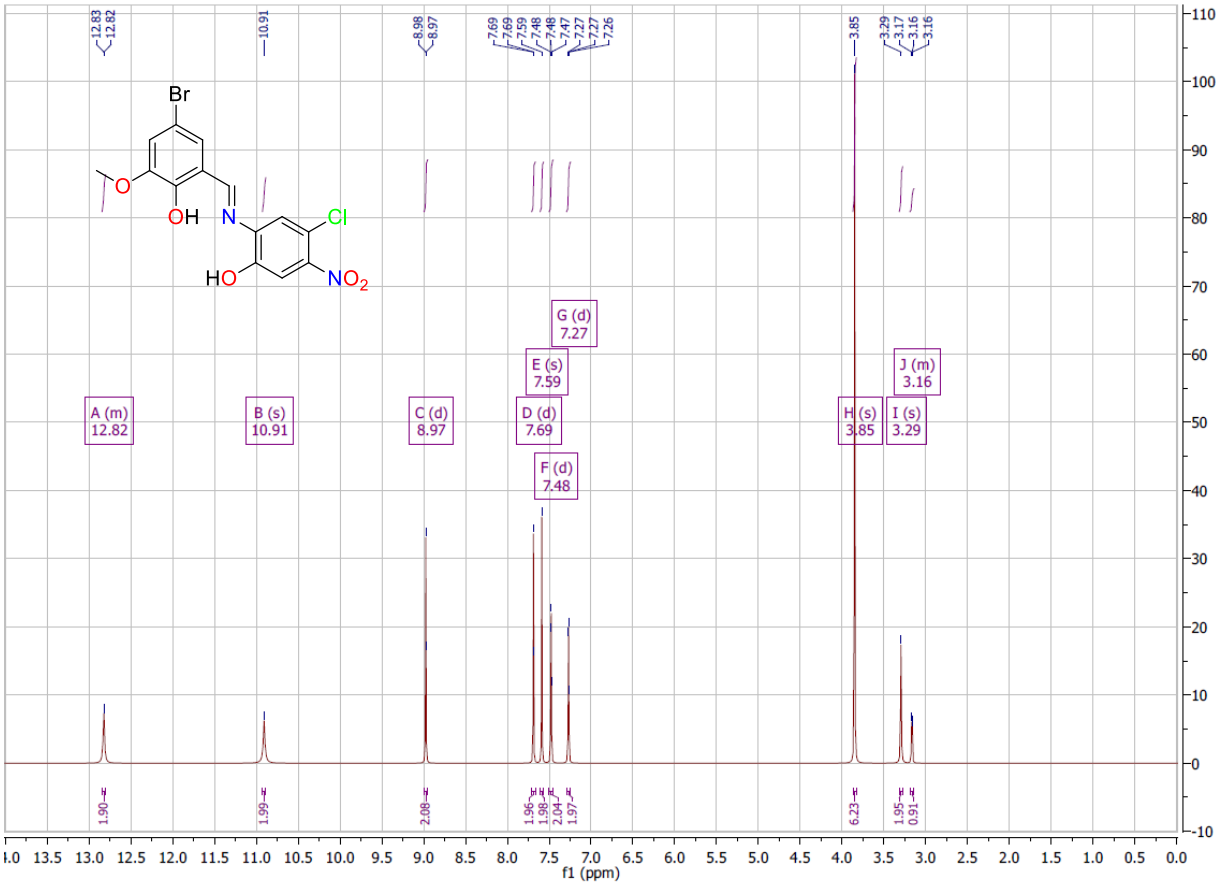

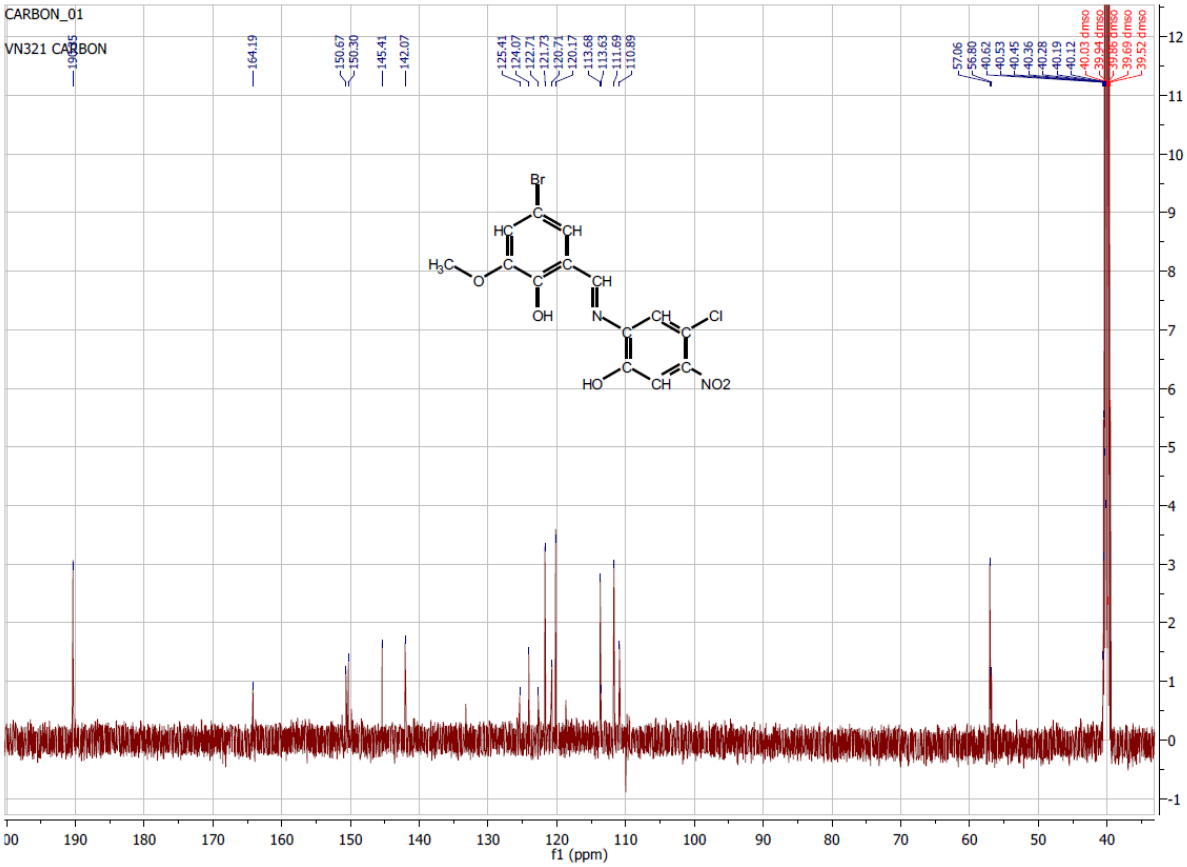

S1.15. (Top) ^{1}H NMR of H_2**L15** **(**Bottom**)** ^{13}C NMR of H_2**L15**

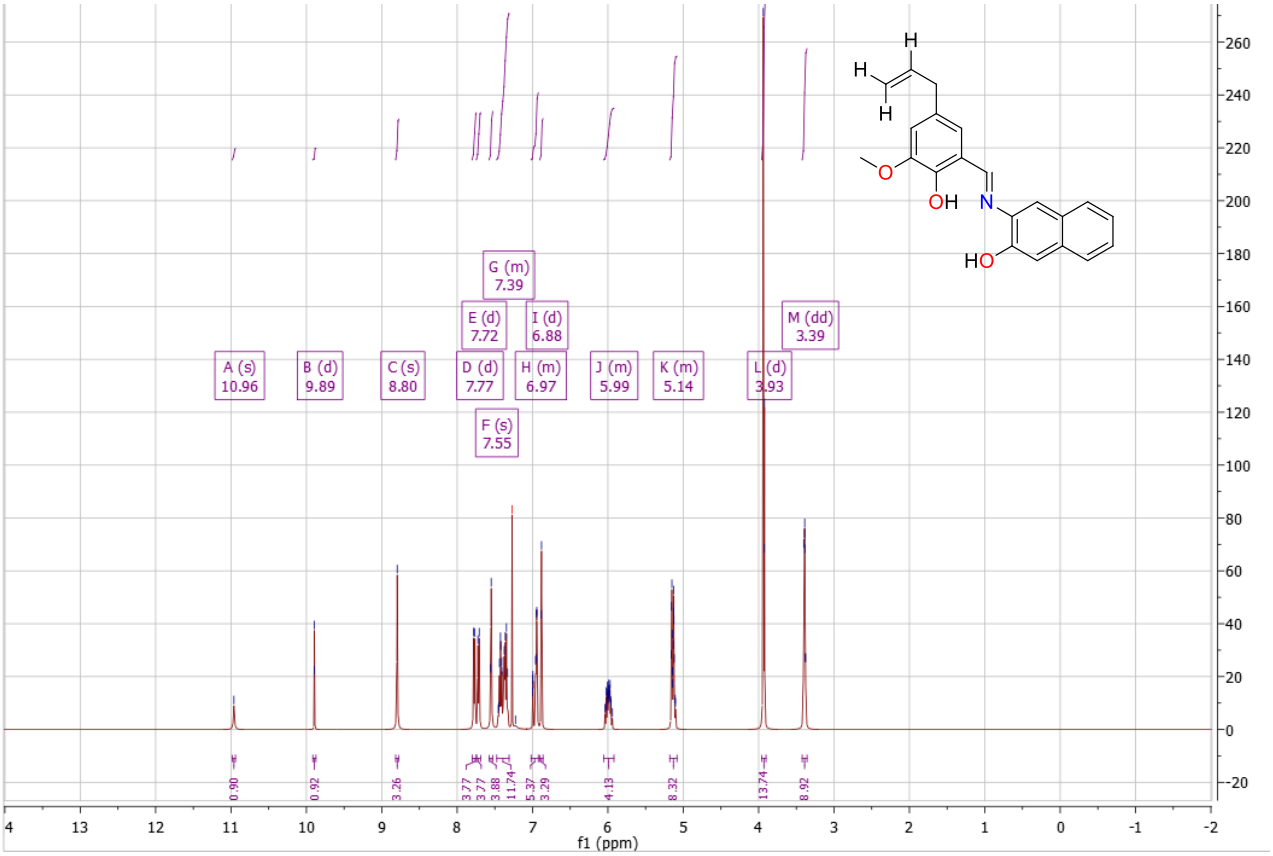

S1.16. ^{1}H NMR of H_2**L16**

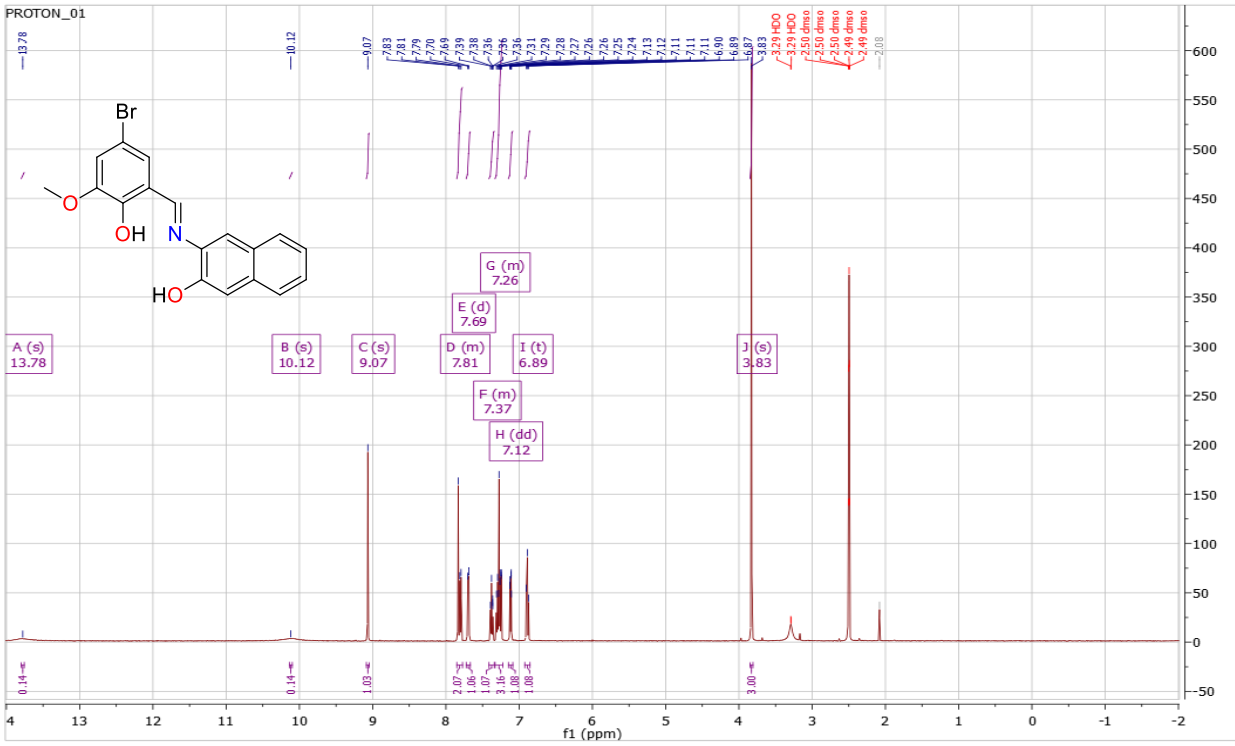

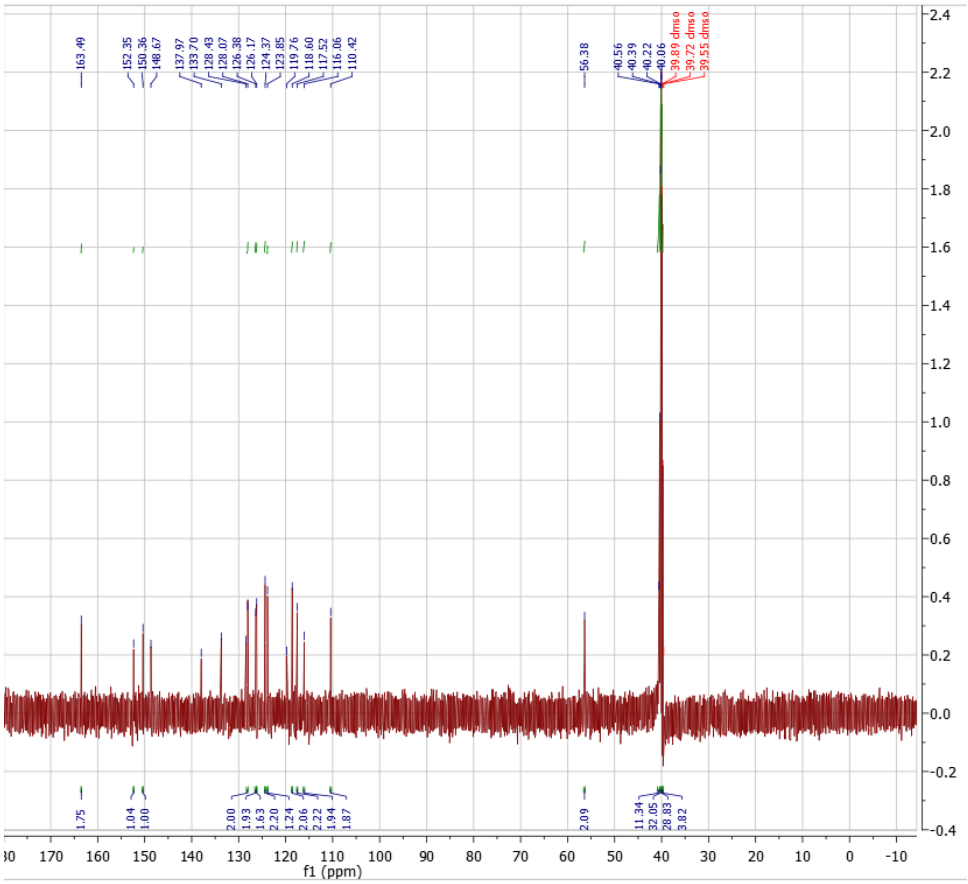

S1.17. (Top) ^{1}H NMR of H_2**L18 (**Bottom**)** ^{13}C NMR of H_2**L18.**

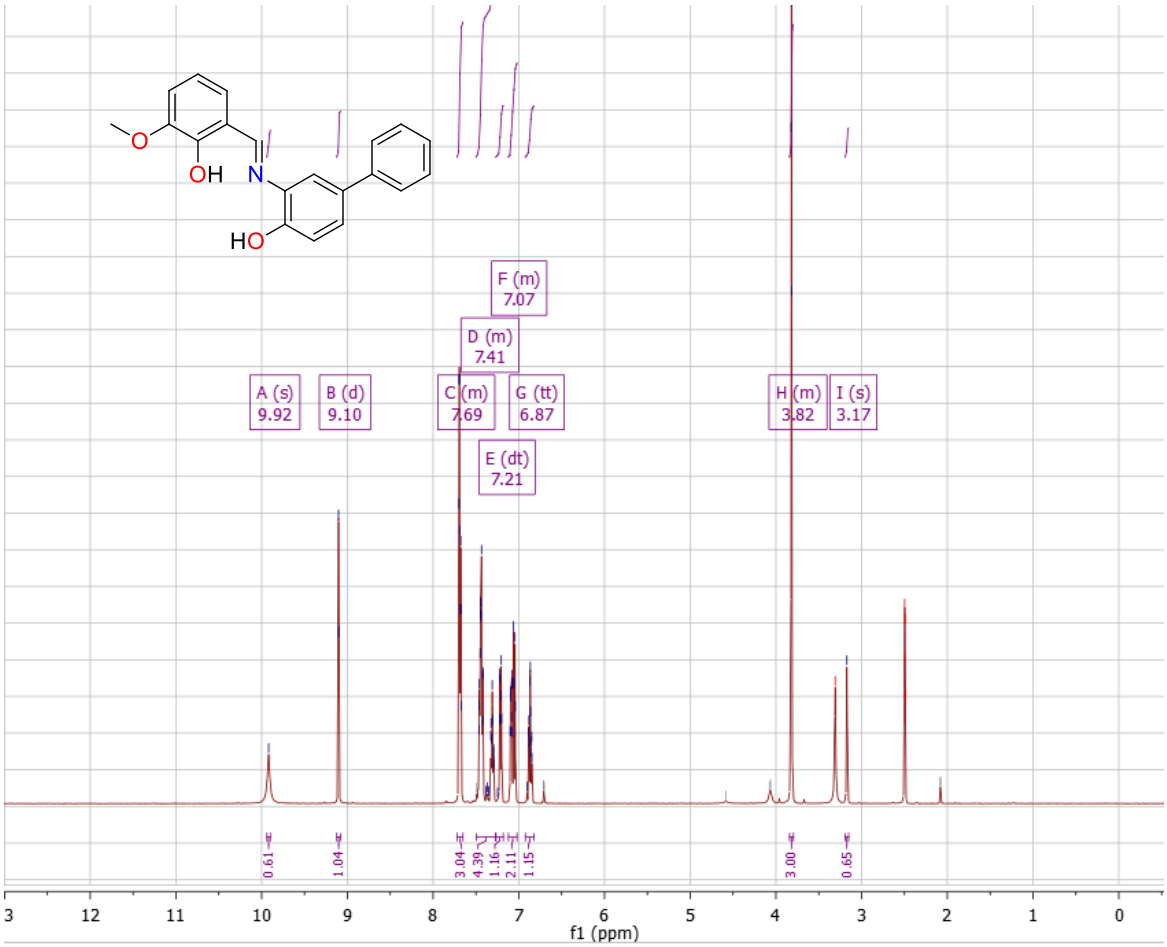

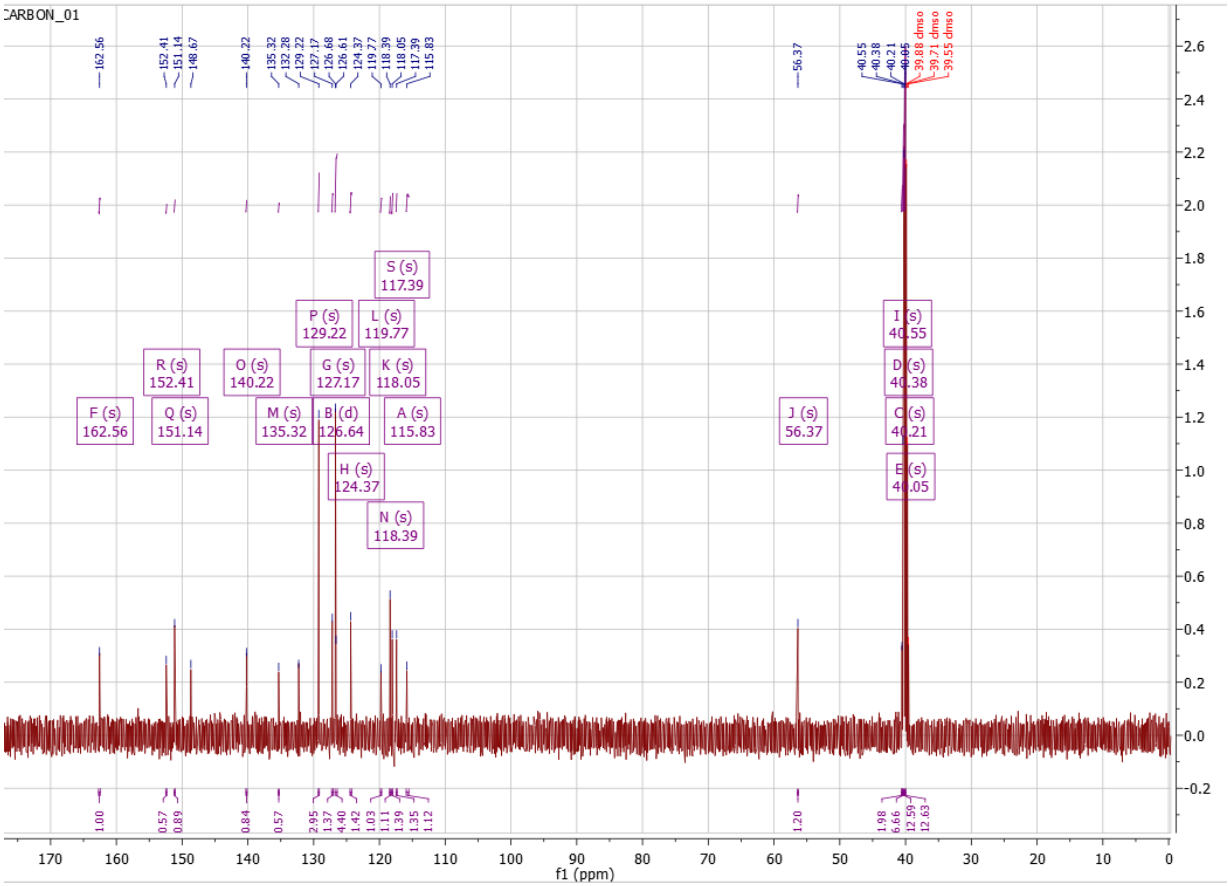

S1.18. (Top) ^{1}H NMR of H_2**L19 (**Bottom**).** ^{13}C NMR of H_2**L19.**

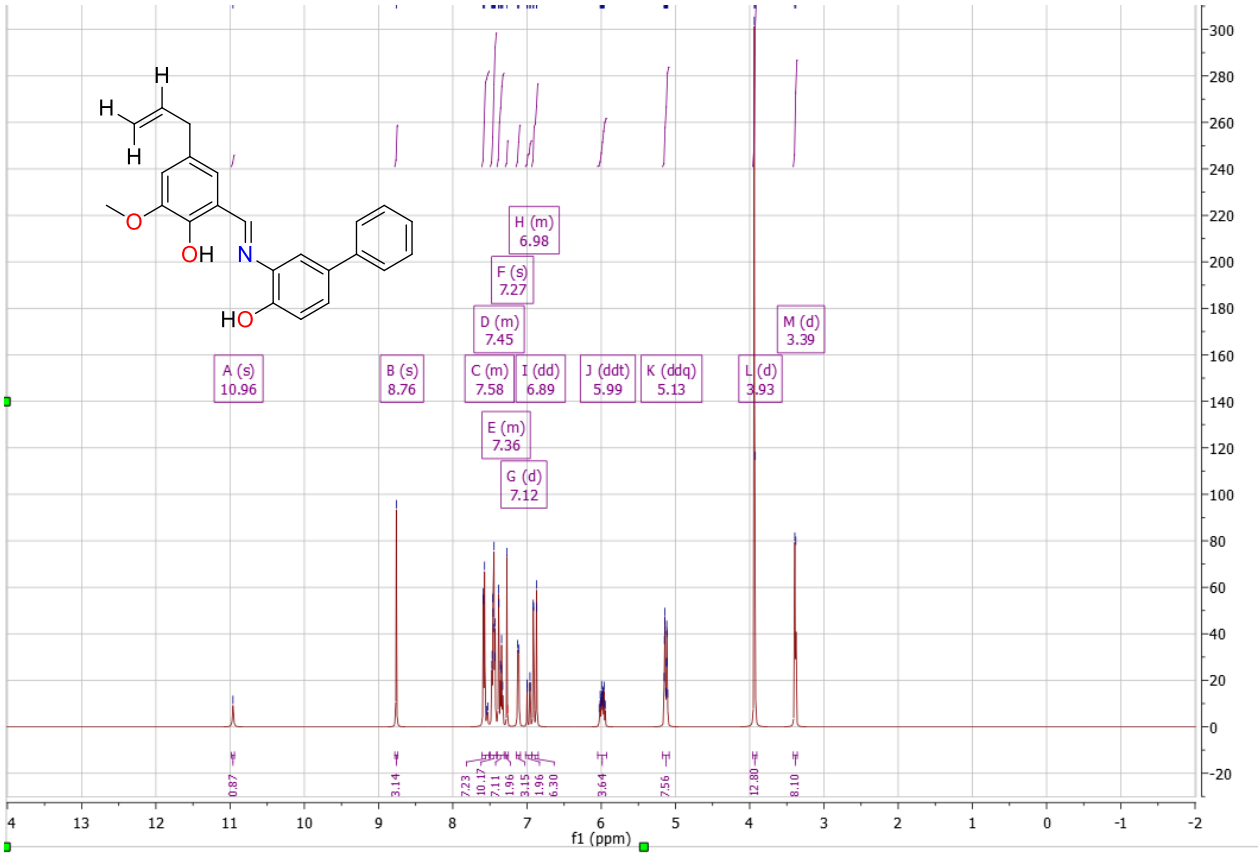

S1.19. ^{1}H NMR of H_2**L20**

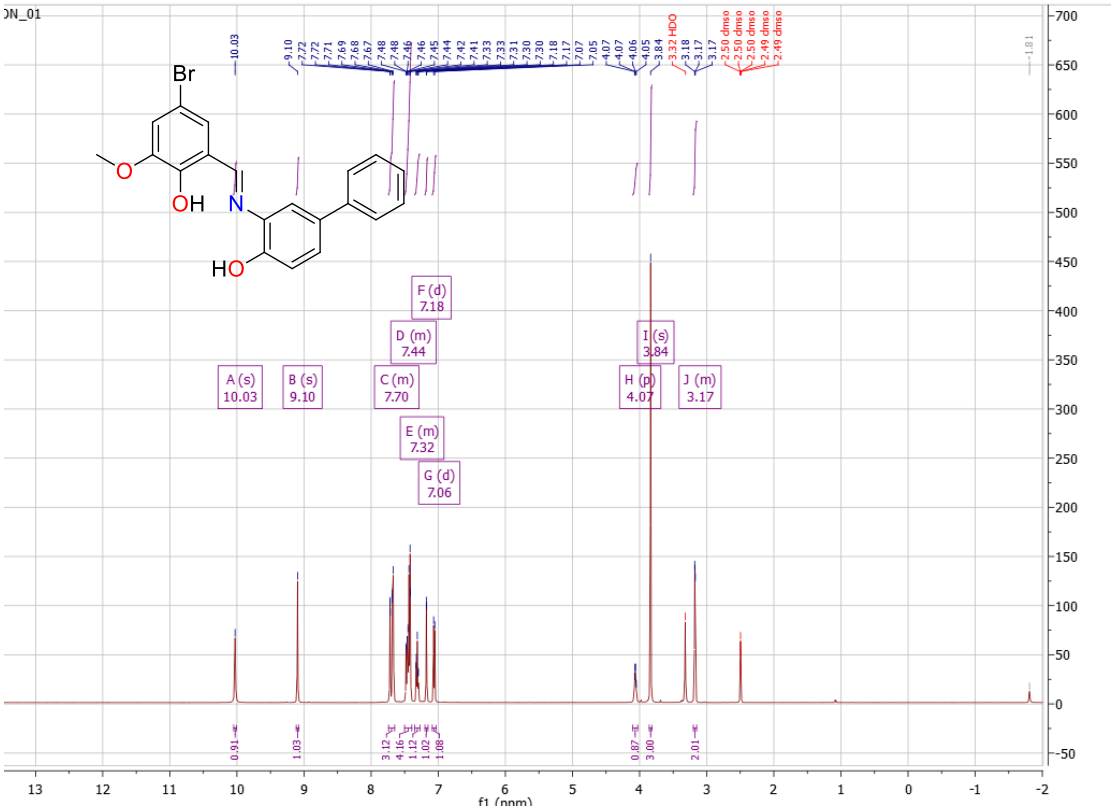

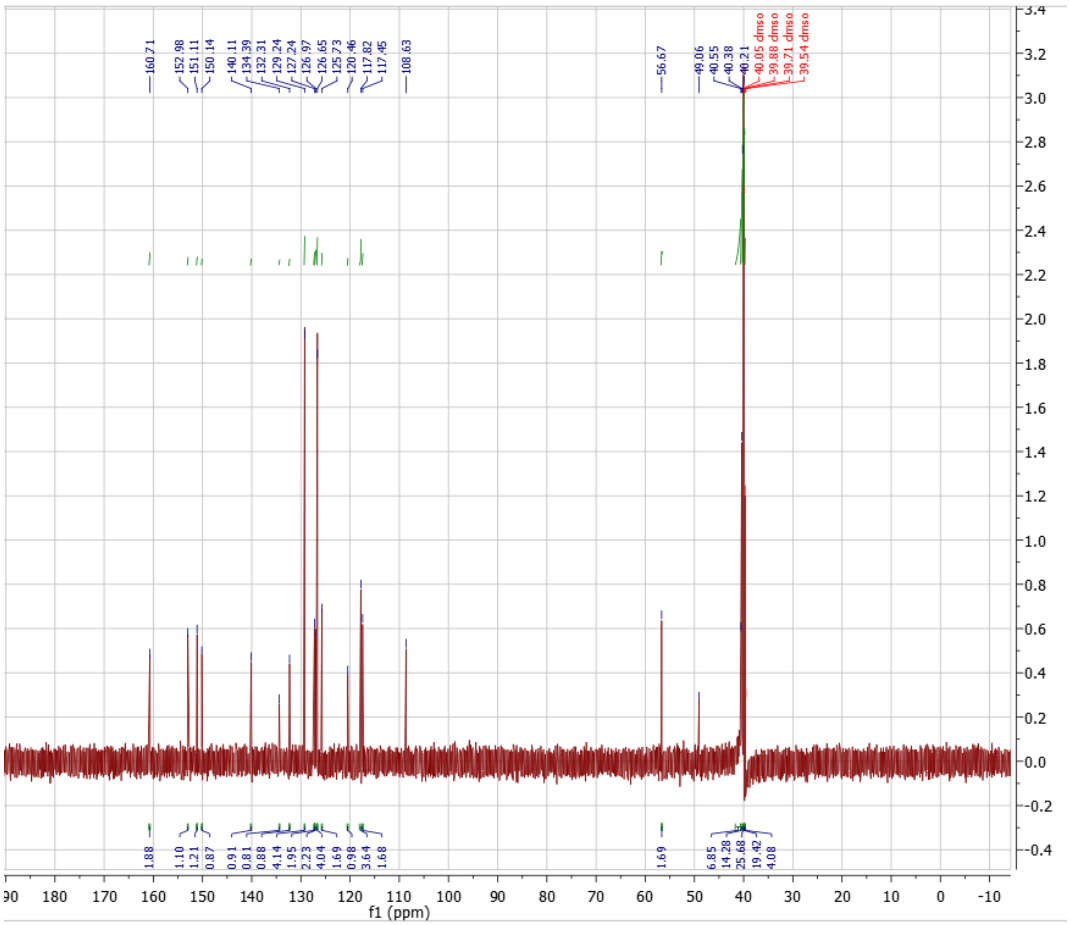

S1.20. (Top) ^{1}H NMR of H_2**L22** (Bottom) ^{13}C NMR of H_2**L22.**

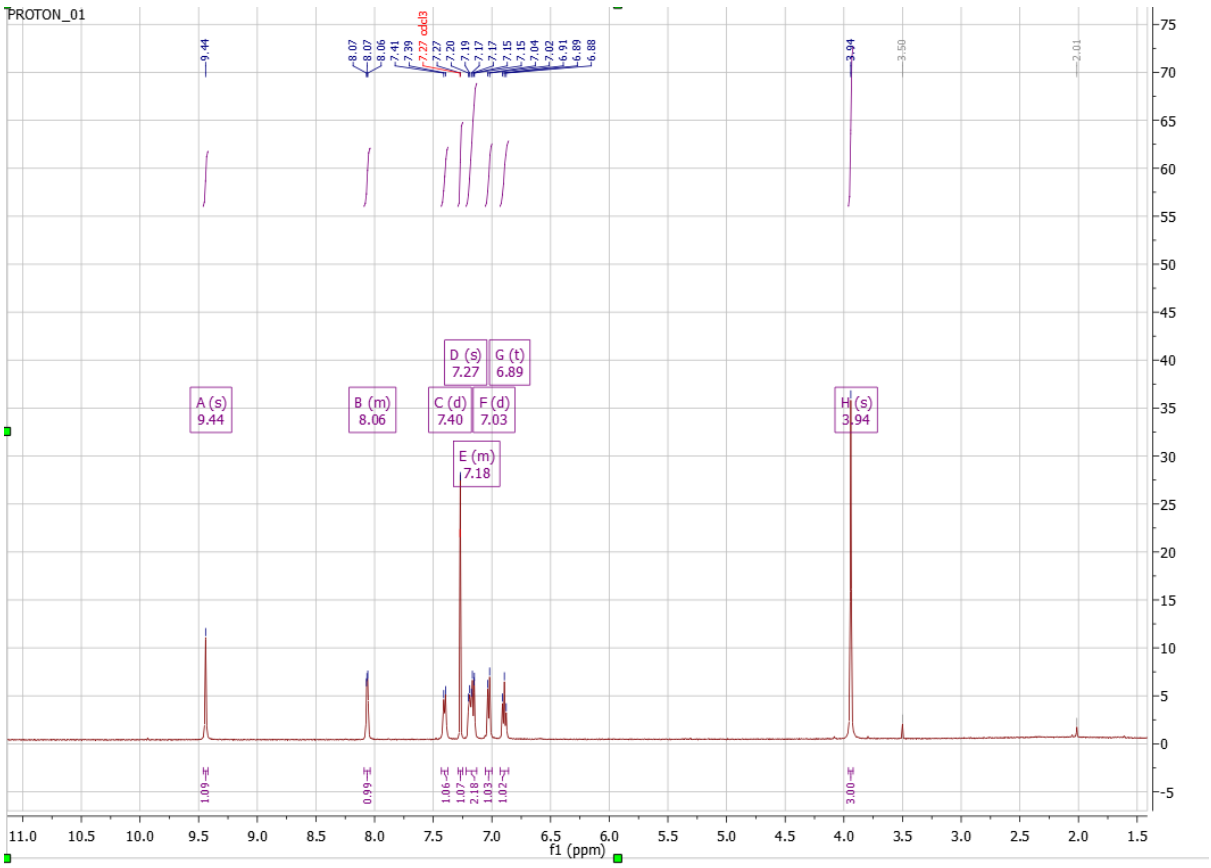

S1.21. ^{1}H NMR of H_2**L24**

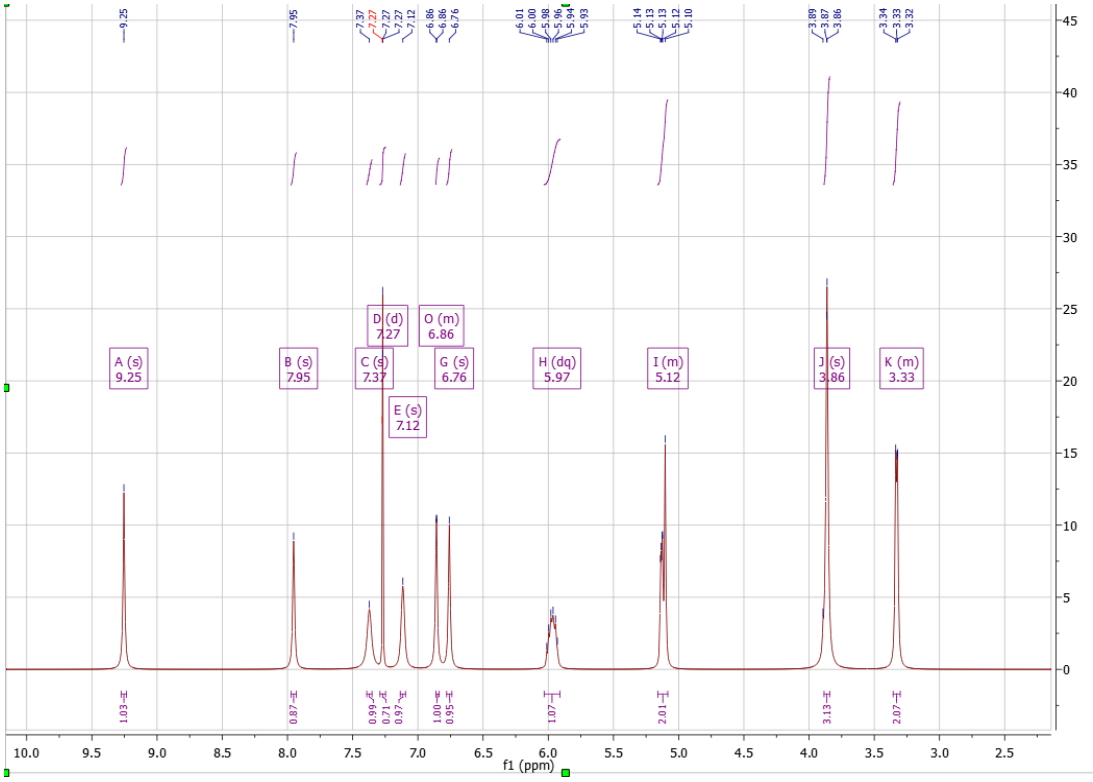

S1.22. ^{1}H NMR of H_2**L25**

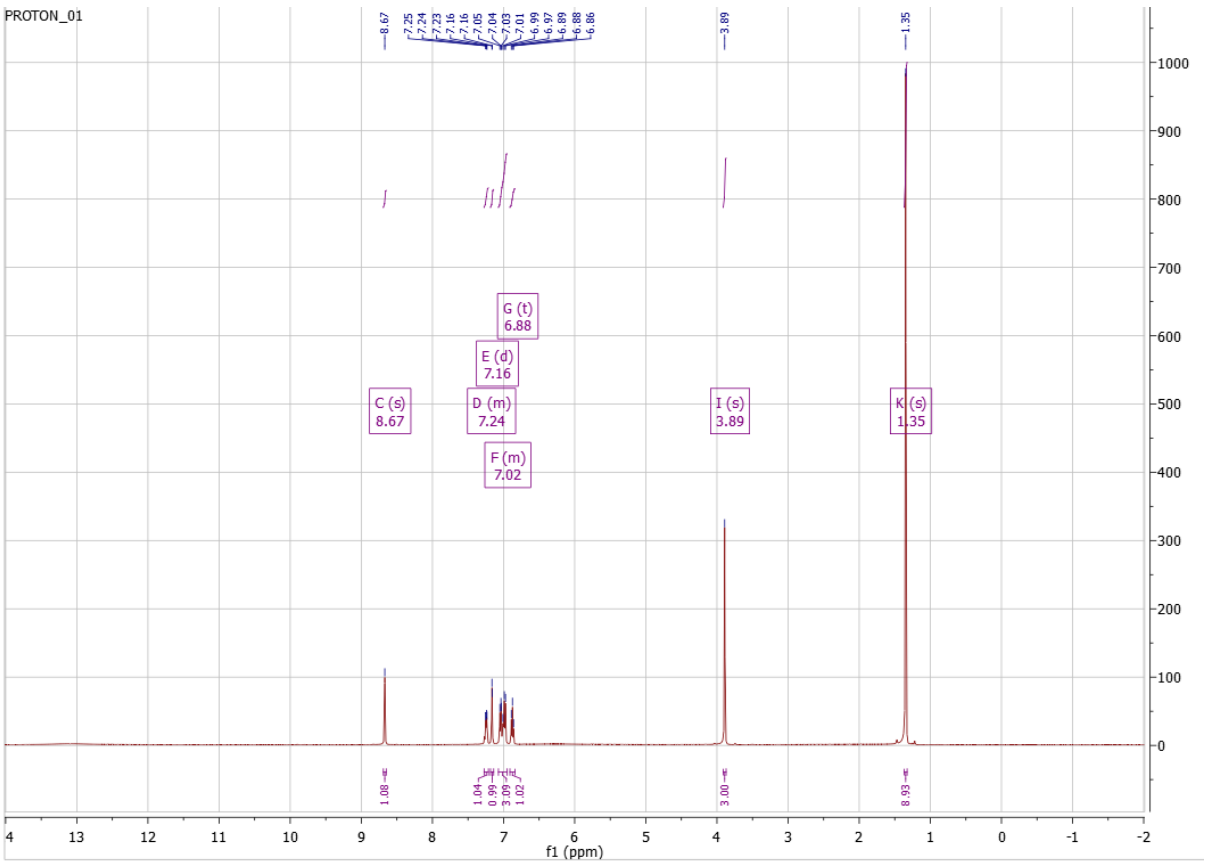

S1.23. ^{1}H NMR of H_2**L27**

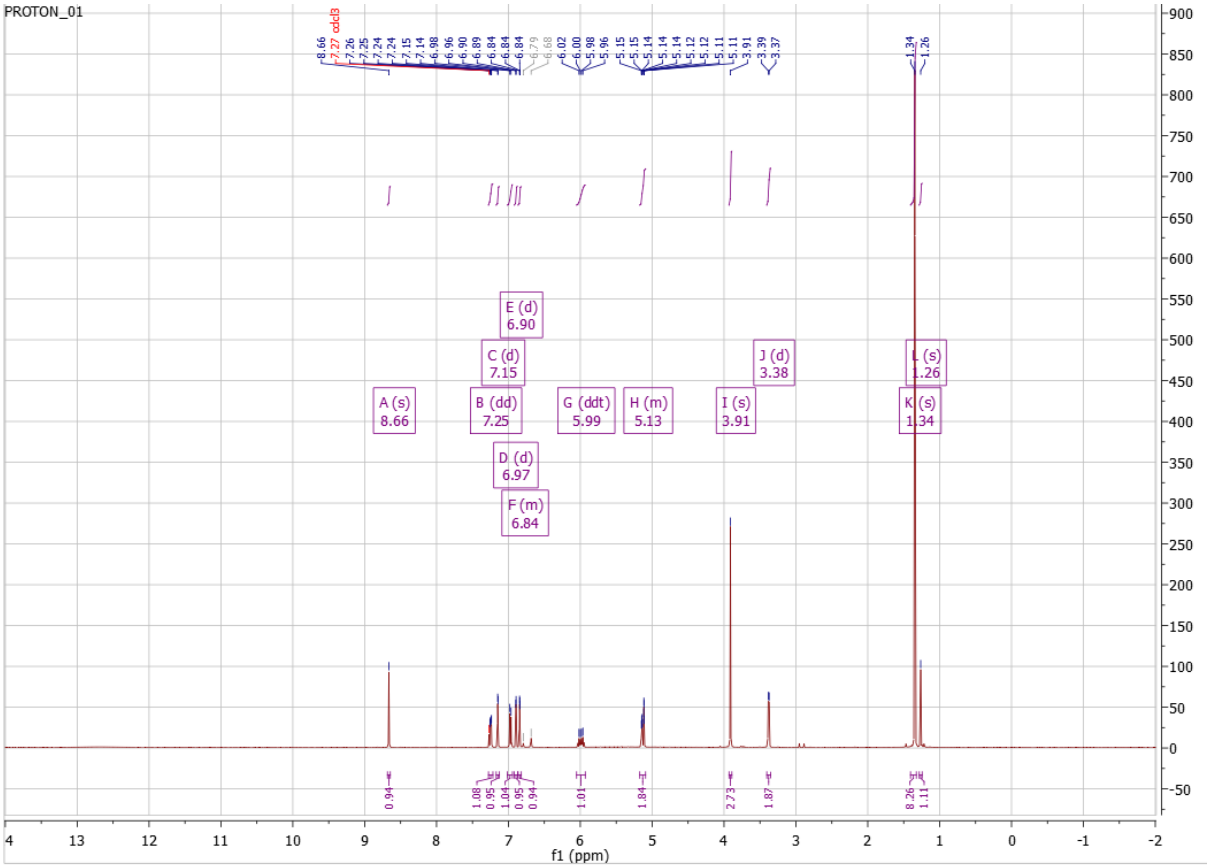

S1.24. ^{1}H NMR of H_2**L28**

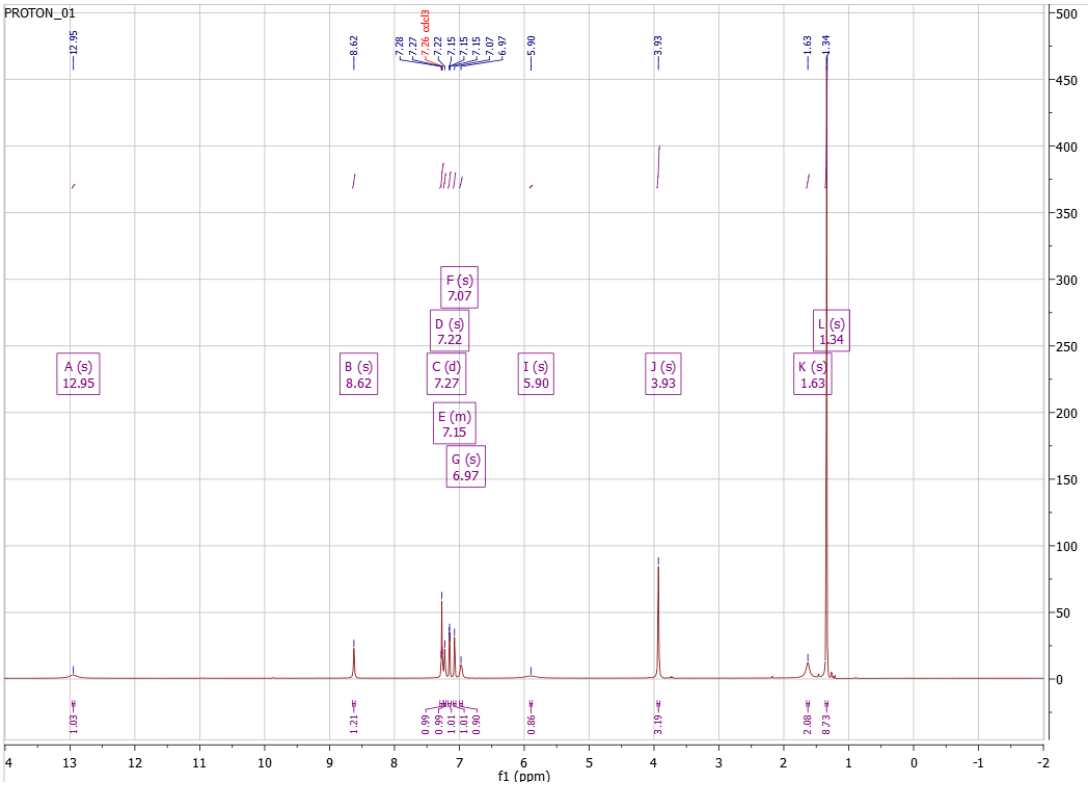

S1.25. ^{1}H NMR of H_2**L29**

Chapter 2

2.1 FT-IR of 1-12

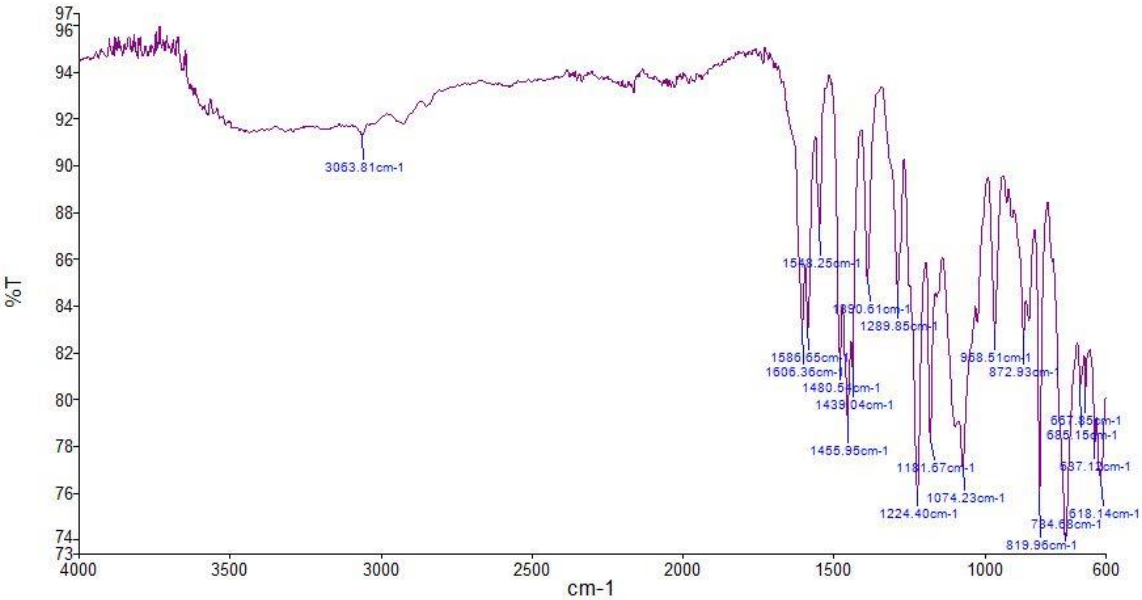

S2.1. FT-IR of 1

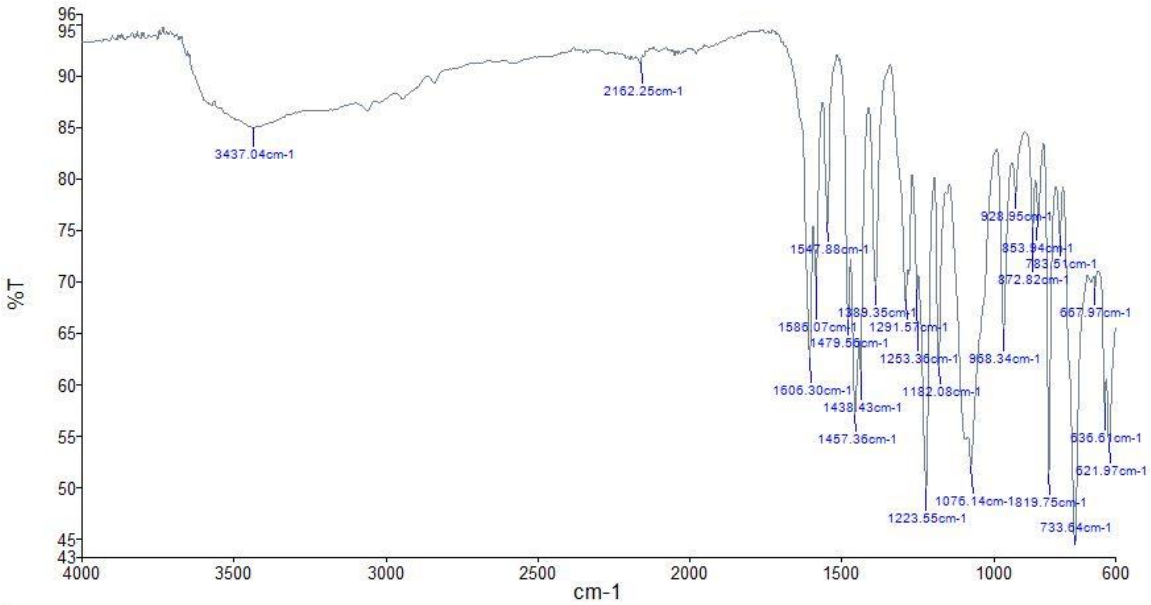

S2.2. FT-IR of 2

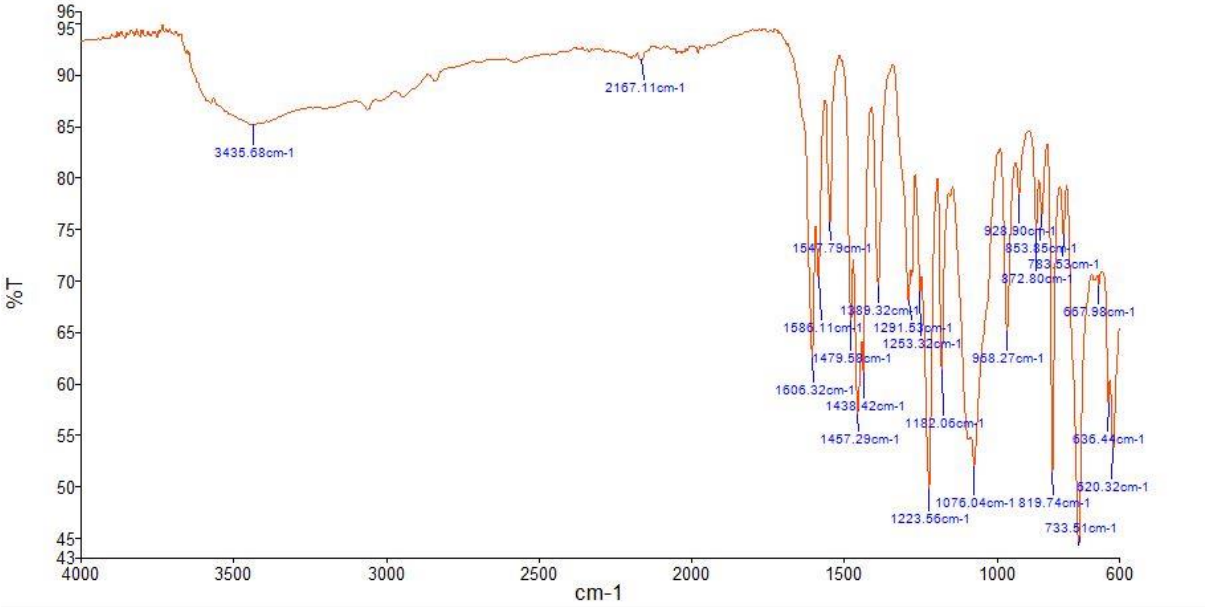

S2.3. FT-IR of 3

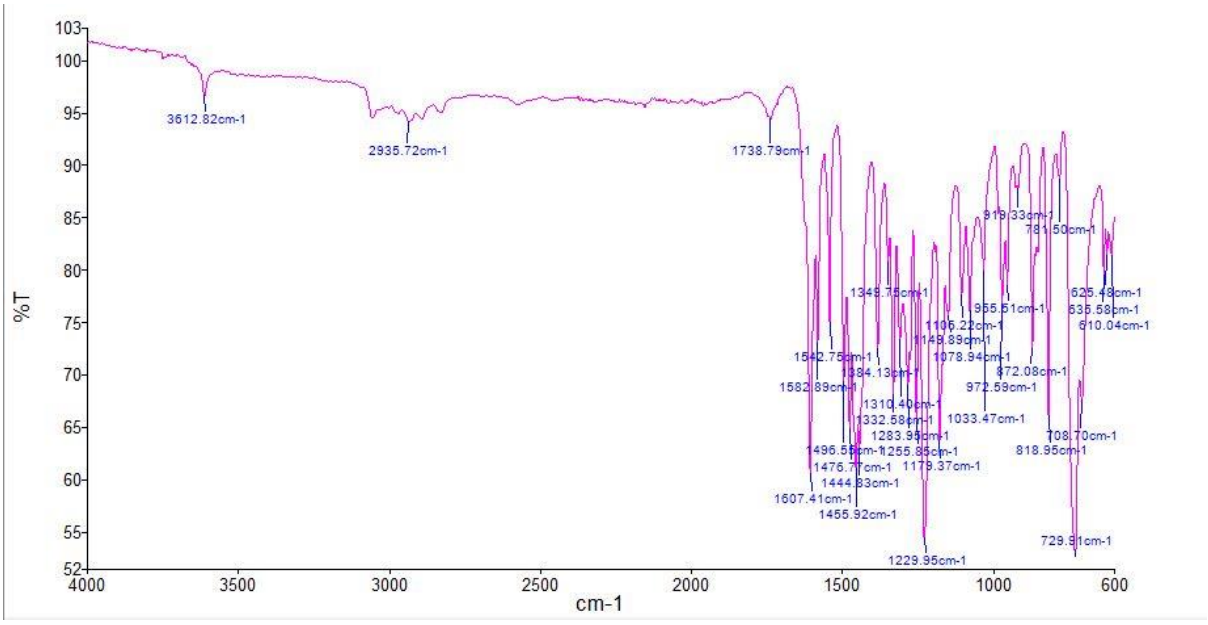

S2.4. FT-IR of 4

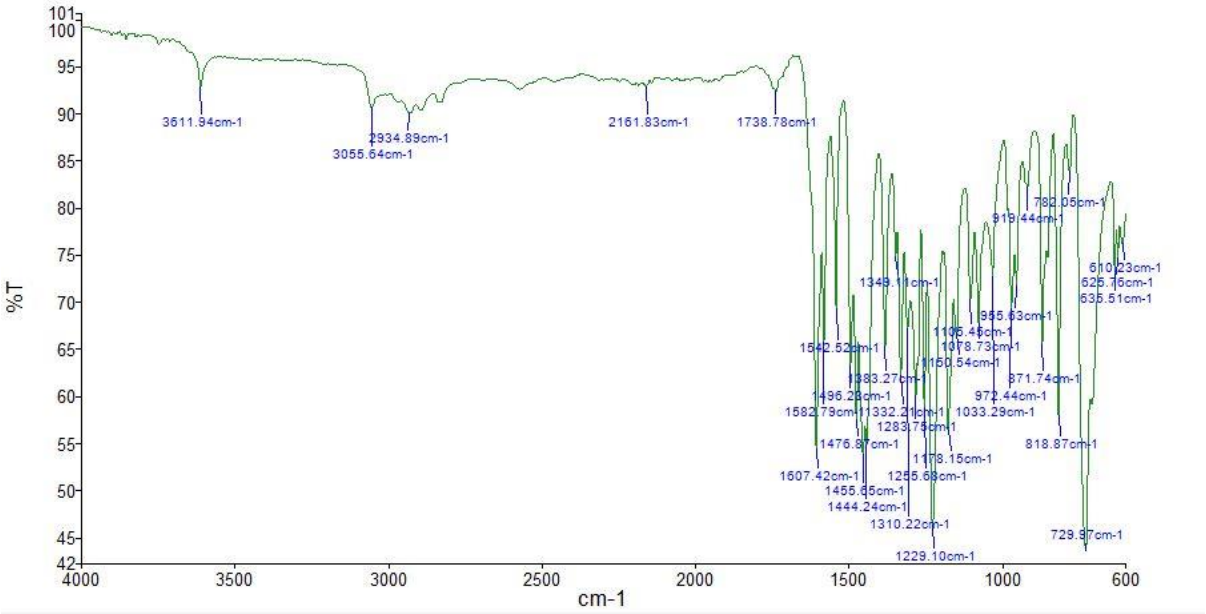

S2.5. FT-IR of 5

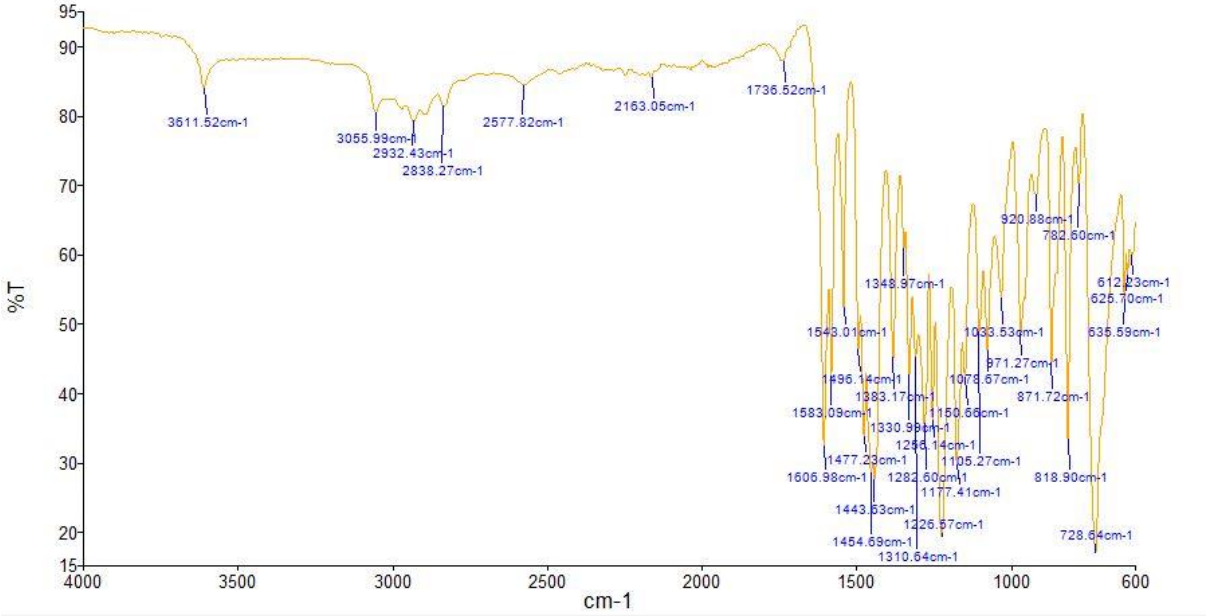

S2.6. FT-IR of 6

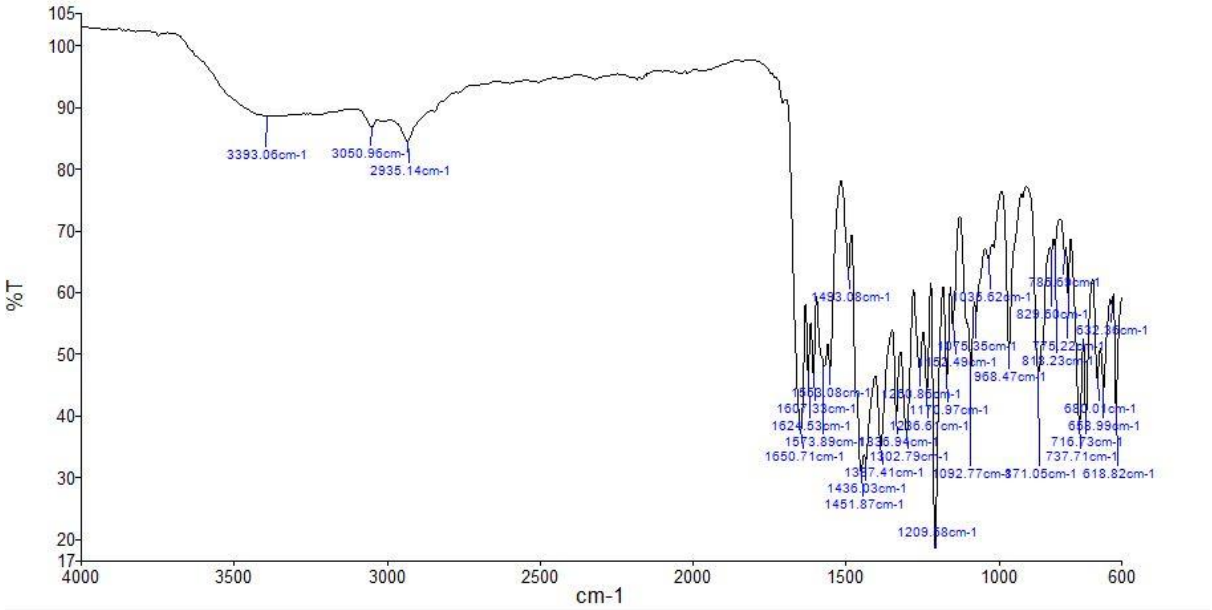

S2.7. FT-IR of 7

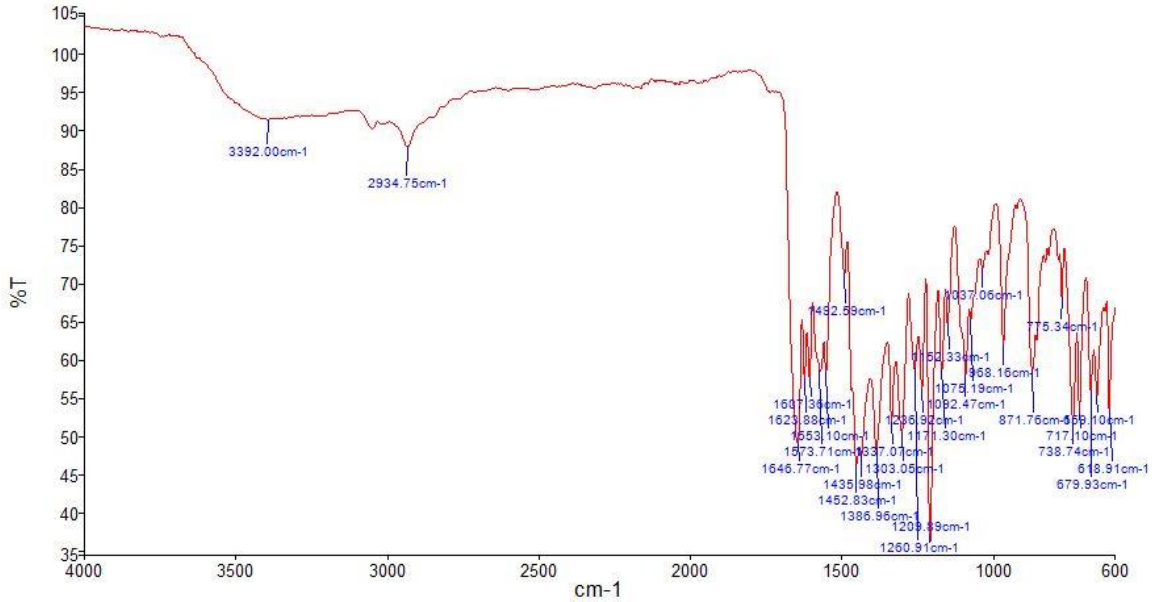

S2.8. FT-IR of 8

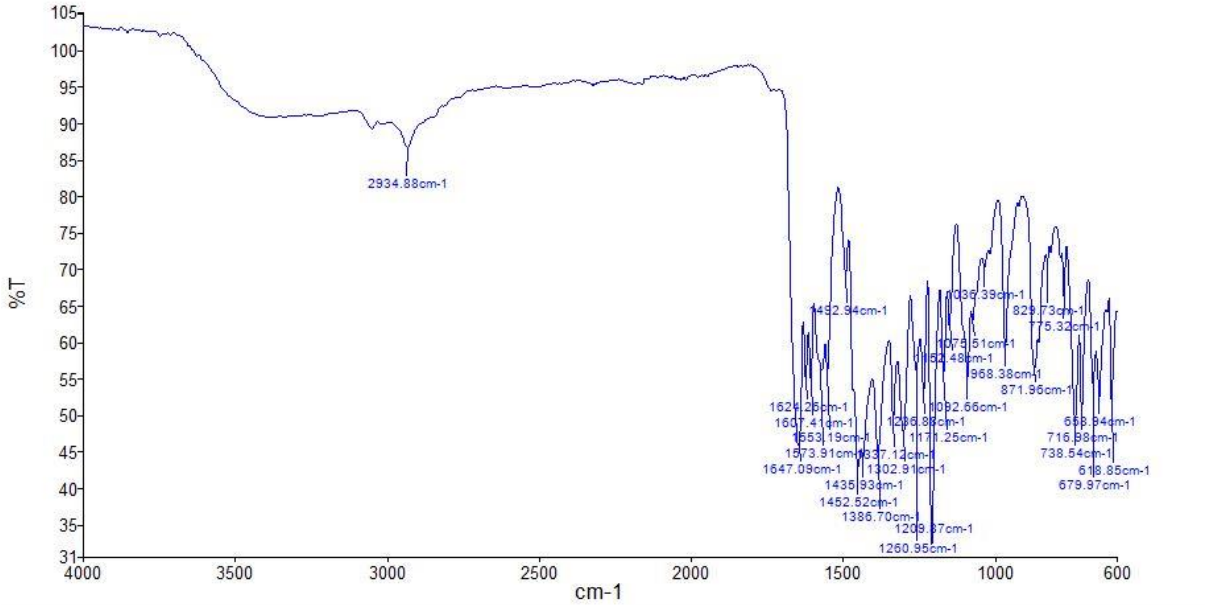

S2.9. FT-IR of 9

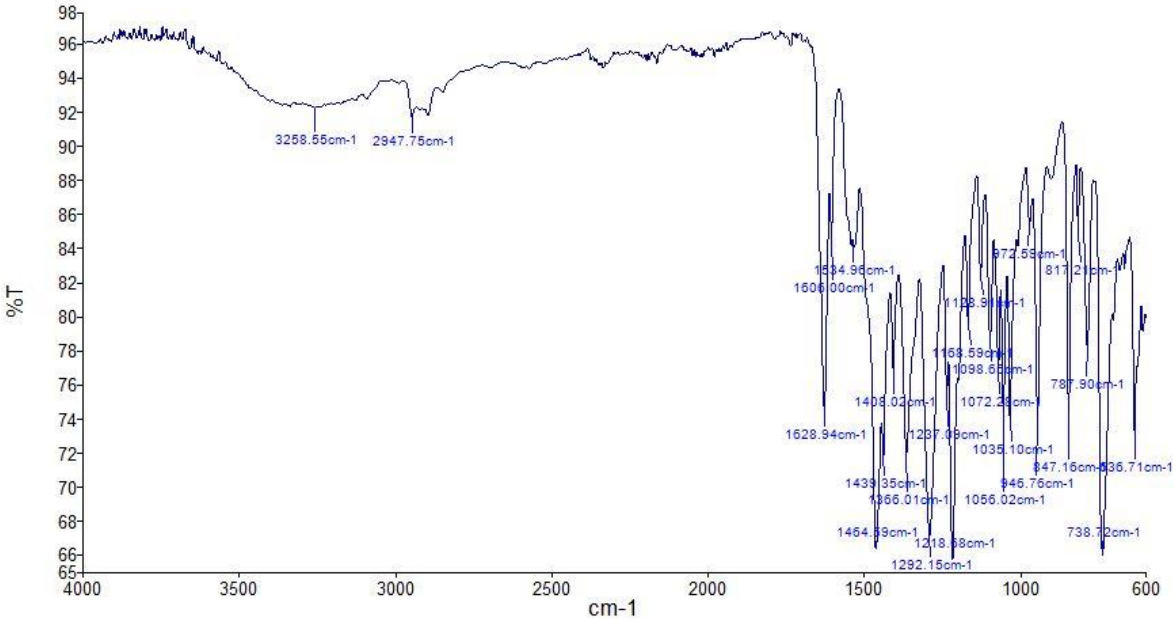

S2.10. FT-IR of 10

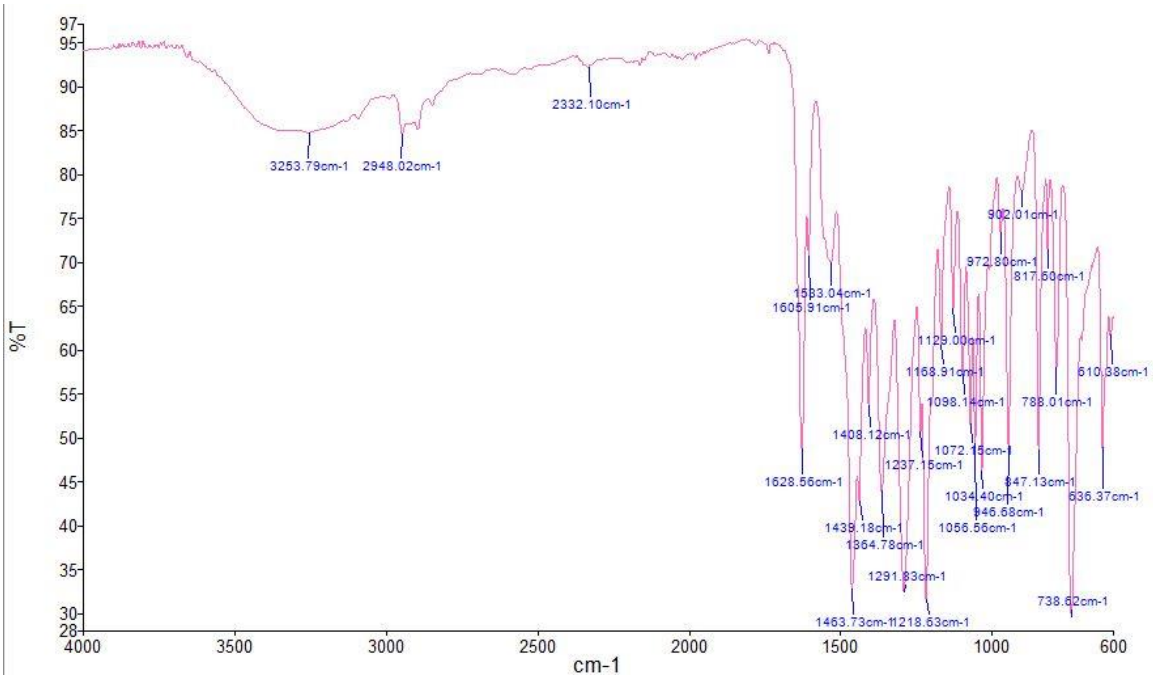

S2.11. FT-IR of 11

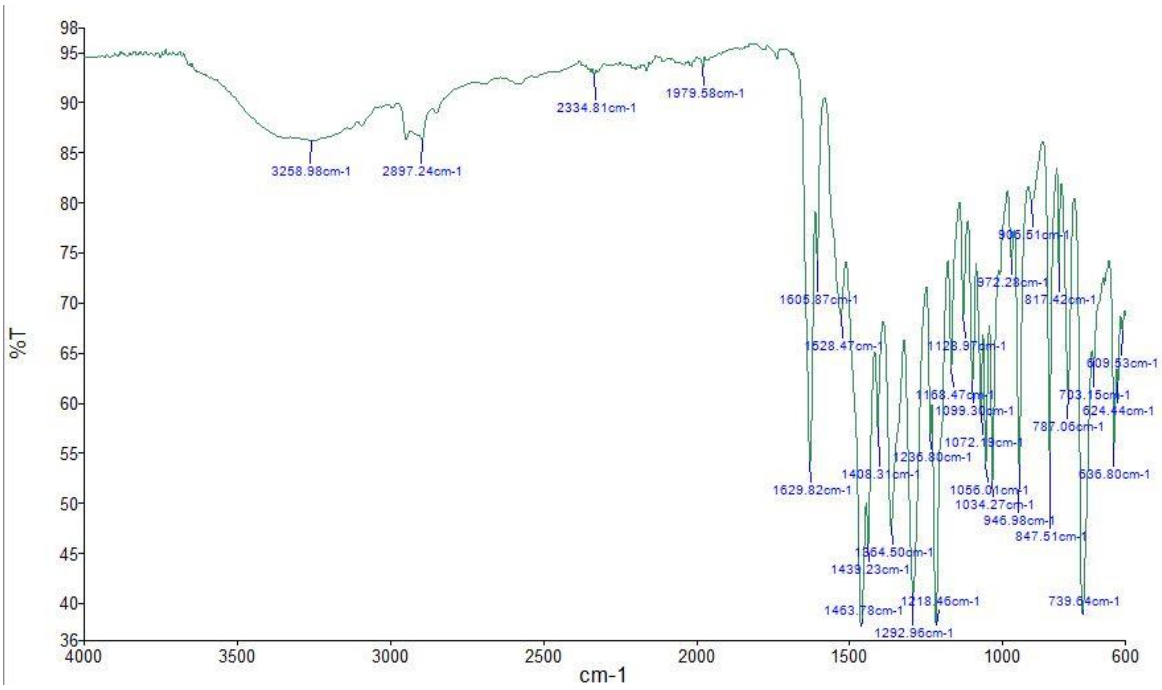

S2.12. FT-IR of 12

2.2 TGA of compounds 1-12

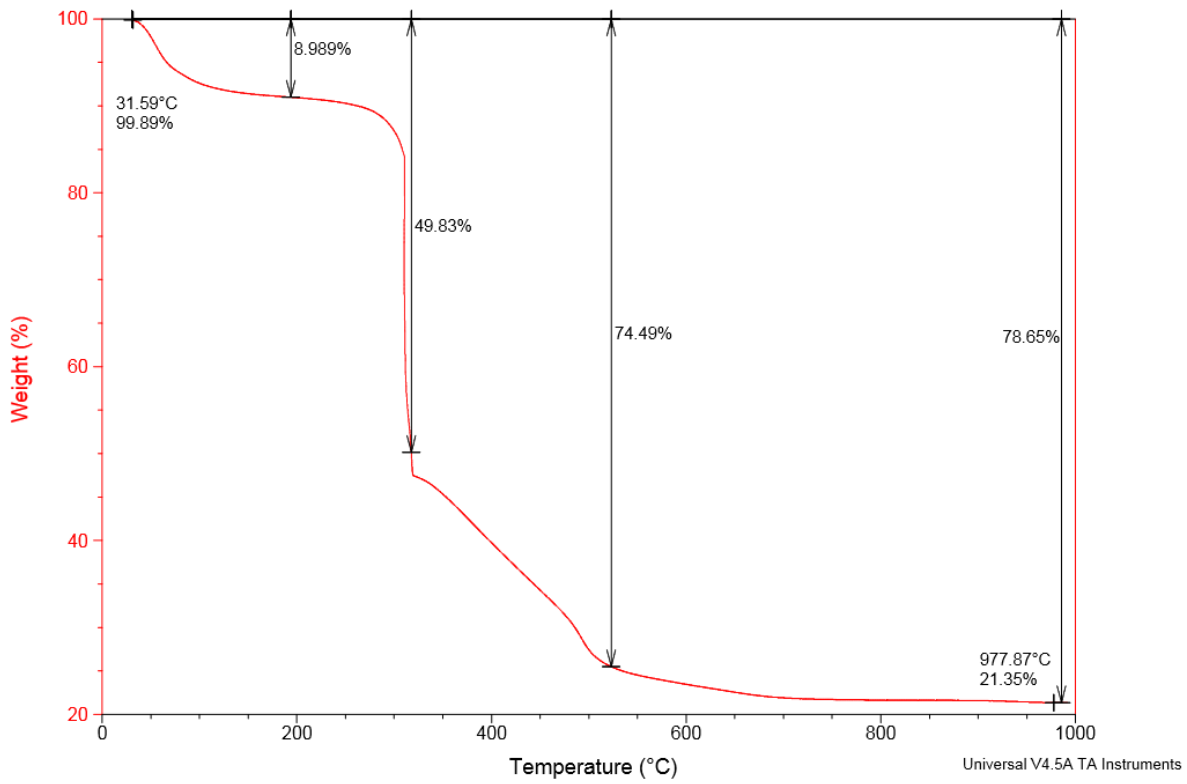

Figure S2.13. TGA of Compound 1

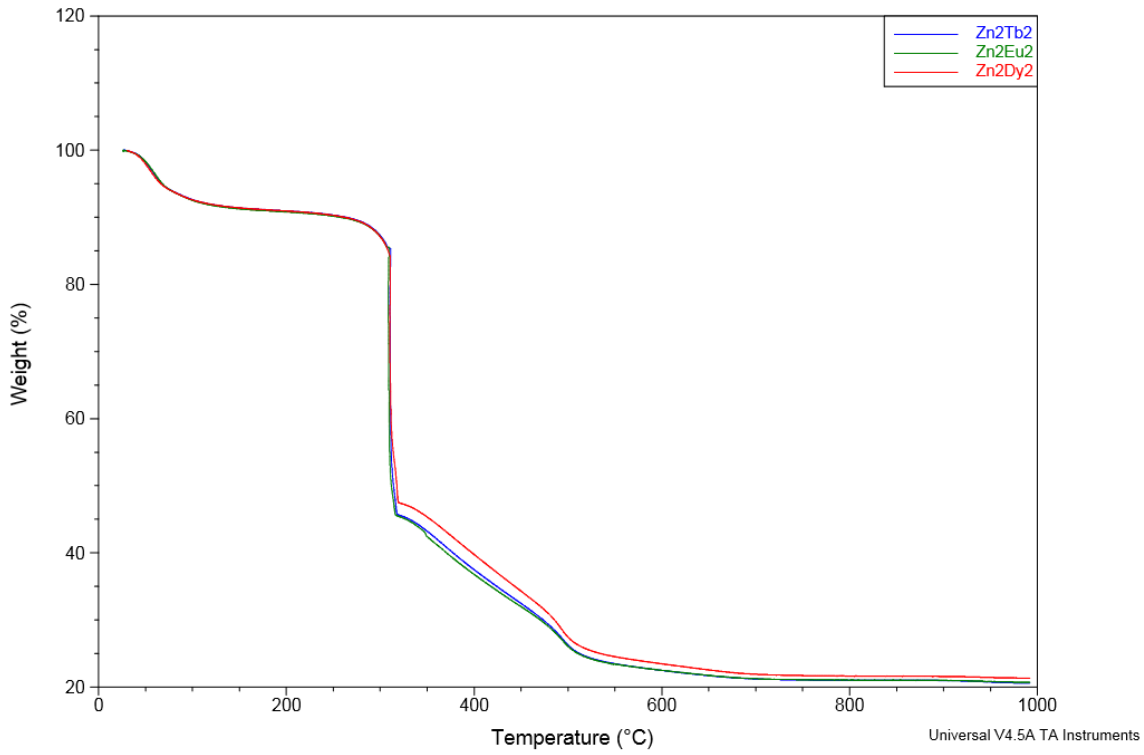

S2.14. Figure S2. Comparative TGA of isoskeletal compounds 1-3

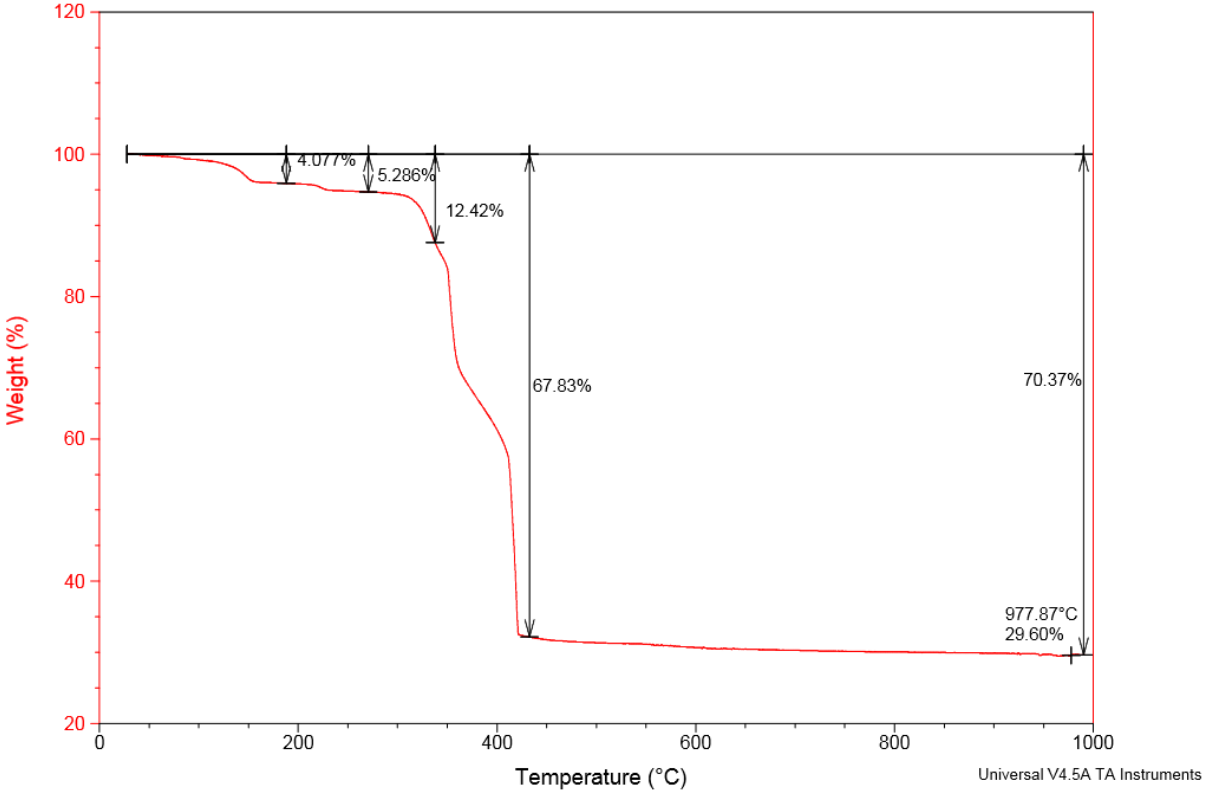

Figure S2.15. TGA of compound 4

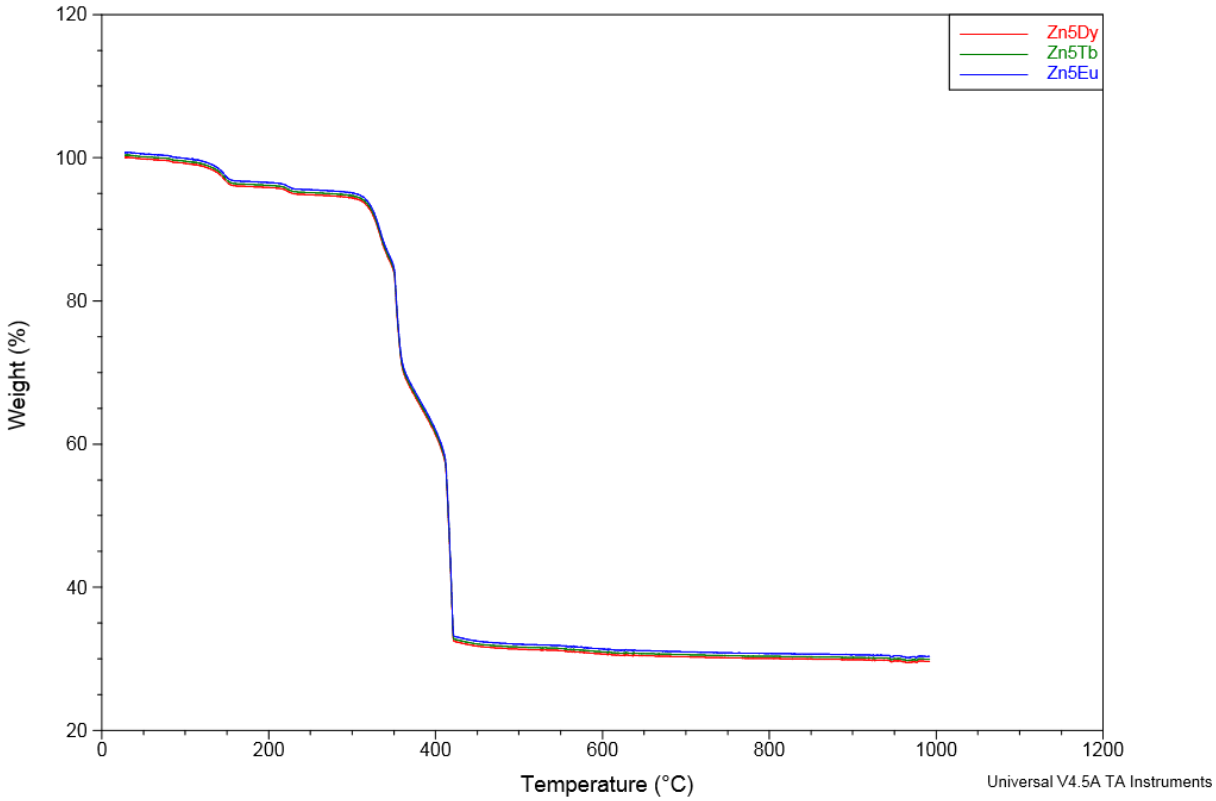

Figure S2.16. Comparative TGA of isoskeletal compounds 4-6

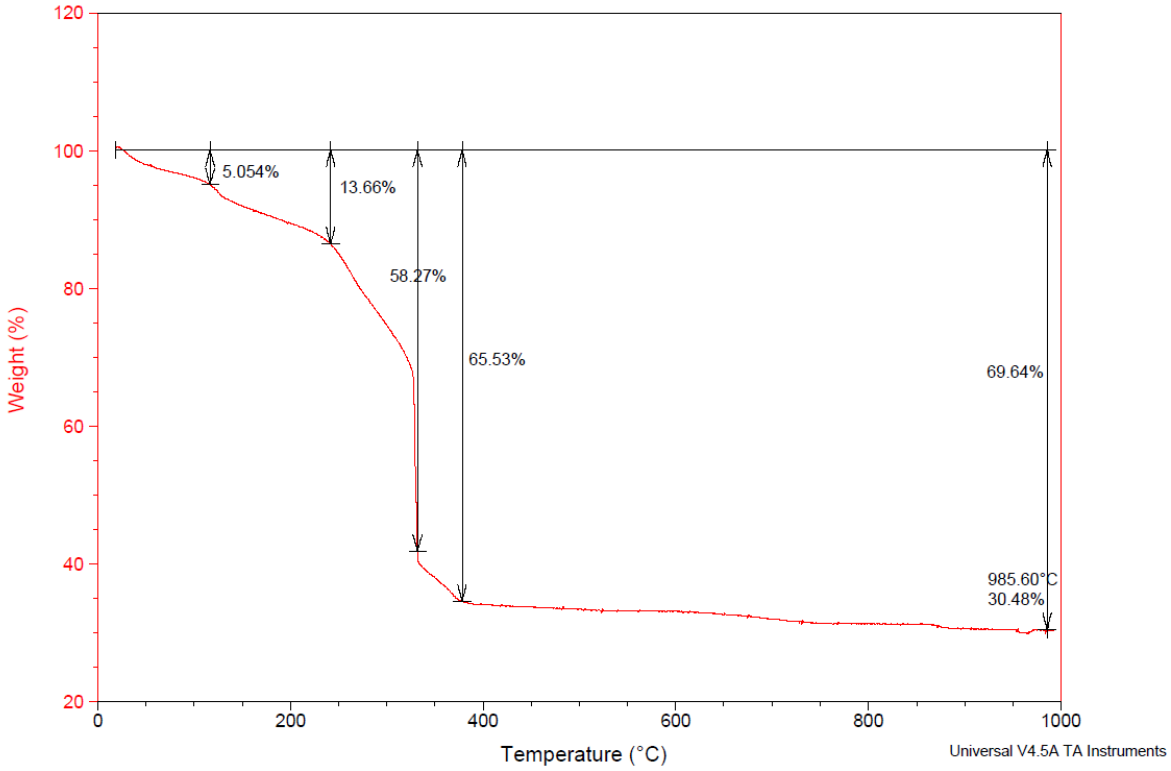

Figure S2.17. TGA of compound 7

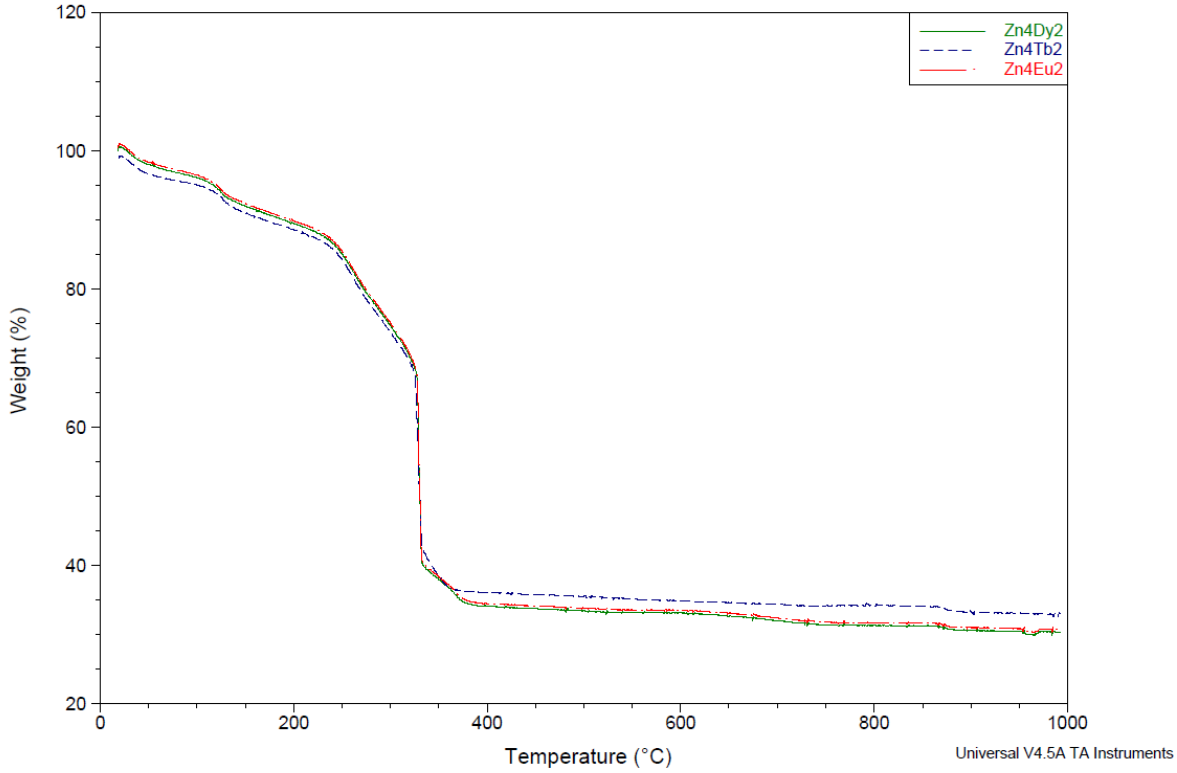

Figure S2.18. Comparative TGA of isoskeletal compounds 7-9

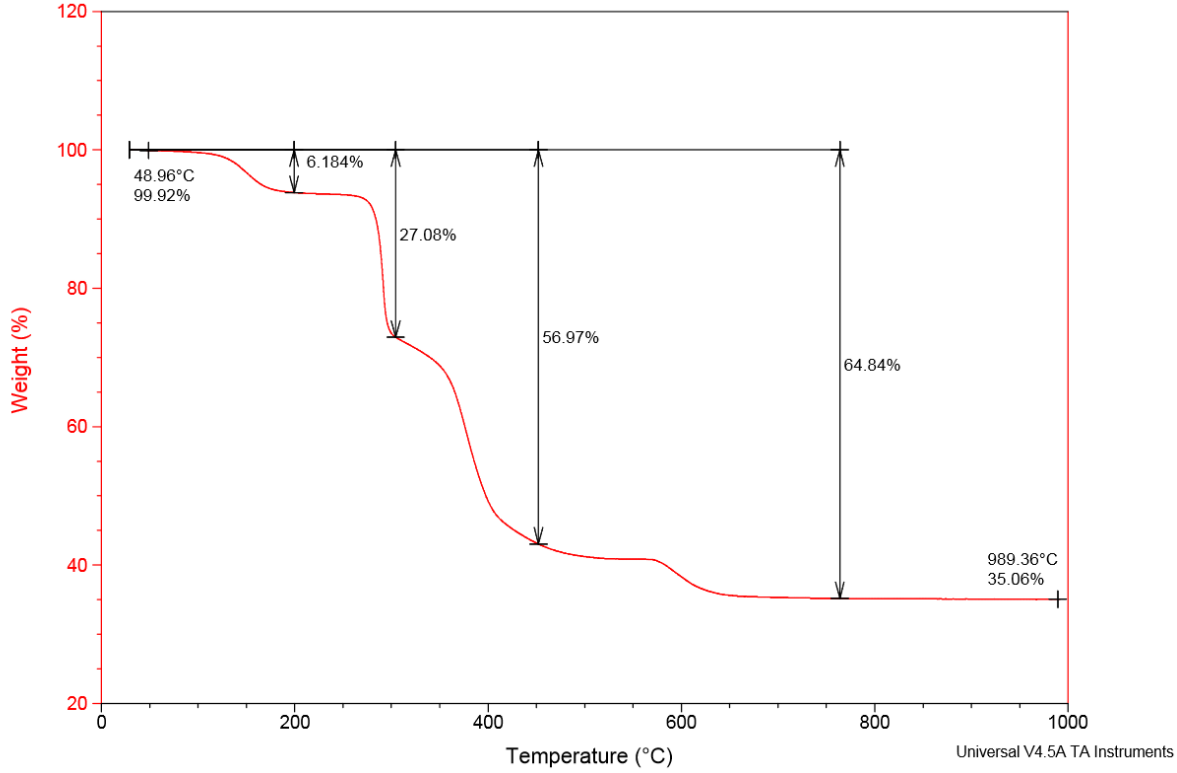

Figure S2.19.TGA of compound 10

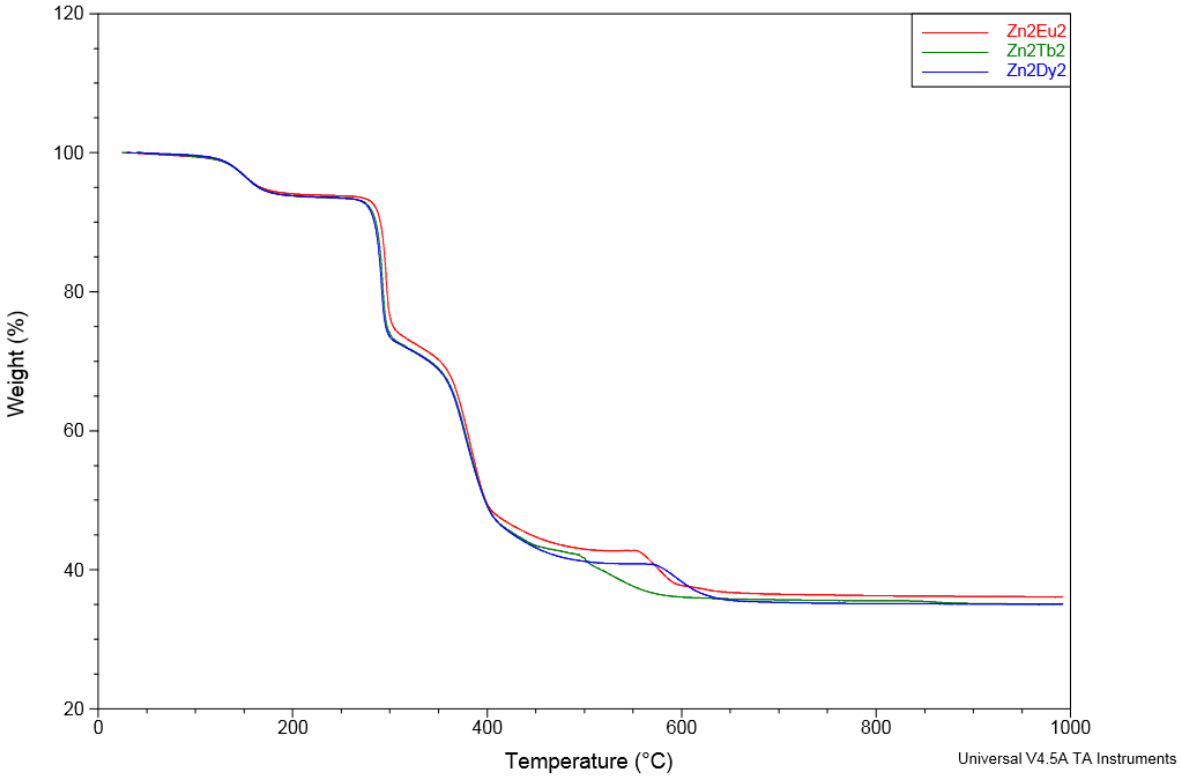

Figure S2.20. Comparative TGA of isostructural compounds 10-12

2.3 Luminescence

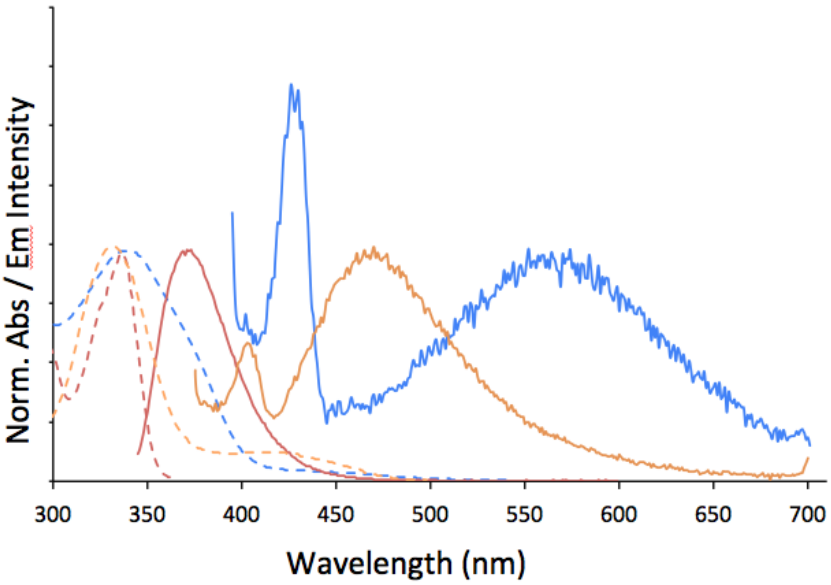

Figure S2.21. Normalised absorption (dashed line) and emission spectra (solid line) of compounds H_2**L1** (blue; λ_{ex} = 330 nm), H_2**L2** (red; λ_{ex} = 330 nm), and H_3**L3** (yellow; λ_{ex} = 330 nm) recorded in DMF ($1x10^{-5}$ mol dm^{-3}, 298 K).

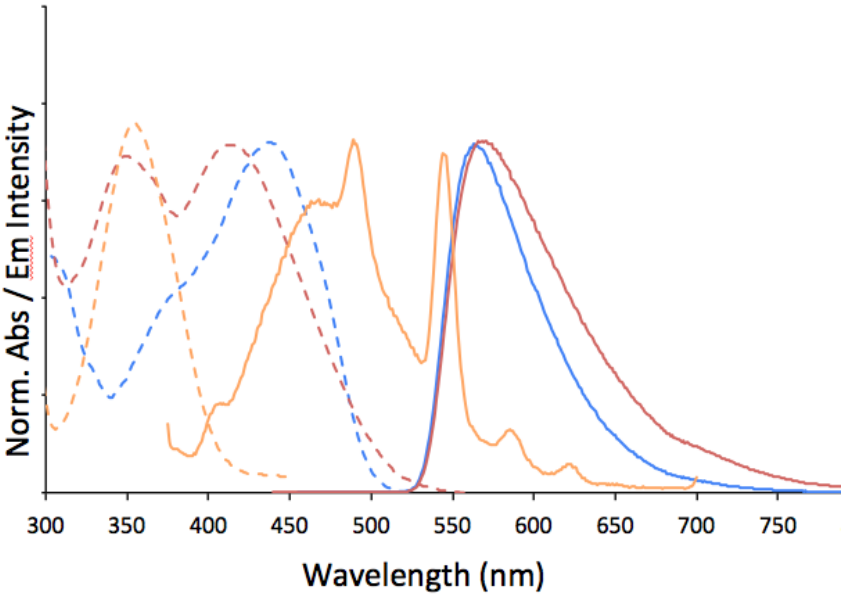

Figure S2.22. Normalised absorption (dashed line) and emission spectra (solid line) of compounds **5** (blue; λ_{ex} = 440 nm), **8** (red; λ_{ex} = 410 nm), and **11** (yellow; λ_{ex} = 350nm) recorded in DMF ($1x10^{-5}$ mol dm^{-3}, 298 K).

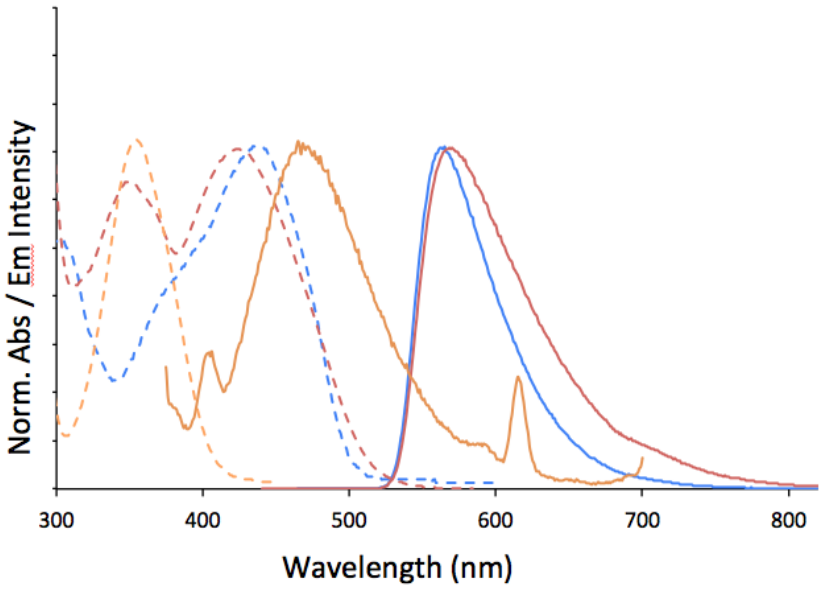

Figure S2.23. Normalised absorption (dashed line) and emission spectra (solid line) of compounds **6** (blue; λ_{ex} = 430 nm), **9** (red; λ_{ex} = 430 nm), and **12** (yellow; λ_{ex} = 350 nm) recorded in DMF ($1x10^{-5}$ mol dm^{-3}, 298 K).

2.4 ESI-MS of 1-3

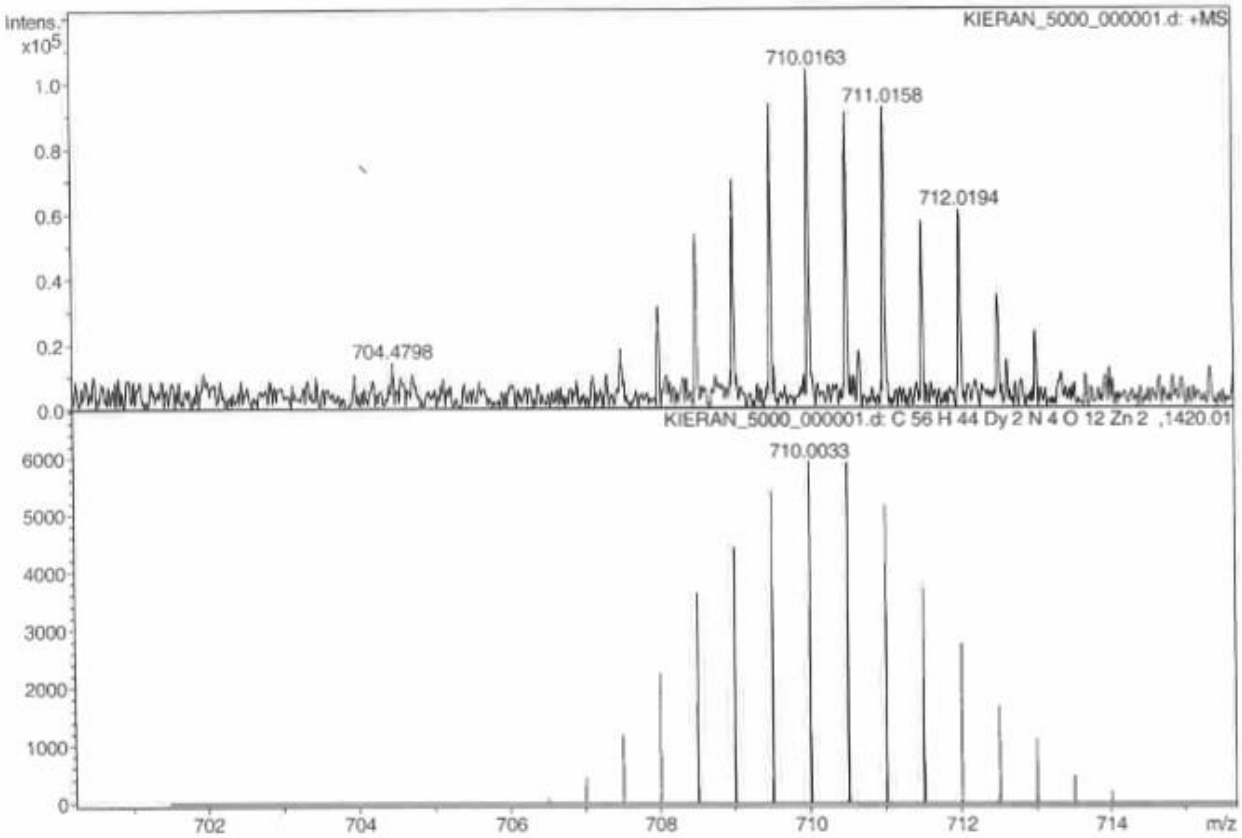

Figure S2.24. ESI-MS of **1**. $[Zn^{II}_2Dy^{III}_2\ (\mathbf{L1})_4]^{2+}$ fragment

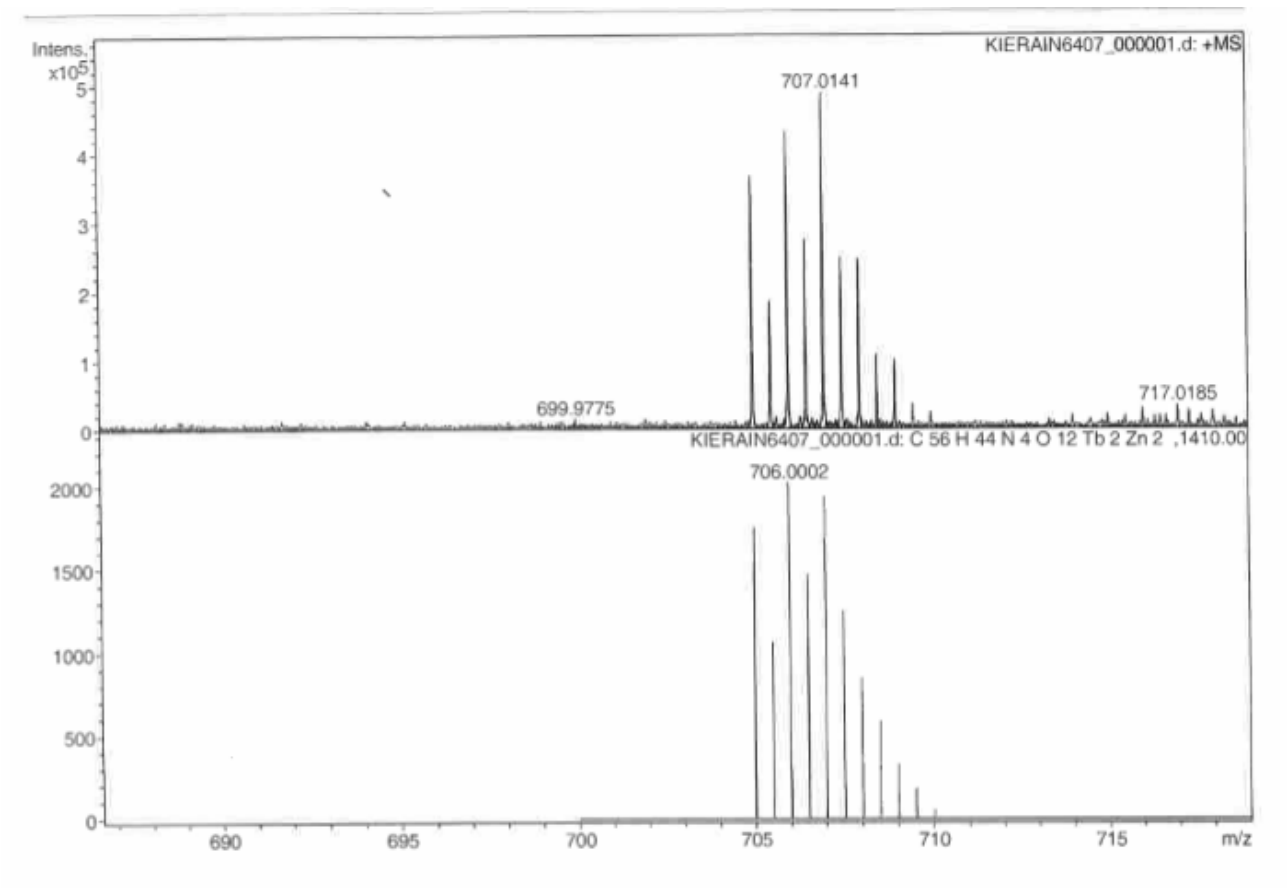

Figure S2.25. ESI-MS of **2**. $[Zn^{II}_2Tb^{III}_2\ (\mathbf{L1})_4]^{2+}$ fragment

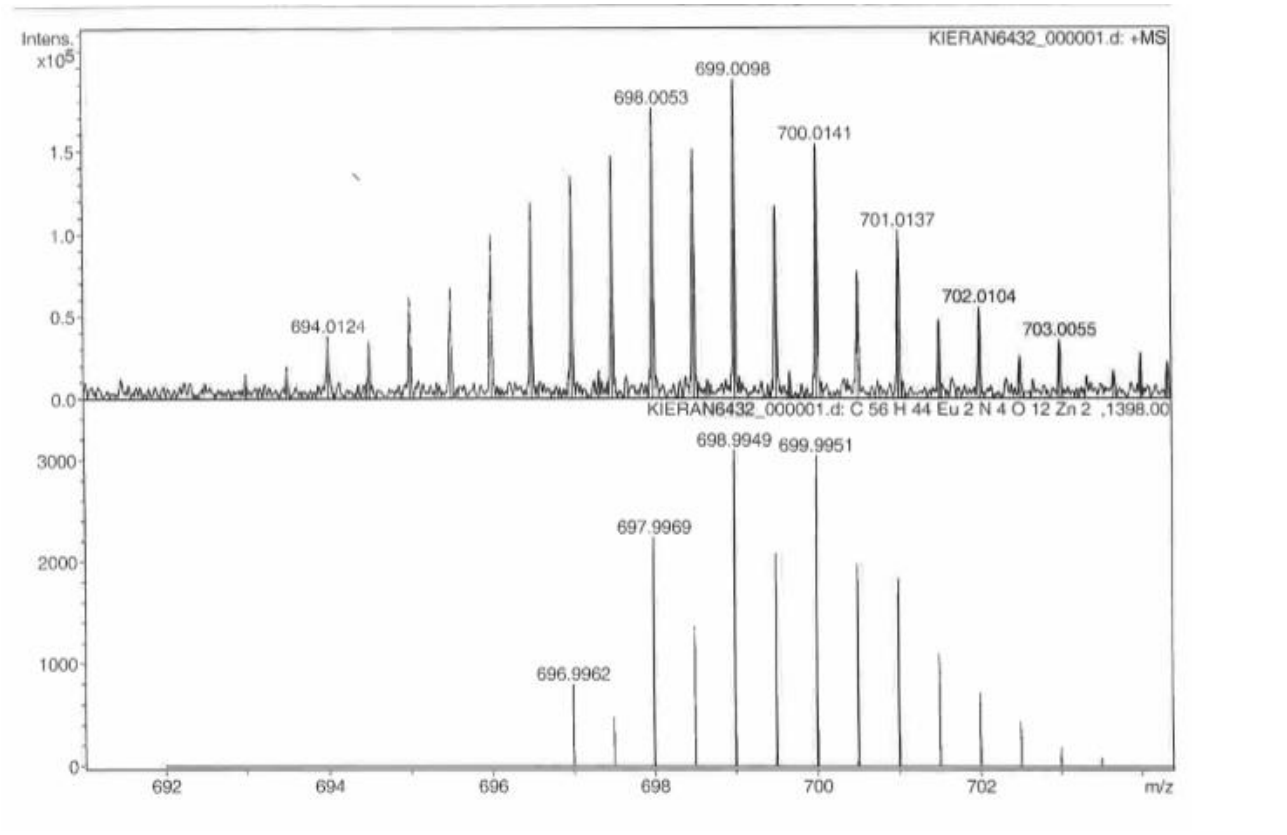

Figure S2.26. ESI-MS of **3**. $[Zn^{II}_2Eu^{III}_2\ (\mathbf{L1})_4]^{2+}$ fragment.

Chapter 3

3.1 ESI-MS of 16

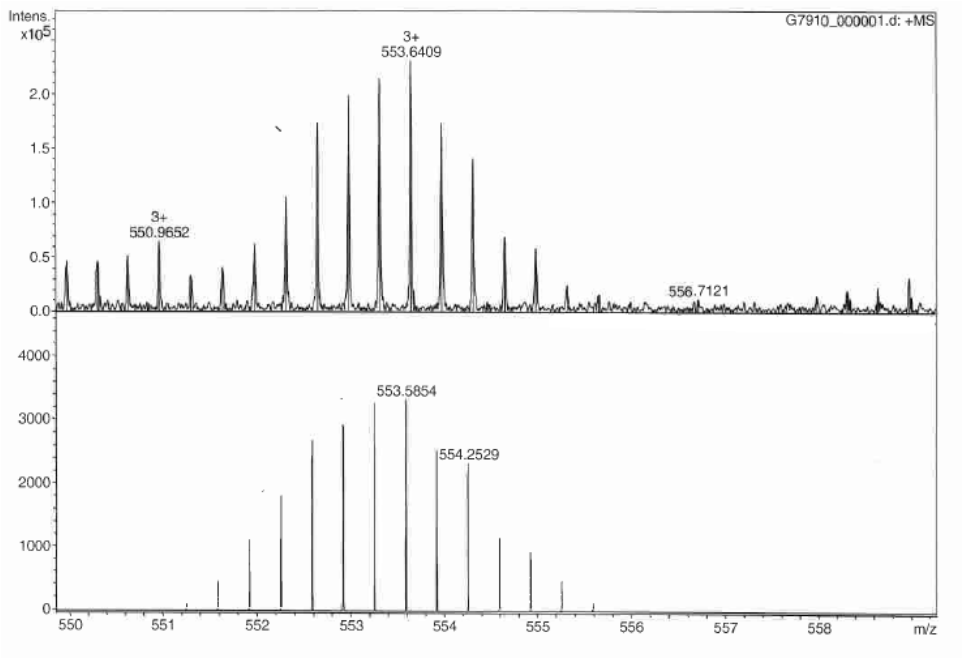

Figure S3.1.ESI-MS of **16** $[Co^{II}_4Gd^{III}_2(C_{14}H_{11}NO_3)_4(OH)_2(Cl)_2(CH_3OH)]^{3+}$ fragment.

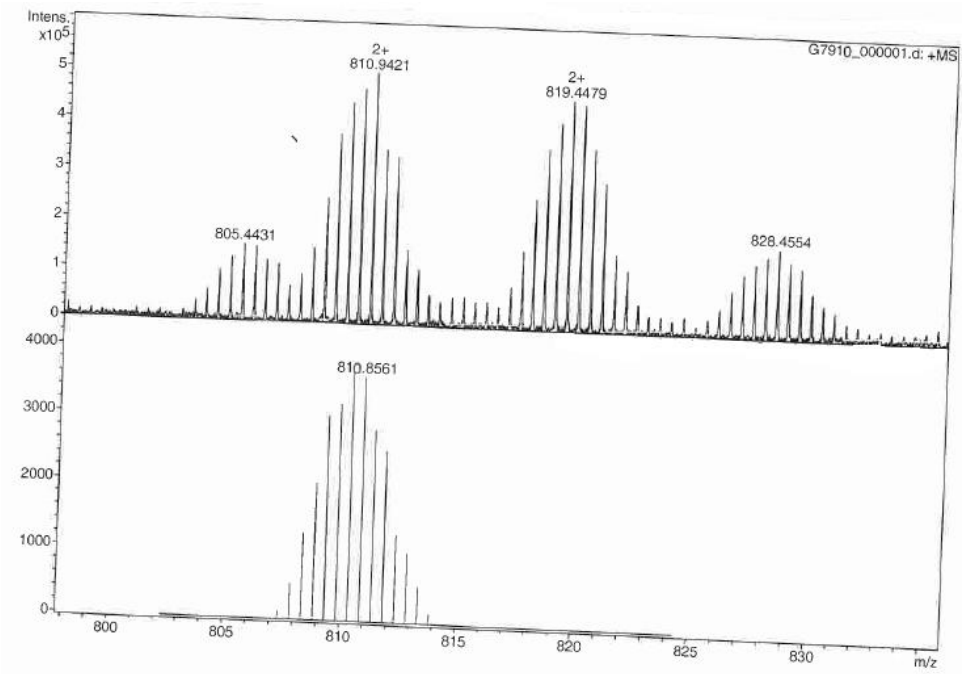

Figure S3.2 ESI-MS of **16** $[Co^{II}_4Gd^{III}_2(C_{14}H_{11}NO_3)_4(OH)_2(Cl)_2+2H]^{2+}$ fragment

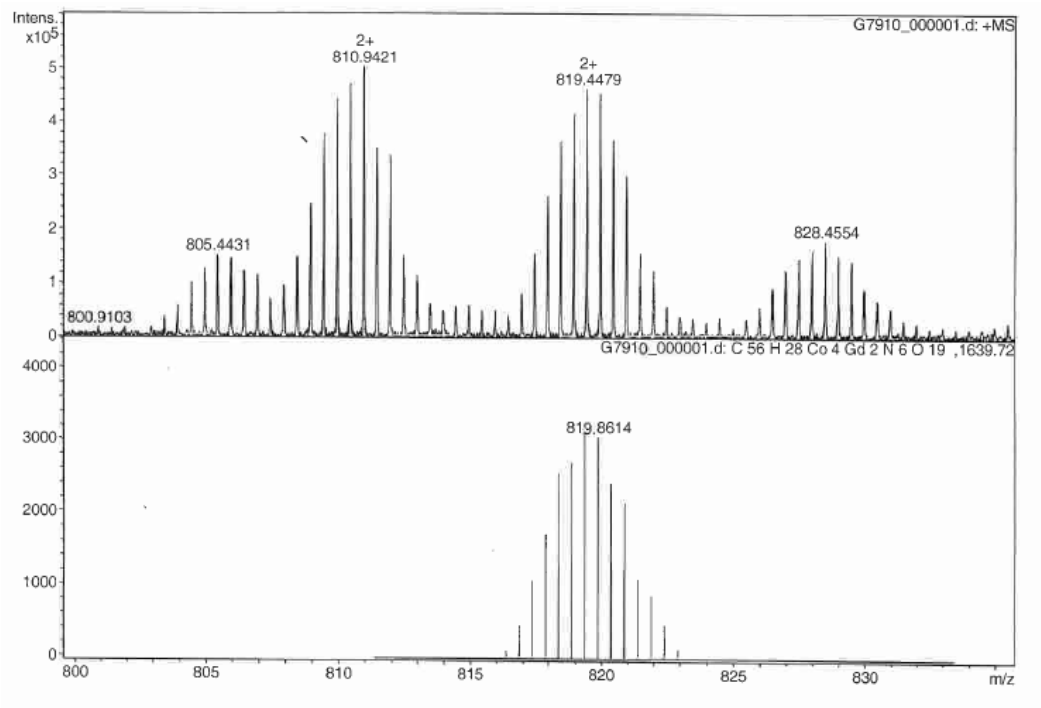

Figure S3.3. ESI-MS of **16-** $[Co^{II}_4Gd^{III}_2(C_{14}H_{11}NO_3)_4(OH)_2(Cl)_2+2H+H_2O]^{2+}$ fragment

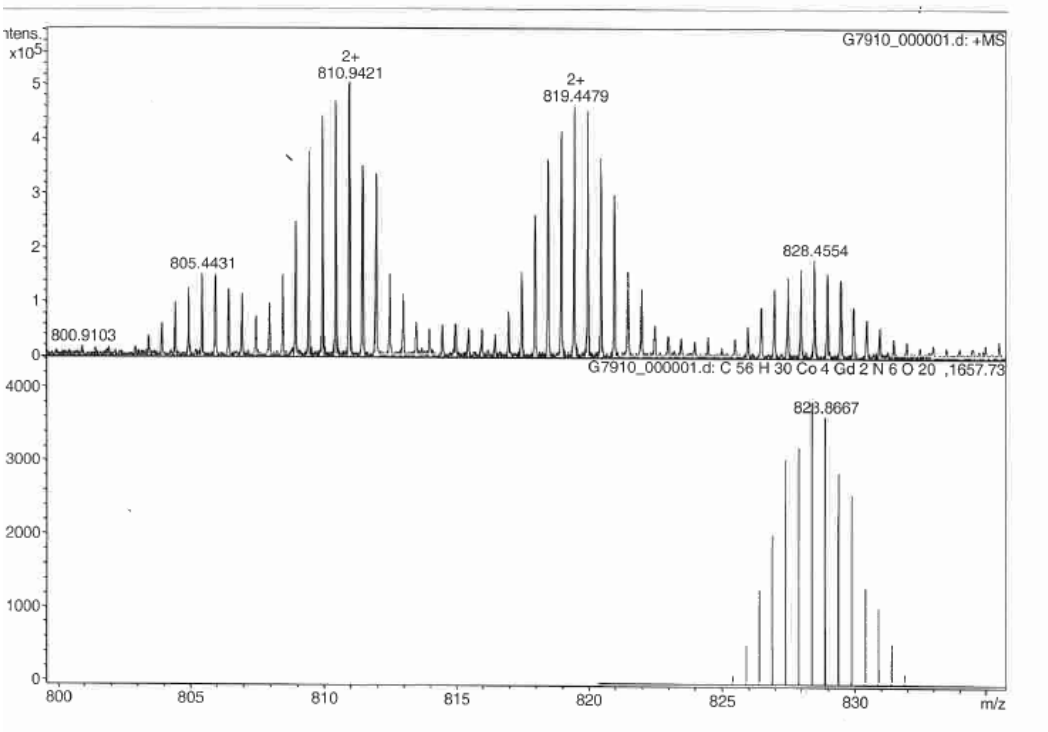

Figure S3.4. ESI-MS of **16** $[Co^{II}_4Gd^{III}_2(C_{14}H_{11}NO_3)_4(OH)_2(Cl)_2+2H+(H_2O)_2]^{2+}$ fragment

3.2 TGA of 16 and 18

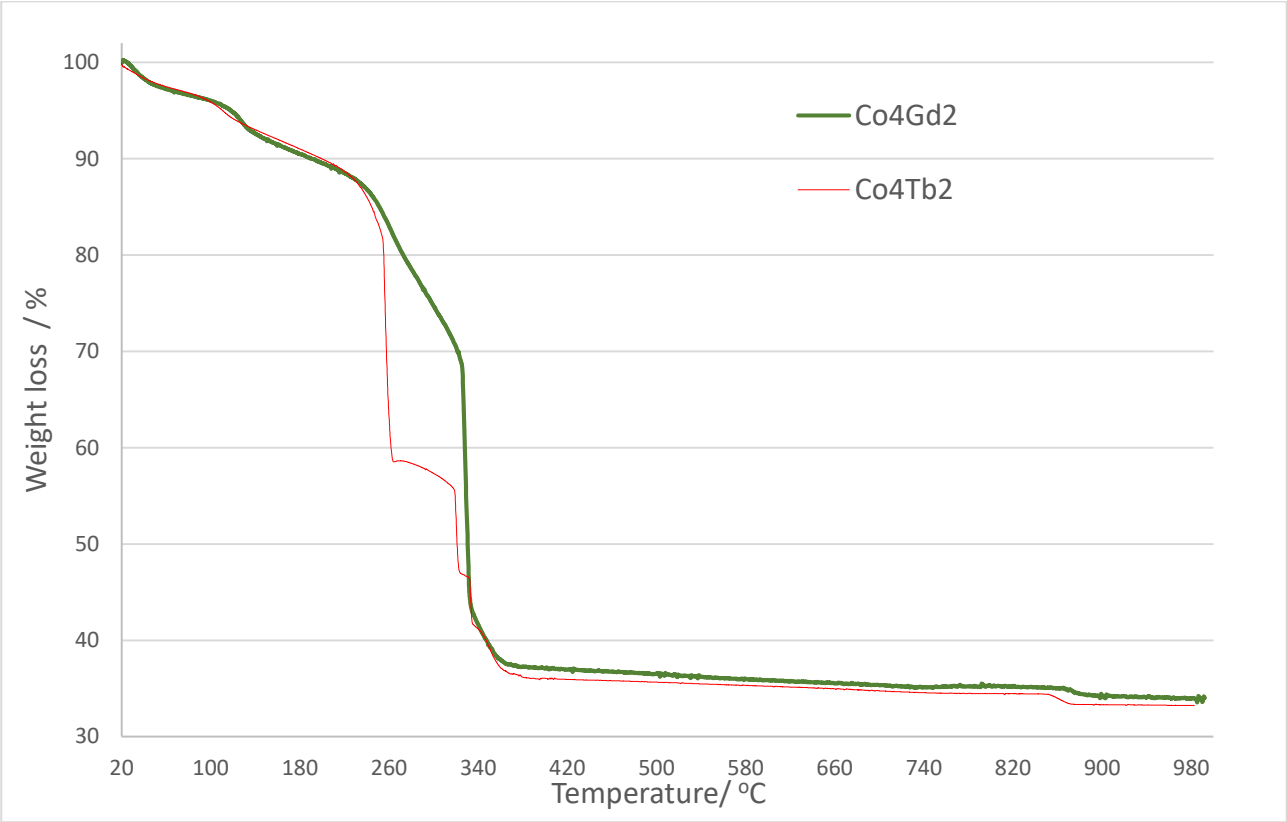

Figure S3.5. TGA of compounds **16** and **18**.

Chapter 4

4.1 FT-IR of 20-24

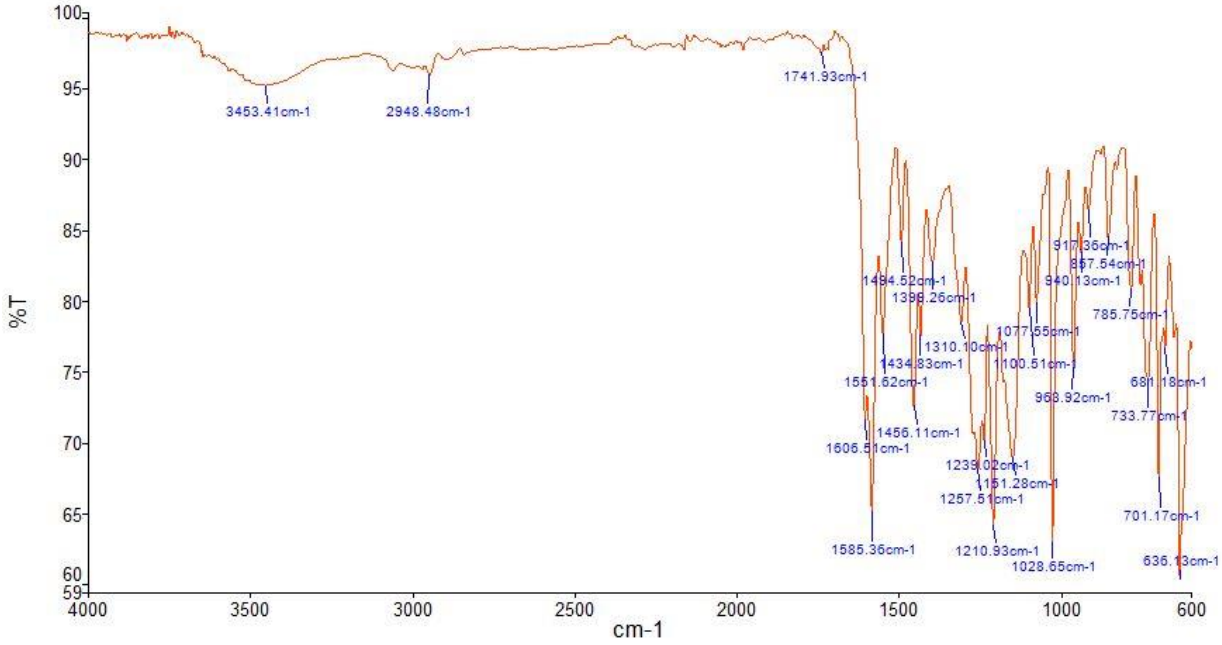

S4.1 FT-IR of **20**

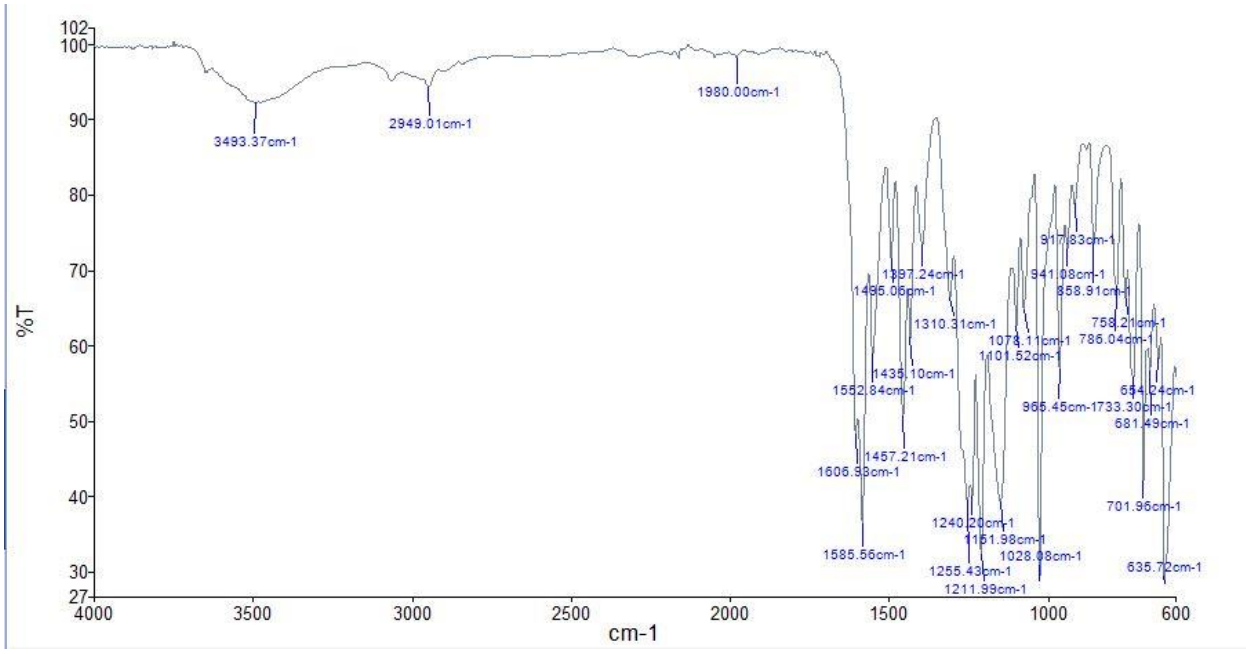

S4.2 FT-IR of **21**

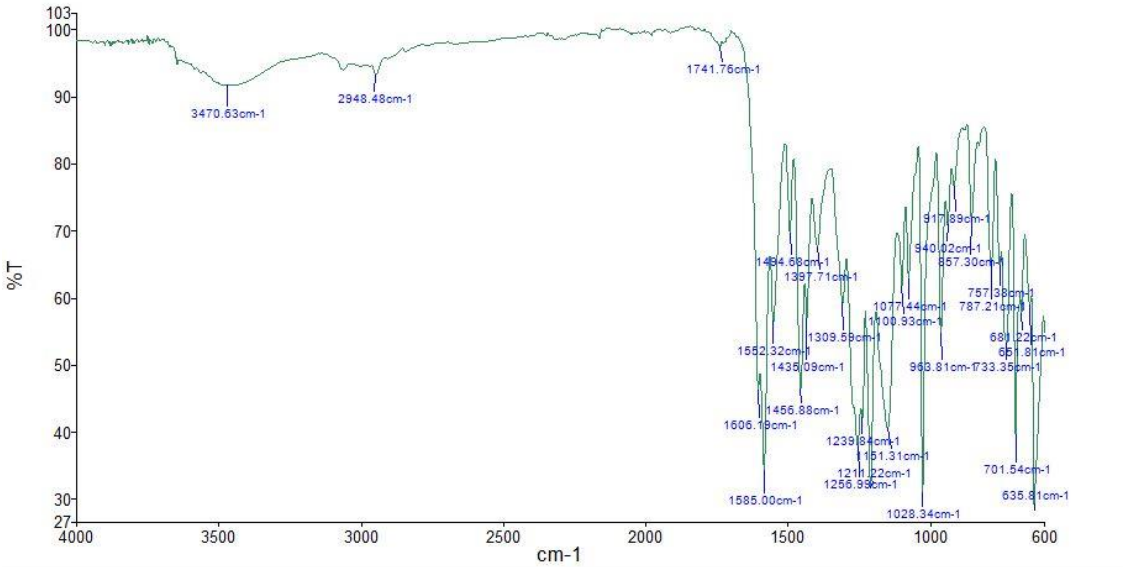

S4.3 FT-IR of **22**

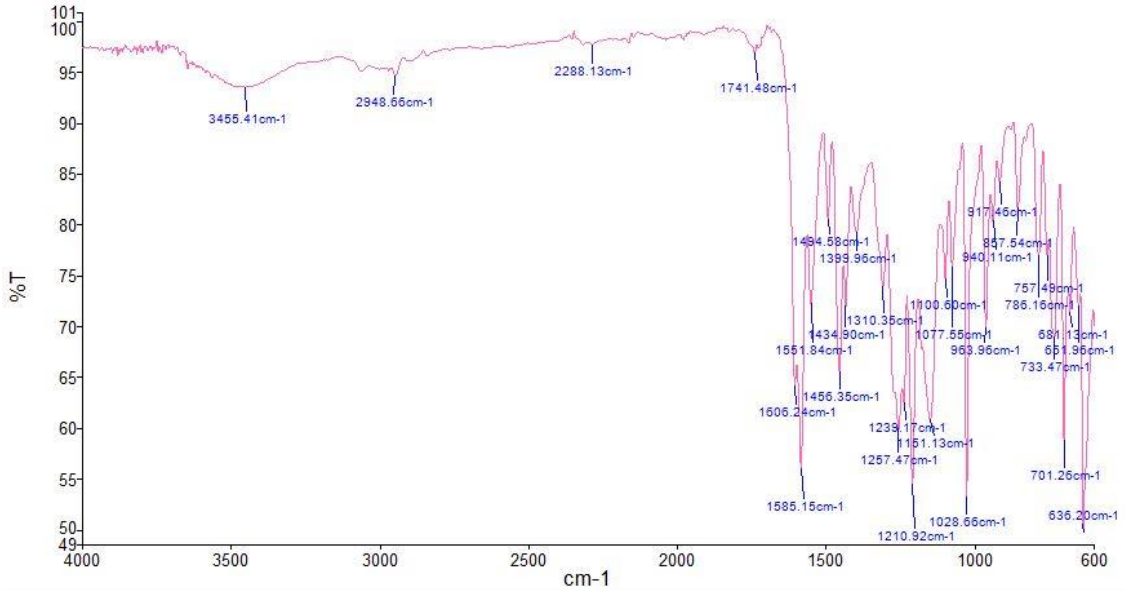

S4.4 FT-IR of **23**

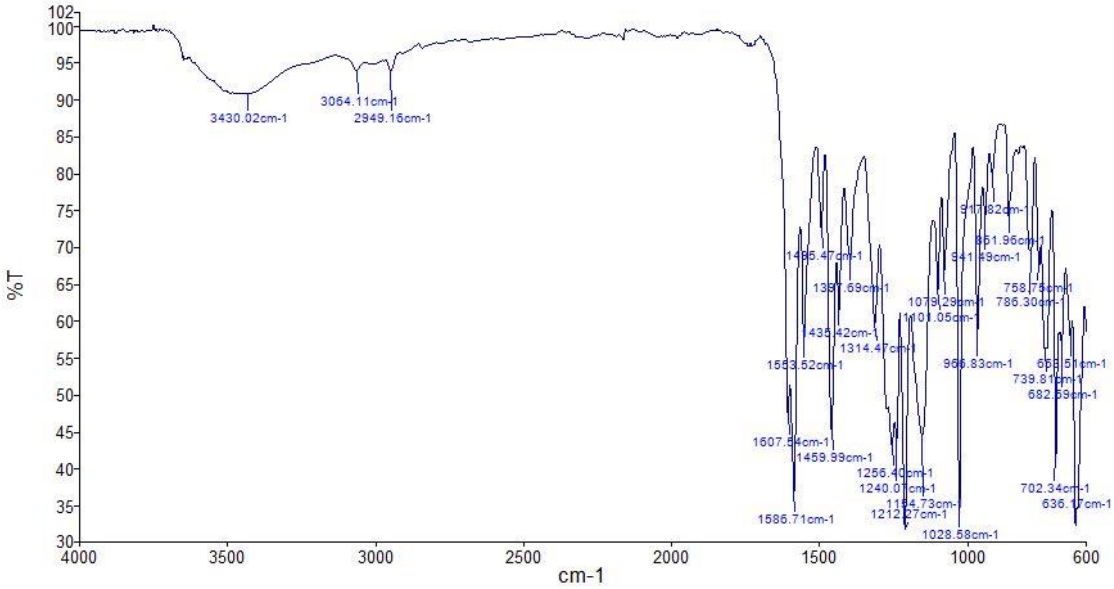

S4.5 FT-IR of **24**

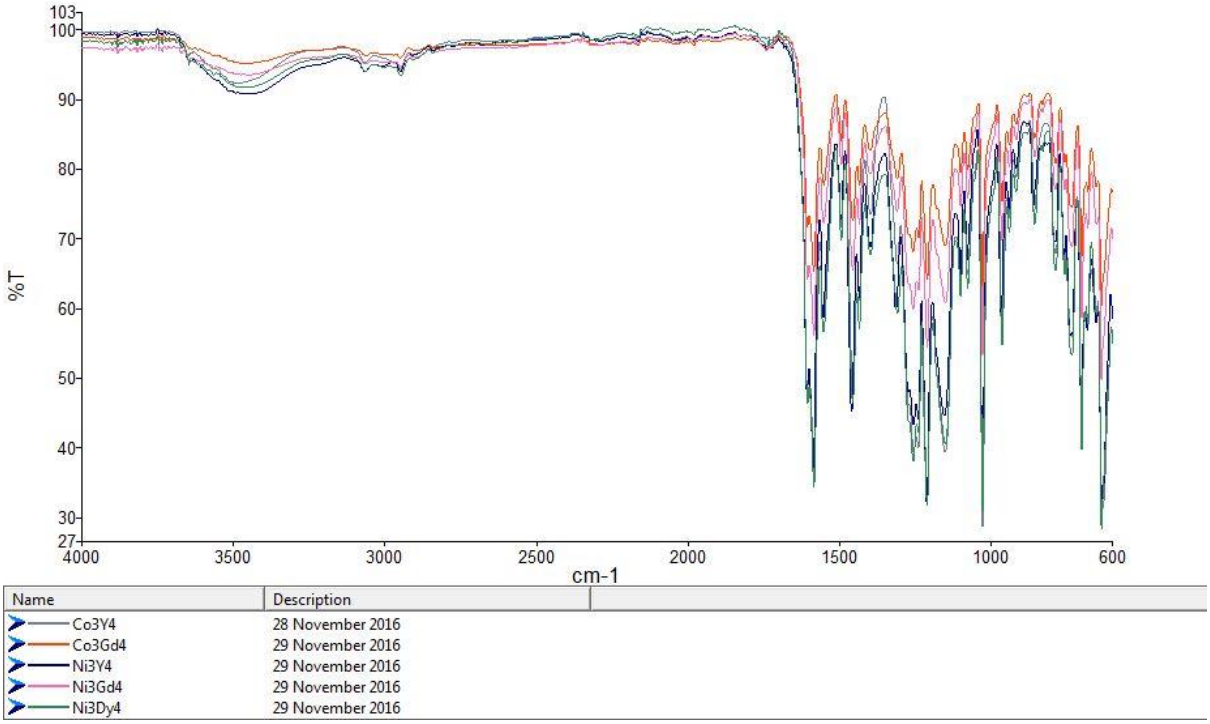

S4.6 FT-IR comparison of **20-24**

4.2 ESI-MS of 20-24

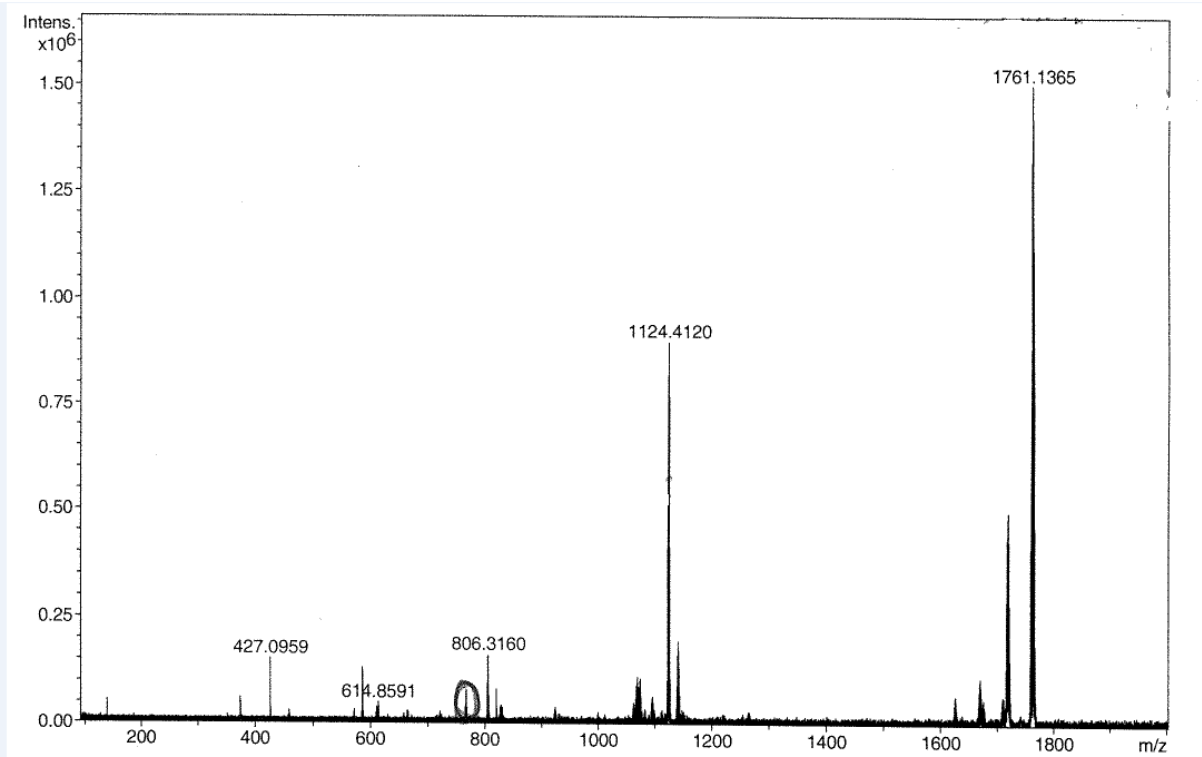

S4.7 ESI-MS of **20** - (807.06m/z $[Co^{II}_3Gd^{III}_4(OH)_6(C_{19}H_{18}N_3O_3)_6(CF_3SO_3)_2]^{4+}$) (1125.39m/z $[Co^{II}_3Gd^{III}_4(OH)_6(C_{19}H_{18}N_3O_3)_6(CF_3SO_3)_3]^{3+}$) (1762.06m/z $[Co^{II}_3Gd^{III}_4(OH)_6(C_{19}H_{18}N_3O_3)_6(CF_3SO_3)_4]^{2+}$)

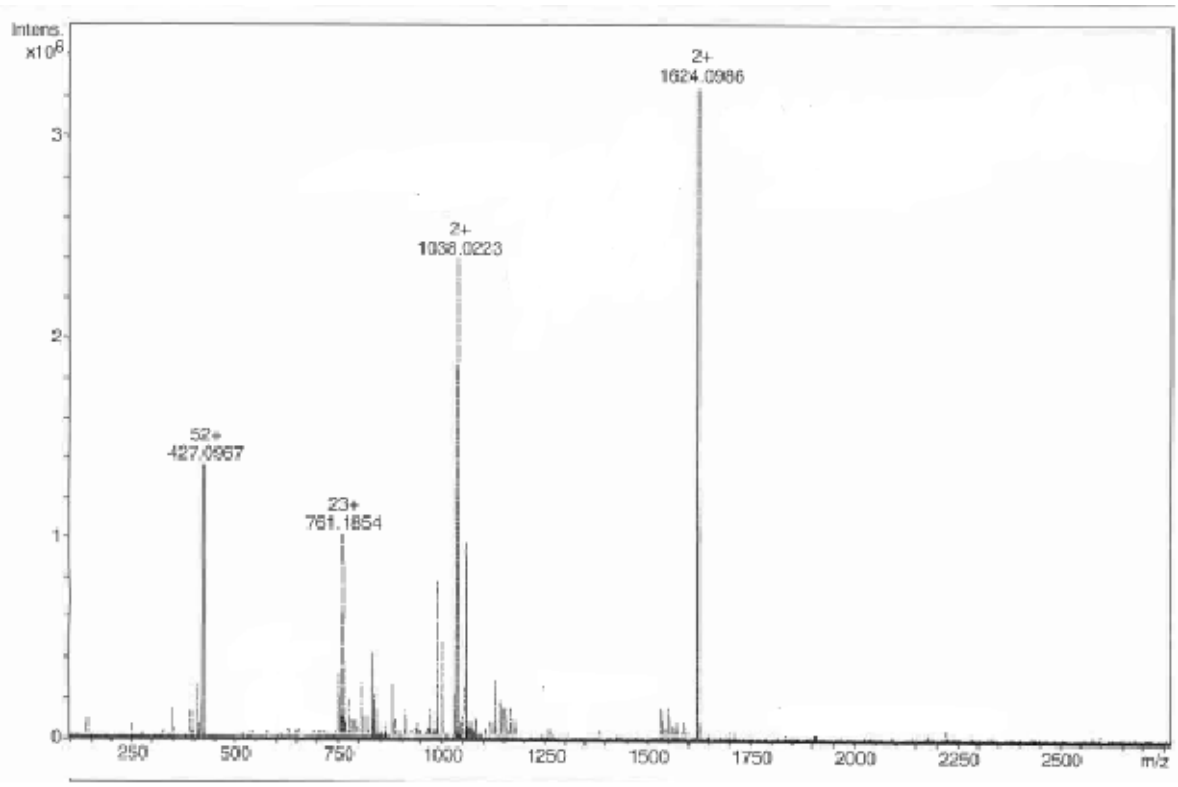

S4.8 ESI-MS of **21** -(761.19 m/z $[Co^{II}_3Y^{III}_4(OH)_6(C_{19}H_{18}N_3O_3)_6(CF_3SO_3)_2]^{4+}$) (1038.02 m/z $[Co^{II}_3Y^{III}_4(OH)_6(C_{19}H_{18}N_3O_3)_6(CF_3SO_3)_3]^{3+}$) (1624.03 m/z $[Co^{II}_3Y^{III}_4(OH)_6(C_{19}H_{18}N_3O_3)_6(CF_3SO_3)_4]^{2+}$)

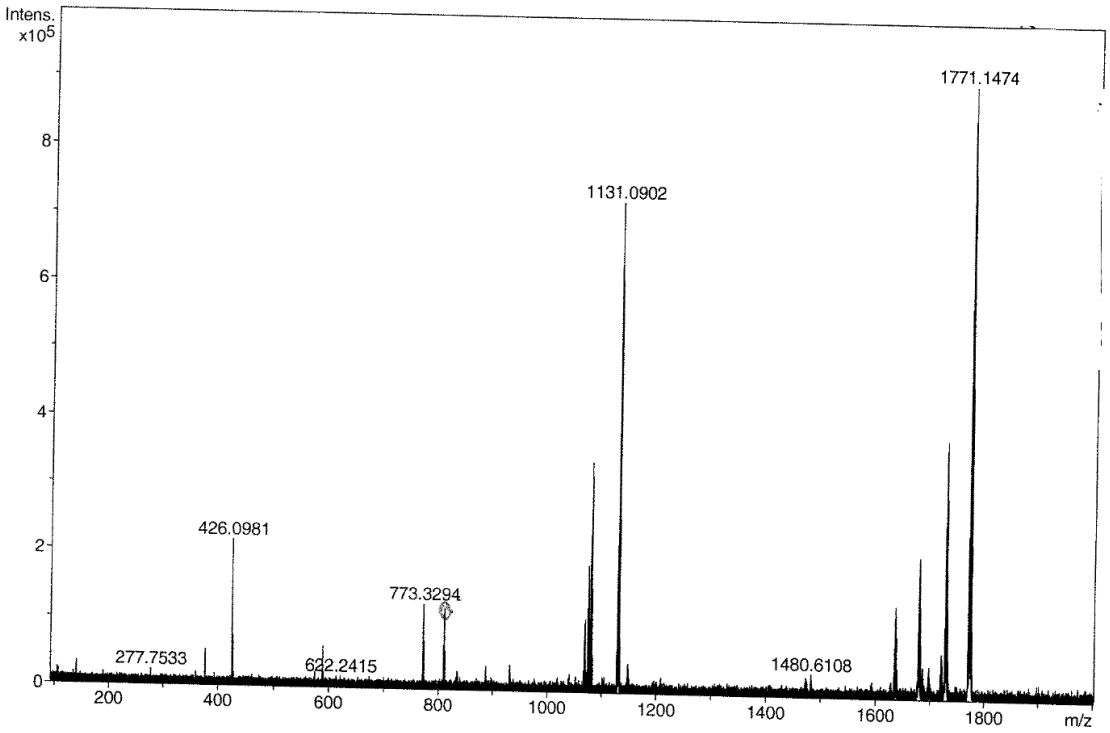

S4.8 ESI-MS of **22** - (774.82 m/z $[Ni^{II}_3Dy^{III}_4(OH)_6(C_{19}H_{18}N_3O_3)_6(CF_3SO_3)]^{4+}$) (1132.07 m/z $[Ni^{II}_3Dy^{III}_4(OH)_6(C_{19}H_{18}N_3O_3)_6(CF_3SO_3)_3]^{3+}$) (1771.14 m/z $[Ni^{II}_3Dy^{III}_4(OH)_6(C_{19}H_{18}N_3O_3)_6(CF_3SO_3)_4]^{2+}$)

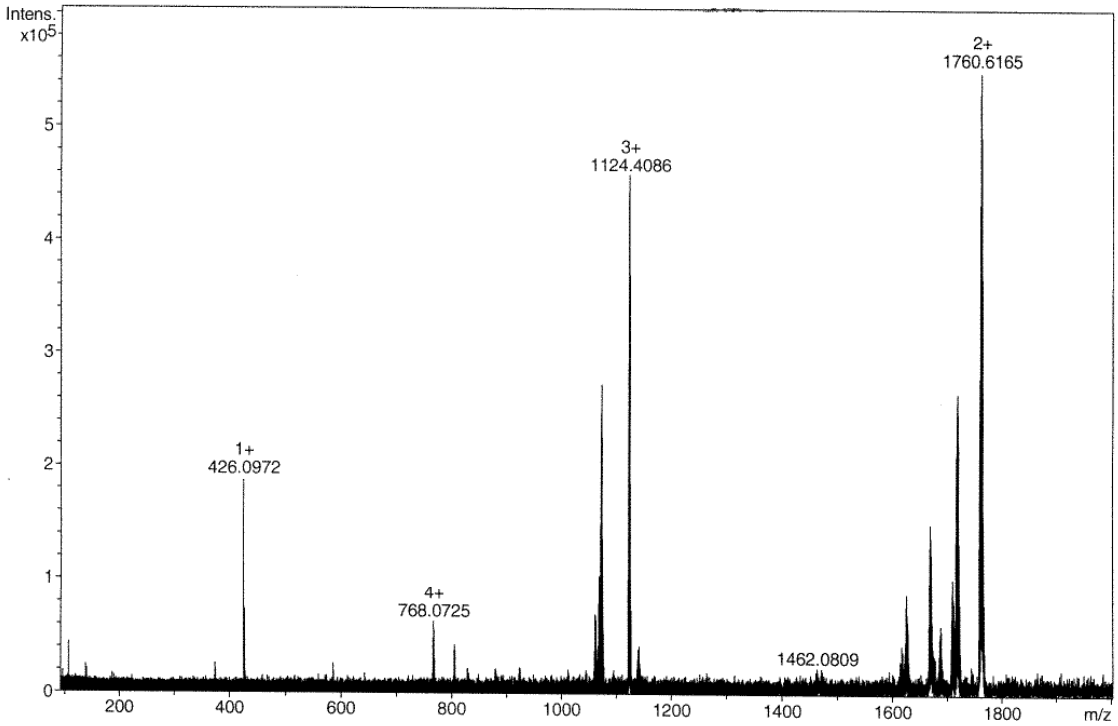

S4.9 ESI-MS of **23** - 768.09 m/z $[Ni^{II}_3Gd^{III}_4(OH)_6(C_{19}H_{18}N_3O_3)_6(CF_3SO_3)]^{4+}$) (1124.41 m/z $[Ni^{II}_3Gd^{III}_4(OH)_6(C_{19}H_{18}N_3O_3)_6(CF_3SO_3)_3]^{3+}$) (1760.61 m/z $[Ni^{II}_3Gd^{III}_4(OH)_6(C_{19}H_{18}N_3O_3)_6(CF_3SO_3)_4]^{2+}$)

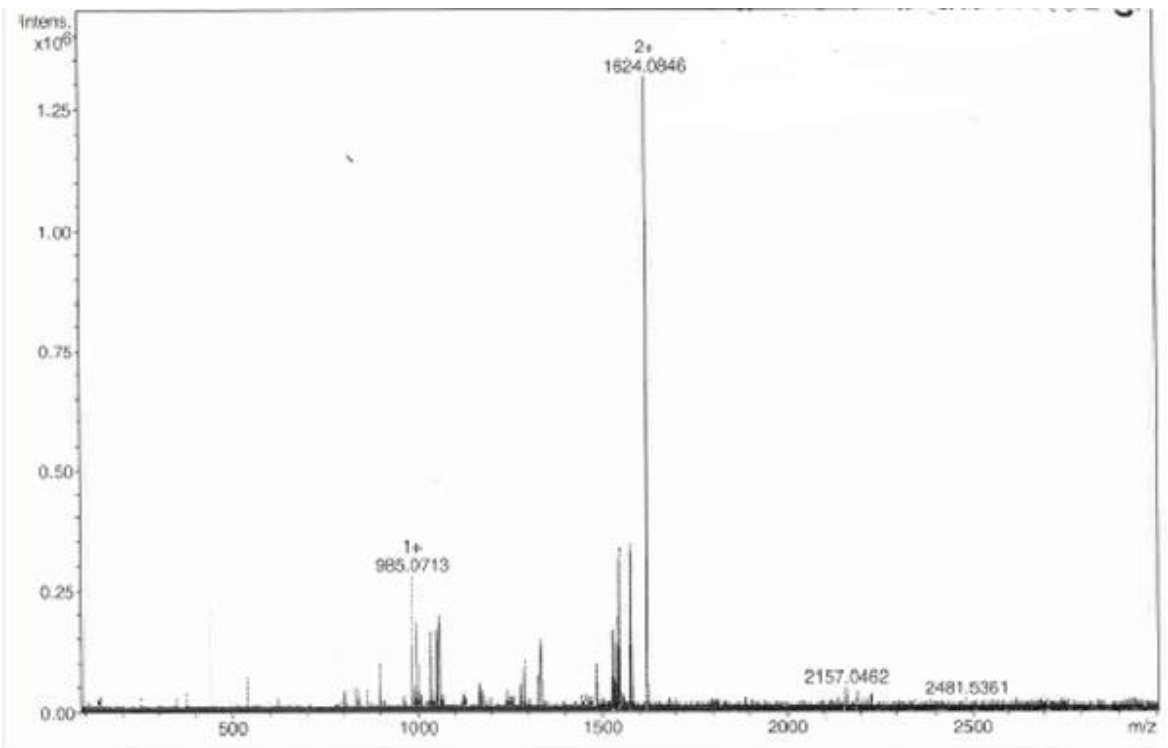

S4.10 ESI-MS of **24 -** (1624.09 m/z $[Ni^{II}_3Y^{III}_4(OH)_6(C_{19}H_{18}N_3O_3)_6(CF_3SO_3)_4]^{2+}$)

4.3 TGA of 20-24

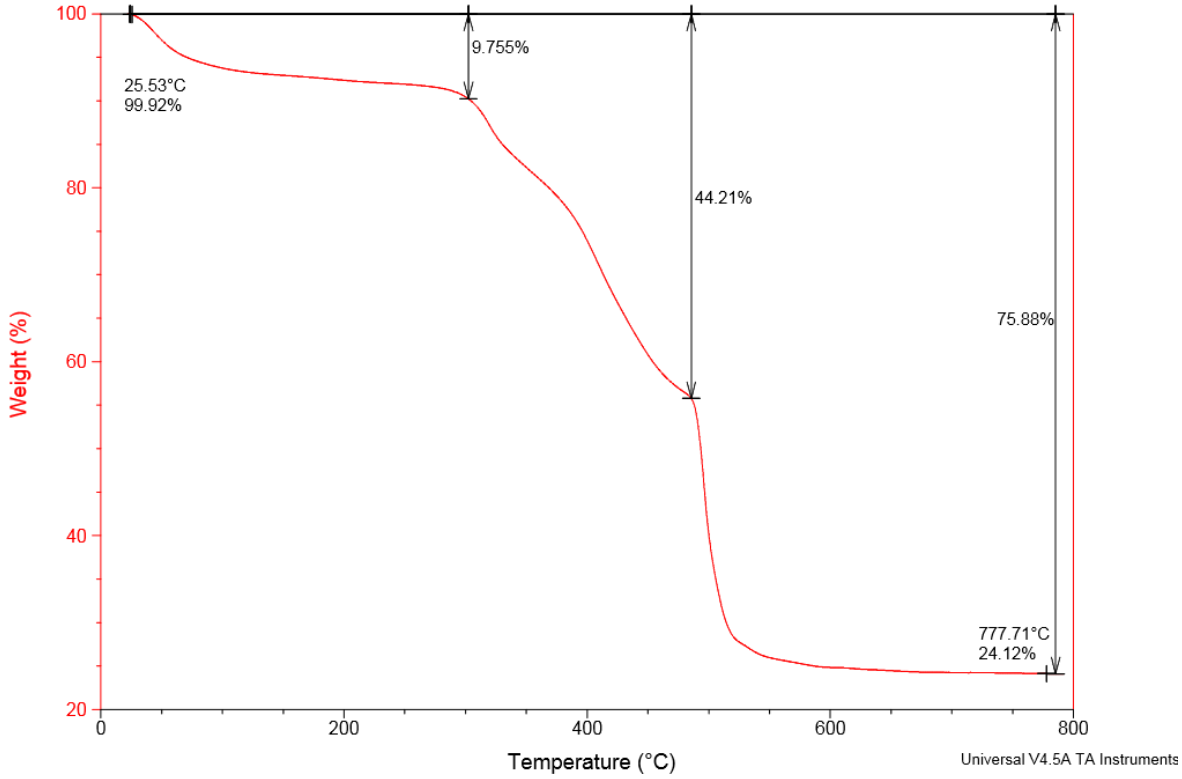

S4.11 TGA of **20**

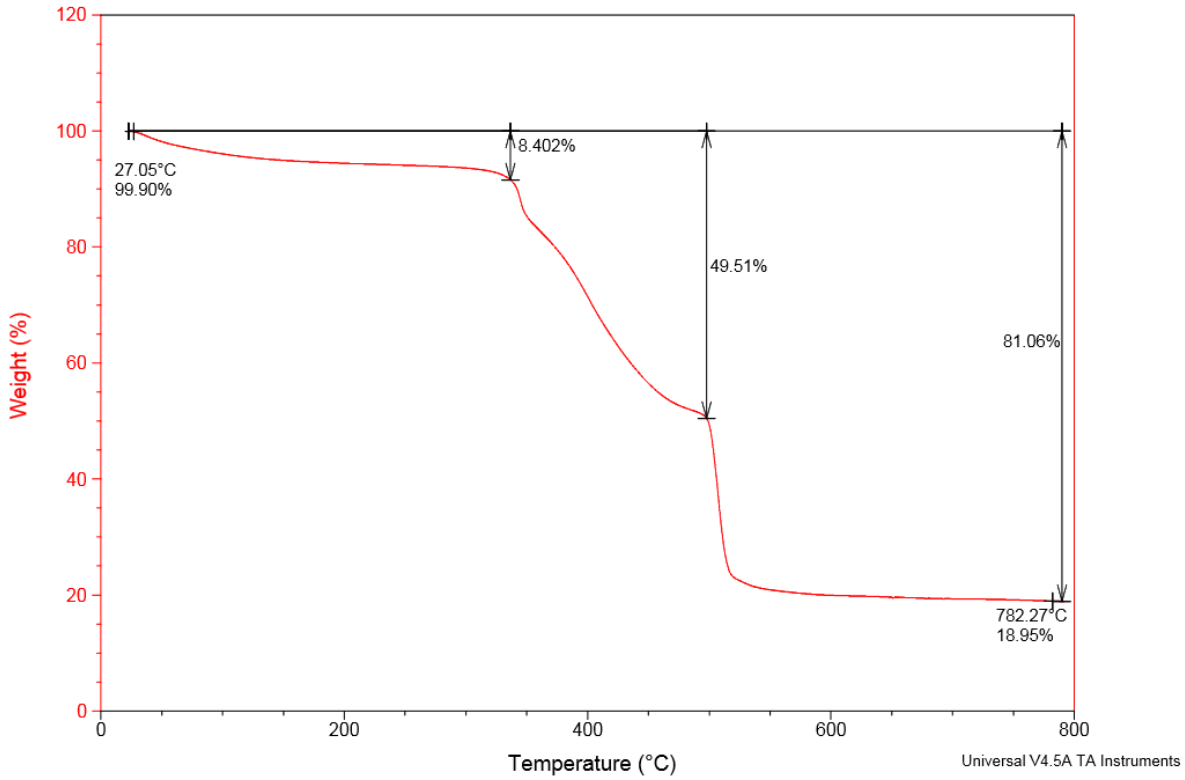

S4.12 TGA of **21**

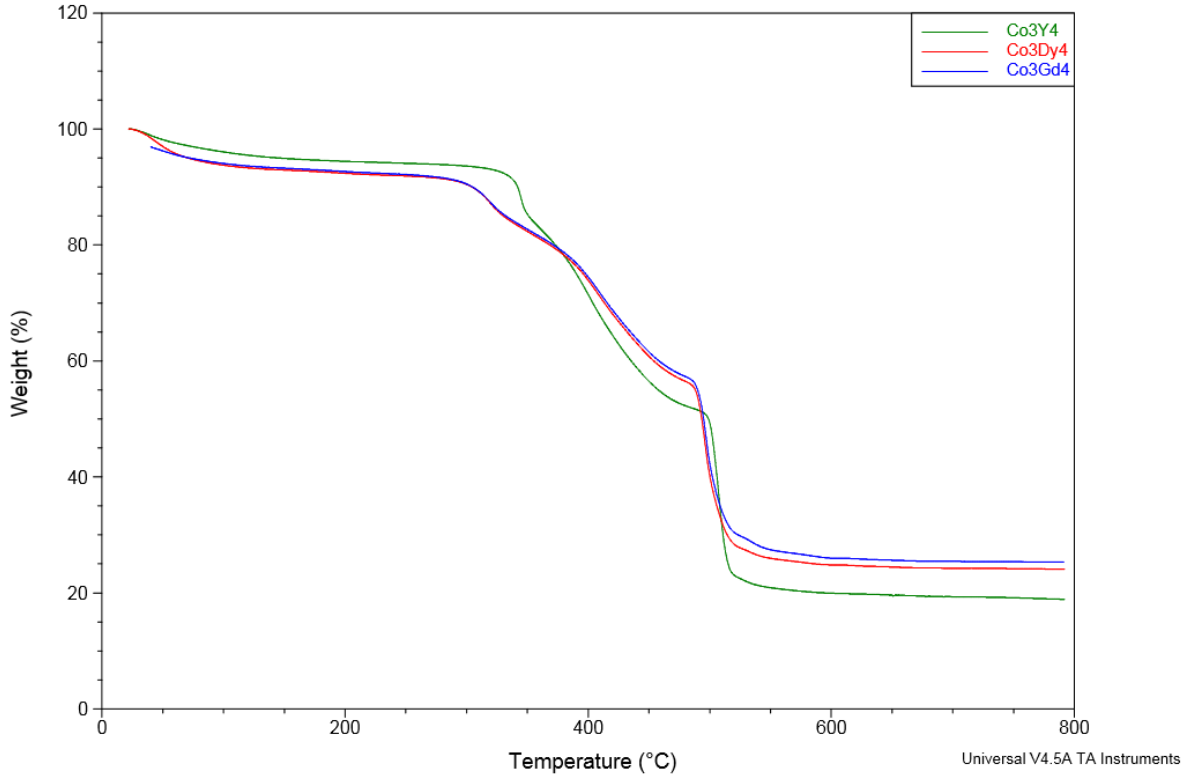

S4.12 TGA comparison of **20** (Blue)**, 21** (green) and **CoDy-EtOH** (red)

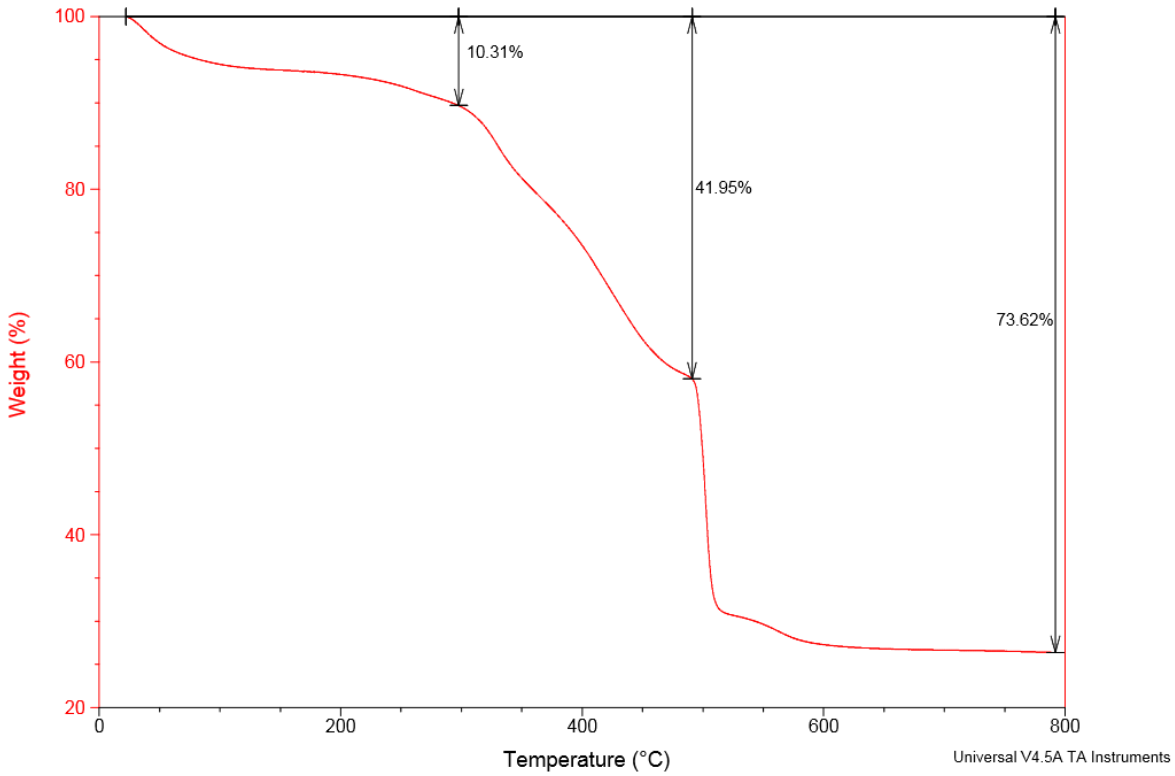

S4.13 TGA of **23**

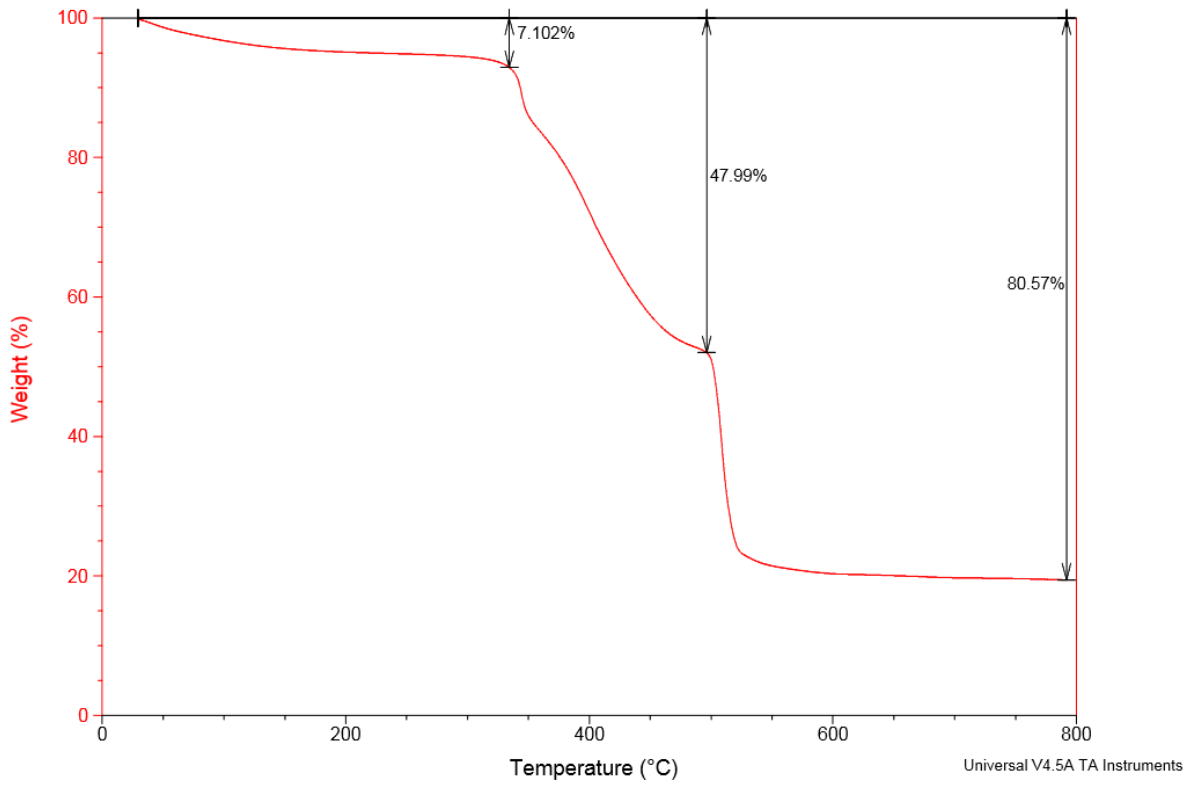

S4.14 TGA of **24**

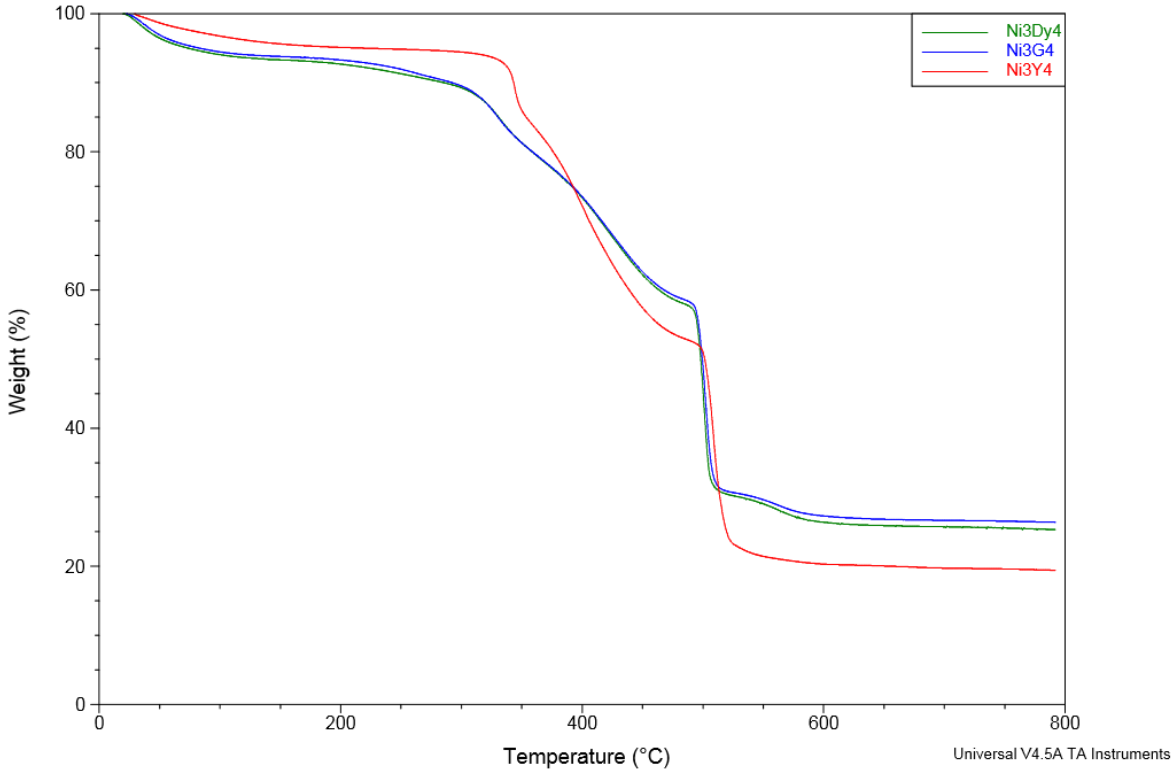

S4.15 TGA comparison of **22** (green)**, 23** (blue) and **24** (red)

Chapter 5

5.1 FT-IR of Complexes 25-42

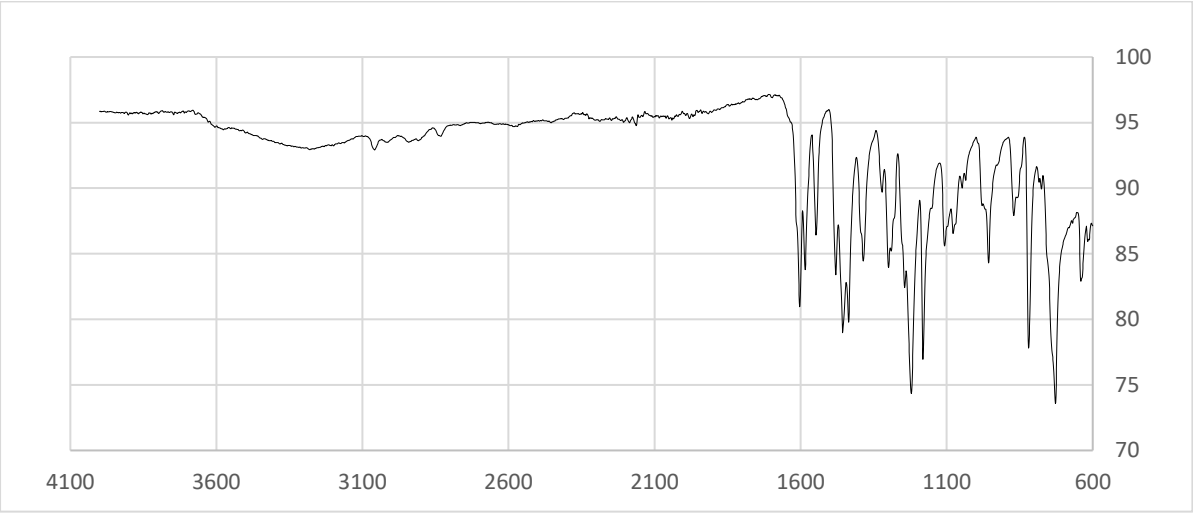

S5.1 FT-IR of **25**

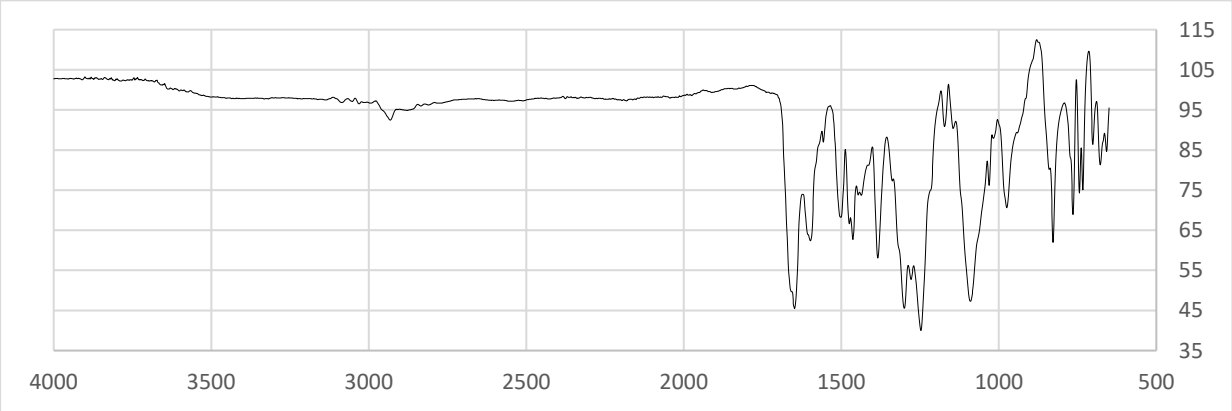

S5.2 FT-IR of **26**

S5.3 FT-IR of **27**

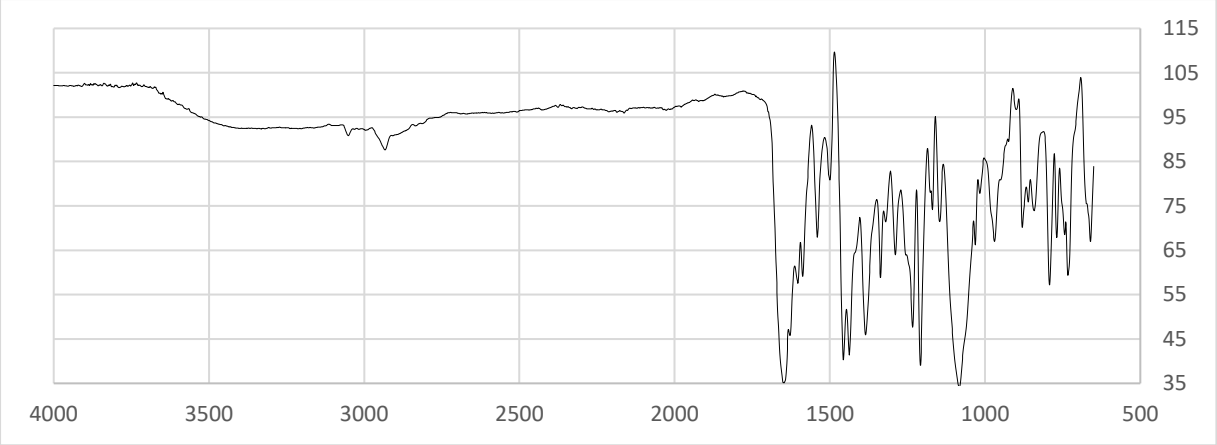

S5.4 FT-IR of **28**

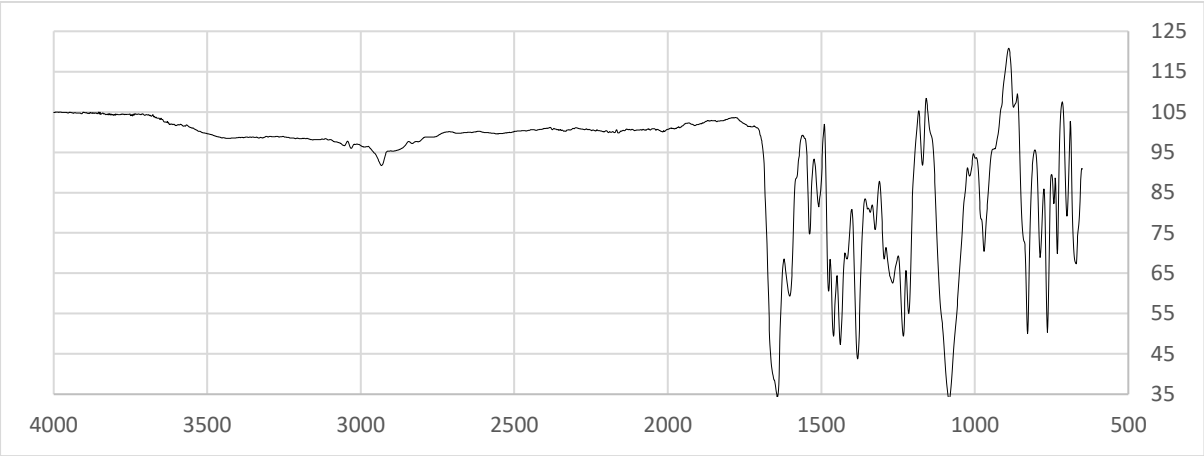

S5.5 FT-IR of **29**

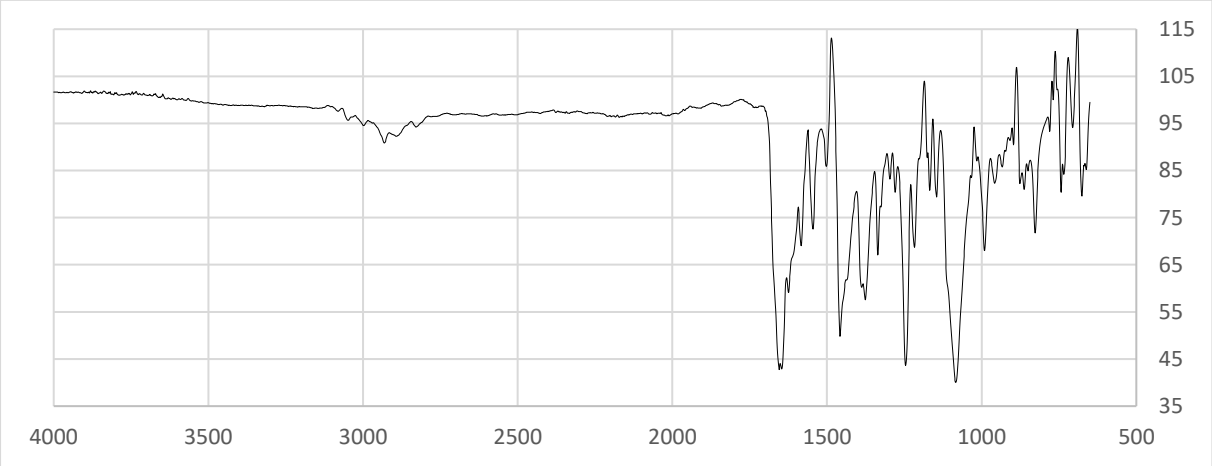

S5.6 FT-IR of **30**

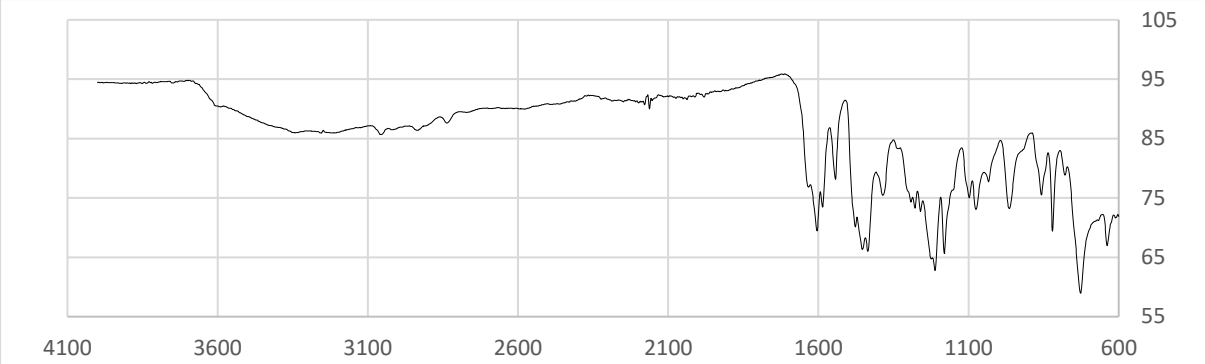

S5.7 FT-IR of **31**

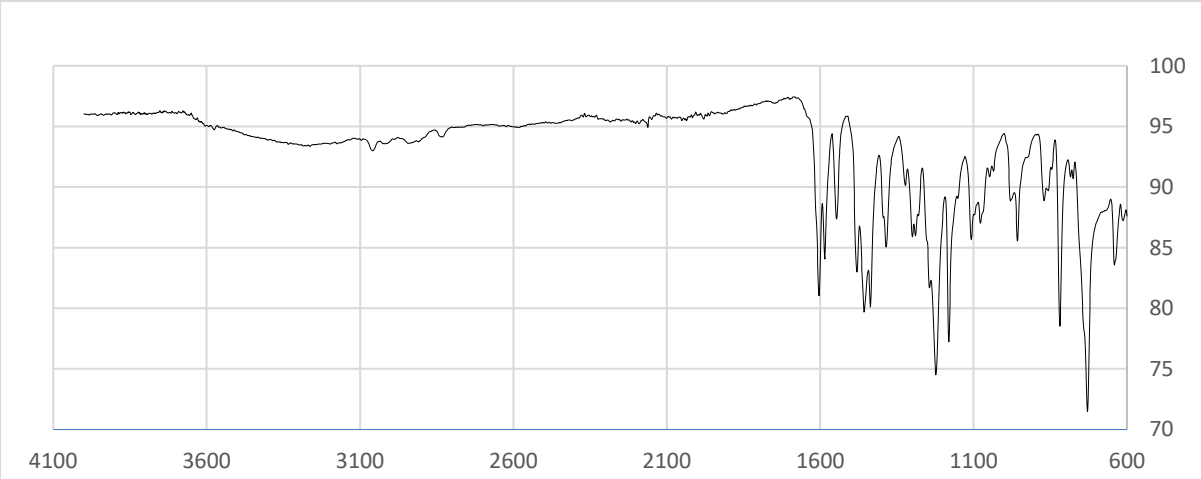

S5.8 FT-IR of **32**

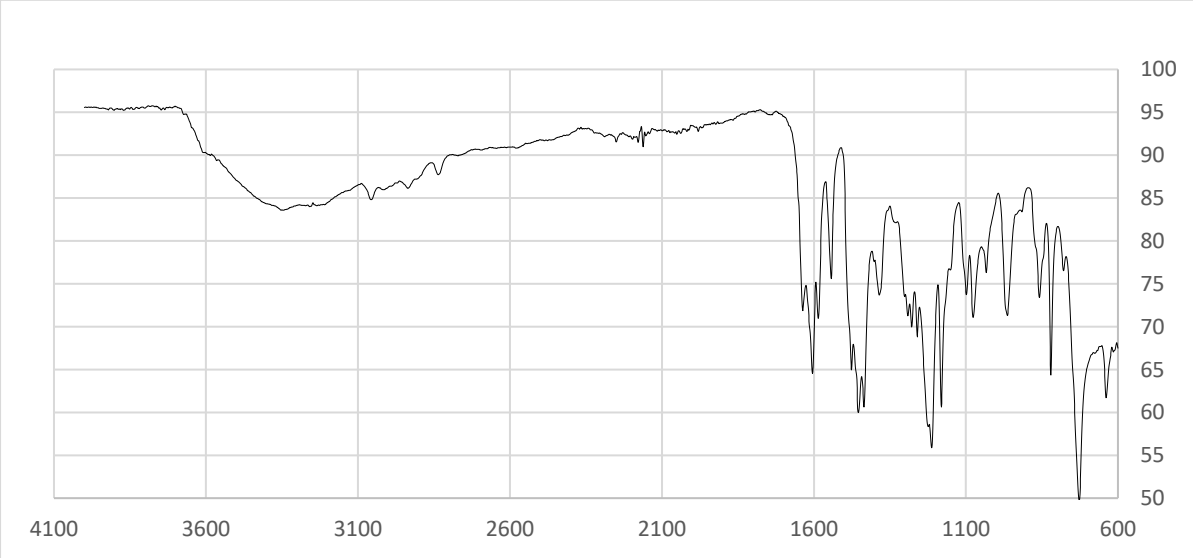

S5.9 FT-IR of **33**

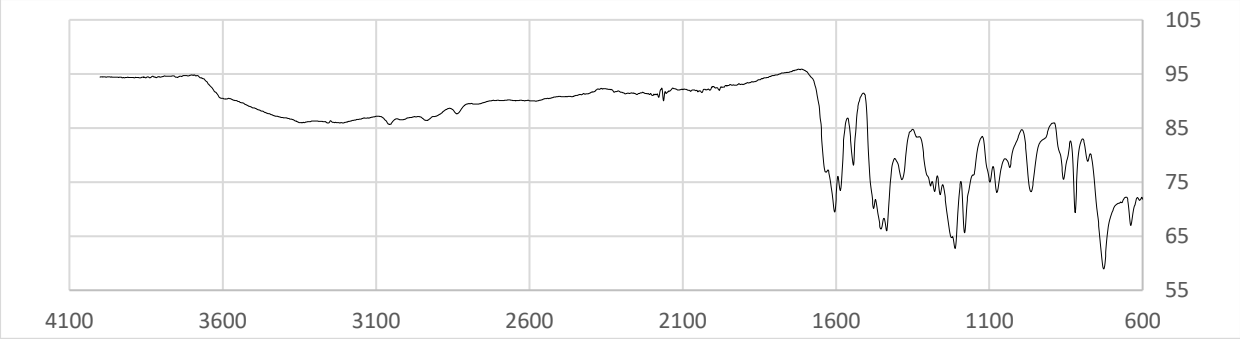

S5.10 FT-IR of **34**

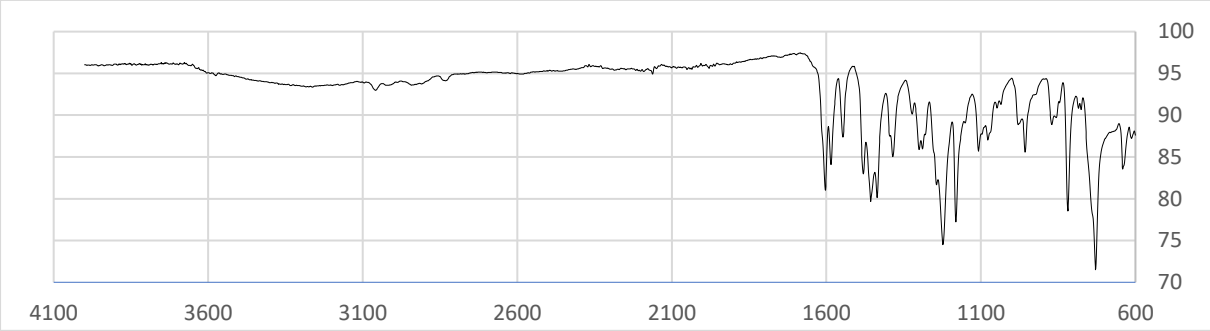

S5.11 FT-IR of **35**

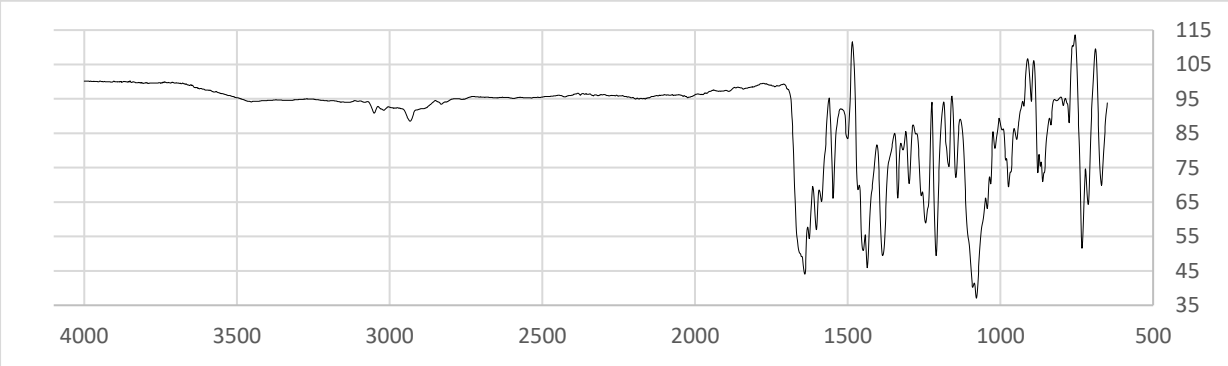

S5.12 FT-IR of **36**

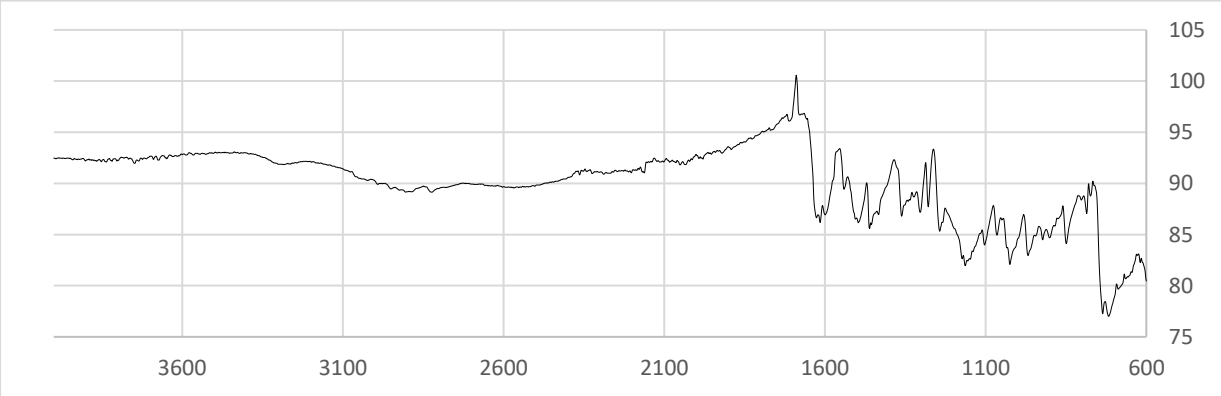

S5.13 FT-IR of **37**

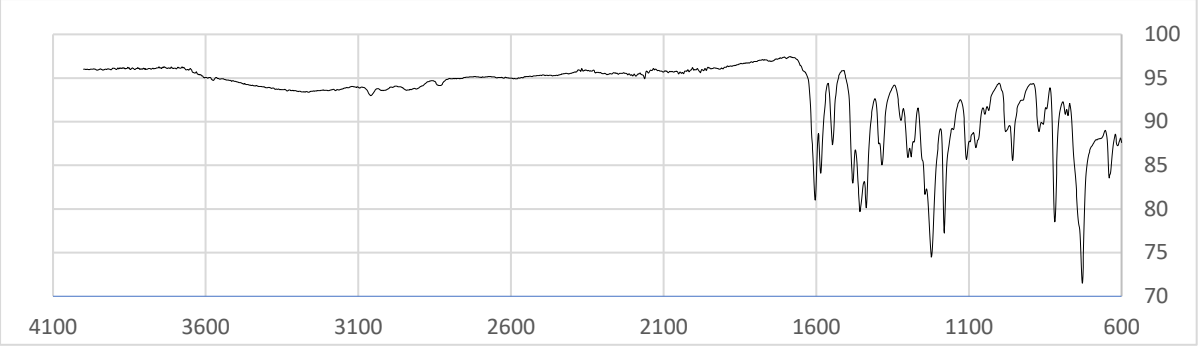

S5.14 FT-IR of **38**

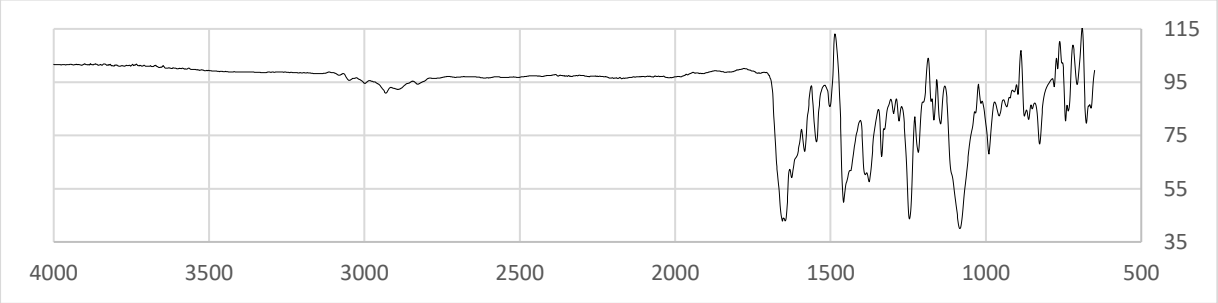

S5.15 FT-IR of **39**

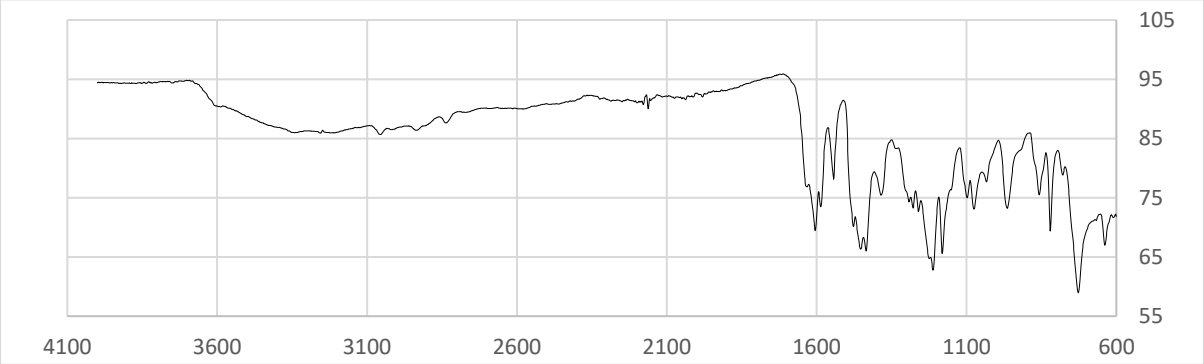

S5.16 FT-IR of **40**

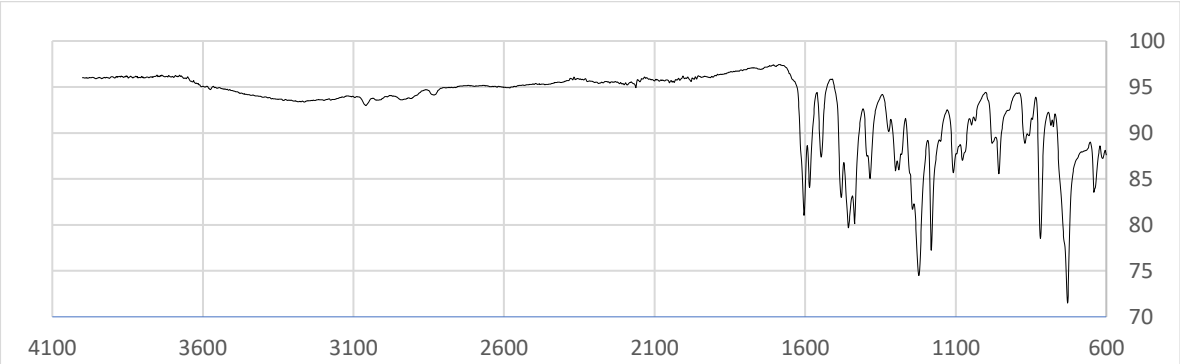

S5.17 FT-IR of **42**

5.2 ESI-MS of Compounds 28, 31 and 37

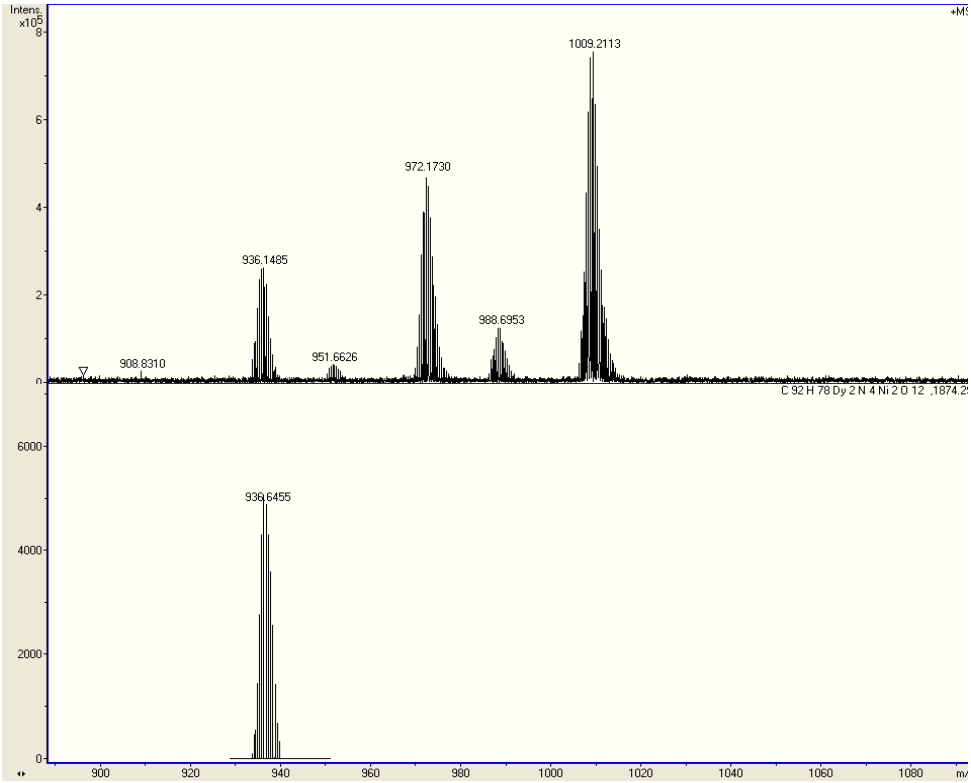

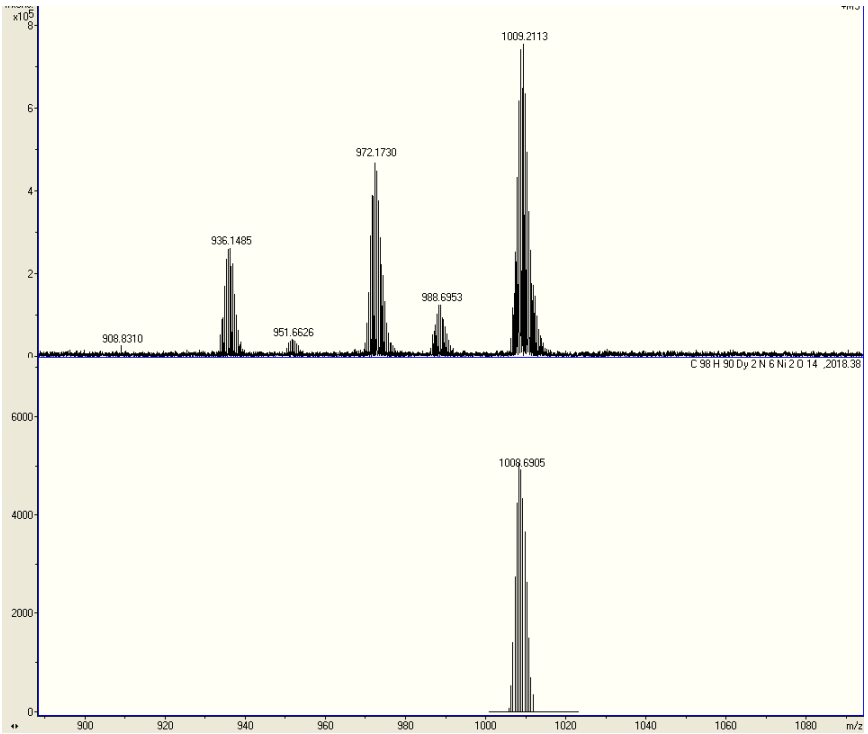

S5.18 ESI-MS of **28**

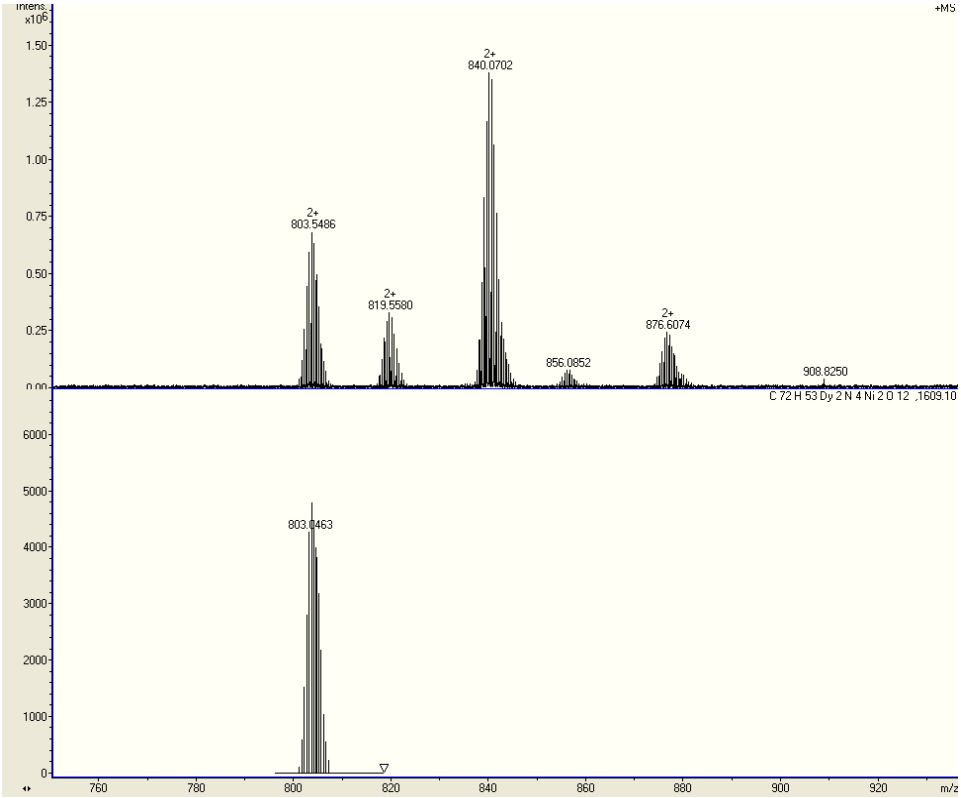
Intens.
x10^6
+MS
2+
840.0702
2+
803.5486
2+
819.5580
2+
876.6074
856.0852
908.8250
C 72 H 53 Dy 2 N 4 Ni 2 O 12 ,1609.10
803.0463
m/z

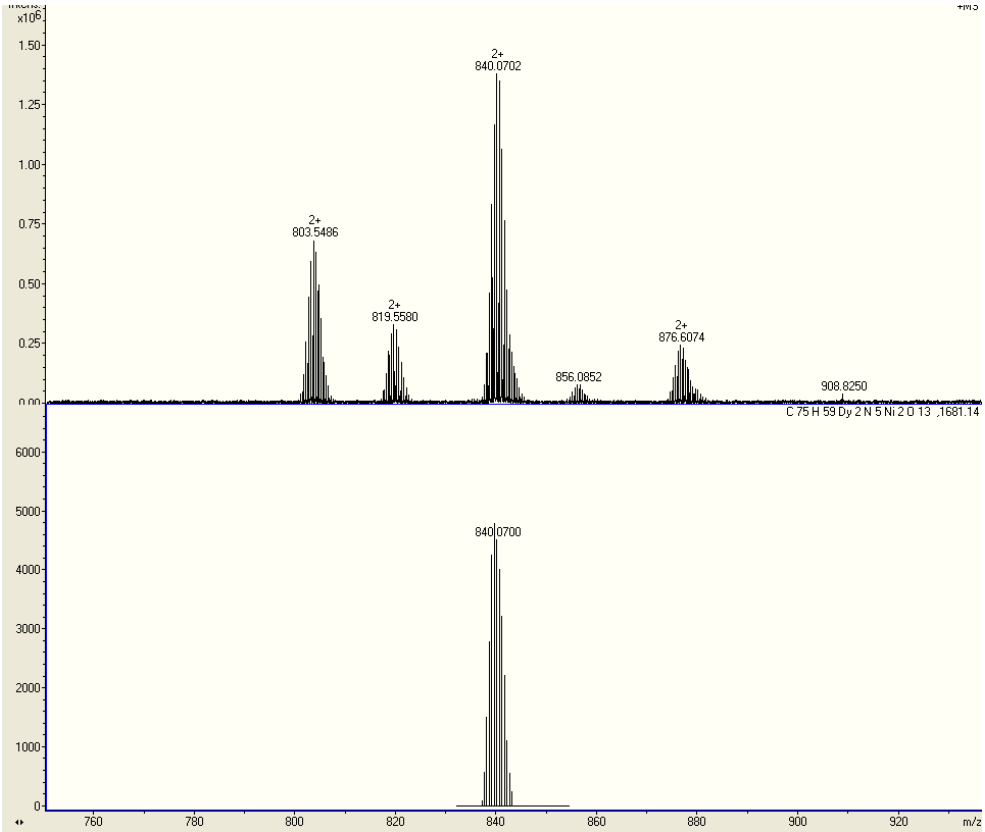
x10^6
2+
840.0702
2+
803.5486
2+
819.5580
2+
876.6074
856.0852
908.8250
C 75 H 59 Dy 2 N 5 Ni 2 O 13 ,1681.14
840.0700
m/z

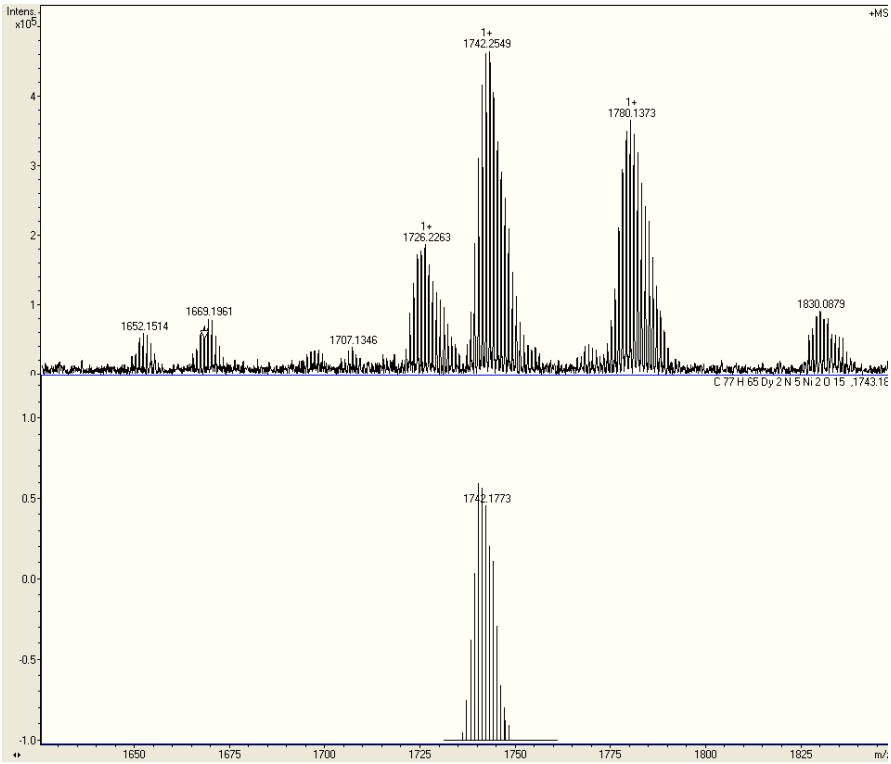

S5.19 ESI-MS of **31**

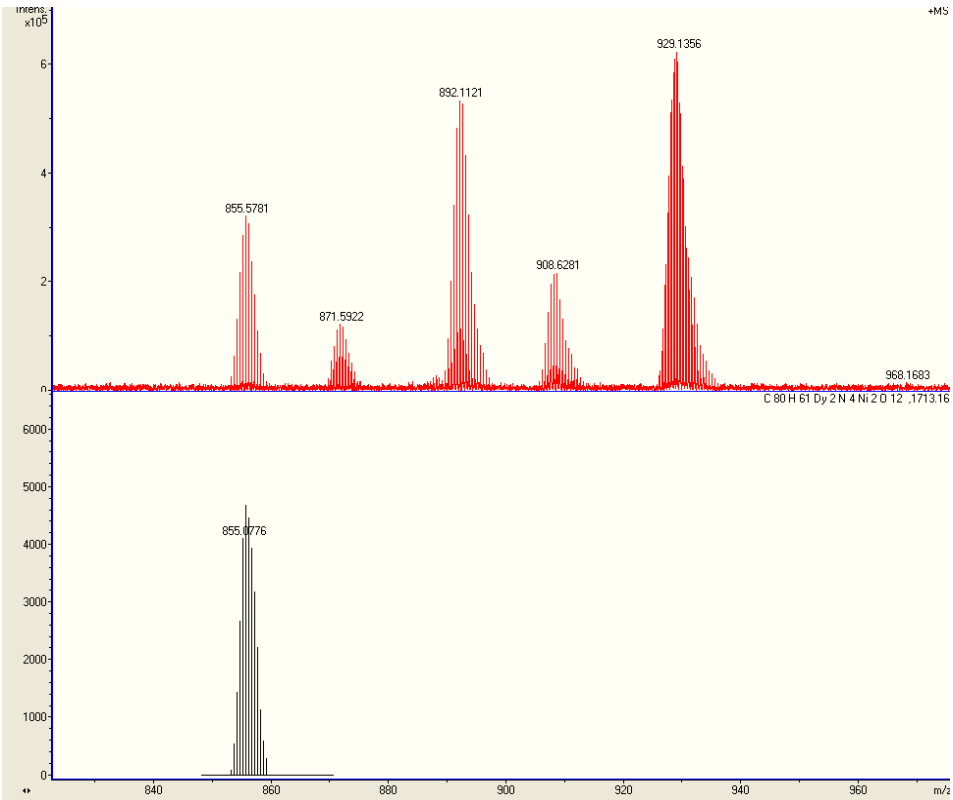

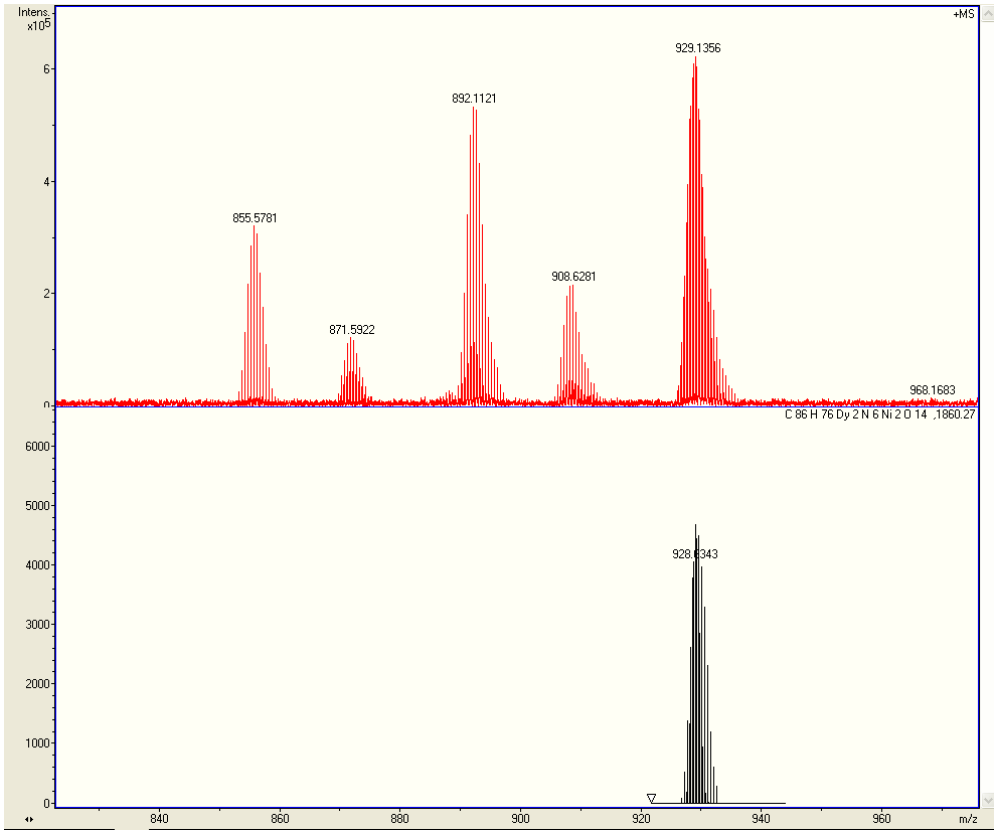

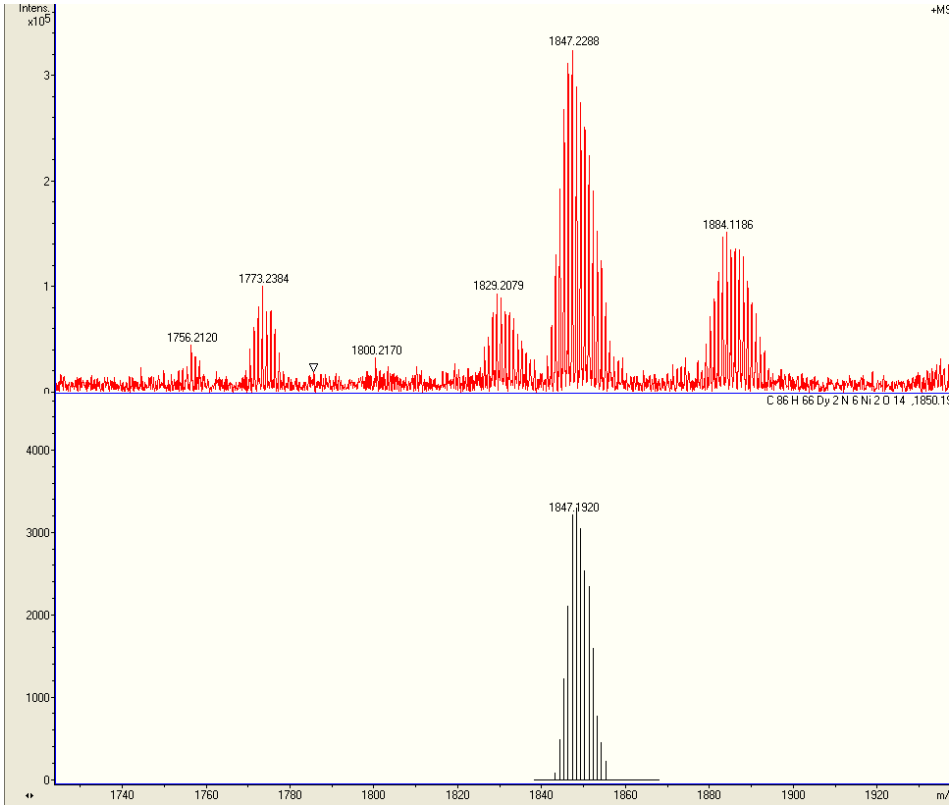

S5.20 ESI-MS of **37**

Chapter 6

6.1 Observed Coordination modes

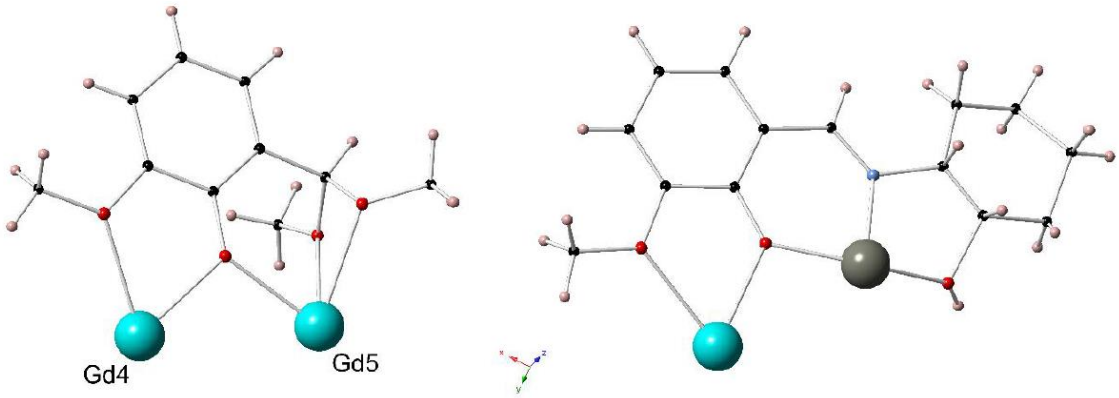

S6.1 The coordination modes of ligands seen in **43** and **44**

6.2 TGA of 43 and 44

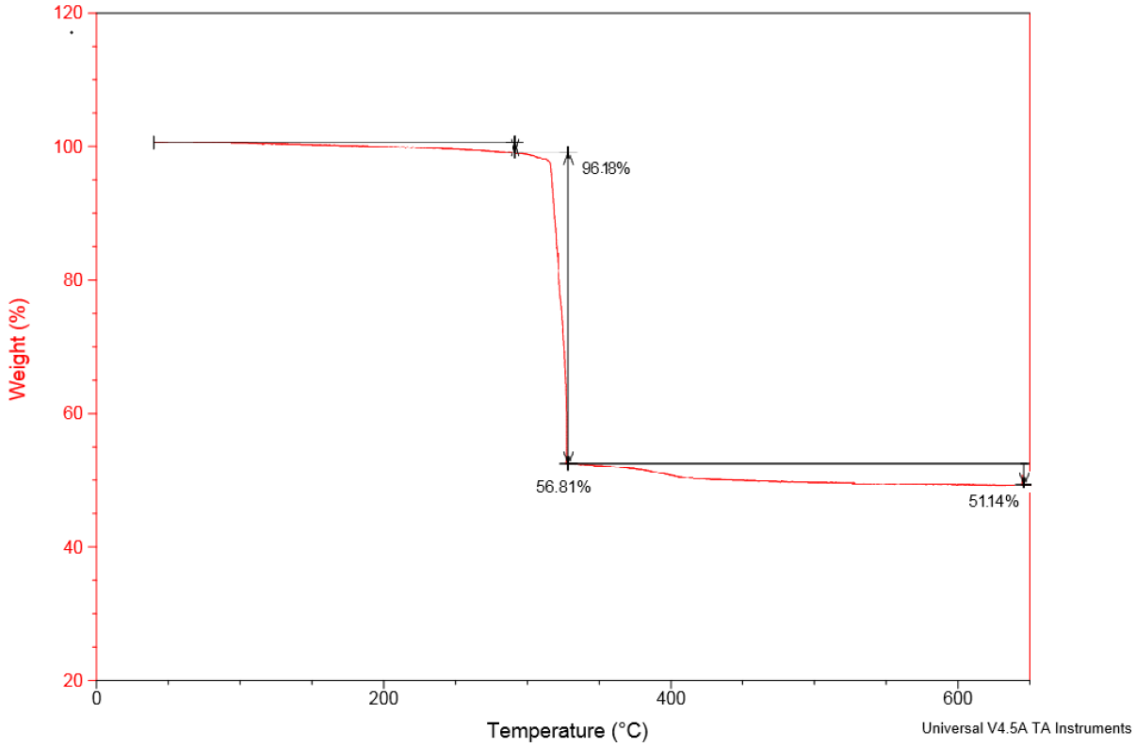

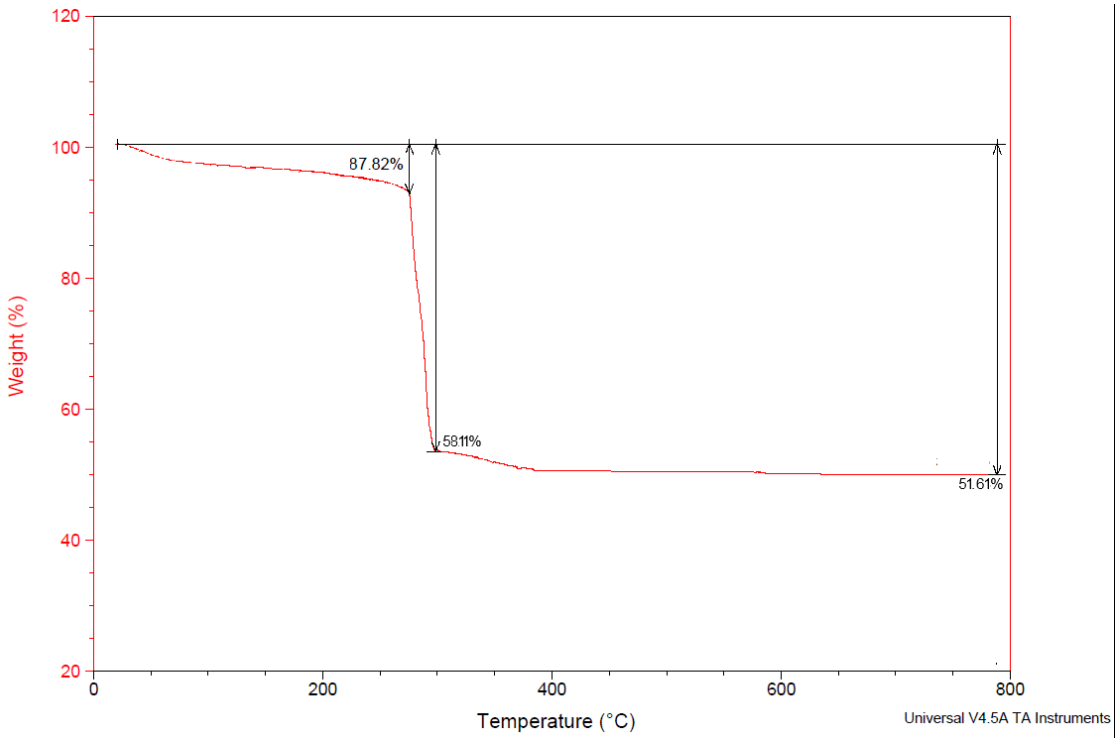

S6.2 (Top) TGA of compound **43** (Bottom) TGA of compound **44**

6.3 Shape Analysis of 43 and 44

S6.3 Complete results of the SHAPE analysis for the nine-coordinated Ln^{III} ions in the complex $Zn^{II}_4Gd^{III}_{11}$ (**43**) and $Zn^{II}_4Dy^{III}_{11}$ (**44**) with the EP-9 = enneagon, OPY = octagonal pyramid, HBPY = heptagonal bipyramid, JTC-9 Johnson trigonal cupola, JCCU-9 = capped cube, CCU-9 spherical-relaxed capped cube, JCSAPR-9 = tricapped trigonal prism,TCTPR-9 = spherical tricapped trigonal prism, JTDIC-9 tridiminished icosahedron, HH-9 == hula-hoop, MFF-9 = muffin.

	Gd2	Dy2	Gd3	Dy3	Gd4	Dy4	Gd5	Dy5
EP-9	32.856	33.888	34.682	34.719	34.565	34.966	33.790	32.915
OPY-9	19.651	19.374	23.307	22.957	23.033	23.182	19.256	19.579
HBPY-9	17.313	18.063	18.576	17.810	17.867	18.510	18.131	17.306
JTC-9	13.795	14.903	14.341	14.070	14.022	14.445	14.826	13.782
JCCU-9	9.709	10.621	10.392	9.305	9.187	10.279	10.719	9.799
CCU-9	9.037	9.625	9.787	9.063	8.946	9.694	9.747	9.126
JCSAPR-9	2.535	2.453	1.869	1.952	2.077	1.863	2.449	2.560
CSAPR-9	**1.873**	**1.674**	**1.411**	**1.493**	**1.526**	**1.426**	**1.680**	**1.881**
JTCTPR-9	3.609	3.814	2.336	2.196	2.234	2.345	3.774	3.650
TCTPR-9	2.326	1.953	2.257	2.158	2.140	2.234	1.972	2.297
JTDIC-9	11.417	11.292	12.087	11.642	11.739	12.280	11.351	11.451
HH-9	10.955	11.810	11.480	11.370	11.413	11.374	11.867	10.978
MFF-9	2.070	2.023	**1.345**	**1.694**	**1.688**	**1.326**	2.055	2.077

S6.4 Complete results of the SHAPE analysis for the eight-coordinated Ln^{III} ions in the complex $Zn^{II}_4Gd^{III}_{11}$ (**43**) and $Zn^{II}_4Dy^{III}_{11}$ (**44**) with OP-8 = octagon, HPY-8 = heptagonal pyramid, HBPY-8= hexagonal bypryramid, CU-8= cube, SAPR-8 = Johnson elongated triangular bipyramid, JBTPR-8 = biaugmented trigonal prism J50, BTPR-8 = biaugmented trigibal prism, JSD-8 = snub diphenoid, TT-8 triakis tetrahedron, ETBPY-8 = elongated trigonal bipyramid.

	Gd6	Dy6	Gd1	Dy1
OP-8	31.768	31.704	31.016	31.225
HPY-8	23.124	23.055	23.510	23.441
HBPY-8	11.900	11.897	16.622	16.472
CU-8	11.657	11.699	9.222	9.053
SAPR-8	5.979	5.957	**0.335**	**0.372**
TDD-8	4.248	4.198	2.444	2.420
JGBF-8	8.139	8.196	16.869	16.824
JETBPY-8	22.734	22.756	29.112	29.098
JBTPR-8	4.258	4.195	3.158	3.196
BTPR-8	**3.861**	**3.831**	2.502	2.547
JSD-8	4.145	4.106	5.594	5.615
TT-8	12.447	12.495	10.087	9.920
ETBPY-8	19.543	19.599	24.829	24.821

6.4 Magellan program

Table S6.5 Input file for Magellan program for complex Zn4Dy11 (**44**) leading to Figure!sites 11 1 2 18 20 36 37 38 39 40 41 42
Dy 9.36027 22.08810 7.25876 3
Dy 9.94045 22.08810 3.78454 3
O 11.03397 24.14126 3.91088 -0.33
N 11.24306 24.18858 5.20250 0
O 8.26675 24.14126 7.13243 -0.33
N 8.05766 24.18858 5.84080 0
O 9.63739 23.37475 1.79962 0
O 9.65036 20.65005 5.52165 -1
O 11.98787 21.23221 3.48814 -0.5
O 8.33567 23.11293 5.17843 -0.33
O 10.96505 23.11293 5.86488 -0.33
O 7.66207 21.46178 2.85447 0
O 9.85848 20.25645 2.41340 -0.5
O 9.66334 23.37475 9.24369 0
O 7.31285 21.23221 7.55517 -0.5
O 11.63865 21.46178 8.18883 0
O 9.44224 20.25645 8.62990 -0.5
Dy 11.74418 26.37177 3.46539 3
O 11.66689 25.25792 5.70298 -0.33
Dy 7.55654 26.37177 7.57791 3
O 7.63383 25.25792 5.34032 -0.33
O 10.99017 28.61349 2.61881 -2
O 9.54633 26.86350 4.06084 -1
O 11.90841 28.00049 5.09185 -1
O 10.39682 26.03004 1.59289 -1
O 13.54765 27.77127 2.83592 -1
O 13.24838 25.13174 1.74330 0
O 13.88692 25.15733 3.87487 0
O 8.31055 28.61349 8.42449 -2
O 9.75439 26.86350 6.98246 -1
O 7.39232 28.00049 5.95146 -1
O 8.90390 26.03004 9.45042 -1
O 5.75307 27.77127 8.20738 -1
O 6.05234 25.13174 9.30001 0
O 5.41380 25.15733 7.16843 0
Dy 10.48151 27.65946 9.03364 3
Dy 9.65036 28.72355 5.52165 3
Dy 12.96595 29.74066 3.94180 3
Dy 9.93471 31.07006 2.55917 3
Dy 6.33477 29.74066 7.10151 3
Dy 9.36601 31.07006 8.48413 3
Dy 8.81921 27.65946 2.00966 3
O 8.40357 30.55695 6.44575 -1
O 10.89715 30.55695 4.59755 -1
O 10.75462 29.42908 7.54147 -1
O 8.54610 29.42908 3.50183 -1
O 6.68450 27.27112 3.22244 -0.33
O 7.40024 25.62137 2.02291 -0.33
O 9.23000 29.66881 0.83554 -1
O 8.50383 27.16528 -0.49938 0

O 6.84262 28.17678 0.57138 0
N 6.47923 26.10505 2.75420 0
O 12.24025 31.05149 2.11347 -0.66
O 13.66344 31.87198 4.30026 -0.5
O 14.88928 29.01305 5.30763 -0.33
O 15.11480 29.87525 2.50904 0
O 13.40112 30.04313 6.50583 -0.33
O 10.73303 33.15757 2.96844 -0.5
O 8.38651 32.24210 4.25609 -0.33
O 7.06047 31.05149 8.92984 -0.66
O 8.56769 33.15757 8.07486 -0.5
O 10.91422 32.24210 6.78721 -0.33
O 11.55665 32.15762 8.88323 -0.33
O 9.37909 32.10926 10.83127 0
O 10.07073 29.66881 10.20777 -1

N 11.78768 32.54982 7.68614 0

O 7.74407 32.15762 2.16007 -0.33
O 9.92163 32.10926 0.21203 0
N 7.51304 32.54982 3.35716 0
O 12.61622 27.27112 7.82087 -0.33
O 11.90048 25.62137 9.02039 -0.33
O 10.79690 27.16528 11.54268 0
O 12.45810 28.17678 10.47192 0
N 12.82149 26.10505 8.28910 0
O 5.63728 31.87198 6.74304 -0.5
O 4.41144 29.01305 5.73567 -0.33
O 5.89960 30.04313 4.53747 -0.33
O 4.18593 29.87525 8.53426 0

Chapter 7

7.1 ESI-MS of LMLn

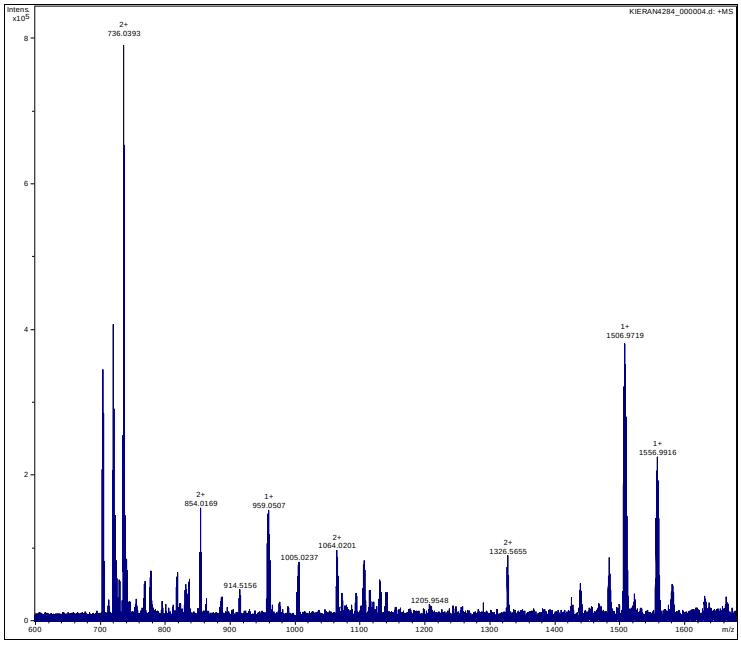

S7.1 ESI-MS of **1CoDy- ClO_4**

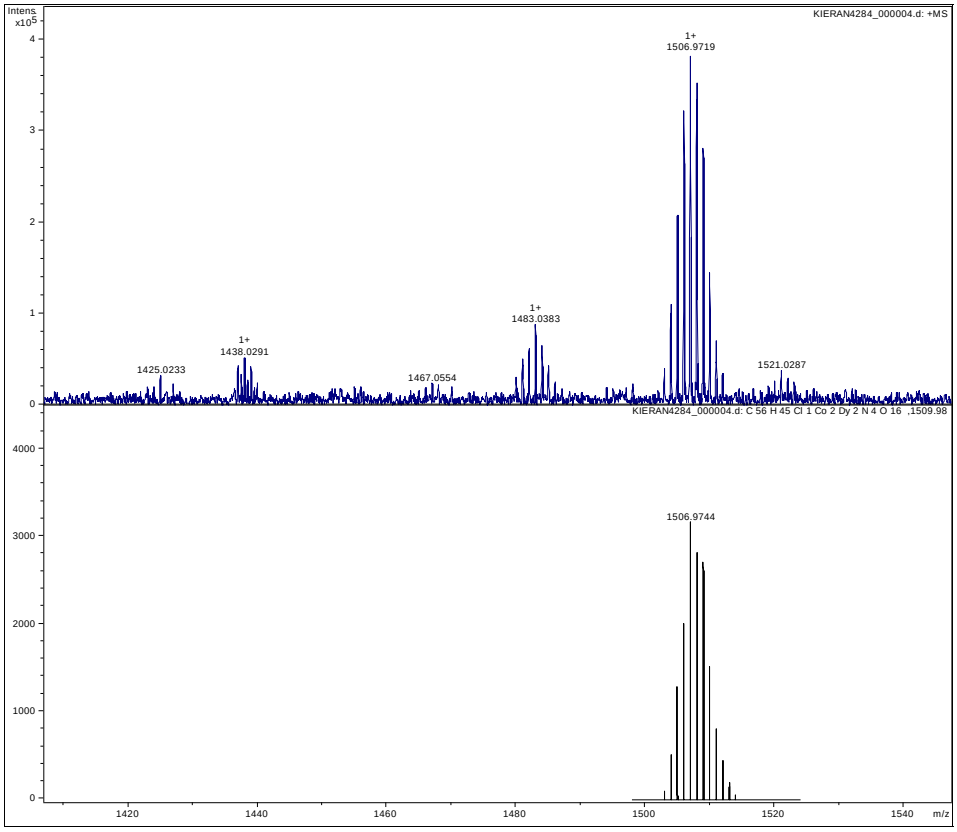

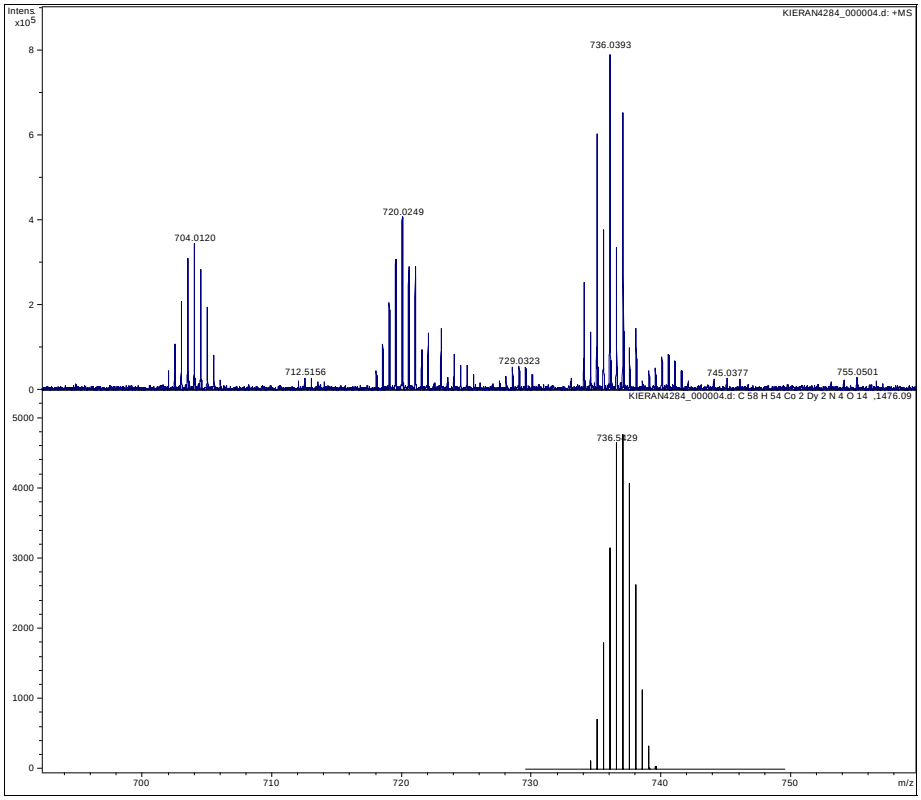

Figure S7.2. Experimental and theoretical ESI-MS patterns of **1CoDy-ClO$_4$** corresponding to $[Co^{II}_2Dy^{III}_2(\mathbf{L1})_4(ClO_4)\text{-}H]^+$ (upper) and $[Co^{II}_2Dy^{III}_2(\mathbf{L1})_4(MeOH)_2\text{-}H]^{2+}$(lower) fragments.

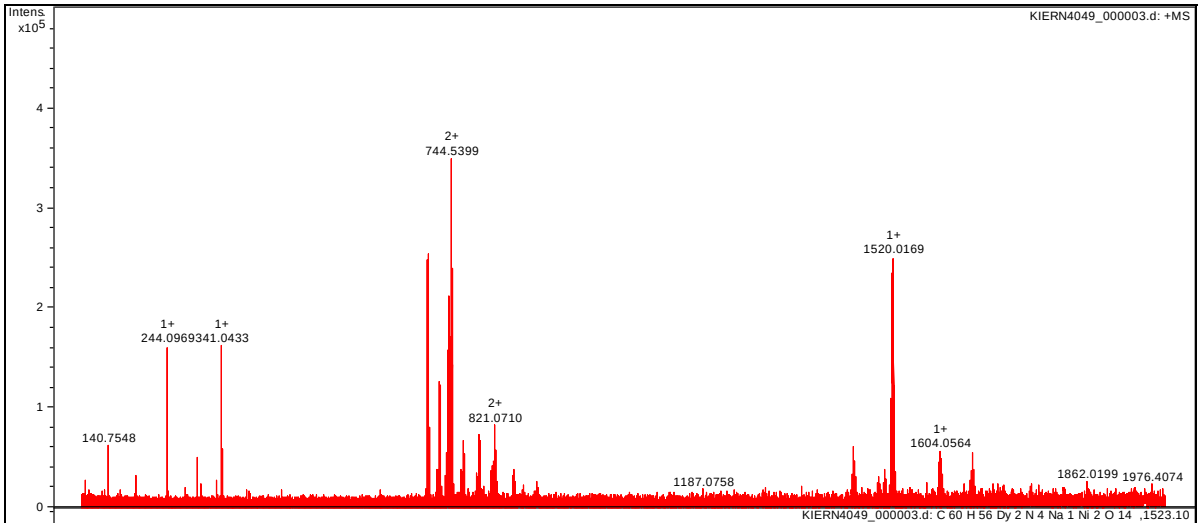

Figure S7.3. ESI-MS of **1NiDy-ClO$_4$**

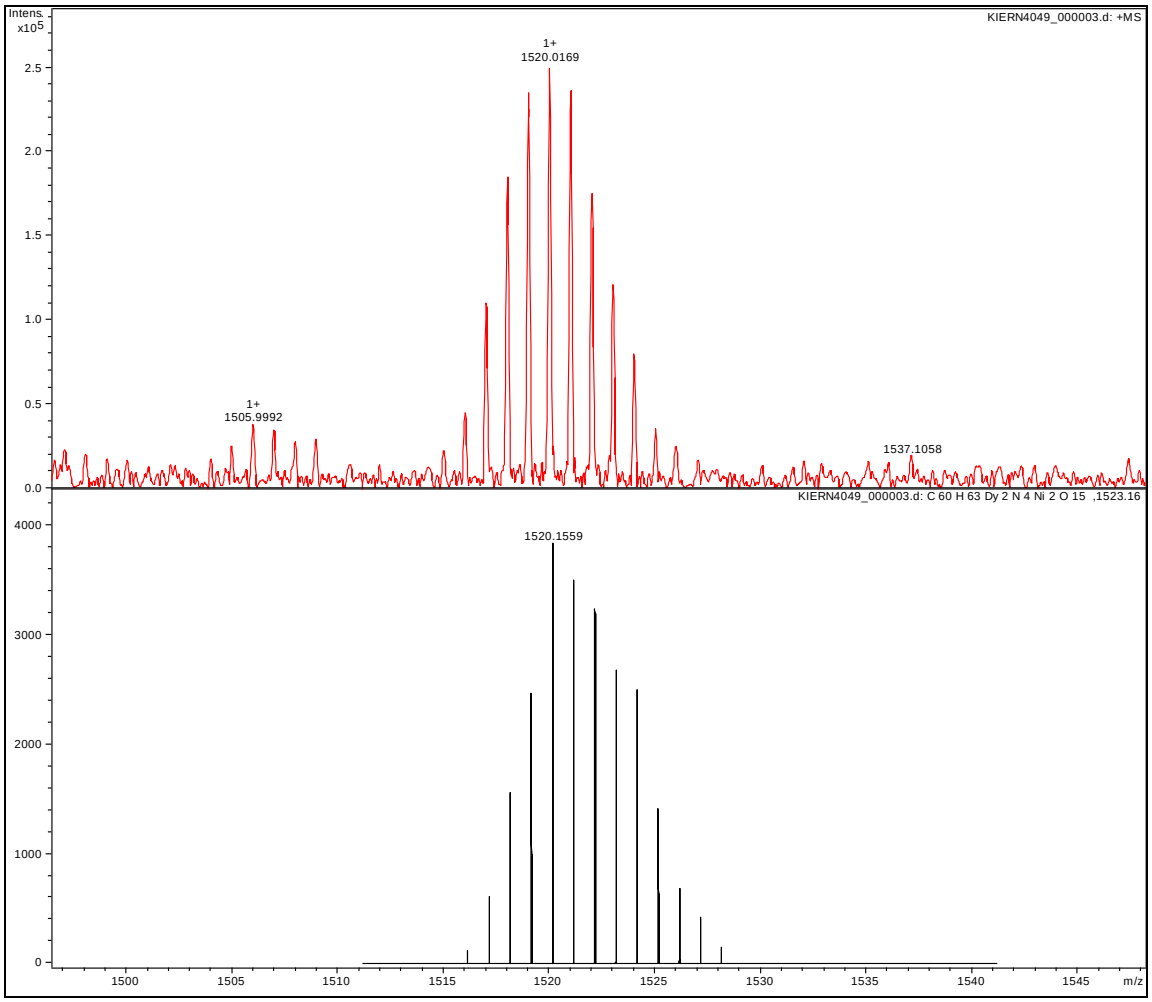

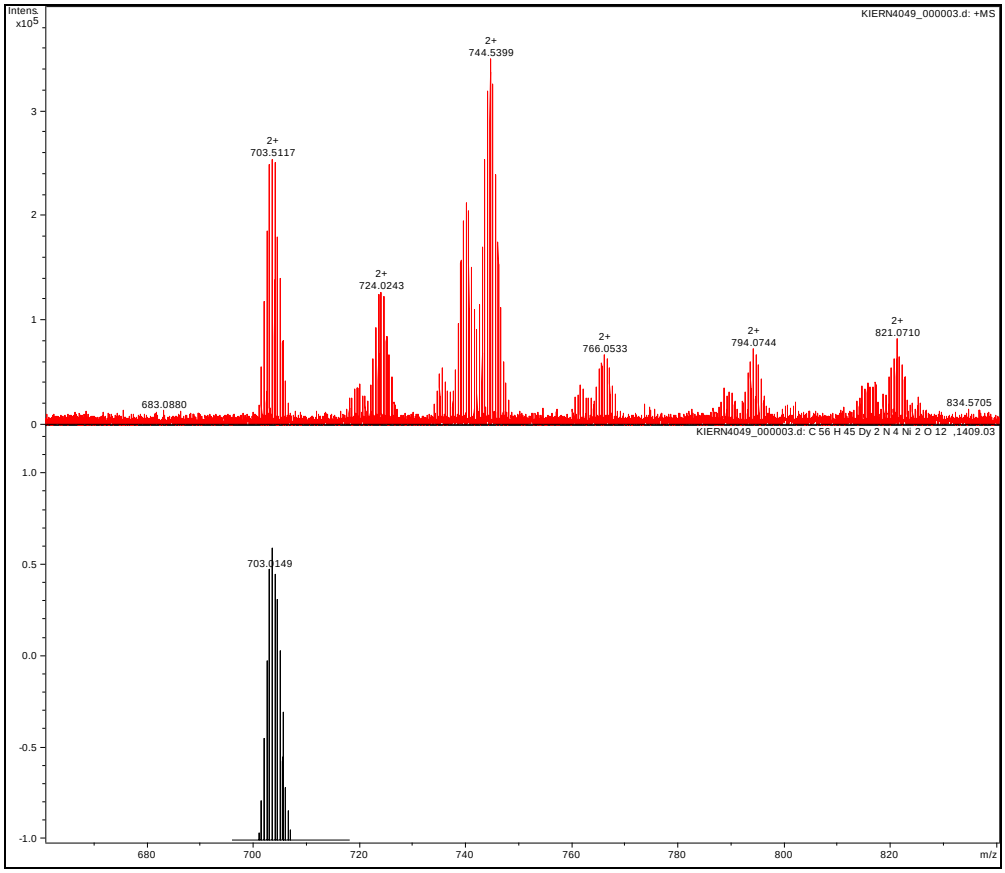

Figure S7.4. Experimental and theoretical ESI-MS patterns of **1NiDy-ClO$_4$** corresponding to $\{[Ni^{II}_2Dy^{III}_2(\mathbf{L1})_4(MeOH)_2(EtOH)]+2H\}^+$ (upper) and $\{[Ni^{II}_2Dy^{III}_2(\mathbf{L1})_4]-H\}^{2+}$ (lower) fragments

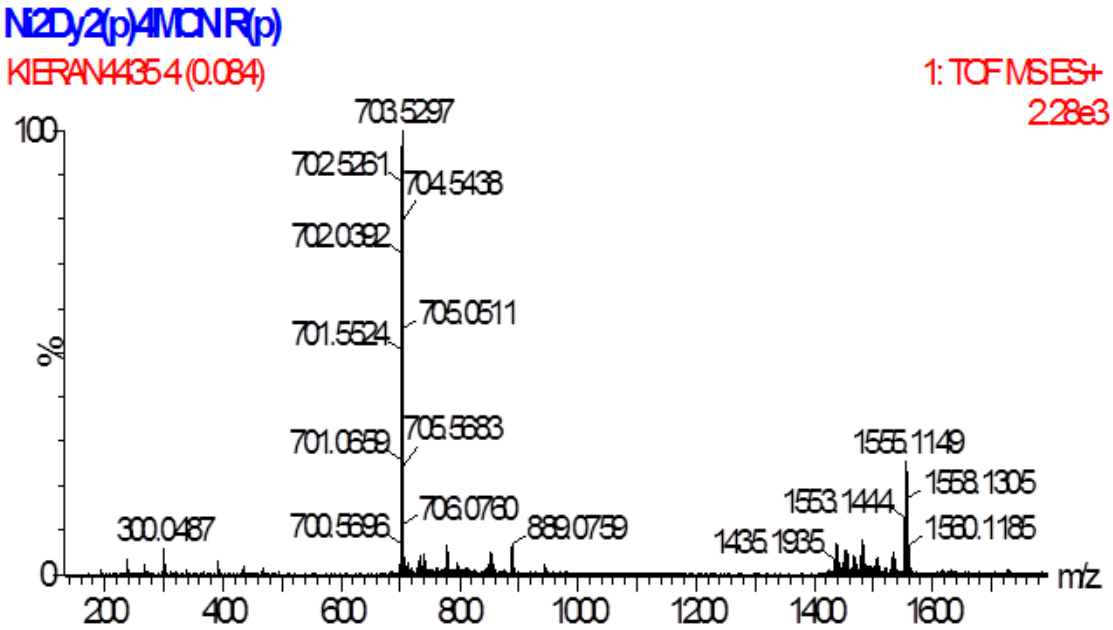

Figure S7.5. ESI-MS of of **1NiDy-Cl**

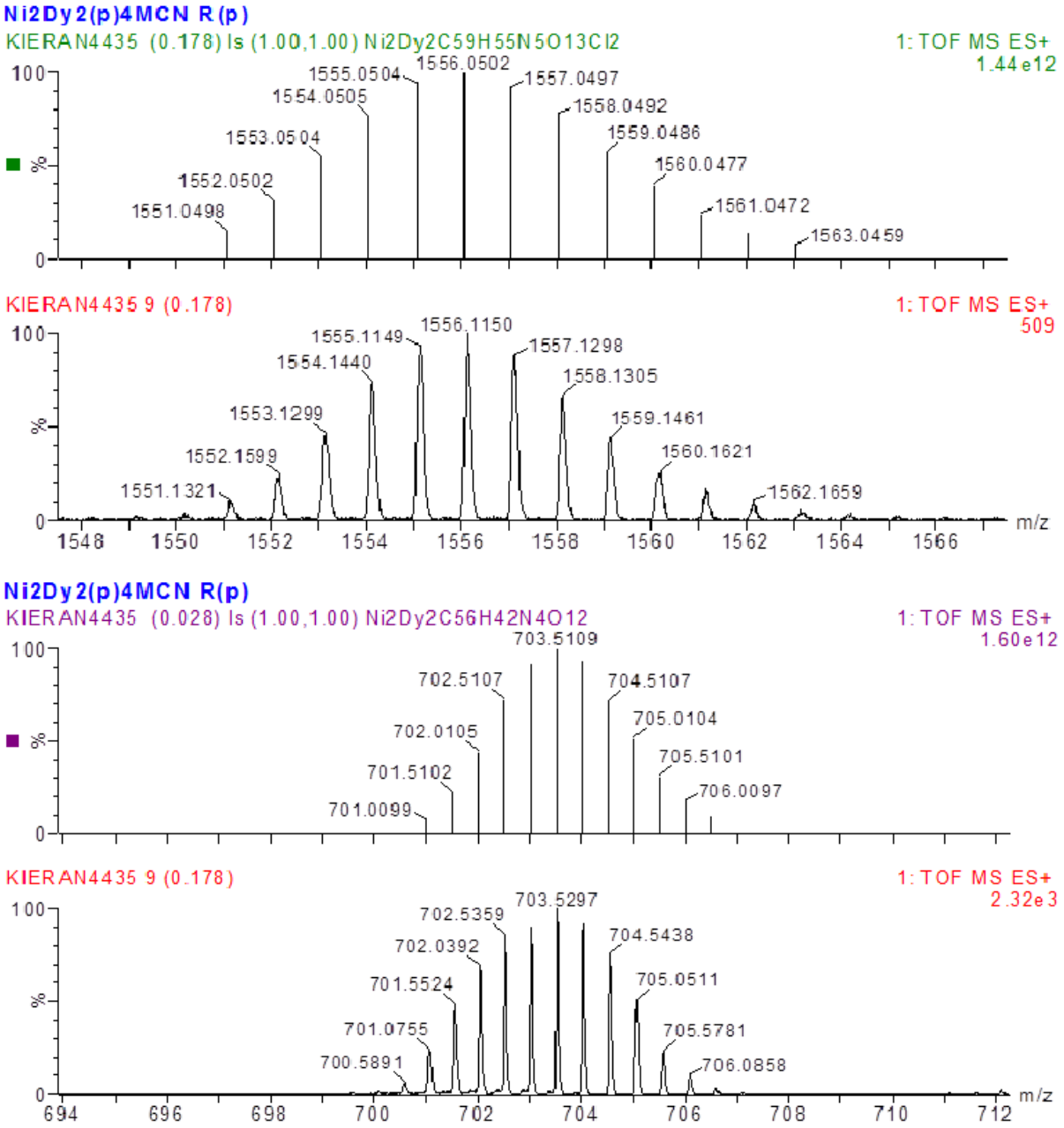

Figure S7.6. Experimental and theoretical ESI-MS patterns of **1NiDy-Cl** corresponding to $\{[Ni^{II}_2Dy^{III}_2(\mathbf{L1})_4Cl_2(CH_3CN)(CH_3OH)]+4H\}^+$ (upper) and $\{[Ni^{II}_2Dy^{III}_2(\mathbf{L1})_4]-H\}^{2+}$ (lower) fragments

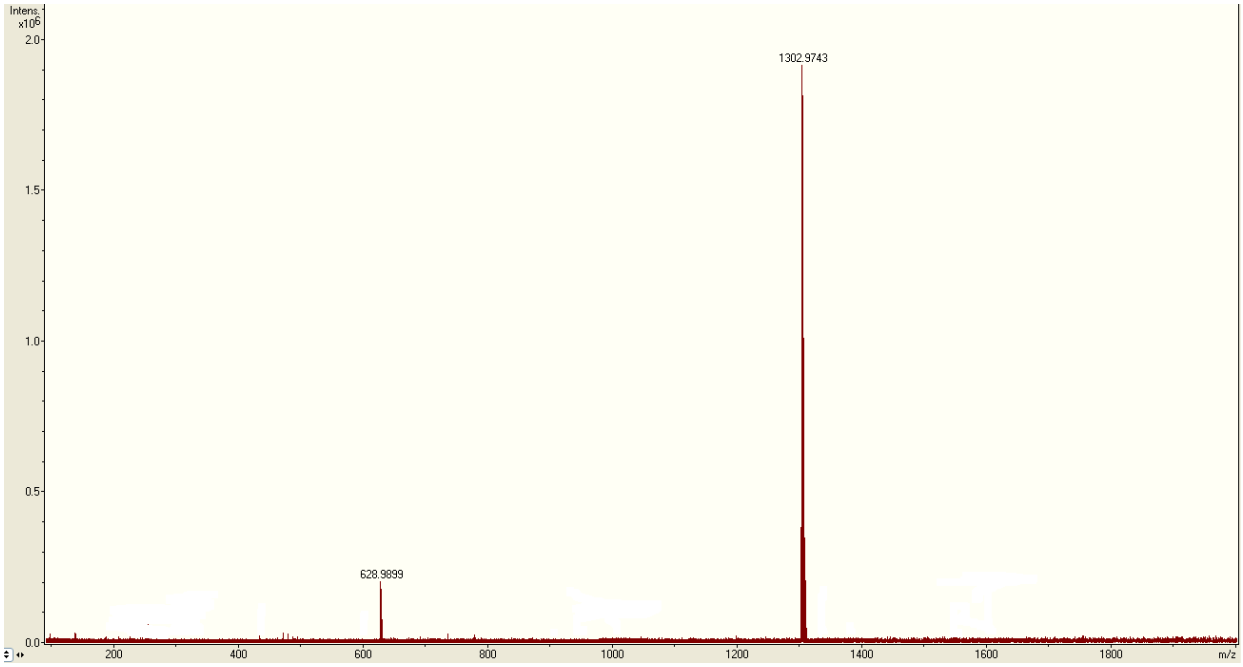

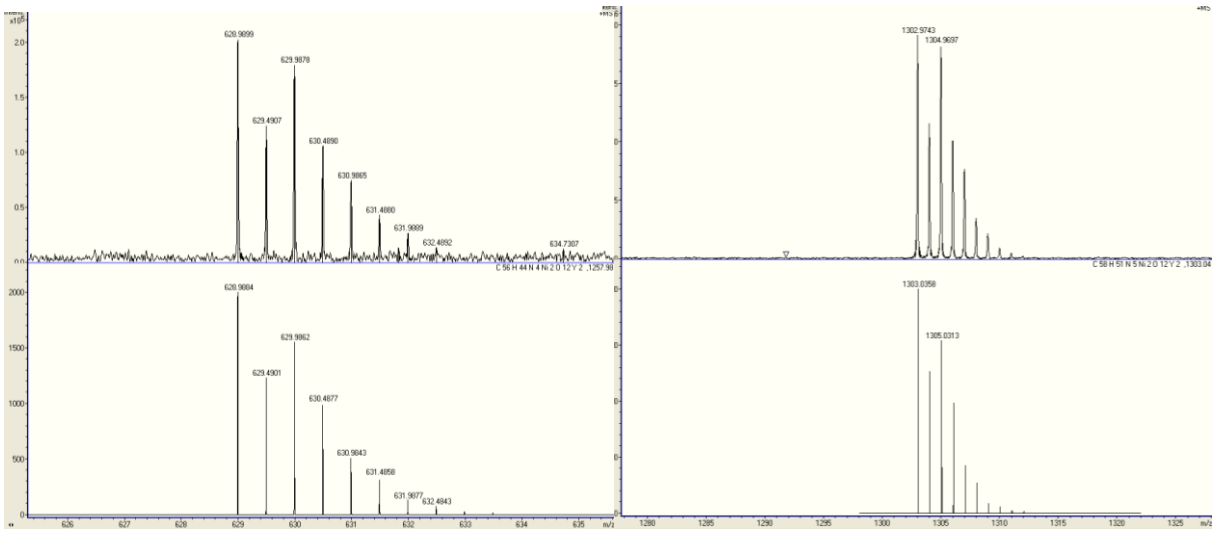

S7.7. ESI-MS of 1NiY-Cl (Top) $[Ni^{II}_2Y^{II}_2(C_{14}H_{11}NO_3)_4(CH_3N)]^{1+}$ Fragment (bottom right) $\{[Ni^{II}_2Y^{II}_2(C_{14}H_{11}NO_3)_4]\text{-}1H\}^{2+}$ (bottom left)

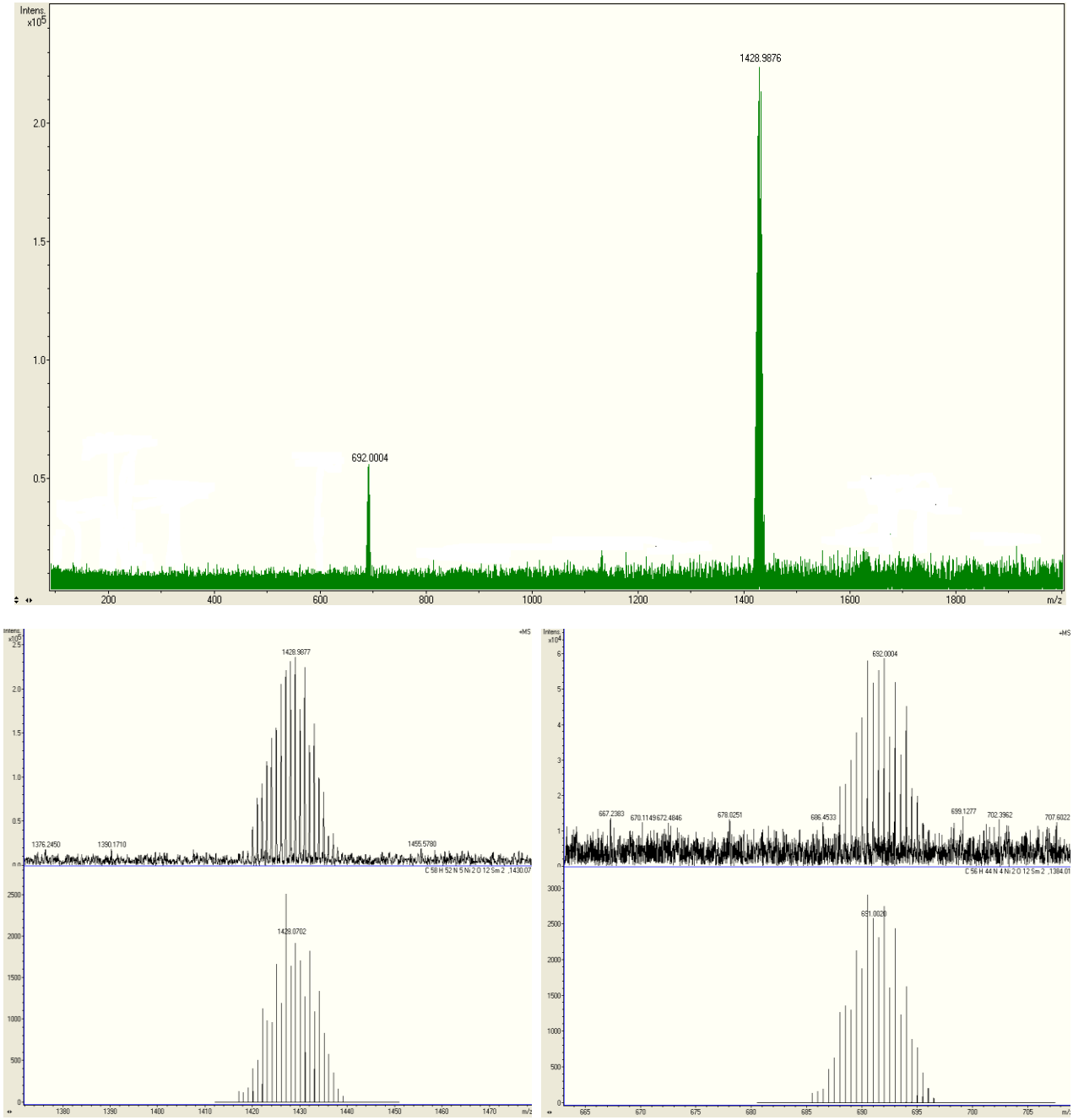

S7.8. ESI-MS of 1NiSm-Cl (Top) $[Ni^{II}_2Sm^{III}_2(C_{14}H_{11}NO_3)_4(CH_3N)]^{1+}$ Fragment (bottom left) $\{[Ni^{II}_2Sm^{III}_2(C_{14}H_{11}NO_3)_4]\text{-}1H\}^{2+}$ (bottom right)

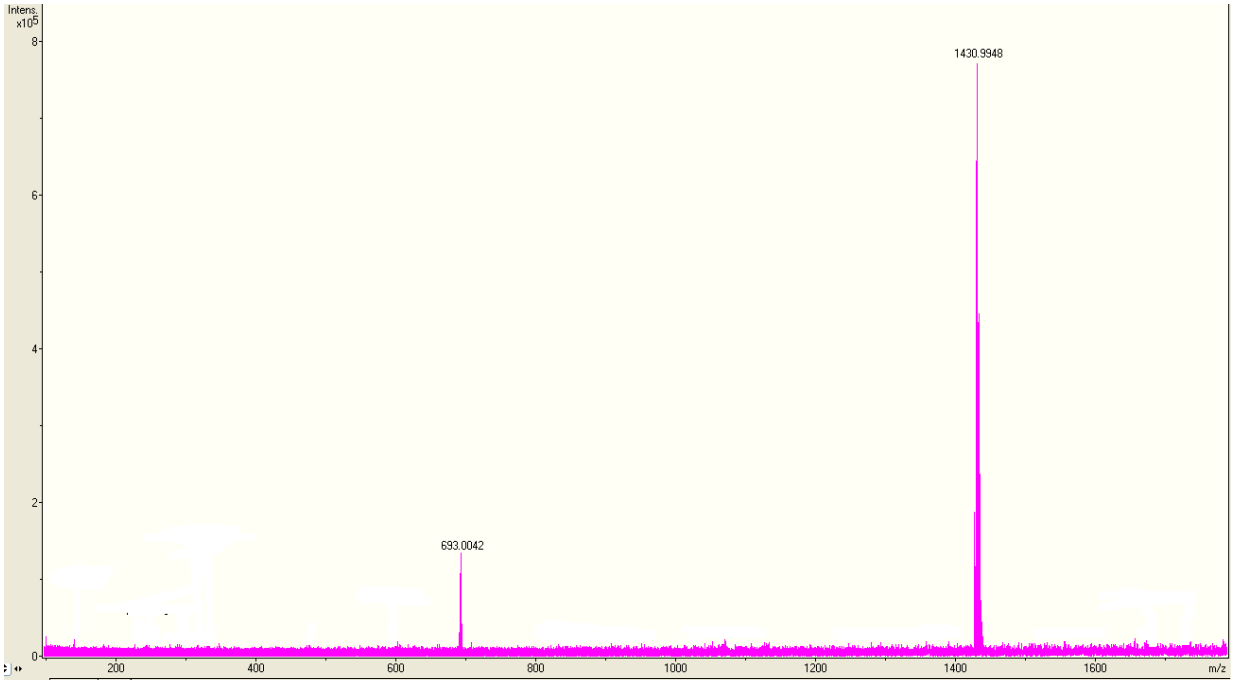

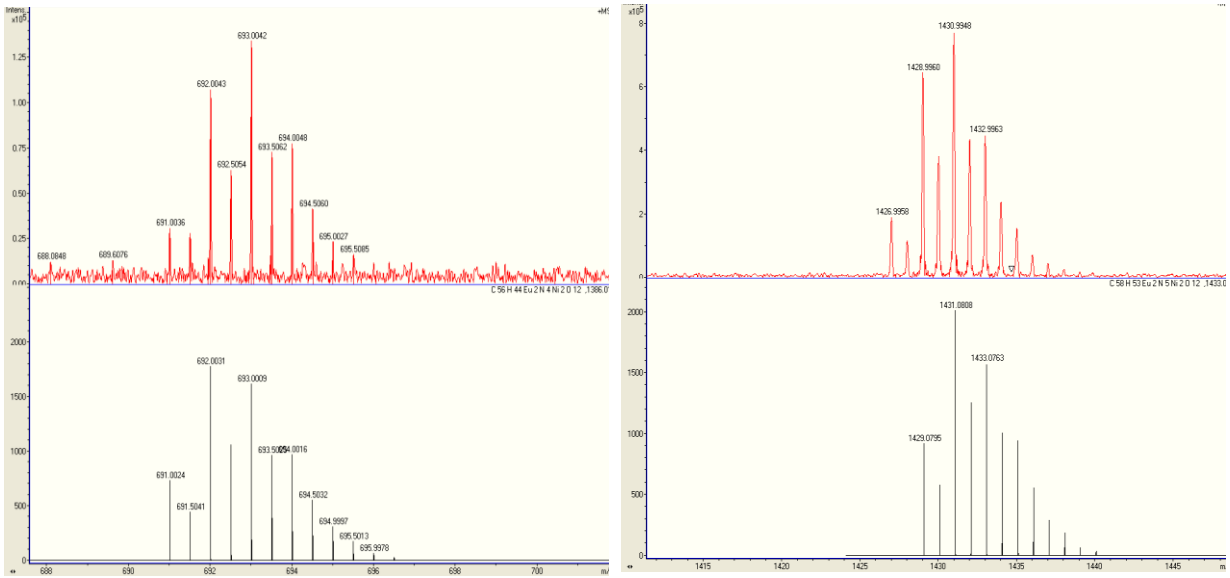

S7.9. ESI-MS of 1-NiEu-Cl (Top) $\{[Ni^{II}_2Eu^{III}_2(C_{14}H_{11}NO_3)_4]\text{-}1H\}^{2+}$ fragment (bottom left) $\{[Ni^{II}_2Eu^{III}_2(C_{14}H_{11}NO_3)_4(CH_3CN)]+1H\}^{1+}$ fragment (bottom right)

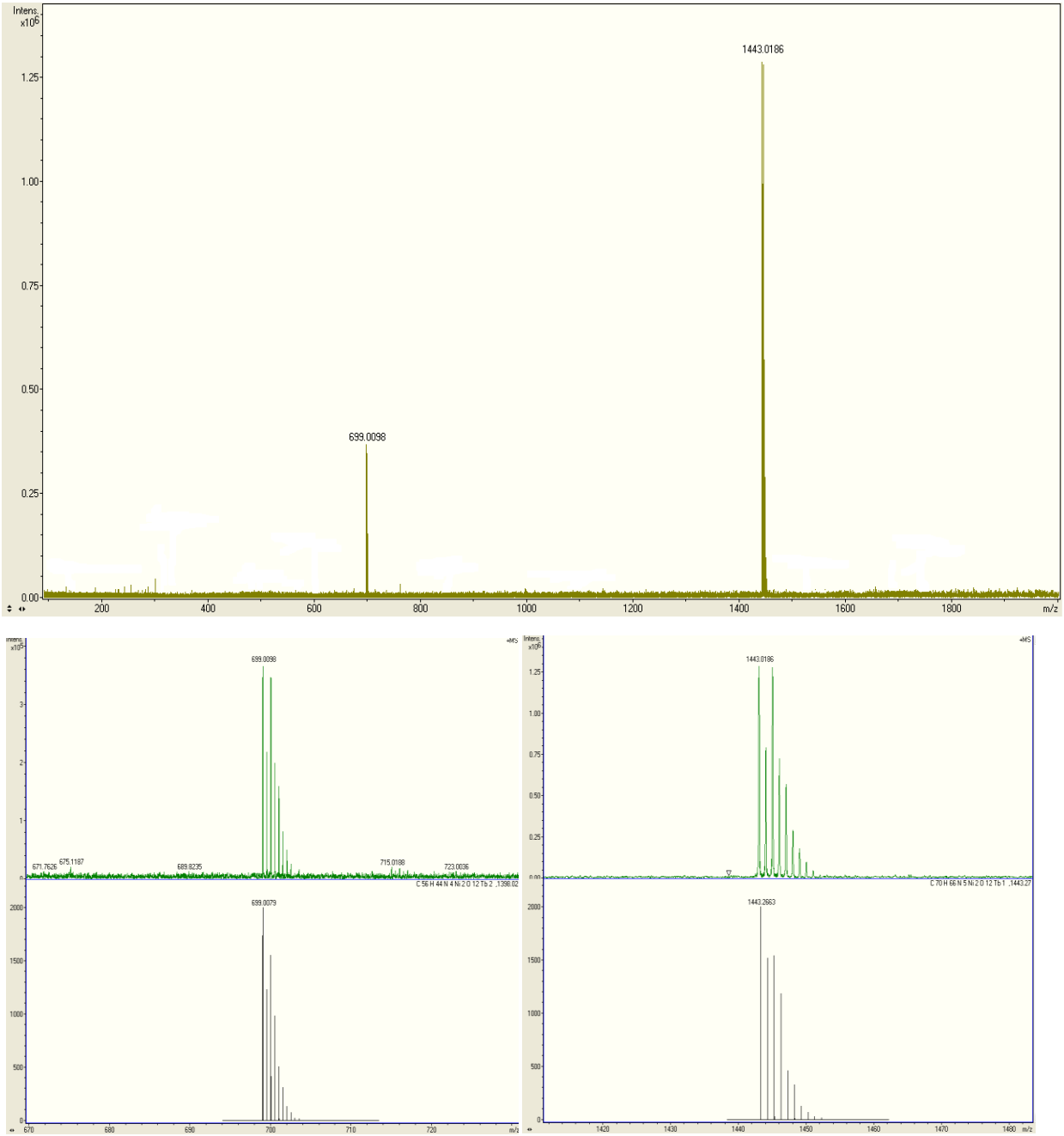

S7.10. ESI-MS of 1NiTb-Cl (Top) $[Ni^{II}_2Tb^{III}_2\ (C_{14}H_{11}NO_3)_4]^{2+}$ fragment (left) $[Ni^{II}_2Tb^{III}_2\ (C_{14}H_{11}NO_3)_4(CH_3CN)]^{1+}$ fragment (right)

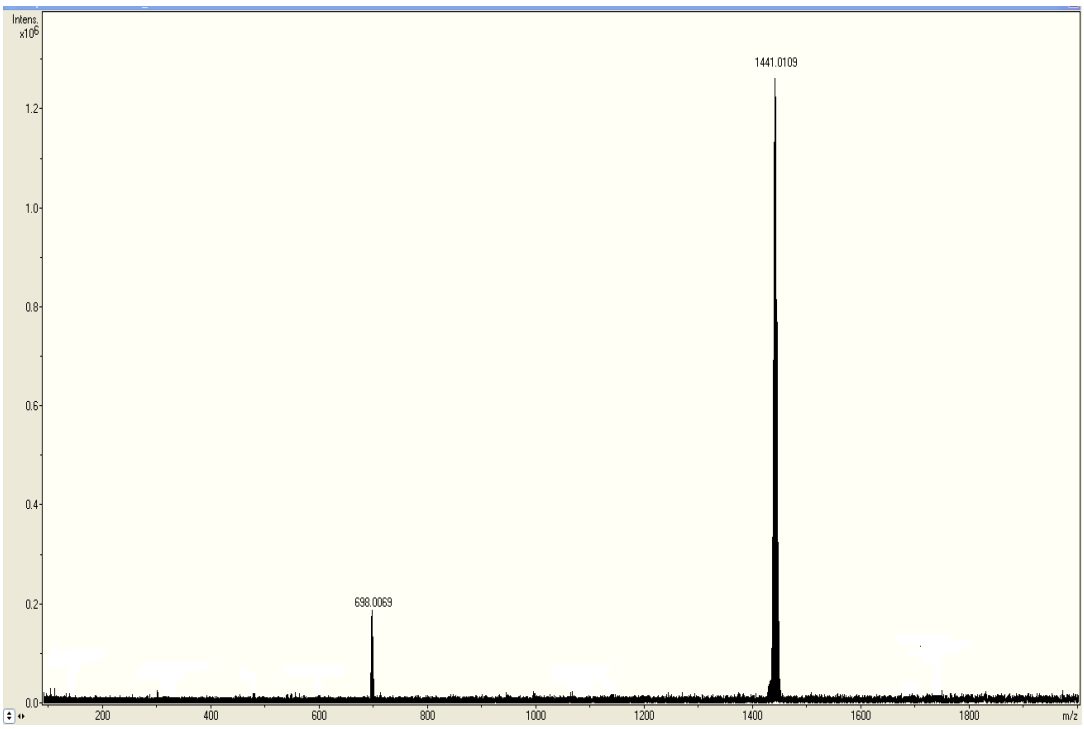

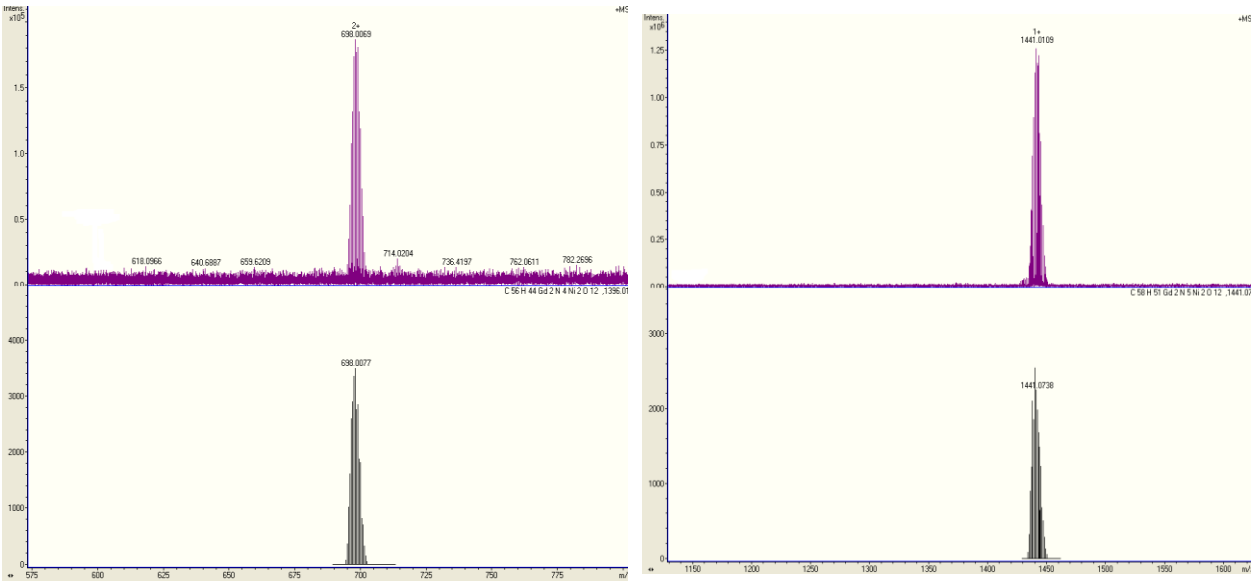

S7.11. ESI-MS of 1NiGd-Cl (Top) $\{[Ni^{II}_2Gd^{III}_2(C_{14}H_{11}NO_3)_4]\text{-}1H\}^{2+}$ fragment (Left) $\{[Ni^{II}_2Gd^{III}_2(C_{14}H_{11}NO_3)_4)(CH_3CN)]+2H\}^{1+}$ fragment (Right)

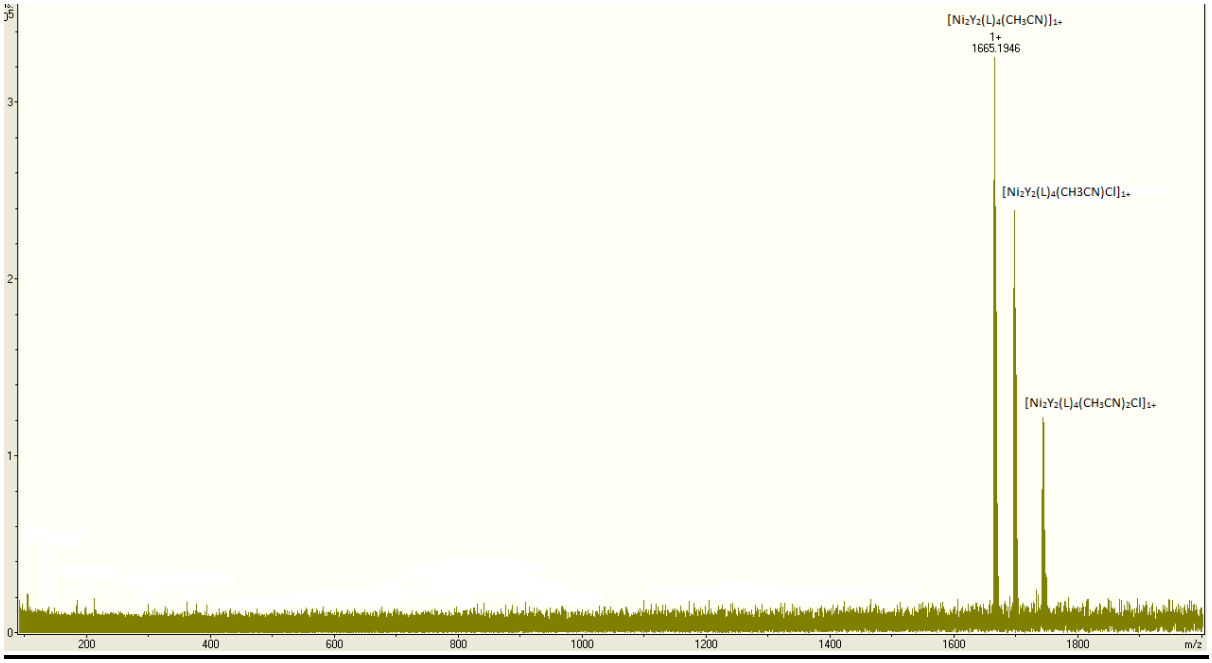

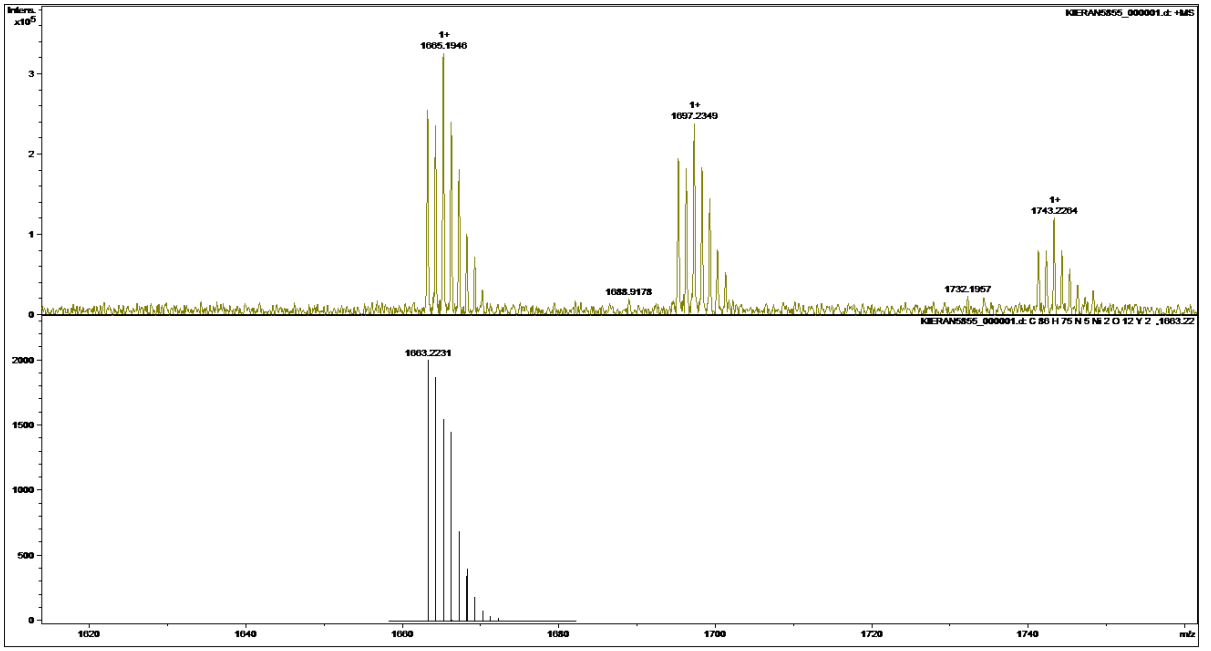

S7.12. ESI-MS of 16NiY-Cl (Upper) $[Ni^{II}_2Y^{II}_2(C_{21}H_{17}NO_3)_4(CH_3CN)]^{1+}$ (Lower)

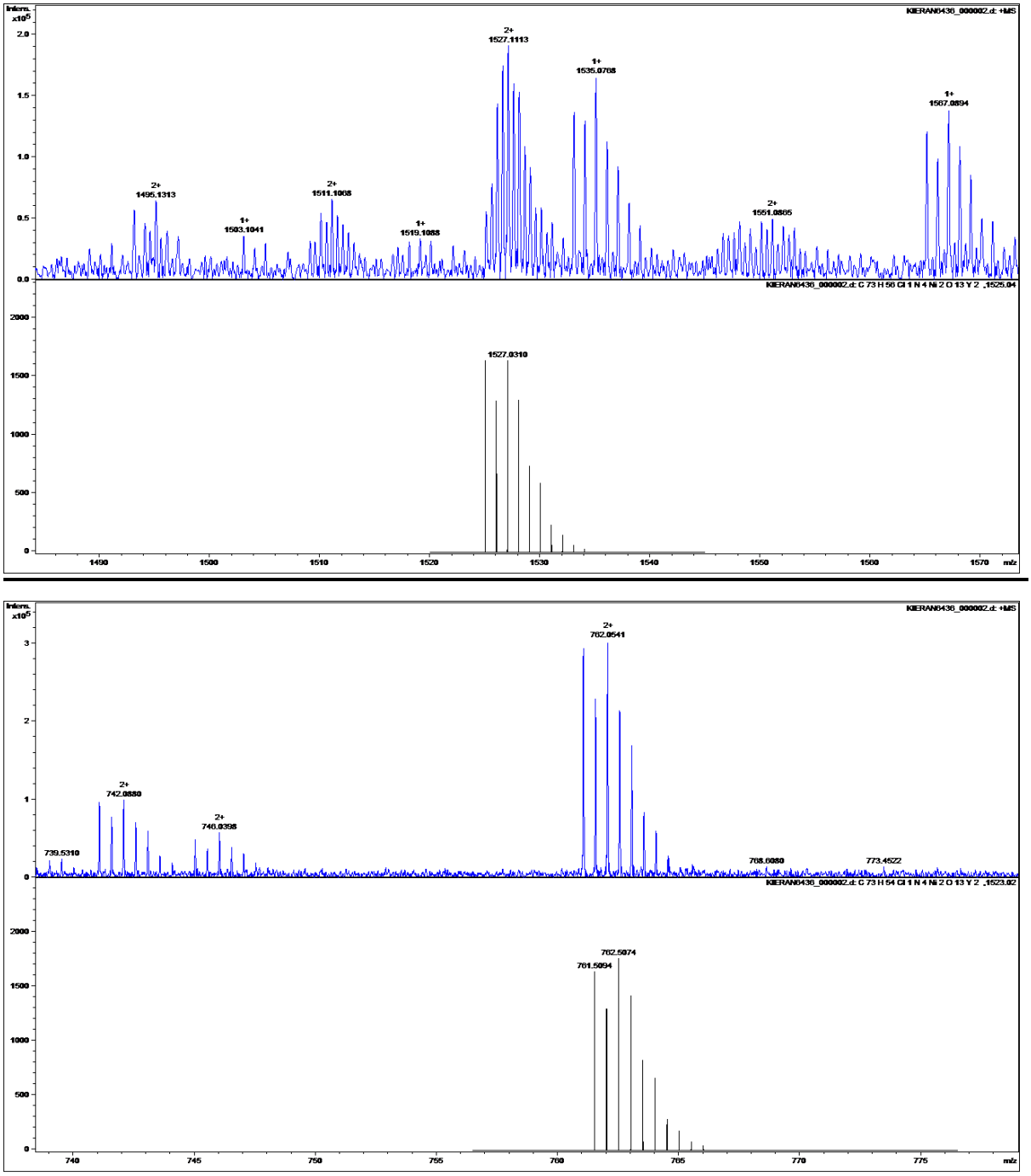

S7.13. ESI-MS of 2NiY-Cl (Upper) $[Ni^{II}_2Y^{III}_2(C_{18}H_{13}NO_3)Cl(CH_3OH)]^{1+}$ fragment. (Lower) $[Ni^{II}_2Y^{III}_2(C_{18}H_{13}NO_3)Cl(CH_3OH)]^{2+}$ fragment.

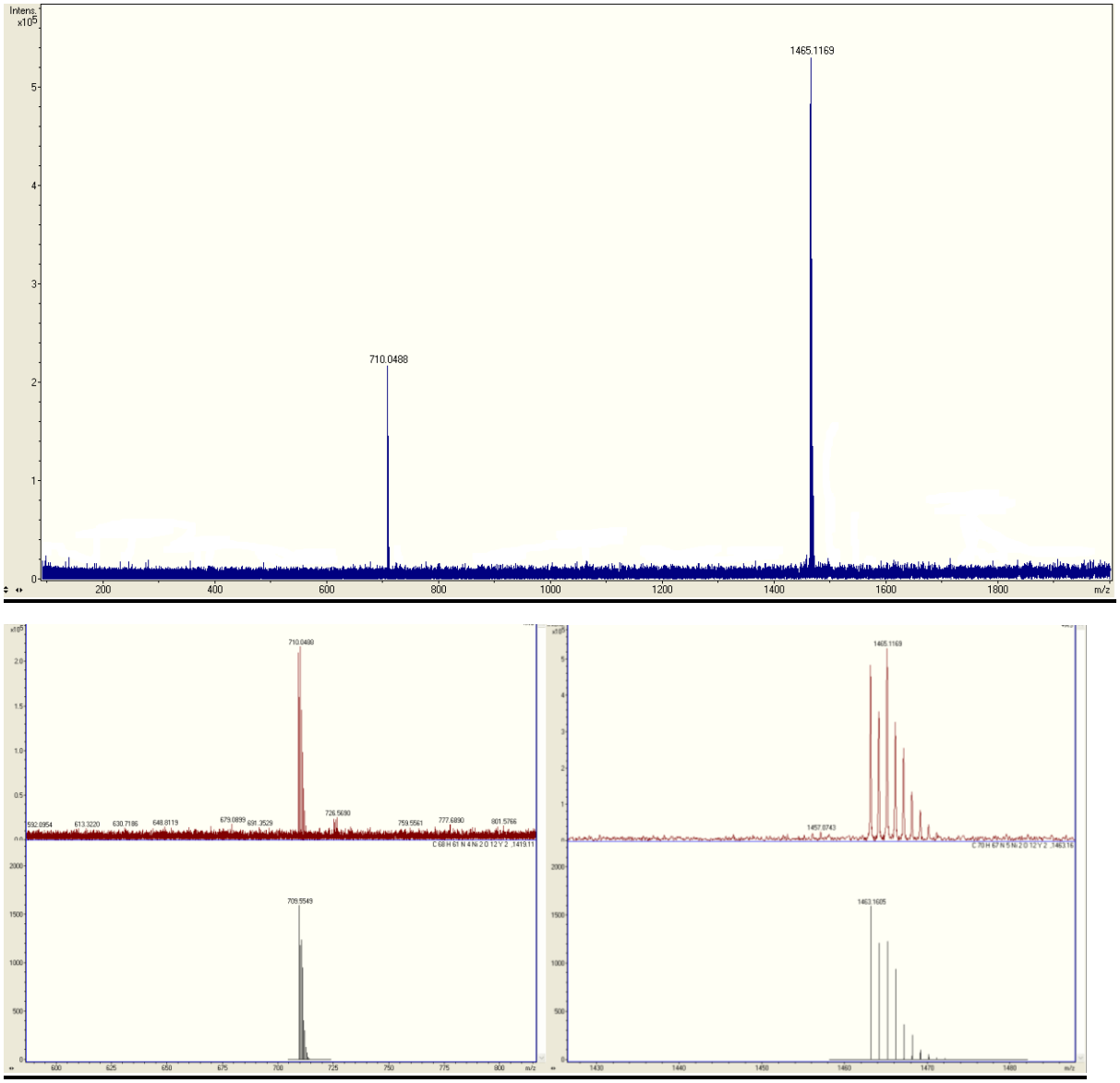

S7.14. ESI-MS of compound 6NiY-Cl $[Y_2Ni_2(C_{17}H_{15}NO_3)]^{2+}$Fragment (Left) $[Ni^{II}_2Y^{III}_2(C_{17}H_{15}NO_3)_4(CH3CN)]^{1+}$Fragment (Right)

7.2 FT-IR of LNiLn-Cl

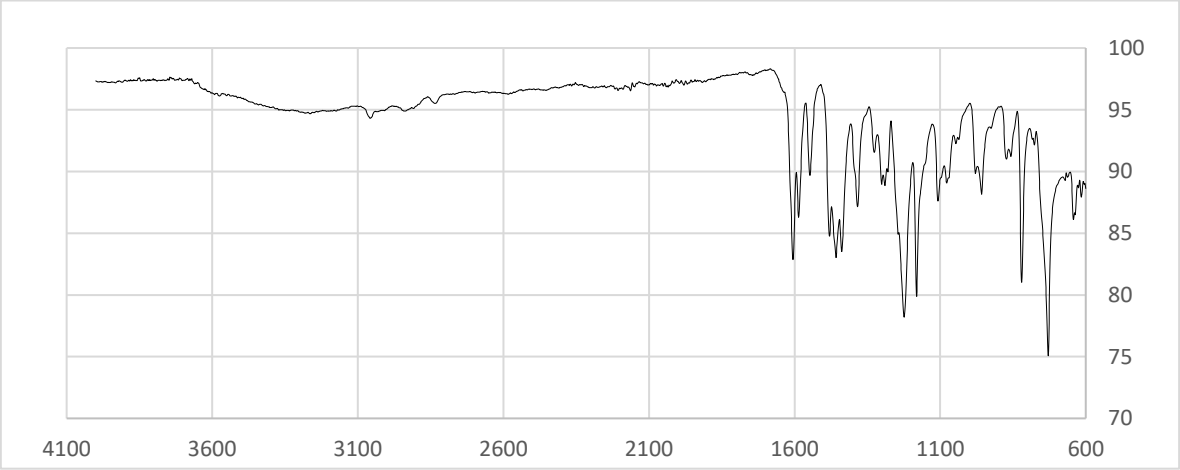

S7.15 FT-IR of 1NiY-Cl

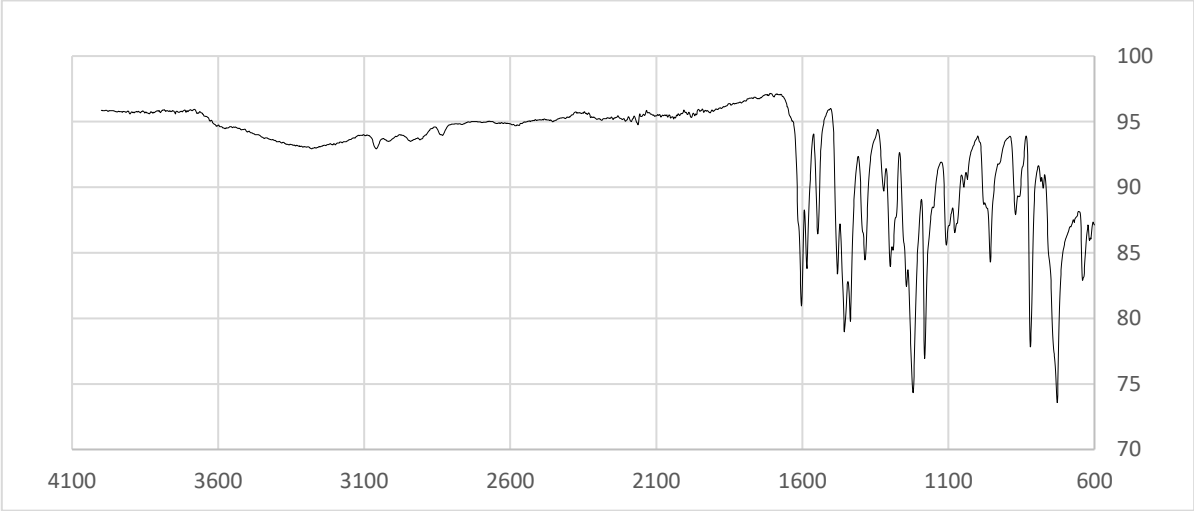

S7.16 FT-IR of 1NiSm-Cl

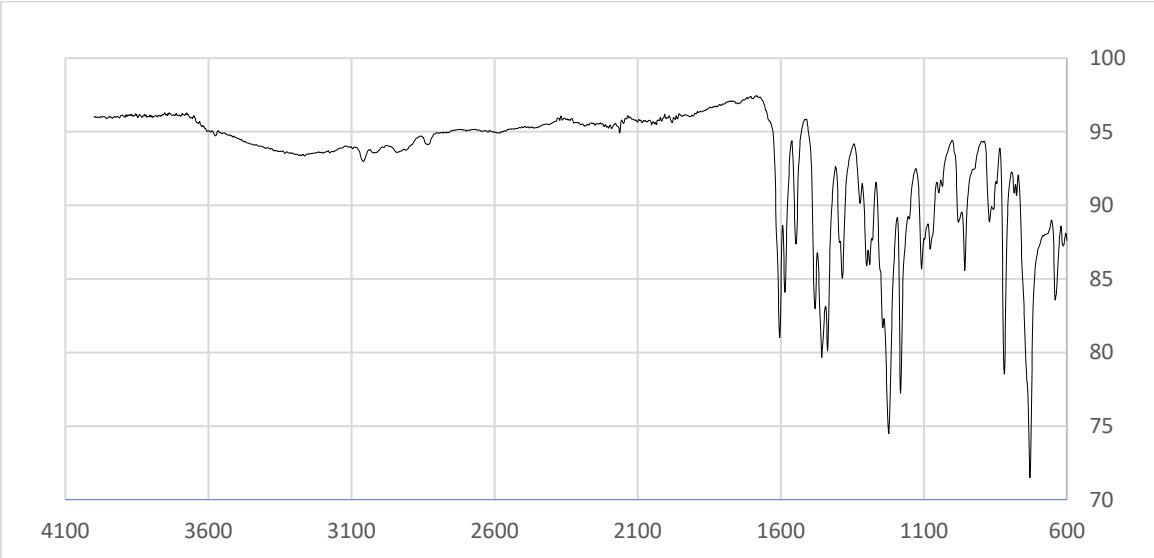

S7.17 FT-IR of 1NiEu-Cl

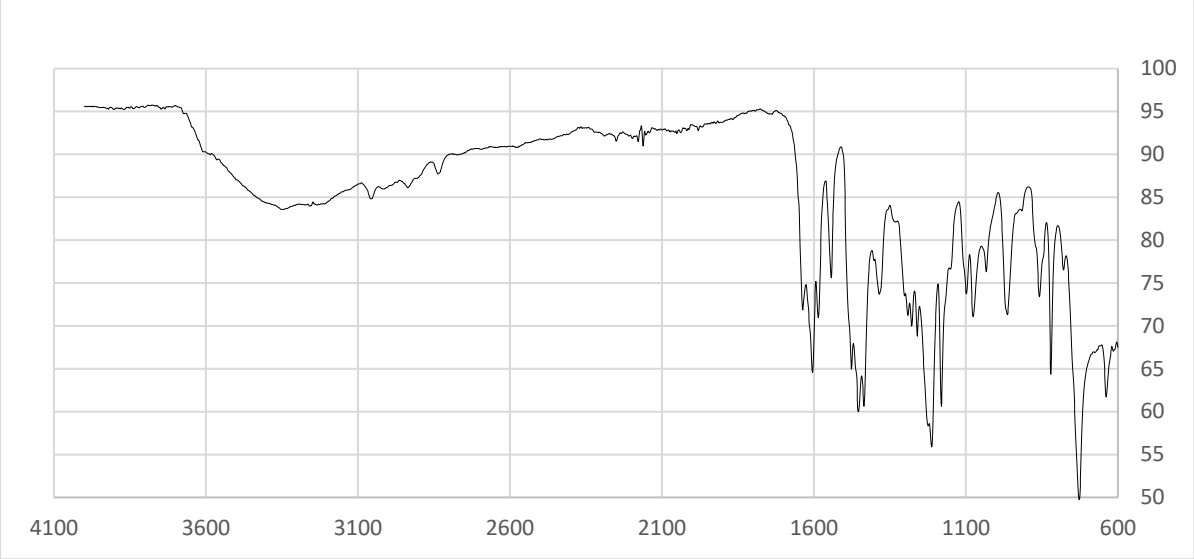

S7.18 FT-IR of 1NiTb-Cl

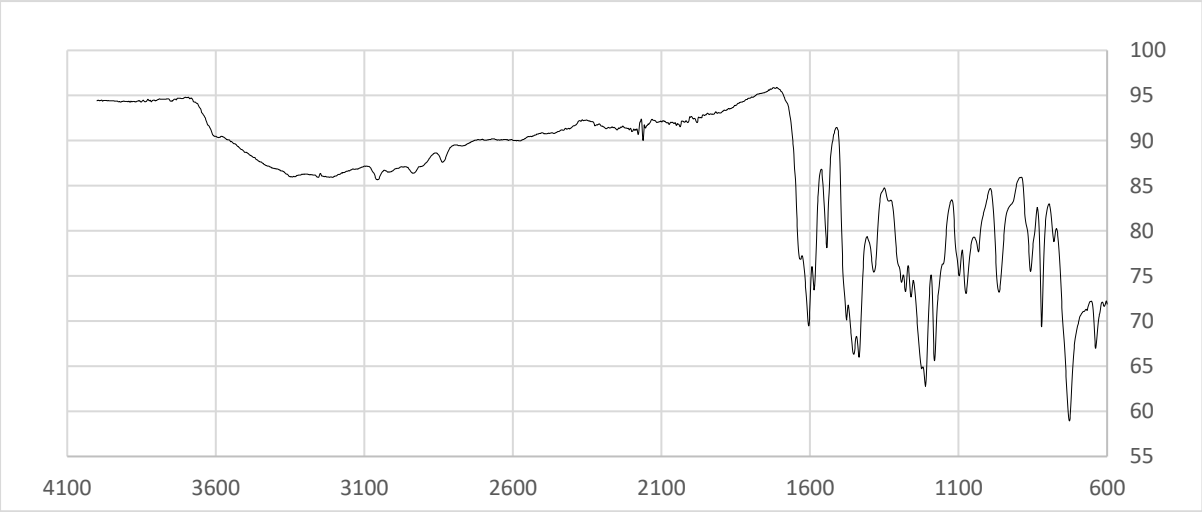

S7.19 FT-IR of 1NiGd-Cl

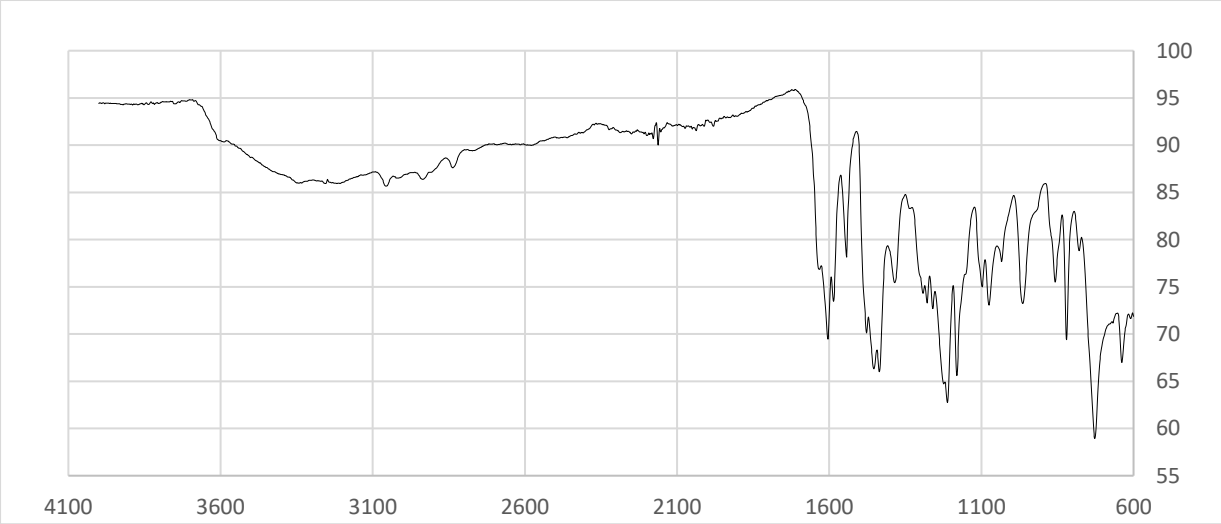

S7.20 FT-IR of 1NiDy-Cl

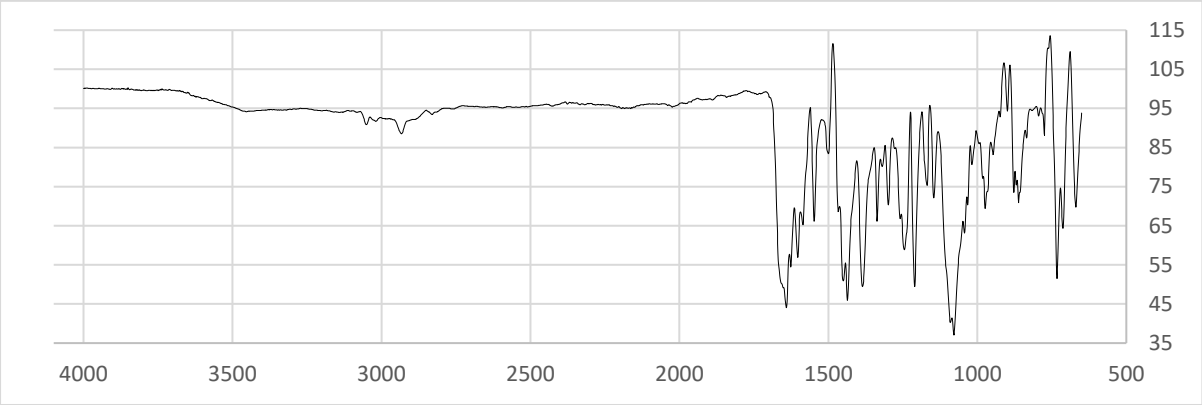

S7.21 FT-IR of 2NiY-Cl

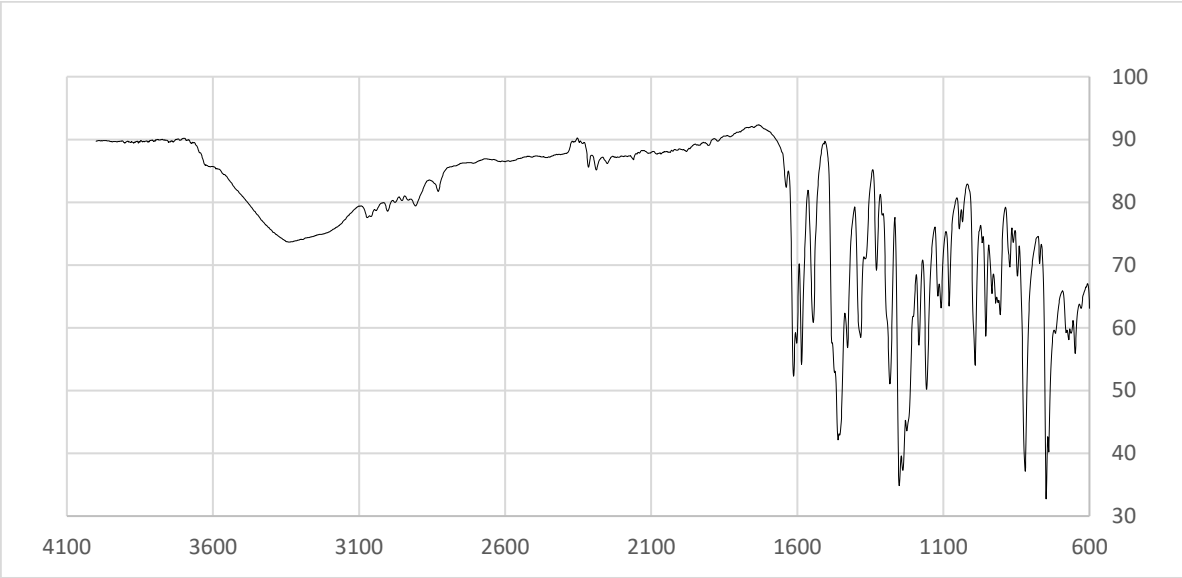

S7.22 FT-IR of 6NiY-Cl

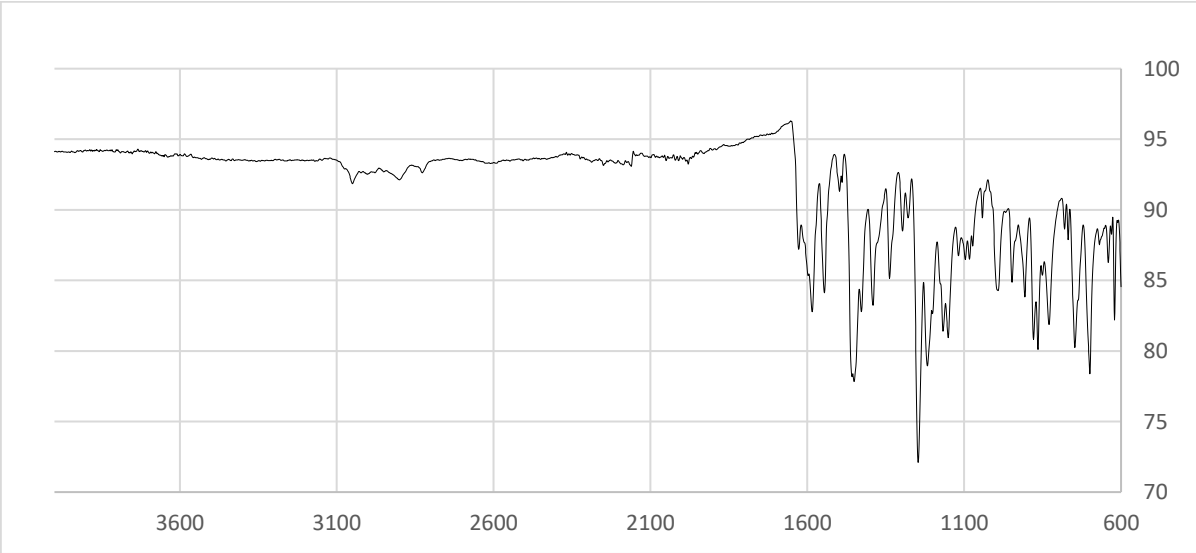

S7.23 FT-IR of 16NiY-Cl

7.3 TGA for LNiLn-Cl

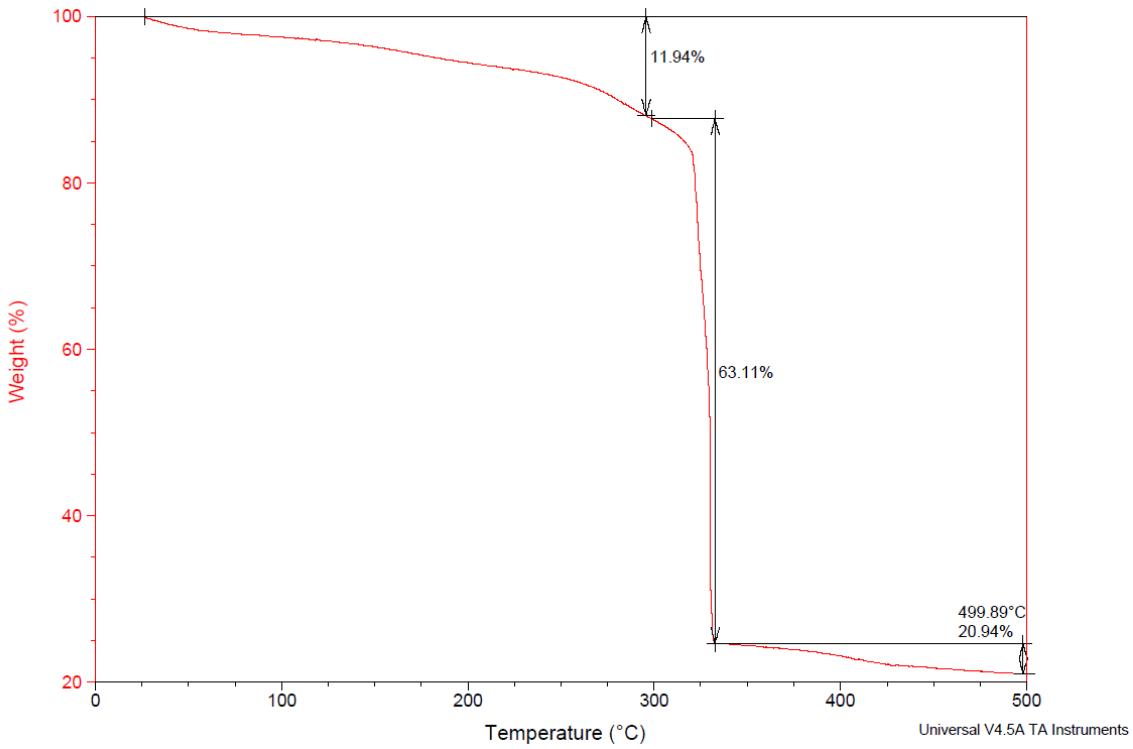

S7.24. TGA for 1NiY-Cl

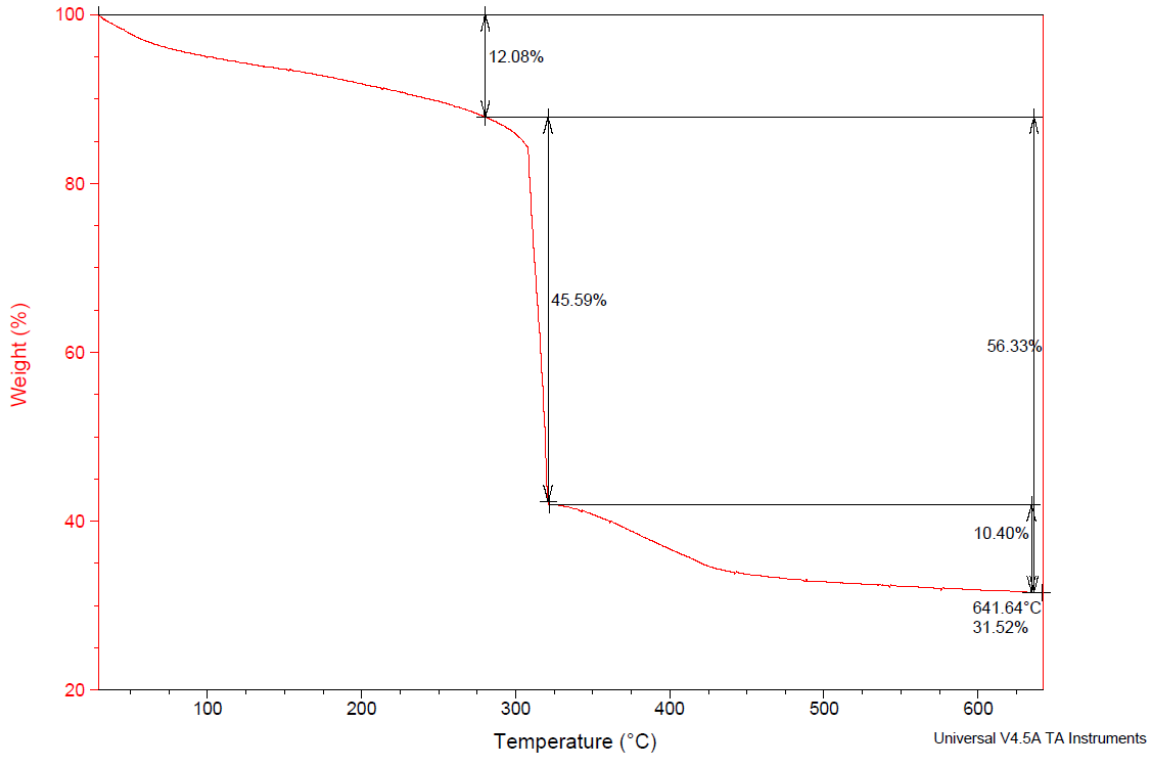

S7.25. TGA for 1NiTb-Cl

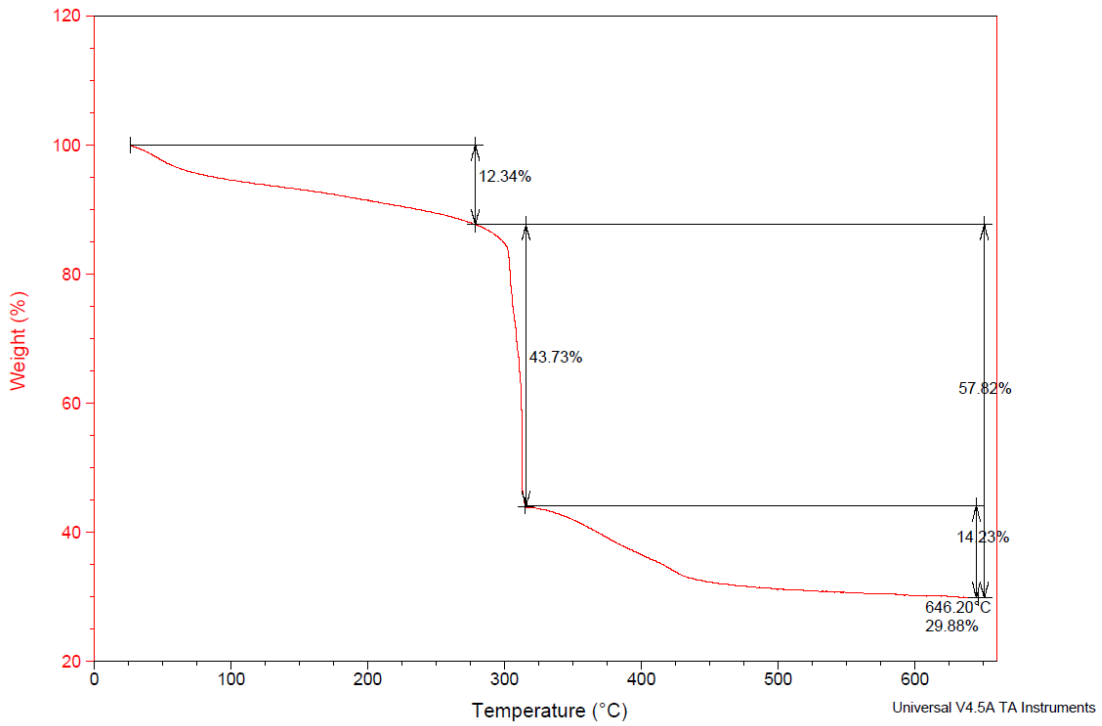

S7.26. TGA for 1NiGd-Cl

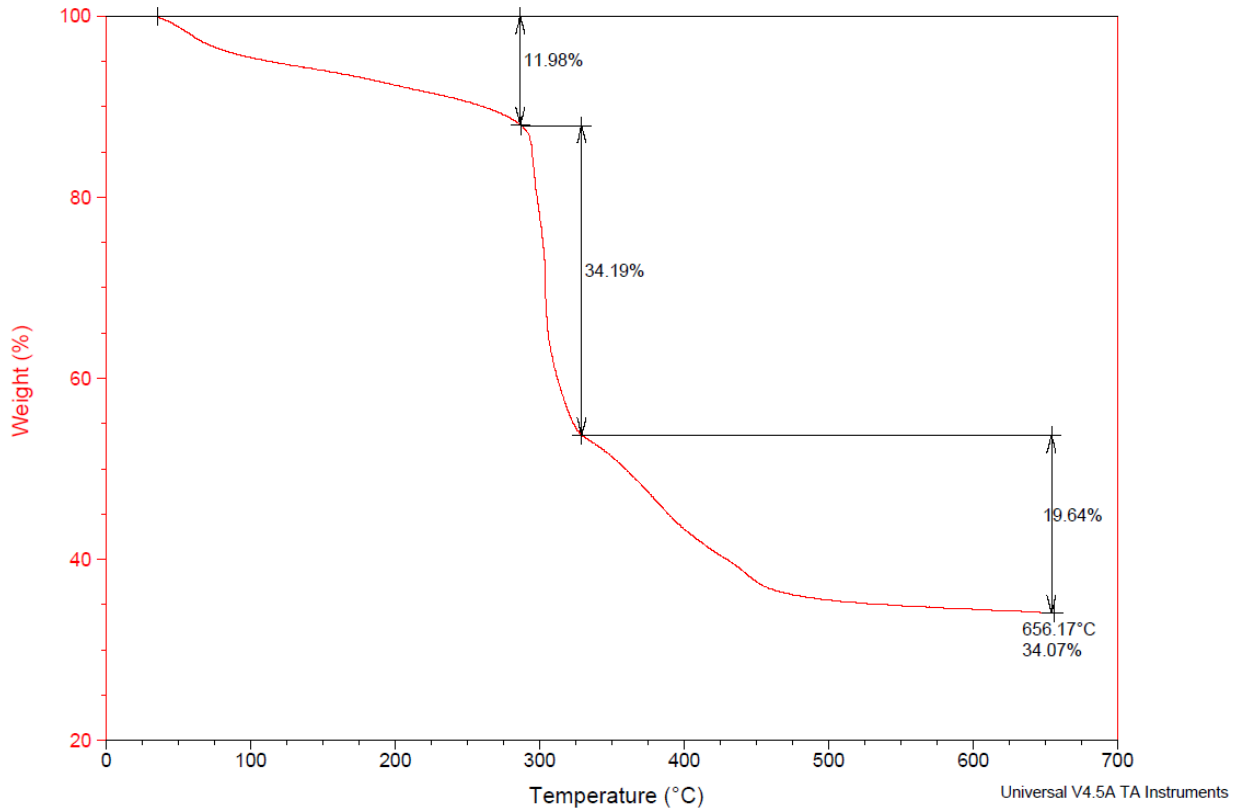

S7.27. TGA for 1NiDy-Cl

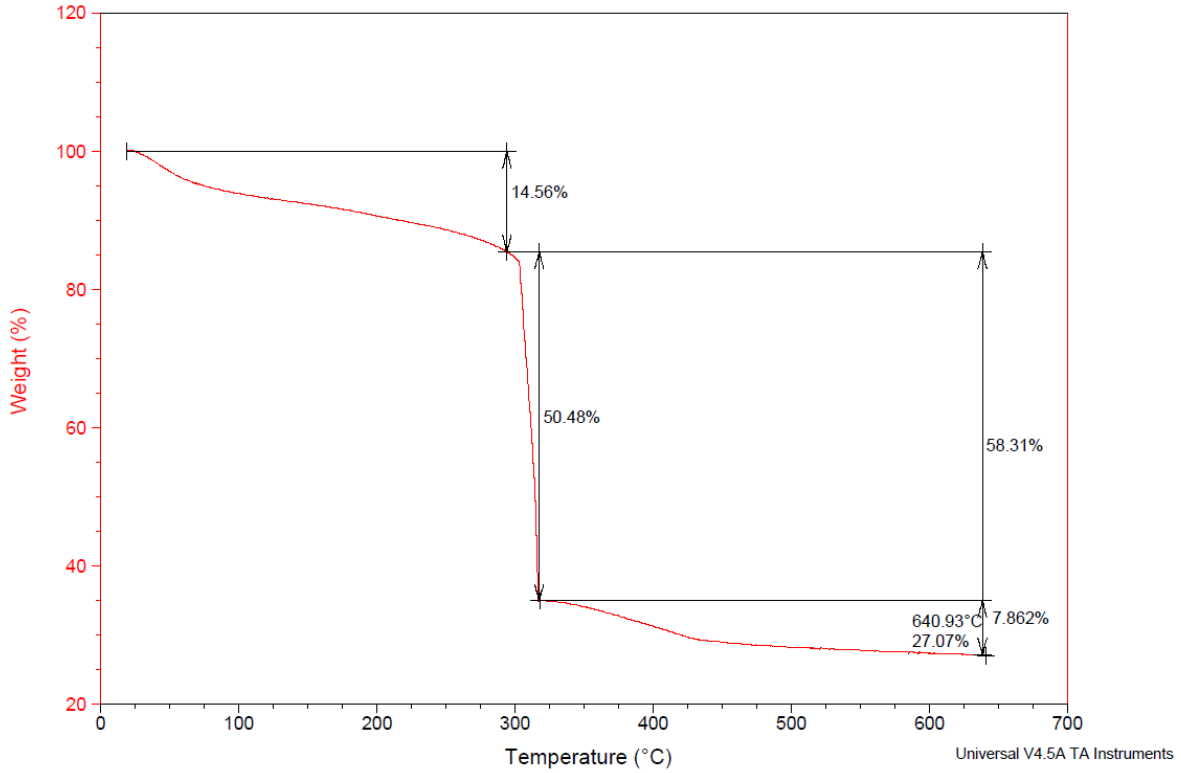

S7.28. TGA for 1NiSm-Cl

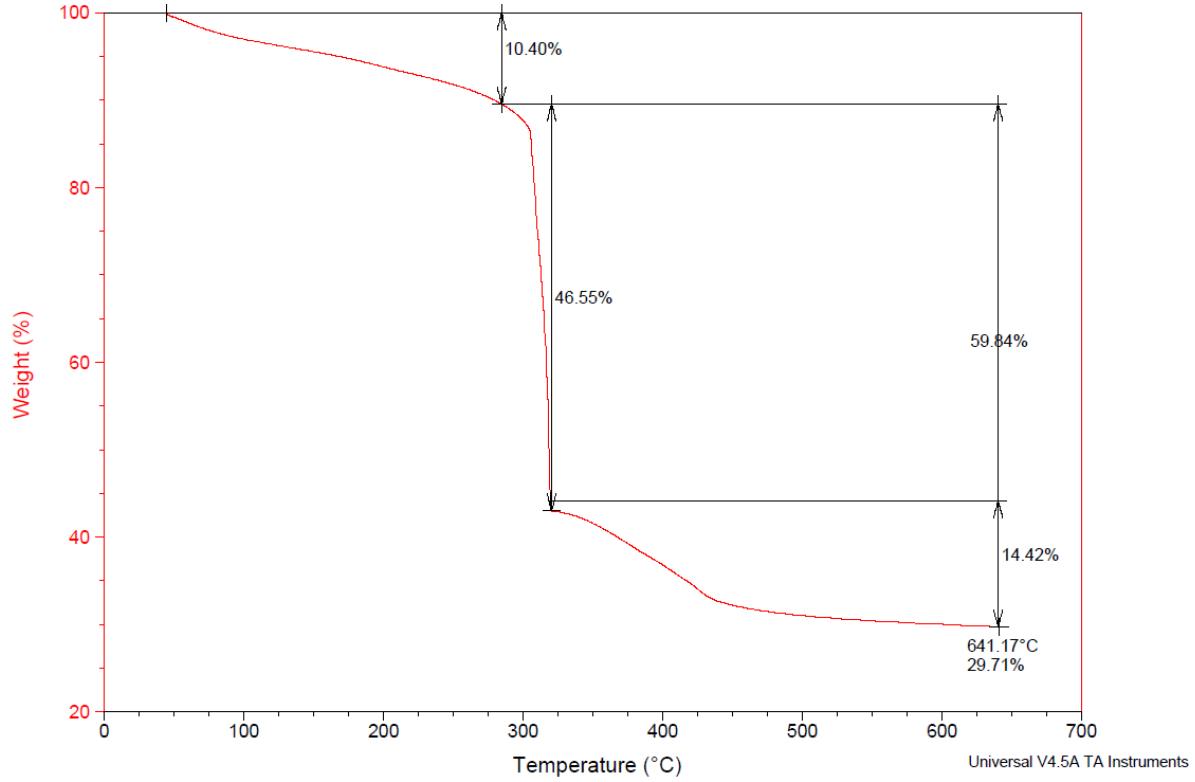

S7.29. TGA for 1NiEu-Cl

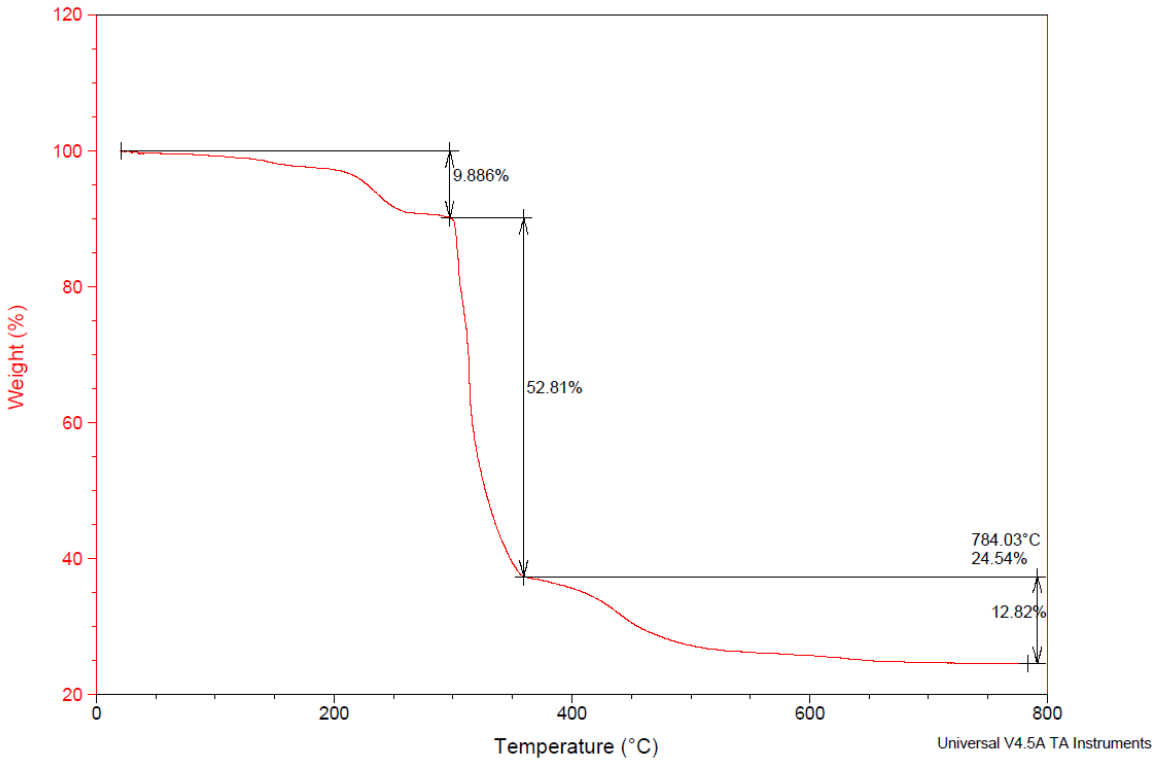

S7.30. TGA for 2NiY-Cl

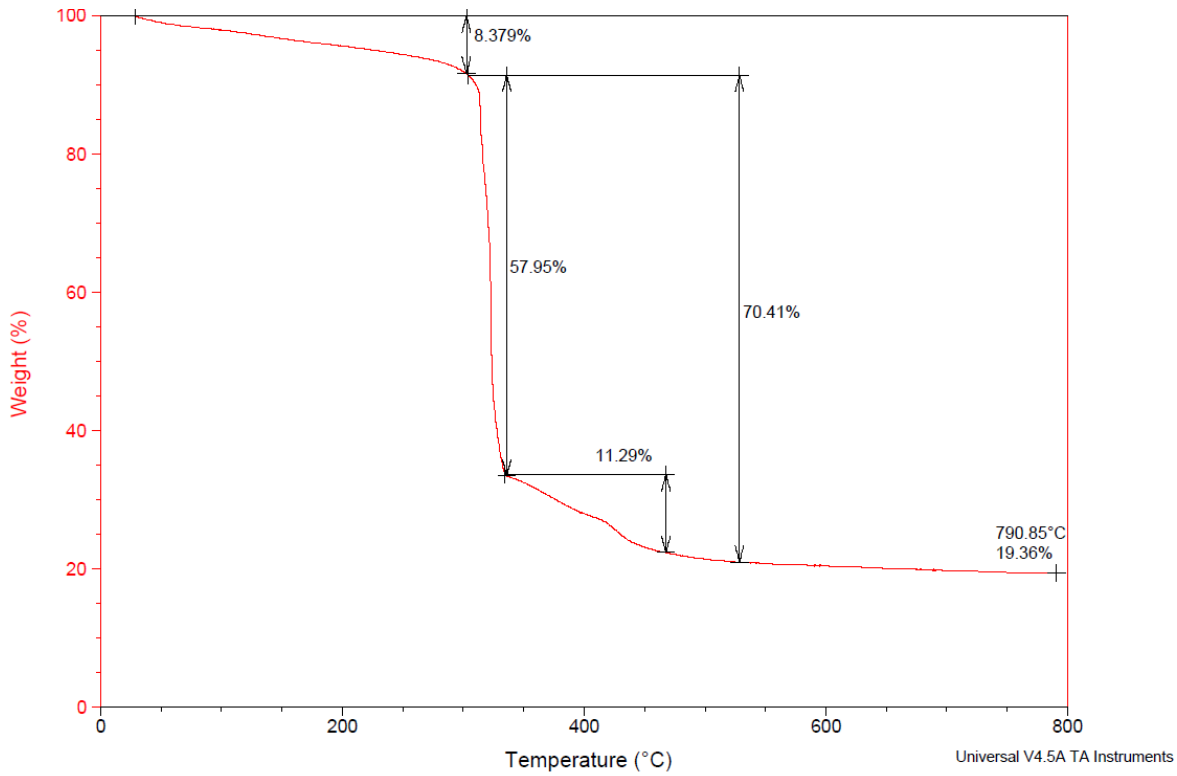

S7.31. TGA for 6NiY-Cl

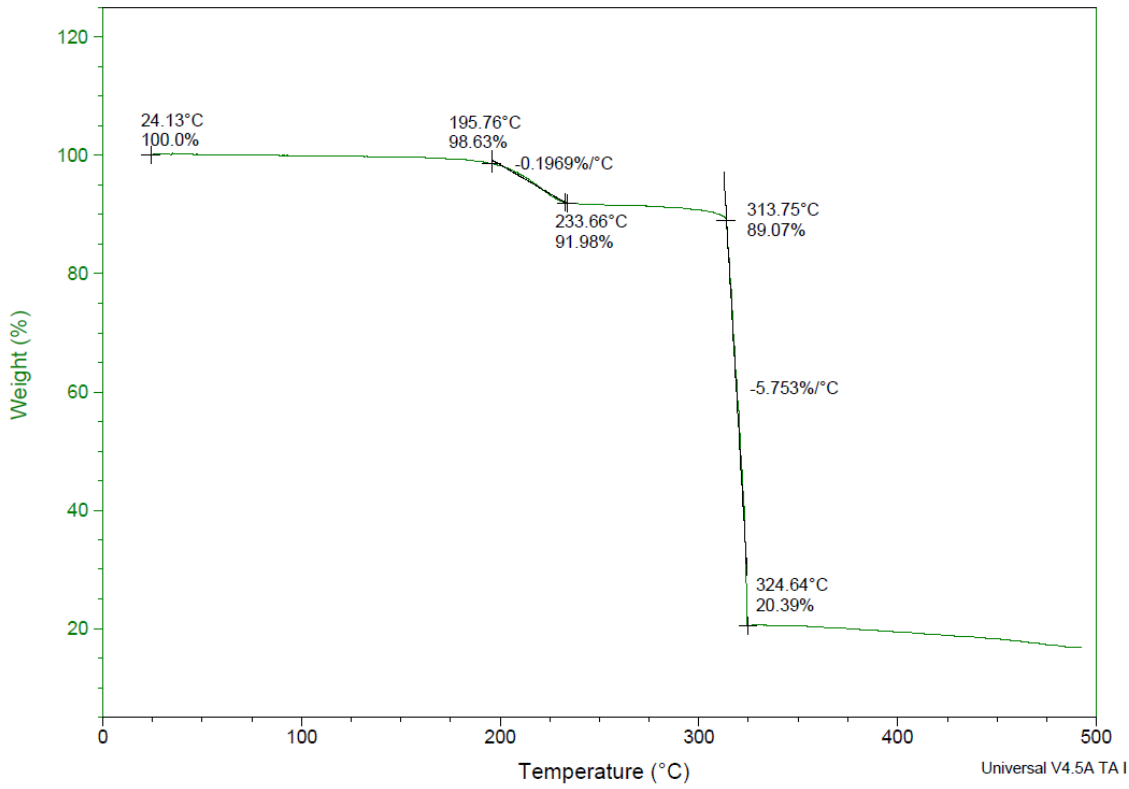

S7.32. TGA for 16NiY-Cl

7.4 Side Product Structures

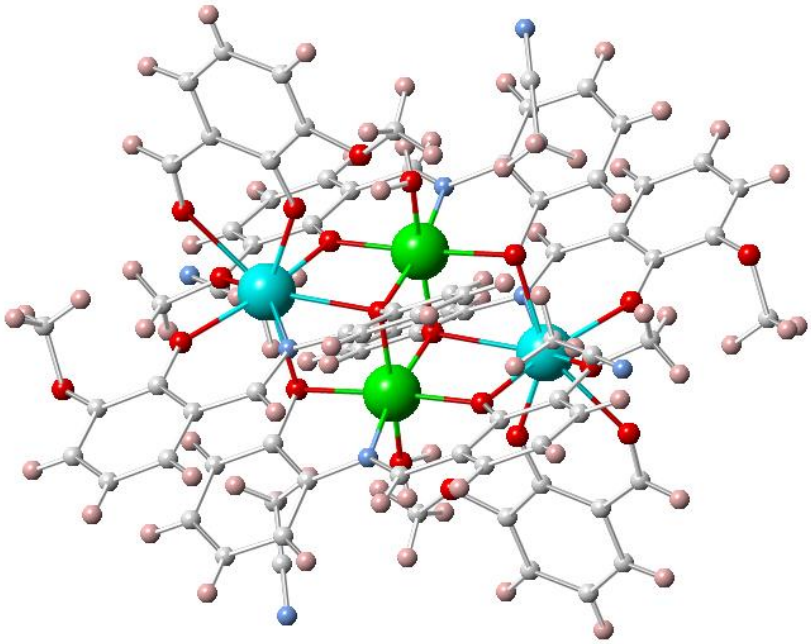

S7.33 Molecular Structure of $[Ni^{II}_2Sm^{III}_2(\mathbf{L1})_4(O\text{-}Van)_2(H_2O)_2]\cdot 4CH_3CN$ (**1NiSm-Cl -B**). Colour code: Ni^{II}, green; Dy^{III}, light blue; O, red; N, blue; C, white. Hydrogen atoms are omitted for clarity.

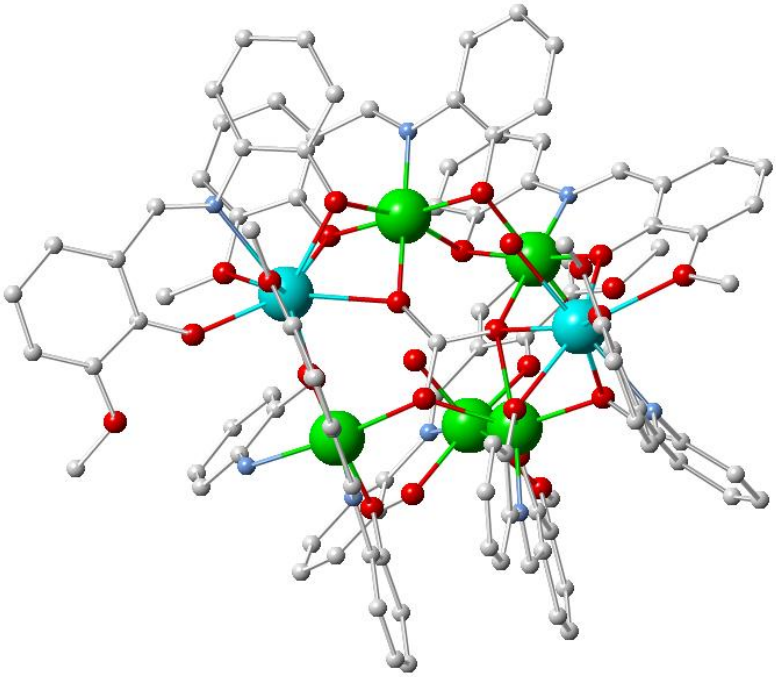

S7.34 Molecular Structure of [$Ni^{II}_5Sm^{III}_2(CO_3)$ (**L1**)$_7$(**L1′**) $(H_2O)_3$] (**1NiSm-Cl -A**) Colour code: Ni^{II}, green; Dy^{III}, light blue; O, red; N, blue; C, white. Hydrogen atoms are omitted for clarity.

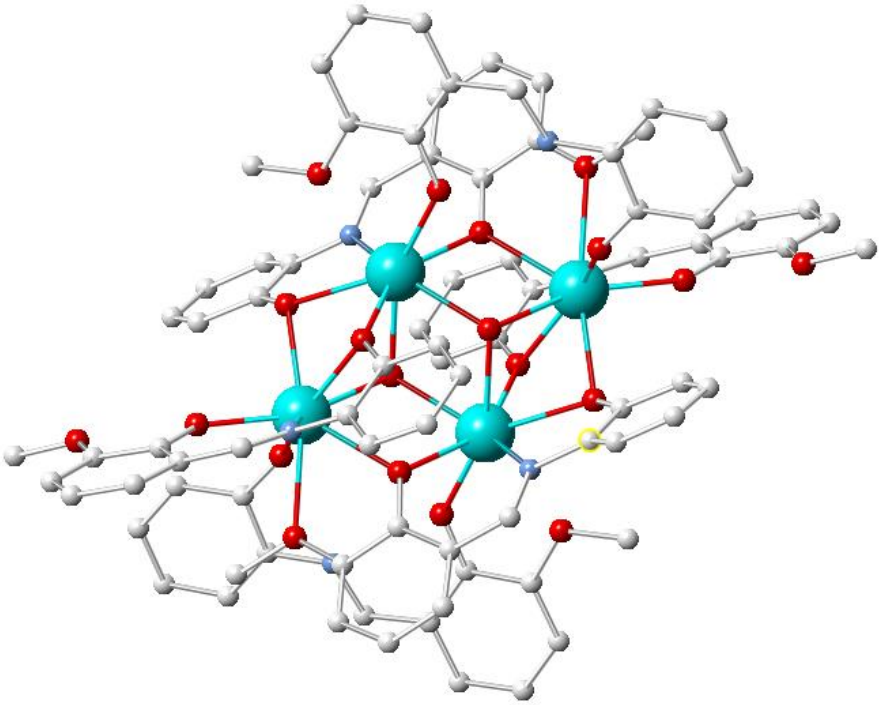

S7.35 [$Sm^{III}_4(OH)_2$(**L1**)$_4$(H**L1**)$_2$] $2CH_3CN$ (**1NiSm-Cl -C**). Colour code: Dy^{III}, light blue; O, red; N, blue; C, white. Hydrogen atoms are omitted for clarity.

7.5 NMR Data of Stenhouse salts

	6	5a	Exp
H1	6.9	8.4	8.30
H3	6.4	6.4	6.97
H4	5.8	5.5	6.56
H5	6.3	7.0	7.62
C1	144.4	155.6	147.80
C3	142.6	123.6	116.17
C4	116.1	105.0	112.22
C5	132.1	137.3	145.60

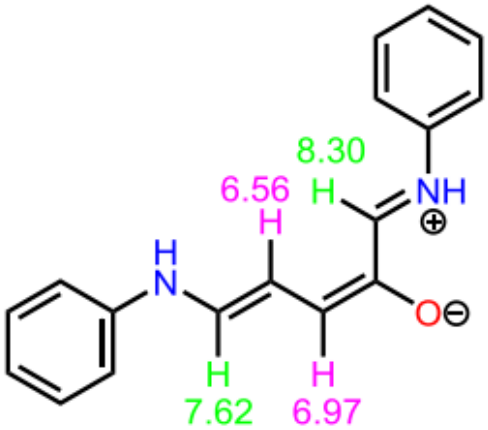

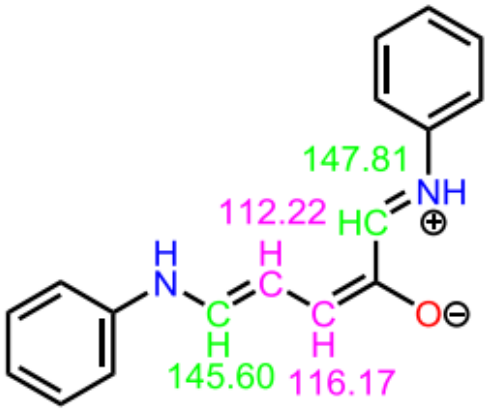

S7.36. Calculated NMR chemical shifts for model compounds **C7f** and **C7f'**

7,6 ^{1}H NMR of Products (C7a-C7k)

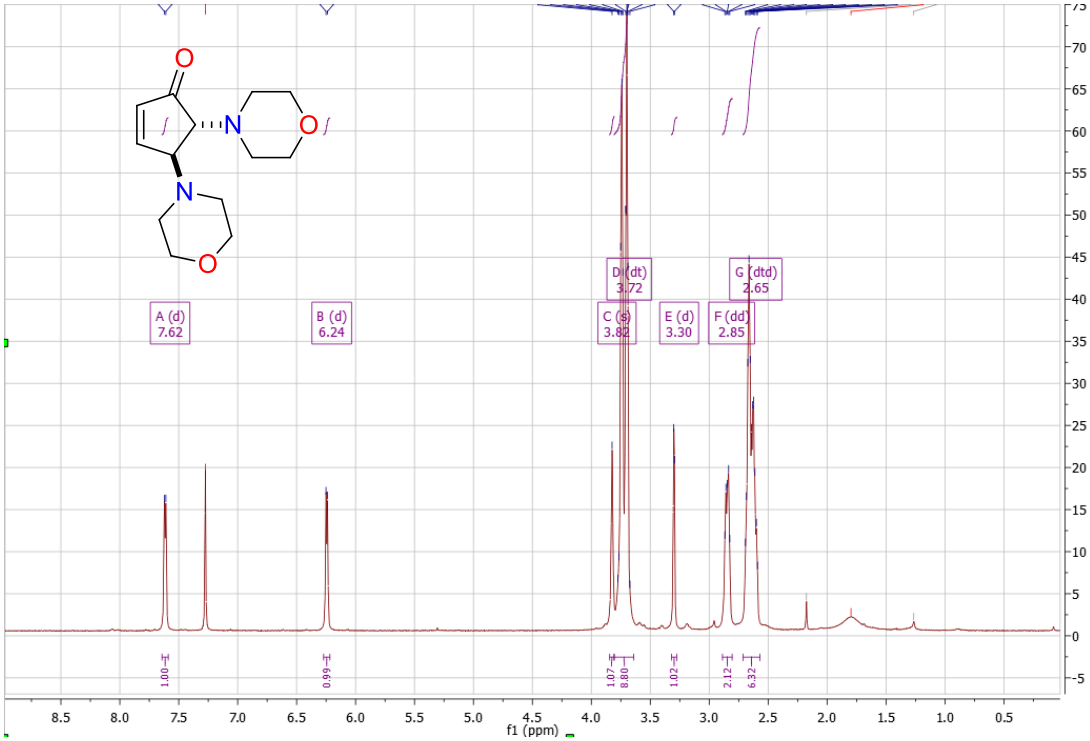

S7.37. ^{1}H NMR of C7a

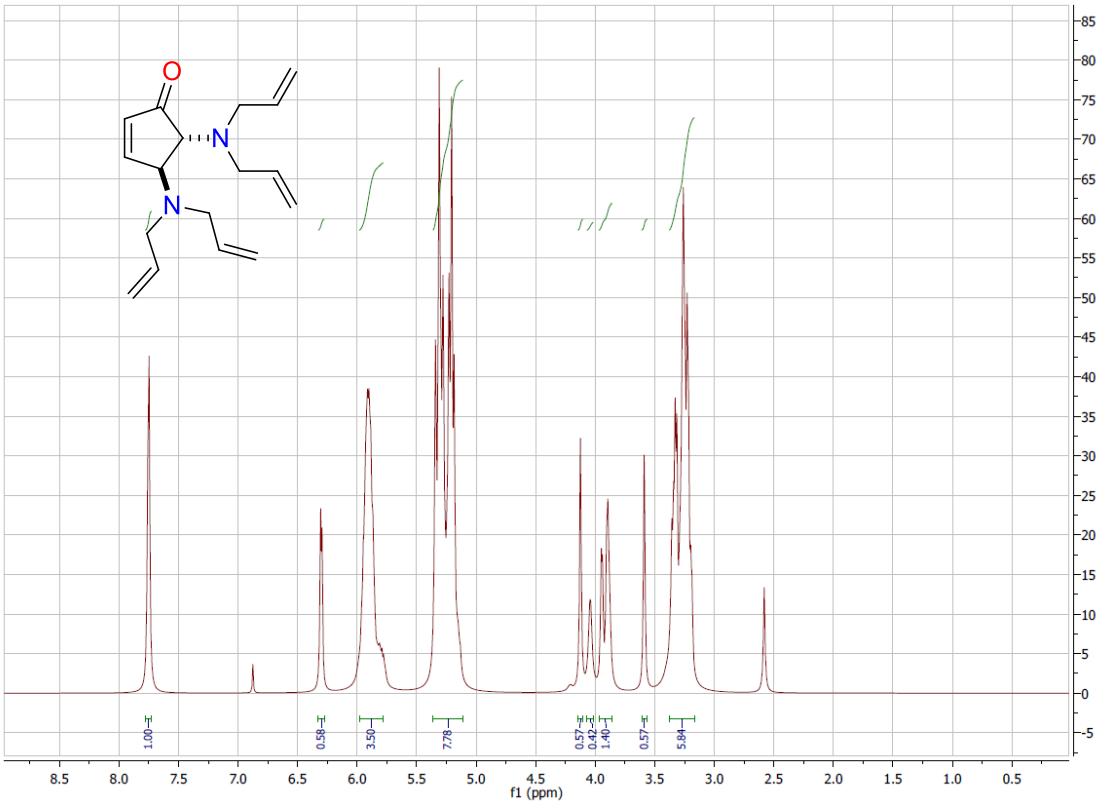

S7.38. ^{1}H NMR of C7b

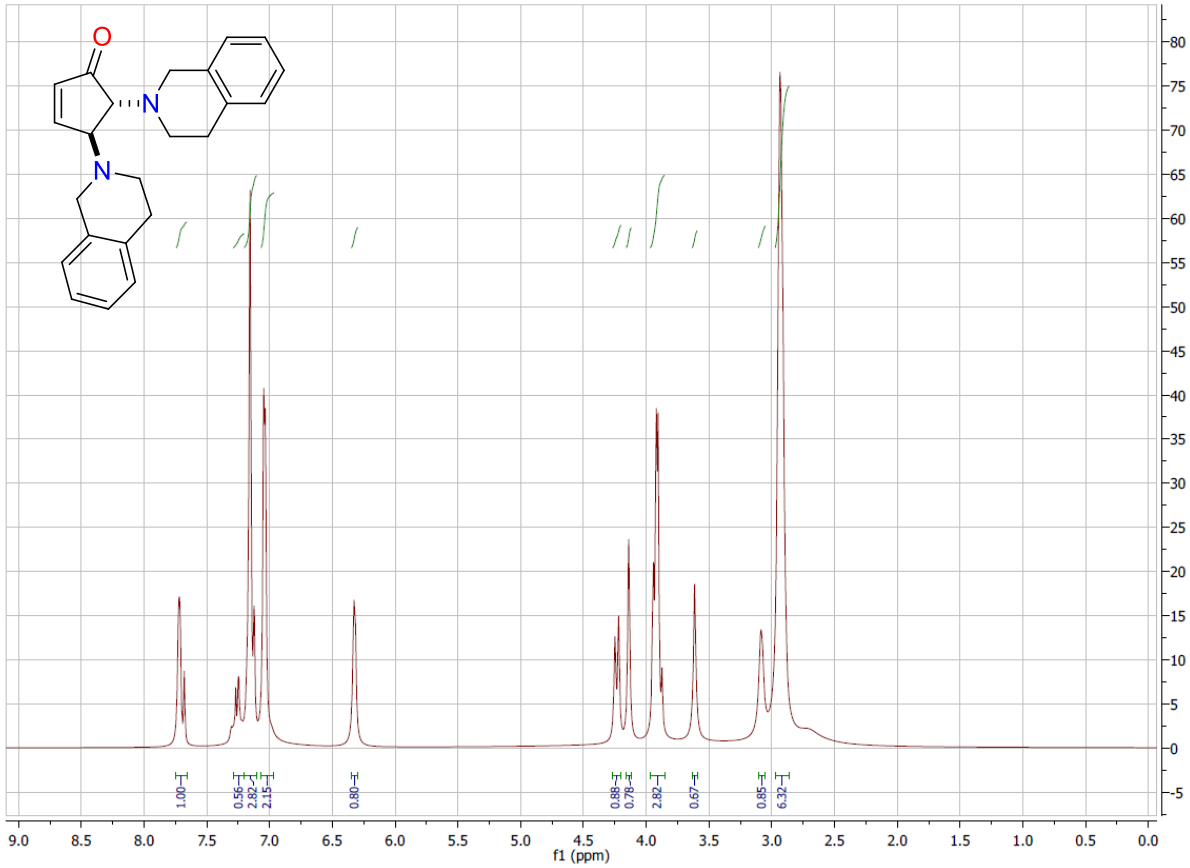

S7.39. ^{1}H NMR of C7e

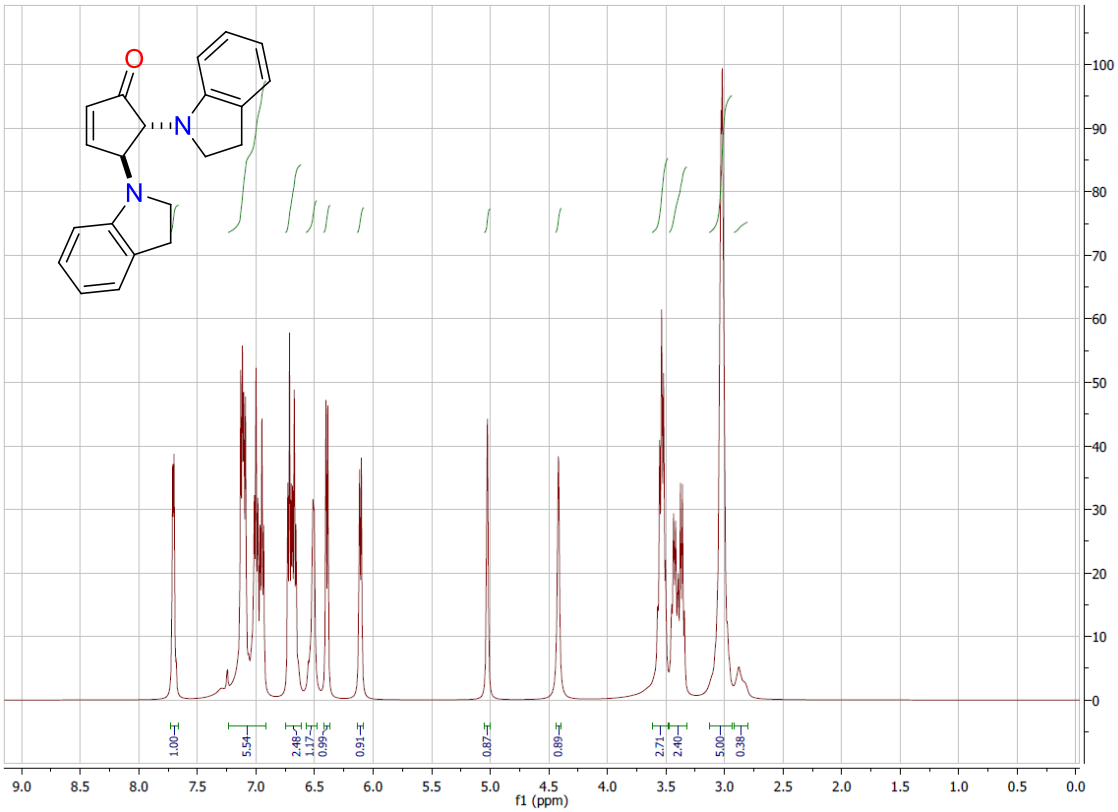

S7.40. ^{1}H NMR of C7c

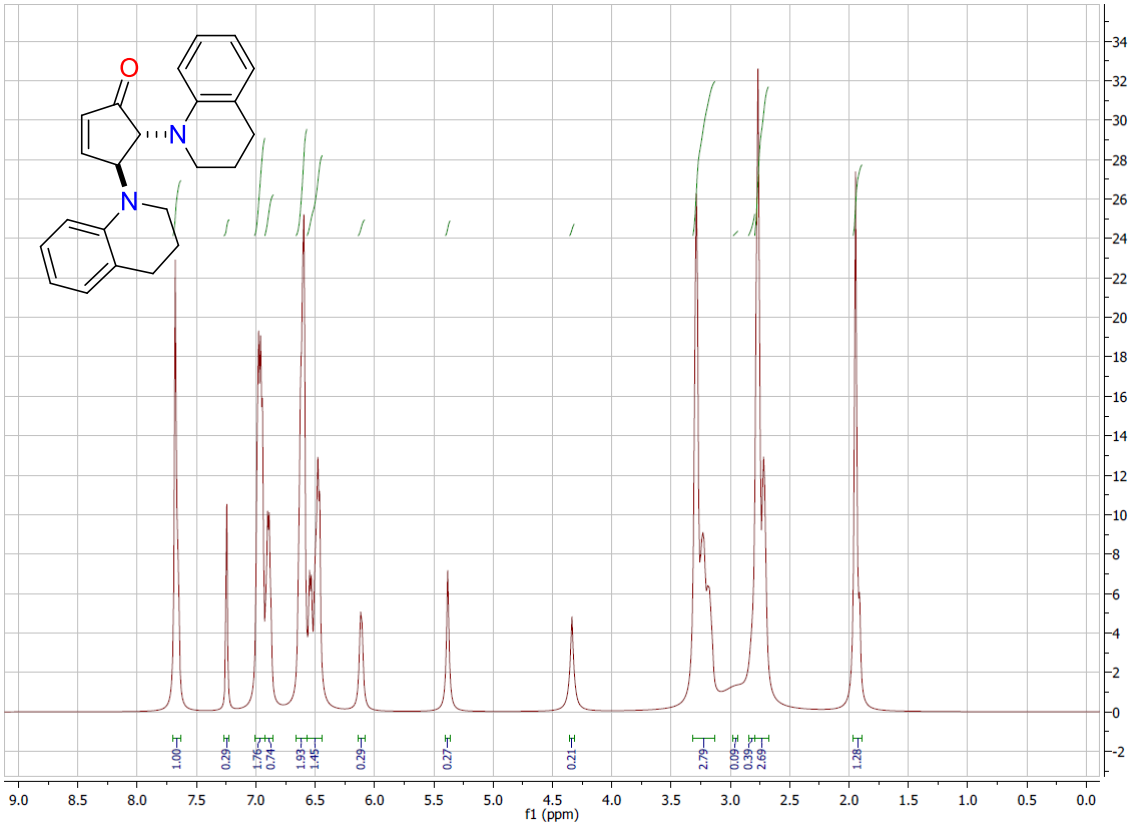

S7.41. ^{1}H NMR of C7d

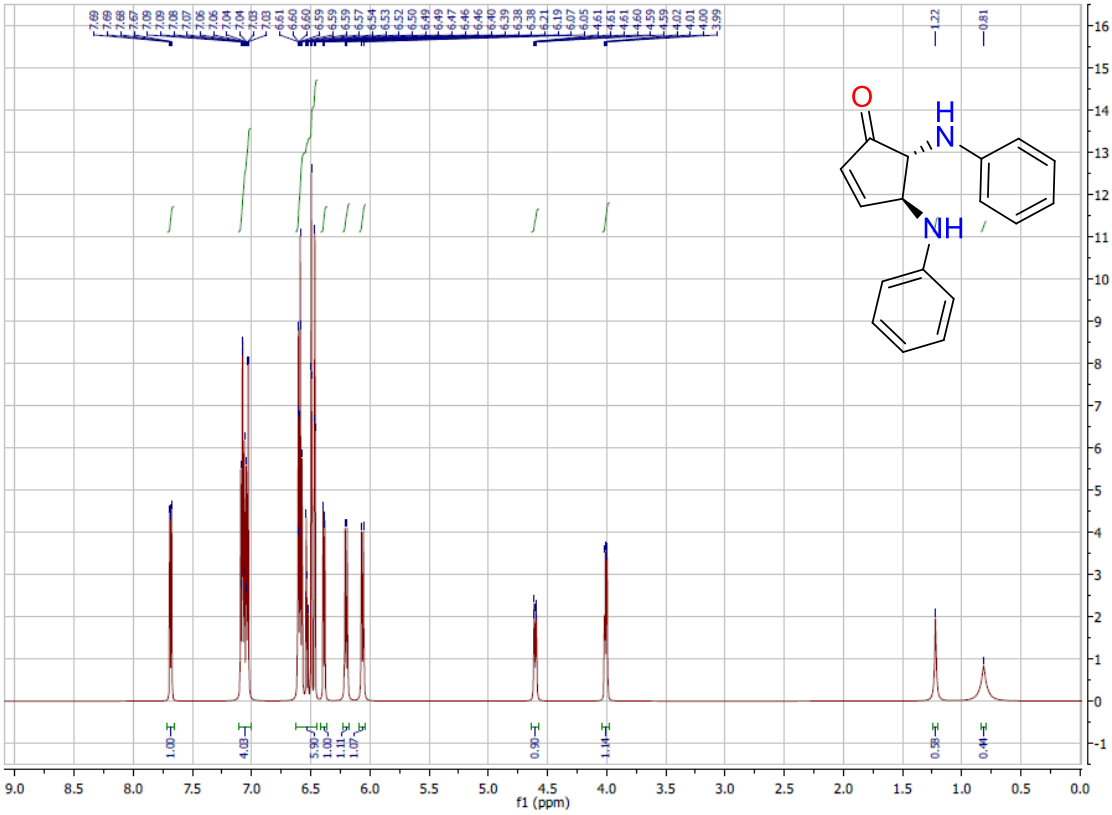

S7.42. ^{1}H NMR of C7j

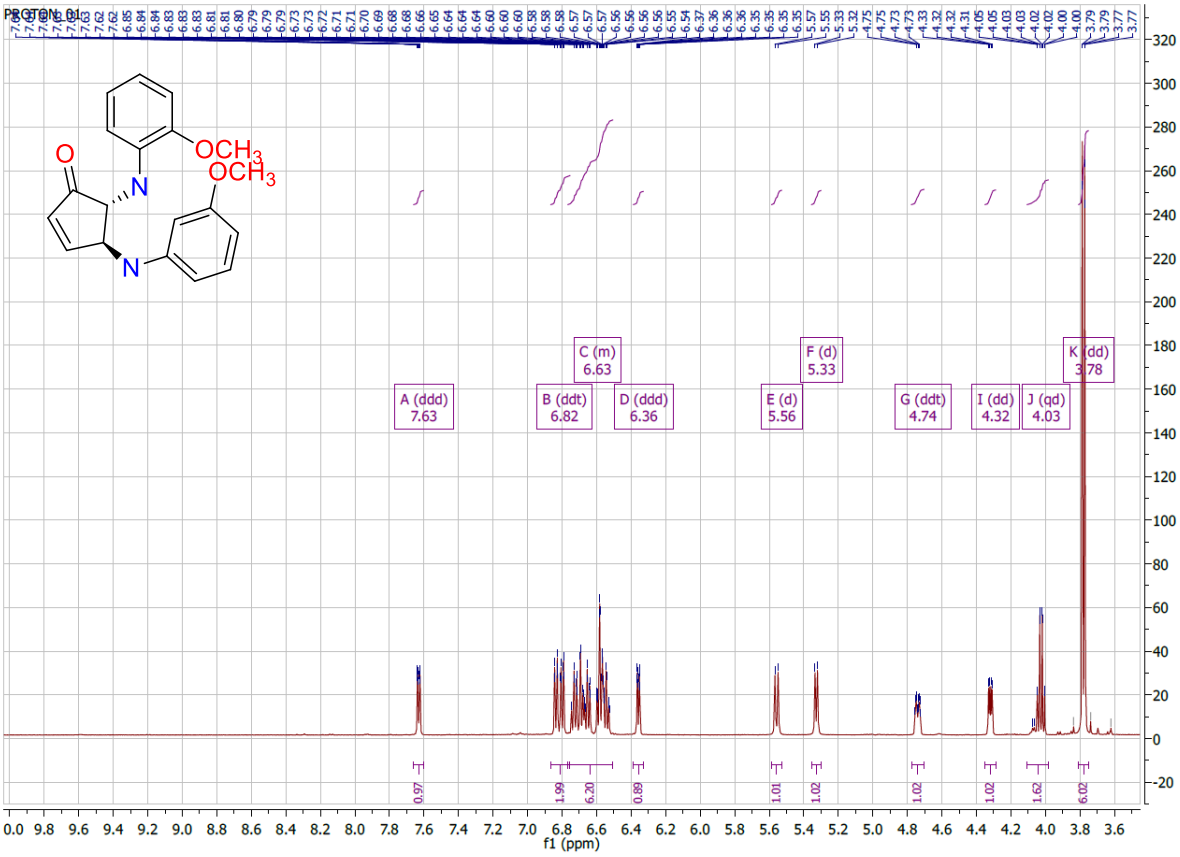

S7.43. ^{1}H NMR of C7k

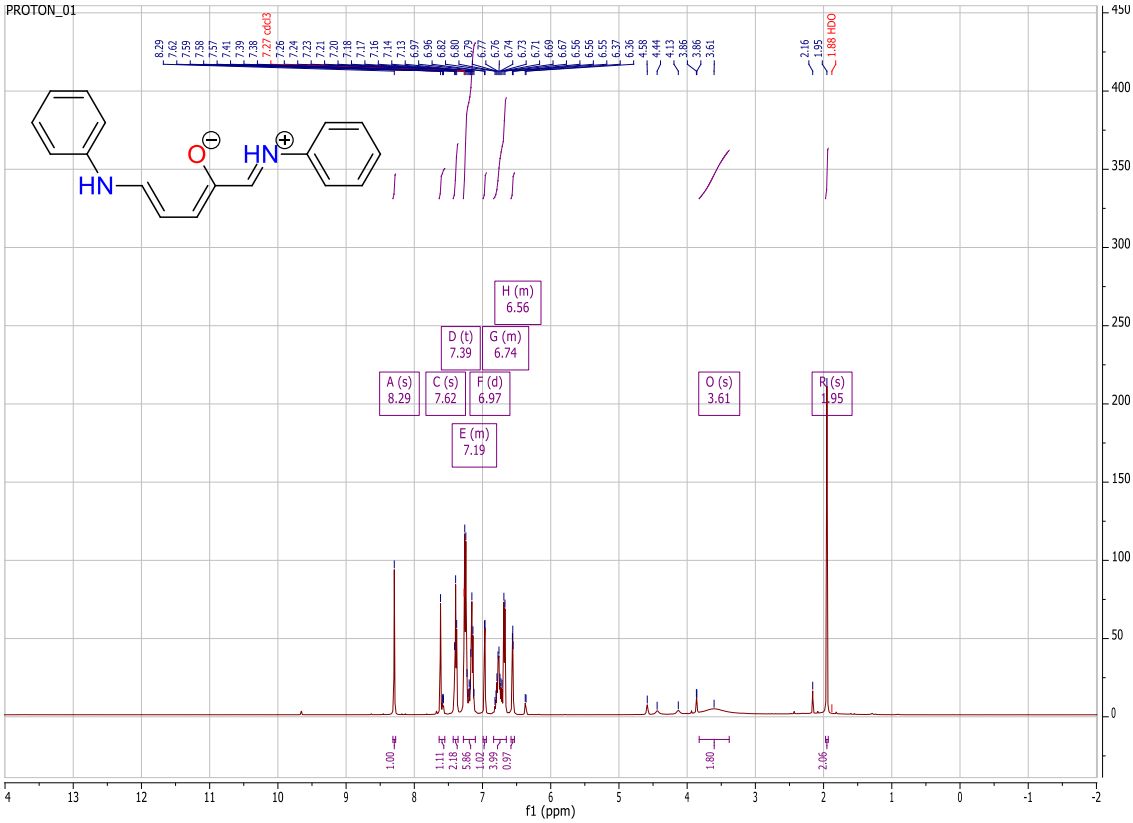

S7.44. ^{1}H NMR of C7f

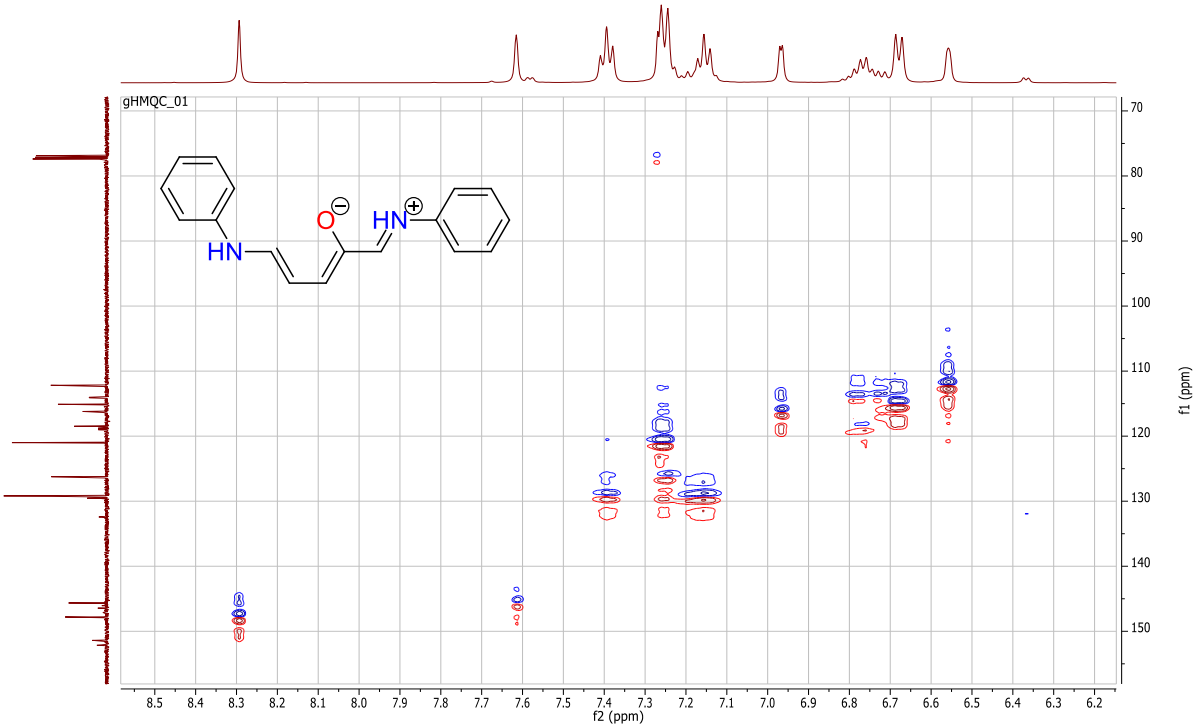

S7.45

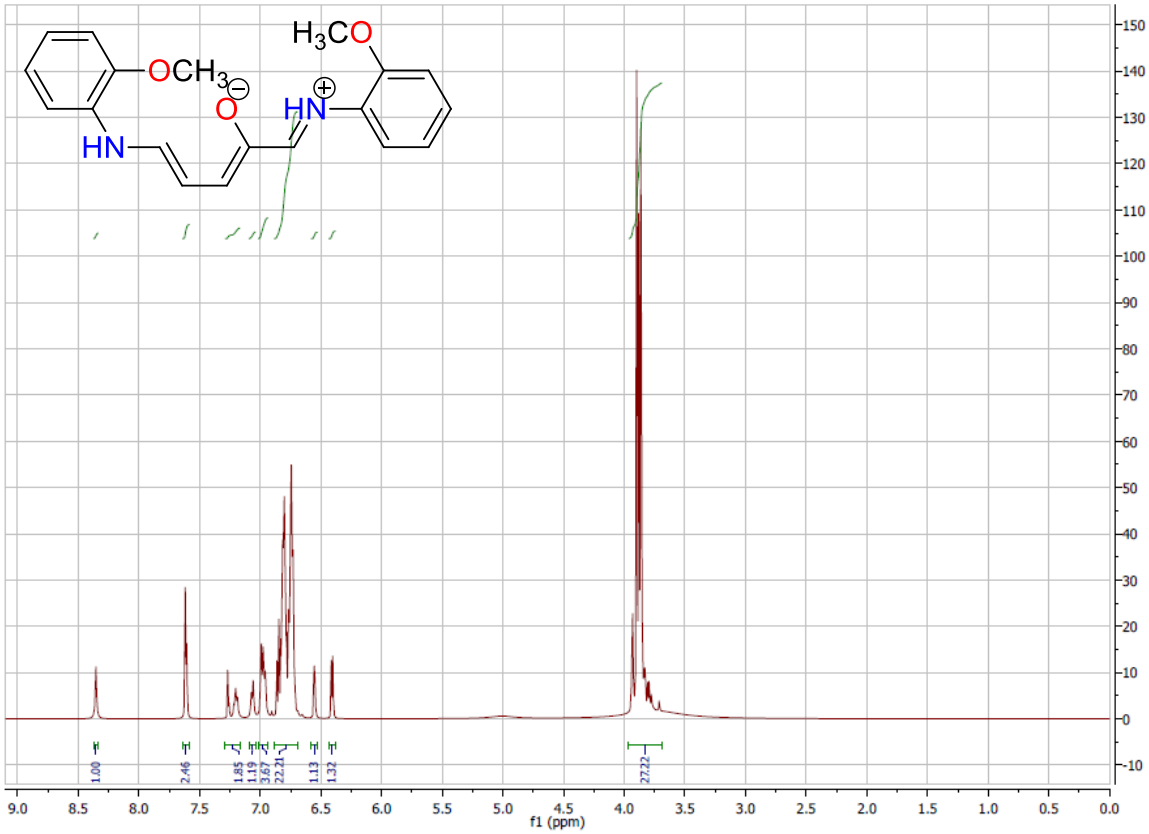

S7.46. ^{1}H NMR of C7g

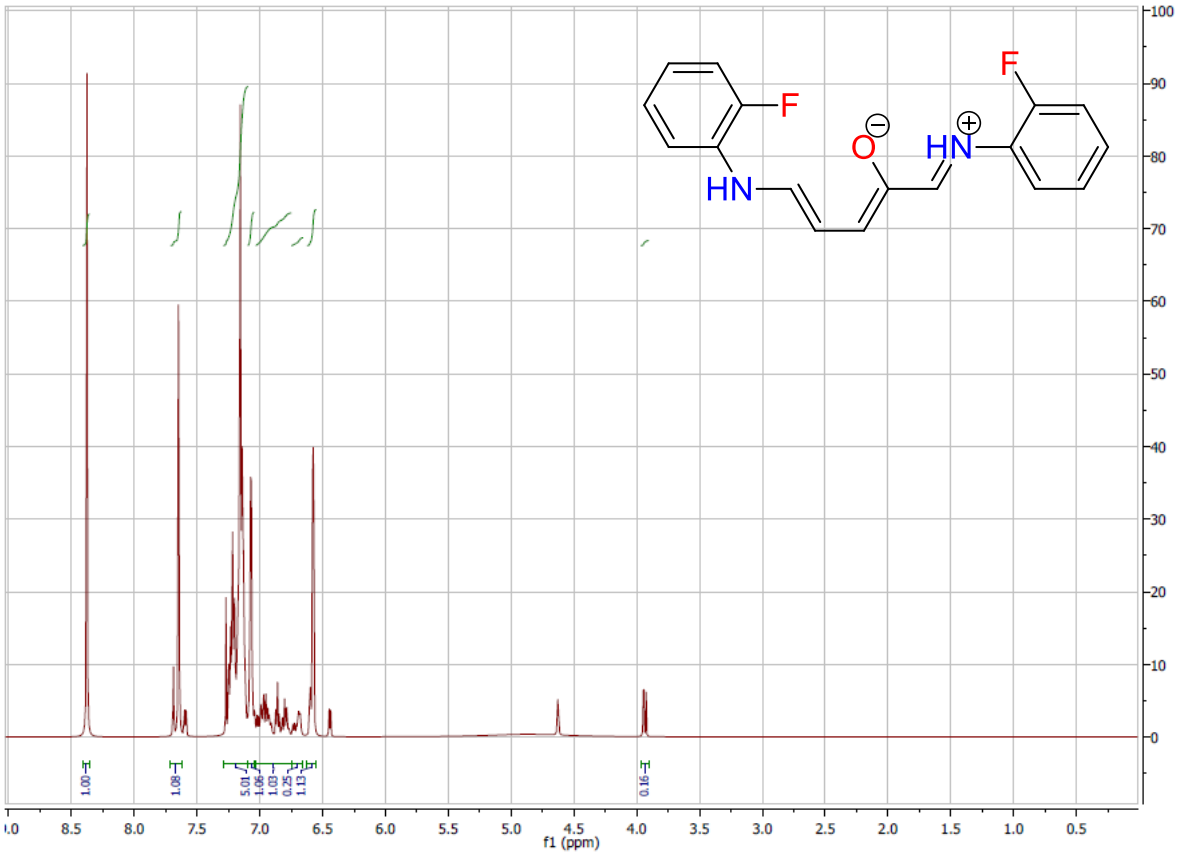

S7.47. ^{1}H NMR of C7h

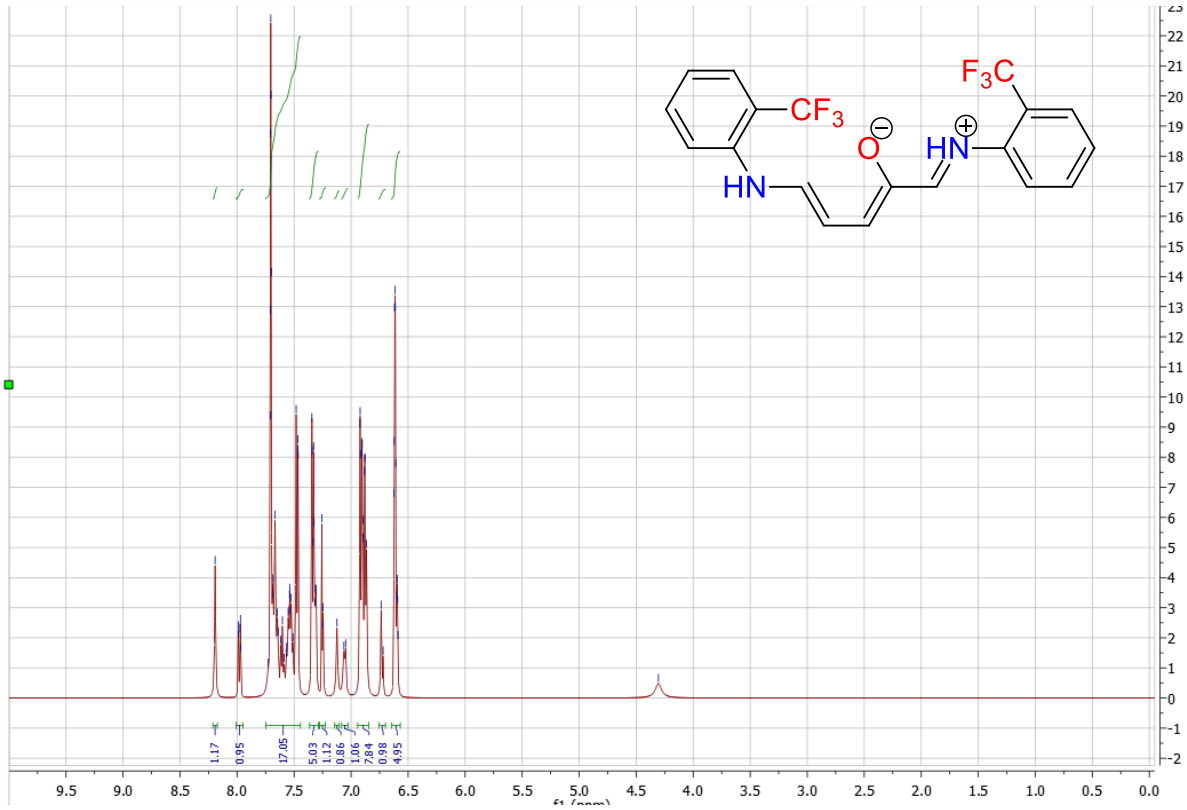

S7.48. ^{1}H NMR of C7i

7.7 ^{13}CNMR of (C7f-C7i)

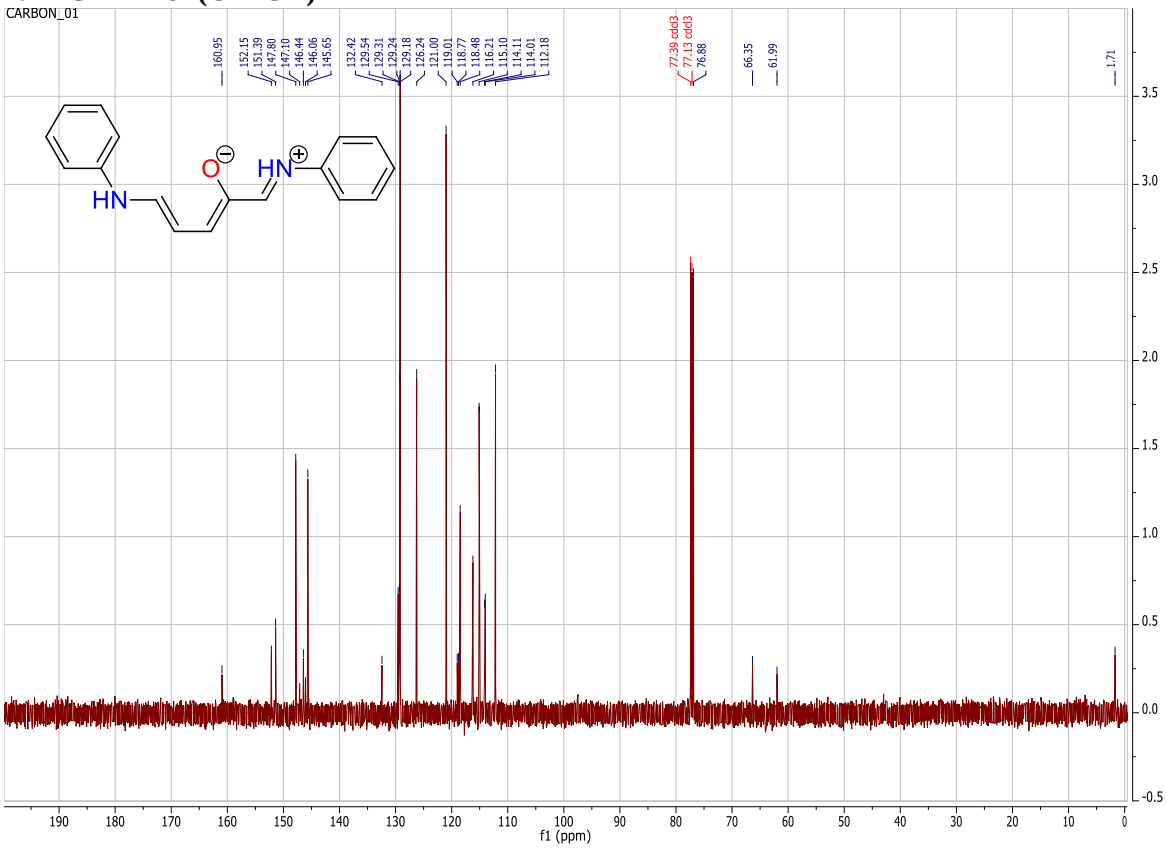

S7.49. ^{13}C NMR of C7f

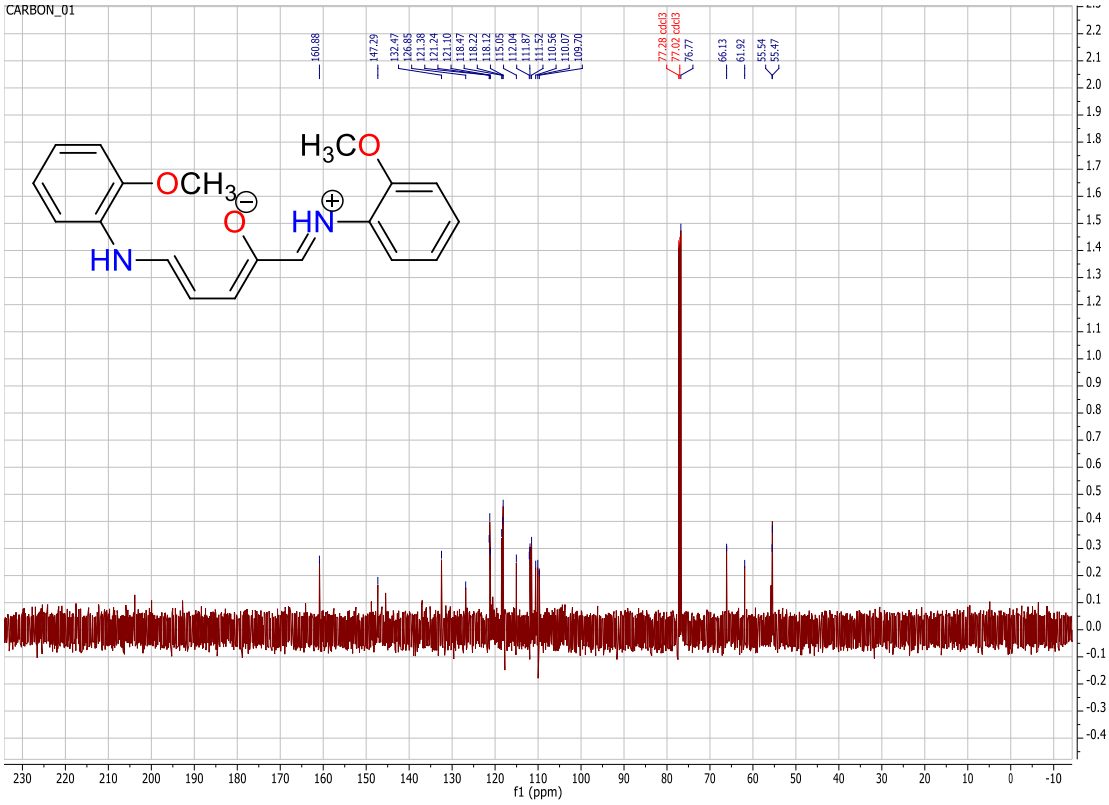

S7.50. ^{13}C NMR of C7g

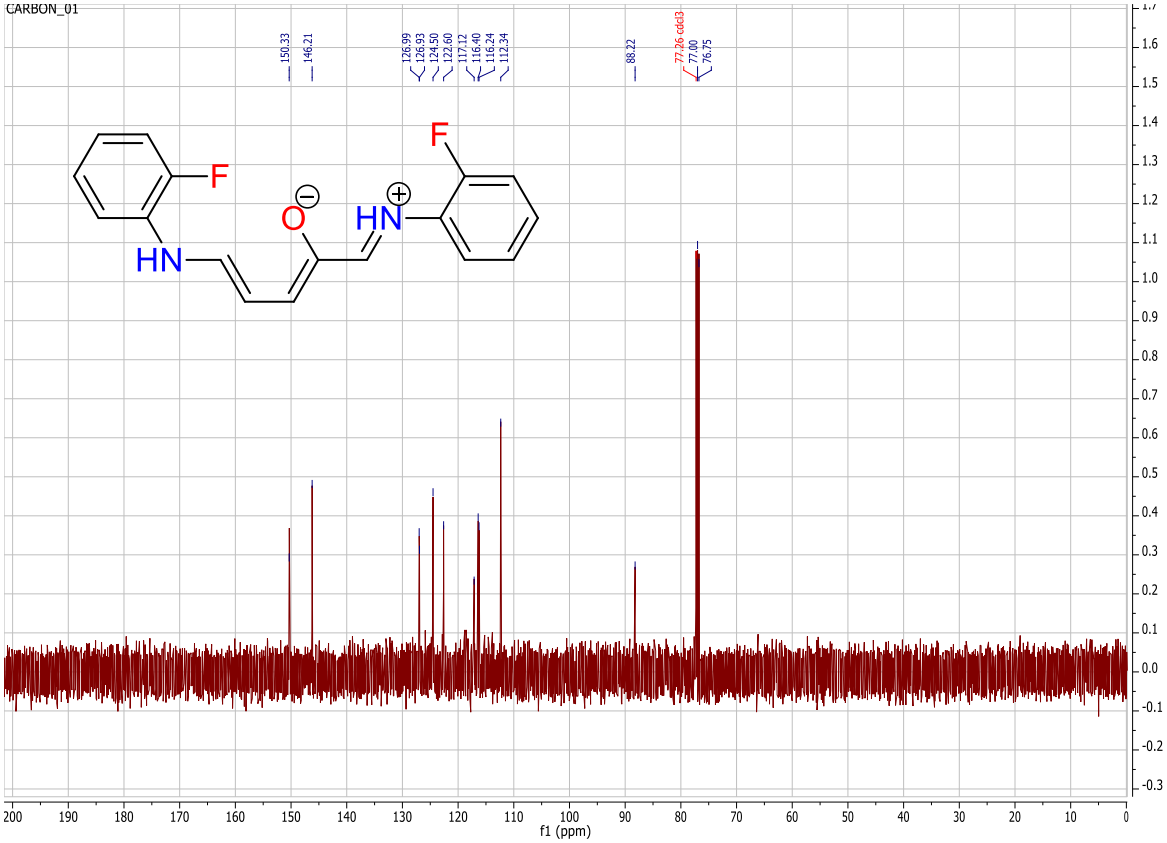

S7.51. ^{13}C NMR of C7h

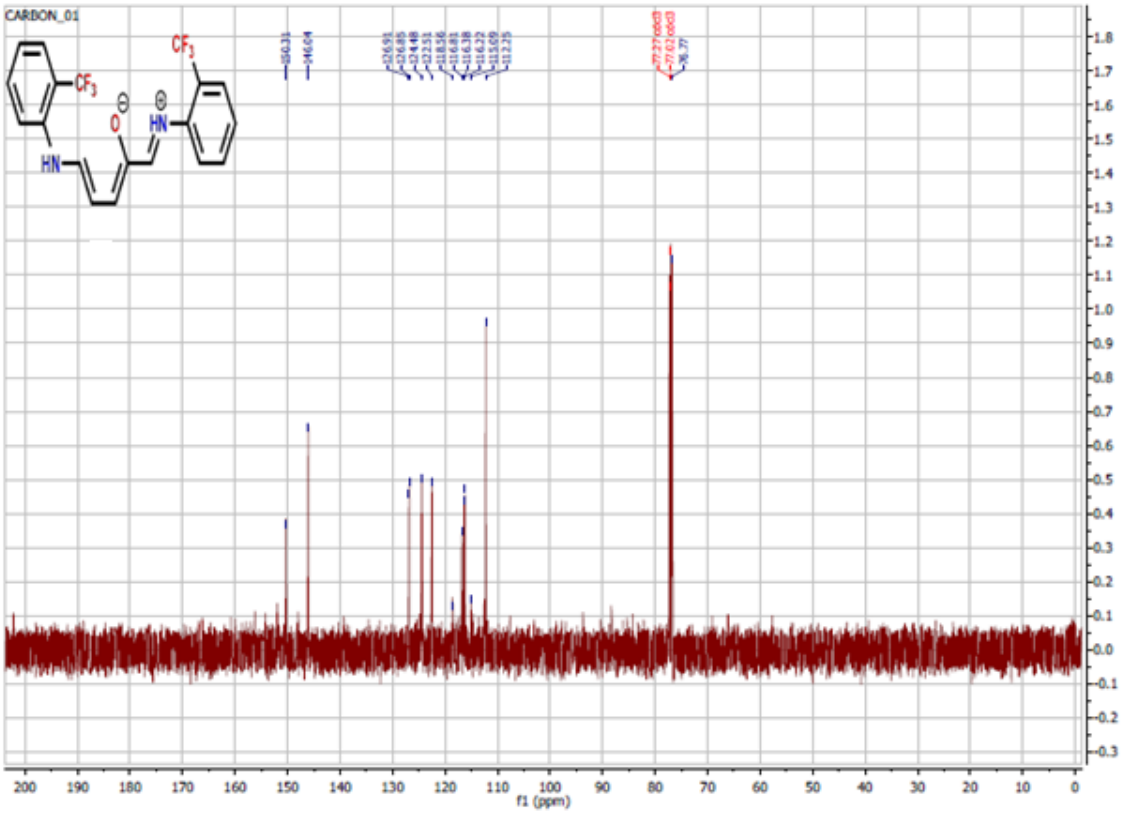

S7.52. ^{13}C NMR of C7i

7.8 ESI-MS of C7f, C7g and C7i

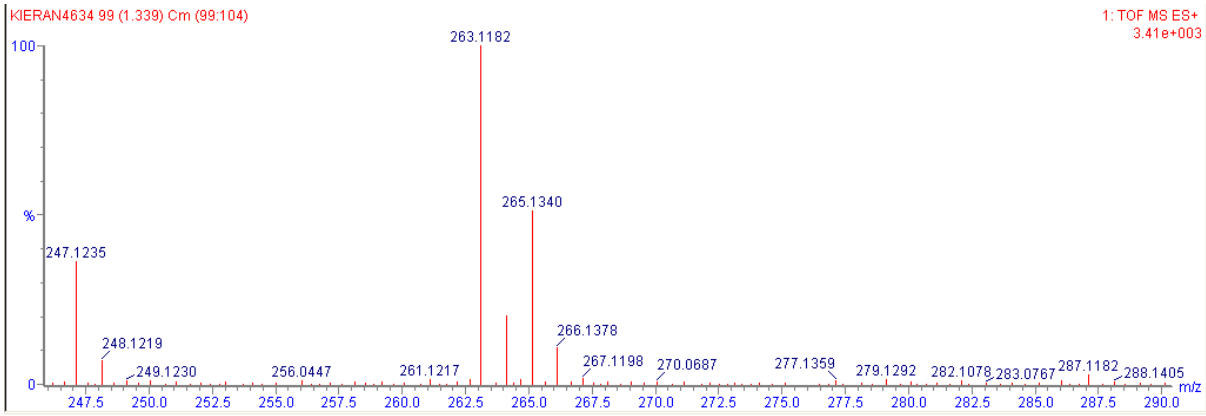

S7.53. ESI-MS of C7f

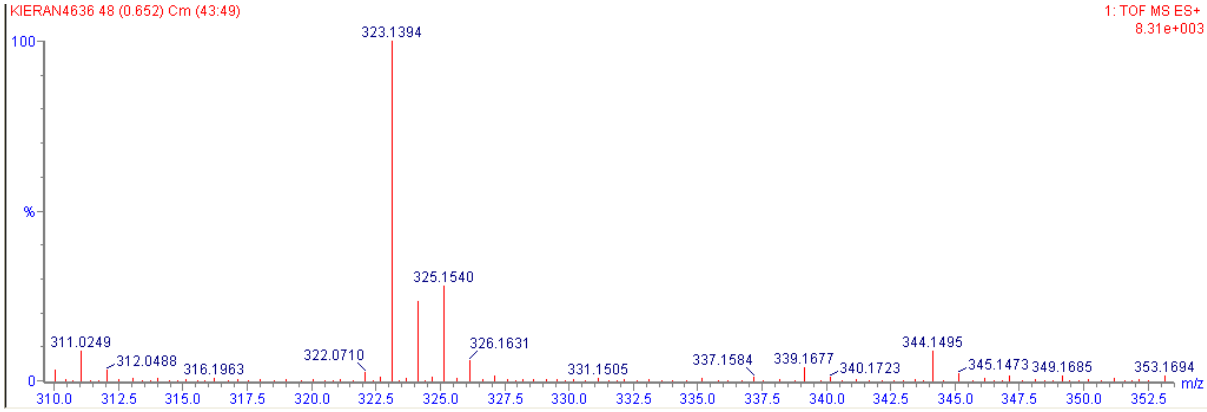

S7.54. ESI-MS of C7g

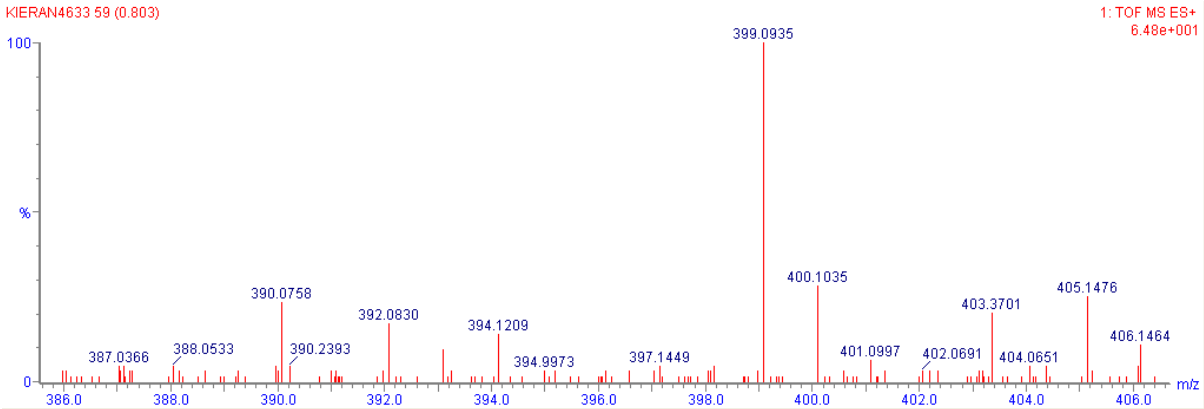

S7.55. ESI-MS of C7i

7.9 FT-IR of C7f and C7g

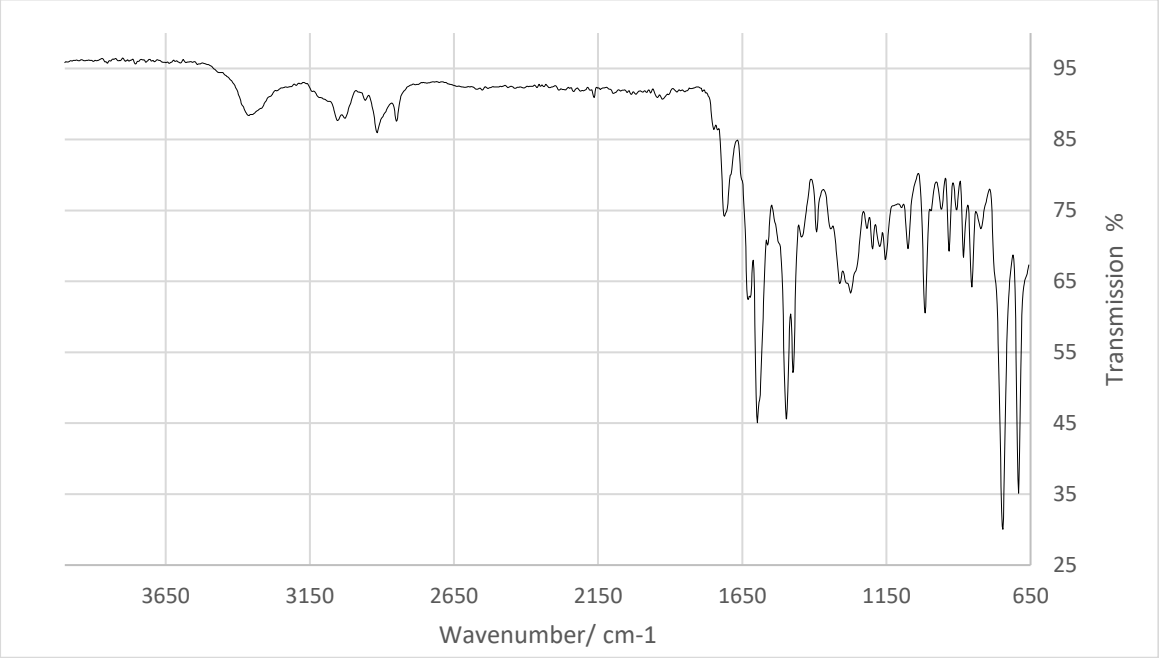

S7.56. FT-IR of C7f

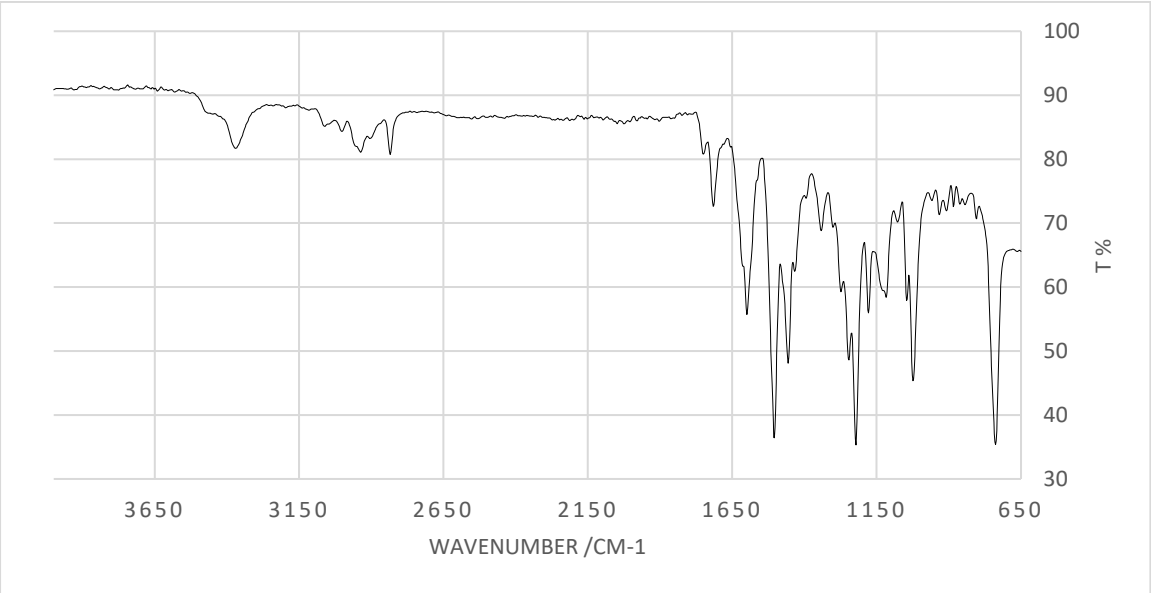

S7.57. FT-IR of C7g

Chapter 8

8.1 FT-IR of 1ZnLn-NO_3

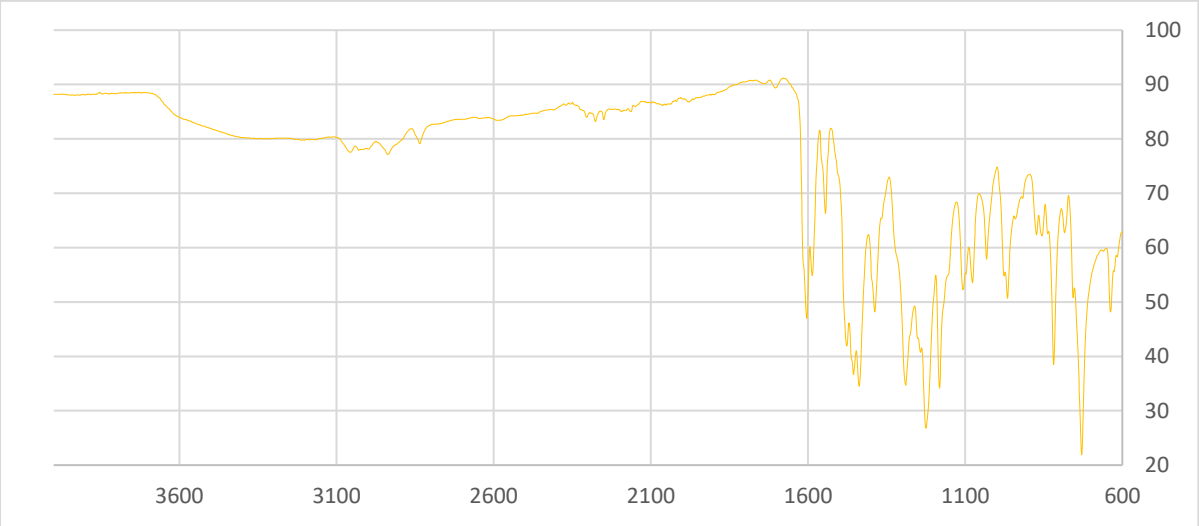

S8.1. FT-IR of 1ZnDy-NO_3

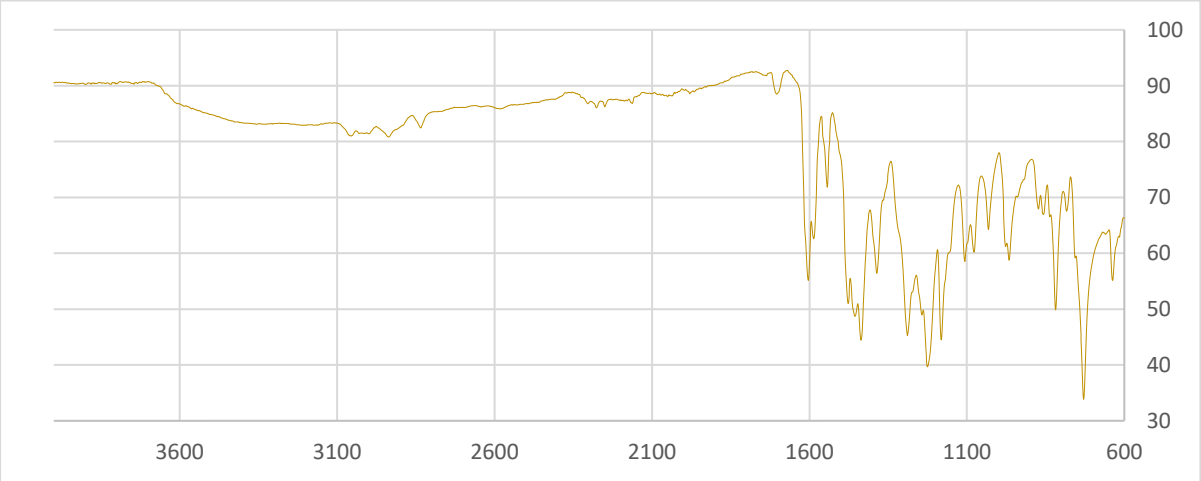

S8.2. FT-IR of 1ZnY-NO_3

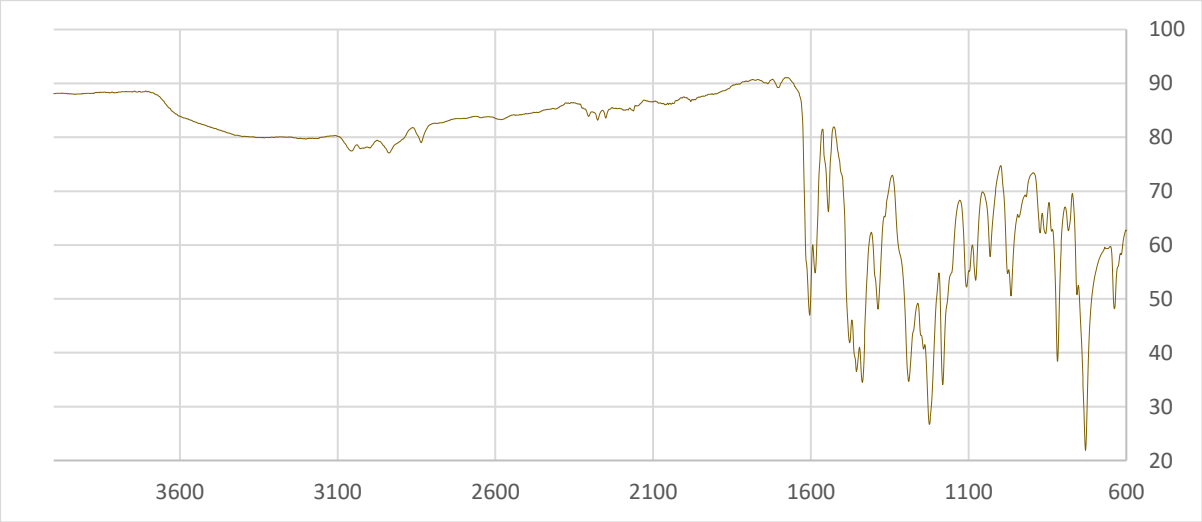

S8.3. FT-IR of 1ZnGd-NO_3

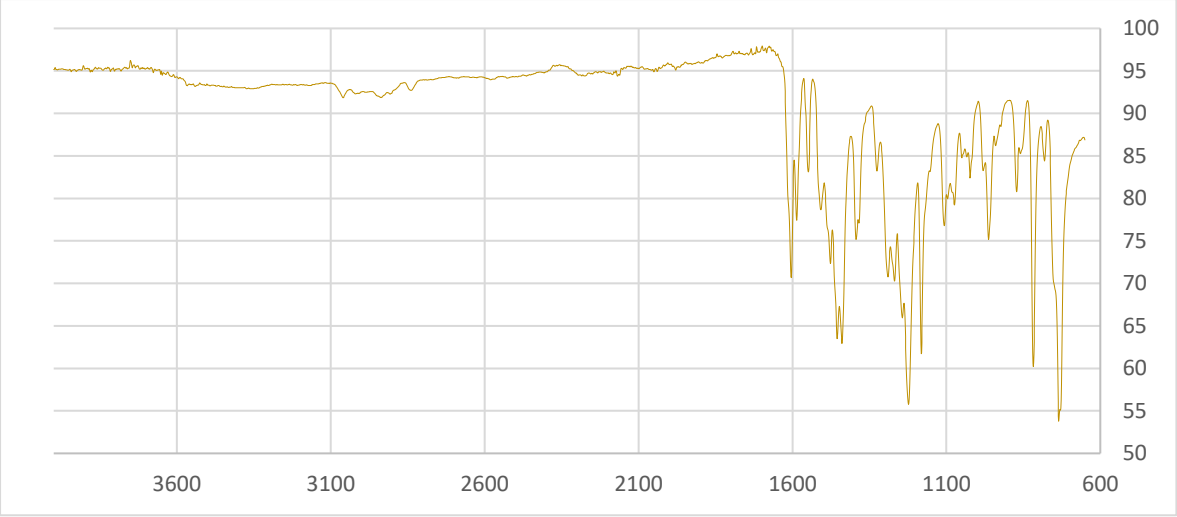

S8.4. FT-IR of 1ZnEu-NO_3

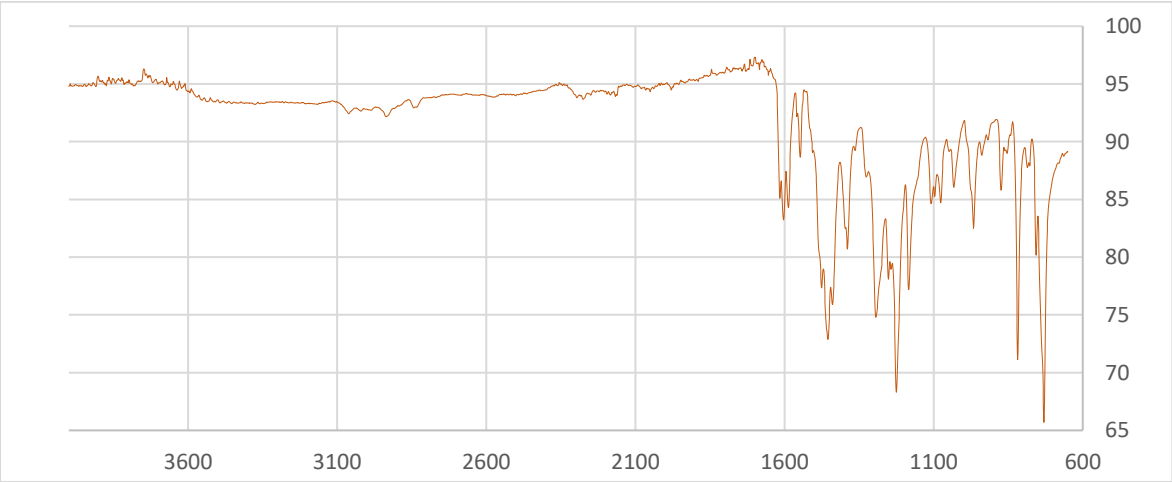

S8.5. FT-IR of 1ZnTb-NO_3

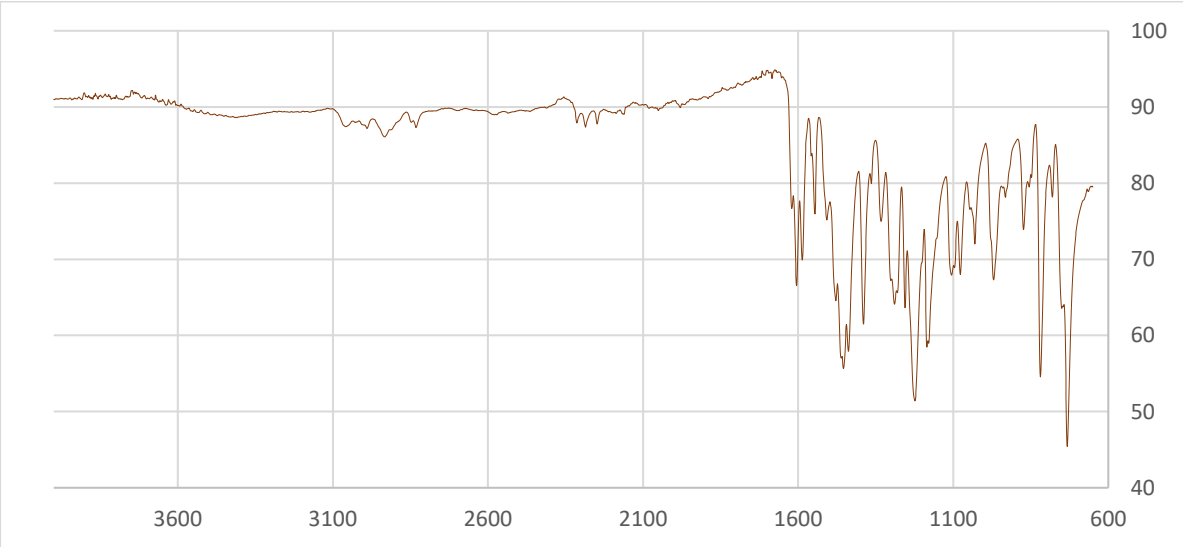

S8.6. FT-IR of 1ZnYb-NO_3

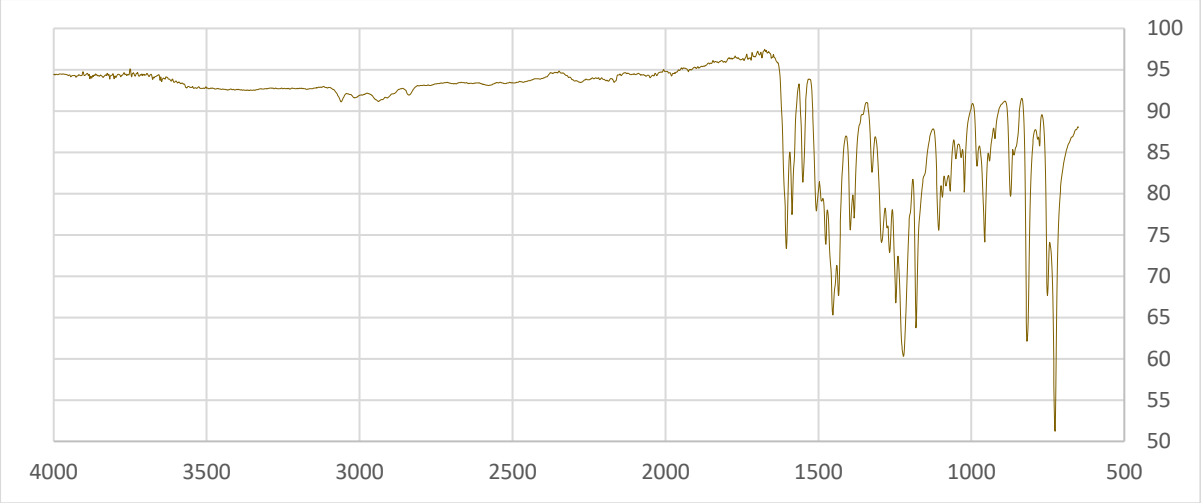

S8.7. FT-IR of 1ZnSm-NO_3

8.2 ESI-MS of 1ZnLn-NO_3

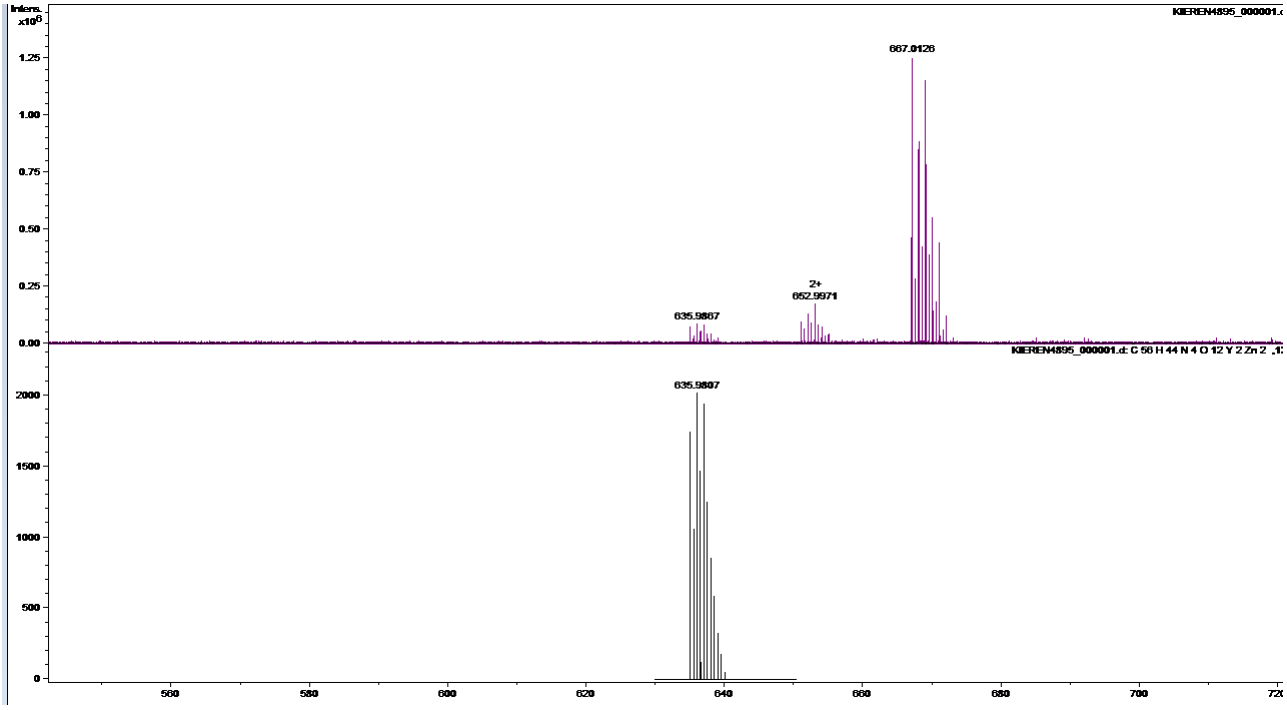

S8.8. ESI-MS of 1ZnY-NO_3. $[Zn^{II}_2Y^{III}_2(C_{14}H_{11}NO_3)_4]^{2+}$ fragment – 635.9867 m/z, $[Zn^{II}_2Y^{III}_2(C_{14}H_{11}NO_3)_4(MeOH)]^{2+}$ fragment – 652.9971 m/z and $[Zn^{II}_2Y^{III}_2(C_{14}H_{11}NO_3)_4(NO_3)]^{2+}$ fragment – 667.0126 m/z.

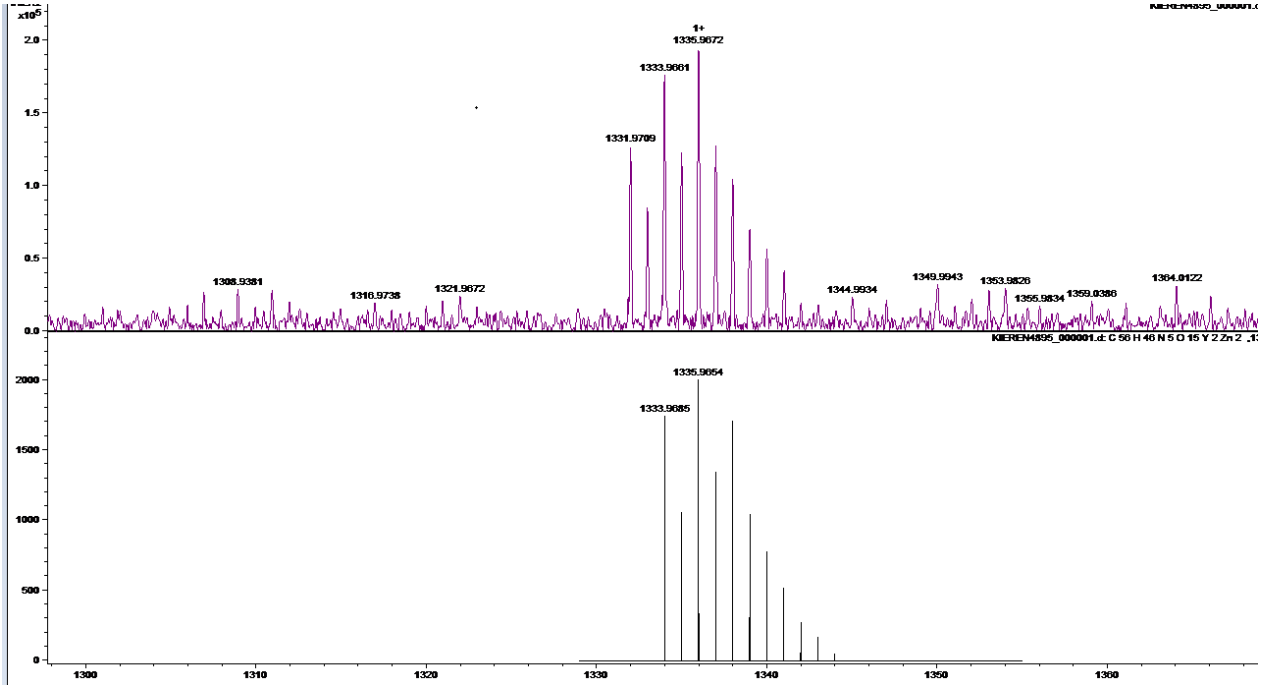

S8.9. ESI-MS of 1ZnY-NO_3. $[Zn^{II}_2Y^{III}_2(C_{14}H_{11}NO_3)_4(NO_3)]^{1+}$ fragment -1335.9672 m/z.

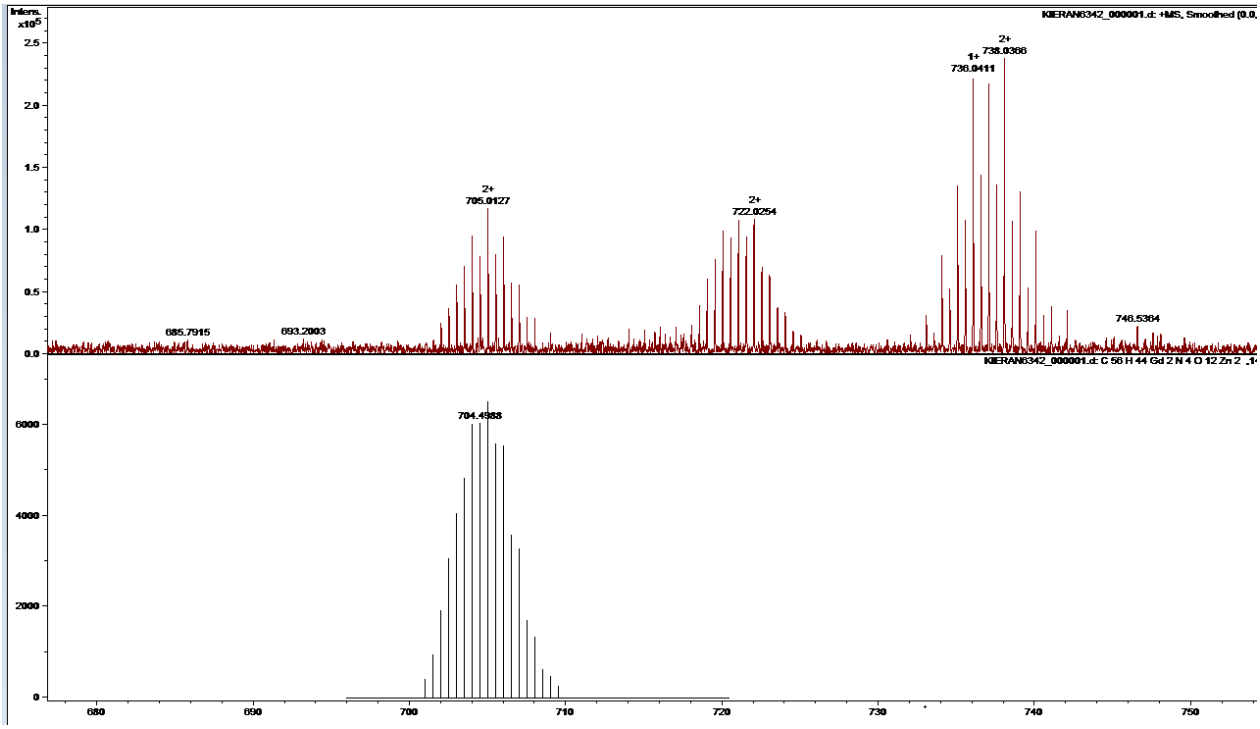

S8.10. ESI-MS of 1ZnGd-NO$_3$. $[Zn^{II}_2Gd^{III}_2(C_{14}H_{11}NO_3)_4]^{2+}$ fragment – 705.0127 m/z, $[Zn^{II}_2Gd^{III}_2(C_{14}H_{11}NO_3)_4(MeOH)]^{2+}$ fragment – 722.0254 m/z and $[Zn^{II}_2Gd^{II}_2(C_{14}H_{11}NO_3)_4(NO_3)]^{2+}$ fragment – 738.0366 m/z.

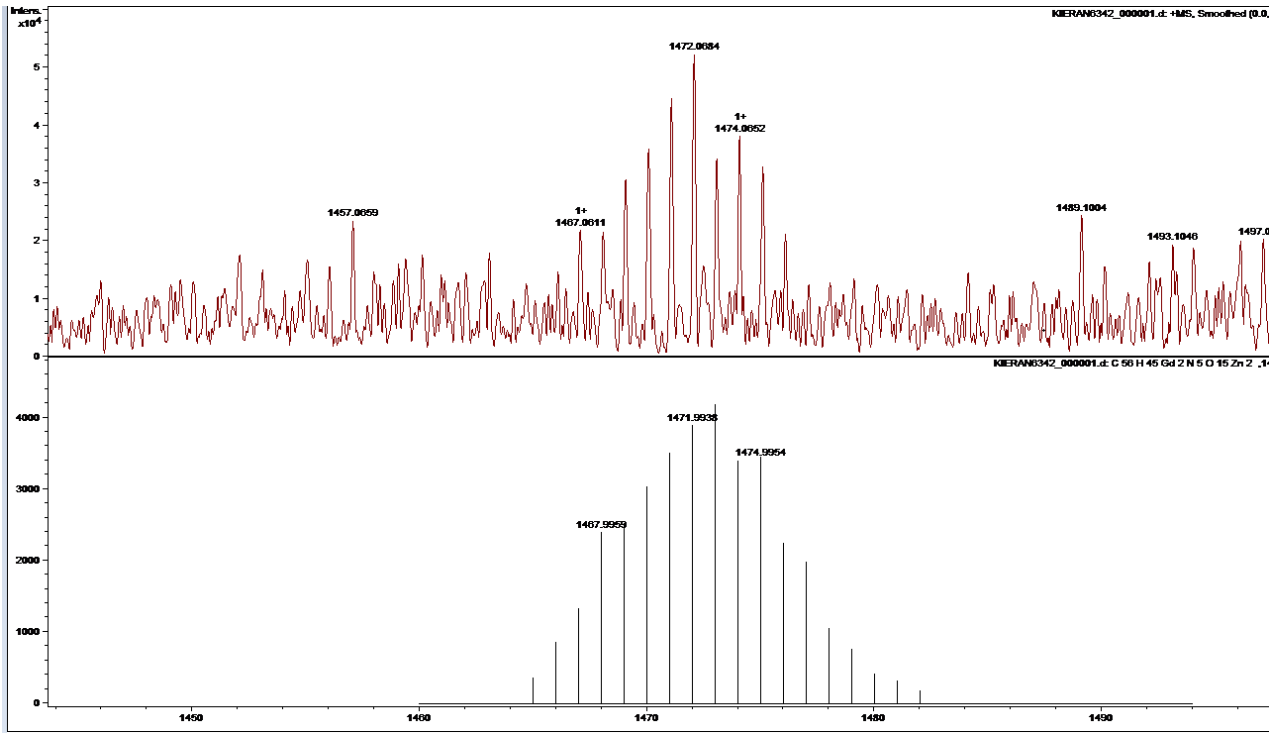

S8.11. ESI-MS of 1ZnGd-NO$_3$. $[Zn^{II}_2Gd^{III}_2(C_{14}H_{11}NO_3)_4(NO_3)]^{1+}$ fragment -1471.9936 m/z.

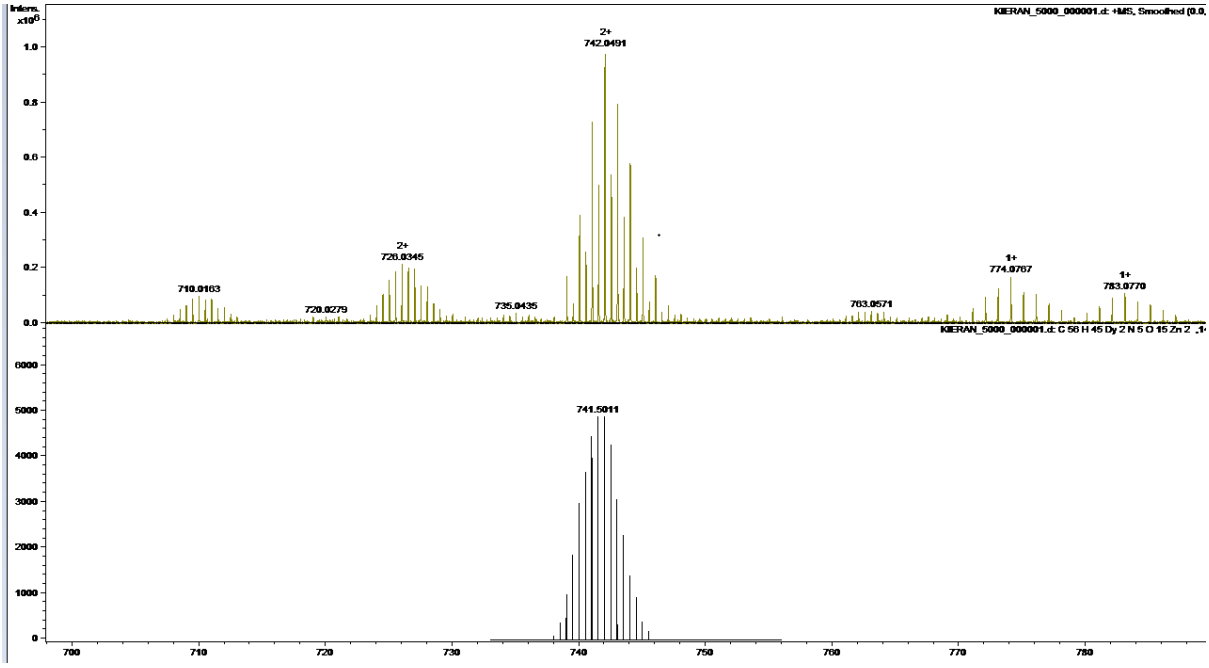

S8.12. ESI-MS of 1ZnDy-NO3. $[Zn^{II}_2Dy^{III}_2(C_{14}H_{11}NO_3)_4]^{2+}$ fragment – 710.0163 m/z, $[Zn^{II}_2Dy^{III}_2(C_{14}H_{11}NO_3)_4(MeOH)]^{2+}$ fragment – 726.0345 m/z and $[Zn^{II}_2Dy^{II}_2(C_{14}H_{11}NO_3)_4(NO_3)]^{2+}$ fragment – 742.0491 m/z.

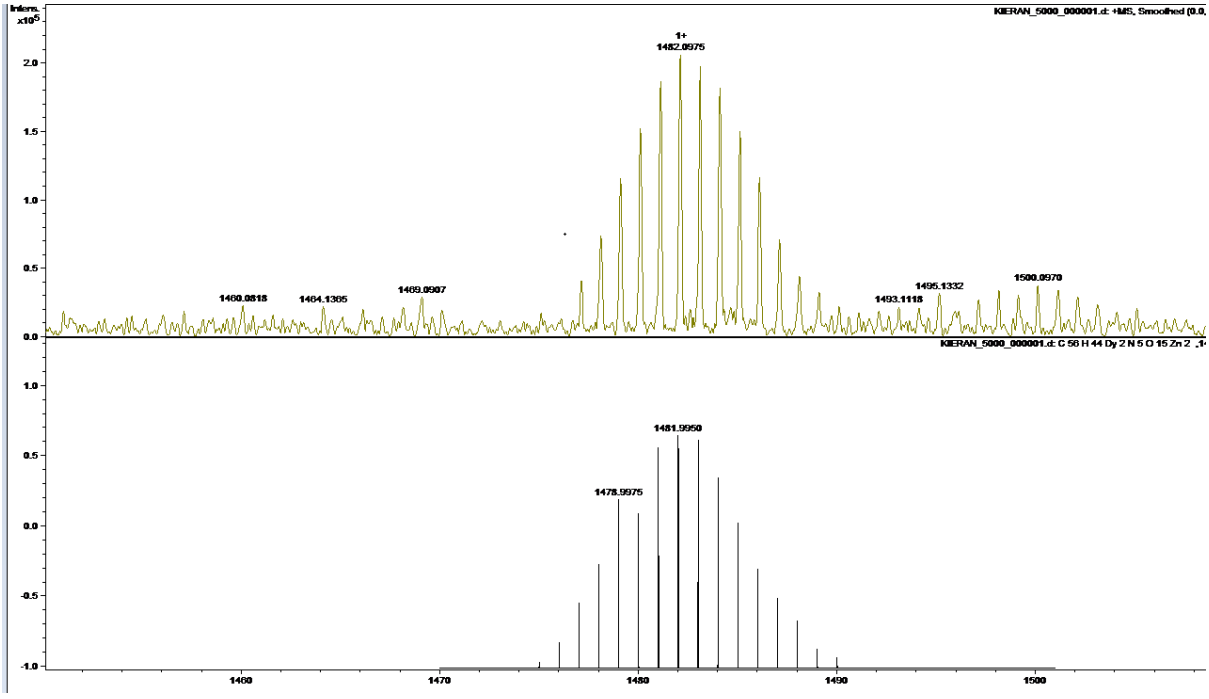

S8.13. ESI-MS of 1ZnDy-NO3. $[Zn^{II}_2Dy^{III}_2(C_{14}H_{11}NO_3)_4(NO_3)]^{1+}$ fragment -1482.0975 m/z.

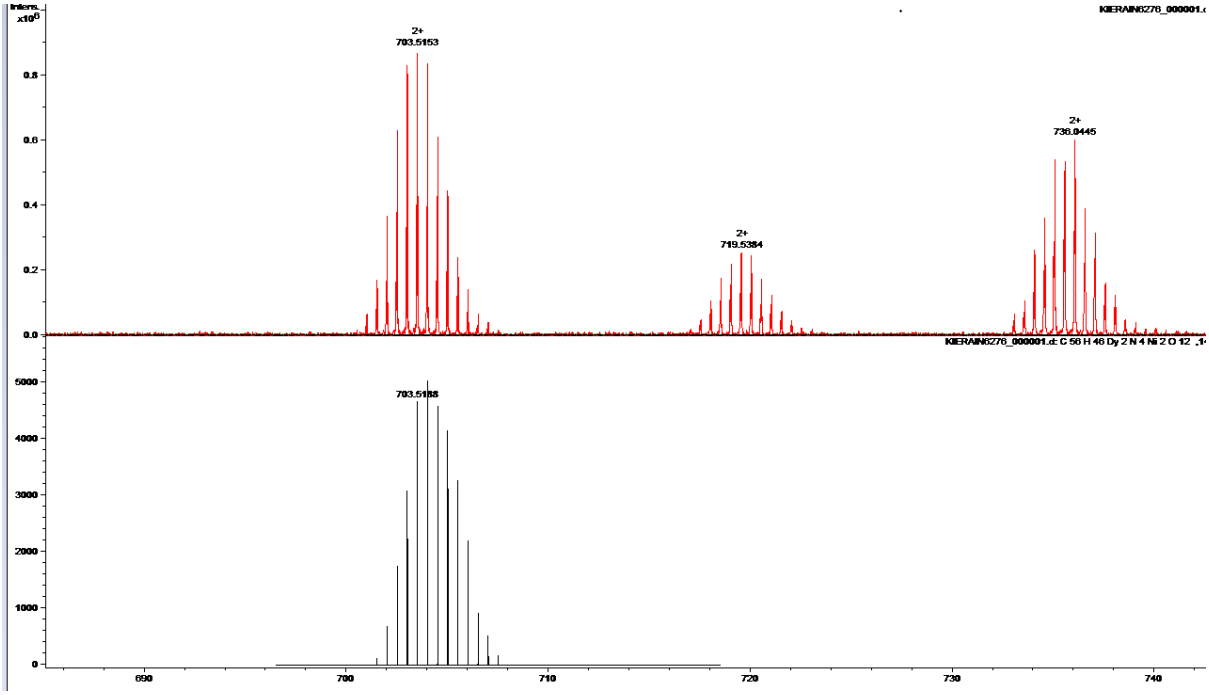

S8.14. ESI-MS of 1NiDy-NO$_3$. $[Ni^{II}_2Dy^{III}_2(C_{14}H_{11}NO_3)_4]^{2+}$ fragment – 703.5153 m/z, $[Ni^{II}_2Dy^{III}_2(C_{14}H_{11}NO_3)_4(MeOH)]^{2+}$ fragment – 719.5384 m/z and $[Ni^{II}_2Dy^{III}_2(C_{14}H_{11}NO_3)_4(NO_3)]^{2+}$ Fragment – 736.0445 m/z.

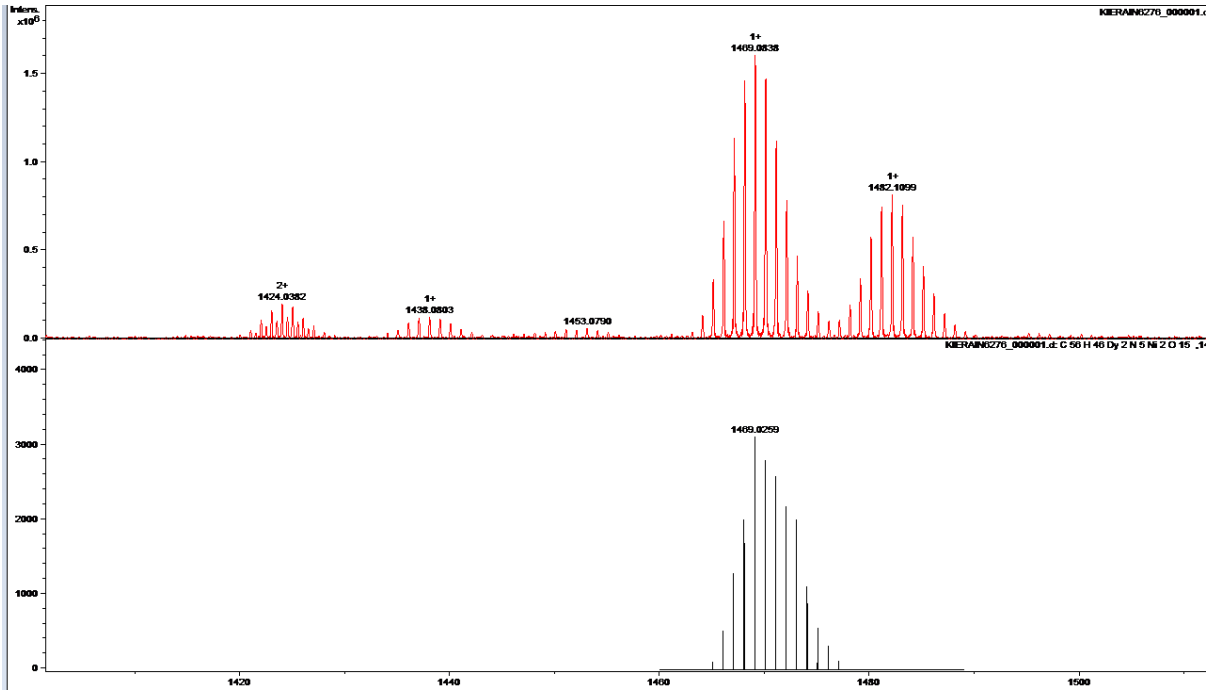

S8.15. ESI-MS of 1NiDy-NO$_3$. $[Ni^{II}_2Dy^{III}_2(C_{14}H_{11}NO_3)_4(NO_3)]^{1+}$ fragment -1469.0383 m/z.

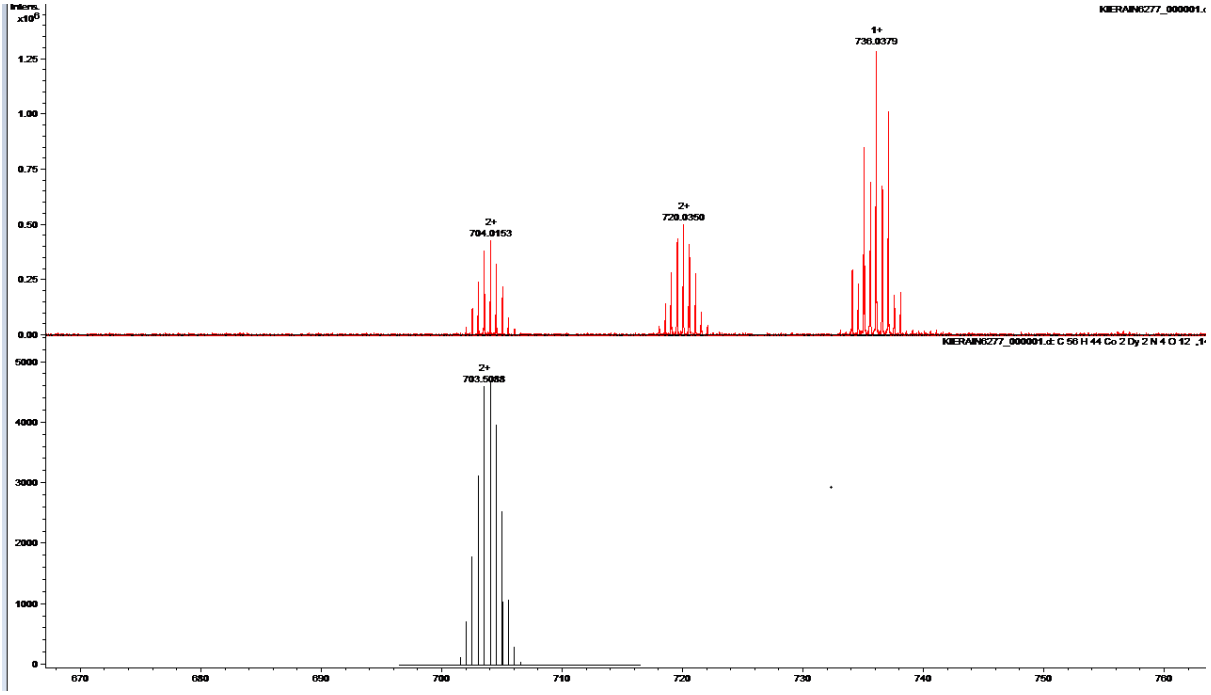

S8.16. ESI-MS of 1CoDy-NO$_3$. [$Co^{II}_2Dy^{III}_2$ ($C_{14}H_{11}NO_3$)$_4$]$^{2+}$ fragment – 704.0153 m/z, [$Co^{II}_2Dy^{III}_2$($C_{14}H_{11}NO_3$)$_4$(MeOH)]$^{2+}$ fragment – 720.0350 m/z and [$Co^{II}_2Dy^{III}_2$ ($C_{14}H_{11}NO_3$)$_4$(NO3)]$^{2+}$ fragment – 736.0379 m/z.

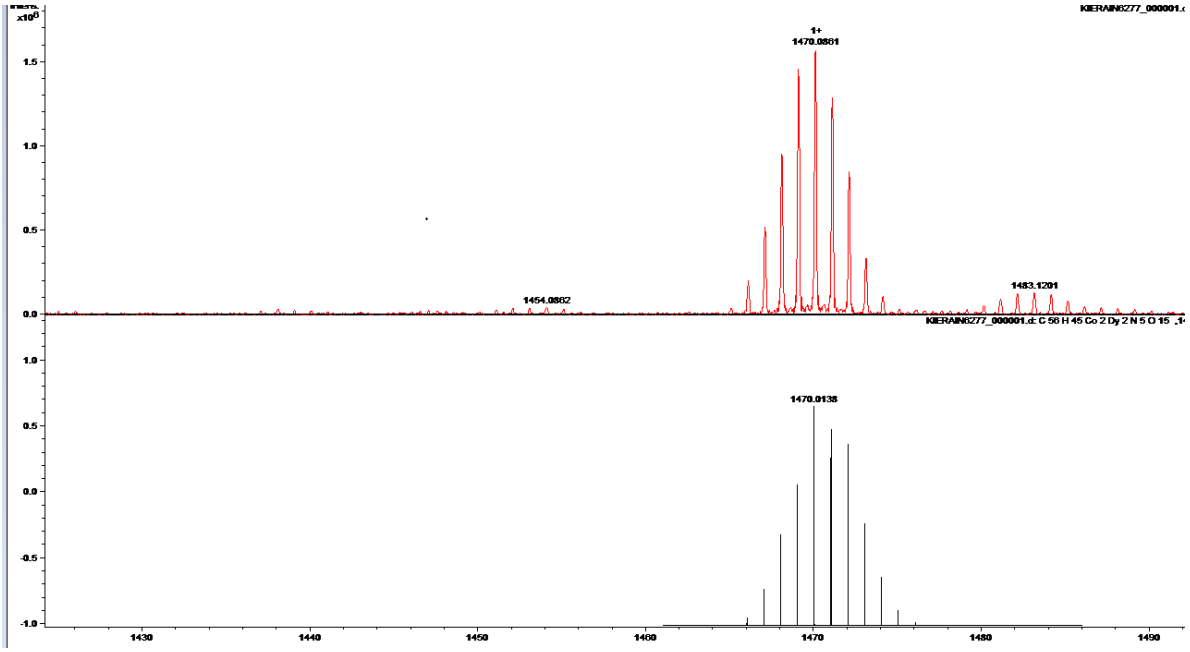

S8.17. ESI-MS of 1CoDy-NO$_3$. [$Co^{II}_2Dy^{III}_2$($C_{14}H_{11}NO_3$)$_4$(NO_3)]$^{1+}$ fragment -1470.0136 m/z.

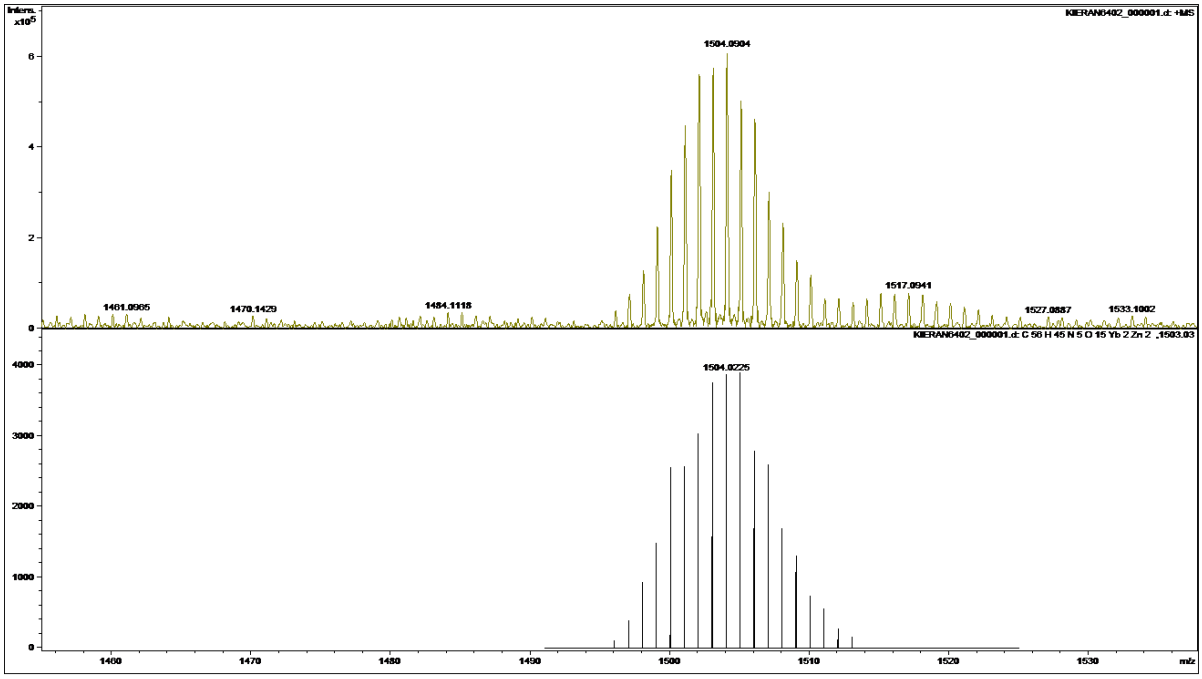

S8.18. ESI-MS of 1ZnYb-NO$_3$. $[Zn^{II}_2Yb^{III}_2(C_{14}H_{11}NO_3)_4(NO_3)]^{1+}$ fragment.

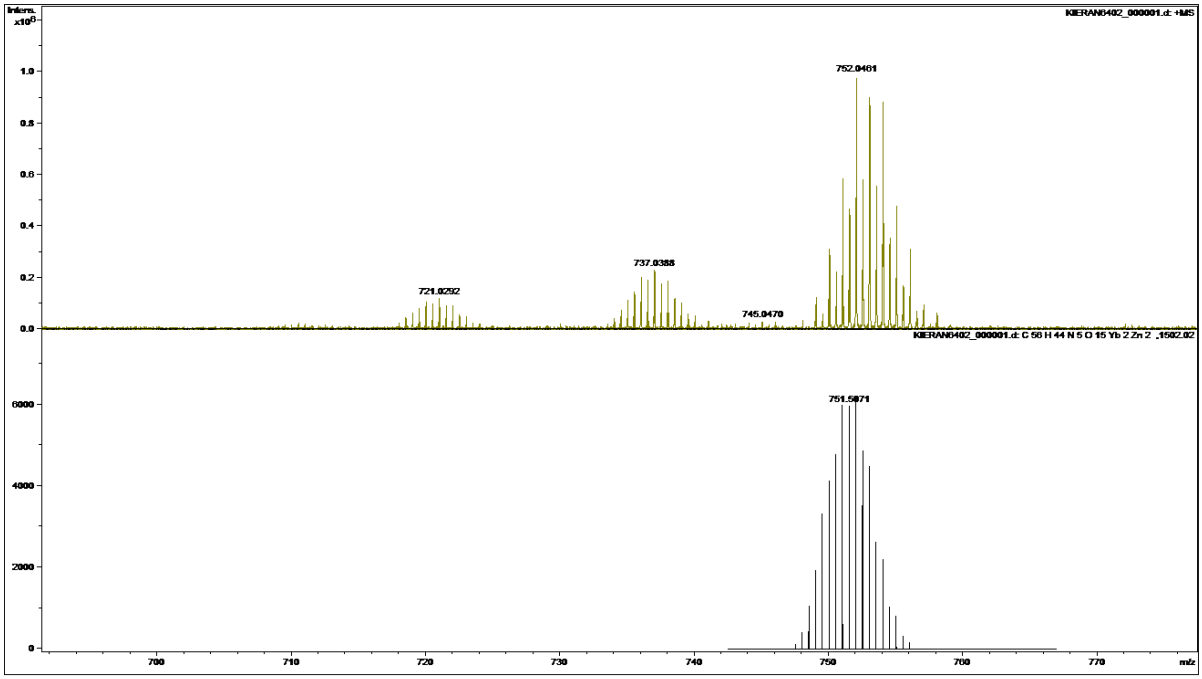

S8.19. ESI-MS of 1ZnYb-NO$_3$. $[Zn^{II}_2Yb^{III}_2(C_{14}H_{11}NO_3)_4(NO_3)]^{2+}$ fragment.

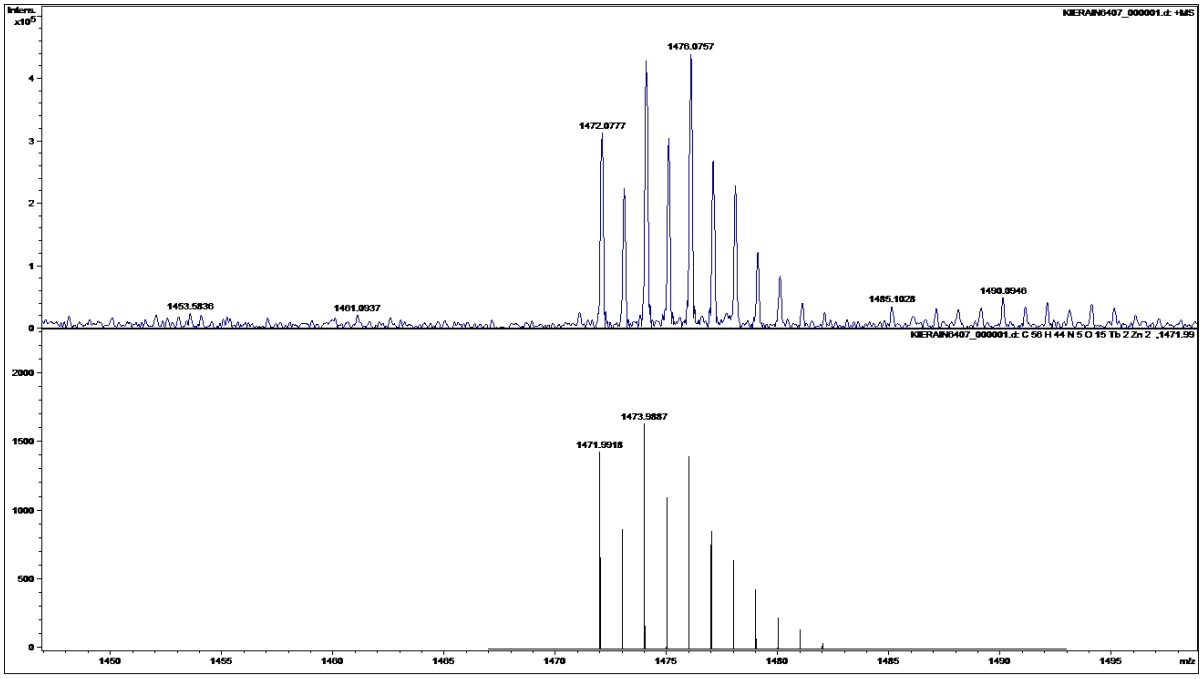

S8.20. ESI-MS of 1ZnTb-NO$_3$. $[Zn^{II}_2Tb^{III}_2(C_{14}H_{11}NO_3)_4(NO_3)]^{1+}$ fragment.

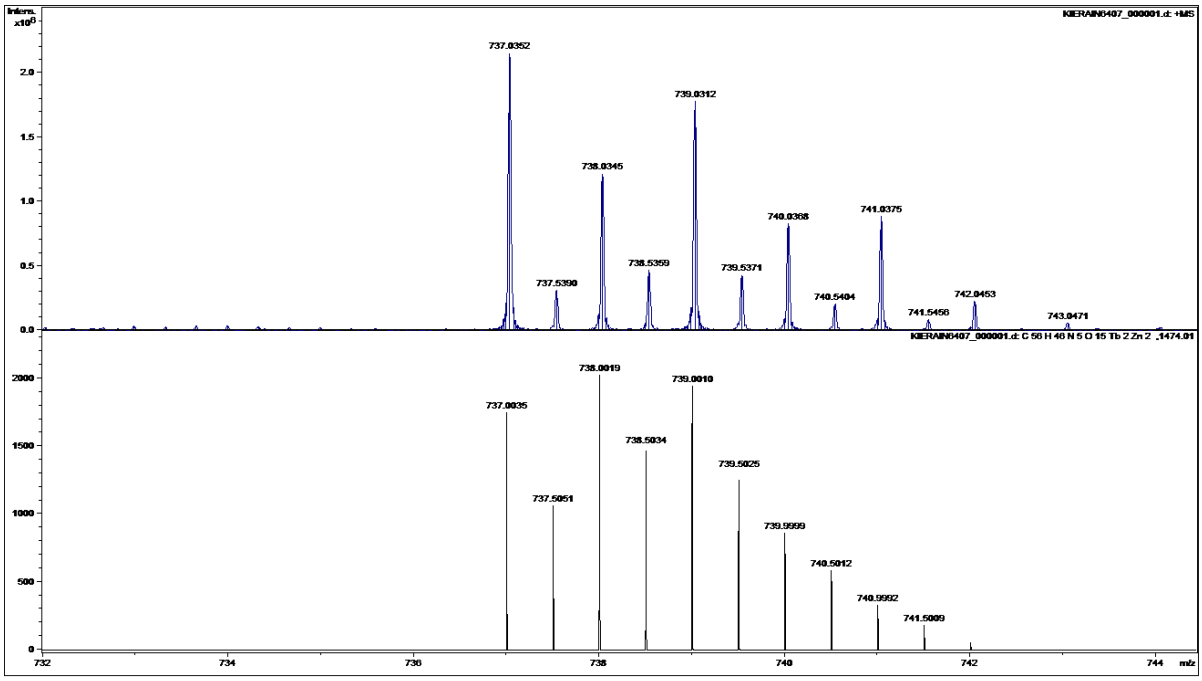

S8.21. ESI-MS of 1ZnTb-NO$_3$. $[Zn^{II}_2Tb^{III}_2(C_{14}H_{11}NO_3)_4(NO_3)]^{2+}$ fragment

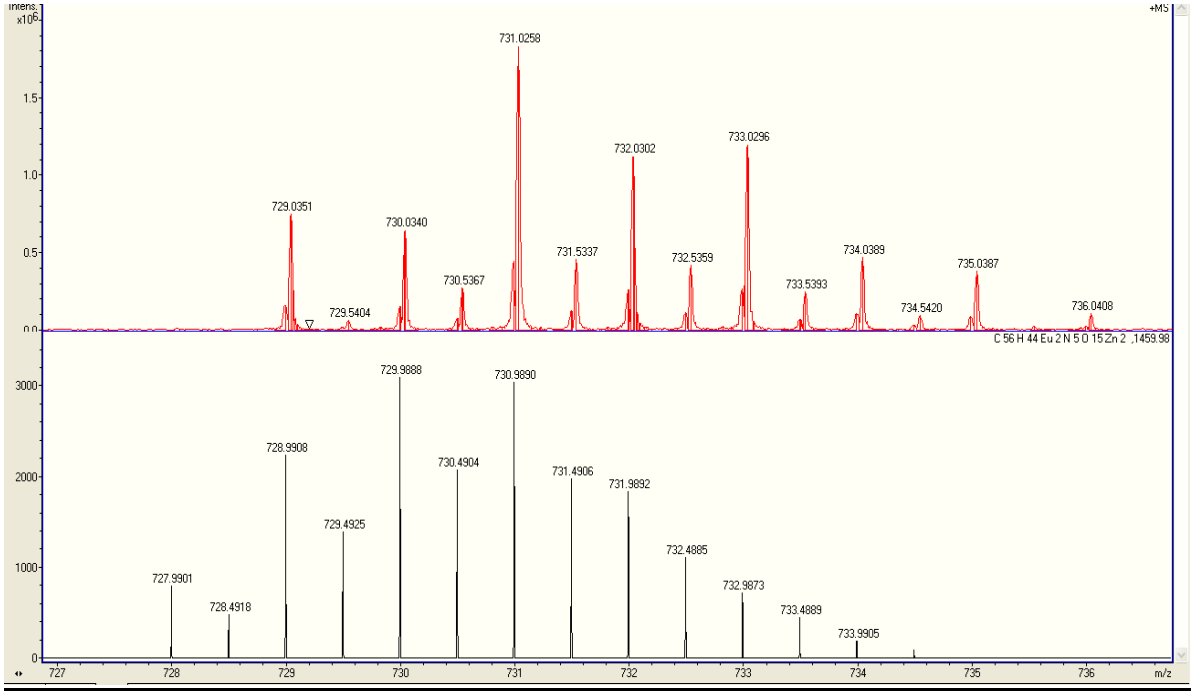

S8.22. ESI-MS of 1ZnEu-NO$_3$. $[Zn^{II}_2Eu^{III}_2(C_{14}H_{11}NO_3)_4(NO_3)]^{2+}$ fragment.

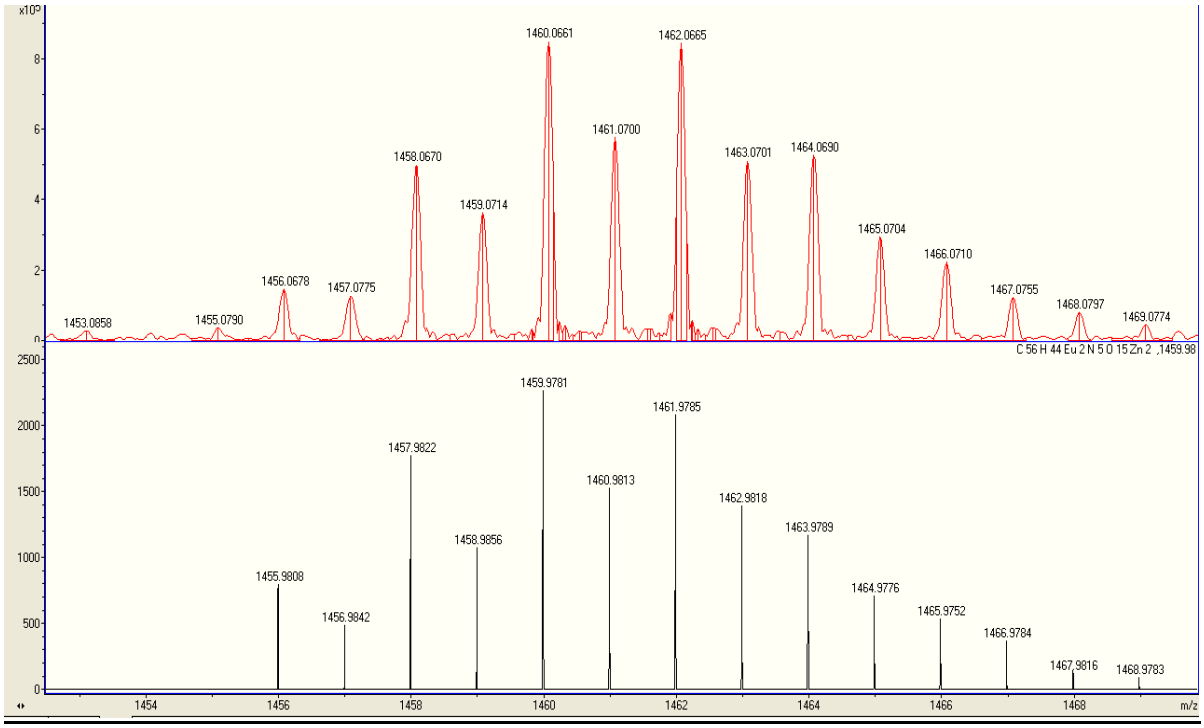

S8.23. ESI-MS of 1ZnEu-NO$_3$. $[Zn^{II}_2Eu^{III}_2(C_{14}H_{11}NO_3)_4(NO_3)]^{1+}$ fragment.

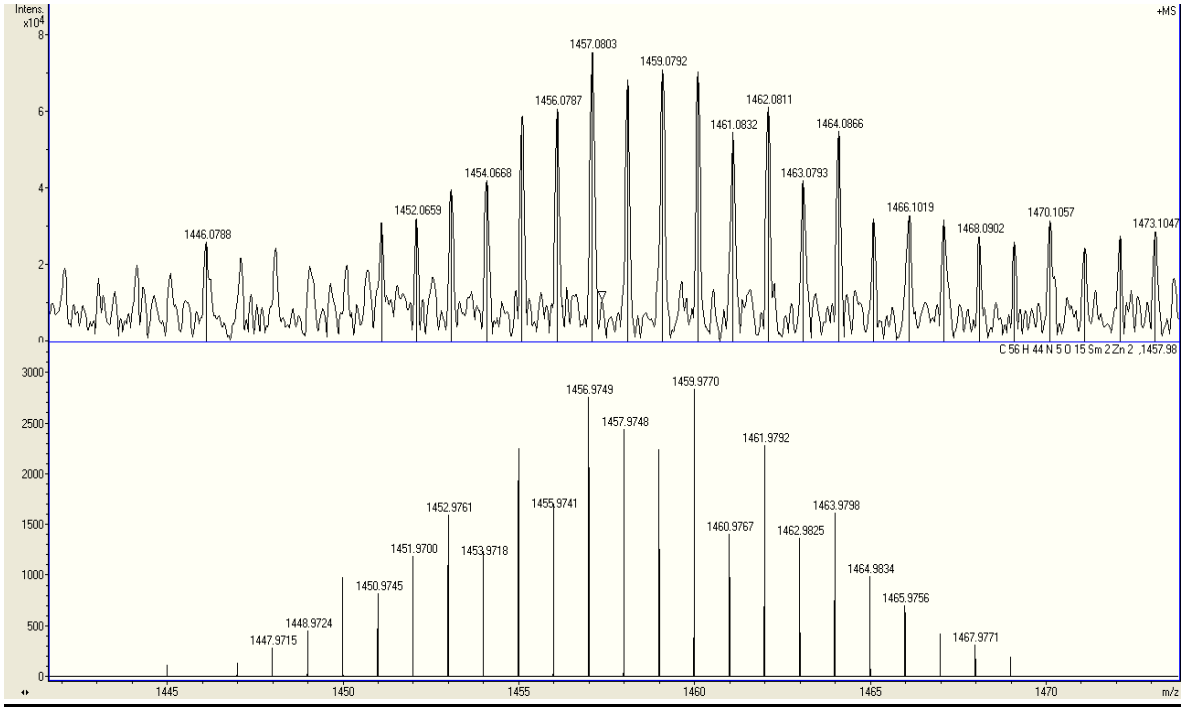

S8.24. ESI-MS of 1ZnSm-NO$_3$. $[Zn^{II}_2Sm^{III}_2\ (C_{14}H_{11}NO_3)_4(NO_3)]^{1+}$ fragment.

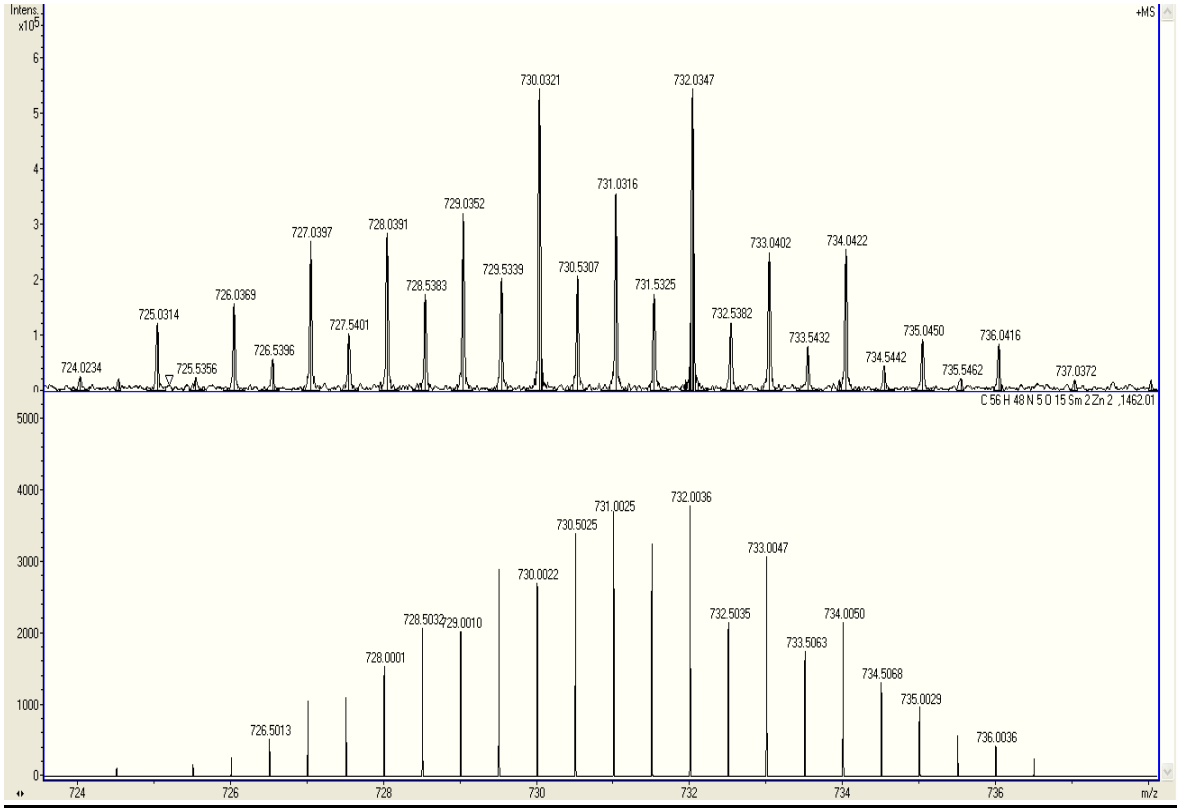

S8.25. ESI-MS of 1ZnSm-NO$_3$. $[Zn^{II}_2Sm^{III}_2\ (C_{14}H_{11}NO_3)_4(NO_3)]^{2+}$ fragment.

8.3 TGA of 1ZnLn-NO_3

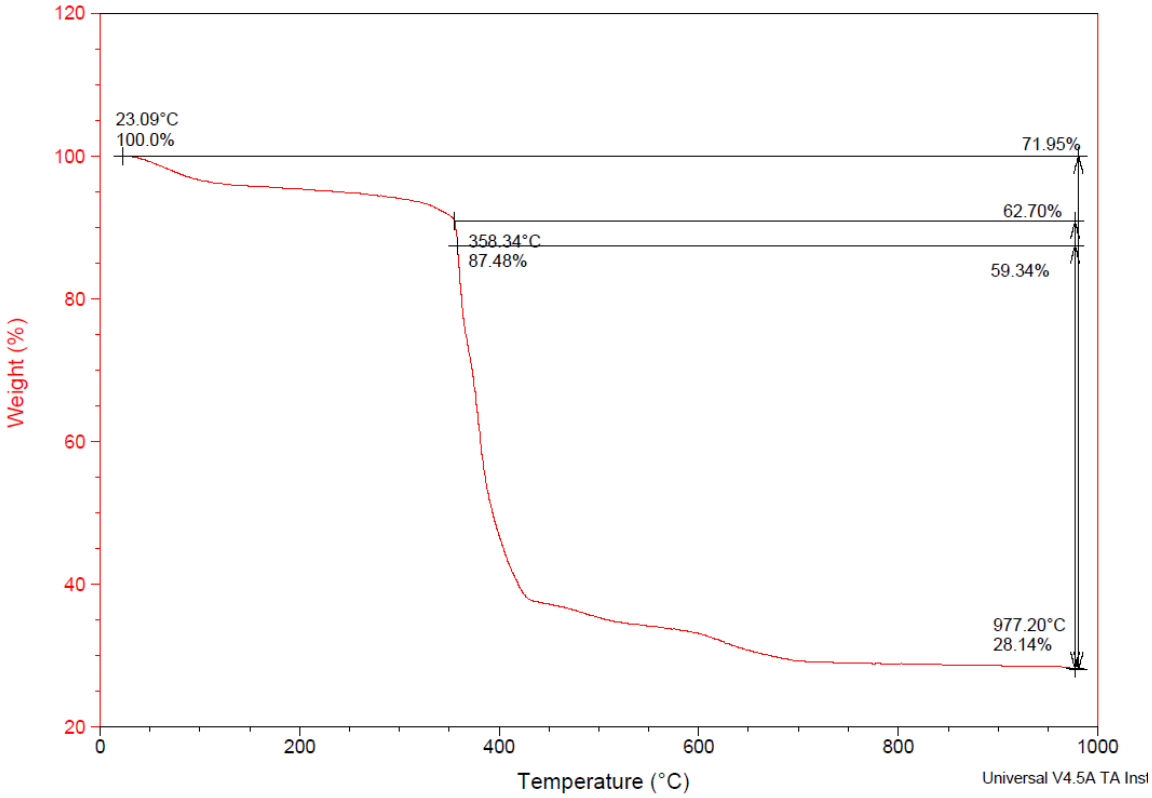

S8.26 TGA of 1ZnY-NO_3

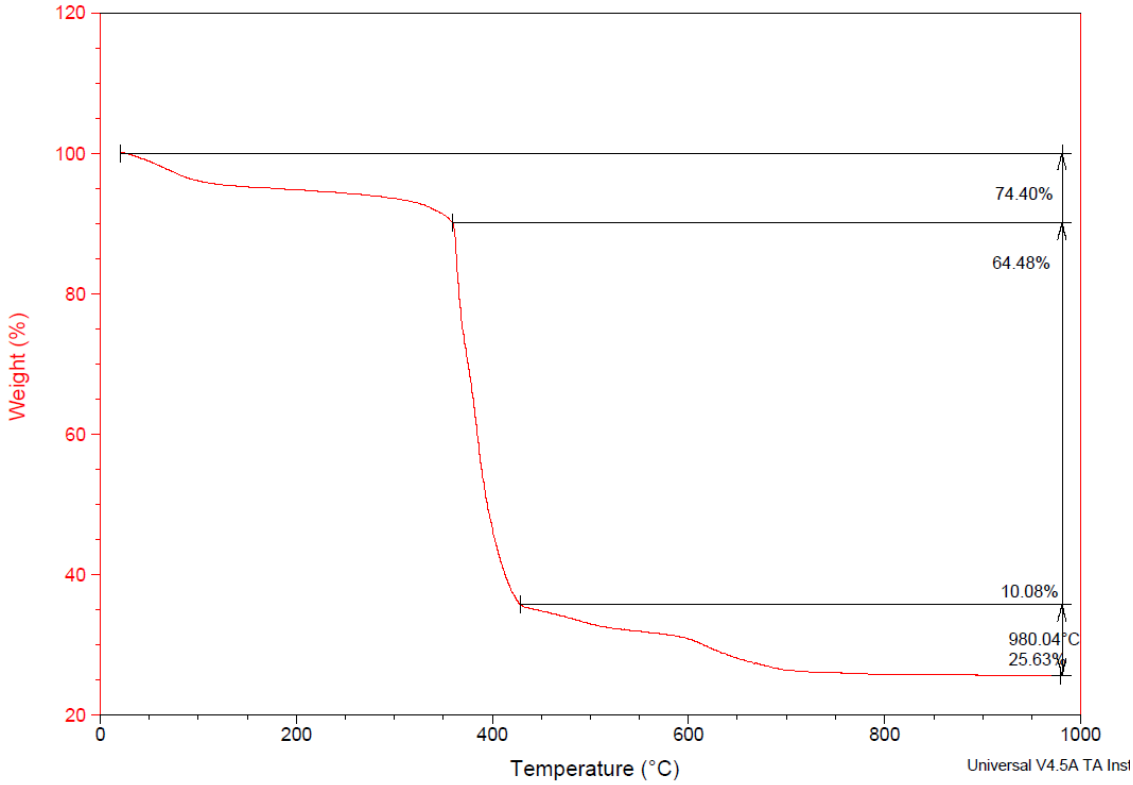

S8.27 TGA of 1ZnDy-NO_3

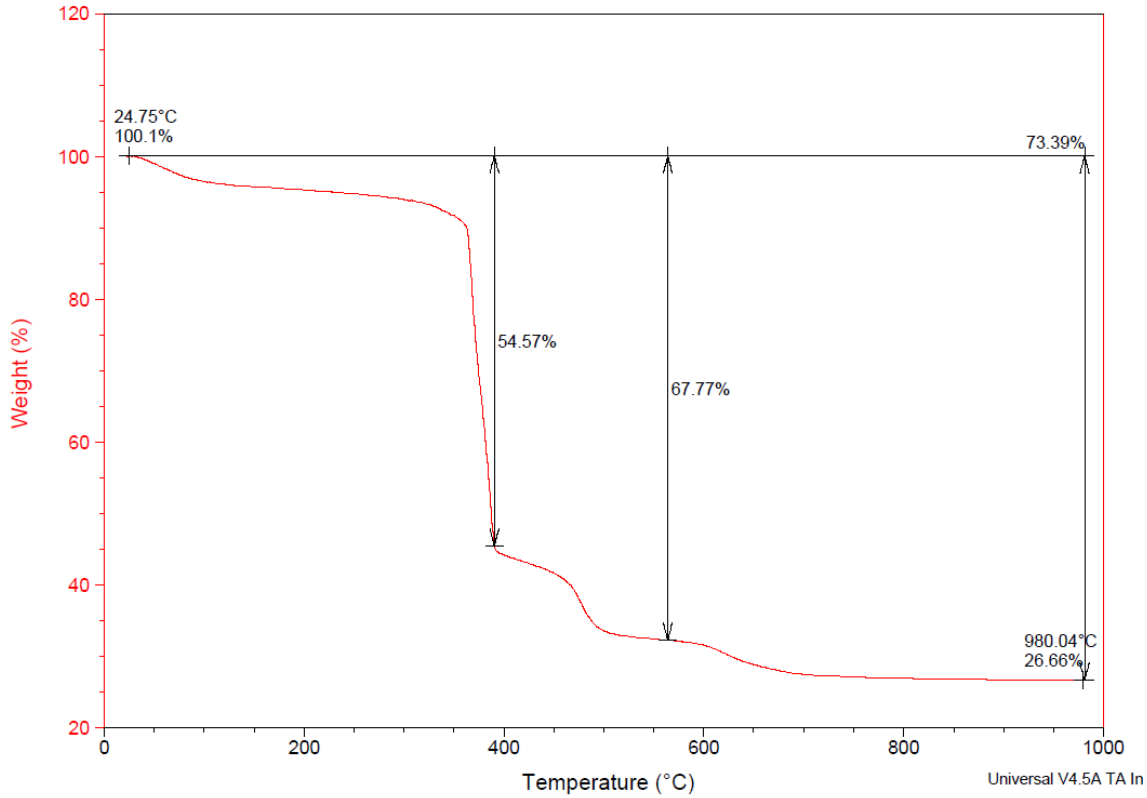

S8.28 TGA of 1ZnGd-NO_3

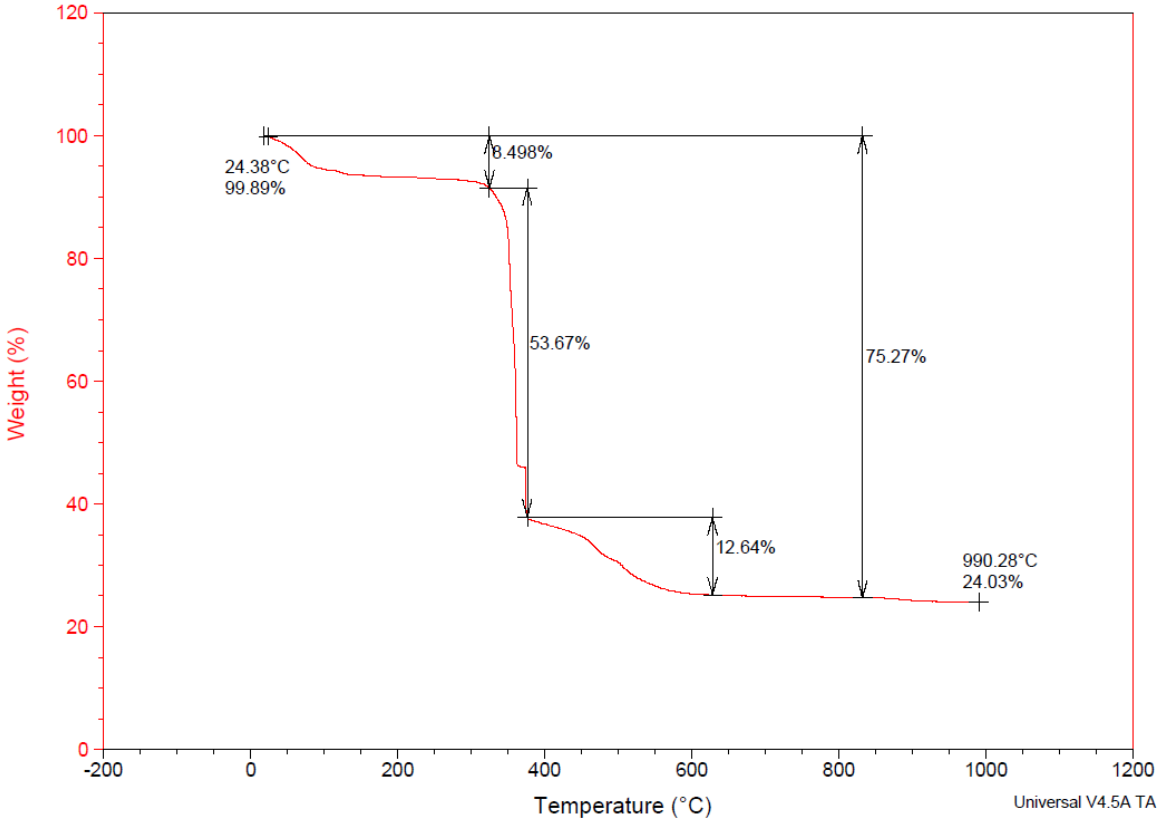

S8.29 TGA of 1ZnTb-NO_3

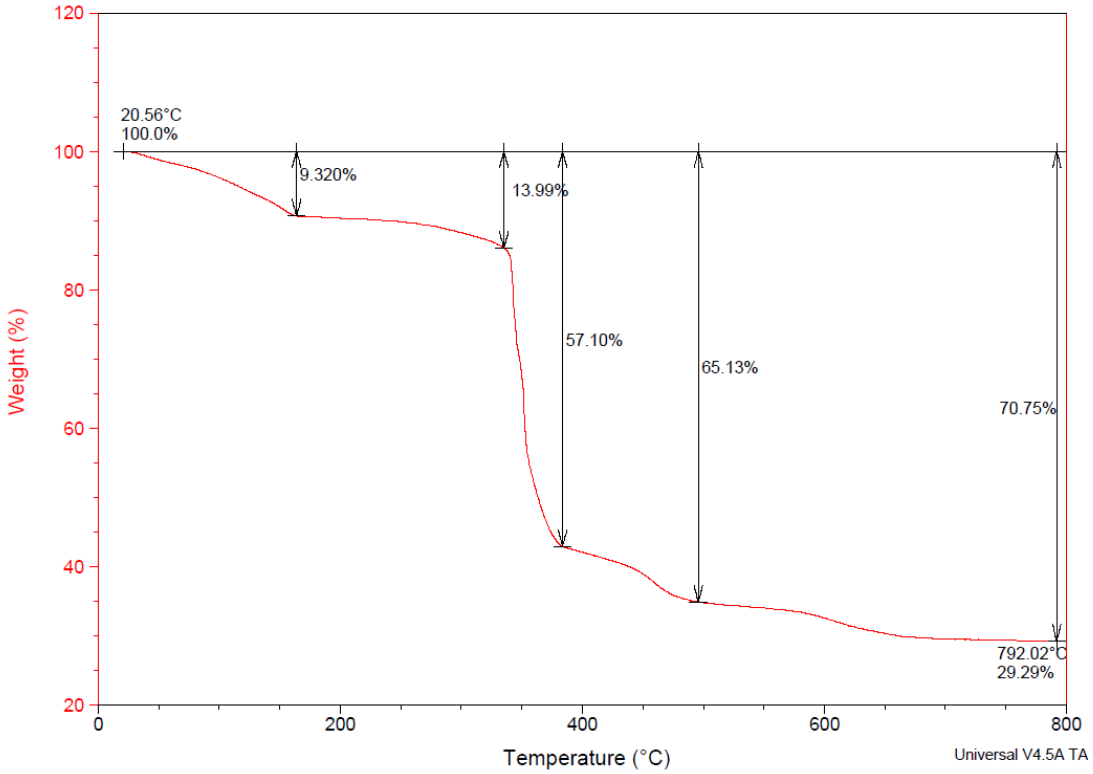

S8.30 TGA of 1ZnYb-NO_3

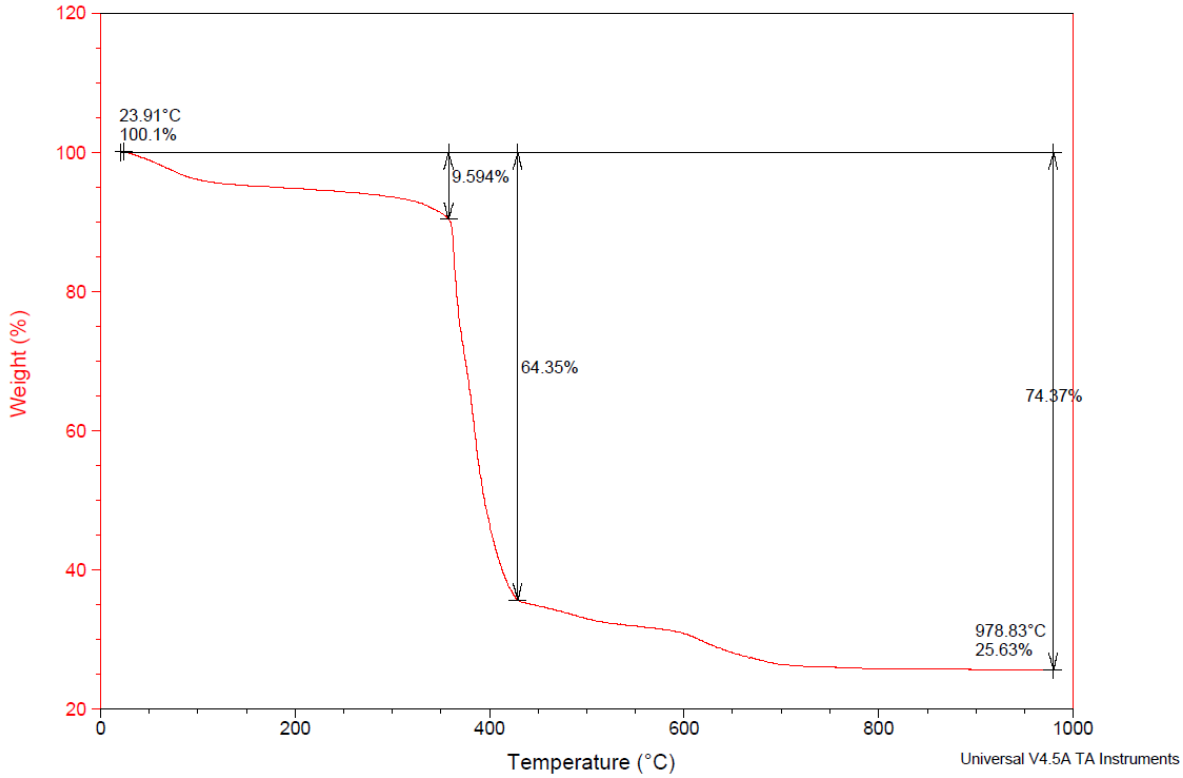

S8.31 TGA of 1ZnEu-NO_3

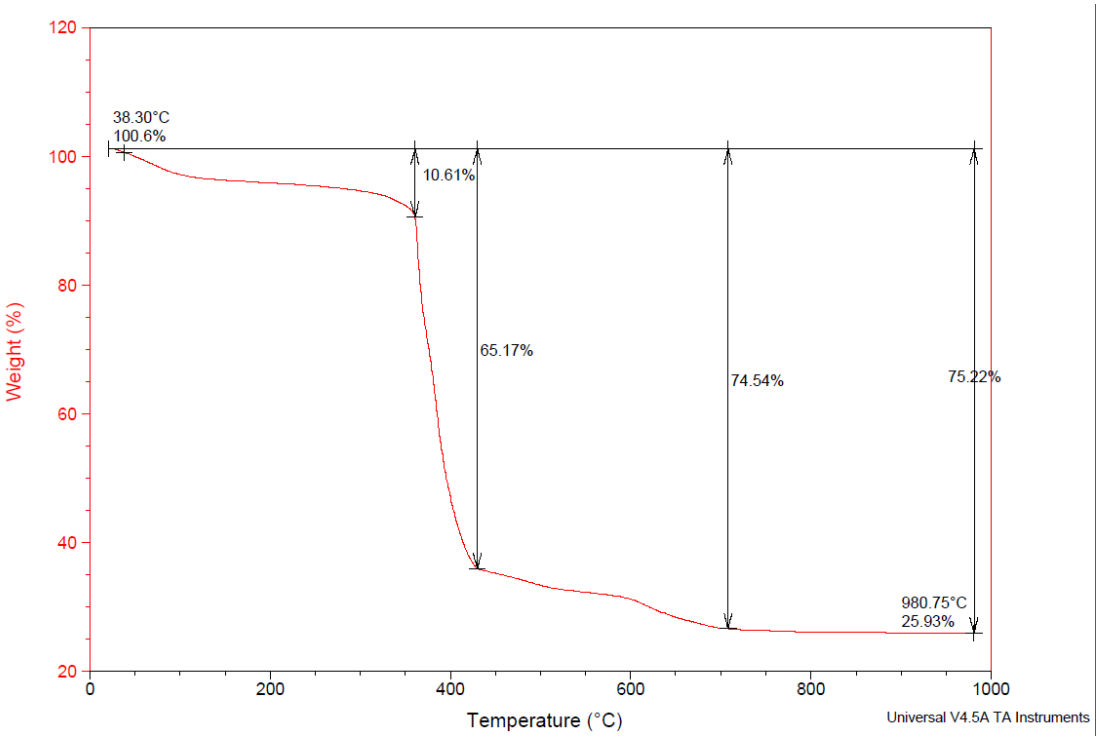

S8.32 TGA of 1ZnSm-NO_3

8.4 EPR of 1GdZn-NO_3

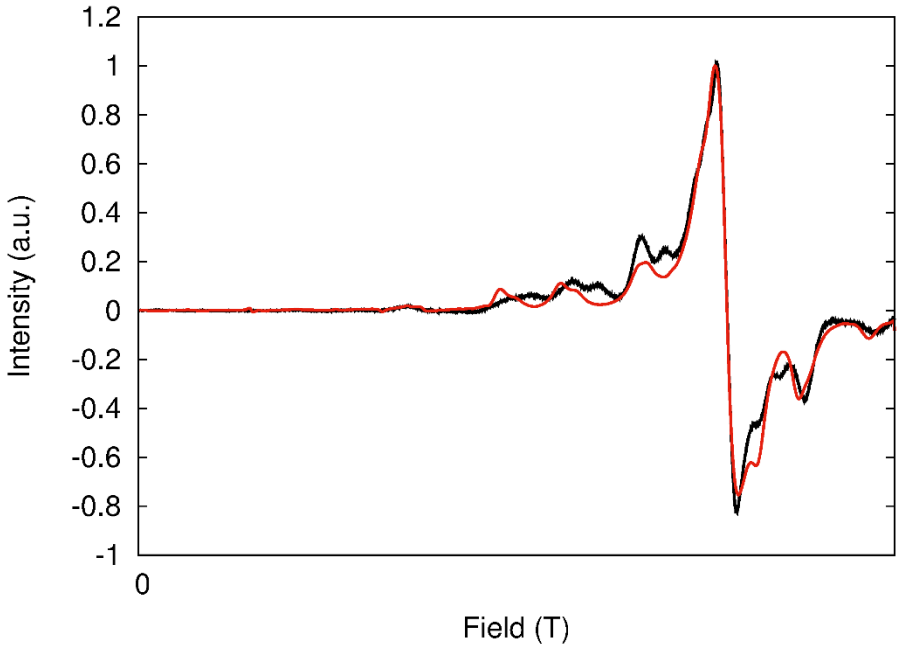

S8.33 . EPR Simulation of solution phase (80% DMF, 20% Et_2O) 1Y at 34.0865 GHz and 7 K. Hamiltonian: $\hat{H} = B_2^0\left(3\hat{S}_z{}^2 - \hat{S}^2\right) + \frac{B_2^2}{2}\left(\hat{S}_+{}^2 + \hat{S}_-{}^2\right) + B_4^0\left(35\hat{S}_z{}^4 - 30\hat{S}^2\hat{S}_z{}^2 + 25\hat{S}_z{}^2 + 3\hat{S}^{2\,2} - 6\hat{S}^2\right) + \frac{B_4^4}{2}\left(\hat{S}_+{}^4 + \hat{S}_-{}^4\right) + \mu_B g\hat{S}\cdot B$. Parameters: g = 1.961(2), B_2^0 = -0.0259(7) cm^{-1}, B_2^2 = 0.0212(6) cm^{-1}, B_4^0 = 0.000018(6) cm^{-1}, B_4^4 = -0.00011(3) cm^{-1}, Lorentzian frequency-space linewidth = 1.13(8) GHz. Given the complexity of the ZFS for the S = 7/2 state, this is likely not the only parameter set

which can approach agreement with the data. We provide this simulation to show a plausible parameter set for the data.

8.5 UV-binding Studies

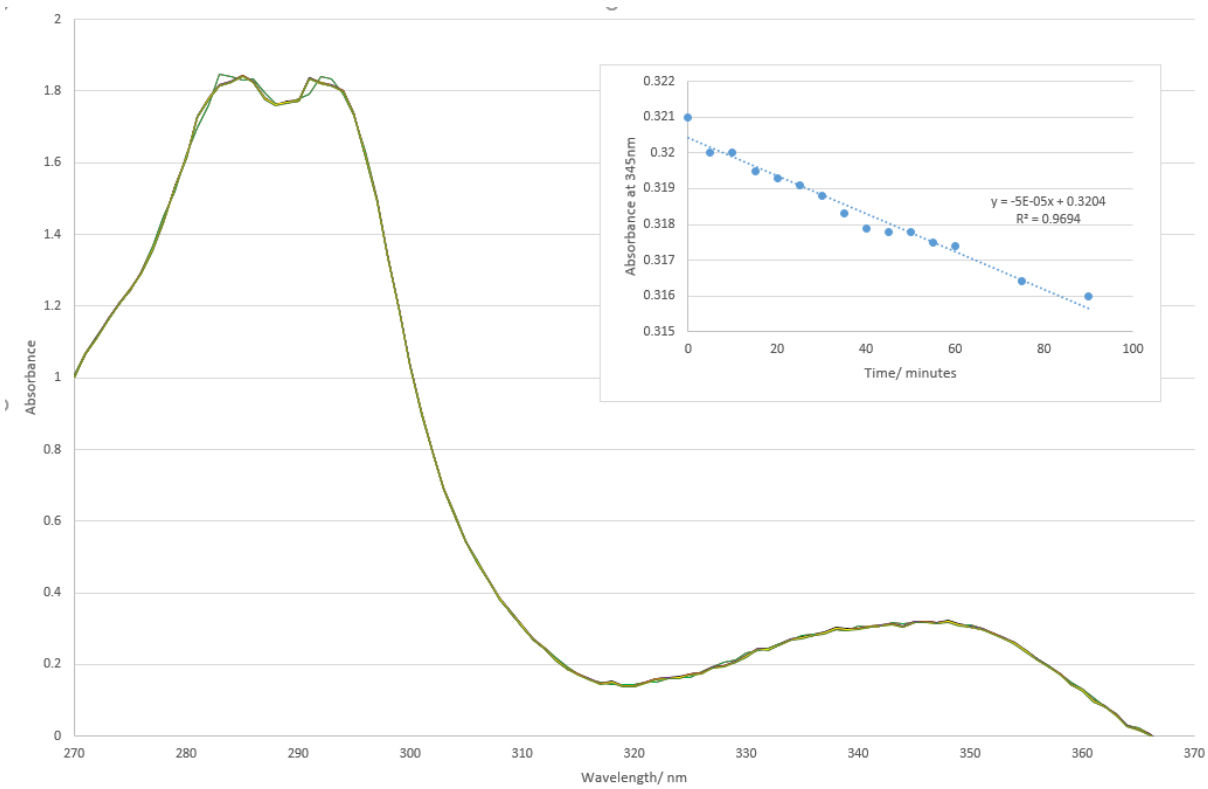

S8.34 UV-Vis binding study of $Zn(OTf)_2$ with 2-napthaldehyde

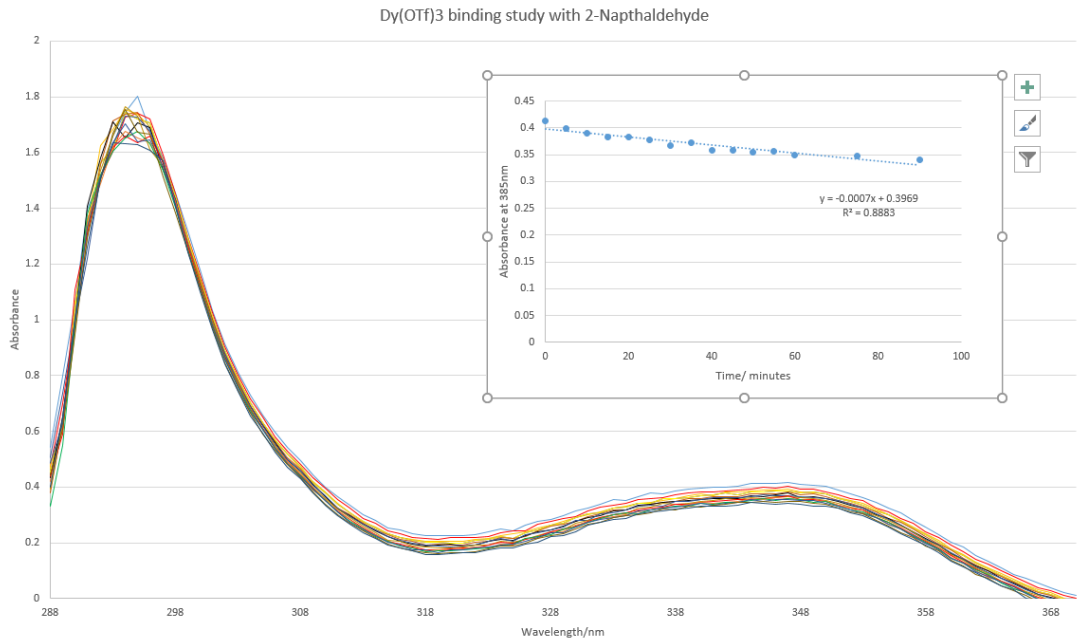

S8.35 UV-Vis binding study of $Dy(OTf)_3$ with 2-napthaldehyde

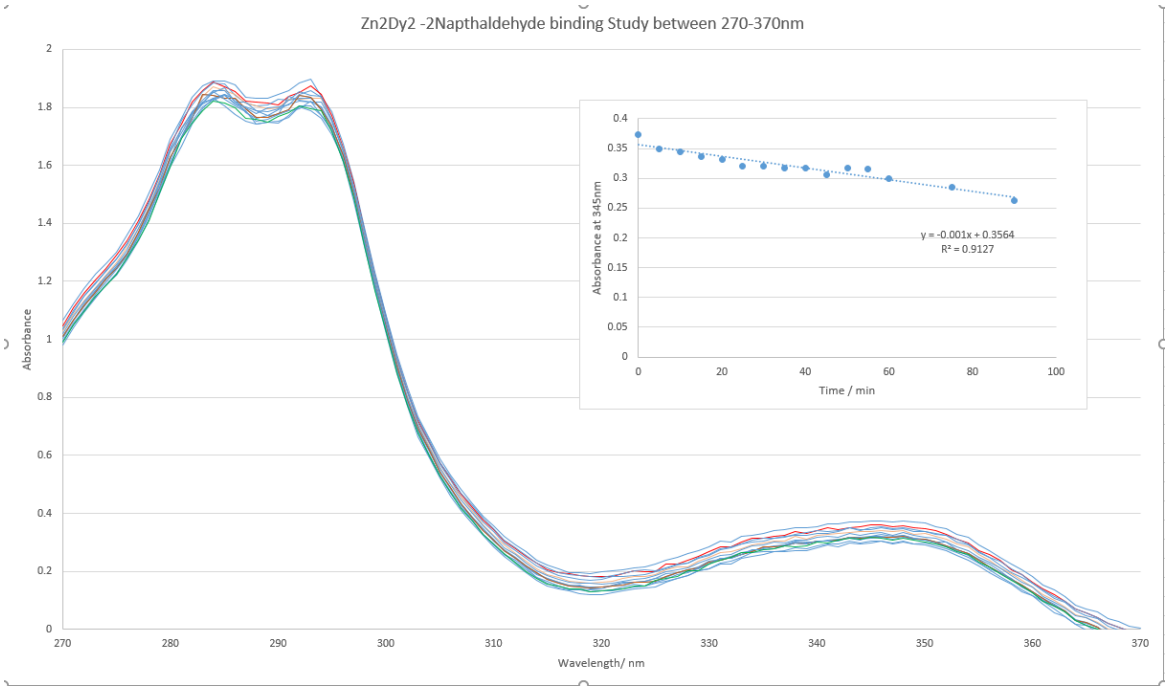

S8.36 UV-Vis binding study of 1ZnDy-NO_3 with 2-napthaldehyde

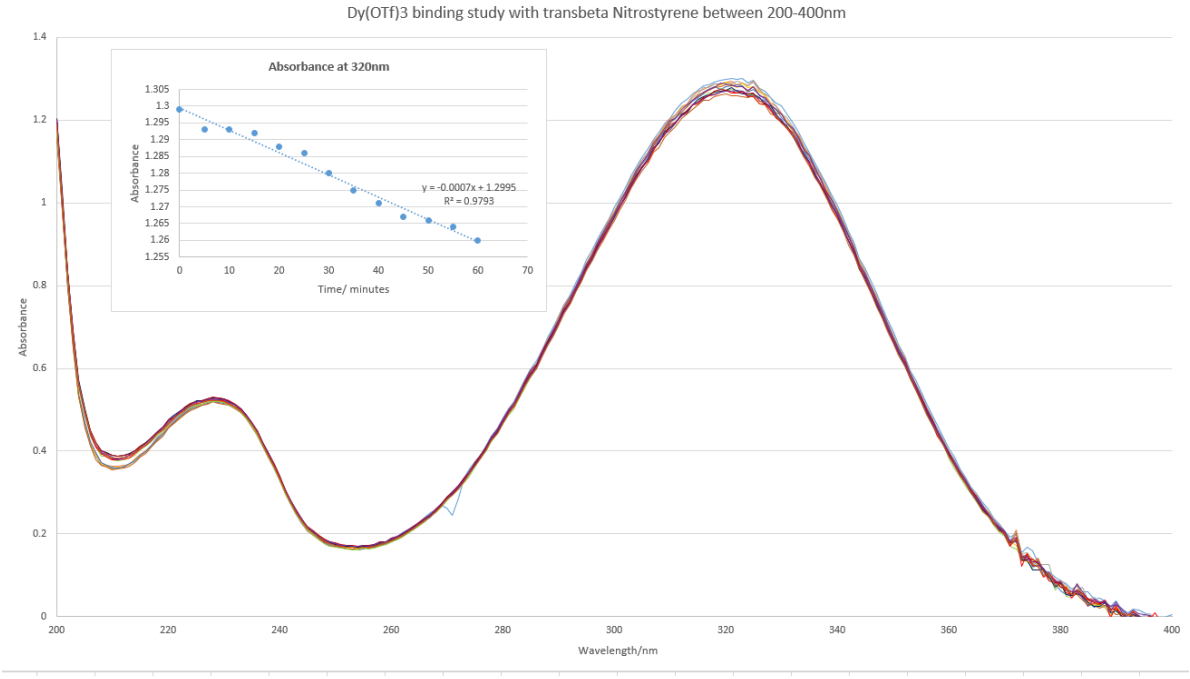

S8.37 UV-Vis binding study of $Dy(OTf)_3$ with trans-β-nitrostyrene

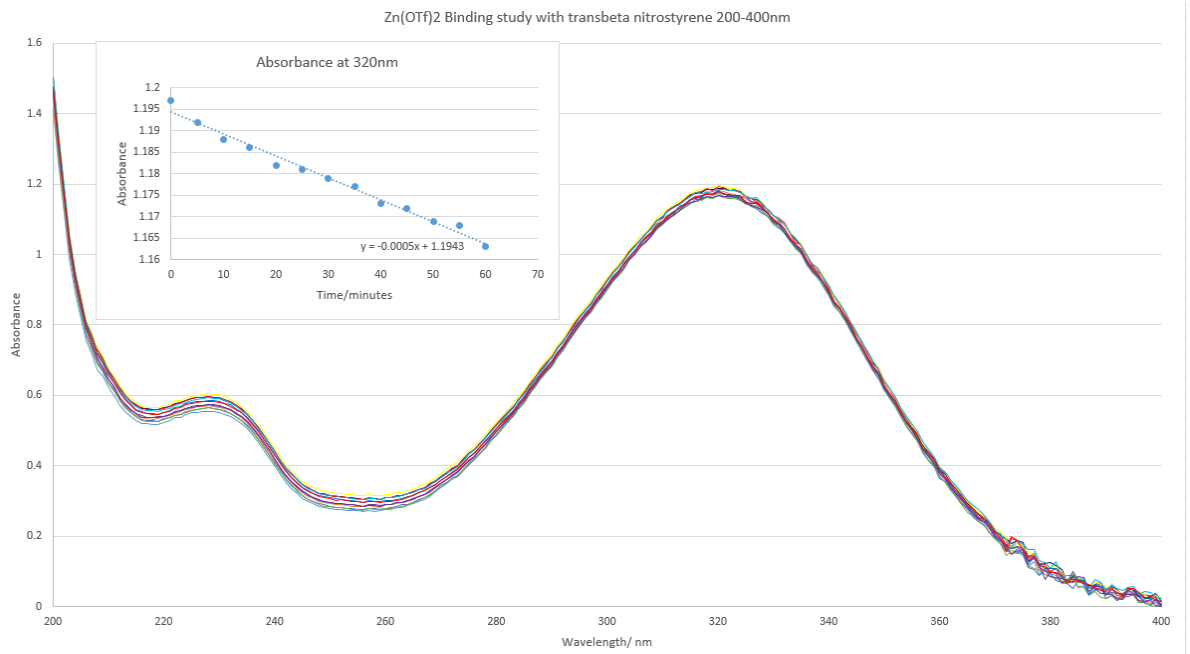

S8.38 UV-Vis binding study of $Zn(OTf)_2$ with trans-β-nitrostyrene

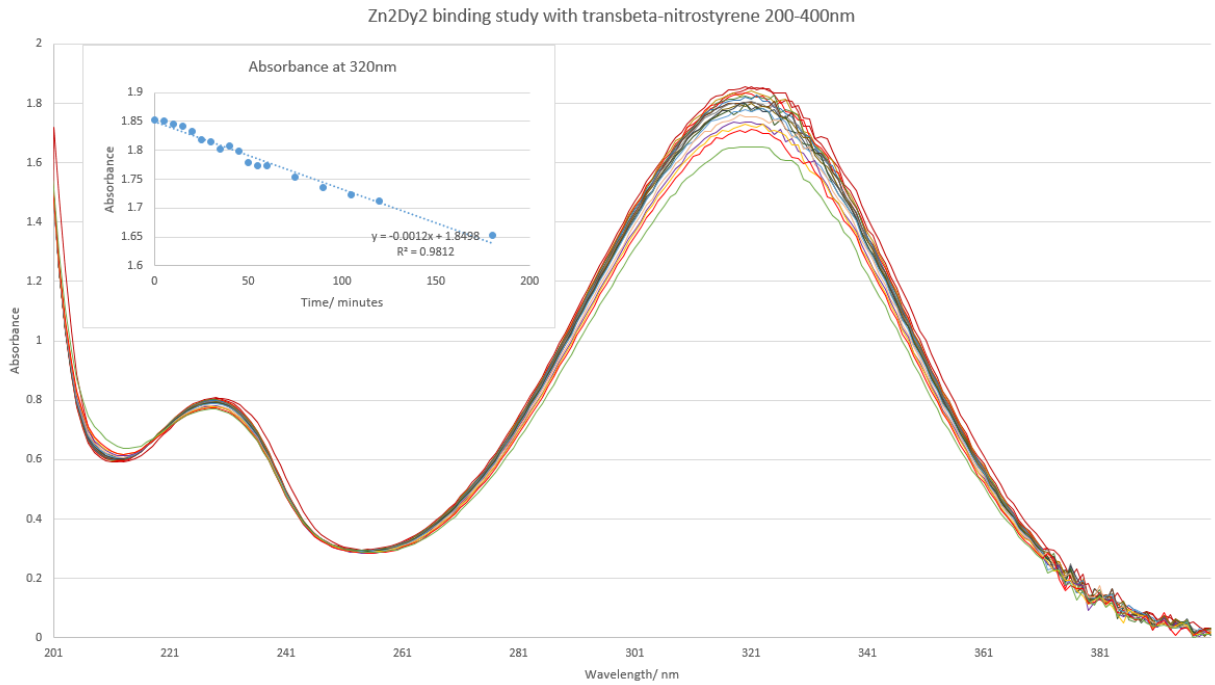

S8.38 UV-Vis binding study of $1ZnDy\text{-}NO_3$ with trans-β-nitrostyrene

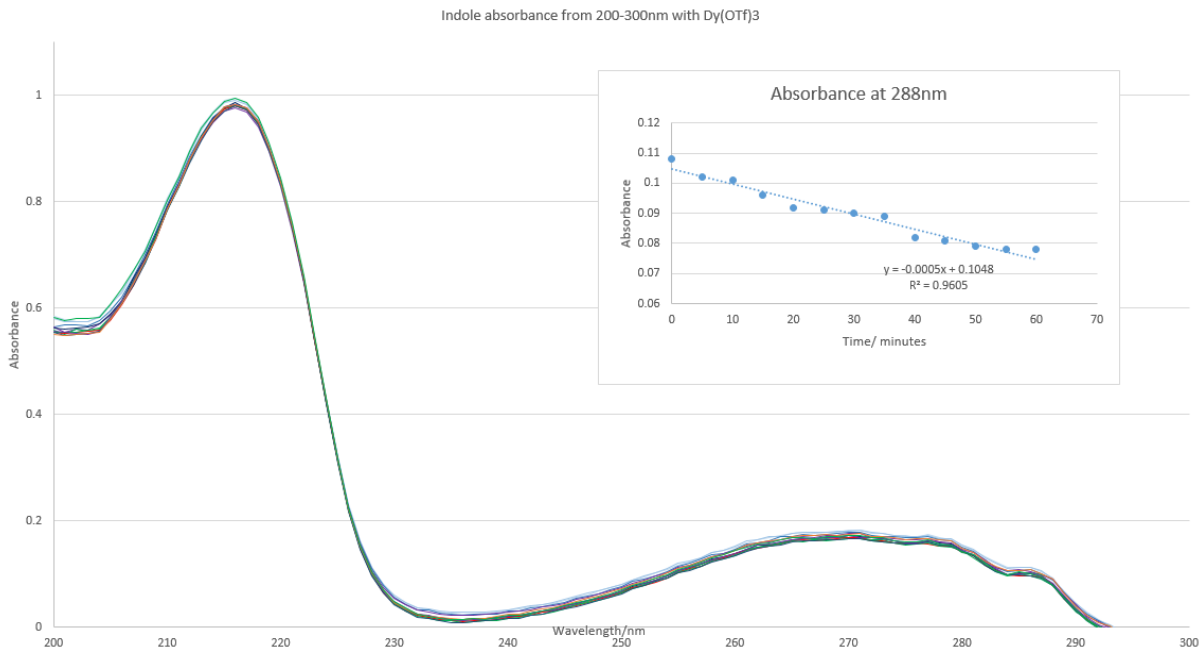

S8.39 UV-Vis binding study of $Dy(OTf)_3$ with indole

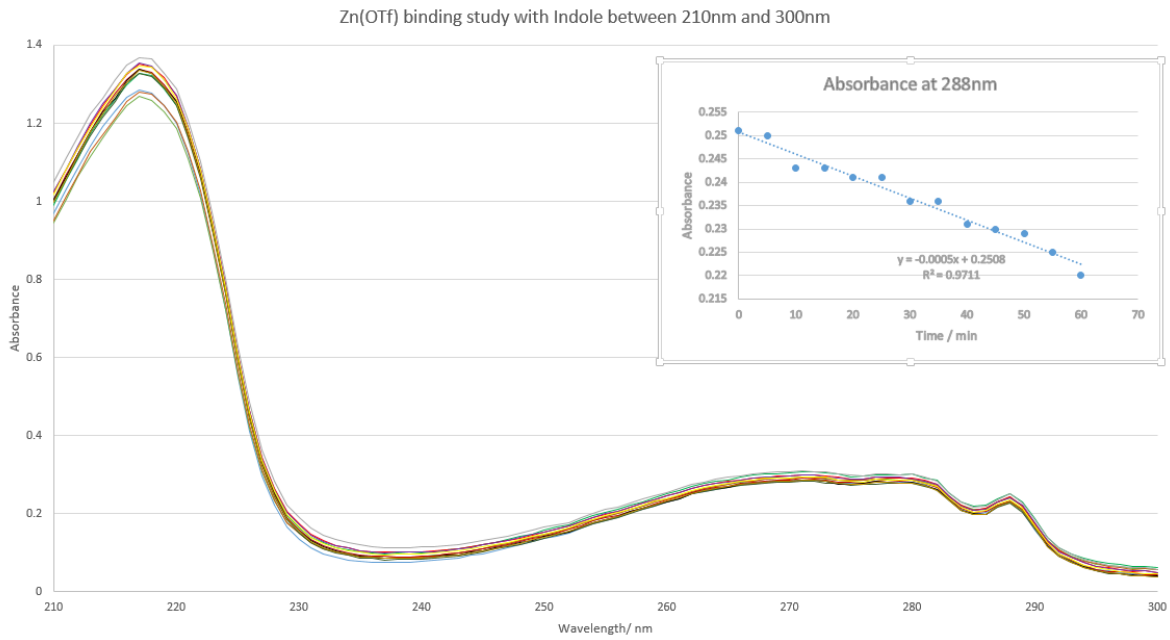

S8.40 UV-Vis binding study of $Zn(OTf)_2$ with indole

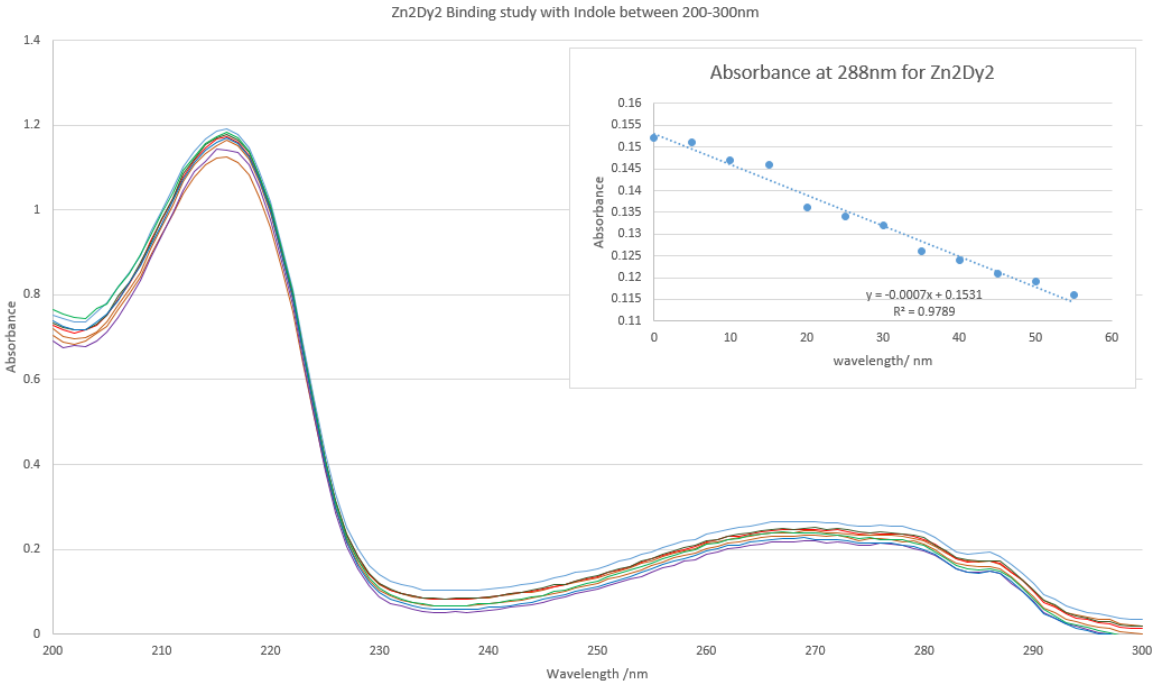

S8.41 UV-Vis binding study of 1ZnDy-NO_3 with indole

8.6 ^{1}H NMR of C8aa-C8au

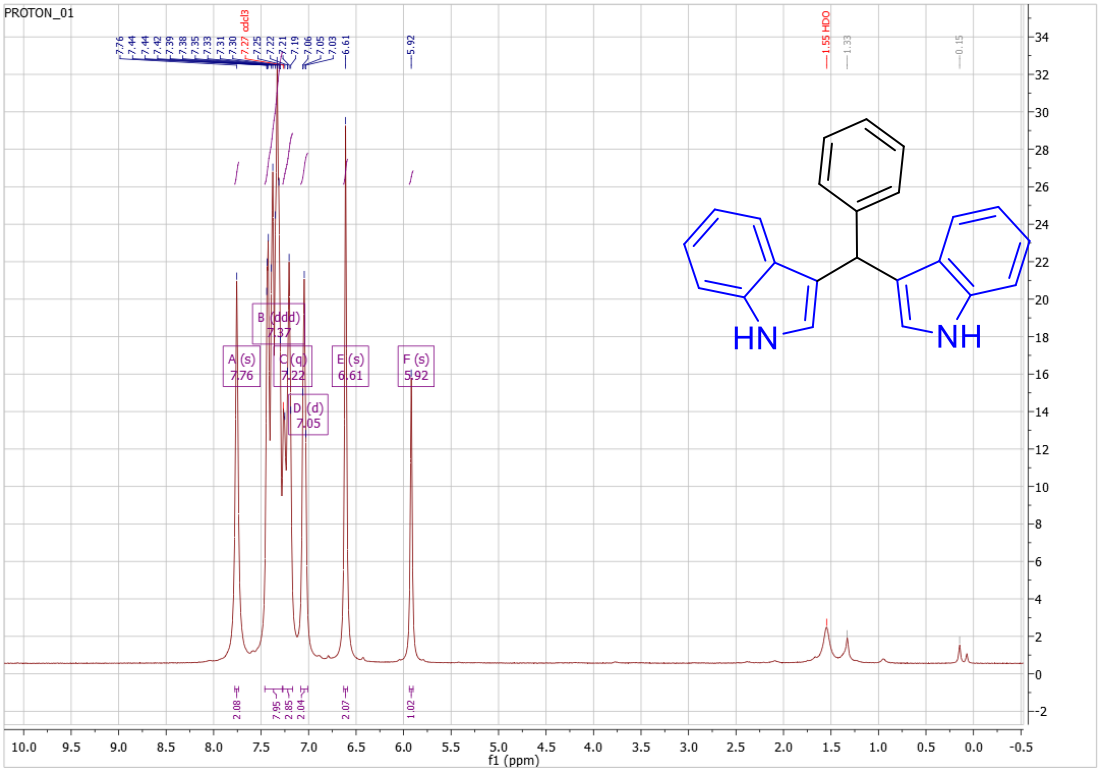

S8.42 ^{1}H NMR of C8aa

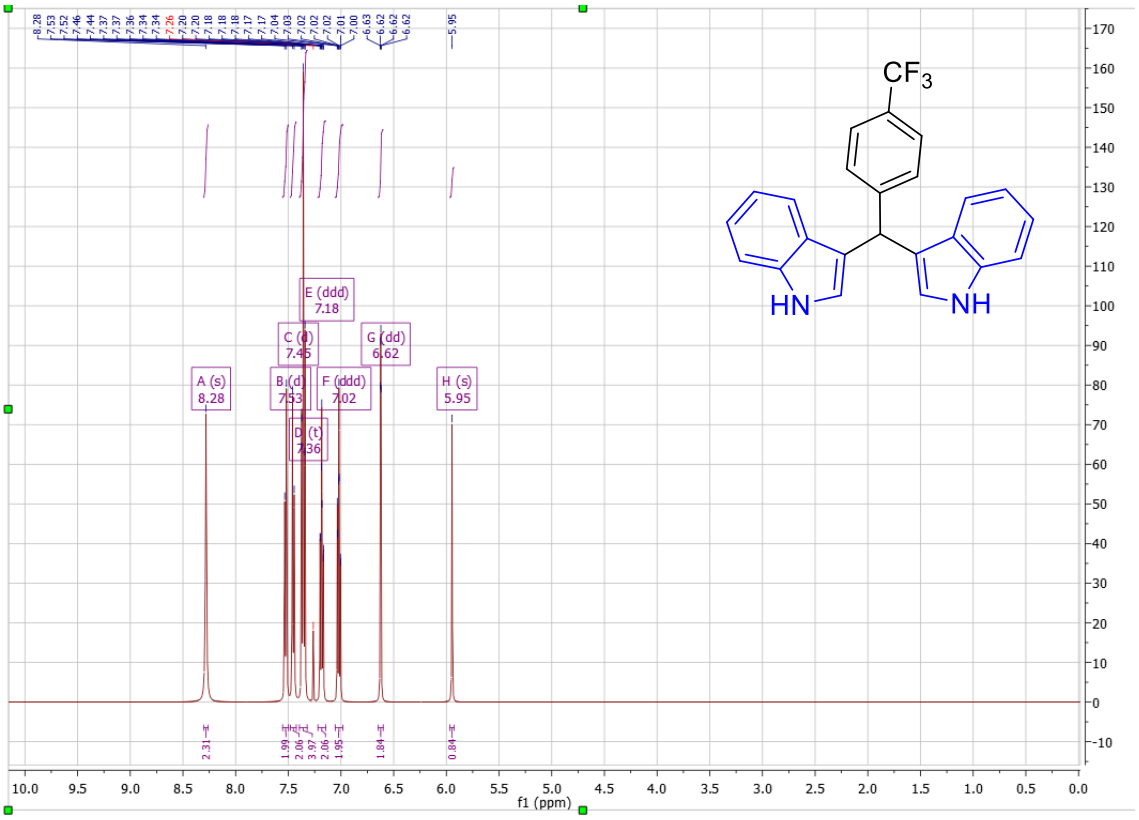

S8.43 ^{1}H NMR of C8ab

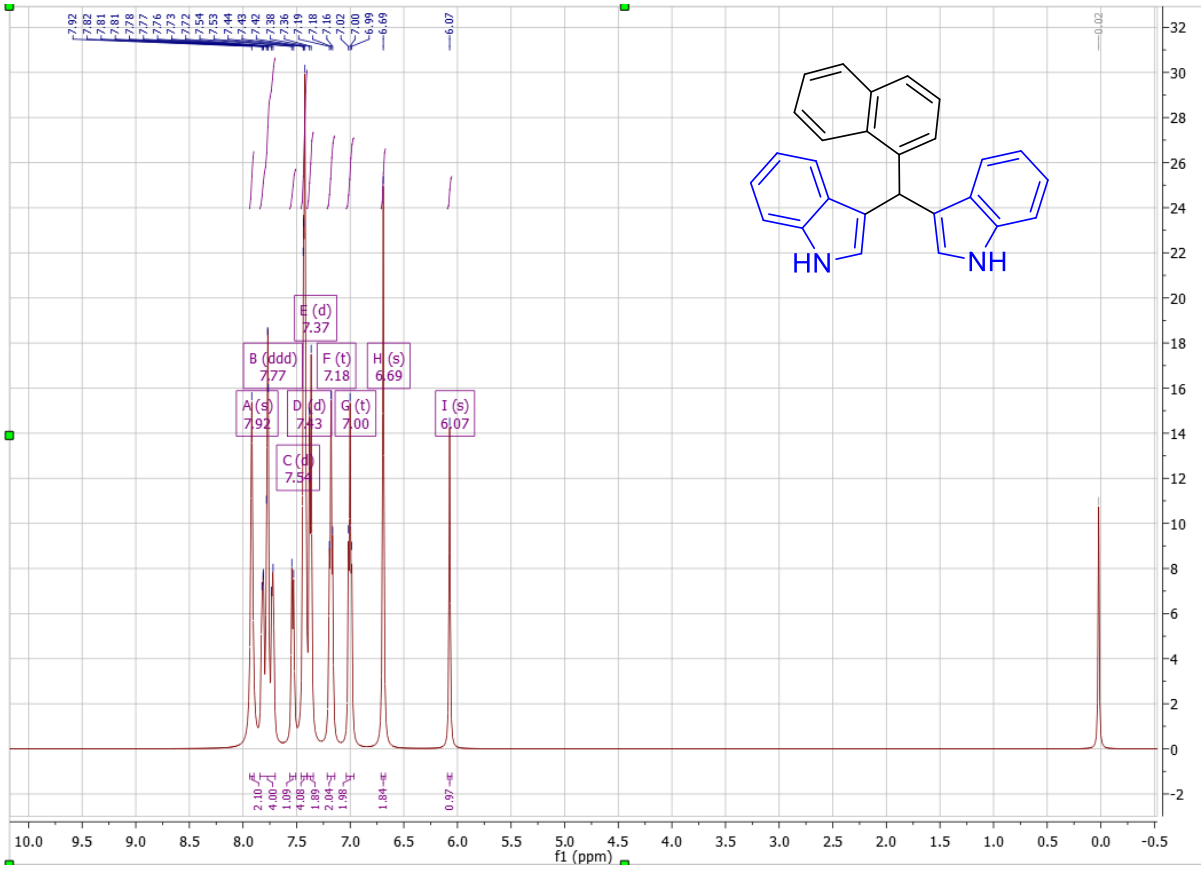

S8.44 ^{1}H NMR of C8ad

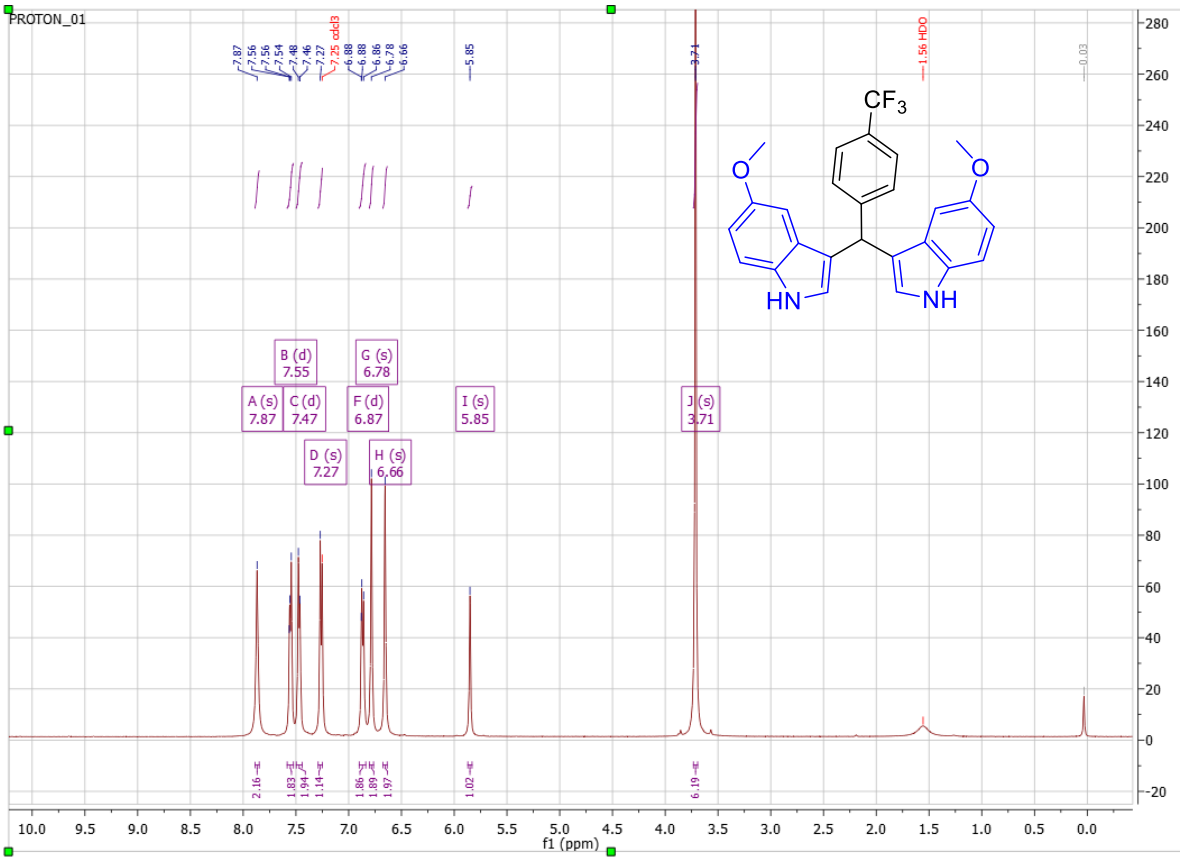

S8.45 ^{1}H NMR of C8ak

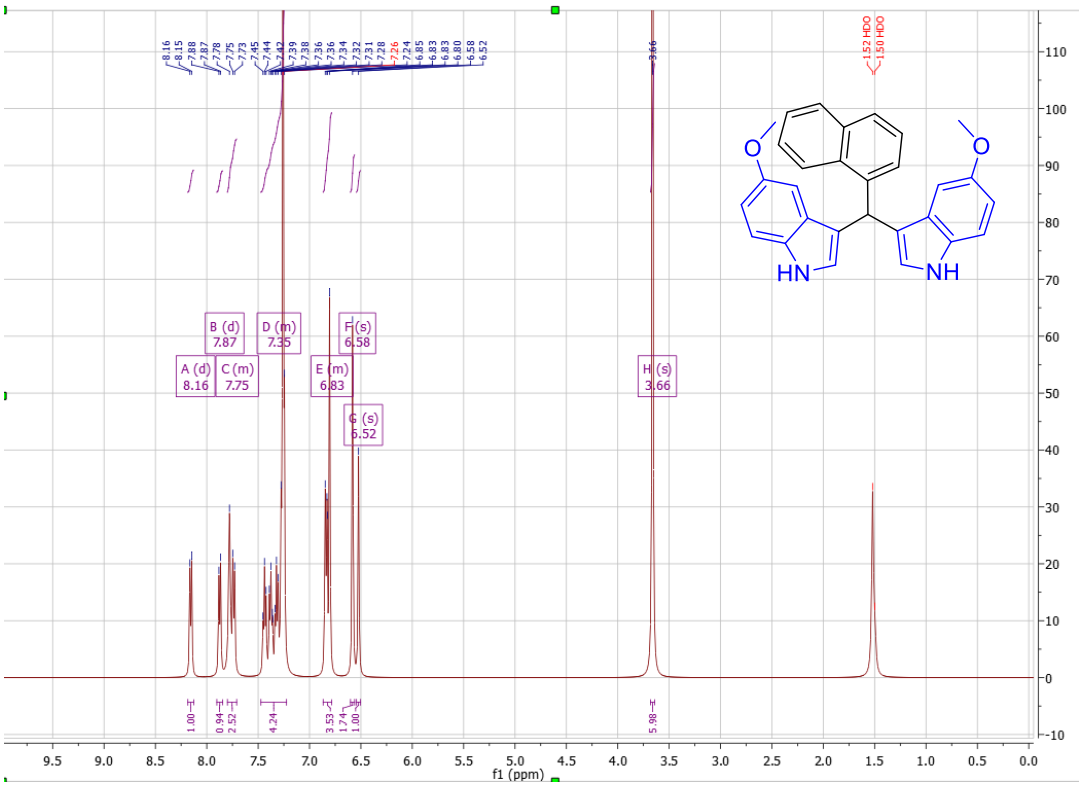

S8.46 ^{1}H NMR of C8am

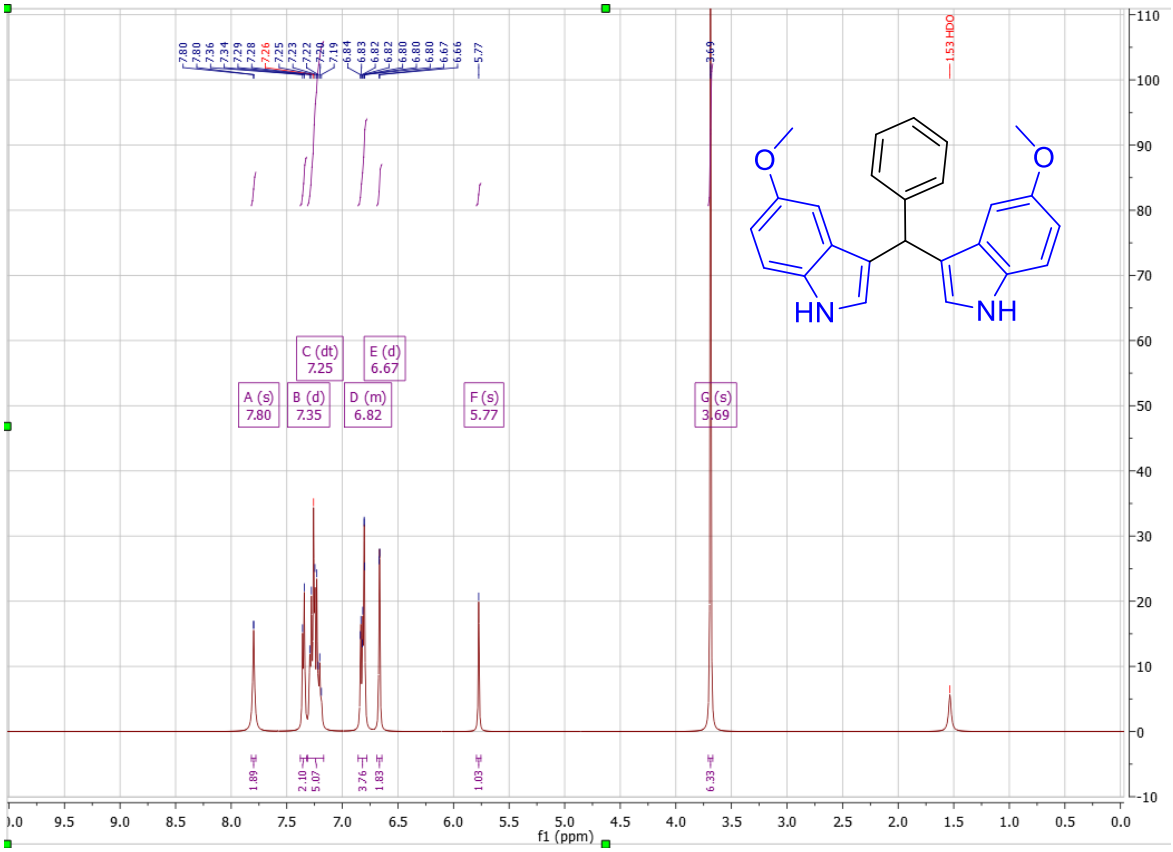

S8.47 ^{1}H NMR of C8aj

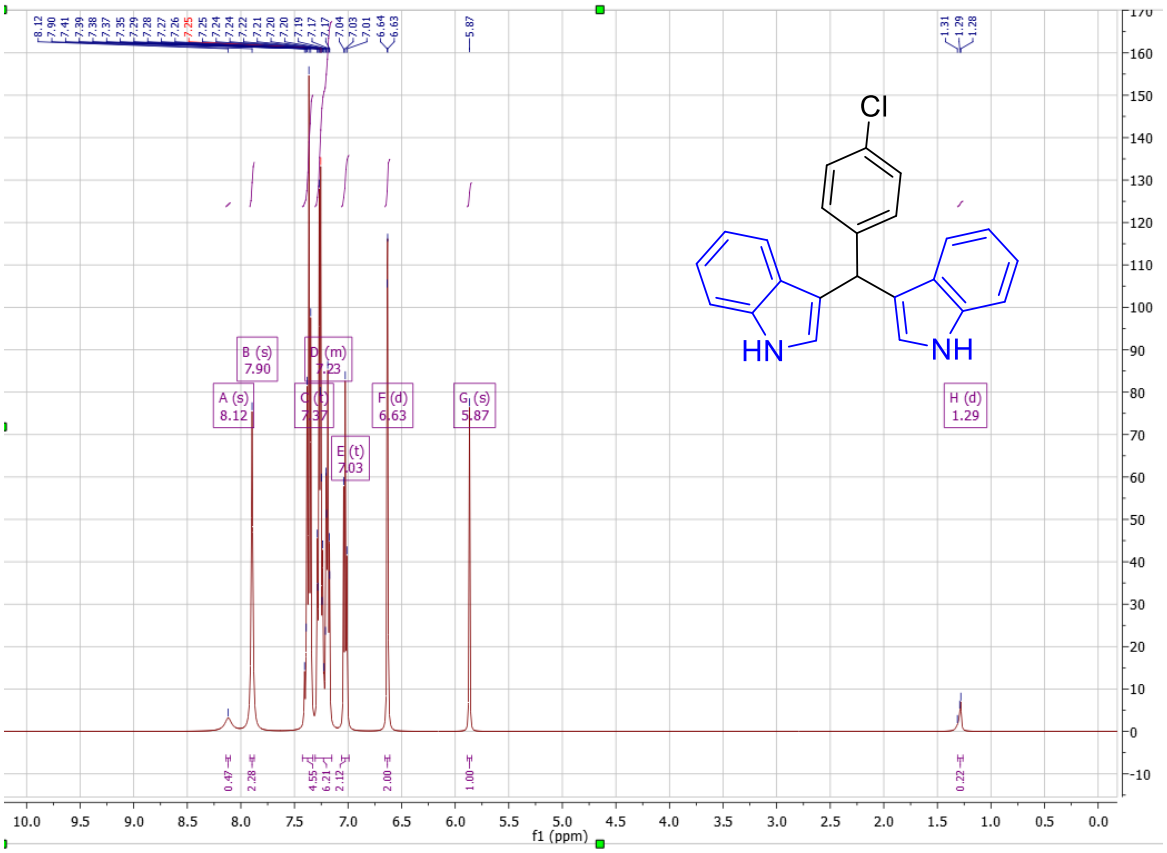

S8.48 ^{1}H NMR of C8ae

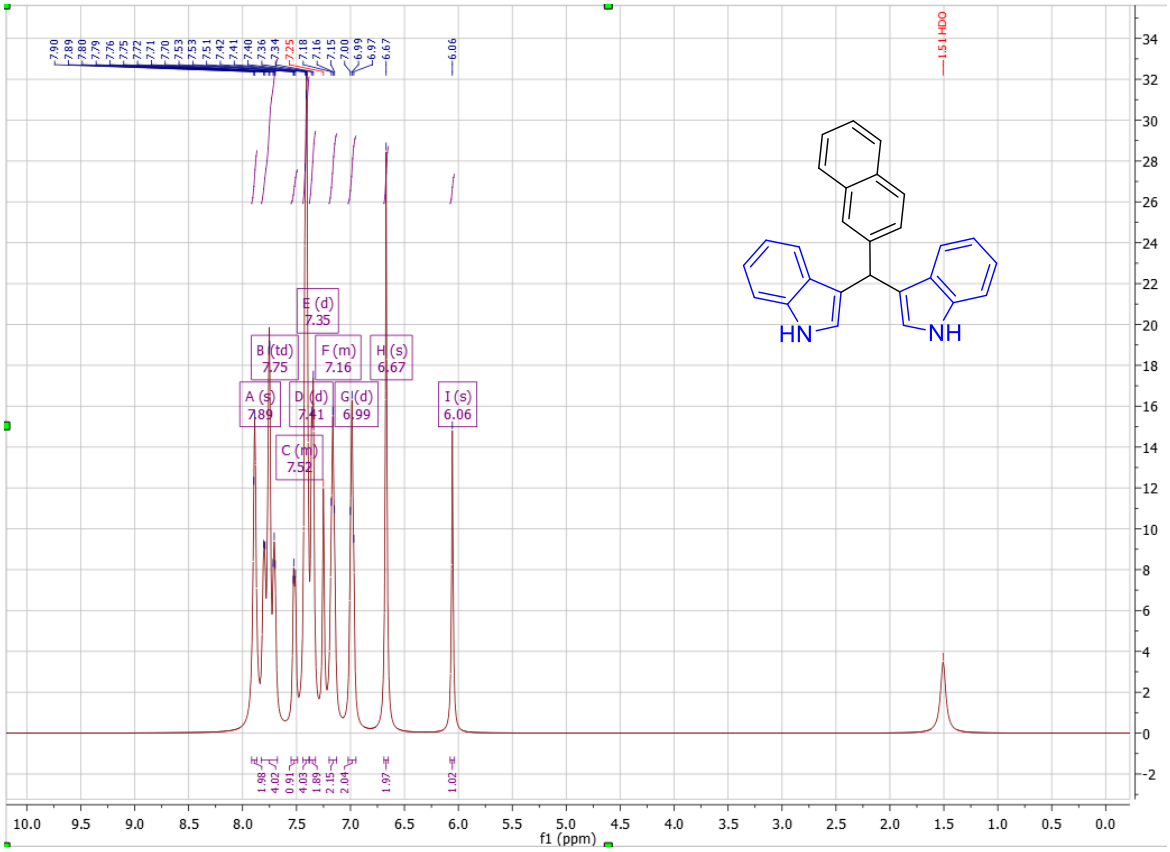

S8.49 ^{1}H NMR of C8ac

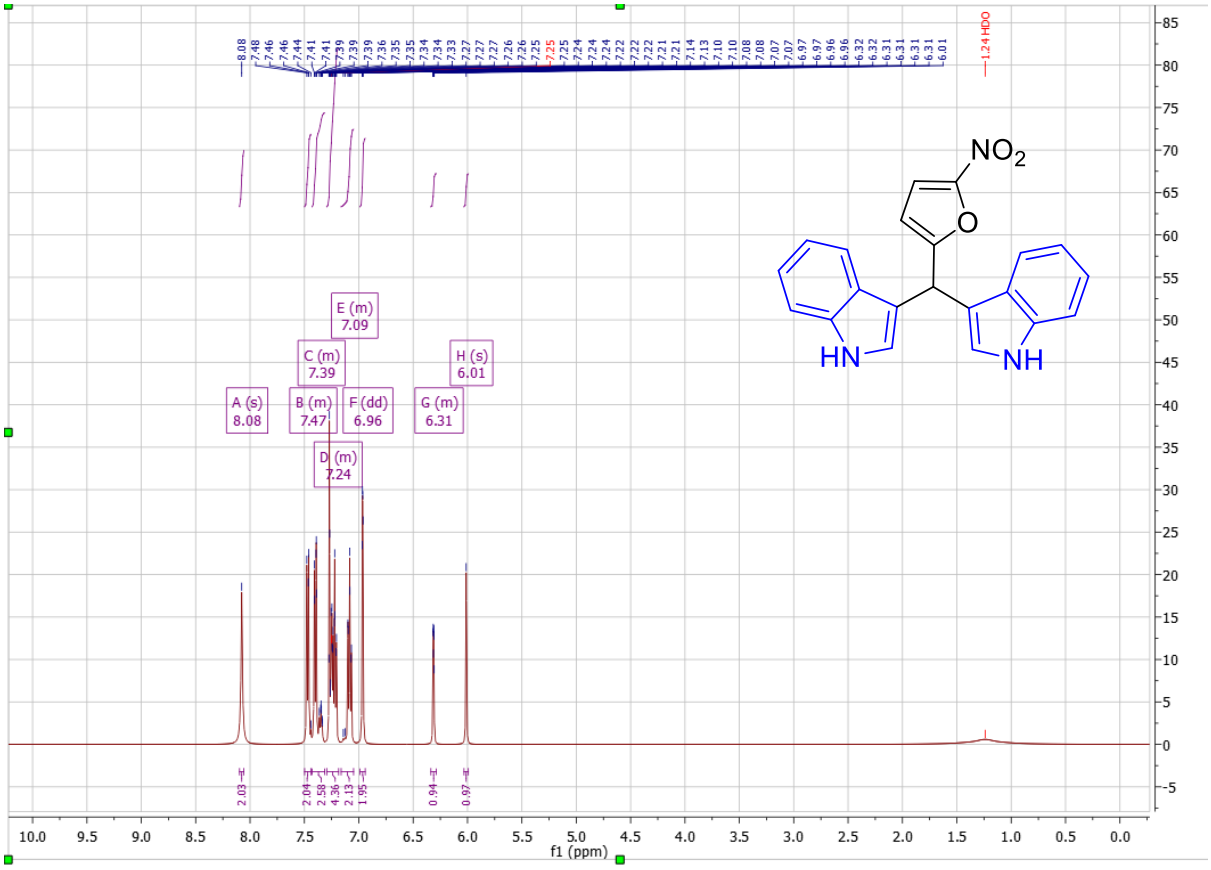

S8.50 ^{1}H NMR of C8af

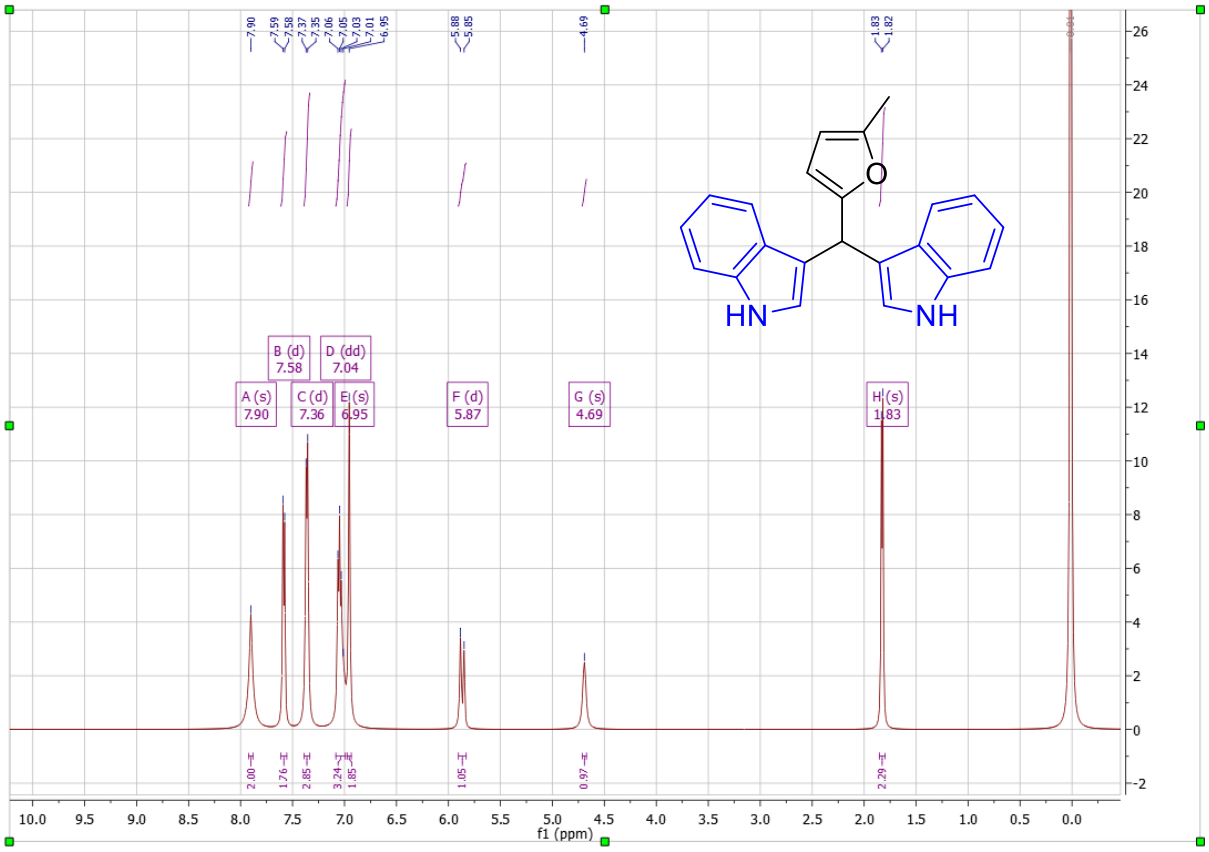

S8.51 ^{1}H NMR of C8ag

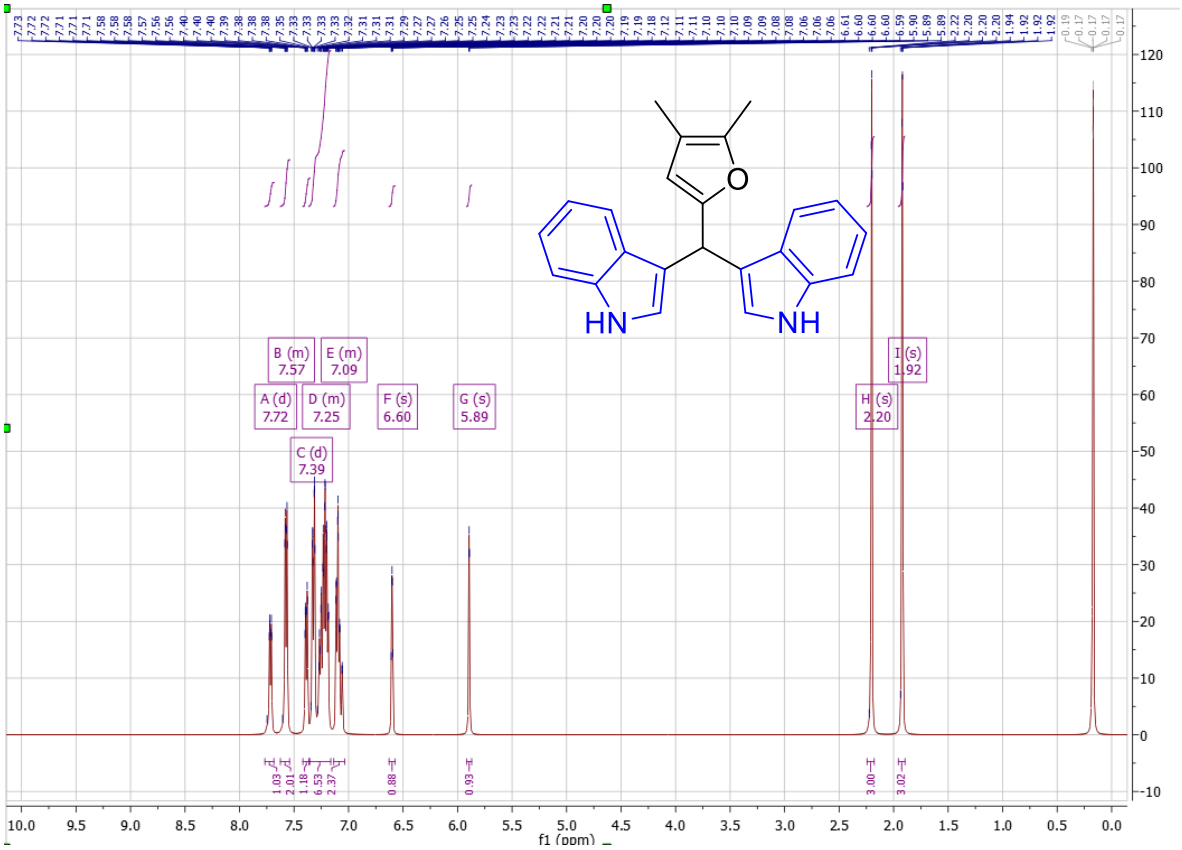

S8.52 ^{1}H NMR of C8ah

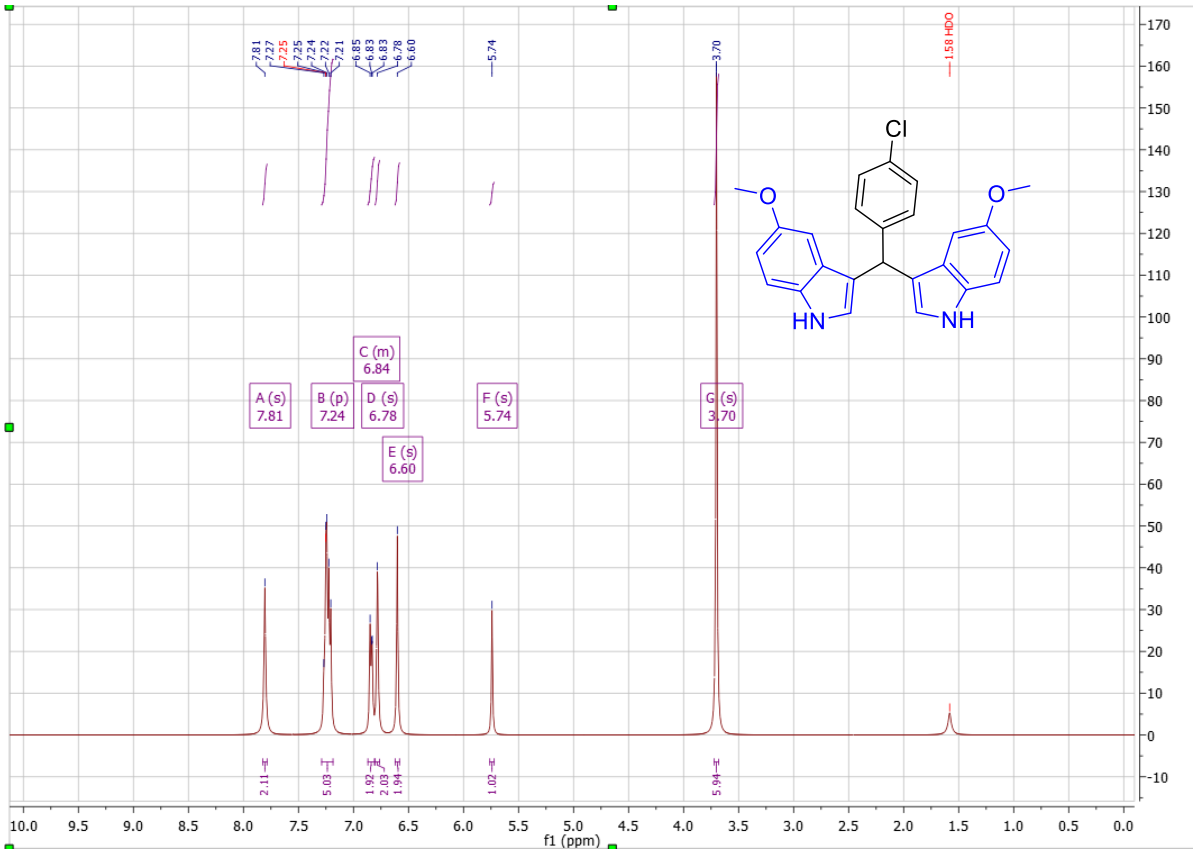

S8.53 ^{1}H NMR of C8an

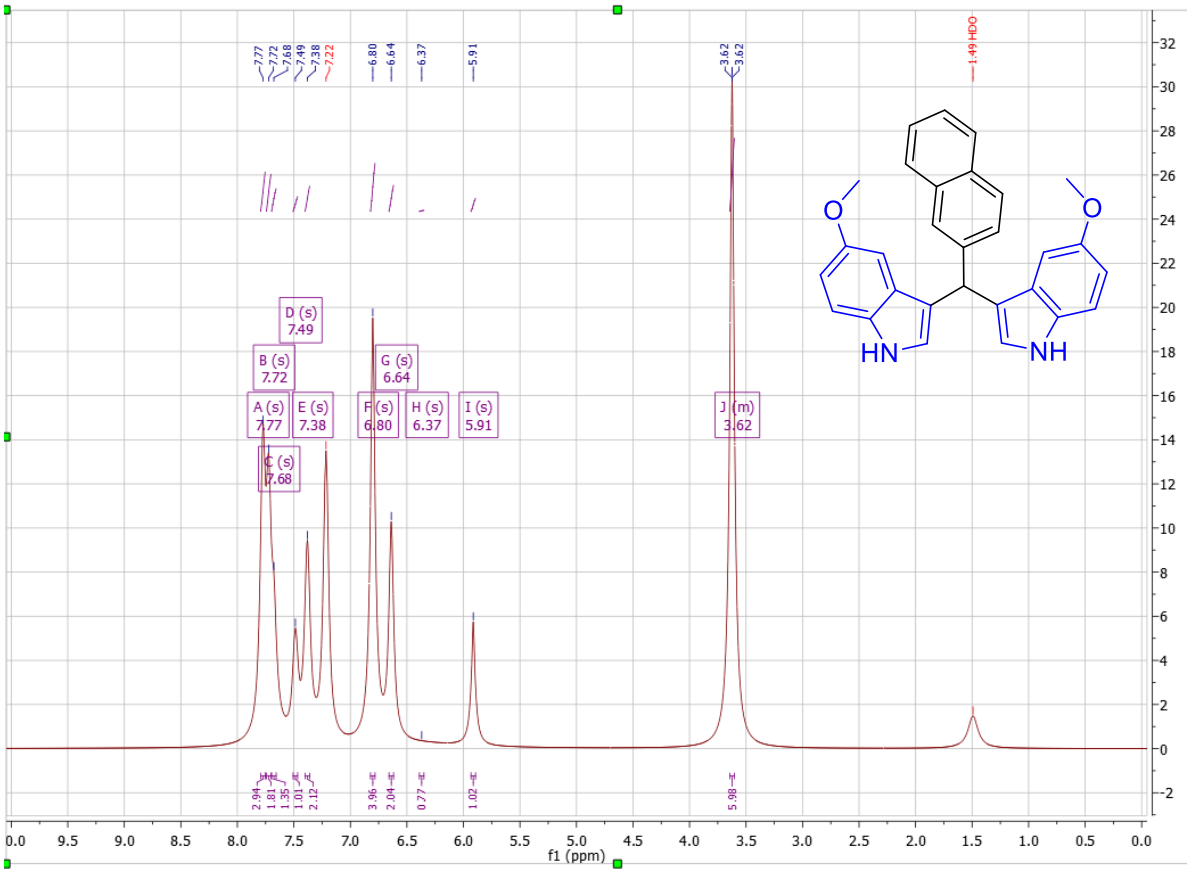

S8.54 ^{1}H NMR of C8ai

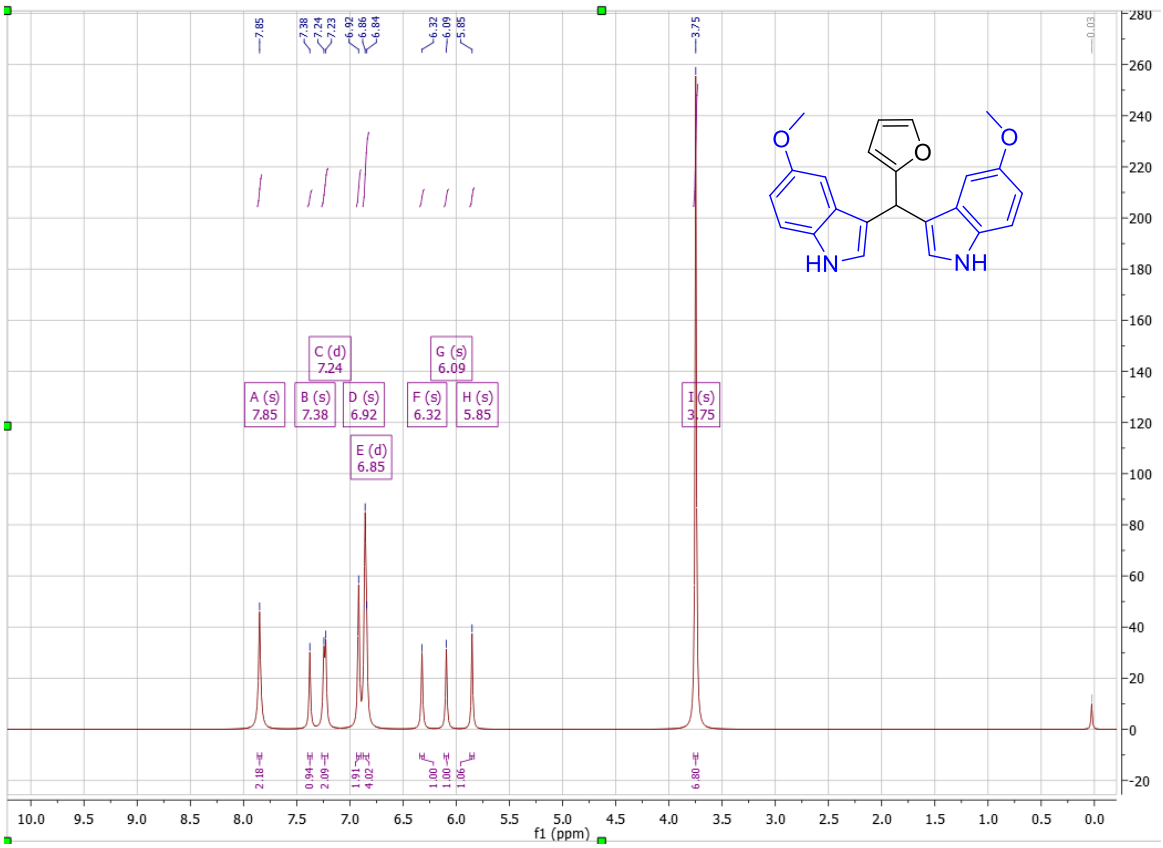

S8.55 ^{1}H NMR of C8af

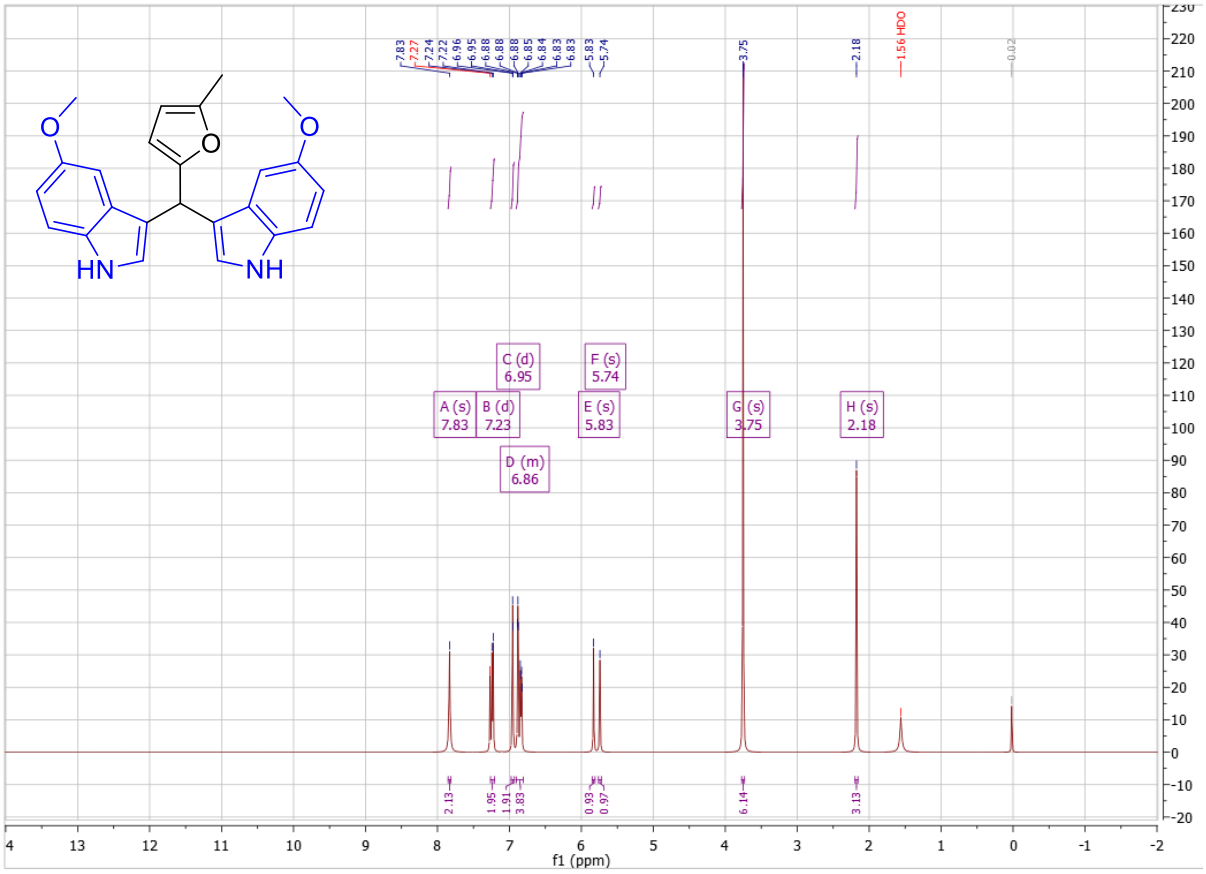

S8.56 ^{1}H NMR of C8ap

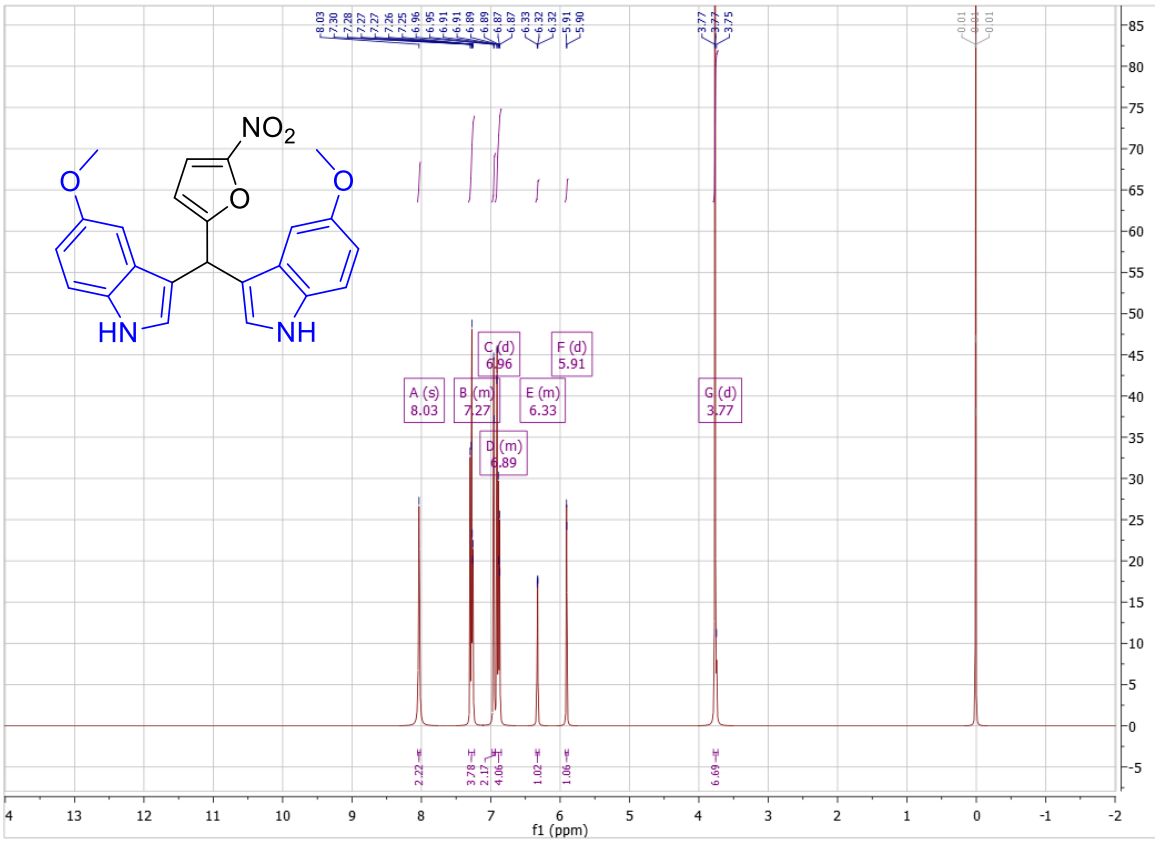

S8.57 ^{1}H NMR of C8aq

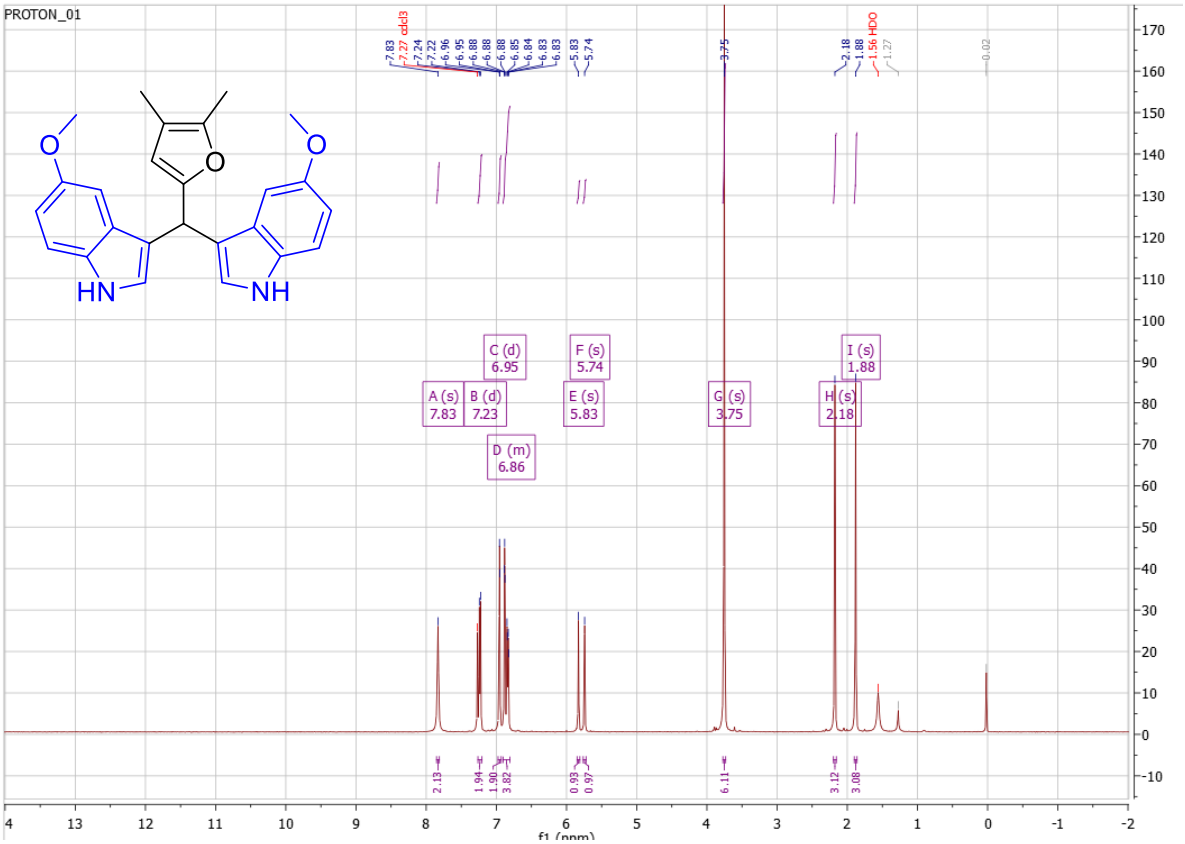

S8.58 ^{1}H NMR of C8ar

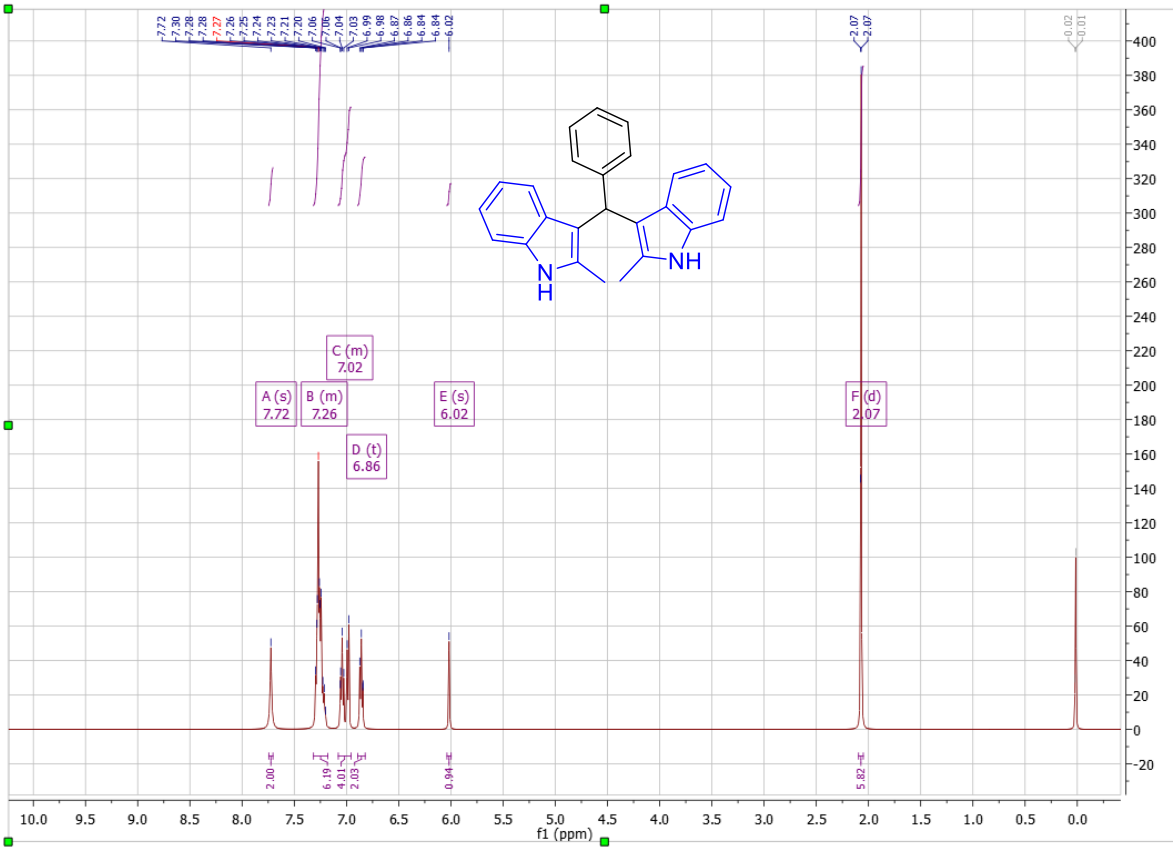

S8.59 ^{1}H NMR of C8at

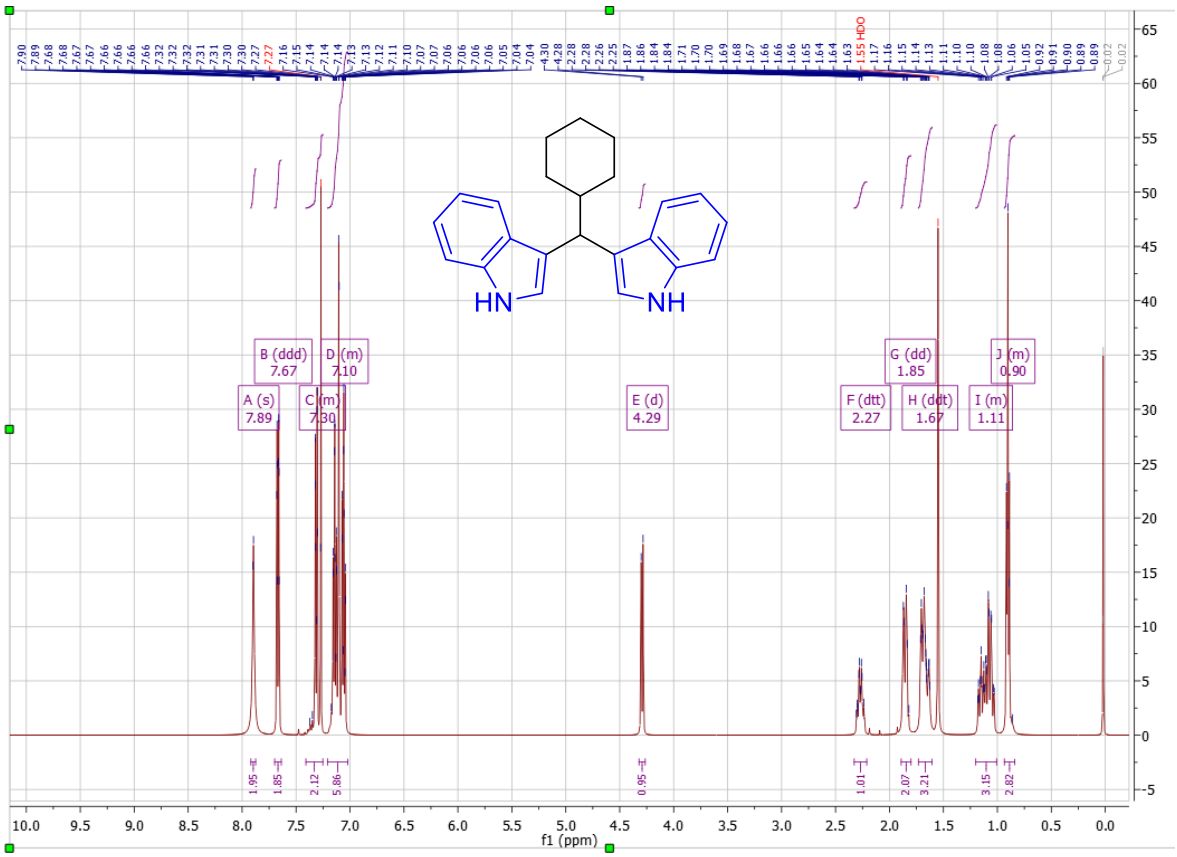

S8.60 ^{1}H NMR of C8as

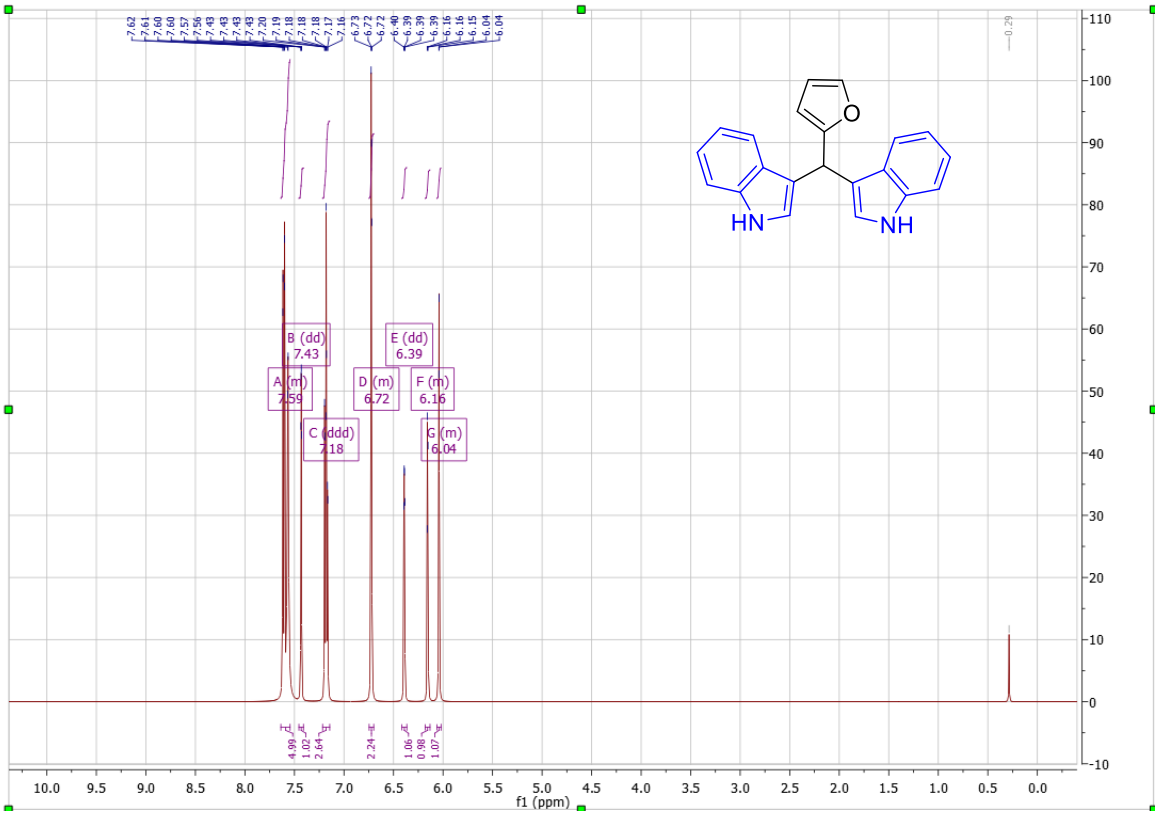

S8.61 ^{1}H NMR of C8af

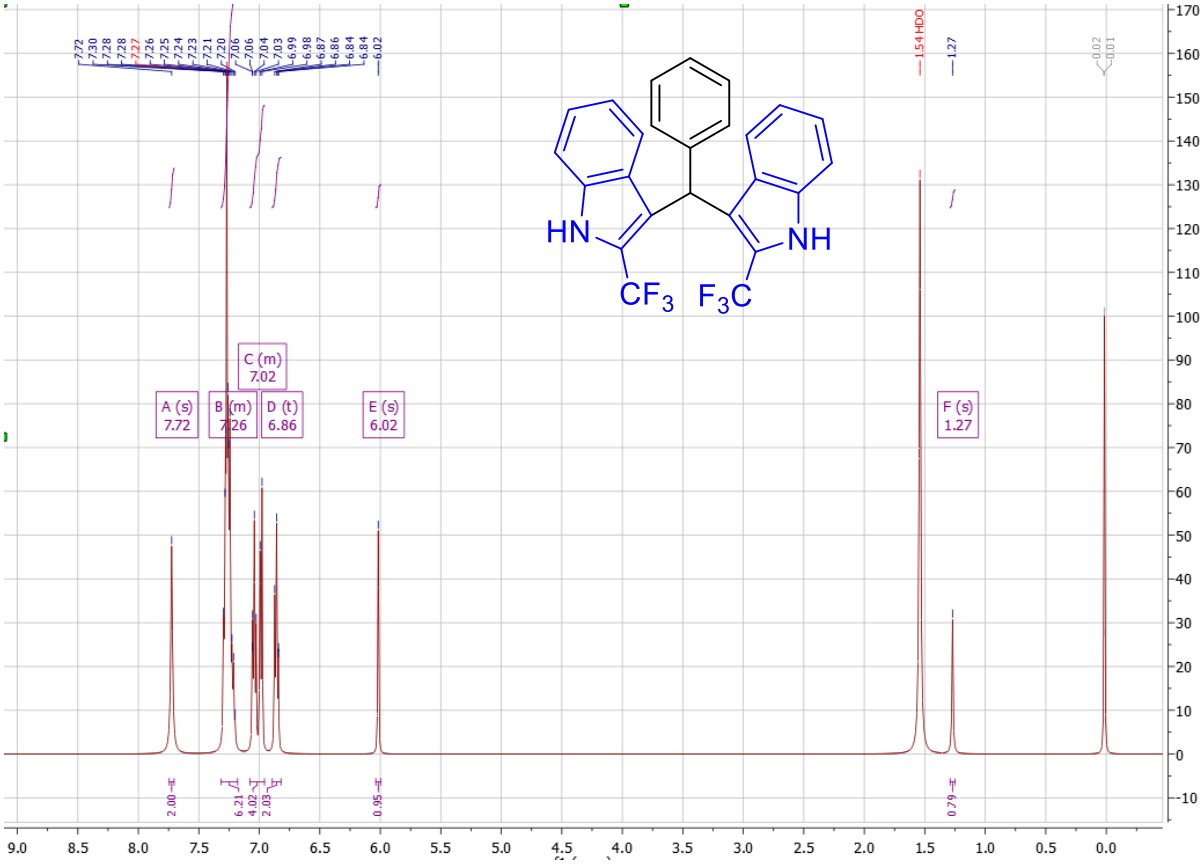

S8.62 ^{1}H NMR of C8au

8.7 ^{13}CNMR C8aa-C8au

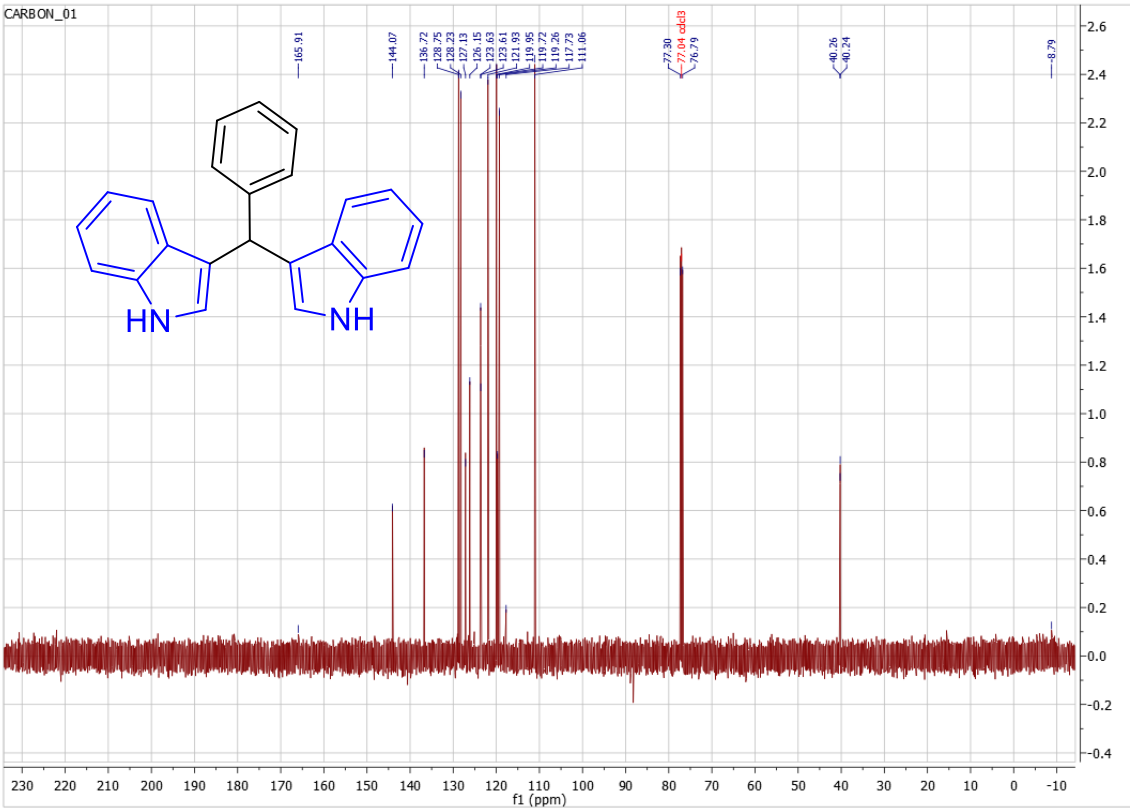

S8.63 ^{13}C NMR of C8au

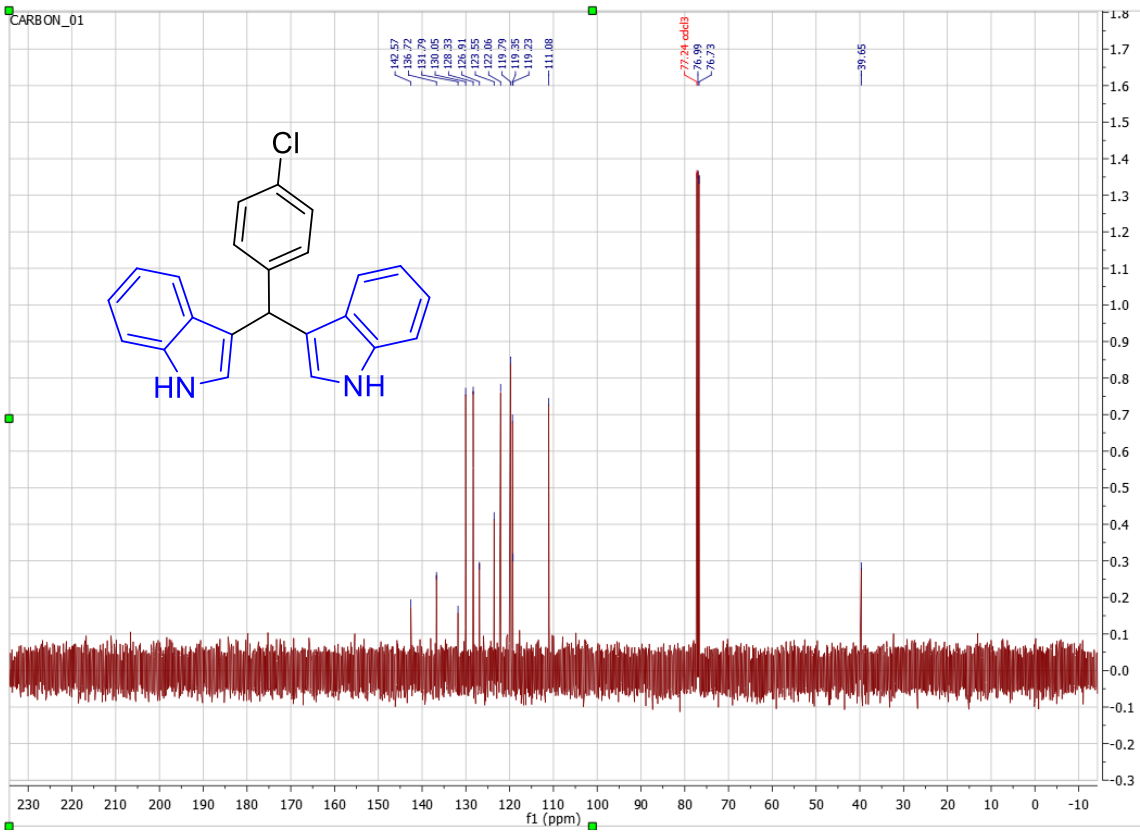

S8.64. ^{13}C NMR of C8ae

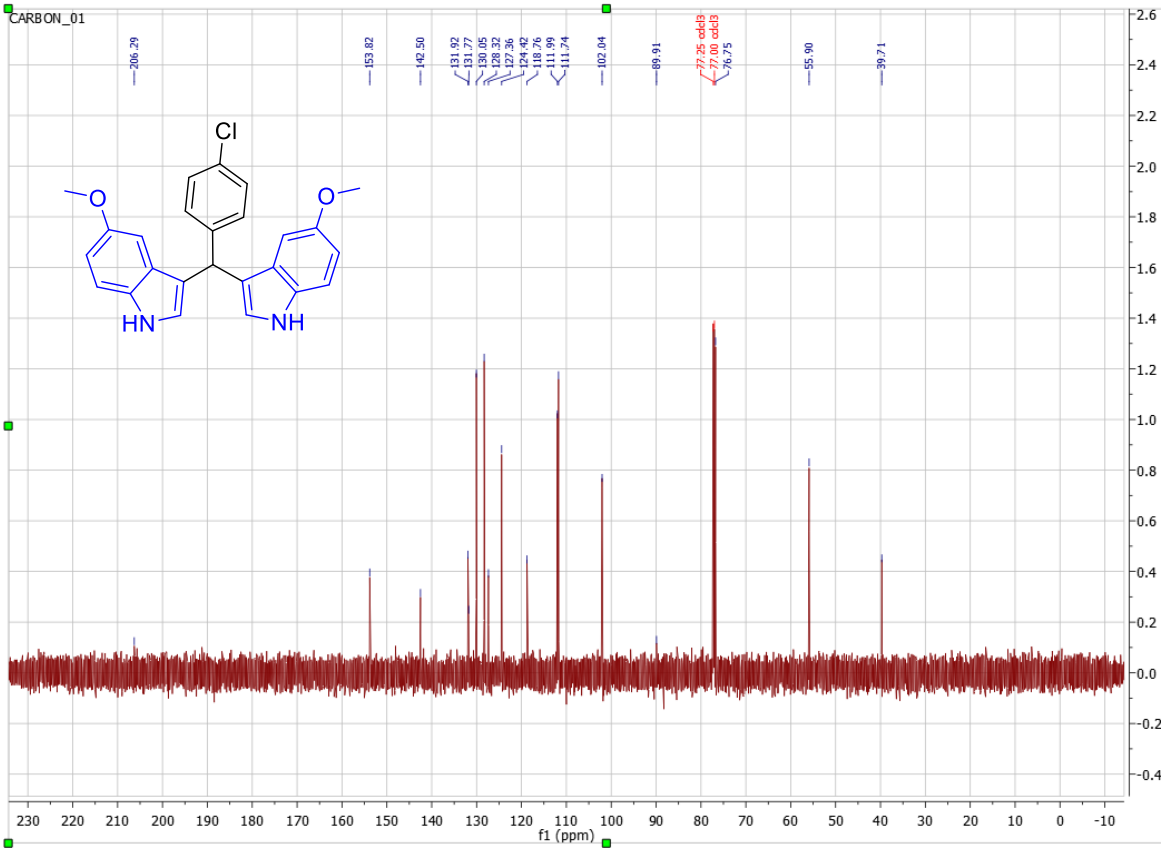

S8.65. ^{13}C NMR of C8an

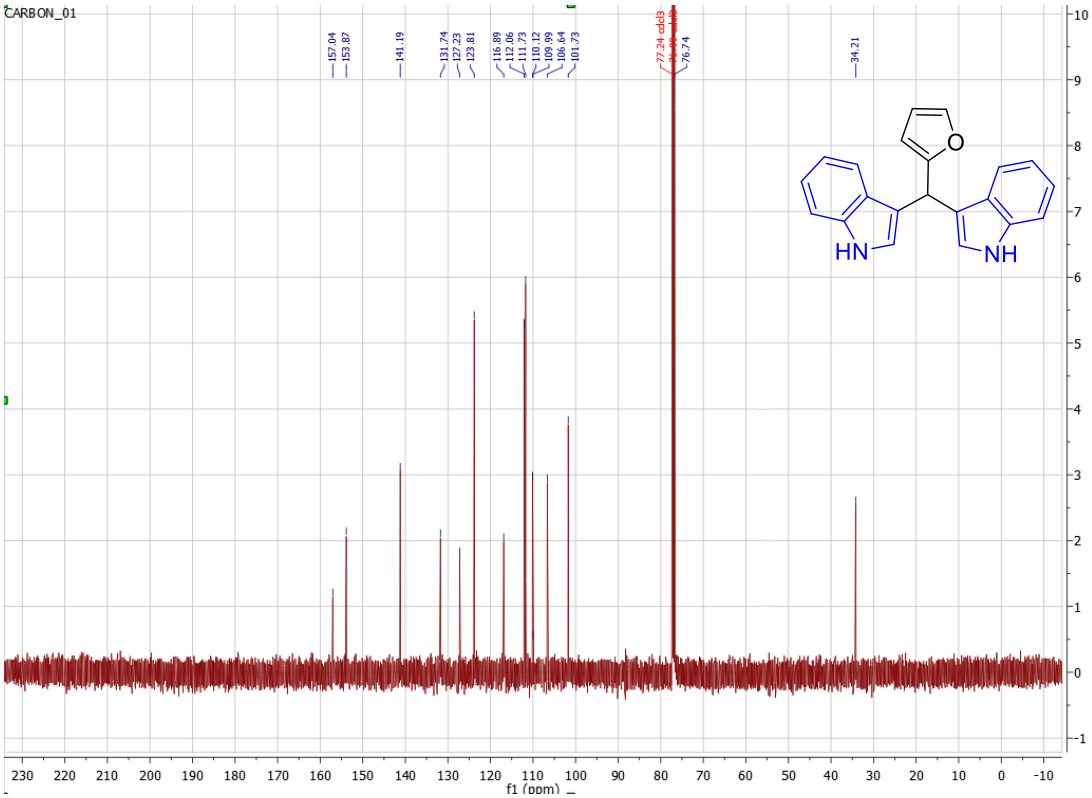

S8.66. ^{13}C NMR of C8af

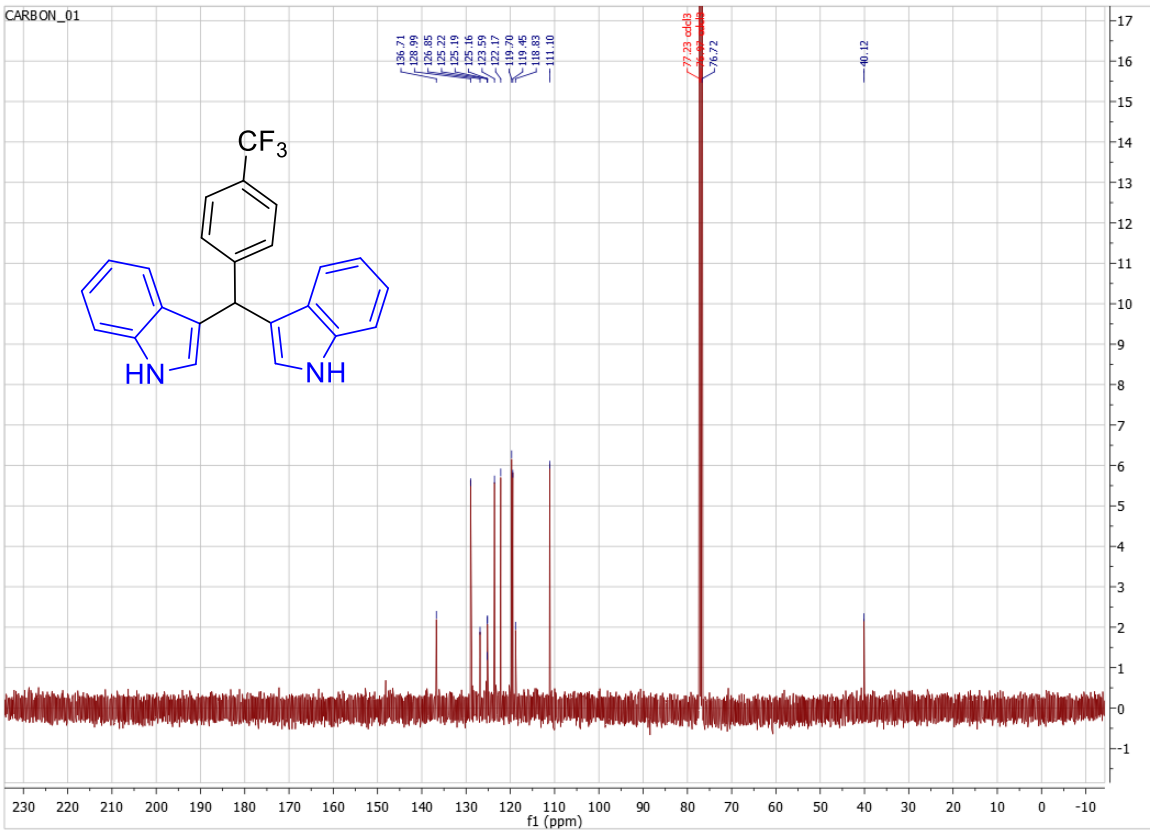

S8.67. ^{13}C NMR of C8ab

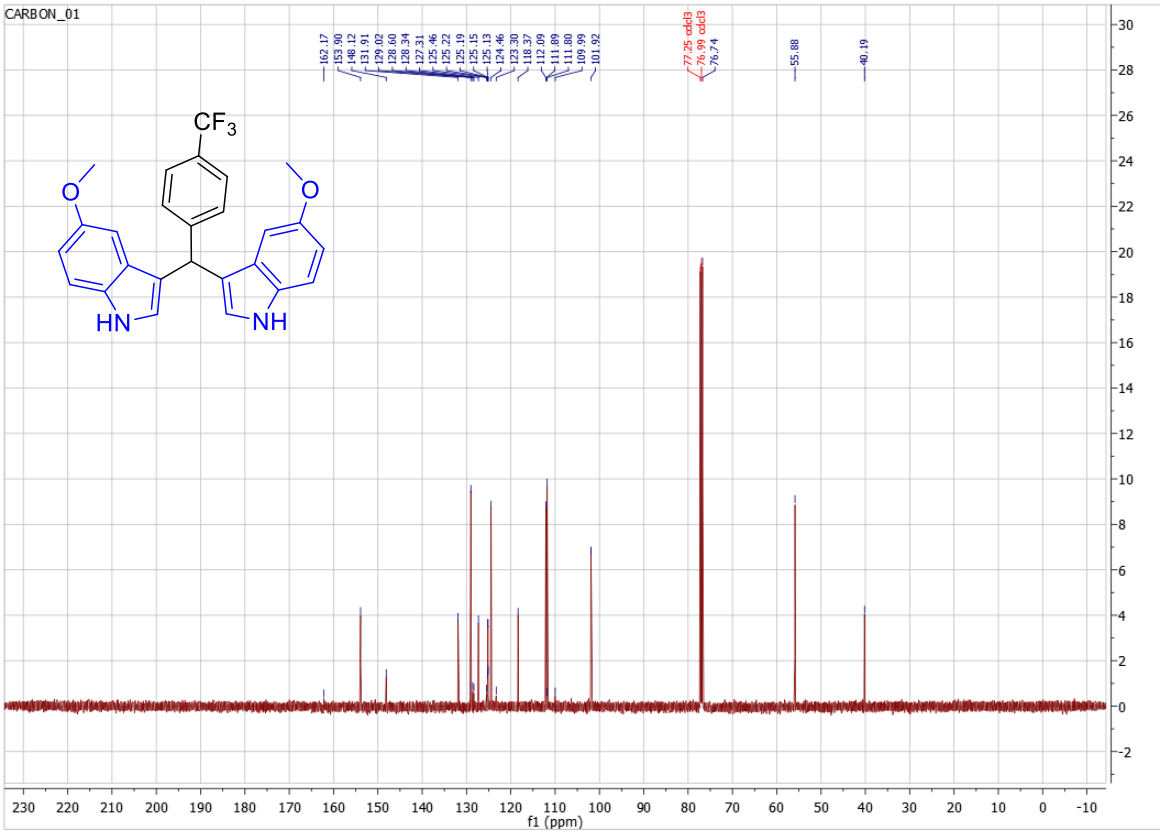

S8.68. ^{13}C NMR of C8ak

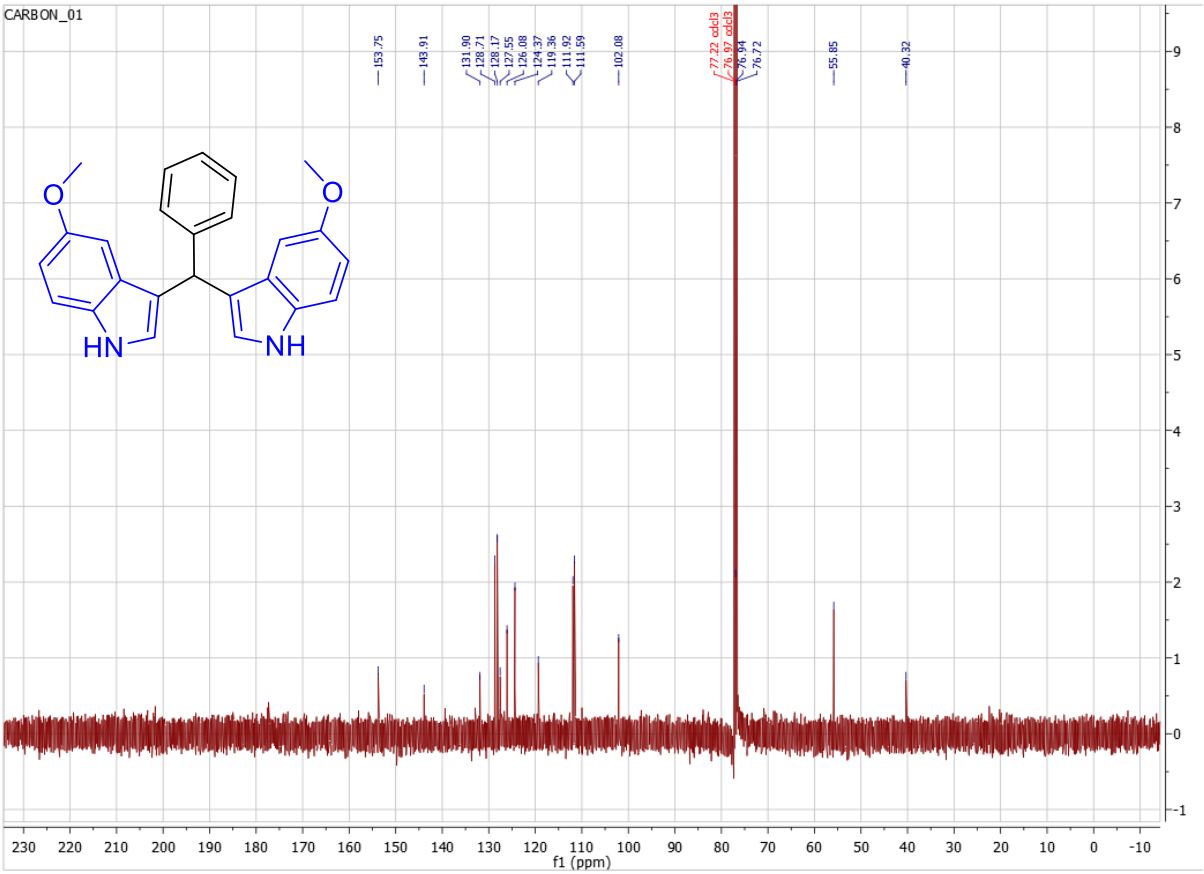

S8.69. ^{13}C NMR of C8aj

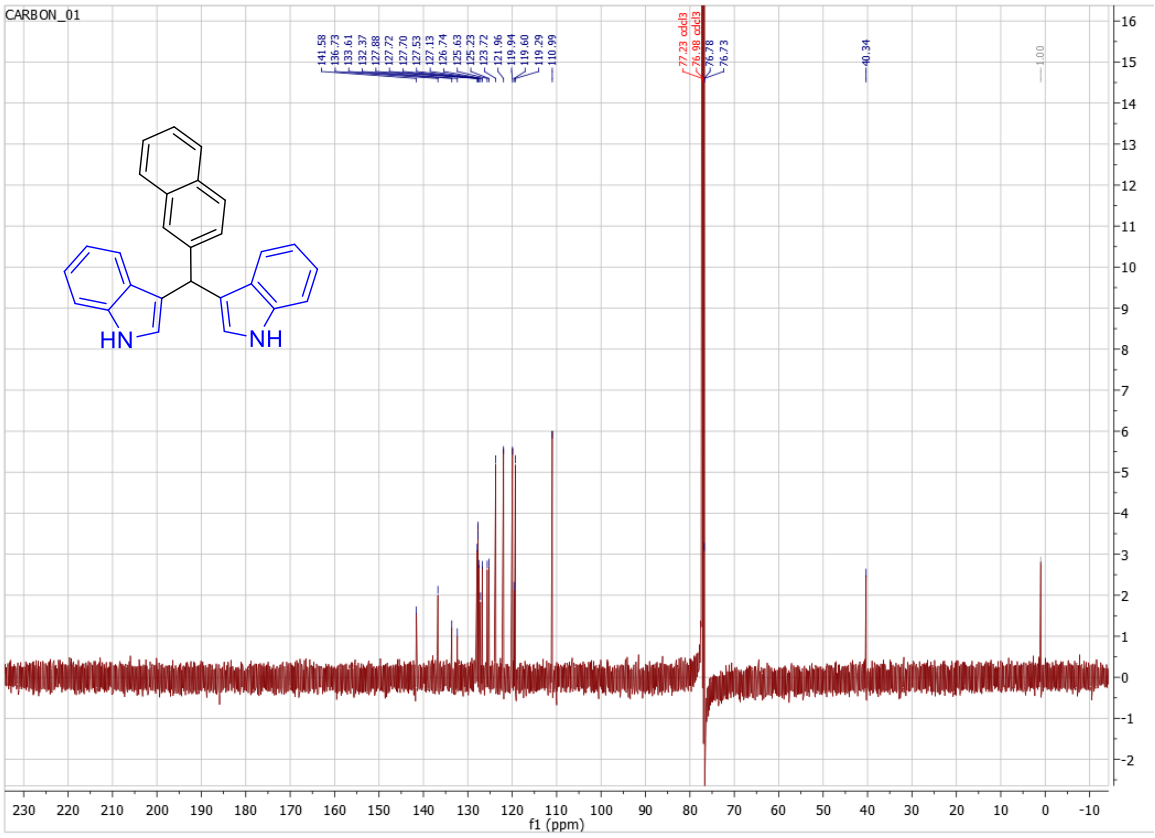

S8.70. ^{13}C NMR of C8ac

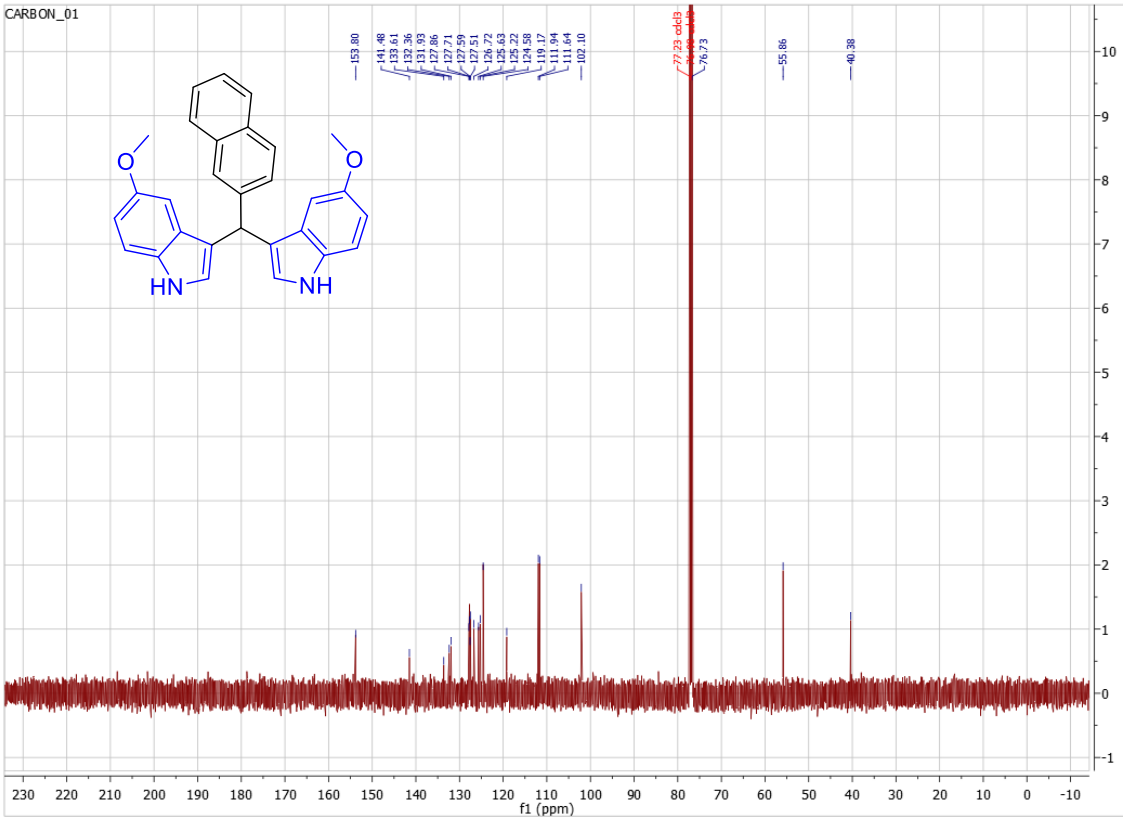

S8.71. ^{13}C NMR of C8ai

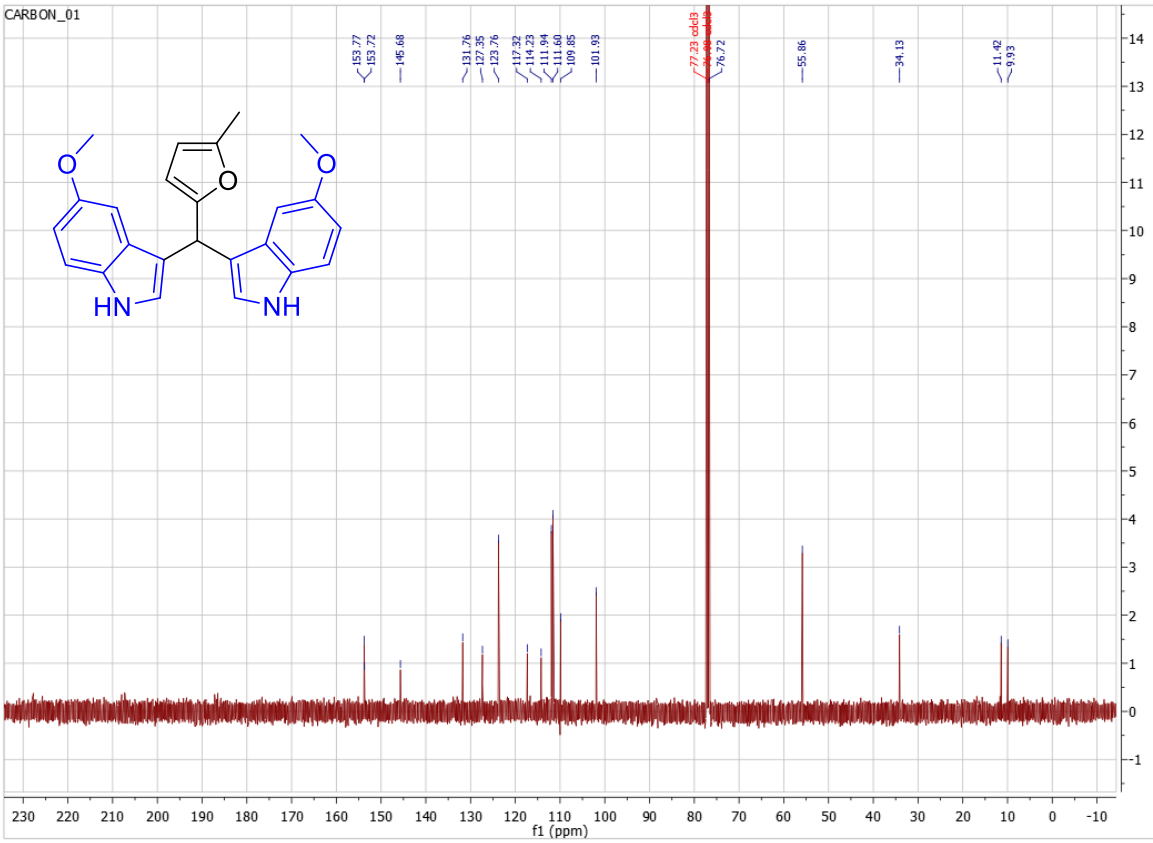

S8.72. ^{13}C NMR of C8ap

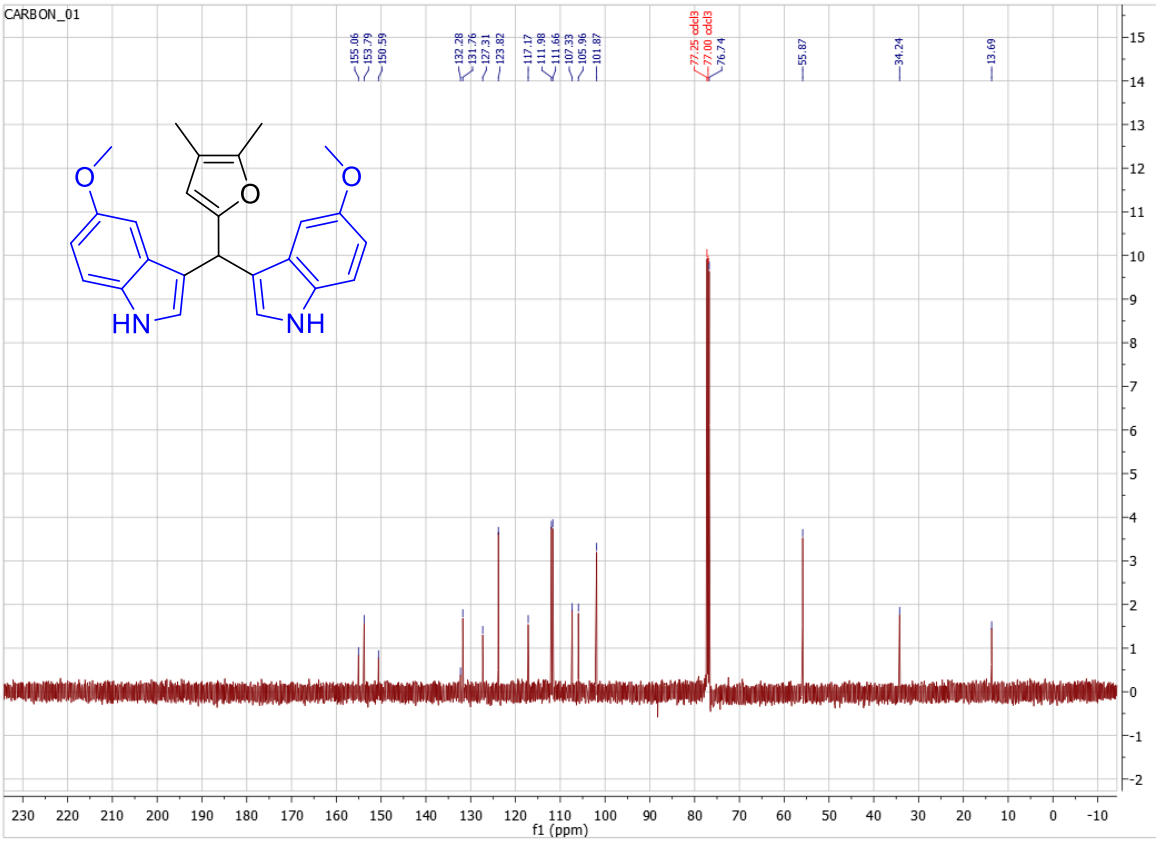

S8.73. ^{13}C NMR of C8ar

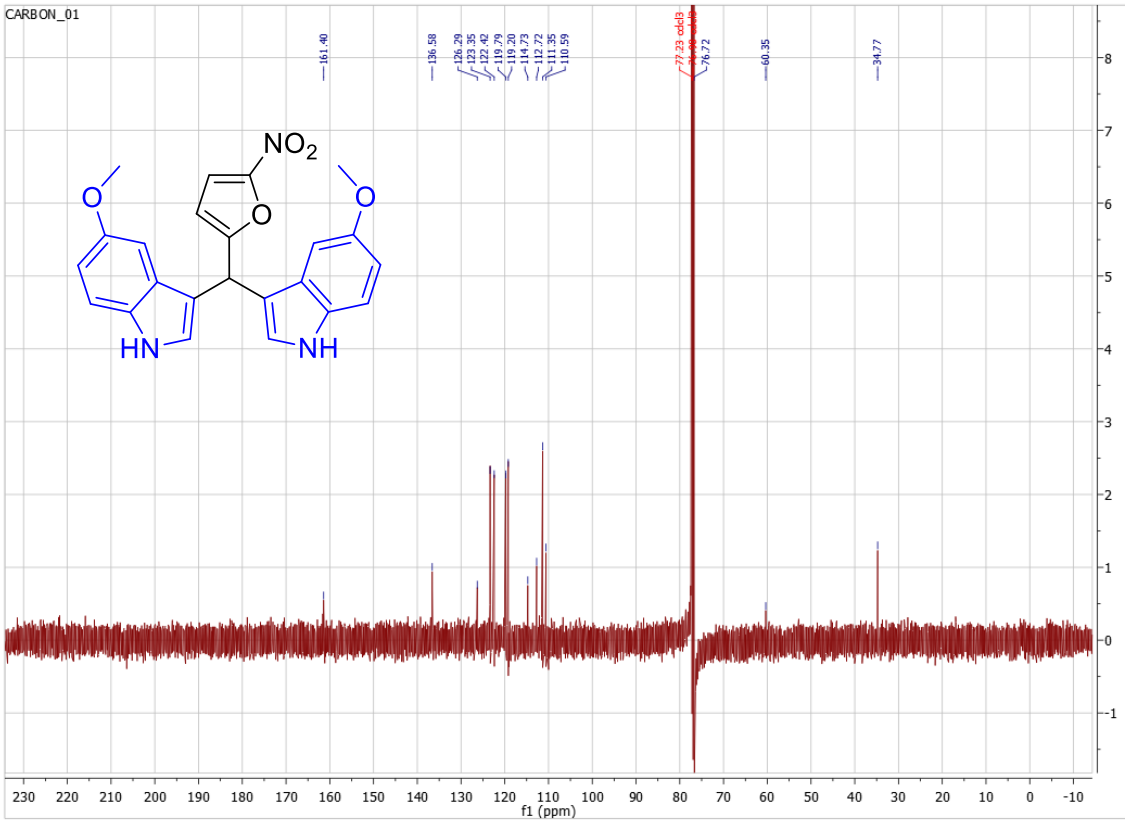

S8.74. ^{13}C NMR of C8aq

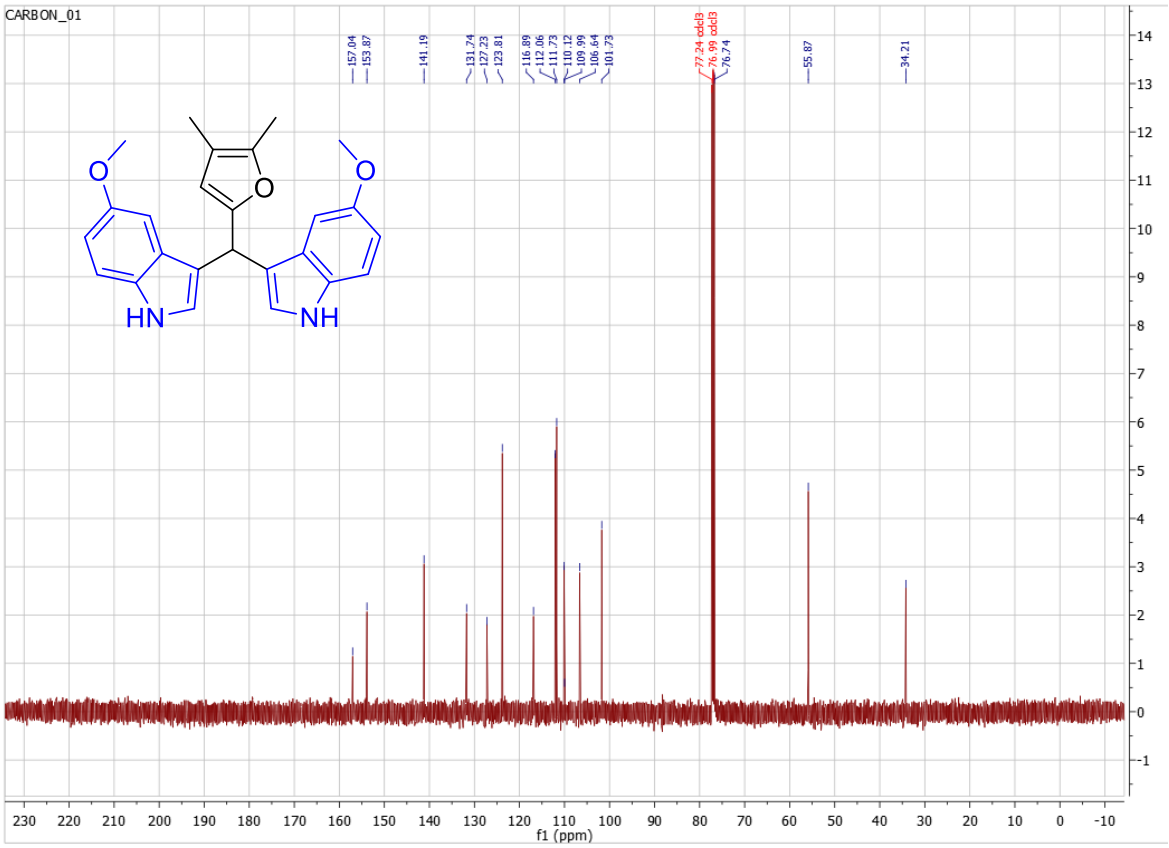

S8.75. ^{13}CNMR of C8ar

8.8 ESI-MS C8aa-C8au

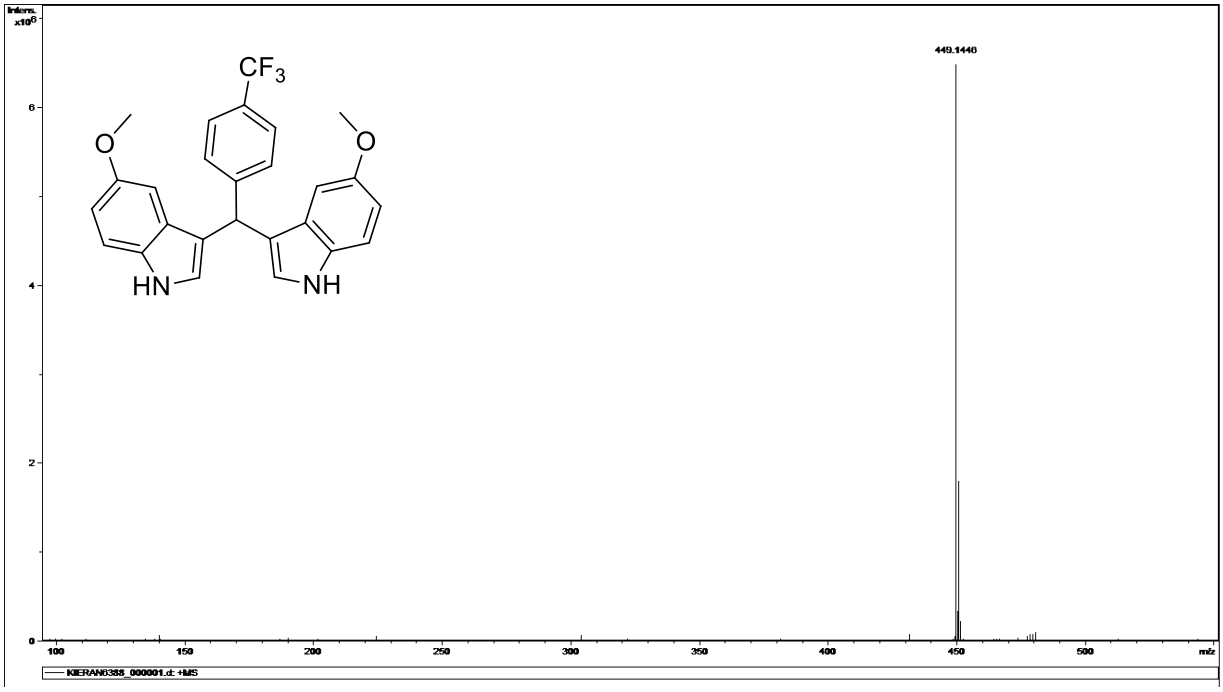

S8.76. ESI-MS of C8ak

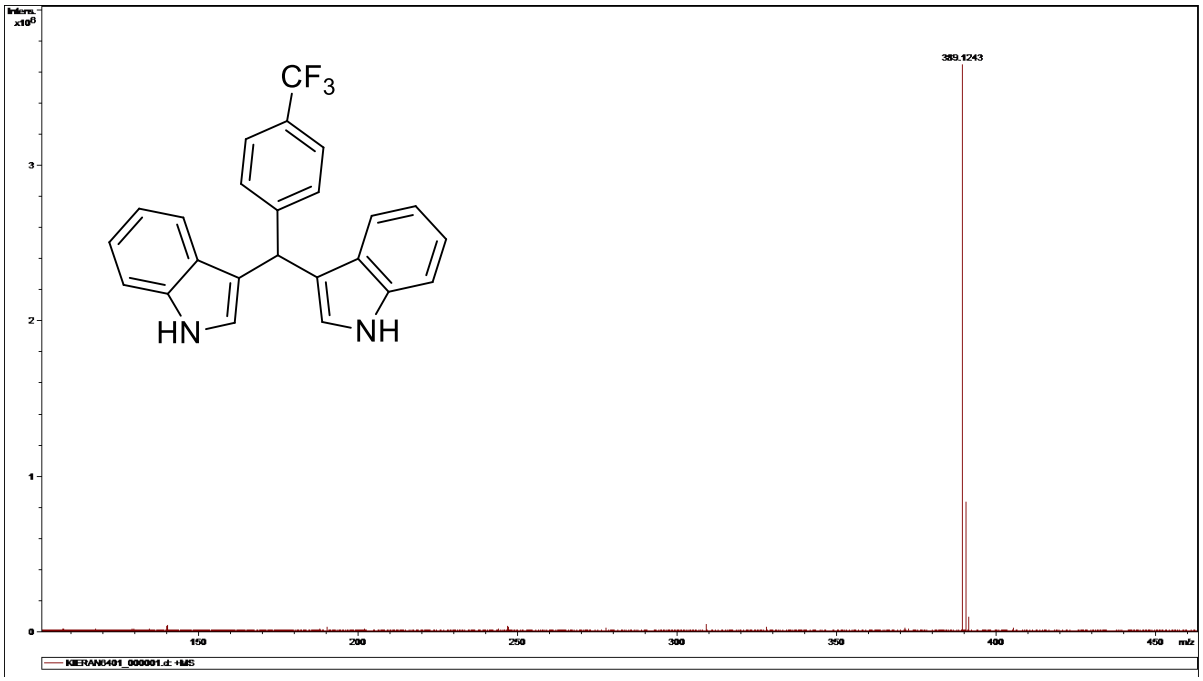

S8.77. ESI-MS of C8ab

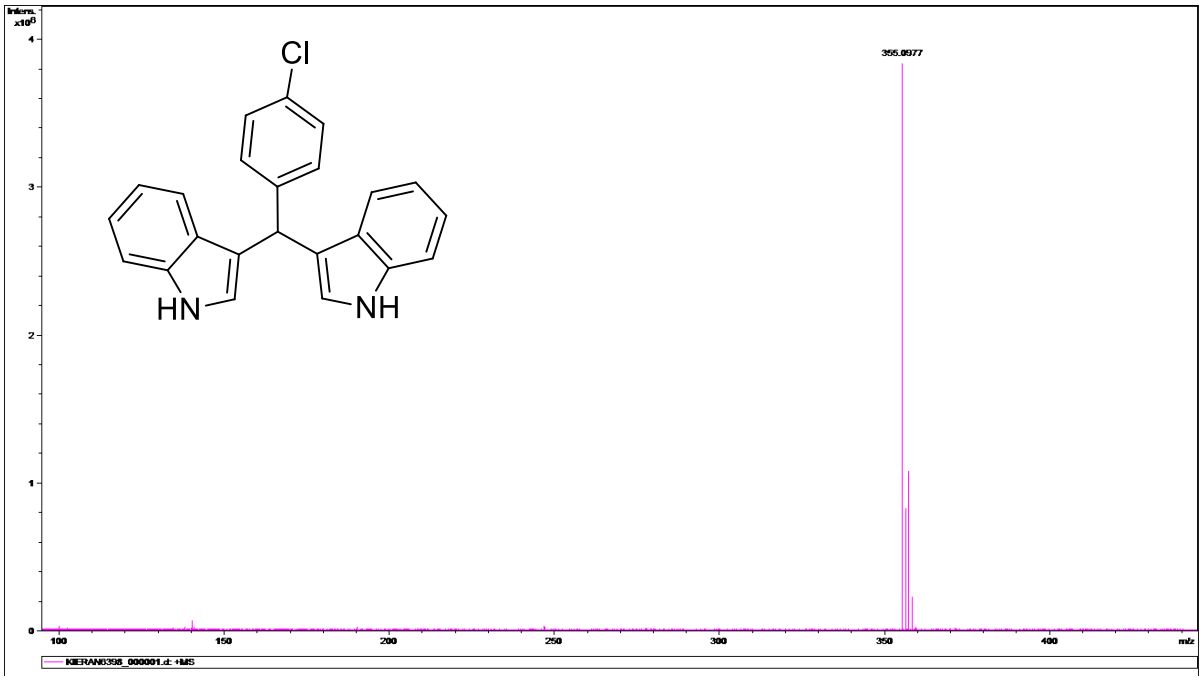

S8.78. ESI-MS of C8ae

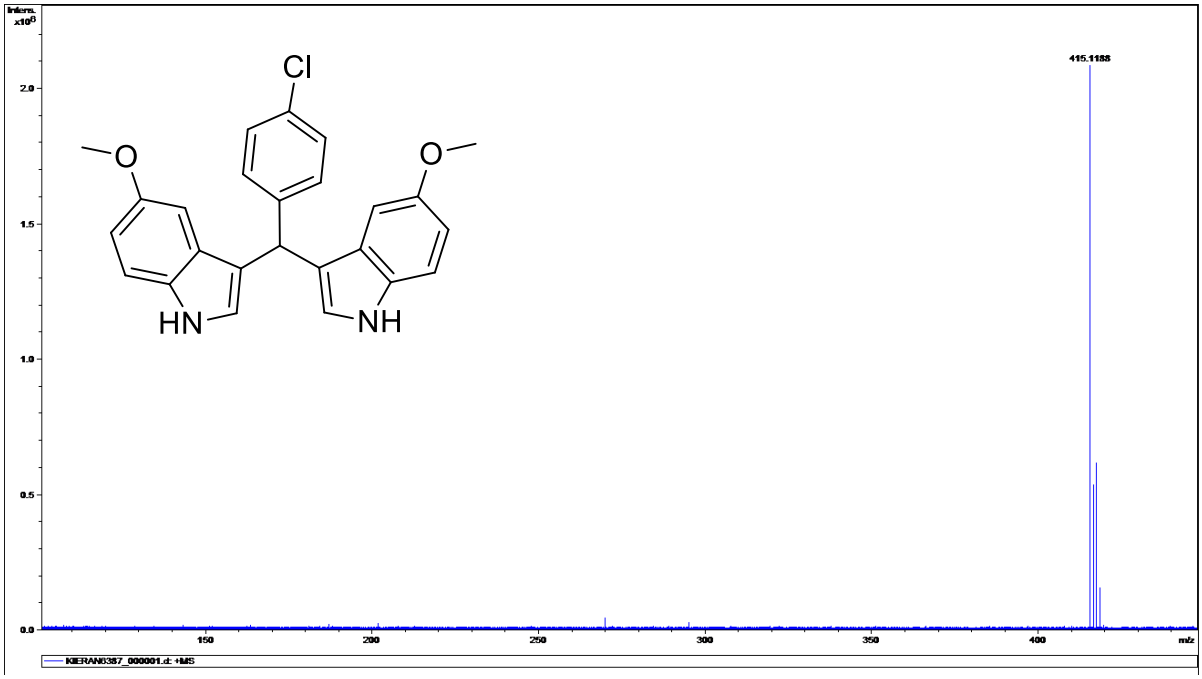

S8.79. ESI-MS of C8an

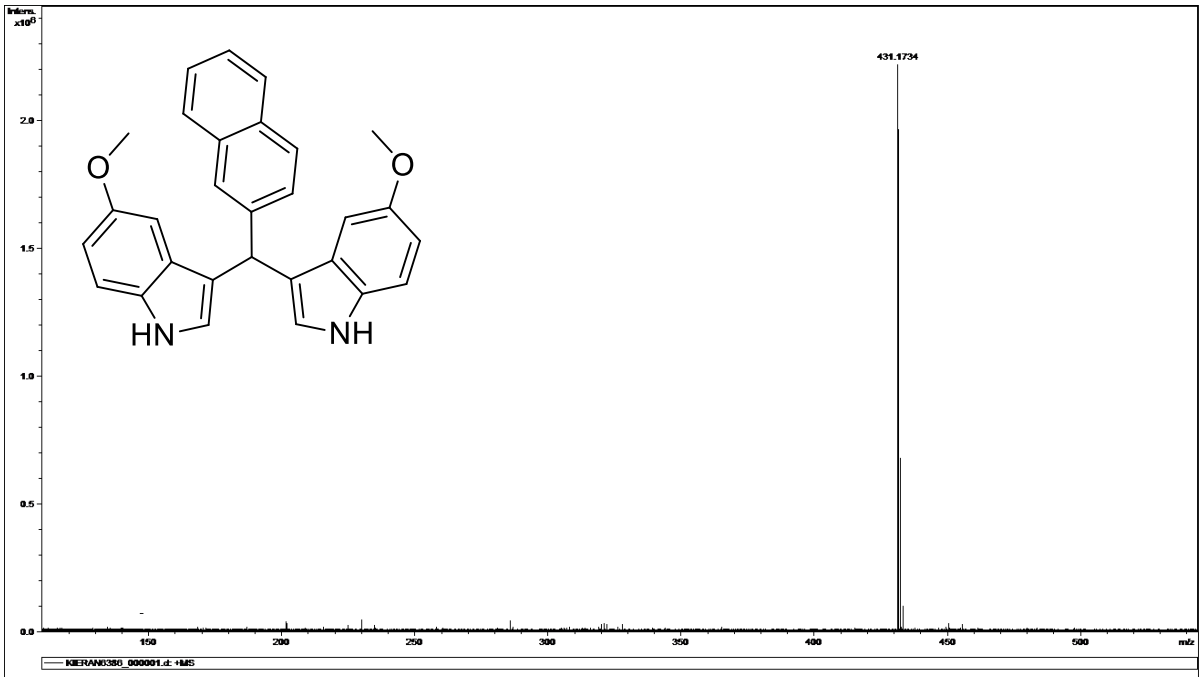

S8.80. ESI-MS of C8al

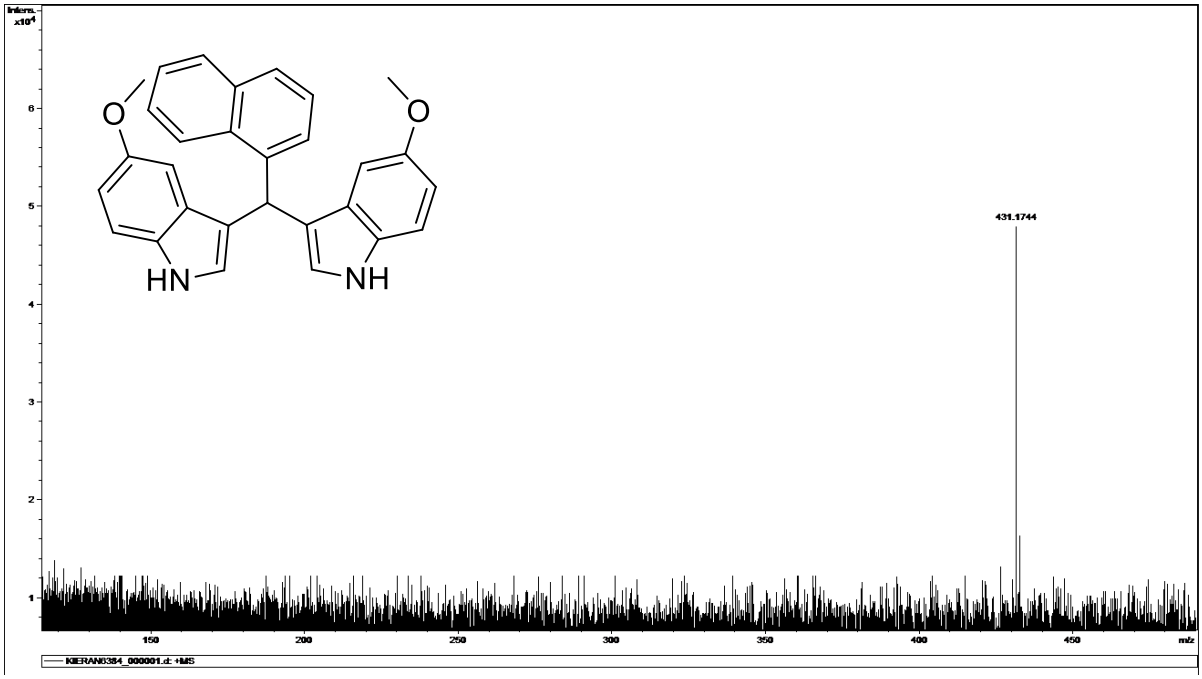

S8.81. ESI-MS of C8am

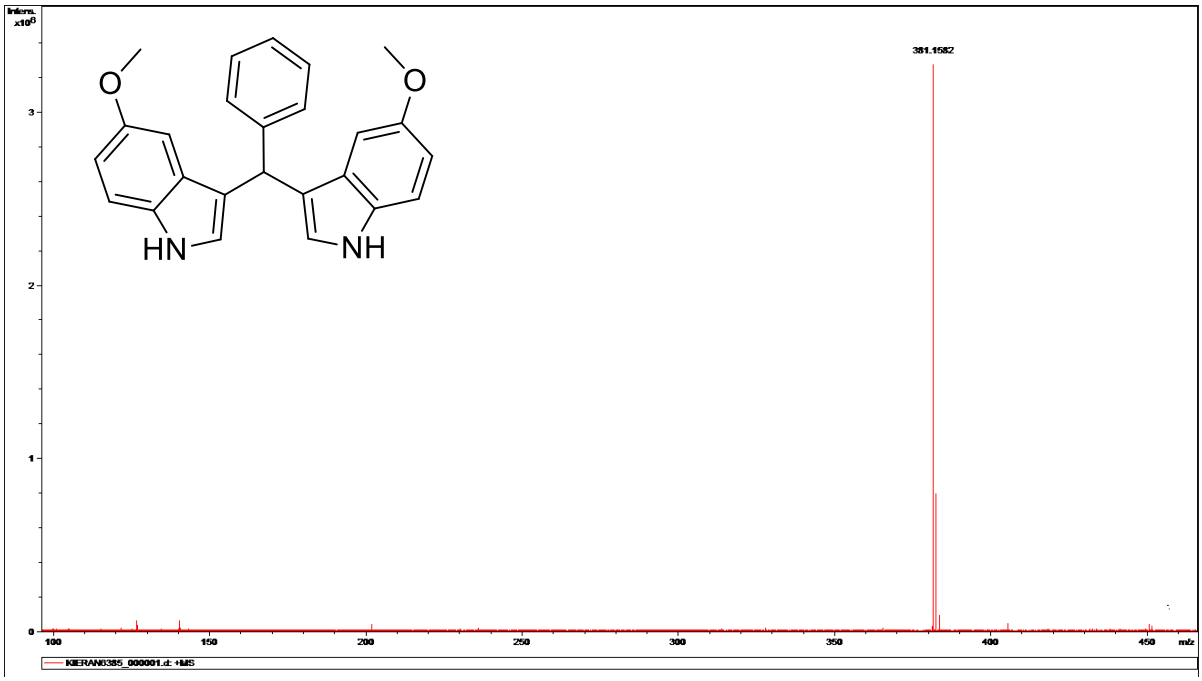

S8.82. ESI-MS of C8aj

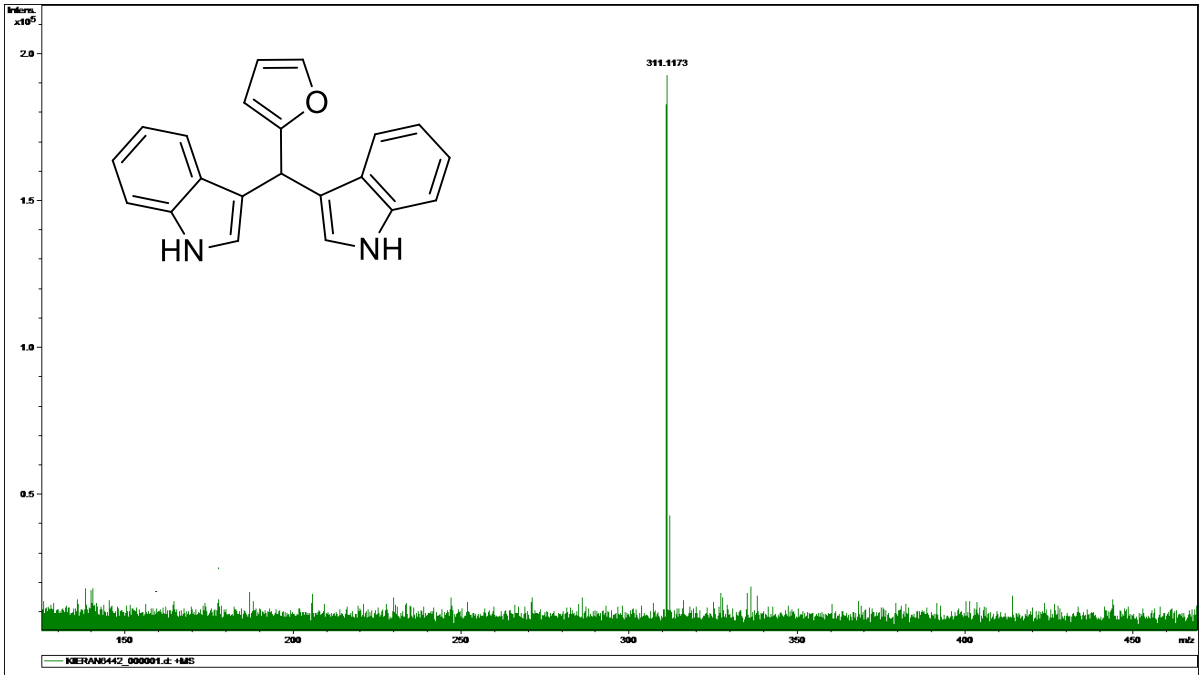

S8.83. ESI-MS of C8ao

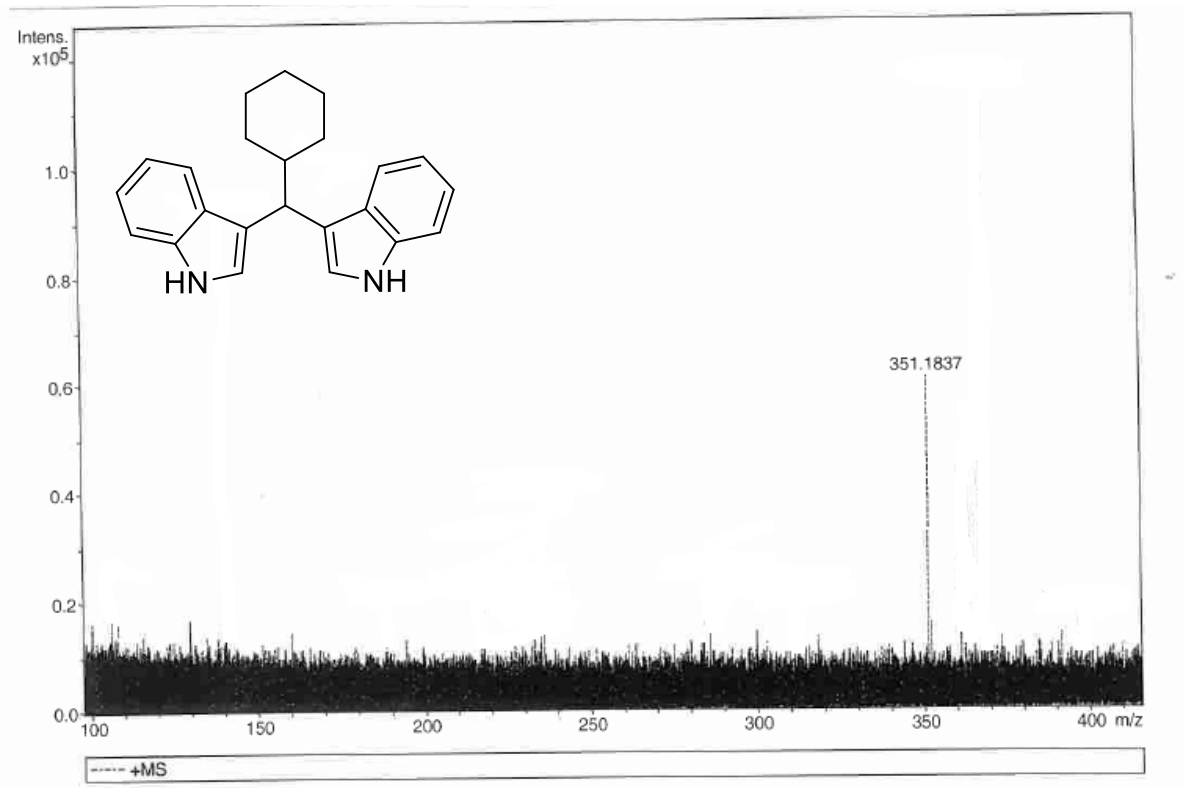

Sum Formula	Sigma	m/z	Err [ppm]	Mean Err [ppm]	Err [mDa]	rdb	N Rule	e⁻
C 23 H 24 N 2 Na 1	0.019	351.1832	-1.38	-1.63	-0.57	12.50	ok	even

S8.84. ESI-MS of C8as

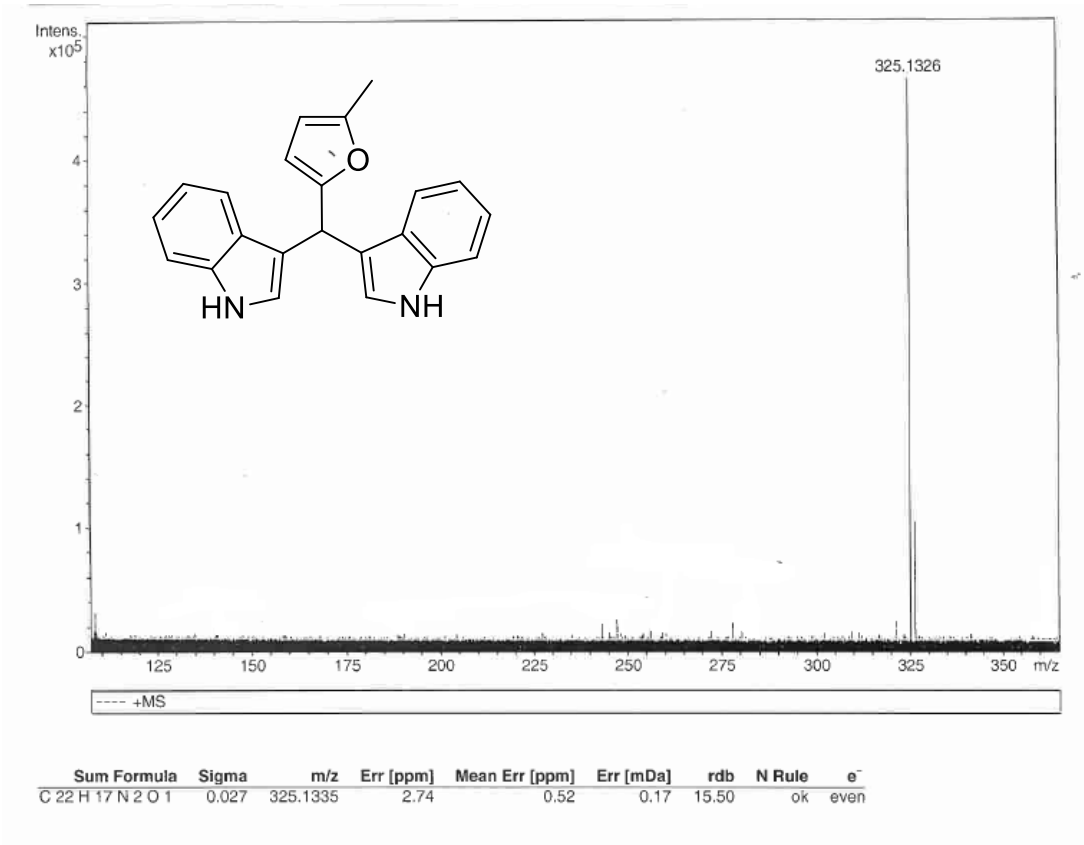

Sum Formula	Sigma	m/z	Err [ppm]	Mean Err [ppm]	Err [mDa]	rdb	N Rule	e⁻
C 22 H 17 N 2 O 1	0.027	325.1335	2.74	0.52	0.17	15.50	ok	even

S8.85. ESI-MS of C8ag

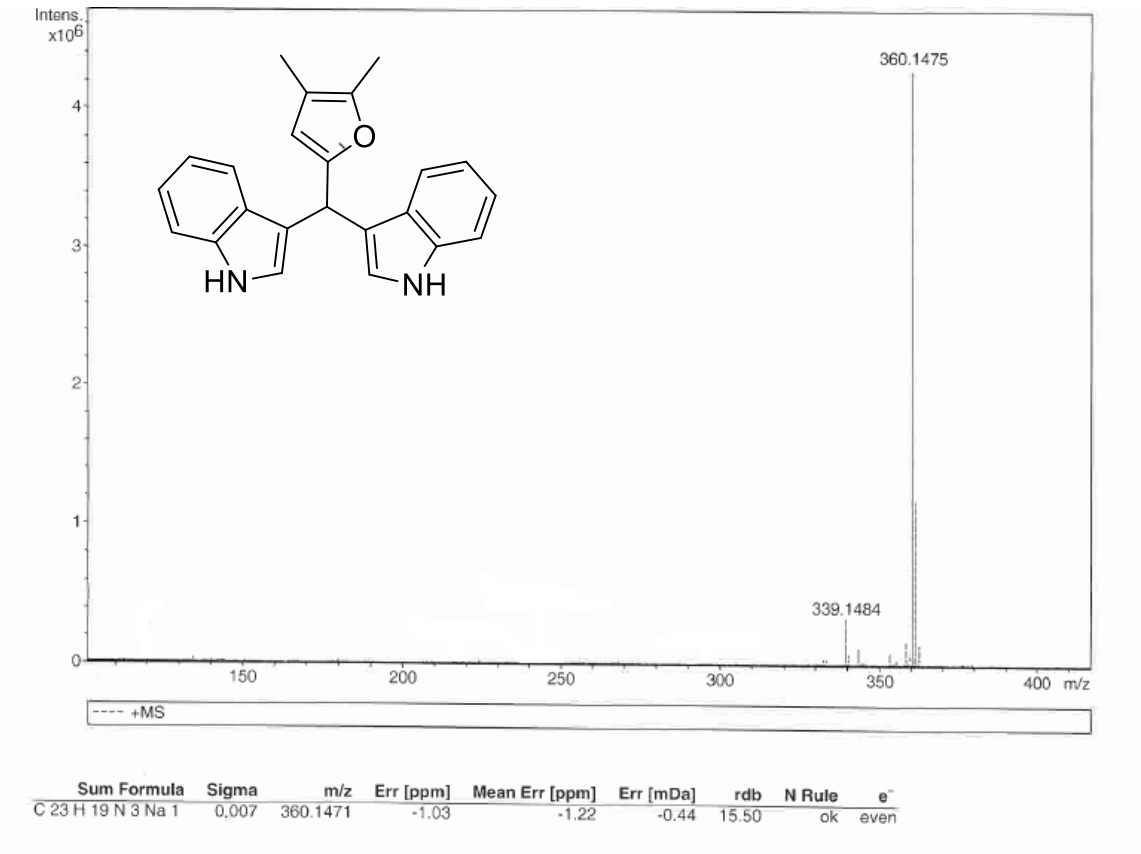

Sum Formula	Sigma	m/z	Err [ppm]	Mean Err [ppm]	Err [mDa]	rdb	N Rule	e⁻
C 23 H 19 N 3 Na 1	0.007	360.1471	-1.03	-1.22	-0.44	15.50	ok	even

S8.86. ESI-MS of C8ah

8.9 ^{1}HNMR of C8ba-C8au

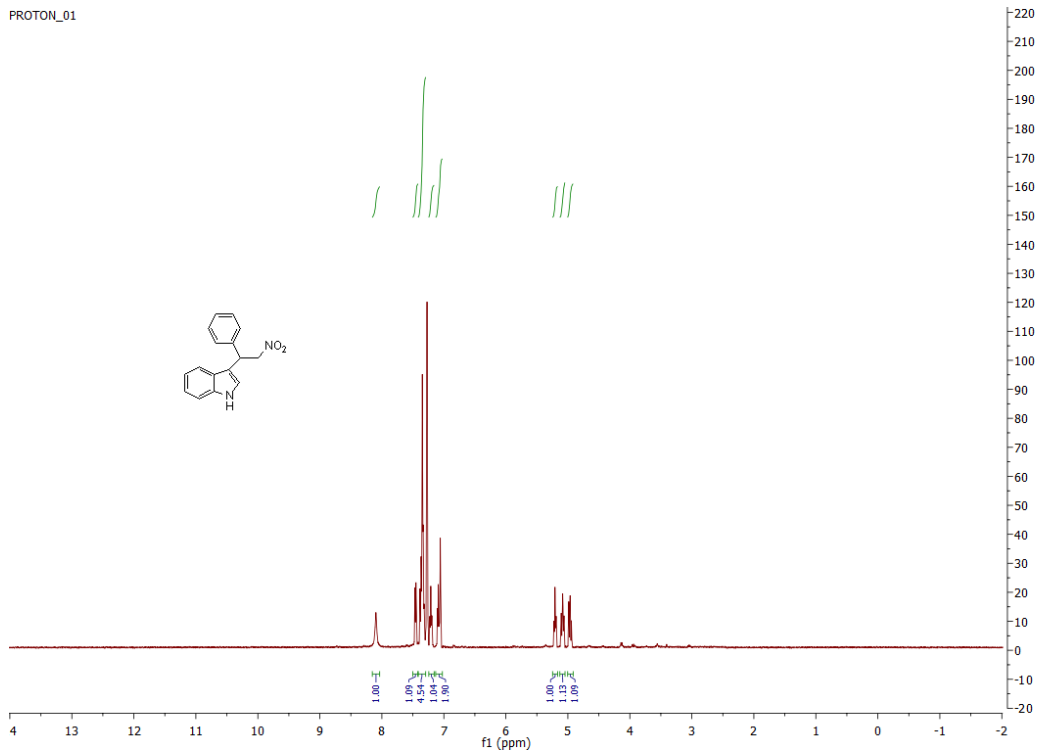

S8.87 ^{1}H NMR of C8ba

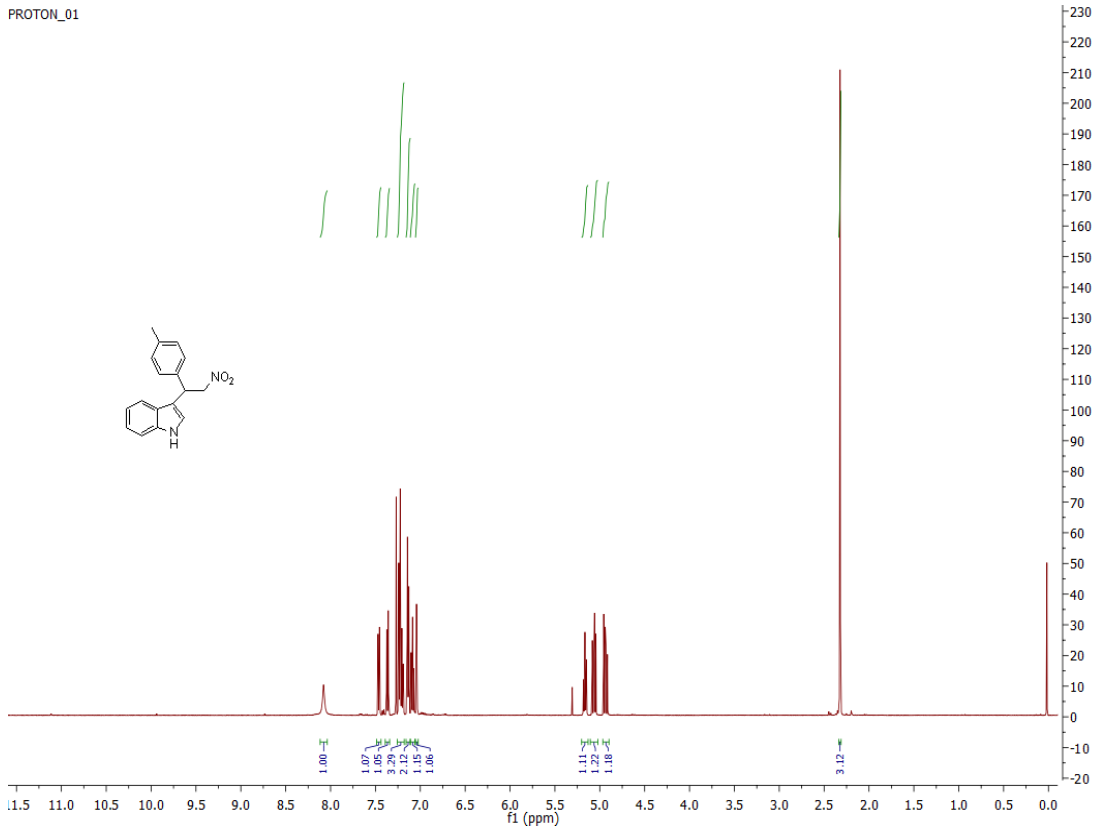

S8.88 ^{1}H NMR of C8bb

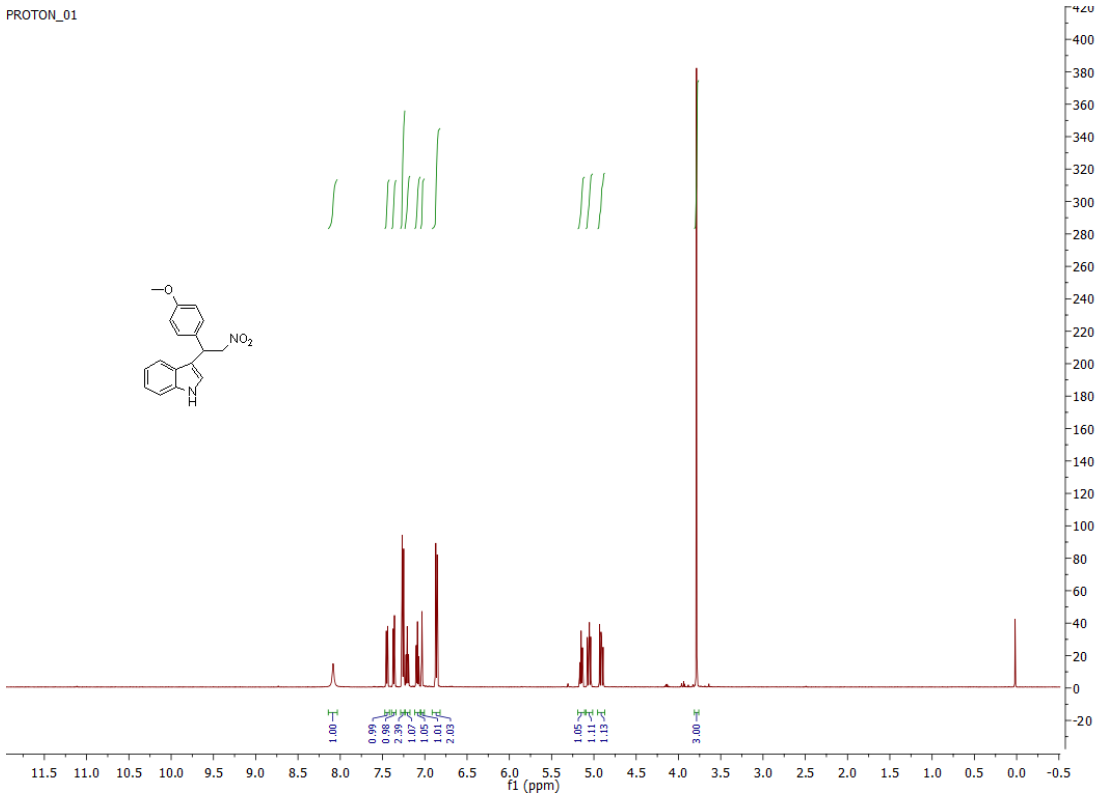

S8.88 ^{1}H NMR of C8bc

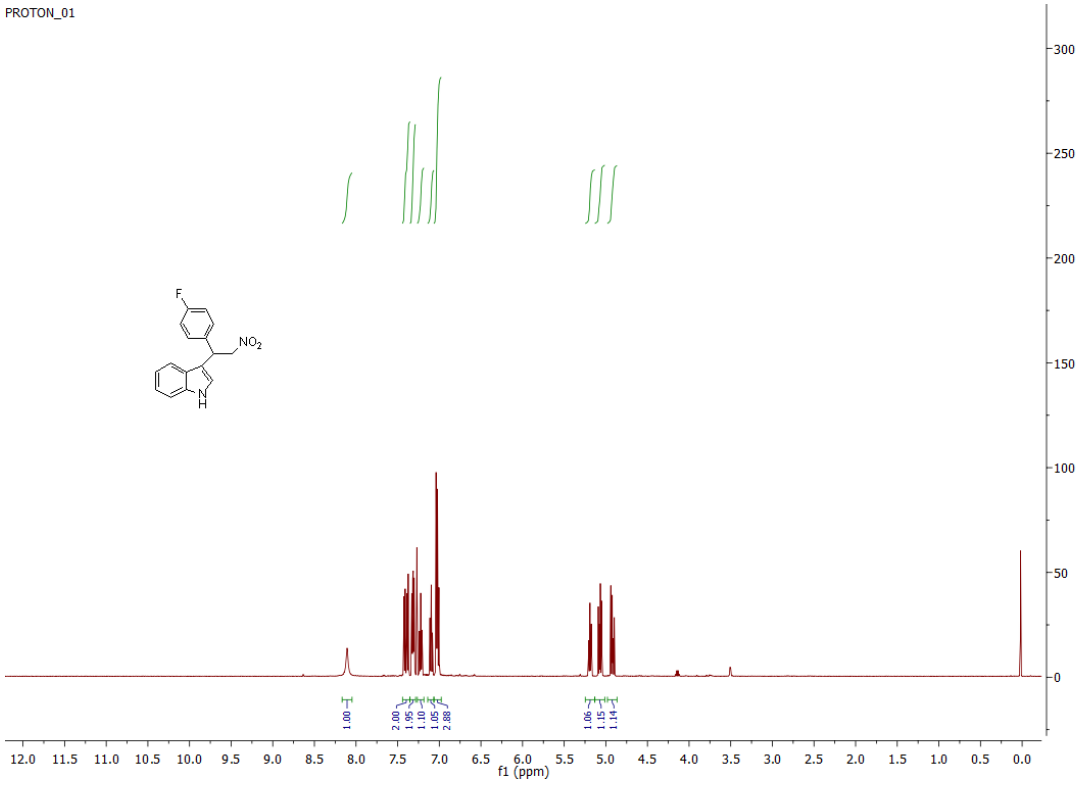

S8.89 ^{1}H NMR of C8bd

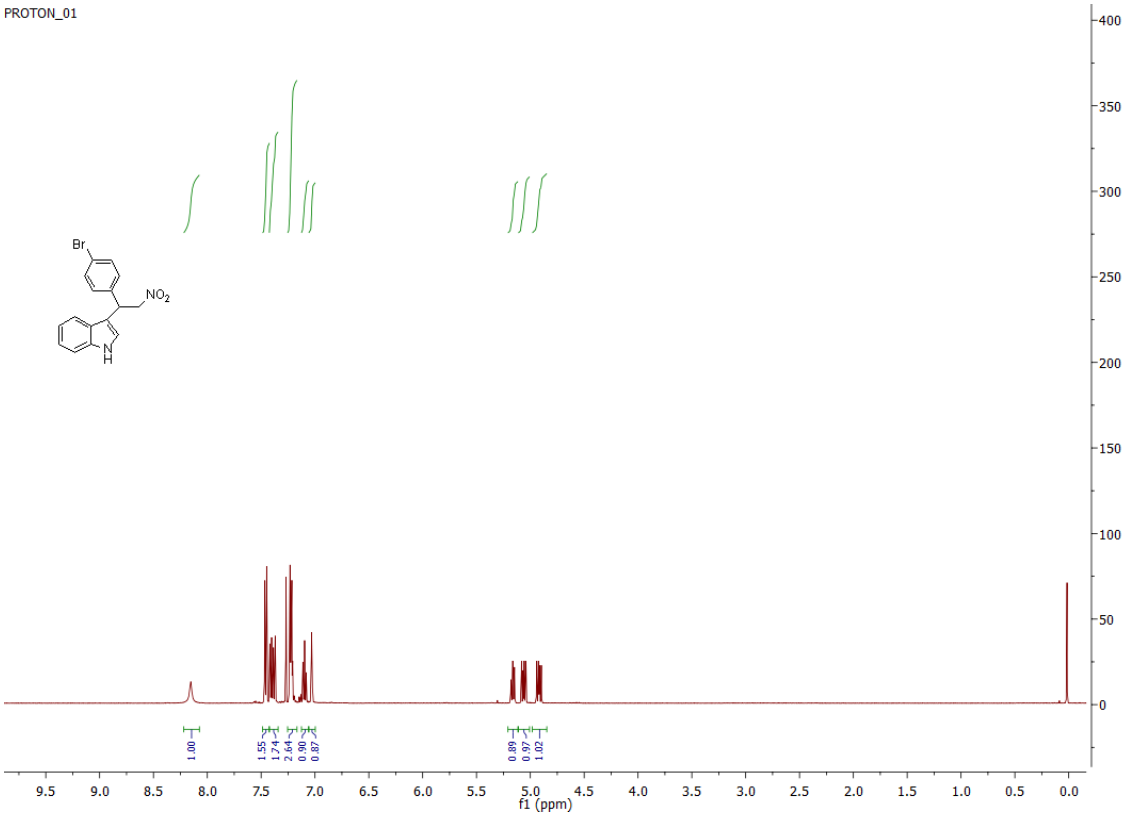

S8.90 ^{1}H NMR of C8be

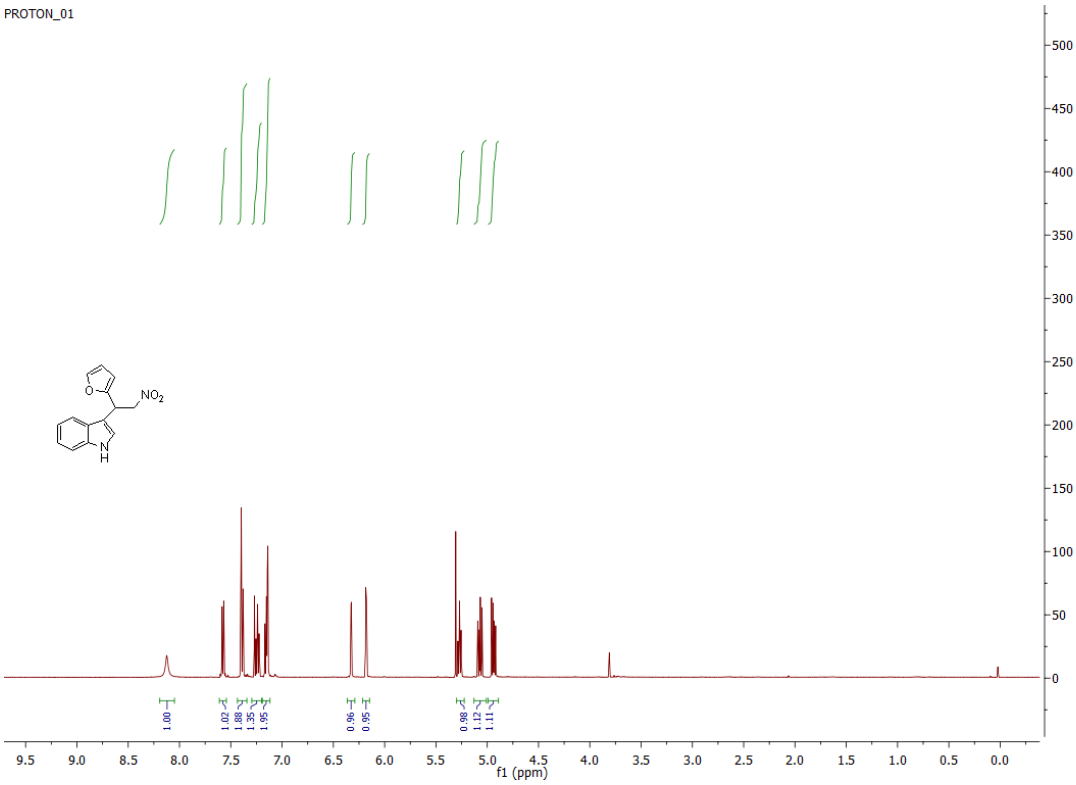

S8.91 ^{1}H NMR of C8bf

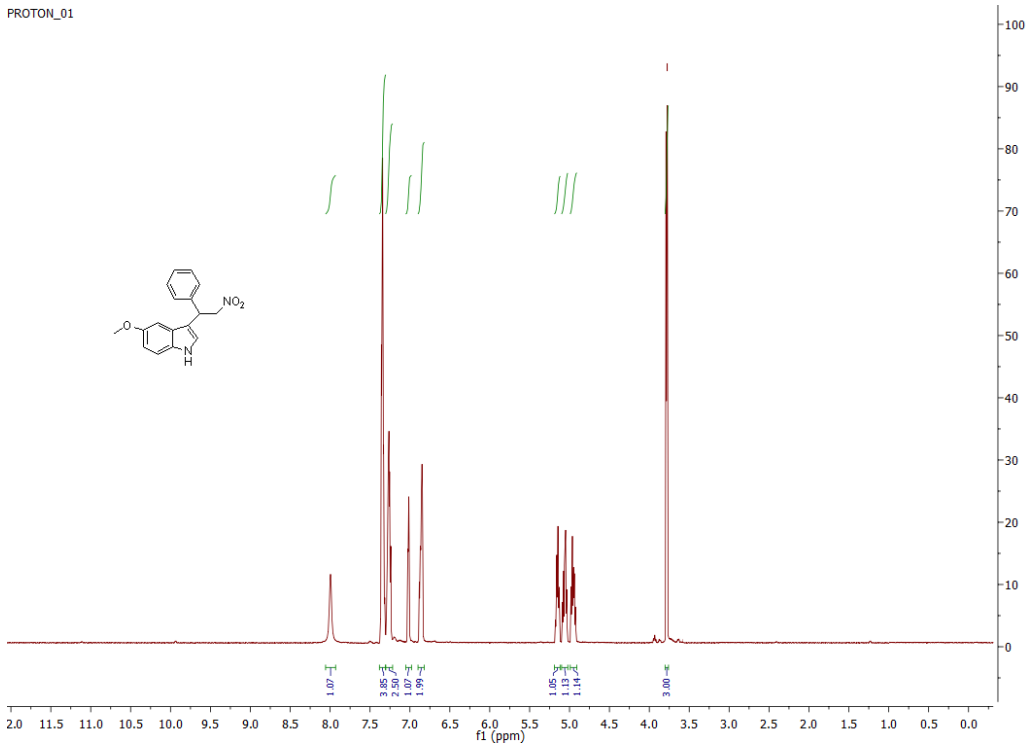

S8.92 ^{1}H NMR of C8bg

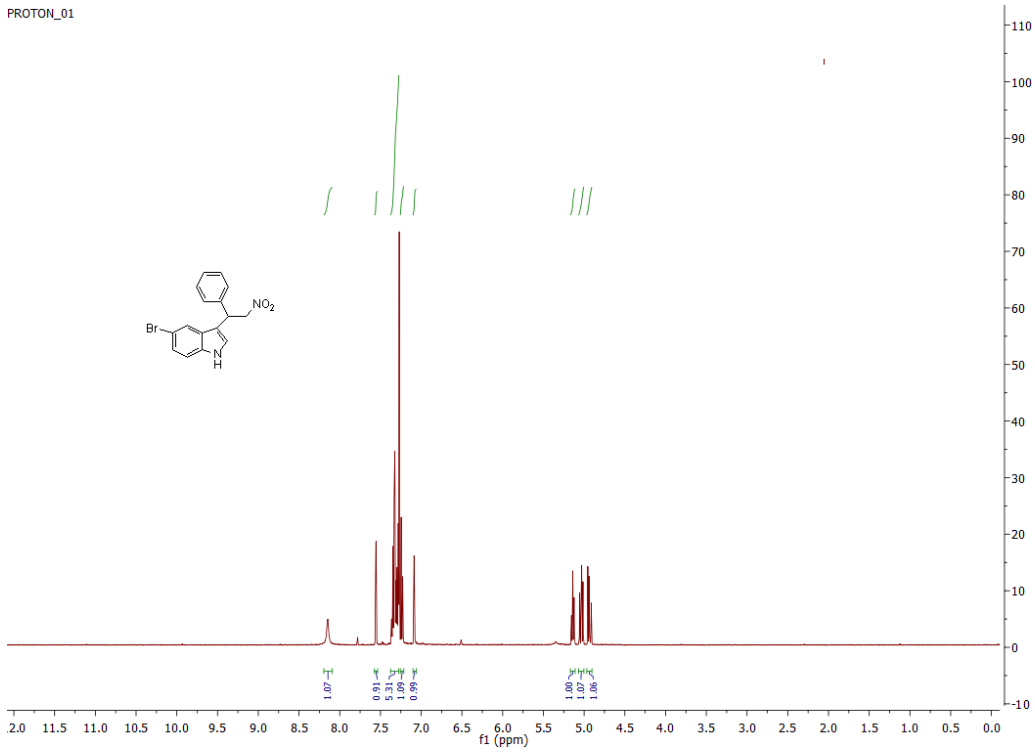

S8.93 ^{1}H NMR of C8bh

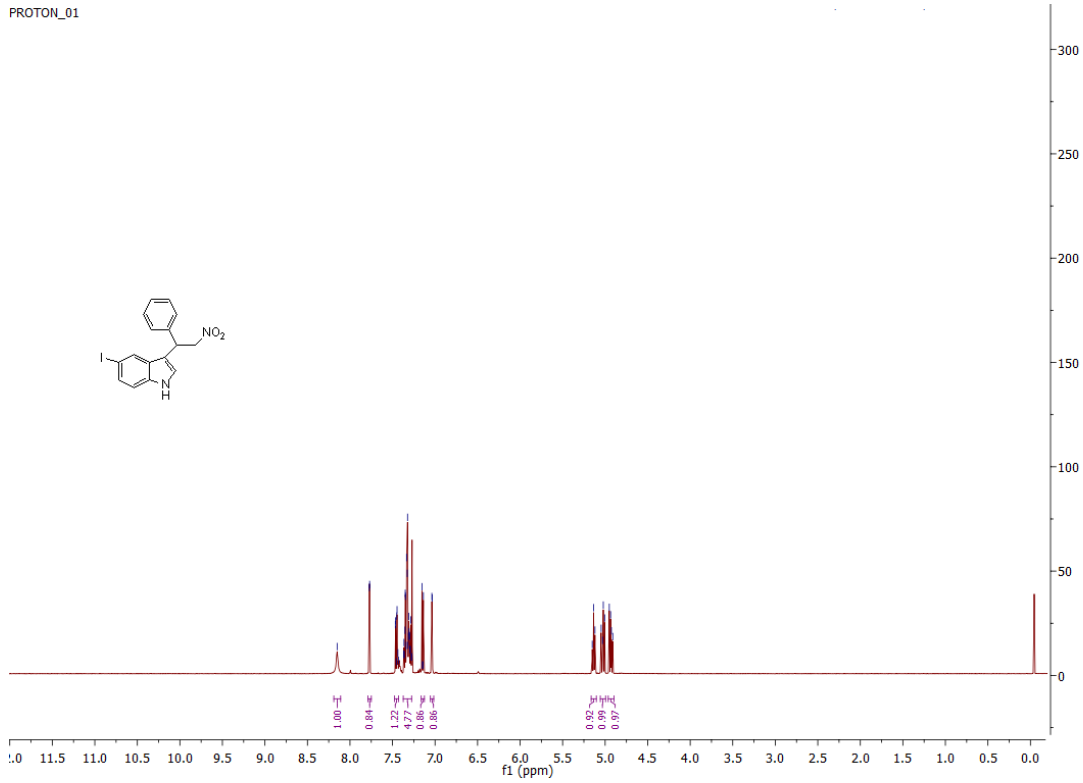

S8.94. ^{1}H NMR of C8bi

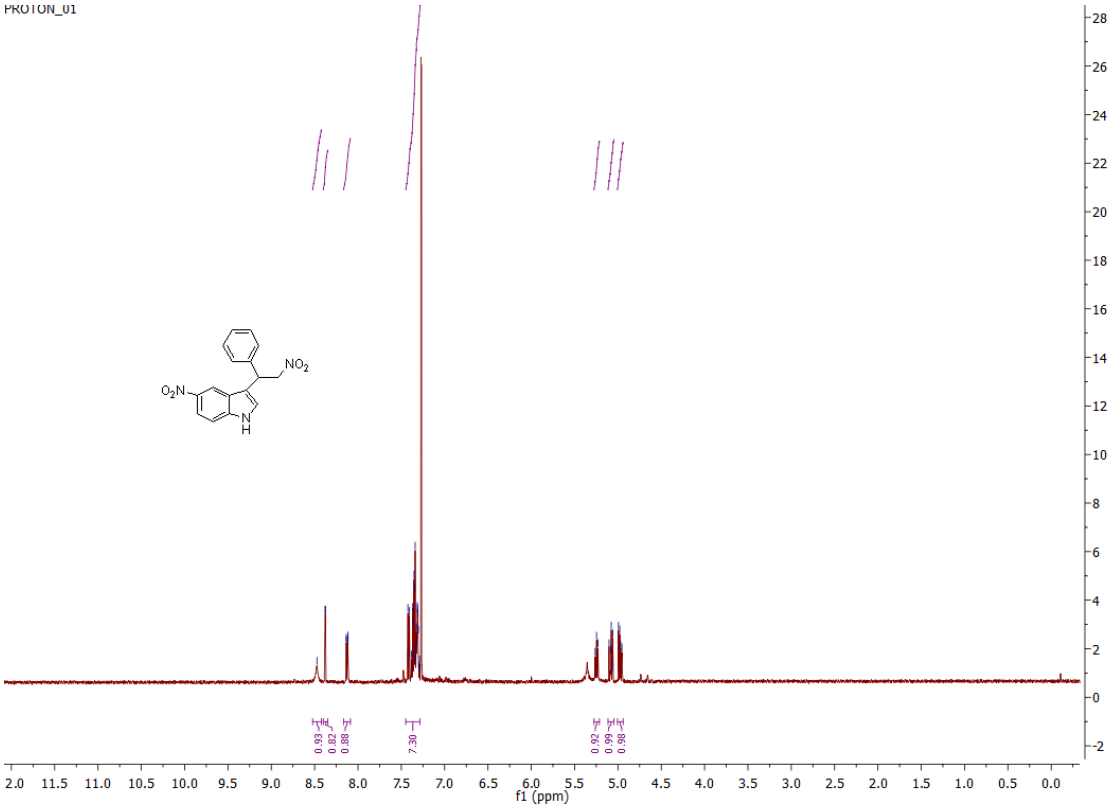

S8.95. ^{1}H NMR of C8bj

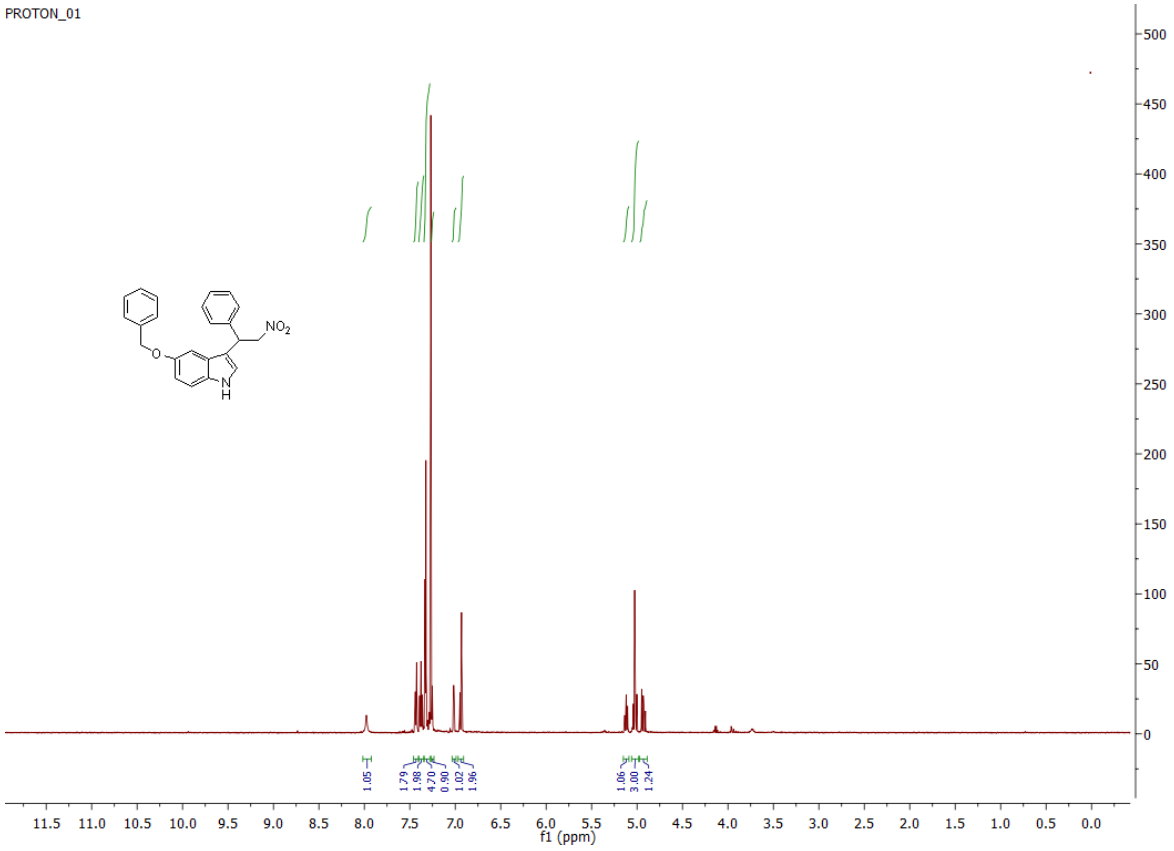

S8.96. ^{1}H NMR of C8bk

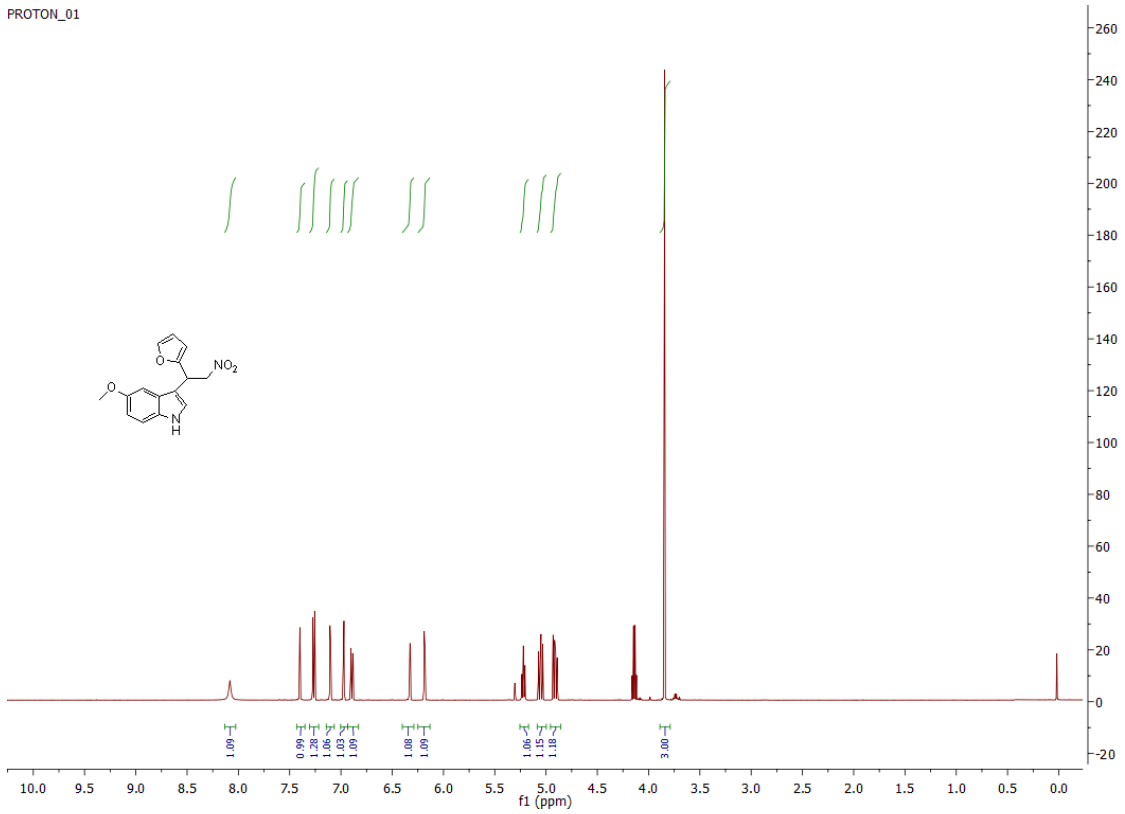

S8.97. ^{1}H NMR of C8bi

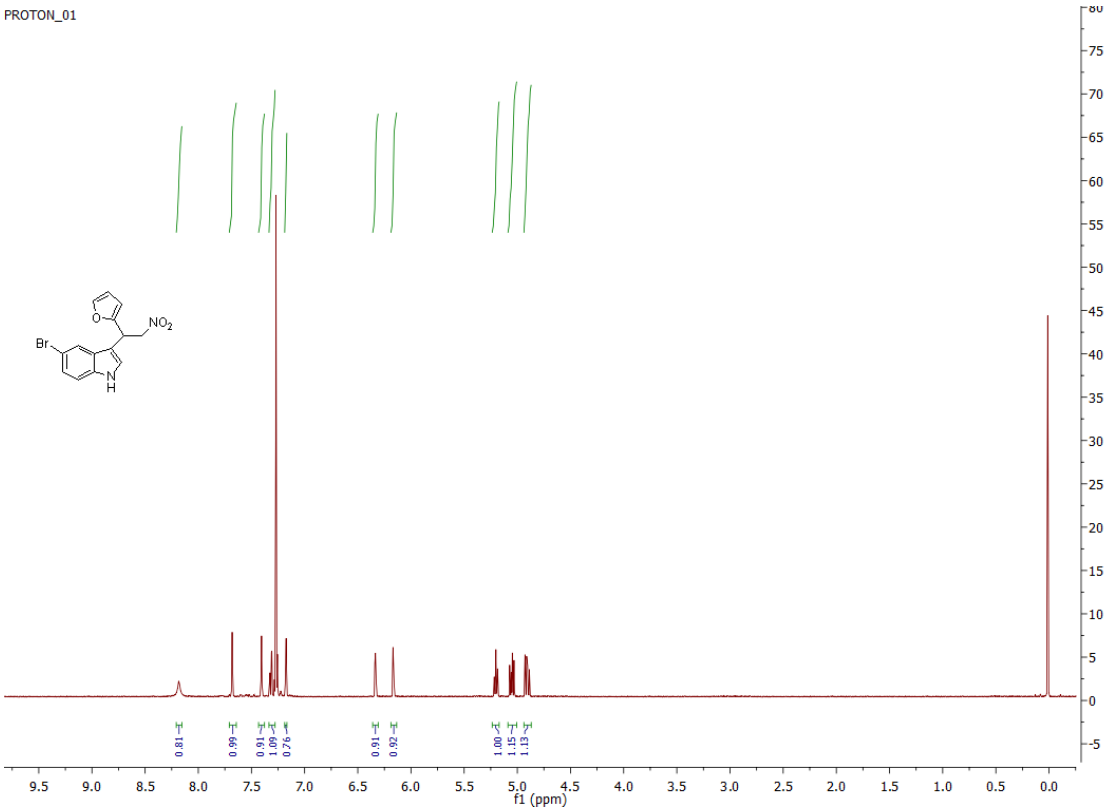

S8.98. ^{1}H NMR of C8bm

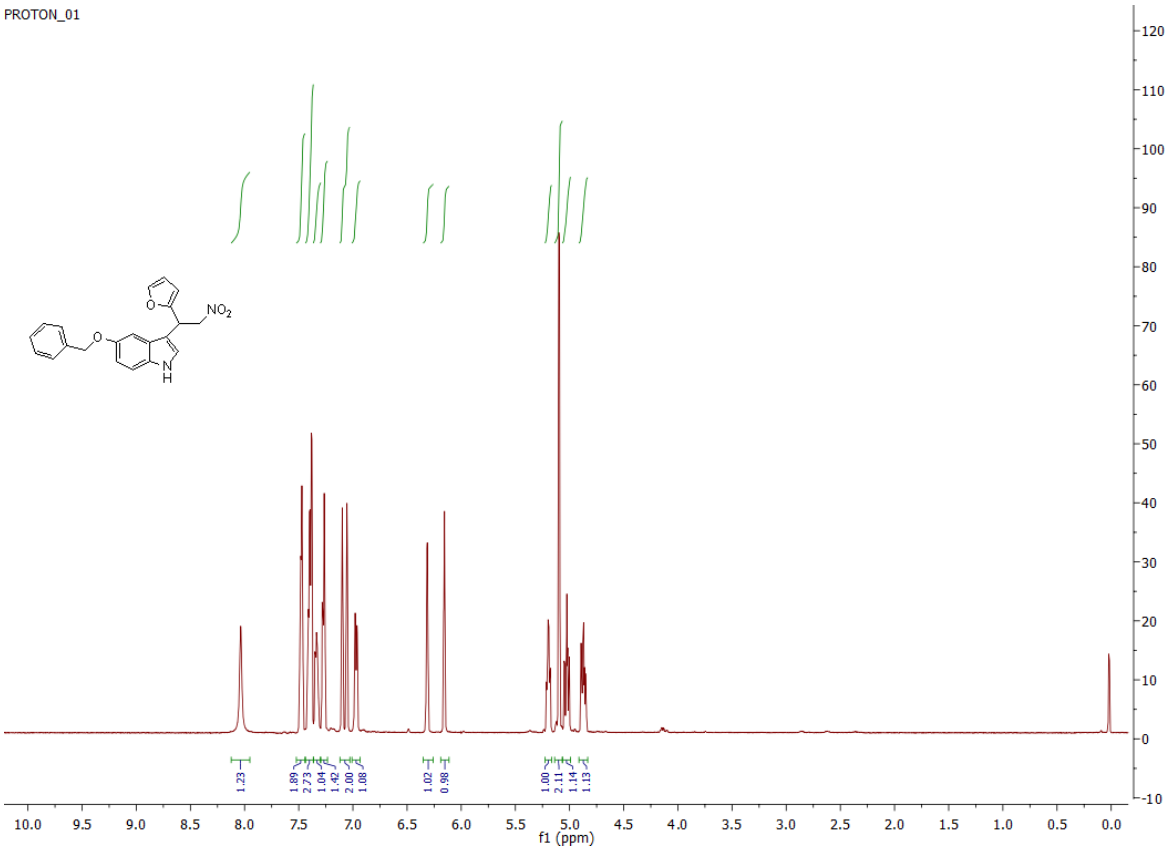

S8.99. ^{1}H NMR of C8bn

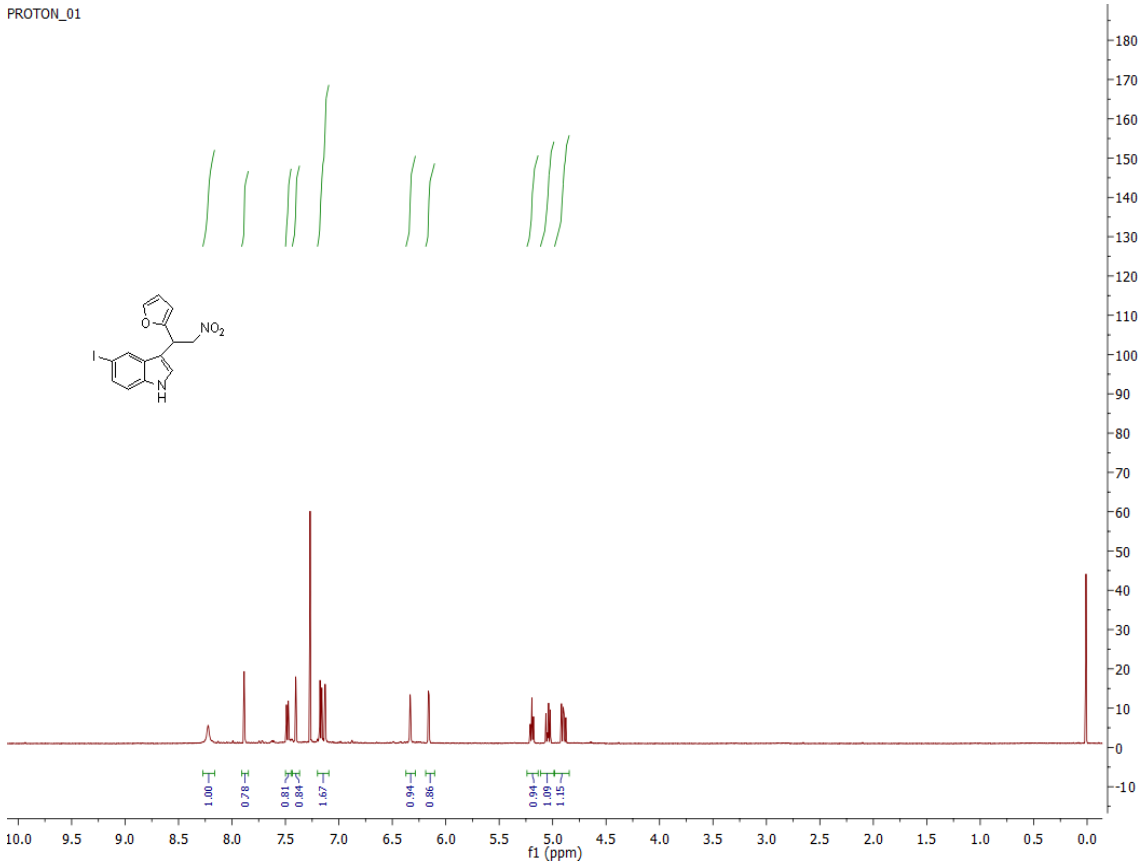

S8.100. ^{1}H NMR of C8bo

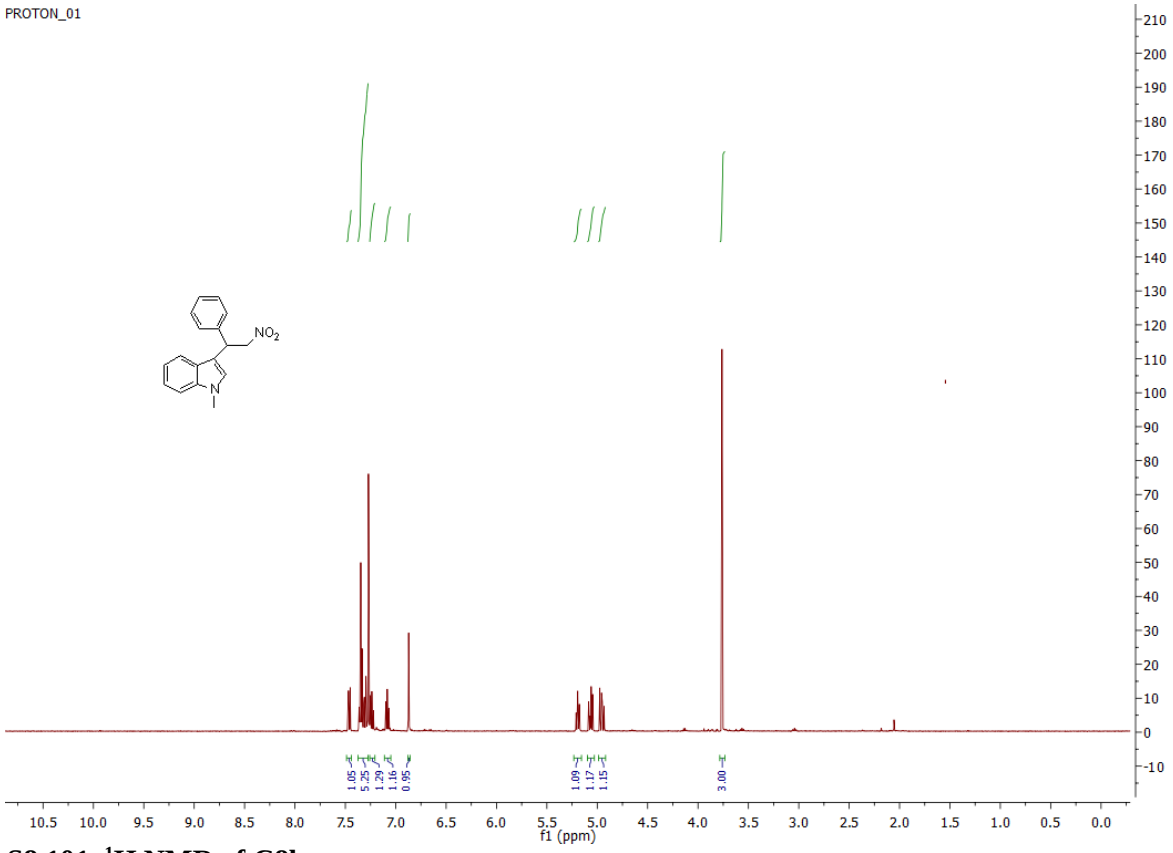

S8.101. ^{1}H NMR of C8bp

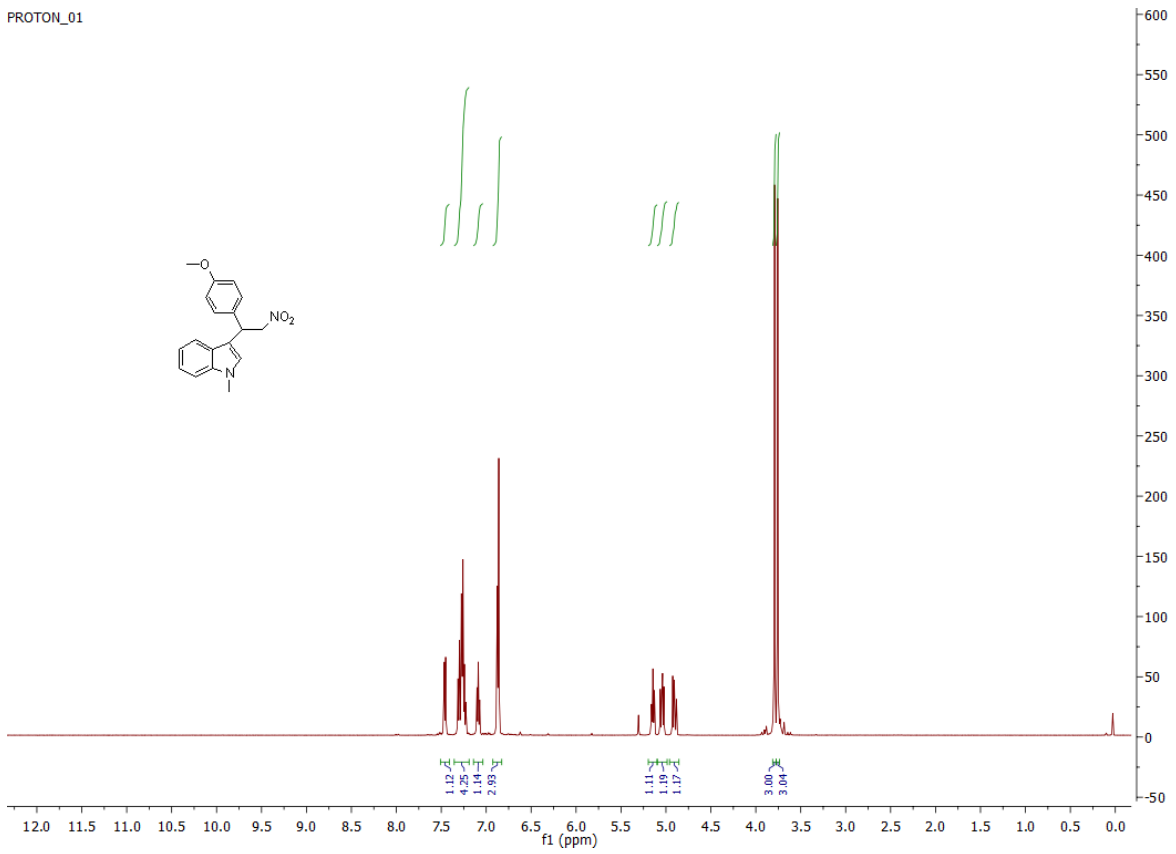

S8.102. ^{1}H NMR of C8bq

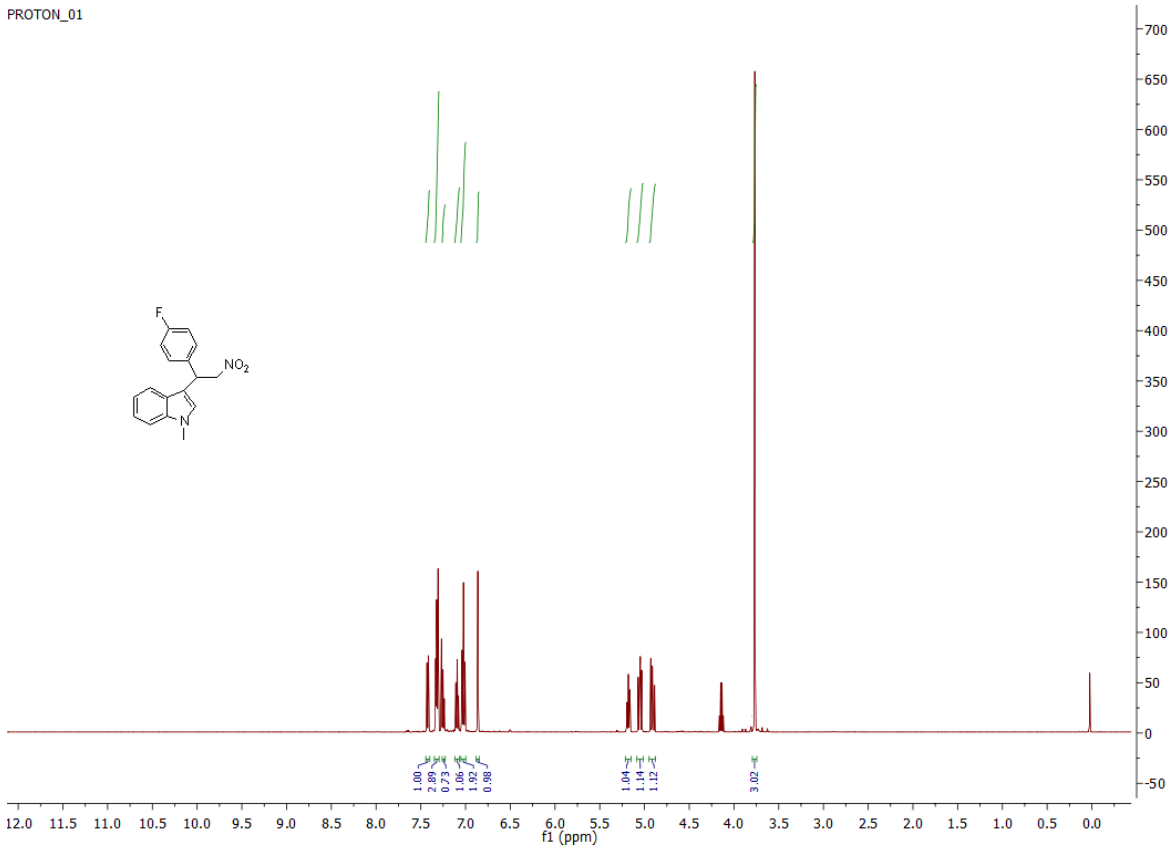

S8.103. ^{1}H NMR of C8br

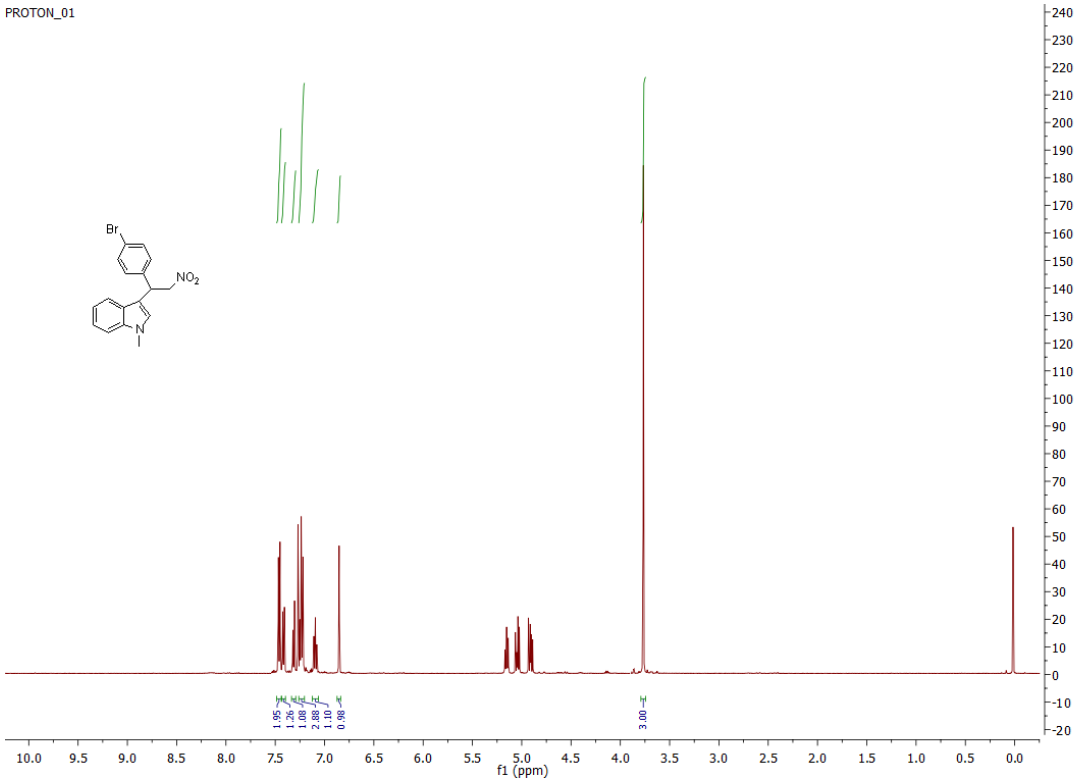

S8.104. ^{1}H NMR of C8bs

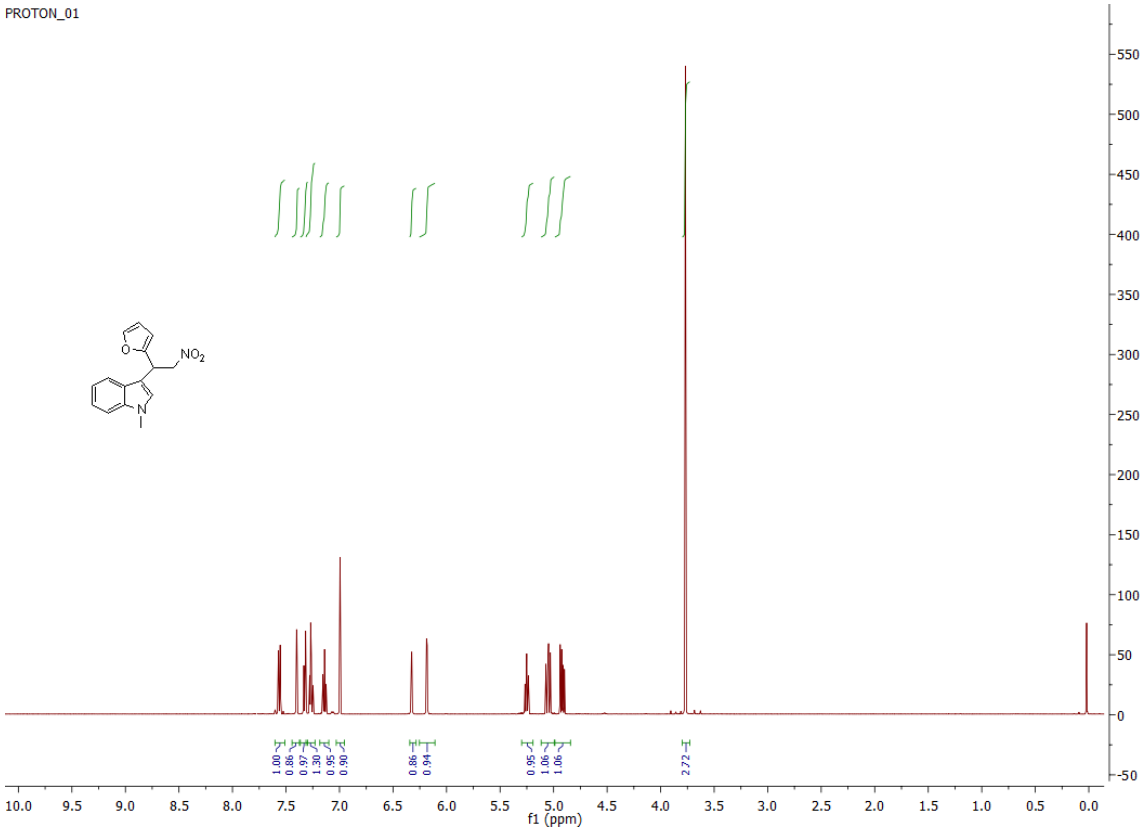

S8.105. ^{1}H NMR of C8bt

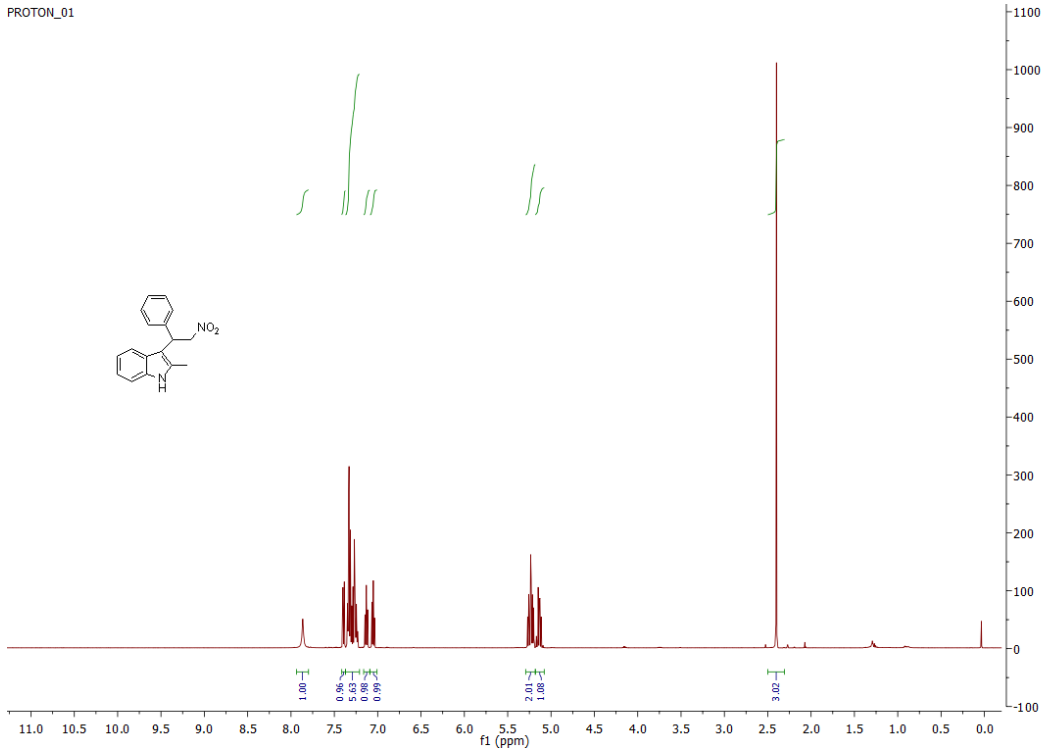

S8.106. ^{1}H NMR of C8bu

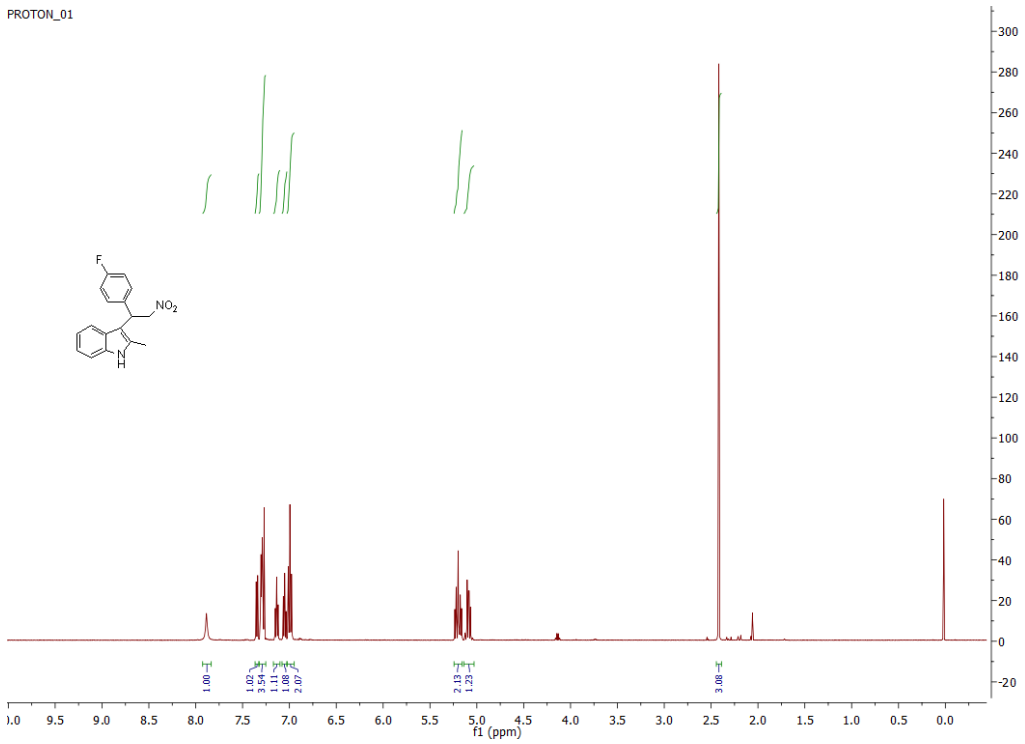

S8.107. ^{1}H NMR of C8bv

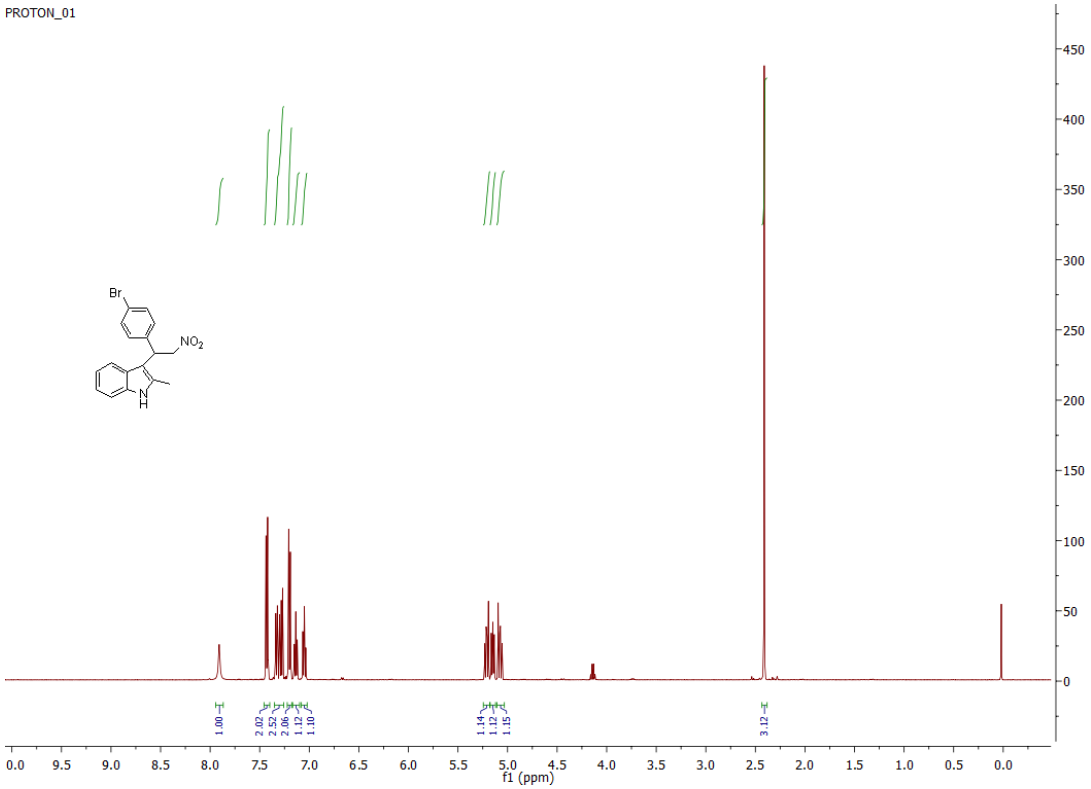

S8.108. ^{1}H NMR of C8bw

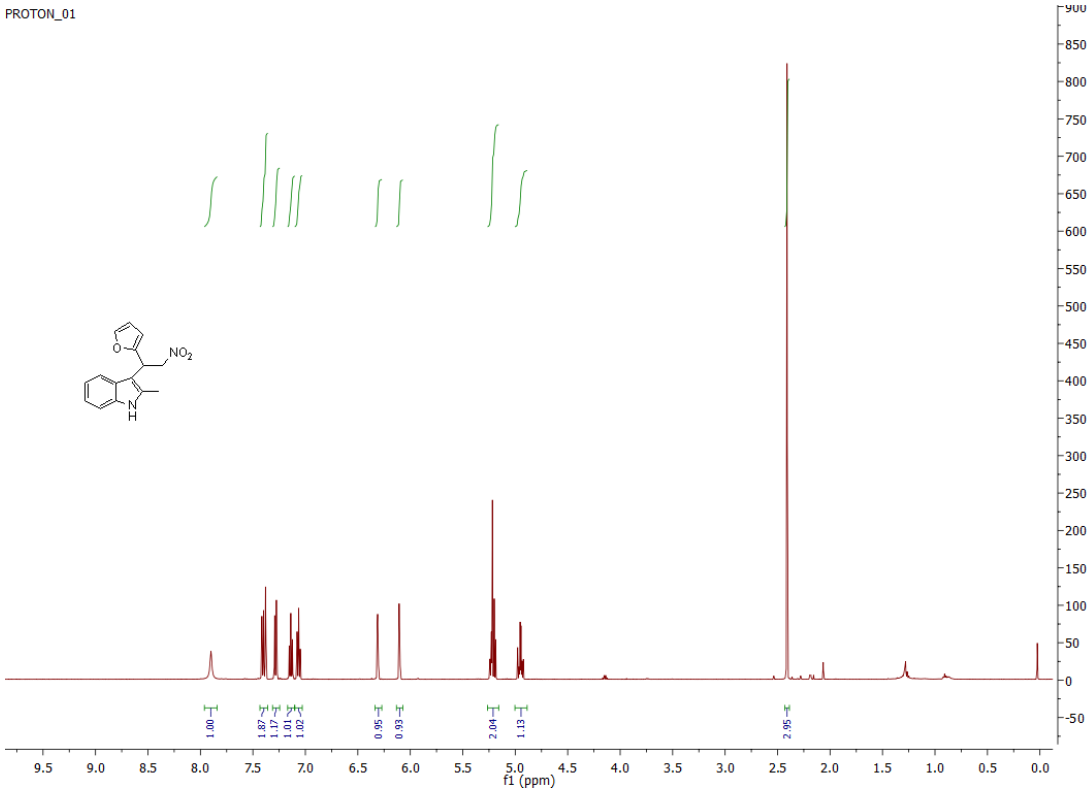

S8.109. ^{1}H NMR of C8bx

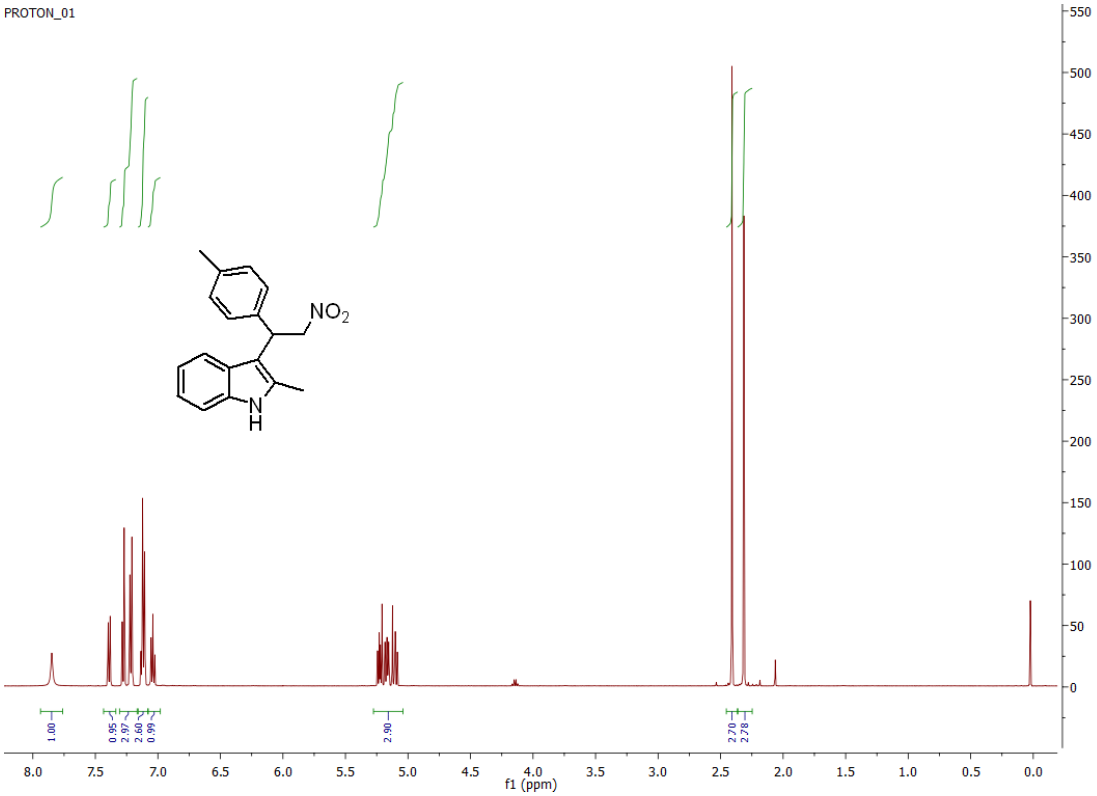

S8.110. ^{1}H NMR of C8by

8.10 ^{13}CNMR of C8ba-C8au

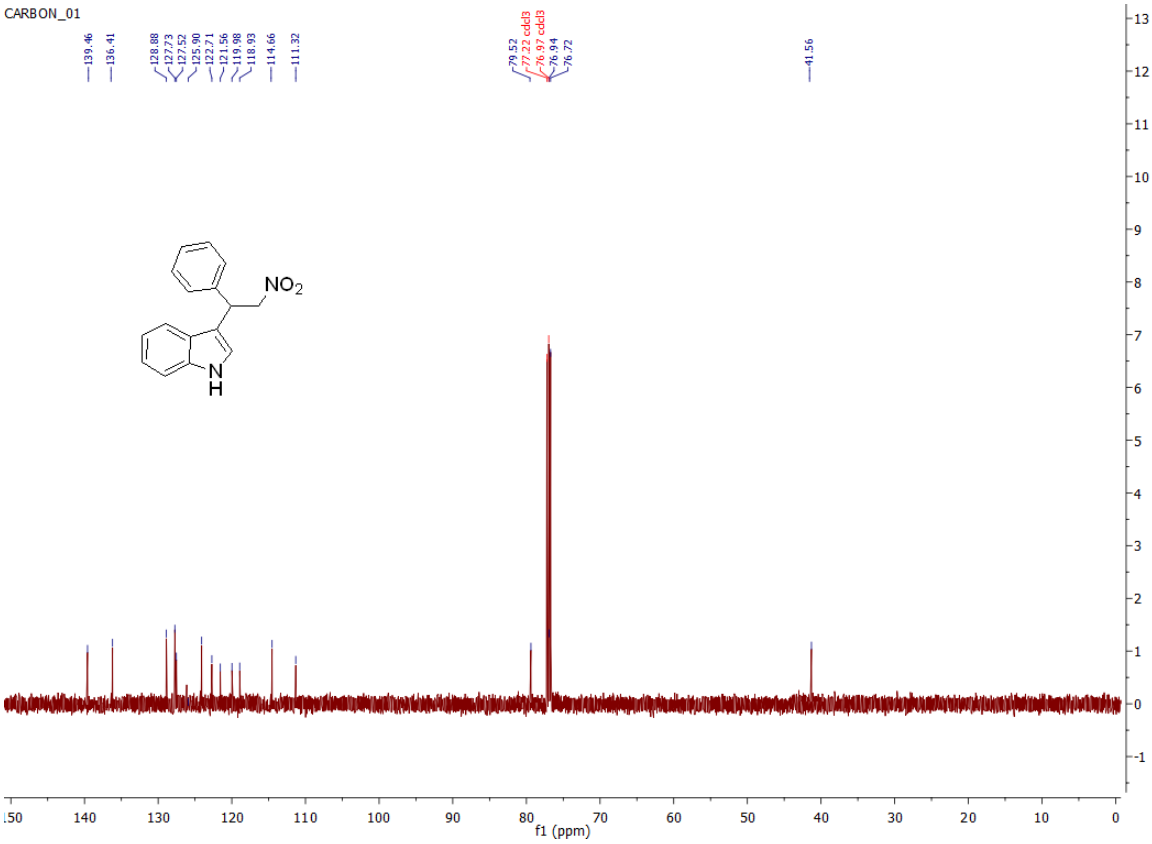

S8.111. ^{13}C NMR of C8ba

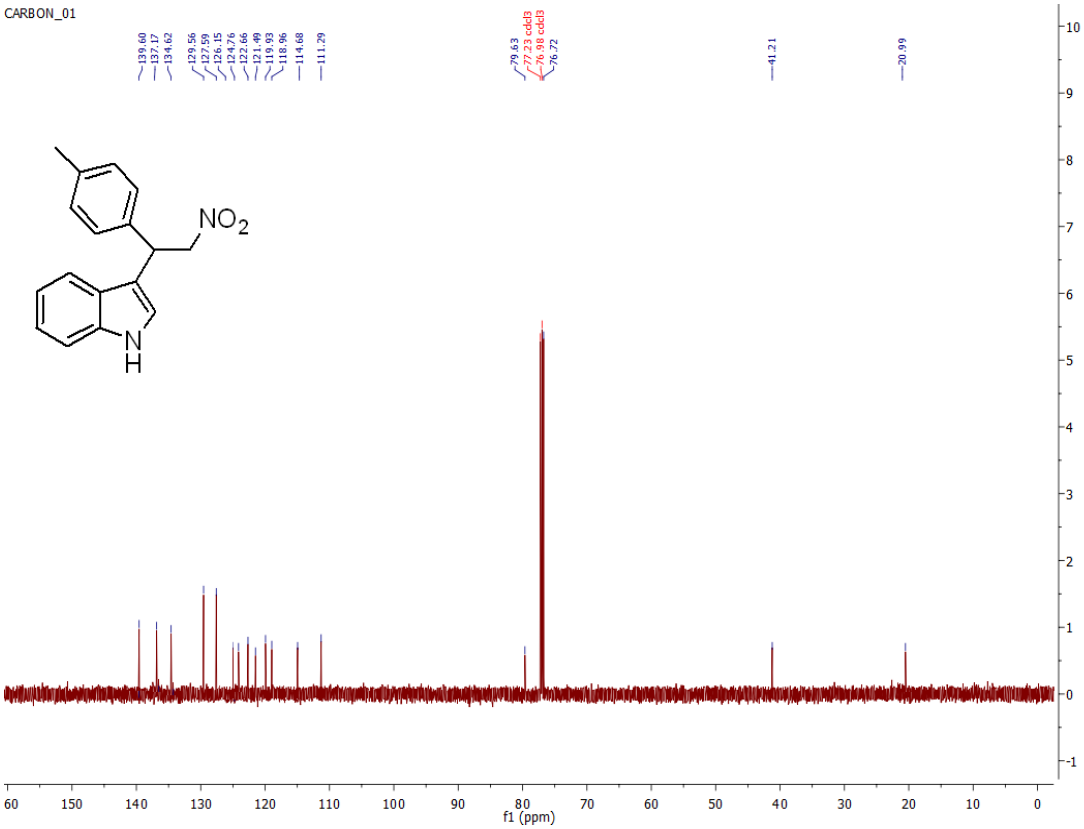

S8.112. ^{13}C NMR of C8bb

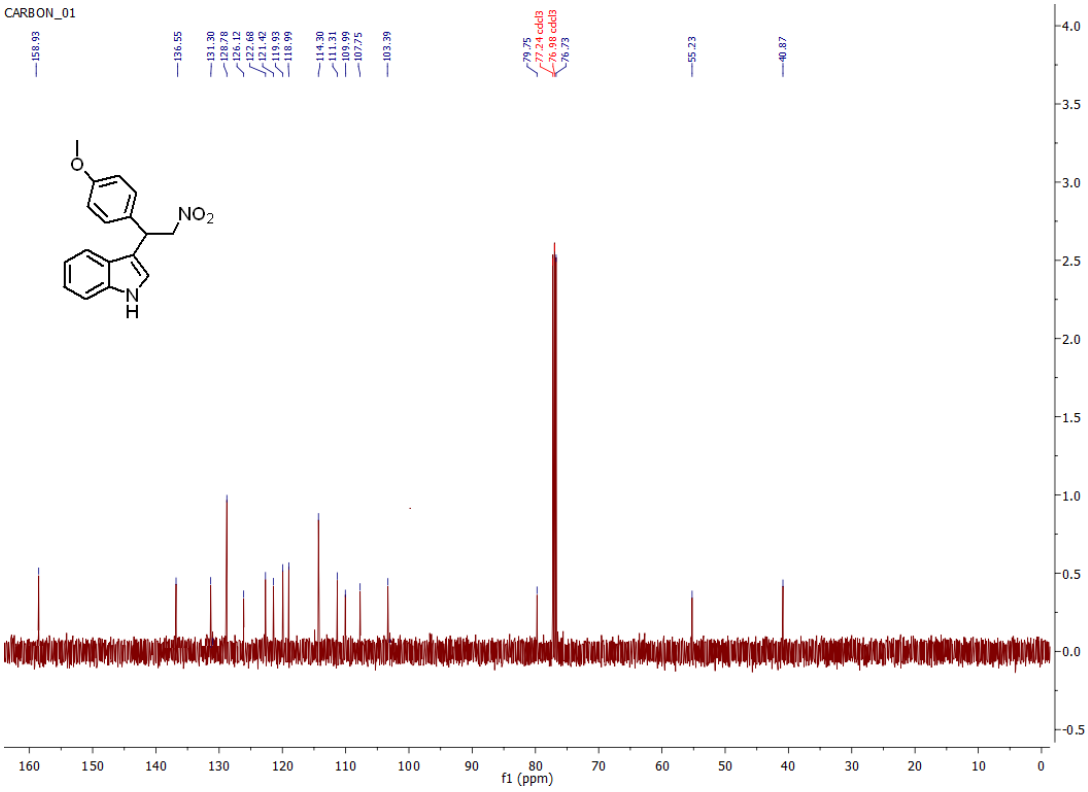

S8.113. ^{13}C NMR of C8bc

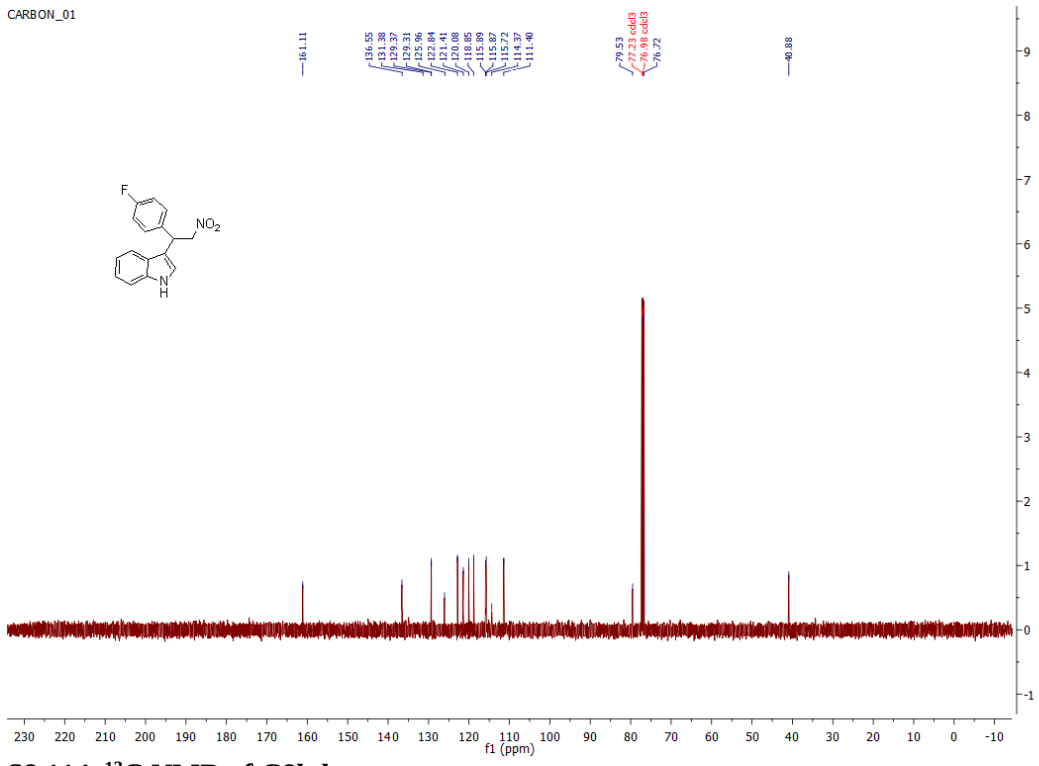

S8.114. ^{13}C NMR of C8bd

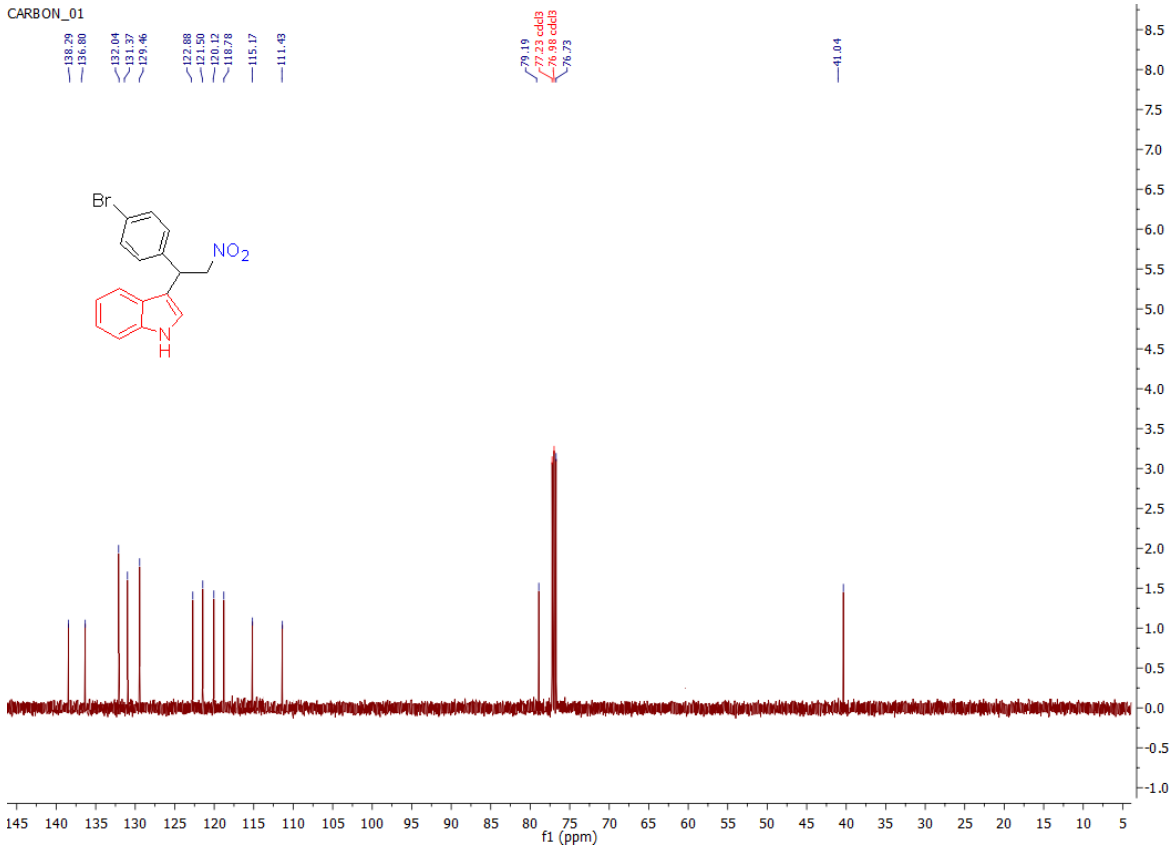

S8.115. ^{13}C NMR of C8be

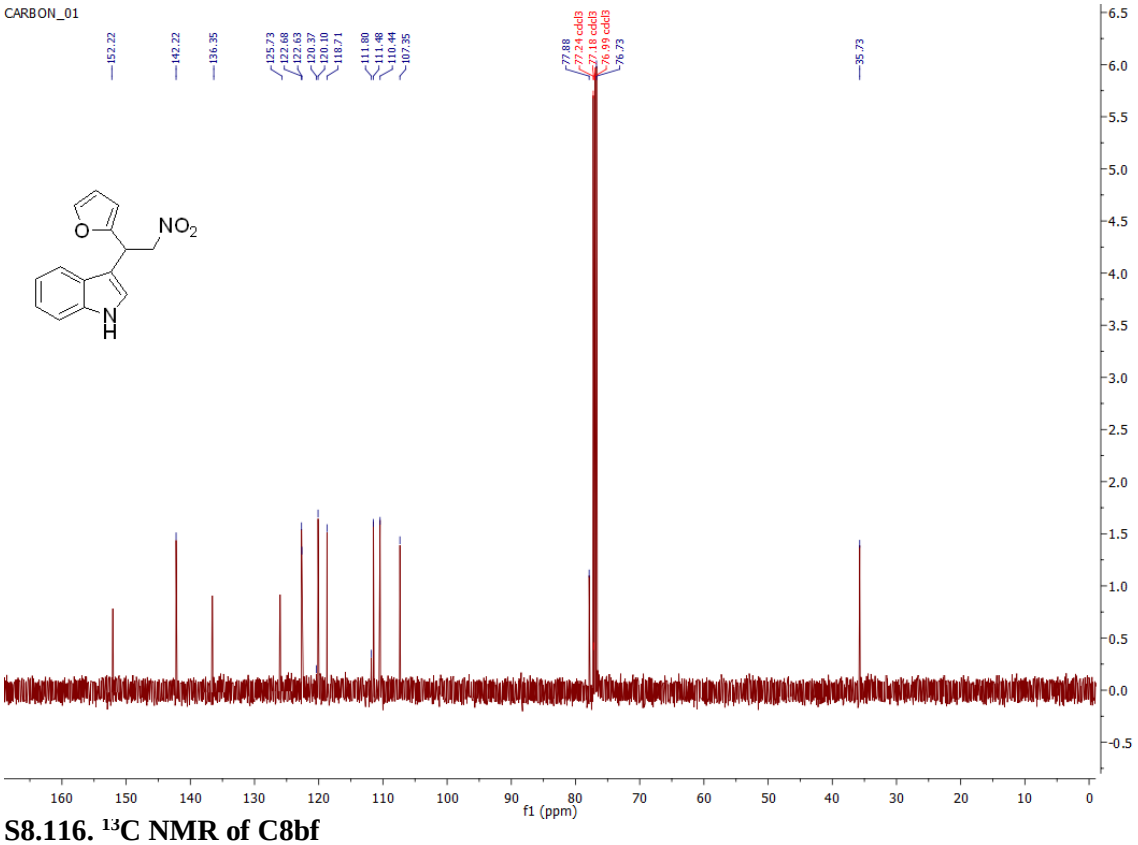

S8.116. ^{13}C NMR of C8bf

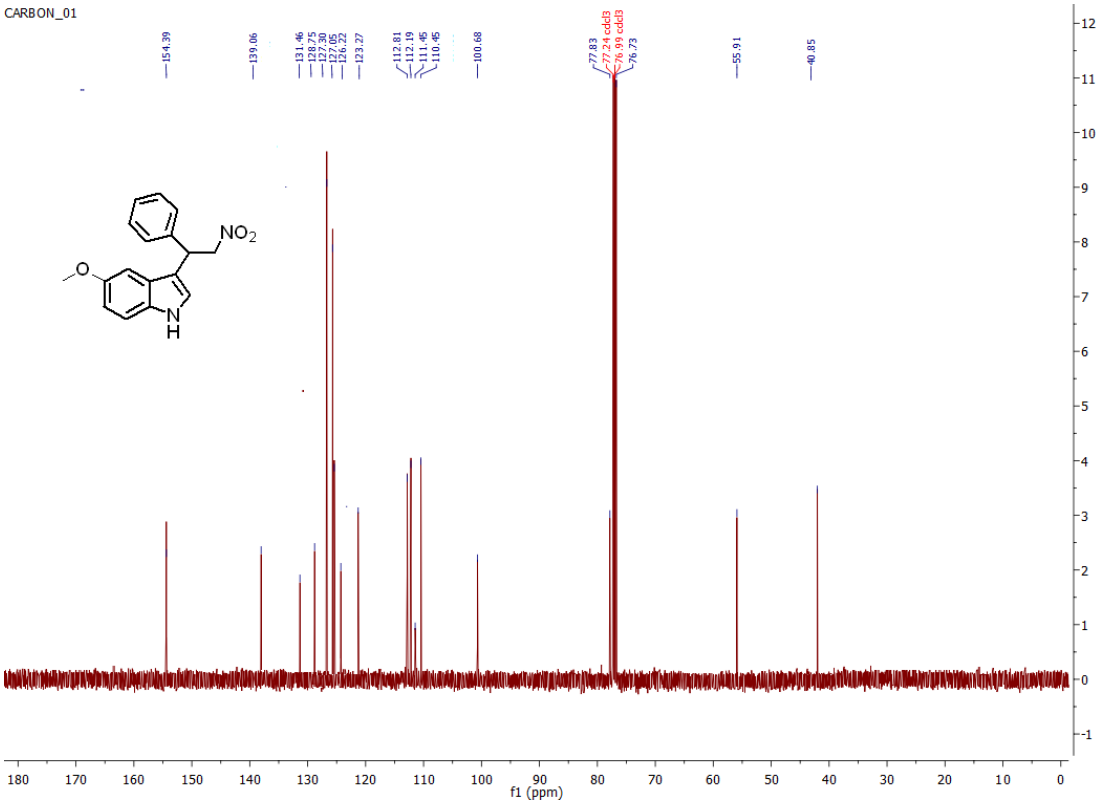

S8.117. ^{13}C NMR of C8bg

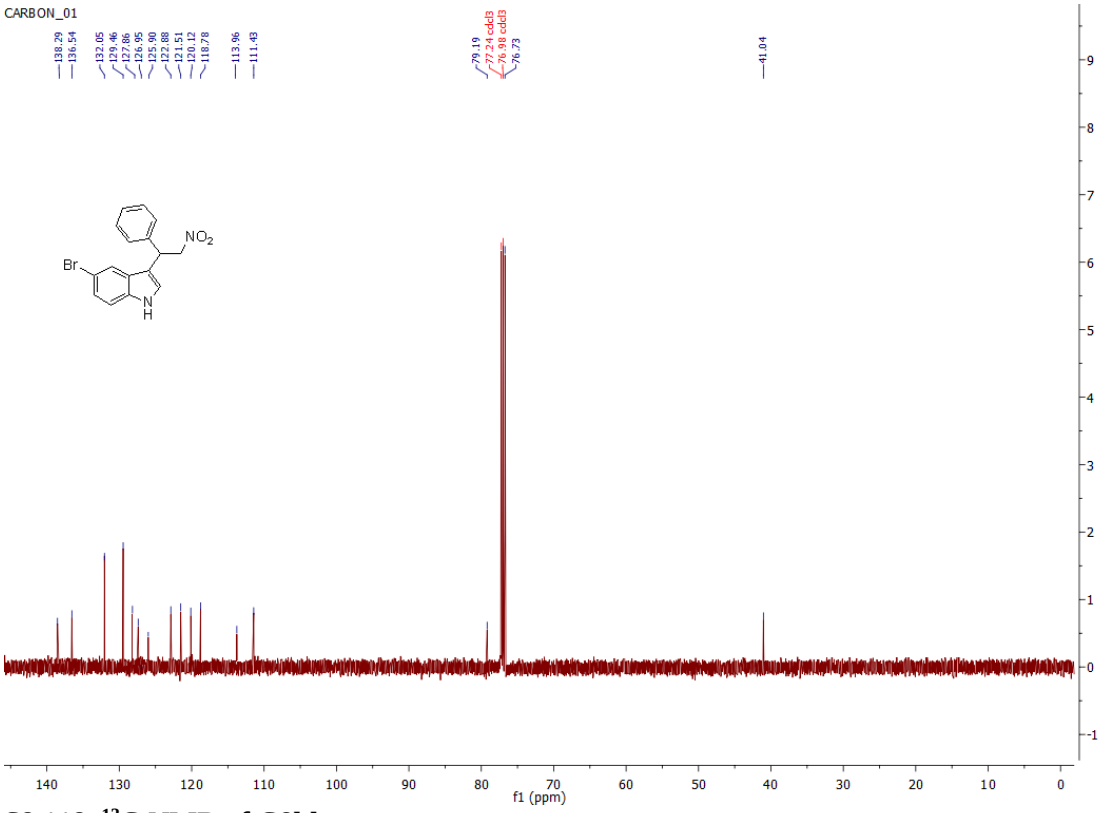

S8.118. ^{13}C NMR of C8bh

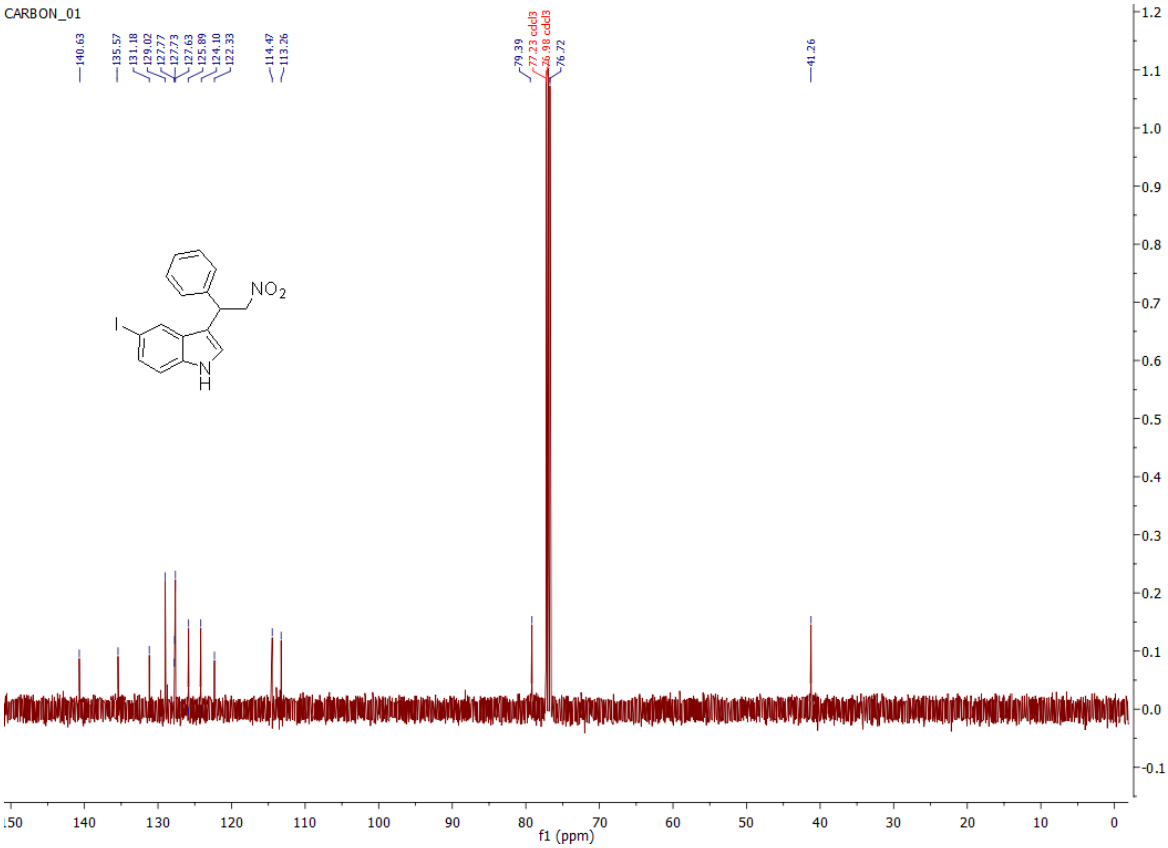

S8.119. ^{13}C NMR of C8bi

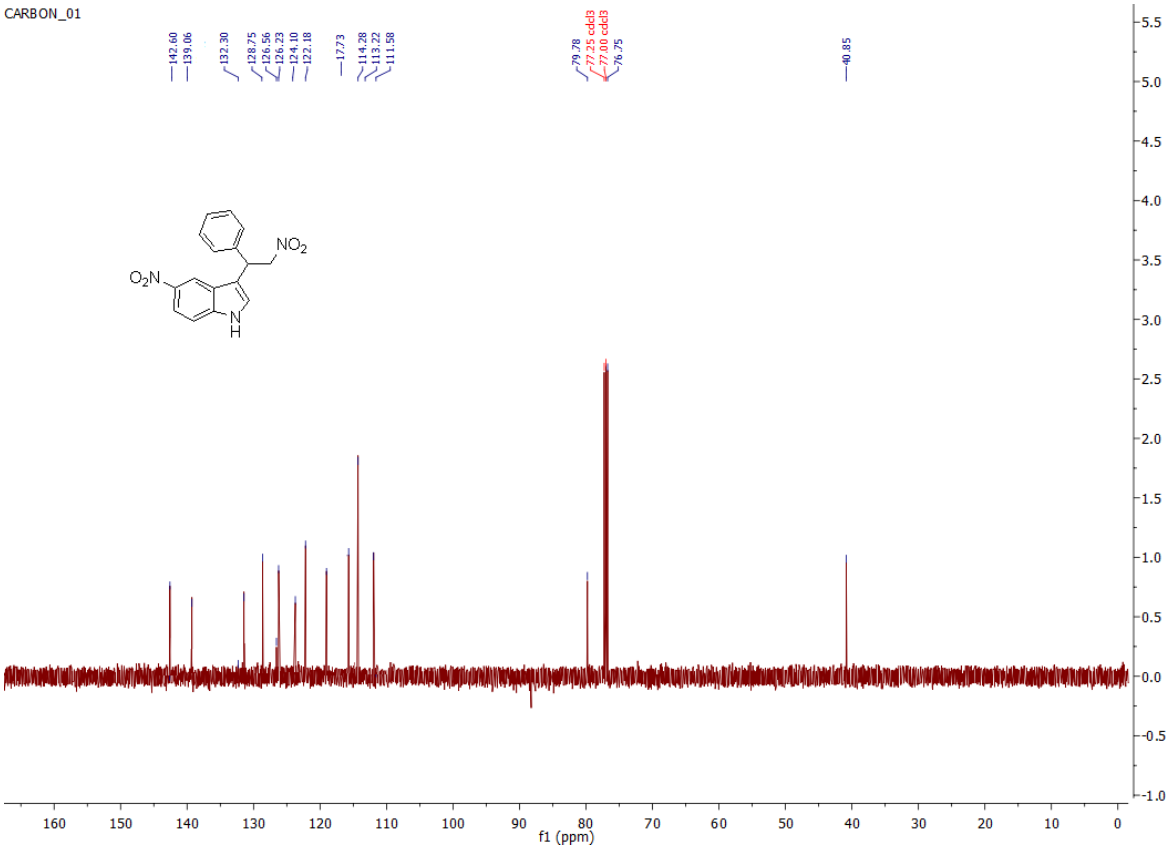

S8.120. ^{13}C NMR of C8bj

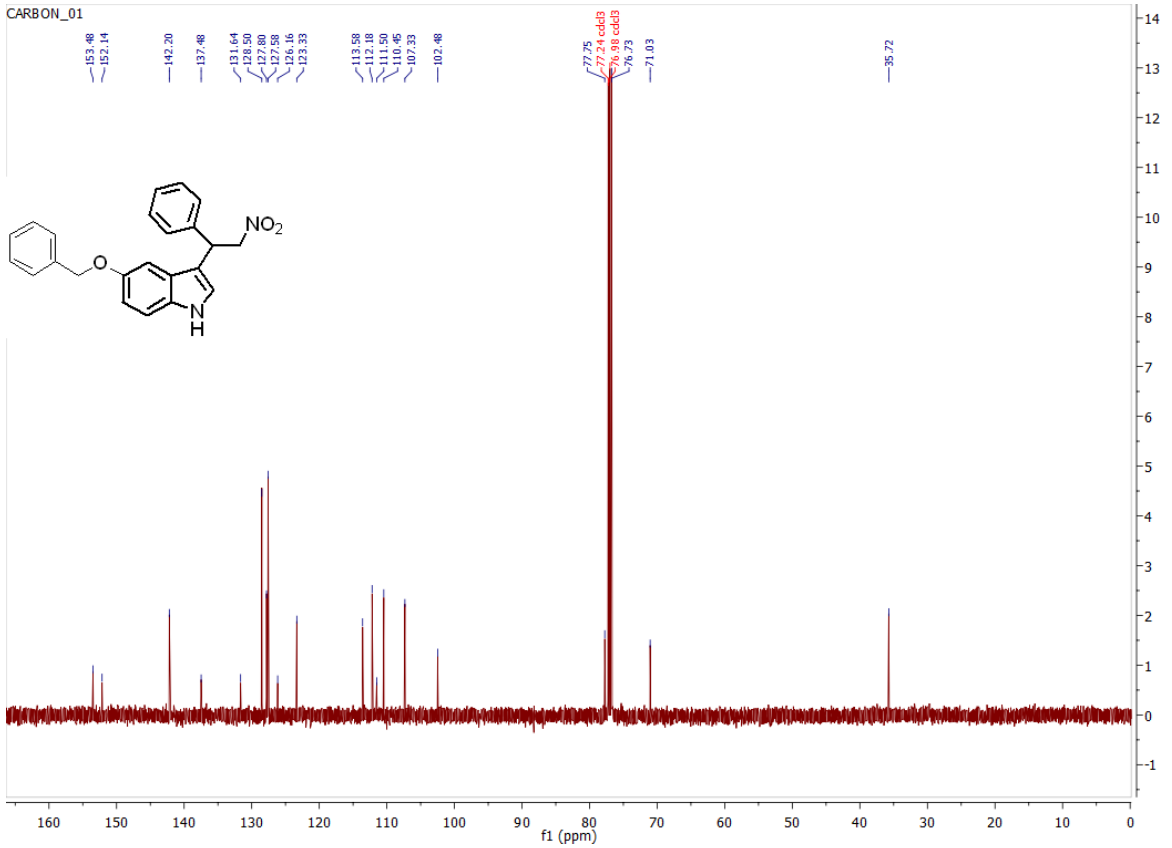

S8.121. ^{13}C NMR of C8bk

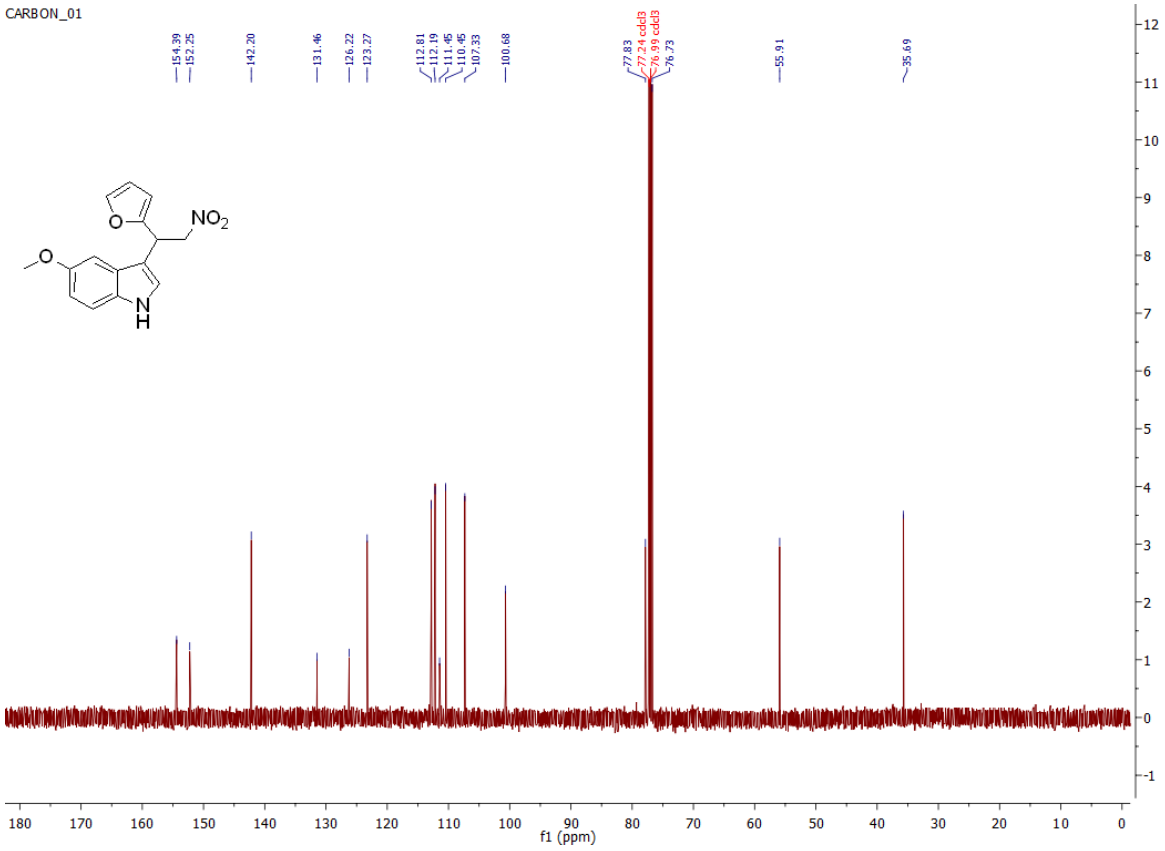

S8.122. ^{13}C NMR of C8bl

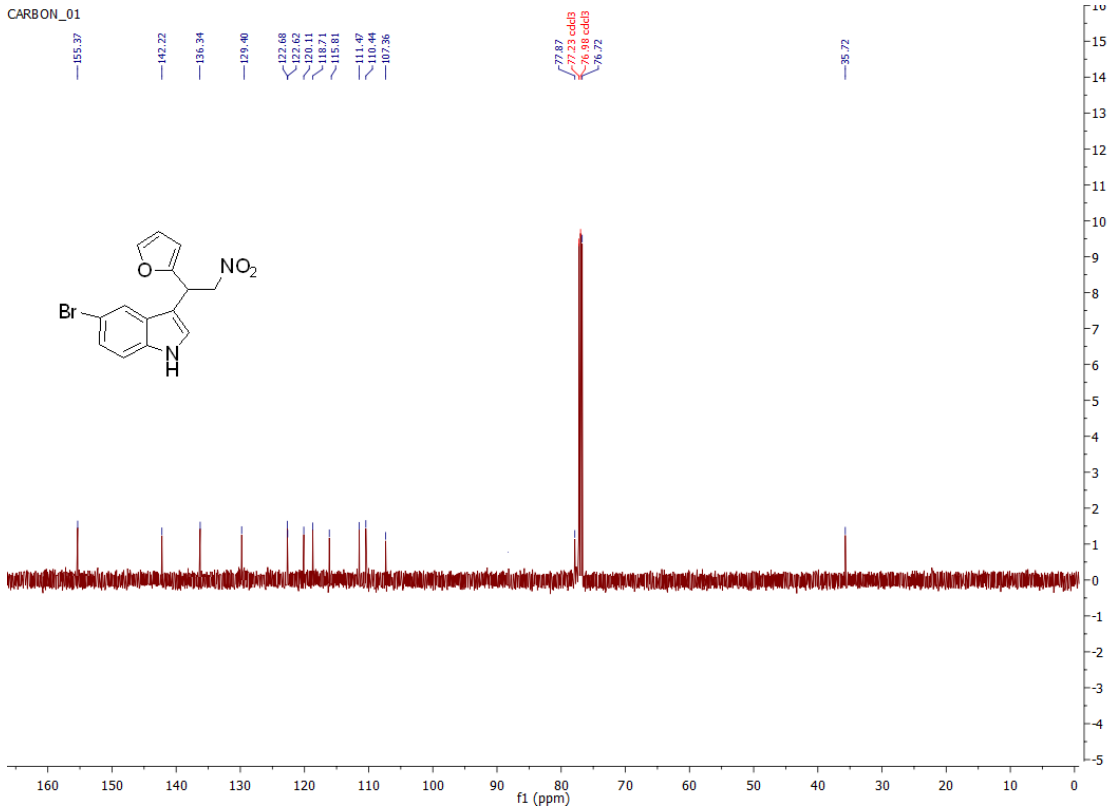

S8.123. ^{13}C NMR of C8bm

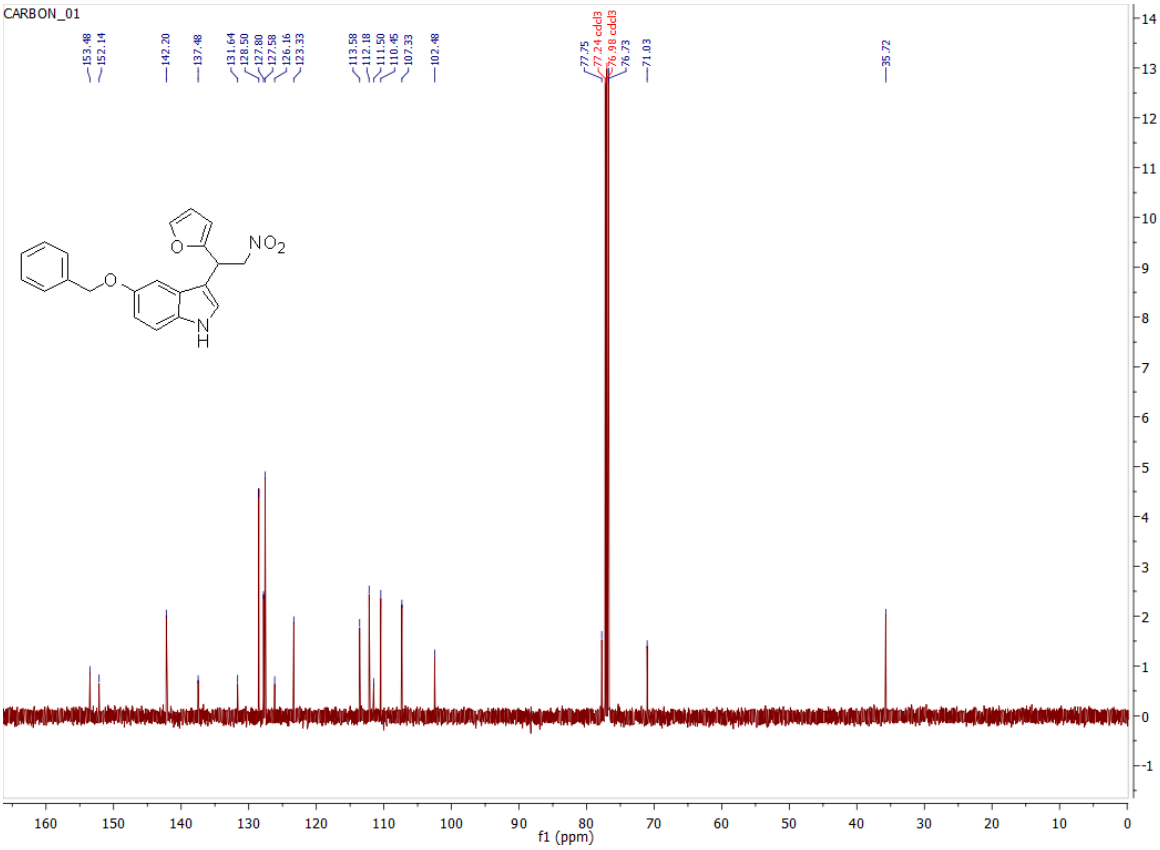

S8.124. ^{13}C NMR of C8bn

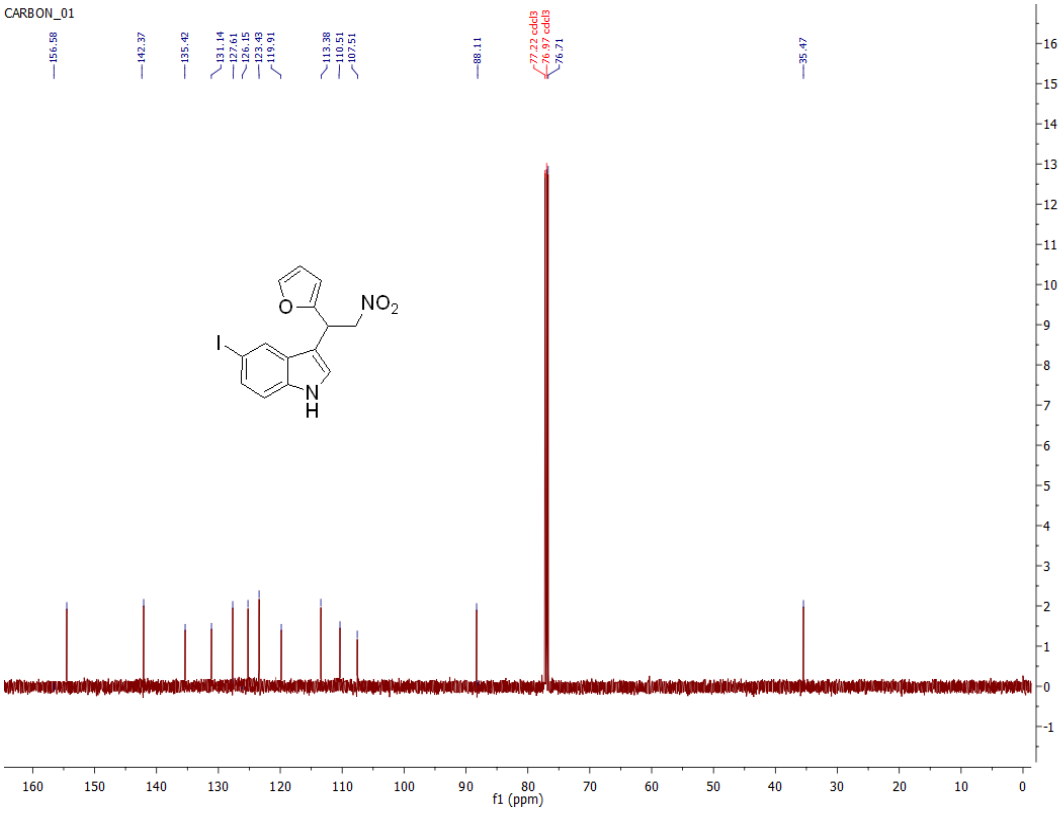

S8.125. ^{13}C NMR of C8bo

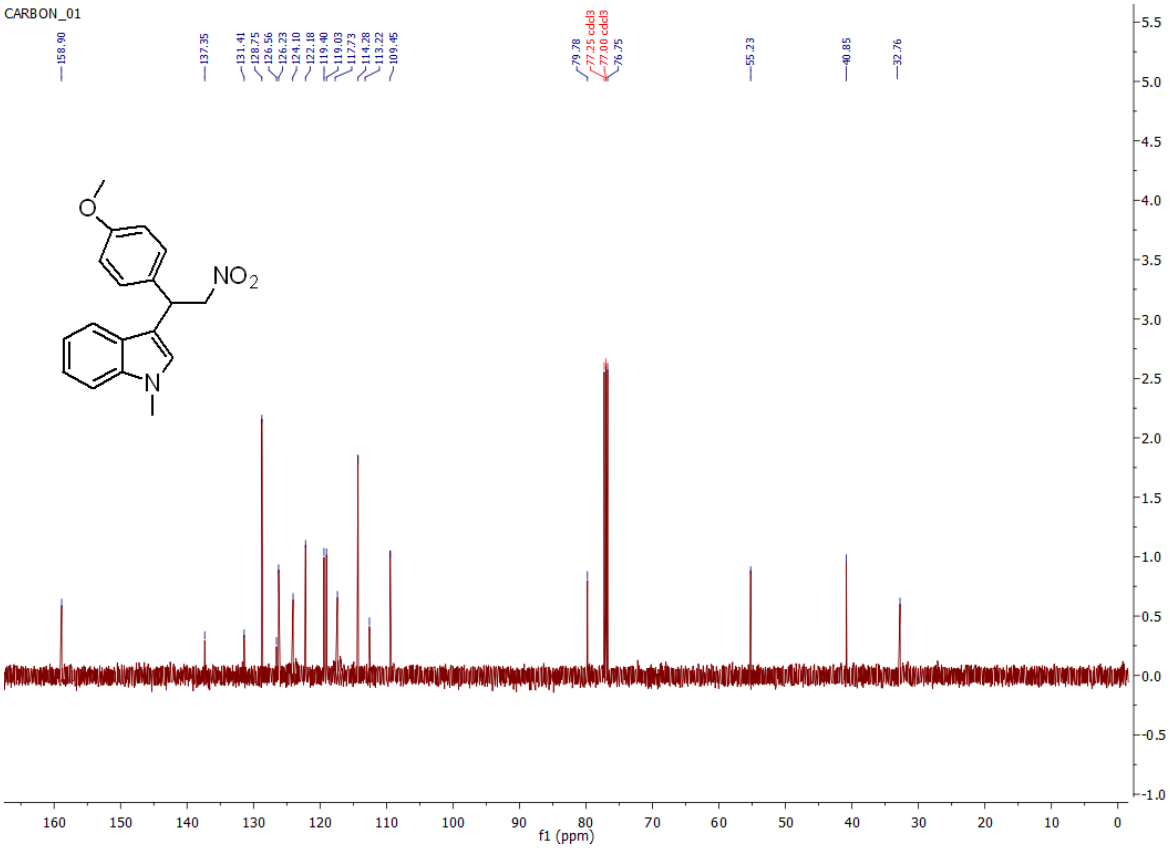

S8.126. ^{13}C NMR of C8bq

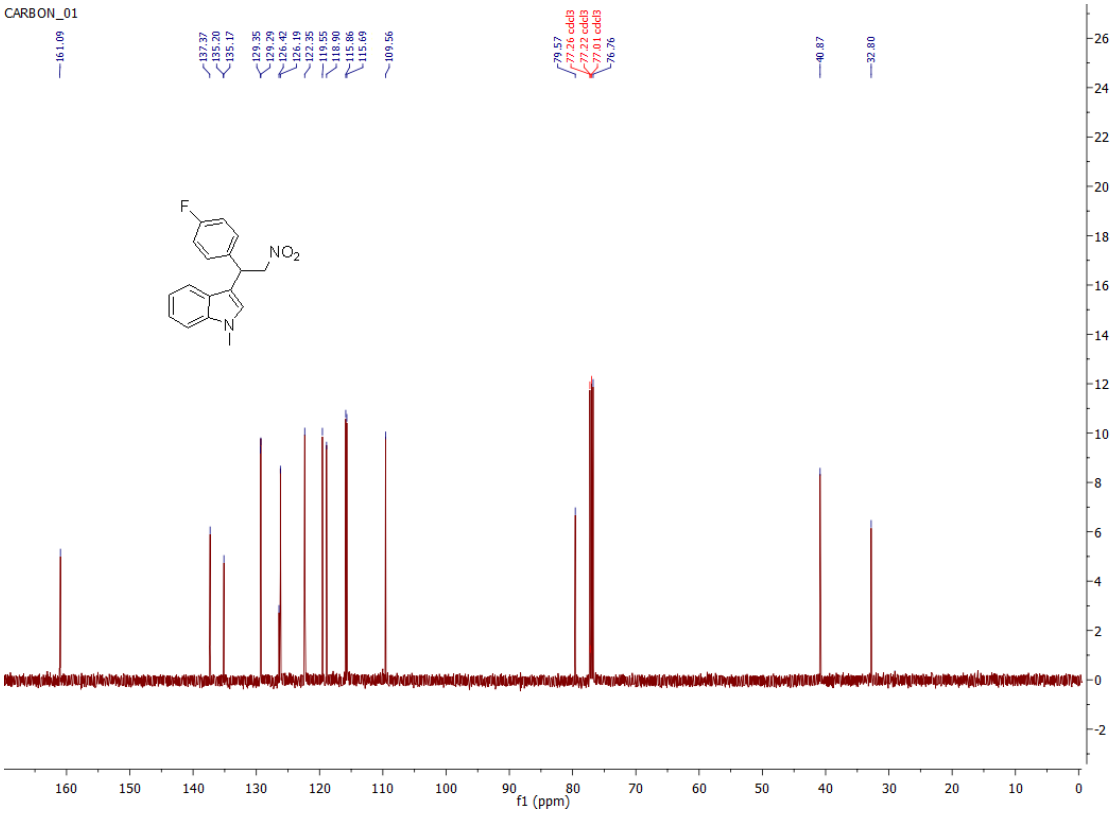

S8.126. ^{13}C NMR of C8br

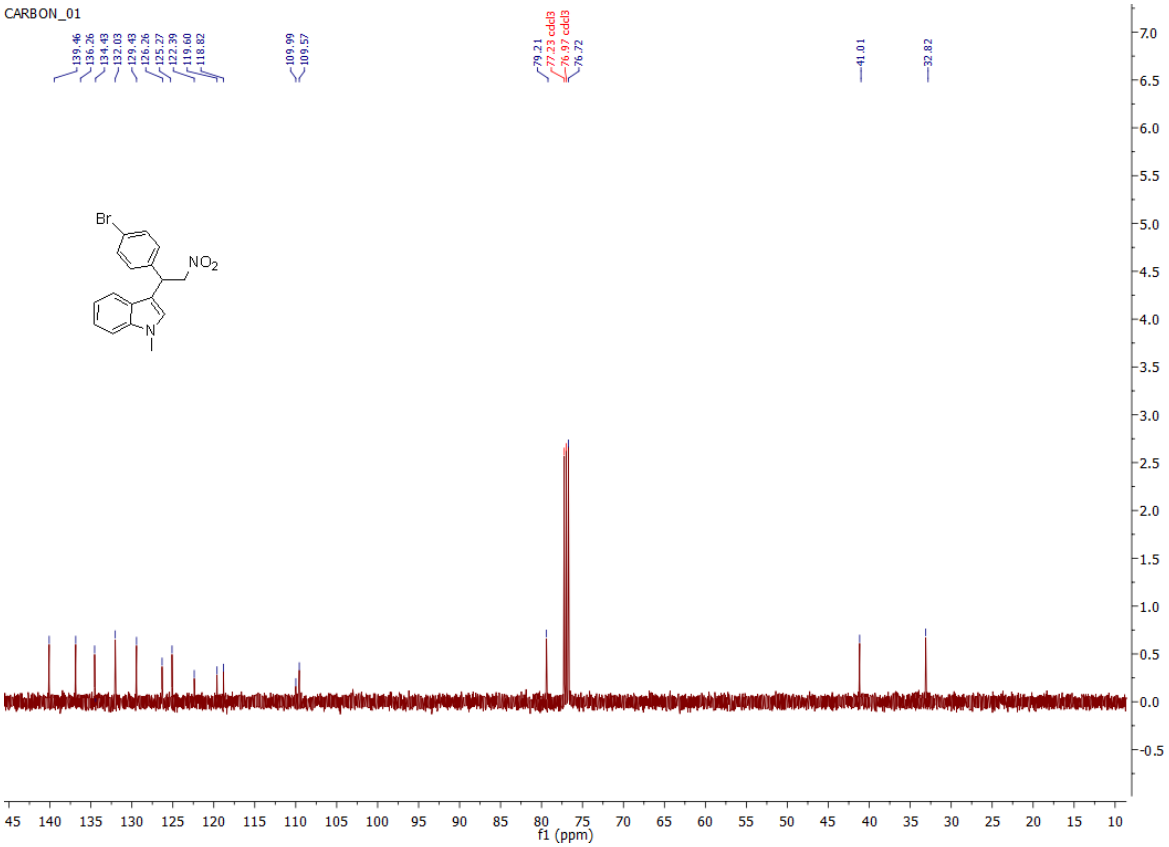

S8.127. ^{13}C NMR of C8bs

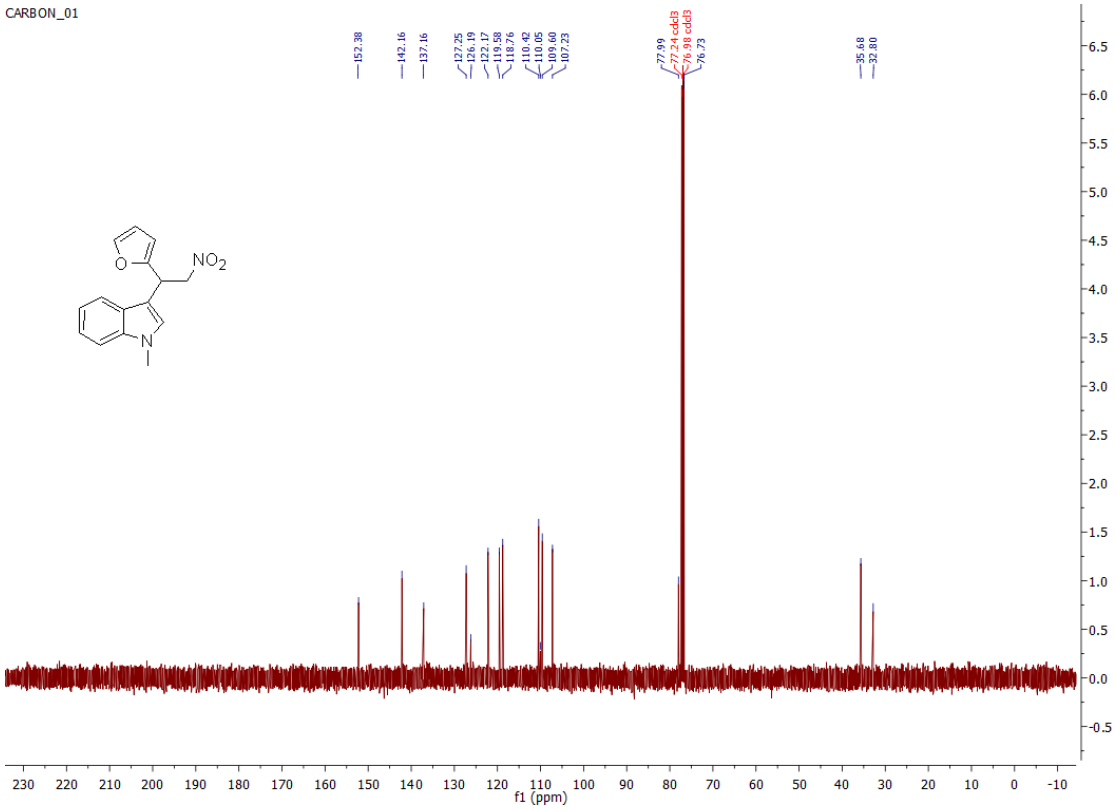

S8.128. ^{13}C NMR of C8bt

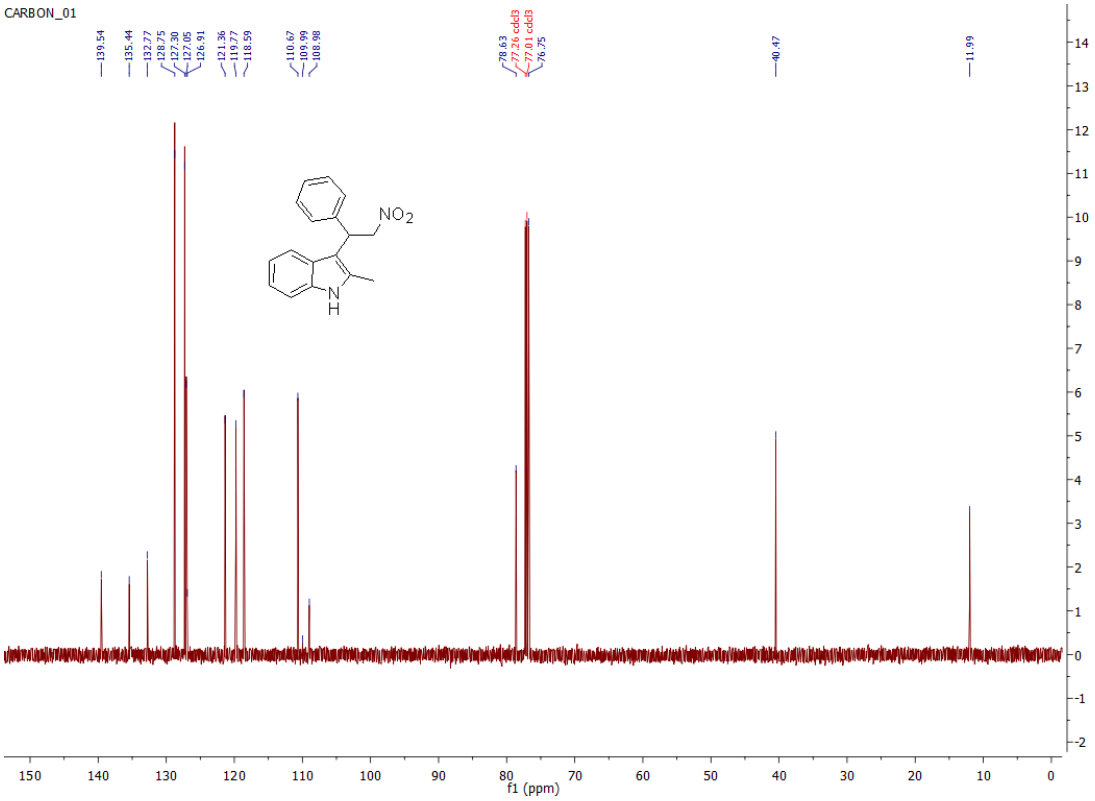

S8.129. ^{13}C NMR of C8bu

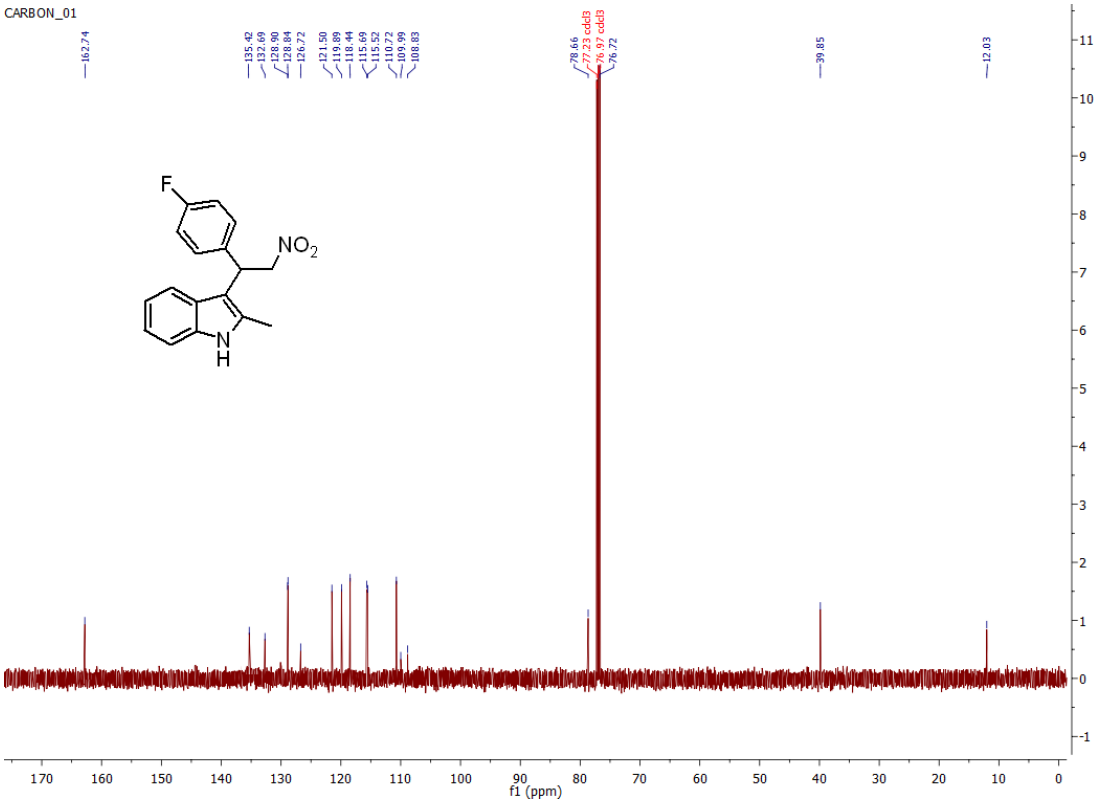

S8.130. ^{13}C NMR of C8bv

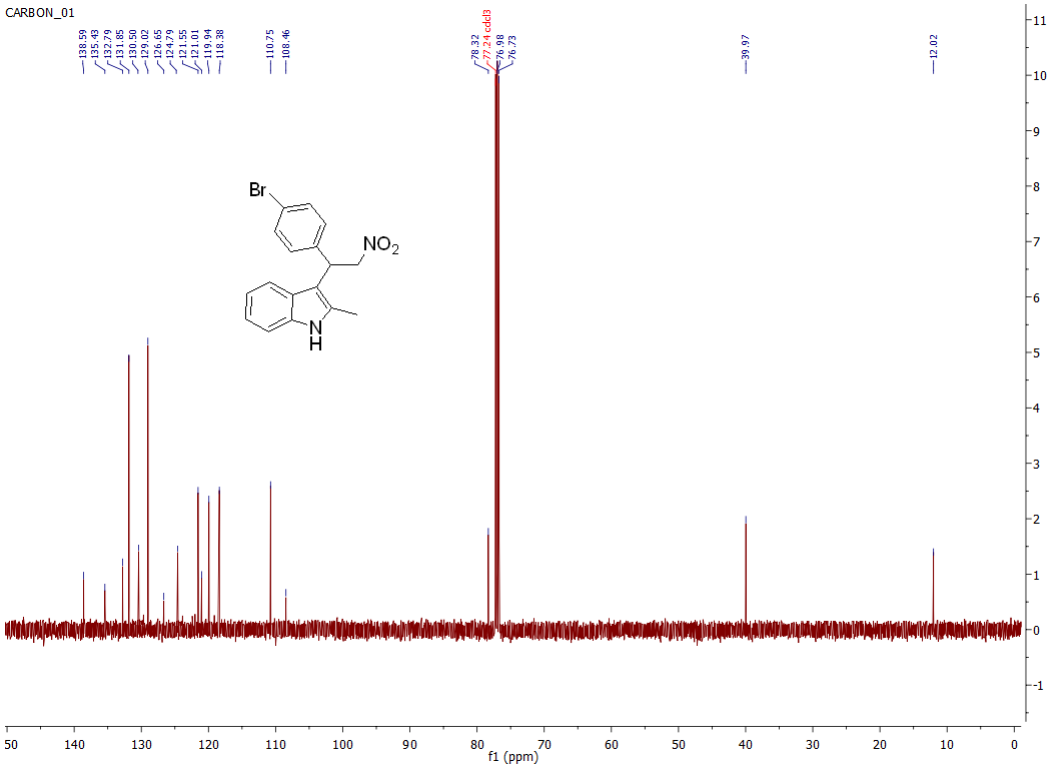

S8.131. ^{13}C NMR of C8bw

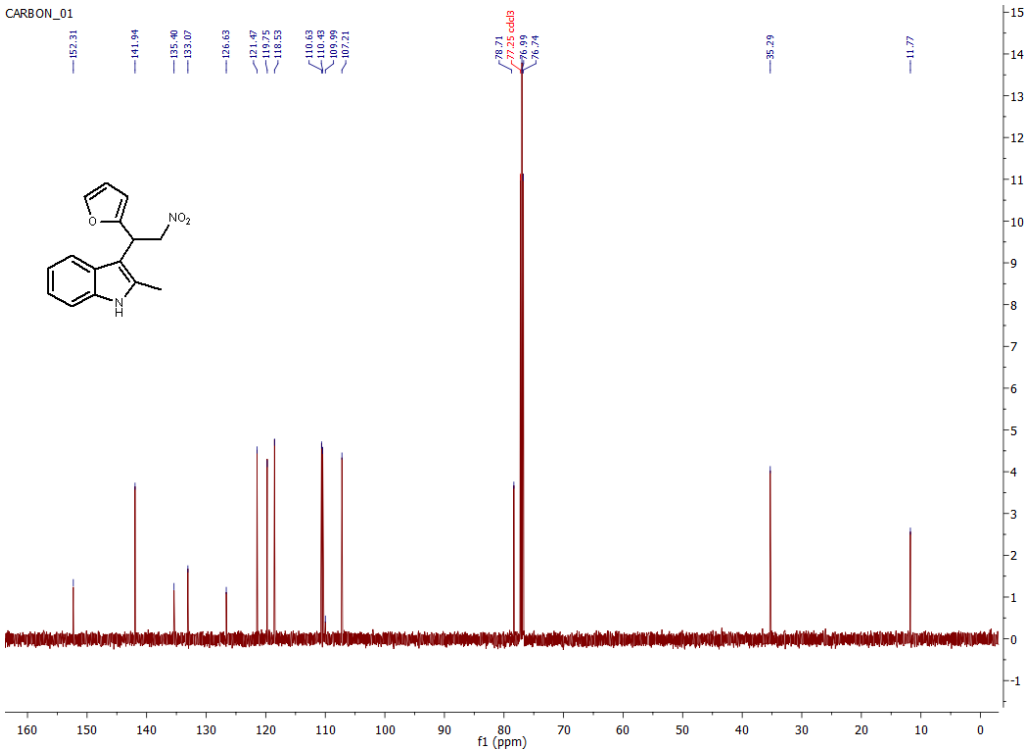

S8.132. ^{13}C NMR of C8bx

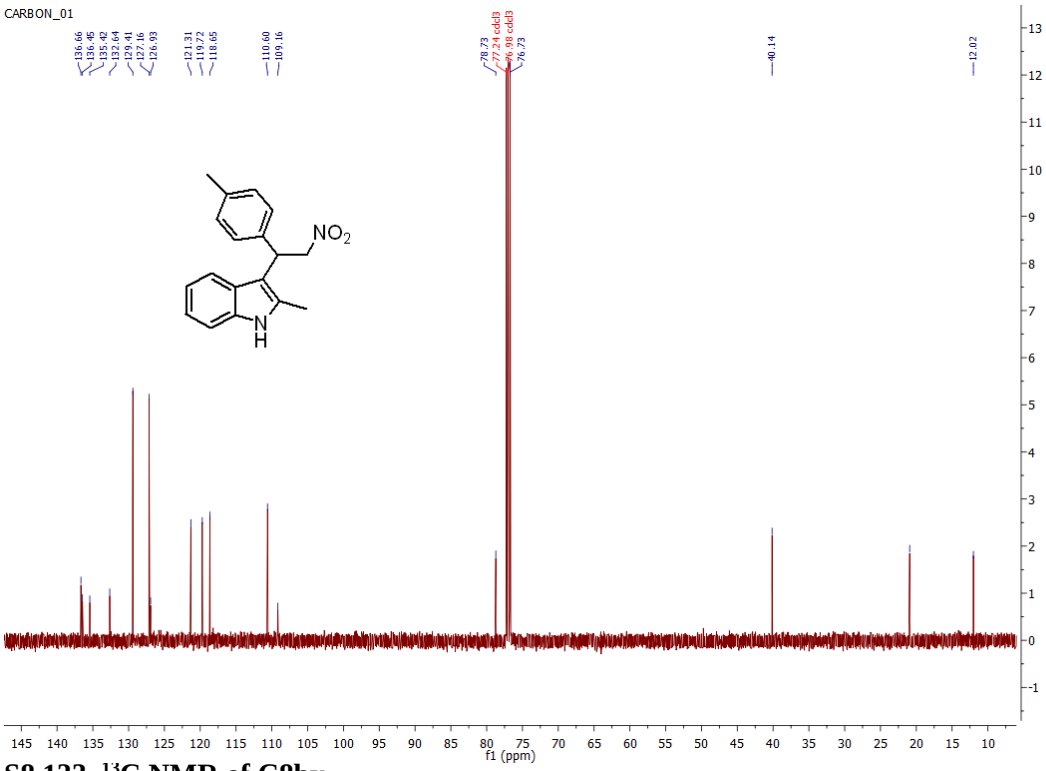

S8.133. ^{13}C NMR of C8by

8.11 ^{1}H NMR of C8ca-C8cq

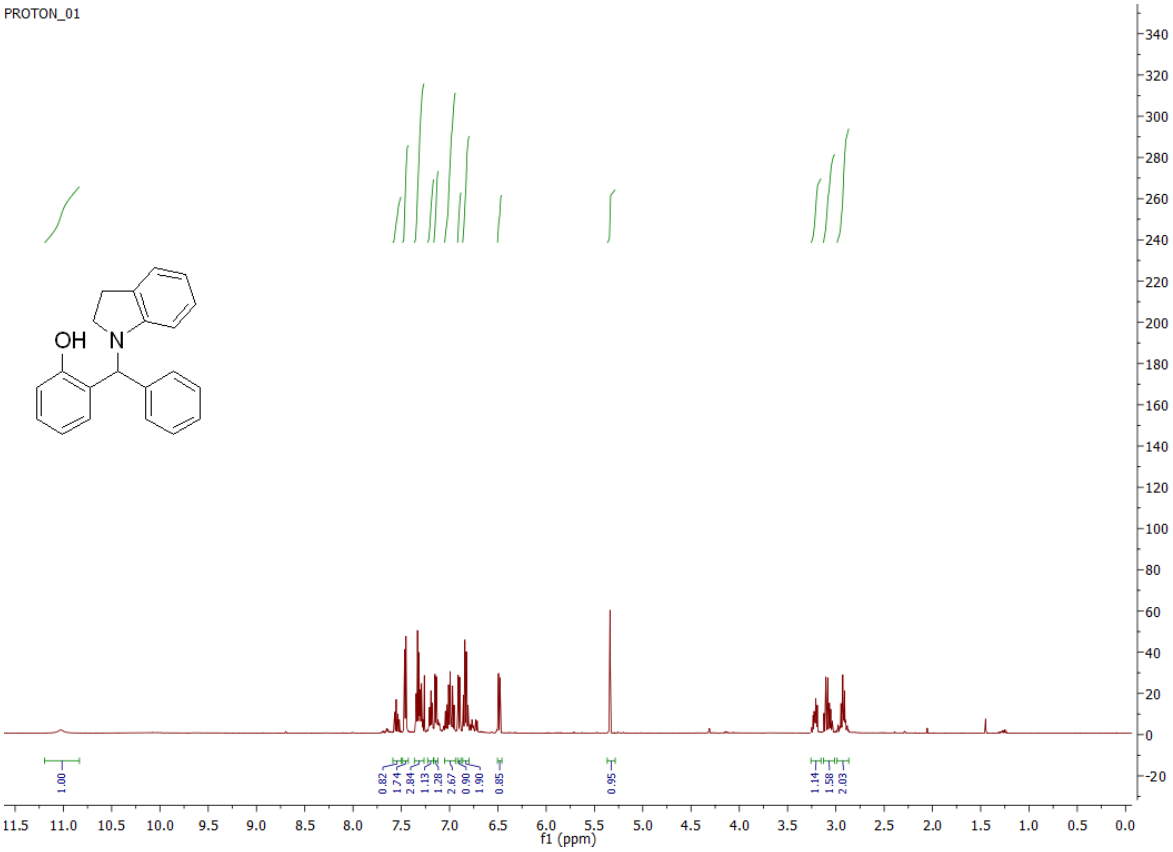

S8.134. ^{1}H NMR of C8ca

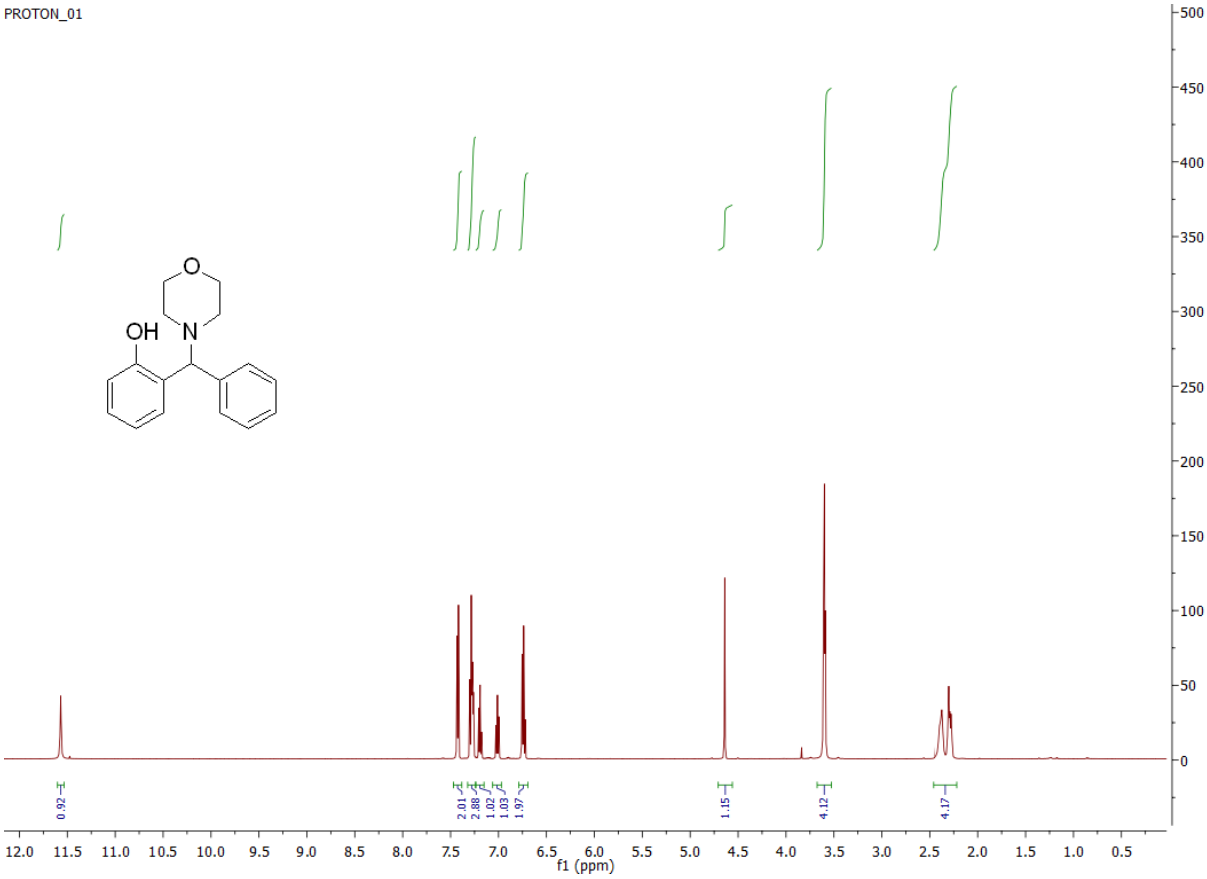

S8.135. ^{1}H NMR of C8cb

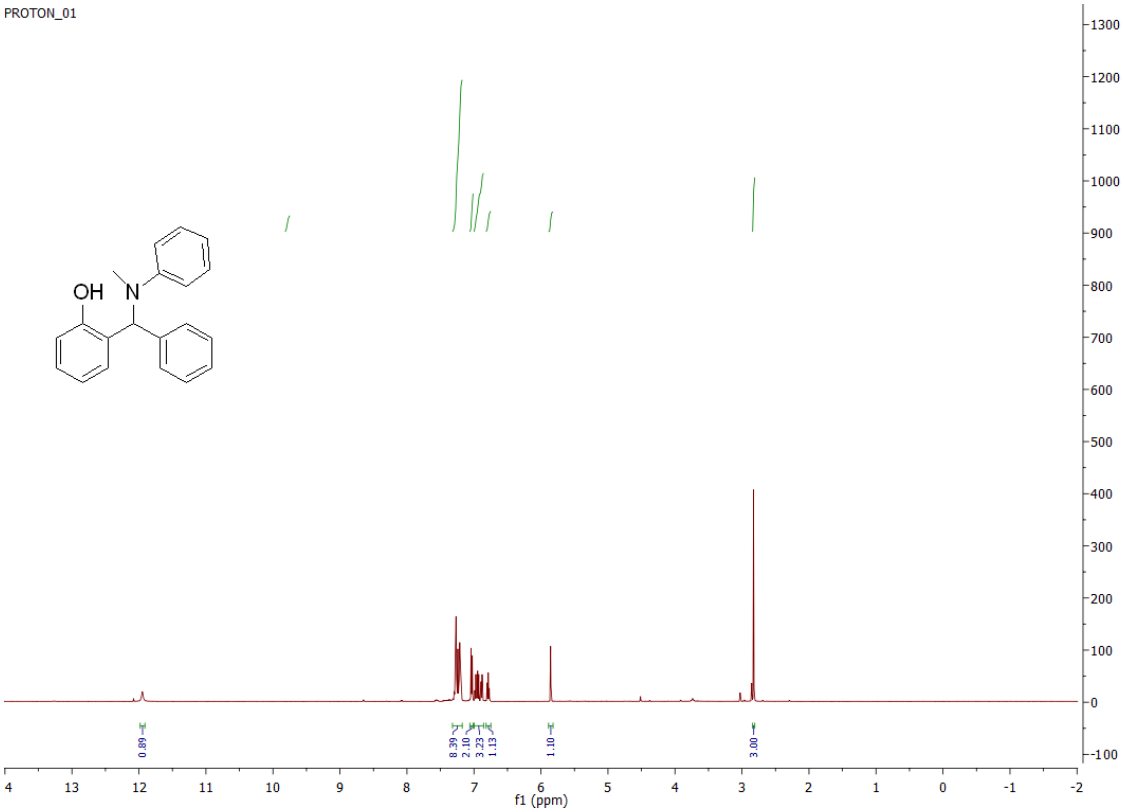

S8.136. ^{1}H NMR of C8cc

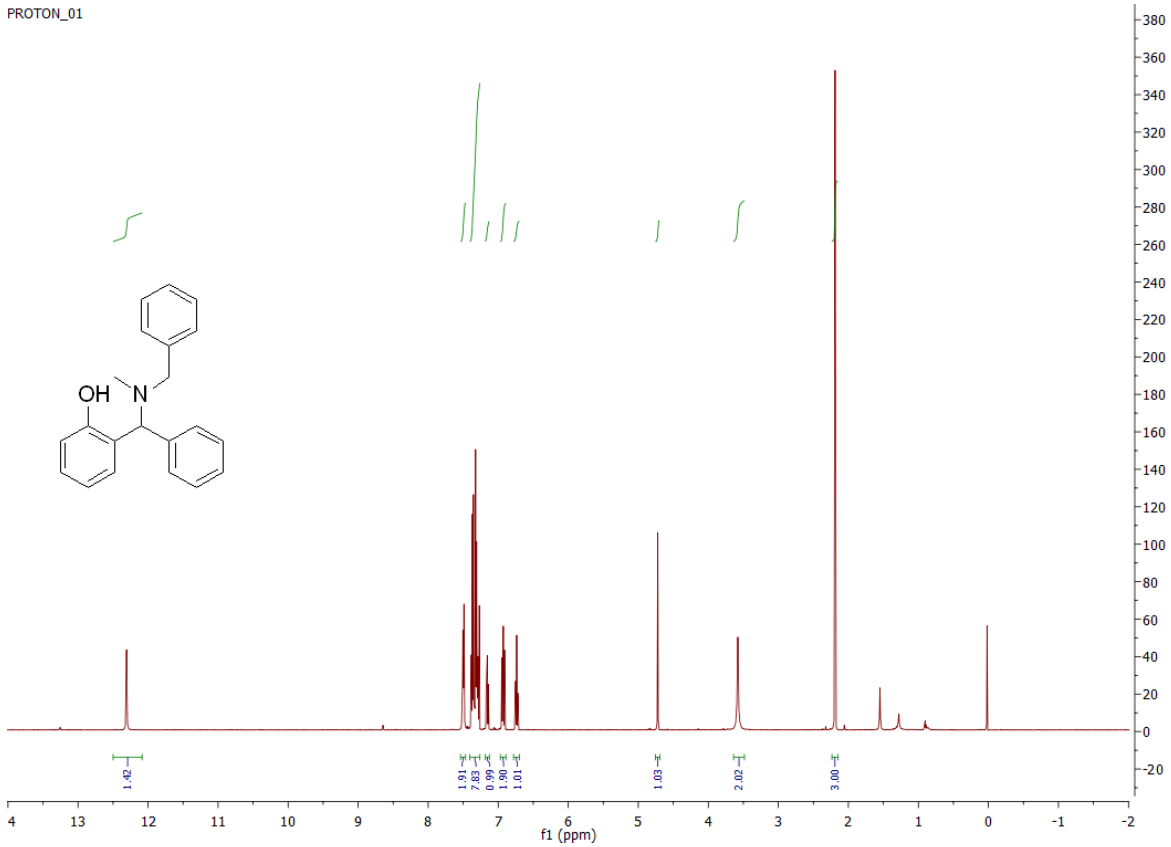

S8.137. ^{1}H NMR of C8cd

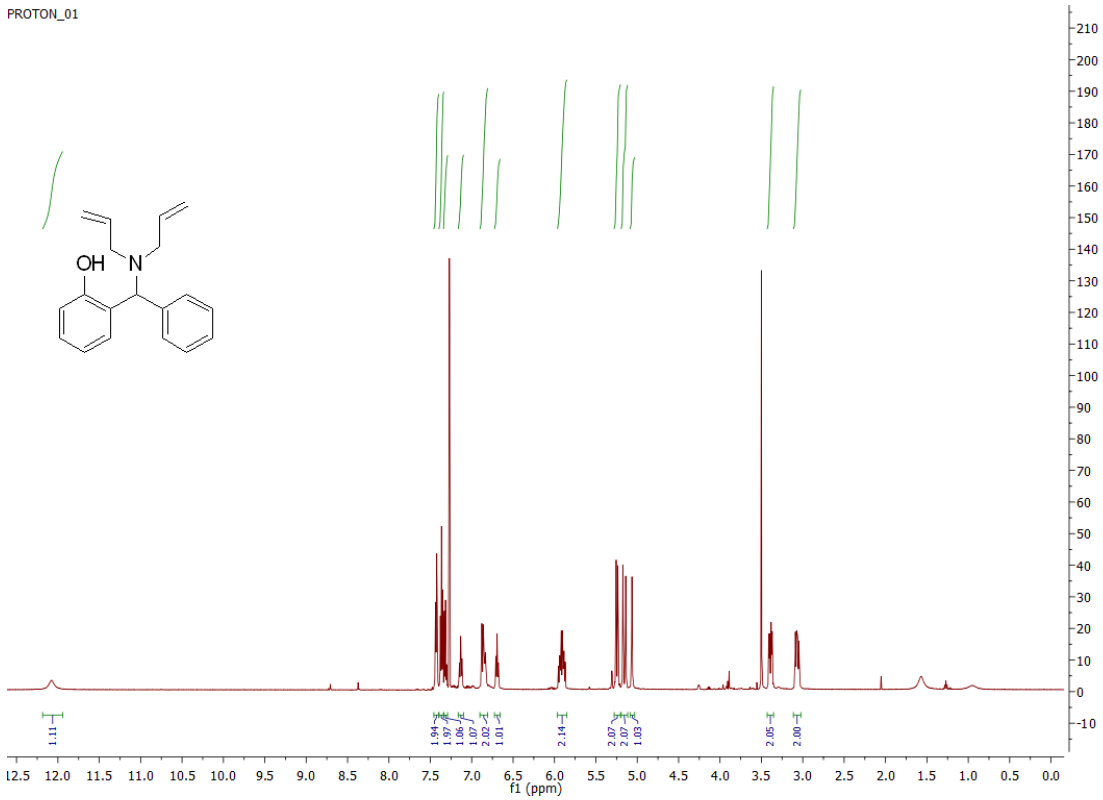

S8.138. ^{1}H NMR of C8ce

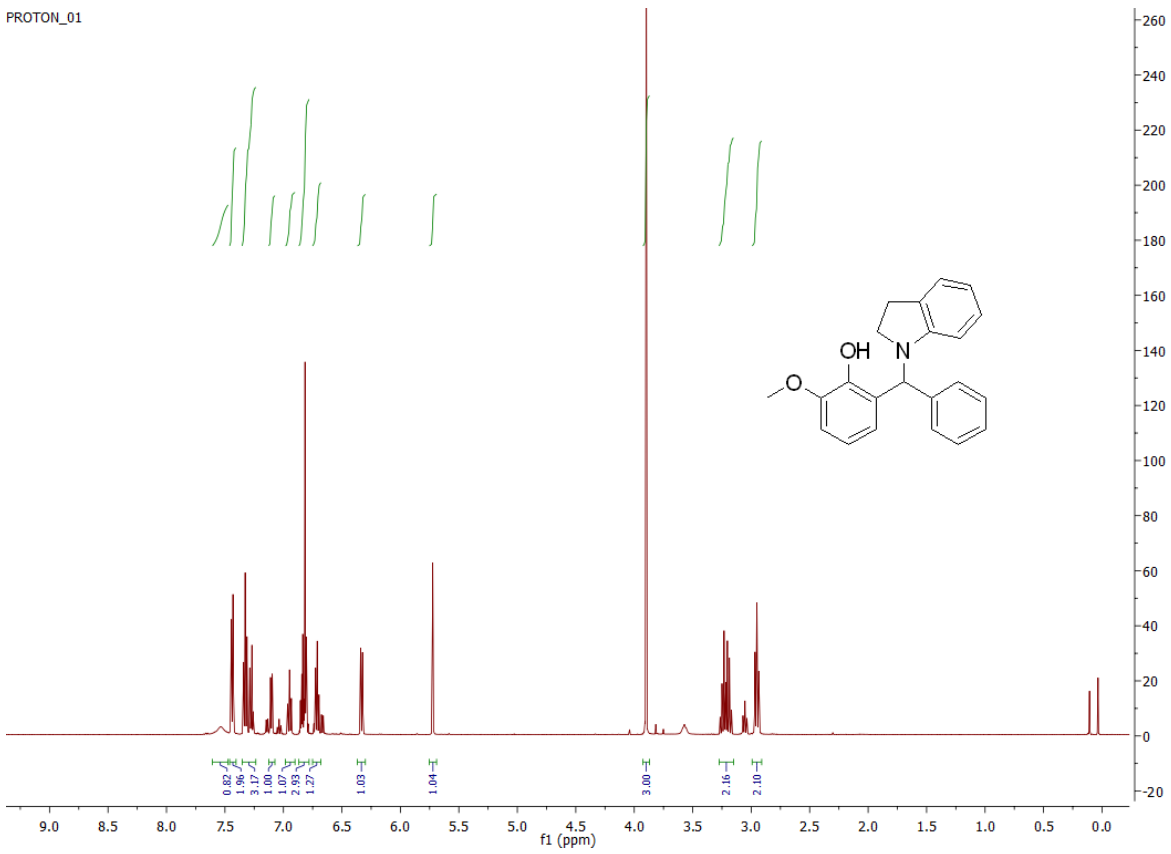

S8.139. ^{1}H NMR of C8cf

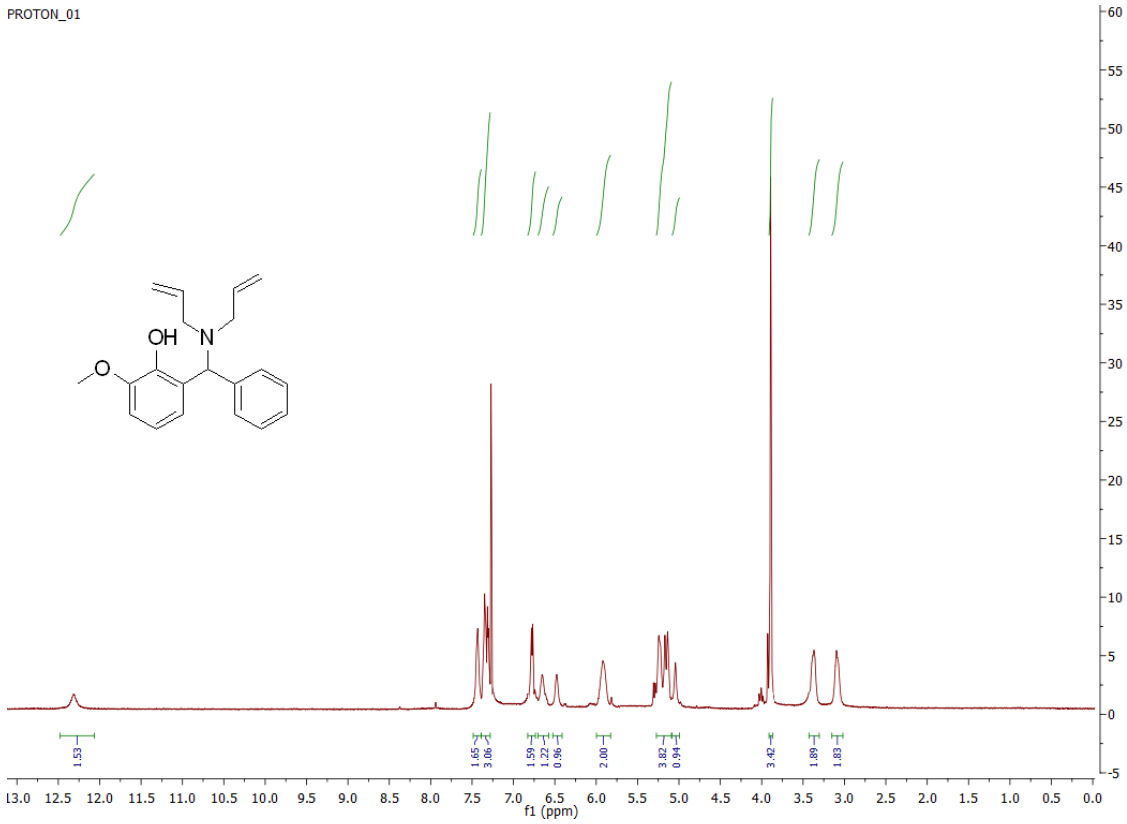

S8.140. ^{1}H NMR of C8cg

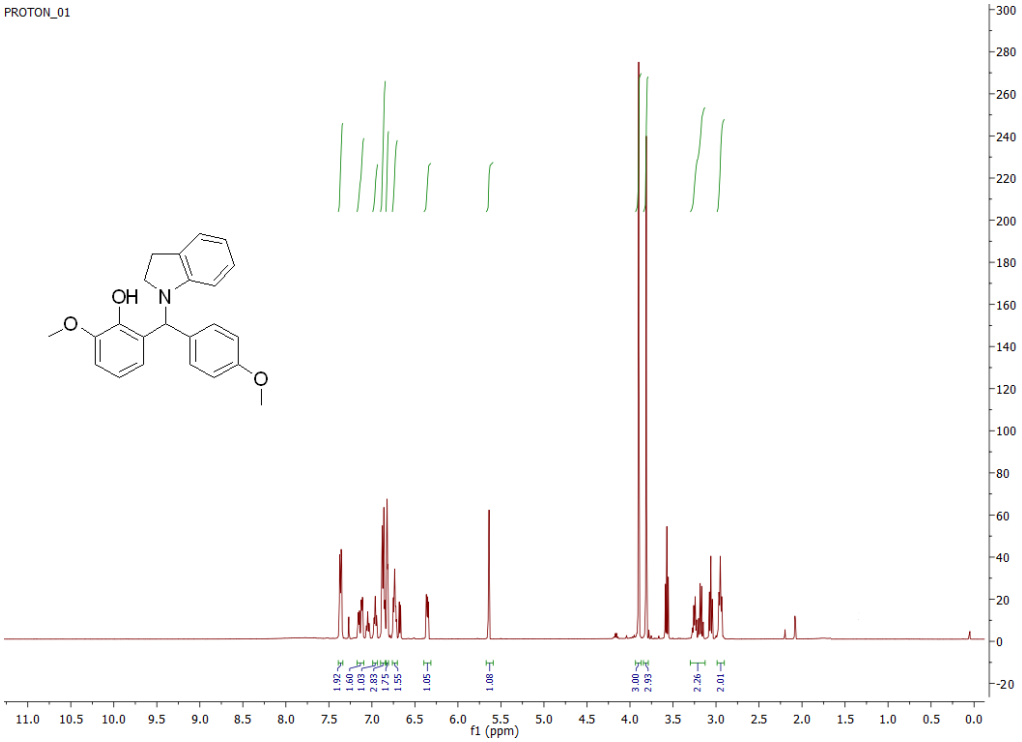

S8.141. ^{1}H NMR of C8ch

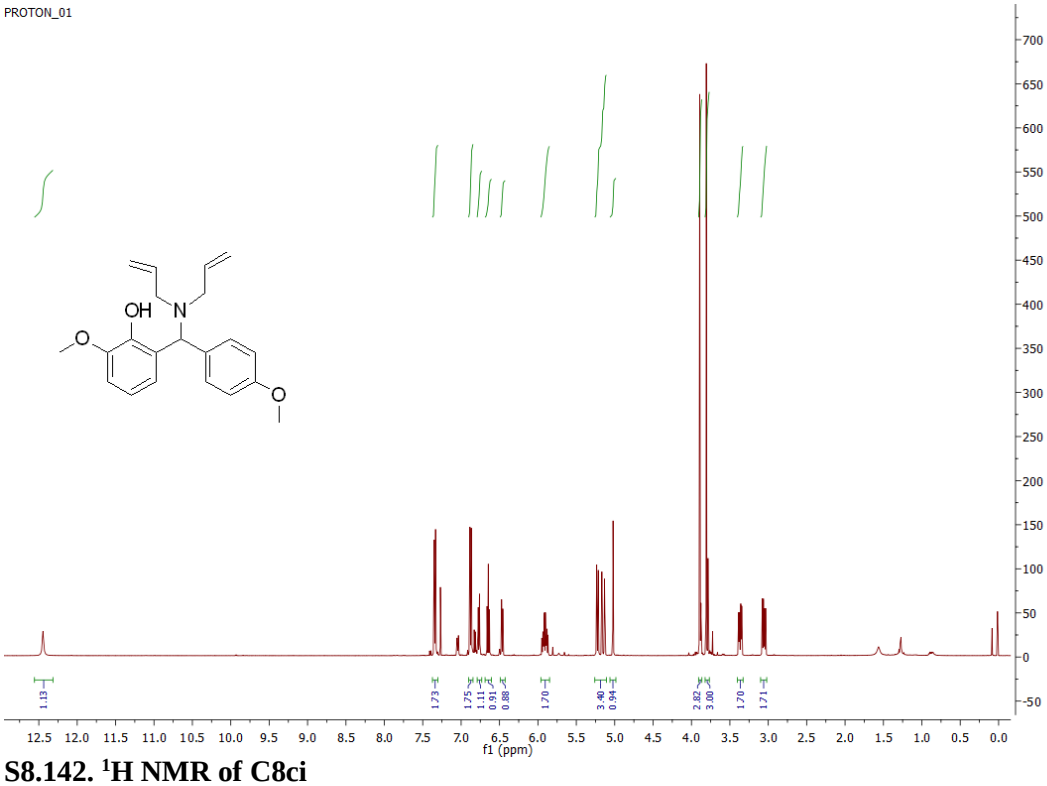

S8.142. ^{1}H NMR of C8ci

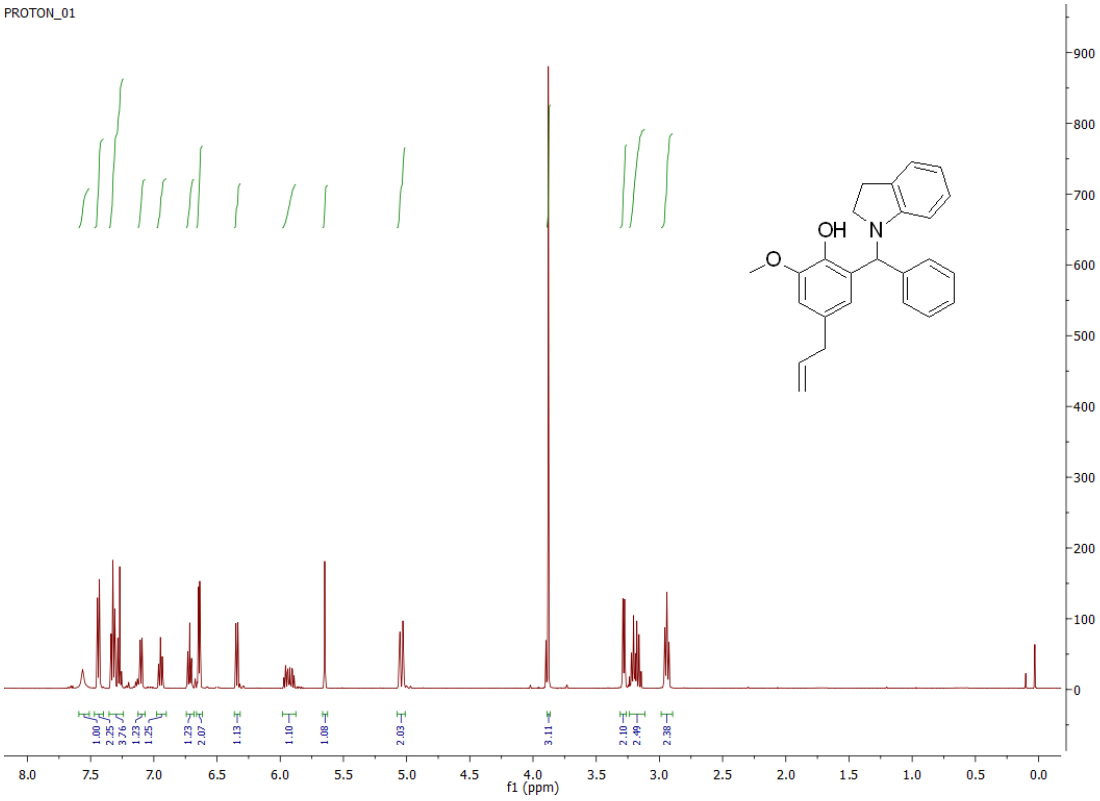

S8.143. ^{1}H NMR of C8cj

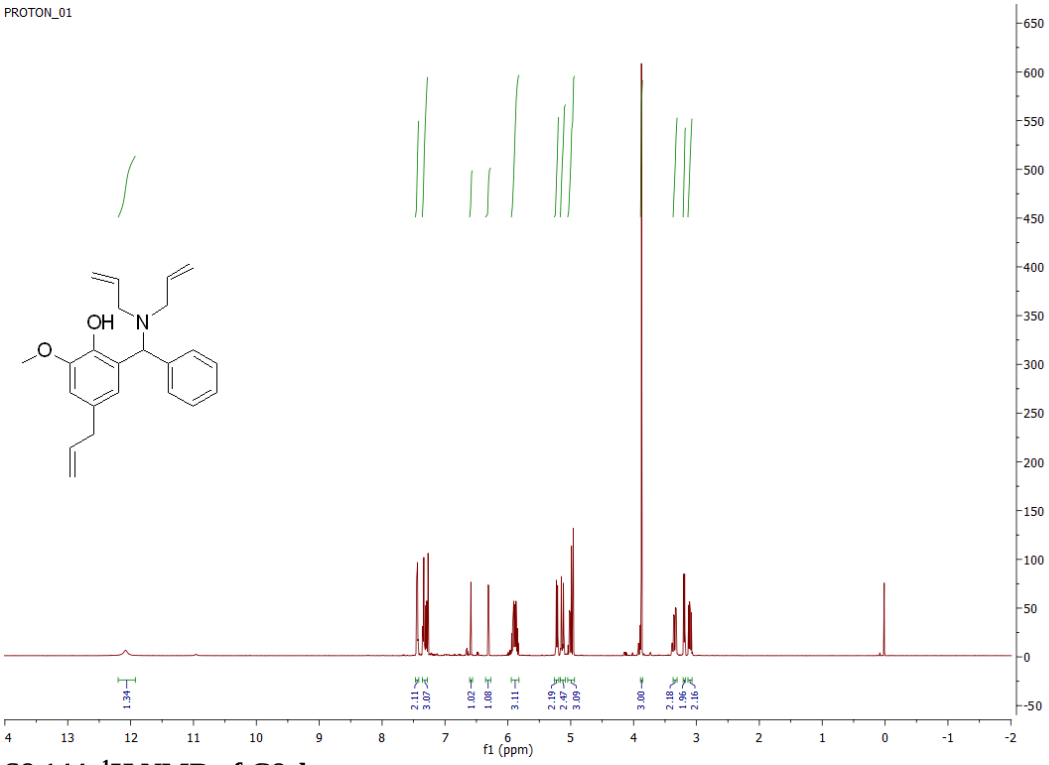

S8.144. ^{1}H NMR of C8ck

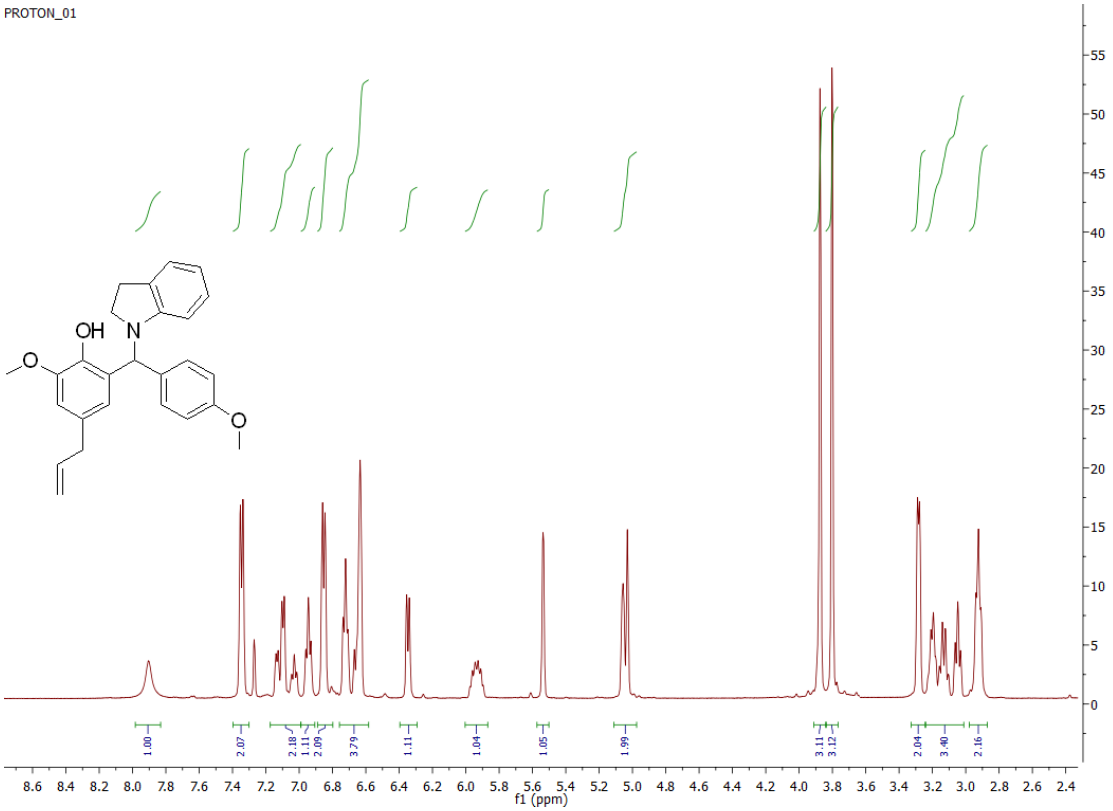

S8.145. ^{1}H NMR of C8cl

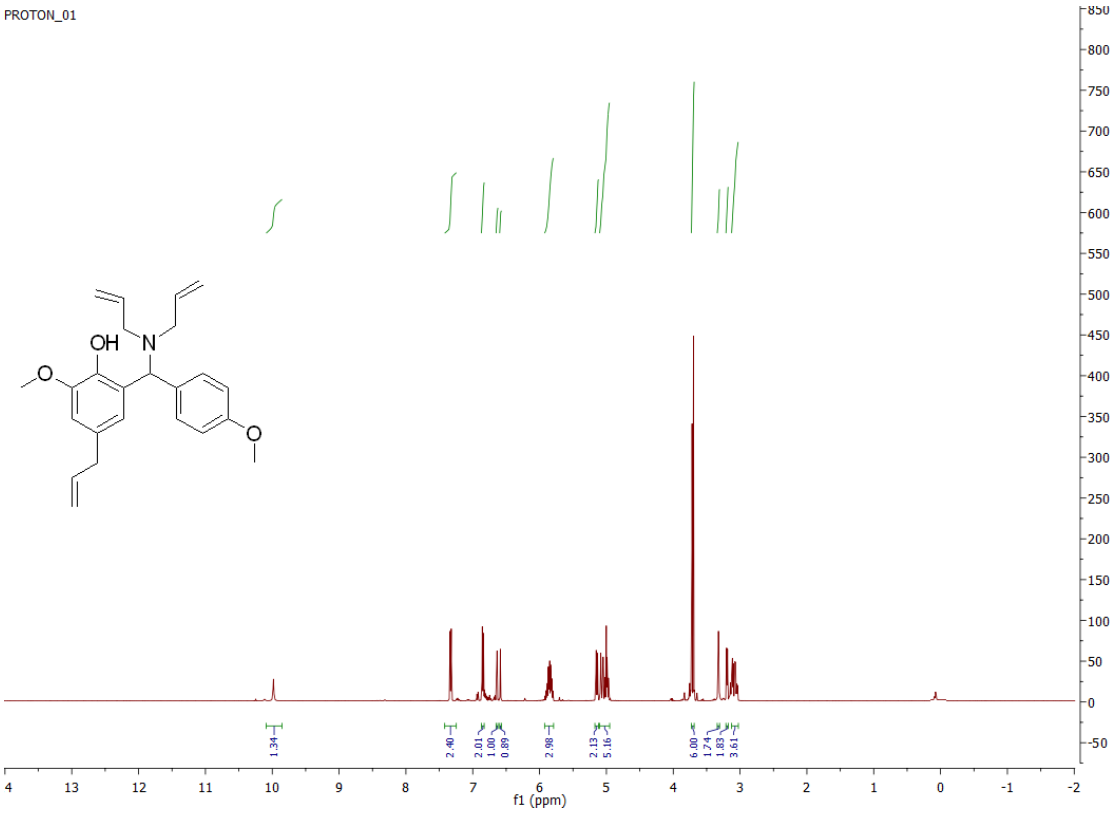

S8.146. ^{1}H NMR of C8cm

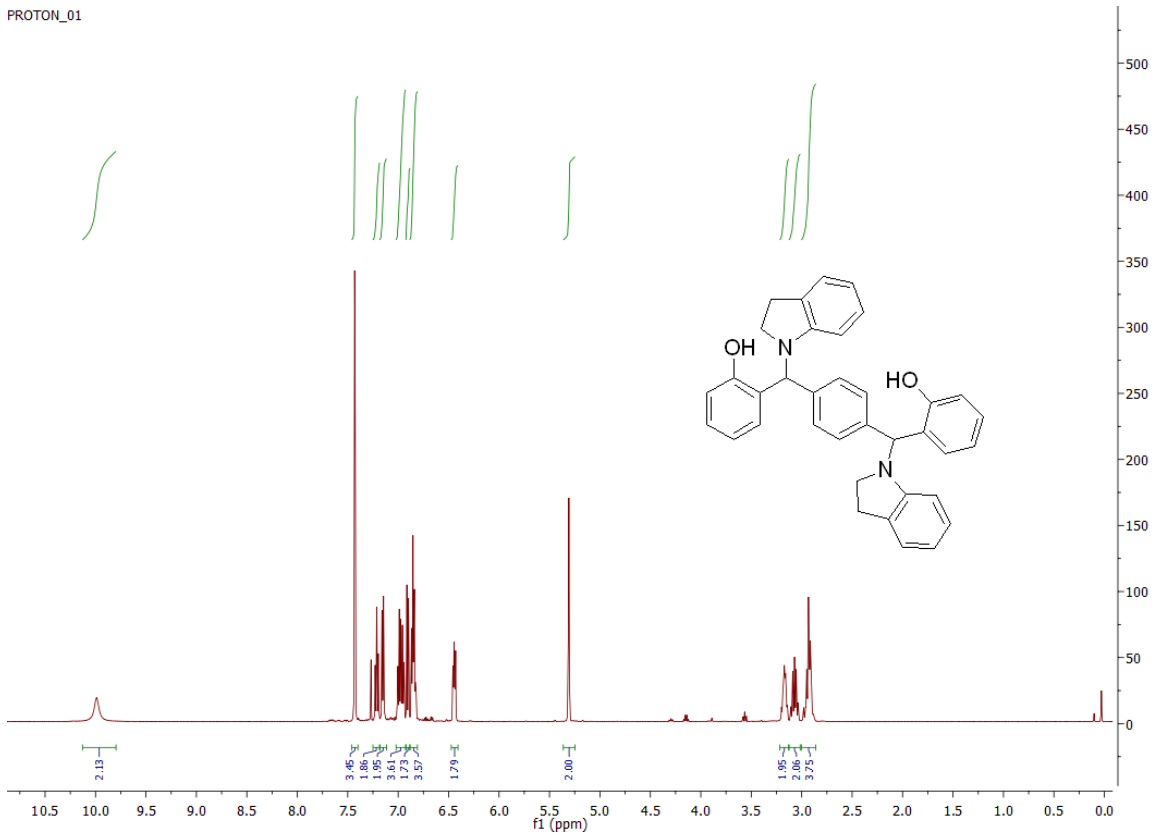

S8.147. ^{1}H NMR of C8cn

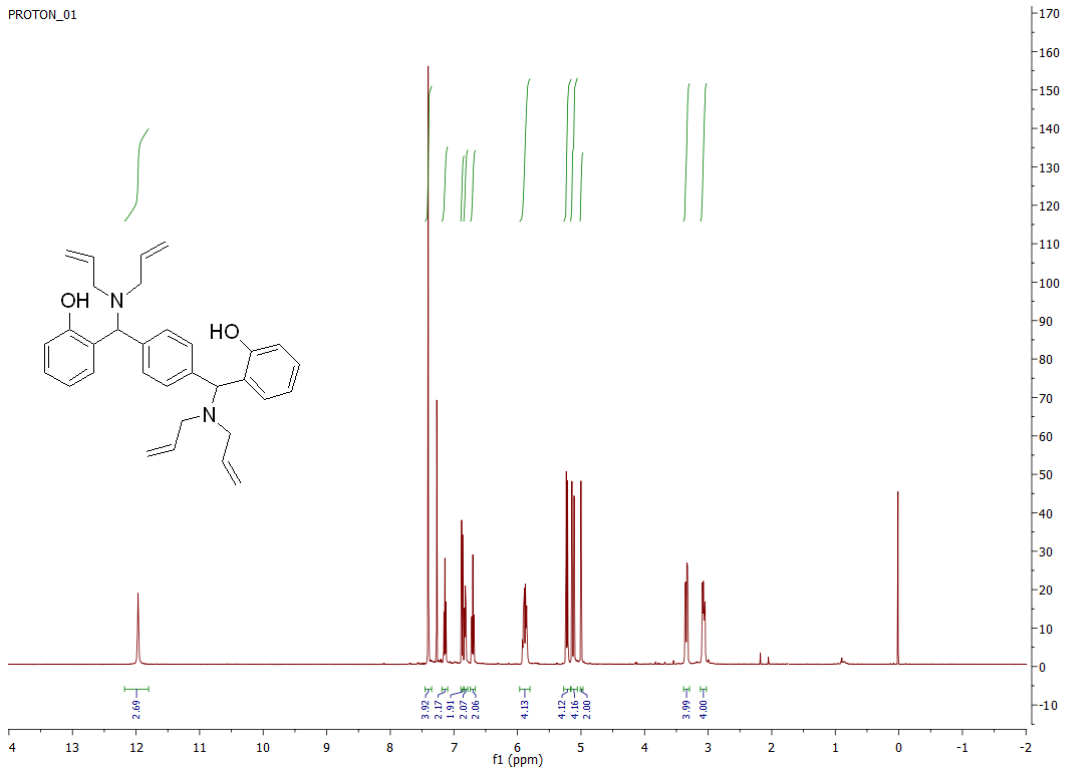

S8.148. ^{1}H NMR of C8co

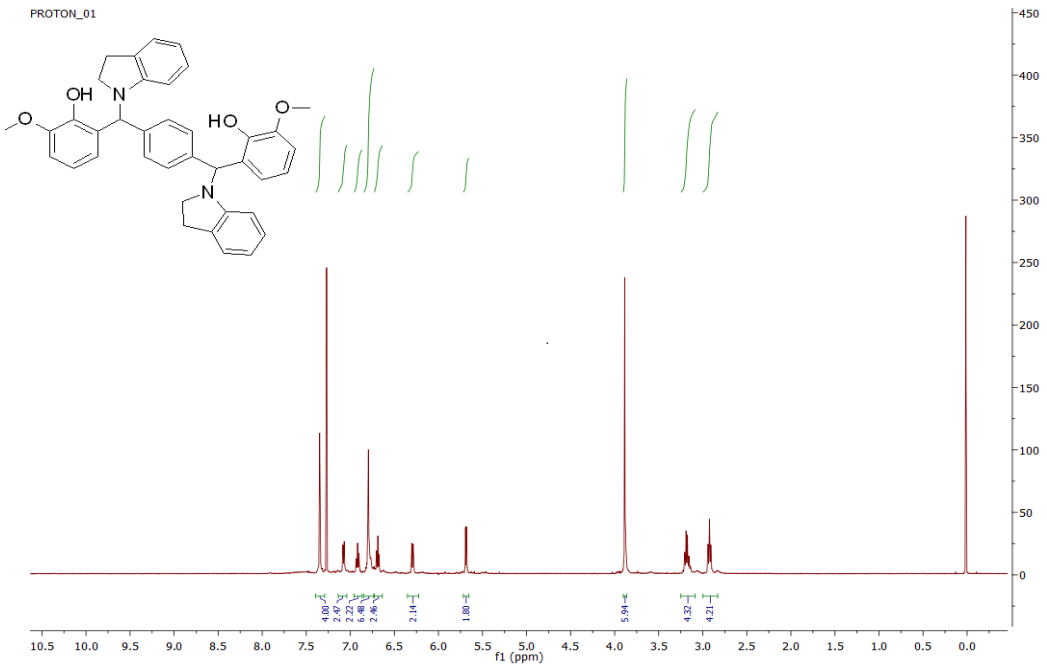

S8.149. ^{1}H NMR of C8cp

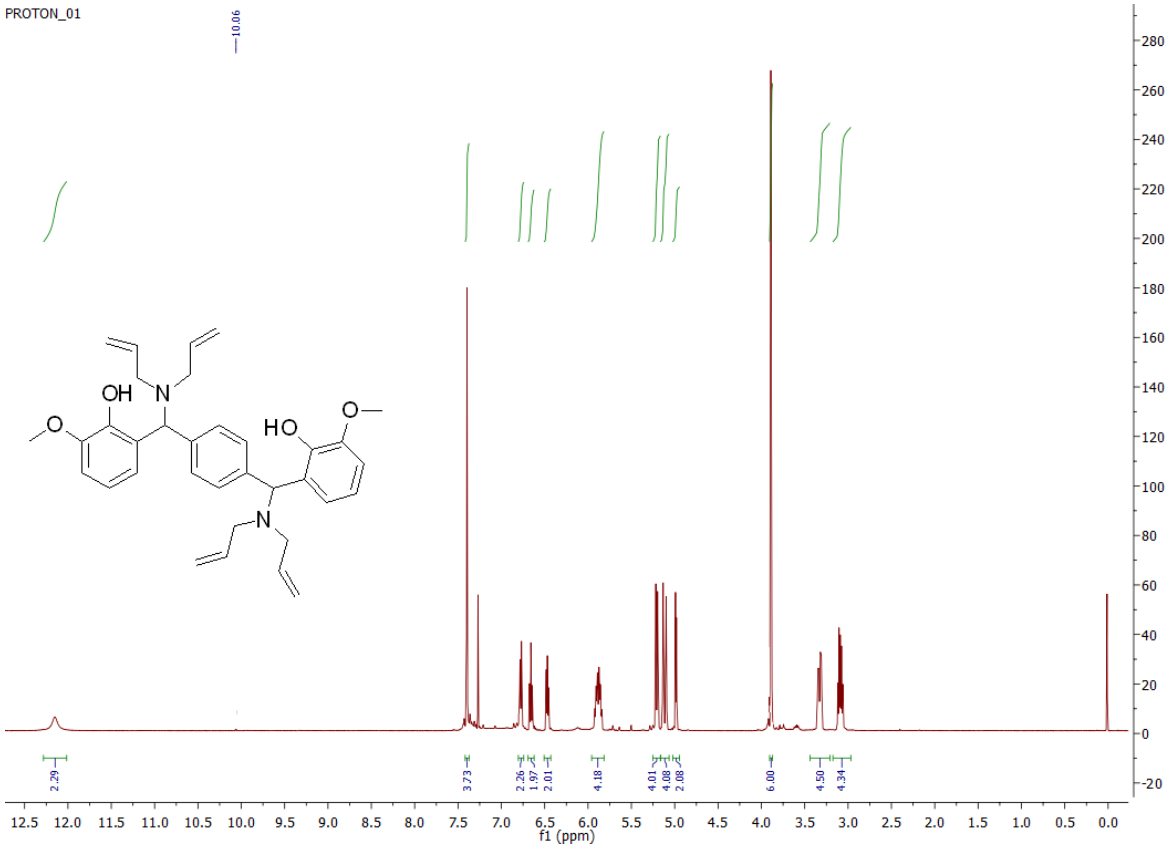

S8.150. ^{1}H NMR of C8cq

8.12 ^{13}C NMR of C8ca-C8aq

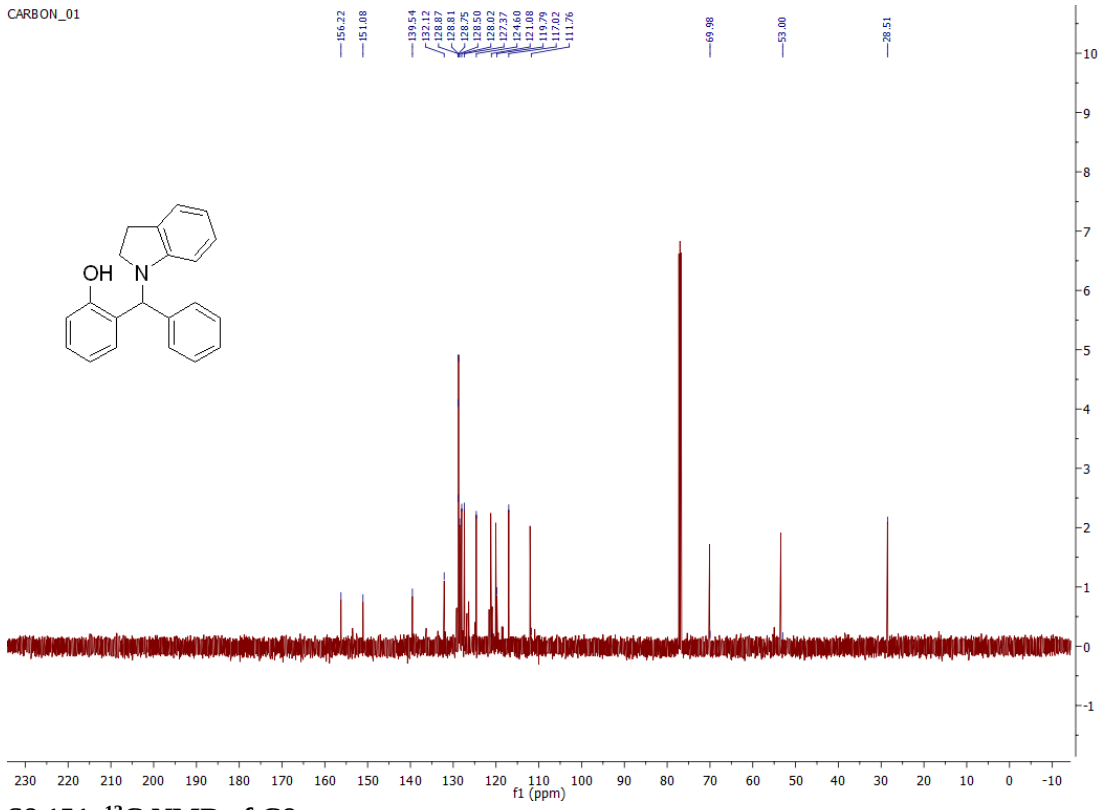

S8.151. ^{13}C NMR of C8ca

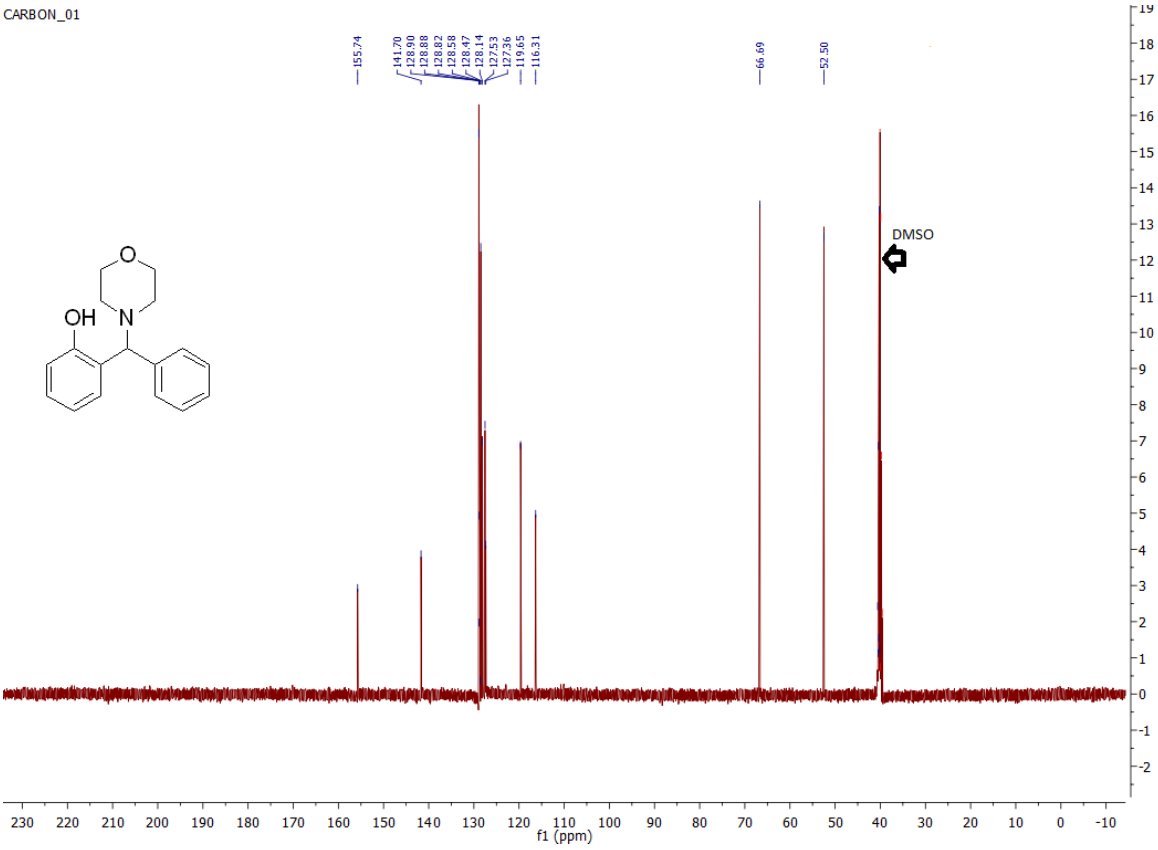

S8.152. ^{13}C NMR of C8cb

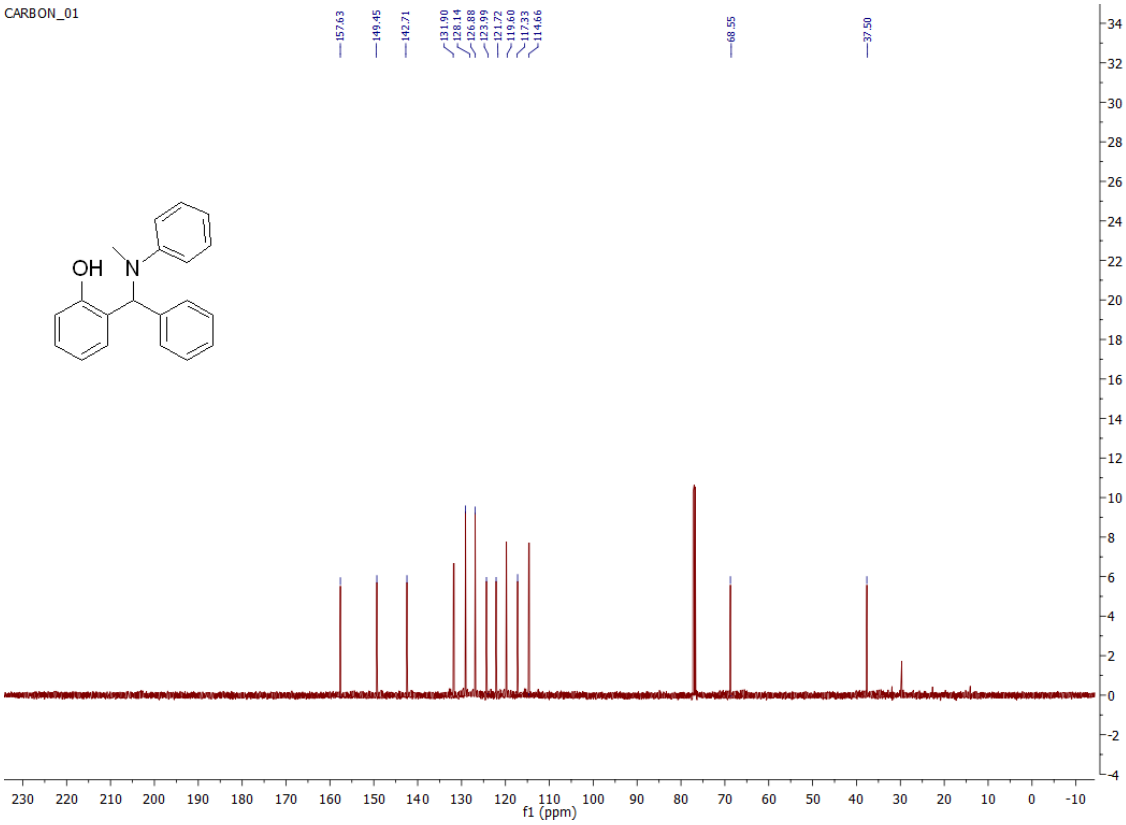

S8.153. ^{13}C NMR of C8cc

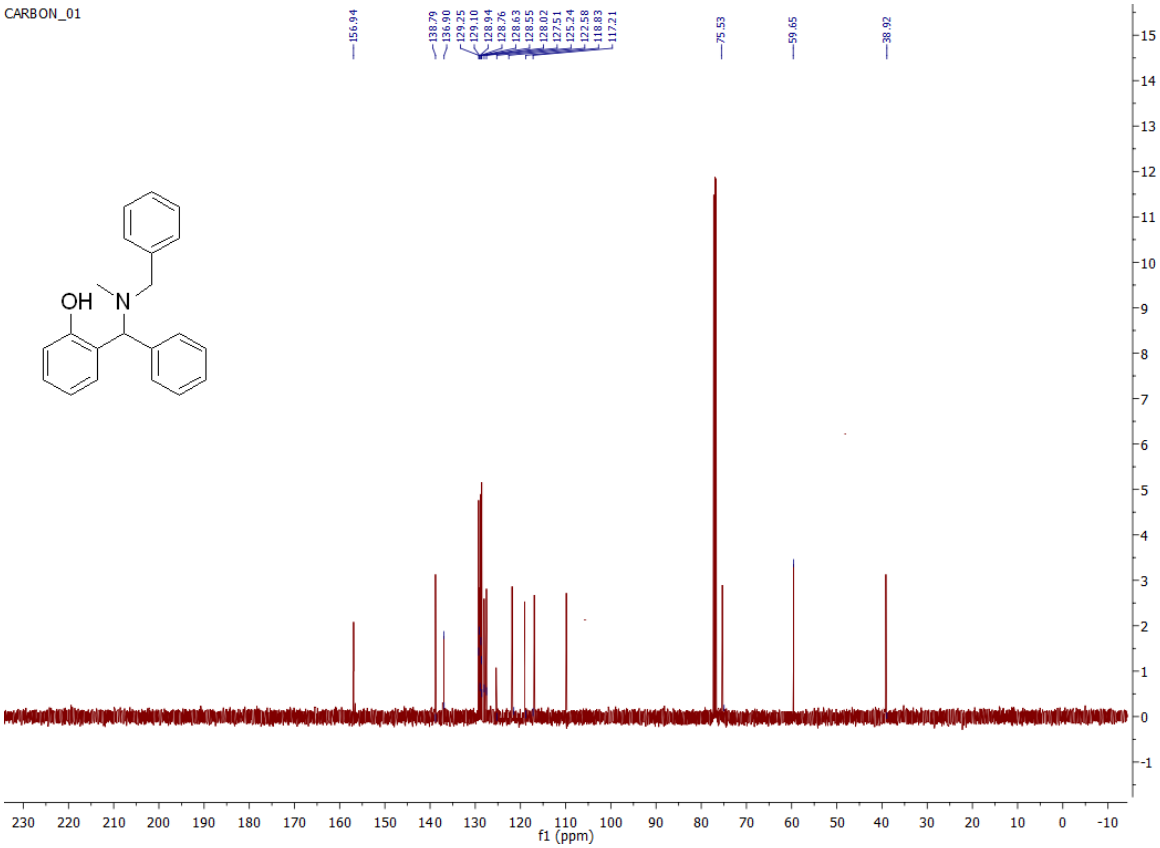

S8.154. ^{13}C NMR of C8cd

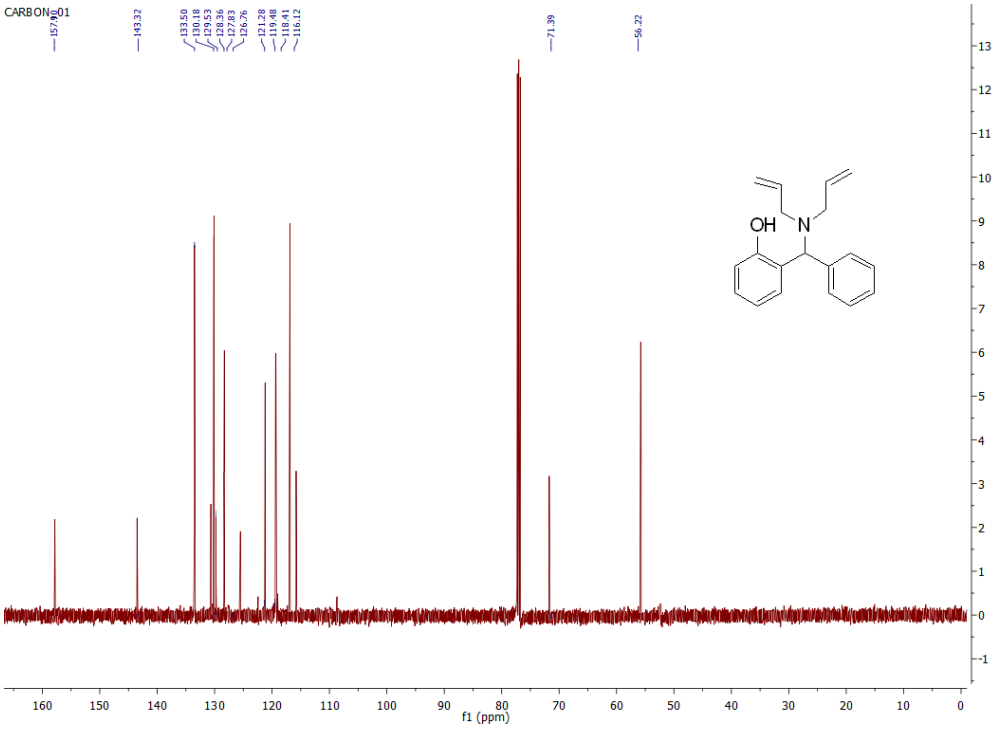

S8.155. ^{13}C NMR of C8ce

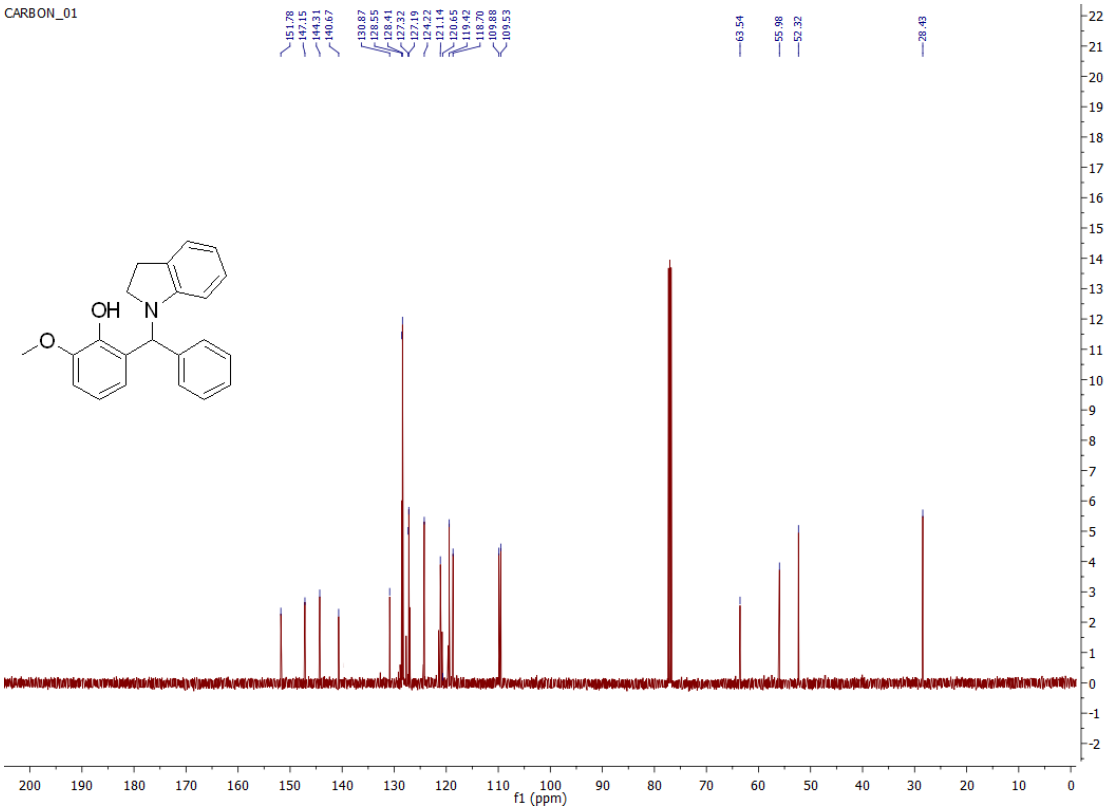

S8.156. ^{13}C NMR of C8cf

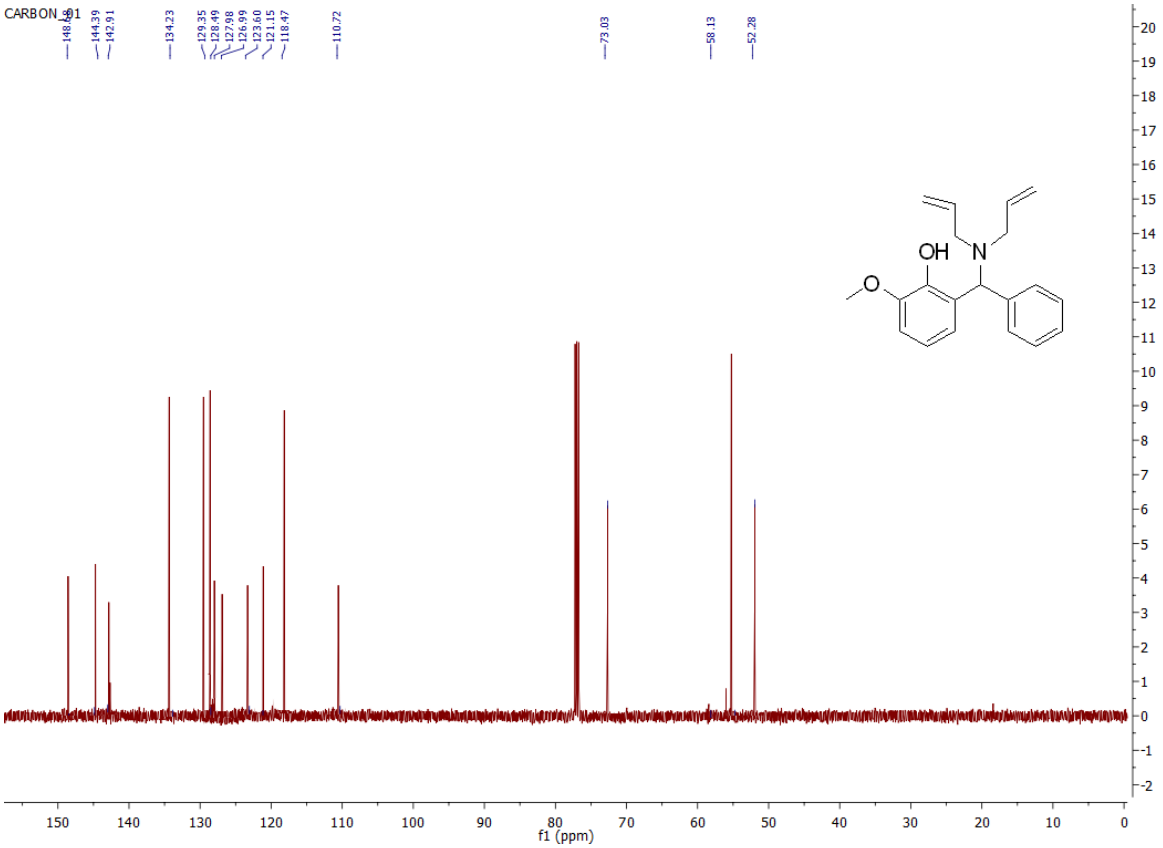

S8.157. ^{13}C NMR of C8cg

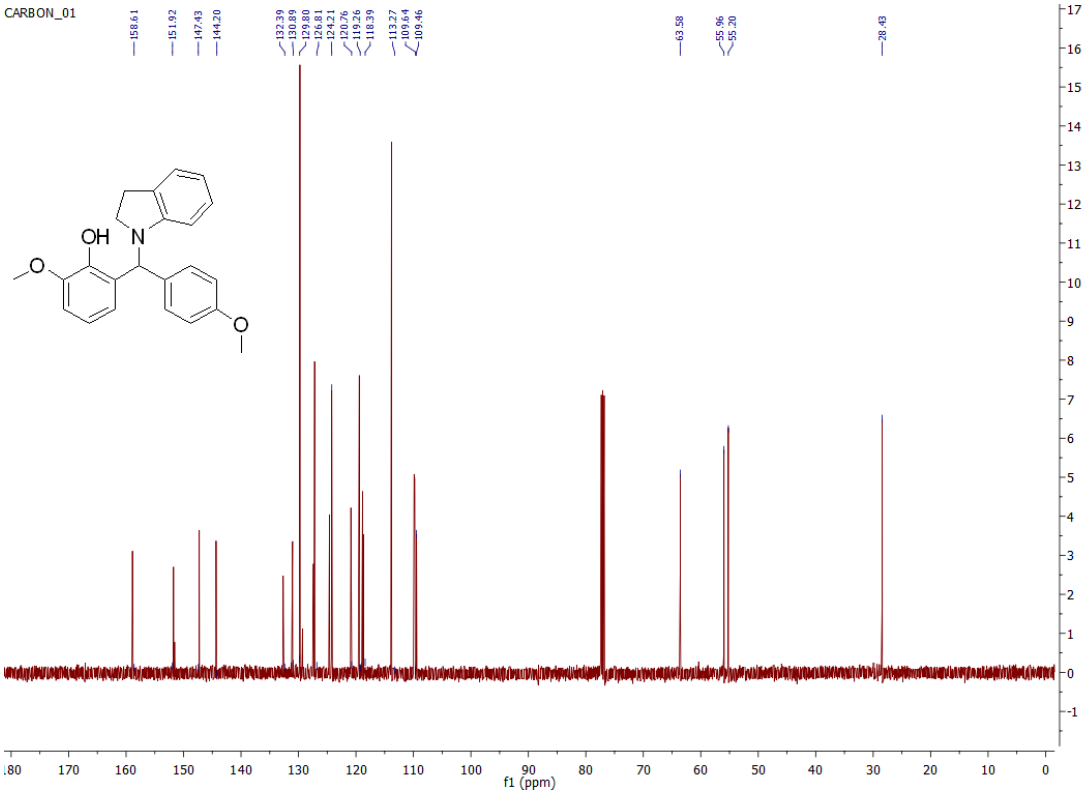

S8.158. ^{13}C NMR of C8ch

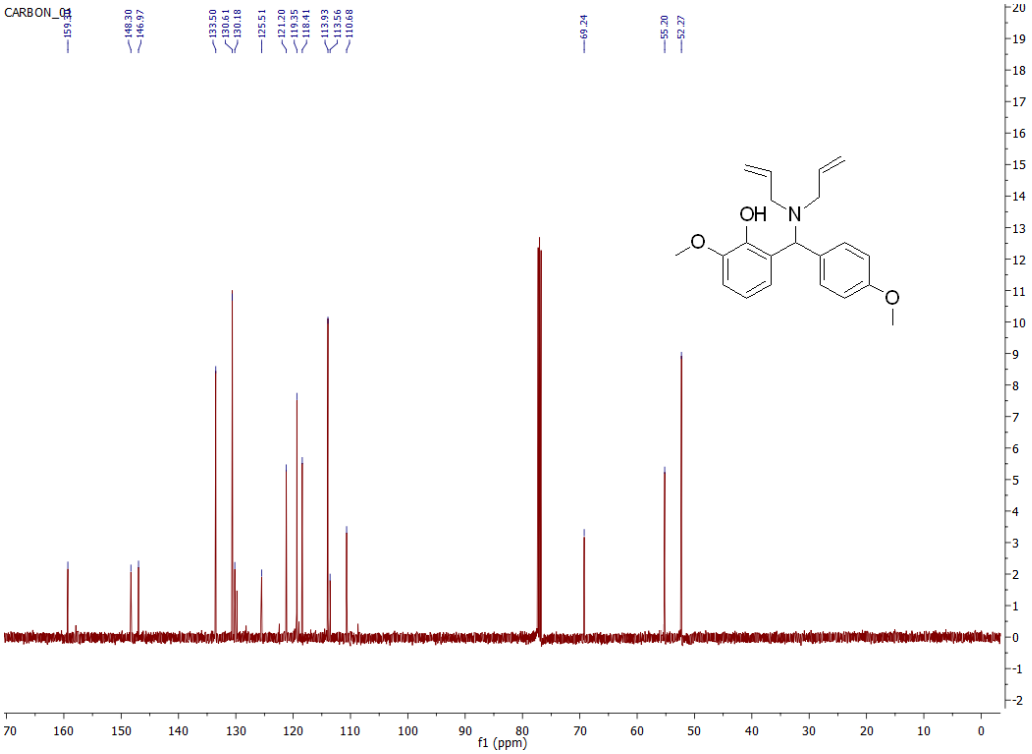

S8.159. ^{13}C NMR of C8ci

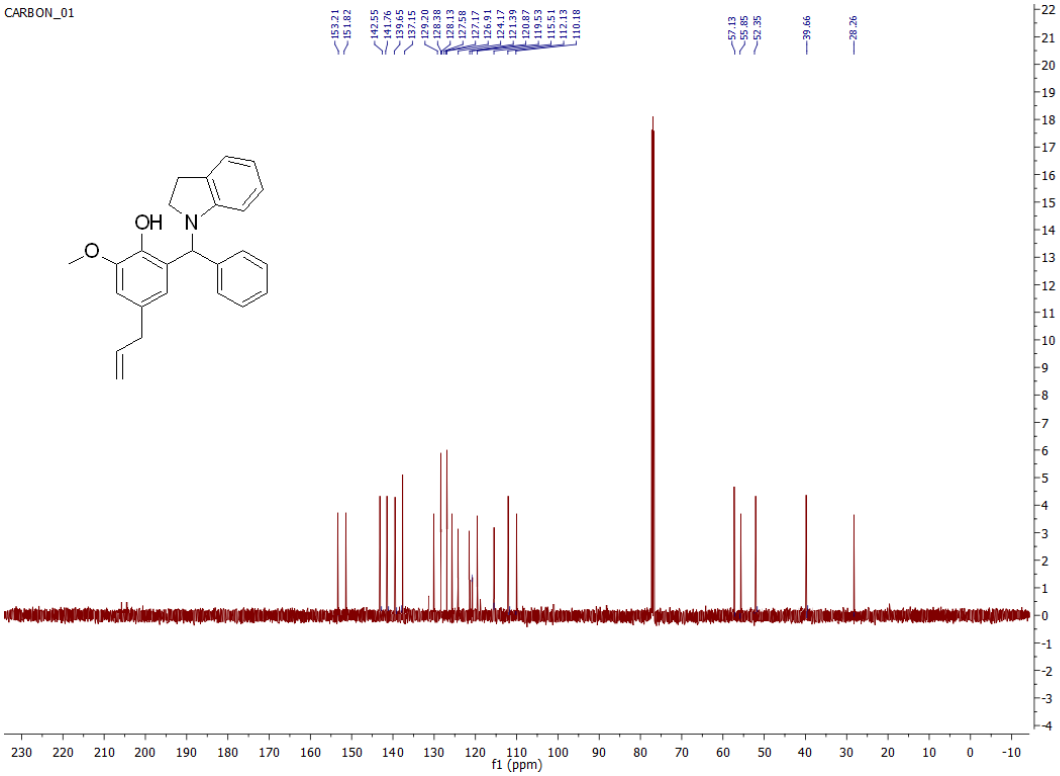

S8.160. ^{13}C NMR of C8cj

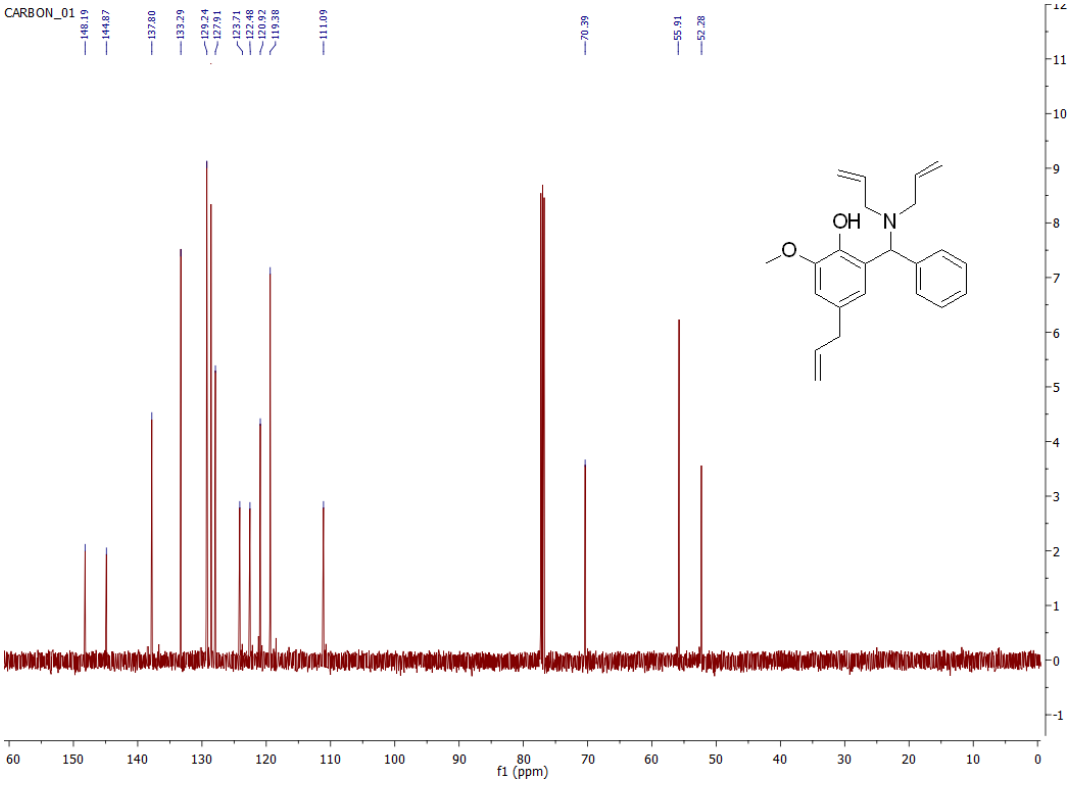

S8.161. ^{13}C NMR of C8ck

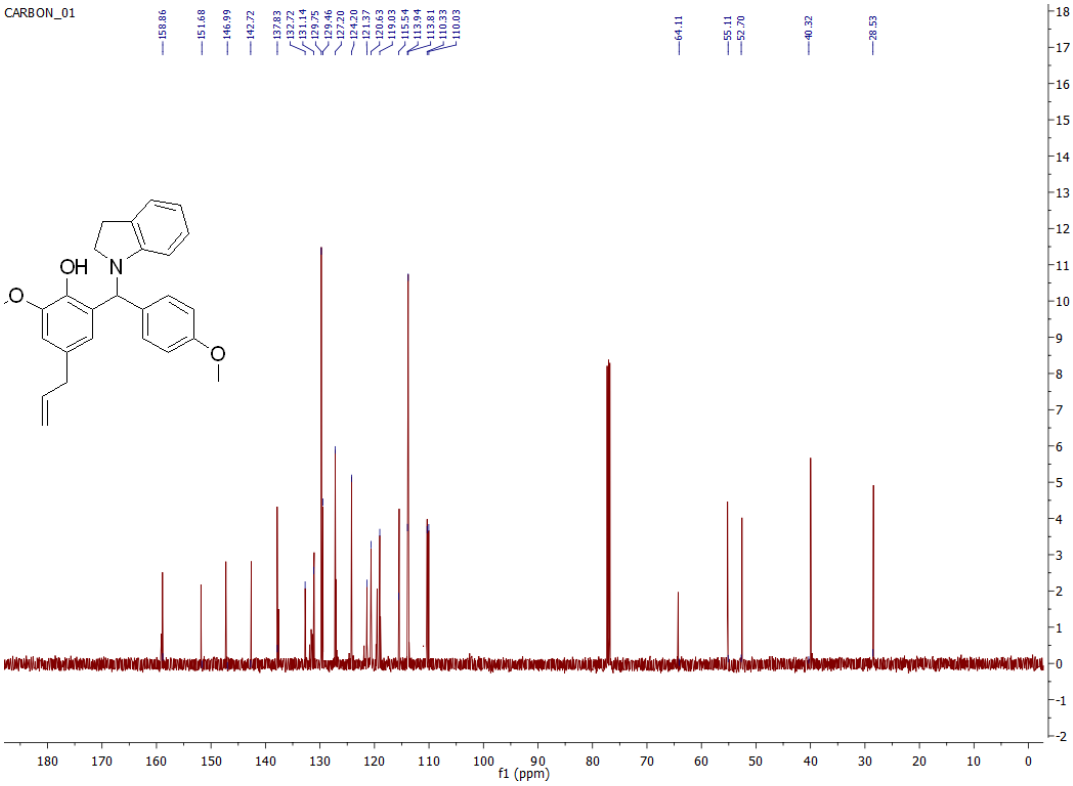

S8.162. ^{13}C NMR of C8cl

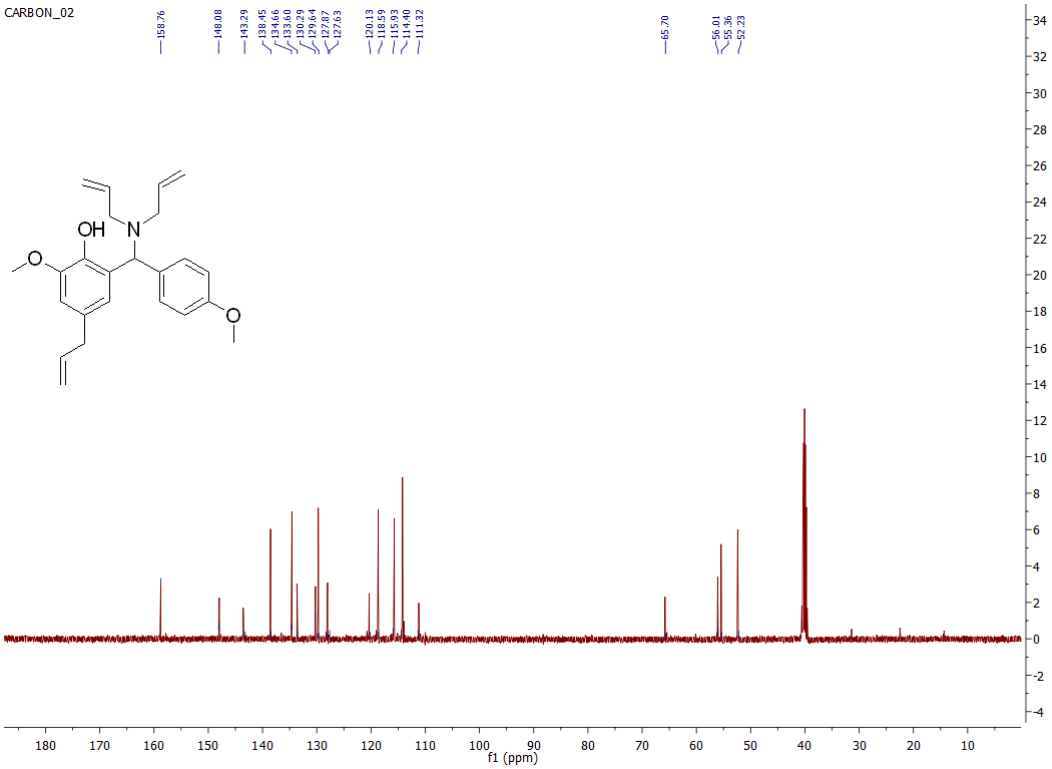

S8.163. ^{13}C NMR of C8cm

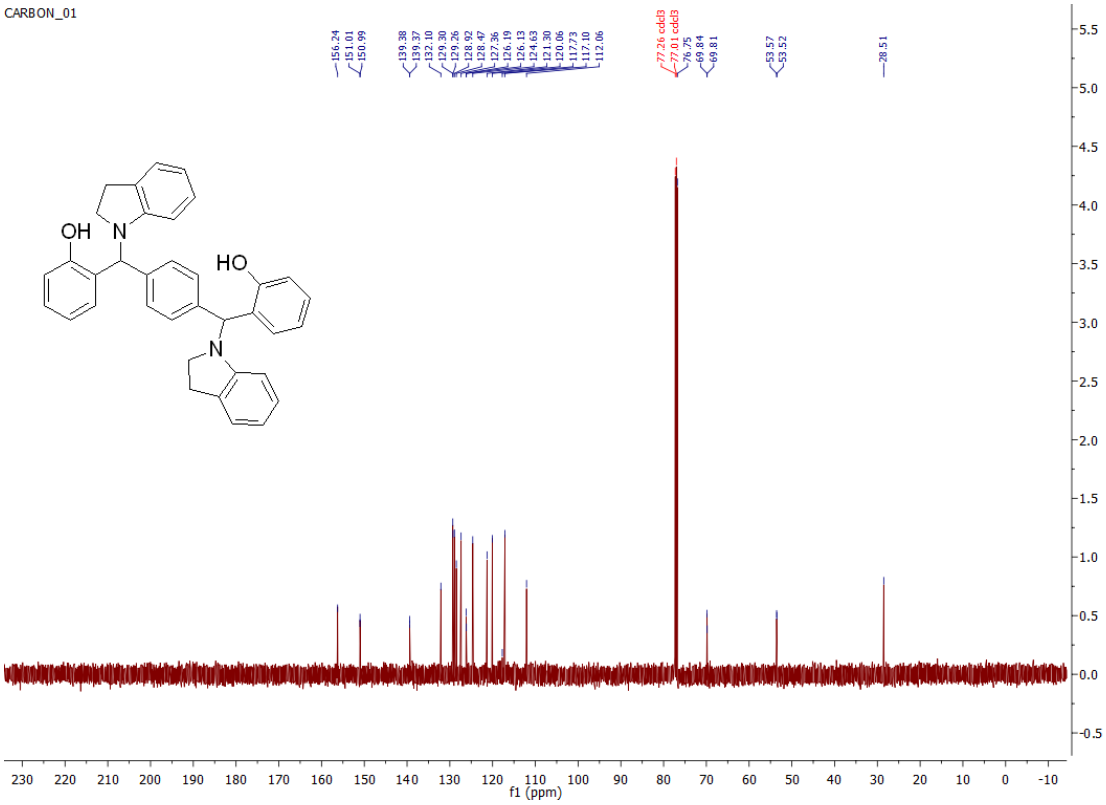

S8.164. ^{13}C NMR of C8cn

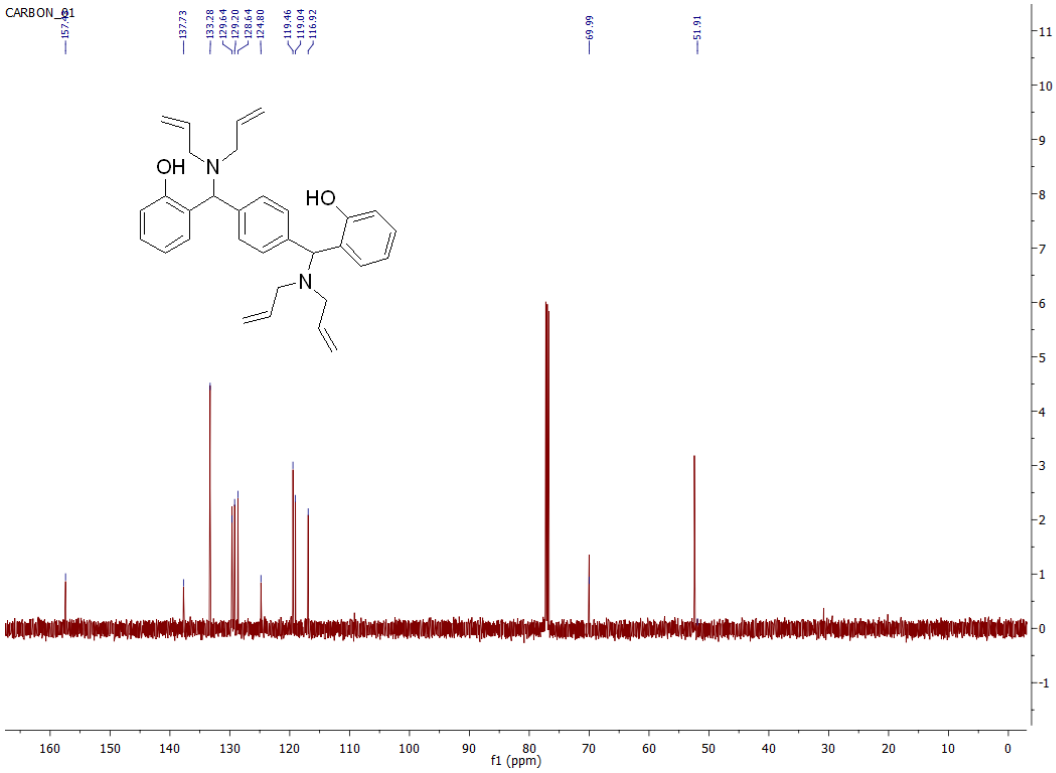

S8.165. ^{13}C NMR of C8co

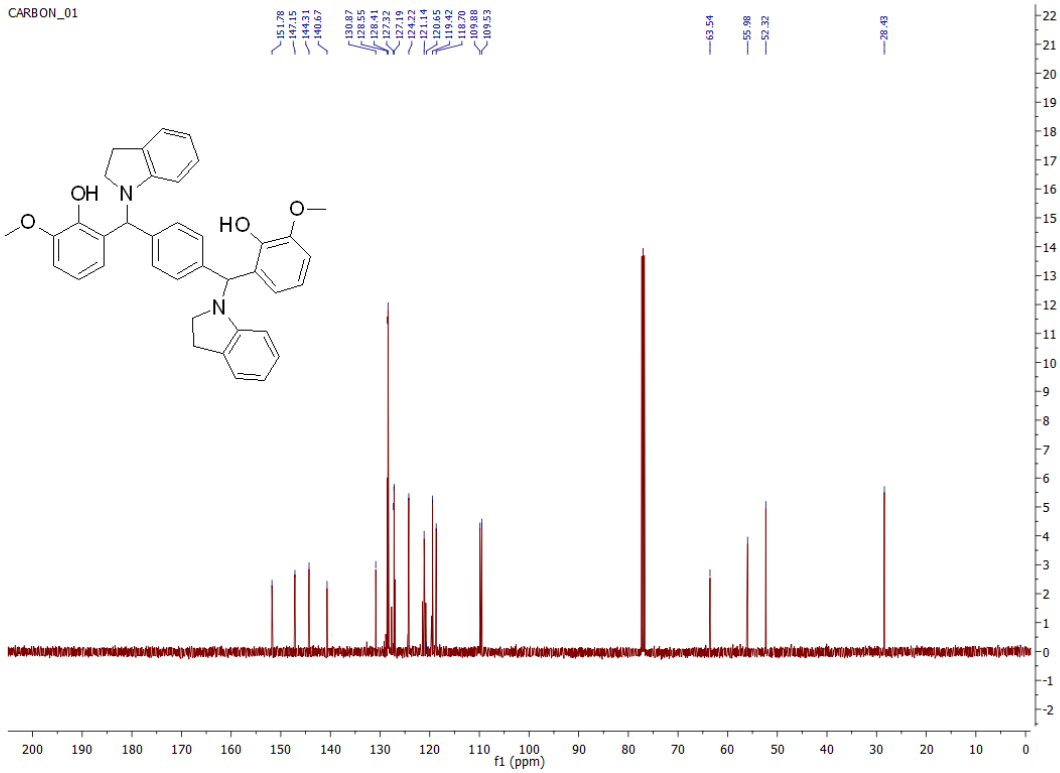

S8.166. ^{13}C NMR of C8cp

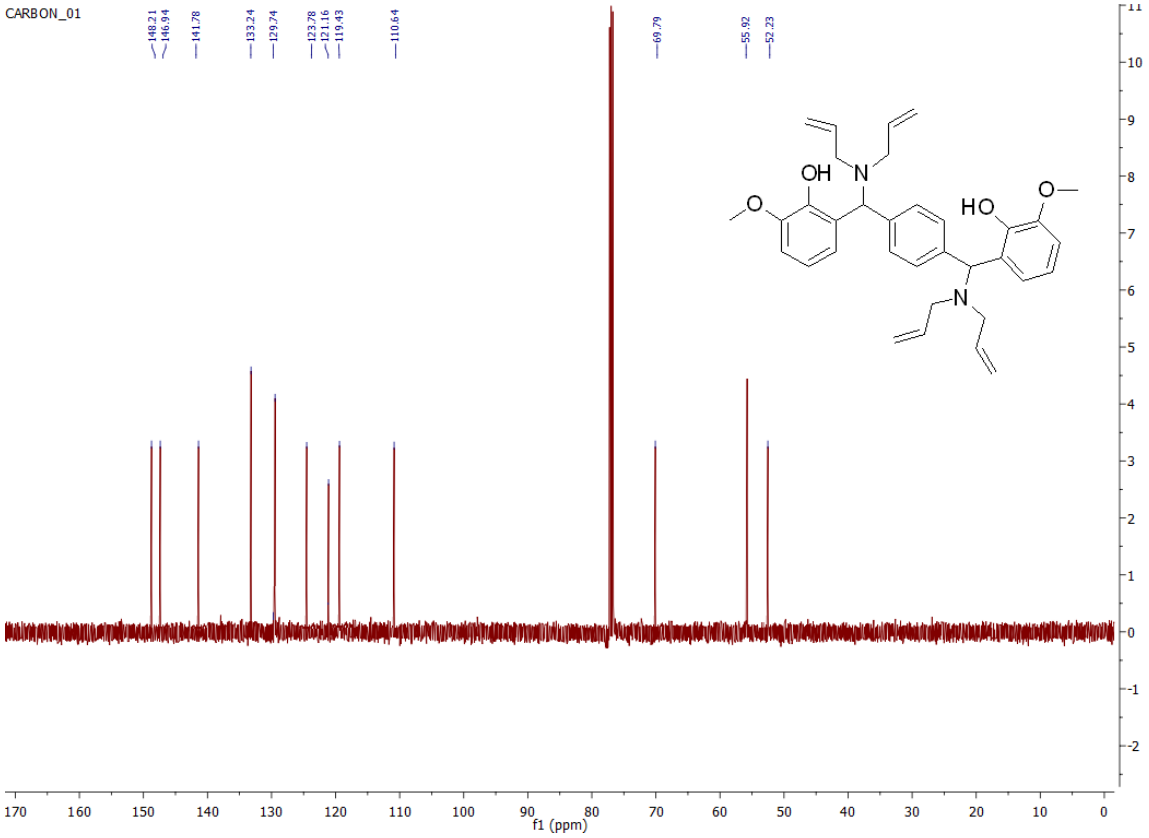

S8.167. ^{13}C NMR of C8cq

Chapter 9

9.1 UV-studies

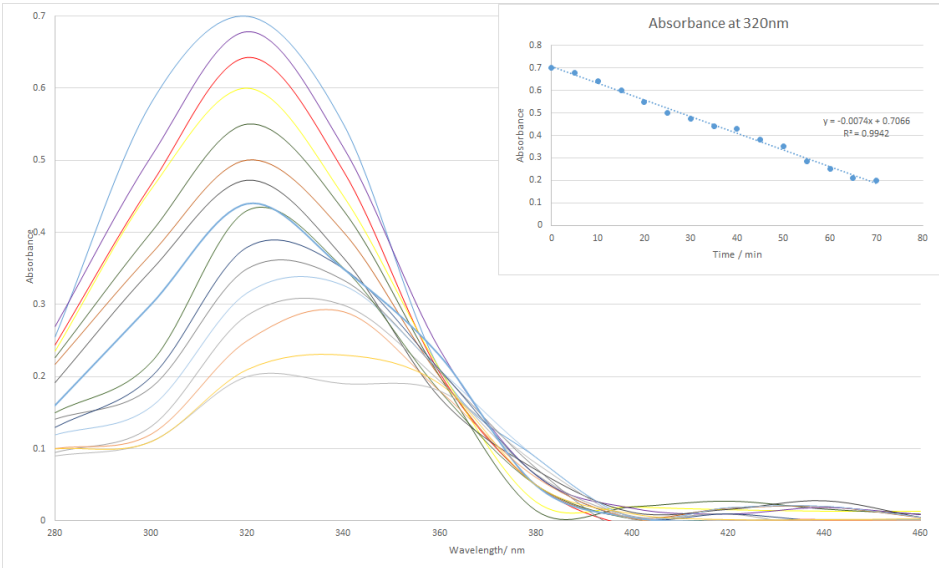

Figure S9.1. *trans*-β-nitrostyrene -1x10^{-5} mmol, dimethylbarbituric acid – 1x10^{-5} mmol, **1ZnY-NO$_3$** – 0.0000125 mmol, concentration of substrates 4x10^{-5} mmol L^{-1} for study. Usual concentration for a reaction 10 mmol L^{-1}, Solution – 250 mL $^{-1}$ of EtOH/H_2O (1:9).

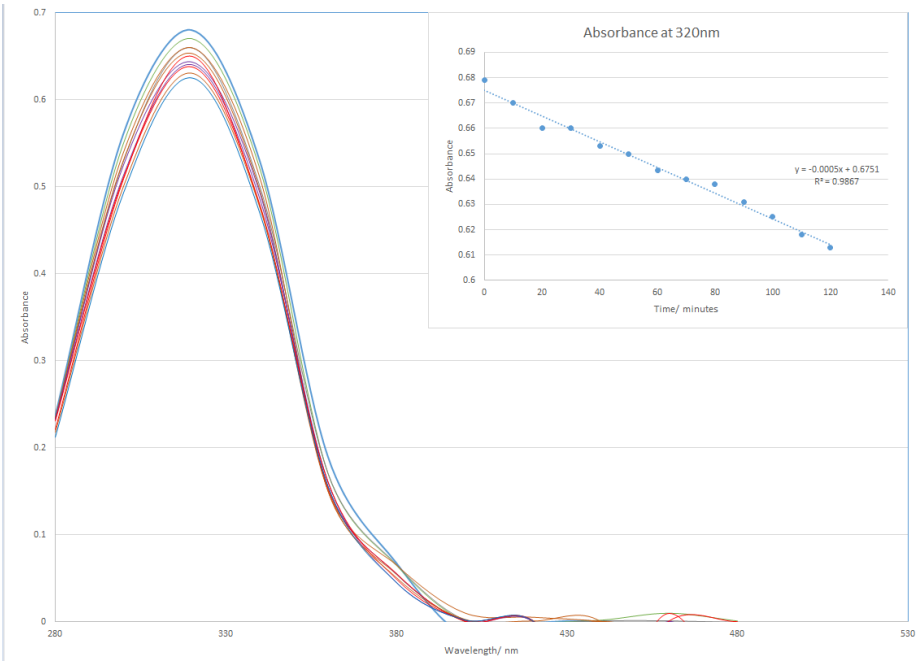

Figure S9.2. *trans*-beta-nitrostyrene -1x10^{-5} mmol, dimethylbarbituric acid – 1x10^{-5} mmol, no catalyst, solution – 250 mL $^{-1}$ of EtOH/H_2O (1:9).

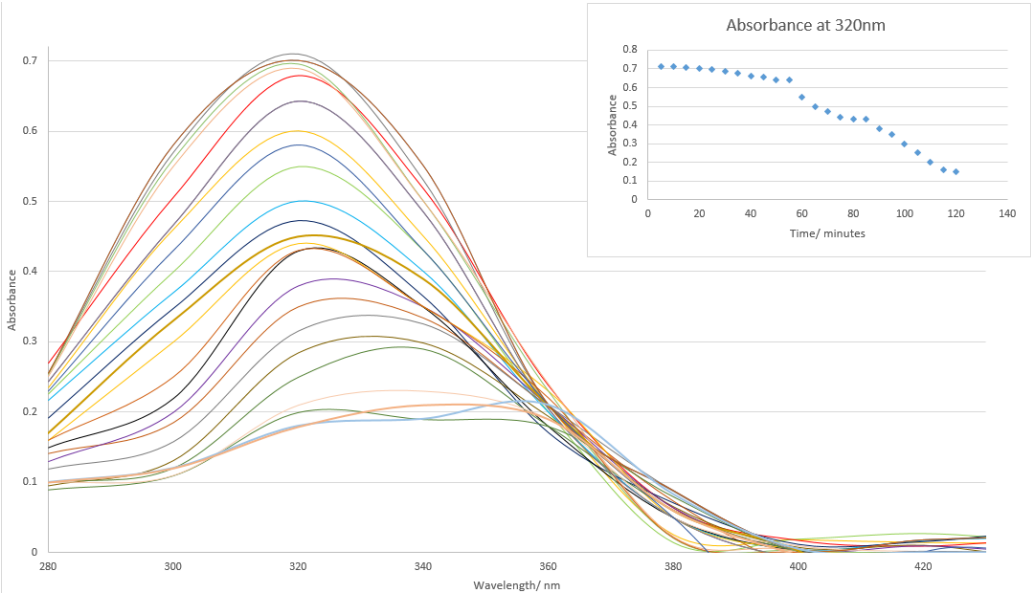

Figure S9.3. *trans*-beta-nitrostyrene -1x10^{-5} mmol, dimethylbarbituric acid – 1x10^{-5} mmol, and at 60 min catalyst **1ZnY-NO$_3$** – 0.0000125 mmol, was added.

9.2 EPR Studies

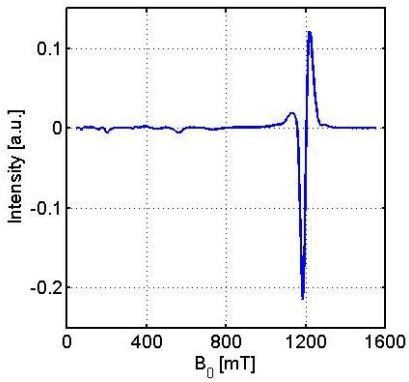

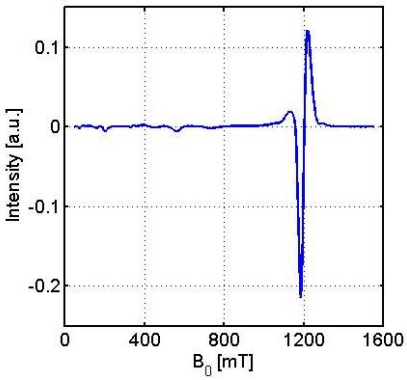

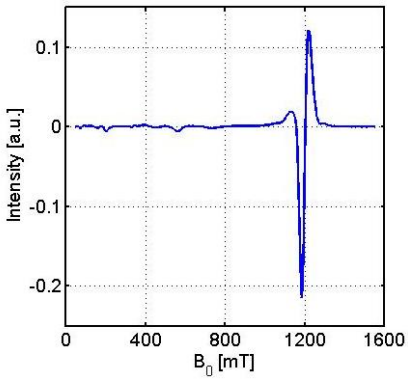

1**ZnGd** with BA (1:1)

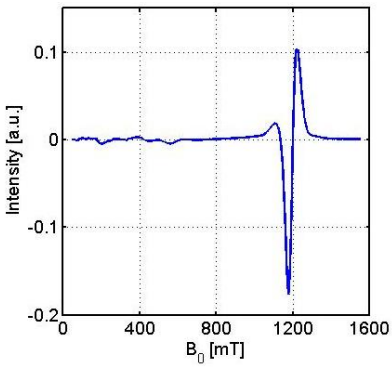

1**ZnGd** with NS (1:1)

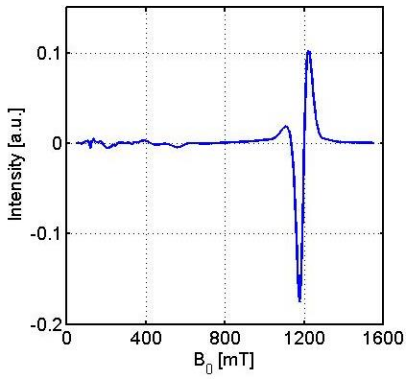

1**ZnGd** with BA and NS (1:1)

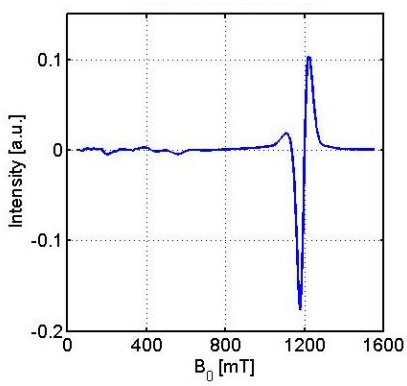

1**ZnGd** with BA (1:20)

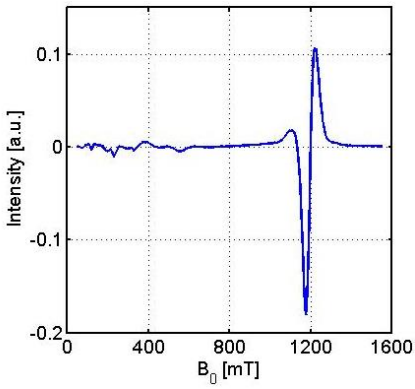

1**ZnGd** with NS (1:20)

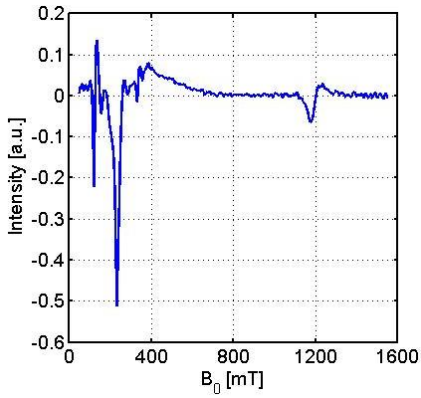

1**ZnGd** with BA and NS (1:20)

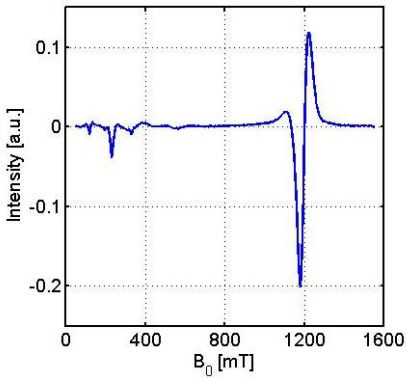

1**ZnGd** with BA (1:40)

1**ZnGd** with NS (1:40)

1**ZnGd** with BA and NS(1:40)

Figure S9.4. The EPR Data

9.3 Theoretical Studies

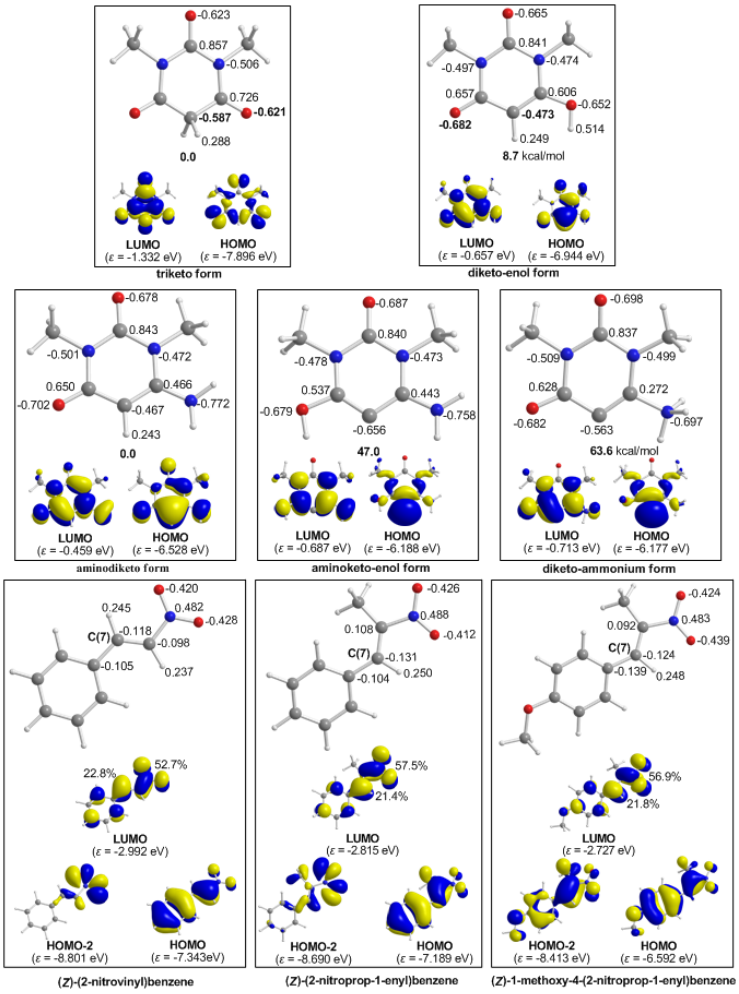

Figure S9.5. Natural atomic charges and the relevant FMOs of the triketo and diketo-enol forms of 1,3-dimethyl barbituric acid, the aminodiketo, aminoketo-enol and diketo-ammonium forms of 6-amino 1,3-dimethyl barbituric acid and the (*Z*)-(2-nitrovinyl)benzene, (*Z*)-(2-nitroprop-1-enyl)benzene and (*Z*)-1-methoxy-4-(2-nitroprop-1-enyl)benzene calculated at the PBE0/6-311++G(d,p) level of theory in aqueous solutions.

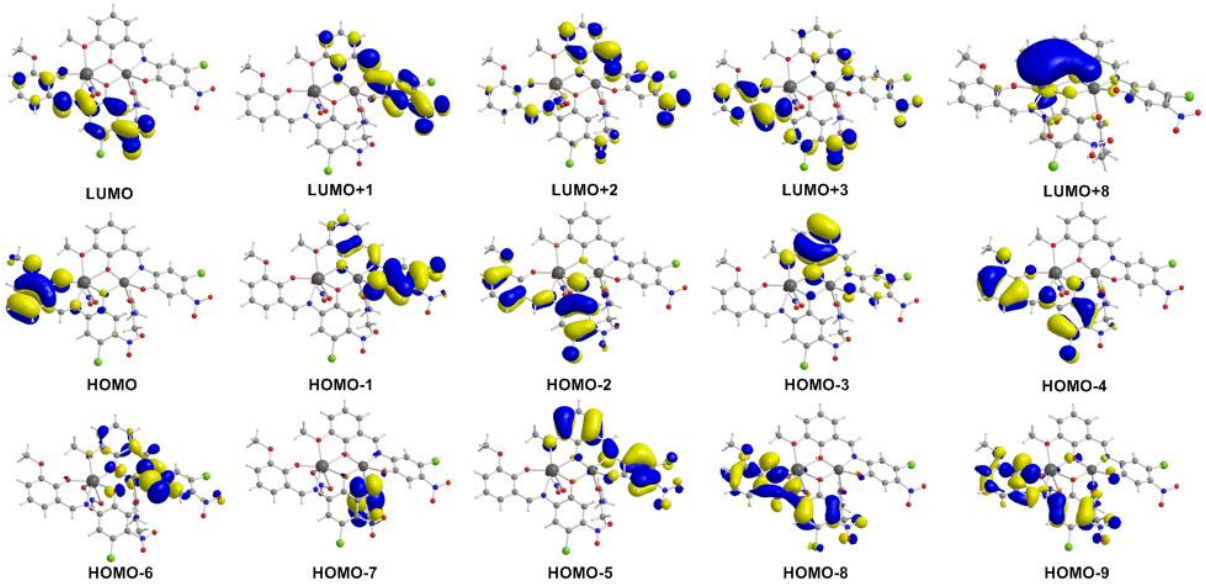

Figure S9.6. 3D plots of FMOs of the representative catalyst **7ZnY** calculated at the PBE0/Def2-TZVP(Zn,Y) ∪ 6-31G(d,p)(E) (E = main group element) level of theory in aqueous solutions.

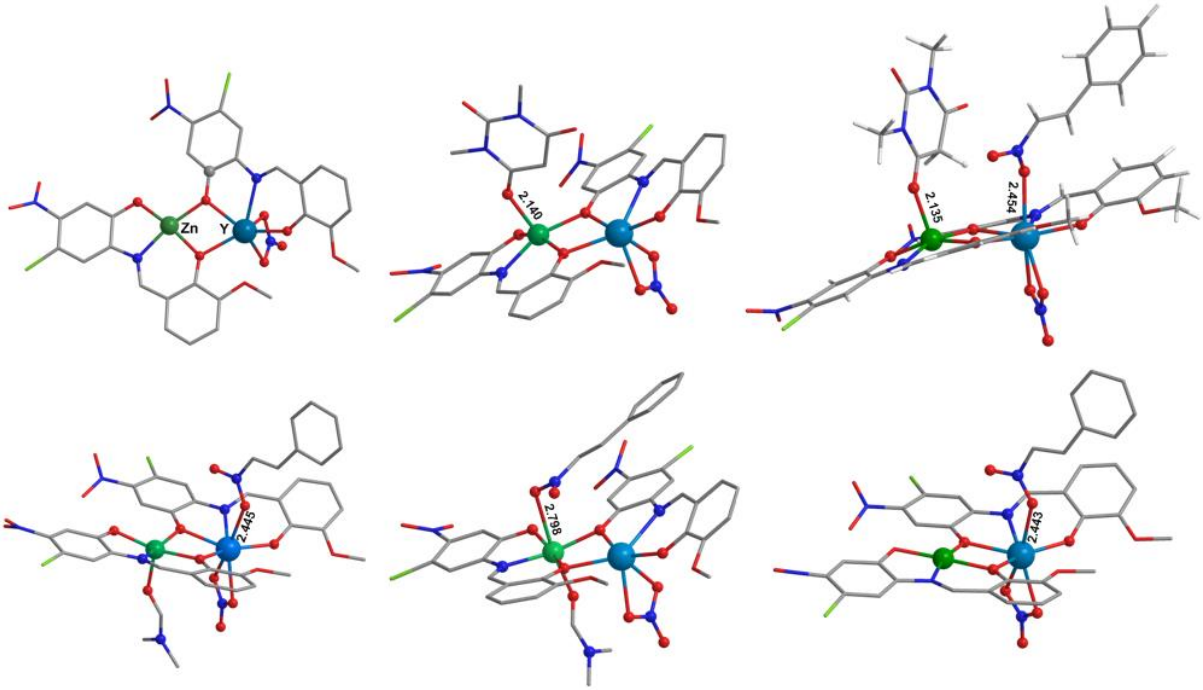

Figure S9.7. The equillibrium geometries of the **7ZnY**-barbiturate and **7ZnY**-*trans*-nitro-styrene adducts optimized at the PBE0/Def2-TZVP(Zn,Y) ∪ 6-31G(d,p)(E) (E = main group element) level of theory in aqueous solutions

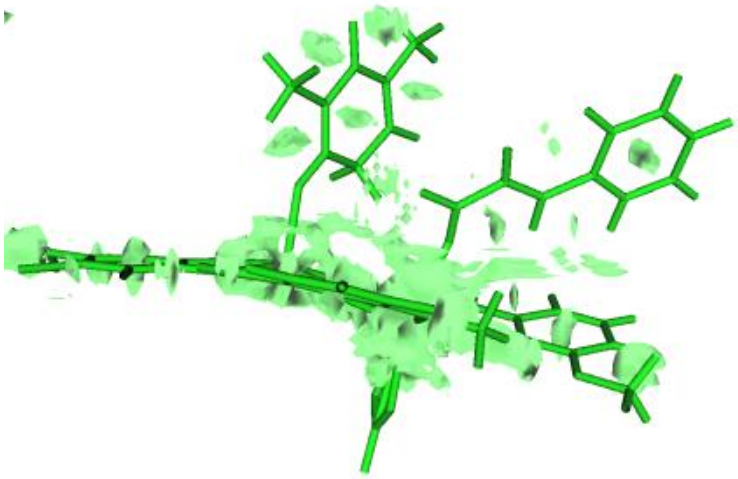

Figure S9.8. 3D plot of the *RDG* (Reduced Density Gradient, isosurface = 0.800 au) of the catalyst-substrate complex **2Im**.

9.4 ESI-MS substrate binding studies

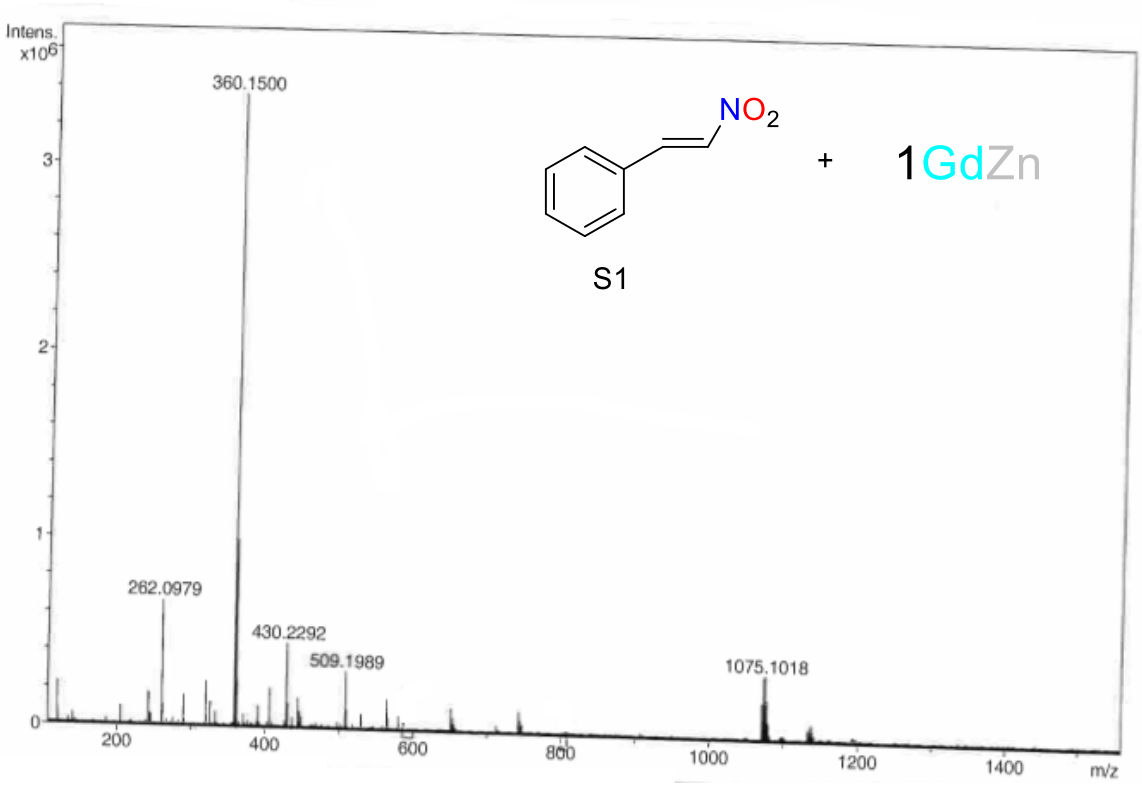

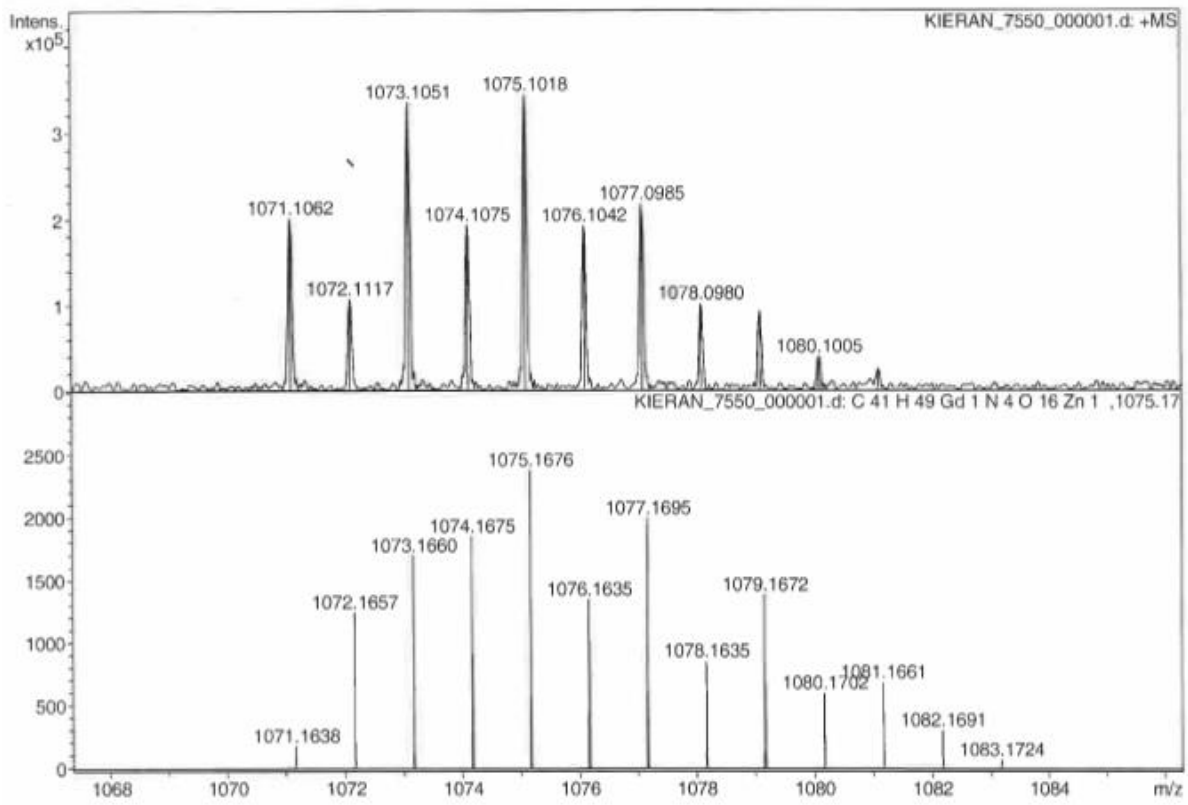

Figure S9.9. ESI-MS Spectra of **1ZnGd-NO$_3$** with trans-β-nitrostyrene (catalytic ratio). Fragment [Zn^{II}Gd^{III}(**L1**)$_2$(S1)(NO$_3$)(CH$_3$OH)$_5$] -1075.1676

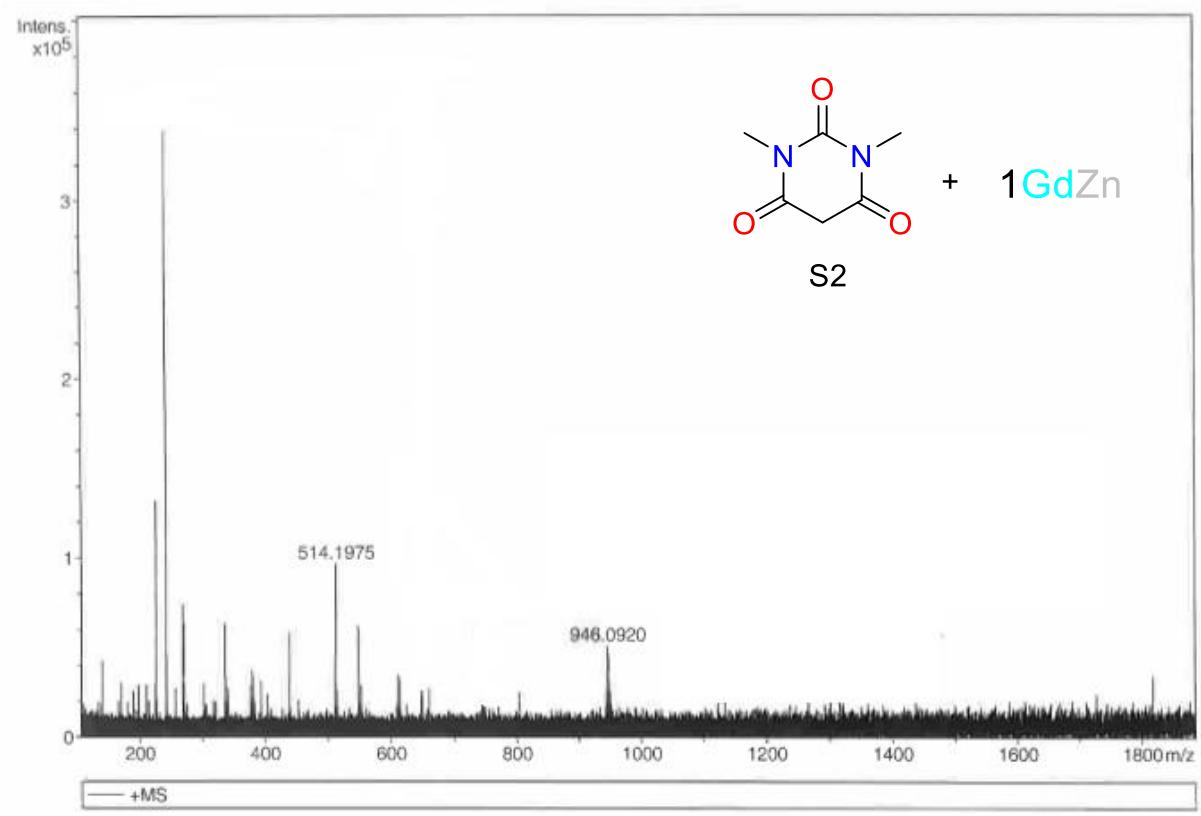

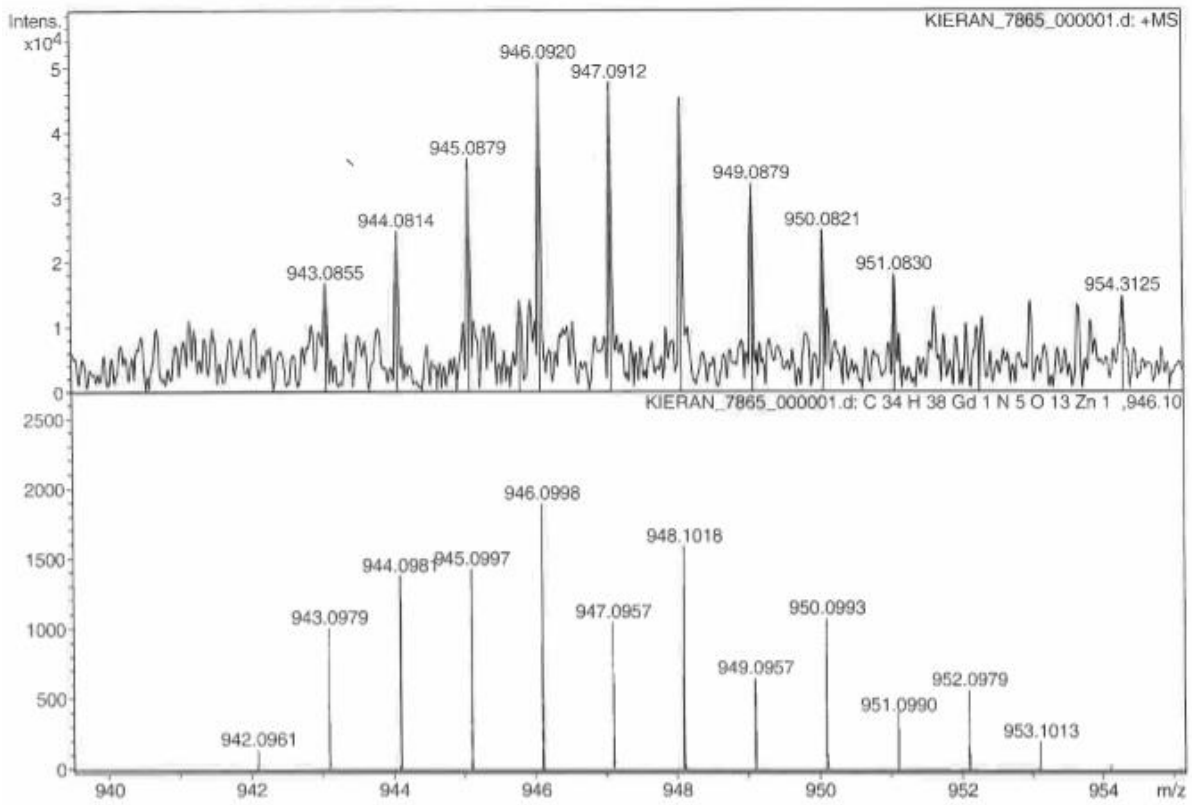

Figure S9.10. ESI-MS spectra of **1ZnGd-NO$_3$** with dimethylbarbituric acid. Fragment [Zn^{II}Gd^{III}(**L1**)$_2$(S2)(NO$_3$)(H$_2$O)] - 946.0998

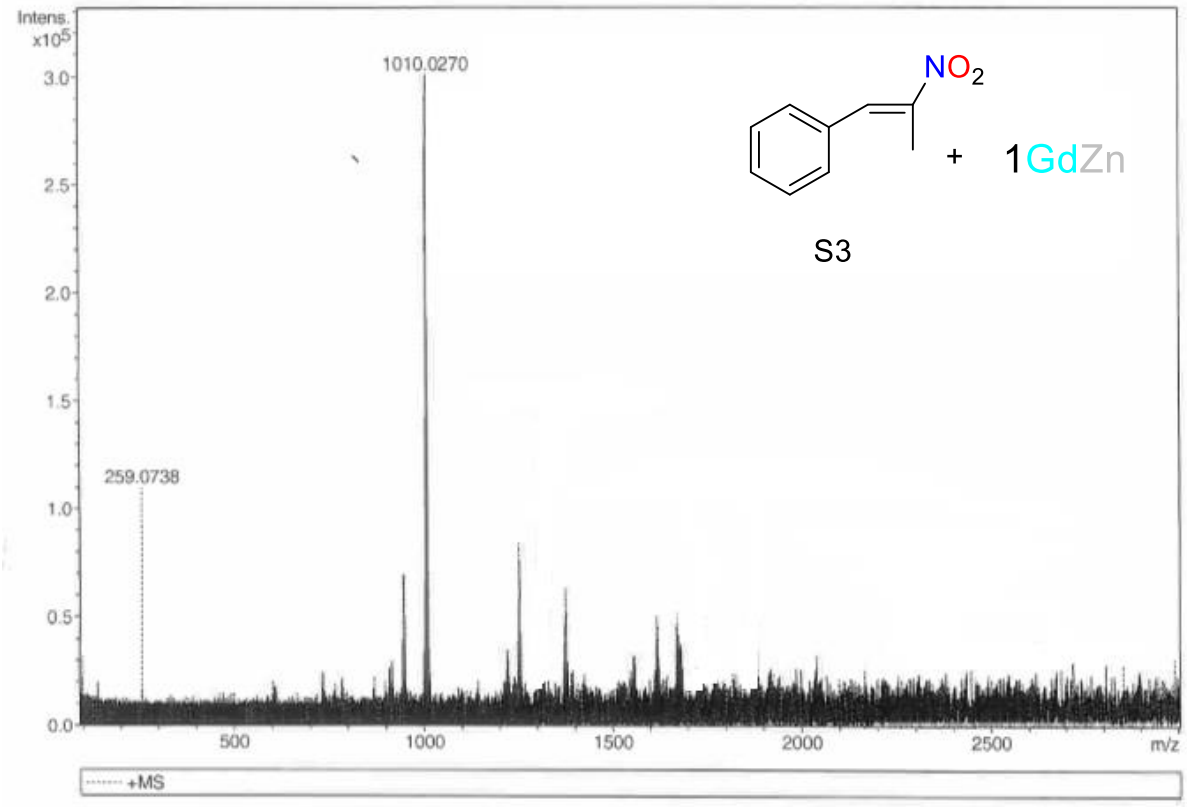

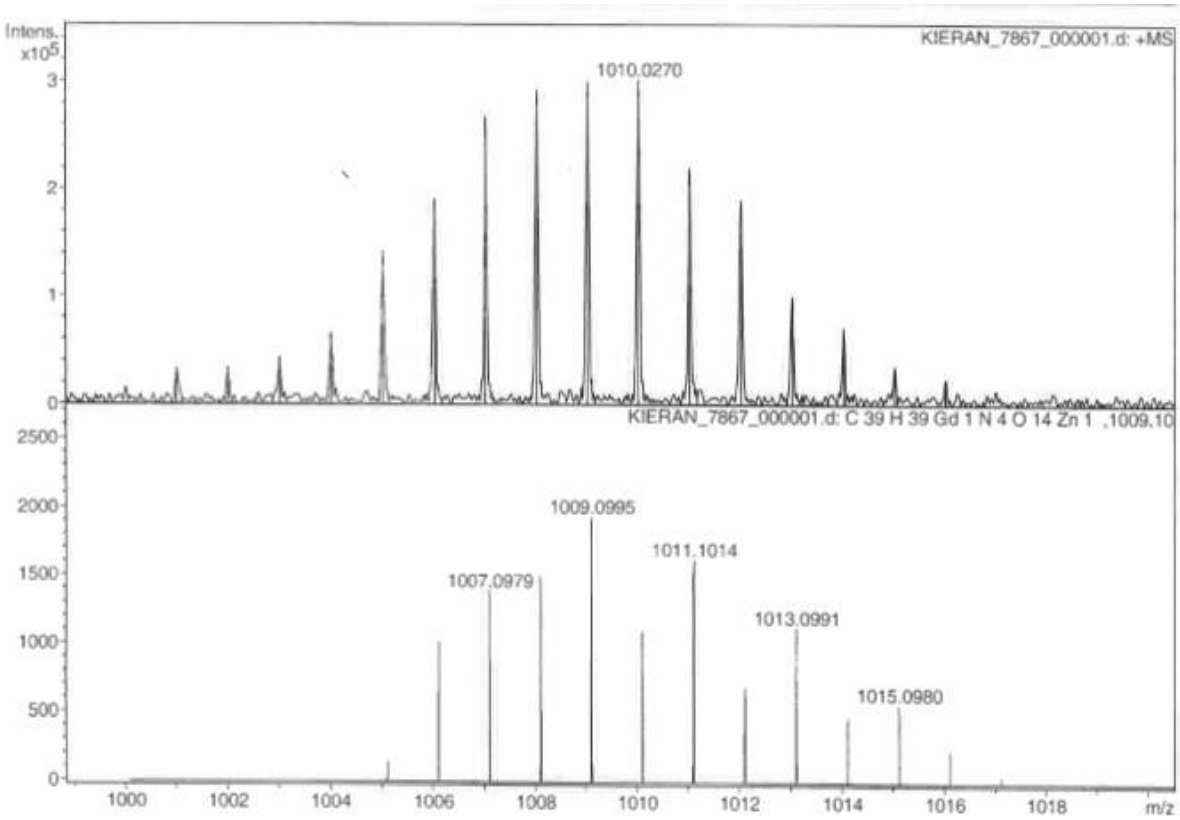

Figure S9.11. ESI-MS spectra of **1ZnGd-NO$_3$** with trans-β-methyl-β nitrostyrene acid (catalytic ratio). Fragment [Zn^{II}Gd^{III}(**L1**)$_2$(S3)(NO$_3$)(CH$_3$OH)$_2$(H$_2$O)] – 1009.0995

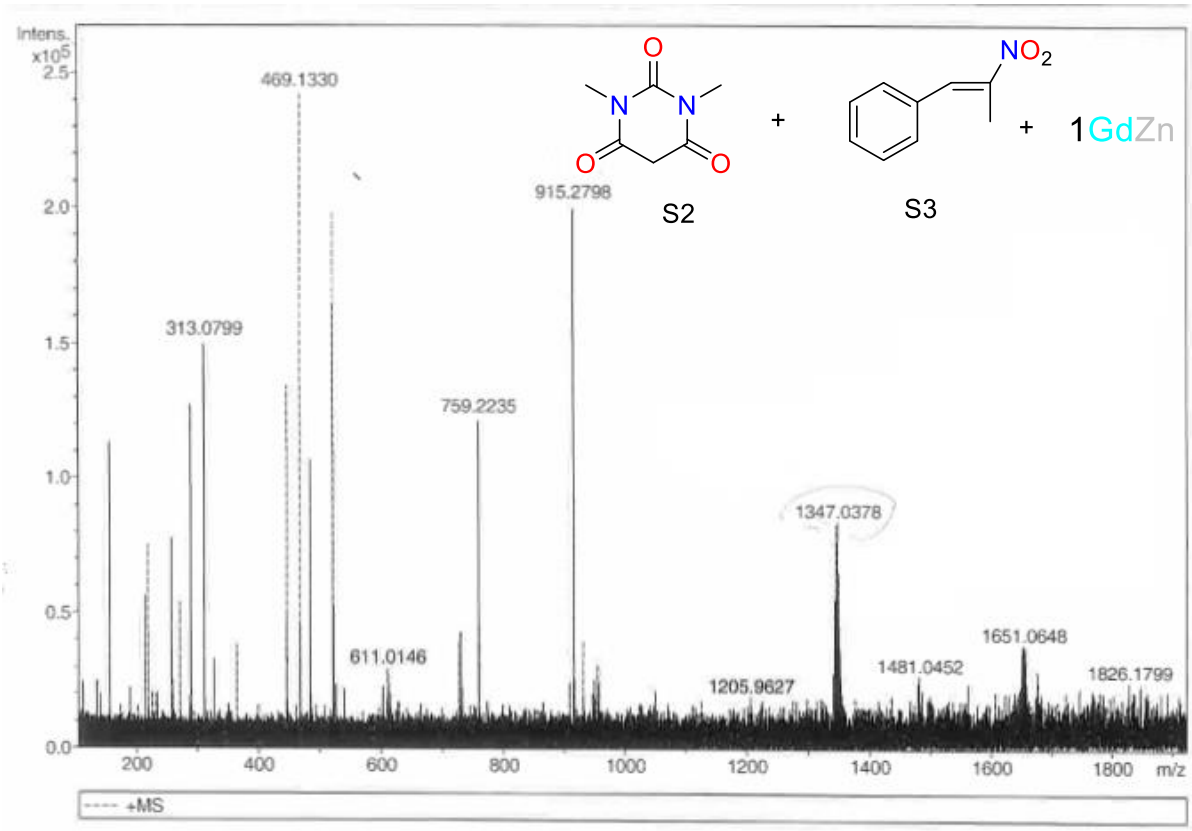

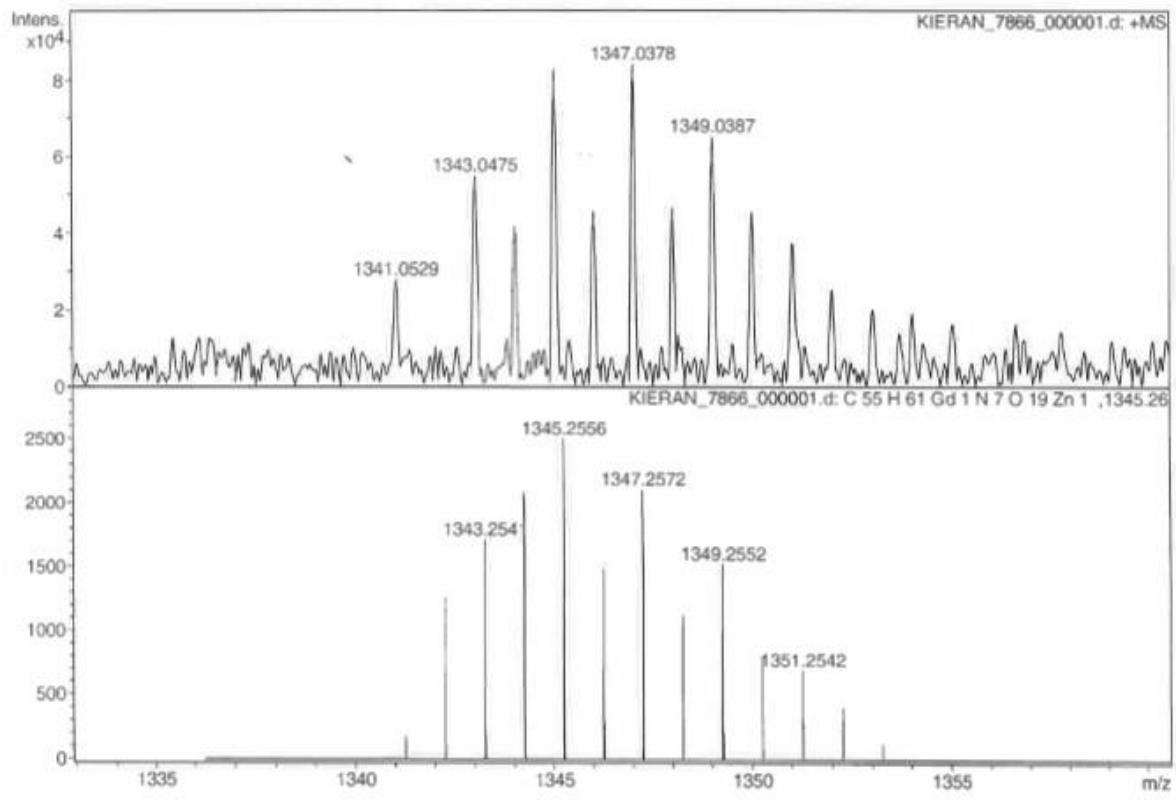

Figure S9.12. ESI-MS spectra of **1ZnGd-NO$_3$** with trans-β-methyl-β Nitrostyrene acid and DMBA(Catalytic Ratio). Fragment [$Zn^{II}Gd^{III}$(**L1**)$_2$(S2)(S3)$_2$(NO_3)(CH_3OH)$_3$] – 1345.2556

9.5 Theoretical Data

Table S9.13. Cartesian Coordinates and energies of 1 calculated at the /6-31G(d,p)/PCM level of theory in aqueous solution.

Triketo form of 1,3-Me$_2$-barbituric acid

N,0,-6.2246702034,1.2061475337,0.0282966307
C,0,-5.5245258923,0.0056207973,0.0489237536
O,0,-4.3242411739,-0.0066010337,0.2117219715
N,0,-6.2287262003,-1.1806062054,-0.120979318
C,0,-7.5915394353,-1.260486692,-0.3118657355
O,0,-8.1622633661,-2.3212491806,-0.4561691526
C,0,-8.3445111697,0.034314701,-0.3332906493
C,0,-7.5872696814,1.3137537374,-0.1501114235
O,0,-8.1545046479,2.3860930435,-0.1600038024
C,0,-5.4250966293,2.4138972756,0.2125282444
C,0,-5.433268778,-2.4045922981,-0.0889380103
H,0,-9.115699291,-0.0130953737,0.4412741323
H,0,-8.8807670146,0.0950223385,-1.2849563449
H,0,-6.101266481,3.2632142721,0.1715166227
H,0,-4.679425817,2.4907798849,-0.578819715
H,0,-4.9214273495,2.3831104046,1.178757387
H,0,-6.1127070278,-3.2400736615,-0.2323315182
H,0,-4.9273567354,-2.4945330731,0.8723838526
H,0,-4.6896331061,-2.3862164706,-0.8857369251

Sum of electronic and zero-point Energies= -568.081435
Sum of electronic and thermal Energies= -568.070797
Sum of electronic and thermal Enthalpies= -568.069853
Sum of electronic and thermal Free Energies= -568.118876

Diketo-enol form of 1,3-Me$_2$-barbituric acid

N,0,-1.1793133356,0.352995236,-0.000660351
C,0,-0.0054205302,1.0684681466,-0.0001813724
O,0,0.014313101,2.2873146442,0.0006522064
N,0,1.1761346905,0.3404300363,-0.0005746777
C,0,1.1607119091,-1.0249035277,-0.0002142247
O,0,2.3715274102,-1.5739243459,0.0000716104
C,0,-0.0027180419,-1.7275341012,-0.0000990666
C,0,-1.2589565395,-1.0517208217,-0.000279931
O,0,-2.3524393294,-1.6089680943,0.0003224193
C,0,-2.4062603179,1.1370538019,-0.0004517374
C,0,2.4138538436,1.1165303865,-0.000152084
H,0,0.0011747326,-2.8087729256,0.0003576147
H,0,-3.2386629893,0.4385768983,-0.0057124605
H,0,-2.445284283,1.7737255362,-0.8854895445
H,0,-2.4505005172,1.7659704486,0.8899624399
H,0,3.2576605349,0.4344779594,-0.0042050411
H,0,2.4510135628,1.7451818522,0.8898332684
H,0,2.4473066935,1.7511848702,-0.8859454508
H,0,2.294959406,-2.5345860001,0.0001663827

Sum of electronic and zero-point Energies= -568.067503
Sum of electronic and thermal Energies= -568.056906
Sum of electronic and thermal Enthalpies= -568.055962
Sum of electronic and thermal Free Energies= -568.104437

1,3-Me$_2$-barbituric carbanion

N,0,1.1729008772,0.4131873397,-0.0405865222
C,0,0.0000004469,1.1251033642,0.0061107638
O,0,0.0000001758,2.3533223226,0.0872170641
N,0,-1.1729011923,0.4132107609,-0.0409182424
C,0,-1.2363443615,-1.0017324455,-0.1356374537
O,0,-2.3563241622,-1.5428697846,-0.1718316048
C,0,-0.0000012508,-1.6628977743,-0.1798622586
C,0,1.236342853,-1.0017460795,-0.1354661663
O,0,2.3563224688,-1.5428872358,-0.1715997188
C,0,2.4017512098,1.1843923101,0.0111749435
C,0,-2.401750029,1.1844379485,0.0105524499
H,0,-0.00000286,-2.7423736646,-0.2518453319
H,0,3.227120783,0.4778826859,-0.0296037215
H,0,2.4531541298,1.7646348173,0.9349973123
H,0,2.4600249212,1.8736335284,-0.8341565863
H,0,-3.2271258485,0.4780617881,-0.0323595559

H,0,-2.4587943904,1.8750286928,-0.8337356654
H,0,-2.4543737708,1.7632114259,0.9352502943

Sum of electronic and zero-point Energies= -567.631214
Sum of electronic and thermal Energies= -567.621088
Sum of electronic and thermal Enthalpies= -567.620144
Sum of electronic and thermal Free Energies= -567.666954

Diketo-6-amino 1,3-dimethyl barbituric acid

H,0,0.6349625761,0.4094326281,-0.3599488656
N,0,-0.2742474727,-1.3571170964,-2.122187326
O,0,-0.6076282567,1.2752912062,1.8029664604
O,0,-4.0782807925,-1.354248656,0.4728795771
N,0,-2.1989851515,-1.3443744067,-0.8190158582
N,0,-2.3498708559,-0.0498416547,1.140192544
C,0,-0.359363711,0.0278801425,-0.1760455046
C,0,-0.9303367287,-0.8661278218,-1.0454993641
C,0,-2.8001738973,-2.3133708403,-1.7258177879
H,0,-3.7544498986,-2.6118711612,-1.3024445517
H,0,-2.1581176371,-3.1913426826,-1.8200892163
H,0,-2.9771876848,-1.869400003,-2.7090701134
C,0,-2.946640739,-0.9371017871,0.2812606054
C,0,-3.1437975433,0.3614592088,2.2887480642
H,0,-3.4101718896,-0.5065039993,2.8938702817
H,0,-4.0591516395,0.855453216,1.9587634279
H,0,-2.5375675636,1.0504332969,2.8707554906
C,0,-1.0503436466,0.4783522445,0.975008177
H,0,-0.787198487,-1.7555113624,-2.8910700131
H,0,0.5904510194,-0.9063904717,-2.3741560274

Sum of electronic and zero-point Energies= -548.201704
Sum of electronic and thermal Energies= -548.190991
Sum of electronic and thermal Enthalpies= -548.190047
Sum of electronic and thermal Free Energies= -548.237744

Diketo-6-amino 1,3-dimethyl barbituric carbanion

N,0,2.494035381,-1.3787877682,-0.0396080546
O,0,-2.2506086972,-1.718747789,-0.2507722461
O,0,-0.2333247701,2.3366905638,0.0794815129
N,0,1.0978824675,0.4848656959,-0.0351899748
N,0,-1.2206666168,0.2892915854,0.0084252922
C,0,0.1192556237,-1.7652300753,-0.0815639279
C,0,1.1814546113,-0.9128952676,-0.0288588161
C,0,2.2833148387,1.3269833139,-0.0797310054
H,0,1.9705772829,2.3424675494,-0.3089400945
H,0,2.9625641504,0.9677738289,-0.8540346868
H,0,2.8049805543,1.3356389866,0.8832595875
C,0,-0.1261666347,1.1089744198,0.0234259776
C,0,-2.5104808345,0.9561715565,0.0775488464

H,0,-2.7045168373,1.5330675097,-0.831222958
H,0,-2.5367515871,1.63795624,0.9293551731
H,0,-3.2684893062,0.1845284173,0.1835717698
C,0,-1.1550951146,-1.1381252209,-0.1272036966
H,0,3.1618143236,-0.8819422019,0.5349390697
H,0,2.5079211654,-2.3724813445,0.1413182318

Sum of electronic and zero-point Energies= -547.672265
Sum of electronic and thermal Energies= -547.661810
Sum of electronic and thermal Enthalpies= -547.660866
Sum of electronic and thermal Free Energies= -547.708262

Diketo-6-ammonium 1,3-dimethyl barbituric acid

H,0,2.877458019,-1.0516487222,-1.135829195
N,0,2.4213505305,-1.3804799813,-0.2808298032
O,0,-2.3030799529,-1.6886646117,0.2291553673
O,0,-0.3287700256,2.3794201463,0.1010469802
N,0,1.0204211134,0.5415029431,0.0209390744
N,0,-1.3048107865,0.324285665,-0.0511554673
C,0,0.0505255593,-1.7204241094,-0.1016251693
C,0,1.0509343475,-0.843060322,-0.0901307075
C,0,2.2086768604,1.3607421903,0.2201847772
H,0,1.8851144845,2.3967177199,0.2784513741
H,0,2.9022504446,1.2644962976,-0.6180917437
H,0,2.7121427647,1.0980833918,1.1543565739
C,0,-0.2112553981,1.1621719836,0.0265711141
C,0,-2.609508126,0.9705236572,-0.0653928276
H,0,-3.325745951,0.2734840075,-0.4939093972
H,0,-2.5526541872,1.8791638719,-0.6615141599
H,0,-2.9320617014,1.2300896204,0.9469719234
C,0,-1.2452882208,-1.0872318565,0.0492691206
H,0,3.057166716,-1.2081198696,0.5017884004
H,0,2.2791335095,-2.3914520218,-0.3603562348

Sum of electronic and zero-point Energies= -548.100426
Sum of electronic and thermal Energies= -548.089600
Sum of electronic and thermal Enthalpies= -548.088656
Sum of electronic and thermal Free Energies= -548.137095

(*Z*)-(2-nitrovinyl)benzene

C,0,-8.5143493794,-0.7502181258,0.0029095475
C,0,-8.4339476887,-2.1429207128,-0.0012202436
C,0,-7.1918758836,-2.768198721,-0.0053818588
C,0,-6.0335653279,-2.0033663401,-0.005408619
C,0,-6.0999809253,-0.602776519,-0.0012742899
C,0,-7.3607140709,0.0153832139,0.0028893239
C,0,-4.8522217208,0.1387805171,-0.0015249579
C,0,-4.7167315967,1.4705559249,0.0021182244

N,0,-3.4095914051,2.0654305786,0.0012936547
O,0,-3.3718003828,3.2892068056,0.0036601611
O,0,-2.4138284678,1.358434371,-0.0020759309
H,0,-9.4835577683,-0.2632629636,0.0061447359
H,0,-9.3416375705,-2.7372609789,-0.0011860851
H,0,-7.12523174,-3.8507188041,-0.0086046159
H,0,-5.0626703284,-2.48895122,-0.0086524818
H,0,-7.4422218602,1.0968165184,0.0061133959
H,0,-3.9362990515,-0.4467019494,-0.0049901305
H,0,-5.5011748322,2.212468405,0.0056901702

Sum of electronic and zero-point Energies= -513.577359
Sum of electronic and thermal Energies= -513.568291
Sum of electronic and thermal Enthalpies= -513.567346
Sum of electronic and thermal Free Energies= -513.612982

Protonated (*Z*)-(2-nitrovinyl)benzene

O,0,-3.6379726488,-0.4835845761,-0.7609654422
N,0,-2.7889846356,0.2057287805,-0.2487428148
C,0,0.9934012985,0.2330433241,-0.024183534
C,0,-0.3513085399,0.5163382908,0.0535446628
H,0,-0.6528288977,1.5464969743,0.2361522387
H,0,-1.5426474077,-1.012397327,0.8852352984
C,0,2.8563608636,-1.2864092725,-0.293442821
H,0,3.2591920802,-2.2780018082,-0.4580280759
C,0,3.2589800215,1.1031211466,0.0800598531
H,0,3.9576300332,1.9216711718,0.1996938034
C,0,3.7282947279,-0.1966575823,-0.1345123748
H,0,4.798399136,-0.3704191851,-0.1812094564
C,0,1.905252667,1.3236767796,0.1366681554
H,0,1.5082610518,2.3188367006,0.3037784619
C,0,1.5027214948,-1.0850474327,-0.2432730769
H,0,0.8243058208,-1.92119677,-0.3659245982
C,0,-1.4471632621,-0.4538225665,-0.0571198329
H,0,-1.3349012935,-1.1793173379,-0.8634585447
O,0,-2.9331925099,1.3404406901,0.1417280981

Sum of electronic and zero-point Energies= -513.948681
Sum of electronic and thermal Energies= -513.939205
Sum of electronic and thermal Enthalpies= -513.938261
Sum of electronic and thermal Free Energies= -513.985141

(*Z*)-(2-nitrovinyl)-p-F-benzene

C,0,-8.5206100106,-0.7426353696,0.0029189805
C,0,-8.4092856245,-2.1258370501,-0.0013319896
C,0,-7.1888153944,-2.7766544924,-0.0055430042
C,0,-6.0371504855,-2.0052210637,-0.005476139
C,0,-6.1017838256,-0.6042460811,-0.0012598535

C,0,-7.3631205204,0.0135797532,0.0029308095
C,0,-4.8552908368,0.1372541596,-0.0014194146
C,0,-4.7201173802,1.4692153179,0.0022621445
N,0,-3.4127065604,2.0626761766,0.0012613019
O,0,-3.3736235093,3.2864223032,0.003240623
O,0,-2.4181004199,1.3541585267,-0.001862983
H,0,-9.5003738672,-0.2796202063,0.006126397
F,0,-9.5329055562,-2.8589778689,-0.0013066142
H,0,-7.1485488657,-3.8594345221,-0.0087756938
H,0,-5.0689924955,-2.4951545269,-0.0087403333
H,0,-7.4481178978,1.0943888704,0.0062272165
H,0,-3.9395648013,-0.4484498446,-0.004868462
H,0,-5.5040919487,2.2117359181,0.0058170144

Sum of electronic and zero-point Energies= -612.765504
Sum of electronic and thermal Energies= -612.755622
Sum of electronic and thermal Enthalpies= -612.754678
Sum of electronic and thermal Free Energies= -612.802303

Protonated (*Z*)-(2-nitrovinyl)-p-F-benzene

O,0,-3.6410356101,-0.4965156018,-0.7352361394
N,0,-2.7859030509,0.2033372797,-0.2479056252
C,0,0.9939608936,0.2356874163,-0.0280652717
C,0,-0.3476073961,0.5167194032,0.0536378882
H,0,-0.6497830716,1.5461092769,0.2372003278
H,0,-1.5410838101,-1.0114317364,0.8900857528
C,0,2.8524604736,-1.2955934833,-0.3020376477
H,0,3.2786726788,-2.2768684313,-0.4683306644
C,0,3.2602383682,1.1138116503,0.0833921737
H,0,3.979336951,1.9140583657,0.203575291
C,0,3.7030078548,-0.1929830731,-0.1340554415
F,0,4.9949208786,-0.4059814486,-0.1869146274
C,0,1.9106198968,1.3244750784,0.1362410405
H,0,1.5183966426,2.3208181875,0.3059777059
C,0,1.5058210488,-1.0832391066,-0.2514392856
H,0,0.8293463758,-1.9201072982,-0.3777592035
C,0,-1.4438947623,-0.4552056424,-0.0530704046
H,0,-1.3336585603,-1.182004831,-0.8584620776
O,0,-2.9252158013,1.3476139947,0.1155662087

Sum of electronic and zero-point Energies= -613.138308
Sum of electronic and thermal Energies= -613.128027
Sum of electronic and thermal Enthalpies= -613.127083
Sum of electronic and thermal Free Energies= -613.176190

(*Z*)-(2-nitrovinyl)-p-Br-benzene

C,0,-8.5120064533,-0.739010561,0.0028509962
C,0,-8.4167901353,-2.1288616673,-0.0013890889
C,0,-7.1852314364,-2.7702197537,-0.0055922304
C,0,-6.0315163258,-2.0004193132,-0.0055190198
C,0,-6.0929650131,-0.6006763876,-0.0013186709
C,0,-7.3531960764,0.0164510714,0.0028624938
C,0,-4.8454828386,0.1404780316,-0.0015061402
C,0,-4.7135151708,1.4720154395,0.0020944998
N,0,-3.4066501014,2.0697384213,0.0014470781
O,0,-3.3717510832,3.2930718815,0.0037216703
O,0,-2.4107166816,1.3636994212,-0.0017571
H,0,-9.4811061459,-0.2550871362,0.0060966226
Br,0,-10.0023494371,-3.162122313,-0.001400869
H,0,-7.1245930771,-3.8516754028,-0.0088652348
H,0,-5.0650657126,-2.4940623154,-0.0087834724
H,0,-7.4396556439,1.0972172995,0.0061715838
H,0,-3.9291745607,-0.4439341874,-0.004861067
H,0,-5.4993341068,2.2124974716,0.0055479488

Sum of electronic and zero-point Energies= -3086.809128
Sum of electronic and thermal Energies= -3086.798590
Sum of electronic and thermal Enthalpies= -3086.797645
Sum of electronic and thermal Free Energies= -3086.847969

Protonated (*Z*)-(2-nitrovinyl)-p-Br-benzene

O,0,-3.6281642347,-0.5160925978,-0.7532939404
N,0,-2.7831336581,0.1962727135,-0.2662998578
C,0,0.9922807046,0.2402507632,-0.0199724608
C,0,-0.350112701,0.5210341334,0.0695489976
H,0,-0.6531161999,1.5491043045,0.2579301439
H,0,-1.555087226,-0.9877112359,0.9202103786
C,0,2.8498764001,-1.2888990856,-0.318027222
H,0,3.2489324655,-2.2789922777,-0.4964978914
C,0,3.263024653,1.1080899786,0.0820401053
H,0,3.9655147545,1.921900863,0.2067510359
C,0,3.7242205113,-0.1966992574,-0.1509939605
Br,0,5.551606401,-0.4992112117,-0.2476419917
C,0,1.9129545601,1.3228579034,0.1461909672
H,0,1.5275647018,2.3203209128,0.3268707002
C,0,1.5025262798,-1.0749972954,-0.2556721823
H,0,0.8260230937,-1.9116523735,-0.3845975927
C,0,-1.4431048399,-0.4544035281,-0.0347429672
H,0,-1.3194088656,-1.2006042262,-0.8198306094
O,0,-2.9315968003,1.3475315167,0.0703283474

Sum of electronic and zero-point Energies= -3087.180339
Sum of electronic and thermal Energies= -3087.169449
Sum of electronic and thermal Enthalpies= -3087.168505
Sum of electronic and thermal Free Energies= -3087.220415

(*Z*)-(2-nitrovinyl)-p-Me-benzene

C,0,-8.4921231374,-0.739859813,-0.0006355948
C,0,-8.4350052512,-2.1416244424,-0.008176655
C,0,-7.1793810435,-2.7495391515,-0.0137037243
C,0,-6.0195434124,-1.9882990437,-0.0119111283
C,0,-6.0774600487,-0.5885208406,-0.0044179643
C,0,-7.342272588,0.0248882529,0.0012369682
C,0,-4.8333672303,0.1512444624,-0.0028353213
C,0,-4.6964794121,1.484844303,0.004715123
N,0,-3.3926994559,2.0788328178,0.0054307127
O,0,-3.3532896809,3.3038003597,0.01254662
O,0,-2.3949434555,1.3726040083,-0.0007831857
H,0,-9.4600006197,-0.247456142,0.0038374395
C,0,-9.6945464609,-2.9521377975,-0.0105893915
H,0,-7.108765959,-3.8327668077,-0.0194809265
H,0,-5.0518468488,-2.4806909699,-0.0163185431
H,0,-7.4280790443,1.1062647371,0.0071237634
H,0,-3.9168882817,-0.4336132172,-0.0082442077
H,0,-5.4821527153,2.2253133174,0.0108171166
H,0,-10.302910774,-2.722606737,-0.8910770324
H,0,-10.3056385606,-2.7241102493,0.8683331937
H,0,-9.4816060199,-4.0224670471,-0.011367262

Sum of electronic and zero-point Energies= -552.830103
Sum of electronic and thermal Energies= -552.819095
Sum of electronic and thermal Enthalpies= -552.818151
Sum of electronic and thermal Free Energies= -552.869679

Protonated (*Z*)-(2-nitrovinyl)-p-Me-benzene

O,0,-4.237000438,-0.9032243942,-0.3978049408
N,0,-3.4377132813,-0.0596729036,-0.0676992471
C,0,0.3246635507,0.2300825126,0.0815866627
C,0,-1.0254476356,0.4575356729,0.1566370213
H,0,-1.3799636915,1.4861685969,0.136201099
H,0,-1.9061200227,-1.475006574,-0.2857726244
H,0,-2.1549480906,-0.8619409221,1.355011738
C,0,2.2630030252,-1.2189280585,0.0425165829
H,0,2.7093679062,-2.2068182734,0.0590601296
C,0,2.5447591878,1.2061941324,-0.080208592
H,0,3.1955938548,2.0693319308,-0.155202626
C,0,3.1077739701,-0.0848770834,-0.0544391944
C,0,4.5758774163,-0.2724839707,-0.1175559157
C,0,1.188496693,1.3684908,-0.0140610268
H,0,0.7477675007,2.359349258,-0.0328002205
C,0,0.9086874155,-1.0778815994,0.1066296698
H,0,0.2777876834,-1.9563386346,0.1758499125
C,0,-2.0676335968,-0.5699758124,0.2987884858

O,0,-3.6537617277,1.1264175295,0.0210000935
H,0,4.8338117188,-1.0382752442,-0.8551361309
H,0,4.9306019203,-0.6484767505,0.850711528
H,0,5.1026849915,0.6531084979,-0.3457177344

Sum of electronic and zero-point Energies= -553.208220
Sum of electronic and thermal Energies= -553.197606
Sum of electronic and thermal Enthalpies= -553.196662
Sum of electronic and thermal Free Energies= -553.247067

(*Z*)-(2-nitrovinyl)-p-MeO-benzene

C,0,-8.5413971588,-0.7170671185,0.0007939973
C,0,-8.4740069767,-2.11701861,-0.003190375
C,0,-7.2254100742,-2.7519730834,-0.0062972147
C,0,-6.0709980943,-1.999482867,-0.0055029121
C,0,-6.115340519,-0.5927722779,-0.0016053002
C,0,-7.3748972485,0.0253064854,0.0015262267
C,0,-4.8705336813,0.1365984872,-0.000989331
C,0,-4.717892215,1.4712079113,0.0022024558
N,0,-3.4108348816,2.047566241,0.0021601556
O,0,-3.3544002113,3.2732541546,0.0038228801
O,0,-2.4196963636,1.329580025,0.0000551579
H,0,-9.4956821493,-0.2059856413,0.0033486707
O,0,-9.5465680136,-2.923480758,-0.0041189525
H,0,-7.1893745442,-3.8356677415,-0.0093068177
H,0,-5.1080558099,-2.5009321868,-0.0079436311
H,0,-7.4541610675,1.1070906364,0.0046348014
H,0,-3.959263689,-0.4565325863,-0.003390948
H,0,-5.4954684764,2.2204565128,0.0046906199
C,0,-10.8419903854,-2.3370873674,-0.0012517171
H,0,-11.5438529988,-3.1688448434,-0.0030363539
H,0,-10.9975913296,-1.7257179968,-0.8949067808
H,0,-10.995984112,-1.7308973754,0.8962053688

Sum of electronic and zero-point Energies= -627.980349
Sum of electronic and thermal Energies= -627.968668
Sum of electronic and thermal Enthalpies= -627.967724
Sum of electronic and thermal Free Energies= -628.019463

Protonated (*Z*)-(2-nitrovinyl)-p-MeO-benzene

O,0,-3.5318279841,-0.301112817,-0.787079238
N,0,-2.6538727605,0.3624573146,-0.2871667735
C,0,1.0883849324,0.1184223776,-0.0441557272
C,0,-0.2112445607,0.5055284255,0.1064264744
H,0,-0.4221045065,1.552329621,0.3118084182
H,0,-1.5799289279,-0.7988087445,1.054220954
C,0,2.8072179304,-1.548626402,-0.4230925123
H,0,3.1418935457,-2.5590725399,-0.6234126054

C,0,3.4291270065,0.8141552268,-0.0275248501
H,0,4.1825274627,1.5829800337,0.0765948499
C,0,3.7965365243,-0.5317132988,-0.2828700435
O,0,5.0259080389,-0.9370485459,-0.4101675219
C,0,2.1095150477,1.1216342318,0.0873490129
H,0,1.8075446484,2.1441740667,0.2859082743
C,0,1.4947574679,-1.2360764083,-0.3109044877
H,0,0.7508711852,-2.0158453364,-0.4226205904
C,0,-1.3878805924,-0.3807468509,0.0564723505
H,0,-1.3184859706,-1.2071097384,-0.6483141409
O,0,-2.7241083041,1.5390946283,-0.0170108494
C,0,6.1239166402,-0.0153684798,-0.2949193317
H,0,6.139190446,0.4253616064,0.7028084722
H,0,6.0479624486,0.7552737831,-1.0629733417
H,0,7.014400282,-0.6168821535,-0.4531767927

Sum of electronic and zero-point Energies= -628.367534
Sum of electronic and thermal Energies= -628.355464
Sum of electronic and thermal Enthalpies= -628.354520
Sum of electronic and thermal Free Energies= -628.407718

(*Z*)-(2-nitroprop-1-enyl)benzene

C,0,-8.5468918436,-0.900601663,0.3013320554
C,0,-8.4269673977,-2.2318385458,-0.0875542852
C,0,-7.1689421441,-2.7633879095,-0.3575449163
C,0,-6.0406006231,-1.9648254007,-0.2443297365
C,0,-6.1499183719,-0.6106717189,0.1087951285
C,0,-7.4215880202,-0.0935845084,0.397051881
C,0,-4.9197577411,0.1649010628,0.1980267161
C,0,-4.7477314126,1.4824590687,0.002129942
N,0,-3.3844889019,1.9832520617,0.2229999768
O,0,-3.219117021,3.1888804469,0.1236100333
O,0,-2.4843765763,1.2063962237,0.4994963012
H,0,-9.5223983103,-0.4899054452,0.539343686
H,0,-9.310167501,-2.8572356856,-0.1648525068
H,0,-7.0667330635,-3.8040516169,-0.646245437
H,0,-5.0587116103,-2.3843829573,-0.4409048326
H,0,-7.5308653345,0.9296278188,0.73553561
H,0,-4.0219603564,-0.4015451728,0.4279228788
C,0,-5.7236456373,2.5137647457,-0.4367939329
H,0,-6.0658131122,3.1347567376,0.3968219218
H,0,-6.5896343849,2.0323218764,-0.8902512038
H,0,-5.2674906359,3.1778705819,-1.17238928

Sum of electronic and zero-point Energies= -552.826234
Sum of electronic and thermal Energies= -552.815763
Sum of electronic and thermal Enthalpies= -552.814818
Sum of electronic and thermal Free Energies= -552.863699

Protonated (*Z*)-(2-nitroprop-1-enyl)benzene

O,0,0.9453835641,7.1231082077,13.8057478086
N,0,1.7816933576,7.2354885066,14.6692697937
C,0,5.4977776961,7.1552959248,14.4390358937
C,0,4.2135380492,7.2116331358,14.9330566255
H,0,4.0179703425,7.8616076932,15.7849410473
C,0,2.9214224041,5.1417662546,15.2993851412
H,0,2.8719871832,5.36937548,16.3648024298
H,0,3.7811400662,4.5004021752,15.1055077352
H,0,2.0139936528,4.6211611781,14.9882886871
C,0,7.1758169364,6.3344300366,12.9002069846
H,0,7.4747578483,5.727351816,12.0547351644
C,0,7.791083401,7.9283053678,14.6576025732
H,0,8.5491985447,8.5266214797,15.1473077413
C,0,8.1286315901,7.1228897875,13.5648978291
H,0,9.1564730923,7.1087828396,13.2171828914
C,0,6.4907670484,7.9493153507,15.0961698012
H,0,6.1971572648,8.562529619,15.9409703707
C,0,5.8723404675,6.3458967566,13.3209818828
H,0,5.1322589889,5.7478637166,12.8032757842
C,0,3.0574272481,6.429199105,14.4658611372
H,0,3.0755908584,6.2014746259,13.4013438861
O,0,1.6763903954,7.8879009432,15.6820287916

Sum of electronic and zero-point Energies= -553.198541
Sum of electronic and thermal Energies= -553.187625
Sum of electronic and thermal Enthalpies= -553.186681
Sum of electronic and thermal Free Energies= -553.236397

(*Z*)-1-methoxy-4-(2-nitroprop-1-enyl)benzene

C,0,1.1339672325,3.1448623368,0.7929989561
C,0,2.5321719472,3.1533371324,0.8868664735
C,0,3.2058653324,1.9833555589,1.2472247616
C,0,2.4773645071,0.8359593445,1.5171658091
C,0,1.0754549075,0.8166984007,1.4719938237
C,0,0.4206396474,2.0014028685,1.08284137
C,0,0.4117143281,-0.4311744386,1.7866283285
C,0,-0.8537799326,-0.6465782233,2.1978879353
N,0,-1.2346034633,-2.046905844,2.3581869166
O,0,-2.3970231036,-2.2745058125,2.6653056917
O,0,-0.4113928084,-2.9343323744,2.1789785243
H,0,0.6276895725,4.0508816234,0.4786069297
O,0,3.1358136547,4.3192583236,0.5969126629
H,0,4.2862151368,1.9552930342,1.3091695678
H,0,3.0099817403,-0.0716932871,1.7842373803
H,0,-0.6553478308,2.0200656897,0.9644300048
H,0,1.0293519943,-1.3201335685,1.6962121974

C,0,-1.916116771,0.3351346085,2.5440955091
H,0,-2.6287618653,0.4792046983,1.7255066936
H,0,-1.4653425918,1.2977931396,2.7849977763
H,0,-2.4813235941,-0.009021673,3.4109479845
C,0,4.5532026861,4.3821902277,0.6631881924
H,0,5.0118890046,3.6922723052,-0.0515016256
H,0,4.9104451685,4.1606094398,1.6733443269
H,0,4.8182251011,5.4047264896,0.4009738097

Sum of electronic and zero-point Energies= -667.228283
Sum of electronic and thermal Energies= -667.215250
Sum of electronic and thermal Enthalpies= -667.214306
Sum of electronic and thermal Free Energies= -667.268970

Protonated (*Z*)-1-methoxy-4-(2-nitroprop-1-enyl)benzene

O,0,-2.7018291273,2.7954596053,0.092694847
N,0,-1.6498587651,2.7219164459,0.6836962658
C,0,0.8304063468,-0.0273738532,0.6428686391
C,0,0.2064331823,1.1482898214,0.9447399982
H,0,0.8168243737,2.0377317143,1.0872106592
C,0,-1.5847830499,1.2583995269,2.6614522636
H,0,-0.9855415463,1.967075508,3.2348905782
H,0,-1.3806191246,0.247673155,3.0162906042
H,0,-2.6457697704,1.4730827152,2.8017543514
C,0,0.8314922858,-2.4073873018,0.1784577597
H,0,0.3370581785,-3.3584763437,0.023124817
C,0,2.9650794548,-1.1574095642,0.2766880755
H,0,4.0440382167,-1.1315808884,0.2062644773
C,0,2.2542345009,-2.372061898,0.0984800632
O,0,2.8209510251,-3.5166047219,-0.1476406219
C,0,2.2649098927,-0.0225127701,0.5425180135
H,0,2.7904247515,0.9151692924,0.68723592
C,0,0.1393934895,-1.2734712052,0.4393068595
H,0,-0.9417229675,-1.3130942769,0.4932141429
C,0,-1.2444066716,1.3376066449,1.1675313402
H,0,-1.8675107003,0.656854417,0.590251934
O,0,-0.9246283634,3.6524586434,0.9537393667
C,0,4.250981637,-3.6279599262,-0.2516320737
H,0,4.7183138887,-3.3385701193,0.6906741104
H,0,4.6152953764,-3.0141544226,-1.07630213
H,0,4.437333486,-4.6784601982,-0.4556102612

Sum of electronic and zero-point Energies= -667.617605
Sum of electronic and thermal Energies= -667.604043
Sum of electronic and thermal Enthalpies= -667.603099
Sum of electronic and thermal Free Energies= -667.659286

Product I

O,0,3.3897828458,2.9747288604,0.2173794992
O,0,2.7990835356,4.2374425921,1.851009913
N,0,2.520671241,3.1963739006,5.8646884825
O,0,4.1050921818,0.3347780359,2.4229838849
O,0,6.8143309238,1.5943070082,5.8370519242
N,0,2.7830154688,3.1840665938,1.2478140662
N,0,4.6796598132,2.3861882332,5.8192975206
N,0,5.4642964532,1.0157557567,4.0966087498
C,0,0.8053214272,1.0539966807,3.7306056484
C,0,1.1012300377,-0.3003439462,3.8908977613
H,0,2.1144647291,-0.6509292991,3.7246398202
C,0,0.1069809336,-1.2011223631,4.2571711684
H,0,0.351897784,-2.2515858775,4.3781625335
C,0,-1.1962541927,-0.7607920328,4.4693117885
H,0,-1.9698693372,-1.464287531,4.7594821793
C,0,-1.5000930801,0.5869895935,4.310885578
H,0,-2.5118631171,0.9420229495,4.4785961326
C,0,-0.5047484794,1.4864198598,3.9413476331
H,0,-0.7513058228,2.53828323,3.8193801432
C,0,1.8715662342,2.0552886966,3.3057625004
H,0,1.5014554265,3.0516413593,3.5690481386
C,0,1.9261562859,2.0711742797,1.7785396315
H,0,0.932414535,2.2774935662,1.3725958533
H,0,2.3276728303,1.1571435803,1.3537855034
C,0,3.2130306894,1.8730894947,3.9828384443
C,0,3.4577564628,2.4950160528,5.1942692426
C,0,4.906985351,3.0298440487,7.1076796024
H,0,5.9022334872,2.7525331878,7.4407409033
H,0,4.1739989006,2.6833468235,7.8390172602
H,0,4.8616967334,4.1179691529,7.0126888339
C,0,5.7308687583,1.658126488,5.2779256602
C,0,6.5211153195,0.2080656762,3.5015981784
H,0,6.3066644727,-0.8553362141,3.6283666837
H,0,7.4560919384,0.4539767175,3.996609724
H,0,6.5840820042,0.4280362849,2.4369131918
C,0,4.2259872289,1.032971999,3.4325561953
H,0,2.7773524514,3.8352505706,6.5975653533
H,0,1.6261775449,3.3600759906,5.4371846724

Sum of electronic and zero-point Energies= -1061.800149
Sum of electronic and thermal Energies= -1061.779398
Sum of electronic and thermal Enthalpies= -1061.778454
Sum of electronic and thermal Free Energies= -1061.852595

Product VI

O,0,12.4433428414,9.9153671296,9.9085592819
O,0,12.9769568712,9.5838866787,11.9614951298
O,0,10.815839274,8.9825246622,7.1990978488
O,0,9.0802544602,12.8080853038,8.869098834

O,0,9.4532319737,9.2957970189,11.6885323999
N,0,12.4595220028,9.2408725731,10.9214331075
N,0,9.1754537526,11.0306513501,10.2668207396
N,0,9.8835974172,10.8806396615,7.9988706495
C,0,9.8872001959,8.8445592007,9.3910449113
C,0,10.8793396309,7.6850728972,9.6992960196
C,0,10.1629712909,6.3530773614,9.8425434194
C,0,9.3584605806,11.6405378064,9.032182544
C,0,10.2692320906,9.5625695624,8.1116299347
C,0,10.4238641771,5.3266749017,8.9347031918
C,0,8.6731693319,11.887919165,11.3384519371
C,0,9.7765030252,4.0996204498,9.0434598418
C,0,8.8591556797,3.8838307698,10.0657909963
C,0,12.9668651294,6.8611785499,10.8905717622
C,0,11.8229060438,7.8671425352,10.8957294685
C,0,9.5150004829,9.7286046639,10.5551717227
C,0,9.2381782656,6.128665446,10.8655610155
C,0,8.591793317,4.9024307489,10.9757594995
C,0,10.1051303073,11.5839479464,6.7374010004
H,0,8.9267819107,8.3733176934,9.1278254812
H,0,11.5025640501,7.6153398815,8.8048510181
H,0,11.1390246951,5.4889293829,8.1334729411
H,0,7.8025458486,12.434779406,10.9814442466
H,0,9.4417398974,12.5972472051,11.6502186943
H,0,8.4033569763,11.2498585664,12.1751122452
H,0,9.9901587932,3.3130314295,8.3269519865
H,0,8.3529307601,2.9278999266,10.1523639348
H,0,13.5546147401,6.9400215283,9.9724260881
H,0,12.552199911,5.854070548,10.9512985885
H,0,13.6164858322,7.0198466856,11.7521776957
H,0,11.2834714785,7.822789999,11.8409475989
H,0,9.0198437002,6.9214111885,11.574707561
H,0,7.8754812497,4.7429470276,11.77540813
H,0,9.1890133016,12.0924520635,6.4411192332
H,0,10.3852633371,10.8450941977,5.9922455142
H,0,10.9045973763,12.3181988877,6.8483987866

Sum of electronic and zero-point Energies= -1120.923057
Sum of electronic and thermal Energies= -1120.901378
Sum of electronic and thermal Enthalpies= -1120.900434
Sum of electronic and thermal Free Energies= -1120.976341

Product XXII

O,0,1.677621887,1.9978135381,-1.7613314021
O,0,2.6377249734,0.089518375,-1.5319224115
O,0,-0.7362325866,3.7950194876,0.9025398275
O,0,1.1680585991,-0.445621406,1.5774854653
O,0,-1.3642368296,1.5287866254,4.7683972058
O,0,3.8808392051,4.4567399954,5.8975525629

N,0,2.3482046106,1.1988970743,-1.137974026
N,0,-1.0255440495,2.6891417299,2.8606222758
N,0,-0.0467196578,0.5423351054,3.1996148113
C,0,4.1963492439,2.3865585346,-0.0995060797
H,0,4.8746350396,1.7704604734,-0.6929512512
H,0,4.6912695243,2.6346548872,0.8400919127
H,0,3.9840114902,3.3131163962,-0.638418733
C,0,2.9107188214,1.6275081468,0.2011378967
H,0,3.1208861426,0.6842040884,0.7025367191
C,0,1.8901363575,2.4758266833,0.9657041022
H,0,1.6805384221,3.3531269899,0.3478744373
C,0,2.4537139216,2.9572908555,2.2864495174
C,0,2.3950919563,4.316982345,2.6096085072
H,0,1.9667655773,5.0184270037,1.8996759664
C,0,2.8754959689,4.7907966475,3.8178913539
H,0,2.8273240656,5.8468991105,4.0606401439
C,0,3.4368853577,3.908335802,4.7443737733
C,0,3.5121677318,2.549709869,4.4375690983
H,0,3.9494927142,1.8423845206,5.1309545219
C,0,3.0216752579,2.09048086,3.2188025571
H,0,3.1045246697,1.0286796664,3.0060593274
C,0,4.4583645581,3.5980092929,6.8668676326
H,0,5.3513458787,3.1007555792,6.4746424093
H,0,3.7398051371,2.8462594029,7.2090090154
H,0,4.7388633221,4.2359813174,7.7033534745
C,0,0.4965192166,1.7875471895,1.1426913483
H,0,0.1434119038,1.4810886846,0.1528063951
C,0,-0.4783956591,2.8415010218,1.6067237037
C,0,-0.8366084244,1.5830186257,3.6805700602
C,0,0.5684335738,0.5357368377,1.9717751792
C,0,0.0790737302,-0.6596520919,4.0205967534
H,0,-0.2635092791,-0.4249377505,5.0236601831
H,0,1.122814943,-0.9695022102,4.0388553606
H,0,-0.5258566433,-1.4658413028,3.601438486
C,0,-1.9130042853,3.7254721545,3.3837150355
H,0,-1.9027127538,4.5524275813,2.6794827664
H,0,-1.5550514128,4.0545954002,4.3583363182
H,0,-2.9268922197,3.3364668623,3.4849977985

Sum of electronic and zero-point Energies= -1235.326912
Sum of electronic and thermal Energies= -1235.302444
Sum of electronic and thermal Enthalpies= -1235.301500
Sum of electronic and thermal Free Energies= -1235.384957

17ZnY catalyst

Y,0,-1.8556052082,-0.3403403094,1.08187914
Zn,0,1.57271329,-0.276694545,0.5096605221
Cl,0,7.7888926741,-2.7013371571,-1.0882091854
Cl,0,-0.7971624273,6.724134444,0.1542132752

O,0,-0.0931897231,0.8906142799,0.2601317592
O,0,0.0076976849,-1.6538827669,0.6533856532
O,0,3.1068843634,0.7551745759,-0.2234731885
O,0,1.8178033512,0.0471104392,2.5443297577
O,0,-3.9826014499,-0.4963939137,0.7248157385
O,0,-2.1965834534,-2.8476064103,1.2187960242
O,0,-1.4372896414,1.0784537187,2.9762284361
O,0,-2.2270972005,-0.8753424934,3.3933159467
O,0,-6.297133195,-1.7282912593,0.7853396957
O,0,1.9375343504,6.2841619181,-0.667879996
N,0,2.8244741114,-1.9045636805,0.0640860081
N,0,-2.5477212612,1.8788408474,0.2352486328
O,0,8.4523444036,-0.1337572017,-2.2659070927
N,0,1.9846920121,5.2119191956,-0.0854134083
O,0,-1.8465683523,0.5019169378,5.0314889927
O,0,3.0073520805,4.7314355212,0.3851752159
N,0,1.3677835058,-0.4043935745,4.7264933661
O,0,7.873753889,1.57894114,-1.0839795329
N,0,-1.8374869882,0.2467787233,3.8487200911
N,0,7.6965665772,0.4416390232,-1.4988189356
C,0,4.1452379151,0.003078131,-0.4420866194
C,0,0.0783420093,-2.9687248419,0.7200542885
C,0,-4.9276923763,1.4889592365,-0.2181537864
C,0,-1.6185871134,4.1800696721,0.1680382163
H,0,-2.5976480585,4.6367945447,0.2603294161
C,0,6.4876157181,-0.2476720806,-1.0698371601
C,0,4.0827789218,-1.4216201398,-0.3097148863
C,0,-6.2936023367,-0.4714880651,0.2775659002
C,0,-7.4042269943,0.1865648356,-0.2201041322
H,0,-8.3712034296,-0.3047961362,-0.2251920817
C,0,5.2173488594,-2.2043499177,-0.52741485
H,0,5.187504395,-3.2783764618,-0.3797084787
C,0,0.7622516812,4.433493212,0.036103548
C,0,-1.4818581555,2.7911929942,0.1778667229
C,0,-0.5108832093,5.0159272101,0.0820808911
C,0,5.3816155182,0.5529368188,-0.8245857895
H,0,5.4693715266,1.6264623837,-0.9412003795
C,0,1.5004167035,-0.7488165924,3.4545648097
H,0,1.3051940913,-1.8081433841,3.2479112481
C,0,-1.1424499375,-5.0464911955,1.1409636687
H,0,-2.0602063255,-5.5622708418,1.3982921587
C,0,2.5310595799,-3.1635784883,0.1268097479
H,0,3.2940008791,-3.9096659017,-0.1125230329
C,0,1.2539940594,-3.7255946059,0.4860651771
C,0,-3.7107352156,2.2408545042,-0.2287203878
H,0,-3.8016451742,3.2278725091,-0.692831461
C,0,-7.2992783664,1.4953527125,-0.7300261696
H,0,-8.184439663,1.9889262016,-1.1173187355
C,0,-1.1117489963,-3.6689043769,1.035376089
C,0,-6.0836222402,2.1333166008,-0.7296838556

H,0,-5.9907934945,3.1458819728,-1.1134943
C,0,0.9205737509,3.0510985065,0.1036488244
H,0,1.9190022393,2.6268666515,0.0652685895
C,0,6.4237010328,-1.6423594729,-0.9203053167
C,0,-0.1881589508,2.2130716179,0.1875423962
C,0,-5.0115270441,0.1611732439,0.2812217238
C,0,0.0276376924,-5.7864585986,0.9102338737
H,0,0.0002689043,-6.8676624984,0.9901504617
C,0,-3.4507594317,-3.4701518958,1.518559515
H,0,-4.1885888621,-2.66983052,1.5234737664
H,0,-3.3988951129,-3.9680403408,2.4911443368
H,0,-3.7030347546,-4.1946172915,0.7388216125
C,0,1.1957529579,-5.1365977614,0.5821714825
H,0,2.1027895515,-5.7053241608,0.3968088056
C,0,-7.5305575702,-2.4186726232,0.8111177126
H,0,-7.935475069,-2.5549739579,-0.1989695788
H,0,-8.2712050323,-1.8950978474,1.4277026245
H,0,-7.3226352602,-3.3948193288,1.2499651953
C,0,1.5661186285,0.9649629433,5.1655945699
H,0,1.8971440416,1.5652018549,4.3200141966
H,0,2.3213953443,0.9913867661,5.9558432023
H,0,0.6240211218,1.3626002563,5.5539898529
C,0,0.981585639,-1.3737408145,5.7350724845
H,0,0.8747001075,-2.3601389196,5.2812012829
H,0,0.0270866076,-1.0802945182,6.1816687457
H,0,1.7437953042,-1.4225892531,6.5178069482

Sum of electronic and zero-point Energies= -5312.291492
Sum of electronic and thermal Energies= -5312.238283
Sum of electronic and thermal Enthalpies= -5312.237339
Sum of electronic and thermal Free Energies= -5312.383479

17ZnY catalyst-DMF

Y,0,2.0922299764,-0.1223759285,-0.9073037974
Zn,0,-1.3533113226,-0.0620537947,-0.3912632984
Cl,0,-7.8538876101,-2.2036571178,-0.424638239
Cl,0,1.151513157,6.5968392721,1.6779973689
O,0,0.2915050991,1.0745485399,-0.1315192174
O,0,0.1368684907,-1.3904111857,-0.8730469469
O,0,-2.9574767528,1.0467838352,-0.1411448975
O,0,4.2240670521,-0.3028139205,-0.6426081969
O,0,2.3575579331,-2.6188746079,-1.2427972094
O,0,2.2896458955,1.5914836955,-2.555360218
O,0,2.388714524,-0.4402416413,-3.250018493
O,0,6.5384006518,-1.5058317613,-0.9113250433
O,0,-1.6726522376,6.114149081,2.0611418091
N,0,-2.7401054251,-1.5776408961,-0.6653617074
N,0,2.7577102701,1.8635609049,0.4238251448
O,0,-8.6143303341,0.2949705725,0.828995855

N,0,-1.683686775,5.2511854379,1.1974651418
O,0,2.5872426946,1.1926530882,-4.6707617618
O,0,-2.6577972584,4.9831284385,0.5067830707
O,0,-7.7651548639,2.0655019549,-0.0709530431
N,0,2.4271426618,0.7994079063,-3.5415893415
N,0,-7.7118316854,0.8893312562,0.2612582527
C,0,-4.0529035687,0.3396045969,-0.1926207914
C,0,0.0269448222,-2.6749959932,-1.1475473423
C,0,5.0972785235,1.2927266008,0.9111072994
C,0,1.8933314398,4.1131595392,1.0278644153
H,0,2.8881806491,4.5220280481,1.1632659877
C,0,-6.4749340241,0.1714350135,-0.0144727006
C,0,-4.0250284186,-1.0646291631,-0.4641846293
C,0,6.4974994674,-0.4582606613,-0.0519487732
C,0,7.5689053529,-0.0015168896,0.6953894612
H,0,8.533485928,-0.4917646879,0.6198694513
C,0,-5.2087005527,-1.8014862293,-0.5089750018
H,0,-5.1951974463,-2.8637318646,-0.7268077974
C,0,-0.479136735,4.4635016632,0.9885237177
C,0,1.7194678354,2.7883671988,0.6218927397
C,0,0.808209323,4.9571781525,1.2345460744
C,0,-5.311067478,0.9265031445,0.0150006665
H,0,-5.3735596358,1.9887655119,0.2183869398
C,0,1.2261359178,-4.734502835,-1.6893267151
H,0,2.1552482639,-5.2640470048,-1.8643845
C,0,-2.4955964014,-2.8016672835,-1.0137369801
H,0,-3.3274655949,-3.4944665842,-1.1654422167
C,0,-1.198484893,-3.3820902991,-1.2340198719
C,0,3.8909373811,2.0512199082,1.0412109588
H,0,3.9677701015,2.8823483963,1.7486847464
C,0,7.4265104437,1.0986471495,1.562884847
H,0,8.2810578522,1.4368226543,2.1394465124
C,0,1.2280677349,-3.389510424,-1.373194742
C,0,6.2138754507,1.7341430671,1.6670979603
H,0,6.0942938513,2.5911860768,2.3245937185
C,0,-0.6690637622,3.1653080821,0.5203143002
H,0,-1.6761974457,2.8103723049,0.3242667637
C,0,-6.4412464343,-1.2073623139,-0.2769661195
C,0,0.4171142294,2.3193211372,0.3234751868
C,0,5.2183494867,0.1703875808,0.0481202286
C,0,0.0069931054,-5.4240208497,-1.7869030312
H,0,0.0094269437,-6.4788651495,-2.0384893415
C,0,3.6179917223,-3.263068201,-1.4665246154
H,0,4.3783590669,-2.5030537275,-1.2931317455
H,0,3.6712541907,-3.6343813616,-2.4941460959
H,0,3.7436505064,-4.0899469787,-0.7616401932
C,0,-1.1765072625,-4.7595714088,-1.5622287724
H,0,-2.1221483646,-5.2898018275,-1.6327202273
C,0,7.7699419555,-2.1858137697,-1.0542649969
H,0,8.0978408755,-2.6266799652,-0.1050635085

H,0,8.5546490529,-1.5190270481,-1.4314105961
H,0,7.5947024029,-2.9810064353,-1.7791659023

Sum of electronic and zero-point Energies= -5064.137461
Sum of electronic and thermal Energies= -5064.091760
Sum of electronic and thermal Enthalpies= -5064.090816
Sum of electronic and thermal Free Energies= -5064.221568

17ZnY catalyst-DMF + barbiturate substrate

Y,0,2.055879763,-0.2440343673,-0.8053964281
Zn,0,-1.3502043819,-0.3075273097,0.0993851173
Cl,0,-7.891703618,-1.9049396894,-1.2039875492
Cl,0,1.2617791229,6.4524985675,1.776824891
O,0,0.3100139562,0.8765919236,0.1853096168
O,0,0.1188198323,-1.5345849292,-0.7005016821
O,0,-2.9065323054,0.9237528717,0.1268885932
O,0,4.1926088686,-0.4622130022,-0.6121808527
O,0,2.3168196594,-2.7380945614,-1.2704576488
O,0,2.0627712732,1.5427794907,-2.3873163375
O,0,2.1098999579,-0.4586931511,-3.1688930001
O,0,6.4801418979,-1.6905967811,-0.9932970891
O,0,-1.5356868807,5.9801684479,2.3334985631
N,0,-2.7656859933,-1.6275674049,-0.6975949237
N,0,2.7999638968,1.6924099043,0.5439666783
O,0,-8.6791528804,0.498573813,0.2118750077
N,0,-1.5928044561,5.0950444047,1.4943742768
O,0,2.1142177969,1.2302523495,-4.5375124737
O,0,-2.6018927744,4.8116261065,0.8627227969
O,0,-7.6040765203,2.2860634237,-0.3482657165
N,0,2.0952032101,0.7923006352,-3.4143595664
N,0,-7.6692118525,1.0802587512,-0.1515540224
C,0,-4.0195776431,0.3120746801,-0.1580764528
C,0,-0.014636837,-2.7672910136,-1.153895572
C,0,5.1562035009,1.1120505996,0.9099072867
C,0,1.9704995324,3.9517787888,1.1547043848
H,0,2.9717675384,4.3629628991,1.2175034405
C,0,-6.4498327029,0.3052379721,-0.3354404992
C,0,-4.0354600528,-1.0521814221,-0.592661013
C,0,6.490061698,-0.6469618963,-0.1282505971
C,0,7.6003581697,-0.2055301927,0.5700461731
H,0,8.5548010871,-0.7057630688,0.446554625
C,0,-5.2417981217,-1.689259572,-0.8849471925
H,0,-5.2578430934,-2.7178141142,-1.2284918616
C,0,-0.4012155299,4.2992751821,1.2433424659
C,0,1.7736646661,2.6176428363,0.7944237463
C,0,0.8971071519,4.8003459272,1.4016855522
C,0,-5.2606379268,0.9640520032,-0.0587560289
H,0,-5.2901160231,2.0000889357,0.2567246923
C,0,1.1457049427,-4.7710654451,-1.9403871593

H,0,2.0653223893,-5.2958837761,-2.1711428998
C,0,-2.5447769521,-2.8110355627,-1.1716298199
H,0,-3.3853356694,-3.4335373253,-1.4908075663
C,0,-1.2542546433,-3.4222985071,-1.3623439976
C,0,3.9623839222,1.8760468495,1.1047196042
H,0,4.0748183077,2.70393837,1.8115023029
C,0,7.5113092929,0.8914185758,1.4484150248
H,0,8.3959940203,1.2176050222,1.9850378784
C,0,1.1722029268,-3.4705829176,-1.4725738424
C,0,6.3115819607,1.5384449165,1.6140077704
H,0,6.23174303,2.3925735171,2.2813092369
C,0,-0.617247043,2.9880168271,0.8251197591
H,0,-1.6326831249,2.6297512081,0.684977995
C,0,-6.4590669156,-1.0363258932,-0.7504244233
C,0,0.457386921,2.1357949528,0.5924295238
C,0,5.2241768136,-0.00491833,0.034322825
C,0,-0.0858311833,-5.4178861714,-2.1252553024
H,0,-0.103538909,-6.4372571453,-2.494969873
C,0,3.5640852249,-3.3834524313,-1.5515281198
H,0,4.3383298054,-2.6551237687,-1.3155060316
H,0,3.6121543488,-3.6639208616,-2.6079731031
H,0,3.6730184863,-4.2719331652,-0.9227840644
C,0,-1.2578686302,-4.7509457047,-1.8499085544
H,0,-2.2146569944,-5.2408049668,-2.008443016
C,0,7.6947249698,-2.387156769,-1.1916335853
H,0,8.0582681498,-2.8339088915,-0.258334041
H,0,8.470863804,-1.7305196131,-1.6026334834
H,0,7.4763588043,-3.1786620917,-1.9088213761
N,0,0.9433204338,-2.0886748418,5.1328191834
C,0,-0.4316287994,-2.1468928065,5.2929007601
O,0,-0.933104294,-2.5156514609,6.3324066227
N,0,-1.2488530356,-1.7607847923,4.2162697954
C,0,-0.7753323865,-1.3354583047,3.0186117693
O,0,-1.5475104096,-0.9910234625,2.1171703883
C,0,0.7026184759,-1.3062862067,2.8240246171
C,0,1.5827776227,-1.6772459174,3.9799704549
O,0,2.7937775913,-1.6247334083,3.8900668723
C,0,1.7370529799,-2.4887286141,6.2912386702
C,0,-2.688692975,-1.8295574667,4.4629516869
H,0,0.9781391,-0.3019658239,2.4878264064
H,0,0.9404915824,-1.9799143993,1.9932227933
H,0,2.7839901149,-2.3974714848,6.0123966436
H,0,1.5052925221,-3.5202321683,6.5597765322
H,0,1.5137696084,-1.8377961134,7.1377313542
H,0,-3.1982704924,-1.5514415849,3.5445110753
H,0,-2.956750605,-1.1416102249,5.265722652
H,0,-2.9580680754,-2.844979858,4.7535386608

17ZnY catalyst-DMF + barbiturate + trans-nitrostyrene substrates

Y,0,1.7427978435,-0.3451948842,-0.6507860989
Zn,0,-1.7401908836,-0.1260579456,-0.284896142
Cl,0,-7.8797576018,-2.2888029959,-2.5115367596
Cl,0,0.7840055839,6.7992854411,-1.1340785282
O,0,-0.0665602586,1.0441034598,-0.2937200969
O,0,-0.219192161,-1.5326147468,-0.4414916026
O,0,-3.2849195707,0.982771679,-0.8357394618
O,0,3.9116573458,-0.3829590166,-0.5067322457
O,0,1.9965624675,-2.7755583771,-0.0418323718
O,0,1.7239094552,0.6421282376,-2.8379267659
O,0,2.0438674218,-1.482051349,-2.7422342223
O,0,6.2174987773,-1.5993752165,-0.2566055631
O,0,-2.0355699488,6.5323561038,-0.5566239992
N,0,-3.0371830589,-1.6925171159,-0.8443124127
N,0,2.40730554,1.9972283682,-0.2321282339
O,0,-8.9253197751,0.364317329,-1.994466361
N,0,-2.0479393531,5.3763460452,-0.9495267551
O,0,2.0596907041,-0.4781824567,-4.6692637409
O,0,-3.0249047235,4.8296727608,-1.4439977717
O,0,-7.7043537372,1.9844784064,-2.7356499461
N,0,1.946255302,-0.441053287,-3.466972989
N,0,-7.8437117064,0.8706127446,-2.2487737804
C,0,-4.3180302403,0.2726116327,-1.190029392
C,0,-0.3248290729,-2.8365009333,-0.2954220948
C,0,4.7562474445,1.668455096,0.3962858861
C,0,1.5333311237,4.2827856821,-0.6369942367
C,0,-6.6360927817,0.1241887222,-1.9258019555
C,0,-4.2738915228,-1.1582311403,-1.2099185809
C,0,6.1700181805,-0.3074406187,0.1499375918
C,0,7.2344159932,0.3955764002,0.6845992053
C,0,-5.3874425666,-1.8961341741,-1.6134901172
C,0,-0.8412243278,4.578745221,-0.796622493
C,0,1.3627957862,2.9149387658,-0.4188475099
C,0,0.4448879508,5.1318864314,-0.80626076
C,0,-5.5278257341,0.8789143073,-1.5673605899
C,0,0.8619908561,-4.93244315,0.1182532993
C,0,-2.8161097689,-2.9576149102,-0.6805441402
C,0,-1.5428676755,-3.5566758748,-0.3727431612
C,0,3.547213481,2.4193166782,0.2354748528
C,0,7.0851434496,1.7396340161,1.0816586886
C,0,0.8681837574,-3.5631951348,-0.0642775957
C,0,5.8691856686,2.3623988094,0.9397360875
C,0,-1.0292043438,3.2064253032,-0.6399192719
C,0,-6.581636248,-1.2784008586,-1.9575456899
C,0,0.0589799481,2.3594657044,-0.4538284529
C,0,4.8881145393,0.3098704456,-0.0086003858
C,0,-0.3524439544,-5.6354203817,0.0584847638
C,0,3.2553650987,-3.438909041,0.1245499594
C,0,-1.5258936342,-4.959833332,-0.1895794996
C,0,7.447793216,-2.2827942124,-0.1181474184

N,0,-0.9449976321,1.3610030097,5.2625795174
C,0,-1.8520439825,0.3146493785,5.2730267682
O,0,-2.3003753674,-0.1255605138,6.3095609159
N,0,-2.2379056271,-0.2480435953,4.0447528324
C,0,-1.7966303884,0.18700191,2.836871823
O,0,-2.155985488,-0.3718304075,1.7952314877
C,0,-0.8851937756,1.3672244445,2.8127228221
C,0,-0.3888712474,1.9075739623,4.1209726487
O,0,0.443966026,2.7910954886,4.1631511832
C,0,-0.5471817284,1.8735414259,6.5702613093
C,0,-3.1595559579,-1.3796362631,4.1341978315
C,0,5.9548875954,-1.2492263337,6.8136457045
C,0,7.0805162843,-0.456426212,6.5712222286
C,0,7.1604733762,0.3148530922,5.4133857962
C,0,6.1170928444,0.2954595489,4.4975390177
C,0,4.9794544526,-0.4998843382,4.7279026852
C,0,4.9116700655,-1.2742292455,5.9028286203
C,0,3.9332579393,-0.4803348675,3.7326744928
C,0,2.7977343814,-1.210643152,3.7512288209
N,0,1.8588799587,-1.1022665588,2.7032524013
O,0,0.867233445,-1.8099732011,2.7446183278
O,0,2.065663975,-0.2799673272,1.7808702483
H,0,2.528227875,4.7072280626,-0.711463876
H,0,8.1996387869,-0.084574212,0.8035811399
H,0,-5.3392835838,-2.9773607259,-1.6840420243
H,0,-5.6022340452,1.9597344017,-1.5634267279
H,0,1.783368702,-5.4715891611,0.3056525401
H,0,-3.6380621575,-3.672343775,-0.7842429833
H,0,3.6272455209,3.463937406,0.5523909123
H,0,7.9364939485,2.2720408112,1.4926784226
H,0,5.7435696543,3.4009153378,1.2344764723
H,0,-2.0348470578,2.7981245628,-0.6747762884
H,0,-0.3533991277,-6.7106238583,0.2003905556
H,0,4.0162399538,-2.6629349983,0.049742695
H,0,3.3960594185,-4.1799785995,-0.6676732523
H,0,3.2955222373,-3.9243920551,1.1041188763
H,0,-2.4654476849,-5.5020293004,-0.2526822623
H,0,7.7628853328,-2.333568102,0.9311403102
H,0,8.2394681847,-1.8068479056,-0.7091239114
H,0,7.2773040013,-3.2924428313,-0.4923695597
H,0,-1.407894604,2.18078705,2.294316661
H,0,-0.0257443332,1.1226170752,2.1809810953
H,0,0.146267504,2.6931736622,6.3981957307
H,0,-0.0622501396,1.0856014181,7.1487077016
H,0,-1.4258213456,2.2272848093,7.1109555301
H,0,-3.3881275549,-1.7044830627,3.1229203562
H,0,-4.0695312608,-1.0671537032,4.6468161288
H,0,-2.6912539722,-2.190145862,4.6938089088
H,0,5.8963444801,-1.8467143,7.7178425851
H,0,7.8947842701,-0.4418960053,7.2895384911

H,0,8.0347416961,0.9300183269,5.2255991034
H,0,6.1758678454,0.8927719454,3.591094001
H,0,4.0424995807,-1.8919241949,6.1055862699
H,0,4.0788907451,0.1832494776,2.8826616353
H,0,2.4893936958,-1.9259995765,4.4998161395

Sum of electronic and zero-point Energies= -6145.538507
Sum of electronic and thermal Energies= -6145.469432
Sum of electronic and thermal Enthalpies= -6145.468487
Sum of electronic and thermal Free Energies= -6145.655539

17ZnY catalyst + trans-nitrostyrene-I

Y,0,-1.3917322277,0.4915678619,1.0659704334
Zn,0,1.9498678951,-0.1243361462,0.3605433307
Cl,0,7.7070683658,-3.7493703035,-0.4598669184
Cl,0,0.301510783,6.3982990826,-2.7969967945
O,0,0.4333249347,1.164575557,-0.1315365305
O,0,0.2584749915,-1.1383972298,1.0357996552
O,0,3.5195223032,0.3729553457,-0.7538522295
O,0,2.4314157963,0.7422608693,2.187191625
O,0,-3.5178397274,0.8428777589,1.3139673072
O,0,-2.073806897,-1.7962274648,1.9010312487
O,0,-0.90440931,2.4139629779,2.4645050943
O,0,-1.1820914915,0.5339092356,3.4697153762
O,0,-5.918184503,0.2461577072,2.1845986756
O,0,2.8339558595,5.2302527412,-3.5588669735
N,0,2.9395709671,-1.9817494718,0.4006606726
N,0,-1.9083144619,2.3959138748,-0.4219845888
O,0,8.5951100159,-1.8411257927,-2.4576693086
N,0,2.855110451,4.5232300857,-2.5631297484
O,0,-0.8028416547,2.3305958208,4.6329649584
O,0,3.8812830971,4.142902618,-2.0145551205
N,0,2.2111795979,0.9119958669,4.4438529663
O,0,8.2926186229,0.2295079413,-1.9229209891
N,0,-0.9565839778,1.7826799151,3.5629967251
N,0,7.9585493055,-0.9475782182,-1.9217068839
C,0,4.449129906,-0.5369989819,-0.7251445773
C,0,0.1222878889,-2.3996462416,1.3858472634
C,0,-4.3630513576,2.3137482467,-0.3741715491
C,0,-0.7601639825,4.2694569248,-1.5769683351
H,0,-1.6623140374,4.8690025542,-1.6189521569
C,0,6.7040757792,-1.2882134707,-1.2657104966
C,0,4.2242071523,-1.8177893413,-0.1258292518
C,0,-5.8502676896,1.1063726887,1.1381116698
C,0,-6.9425659219,1.6670356068,0.5005659515
H,0,-7.9477578104,1.4262332444,0.8294499917
C,0,5.2448127574,-2.7673902169,-0.0741141933
H,0,5.0966995758,-3.7114436202,0.4390772378
C,0,1.5907626709,4.0735725065,-2.0041942543

C,0,-0.769825733,3.0162313487,-0.960992681
C,0,0.4020802703,4.8052599955,-2.119441474
C,0,5.7170452633,-0.3127776012,-1.288797758
H,0,5.9251071105,0.6389466883,-1.7628173689
C,0,2.1199177541,0.2566133708,3.2970596866
H,0,1.7383193911,-0.767101785,3.3859730411
C,0,-1.3882283761,-4.1074449902,2.2721459206
H,0,-2.3612872288,-4.397978311,2.6507526397
C,0,2.4658532663,-3.1270852271,0.7745069793
H,0,3.0892278986,-4.0220493159,0.6884045386
C,0,1.1461728454,-3.3764397711,1.2946140898
C,0,-3.0859103726,2.7511071573,-0.8520319476
H,0,-3.1473727783,3.468718831,-1.6760614453
C,0,-6.7700863052,2.552739755,-0.5809142857
H,0,-7.6422147636,2.9793436396,-1.0651884522
C,0,-1.1453662829,-2.8073164253,1.8723765668
C,0,-5.5042552175,2.8706010608,-1.0073334772
H,0,-5.3576755229,3.5610888525,-1.8338510685
C,0,1.6149142905,2.8520669498,-1.3351370038
H,0,2.5498847318,2.3068282016,-1.2520652967
C,0,6.4854502443,-2.5307435226,-0.6499053081
C,0,0.4506332133,2.3136095581,-0.7929647653
C,0,-4.5191107215,1.4052779428,0.7091108188
C,0,-0.3650240029,-5.0651848506,2.1848078435
H,0,-0.5604224321,-6.085082229,2.4976078924
C,0,-3.383909002,-2.1208039334,2.3761897089
H,0,-3.9691435829,-1.2060181793,2.2926325923
H,0,-3.3337851531,-2.4529519172,3.4174497643
H,0,-3.8248546421,-2.9060821306,1.7544381587
C,0,0.8709746316,-4.7049442439,1.6990322552
H,0,1.6633557666,-5.4442925112,1.6206100288
C,0,-7.2031659599,-0.1097199635,2.6542567432
H,0,-7.7918394954,-0.609161561,1.8750803452
H,0,-7.7554106502,0.7662303491,3.0155054924
H,0,-7.0430329273,-0.800289488,3.4825937515
C,0,2.6760483707,2.2858843078,4.4975459552
H,0,2.9968604713,2.5922848195,3.5033603109
H,0,3.5138968731,2.3626410544,5.1959507876
H,0,1.8640809964,2.9346252192,4.839203051
C,0,1.7850755937,0.3075287194,5.692117372
H,0,1.4961486663,-0.7307588441,5.5226000799
H,0,0.9273955289,0.855928812,6.0922195003
H,0,2.602659064,0.3353085233,6.4176925709
C,0,-5.2634258789,-4.3784849999,-5.2325446491
C,0,-6.0594025728,-5.2649893536,-4.5018990582
C,0,-6.0561349482,-5.2260909908,-3.1089745361
C,0,-5.2580367164,-4.3025580048,-2.4469873982
C,0,-4.4516813248,-3.4050163183,-3.1692590974
C,0,-4.4654719962,-3.4552670351,-4.5762905335
C,0,-3.6443529877,-2.4688817586,-2.4189924414

C,0,-2.8123588545,-1.5397595252,-2.929856269
N,0,-2.0792980506,-0.6822351072,-2.0738088901
O,0,-1.3376387058,0.1370899874,-2.5850746956
O,0,-2.2199743322,-0.7996974963,-0.8379324958
H,0,-5.2691600176,-4.4117595164,-6.3174040846
H,0,-6.6823731269,-5.9860186989,-5.0226345318
H,0,-6.6743884025,-5.9141104536,-2.541255512
H,0,-5.2512710758,-4.2672158827,-1.3610013202
H,0,-3.8529637449,-2.7724224195,-5.1564822108
H,0,-3.7156457979,-2.521143121,-1.3350730837
H,0,-2.6081122253,-1.3414261932,-3.9720636291

Sum of electronic and zero-point Energies= -5825.751729
Sum of electronic and thermal Energies= -5825.688221
Sum of electronic and thermal Enthalpies= -5825.687276
Sum of electronic and thermal Free Energies= -5825.858981

17ZnY catalyst + trans-nitrostyrene-II

Y,0,1.8118985949,-0.7949250889,-1.3920033865
Zn,0,-1.524175326,-0.5444746464,-0.47208726
Cl,0,-8.0048777106,-2.5004748169,0.4684562197
Cl,0,1.6554510674,5.8605619081,1.5219913353
O,0,0.2628616886,0.4289964714,-0.2321234202
O,0,-0.1525710774,-1.9799647068,-1.1139435849
O,0,-2.9132592537,0.447936605,0.5458487693
O,0,-1.8771997274,0.1999090459,-2.3987726167
O,0,3.9419684855,-0.9638906585,-1.7173789404
O,0,1.987675127,-3.2932407893,-1.6807481642
O,0,1.6726972609,0.9240590929,-3.0561053441
O,0,1.4283837146,-1.0998858116,-3.7332205603
O,0,6.1013105519,-2.1818229034,-2.5695153221
O,0,-1.0313005648,5.4228226602,2.4914082699
N,0,-2.9316666252,-2.0873807892,-0.3476575888
N,0,2.8150516679,1.1527941391,-0.221690425
O,0,-8.4201334999,-0.2311759886,2.2244574016
N,0,-1.2536191927,4.5925438262,1.6240638202
O,0,1.3951895248,0.5273574894,-5.1747748841
O,0,-2.3615358697,4.3711980731,1.1535069596
N,0,-1.8374254741,-0.0264654833,-4.6613174438
O,0,-7.5828157937,1.6298509341,1.5175396029
N,0,1.494704011,0.1350482309,-4.0349213364
N,0,-7.5627962922,0.4124872666,1.6399341072
C,0,-4.0423807995,-0.198082332,0.5666859662
C,0,-0.298706297,-3.2849628168,-1.1944691094
C,0,5.1873866416,0.5229155852,-0.3146839267
C,0,2.1674108865,3.3898538218,0.6407370241
H,0,3.1788551463,3.7734372179,0.5686171183
C,0,-6.4238975763,-0.2999290111,1.0783508873
C,0,-4.1394063508,-1.5518191033,0.108387272

C,0,6.2848685896,-1.18691714,-1.6664080172
C,0,7.5093862042,-0.7942575447,-1.1552113087
H,0,8.417617942,-1.2946963192,-1.4731662596
C,0,-5.3661279237,-2.2155989683,0.10437522
H,0,-5.4515969784,-3.2145459425,-0.3097323116
C,0,-0.1459231471,3.7883203411,1.1329418065
C,0,1.8723116596,2.0864432406,0.2357315618
C,0,1.1772942698,4.2466513336,1.108573368
C,0,-5.2220830729,0.3940082512,1.0496340214
H,0,-5.1912018084,1.4125973453,1.417380249
C,0,-1.8127533464,-0.5077213536,-3.4269554283
H,0,-1.7246263929,-1.5987105919,-3.3636066617
C,0,0.7951829733,-5.4223463186,-1.6621401696
H,0,1.6814927267,-5.988360929,-1.9239139297
C,0,-2.7422564662,-3.3527938633,-0.540588788
H,0,-3.5582027826,-4.0550116166,-0.3447876498
C,0,-1.5155043056,-3.9766513764,-0.9660782434
C,0,4.0644076248,1.2948580792,0.1238406236
H,0,4.3242214042,2.0914047114,0.827621013
C,0,7.5971473947,0.2523305371,-0.2170419231
H,0,8.5685423157,0.5399846558,0.1711783905
C,0,0.8482851952,-4.0489414718,-1.5234003534
C,0,6.4576473941,0.8995415648,0.1931133961
H,0,6.5122702926,1.7132047639,0.9114927192
C,0,-0.4694978295,2.5124105622,0.6761411108
H,0,-1.5038071826,2.182941387,0.6972694415
C,0,-6.5168437068,-1.6156774782,0.597704289
C,0,0.5228444778,1.6518001347,0.2148446087
C,0,5.0788179965,-0.5467005076,-1.2447491934
C,0,-0.4198951642,-6.0953110355,-1.4567597045
H,0,-0.4583517294,-7.1734996191,-1.5670358993
C,0,3.184962033,-3.988409415,-2.0494539242
H,0,3.9596361174,-3.228214344,-2.1366842479
H,0,3.0406909886,-4.4977275898,-3.0067194132
H,0,3.449544349,-4.7140587178,-1.2748730996
C,0,-1.5454108047,-5.3847322423,-1.1078794218
H,0,-2.4845211988,-5.9022336034,-0.9317996354
C,0,7.2476722988,-2.8817470487,-3.0118700863
H,0,7.7592709101,-3.3808967349,-2.1799569217
H,0,7.9539626926,-2.2143620069,-3.520091917
H,0,6.8908933525,-3.6321914558,-3.717620928
C,0,-1.9359206797,1.3986857513,-4.9172989735
H,0,-2.0768280806,1.9208146567,-3.9724290452
H,0,-2.7850615538,1.5948551728,-5.5778132574
H,0,-1.0188634186,1.7506520806,-5.3991031001
C,0,-1.7007277445,-0.8977191565,-5.8130997376
H,0,-1.6709467977,-1.9396382403,-5.4907065714
H,0,-0.7739535581,-0.6627342289,-6.3447526603
H,0,-2.5490368399,-0.758561443,-6.4889444541
C,0,3.853340603,2.6291722787,4.4436500578

C,0,5.2032859488,2.3044533993,4.5989164159
C,0,5.6622776379,1.0373103075,4.245232649
C,0,4.7739504251,0.0974134641,3.7368379672
C,0,3.4132507643,0.4094915233,3.5776832444
C,0,2.9634447277,1.6930051757,3.9386216009
C,0,2.5412805493,-0.608764866,3.02247102
C,0,1.2186252005,-0.5051543914,2.8126745769
N,0,0.5033145911,-1.5843746394,2.2065569896
O,0,-0.7090041575,-1.418768522,2.0574704017
O,0,1.0952204952,-2.6007177074,1.8622099322
H,0,3.4974496516,3.6177685996,4.7166793562
H,0,5.8951957765,3.0418670874,4.9947284599
H,0,6.7107356617,0.7825466294,4.3641004195
H,0,5.128792149,-0.890751074,3.4567986536
H,0,1.918626206,1.9619135343,3.8188868326
H,0,3.0070613473,-1.5488444762,2.734560909
H,0,0.5781467947,0.3341199896,3.0423804901

Sum of electronic and zero-point Energies= -5825.745649
Sum of electronic and thermal Energies= -5825.681056
Sum of electronic and thermal Enthalpies= -5825.680112
Sum of electronic and thermal Free Energies= -5825.856039

-N(O)OH Michael addition product

O,0,-1.286231384,-1.6895695387,1.091401106
O,0,-0.2536400296,-3.5912509089,0.7260784877
O,0,-0.7716177911,1.4044669942,2.1863328382
O,0,-4.2718273931,1.0013166981,-0.6617762484
O,0,-0.3028461081,-0.7470952919,-1.9599259812
N,0,-0.1957747142,-2.2035255635,0.7756613468
N,0,-2.2607098787,0.230700829,-1.3793513195
N,0,-2.5109013661,1.2806158509,0.7390809298
C,0,-0.2529688262,0.6540937482,-0.0237514232
C,0,0.980816516,-0.0964590252,0.5629603596
C,0,2.3013208837,0.4055351003,0.0074857893
C,0,-3.0833231554,0.8508568638,-0.4497812818
C,0,-1.1852427176,1.1111955334,1.080168046
C,0,3.1498855037,1.1537977837,0.8265437984
C,0,-2.9156148719,-0.2911204345,-2.5739528014
C,0,4.3643829747,1.6344647915,0.3420310545
C,0,4.7462021418,1.3673919895,-0.9699632758
H,0,1.7542463283,-2.1819069188,0.1656945776
C,0,0.9021691097,-1.58805496,0.4673029607
C,0,-0.9220775039,-0.0442516035,-1.181458164
C,0,2.6907743234,0.1432129847,-1.3101632449
C,0,3.9058577658,0.6206533089,-1.7936713516
C,0,-3.4293236143,1.8560517584,1.7162225895
H,0,0.1294717267,1.5927714061,-0.4544595822

H,0,0.9579535581,0.1696546016,1.6283059432
H,0,2.8574849461,1.3627166222,1.852682739
H,0,-3.6049855478,0.4593526631,-2.957227265
H,0,-3.4708243363,-1.2034052702,-2.3419042437
H,0,-2.1429997154,-0.5128873012,-3.3062467933
H,0,5.0123838414,2.214866671,0.9924119738
H,0,5.6935608909,1.7391655631,-1.3494090979
H,0,0.6579650956,-3.9119176,0.643336065
H,0,2.0269035046,-0.4265993303,-1.9536826639
H,0,4.1965847374,0.4097818235,-2.8189355201
H,0,-4.0027419739,2.6562015813,1.2485362491
H,0,-2.8322748189,2.244150878,2.5375430619
H,0,-4.1176381016,1.0933277021,2.0864803416

Sum of electronic and zero-point Energies= -1081.384739
Sum of electronic and thermal Energies= -1081.364105
Sum of electronic and thermal Enthalpies= -1081.363161
Sum of electronic and thermal Free Energies= -1081.436745

-NO_2 Michael addition product

O,0,-1.2346208963,-1.7053022181,1.0904645873
O,0,0.075859554,-3.3201299198,1.6633049276
O,0,-0.7773142792,1.4575373542,2.0899890782
O,0,-4.2923482074,0.8987542313,-0.7109167629
O,0,-0.2883779996,-0.7411390564,-2.0473224091
N,0,-0.138891769,-2.2505924958,1.1264423359
N,0,-2.2761725369,0.1361005858,-1.4174527965
N,0,-2.5255818347,1.2617262096,0.6636599637
C,0,-0.2598423332,0.6456929648,-0.0994989707
C,0,0.9799664936,-0.0610312302,0.5126725805
C,0,2.3052338971,0.448215724,-0.0305482602
C,0,-3.1009655772,0.7788495901,-0.5021930239
C,0,-1.1944576814,1.126555525,0.9962681725
C,0,3.305810721,0.8282932079,0.8686583155
C,0,-2.9427391771,-0.4209885385,-2.5909671398
C,0,4.5403069503,1.2813721939,0.4109589298
C,0,4.7908541027,1.3595745724,-0.9567149228
H,0,1.8997175971,-1.9846160287,0.9024554512
C,0,1.0020859791,-1.5873581693,0.4307273314
C,0,-0.9248777622,-0.0720372833,-1.2495475457
C,0,2.5675407841,0.5235670273,-1.4023442933
C,0,3.8012005086,0.9795943405,-1.8603881064
C,0,-3.4446373108,1.8598335586,1.6272247349
H,0,0.1037446643,1.5821499149,-0.5536058698

H,0,0.9512989349,0.2102676175,1.5725583993
H,0,3.1145018342,0.7742875152,1.9376972832
H,0,-3.5481098116,0.3521952207,-3.0631473012
H,0,-3.5875267145,-1.2531965774,-2.3010877899
H,0,-2.1715140311,-0.7713849984,-3.2719750498
H,0,5.3037123822,1.5779105025,1.1243682219
H,0,5.7517404801,1.7157768581,-1.31642127
H,0,0.9473925726,-1.9383633094,-0.6028270963
H,0,1.8013592941,0.2191112965,-2.1096052608
H,0,3.9892610649,1.0362339044,-2.9287672498
H,0,-4.0326951766,2.633941268,1.1346173665
H,0,-2.8468689487,2.2864397223,2.428576397
H,0,-4.1184457674,1.1011589199,2.0305870424

Sum of electronic and zero-point Energies= -1081.410627
Sum of electronic and thermal Energies= -1081.390523
Sum of electronic and thermal Enthalpies= -1081.389579
Sum of electronic and thermal Free Energies= -1081.462764

1Im

Y,0,-2.0960341887,-1.599042146,0.6994400105
Zn,0,1.3376966806,-1.0685472828,0.3642025698
Cl,0,7.7982603627,-3.1137658866,-0.5448246748
Cl,0,-0.9098467363,3.2853211792,5.8859232221
O,0,-0.2698850972,-0.2820468142,1.2610538396
O,0,-0.1614584707,-2.2579705366,-0.385560509
O,0,2.9623592362,-0.0876279694,0.8997910395
O,0,-4.2354941021,-1.409178255,0.4974185725
O,0,-2.4078389278,-3.0798610599,-1.3114831598
O,0,-1.4474308631,-2.4694457527,2.8486226845
O,0,-2.4982311074,-3.8051814283,1.5328698861
O,0,-6.5691908842,-2.0927815691,-0.4869674958
O,0,1.8479045072,3.5983150577,5.0781387482
N,0,2.7050488374,-2.3275761177,-0.5622106927
N,0,-2.7123595264,0.4019526297,2.017739006
O,0,8.7094832068,-0.4892793323,0.2851187824
N,0,1.8646717995,2.4936882178,4.558198458
O,0,-1.9064536743,-4.4880127839,3.5092315328
O,0,2.8656719716,1.7963313826,4.4598769779
O,0,7.727954135,0.2937701039,2.0427165469
N,0,-1.9495817833,-3.6239050711,2.6669772538
N,0,7.7309091103,-0.3479377108,1.0011685429
C,0,4.0478904401,-0.7312057474,0.5664874628
C,0,-0.0764593342,-3.149450635,-1.3540185202
C,0,-5.0810817126,0.6301744111,1.4124608151
C,0,-1.7555616857,1.7886446728,3.8395828206
C,0,6.4729022043,-0.9498281046,0.5809927041
C,0,3.997868431,-1.9293556535,-0.2136572445
C,0,-6.5131647218,-0.9102680745,0.1732068069

C,0,-7.5796779062,-0.0472319012,0.3499168386
C,0,5.1665229096,-2.6197178692,-0.5342223559
C,0,0.6308058173,1.9758489445,3.9882702277
C,0,-1.6337936394,0.9556161298,2.726534426
C,0,-0.6373124851,2.3209892547,4.4721146135
C,0,5.318317253,-0.2723834926,0.9487242946
C,0,-1.3159844653,-4.5820202027,-2.8963614363
C,0,2.4464954909,-3.2153587602,-1.4699420998
C,0,1.1386151341,-3.6447159096,-1.8886893446
C,0,-3.8505848274,1.0391669078,2.0154422745
C,0,-7.4199828881,1.1640141764,1.0519018658
C,0,-1.2931161631,-3.6370853617,-1.8882593629
C,0,-6.1940337765,1.4960426162,1.572547944
C,0,0.77287409,1.0976563482,2.9157075624
C,0,6.4145803277,-2.1396799137,-0.161534835
C,0,-0.3461970692,0.569782092,2.2805289698
C,0,-5.2216694347,-0.5896508675,0.696042986
C,0,-0.1074306184,-5.0738133064,-3.4150296206
C,0,-3.6846036206,-3.5273728714,-1.783312064
C,0,1.0913253734,-4.6110804905,-2.9221844329
C,0,-7.8127700273,-2.4724708224,-1.0422363233
H,0,-2.7325182747,2.0115361598,4.2538044706
H,0,-8.5543875581,-0.2961139099,-0.0557327507
H,0,5.1228151329,-3.5641867823,-1.0658608849
H,0,5.4013511655,0.6354738692,1.5341555035
H,0,-2.256322801,-4.9478577161,-3.2919859854
H,0,3.272955009,-3.689400199,-2.0071146978
H,0,-3.902738256,2.0100954043,2.5178488223
H,0,-8.2722003871,1.8239215739,1.1757368518
H,0,-6.0596669334,2.424480924,2.1213768101
H,0,1.7675682103,0.8367286759,2.566791816
H,0,-0.1295711834,-5.8161535163,-4.2053074672
H,0,-4.4262087946,-2.9681604312,-1.2151347406
H,0,-3.791952868,-4.6013107861,-1.6049023018
H,0,-3.7837222404,-3.3094667123,-2.8501287621
H,0,2.0283070143,-4.9856332575,-3.3248244878
H,0,-8.1572076234,-1.7473746733,-1.7895999194
H,0,-8.5810125878,-2.5828187749,-0.2674426315
H,0,-7.6478056833,-3.4360344161,-1.5248590894
O,0,-1.9860820076,0.1241654024,-1.0723694225
O,0,-3.5154697888,-0.2647234988,-2.5470403163
O,0,-1.5034090058,3.8051602323,-0.8593098145
O,0,2.8659088943,5.0154951073,-0.7567040902
O,0,1.8986992999,0.9057424913,-2.4184849675
N,0,-2.6202495497,0.4041231759,-2.0978924761
N,0,2.4000887787,2.948748454,-1.5650393646
N,0,0.6763823224,4.4303336654,-0.8324384485
C,0,0.0498074036,2.1997978647,-1.6753194897
C,0,-0.7360714119,1.8365061616,-2.969234695
C,0,-0.4598925044,2.8244815277,-4.0892808748

C,0,2.0300653628,4.1808114244,-1.036956651
C,0,-0.3351336845,3.5381890589,-1.1003018355
C,0,0.4696978089,2.4906974552,-5.0796600761
C,0,3.8339221643,2.738712419,-1.744029073
C,0,0.7632321535,3.3825406576,-6.1078848369
C,0,0.1258190091,4.6196421197,-6.1629008022
H,0,-2.7586472587,1.6312742939,-3.7458192436
C,0,-2.2487393553,1.6711138616,-2.7849267607
C,0,1.5201329282,1.9561064573,-1.9270705219
C,0,-1.0963330624,4.0701188873,-4.1526181536
C,0,-0.8048401064,4.9596278181,-5.1838334969
C,0,0.3521669482,5.7339758732,-0.2598289074
H,0,-0.2299718263,1.467206502,-0.9068984846
H,0,-0.3291380422,0.8683808176,-3.2770928442
H,0,0.9686881769,1.5262421845,-5.0397282942
H,0,4.3371360862,2.7668569931,-0.7761023208
H,0,4.2442570407,3.5195305065,-2.385251875
H,0,3.9648310688,1.7633675287,-2.2057195705
H,0,1.4876263927,3.106733293,-6.8686266512
H,0,0.3507308615,5.3146474959,-6.9665252528
H,0,-2.6698315609,2.4641355129,-2.1603242716
H,0,-1.8219669413,4.3554056595,-3.3962222089
H,0,-1.3091080535,5.9207830182,-5.221030006
H,0,0.8324983344,5.8418726758,0.7137028112
H,0,-0.7285671481,5.7833718389,-0.153932166
H,0,0.7039383497,6.5255672077,-0.9227152165

Sum of electronic and zero-point Energies= -6145.547670
Sum of electronic and thermal Energies= -6145.479678
Sum of electronic and thermal Enthalpies= -6145.478734
Sum of electronic and thermal Free Energies= -6145.664358

2Im

Y,0,-1.0947329209,0.1148115111,1.5472588127
Zn,0,2.2378752717,0.1767668308,0.5978656357
Cl,0,8.7483197385,-1.8977677453,0.3986105465
Cl,0,0.4495625794,7.041508129,2.4565528977
O,0,0.6078752332,1.464197786,0.5767390466
O,0,0.783442,-1.1535090824,1.05081978
O,0,3.7780299179,1.2270419325,-0.0082419638
O,0,-3.2464041861,0.1371445187,1.740322269
O,0,-1.4458056419,-2.3789564298,1.4572260935
O,0,0.1874590404,0.9713479975,3.3934268916
O,0,-0.9818421729,-0.7909210892,3.7742605106
O,0,-5.612365539,-0.9643928519,1.9295914897
O,0,2.9526252037,6.7982733117,1.0369633494
N,0,3.6279868839,-1.3655066469,0.6749092771
N,0,-1.7030548657,2.4832622019,1.4343034843
O,0,9.4188481327,0.5000952056,-1.0884271611

N,0,2.9962872153,5.5941304966,1.2313243503
O,0,0.2342269553,0.0562561039,5.3632900748
O,0,4.0318226547,4.9480313048,1.3180567357
O,0,8.5648240303,2.3169183213,-0.2905480884
N,0,-0.1710556422,0.0777877354,4.2254506586
N,0,8.5232430692,1.1197440639,-0.5374222254
C,0,4.8892313904,0.5425480897,0.0569204083
C,0,0.8748926777,-2.4664800384,1.1704051382
C,0,-4.1516811281,2.3248031916,1.3891606754
C,0,-0.5896200209,4.6552220295,1.862319608
C,0,7.3070660274,0.4031210804,-0.1764721483
C,0,4.8957712484,-0.8434930488,0.4091201704
C,0,-5.5855272862,0.3718007304,1.7047858354
C,0,-6.7000441051,1.1776811866,1.5610982123
C,0,6.0949684915,-1.5508051534,0.4950932255
C,0,1.7435200307,4.8625755105,1.3384192677
C,0,-0.5866555009,3.3320547369,1.4162679577
C,0,0.5586787655,5.4378800872,1.8141906293
C,0,6.1294307584,1.1352665674,-0.2263081617
C,0,-0.3440731685,-4.5537160566,1.548142632
C,0,3.3742121415,-2.6273217553,0.8119066936
C,0,2.0795623619,-3.2058750984,1.0668908047
C,0,-2.8952889654,3.0023094463,1.3207863405
C,0,-6.5660776504,2.561273024,1.3274594848
C,0,-0.3280651426,-3.1777569438,1.4072448591
C,0,-5.3170689098,3.1230227713,1.2434088809
C,0,1.7768331453,3.5284442659,0.9362270668
C,0,7.309251961,-0.9518747394,0.1913053304
C,0,0.6262546168,2.7561659094,0.9749755523
C,0,-4.269407581,0.9244323485,1.6157304325
C,0,0.8540408283,-5.2768285732,1.4448601515
C,0,-2.689134089,-2.9942747086,1.8270179817
C,0,2.0371376711,-4.6135498047,1.2058008062
C,0,-6.8795995948,-1.5832147312,2.0316401486
H,0,-1.487471268,5.0859889326,2.2912106694
H,0,-7.6942209422,0.7486995074,1.6254420845
H,0,6.1060491554,-2.5852528792,0.8208517658
H,0,6.1677898361,2.1823723479,-0.5015225916
H,0,-1.2735318314,-5.0793360362,1.7350310647
H,0,4.1850571311,-3.3552236871,0.7192347763
H,0,-2.9763466003,4.0790365736,1.1424130675
H,0,-7.4566486255,3.1711571463,1.2181523348
H,0,-5.2011746071,4.1895644401,1.0695601365
H,0,2.7098986824,3.0969805234,0.5853041345
H,0,0.8379537831,-6.3554175658,1.5551656517
H,0,-3.4187503596,-2.1857816834,1.8683670944
H,0,-2.5909849561,-3.4724572312,2.8055052995
H,0,-2.9848699593,-3.7265395115,1.0713451022
H,0,2.9671035481,-5.1695117538,1.1263986033
H,0,-7.4555755827,-1.4741799246,1.1047399511

H,0,-7.460329452,-1.1726475443,2.8664674336
H,0,-6.6868344737,-2.6407772437,2.2130709317
O,0,-1.5466934046,-0.1378718354,-0.7549080513
O,0,-0.2840481278,1.3663718181,-1.8641570415
O,0,1.1113347437,-2.3808598602,-2.7106654866
O,0,0.0827581066,-6.7696638803,-2.1829592102
O,0,-3.2817835031,-3.7707069497,-1.6444258289
N,0,-0.9419431198,0.1807208115,-1.8432668825
N,0,-1.6111179296,-5.2847557911,-1.923489362
N,0,0.6090554622,-4.5805306255,-2.4544324231
C,0,-1.1218642142,-2.8756588641,-2.0673319314
C,0,-1.735167524,-1.7863209438,-2.9964469014
C,0,-1.9357419202,-2.263840172,-4.4205678772
C,0,-0.2848370248,-5.6128407485,-2.1834405289
C,0,0.2873987653,-3.2442158663,-2.4523766993
C,0,-3.2120293177,-2.6612693146,-4.8304667825
C,0,-2.5059187611,-6.4101904329,-1.6686814011
C,0,-3.4281413253,-3.1288340075,-6.1241839467
C,0,-2.3698664841,-3.2011678057,-7.0266377668
H,0,-0.387141012,-0.1120450422,-3.7502793786
C,0,-0.9505923107,-0.5200182875,-2.9233586655
C,0,-2.1074409388,-4.0023549936,-1.8750880176
C,0,-0.8773287338,-2.3402794031,-5.3331600448
C,0,-1.0951938158,-2.805215476,-6.6276459021
C,0,1.9819892902,-4.9889319895,-2.738043211
H,0,-1.0412049224,-2.4072488373,-1.0751571304
H,0,-2.7171808752,-1.5870550338,-2.5501901496
H,0,-4.0391910824,-2.606642095,-4.1281096983
H,0,-2.1891034885,-6.9401922403,-0.7687733899
H,0,-2.4851320737,-7.0967097483,-2.5156161887
H,0,-3.5061650287,-6.0062368227,-1.5339563564
H,0,-4.4262009611,-3.4316648946,-6.4270444426
H,0,-2.5377015615,-3.5616269981,-8.0372751736
H,0,0.1004861878,1.4474159929,-0.9368517576
H,0,0.1236720039,-2.0410603907,-5.0352230183
H,0,-0.2649180639,-2.8563279865,-7.3258968708
H,0,2.4090017062,-5.4813861584,-1.8627669745
H,0,2.5461104557,-4.090737638,-2.9763634807
H,0,1.9943513942,-5.6794958288,-3.5818299862

Sum of electronic and zero-point Energies= -6145.544478
Sum of electronic and thermal Energies= -6145.477122
Sum of electronic and thermal Enthalpies= -6145.476178
Sum of electronic and thermal Free Energies= -6145.656179

9.6 ESI-MS of LMLn-NO_3

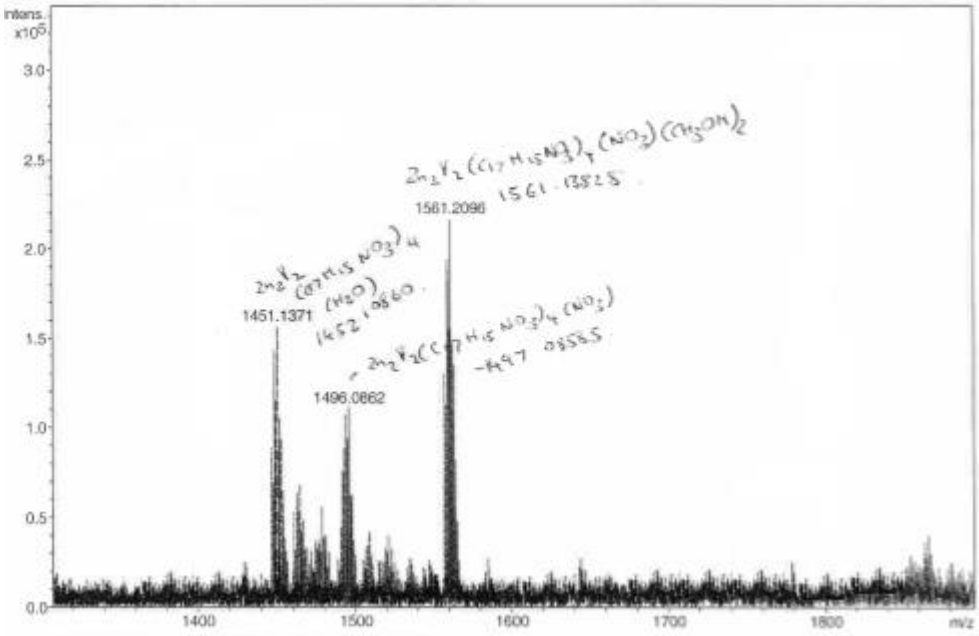

Figure S9.14. ESI-MS of **6ZnY-NO_3**

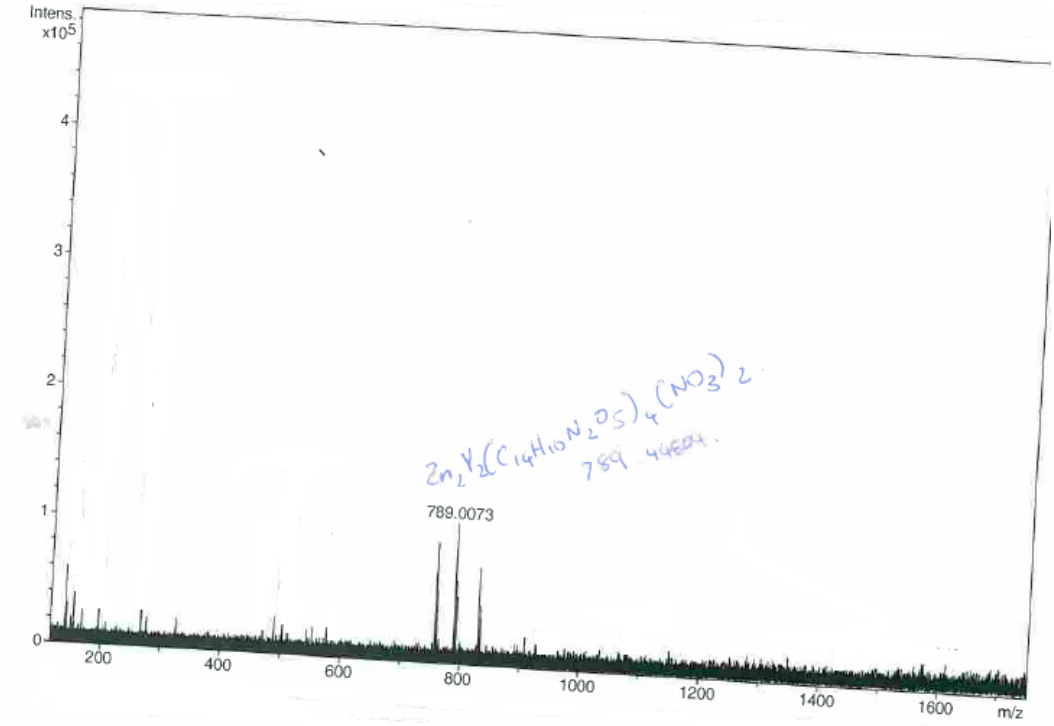

Figure S9.15. ESI-MS of **8ZnY-NO_3.** 789.85 m/z peak corresponds to- $[Zn^{II}_2Y^{III}_2(\mathbf{L8})_4(NO_3)_2]^{2+}$

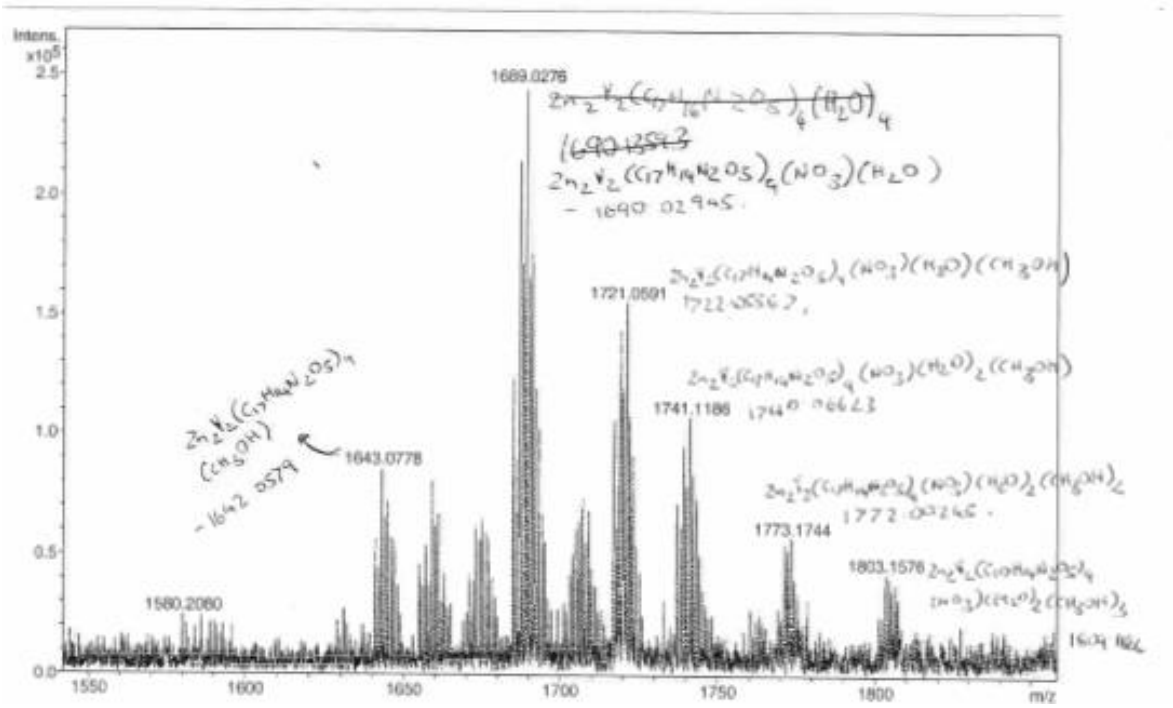

Figure S9.16. ESI-MS of **9ZnY-NO$_3$** 789.85 m/z peak corresponds to a $[Zn^{II}_2Y^{III}_2(\mathbf{L9})_4(NO_3)_2]^{2+}$ fragment.

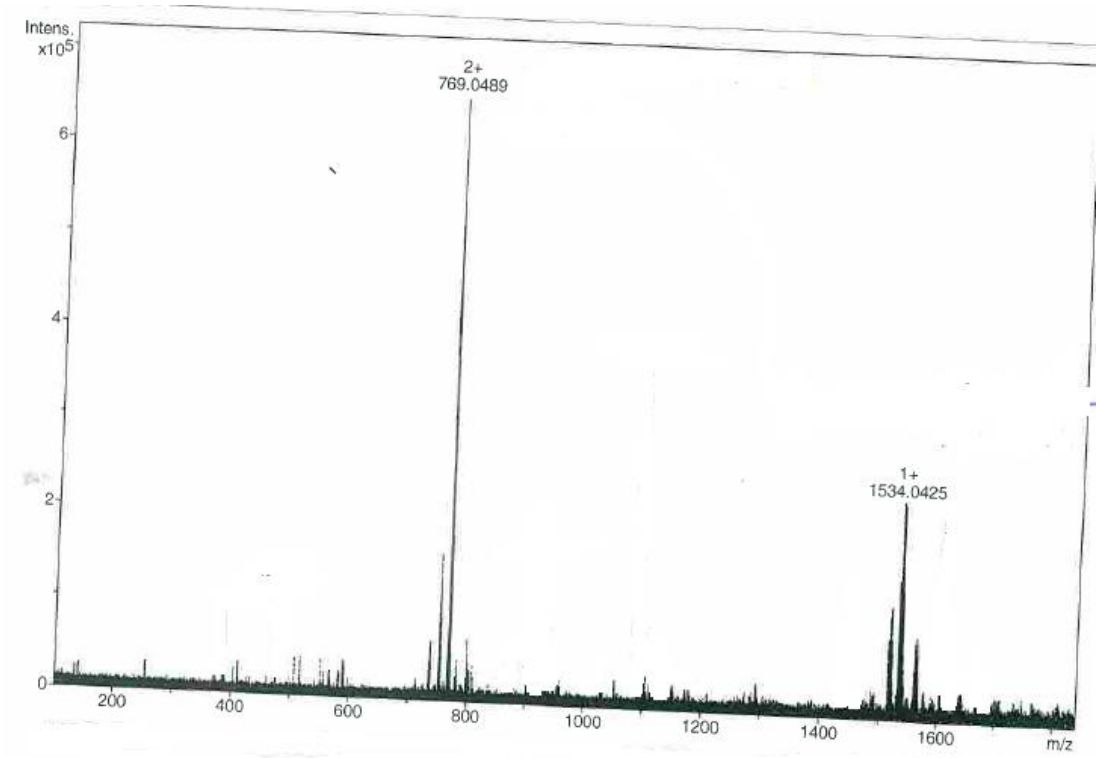

Figure S9.17. ESI-MS of **2ZnY-NO$_3$.** 1534.08 m/z m/z peak corresponds to a - $[Zn^{II}_2Y^{III}_2(\mathbf{L2})_4(CH_3OH)_2]^{1+}$ fragment.

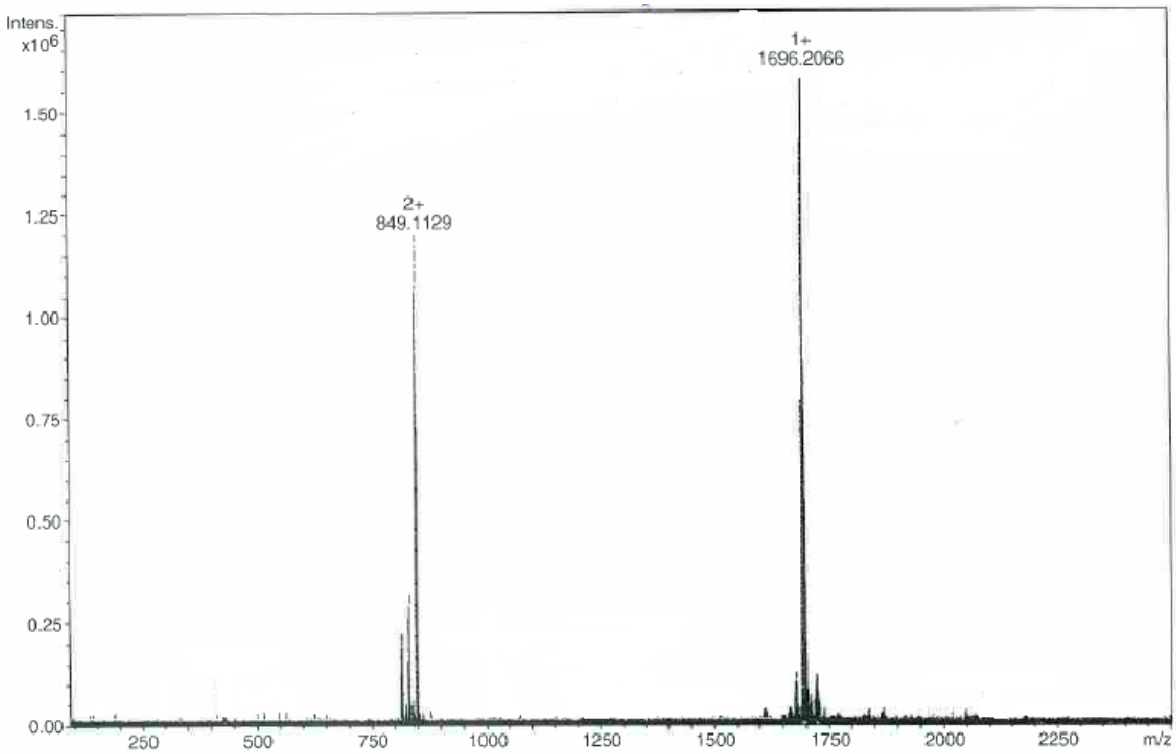

Figure S9.18. ESI-MS of 1**6ZnY-NO$_3$** 849.1129 m/z peak corresponds to a $[Zn^{II}_2Y^{III}_2(\mathbf{L16})_4(NO_3)]^{2+}$ fragment and the 1697.15 m/z peak corresponds to a $[Zn^{II}_2Y^{III}_2(\mathbf{L11})_4(NO_3)]^{1+}$ fragment.

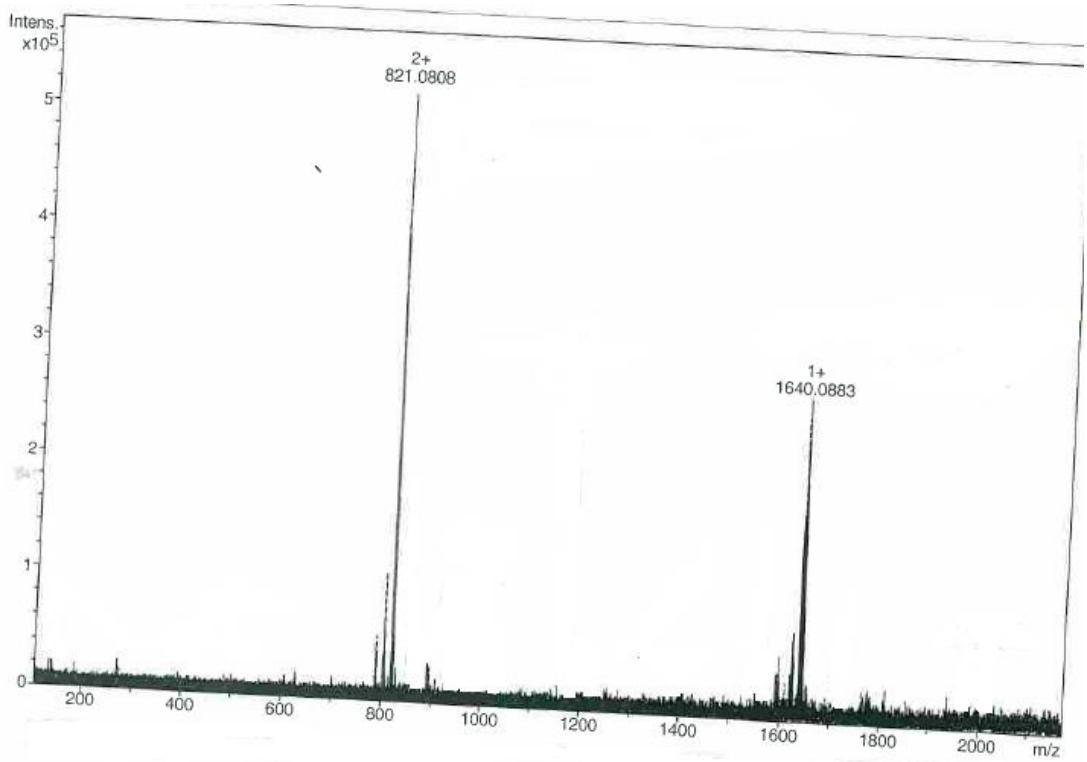

Figure S9.19. ESI-MS of **19ZnY-NO$_3$** 821.04 m/z peak corresponds to a $[Zn^{II}_2Y^{III}_2(\mathbf{L19})_4(NO_3)]^{2+}$ fragment; 1641.09 m/z peak corresponds to a $[Zn^{II}_2Y^{III}_2(\mathbf{L19})_4(NO_3)]^{1+}$ fragment.

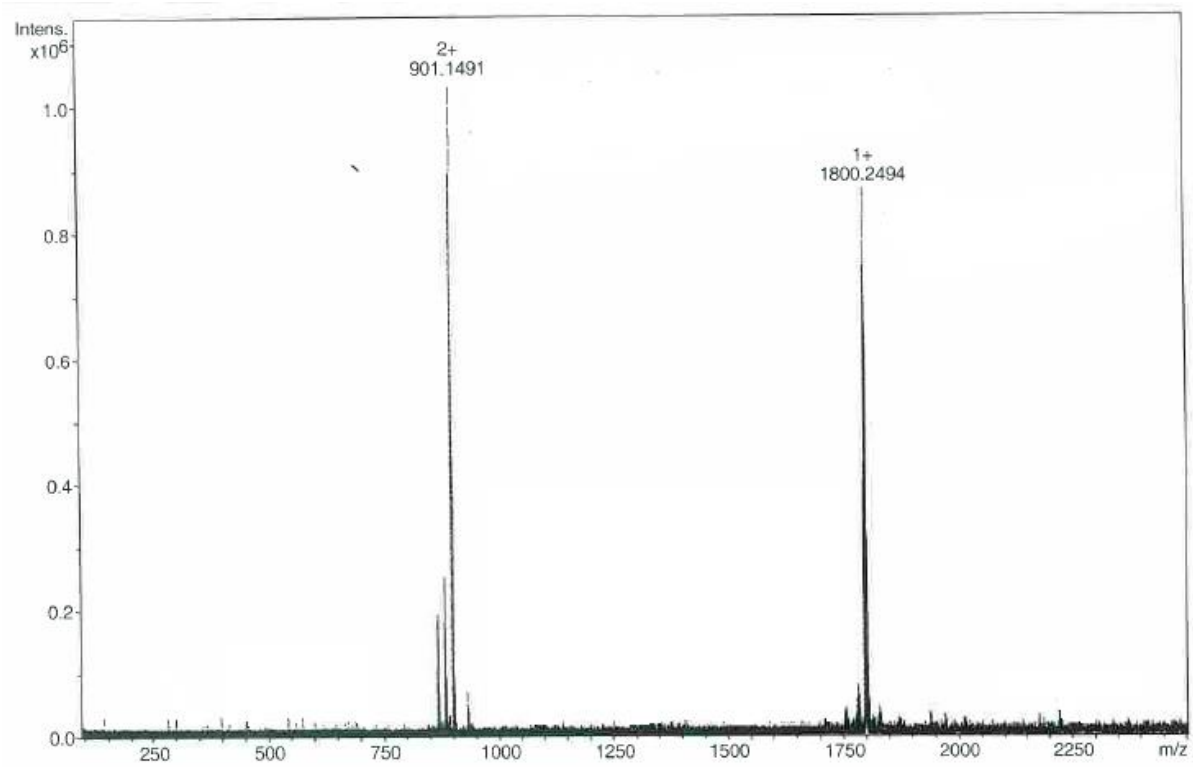

Figure S9.20. ESI-MS of **20ZnY-NO$_3$.** 901.11 m/z peak corresponds to a $[Zn^{II}_2Y^{III}_2(\mathbf{L20})_4(NO_3)]^{2+}$ fragment; 1801.21 m/z peak corresponds to a $Zn^{II}_2Y^{III}_2(\mathbf{L20})_4(NO_3)]^{1+}$fragment.

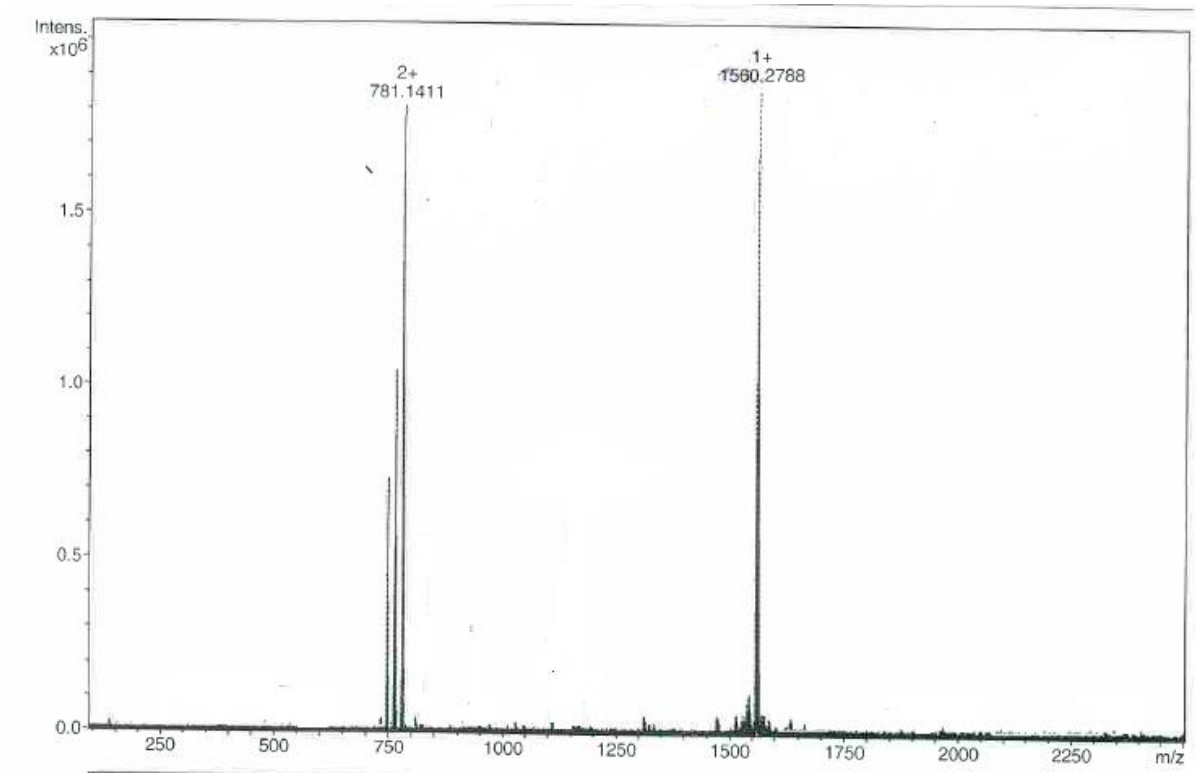

Figure S9.21. ESI-MS of **27ZnY-NO$_3$.** 781.11 m/z peak corresponds to a $[Zn^{II}_2Y^{III}_2(\mathbf{L27})_4(NO_3)]^{2+}$ fragment; 1561.21 m/z peak corresponds to a $[Zn^{II}_2Y^{III}_2(\mathbf{L27})_4(NO_3)]^{+}$ fragment.

ZnY17

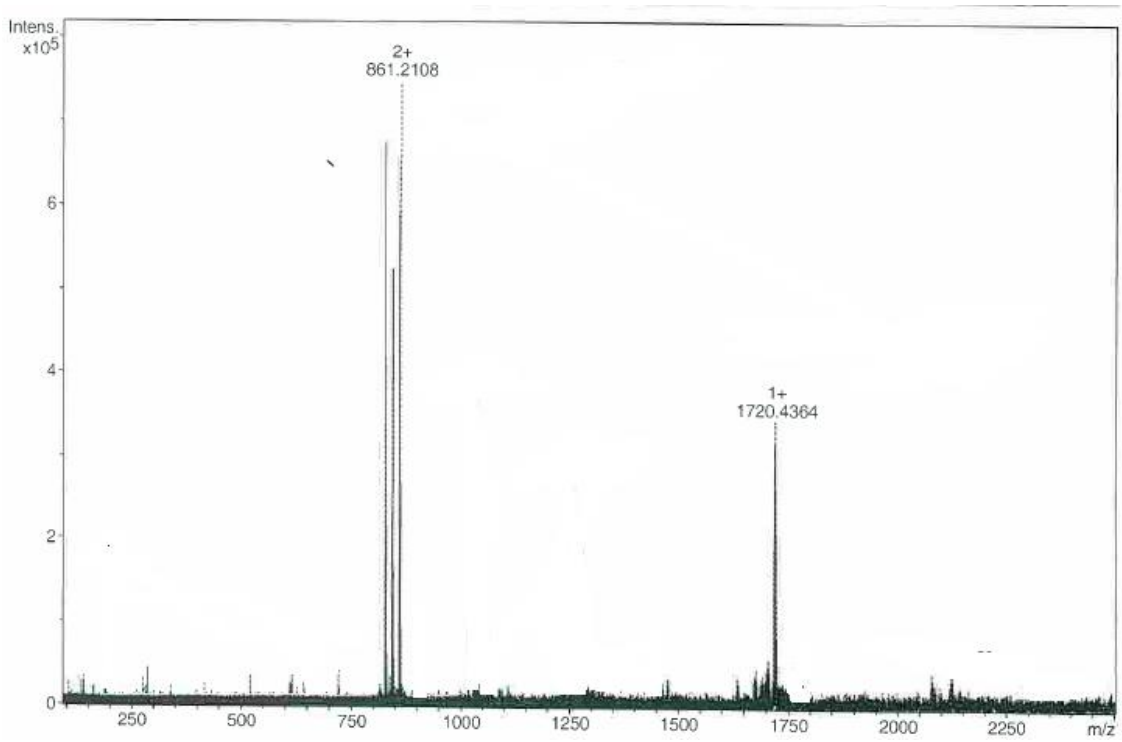

Figure S9.22. ESI-MS of **28ZnY-NO$_3$.** 861.11 m/z peak corresponds to a $[Zn^{II}_2Y^{III}_2(\mathbf{L28})_4(NO_3)]^{2+}$ fragment; 1720.21 m/z peak corresponds to a $[Zn^{II}_2Y^{III}_2(\mathbf{L28})_4(NO_3)]^{+}$.

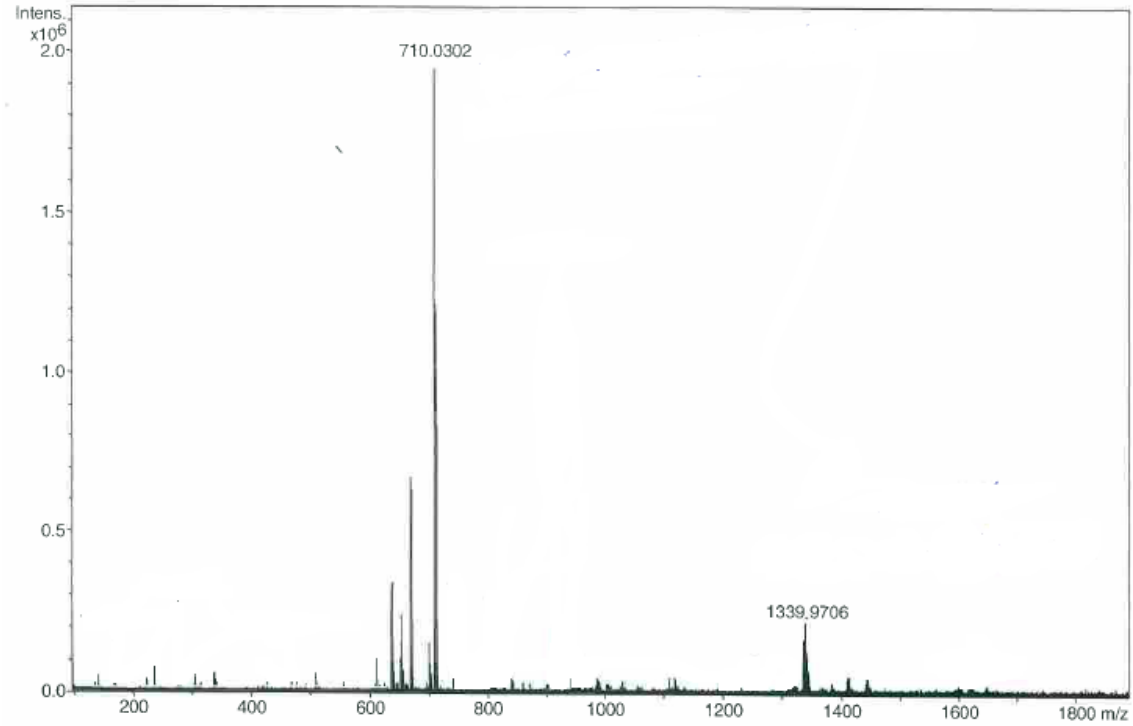

Figure S9.23. ESI-MS of **24ZnY-NO$_3$.** 710.97 m/z peak corresponds to a $[Zn^{II}_2Y^{III}_2(\mathbf{L24})_4(NO_3)_2(H_2O)]$ fragment ;1336.94 m/z peak corresponds to a $[Zn^{II}_2Y^{III}_2(\mathbf{L24})_4(NO3)]^{+}$ fragment.

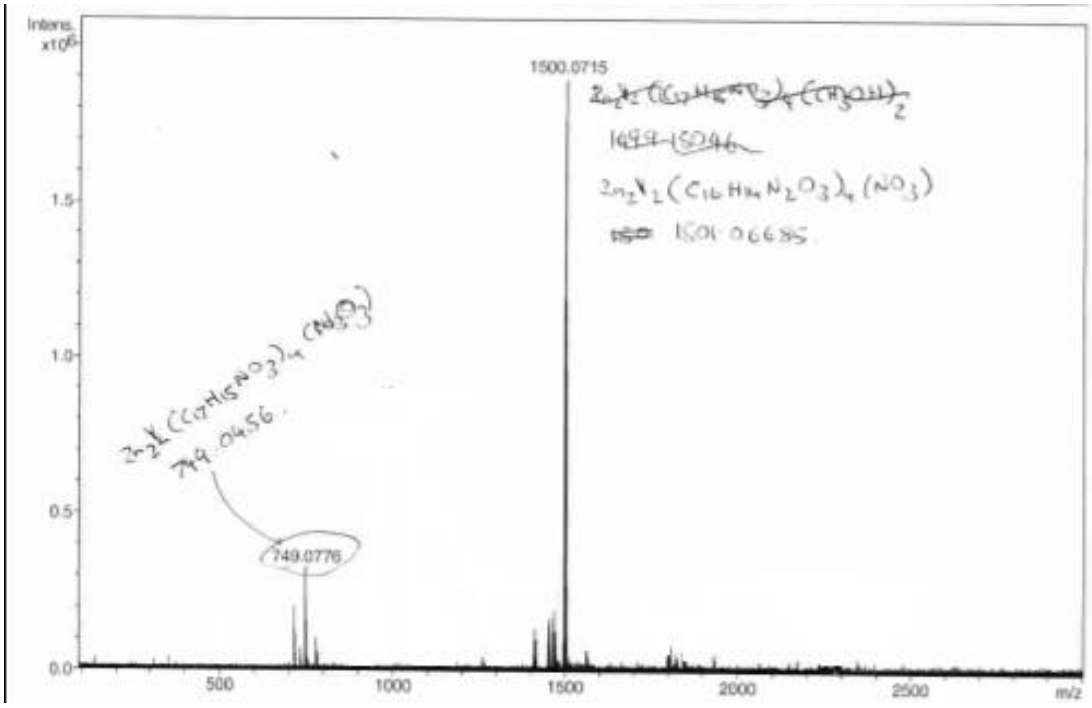

Figure S9.24. ESI-MS of **25ZnY-NO$_3$**

9.7 TGA of LMLn-NO_3

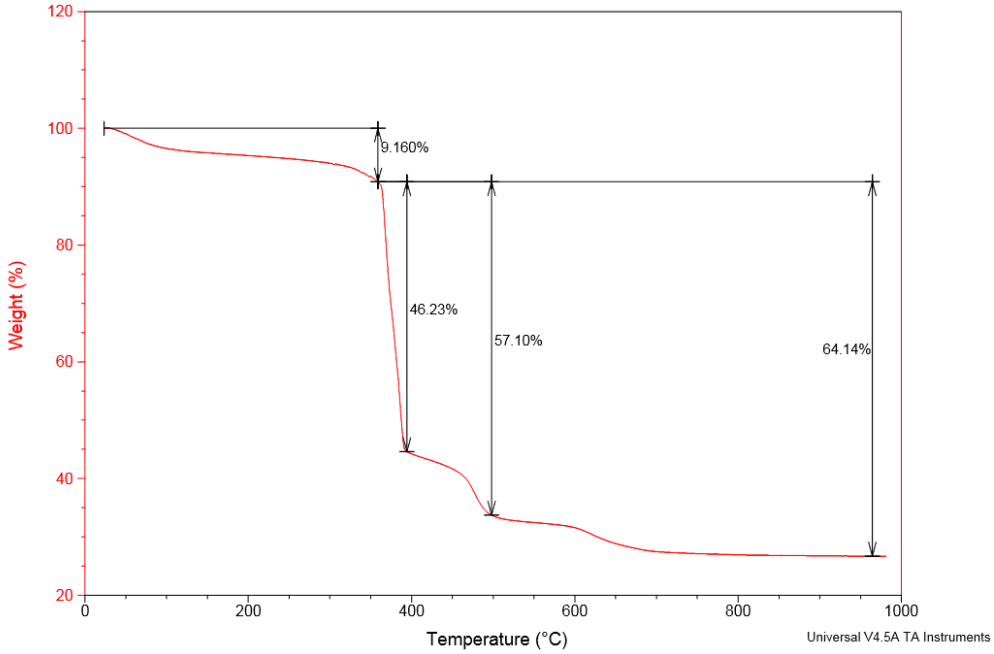

Figure S9.25. TGA of **6ZnY-NO_3**

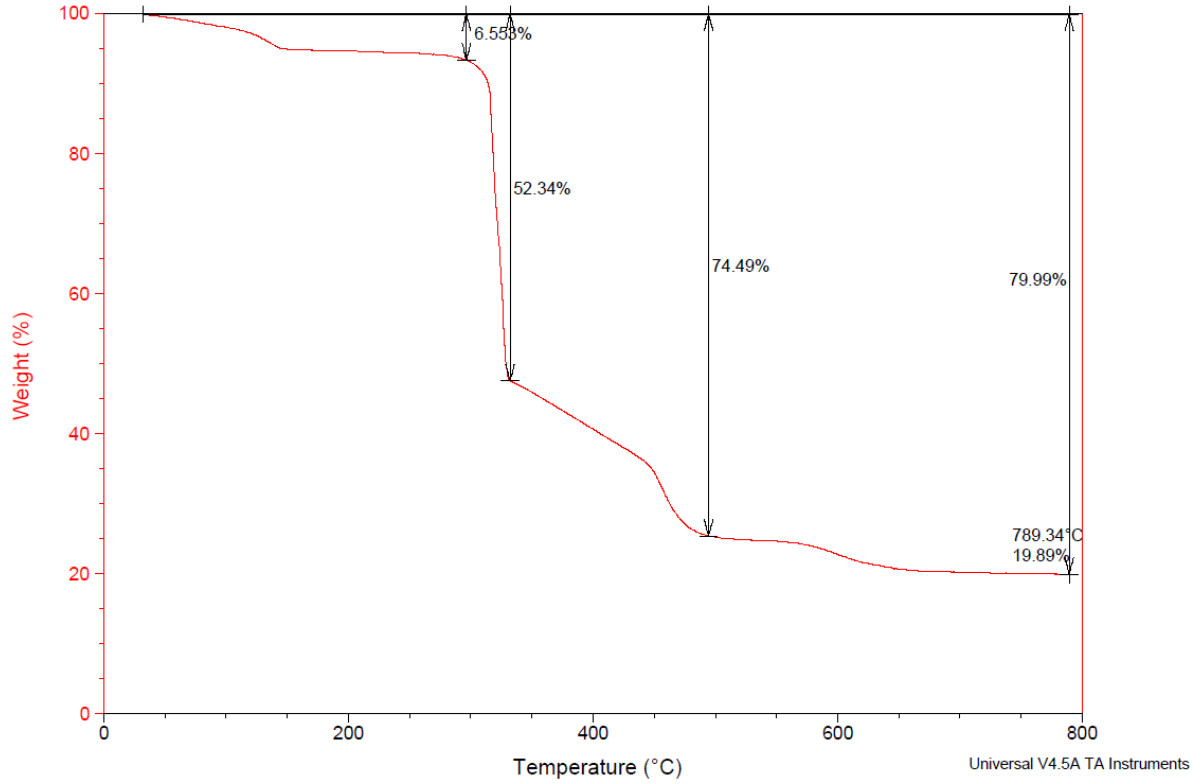

Figure S9.26. TGA of **5ZnY-NO_3**

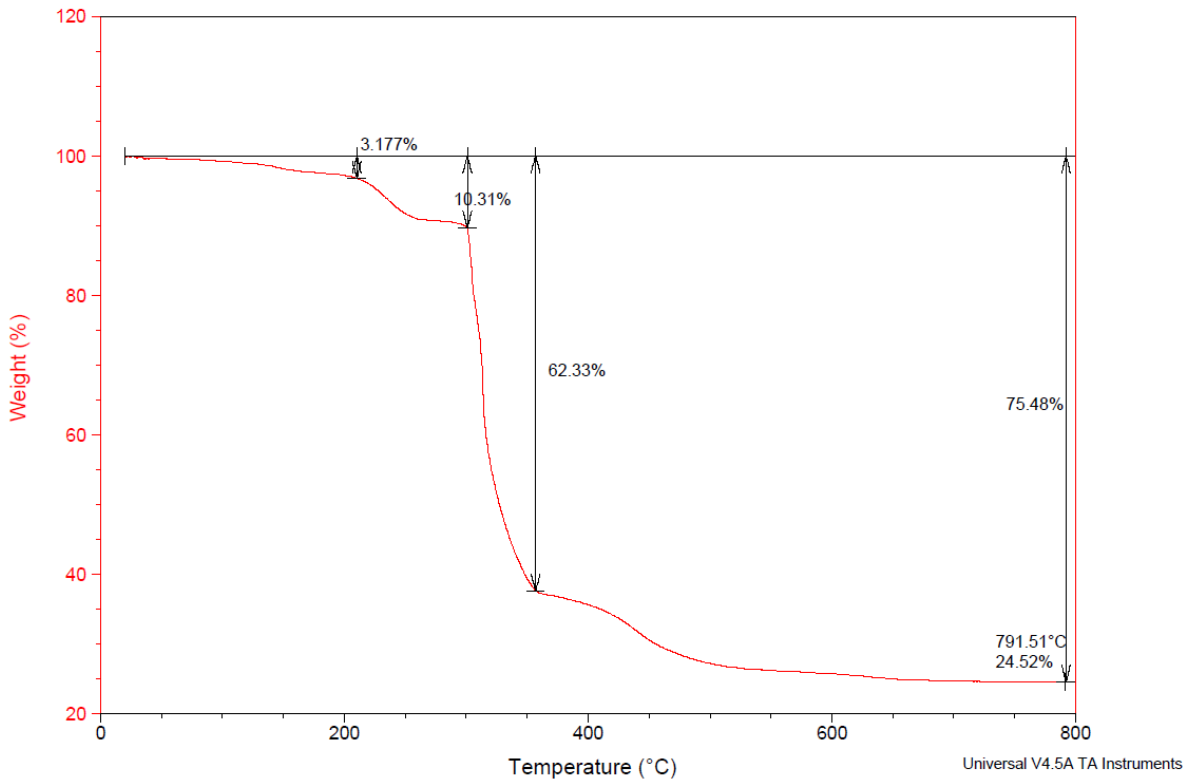

Figure S9.27. TGA of **8ZnY-NO$_3$**

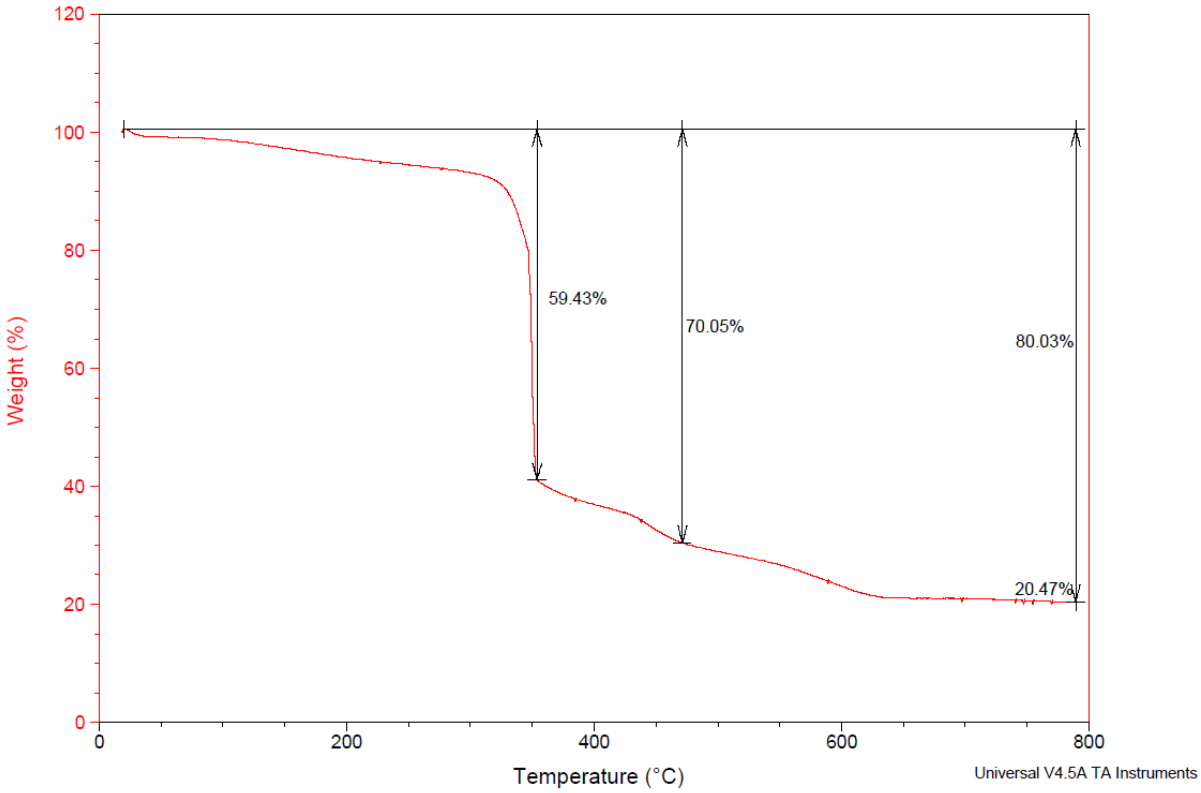

Figure S9.28. TGA of **9ZnY-NO$_3$**

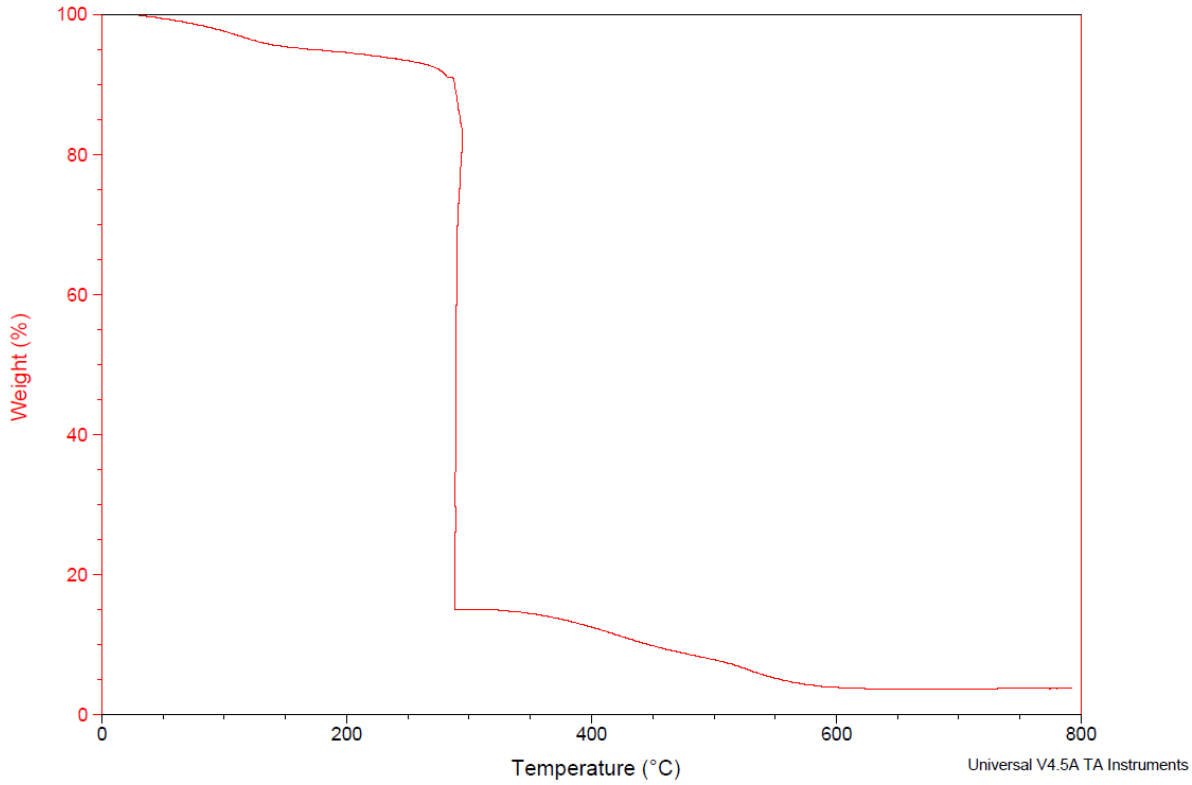

Figure S9.29. TGA of **11ZnY-NO$_3$**

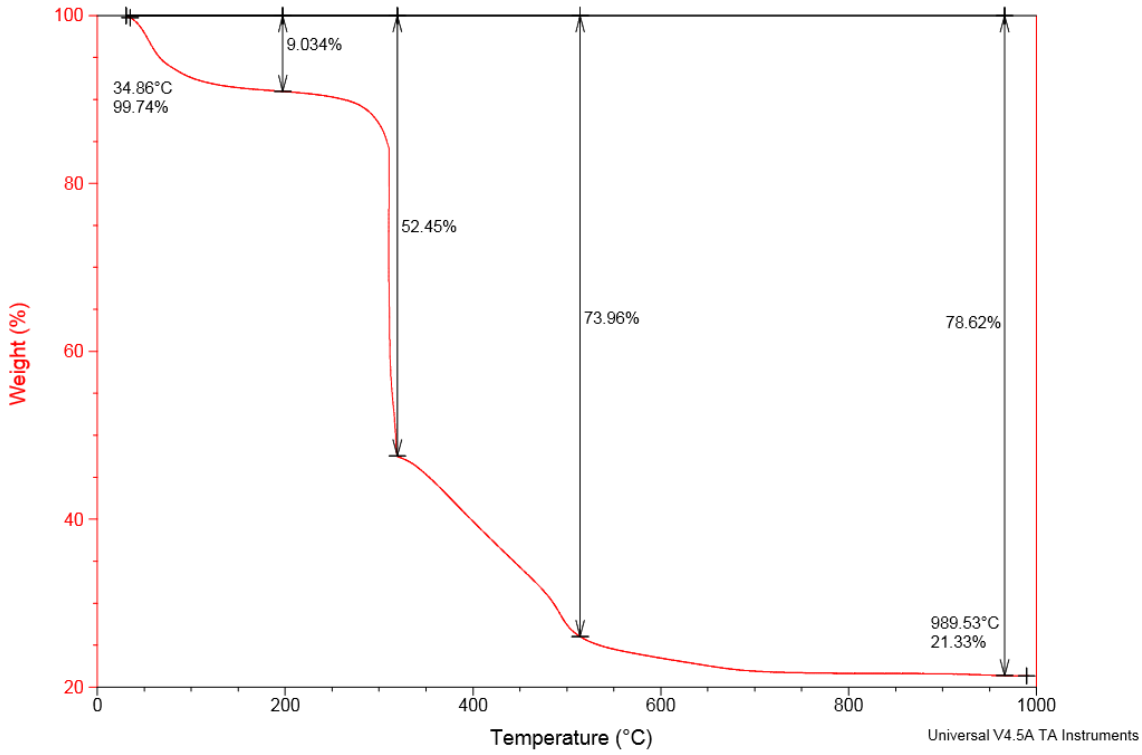

Figure S9.30. TGA of **12ZnY-NO$_3$**

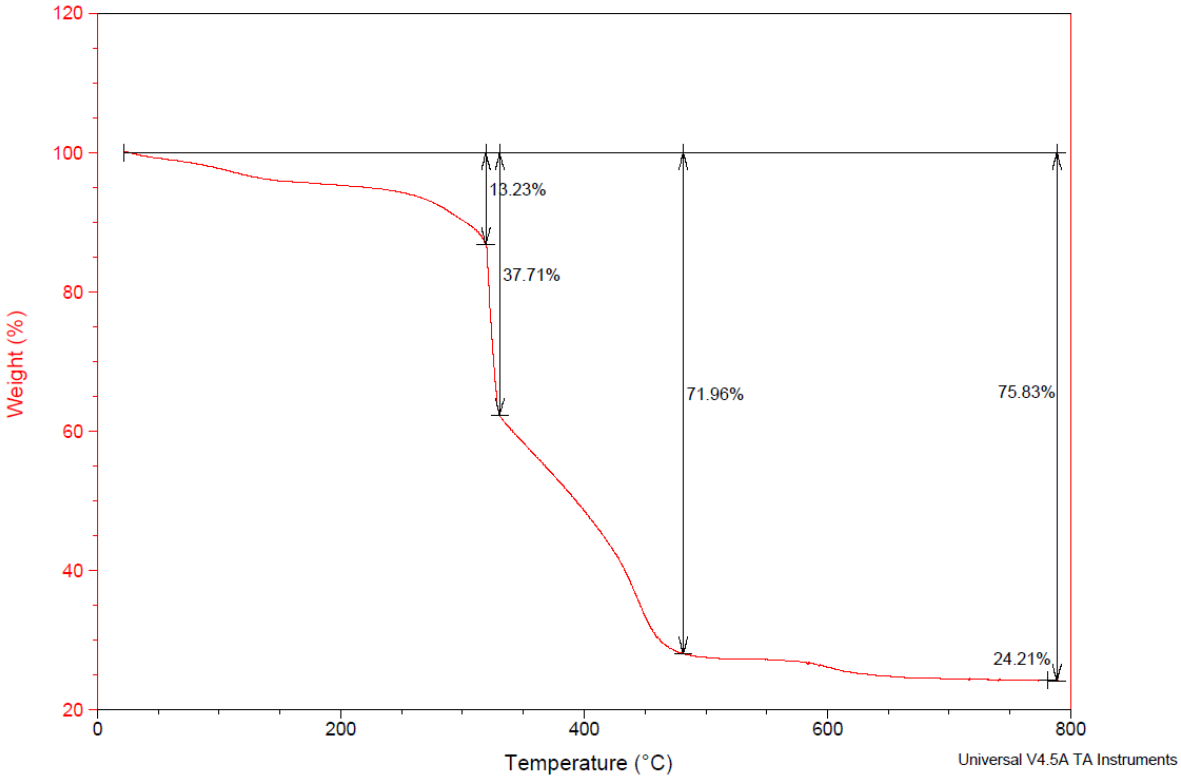

Figure S9.31. TGA of **13ZnY-NO$_3$**

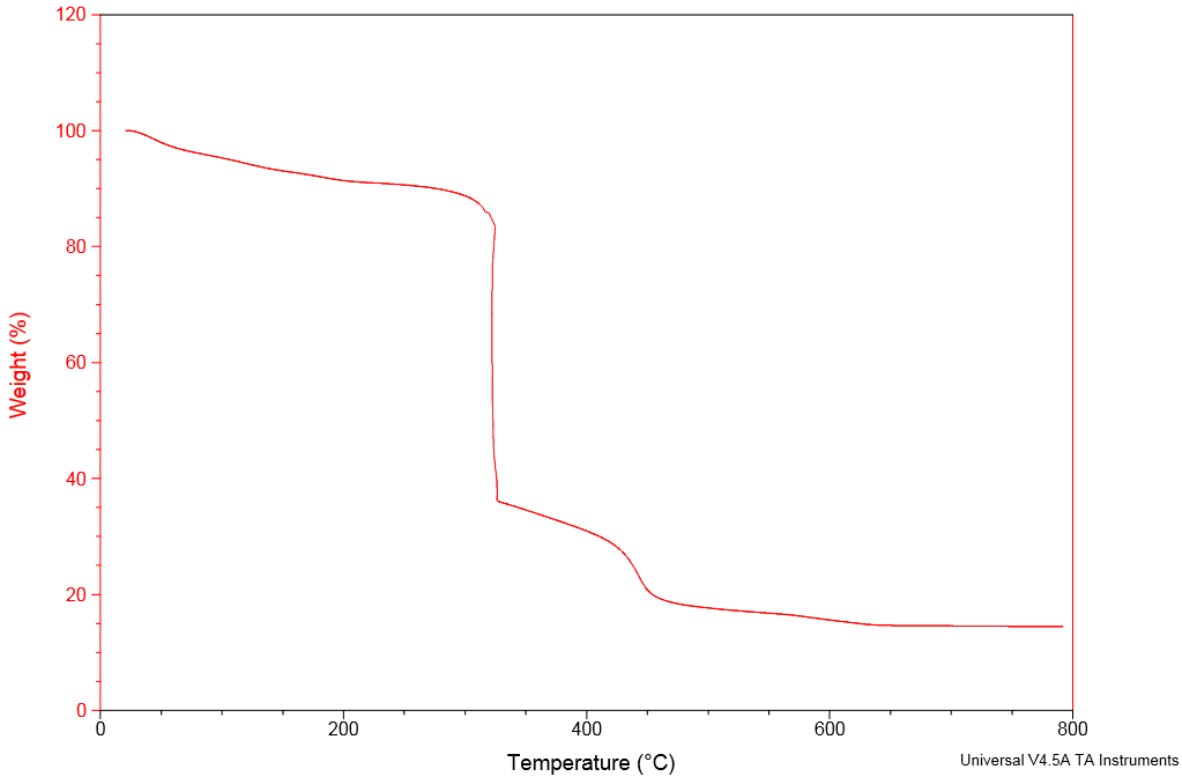

Figure S9.32. TGA of **15ZnY-NO$_3$**

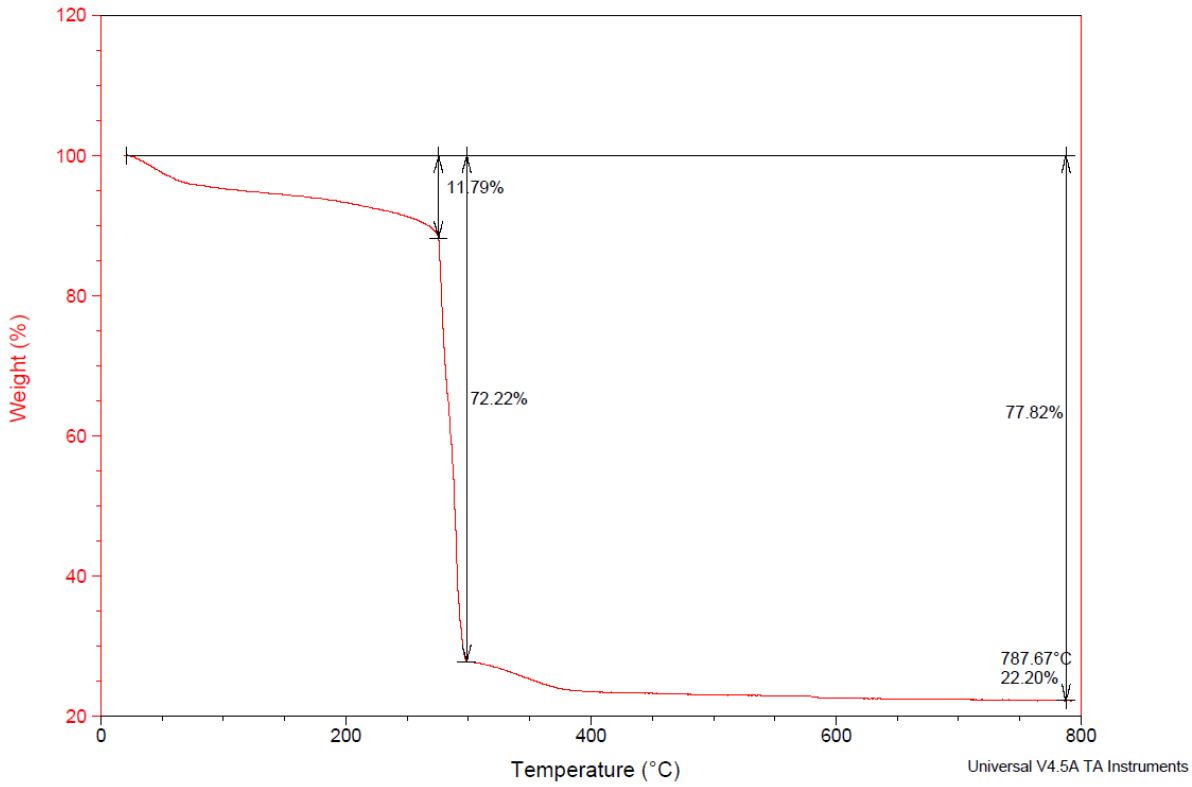

Figure S9.33. TGA of **2ZnY-NO$_3$**

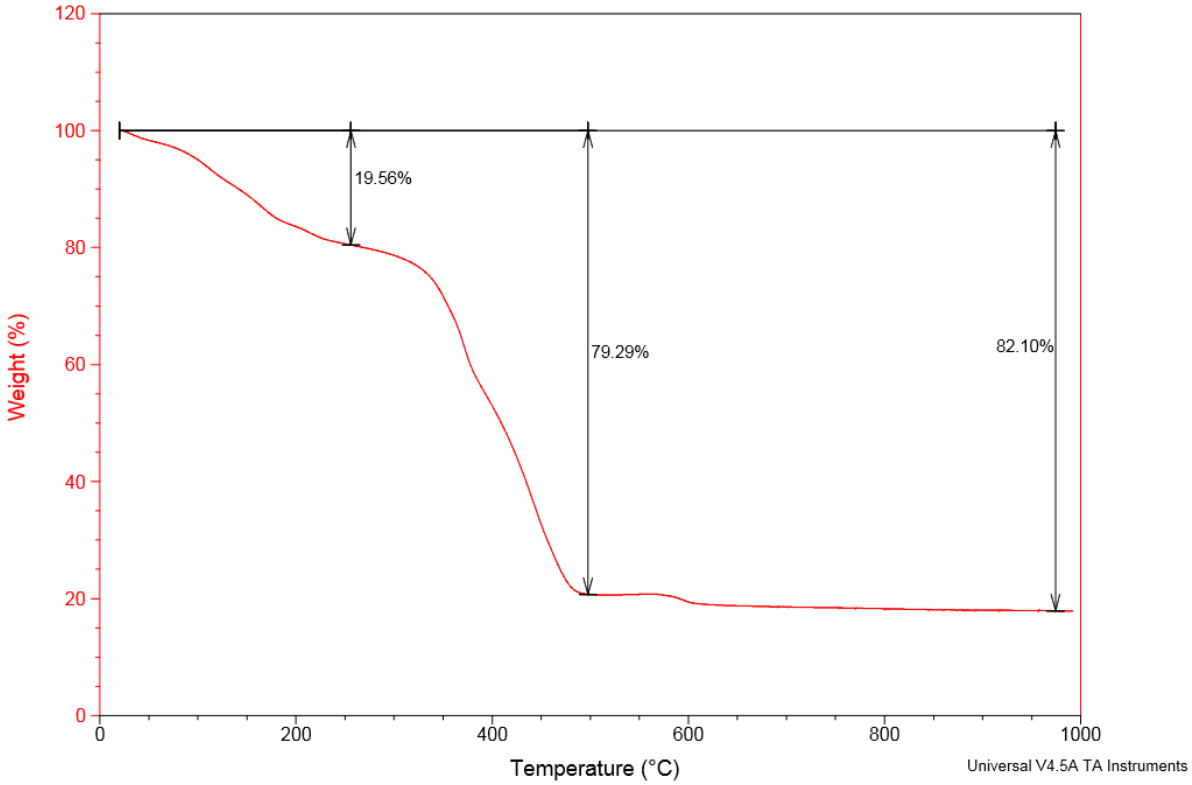

Figure S9.34. TGA of **16ZnY-NO$_3$**

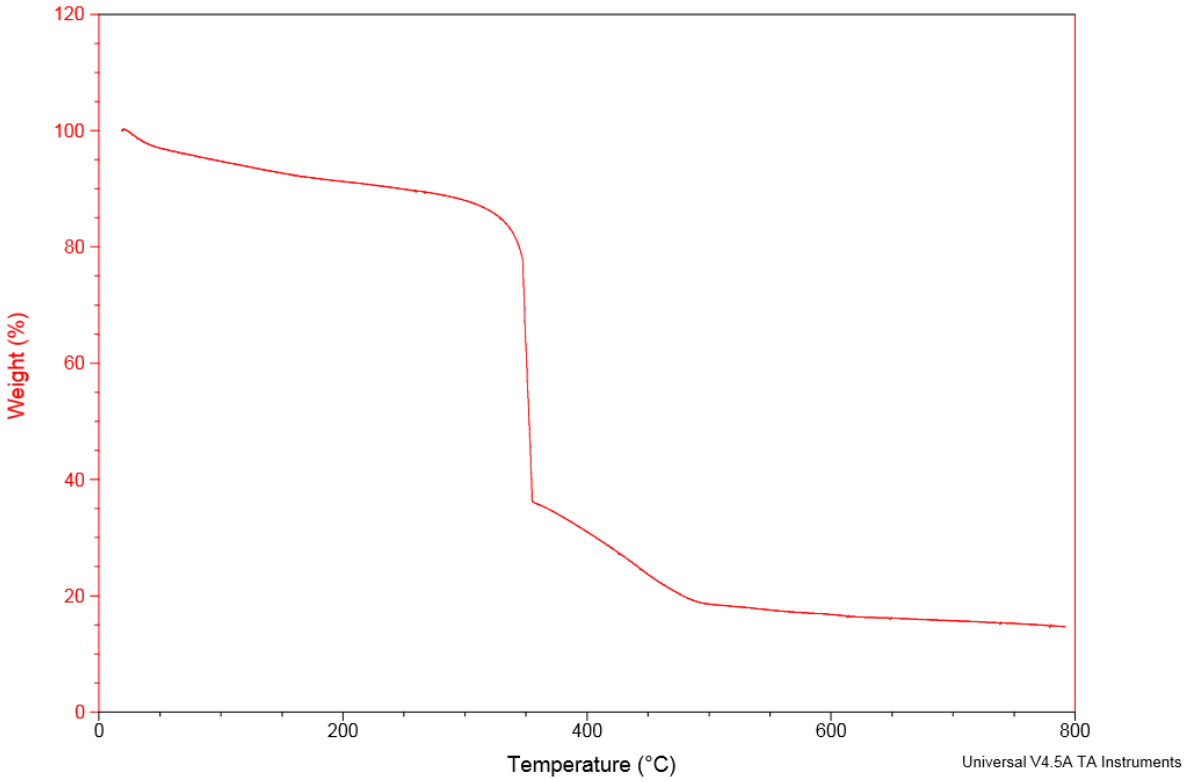

Figure S9.35. TGA of **18ZnY-NO$_3$**

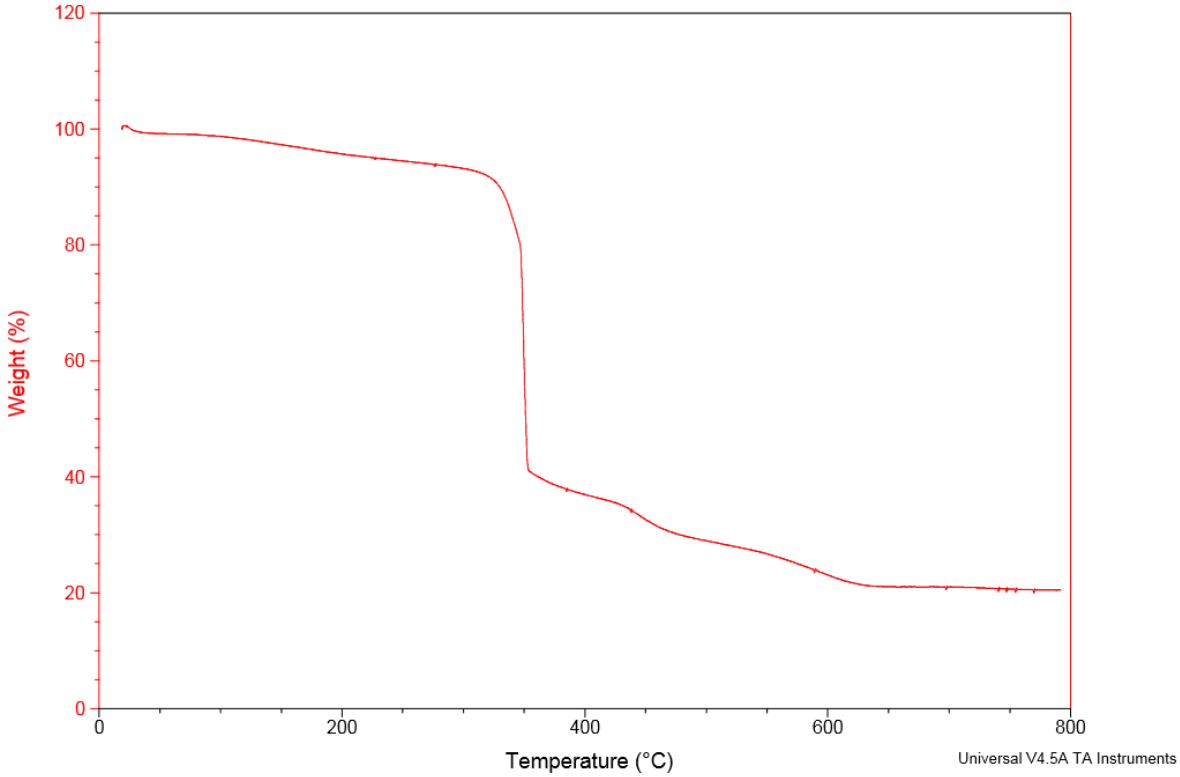

Figure S9.36. TGA of **19ZnY-NO$_3$**

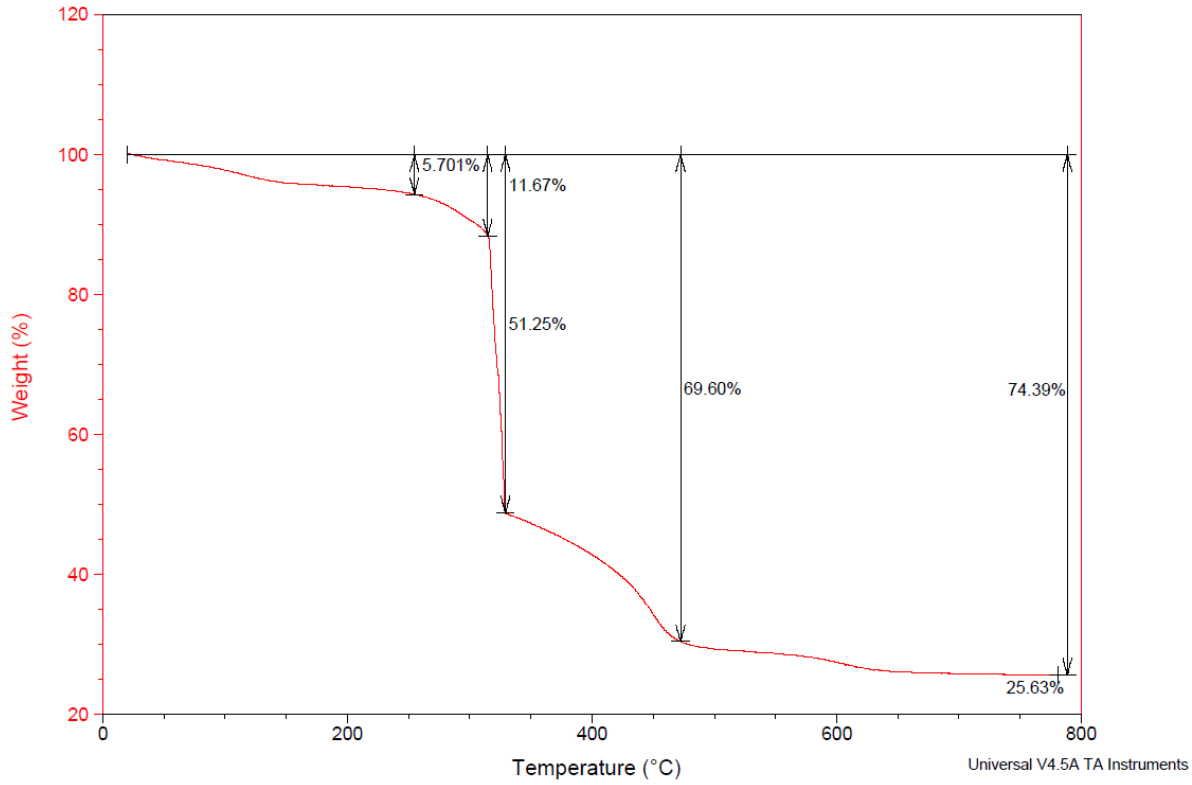

Figure S9.37. TGA of **20ZnY-NO$_3$**

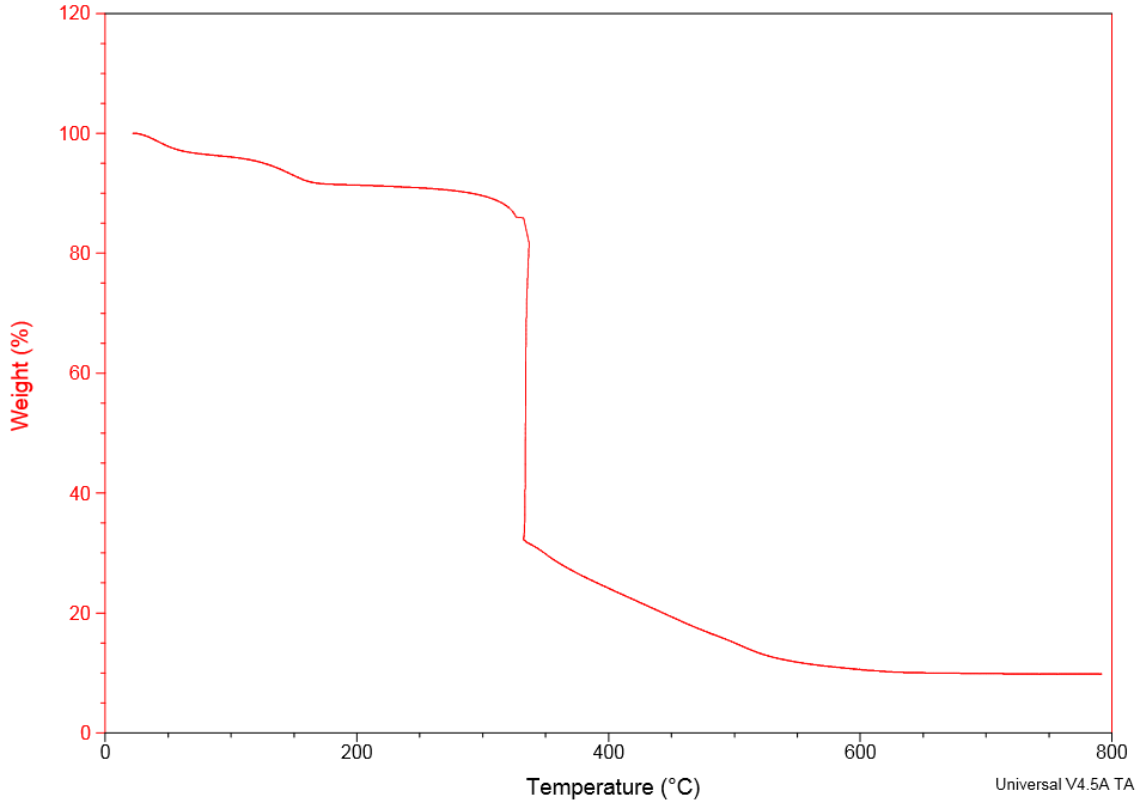

Figure S9.38. TGA of **22ZnY-NO$_3$**

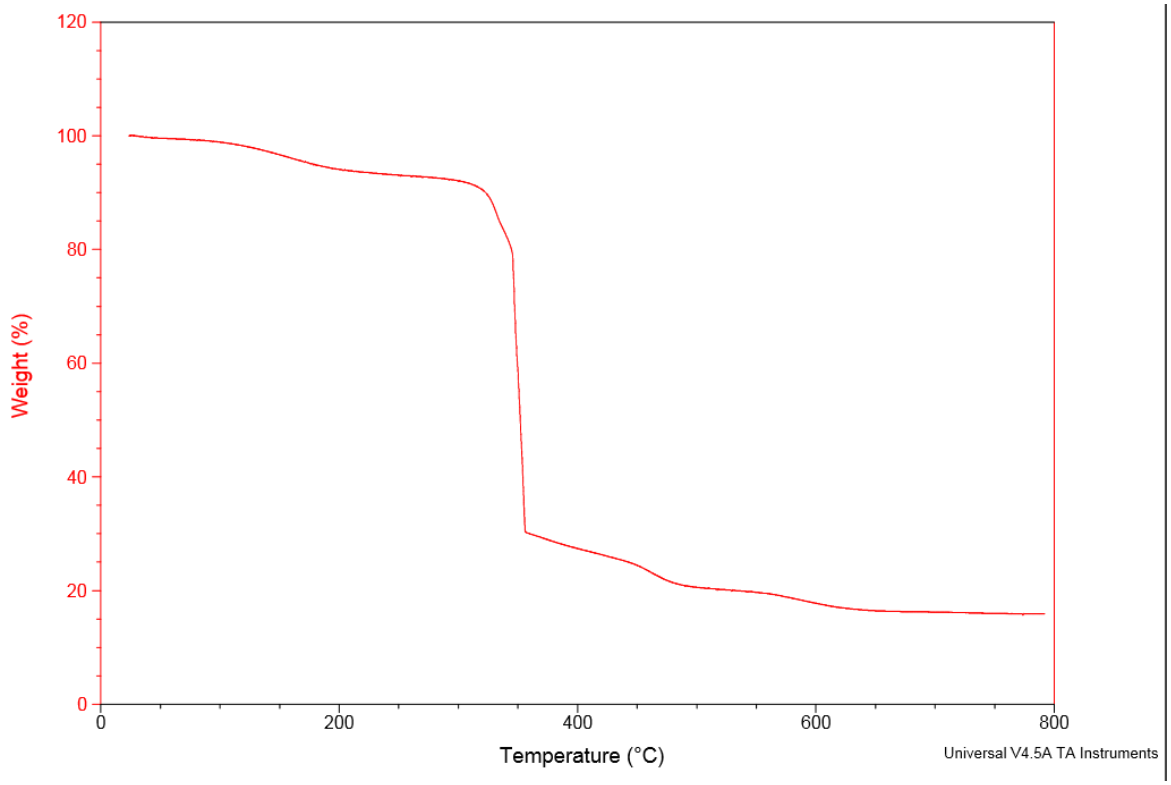

Figure S9.39. TGA of **27ZnY-NO$_3$**

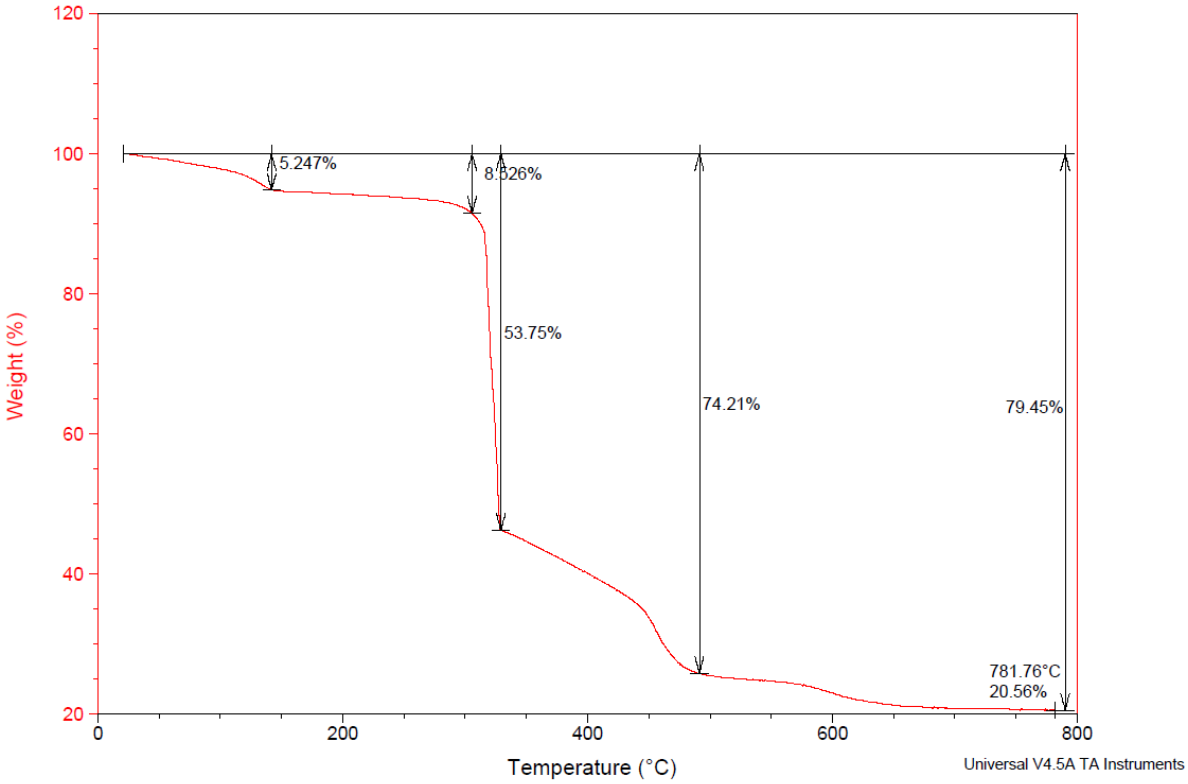

Figure S9.40. TGA of **28ZnY-NO$_3$**

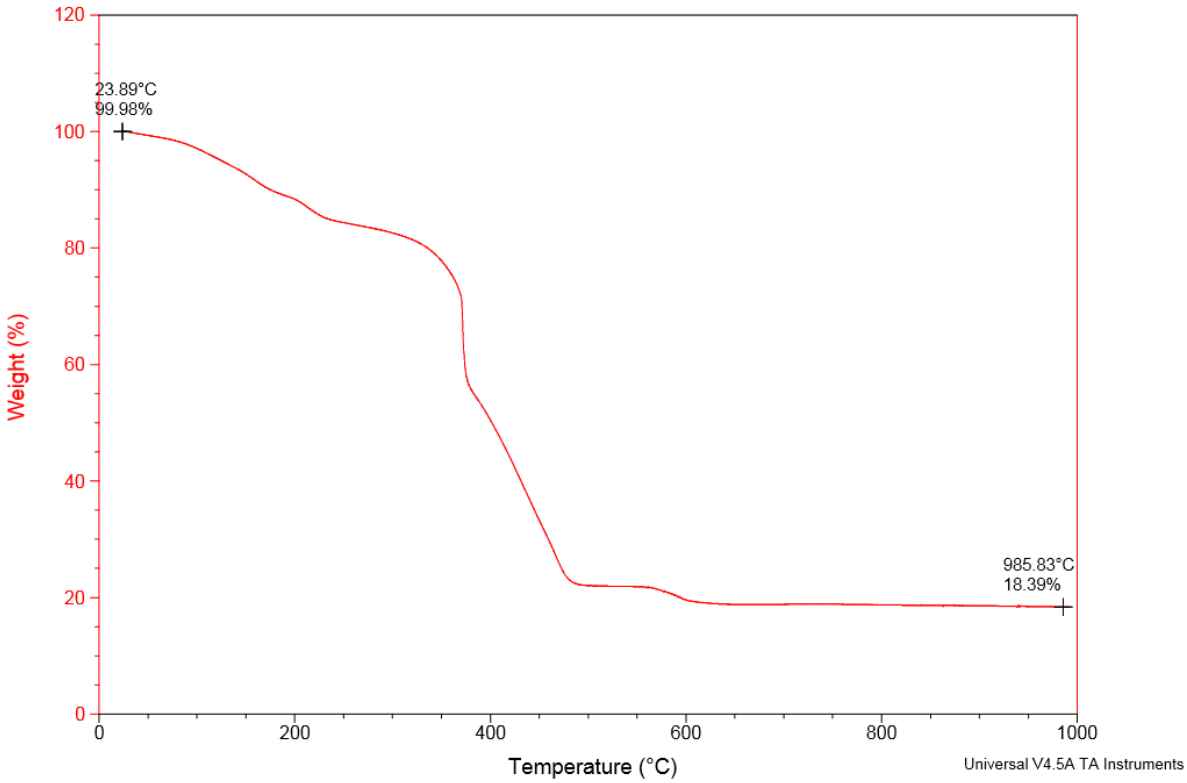

Figure S9.41. TGA of **29ZnY-NO$_3$**

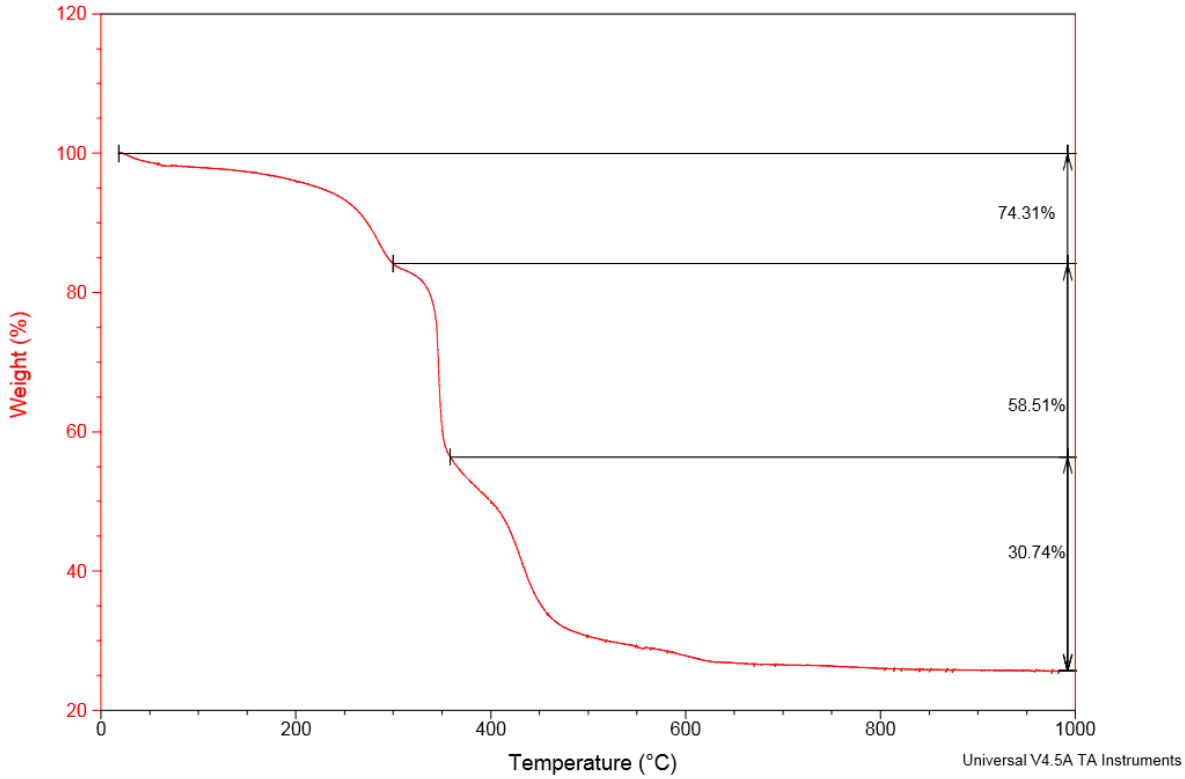

Figure S9.42. TGA of **24ZnY-NO$_3$**

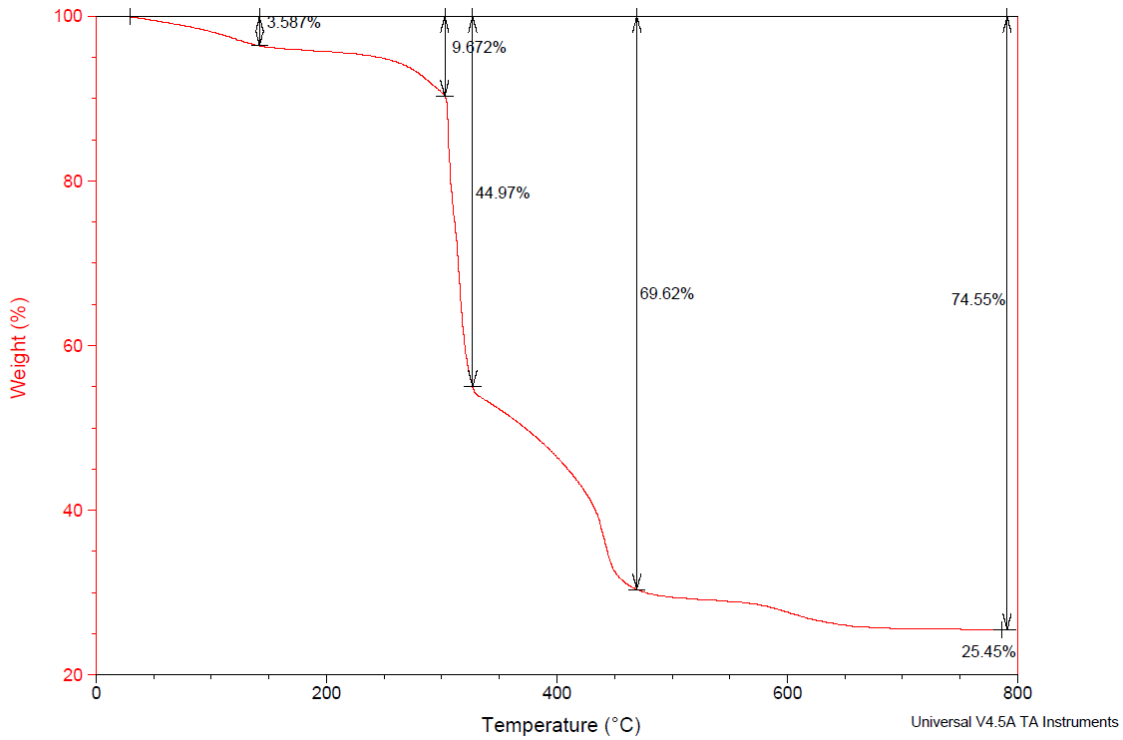

Figure S9.43. TGA of **25ZnY-NO$_3$**

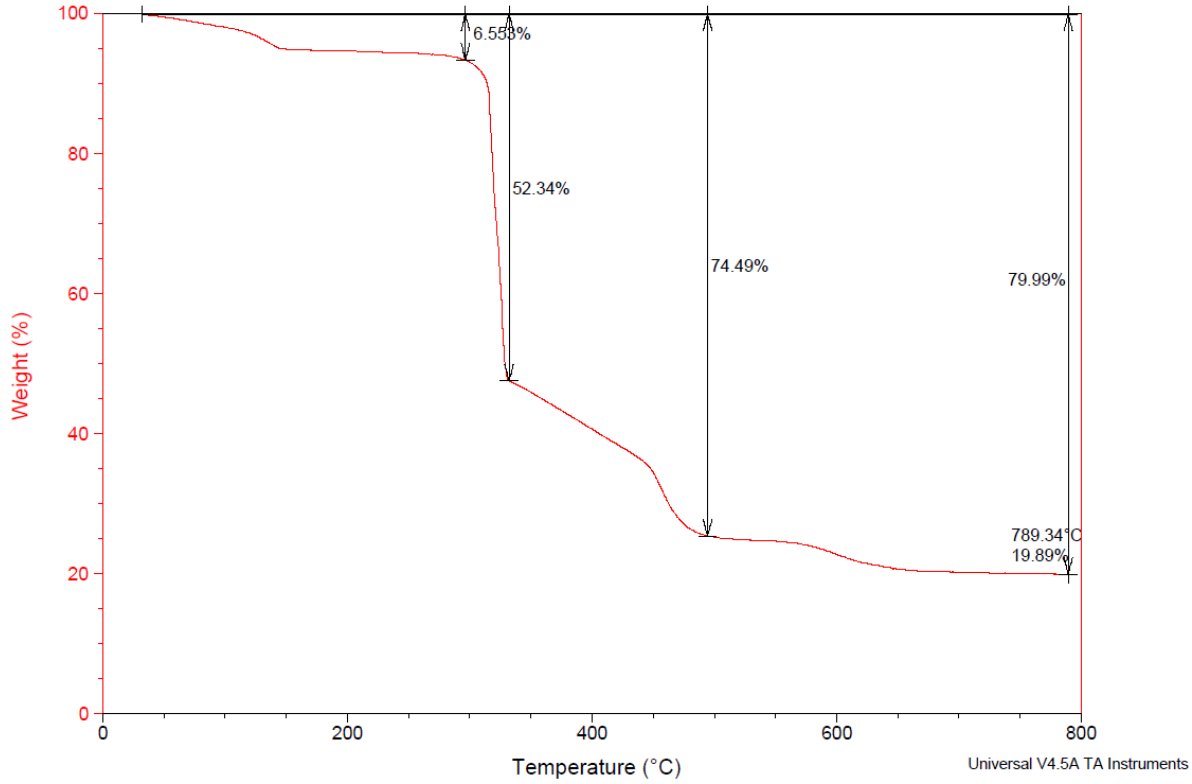

Figure S9.44. TGA of **26ZnY-NO$_3$**

9.8 FT-IR of LMLn-NO_3

Figure S9.45. FT-IR of **6ZnY-NO_3**

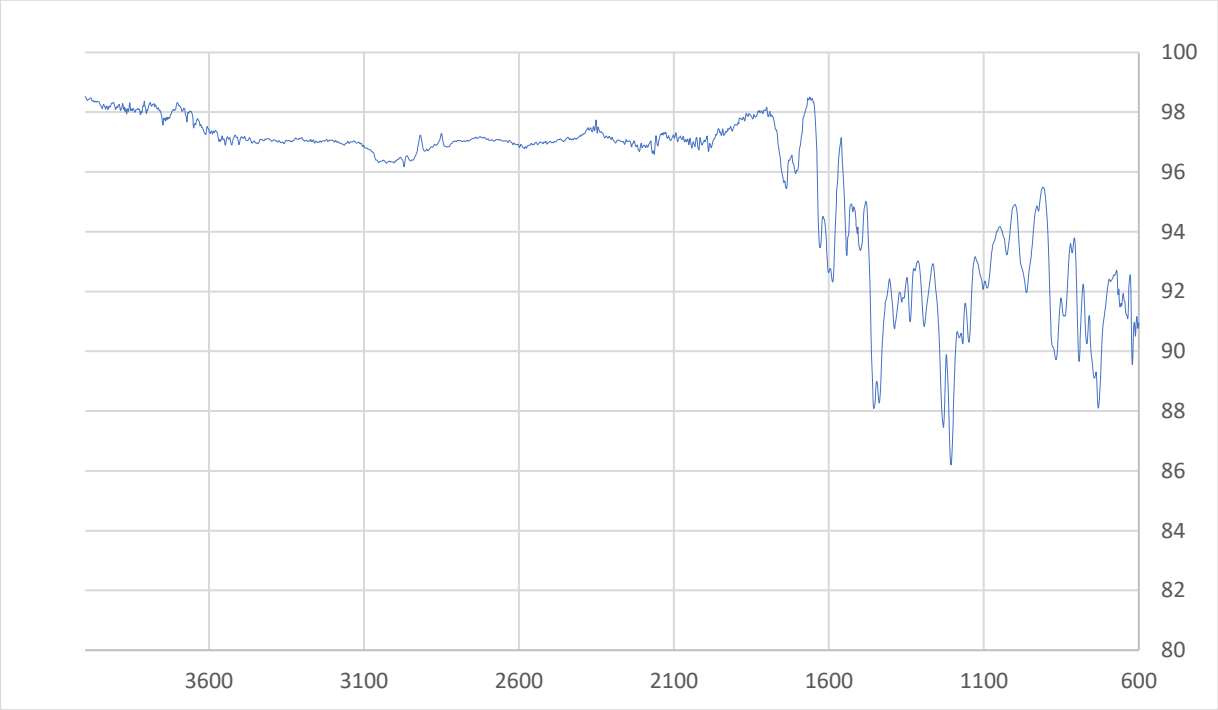

Figure S9.46. FT-IR of **5ZnY-NO_3**

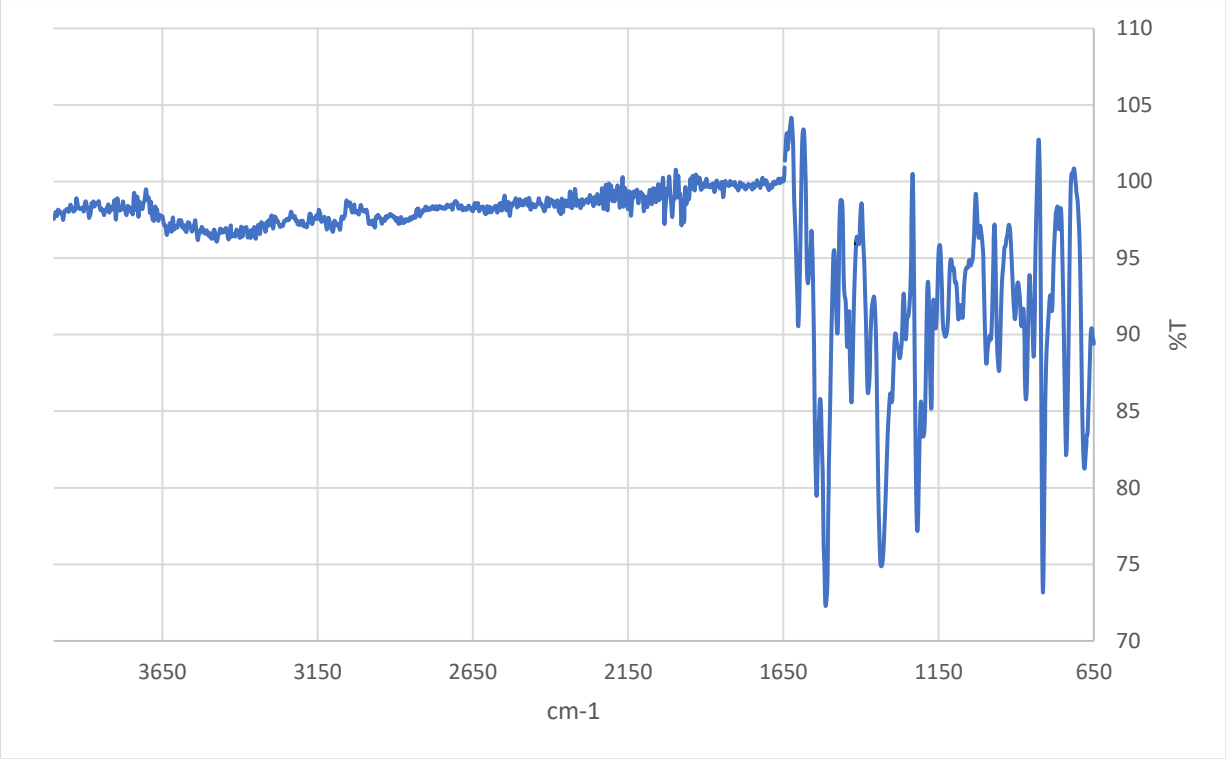

Figure S9.47. FT-IR of **8ZnY-NO$_3$**

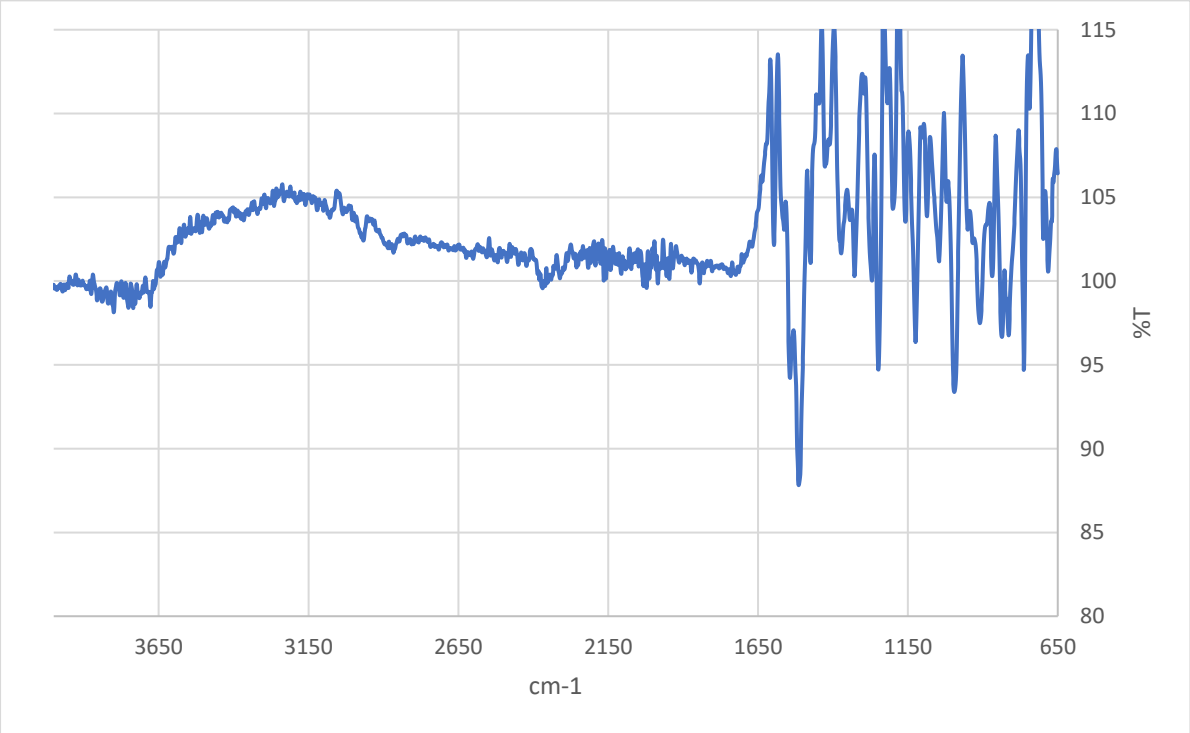

Figure S9.48. FT-IR of **9ZnY-NO$_3$**

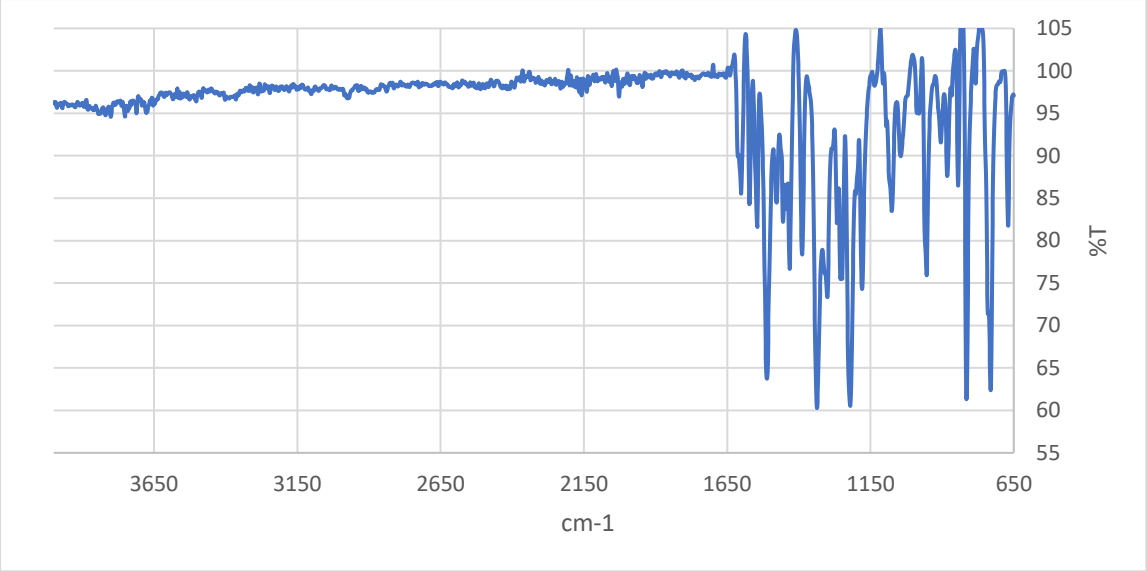

Figure S9.49. FT-IR of **11ZnY-NO$_3$**

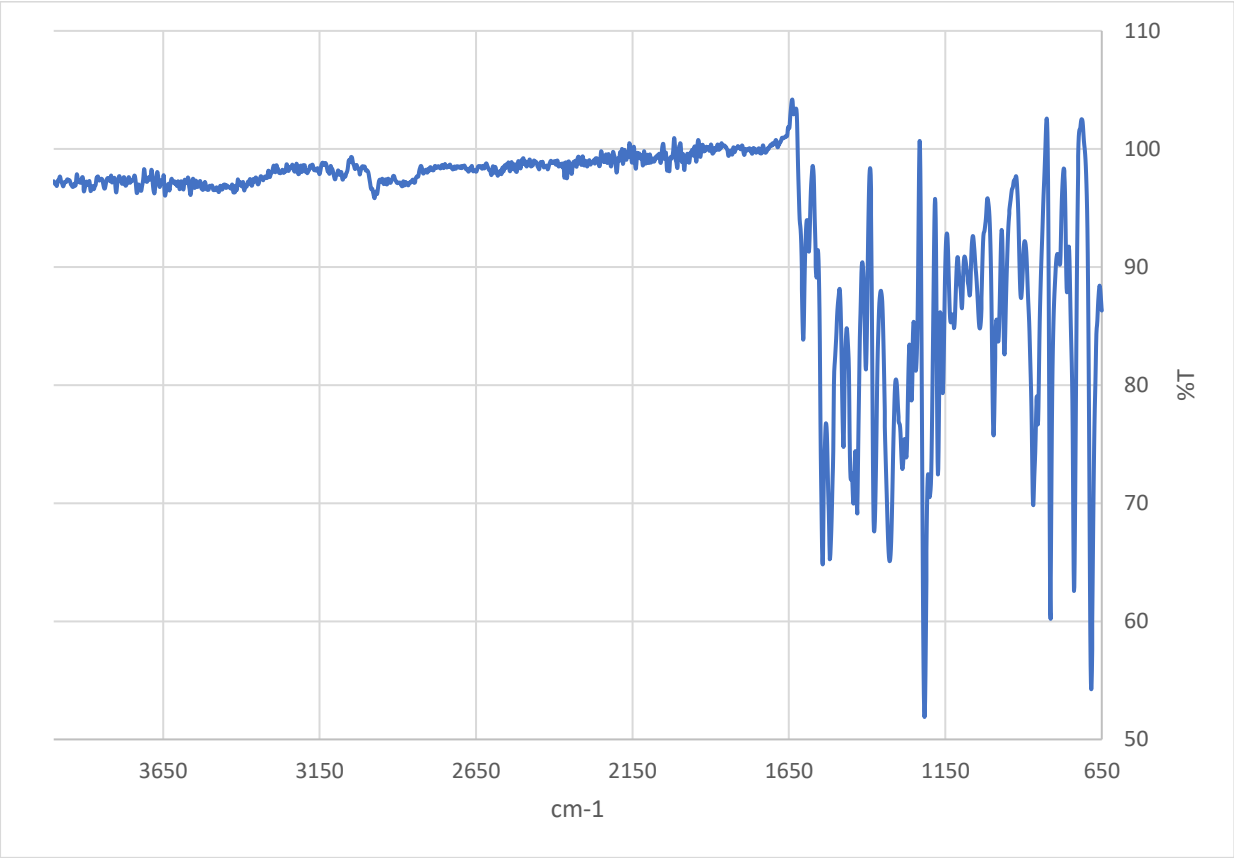

Figure S9.50. FT-IR of **12ZnY-NO$_3$**

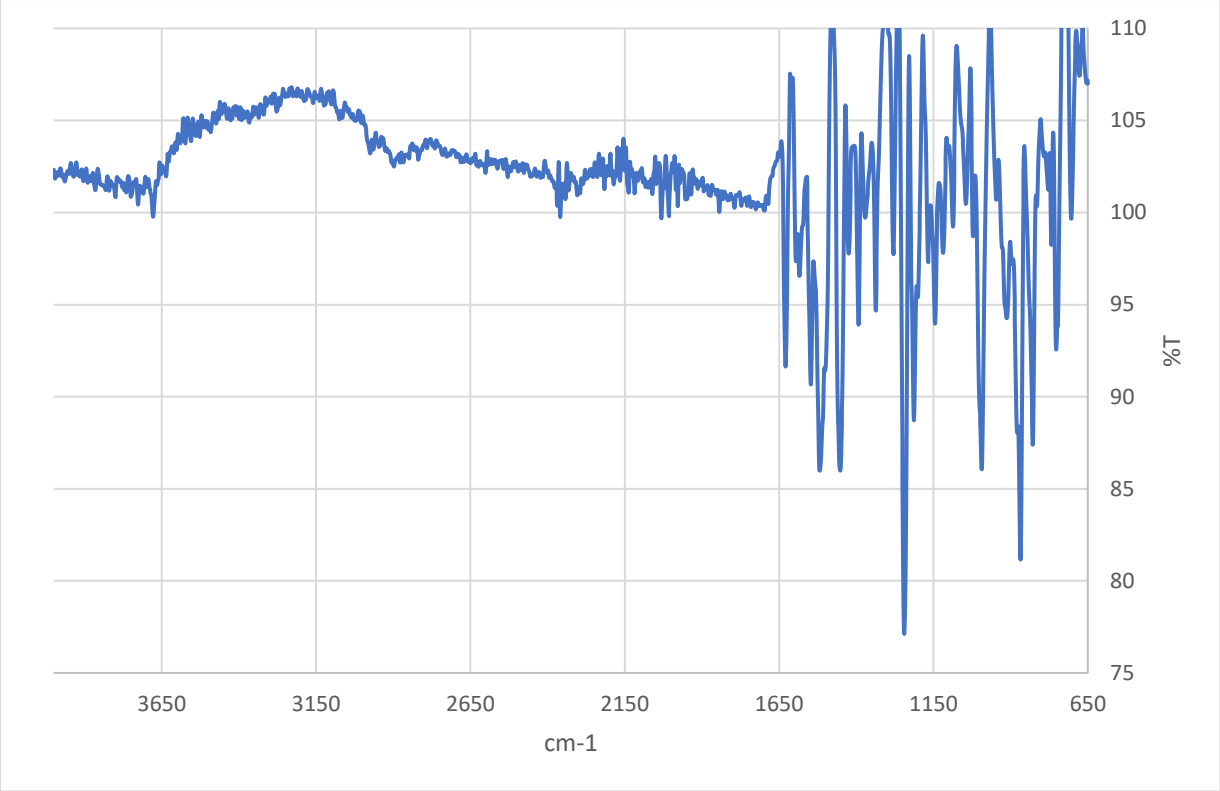

Figure S9.51. FT-IR of **13ZnY-NO$_3$**

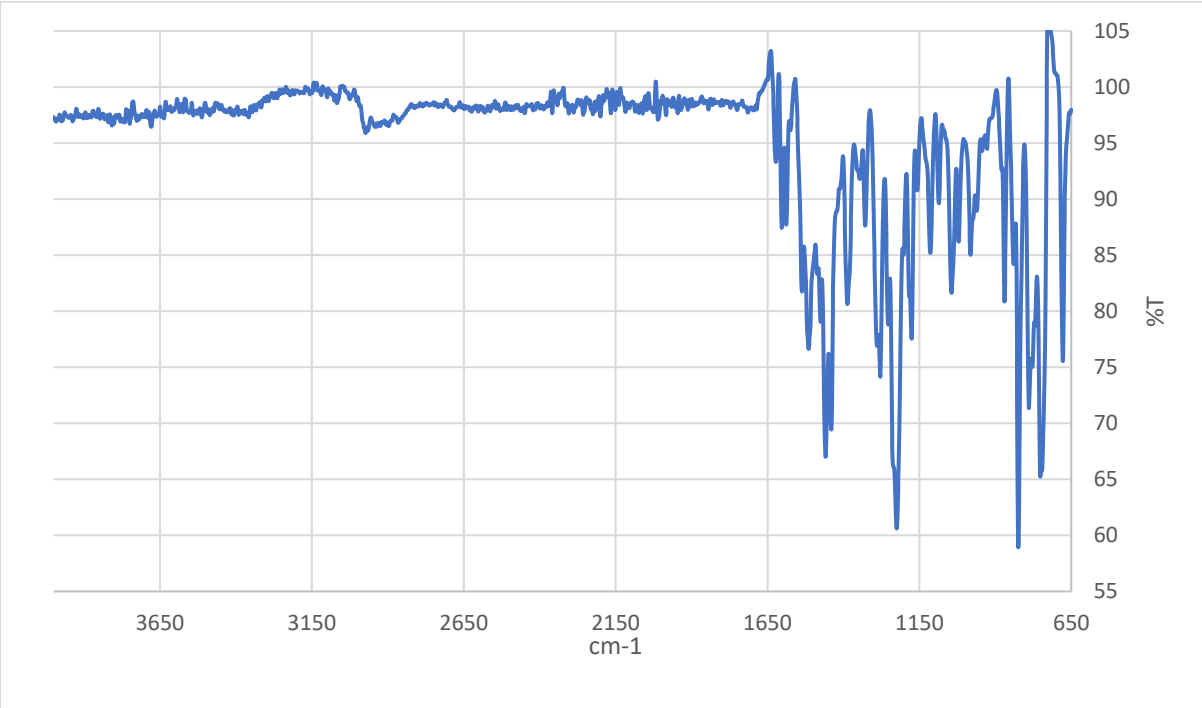

Figure S9.52 FT-IR of **15ZnY-NO$_3$**

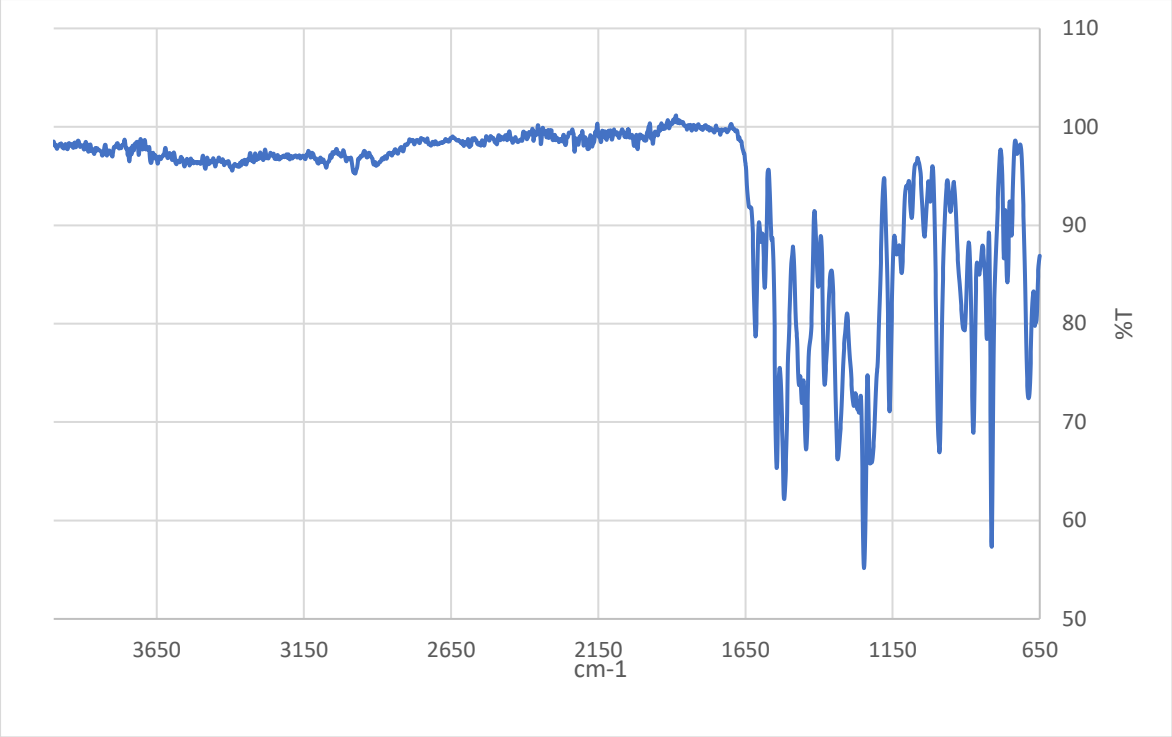

Figure S9.53. FT-IR of **2ZnY-NO$_3$**

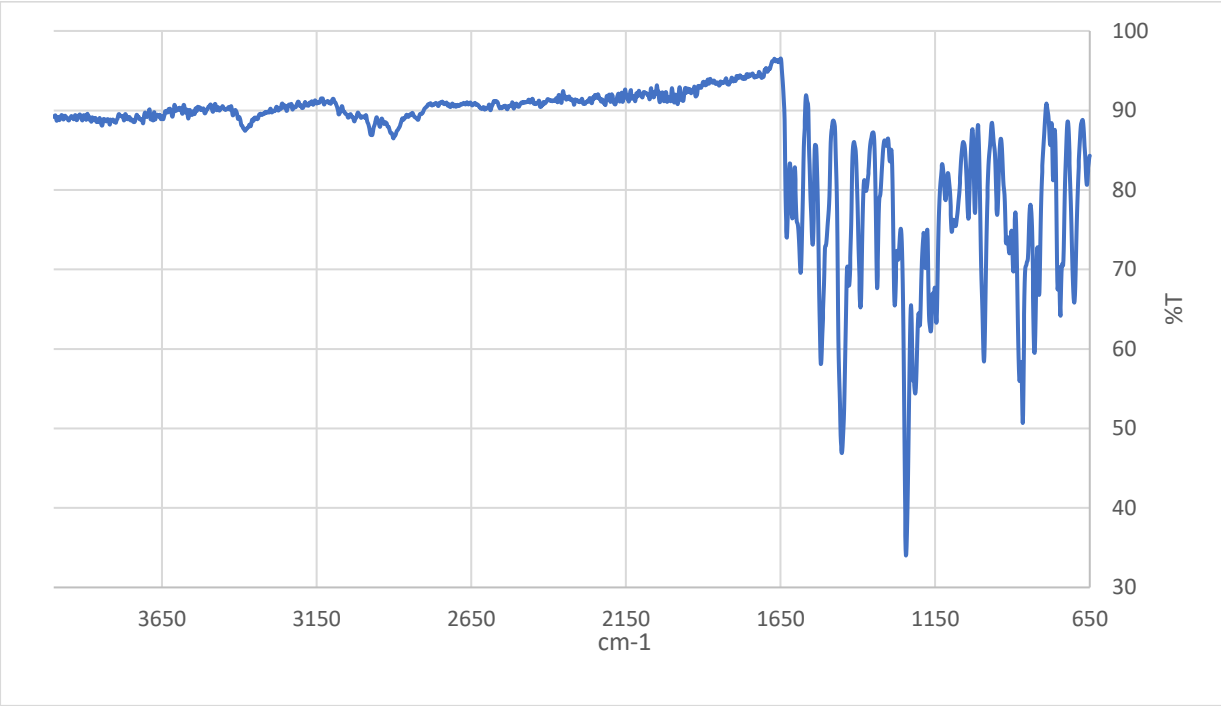

Figure S9.54. FT-IR of **16ZnY-NO$_3$**

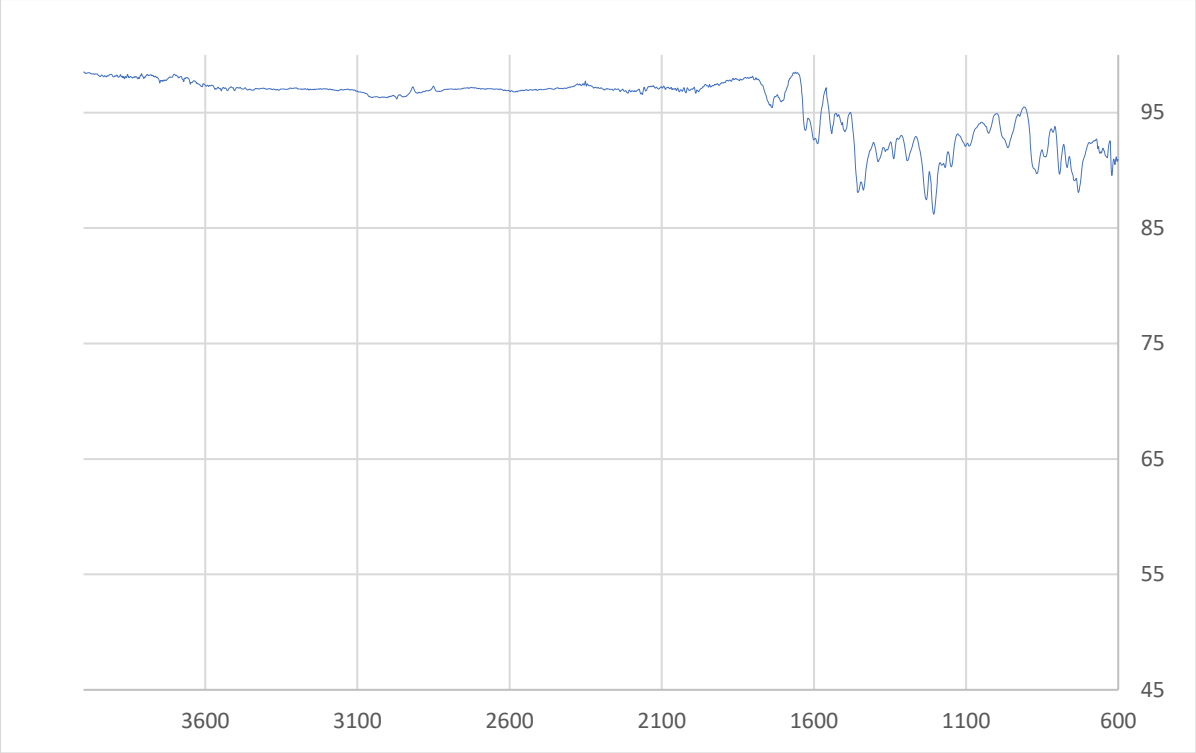

Figure S9.55. FT-IR of **18ZnY-NO$_3$**

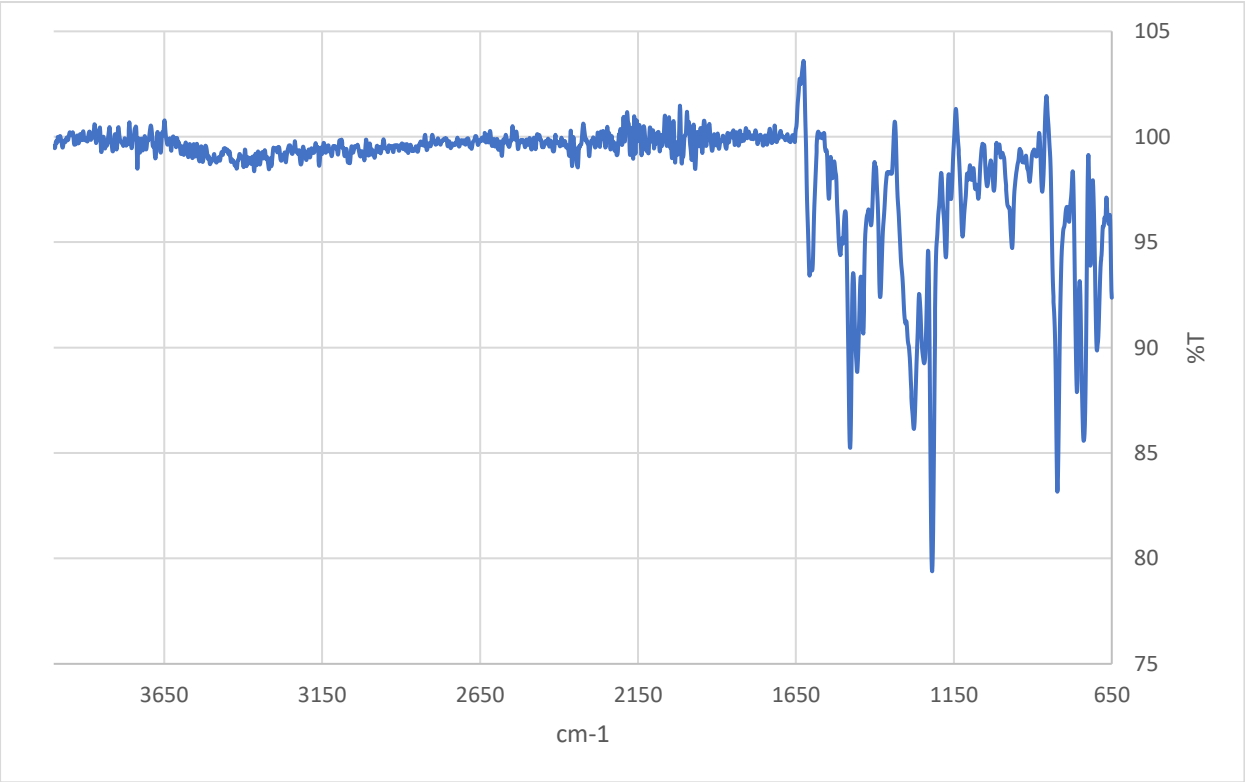

Figure S9.56. FT-IR of **19ZnY-NO$_3$**

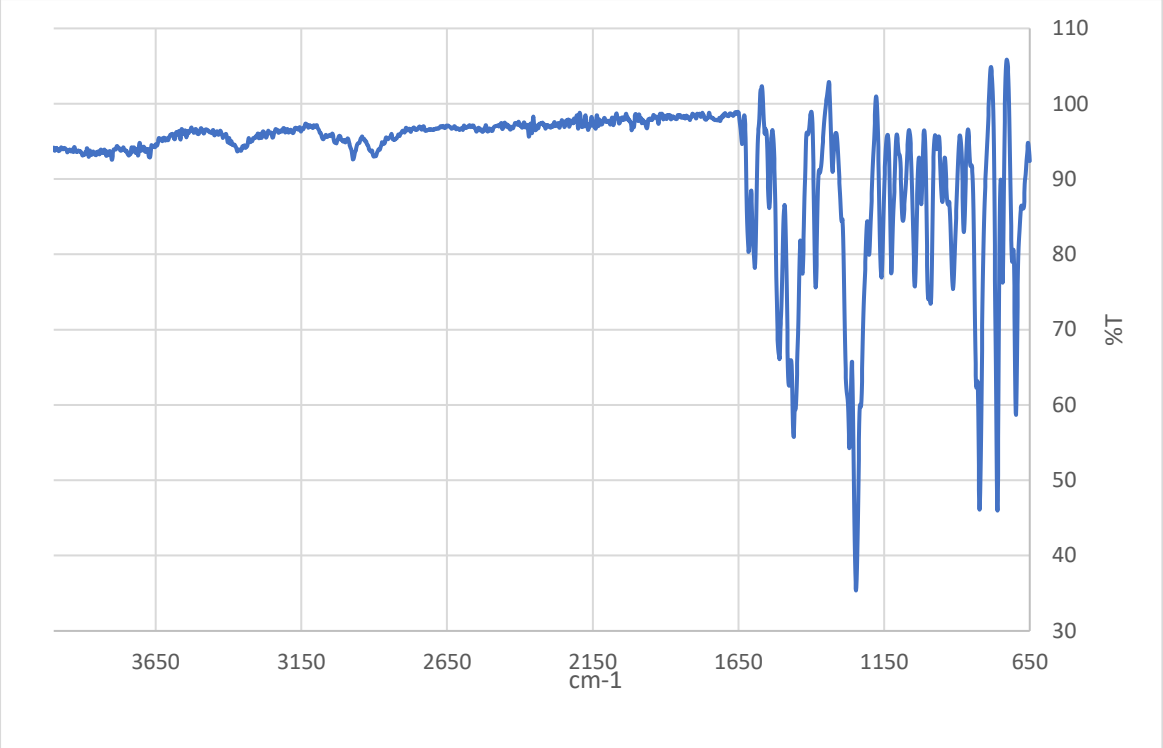

Figure S9.57. FT-IR of **20ZnY-NO$_3$**

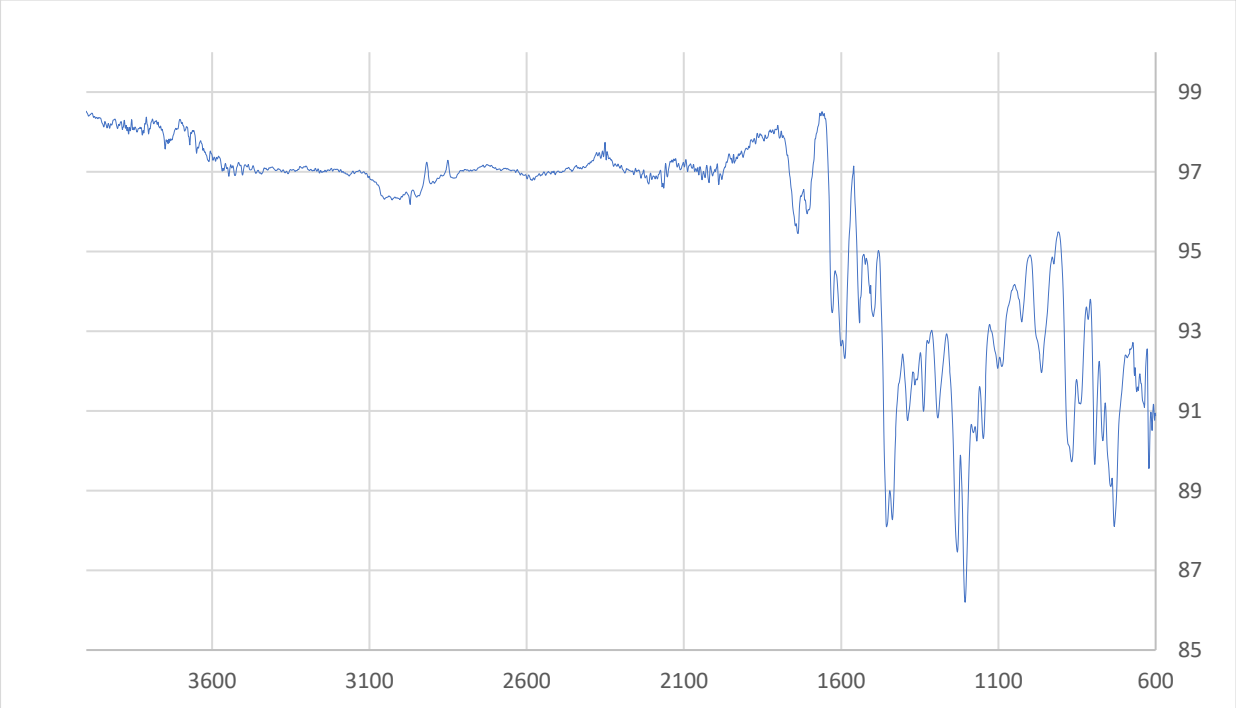

Figure S9.58. FT-IR of **22ZnY-NO$_3$**

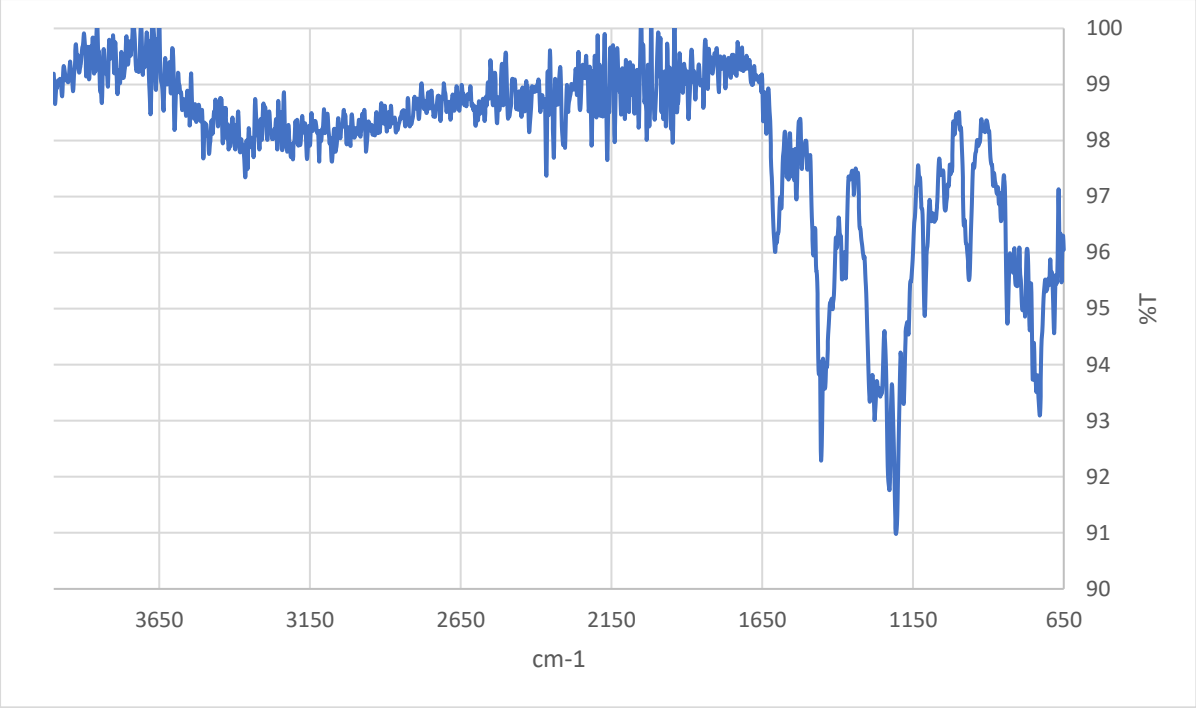

Figure S9.59. FT-IR of **27ZnY-NO$_3$**

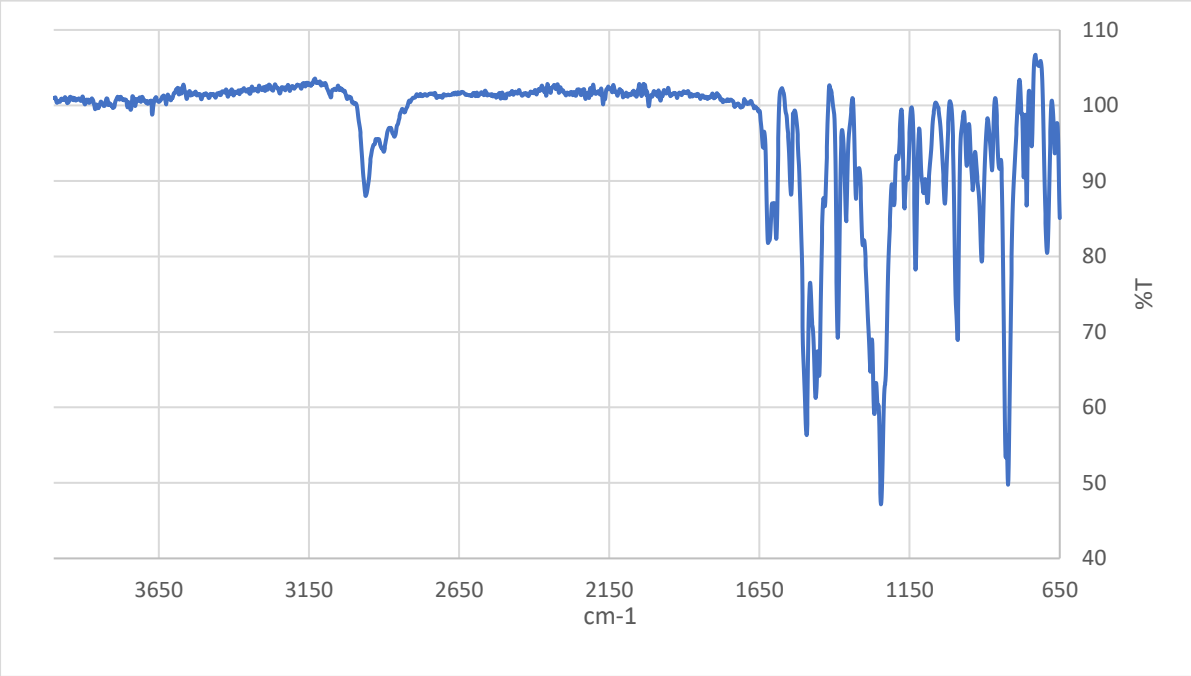

Figure S9.60. FT-IR of **28ZnY-NO$_3$**

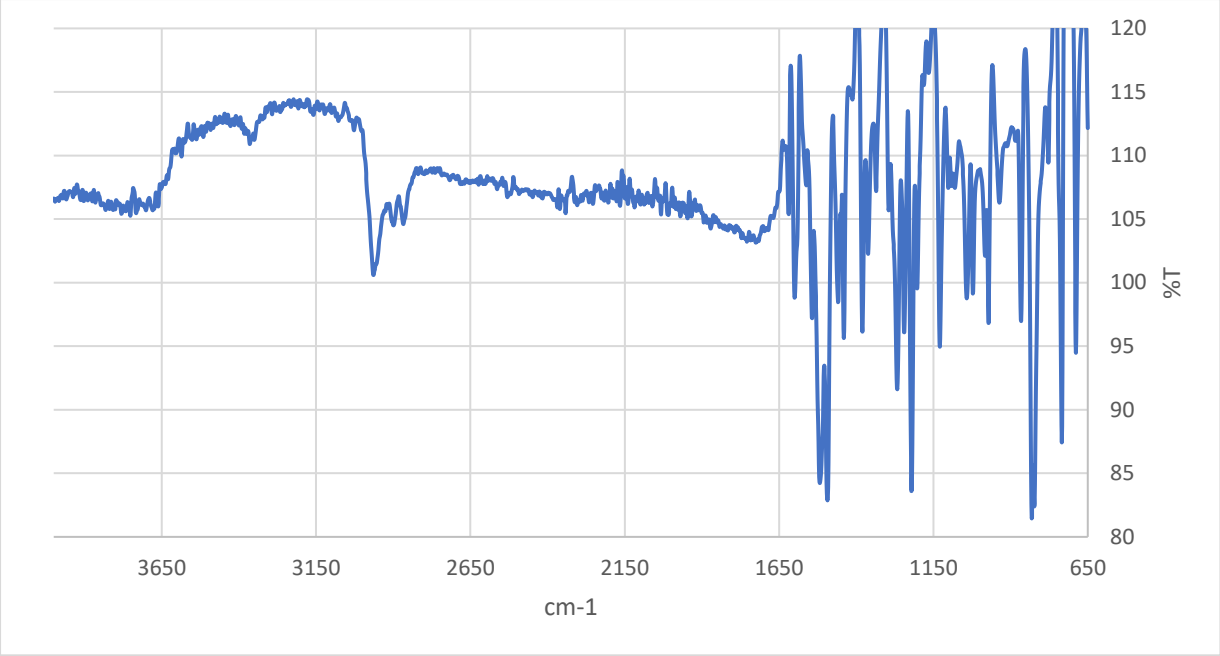

Figure S9.61. FT-IR of **29ZnY-NO$_3$**

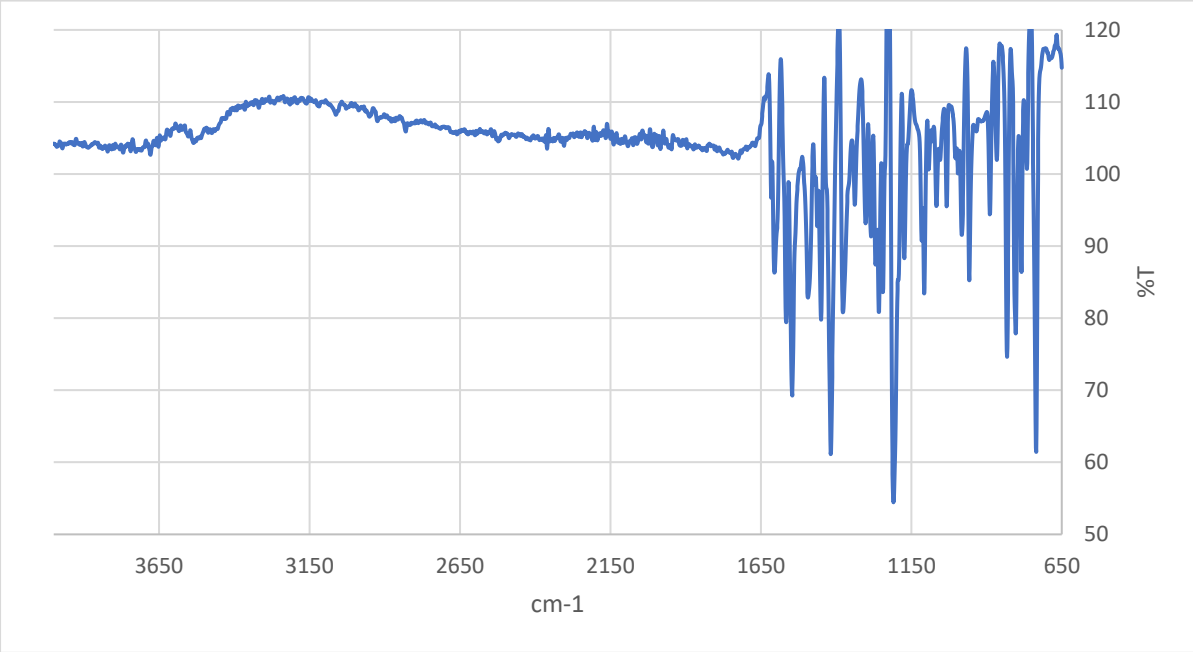

Figure S9.62. FT-IR of **24ZnY-NO$_3$**

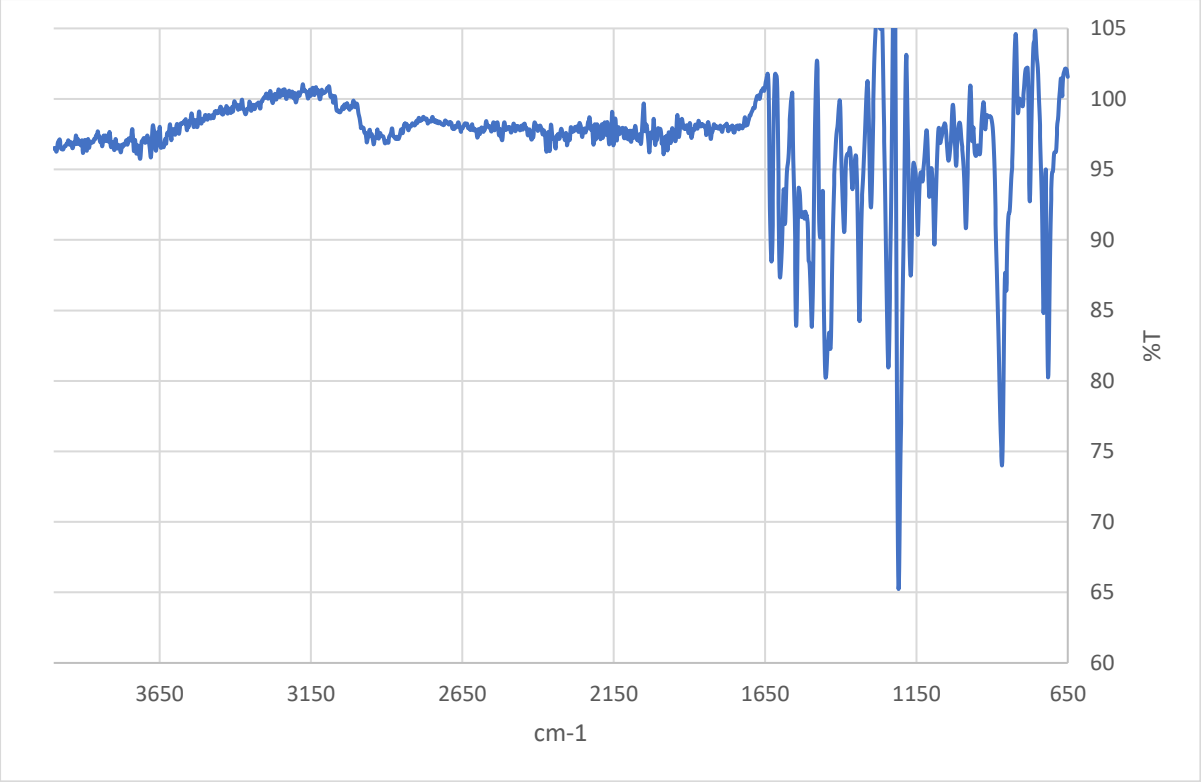

Figure S9.63. FT-IR of **25ZnY-NO$_3$**

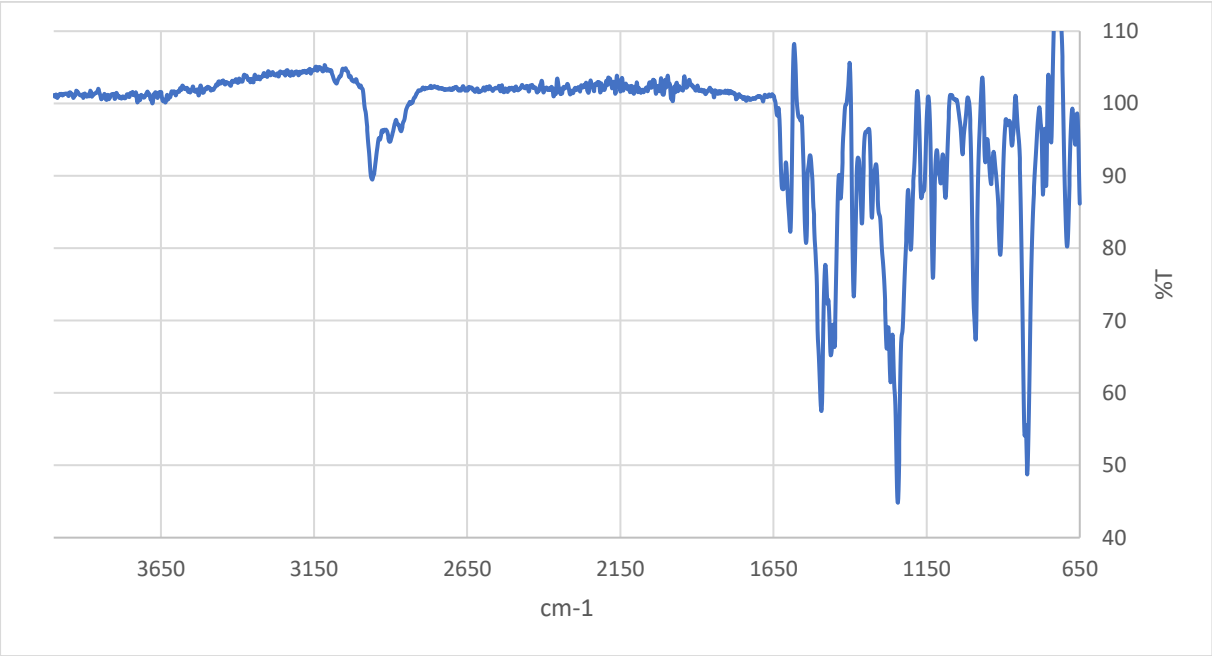

Figure S9.64. FT-IR of **26ZnY-NO$_3$**

9.9 ^{1}HNMR and 13CNMR of C9a-C9v

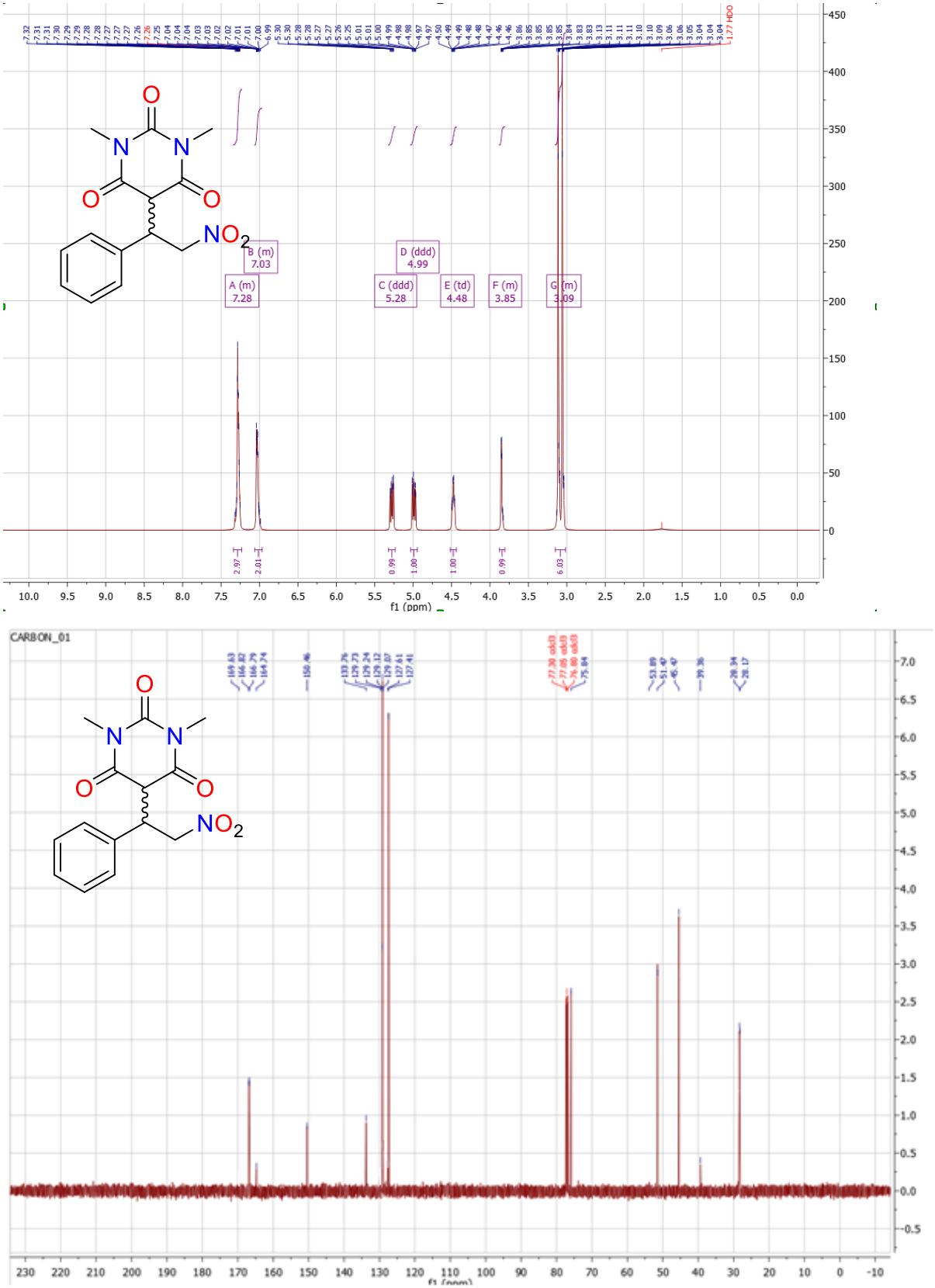

Figure S9.65. (Top) ^{1}H NMR of **C9a** (Bottom) ^{13}C NMR of **C9a**

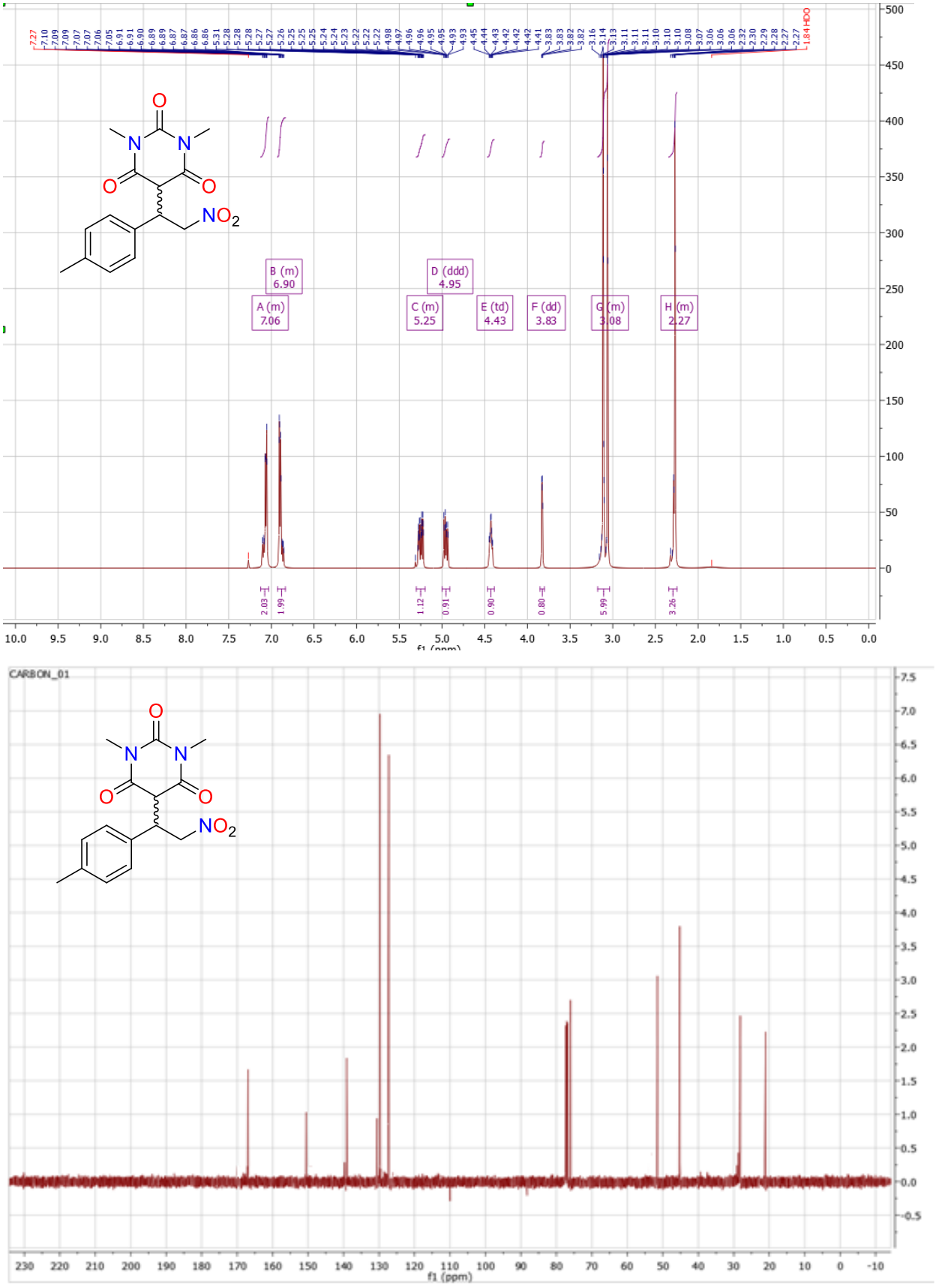

Figure S9.66. (Top) ^{1}H NMR of **C9c** (Bottom) ^{13}C NMR of **C9c**

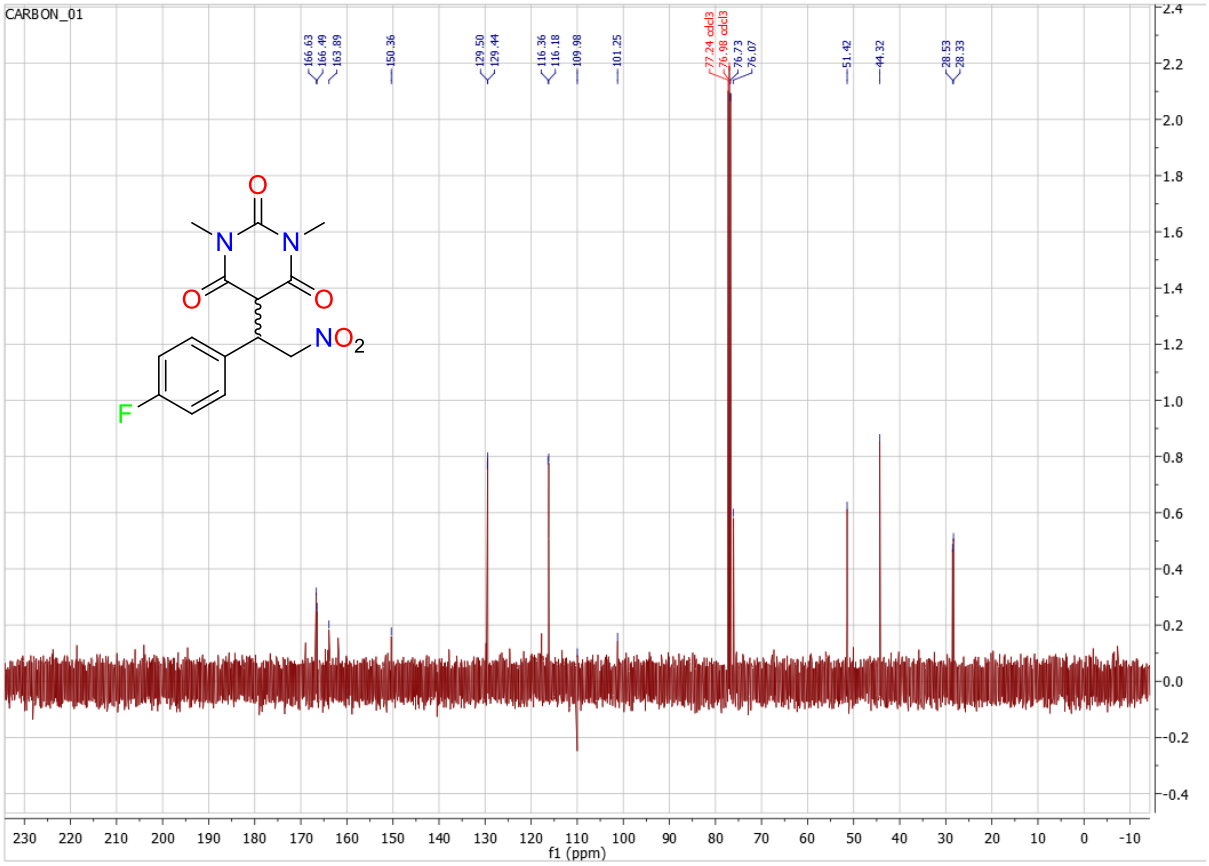

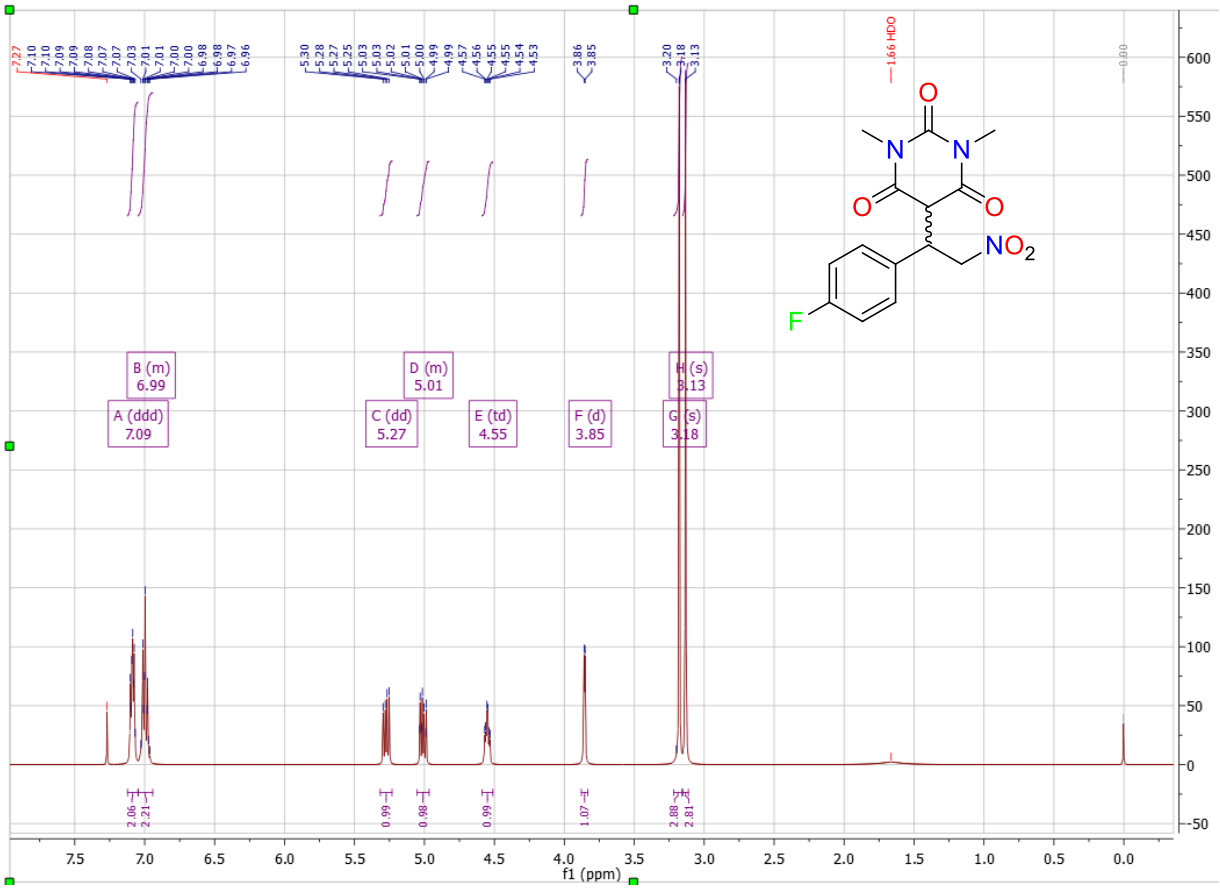

Figure S9.67. (Top) ^{1}H NMR of **C9e** (Bottom) ^{13}C NMR of **C9e**

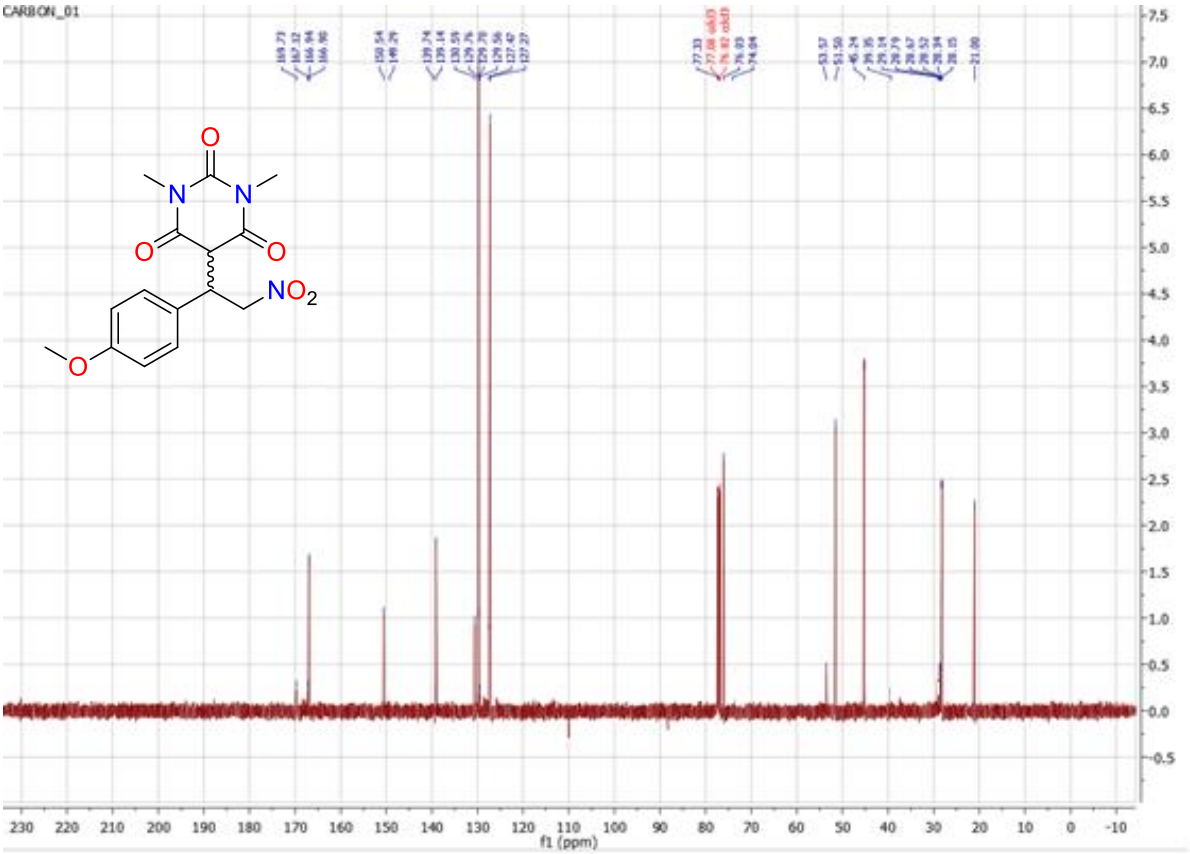

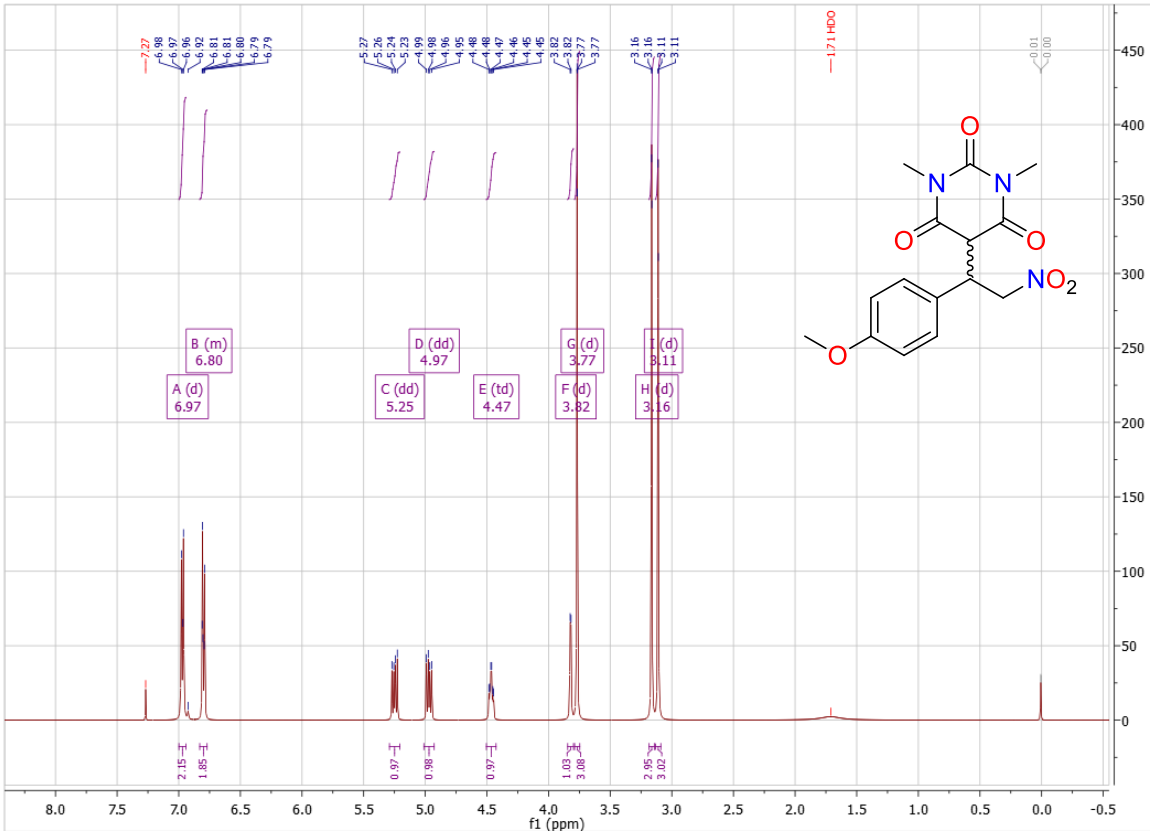

. **Figure S9.68**. (Top) ^{1}H NMR of **C9b** (Bottom) ^{13}C NMR of **C9b**

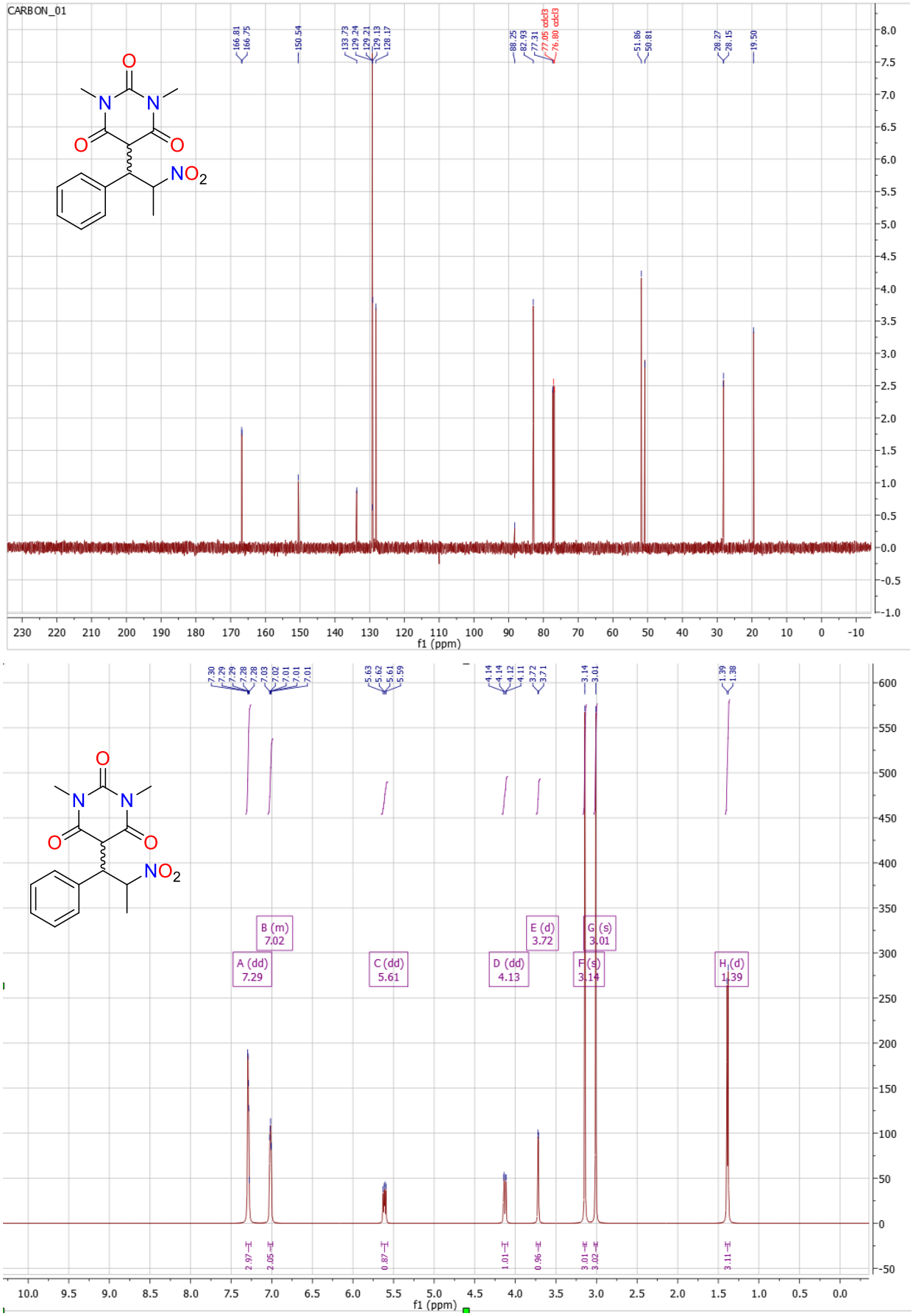

Figure S9.69. (Top) ^{1}H NMR of **C9f** (Bottom) ^{13}C NMR of **C9f**

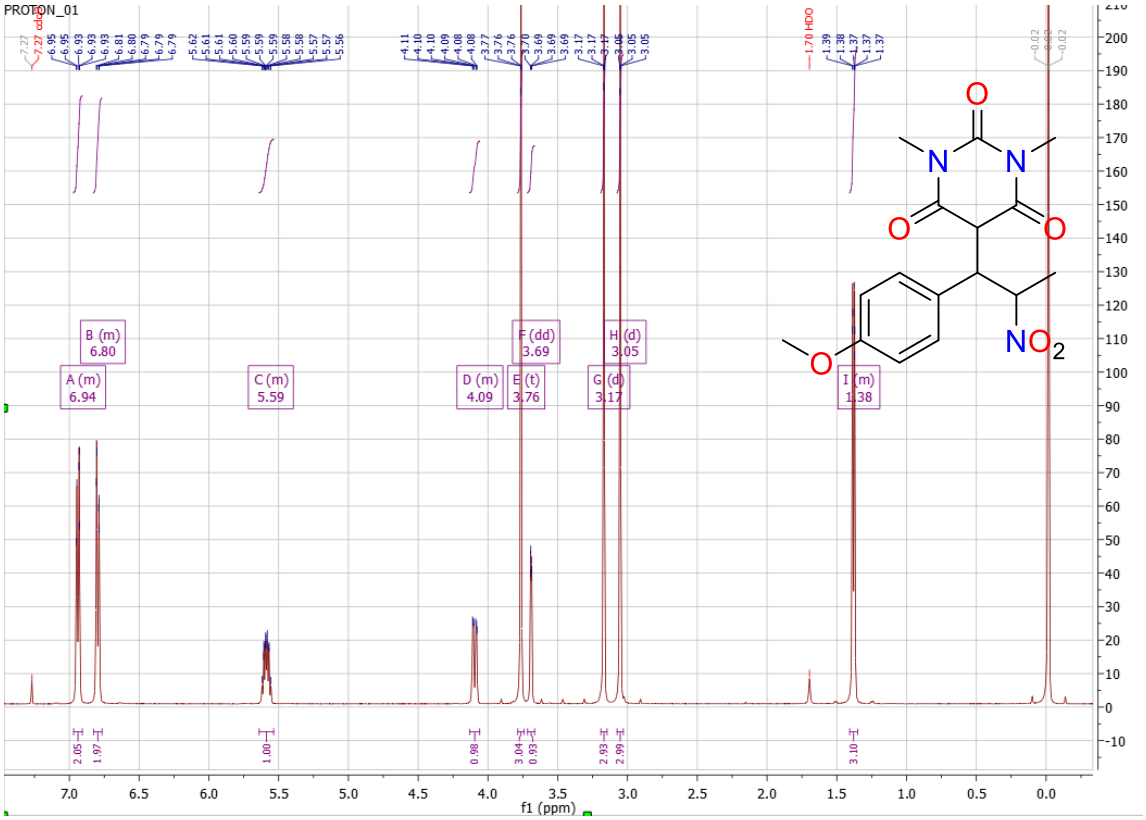

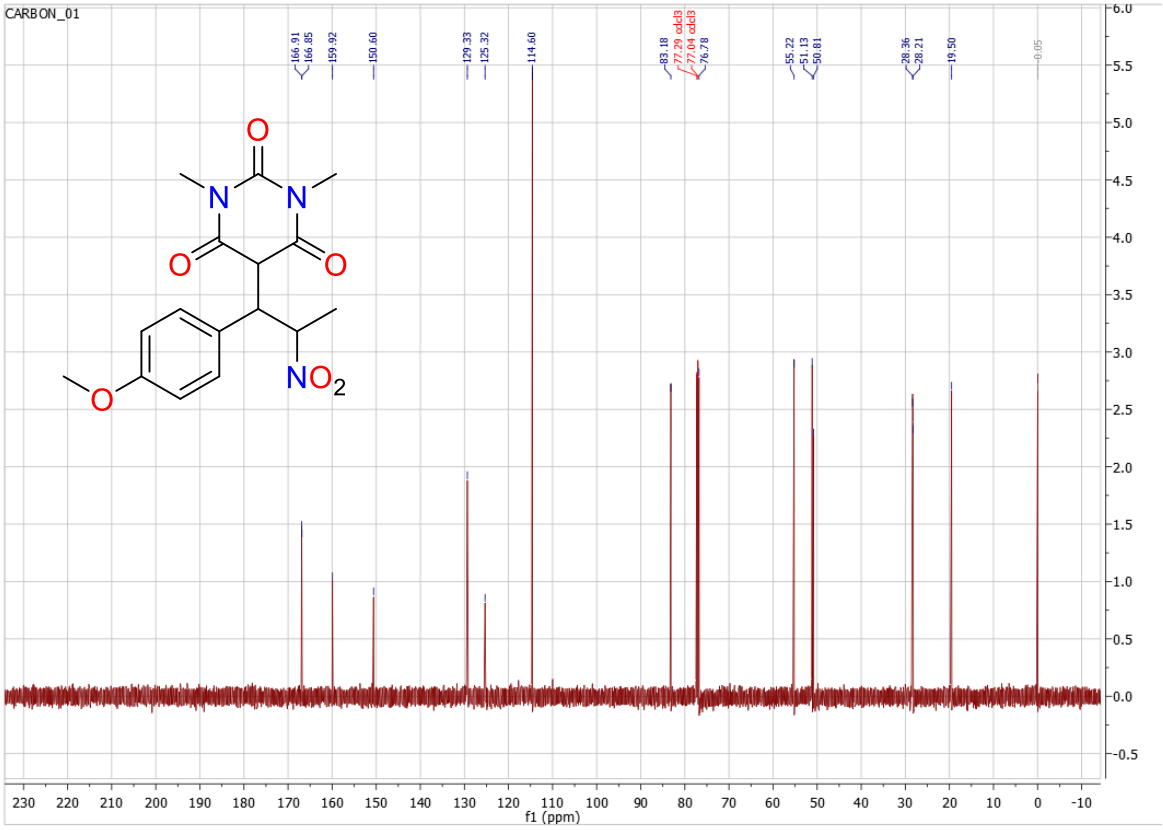

Figure S9.70. (Top) ^{1}H NMR of **C9v** (Bottom) ^{13}C NMR of **C9v**

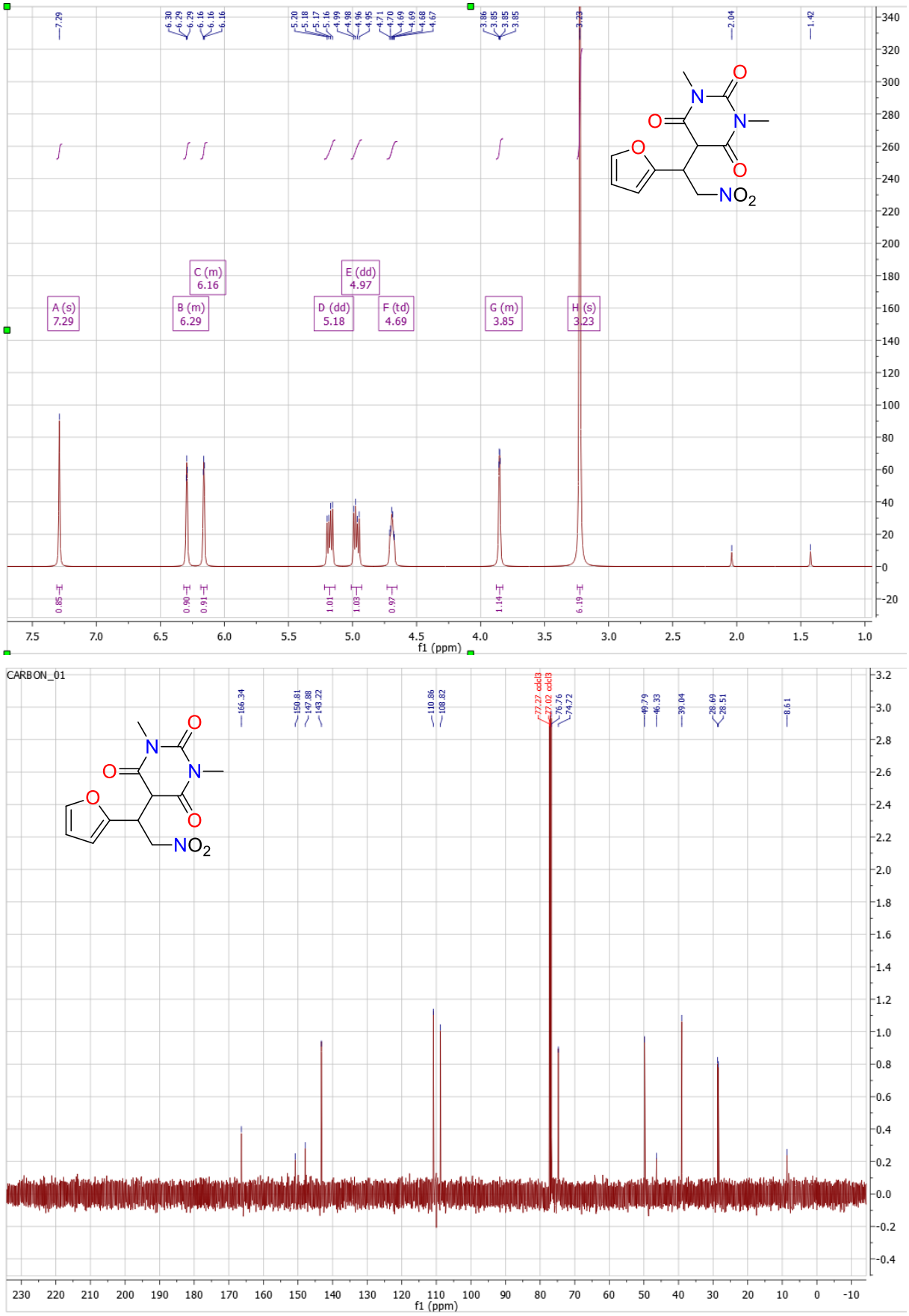

Figure S9.71. (Top) ^{1}H NMR of **C9g** (Bottom) ^{13}C NMR of **C9g**

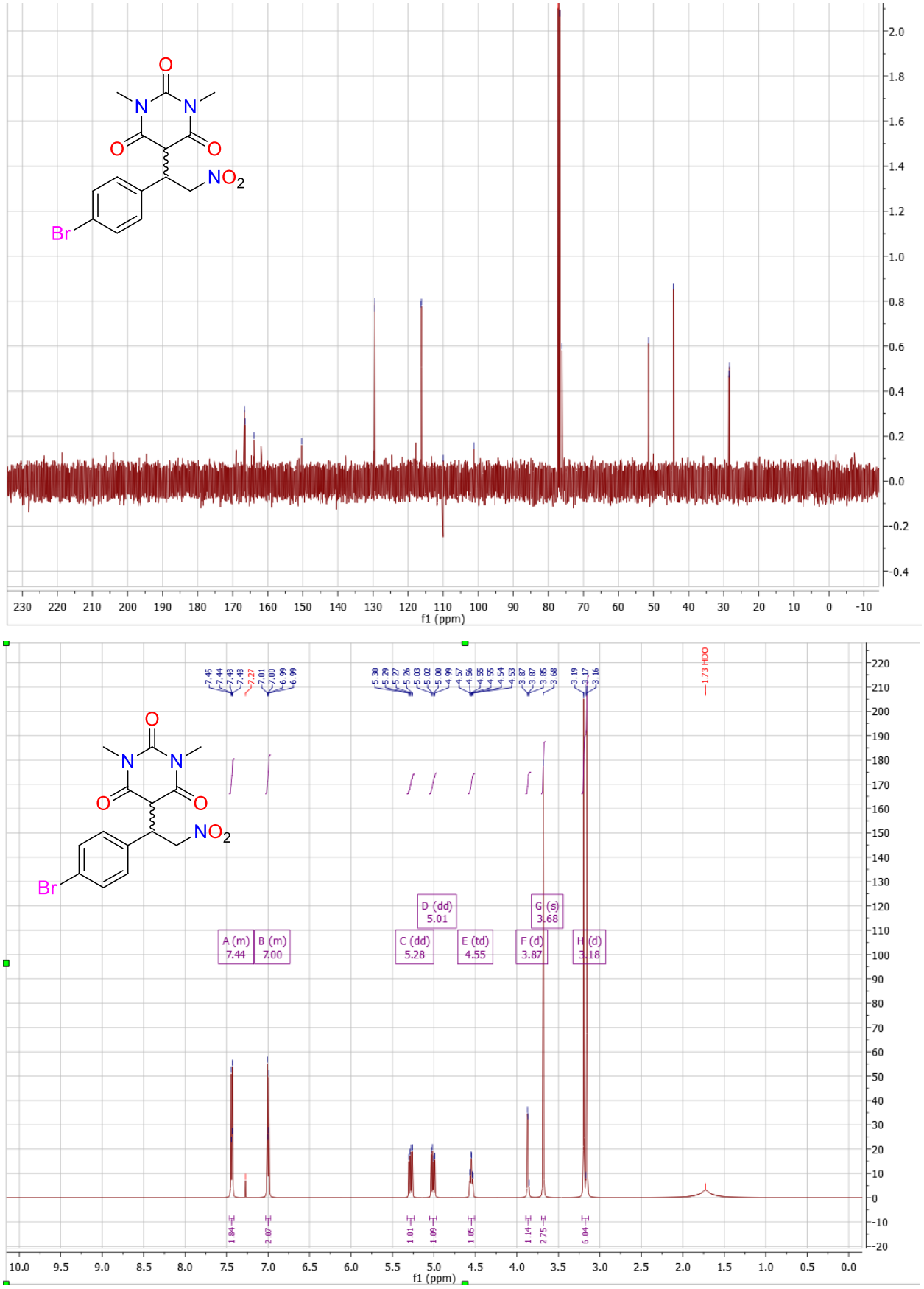

Figure S9.72. (Top) ^{1}H NMR of **C9d** (Bottom) ^{13}C NMR of **C9d**

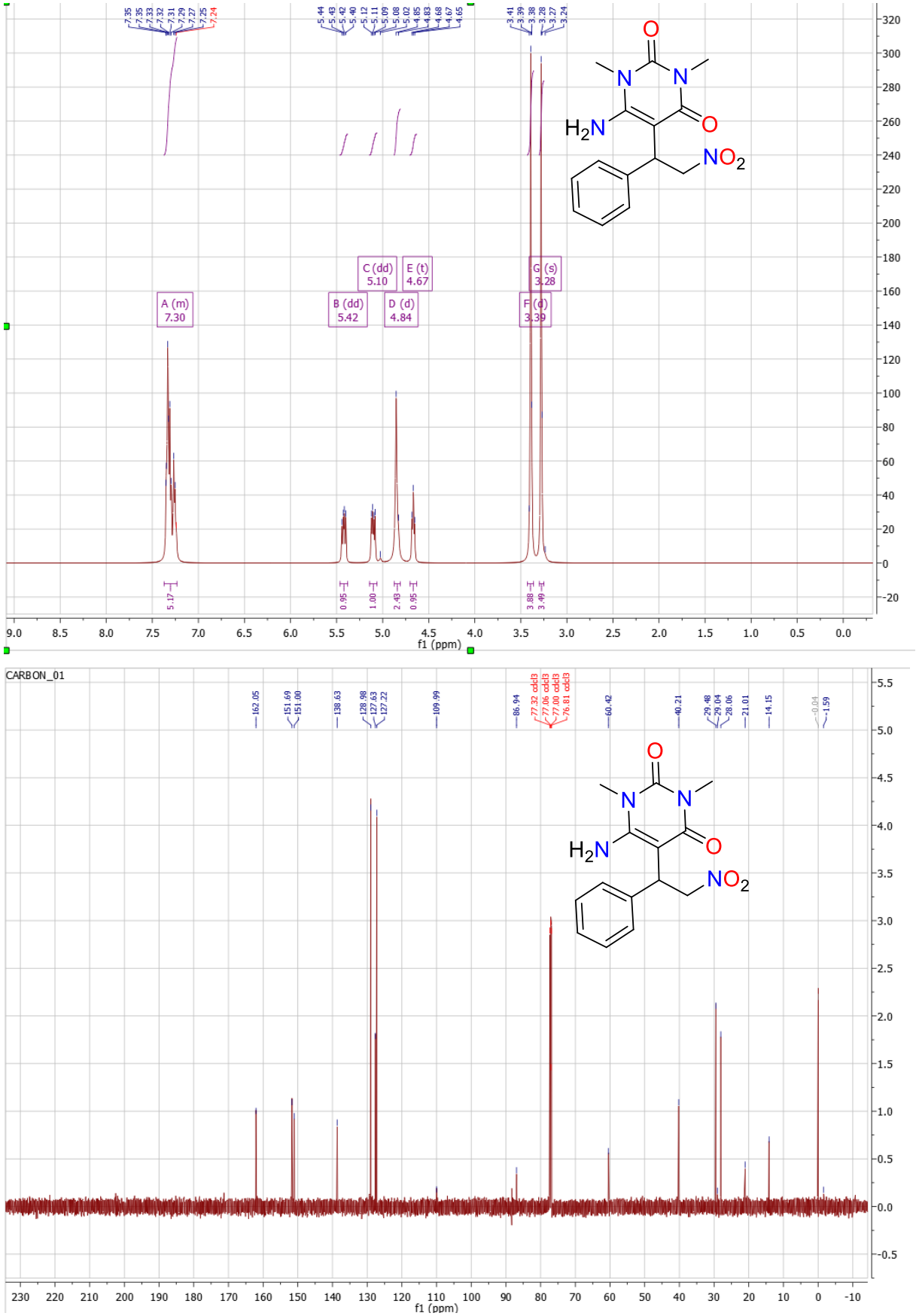

Figure S9.73. (Top) ^{1}H NMR of **C9h** (Bottom) ^{13}C NMR of **C9h**

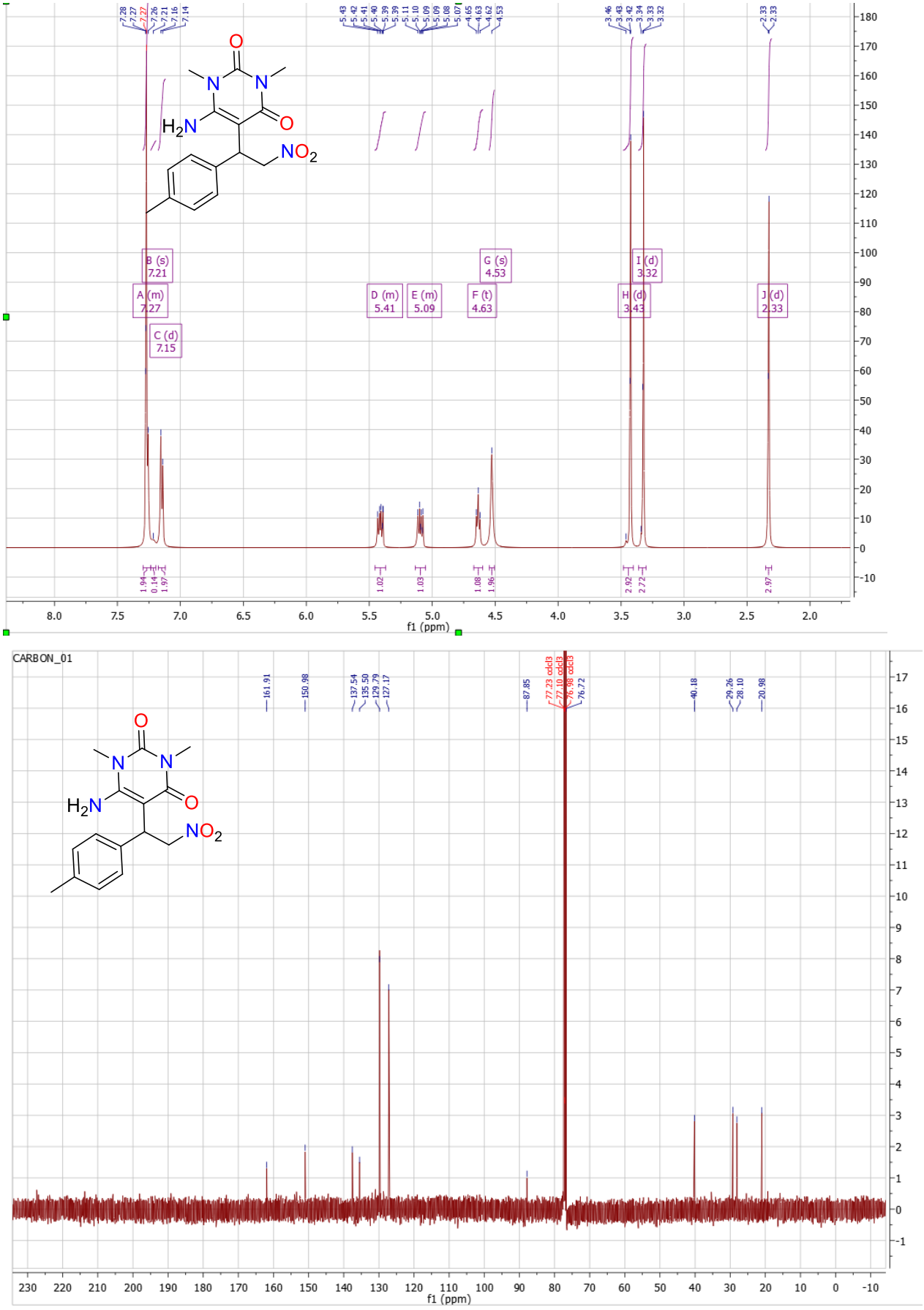

Figure S9.74. (Top) ^{1}H NMR of **C9g** (Bottom) ^{13}C NMR of **C9g**

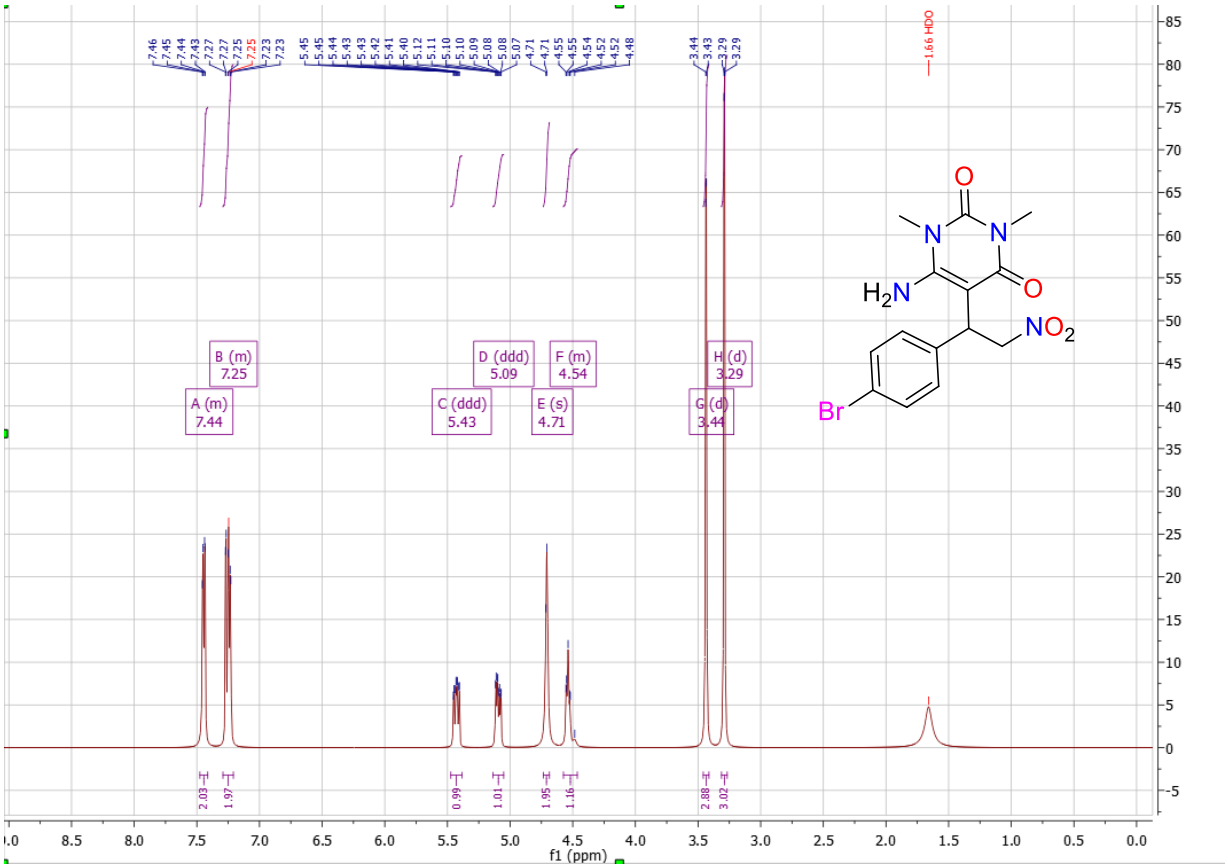

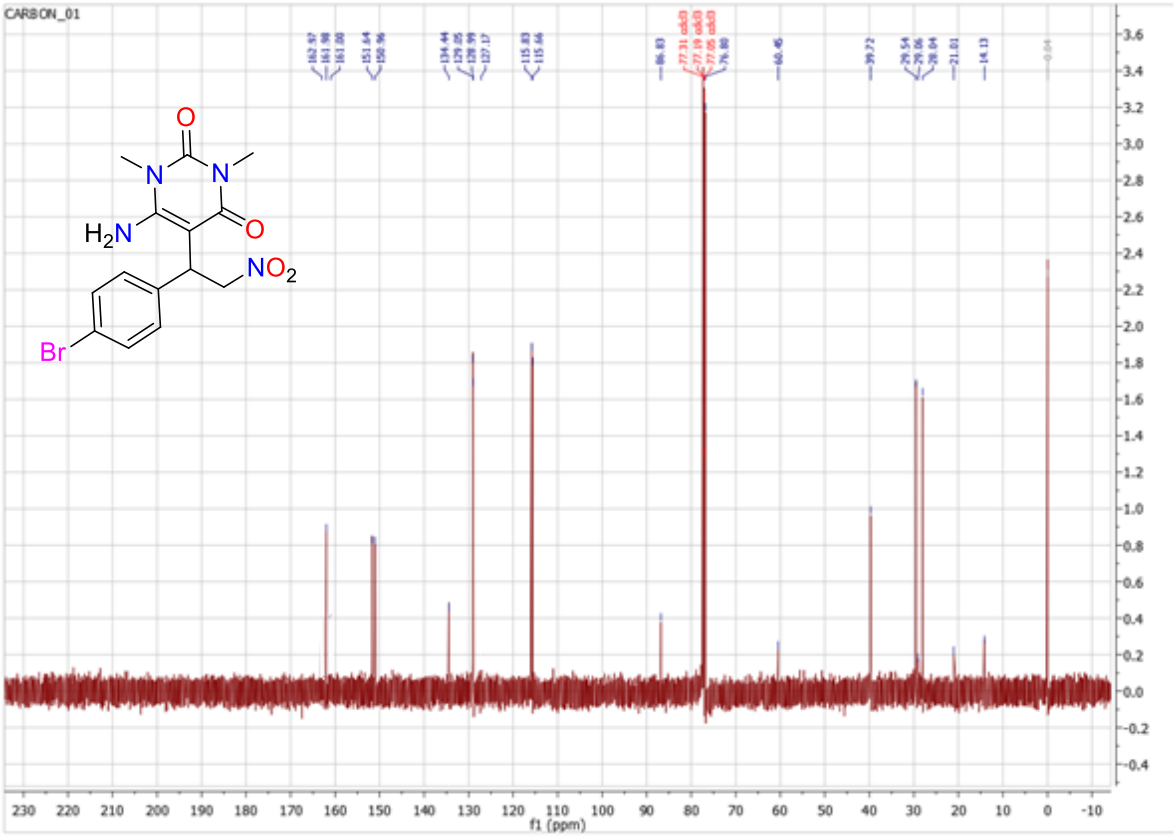

Figure S9.75. (Top) ^{1}H NMR of **C9k** (Bottom) ^{13}C NMR of **C9k**

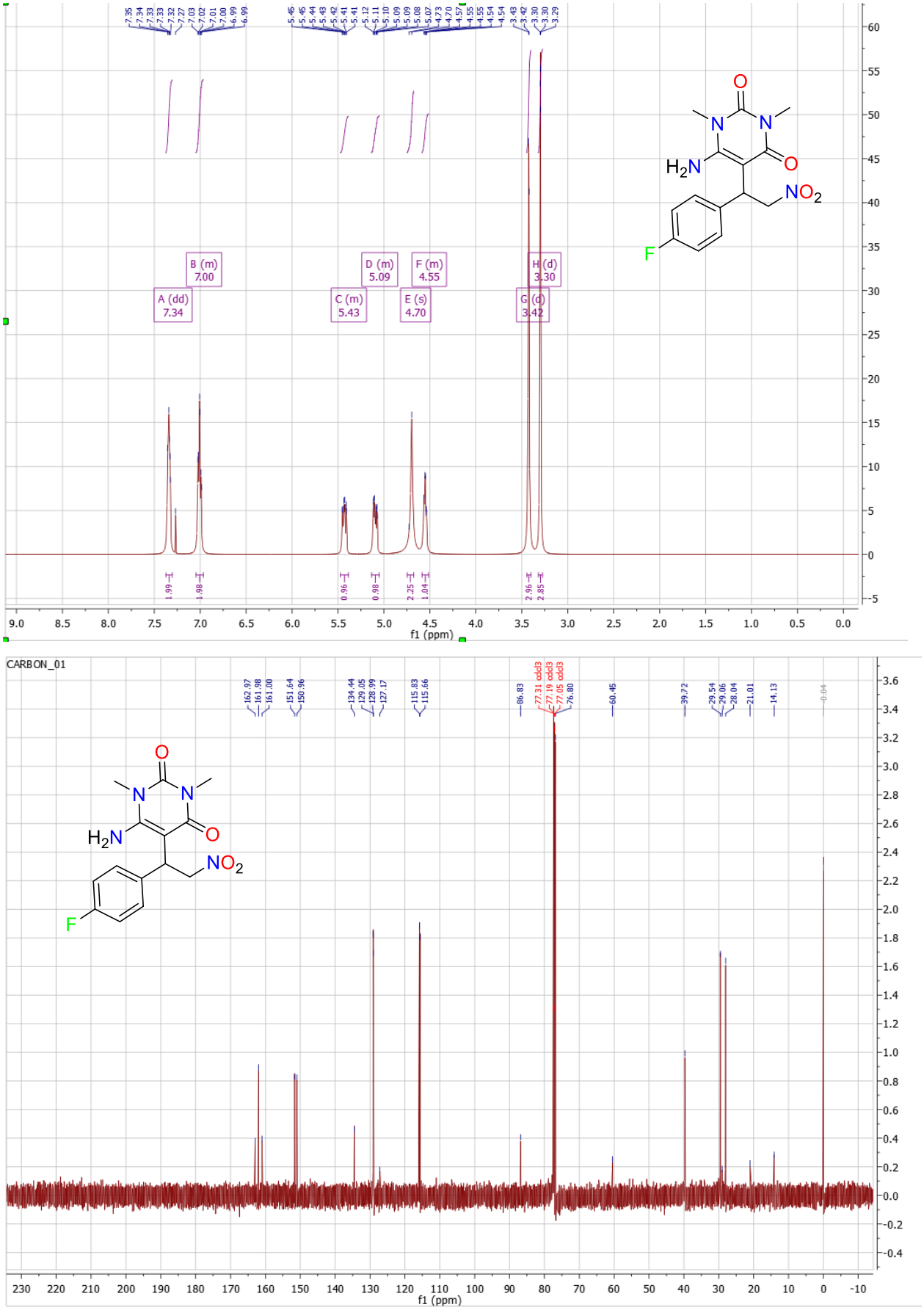

Figure S9.76. (Top) ^{1}H NMR of **C9l** (Bottom) ^{13}C NMR of **C9l**

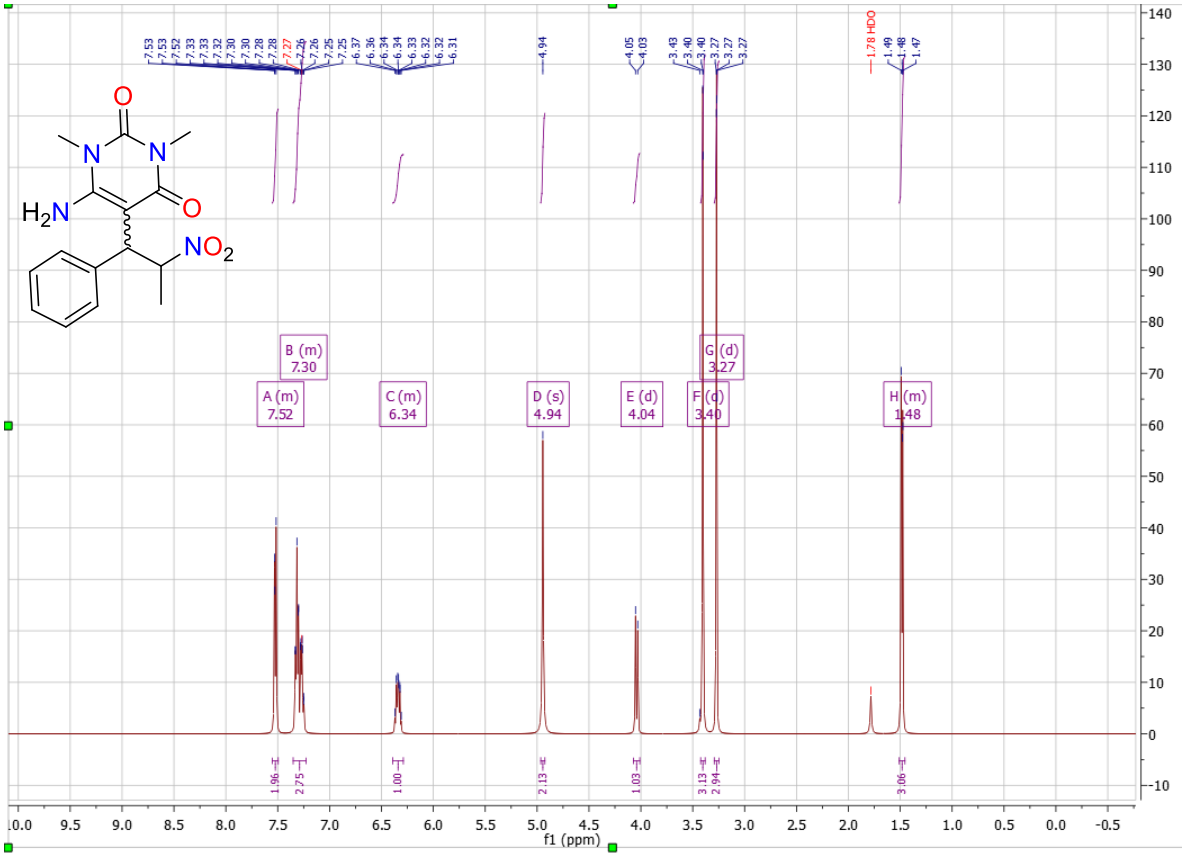

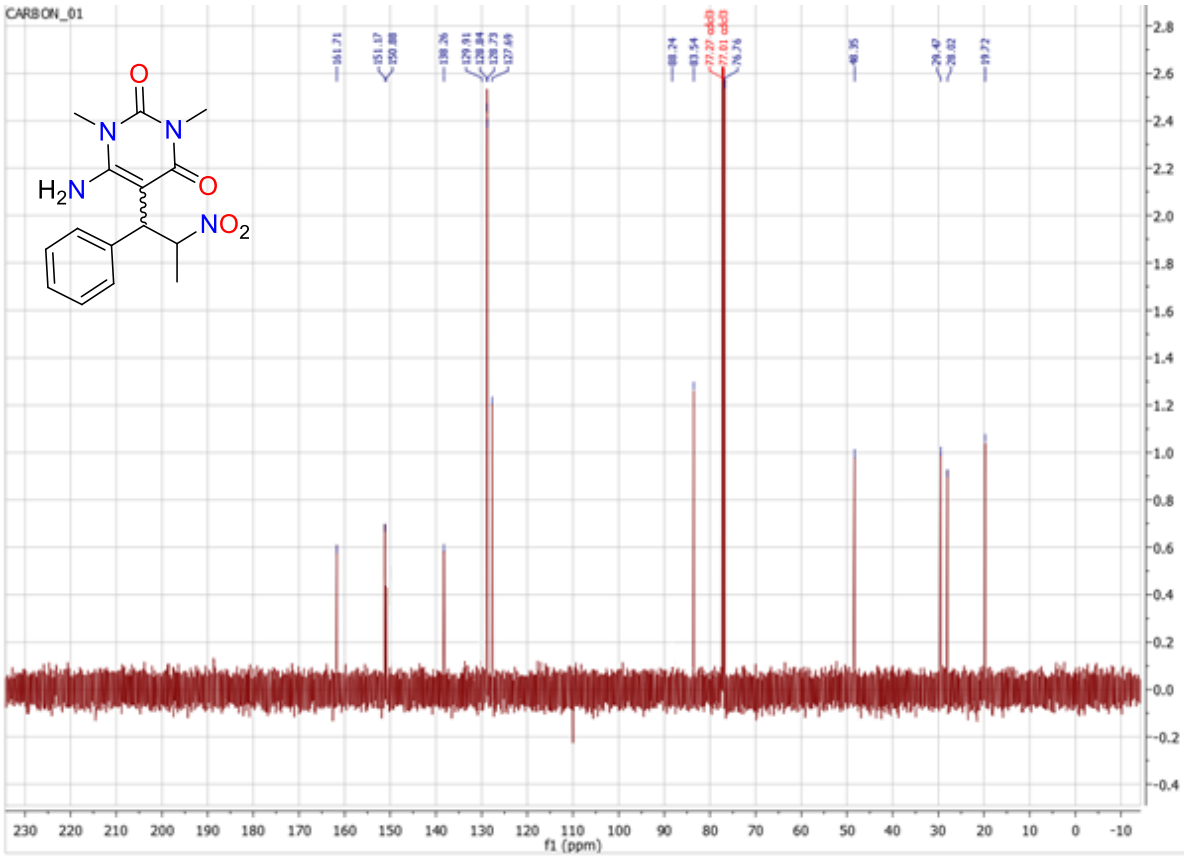

Figure S9.77. (Top) ^{1}H NMR of **C9m** (Bottom) ^{13}C NMR of **C9m**

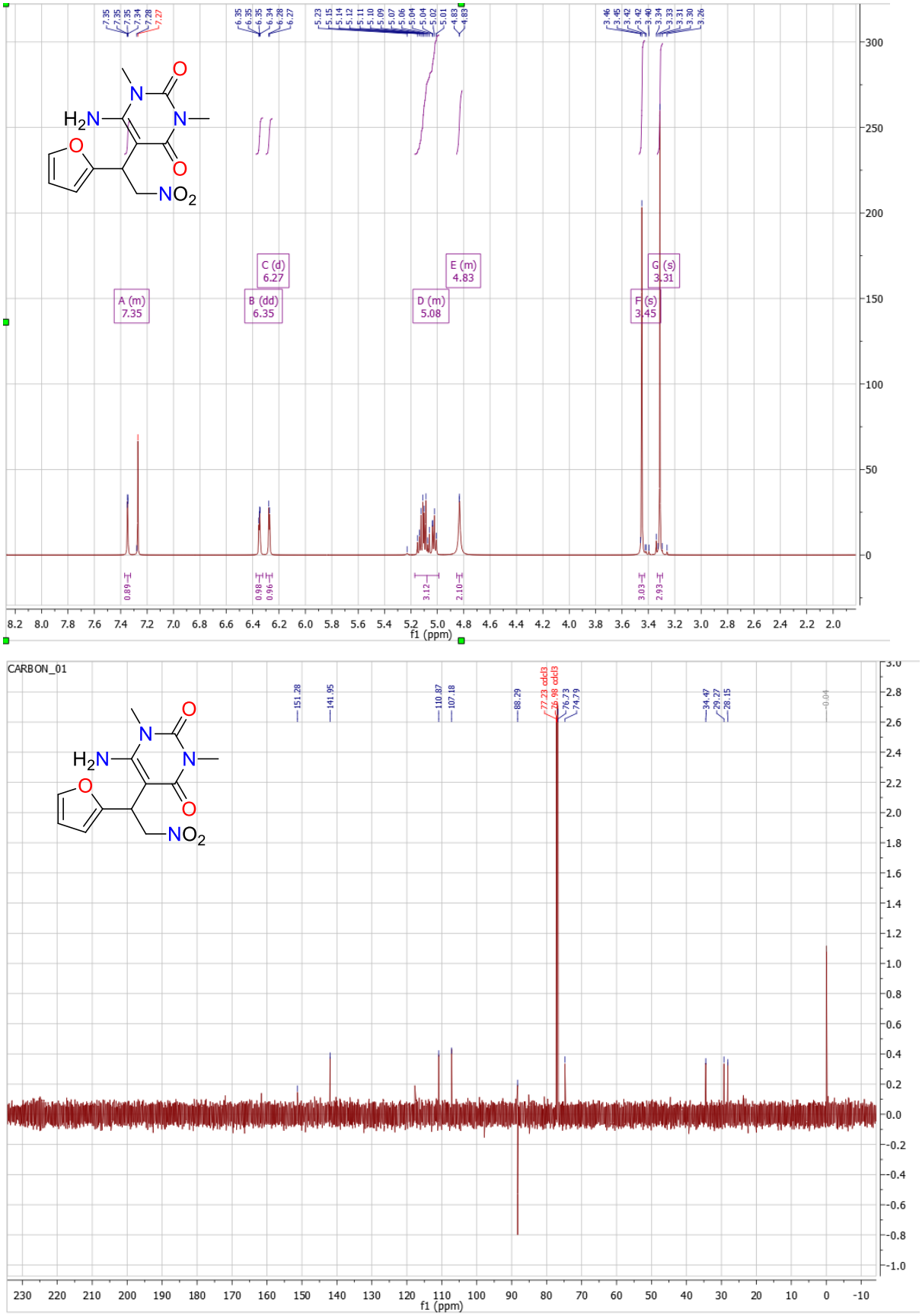

Figure S9.78. (Top) ^{1}H NMR of **C9n**(Bottom) ^{13}C NMR of **C9n**

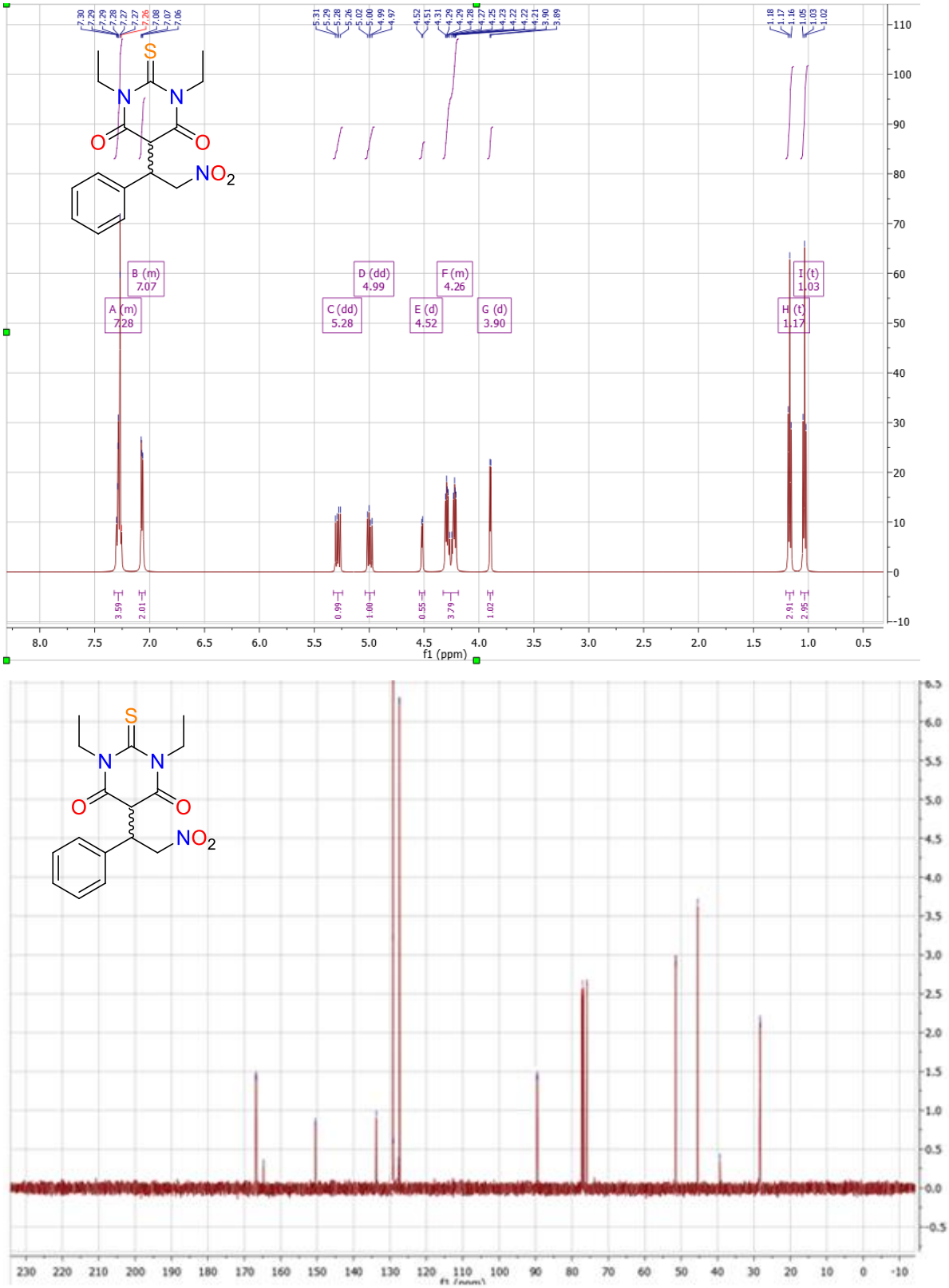

Figure S9.79. (Top) ^{1}H NMR of **C9o** (Bottom) ^{13}C NMR of **C9o**

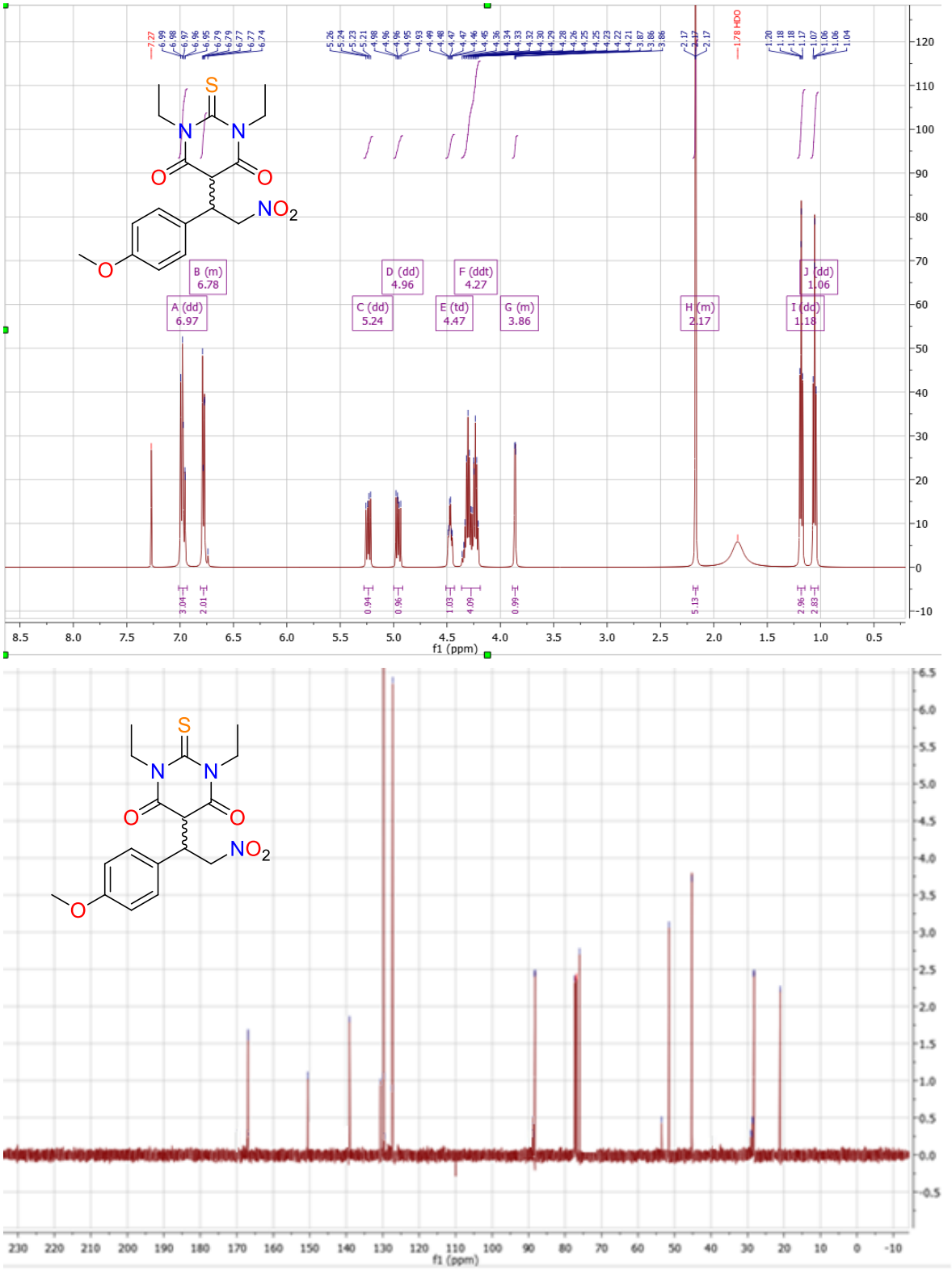

Figure S9.80. (Top) ^{1}H NMR of **C9p** (Bottom) ^{13}C NMR of **C9p**

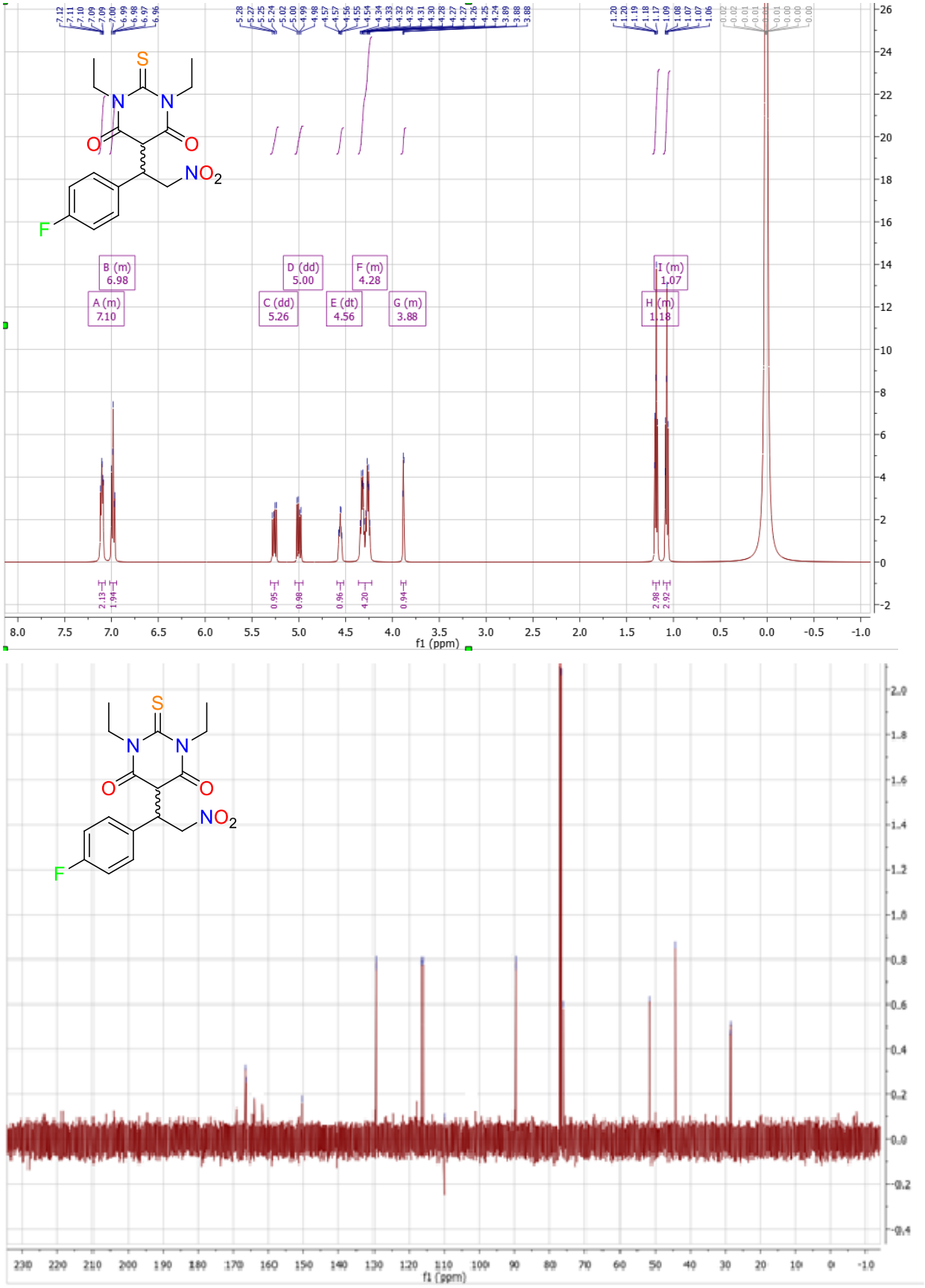

Figure S9.81. (Top) ^{1}H NMR of **C9s** (Bottom) ^{13}C NMR of **C9s**

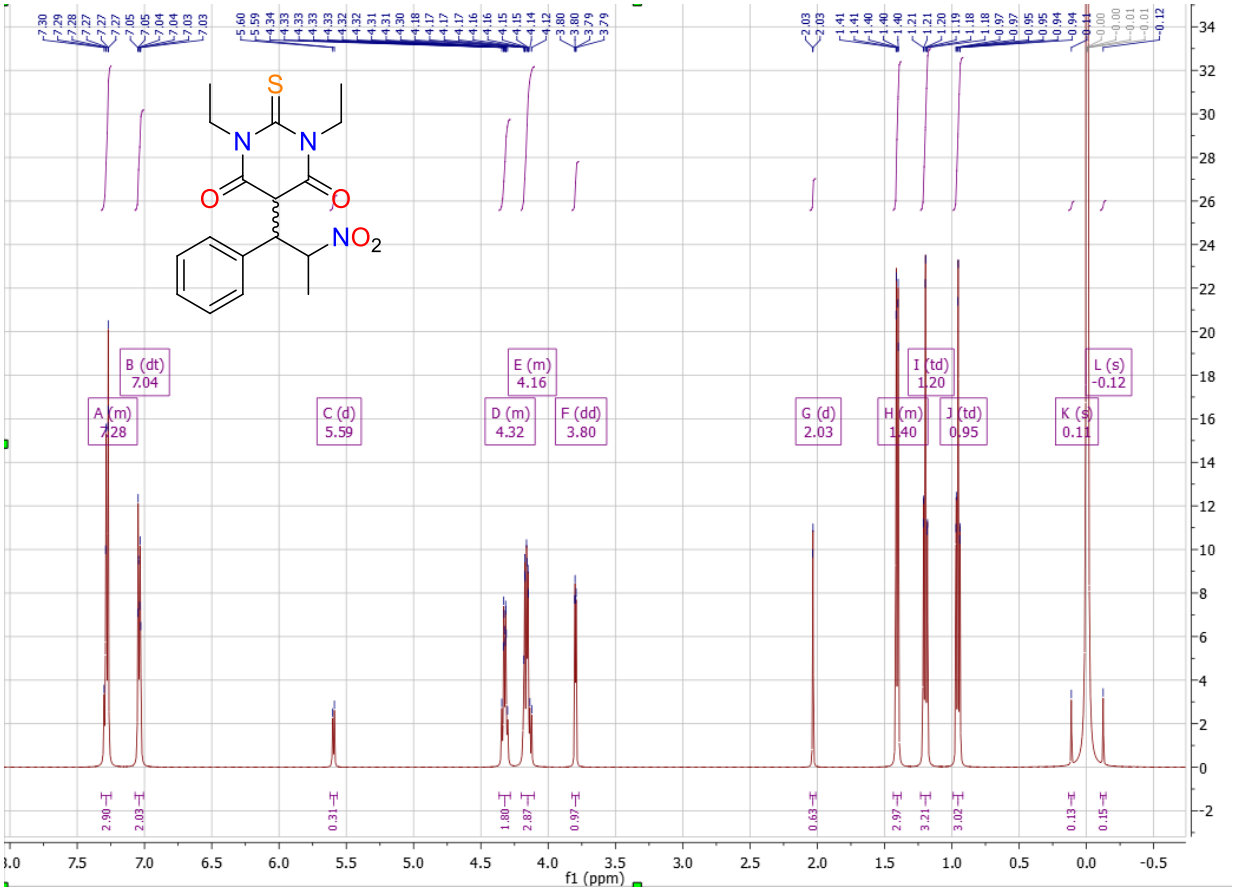

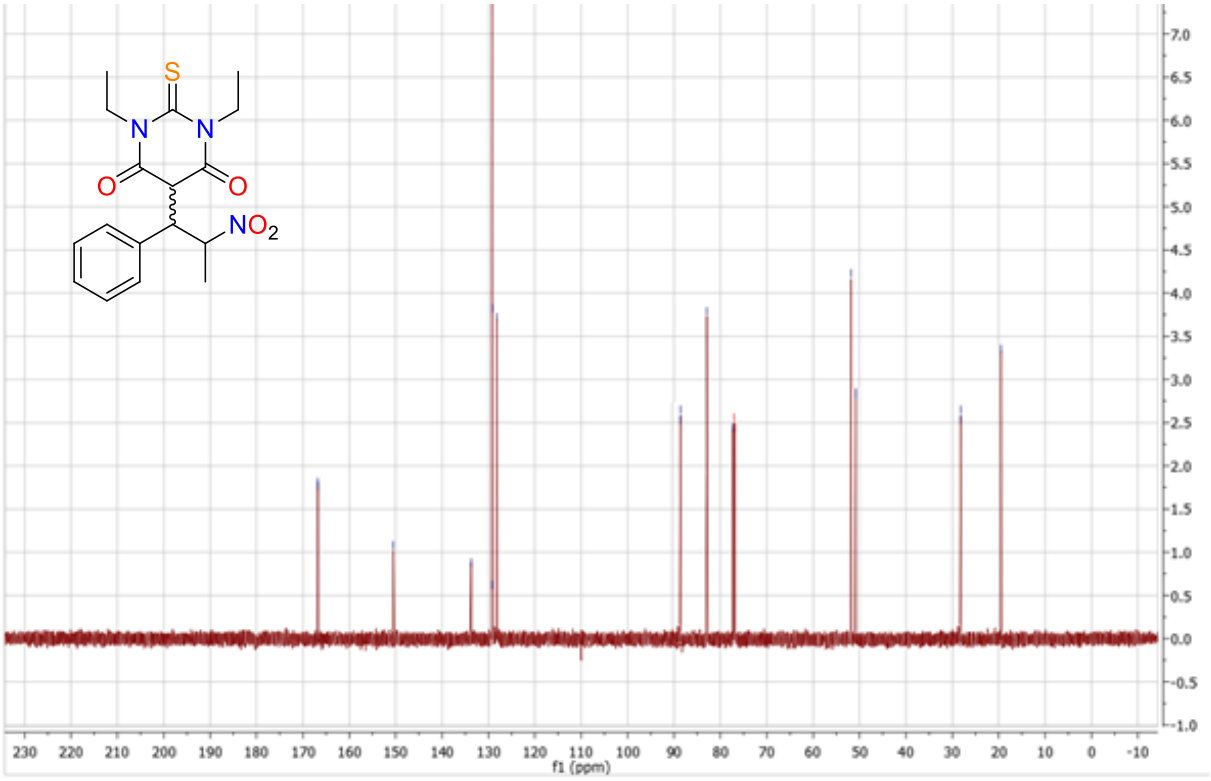

Figure S9.82. (Top) ^{1}H NMR of **C9t** (Bottom) ^{13}C NMR of **C9t**

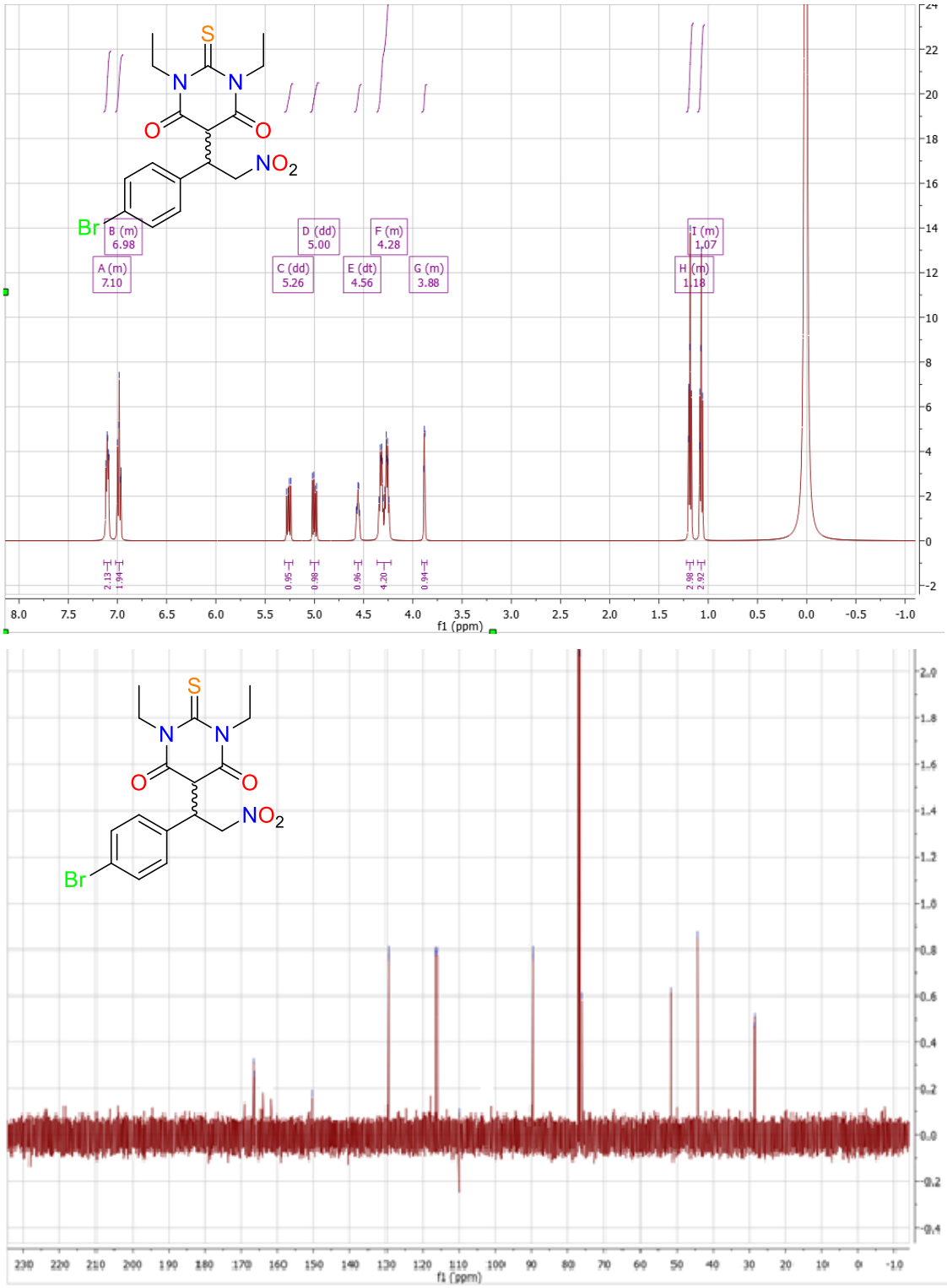

Figure S9.83. (Top) ^{1}H NMR of **C9r** (Bottom) ^{13}C NMR of **C9r**

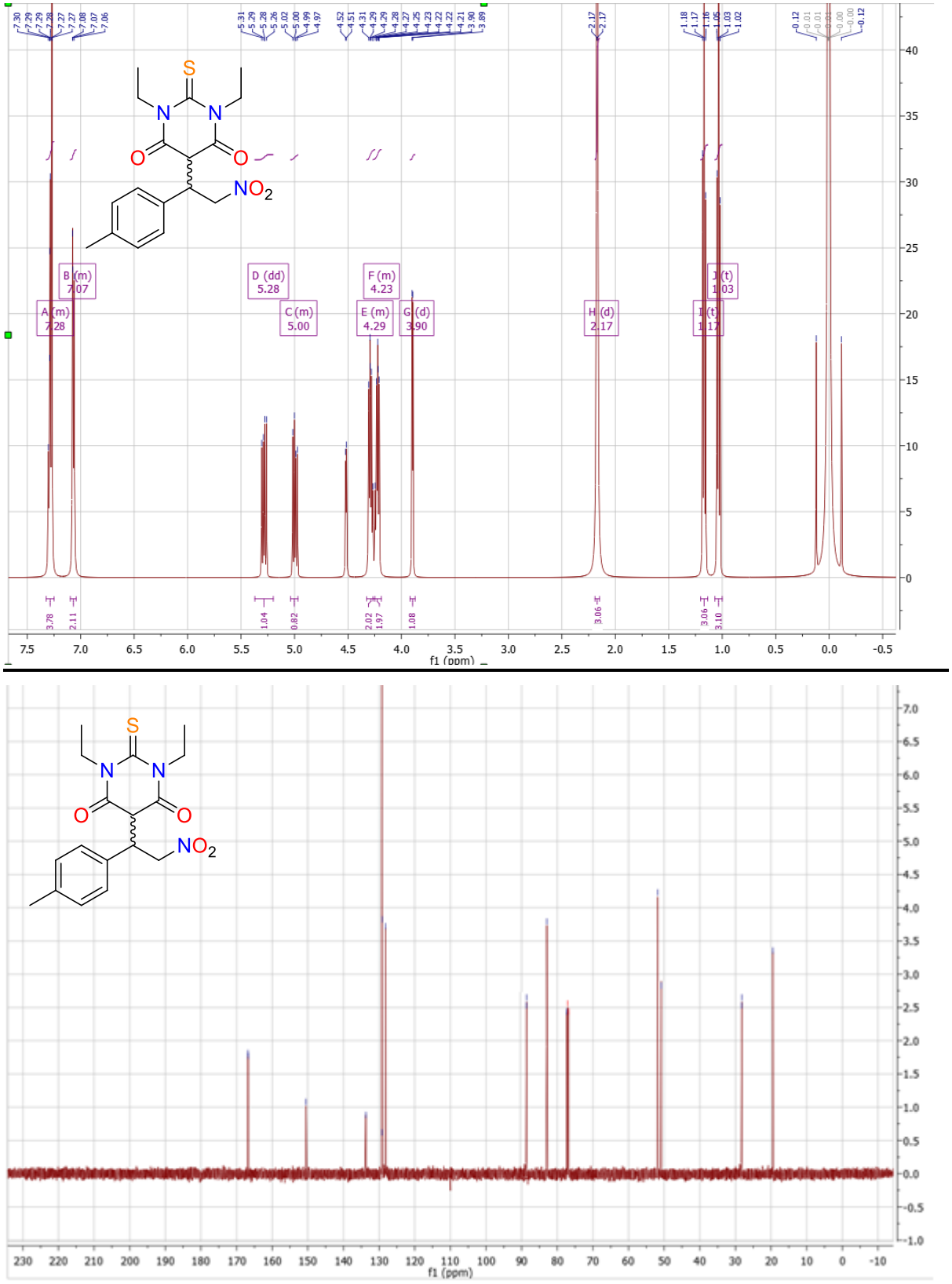

Figure S9.84. (Top) ^{1}H NMR of **C9q** (Bottom) ^{13}C NMR of **C9q**

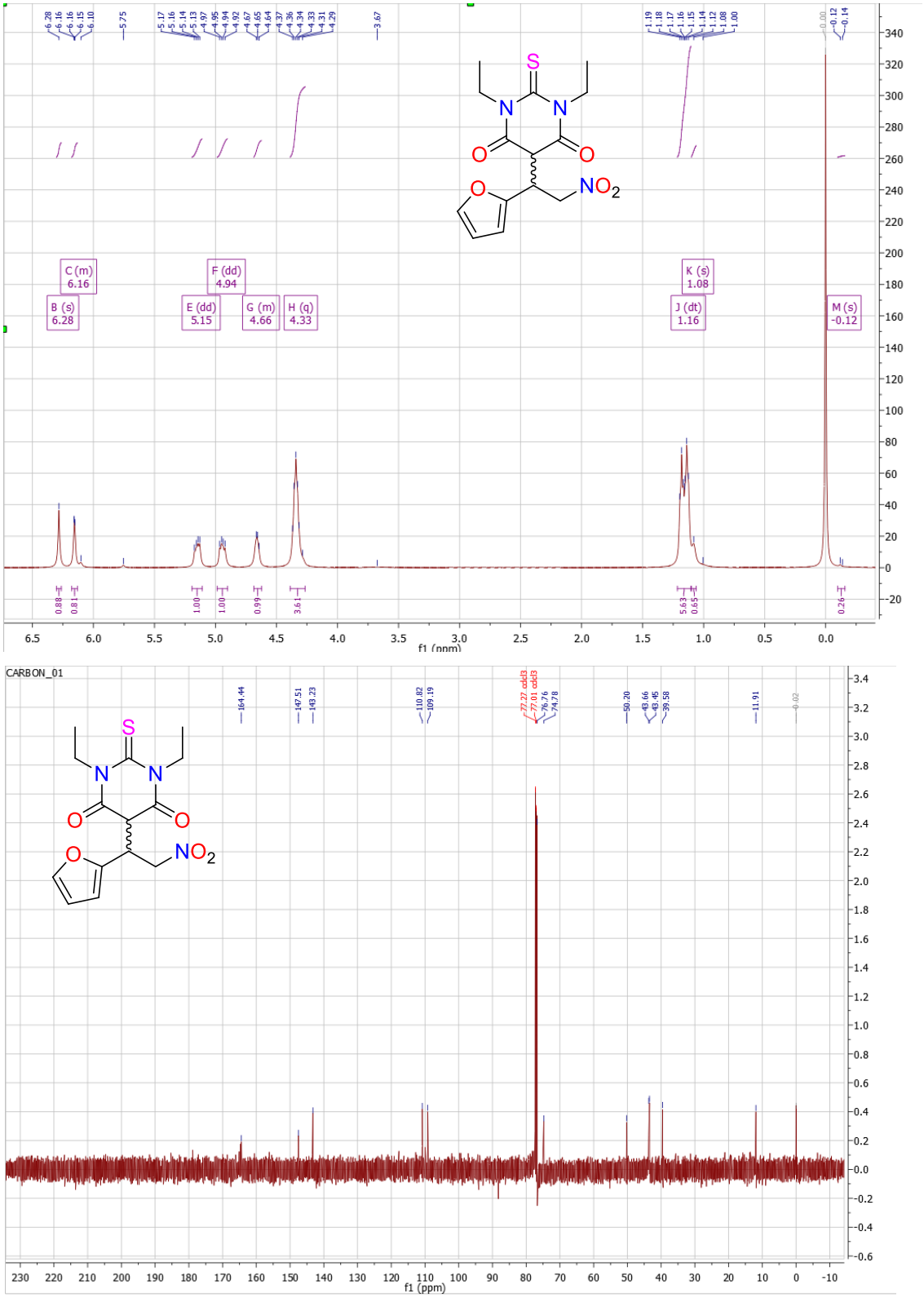

Figure S9.85. (Top) ^{1}H NMR of **C9u** (Bottom) ^{13}C NMR of **C9u**

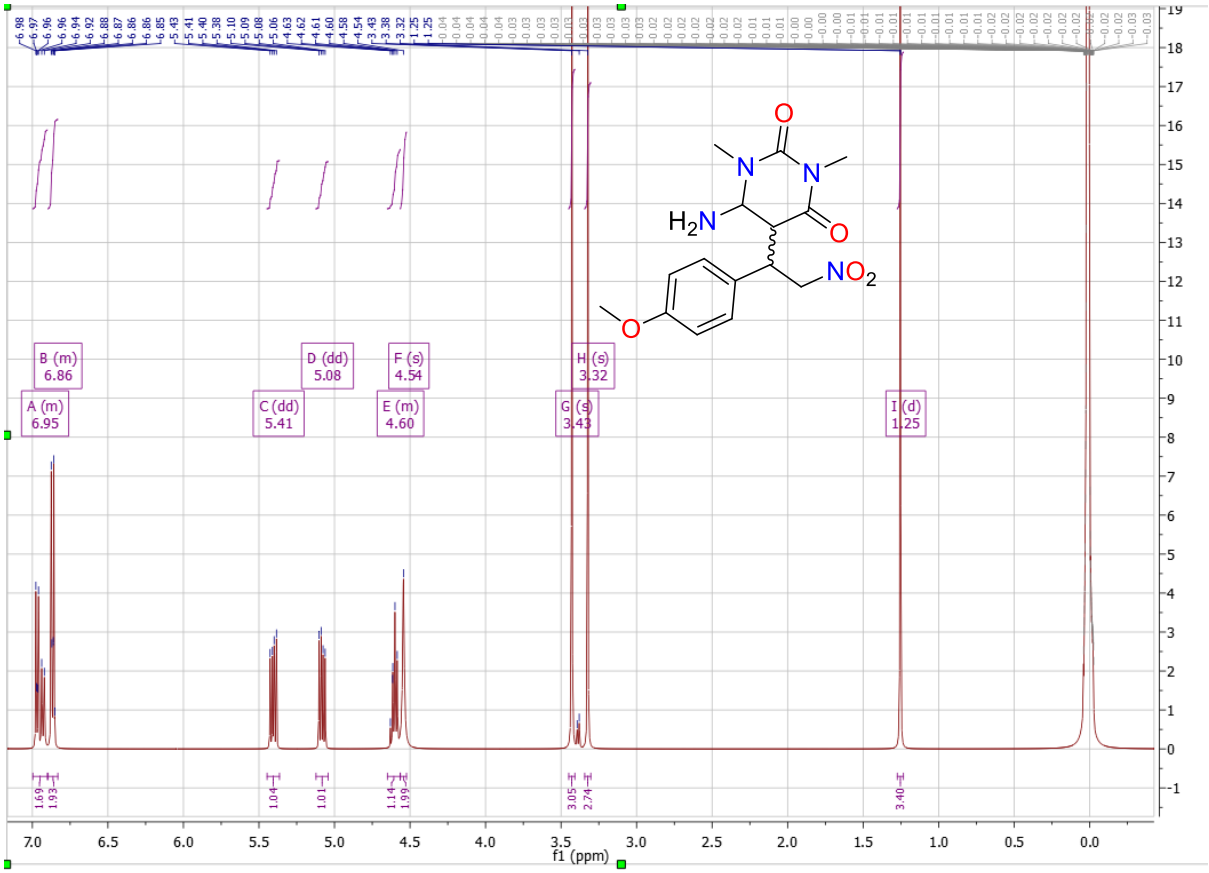

Figure S9.86.^{1}H NMR of **C9g**

9.10 Crude ^{1}HNMR Stereo selectivity

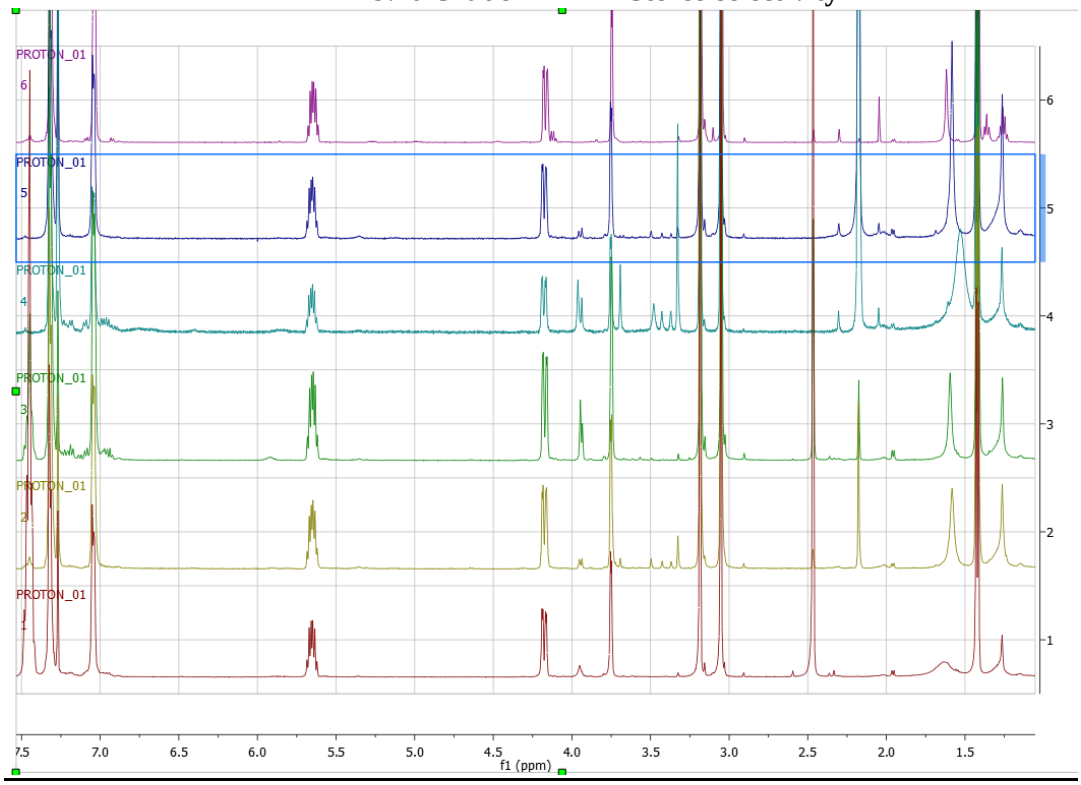

Figure S9.87. *Trans* 1-Ln Crude ^{1}H NMR

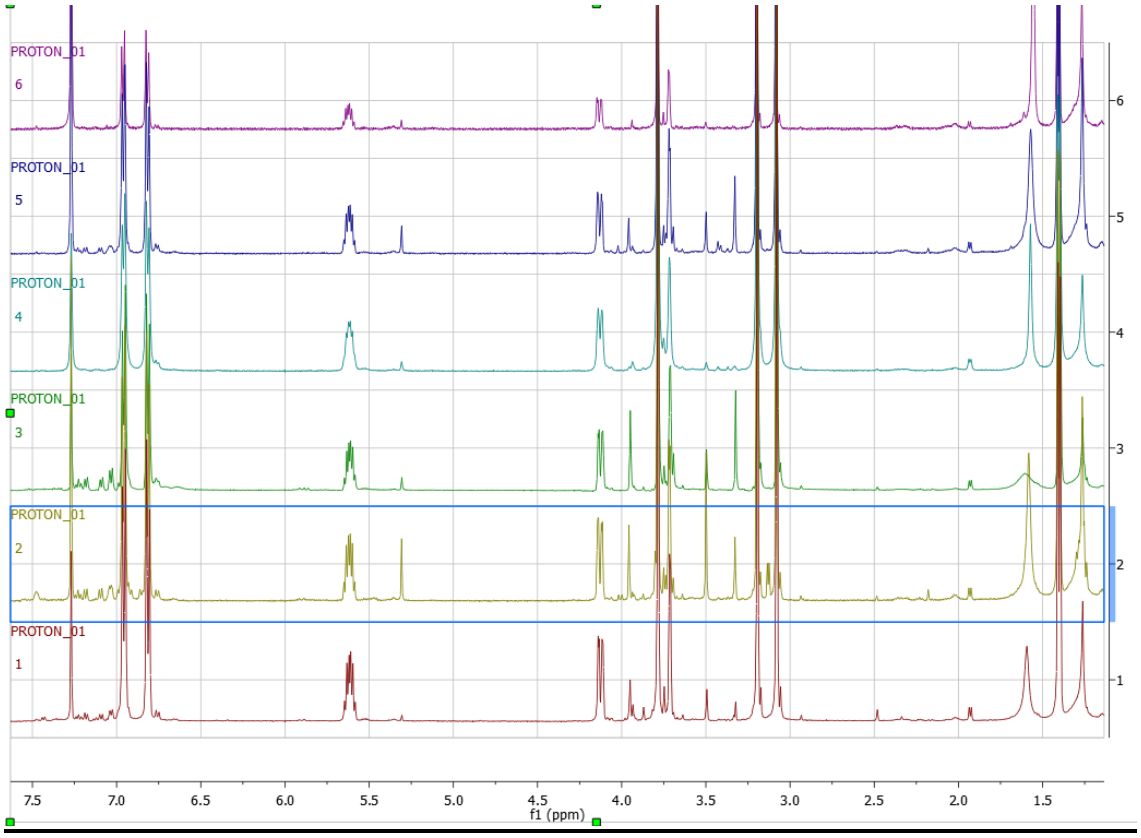

Figure S9.88. *Cis* 1-Ln Crude ^{1}H NMR

9.11 ESI-MS C9a-C9v

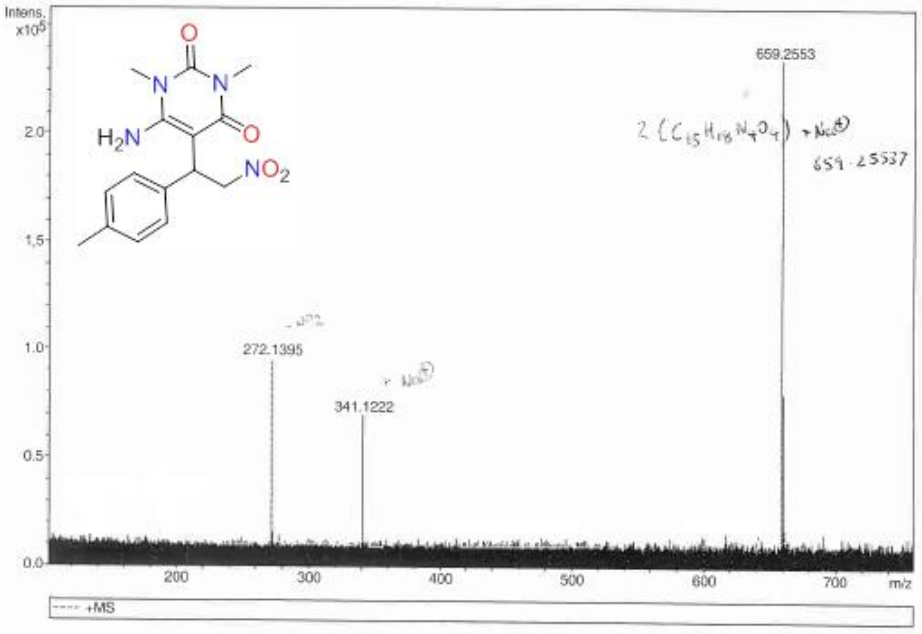

Sum Formula	Sigma	m/z	Err [ppm]	Mean Err [ppm]	Err [mDa]	rdb	N Rule	e⁻
C 15 H 18 N 4 Na 1 O 4	0.018	341.1220	-0.47	-1.54	-0.52	8.50	ok	even

Figure S9.89. ESI-MS of C9j

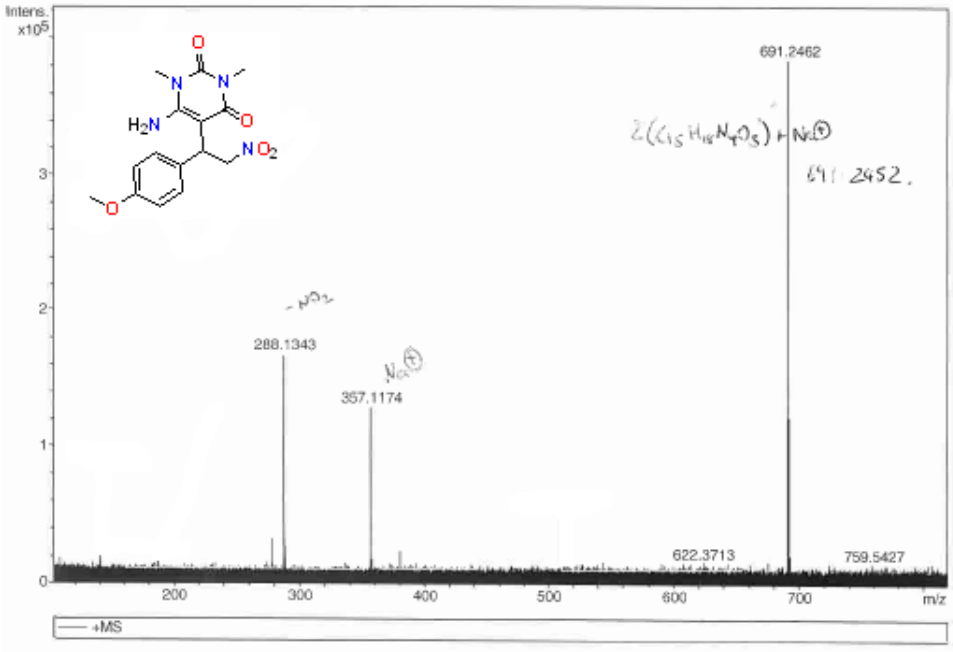

Sum Formula	Sigma	m/z	Err [ppm]	Mean Err [ppm]	Err [mDa]	rdb	N Rule	e⁻
C 15 H 18 N 4 Na 1 O 5	0.031	357.1169	-1.24	-1.28	-0.46	8.50	ok	even

Figure S9.90. ESI-MS of C9i

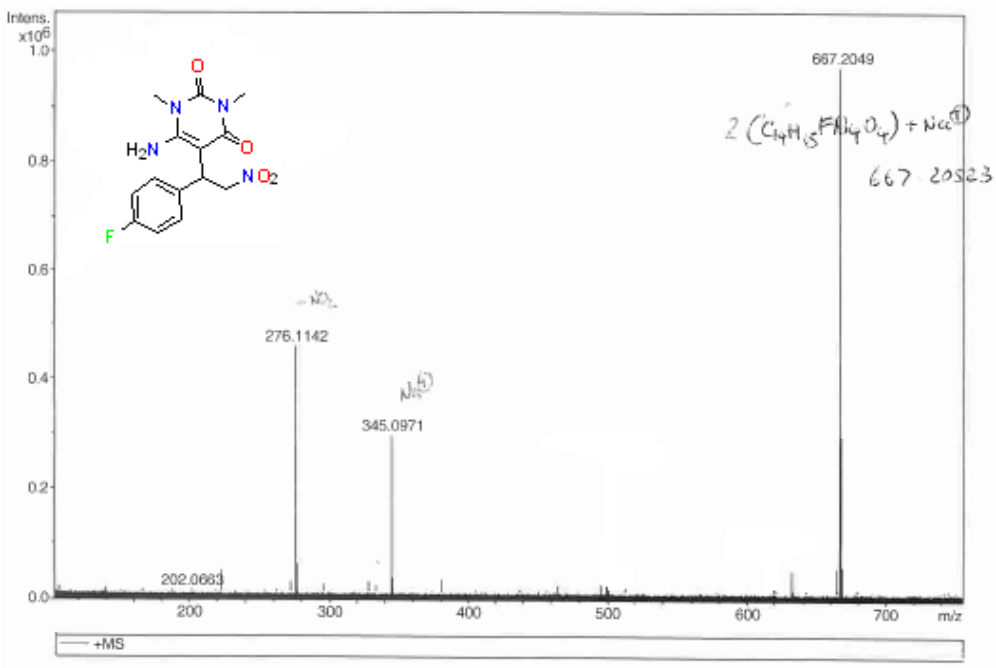

Sum Formula	Sigma	m/z	Err [ppm]	Mean Err [ppm]	Err [mDa]	rdb	N Rule	e⁻
C 14 H 15 F 1 N 4 Na 1 O 4	0.028	345.0970	-0.49	0.71	0.24	8.50	ok	even

Figure S9.91. ESI-MS of C9j

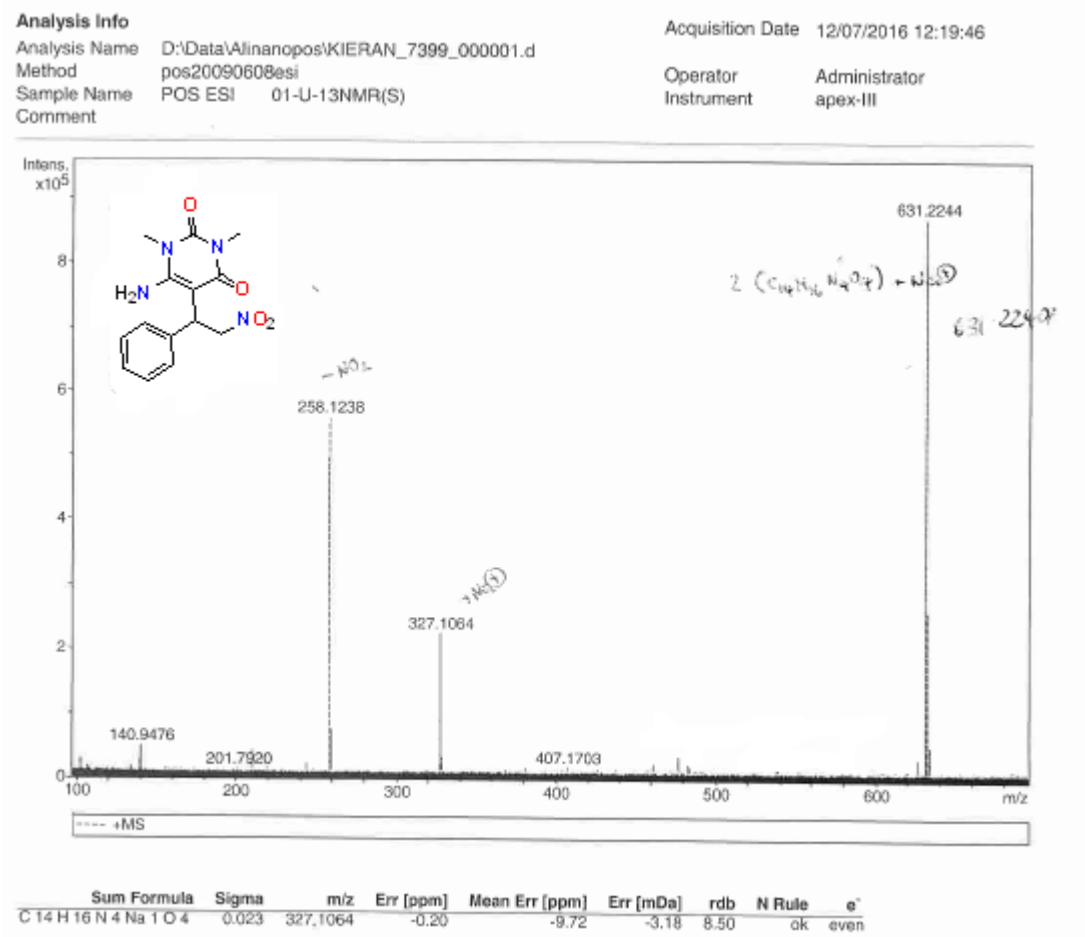

Sum Formula	Sigma	m/z	Err [ppm]	Mean Err [ppm]	Err [mDa]	rdb	N Rule	e⁻
C 14 H 16 N 4 Na 1 O 4	0.023	327.1064	-0.20	-9.72	-3.18	8.50	ok	even

Figure S9.92. ESI-MS of C9h

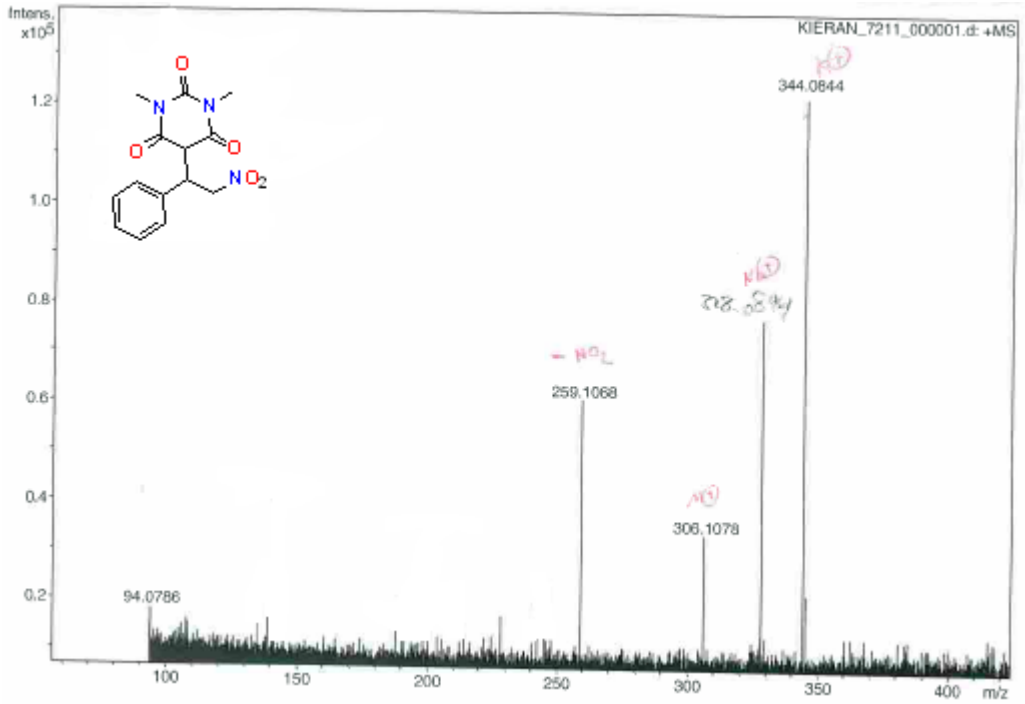

Figure S9.93. ESI-MS of C9a

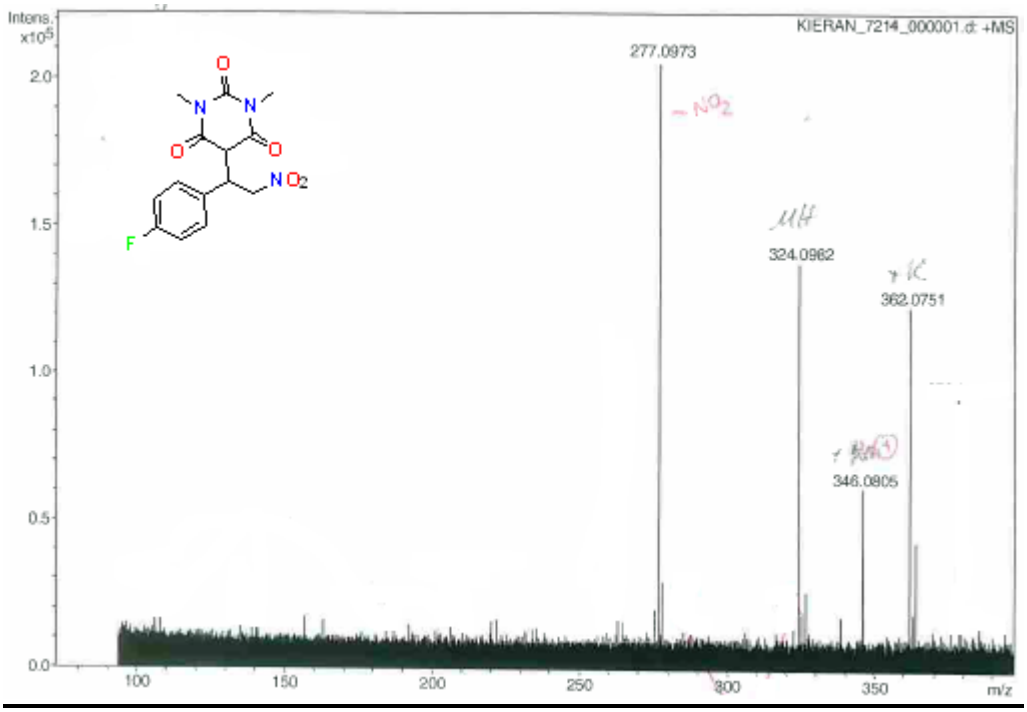

Figure S9.94. ESI-MS of C9e

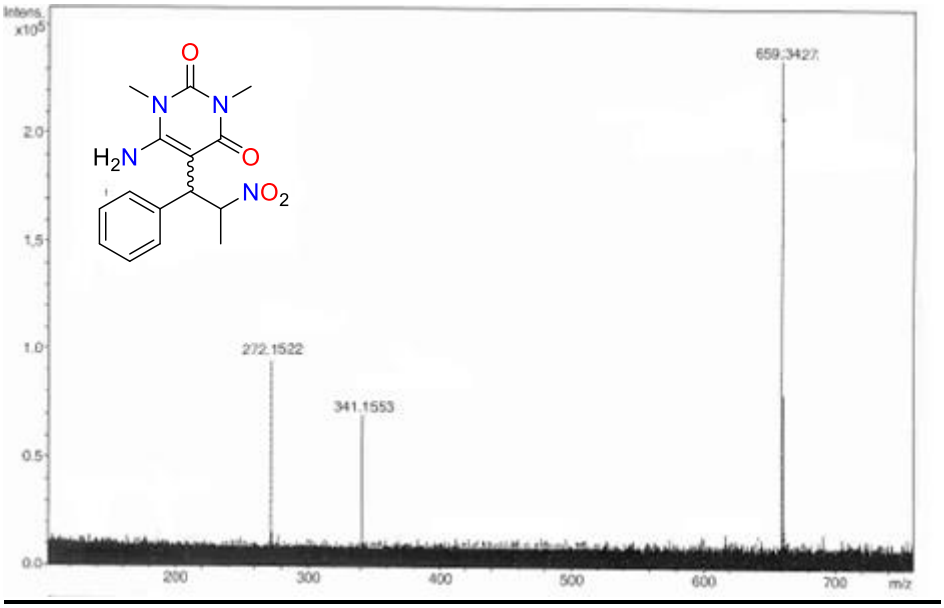

Figure S9.89. ESI-MS of C9m

Chapter 10

10.1 Reported PCCs in this thesis

Table S10.1 List of PCCs synthesised

Entry	Formula	Ligand	Topology	Chapter	Ref
1	$[Zn^{II}_2Ln^{III}_2(\mathbf{L1})_4(EtOH)_6](ClO_4)_2$	H_2**L1**	**2,3M4-1**	2	[1]
	Ln = Dy (**1**), Tb (**2**), Eu (**3**)				
2	$[Zn^{II}_5Ln(OH)(\mathbf{L1})_6(H_2O)]$	H_2**L1**	**2,3,4M6-1**	2	[1]
	Ln= Dy (**4**), Tb (**5**), Eu (**6**)				
3	$[(Zn^{II}_4Ln^{III}_2(OH)_2(\mathbf{L2})_4(OAc)_2(NO_3)_2(DMF)_3]$	H_2**L2**	**2,3,4M6-1**	2	[1]
	Ln = Dy (**7**), Tb (**8**), Eu (**9**)				
4	$[Zn^{II}_2Ln^{III}_2(\mathbf{L3})_2(NO_3)_2(CO_3)_2(CH_3OH)_2]$	H_3**L3**	**1,2,4M-1**	2	[1]
	Ln = Dy (**10**), Tb (**11**), Eu (**12**)				
5	$[Zn^{II}_4Dy^{III}_7(OH)_4(O_2)_2(\mathbf{L1})_8Cl_4(H_2O)_4]Cl_5$ (**13**)	H_2**L1**	**2,4,4,4M11-1**	2	[1]
6	$[Zn^{II}_6Dy^{III}_4(OH)_2(\mathbf{L1})_{10}(MeOH)_2(H_2O)_4]Cl_2$ (**14**)	H_2**L1**	**2,2,3,3M10-1**	2	[1]

7	$[Co^{II}_4Ln^{III}_2(\mu_3\text{-}OH)_2(\mathbf{L1})_4Cl_2(NO_3)_2(MeOH)_4]$ 3(Et_2O)	H_2**L1**	**2,3,4M6-1**	3	[2]
	Ln = Y (**15**), Gd (**16**), Dy(**17**), Tb (**18**)				
8	$[Co^{II}_4Dy^{III}_2(\mu_3\text{-}OH)_2(\mathbf{L5})_4Cl_2(NO_3)_2(MeOH)_4]$ (**19**)	H_2**L5**	**2,3,4M6-1**	3	[2]
10	$[Co^{II}_3Ln^{III}_4(\mu_3\text{-}OH)_6(\mathbf{L4})_6(CF_3SO_3)](CF_3SO_3)_5]$	H**L4**	**3,6M7-1**	4	[3]
	Ln = Gd (**20**), Y (**21**)				
11	$[Ni^{II}_3Ln^{III}_4(\mu_3\text{-}OH)_6(\mathbf{L4})_6(CF_3SO_3)](CF_3SO_3)_5]$	H**L4**	**3,6M7-1**	4	[3]
	Ln = Dy (**22**) Gd (**23**), Y (**24**)				
12	$(Et_3NH)[Co^{III}(\mathbf{L8})_2]\cdot 3MeOH$ (**25**)	H_2**L8**	**(0)**	5	[4]
13	$(Et_3NH)[Co^{III}(\mathbf{L18})_2]\cdot 2MeOH$ (**26**)	H_2**L18**	**(0)**	5	[4]
14	$[Ni^{II}_2Dy^{III}_2(\mathbf{L20})_4(\text{allyl-o-vanillin})_2(EtOH)_2]\cdot 3CH_2Cl_2$ (**27**)	H_2**L20**	**2,3M4-1**	5	[4]
15	$[Ni^{II}_2Dy^{III}_2(\mathbf{L20})_4(DMF)_6](ClO_4)_2$.4DMF (**28**)	H_2**L20**	**2,3M4-1**	5	[4]
16	$[Ni^{II}_2Dy^{III}_2(\mathbf{L22})_4(\text{bromo-o-vanillin})_2(EtOH)_2]$.6EtOH (**29**)	H_2**L22**	**2,3M4-1**	5	[4]
17	$[Ni^{II}_2Dy^{III}_2(\mathbf{L16})_4(\text{allyl-o-vanillin})_2(EtOH)_2]$ 2THF 2EtOH (**30**)	H_2**L16**	**2,3M4-1**	5	[4]
18	$[Ni^{II}_2Dy^{III}_2(\mathbf{L16})_4(DMF)_2](ClO_4)_2$ (**31**)	H_2**L16**	**2,3M4-1**	5	[4]
19	$[Ni^{II}_2Dy^{III}_2(\mathbf{L1})_4(EtOH)_4(H_2O)_2](ClO_4)_2$ (**32**)	H_2**L1**	**2,3M4-1**	5	[4]
20	$[Ni^{II}_2Dy^{III}_2(\mathbf{L1})_4(DMF)_6](OTf_3)_2\cdot 2DMF$ (**33**)	H_2**L**1	**2,3M4-1**	5	[4]

21	$[Ni^{II}_2Dy^{III}_2(\mathbf{L18})_4(DMF)_6]$ $[Ni^{II}_2Dy^{III}_2(\mathbf{L18})_4(DMF)_4(H_2O)_2]$ $(ClO_4)_4$ 5DMF (**34**)	H_2**L18**	**(2,3M4-1)+ (2,3M4-1)**	5	[4]
22	$[Ni^{II}_4(\mathbf{L2})_4(MeOH)_4]$ (**35**)	H_2**L2**	**3M4-1**	5	[4]
23	$[Ni^{II}_2Dy^{III}_2(\mathbf{L2})_4(EtOH)_6](ClO_4)_2$ 4EtOH (**36**)	H_2**L2**	**2,3M4-1**	5	[4]
24	$[Ni^{II}_2Dy^{III}_2(\mathbf{L19})_4(DMF)_6](ClO_4)_2 \cdot 2Et_2O$ (**37**)	H_2**L19**	**2,3M4-1**	5	[4]
25	$[Ni^{II}_2Dy^{III}_2(\mathbf{L1})_4(OAc)_2(MeOH)_2]$ ·2MeOH (**38**)	H_2**L1**	**2,3M4-1**	5	[4]
26	$[Co^{II}_2Dy^{III}_2(\mathbf{L9})_4(\mathbf{M1})_2(DMF)_2]$ (**39**)	H_2**L9**	**2,3M4-1**	5	[4]
27	$[Co^{II}_2Dy^{III}_2(\mathbf{L9})_4(\mathbf{M2})_2(DMF)_2]$ · 2DMF (**40**)	H_2**L9**	**2,3M4-1**	5	[4]
28	$[Dy^{III}(\mathbf{M1})_3(DMF)_2]$ (**41**)	M1	**(0)**	5	[4]
29	$[Ni^{II}_2Dy^{III}_2(OH)(\mathbf{L2})_3(\mathbf{M1})_3(DMF)_2]$ (**42**)	H_2**L2**	**2,3M4-1**	5	[4]
30	$[Zn^{II}_4Ln^{III}_{11}(\mu_4\text{-}OH)_2(\mu_3\text{-}OH)_8(\mu_2\text{-}OH_2)_2(\mu_3\text{-}NO_3)_2(NO_3)_6Cl_4(HL)_2(L')_4(\mu_2\text{-}MeO)_7(\mu_3\text{-}MeO)_2(MeOH)_2(H_2O)_2]$ Ln = Dy (**43**), Gd (**44**)	H_2**L**	**1,2,3,4,5,5,5,8M15--1**	6	This work
31	$[Ni^{II}_2Dy^{III}_2(\mathbf{L1})_4(EtOH)_6](ClO_4)_2 \cdot 2(EtOH)$ (**1NiDy-ClO$_4$)**	H_2**L1**	**2,3M4-1**	7	[5]
32	$[Co^{II}_2Dy^{III}_2(\mathbf{L1})_4(EtOH)_6](ClO_4)_2 \cdot 2(EtOH)$ (**1CoDy-ClO$_4$**)	H_2**L1**	**2,3M4-1**	7	[5]
33	$[Ni^{II}_2Ln^{III}_2(\mathbf{L1})_4Cl_2(CH_3CN)_2] \cdot 2(CH_3CN)_2$	H_2**L1**	**2,3M4-1**	7	[5,6]

	Ln = Dy (**1NiDy-Cl**), Sm (**1NiSm-Cl**), Eu (**1NiEu -Cl**), Gd (**1NiGd-Cl)**, Tb (**1NiTb-Cl**), Y (**1NiY-Cl**)				
34	$[Co^{II}_2Ln^{III}_2(\mathbf{L1})_4Cl_2(CH_3CN)_2]\cdot 2(CH_3CN)_2$ (**1CoDy-Cl**)	H_2**L1**	**2,3M4-1**	7	
35	$[Ni^{II}_2Ln^{III}_2(\mathbf{L6})_4Cl_2(DMF)_2]$ (**6NiY-Cl**)	H_2**L6**	**2,3M4-1**	7	6
36	$[Ni^{II}_2Ln^{III}_2(\mathbf{L2})_4Cl_2(DMF)_2]$ (**2NiY-Cl**)	H_2**L2**	**2,3M4-1**	7	6
37	$[Ni^{II}_2Ln^{III}_2(\mathbf{L16})_4Cl_2(DMF)_2]$ (**16NiY- Cl**)	H_2**L16**	**2,3M4-1**	7	6
38	$[Ni^{II}_5Sm^{III}_2(CO_3)(\mathbf{L1})_7(L')(H_2O)_3]$ (**1NiSm-Cl-A**)	H_2**L1**		7	6
39	$[Ni^{II}_2Sm^{III}_2(\mathbf{L1})_4(O\text{-}Van)_2(H_2O)_2]$ (**1NiSm-Cl-B**)	H_2**L1**	**2,3M4-1**	7	6
40	$[Sm^{III}_4(OH)_2(\mathbf{L1})_4(H\mathbf{L1})_2]$ (**1NiSm-Cl-C**)	H_2**L1**		7	6
41	$[Ni^{II}_8Eu^{III}_4(\mathbf{L1})_8(CO_3)_4Cl_4(H_2O)_{14}]$ (**1NiEu-Cl-A**)	H_2**L1**		7	6
42	$[Zn^{II}_2Ln^{III}_2(\mathbf{L1})4(NO_3)_2(DMF)_2]$	H_2**L1**	**2,3M4-1**	8	7
	Ln = Y(**1ZnY-NO$_3$**), Sm (**1ZnSm-NO$_3$**), Eu (**1ZnEu-NO$_3$**), Gd(**1ZnGd-NO$_3$**), Dy (**1ZnDy-NO$_3$**), Tb (**1ZnTb-NO$_3$**), Yb (**1ZnYb-NO$_3$**)				
44	$[Zn^{II}_2Y^{III}_2(\mathbf{L5})_4(NO_3)_2(DMF)_2]$ (**5ZnY-NO$_3$**)	H_2**L5**	**2,3M4-1**	9	8
45	$[Zn^{II}_2Y^{III}_2(\mathbf{L6})_4(NO_3)_2(DMF)_2]$ (**6ZnY-NO$_3$**)	H_2**L6**	**2,3M4-1**	9	8
46	$[Zn^{II}_2Y^{III}_2(\mathbf{L8})_4(NO_3)_2(DMF)_2]$ (**8ZnY-NO$_3$**)	H_2**L8**	**2,3M4-1**	9	8
47	$[Zn^{II}_2Y^{III}_2(\mathbf{L9})_4(NO_3)_2(DMF)_2]$ (**9ZnY-NO$_3$**)	H_2**L9**	**2,3M4-1**	9	8

48	$[Zn^{II}_2Y^{III}_2(\mathbf{L11})_4(NO_3)_2(DMF)_2]$ (**11ZnY-NO$_3$**)	H_2**L11**	**2,3M4-1**	9	[8]
49	$[Zn^{II}_2Y^{III}_2(\mathbf{L12})_4(NO_3)_2(DMF)_2]$ (**12ZnY-NO$_3$**)	H_2**L12**	**2,3M4-1**	9	[8]
50	$[Zn^{II}_2Y^{III}_2(\mathbf{L13})_4(NO_3)_2(DMF)_2]$ (**13ZnY-NO$_3$**)	H_2**L13**	**2,3M4-1**	9	[8]
51	$[Zn^{II}_2Y^{III}_2(\mathbf{L15})_4(NO_3)_2(DMF)_2]$ (**15ZnY-NO$_3$**)	H_2**L15**	**2,3M4-1**	9	[8]
	$Zn^{II}_2Y^{III}_2(\mathbf{L2})_4(NO_3)_2(DMF)_2]$ (**2ZnY-NO$_3$**)	H_2**L2**	**2,3M4-1**	9	[8]
52	$[Zn^{II}_2Y^{III}_2(\mathbf{L16})_4(NO_3)_2(DMF)_2]$ (**16ZnY-NO$_3$**)	H_2**L16**	**2,3M4-1**	9	[8]
53	$[Zn^{II}_2Y^{III}_2(\mathbf{L18})_4(NO_3)_2(DMF)_2]$ (**18ZnY-NO$_3$**)	H_2**L18**	**2,3M4-1**	9	[8]
54	$[Zn^{II}_2Y^{III}_2(\mathbf{L19})_4(NO_3)_2(DMF)_2]$ (**19ZnY-NO$_3$**)	H_2**L19**	**2,3M4-1**	9	[8]
55	$[Zn^{II}_2Y^{III}_2(\mathbf{L20})_4(NO_3)_2(DMF)_2]$ (**20ZnY-NO$_3$**)	H_2**L20**	**2,3M4-1**	9	[8]
56	$[Zn^{II}_2Y^{III}_2(\mathbf{L22})_4(NO_3)_2(DMF)_2]$ (**22ZnY-NO$_3$**)	H_2**L22**	**2,3M4-1**	9	[8]
57	$[Zn^{II}_2Y^{III}_2(\mathbf{L24})_4(NO_3)_2(DMF)_2]$ (**24ZnY-NO$_3$**)	H_2**L24**	**2,3M4-1**	9	[8]
58	$[Zn^{II}_2Y^{III}_2(\mathbf{L25})_4(NO_3)_2(DMF)_2]$ (**25ZnY-NO$_3$**)	H_2**L25**	**2,3M4-1**	9	[8]
59	$[Zn^{II}_2Y^{III}_2(\mathbf{L26})_4(NO_3)_2(DMF)_2]$ (**26ZnY-NO$_3$**)	H_2**L26**	**2,3M4-1**	9	[8]
60	$[Zn^{II}_2Y^{III}_2(\mathbf{L27})_4(NO_3)_2(DMF)_2]$ (**27ZnY-NO$_3$**)	H_2**L27**	**2,3M4-1**	9	[8]
61	$[Zn^{II}_2Y^{III}_2(\mathbf{L28})_4(NO_3)_2(DMF)_2]$ (**28ZnY-NO$_3$**)	H_2**L28**	**2,3M4-1**	9	[8]
62	$[Zn^{II}_2Y^{III}_2(\mathbf{L29})_4(NO_3)_2(DMF)_2]$ (**29ZnY-NO$_3$**)	H_2**L29**	**2,3M4-1**	9	[8]

63	$[Cu^{II}_2Dy^{II}_2(\mathbf{L1})_4(NO_3)_2]$.4MeCN (**1CuDy-NO$_3$**)	H_2**L1**	**2,3M4-1**	9	[8]

Bibliography

1 K. Griffiths, J. Mayans, M. A. Shipman, G. J. Tizzard, S. J. Coles, B. A. Blight, A. Escuer and G. E. Kostakis, *Cryst. Growth Des.*, 2017, **17**, 1524–1538.

2 K. Griffiths, G. Novitchi and G. E. Kostakis, *Eur. J. Inorg. Chem.*, 2016, **2016**, 2750–2756.

3 K. Griffiths, C. Harding, V. N. Dokorou, E. Loukopoulos, S. I. Sampani, A. Abdul-Sada, G. J. Tizzard, S. J. Coles, G. Lorusso, M. Evangelisti, A. Escuer and G. E. Kostakis, *Eur. J. Inorg. Chem.*, 2017, **2017**, 3938–3945.

4 K. Griffiths, V. N. Dokorou, J. Spencer, A. Abdul-Sada, A. Vargas and G. E. Kostakis, *CrystEngComm*, 2016, **18**, 704–713.

5 K. Griffiths, C. W. D. Gallop, A. Abdul-Sada, A. Vargas, O. Navarro and G. E. Kostakis, *Chem. Eur. J.*, 2015, **21**, 6358–6361.

6 K. Griffiths, P. Kumar, J. D. Mattock, A. Abdul-Sada, M. B. Pitak, S. J. Coles, O. Navarro, A. Vargas and G. E. Kostakis, *Inorg. Chem.*, 2016, **55**, 6988–6994.

7 K. Griffiths, P. Kumar, G. Akien, N. F. Chilton, A. Abdul-Sada, G. J. Tizzard, S. Coles and G. E. Kostakis, *Chem. Commun.*, 2016, **52**.

8 K. Griffiths, A. C. Tsipis, P. Kumar, O. P. E. Townrow, A. Abdul-Sada, G. R. Akien, A. Baldansuren, A. C. Spivey and G. E. Kostakis, *Inorg. Chem.*, 2017, **56**, 9563–9573.